

ΔΕΛΤΙΟ ΤΗΣ ΕΛΛΗΝΙΚΗΣ ΓΕΩΛΟΓΙΚΗΣ ΕΤΑΙΡΙΑΣ
Τόμος XLIII, No 3

BULLETIN OF THE GEOLOGICAL SOCIETY OF GREECE
Volume XLIII, No 3

ΕΙΚΟΝΑ ΕΞΩΦΥΛΛΟΥ - COVER PAGE

Γενική άποψη της γέφυρας Ρίου-Αντιρρίου. Οι πυλώνες της γέφυρας διασκοπήθηκαν γεωφυσικά με χρήση ηχοβολιστή πλευρικής σάρωσης (EG&G 4100P και EG&G 272TD) με σκοπό την αποτύπωση του πυθμένα στην περιοχή του έργου, όσο και των βάθρων των πυλώνων. (Εργαστήριο Θαλάσσιας Γεωλογίας & Φυσικής Ωκεανογραφίας, Πανεπιστήμιο Πατρών. Συλλογή και επεξεργασία: Δ.Χριστοδούλου, Η. Φακίρης).

General view of the Rion-Antirion bridge, from a marine geophysical survey conducted by side scan sonar (EG&G 4100P and EG&G 272TD) in order to map the seafloor at the site of the construction (pylons and piers) (Gallery of the Laboratory of Marine Geology and Physical Oceanography, University of Patras. Data acquisition and Processing: D. Christodoulou, E. Fakiris).

ΔΕΛΤΙΟ ΤΗΣ ΕΛΛΗΝΙΚΗΣ ΓΕΩΛΟΓΙΚΗΣ ΕΤΑΙΡΙΑΣ
Τόμος XLIII, Νο 3

BULLETIN OF THE GEOLOGICAL SOCIETY OF GREECE
Volume XLIII, No 3

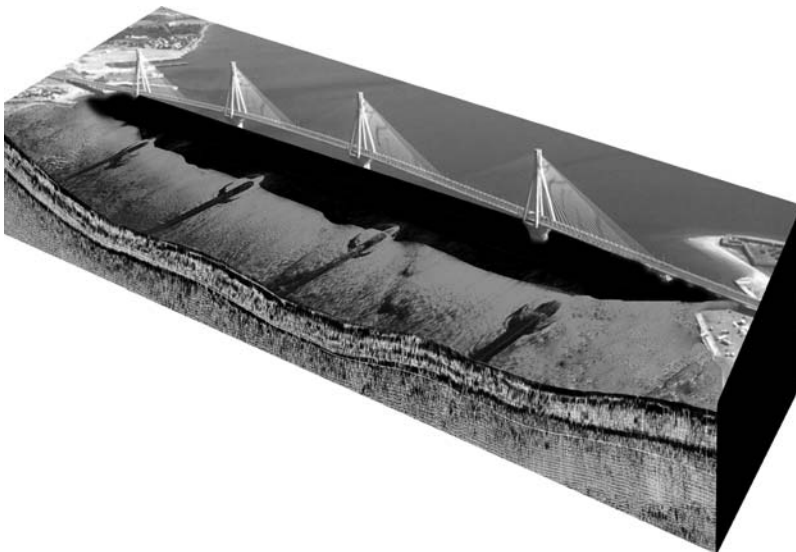


**12ο ΔΙΕΘΝΕΣ ΣΥΝΕΔΡΙΟ
ΤΗΣ ΕΛΛΗΝΙΚΗΣ ΓΕΩΛΟΓΙΚΗΣ ΕΤΑΙΡΙΑΣ**

ΠΛΑΝΗΤΗΣ ΓΗ:
Γεωλογικές Διεργασίες και Βιώσιμη Ανάπτυξη

**12th INTERNATIONAL CONGRESS
OF THE GEOLOGICAL SOCIETY OF GREECE**

PLANET EARTH:
Geological Processes and Sustainable Development



ΠΑΤΡΑ / PATRAS 2010

ISSN 0438-9557

Copyright © από την Ελληνική Γεωλογική Εταιρεία
Copyright © by the Geological Society of Greece

12ο ΔΙΕΘΝΕΣ ΣΥΝΕΔΡΙΟ
ΤΗΣ ΕΛΛΗΝΙΚΗΣ ΓΕΩΛΟΓΙΚΗΣ ΕΤΑΙΡΙΑΣ

ΠΛΑΝΗΤΗΣ ΓΗ:
Γεωλογικές Διεργασίες και Βιώσιμη Ανάπτυξη

Υπό την Αιγίδα του
Υπουργείου Περιβάλλοντος, Ενέργειας και Κλιματικής Αλλαγής

12th INTERNATIONAL CONGRESS
OF THE GEOLOGICAL SOCIETY OF GREECE

PLANET EARTH:
Geological Processes and Sustainable Development

Under the Aegis of the
Ministry of Environment, Energy and Climate Change



ΠΡΑΚΤΙΚΑ / PROCEEDINGS

ΕΠΙΜΕΛΕΙΑ ΕΚΔΟΣΗΣ

Γ. ΚΟΥΚΗΣ

Πανεπιστήμιο Πατρών

Α. ΖΕΛΗΛΙΔΗΣ

Πανεπιστήμιο Πατρών

Ι. ΚΟΥΚΟΥΒΕΛΑΣ

Πανεπιστήμιο Πατρών

Γ. ΠΑΠΑΘΕΟΔΩΡΟΥ

Πανεπιστήμιο Πατρών

Μ. ΓΕΡΑΓΑ

Πανεπιστήμιο Πατρών

Β. ΖΥΓΟΥΡΗ

Πανεπιστήμιο Πατρών

EDITORS

G. KOUKIS

University of Patras

A. ZELILIDIS

University of Patras

I. KOUKOUVELAS

University of Patras

G. PAPATHEODOROU

University of Patras

M. GERAGA

University of Patras

V. ZYGOURI

University of Patras

PATRAS, May 2010

ΕΛΛΗΝΙΚΗ ΓΕΩΛΟΓΙΚΗ ΕΤΑΙΡΙΑ



ΔΙΟΙΚΗΤΙΚΟ ΣΥΜΒΟΥΛΙΟ

(που εξελέγη στη Γενική Συνέλευση των μελών της Εταιρίας το Μάρτιο του 2010)

ΠΡΟΕΔΡΟΣ

Απόστολος ΑΛΕΞΟΠΟΥΛΟΣ

ΑΝΤΙΠΡΟΕΔΡΟΣ

Αλεξάνδρα ΖΑΜΠΕΤΑΚΗ-ΛΕΚΚΑ

ΓΕΝ. ΓΡΑΜΜΑΤΕΑΣ

Ευγενία ΜΩΡΑΪΤΗ

ΕΙΔ. ΓΡΑΜΜΑΤΕΑΣ

Δημήτριος ΓΑΛΑΝΑΚΗΣ

ΤΑΜΙΑΣ

Ασημίνα ΑΝΤΩΝΑΡΑΚΟΥ

ΕΦΟΡΟΣ

Χαράλαμπος ΚΡΑΝΗΣ

ΜΕΛΗ

Κωνσταντίνος ΒΟΥΔΟΥΡΗΣ

Χρυσάνθη ΙΩΑΚΕΙΜ

Αθανάσιος ΓΚΑΝΑΣ

GEOLOGICAL SOCIETY OF GREECE



BOARD OF DIRECTORS

(elected at the General Assembly of the members of the Society on March 2010)

PRESIDENT

Apostolos ALEXOPOULOS

VICE-PRESIDENT

Alexandra ZAMBETAKIS-LEKKAS

GENERAL SECRETARY

Evgenia MORAITI

EXECUTIVE SECRETARY

Dimitrios GALANAKIS

TREASURER

Asimina ANTONARAKOU

TRUSTEE

Charalambos KRANIS

MEMBERS

Konstantinos VOUDOURIS

Chyssanthi IOAKIM

Athanasios GANAS

ΟΡΓΑΝΩΤΙΚΗ ΕΠΙΤΡΟΠΗ 12ου ΔΙΕΘΝΟΥΣ ΣΥΝΕΔΡΙΟΥ



ΠΡΟΕΔΡΟΣ

Γεώργιος ΚΟΥΚΗΣ, Καθηγητής Πανεπιστημίου Πατρών

ΑΝΤΙΠΡΟΕΔΡΟΣ

Αβραάμ ΖΕΛΗΛΙΔΗΣ, Καθηγητής Πανεπιστημίου Πατρών

ΓΕΝΙΚΟΣ ΓΡΑΜΜΑΤΕΑΣ

Ιωάννης ΚΟΥΚΟΥΒΕΛΑΣ, Αν. Καθηγητής Πανεπιστημίου Πατρών

ΕΙΔΙΚΟΣ ΓΡΑΜΜΑΤΕΑΣ

Γεώργιος ΠΑΠΑΘΕΟΔΩΡΟΥ, Αν. Καθηγητής Πανεπιστημίου Πατρών

ΤΑΜΙΑΣ

Μαρία ΓΕΡΑΓΑ, Λέκτορας Πανεπιστημίου Πατρών

ΜΕΛΗ

Νικόλαος ΚΟΝΤΟΠΟΥΛΟΣ, Καθηγητής Πανεπιστημίου Πατρών

Νικόλαος ΛΑΜΠΡΑΚΗΣ, Καθηγητής Πανεπιστημίου Πατρών

Νικόλαος ΣΑΜΠΑΤΑΚΑΚΗΣ, Αν. Καθηγητής Πανεπιστημίου Πατρών

Ευθύμιος ΣΩΚΟΣ, Επ. Καθηγητής Πανεπιστημίου Πατρών

Δημήτριος ΠΑΠΟΥΛΗΣ, Λέκτορας Πανεπιστημίου Πατρών

Μιχαήλ ΣΤΑΜΑΤΑΚΗΣ, Καθηγητής Εθνικού και Καποδιστριακού
Πανεπιστημίου Αθηνών

Απόστολος ΑΛΕΞΟΠΟΥΛΟΣ, Καθηγητής Εθνικού και Καποδιστριακού Πανεπι-
στημίου Αθηνών, Πρόεδρος Ε.Γ.Ε.

Κωνσταντίνος ΠΑΠΑΒΑΣΙΛΕΙΟΥ, Αν. Καθηγητής Εθνικού και Καποδιστριακού
Πανεπιστημίου Αθηνών, Γενικός Δ/ντής Ι.Γ.Μ.Ε.

Κωνσταντίνος ΜΑΚΡΟΠΟΥΛΟΣ, Καθηγητής Εθνικού και Καποδιστριακού
Πανεπιστημίου Αθηνών, Δ/ντής Γεωδυναμικού Ινστιτούτου Ε.Α.Α.

Εμμανουήλ ΜΑΝΟΥΤΣΟΓΛΟΥ, Αν. Καθηγητής Πολυτεχνείου Κρήτης

Σπυρίδων ΠΑΥΛΙΔΗΣ, Καθηγητής Αριστοτελείου Πανεπιστημίου Θεσσαλονίκης

Κωνσταντίνος ΠΑΠΑΚΩΝΣΤΑΝΤΙΝΟΥ, Πρόεδρος ΕΛ.ΚΕ.Θ.Ε.

Γραμματεία Συνεδρίου

Συνέδρα

Ηρ. Πολυτεχνείου 92, 26442 Πάτρα • Τηλ.: 2610 432.200 • Fax: 2610 430.884

URL: www.synedra.gr • E-mail: synedra@synedra.gr

ORGANIZING COMMITTEE OF THE 12th INTERNATIONAL CONGRESS



PRESIDENT

George KOUKIS, Professor, University of Patras

VICE-PRESIDENT

Abraham ZELILIDIS, Professor, University of Patras

GENERAL SECRETARY

Ioannis KOUKOUVELAS, Assoc. Professor, University of Patras

EXECUTIVE SECRETARY

George PAPTAEODOROU, Assoc. Professor, University of Patras

TREASURER

Maria GERAGA, Lecturer, University of Patras

MEMBERS

Nikolaos KONTOPOULOS, Professor, University of Patras

Nikolaos LAMBRAKIS, Professor, University of Patras

Nikolaos SABATAKAKIS, Assoc. Professor, University of Patras

Eythimios SOKOS, Assist. Professor, University of Patras

Dimitrios PAPOULIS, Lecturer, University of Patras

Michael STAMATAKIS, Professor, National and Kapodistrian
University of Athens

Apostolos ALEXOPOULOS, Professor, National and Kapodistrian University of Athens.
President of G.S.G.

Constantinos PAPAASSILEIOU, Assoc. Professor, National and Kapodistrian University of
Athens, Gen. Director of I.G.M.E.

Konstantinos MAKROPOULOS, Professor, National and Kapodistrian University of Athens,
Director of Institute of Geodynamics, N.O.A.

Emmanouil MANOUTSOGLU, Assoc. Professor, Technical University of Crete

Spyridon PAVLIDES, Professor, Aristotle University of Thessaloniki

Konstantinos PAPACONSTANTINOY, President of H.C.M.R.

Congress Secretariat

Synedra

Iroon Polytechniou 92, GR 26442 Patras • Ph.: +302610 432.200 • Fax: +302610 430.884
URL: www.synedra.gr • E-mail: synedra@synedra.gr

ΧΟΡΗΓΟΙ
ΤΟΥ 12ου ΔΙΕΘΝΟΥΣ ΣΥΝΕΔΡΙΟΥ ΤΗΣ ΕΛΛΗΝΙΚΗΣ ΓΕΩΛΟΓΙΚΗΣ ΕΤΑΙΡΙΑΣ



Υπό την Αιγίδα του
ΥΠΟΥΡΓΕΙΟΥ ΠΕΡΙΒΑΛΛΟΝΤΟΣ, ΕΝΕΡΓΕΙΑΣ & ΚΛΙΜΑΤΙΚΗΣ ΑΛΛΑΓΗΣ

και τη Συμβολή των
ΤΜΗΜΑ ΓΕΩΛΟΓΙΑΣ ΠΑΝΕΠΙΣΤΗΜΙΟΥ ΠΑΤΡΩΝ
ΙΝΣΤΙΤΟΥΤΟ ΓΕΩΛΟΓΙΚΩΝ ΚΑΙ ΜΕΤΑΛΛΕΥΤΙΚΩΝ ΕΡΕΥΝΩΝ
ΓΕΩΤΕΧΝΙΚΟ ΕΠΙΜΕΛΗΤΗΡΙΟ ΕΛΛΑΔΑΣ

ΚΟΙΝΩΦΕΛΕΣ ΙΔΡΥΜΑ
ΙΩΑΝΝΗ Σ. ΛΑΤΣΗ

ΠΑΝΕΠΙΣΤΗΜΙΟ ΠΑΤΡΩΝ

ΟΡΓΑΝΙΣΜΟΣ ΑΝΤΙΣΕΙΣΜΙΚΟΥ
ΣΧΕΔΙΑΣΜΟΥ ΚΑΙ ΠΡΟΣΤΑΣΙΑΣ

ΑΚΤΩΡ Α.Τ.Ε.

ΕΜΒΕΛΕΙΑ Α.Ε.

ΕΛΛΗΝΙΚΑ ΛΑΤΟΜΕΙΑ Α.Ε.

ΟΜΙΛΟΣ ΤΕΧΝΙΚΩΝ ΜΕΛΕΤΩΝ
(ΟΤΜ) Α.Τ.Ε.

ΓΕΦΥΡΑ Α.Ε.

ΓΕΝΙΚΗ ΜΕΛΕΤΩΝ Ε.Π.Ε. «ΙΣΤΡΙΑ»

ΣΥΝΔΕΣΜΟΣ ΜΕΤΑΛΛΕΥΤΙΚΩΝ
ΕΠΙΧΕΙΡΗΣΕΩΝ

ΔΕΛΦΟΙ-ΔΙΣΤΟΜΟΝ Α.Μ.Ε.

ΓΕΩΜΗΧΑΝΙΚΗ Α.Τ.Ε.

Α.Ε. ΤΣΙΜΕΝΤΩΝ ΤΙΤΑΝ

ΕΛΑΦΟΣ ΣΥΜΒΟΥΛΟΙ
ΜΗΧΑΝΙΚΟΙ Α.Ε.

ΓΕΩΣΚΟΠΙΟ Α.Τ.Ε.

Η Οργανωτική Επιτροπή του 12ου Διεθνούς Συνεδρίου της Ελληνικής Γεωλογικής Εταιρείας ευχαριστεί θερμά τα ανωτέρω Ιδρύματα, Ινστιτούτα Ερευνών, Οργανισμούς, Τεχνικές και Μελετητικές Εταιρείες για την οικονομική υποστήριξη και συμβολή τους στην οργάνωση και υλοποίηση του Συνεδρίου.

SPONSORS
OF THE 12th INTERNATIONAL CONGRESS OF THE GEOLOGICAL SOCIETY OF GREECE



Under the Aegis of the
MINISTRY OF ENVIRONMENT, ENERGY AND CLIMATE CHANGE

and the Contribution of the
DEPARTMENT OF GEOLOGY, UNIVERSITY OF PATRAS
INSTITUTE OF GEOLOGY AND MINERAL EXPLORATION
GEOTECHNICAL CHAMBER OF GREECE

JOHN S. LATSIS, PUBLIC BENEFIT
FOUNDATION

UNIVERSITY OF PATRAS

EARTHQUAKE PLANNING AND
PROTECTION ORGANIZATION

AKTOR S.A.

EMBELIA S.A.

HELLENIC QUARRIES S.A..

CONSULTING ENGINEERING
COMPANY (OTM) S.A.

GEFYRA S.A.

GENERAL CONSULTING LTD "ISTRIA"

GREEK MINING ENTERPRISES
ASSOCIATION

DELFI-DISTOMON BAUXITE S.A.

GEOMECHANIKI S.A.

TITAN CEMENT COMPANY S.A.

EDAFOS ENGINEERING
CONSULTANTS S.A.

GEOSCOPIO S.A.

The Organizing Committee of the 12th International Congress of the Geological Society of Greece expresses its grateful thanks to the above Foundations, Institutes, Organizations, Construction and Consulting Companies for their substantial support.

ΕΠΙΣΤΗΜΟΝΙΚΗ ΕΠΙΤΡΟΠΗ – SCIENTIFIC COMMITTEE



Η Οργανωτική Επιτροπή ευχαριστεί θερμά τους κριτές για τη συμβολή τους στην κρίση όλων των εργασιών. Κάθε εργασία κρίθηκε από δύο κριτές για την απόκτηση Πρακτικών υψηλού επιστημονικού επιπέδου. Η Οργανωτική Επιτροπή δεν έχει ευθύνη για το περιεχόμενο και τις απόψεις που εκφράζονται στις εργασίες από τους συγγραφείς.

The Organizing Committee expresses sincere thanks to the reviewers for their contribution in evaluating and approving of the submitted papers. Each paper has passed through two reviewers, producing Proceedings of high scientific level. The Organizing Committee is not responsible for the content and the views expressed by the authors in the papers.

Alexopoulos A., Alexopoulos I., Alexouli A., Anagnostou C., Antonarakou A., Argyraki A., Avramidis P., Bersezio R., Bogdanov K., Caputo R., Christanis K., Christaras B., Christidis G., Depountis N., Drakatos G., Dresnier Th. Drinia H., Economou G., Fassoulas C., Ferentinos G., Fermeli G., Filippidis A., Fountoulis I. Frey M.L., Gaki – Papanastassiou K., Ganas A., Georgakopoulos A., Geraga M., Godelitsas A., Hatzipanagioutou K., Iliopoulos I., Ioakim C., Kalavrouziotis I., Kaleris V., Kallergis G., Kamberis E., Karakaisis G.F., Karakitsios V., Karastathis V., Karipi S., Katagas C., Kati M., Katsonopoulou D., Kiliass A., Kiratzi A., Kitsou D., Kokkalas S., Kollaman H., Kondopoulou D., Konispoliatis N., Konstantinou C., Kontopoulos N., Koroneos A., Koukis G., Koukouvelas I., Lambrakis N., Laskou M., Lekkas E., Loupasakis C., Lykousis V., Magganas A., Manoutsoglou E., Marinou P.V., Markopoulos Th., Migiros G., Mladenova Th., Mountrakis D., Mposkos E., Mylonakis G., Nakov R., Nikolaou N., Oprsal I., Papadimitriou E., Papadimitriou P., Papadopoulos T., Papaioannou Ch., Papamarinopoulos S., Papanastassiou D., Papanikolaou D., Papatheodorou G., Papazachos C.B., Papoulis D., Paraskevopoulos P., Parcharidis I., Pavlides S., Pavlopoulos A., Pe – Piper G., Perdikakis V., Perrakis M., Perraki Th., Petalas C., Pomoni – Papaioannou F., Pomonis P., Ritolo S., Rokka A., Rondoyanni Th., Roumelioti Z., Rozos D., Ruiz – Ortiz P.A., Sabatakakis N., Sachpazi M., Sakellariou D., Scordilis Em., Seifert Th., Skarpelis N., Skias S., Sokos E., Soulios G., Soupios P., Stamatakis M., Stamatelopoulou - Seymour K., Stamatis G., Stiros S., Stournaras G., Syrides G., Theodorou G., Theodosiou I., Torok A., Tranos M., Triantafyllou M.V., Tsapanos T.M., Tselentis G-A., Tsiambaos G., Tsikouras B., Tshipoura – Vlahou M., Tsirambides A., Tsokas G., Tsolis–Katagas P., Tsombos P., Tsourlos P., Tucker M.E., Tulipano L., Tzani A., Varnavas S., Vavelidis M., Voudouris K., Voulgaris N., Xypolias P., Zagana E., Zambetakis – Lekkas A., Zelilidis A., Zouros N., Zygori V.

ΔΟΜΗ ΤΩΝ ΠΡΑΚΤΙΚΩΝ / SCHEME OF THE PROCEEDINGS



TOMOS 1 / VOLUME 1

Εναρκτήρια Ομιλία / Opening Lectures
Κεντρικές και Θεματικές Ομιλίες / Special and Keynote Lectures
Γενική και Τεκτονική Γεωλογία / General and Structural Geology
Νεοτεκτονική και Γεωμορφολογία / Neotectonics and Geomorphology

TOMOS 2 / VOLUME 2

Παλαιοντολογία, Στρωματογραφία και Ιζηματολογία /
Palaeontology, Stratigraphy and Sedimentology
Γεωαρχαιολογία / Geoarchaeology
Γεώτοποι / Geosites
Διδακτική των Γεωεπιστημών / Teaching Earth Sciences
Θαλάσσια Γεωλογία και Ωκεανογραφία / Marine Geology and Oceanography

TOMOS 3 / VOLUME 3

Τεχνική Γεωλογία και Γεωτεχνική Μηχανική /
Engineering Geology and Geotechnical Engineering
Φυσικές Καταστροφές / Natural Hazards
Αστική Γεωλογία / Urban Geology
Γ.Σ.Π. στις Γεωεπιστήμες / G.I.S. in Earth Sciences

TOMOS 4 / VOLUME 4

Υδρογεωλογία και Υδρολογία / Hydrogeology and Hydrology
Γεωφυσική / Geophysics
Σεισμολογία / Seismology

TOMOS 5 / VOLUME 5

Ενεργειακές Πρώτες Υλες και Γεωθερμία / Energy Resources and Geothermics
Γεωχημεία και Κοιτασματολογία / Geochemistry and Ore Deposit Geology
Βιομηχανικά Ορυκτά και Πετρώματα / Industrial Minerals and Rocks
Ορυκτολογία και Πετρολογία / Mineralogy and Petrology

ΤΑ ΣΥΝΕΔΡΙΑ ΤΗΣ Ε.Γ.Ε.

- 1ο ΔΙΗΜΕΡΟ, ΑΘΗΝΑ, 1983, Δελτίο XVII
- 2ο ΔΙΗΜΕΡΟ, ΑΘΗΝΑ, 1984, Δελτίο XIX
- 3ο ΣΥΝΕΔΡΙΟ, ΑΘΗΝΑ, 1986, Δελτίο XX
- 4ο ΣΥΝΕΔΡΙΟ, ΑΘΗΝΑ, 1988, Δελτίο XXIII
- 5ο ΣΥΝΕΔΡΙΟ, ΘΕΣΣΑΛΟΝΙΚΗ, 1990, Δελτίο XXV
- 6ο ΣΥΝΕΔΡΙΟ, ΑΘΗΝΑ, 1992, Δελτίο XXVIII
- 7ο ΣΥΝΕΔΡΙΟ, ΘΕΣΣΑΛΟΝΙΚΗ, 1994, Δελτίο XXX
- 8ο ΣΥΝΕΔΡΙΟ, ΠΑΤΡΑ, 1998, Δελτίο XXXII
- 9ο ΣΥΝΕΔΡΙΟ, ΑΘΗΝΑ, 2001, Δελτίο XXXIV
- 10ο ΣΥΝΕΔΡΙΟ, ΘΕΣΣΑΛΟΝΙΚΗ, 2004, Δελτίο XXXVI
- 11ο ΣΥΝΕΔΡΙΟ, ΑΘΗΝΑ, 2007, Δελτίο XXXX



THE CONGRESSES OF G.S.G.

- 1st MEETING, ATHENS, 1983, Bull. XVII
- 2nd MEETING, ATHENS, 1984, Bull. XIX
- 3rd CONGRESS, ATHENS, 1986, Bull. XX
- 4th CONGRESS, ATHENS, 1988, Bull. XXIII
- 5th CONGRESS, THESSALONIKI, 1990, Bull. XXV
- 6th CONGRESS, ATHENS, 1992, Bull. XXVIII
- 7th CONGRESS, THESSALONIKI, 1994, Bull. XXX
- 8th CONGRESS, PATRAS, 1998, Bull. XXXII
- 9th CONGRESS, ATHENS, 2001, Bull. XXXIV
- 10th CONGRESS, THESSALONIKI, 2004, Bull. XXXVI
- 11th CONGRESS, ATHENS, 2007, Bull. XXXX

ΠΡΟΛΟΓΟΣ



Η Γη είναι ένας πλανήτης με συνεχή και δυναμική εξέλιξη στην ιστορία του. Η γνώση και κατανόηση από τον άνθρωπο της εξέλιξης αυτής είναι μεγάλης σημασίας για τον εντοπισμό, την εκμετάλλευση και τη χρήση των φυσικών πόρων, καθώς και για την ανάδειξη και αντιμετώπιση των περιβαλλοντικών προκλήσεων-προβλημάτων από τη χρήση των πόρων αυτών.

Η περιβαλλοντική αυτή διάσταση απαιτεί μια ολοκληρωμένη, πολυ-επιστημονική θεώρηση του Πλανήτη, που θα περιλαμβάνει τη μελέτη όλων των παραγόντων, όπως της λιθόσφαιρας, της υδρόσφαιρας, της ατμόσφαιρας και της βιόσφαιρας, οι οποίοι συνδέονται μεταξύ τους σε πολύ σημαντικά συστήματα. Τα συστήματα αυτά απαιτούν τη συνεργασία, χωρίς σύνορα και περιορισμούς, των φυσικών επιστημών, όπως η Γεωλογία, η Βιολογία, η Χημεία και η Φυσική. Έτσι μόνο θα κατανοήσουμε τον Πλανήτη μας, θα αναδείξουμε τα περιβαλλοντικά προβλήματα και θα δημιουργήσουμε ενημερωμένες-ευαισθητοποιημένες κοινωνίες, οι οποίες θα μπορούν να αποφασίσουν για το παρόν και το μέλλον του.

Σήμερα είναι γεγονός ότι υπάρχει μια εμπεριστατωμένη άποψη σχετικά με την εξελικτική πορεία της Γης στη διάρκεια των 4,6 δισεκατομμυρίων ετών της ύπαρξής της. Παράλληλα αποτελεί κοινή συνείδηση ότι η ισορροπία του πλανήτη από την καθημερινή πίεση των έξι (6) περίπου δισεκατομμυρίων ανθρώπων που φιλοξενούνται σε αυτόν, είναι πλέον εύθραυστη. Ειδικότερα όσον αφορά στις Γεωεπιστήμες, υπάρχει σοβαρή γνώση σχετικά με τις **Γεωλογικές Διεργασίες**, που έχουν λάβει χώρα στα πλαίσια της ιστορίας αυτής με τη δημιουργία των ορέων και των ωκεανών, τους σεισμούς, την ηφαιστειακή δραστηριότητα, καθώς και την εκδήλωση εξωγενών φαινομένων, όπως οι κατολισθήσεις, οι πλημμύρες, οι ξηρασίες, τα τσουνάμι.

Όσον αφορά στη **Βιώσιμη Ανάπτυξη**, είναι γνωστό ότι τις τελευταίες δεκαετίες η τεχνολογική εξέλιξη και η πληθυσμιακή έκρηξη επέβαλαν μια αλόγιστη και χωρίς σχεδιασμό υπερεκμετάλλευση των φυσικών πόρων, με αποτέλεσμα την υποβάθμιση του περιβάλλοντος για πρώτη φορά στην ιστορία του Πλανήτη μας.

Έτσι, μερικά από τα ερωτήματα που τίθενται επιτακτικά και αναμένουν απαντήσεις από την επιστημονική κοινότητα, δεδομένου ότι εκφράζουν την αγωνία όλης της ανθρωπότητας, είναι τα εξής: α) Οι ανθρώπινες δραστηριότητες έχουν προκαλέσει πράγματι επικίνδυνες τροποποιήσεις του περιβάλλοντος και μάλιστα μη αναστρέψιμες ή οι κλιματικές μεταβολές που παρατηρούνται σήμερα αποτελούν φυσικές διακυμάνσεις; β) Ειδικότερα η βιομηχανική ανάπτυξη και η υπερκατανάλωση ενεργειακών πρώτων υλών αποτελούν κίνδυνο για το περιβάλλον ή θεωρούνται μηδαμνής επίδρασης σε σχέση με τις ηφαιστειακές εκρήξεις και τις αλλαγές των ρευμάτων στους ωκεανούς, οι οποίες προκαλούν δραματικές αλλαγές στο περιβάλλον;

γ) Είναι ακόμα δυνατή μια Βιώσιμη Ανάπτυξη και εάν ναι, ποιο είναι το είδος αυτής στα όρια αντοχής και αποδοχής του πλανήτη μας;

Στα παραπάνω ερωτήματα και προβληματισμούς η επιστήμη της Γεωλογίας έχει να προσφέρει πολλά, δεδομένου ότι οι φυσικές διεργασίες κατά τη διάρκεια της εξέλιξης της Γης έχουν καταγραφεί στους εδαφικούς και βραχώδεις γεωλογικούς σχηματισμούς, χωρίς επηρεασμούς από τις παρεμβάσεις του ανθρώπου. Έτσι οι ανθρώπινες παρεμβάσεις της σύγχρονης εποχής μπορούν να διαχωριστούν και να επισημανθούν, ώστε να αντιμετωπιστούν σωστά. Γενικότερα, η γνώση και κατανόηση της εξέλιξης της Γης μέσα από τις φυσικές διεργασίες μπορούν να συμβάλουν στην αποτύπωση των ρυθμών αλλαγής της Γης στο γεωλογικό χρόνο. Επιπλέον οι ρυθμοί αλλαγής και οι διεργασίες, που είναι υπεύθυνες για αυτούς, μπορούν παράλληλα να αποτελούν δείκτες πρόγνωσης για την πορεία του πλανήτη στο μέλλον. Με άλλα λόγια, το παρελθόν και γενικότερα η γεωλογική ιστορία του Πλανήτη μπορεί να αποτελέσει το «κλειδί» για το παρόν και το μέλλον αυτού.

Συμπερασματικά, η συμβολή της Γεωλογίας και γενικότερα των Φυσικών Επιστημών στην κοινωνία μας είναι πολύ σημαντική για τη γνώση της εξέλιξης της Γης, την έρευνα και αξιολόγηση των φυσικών πόρων, την εκτίμηση των περιβαλλοντικών επιπτώσεων λόγω εκμετάλλευσης των πόρων αυτών, καθώς και την πρόγνωση-αντιμετώπιση των διάφορων φυσικών επικινδυνοτήτων από γεωλογικές διεργασίες και καταστροφικά καιρικά φαινόμενα.

Το 12ο Διεθνές Συνέδριο της Ελληνικής Γεωλογικής Εταιρίας με τίτλο «**Πλανήτη Γη: Γεωλογικές Διεργασίες και Βιώσιμη Ανάπτυξη**» διοργανώνεται από το Τμήμα Γεωλογίας του Πανεπιστημίου Πατρών και πραγματοποιείται στο Συνεδριακό και Πολιτιστικό Κέντρο του Πανεπιστημίου από τις 19 έως 22 Μαΐου 2010. Το Δελτίο της Ελληνικής Γεωλογικής Εταιρίας περιλαμβάνει τα Πρακτικά του Συνεδρίου σε πέντε (5) τόμους των 2.992 σελίδων συνολικά. Οι τόμοι αυτοί καλύπτουν όλο το φάσμα των Γεωεπιστημών σε θέματα της βασικής και εφαρμοσμένης έρευνας. Στα πρακτικά περιλαμβάνονται 267 συνολικά εργασίες από 605 συγγραφείς, όλες στην Αγγλική γλώσσα, δίνοντας έτσι τη δυνατότητα διεθνούς προβολής και χρήσης του επιστημονικού Δελτίου της Εταιρίας. Οι επίσημες γλώσσες του Συνεδρίου είναι η Ελληνική και η Αγγλική.

Στο Συνέδριο υπάρχει σημαντικός αριθμός εργασιών από τον ευρύτερο γεωγραφικό μας χώρο, έχουν δε δηλώσει συμμετοχή πολλοί αξιόλογοι επιστήμονες από την Ελλάδα και το εξωτερικό, καθώς και νέοι ερευνητές και φοιτητές.

Όλες οι εργασίες που δημοσιεύονται, υπεβλήθησαν σε επιστημονική κρίση από εξωτερικούς κριτές, ακολουθώντας τη διαδικασία που είναι διεθνώς καθιερωμένη στα επιστημονικά περιοδικά. Πολλοί αναγνωρισμένοι επιστήμονες, Έλληνες και ξένοι, όλων των ειδικοτήτων, συμμετείχαν στη διαδικασία αυτή. Εκ μέρους της Οργανωτικής Επιτροπής τους ευχαριστώ για τη συμμετοχή και τη συμβολή τους με το σοβαρό έργο που προσέφεραν στην απόκτηση Πρακτικών υψηλού επιπέδου.

Οι επιστημονικές εργασίες εντάχθηκαν σε επιμέρους θεματικές ενότητες, στις οποίες διαχωρίστηκαν τα Πρακτικά και αποτέλεσαν αντικείμενο στις αντίστοιχες Συνεδρίες. Τα κείμενα των ειδικών και προσκεκλημένων ομιλιών, που καλύπτουν το ευρύτερο αντικείμενο της κάθε ενότητας και παρουσιάζουν υψηλού επιπέδου θεώρηση σχετικά με την υφιστάμενη γνώση, τις νέες απόψεις και τάσεις της έρευνας, αποτέλεσαν ιδιαίτερη ενότητα.

Στο Συνέδριο αυτό δίνεται ιδιαίτερη έμφαση στις Γεωλογικές Διεργασίες και τη Βιώσιμη Ανάπτυξη. Όπως αναφέρθηκε διεξοδικά παραπάνω, η κατανόηση της εξέλιξης του πλανήτη Γη μέσα από τις γεωλογικές διεργασίες επιτρέπει στον άνθρωπο να αξιολογήσει τις διάφορες δραστηριότητές του, όπως την αναζήτηση, εκμετάλλευση και χρήση των φυσικών πόρων, καθώς και την κατασκευή διαφόρων έργων υποδομής, χωρίς να προκαλεί επικίνδυνες μεταβολές στο φυσικό και το ανθρωπογενές περιβάλλον. Έτσι μόνο μπορεί να εξασφαλιστεί η Βιώσιμη Ανάπτυξη και να προβλεφθεί η πορεία του Πλανήτη.

Η έγκαιρη εκτύπωση και παράδοση των τόμων του Συνεδρίου στους συνέδρους και στην επιστημονική κοινότητα, καθώς και η γενικότερη οργάνωση του Συνεδρίου γίνεται με την οικονομική στήριξη πολλών φορέων, δημόσιων και ιδιωτικών. Εκφράζονται θερμές ευχαριστίες στο Υπουργείο Περιβάλλοντος, Ενέργειας και Κλιματικής Αλλαγής, που έθεσε το Συνέδριο υπό την αιγίδα του, καθώς και στο Τμήμα Γεωλογίας του Πανεπιστημίου Πατρών, το Ι.Γ.Μ.Ε., και το ΓΕΩΤ.Ε.Ε. Θερμές ευχαριστίες εκφράζονται επίσης στο Κοινοφελές Ίδρυμα Ιωάννη Σ. Λάτση, το Πανεπιστήμιο Πατρών, αλλά και σε ιδιωτικές Τεχνικές και Μελετητικές Εταιρίες, που με τόση προθυμία ανταποκρίθηκαν στην πρόσκλησή μας.

Τέλος, θα ήθελα να εκφράσω τις προσωπικές μου ευχαριστίες στους συναδέλφους της Οργανωτικής Επιτροπής για την αμέριστη βοήθειά τους και την άριστη συνεργασία στη συλλογική αυτή προσπάθεια, καθώς και στο Γραφείο Οργάνωσης Συνεδρίων «Συνέδρα», όπως επίσης στους φοιτητές του Τμήματος Γεωλογίας, που αγάλιασαν και βοήθησαν στην οργάνωση του Συνεδρίου με απαράμιλλο ζήλο.

Πάτρα, 14 Απριλίου 2010

Γεώργιος Χρ. Κούκης
Πρόεδρος
της Οργανωτικής Επιτροπής

PROLOGUE



Earth is a dynamic Planet that has been continuously changing and evolving throughout its whole history. Knowledge and understanding of the evolution processes is of crucial importance not only to explore and take advantage of the natural recourses that our planet provides, but also to access the degree of environmental impacts that the exploitation of these causes.

This environmental aspect demands to consider a comprehensive and multi-scientific view of our Planet, which involves the study of lithosphere, hydrosphere, biosphere and atmosphere. All the above are closely connected together to form very important and complex natural systems, which need the close cooperation of all sciences involved, such as Geology, Biology, Chemistry and Physics. This is the most effective way to understand our Planet, to consider the environmental problems and enforce societies to become informed and conscious of its present and future.

Nowadays an almost complete and comprehensive knowledge about the evolution of Earth during the 4.6 billion years of its age has been gained. In parallel, it is common sense that our Planet's equilibrium is fragile due to environmental pressures that human causes, since Earth's population exceeds 6 billion people.

In the field of Geo-Sciences, in special, there has been gained sufficient experience about the **Geological Processes** that have been taken place during Earth's history and are evident in the formation of mountains and oceans, by the manifestation of earthquakes, by volcanic activity, as well as in natural phenomena as landslides, floods, droughts and tsunamis.

Concerning **Sustainable Development**, it is well known that during the last decades technological evolution and population growth have imposed an unreasonable and sometimes without design overconsumption of natural resources, which leads to gradual degradation of the environment for the first time in our Planet's history.

Thus, some of the "hot" questions that have been arisen and need to be answered by the Scientific Community, since they express the concern of the whole humanity, are: a) Human activities have indeed caused dangerous and non-reversible modifications of the environment or present climatic changes are a result of normal and natural fluctuations? b) Industrial development and overconsumption of natural recourses are a "red flag" for the environment or they can be considered as of minor effect when compared with volcanic eruptions and changes in the regime of ocean current circulation, which cause dramatic environmental changes? c) Is Sustainable Development still achievable and, if yes, in which form and within our Planet's bearing thresholds?

In the above questions Scientific Community can offer a lot, regarding that natural processes

during Earth's evolution have been imprinted on soil and rock geological formations, without any influence by human activities. Present human actions can be clearly distinguished and identified in order to be treated in the right way. The deep knowledge and understanding of Earth's evolution through natural processes can contribute to imprint the rates of Earth's changes through geological time. The changing rates and the processes responsible for them also contribute to obtain indices to predict similar phenomena for the future. In other words the Past and, generally, the geological history of our Planet is the "key" for the Present and Future.

In conclusion, the contribution of Geology and generally of Natural Sciences in our society is very important to understand Earth's evolution, to assist the research and assessment of natural resources, as well as to estimate the environmental impacts from their exploitation. Furthermore, they can provide solutions to the direction of the prevention and confrontation of natural hazards that are triggered by Geological Processes and catastrophic climatic events.

The 12th International Congress of the Geological Society of Greece entitled "**Planet Earth: Geological Processes & Sustainable Development**" is organized by the Department of Geology of the University of Patras in Greece and is held at the Conference and Cultural Center of the University between the 19th and 22nd of May 2010. The *Bulletin of the Geological Society of Greece* includes the Congress's Proceedings in 5 Volumes of 2.992 pages. These volumes cover the whole spectrum of Geo-Sciences in themes of basic and applied research. They include 267 research papers by 605 authors, all written in English making them easily accessible and promoted internationally. Official languages of the Congress are Greek and English. Many renowned scientists from Greece and abroad participate, covering scientific issues from our broad geographic region, as well as new researchers and students.

All submitted papers were reviewed by external reviewers, following the procedure that is established in scientific magazines. Many renowned scientists, Greek and foreigners, of all specialties, participated in this process. On behalf of the Organizing Committee I would like to thank them for their participation and contribution to acquire Proceedings of high quality.

The research papers were included in specific thematic units to which the Proceedings were divided and covered each Congress's session. Special and Keynote lectures about currently acquired knowledge, new insights and modern research trends for each area of interest comprised a special thematic unit.

This Congress focuses on Geological Processes and Sustainable Development. As it was mentioned above, the understanding of Earth's evolution through geological processes allows human to assess his activities, such as investigation and exploitation of natural resources and construction of Infrastructure Works, without causing serious and dangerous damages to the natural and human environment. This is the only way to secure sustainable development and forecast Earth's future.

The on-time production and delivering of the proceedings to the participants and scientific community, as well as the organization of the Congress is sponsored by many public and pri-

vate Organizations, Services and Companies. I would like to express my special thanks to the Ministry of Environment, Energy and Climate Change, which held the Congress under its aegis, as well as to the Department of Geology of the University of Patras, the Institute of Geology and Mineral Exploration (I.G.M.E.) and the Geotechnical Chamber of Greece for their contribution to organize this Congress. Special thanks are also expressed to the Public Benefit Foundation “John S. Latsis”, to the University of Patras and to many private technical and consulting companies which willingly accepted our invitation.

Finally, I would like to personally thank the colleagues of the Organizing Committee for their generous help, support and cooperation to this teamwork, the Congress Organizing firm “Synedra”, as well as the students of the Department of Geology for their precious contribution.

Patras, 14 of April 2010

George Ch. Koukis
President
of the Organizing Committee

ΠΕΡΙΕΧΟΜΕΝΑ / CONTENTS



ΤΟΜΟΣ 1 / VOLUME 1

Εναρκτήρια Ομιλία / Opening Lectures
Κεντρικές και Θεματικές Ομιλίες / Special and Keynote Lectures
Γενική και Τεκτονική Γεωλογία / General and Structural Geology
Νεοτεκτονική και Γεωμορφολογία / Neotectonics and Geomorphology

ΕΝΑΡΚΤΗΡΙΑ ΟΜΙΛΙΑ / OPENING LECTURE

Zerefos C.S.: The “Anthropocene” in the Mediterranean 2

ΚΕΝΤΡΙΚΕΣ ΟΜΙΛΙΕΣ / SPECIAL LECTURES

Foscolos, A.E.: Climatic Changes: Anthropogenic Influence or Naturally Induced Phenomenon 8

Makris, J.: Geophysical studies and tectonism of the Hellenides 32

Papazachos, B.C., Karakaisis, G.F., Papazachos, C.B., Scordilis E.M.: Intermediate Term
Earthquake Prediction Based on Interevent Times of Mainshocks and on Seismic Triggering 46

Rausch, R., Schüth, C., Kallioras, A.: Groundwater Resources Management in Arid Countries 69

ΘΕΜΑΤΙΚΕΣ ΟΜΙΛΙΕΣ / KEYNOTE LECTURES

Νεοτεκτονική και Γεωμορφολογία – Neotectonics and Geomorphology

Papanikolaou, D.: Major Paleogeographic, tectonic and geodynamic changes from the last
stage of the Hellenides to the actual Hellenic Arc and Trench System 72

*Παλαιοντολογία, Στρωματογραφία και Ιζηματολογία – Paleontology, Stratigraphy
and Sedimentology*

Dermitzakis, M.D.: The Status of Stratigraphy in the 21st Century 86

Γεωαρχαιολογία – Geoarchaeology

Mariolakos, I.D.: The forgotten geographical and physical – oceanographic knowledge of the
Prehistoric Greeks 92

Papamarinopoulos, S.P.: Atlantis in Spain (Part I, II, III, IV, V, VI) 105

Γεώτοποι – Geosites

Zouros, N.: Geodiversity and Sustainable Development: Geoparks - A new challenge for Research
and Education in Earth Sciences 159

Διδακτική των Γεωεπιστημών – Teaching Earth Sciences

Makri, K., Pavlides, S.B., Kastanis, N.: An analysis of Geological Textbooks, at 1830-1930 169

Θαλάσσια Γεωλογία και Ωκεανογραφία – Marine Geology and Oceanography

Ferentinos, G.: The contribution of Marine Geology to the Socio-economic Development of Greece:

Marine Resources, Infrastructure, Environment Sustainability, Cultural Heritage. A brief account of the 30 years contribution of the laboratory of Marine Geology and Physical Oceanography	176
<i>Τεχνική Γεωλογία και Γεωτεχνική Μηχανική – Engineering Geology and Geotechnical Engineering</i>	
Tsiambaos, G.: Engineering Geological Behaviour of Heterogeneous and Chaotic Rock masses	183
<i>Υδρογεωλογία και Υδρολογία – Hydrogeology and Hydrology</i>	
Soulios, G.: Springs (Classification, Function, Capturing)	196
<i>Σεισμολογία – Seismology</i>	
Makropoulos, K.C.: Earthquakes and Preventive Measures	216
<i>Ενεργειακές Πρώτες Ύλες και Γεωθερμία - Energy Resources and Geothermics</i>	
Christanis, K.: Energy Resources of Greece: Facts and Myths	224
<i>Γεωχημεία και Κοιτασματολογία – Geochemistry and Ore Deposit Geology</i>	
Varnavas, S.: Medical Geochemistry. A key in the Precautionary Measures against the Development of Cancer and other Diseases	234
<i>Ορυκτολογία και Πετρολογία – Mineralogy and Petrology</i>	
Katagas, Ch.: Wandering about Mineralogy and Petrology	247

ΓΕΝΙΚΗ ΚΑΙ ΤΕΚΤΟΝΙΚΗ ΓΕΩΛΟΓΙΑ / GENERAL AND STRUCTURAL GEOLOGY

Argyriadis, I., Midoun, M., Ntontos, P.: A new interpretation of the Structure of Internal Hellenides	264
Kilias, Ad., Frisch, W., Avgerinas, A., Dunkl, I., Falalakis, G., Gawlick, H.-J., Mountrakis, D.: The Pelagonian nappe pile in Northern Greece and FYROM. Structural Evolution during the Alpine Orogeny: A new approach	276
Kokinou, E., Kamberis, E., Sarris, A., Tzanaki, I.: Geological and Magnetic Susceptibility Mapping of Mount Giouchta (Central Crete)	289
Kurz, W., Wölfler, A., Handler, R.: Cenozoic Tectonic Evolution of the Eastern Alps – A reconstruction based on ⁴⁰ AR/ ³⁹ AR Mica, Zircon and Apatite Fission track and Apatite (U/TH) – HE Thermochronology	299
Marsellos, A.E., Kidd, W.S.F., Garver, J.I., Kyriakopoulos, K.G.: Exhumation of the Hellenic Accretionary Prism – Evidence from the Fission Track Thermochronology	309
Migiros, G., Antoniou, Vas., Papanikolaou, I., Antoniou, Var.: Tectonic setting and deformation of the Kallidromo Mt, Central Greece	320
Papageorgiou, E.: Crustal Movements along the Hellenic Volcanic Arc from DGPS measurements	331
Papageorgiou, E., Tzanis, A., Sotiropoulos, P., Lagios, E.: DGPS and Magnetotelluric constraints on the Contemporary Tectonics of the Santorini Volcanic Complex, Greece	344
Papoulia, J., Makris, J.: Tectonic processes and crustal evolution on/offshore western Peloponnese derived from active and passive seismics	357
Spanos, D., Koukouvelas, I., Kokkalas, S., Xypolias, P.: Patterns of Ductile Deformation in Attico – Cycladic Massif	368

Tselepidis, V., Rondoyanni, Th.: A contribution to the Geological Structure of Chios Island, Eastern Aegean Sea	379
Xypolias, P., Chatzaras, V.: The nature of Ductile deformation in the Phyllite – Quartzite unit (External Hellenides)	387

NEOTEKTONIKH KAI GEOMORFOLOGIA / NEOTECTONICS AND GEOMORPHOLOGY

Caputo, R., Catalano, S., Monaco, C., Romagnoli, G., Tortorici, G., Tortorici, L.: Middle – Late Quaternary Geodynamics of Crete, Southern Aegean, and Seismotectonic Implications	400
Gaki – Papanastassiou, K., Karymbalis, E., Maroukian, H.: Recent Geomorphic changes and Anthropogenic Activities in the Deltaic Plain of Pinios River in Central Greece	409
Gaki – Papanastassiou, K., Karymbalis, E., Maroukian, H., Tsanakas, K.: Geomorphic evolution of Western (Paliki) Kephalaria Island (Greece) during the Quaternary	418
Kokkalas, S.: Segmentation and Interaction of Normal Faults in Central Greece	428
Metaxas, Ch.P., Lalechos, N.S., Lalechos, S.N.: Kastoria “Blind” Active Fault: Hazardous Seismogenic Fault of the NW Greece	442
Mourtzas, N.D.: Sea level changes along the coast of Kea Island and Paleogeographical coastal reconstruction of Archaeological sites	453
Nomikou, P., Papanikolaou, D.: A comparative morphological study of the Kos – Nisyros – Tilos volcanosedimentary basins	464
Papanikolaou, M., Papanikolaou, D., Triantaphyllou, M.: Post – Alpine Late Pliocene – Middle Pleistocene uplifted Marine sequences in Zakynthos Islands	475
Pavlidis, S., Caputo, R., Sboras, S., Chatzipetros, A., Papathanasiou, G., Valkaniotis, S.: The Greek Catalogue of Active Faults and Database of Seismogenic Sources	486
Tranos, M.D., Mountrakis, D.M., Papazachos, C.B., Karagianni, E., Vamvakaris, D.: Faulting deformation of the Mesohellenic Trough in the Kastoria – Nestorion Region (Western Macedonia, Greece)	495
Tsanakas, K., Gaki-Papanastassiou, K., Poulos, S.E., Maroukian, H.: Geomorphology and Sedimentological processes along the coastal zone between Livanates and Agios konstantinos (N. Evoikos Gulf, Central Greece)	506
Vassilopoulou, S.: Morphotectonic analysis of Southern Argolis Peninsula (Greece) based on Ground and Satellite Data by GIS Development	516
Zygouri, V.: Probabilistic Hazard Assessment, using Arias Intensity Equation, in the eastern part of the Gulf of Corinth (Greece)	527
Ευρετήριο συγγραφέων / Author index	537



ΤΟΜΟΣ 2 / VOLUME 2

Παλαιοντολογία, Στρωματογραφία και Ιζηματολογία /
Palaeontology, Stratigraphy and Sedimentology

Γεωαρχαιολογία / Geoarchaeology

Γεώτοποι / Geosites

Διδακτική των Γεωεπιστημών / Teaching the Earth Sciences

Θαλάσσια Γεωλογία και Ωκεανογραφία / Marine Geology and Oceanography

ΠΑΛΑΙΟΝΤΟΛΟΓΙΑ, ΣΤΡΩΜΑΤΟΓΡΑΦΙΑ ΚΑΙ ΙΖΗΜΑΤΟΛΟΓΙΑ / PALAEOLOGY, STRATIGRAPHY AND SEDIMENTOLOGY

Anagnostoudi, Th., Papadopoulou, S., Ktenas, D., Gkadri, E., Pyliotis, I., Kokkidis, N., Panagiotopoulos, V.: The Olvios, Rethis and Inachos Drainage System Evolution and Human activities influence of their future evolution	548
Avramidis, P., Panagiotaras, D., Papoulis, D., Kontopoulos, N.: Sedimentological and Geochemical characterization of Holocene sediments, from Alikes Lagoon, Zakynthos Island, Western Greece	558
Antonarakou, A.: Plankton Biostratigraphy and Paleoclimatic implications of an Early Late Miocene sequence of Levkas Island, Ionian Sea, Greece	568
Bellas, S., Keupp, H.: Contribution to the late Neogene stratigraphy of the Ancient Gortys area (Southern Central Crete, Greece)	579
Codrea, V., Barbu, O., Jipa-Murzea, C.: Upper Cretaceous (Maastrichtian) land vertebrate diversity in Alba district (Romania)	594
Dimiza, M.D., Triantaphyllou, M.V.: Comparing living and Holocene coccolithophore assemblages in the Aegean marine environments)	602
Drinia, H., Koskeridou, E., Antonarakou, A., Tzortzaki, E.: Benthic Foraminifera associated with the zooxanthellate coral <i>Cladocora</i> in the Pleistocene of the Kos Island (Aegean Sea, Greece): sea level changes and palaeoenvironmental conditions	613
Drinia, H., Pomoni-Papaioannou, F., Tsaparas, N., Antonarakou, A.: Miocene Scleractinian corals of Gavdos Island, Southern Greece: Implications for tectonic control and sea level changes	620
Kafousia, N., Karakitsios, V., Jenkyns, H.C.: Preliminary data from the first record of the Early Toarcian oceanic anoxic event in the sediments of the Pindos Zone (Greece)	627
Karakitsios, V. Triantaphyllou, M. Panoussi, P.: Preliminary study on the slump structures of the Early Oligocene sediments of the Pre-Apulian zone (Antipaxos Island, North-western Greece)	634
Kourkounis, S., Panagiotakopoulou, O., Zelilidis, A., Kontopoulos, N.: Texture versus distance of travel of gravels on a stream bed: a case study from four streams in NW Peloponnese, Greece	643
Koutsios, A., Kontopoulos, N., Kalisperi, D., Soupios, P. Avramidis, P.: Sedimentological and Geophysical observations in the Delta Plain of Selinous River, Ancient Helike, Northern Peloponnesus Greece	654
Kyriakopoulos, K., Karakitsios, V., Tshipoura-Vlachou, M., Barbera G., Mazzoleni, P. Puglisi, D.: Petrological characters of the Early Cretaceous Boeothian Flysch, (Central Greece)	663

Makrodimitras, G., Stoykova, K., Vakalas, I., Zelilidis, A.: Age determination and Palaeogeographic reconstruction of Diapondia Islands in NW Greece, based on Calcareous Nannofossils	675
Maneta, V., Voudouris, P.: Quartz megacrysts in Greece: Mineralogy and Environment of Formation	685
Manoutsoglou, E., Batsalas, A., Stamboliadis, E., Pantelaki, O., Vakalas, I., Zelilidis, A.: The Auriferous submarine fans sandstones of the Ionian zone (Epirus, Greece)	697
Moumou, Ch., Vouvalidis, K., Pechlivanidou, S., Nikolaou, P.: The Fluvial action of the Karla basin streams in a natural and man-made environment	706
Pavlopoulos, A., Kamperis, E., Sotiropoulos, S., Triantaphyllou, M.: Tectonosedimentary significance of the Messinia conglomerates (SW Peloponnese, Greece)	715
Photiades, A., Pomoni-Papaioannou, F.A., Kostopoulou, V.: Correlation of Late Triassic and Early Jurassic Lofer – type carbonates from the Peloponnesus peninsula, Greece	726
Sigalos, G., Loukaidi, V., Dasaklis, S., Alexouli-Livaditi, A.: Assessment of the Quantity of the material transported downstream of Sperchios River, Central Greece	737
Svana, K., Iliopoulos, G., Fassoulas, C.: New Sirenian findings from Crete Island	746
Triantaphyllou, M.V.: Calcareous nannofossil Biostratigraphy of Langhian deposits in Lefkas (Ionian Islands)	754
Triantaphyllou, M.V., Antonarakou, A., Drinia, H., Dimiza M.D., Kontakiotis, G., Tsolakis, E. Theodorou, G.: High resolution Biostratigraphy and Paleocology of the Early Pliocene succession of Pissouri Basin (Cyprus Island)	763
Zambetakis – Lekkas, A.: On the occurrence of primitive <i>Orbitoides</i> species in Gavrovo – Tripolitza platform (Mainalon Mountain, Peloponnesus, Greece)	773
Zidianakis, G., Iliopoulos, G., Fassoulas, C.: A new late Miocene plant assemblage from Messara Basin (Crete, Greece)	781
Zoumpoulis, E., Pomoni-Papaioannou, F., Zelilidis, A.: Studying in the Paxos zone the carbonate depositional environment changes during Upper Cretaceous, in Sami area of Kefallinia Island, Greece	793

ΓΕΩΑΡΧΑΙΟΛΟΓΙΑ / GEOARCHAEOLOGY

Economou, G., Kougemitrou, I., Perraki, M., Konstantinidi-Syvridi, E., Smith, D.C.: A Mineralogical study of some Mycenaean Seals employing Mobile Raman Microscopy	804
Katsonopoulou, D.: Earth Science Applications in the field of Archaeology: the Helike example	812
Mariolakas, I., Theocharis, D.: Geomythological approach of Asopos River (Aegina, Greece)	821
Mariolakas, I., Nikolopoulos, V., Bantekas, I., Palyvos, N.: Oracles on faults: a probable location of a “lost” oracle of Apollo near Oroviai (Northern Euboea Island, Greece) viewed in its Geological and Geomorphological context	829
Melfos, V., Voudouris, P., Papadopoulou, L., Sdrolia, S., Helly, B.: Mineralogical, Petrographic and stable isotopic study of Ancient white marble quarries in Thessaly, Greece - II. Chasanbali, Tempi, Atrax, Tisaion Mountain	845
Rathossi, C., Pontikes, Y., Tsolis-Katagas, P.: Mineralogical differences between ancient sherds	

and experimental ceramics: Indices for Firing conditions and Post - burial alteration	856
Stiros, S., Kontogianni, V.: Selection of the path of the Eupalinos aqueduct at Ancient Samos on the basis of Geodetic and Geological / Geotechnical criteria	866

ΓΕΩΤΟΠΟΙ / GEOSITES

Antonelou, A., Tsikouras, B., Papoulis, D., Hatzipanagiotou, K.: Investigation of the formation of speleothems in the Agios Georgios Cave, Kilkis (N. Greece)	876
Dotsika, E., Psomiadis, D., Zanchetta, G., Spyropoulos, N., Leone, G., Tzavidopoulos, I., Poutoukis, D.: Pleistocene Palaeoclimatic evolution from Agios Georgios Cave speleothem (Kilkis, N. Greece)	886
Fassoulas, C., Zouros, N.: Evaluating the influence of Greek Geoparks to the local communities	896
Haidarlis, M., Sifakis, A., Brachou C.: Geoconservation legal status and Geopark establishment in Greece	907
Illiopoulos, G., Eikamp, H., Fassoulas, C.: A new Late Pleistocene mammal locality from Western Crete	918
Theodosiou, Ir.: Designation of Geosites – Proposals for Geoparks in Greece	926
Theodosiou, Ir., Athanassouli, E., Epitropou, N., Janikian, Z., Kossiaris, G., Michail, K., Nicolaou, E., Papanikos, D., Pashos, P., Pavlidou, S., Vougioukalakis, G.: Geotrails in Greece	939
Vaxevanopoulos, M., Melfos, V.: Hypogenic features in Maronia Cave, Thrace, Greece. Evidence from morphologies and fluid inclusions	948
Zisi, N., Dotsika, E., Tsoukala, E., Giannakopoulos, A., Psomiadis, D.: Palaeoclimatic evolution in Loutra Arideas Cave (Almopia Speleopark, Macedonia, N. Greece) by stable isotopic analysis of fossil bear bones and teeth	958
Zouros, N., Valiakos, I.: Geoparks management and assessment	965

ΔΙΔΑΚΤΙΚΗ ΤΩΝ ΓΕΩΕΠΙΣΤΗΜΩΝ / TEACHING EARTH SCIENCES

Fermeli, G., Dermitzakis, M.: The contribution of Museums’ digitalized Palaeontological collections to the scientific literacy of compulsory education students: the case of an interactive multimedia production of the Palaeontological and Geological Museum of the University of Athens	978
Fermeli, G., Vitsas, T., Foundas, P., Sokos, E., Alexandropoulou, S., Papatheodoropoulos, P., Germanis, N., Nikolaidis, A., Zevgitis, T.: The use of Educational seismographs in the Seismology School Network “EGELADOS”	989
Katrivanos, D.E., Makri, K.: Perception of first-year geology students on the Tectonic Plates Theory	999
Kritikou, S., Malegiannaki, I.: Following the traces of Naxian emery – an implementation of environmental education in geodidactics	1007

ΘΑΛΑΣΣΙΑ ΓΕΩΛΟΓΙΑ ΚΑΙ ΩΚΕΑΝΟΓΡΑΦΙΑ / MARINE GEOLOGY AND OCEANOGRAPHY

Iatrou, M., Papatheodorou, G., Geraga, M., Ferentinos, G.: The study of Heavy Metal concentrations in the Red Mud deposits at the Gulf of Corinth, using multivariate techniques	1018
---	------

Lycourghiotis, S., Stiros, S.: Sea surface topography in the Gulf of Patras and the Southern Ionian Sea using GPS	1029
Perissoratis, C., Ioakim, Chr.: Research projects to study the Sea floor and Sub-bottom sediments funded by the recent European Commission Framework Programs: The IGME Participation	1035
Sakellariou, D., Fountoulis, I., Lykousis, V.: Evidence of cold seeping in Plio-Pleistocene sediments of SE Peloponnes: The fossil carbonate chimneys of Neapolis Region	1046
Sakellariou, D., Sigurdsson, H., Alexandri, M., Carey, S., Rousakis, G., Nomikou, P., Georgiou P., Ballas, D.: Active tectonics in the Hellenic Volcanic Arc: The Kolumbo submarine volcanic zone	1056
Thomopoulos, K., Geraga, M., Fakiris, E., Papatheodorou, G., Ferentinos, G.: Palaeoclimatic and Palaeoceanographic evolution of the Mediterranean Sea over the last 18ka	1064
Xeidakis, G., Georgoulas, A., Kotsovinos, N., Delimani, P., Varaggouli, E.: Environmental Degradation of the coastal zone of the West part of Nestos River Delta, N. Greece	1074
Ευρετήριο συγγραφέων / Author index	1085



ΤΟΜΟΣ 3 / VOLUME 3

Τεχνική Γεωλογία και Γεωτεχνική Μηχανική /
 Engineering geology and Geotechnical Engineering
 Φυσικές Καταστροφές / Natural Hazards
 Αστική Γεωλογία / Urban Geology
 Γ.Σ.Π. στις Γεωεπιστήμες / GIS in Earth Sciences

ΤΕΧΝΙΚΗ ΓΕΩΛΟΓΙΑ ΚΑΙ ΓΕΩΤΕΧΝΙΚΗ ΜΗΧΑΝΙΚΗ / ENGINEERING GEOLOGY AND GEOTECHNICAL ENGINEERING

Angelopoulos, A., Soulis, V.J., Malandraki, V.: Geological and geotechnical behaviour of Evinos Dam following the impoundment	1094
Antonioni, A.A., Tsiambaos, G.: Engineering geological aspects for the microzonation of the city of Volos, Greece	1104
Chatziangelou, M., Thomopoulos, Ach., Christaras, B.: Excavation data and failure investigation along tunnel of Symbol Mountain	1112
Christaras, B., Papathanassiou G., Vouvalidis, K., Pavlides, S.: Preliminary results regarding the rock falls of December 17, 2009 at Tempi, Greece	1122
Christaras, B., Syrides, G., Papathanassiou, G., Chatzipetros, A., Mavromatis, T., Pavlides, Sp.: Evaluating the triggering factors of the rock falls of 16 th and 21 st December 2009 in Nea Fokea, Chalkidiki, Norderh Greece	1131
Depountis, N., Lainas, S., Pyrgakis, D., Sabatakakis, N., Koukis, G.: Engineering Geological and geotechnical investigation of landslide events in wildfire affected areas of Iliia Prefecture, Western Greece	1138

Diasakos, N., Amerikanos, P., Tryfonas, G., Vagioutou, E., Baltzois, V., Bloukas, S., Tagkas, Th., Malandrakis, E., Poulakis, N., Kalogerogiannis, G., Tsirigotis, N.: Tunnel excavation in clayey-marly formations: The case of Kallidromo Tunnel	1149
Hagiou, E., Konstantopoulou, G.: Environmental planning of abandoned Quarries rehabilitation – A methodology	1157
Karagianni, A., Karoutzos, G., Ktena, S., Vagenas, N., Vlachopoulos, I., Sabatakakis, N., Koukis, G.: Elastic Properties of Rocks	1165
Kouki, A.: Mineralogical composition and fabric as related to the mechanical behavior of the fine – grained Plio – Pleistocene sediments of Achaia, Greece	1169
Kouki, A., Rozos, D.: The fine – grained Plio – Pleistocene deposits in Achaia – Greece and their distinction in characteristic geotechnical units	1177
Kouki, A., Rozos, D.: Engineering – Geotechnical conditions in Patras ring road wider area, Greece. Compilation of the relevant map at scale of 1:5000	1184
Kozyreva, E.A., Khak, V.A.: The anthropogenic changes in the Geological Environment in the South of East Siberia	1192
Kynigalaki, M., Kanaris, D., Nikolaou, N., Kontogianni, V.: Buildings’ damage at Horemi Village, Arkadia, Greece: evaluation of the Geotechnical conditions at shallow depths	1202
Lainas, S., Koulouris, S., Vagenas, S., Depountis, N., Sabatakakis, N., Koukis, G.: Earthquake-induced rockfalls in Santomeri Village, Western Greece	1210
Loupasakis, C., Rozos, D.: Land subsidence induced by the overexploitation of the aquifers in Kalochori village – new approach by means of the computational geotechnical engineering	1219
Loupasakis, C., Spanou, N., Kanaris, D., Exioglou, D., Georgakopoulos, A.: Geotechnical investigation of the rock slope stability problems occurred at the foundations of the coastal byzantine wall of Kavala city, Greece	1230
Marinos, P.V.: Engineering geological behaviour of rock masses in underground excavations	1238
Marinos, P.V.: New proposed GSI classification charts for weak or complex rock masses	1248
Marinos, P.V., Tsiambaos, G.: Strength and deformability of specific sedimentary and ophiolitic rocks	1259
Moraiti, E., Christaras, B., Brauer, R.: Landslide in Nachterstedt of Germany	1267
Mourtzas, N., Gkiolas, A.: Tunneling in ophiolitic series formations: Tunnels of the new high-speed railway double track line - section Lianokladi – Domokos	1272
Mourtzas, N.D., Symeonidis, K., Passas, N., Alkalais, E., Kolaiti, E.: Slope stabilization on Chalkoutsí – Dilesi road, at Pigadakia location, Attica Prefecture	1286
Parcharidis, I., Foulmelis, M., Kourkouli, P.: Slope instability monitoring by space-borne SAR interferometry: Preliminary results from Panachaiko Mountain (Western Greece)	1301

ΦΥΣΙΚΕΣ ΚΑΤΑΣΤΡΟΦΕΣ / NATURAL HAZARDS

Bizoura, A., Lykoudi, E., Spyridonos, E., Manoutsoglou, E.: Assessment of the vulnerability degree of different lithological formations in the catchment area of Agia Eirini Gorge, Western Crete	1314
--	------

Diakakis, M.: Flood history analysis and its contribution to flood hazard assessment. The case of Marathonas, Greece	1323
Gournelos, T., Nastos, P.T., Chalkias, D., Tsagas, D., Theodorou, D.: Landslide movements related to precipitation. Analysis of a statistical sample from the Greek area	1335
Kadetova, A.V., Kozireva, E.A.: The potential natural hazards to be considered in the design and exploitation of the aerial rope-way in the “Gora Sobolinaya” mountain-skiing resort (Southern Pribaikalia, Russia)	1341
Kalantzi, F., Doutsou, I., Koukouvelas, I.: Historical landslides in the Prefecture of Ioannina – collection and analysis of data	1350
Lekkas, E.: Macroseismicity and geological effects of the Wenchuan earthquake (Ms 8.0r - 12 May 2008), Sichuan, China: Macro-distribution and comparison of EMS ₁₉₉₈ and ESI ₂₀₀₇ intensities	1361
Papathanassiou, G., Pavlides, S.: Probabilistic evaluation of liquefaction-induced ground failures triggered by seismic loading in urban environment; case studies from Greece	1373
Papathanassiou, G., Valkaniotis, S., Chatzipetros, Al., Pavlides S.: Liquefaction susceptibility map of Greece	1383
Poyiadji, E., Nikolaou, N., Karmis, P.: Ground failure due to Gypsum dissolution	1393
Rozos, D., Lykoudi, E., Tsangaratos, P., Markantonis, K., Georgiadis, P., Rondoyanni, Th., Leivaditi, A., Kyrousis, I.: Evaluation of soil erosion and susceptibility to landslide manifestation as a consequence of wildfire events affected the Zacharo municipality, Peloponnesus, Greece	1406

ΑΣΤΙΚΗ ΓΕΩΛΟΓΙΑ / URBAN GEOLOGY

Apostolidis, Em., Koutsouveli, An.: Engineering geological mapping in the urban and suburban region of Nafplion city (Argolis, Greece)	1418
Georgiou, Ch., Galanakis, D.: Neotectonic study of urban and suburban Nafplio area (Argolida-Greece)	1428
Karastathis, V.K., Karmis, P., Novikova, T., Roumelioti, Z., Gerolymatou, E., Papanastassiou, D., Liakopoulos, S., Giannouloupoulos, P., Tsombos, P., Papadopoulos, G. A.: Liquefaction risk assessment by the use of Geophysical techniques: The test area of Nafplion city, Greece	1438
Karmis, P.D., Giannouloupoulos, P., Tsombos, P.: Geophysical investigations at Nafplion city, Greece. Hydrogeological implications	1447
Koukoulis, A., Karageorgiou, D.E.: Radon: Geoinformation for the planning of urban – suburban regions. The case of Nafplion city, Greece	1457
Loupasakis, C., Galanakis, D., Rozos, D.: Rock slope stability problems in natural sightseeing areas - an example from Arvanitia, Nafplio, Greece	1465
Mitropoulos, D., Zananiri, I.: Upper Quaternary evolution of the Northern Argolis Gulf, Nafplio area	1474
Nikolakopoulos, K., Tsompos, P.: Remote sensing applications in the frame of “Urban Geology” project	1486

Photiades, A.: Geological contribution to the tectono- stratigraphy of the Nafplion area (NW Argolis, Greece)	1495
Sabatakakis, P., Koukis, G.: Aqueous environment and effects on the civil areas: The case of Nafplio	1508
Tassiou, S., Vassiliades, E.: Geochemical study of the urban and suburban area of Nafplion city, Argolidha Prefecture, Hellas	1520
Tsombos, P.I., Zervakou, A.D.: The “Urban Geology” project of IGME: The case study of Nafplio, Argolis Prefecture, Greece	1528
Zananiri, I., Chiotis, E., Tsombos, P., Hademenos, V., Zervakou, A.: Geoarchaeological studies in urban and suburban areas of the Argolis Prefecture	1539
Zananiri, I., Zervakou, A., Tsombos, P., Chiotis, E.: Visualization of datasets from urban geology studies using Google Earth: The case study of Nafplio, Argolis Prefecture	1549
Zervakou, A.D., Tsombos, P.I.: GIS in urban geology: The case study of Nafplio, Argolis Prefecture, Greece	1559

Γ.Σ.Π. ΣΤΙΣ ΓΕΩΕΠΙΣΤΗΜΕΣ / G.I.S. IN EARTH SCIENCES

Bathrellos, G.D., Skilodimou, H.D., Chousianitis, K.G.: Soil erosion assessment in Southern Evia Island using USLE and GIS	1572
Golubović Deliganni, M., Parcharidis, I., Pavlopoulos, K.: Karstic landscape study based on Remote Sensing Data: the case of Ksiromero region, Aitolokarnania - Western Greece	1582
Ilia, I., Tsangaratos, P., Koumantakis, I., Rozos, D.: Application of a Bayesian approach in GIS based model for evaluating landslide susceptibility. Case study Kimi area, Euboea, Greece	1590
Karageorgiou, M.M.D., Karymbalis, E., Karageorgiou, D.E.: The use of the Geographical Information Systems (G.I.S.) in the geological – mineralogical mapping of the Paranesti area	1601
Sboras, S., Ganas, A., Pavlides, S. : Morphotectonic analysis of the neotectonic and active faults of Beotia (Central Greece), using G.I.S. techniques	1607
Kynigalaki, M., Nikolaou, N., Karfakis, J., Koutsouveli, An., Poyiadji, El., Pyrgiotis, L., Konstantopoulou, G., Bellas, M., Apostolidis, Em., Loupasakis, K., Spanou, N., Sabatakakis, N., Koukis, G.: Digital engineering geological map of the Athens Prefecture area and related Database Management System	1619
Nikolakopoulos, K., Gioti, Ev., Skianis, G., Vaiopoulos, D.: Ameliorating the Spatial Resolution of Hyperion Hyperspectral Data. The case of Antiparos Island	1627
Rozos, D., Bathrellos, D.G., Skilodimou, D.H.: Landslide susceptibility mapping of the Northeastern part of Achaia Prefecture using Analytical Hierarchical Process and GIS techniques	1637
Skianis, G.Aim., Gournelos, Th., Vaiopoulos, D., Nikolakopoulos, K.: A study of the performance of the Modified Transformed Vegetation Index MTVI	1647
Tsangaratos, P., Koumantakis, I., Rozos, D.: GIS-Based application for geotechnical data managing	1656
Ευρετήριο συγγραφέων / Author index	1667



TOMOS 4 / VOLUME 4

Υδρογεωλογία και Υδρολογία / Hydrogeology and Hydrology
Γεωφυσική / Geophysics
Σεισμολογία / Seismology

ΥΔΡΟΓΕΩΛΟΓΙΑ ΚΑΙ ΥΔΡΟΛΟΓΙΑ / HYDROGEOLOGY AND HYDROLOGY

Christaras, B.: Could water co-management contribute to Peace, in Middle East?	1672
Christoforidou, P., Panagopoulos, A., Voudouris, K.: Towards a new procedure to set up groundwater threshold values in accordance with the provisions of the EC Directive 2006/118: A case study from Achaia and Corinthia (Greece)	1678
Dimitrakopoulos, D., Vassiliou, E., Tsangaratos, P., Ilija, I.: Environmental management of mine water, considering European Water Legislation. Case study of Megalopolis mines	1688
Gkioungkis, I., Mwila, G., Pliakas, F., Kallioras, A., Diamantis, I.: Hydrogeological assessment of groundwater degradation at the Eastern Nestos river delta, N.E. Greece	1697
Karalemas, N., Lekkas, S.: Operational mechanism of karst spring “Logaras”, near the village “Skortsinou”, Arcadia, (Peloponnesus)	1707
Karapanos, E., Burgess, W., Lambrakis, N.: Groundwater flow modelling of the alluvial aquifer in the Mouria area, SW Greece	1716
Katsanou, K., Stratikopoulos, K., Zagana, E. Lambrakis, N.: Radon changes along main faults in the broader Aigion region, NW Peloponnese	1726
Kelepertzis, E., Argyraki, A., Daftsis, E., Ballas, D.: Quality characteristics of surface waters at Asprolakkas River Basin, N.E. Chalkidiki, Greece	1737
Koukidou, I., Panagopoulos, A.: Application of feflow for the simulation of groundwater flow at the Tirnavos (Central Greece) alluvial basin aquifer system	1747
Kounis, G.D., Kounis, K.G.: Infiltration, effective porosity, transmissibility and critical yield of water wells in the carbonate fissured aquifers of Attica – A contribution to the regional and managerial hydrogeology	1758
Kounis, G.D., Kounis, K.G.: Relationship between the transmissibility of the “Athens Schists” and the percentage of their competent rock component	1767
Maramathas, A., Gialamas, J., Pambuku, A., Beshku, H., Vako, E.: Brackish karst springs simulation with “modkarst” model under not enough data conditions (the case of the “Potami” spring at Himara Albania)	1777
Mariolakos, I., Spyridonos, E.: Remarks on the karstification in the wider area of the Upper Messinia closed hydrogeological basin (SW Peloponnesus, Greece)	1785
Matiatos, I., Alexopoulos, A., Zouridakis, N.: Use of stable isotopes in the determination of the mean altitude of recharge and the investigation of function mechanism of spring waters in Argolis Peninsula (Greece)	1792
Mertzanides, Y., Economou, N., Hamdan, H., Vafidis, A.: Imaging sea water intrusion in coastal	

zone of Kavala (N. Greece) with electrical resistivity tomography	1802
Mertzanides, Y., Ziannos, V., Tsobanoglou, C., Kosmidis, E.: Telemetry network for monitoring quality of irrigation water in Kavala (N. Greece)	1812
Nikas, K., Antonakos, A., Kallergis, G., Kounis, G.: International hydrogeological map of Europe: sheet D6 “Athina”	1821
Papafotiou, A., Schütz, C., Lehmann, P., Vontobel, P., Or, D., Neuweiler, I.: Measurement of preferential flow during infiltration and evaporation in porous media	1831
Raco, B., Dotsika, E., Psomiadis, D., Doveri, M., Lelli, M., Zisi, N., Papakonstantinou, K., Lazaridis, A.: Geochemical investigation of aquifer pollution from waste management. The case of Komotini landfill (Greece)	1840
Rozos, D., Sideri, D., Loupasakis, C. Apostolidis, E.: Land subsidence due to excessive ground water withdrawal. A case study from Stavros - Farsala site, West Thessaly Greece	1850
Skordas, K., Tziritis, E., Kelepertsis, A.: Groundwater quality of the hydrological basin of Amyros River, Agia area Thessaly, Greece	1858
Stamatis, G.: Groundwater quality of the Ag. Paraskevi/Tempi valley karstic springs - application of a tracing test for research of the microbial pollution (Kato Olympos/NE Thessaly)	1868
Zagana, E., Lemesios, I., Charalambopoulos, S., Katsanou, K., Stamatis, G., Lambrakis, N.: Environmental – hydrogeological investigations on the clay deposits in the broad area of Mesologgi – Aitoliko lagoons	1878

ΓΕΩΦΥΣΙΚΗ / GEOPHYSICS

Aidona, E., Kondopoulou, D., Alexandrou, M., Ioannidis, N.: Archaeomagnetic studies in Kilns from N. Greece	1888
Alexopoulos, J.D., Dilalos, S.: Geophysical research for geological structure determination in the region of South Mesogheia (Attica)	1898
Arvanitis, A.A., Stampolidis, A.D., Tsokas, G.N.: Contribution of geophysical methods to the investigation of geothermal conditions in the Southwestern part of the Strymon Basin (Macedonia, Northern Greece)	1907
Chailas, S., Tzanis, A., Kranis, H., Karmis, P.: Compilation of a unified and homogeneous aeromagnetic map of the Greek mainland	1919
Skarlatoudis, A.A., Papazachos, C.B.: Implementation of a non-splitting formulation of perfectly matched layer in a 3D – 4 th order staggered-grid velocity-stress finite-difference scheme	1930
Tzanis, A.: A Matlab program for the analysis and interpretation of transient electromagnetic sounding data	1941
Vargemezis, G., Fikos, I.: Large scale vertical electrical soundings survey in Anthemountas River Basin for evaluating hydraulic communication between sub basin aquifers	1953
Vargemezis, G., Tsourlos, P., Mertzanides, I.: Contribution of deep electrical resistivity tomography technique to hydrogeological studies: Cases from areas in Kavala (North Greece)	1962
Zananiri, I., Kondopoulou, D., Spassov, S.: The application of environmental magnetism techniques for pollution assessment in urban and suburban areas in Greece: State of the art and case studies	1972

ΣΕΙΣΜΟΛΟΓΙΑ / SEISMOLOGY

Adamaki, A.K., Tsaklidis, G.M., Papadimitriou, E.E., Karakostas, V.G.: Evidence for induced seismicity following the 2001 Skyros mainshock	1984
Astiopoulos, A.C., Papadimitriou, E., Karakostas, V., Gospodinov, D., Drakatos, G.: Seismicity changes detection during the seismic sequences evolution as evidence of stress changes	1994
Chousianitis, K., Agalos, A., Papadimitriou, P., Lagios, E., Makropoulos, K.: Source parameters of moderate and strong earthquakes in the broader area of Zakynthos Island (W. Greece) from regional and teleseismic digital recordings	2005
Kapetanidis, V., Papadimitriou, P., Makropoulos, K.: A cross-correlation technique for relocation of seismicity in the Western Corinth Rift	2015
Karakaisis, G.F., Papazachos, C.B., Scordilis, E.M.: Seismic sources and main seismic faults in the Aegean and surrounding area	2026
Karakonstantis, A., Papadimitriou, P.: Earthquake relocation in Greece using a unified and homogenized seismological catalogue	2043
Karakostas, V.G., Papadimitriou, E.E., Karamanos, Ch.K. Kementzetzidou, D. A.: Microseismicity and seismotectonic properties of the Lefkada – Kefalonia seismic zone	2053
Karakostas, V.G., Papadimitriou, E. E., Tranos, M.D., Papazachos, C.B.: Active seismotectonic structures in the area of Chios Island, North Aegean Sea, revealed from microseismicity and fault plane solutions	2064
Karamanos, Ch.K., Karakostas, V.G., Seeber, L., Papadimitriou, E.E., Kilias, A.A.: Recent seismic activity in Central Greece revealing local seismotectonic properties	2075
Kaviris, G., Papadimitriou, P., Makropoulos, K.: Anisotropy study of the February 4th 2008 swarm in NW Peloponnesus (Greece)	2084
Leptokaropoulos, K.M., Papadimitriou, E.E., Orlecka–Sikora, B., Karakostas, V.G.: Seismicity rate changes in association with time dependent stress transfer in the region of Northern Aegean Sea, Greece	2093
Moshou, A., Papadimitriou, P., Makropoulos, K.: Moment tensor determination using a new waveform inversion technique	2104
Paradisopoulou, P.M., Papadimitriou, E.E., Karakostas, V.G., Lasocki, S., Mirek, J., Kilias, A.: Influence of stress transfer in probability estimates of $M \geq 6.5$ earthquakes in Greece and surrounding areas	2114
Popandopoulos, G., Baskoutas, I.: Space regularity manifestation of the temporal variation of seismic parameters: Possibility for the strong seismic activity assessment	2125
Roumelioti, Z., Kiratzi, A.: Incorporating different source rupture characteristics into simulations of strong ground motion from the 1867, M7.0 earthquake on the Island of Lesbos (NE Aegean Sea, Greece)	2135
Roumelioti, Z., Kiratzi, A.: Moderate magnitude earthquake sequences in Central Greece (for the year 2008)	2144
Scordilis, E.M.: Correlations of the mean time and mean magnitude of accelerating preshocks with the origin time and magnitude of the mainshock	2154

Segou, M., Voulgaris, N., Makropoulos, K.: On the sensitivity of ground motion prediction equations in Greece	2163
Serpetsidaki, A., Sokos, E., Tselentis, G-A.: Study of the 2 nd December 2002 Vartholomio earthquake (Western Peloponnese), M5.5 aftershock sequence	2174
Sokos, E., Pikoulis, V.E., Psarakis, E.Z., Lois, A.: The April 2007 swarm in Trichonis Lake using data from a microseismic network	2183
Tsapanos, T.M., Koravos, G.Ch., Plessa, A., Vythoulkas, N.K., Pitsonis, I.S.: Decay parameters of aftershock sequences globally distributed	2193
Votsi, I., Limnios, N., Tsaklidis, G., Papadimitriou, E.: Semi-Markov models for seismic hazard assessment in certain areas of Greece	2200
Ευρετήριο συγγραφέων / Author index	2211



ΤΟΜΟΣ 5 / VOLUME 5

Ενεργειακές Πρώτες Ύλες και Γεωθερμία / Energy resources and Geothermics
Γεωχημεία και Κοιτασματολογία / Geochemistry and Ore Deposit Geology
Βιομηχανικά Ορυκτά και Πετρώματα / Industrial Minerals and Rocks
Ορυκτολογία και Πετρολογία / Mineralogy and Petrology

ΕΝΕΡΓΕΙΑΚΕΣ ΠΡΩΤΕΣ ΥΛΕΣ ΚΑΙ ΓΕΩΘΕΡΜΙΑ / ENERGY RESOURCES AND GEOTHERMICS

Fotopoulou, M., Siavalas, G., İnaner, H., Katsanou, K., Lambrakis, N., Christanis, K.: Combustion and leaching behavior of trace elements in lignite and combustion by products from the Muğla basin, SW Turkey	2218
Karageorgiou, D.E., Metaxas, A., Dimitriou, D., Arapogiannis, E., Varvarousis, G.: Contribution of lignite in the Greek economy	2229
Karageorgiou, D.E., Metaxas, A., Karageorgiou, M.M.D., Papanikolaou, G., Georgakopoulos, A.N., Vrettos, K.: Development of lignite in Crete. Comparison of basins, possibilities of exploitation	2236
Kolios, N., Arvanitis, A., Karydakis, G., Koutsinos, S.: Geothermal drilling activity in the Akropotamos Area (Macedonia, Northern Greece)	2246
Mertzanides, Y., Kargiotis, E., Mitropoulos, A.: Geological and geophysical data of “Epsilon” field in Prinos oil basin	2257
Metaxas, A., Varvarousis, G., Karydakis, Gr., Dotsika, E., Papanikolaou, G.: Geothermic status of Thermopylae - Anthili area in Fthiotida Prefecture	2265
Metaxas, A., Georgakopoulos, A.N., Karageorgiou, D.M.M., Papanikolaou, G., Karageorgiou, E.D.: CO ₂ Content of Greek lignite: the case of Proastio Lignite deposit in Ptolemais Basin, Northern Greece	2274
Oikonomopoulos, I., Perraki, Th., Tougiannidis, N.: FTIR study of two different lignite lithotypes from Neocene Achlada lignite deposits in NW Greece	2284

Papanicolaou, C., Triantafyllou, G., Pasadakis, N., Foscolos, A.E.: Adsorption of phenols from olive oil mill wastewater as well as n and p from a simulated city wastewater liquid on activated Greek lignites	2294
--	------

ΓΕΩΧΗΜΕΙΑ ΚΑΙ ΚΟΙΤΑΣΜΑΤΟΛΟΓΙΑ / GEOCHEMISTRY AND ORE DEPOSIT GEOLOGY

Alexandratos, V.G., Behrends, T., Van Cappellen, P.: The influence of reductive dissolution of iron oxides by S(-II) on uranium mobility	2310
Argyraiki, A., Petrakaki, N.: Heterogeneity in heavy metal concentrations in the soil of a firing range area at Kesariani, Athens, Greece	2319
D' Alessandro, W., Brusca, L., Martelli, M., Rizzo, A., Kyriakopoulos, K.: Geochemical characterization of natural gas manifestations in Greece	2327
Demetriades, A., Birke, M., Locutura, J., Bel-lan, A.B., Duris, M., EuroGeoSurveys Geochemistry Expert Group: Urban geochemical studies in Europe	2338
Demetriades, A., Reimann, C., Birke, M., Salminen, R., De Vos, W., Tarvainen, T., EuroGeoSurveys Geochemistry Expert Group: Geochemical Atlases of Europe produced by the EuroGeoSurveys Geochemistry Expert Group: State of progress and potential uses	2350
Kyriakopoulos, G.K.: Natural degassing of carbon dioxide and hydrogen sulphide and its environmental impact at Milos Island, Greece	2361
Papastergios, G., Filippidis, A., Fernandez-Turiel, J.L., Gimeno, D., Sikalidis, C.: Natural and anthropogenic effects on the soil geochemistry of Kavala Area, Northern Greece	2373
Psomiadis, D., Dotsika, E., Albanakis, K., Zisi, N., Poutoukis, D., Lazaridis, A.: Comparison of sampling techniques for isotopic analysis of shallow marine carbonates	2383
Serelis, K.G., Kafkala, I.G., Parpodis, K., Lazaris, S.: Anthropogenic and Geogenic contamination due to heavy metals in the vast area of Vari, Attica	2390
Stefanova, M., Marinov, S.P.: Organic geochemistry of humic acids from a Neogene lignite sample, Bulgaria	2398
Tombros, S.F., St. Seymour, K., Spry, P.G., Bonsall, T.A.: The isotopic signature of the mineralizing fluid of the Lavrion carbonate-replacement Pb-Zn-Ag district	2406
Triantafyllidis, S., Skarpelis, N.: Geochemical investigation and modelling of an acid pit lake from a high sulfidation ore deposit: Kirki, NE Greece	2417

ΒΙΟΜΗΧΑΝΙΚΑ ΟΡΥΚΤΑ ΚΑΙ ΠΕΤΡΩΜΑΤΑ / INDUSTRIAL MINERALS AND ROCKS

Anagnostou, Ch.: Bauxite resource exploitation in Greece vs sustainability	2426
Arvanitidis, N.D.: New metallogenetic concepts and sustainability perspectives for non-energy metallic minerals in Central Macedonia, Greece	2437
Fadda, S., Fiori, M., Pretti, S., Valera, P.: Volcanic – sedimentary metal deposition in Paleomargin environment: A “ Protore ” occurrence in Central Sardinia (Italy)	2446
Kitsopoulos, K.: Immobile trace elements discrimination diagrams with zeolitized volcanics from the Evros - Thrace - Rhodope volcanic terrain	2455

Lampropoulou, P., Tzeveleku, Th., Papamantellos, D., Stivanakis, V., Papaefthymiou, S.: Human interferences to the environment, consequences and care	2465
Laskaridis, K., Patronis, M.: “Karystía líthos”: a timeless structural ornamental stone	2475
Leontakianakos, G., Baziotis, I., Ekonomou, G., Delagrammatikas, G., Galbenis, C.T., Tsimas, S.: A Case study of different limestones during quick lime and slaked-lime production	2485
Manoutsoglou, E., Panagopoulos, G., Spyridonos, E., Georgiou, A.: Methodology for optimal determination of new drilling program in an active open pit: Example from an active sulfate open pit in Altsi, Lasithi Prefecture, Eastern Crete	2492
Mpalatsas, I., Rigopoulos, I., Tsikouras, B., Hatzipanagiotou, K.: Suitability assessment of Cretaceous limestones from Thermo (Aitoloakarnania, Western Greece) for their use as base and sub-base aggregates in road-construction	2501
Papastamatiou, D., Skarpelis, N., Argyraki, A.: Air quality in mining areas: The case of Stratoni, Chalkidiki, Greece	2510

ΟΡΥΚΤΟΛΟΓΙΑ ΚΑΙ ΠΕΤΡΟΛΟΓΙΑ / MINERALOGY AND PETROLOGY

Baziotis, I., Mposkos, E.: Geochemistry and tectonic setting of eclogite protoliths from Kechros Complex in East Rhodope (N.E. Greece)	2522
Bourliva, A., Michailidis, K., Sikalidis, C., Filippidis, A., Apostolidis, N.: Municipal wastewater treatment with bentonite from Milos Island, Greece	2532
Bourouni, P., Tsikouras, B., Hatzipanagiotou, K.: Petrological investigation of carbonate rocks from the Ionian Zone (Etolokarnania, Western Greece)	2540
Christidis, G.E., Skarpelis, N.: Clay mineralogy of the sedimentary iron-nickel ore of Agios Ioannis, NE Boeotia: new data and implication for diagenetic modifications	2553
Christidis, G.E., Katsiki, P., Pratikakis, A., Kacandes, G.: Rheological properties of Palygorskite- Smectite suspensions from the Ventzia Basin, W. Macedonia, Greece	2562
Christidis, G.E., Perdikatsis, V., Apostolaki, Ch.: Mineralogy of the Saharan Aeolian Dust in Crete: Examples from the period 2004-2009	2570
Çina, A.: Mineralogy of chromitite, Bulqiza ultramafic massif, Albanian ophiolitic complex	2577
Fadda, S., Fiori, M., Pretti, S., Valera, P.: Manganese mineralisations at the base of Miocene sediments in Northern Sardinia (Italy)	2588
Filippidis, A., Papastergios, G., Apostolidis, N., Filippidis, S., Paragios, I., Sikalidis, C.: Purification of urban wastewaters by Hellenic natural Zeolite	2597
Georgiadis, I.K., Koronaios, A., Tsirambides, A., Stamatakis, M.: Textural and petrological study of modern sands from the Vertiskos Unit of Serbomacedonian Massif (Macedonia, Greece)	2606
Karipi, S., Tsikouras, B., Rigopoulos, I., Hatzipanagiotou, K., Pomonis, P.: Insights into hydrothermal activity in the Iti Ophiolite (Central Greece)	2617
Kitsopoulos, K.: Magma generation and mixing in the earliest volcanic centre of Santorini (Akrotiri Peninsula). Mineral chemistry evidence from the Akrotiri Pyroclastics	2625
Koutsopoulou, E., Tsolis-Katagas, P., Papoulis, D.: Heavy metals in stream sediments affected by a landfill and associated impact on groundwater quality	2635

Lykakis, N. Kiliyas, S. P.: Epithermal Manganese Mineralization, Kimolos Island, South Aegean Volcanic Arc, Greece	2646
Michailidis, K., Trontzios, G., Sofianska, E.: Chemical and mineralogical assessment of clays from Peloponnese (S. Greece) and their evaluation for utilization in ceramics industry	2657
Mposkos, E., Baziotis, I.: Study of the metamorphic evolution of a carbonate – bearing metaperidotite from the Sidironero Complex (Central Rhodope, Greece) using P-T and P(T)- X_{CO_2} Pseudosections	2667
Papadopoulos, A., Christofides, G., Papastefanou, C., Koroneos, A., Stoulos, S.: Radioactivity of granitic rocks from Northern Greece	2680
Persianis, D., Katsikis, J., Karageorgiou, D.E.: The genetic hypothesis of the uraniferous mineralization, Eastern Chalkidiki (Northern Greece)	2692
Ploumis, P., Chatzipanagis, I.: Geological, petrological and tectonic features characterizing the commerciality of the marbles of Southern Vermion Mountain	2702
Rigopoulos, I., Tsikoura, B., Pomonis, P., Karipi, S., Hatzipanagiotou, K.: Quantitative analysis of Asbestos fibres in ophiolitic rocks used as aggregates and hazard risk assessment for human health	2712
Solomonidou, A., Dominic Fortes, A., Kyriakopoulos, K.: Modelling of volcanic eruptions on Titan	2726
Stamatakis, M., Stamatakis, G.: The use of diatomaceous rocks of Greek origin as absorbents of olive-oil wastes	2739
Theodosoglou, E., Koroneos, A., Soldatos, T., Zorba, T., Paraskevopoulos, K.M.: Comparative Fourier Transform infrared and X-Ray powder diffraction analysis of naturally occurred K-feldspars	2752
Tzamos, E., Filippidis, A., Kantiranis, N., Sikalidis, C., Tsirambides, A., Papastergios, G., Vogiatzis, D.: Uptake ability of zeolitic rock from South Xerovouni, Avdella, Evros, Hellas	2762
Vasilatos, Ch., Vlachou-Tsipoura, M., Stamatakis, M.G.: On the occurrence of a volcanic ash layer in the Xylokastro Area, North Peloponnesus, Greece: Mineralogy and geochemistry	2773
Voudouris, P., Magganas, A., Kati, M., Gerogianni, N., Kastanioti, G., Sakelaris, G.: Mineralogical constraints to the formation of vein-type zeolites from Kizari area, Thrace Northern Greece	2786
Ευετήσιο συγγραφέων / Author index	2799

12ο ΔΙΕΘΝΕΣ ΣΥΝΕΔΡΙΟ ΤΗΣ ΕΛΛΗΝΙΚΗΣ ΓΕΩΛΟΓΙΚΗΣ ΕΤΑΙΡΙΑΣ
ΠΛΑΝΗΤΗΣ ΓΗ: Γεωλογικές Διεργασίες και Βιώσιμη Ανάπτυξη

12th INTERNATIONAL CONGRESS OF THE GEOLOGICAL SOCIETY OF GREECE
PLANET EARTH: Geological Processes and Sustainable Development



ΤΕΧΝΙΚΗ ΓΕΩΛΟΓΙΑ ΚΑΙ ΓΕΩΤΕΧΝΙΚΗ ΜΗΧΑΝΙΚΗ
ENGINEERING GEOLOGY AND GEOTECHNICAL ENGINEERING

GEOLOGICAL AND GEOTECHNICAL BEHAVIOUR OF EVINOS DAM FOLLOWING THE IMPOUNDMENT

Angelopoulos A.¹, Soulis V.J.², Malandraki V.³

¹ Geologist, Geophysist, Division of Raw Water Intake, Athens Water Supply and Sewage Company S.A (E.YD.A.P S.A), Galatsiou 16, Athens, Greece, angelopoulos@eydap.gr

² Dr Civil Engineer, Division of Raw Water Intake, Athens Water Supply and Sewage Company S.A (E.YD.A.P S.A), Galatsiou 16, Athens, Greece, vsoulis@eydap.gr

³ Dr Civil Engineer, Division of Raw Water Intake, Athens Water Supply and Sewage Company S.A (E.YD.A.P S.A), Galatsiou 16, Athens, Greece, malavas@eydap.gr

Abstract

The Evinos dam built between 1993 and 1997. The period of construction followed a period of rest until 2001. The impoundment of the Evinos Dam and the subsequent 3rd operational period took place between 2001 and 2005. The 4th period of operation commenced in February 2005 and concerns the period of regular operation of Dam Evinos after completion. During this period, sufficient data have been gathered for the evaluation of the geotechnical behaviour of both Evinos Dam itself and the stabilization works on the two landslides that occurred (Landslide of the left abutment '93, Landslide of Ag.Demetrios-Arahova country road). Specialized personnel of the Department of the Evinos Dam of the Athens Water Supply and Sewage Company S.A are responsible for the in-situ collection of instrumental readings. On the other hand specialized personnel of the Division of Raw Water Intake of Athens Water Supply and Sewage Company S.A are assigned to evaluate the dam's behaviour. The infiltration of water within the Dam's core is continuously monitored together with the horizontal movement and settlement upstream and downstream the dam's body through a considerable number of vibrating wire piezometers, earth pressure cells, extensimeters, inclinometers and surface monumental stations. The behaviour of the stabilization interventions in the landslide area's are evaluated through measurement of topographic monuments ,open piezometers and drainage measurements. The evaluation of the instrumental measurements confirms the expected behavior of the dam and the satisfactory performance of the stabilization interventions in the landslide area's.

Key words: Evinos Dam, evaluation, geotechnical behaviour, landslides, piezometers, settlement, movement

1. Introduction

The Evinos Project, Dam and tunnel of Evinos – Mornos belongs to the second phase of the water supply scheme for the city of Athens and its wider area. The geological formations of the reservoir and the area of the dam foundation consists of flysch a highly deformed complex of sandstones ,siltstones and mudstones Fig.1. The intersection of the dam comprises a central core with material from the clay phase of the flysch, filter transition zones and support bodies of the river's sandstone. The lower parts consist of rocky materials from excavations. Dounias & Papageorgiou, 2001 are de-

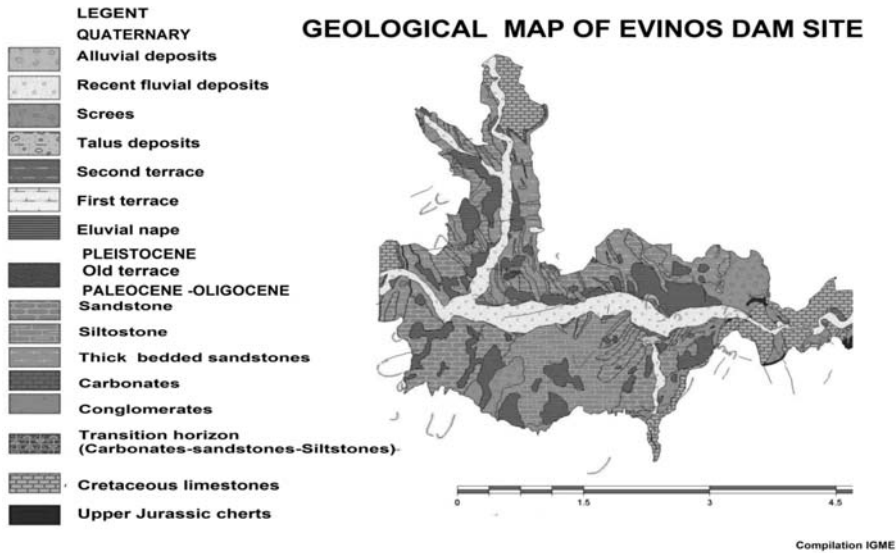


Fig. 1: Geological map of Evinos dam site.

describing the construction materials and the impermeable clay core made from flysch siltstones of Evinos Dam. The reasons that an earth fill dam with impermeable clay core was initially selected for the design of Evinos Dam were the high fractured geological formation of the area, the high seismic demands and the satisfactory performance of similar projects in analogous geological conditions (e.g. Kremasta, Kastraki Pournari, Mornos, Dounias & Papageorgiou, 2001). During the construction of Evinos Dam two landslides occurred. The first initiated in the Agios Demetrios-Arahouva Country Road in the left abutment of the dam, while the second one occurred in August 1993, in the same abutment, just before the spillway entrance. The behaviour of the Dam's core is continuously monitored utilizing a number of instruments (vibrating wire piezometers, earth pressure cells, extensimeters, inclinometers, surface monumental stations). These instruments are placed in three sections IV, IX, XI, within the dam's body Fig 6. The evolution of the two landslides is also monitored (Angelopoulos et al., 2007, 2008).

2. Evinos dam

2.1. Piezometers

A large number of vibrating wire piezometers were installed in the shoulders and the core of the dam. The pore water pressure development differs through the dam due to the partial saturation and the low permeability values of the core. Piezometers Pz11-19 are placed in Section VI of the Evinos dam. In fig. 2 piezometers Pz11, Pz12 and Pz17 initially show no response in the changes of the reservoir level. In March 2006 the reservoir has overflowed. This period lasted for 3 months initiating the response of piezometers to the changes of the reservoir level. Piezometer Pz11 is more sensible to changes of reservoir level. This behaviour indicates that a flow net has been gradually started to establish in the core even for higher values of the reservoir level. Piezometers Pz14 and Pz 19 which are installed in the filter zone (free drainage material), showed a constant piezometric level through time. In fig. 3 the changes in the piezometric level of piezometers Pz31-33-34 are

Evolution of piezometric level with time in Section VI
Pz in El. 448 down to 425m

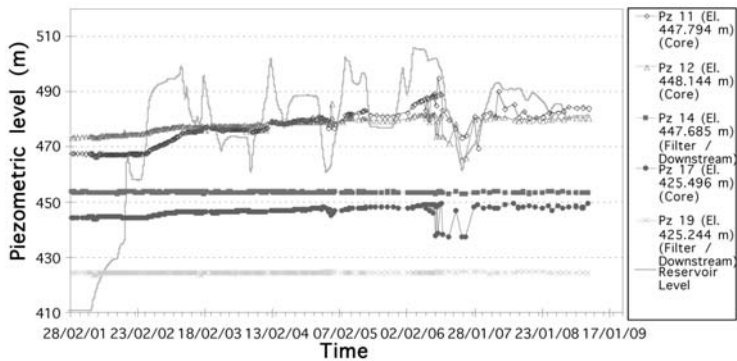


Fig. 2: Evolution of piezometric level in piezometers located in Section VI of the dam.

Evolution of piezometric level with time in Section IX-
Pz in El. 447 down to 423m

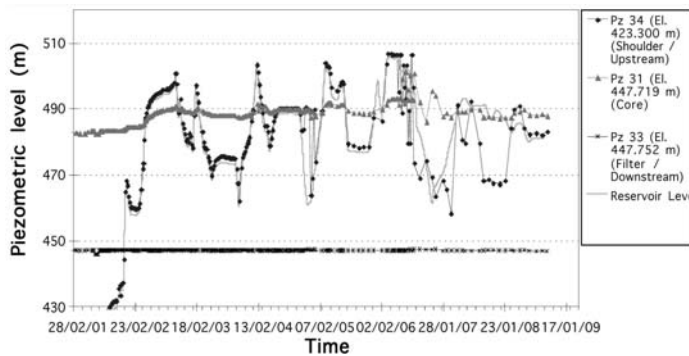


Fig. 3: Evolution of piezometric level in piezometers located in Section IX of the dam.

shown. These piezometers are placed upstream, downstream and at the core of the dam's body in section IX. Piezometer Pz34 which is installed upstream generally follows the fluctuation of the reservoir level. However, there was a period of drop of the reservoir level in the end of 2007 that Piezometer Pz34 didn't follow. Piezometer Pz 33 is placed in the filter zone downstream the dam's body. It shows no changes in its piezometric level as it is a free drained material. The study of the pore pressure development generally confirms the successful response of dam's core.

Piezometers are also placed in the foundation of the dam to inspect both the piezometric level in the foundation and the effectiveness of the grout curtain. In fig. 4 changes of the piezometric level measured in piezometers placed along Section VI can be depicted. Piezometers Pzf 11, Pzf 12, Pzf 26 show constant piezometric level through time. Piezometers installed upstream Pzf9, Pzf 10 show roughly constant piezometric level (about +420), which is influenced by the level of rainfall. Hydraulic piezometers are also installed through the grout curtain tunnel. Phc 2 follows the changes observed in the reservoir level. Phc 3 is less sensible to changes of the reservoir level. The response of piezometers placed in the foundation of Evinos Dam show little infiltration from the reservoir.

Evolution of piezometric level with time in Section VI-Pzf9 up to 10, 11, 12, 26 and Ph2, Ph3

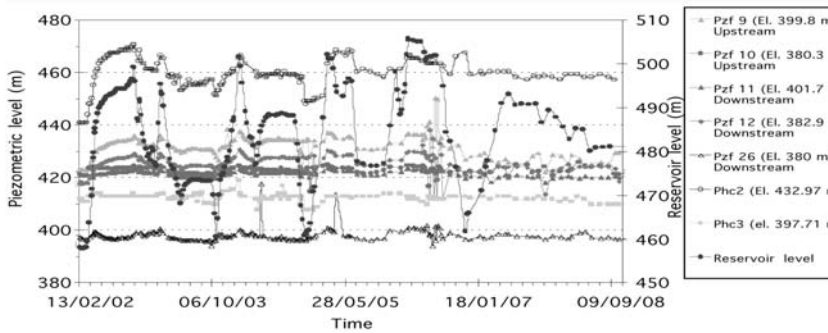


Fig. 4: Evolution of piezometric level in piezometers located in the foundation of the dam.

Evolution of movement and settlement at Dam's Crest
Group of Stations S68-S72

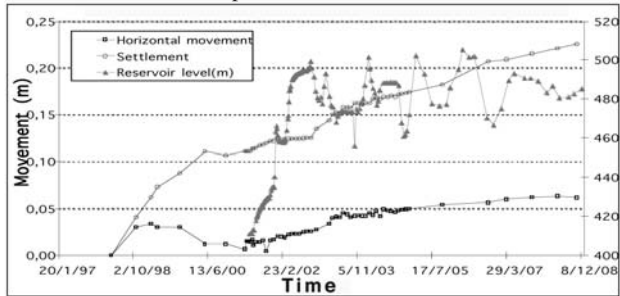


Fig. 5: Cumulative mean displacements and settlement in the dam's Crest.

2.2 Settlement and horizontal movement

Additionally the evaluation of the stability of Evinos Dam is carried out through the systematic measurement of horizontal and vertical movement of the dam's crest. In the dam's crest a number of surface monumental stations have been positioned upstream and downstream the dam's longitudinal axis (S24 -S33 upstream, S64-S73 upstream, Dounias, 2006). In fig. 5, the evolution of horizontal and vertical movements in respect with time are depicted for the same group of stations. The horizontal movement of the dam's crest is gradually increasing through time, although its magnitude is negligible. The settlement of the dam is increased following the impoundment of the reservoir. A slight increase of settlement rate is recorded even in the 4th period of operation in the dam's crest (February 2005-November 2008, Angelopoulos et.al., 2007,2008). During this period of operation the maximum settlement recorded is of the order of 5.2cm. The total settlement of the dam's crest is of the order of 22.6 cm and is regarded as safe. In fig. 6 the cumulative horizontal displacements D_x and settlement D_v for the group of stations S68-S72 in the dam's crest is presented. In the same figure the cumulative displacements D_x and settlement D_v for the group of stations B03-B07 in the area of the landslide of the left abutment '93 is also presented. The small vector denotes the displacements values and settlement in the date of impoundment (11/2001), the large vector denotes the displacement and settlement in the end of 2008 (12/2008).

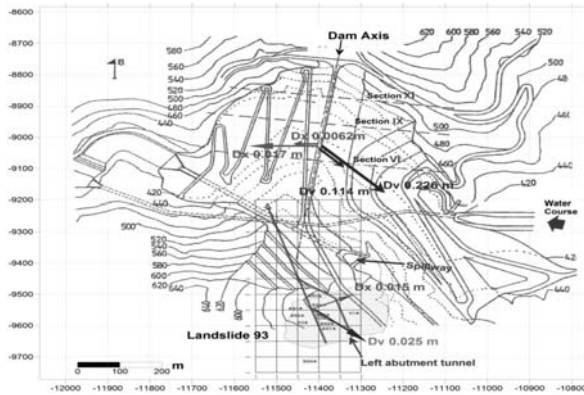


Fig. 6: Cumulative displacements D_x and settlement D_v for the group of stations S68-S72 in the dam's Crest, for the group of stations B03-B07 in the area of 1993 Landslide.

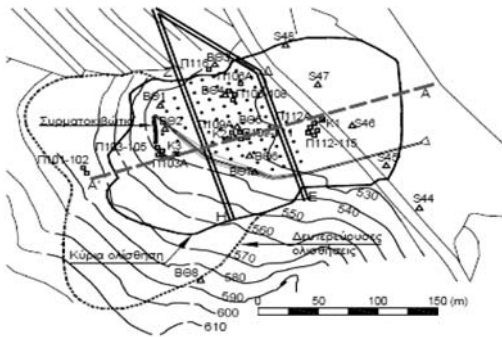


Fig. 7: Drainage tunnels and piezometers located in the area of the Landslide of the left abutment '93.

3. Landslide of the left abutment '93

In August 1993 a landslide occurred in the left abutment of Agios Demetrios just before the entrance of the spillway. The stabilization works included the construction of a drainage tunnels together with the construction of wells. The behaviour of the stabilization measurements are monitored by in-situ measurements in a) piezometers, b) inclinometric - settlement columns, c) surface monumental stations, d) devices measuring the flow in the exit of the drainage tunnels. In fig. 7, the stabilization measurements are depicted together with the positions of piezometers and surface monumental stations (Dounias & Dede, 2006).

4. Piezometers

The piezometric levels are continuously monitored after the completion of stabilization works. Piezometers are placed in different depths within the landslide's body. The deepest one is placed inside the substratum. In figs. 8, 9 the fluctuation of piezometric level in respect with time can be depicted. In the same figures the fluctuation of rainfall and the fluctuation of the reservoir's water level are recorded during the monitoring period. The stabilization works succeeded in reducing the piezometric level of deep piezometers that exhibit an immediate response in respect to the rainfall but they also exhibit an immediate pore pressure decrease. The piezometers located in depth up to 15.00m (i.e Π105 depth 4.25m, Π108 depth 12.30m, Π111 depth 12.20m, Π115 depth 11.40m) ex-

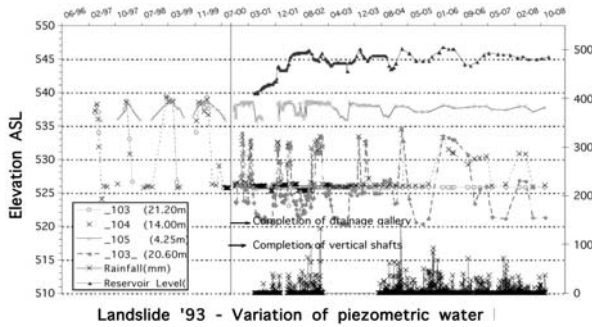


Fig. 8: Piezometric measurements of group Π103-Π105

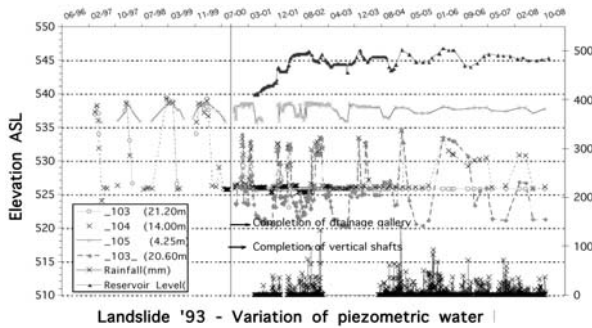


Fig. 9: Piezometric measurements of group Π112-Π115.

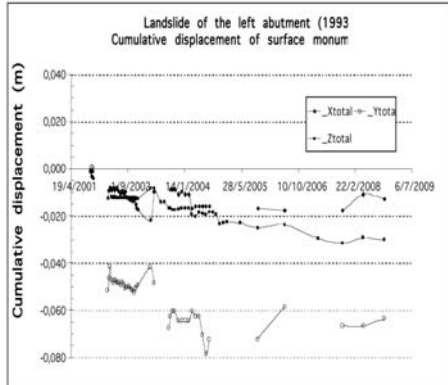


Fig. 10: Measurement of displacements in station K1 nearby piezometers Π112-115.

cept the piezometer Π104 (depth 14.00m) show reduced fluctuation of piezometric level after the completion of drainage tunnels. Piezometers placed in deeper levels (i.e Π106 depth 30.00m, Π109 depth 32.80m) do not exhibit any fluctuation of their piezometric level and they are considered as dry. In spring 2006 the dam has overflowed for a total period of three months. Piezometers Π103A and Π104 maintained their high piezometric level besides the substantial drop in the reservoir's level.

3.2 Settlement and horizontal movement

The surface monumental stations (K1, K2, K3 and BΘ1-BΘ8) have been placed inside the area of the landslide aiming to capture possible excessive settlement and horizontal movement (Figs 10, 11).

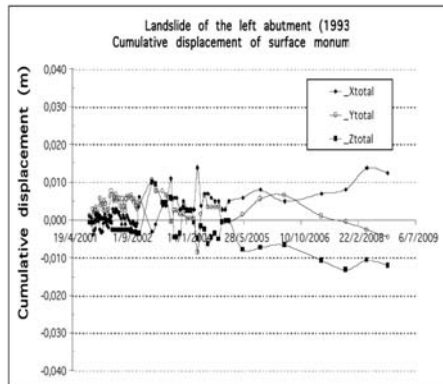


Fig. 11: Measurement of displacements in station K2 nearby piezometers Π109-111.

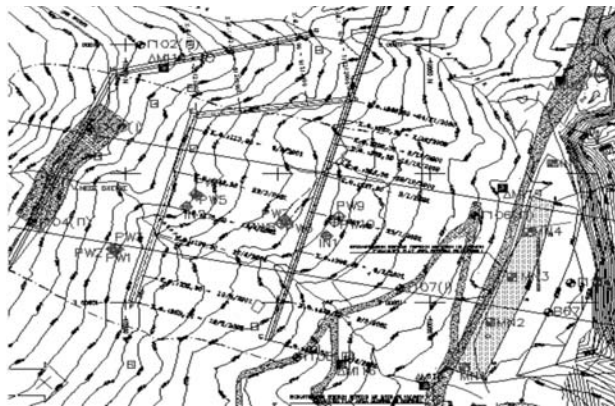


Fig. 12: Drainage tunnels and piezometers located in the area of the Road Landslide.

The stabilization works succeeded in reducing the overall movements to values between the limits of the instrumental measuring fault. Station K1 is located near by the group of piezometers Π112-115, while station K2 is located nearby the group of piezometers Π109-111.

4. The landslide of the Agios Demetrios- Arahova Country Road

The landslide occurred at the Agios Demetrios – Arahova Country Road during the construction of the Evinos reservoir project (1993). The stabilization interventions included the construction of toe berms, drainage tunnels, and surface runoff collection works. The behaviour of the stabilization interventions are monitored by in-situ measurements in a) piezometers, b) inclinometric-settlement columns, c) surface monumental stations, d) devices measuring the flow in the outlet of drainage tunnels. In fig. 12, the stabilization interventions are depicted together with the piezometers and surface monumental stations (Dounias et al., 2006).

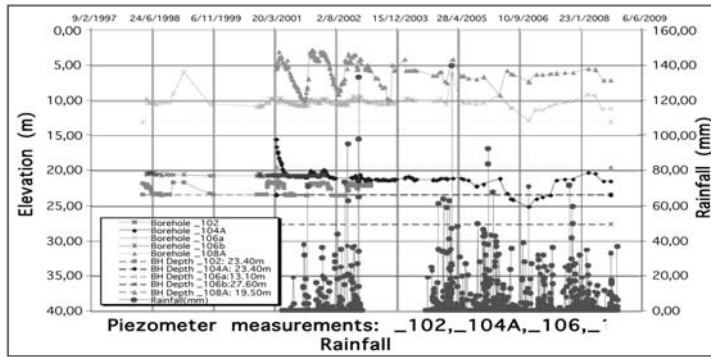


Fig. 13: Piezometric Measurements of Group Γ102, Γ104A, Γ108A and Γ106a & b.

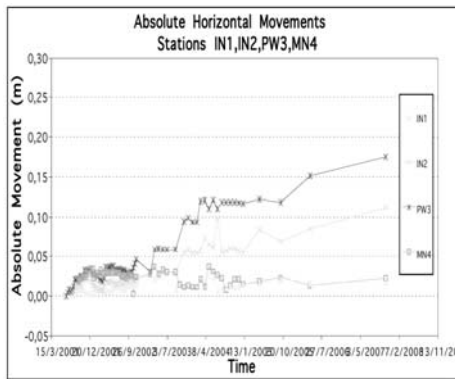


Fig. 14: Measurement of horizontal displacements in the area of Road Landslide.

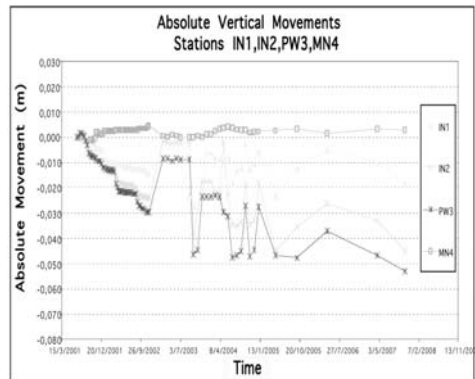


Fig. 15: Measurement of settlement in the area of Road Landslide.

4.1 Piezometers

Piezometers are installed in the area of Agios Demetrios-Arahova Country Road Landslide to record the fluctuation of piezometric level upstream and downstream the drainage tunnel. In fig. 13, the history of fluctuation of the piezometric levels of piezometers Γ102, Γ104A, Γ108A and Γ106a & b is presented. In the same fig. 13 the rainfall level curve is also depicted. The piezometers that are located in depth levels greater than 15m are affected by the drainage tunnel and show decreased piezometric levels in respect with piezometers placed in depth levels smaller than 15m. The measurements of piezometers placed deeply in the area of landslide are affected by the reservoir’s water level rise.

4.2 Settlement and horizontal movement

In figs 14, 15 the horizontal displacement measurements together with the settlement measurements are shown for the area of the landslide. The horizontal displacements measured downstream the drainage tunnels appear to be reduced in MN4, IN1 stations compared to the horizontal displacements measured in stations located upstream the drainage tunnels (PW3, IN2 upper part of landslide). The settlement (1,9 cm) of the lower parts of landslide MN4, IN1 are smaller compared to the settlement recorded (5.3cm) in stations PW3, IN2.

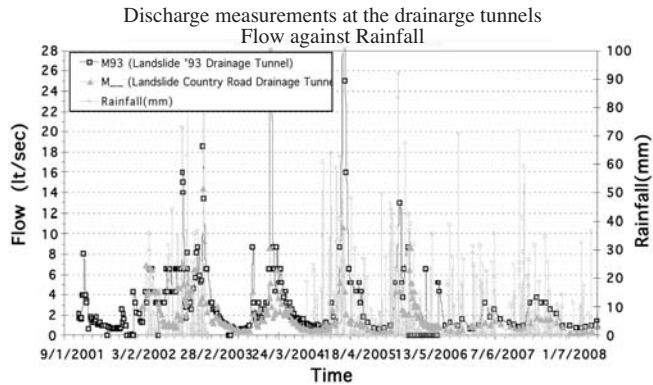


Fig. 16: Discharge measurements at the drainage tunnels in the areas of 1993 Landslide, and Country Road Landslide in relation to the rainfall.

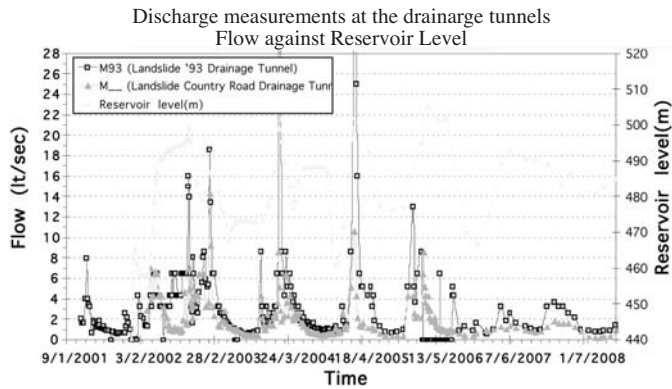


Fig. 17: Discharge measurements at the drainage tunnels in the areas of 1993 Landslide, and Country Road Landslide in relation to the reservoir level.

5. Discharge through drainage tunnels

In figs. 16, 17 the discharge measurements at the drainage tunnels of: a) Landslide of the left abutment '93 and b) Agios Demetrios-Arahova Country Road Landslide are depicted respectively. It is observed that the discharge at the outlets of these two drainage tunnels depends on the level of rainfall and exhibits immediate response. The discharge of the drainage tunnel within the landslide of the left abutment '93 depends on the reservoir level. It is shown that the discharge of the drainage tunnel within the landslide of the left abutment '93 is increased remarkably when the reservoir water level is above +485m.

6. Conclusions-Results

- Upstream piezometers show piezometric level that follows the fluctuation of the reservoir's water level as expected.
- Downstream piezometers placed in the free draining material, present a constant low piezometric level through time, as expected.

- Piezometers placed downstream the grout curtain show considerably low piezometric level which demonstrates the efficiency of the grout curtain.
- Surface monumental stations placed on the dam crest (S68-72 downstream), indicate “extension” of the dam’s crest towards downstream, as well as a normal evolution of settlement.
- Drainage interventions are considered effective; as it is proved they have led to a considerable water level decrease in the deeper piezometers in both landslides.
- The horizontal displacements and settlement measured in surface monumental stations (K1, K2, K3) suggest that the landslide of the left abutment '93 is not active.
- The horizontal displacements and settlement measured downstream the drainage tunnels in the area of Agios Demetrios-Arahoa Country Road Landslide appear to be reduced in comparison to the horizontal displacements and settlement measured in stations located upstream the drainage tunnels.

7. Acknowledgments

The authors would like to thank the personnel of the Department of Evinos Dam, Division of Raw Water Intake, Athens Water Supply and Sewage Company S.A for their help during fieldwork and their effort during field measurements. We thank the head of the Division of Raw Water Intake, Athens Water Supply and Sewage Company S.A, Mr. George Valavanis, for his persistent support in the preparation of this work.

8. References

- Angelopoulos A., Soulis V., Malandraki V., 2007. Evaluation of instrumental results during the 4th operational period of Evinos Dam, October 2006-September 2007, *Internal Report Issue No 16, Division of Raw Water Intake*, E.YD.A.P.S.A, Greece, Athens .
- Angelopoulos A., Soulis .V., Malandraki V., 2008. Evaluation of instrumental results during the 4th operational period of Evinos Dam, October 2007-September 2008, *Internal Report Issue No 17”*, *Division of Raw Water Intake*, E.YD.A.P.S.A, Greece, Athens .
- Dounias G., Dede V., 2006. Stabilization of the '93 landslide at the Evinos reservoir with drainage galleries. *Proceedings of the 5th Greek Conference on Geotechnical and Geoenvironmental Engineering*, Greece, Xanthi.
- Dounias G., Belokas G., Marinos P., 2006. The Landslide of the Agios Demetrios-Arahoa Country Road, at the Evinos river Basin. *Proceedings of the 5th Greek Conference on Geotechnical and Geoenvironmental Engineering*, Greece, Xanthi.
- Dounias G., 2006. The behaviour of clay core of the Evinos dam. *Proceedings of the 5th Greek Conference on Geotechnical and Geoenvironmental Engineering*, Greece, Xanthi.
- Dounias, G. & Papageorgiou, E., 2001, “Stresses and Strains in the Evinos dam, Greece”, *XVth International Conference on Soil Mechanics & Geotechnical Engineering*. Istanbul, Vol. 1, pp. 401-404.

ENGINEERING GEOLOGICAL ASPECTS FOR THE MICROZONATION OF THE CITY OF VOLOS, GREECE

Antoniou A. A.¹ and Tsiambaos G.¹

¹ National Technical University of Athens, School of Civil Engineering, Department of Geotechnical Engineering, 9 Iroon Polytechniou street, 15780 Zografou, Athens, Greece

Abstract

The city of Volos located at the foot of the Peninsula of Pelion at Central Greece experienced several strong earthquakes during the previous century. The engineering geological conditions of the city have been analyzed using a relational geotechnical database management system, while the city subsoil has been grouped into five geotechnical units. The maps showing the contours of the depth to bedrock head and the ground zoning against seismic hazard were compiled through GIS. For the compilation of the latter map, a set of unified classification criteria was proposed based on the Greek Seismic Code (EAK 2000).

Key words: seismic microzonation, GIS, engineering geological mapping, geotechnical data, Volos

1. Introduction

The city of Volos, the capital of the Magnesia prefecture, is located at the foot of the Peninsula of Pelion at Central Greece and constitutes an important commercial harbor and export centre. The urban development of the city was primarily based on economic and social determinants such as the establishment of the industrial estate, the upgrading of the port and the rapid growth of tourism. The broader area of the city is located in a narrow strip of the Pagasitikos gulf basin and west of the Pelion mountain range. Three main streams run through the region i.e. Xerias, Kravsidonas and Anavros (Fig. 1).

As regarding seismicity of the broader area, which constitutes the main natural hazard for the city, medium to strong earthquakes are closely related to the active fault zones crossing the Magnesia area and Pagasitikos gulf.

Due to this seismic activity, the city of Volos presents a high risk against earthquake, while severe structural damage has been occurred in the past. It must be noted that the engineering geological environment and the intense geodynamic processes were not taken into account for the urban planning of the city. The aim of this work was to collect and evaluate the data referred to engineering geological and geotechnical conditions of the area and to define the earthquake hazard zones in the city of Volos. This type of zonation is commonly referred to the preliminary phase of the seismic microzonation and seismic risk analysis and mitigation strategy for an urban area.

2. Geological setting

The bedrock of the city belongs to the Pelagonian geotectonic zone. It consists, according to the ge-

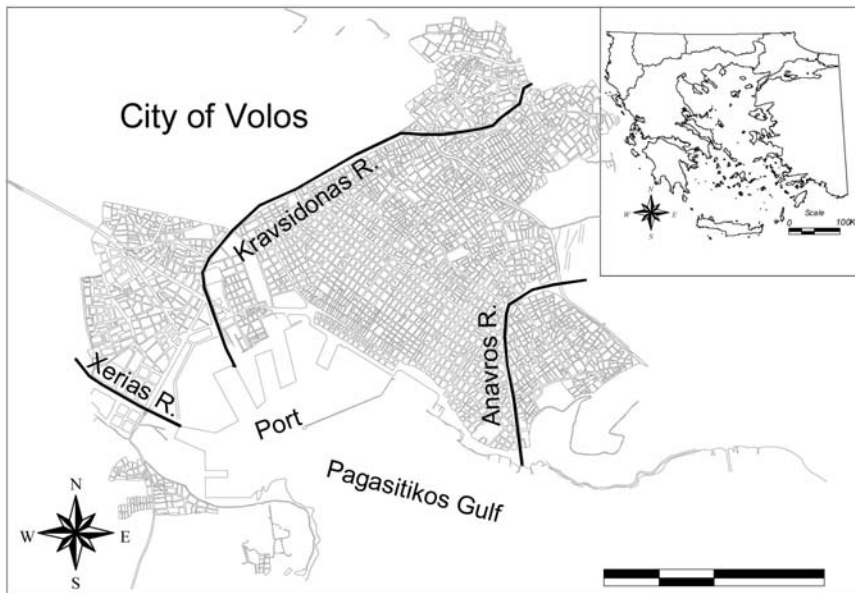


Fig. 1: General reference map of the city of Volos.

ological map of Greece of scale 1:50.000 (Katsikatsos et al., 1986) mainly of:

- Neopaleozoic to Middle Triassic schists, prasinites, quartzites and phyllites with intercalations of marbles and cipolins, of a total thickness of 800 m. These formations outcrop at the eastern part of the broader area of the city.
- Middle Triassic to Upper Jurassic marbles, with schists and metabasite rocks intercalations, which are intensively folded and recognized. They have a total thickness of 800 m and dominate at the north-eastern, south-eastern and south-western part.
- Amphibolitic schists accompanied by crystalline limestones and marbles, belonging to the Eohellenic (pre-upper Cretaceous) tectonic nappe. They have a maximum thickness of 300 m and cover the area north of the city.
- Neogene deposits, such as red clay, silt and clayey-sandy material of low cohesion with breccia and conglomerate intercalations with a maximum thickness of 100 m, outcrop west of the city.
- The quaternary deposits are of great extent dominating at the Volos city. They are fluvial-torrential terraces (mainly loose conglomerates) covering the western part, and plain deposits (consisting of sand, silt and clay with low percentage of coarse grained material) which cover the central part of the city. Pleistocene and Holocene scree and talus cones develop at places in the eastern city borders.

3. Seismological aspects

The geomorphology of Thessaly is mainly controlled by two systems of normal faults. The first NW-SE trending fault-system formed the basins of Larissa and Karditsa and probably controlled the orientation of coastline (Goldsworthy et al., 2002). The second system, striking E-W developed

in numerous fault zones in Thessaly district, which have formed new small grabens and offset the plio-quadernary deposits (Caputo,1990), This phase is very important for the tectonic evolution of the whole Thessaly region and also the Volos area, during which new faults have been formed and the recent morphology has been established. The focal mechanism of strong earthquakes and microearthquakes indicates a N-S trending extension along the E-W striking faults, the same also deduced by the tectonic analysis of recent faults (Papazachos et al. 1983, Hatzfeld et al, 1999).

The region experienced several strong earthquakes during historical time, such as in 743 and 1773 as well as in the recent time (Papazachos and Papazachou, 1989). In more detail, on April 19, 1955 an earthquake of $M_s=6.2$ caused extensive damage in the area of Volos. Its epicenter was located at Lechonia (less than 50km from the city of Volos). Damage was observed in the Magnesia prefecture, where 449 buildings were destroyed, 7609 suffered serious damage and 3540 lighter damage. Most of these structural damages were observed in the villages of Pelio mountain, where buildings were founded on the loose mantle of weathering, on steep slopes suffering landslide phenomena. The extended damage is also attributed to the weakening of the buildings by the prior Sophades earthquake ($M_s = 7.0$) of 30 April 1954.

Moreover, on March 8, 1957 an earthquake of $M_s = 6.8$ caused serious damage in the prefectures of Magnesia, Larissa, Karditsa and Trikala. Seven minutes before the main shock a large foreshock ($M_s = 6.5$) occurred, the consequence of which cannot be distinguished from those of main shock.

Finally, on July 9, 1980 an earthquake of $M_s=6.5$ caused severe damage in the prefectures of Magnesia, Phthiotida and Larissa. The epicenter was located at Almyros town, approximately 50km from the city of Volos. In total 5222 buildings were destroyed, 14726 suffered serious damage and 10688 light damage. In Nea Agchialos town, small ground fissures with an east-west direction were observed. These fissures were considered as shallow traces of small faults which were generated in the superficial deposits striking parallel to the main seismic fault which was not observed on the surface.

4. Geotechnical investigation and ground conditions

In order to determine the geotechnical characteristics of the subsoil of the city of Volos data collected from about 120 sampling boreholes and trial pits. The location of the investigations sites are shown in Fig. 2.

The information was implemented, after a thorough inspection and modification to standardize the terminology, in a geotechnical database under the name HelGeoRDaS (Hellenic Geotechnical Relational Database management System). The objects that are included in the database are:

- Tables: Seven primary tables and several auxiliary ones were formed and all are related with each other in the common field “*code of geotechnical research*”.
- Queries: The built in queries are retrieving data from one or more tables.
- Forms: For the easy implementation of data seven forms were built, one for each main table.

An extensive description of the system can be found in Antoniou et al (2001, 2008).

Moreover, the geotechnical database cites geographical information (e.g. coordinates), therefore the import of topology that concerns the territorial information, has been achieved with the connection of programs MS Access and ArcInfo of ESRI via Structured Query Language (SQL).

The majority of the geotechnical investigations were executed mainly for the construction of public buildings and engineering works at the port of Volos. Due to their vicinity with the coast, the

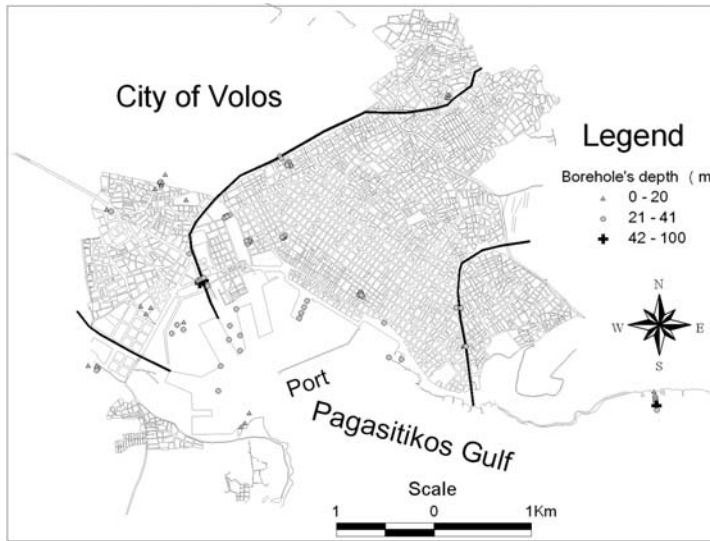


Fig. 2: Geotechnical investigation sites at the city of Volos.

Table 1. Description of geotechnical units with the range of measured parameters

Unit	Soil classification	Physical and mechanicals properties
I	Earth fills	
II	ML, CL, OH	LL = 40 – 60, PI = 20 – 25, w = 20 – 40% $c_u = 40$ KPa, $N_{SPT} = 1$ to 10
IIIa	CL, ML	LL = 20 – 40, PI = 5 – 20, w = 20 – 30% $c_u = 15 - 80$ KPa, $N_{SPT} = 2$ to >50
IIIb	SC, SM, SG, GM	LL = 20 – 40, PI = 5 – 10, w = 20%, $N_{SPT} = 15$ to >50
IV	GW, GM, GC, GP	LL = 20 – 40, PI = 5 $N_{SPT} = 15$ to >50
V	Bedrock	

depth of sampling boreholes was usually greater than 20m and in some cases over 140m, including the execution of Standard Penetration Tests (SPT).

To describe in detail the engineering geological conditions of the urban area, the soil formations were grouped into five individual geotechnical units, based on the evaluation of the existing geotechnical database taking into account the origin and age as well as the physical and mechanical characteristics of soil formations. Table 1 summarizes the physical and mechanical properties of the geotechnical units, as described hereafter:

Unit I: Earth fill materials which cover the major part of the city with a maximum thickness of 3m.

Unit II: Very loose to soft grey silt of low plasticity (ML) with intercalations of soft grey to brown clay of low plasticity (CL) or organics of high plasticity (OH). This unit underlies the backfill ma-

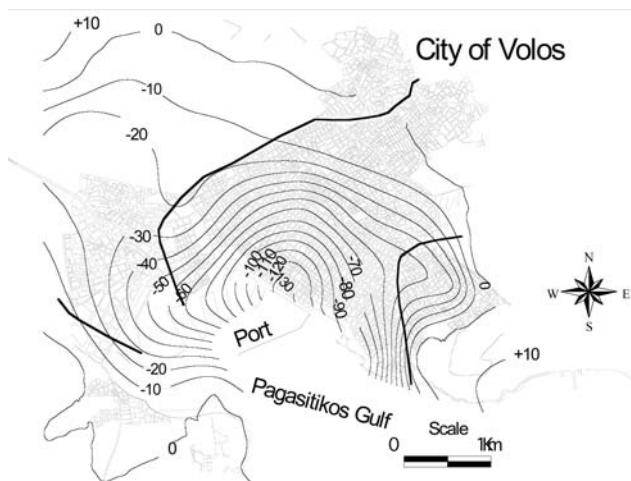


Fig. 3: Contour map showing the depth to bedrock head.

terials and covers mainly the coastal line and extends for about 200m towards the central part of the city. Its maximum thickness is 30m.

Unit III: Mixed phases of alluvial deposits which underlie directly unit I (at the central part of the city) or unit II (at the coastal area). Moreover, this unit can be subdivided to:

Unit IIIa (fine grained materials): Cohesive to stiff clay of low plasticity (CL) or silts of low plasticity (ML). The maximum thickness is 20m.

Unit IIIb (coarse grained materials): Medium dense clayey to silty sand (SC, SM) or dense sandy gravel (SG) or silty gravel (GM) with a maximum thickness of 30m.

Unit IV: Dense to very dense clayey to silty gravel well to poor graded (GW, GM, GC, GP). This unit underlies directly unit I or III at the northern part of the city. The maximum thickness is about 25m and locally in the coastal area exceeds 60m.

Unit V: This unit refers to bedrock and consists of schists, crystalline limestones and marbles. The bedrock outcrops at the surrounded hills and at Pelion mountain and usually develops a thick mantle of weathering.

The evaluation of the processed geotechnical data, led to the compilation of an engineering geological map (Fig. 3) showing the depth to bedrock head with contours at 10 m intervals. The maximum depth in the coastal area is greater than 130 m while to the north east and west part of the city the bedrock crops out.

5. Ground zoning for earthquake hazard

The available geological and geotechnical data, obtained from data retrieval options using Hel-GeoRDaS, as well as in situ observations, were evaluated with reference to the ground categories provided by the Greek Seismic Code (EAK 2000, Table 2).

Table 3 defines four zones for the city of Volos, each zone described in terms of the basic engineering geological characteristics, such as lithology, mechanical behaviour, stiffness, thickness etc (Marinos et al., 2001). Based on the aforementioned ground zoning, an engineering geological zoning map referring to earthquake hazard was compiled and presented in Fig. 4.

Table 2. Ground categories according to the Greek seismic code (EAK).

Category	Description
A	Hard or soft rock formations, with no intense weathering
	Layers of dense granular material with little silt or clay, and thickness over 70m
	Layers of very stiff overconsolidated clay, less than 70m thick
B	Highly weathered rock
	Layers of granular material of medium density and thickness over 5m or of high density and thickness over 70m
	Layers of hard overconsolidated clay more than 70m thick
C	Layers of granular material of low relative density and thickness over 5m or of medium density and thickness over 70m
D	Soft clays with plasticity index $I_p > 50$; thickness $> 10m$
X	Loose silty-sand soils under ground water level liquefaction risk
	Soils close to identified active faults
	Steep slopes with loose scree
	Loose granular soils or soft clayey-silty soils prone to dynamic consolidation or strength loss
	Recent loose earthfill, organic soils, rubble
	Soils of category C in very steep slopes

Table 3. Description of earthquake hazard zones in the city of Volos.

Zone	Description
1	Bedrock formations. Hard or soft rock including crystalline limestones, schists,, marbles, marls and well-cemented conglomerates. According to the Greek Seismic Code (EAK) this zone corresponds to ground category A. The highly weathered mantle of these formations with thickness greater than 5m compares to stiff soils formations and corresponds to ground category B. Stiff or dense soils. Includes mainly debris, talus cones and conglomerates of various cementation, clayey sand and gravel, stiff and hard clays. According to the EAK this zone corresponds to ground category A (very dense or cohesive soils) or B (looser soils with a thickness greater than 5 to 10m).
2	Medium stiff or dense soils. Includes recent deposits and non-cemented debris consisting mainly of silty-clayey soils of low strength and low to medium dense clayey sand and gravel. According to the EAK, this zone corresponds to ground category B, except those with low strength and low density with thickness greater than 10 –20 m which correspond to category C.
3	Coastal deposits. Includes recent loose sands and silts as well as soft clays of low to medium plasticity. According to the EAK, this zone corresponds to ground category C. Loose silty-sand soils under ground water level with liquefaction risk.
4	Rivers and watercourses. Includes areas along main rivers (Xerias, Kravsidonas and Anavros). The limits of this zone are only indicative on the map and its exact extent should result from detailed investigations, as foreseen in EAK for ground category X.

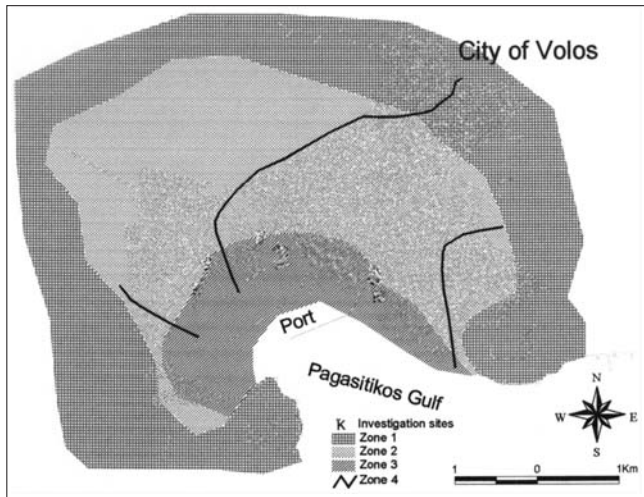


Fig. 4: Ground zoning map of Volos basin concerning earthquake hazard.

6. Conclusions

The engineering geological conditions of the urban area of Volos have been studied by using information derived from HelGeoRDaS geotechnical data base obtained from detailed geotechnical survey, as well as from in situ observations. In particular, the soil formations of the urban area were grouped into five geotechnical units, while thematic maps were compiled to illustrate information such as the depth to bedrock head. Moreover, an engineering geological zoning map referring to earthquake hazard was compiled with reference to the ground categories provided by the Greek Seismic code, EAK 2000. This mapping is considered appropriate for use at a preliminary local urban planning level, while more detailed geotechnical investigation is required for specific foundation works.

7. References

- Antoniou, A.A., Papadimitriou, A.G., Tsiambaos, G. 2008. A Geographical Information System managing geotechnical data for Athens (Greece) and its use for automated seismic microzonation. *Natural Hazards*, 47:369-395.
- Antoniou, A., Marinou, P., Kavvadas, M., Tsiambaos, G., Tsatsanifos, C. 2001. A geotechnical relational database management system *In: Proceedings of the 4th Hellenic Symposium in Geotechnical Engineering and Geoenvironment*. 1, 29-34.
- Caputo R., 1990. Geological and structural study of the recent and active brittle deformation of the neo-gene- quaternary basins of Thessaly. Ph.D. thesis, Univ. of Thessaloniki, Greece, 251 p.
- EAK, 2000. Earthquake Design Code, Earthquake Planning and Protection Organization, Athens (in Greek)
- Goldsworthy, M., Jackson, J., Haines, A.J. 2002. The continuity of active fault systems in Greece, *Geophysical Journal International*, 148, 3, F596-618.
- Hatzfeld, D., Ziazia, M., Kementzetzidou, D., Hatzidimitriou, P., Panagiotopoulos, D., Makropoulos, K., Papadimitriou, P., and Deschamps, A., 1999. Microseismicity and Focal Mechanisms at the Western Termination of the North Anatolian Fault and their Implications for Continental Tectonics. *Geophys. J. Int.*, 137, 891-908.

- Katsikatsos G., Mylonakis J., Vidakis M., Hecht J and Papadeas G., 1986. Geological map of Greece scale 1:50.000, sheet "Volos". Institute of Geology and Mineral Exploration, Athens.
- Marinos, P., Bouckovalas, G., Tsiambaos, G., Sabatakakis, N., Antoniou, A. 2001. Ground zoning against seismic hazard in Athens, Greece. *Engineering Geology*, 62, 343-356.
- Papazachos, B. C., Panagiotopoulos, D. G., Tsapanos, T. M., Mountrakis, D. M. and Dimopoulos, G. Ch., 1983. A study of the 1980 summer seismic sequence in the Magnesia region of central Greece. *Geophysical J. R. Astron. Society*, 75, 155-168, 1983.
- Papazachos B., Papazachou K. 1989. Earthquakes in Greece, Thessaloniki, Greece.

EXCAVATION DATA AND FAILURE INVESTIGATION ALONG TUNNEL OF SYMBOL MOUNTAIN

Chatziangelou M., Thomopoulos Ach., Christaras B.

*Department of Geology, Aristotle University of Thessaloniki, Greece, mcha@geo.auth.gr,
christar@geo.auth.gr*

Abstract

The tunnel of Symbol Mountain, which is 1160m long, is placed on South-west of Kavala City at Northern Greece. The tunnel consists of two bores with NW-SE direction, which are connected with two small tunnels. The stability of the rock mass was limited, during the excavation, because the rock mass was often changing, the faults are open, and the aquifer is placed above the excavation.

The aim of the present paper is to describe the dangerous geological status of Symbol Mountain and to propose excavation solutions of the unexpected failure conditions.

For the above reasons, the sudden changes of the rock mass quality along the tunnel excavation are described. The causes of the geological failures were investigated and the failures were classified. Furthermore, the efficacy of support measures was tested and a relationship between the apparent face of wedges and the shotcrete thickness was proposed.

Key words: *Tunnels, support measures, wedges, slidings, decollement, anchors, bolts, shotcrete, swellex, excavation.*

1. Introduction

The tunnel of Symbol Mountain is geotechnical located on Rodope mass. The excavation of the tunnel passed through alternations of gneiss, schists and marbles. The quality of the rock formations often changes from sound to weathered. It is, usually, heavily jointed and in many cases is folded. Furthermore, the presence of chloritic schist, lengthen 400m, caused numerous unexpected failures and support problems. So, the excavation needed to be extremely careful, and for this reason a combination of excavation methods were used. The presence of an opened vertical fault, which is just placed at the exit of the tunnel and creates a shear zone about 400m long, increased the stability problems. The water table is placed above the tunnel.

2. Rock mass quality

The beginning of the tunnel, the rock mass consists of fair quality gneiss with pegmatite veins, although there is a part of the tunnel between ch.36+300-ch.36+400 where the quality of a part of gneiss is very poor (Bieniawski, 1989, Hook, 2004). Walking along the tunnel, the rock mass quality becomes poor and or very poor near the schist formation. At the middle of the tunnel (ch. 35+800-ch.36+300), there is a fair quality lens of marble. Walking to the outlet of the tunnel, we met alternations of gneiss and marble medium and poor qualified. Between ch. 36+500-ch. 36+700, there is a formation of chloritic schistolite of poor quality. That geological formation caused numerous problems during the excavation, as it deformed very quickly after it was excavated. The last part of the tunnel is placed along a shear zone of an opened vertical fault 150/70 F (Fig.1).

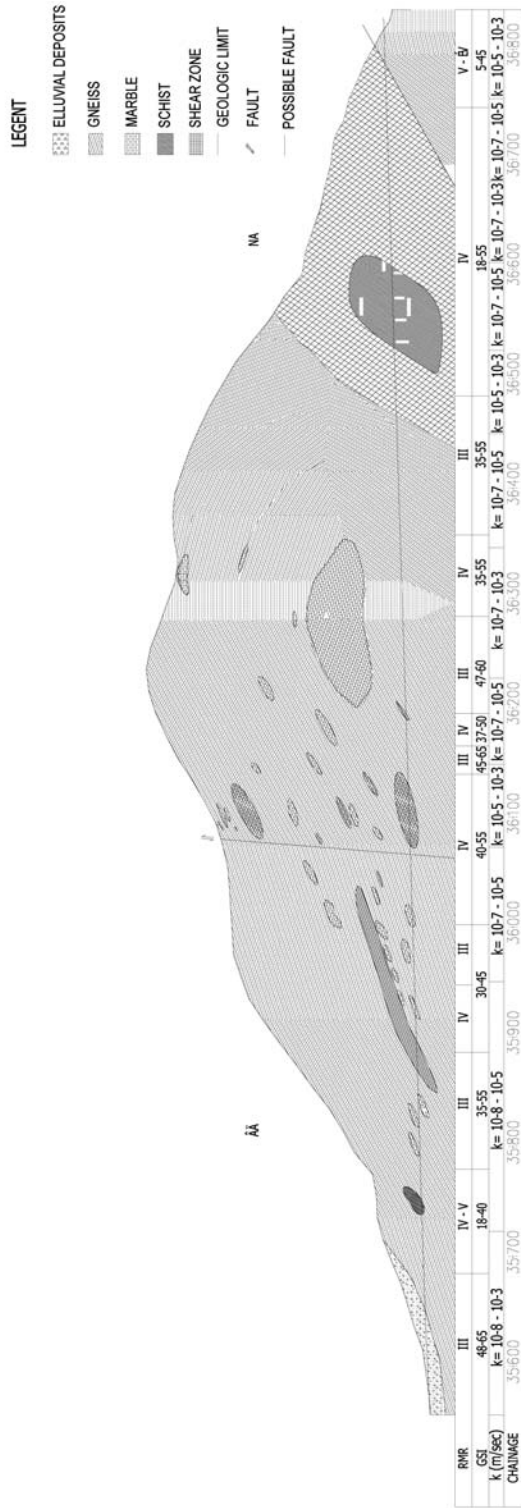


Fig. 1: Geological section along the right bore of the tunnel .

Table 1. Slidings and décollements along the tunnel

Chainage	Geological formations	Sliding	Décollement	J1	J2	J3	J4	J5
35677,1 - 35680,70	Gneiss with pegmatitic intercalations	239/38 S		173/38 S	239/38 S			
35684,3 - 5695,10	Gneiss with pegmatitic intercalations	235/54 F		235/54 F	360/32 S			
35697,5 - 35706	Gneiss with pegmatitic intercalations	224/58		224/58	146/4 S	174/72	145/38	
35716,5 - 35724	Gneiss with pegmatitic intercalations	249/41, 153/67		153/67	249/41	100/6 S		
35728,8 - 35733,3	Gneiss with pegmatitic intercalations	308/59, 212/47		212/47	308/59	97/12 S		
35733,3 - 35741,4	Gneiss with pegmatitic intercalations and schist	272/54		33/18 S	206/46	272/54		
35741,9 - 35744,7	Schist	71/51		343/19 S	71/51	119/31		
35744,7 - 35749,4	Schist and gneiss with pegmatitic intercalations	31/73, 238/45 S		154/25	238/45 S	20/18	31/73	
35749,4 - 35765,2	Gneiss with pegmatitic intercalations	64/53, 275/52		275/52	344/30 S	64/53		
35765,2 - 35774,2	Gneiss with pegmatitic intercalations and schist	285/63 F		181/26 F	285/63 F	339/28 S	56/65	
35774,4 - 35776	Gneiss and schist	226/46		226/46	351/18 S			
35776 - 35785	Marble and gneiss	238/61		174/69	238/61	4/12 S		
35785 - 35790,4	Gneiss	252/59		252/59	110/79	8/22 S		
35790,4 - 35802,9	Marble and gneiss	204/65	161/77	161/77	204/65	247/31	5/30 S	
35802,9 - 35864,4	Gneiss	54/60 S		54/60 S	243/43	10/24F		
35864,4 - 35880	Gneiss and marble	275/40 S, 71/77	Flow of weathered material, fall of soiled material	71/77	275/40 S	65/41	150/15 S	200/75
35880 - 35882	Marble	100/64	Soil material	258/29 F	358/68	100/64		
35882 - 35906,6	Gneiss and marble and chlorite	112/63, 175/67, 9/62 S	Soil material	237/34 F	9/62 S	112/63	175/67	
35906,6 - 35934,626	Marble	204/62 F		155/64	204/62 F	258/19 S		
35934,626 - 35941,635	Gneiss, marble, pegmatite and quartzite	55/62, 198/72	283/12 S	55/62	198/72	250/70	283/12 S	
35941,63535948,349	Marble	66/56		100/68	66/56	288/8 S		
35948,349 - 35957,379	Gneiss and marble	191/62, 313/36 S	313/36 S	313/36 S	191/60			
36008,125 - 082,468	Gneiss and marble	34/73, 267/29 S	267/29 S	267/29 S	151/60	34/73		
36082,468 - 36114,909	Marble	191/59, 270/58	318/16 S	66/88	191/59	270/58	318/16 S	

Chainage	Geological formations	Sliding	Décollement	J1	J2	J3	J4	J5
36114,909 - 36124,729	Marble	310/5 S		240/38	310/5 S			
36134,729 - 36139,41	Marble and schistolite	254/64, 349/26 S		254/64	349/26 S			
36139,41 - 36176,222	Marble	224/60, 33/68	348/13 F	224/60	140/68	33/68	348/13 F	
36176,222 - 36188,494	Marble and gneiss	65/67		240/71	312/33 S	65/67		
36188,494 - 36240,379	Gneiss	310/11 S, 43/78, 233/66	310/11 S	233/66	332/68	43/78	310/11 S	
36240,379 - 36312,44	Gneiss and marble	224/72		224/72	247/3 F			
36312,44 - 364327,74	Gneiss and marble	210/37	10/10 S	210/37	10/10 S			
36327,74 - 36350,746	Gneiss and marble		358/22 S	232/43	152/32 F	358/22 S		
36425,28 - 36387,1	Gneiss	137/52 S, 227/78	19/27 S, 137/52 S	227/78	137/52 S	238/39	19/27 S	
36387,1-36481,783	Chloritic schist and gneiss	123/70 S		123/70 S				
36481,783 - 36443,87	Gneiss	80/55, 197/55 F		197/55 F	80/55	03 / 015 S		
36443,87 - 36499,58	Chloritic schist and gneiss	221/72, 26/74		221/72	26/74	137/16 S	147/60	
36499,58 - 36537,046	Chloritic schist	219/72	cracked material, 138/44 S	219/72	212/11 S	138/44 S	04/016 S	
36537,46 - 36659,4	Gneiss	2875, 149/74, 252/74	155/20 S, cracked material	246/74	155/20 S	149/74	2875	
36659,4 - 36717,5	Gneiss and granite	220/63, 135/37		135/37	220/63	49/75	267/6 S	
36717,5 - 36740,9	Gneiss and marble	30/58 S, 120/70		140/52	265/82	30/58 S		
36740,9 - 36746	Gneiss	38/85		61/15 S	333/90	38/85		
36746 - 36749	Melange of granite, gneiss and marble	221/59, 128/68 F		128/68 F	221/59			
36749 - 36763,1	Granite and kaolinite	117/70 F		48/16 S	117/70 F	210/19	2684	
36763,73 - 36766,7	Gneiss	15/60 F		45/84	348/38 S	108/46 S	158/60 F	
36766,7 - 36771,5	Gneiss	132/74 F, 117/43 S		132/74 F	117/43 S			
36771,5 - 36777,5	Gneiss	100/43		90/10 S	100/43			
36777,5 - 36779,5	Gneiss and marble	124/40 S		188/70 F	287/63	35/63	120/70 F	124/40 S
36779,5 - 36789	Gneiss			36/83	81/89	153/68 S	171/36	

Table 2. Geometrical characteristics of most important wedges along the tunnel of Symbol Mountain

Chainage	Geological formations	Distance of the roof from the surface (m)	J1	J2	J3	J4	J5	Type of failure	Position of the wedge	FS.	Volume (m ³)	Weight (tms)	z-length (m)	Apparent face (m ²)	Height (m)
335675,9-35677,10	Gneiss	0	300/49	166/43	40/20			Collapse	Upper left wedge	0	201,825	544,928	20,26	72,54	9,53
35698,8 - 35707,2	Gneiss with pegmatitic intercalations	15	224/58	146/4 S	174/72	145/38		Collapse	Lower right wedge	0	208,672	563,414	16,12	66,51	9,85
								Upper left wedge	0	778,222	2101,198	40,39	210,56	12,68	
35707,2 - 35710,1	Gneiss and granite	15	158/48	226/52	80/5 S			Collapse	Upper right wedge	0	187,967	507,51	13,17	80,02	8,66
							Upper left wedge	0	620,66	1675,781	45,56	221,48	9,34		
35710,1 - 35718	Gneiss with pegmatitic intercalations	15	146/46	199/13 S	236/53	330/58		Collapse	Upper left wedge	0	1646,741	446,2	40,72	276,07	22,14
								Upper right wedge	0	1036,954	2799,776	18,51	121,47	35,26	
35718 - 35725,8	Gneiss with pegmatitic intercalations	15	153/67	249/41	100/6 S			Collapse	Upper left wedge	0	428,827	1157,833	25,85	124,25	11,71
5725,8 - 35730,3	Gneiss with pegmatitic intercalations	15	234/32	108/17 S	350/58			Collapse	Upper left wedge	0	232,963	629	23,27	99,42	7,5
35730,3 - 35734,8	Gneiss with pegmatitic intercalations	15	212/47	308/59	97/12 S			Collapse	Upper left wedge	0	967,241	2611,551	59,67	326,68	9,71
35734,8 - 35742,9	Gneiss with pegmatitic intercalations and schist	18	33/18 S	206/46	272/54			Collapse	Upper left wedge	0	1004,184	2711,296	147,98	577,23	6,4
35746,2 - 35749,4	Gneiss with pegmatitic intercalations and schist	18	154/25	238/45 S	20/18	31/73		Collapse	Upper right wedge	0	1009,331	2725,194	26,31	141,8	22,61
								Collapse	Lower right wedge	0	591,184	1596,196	23,67	112,33	18,47
35768,8 - 35774,2	Gneiss with pegmatitic intercalations and schist	34	181/26 F	285/63 F	339/28 S	56/65		Collapse	Upper right wedge	0	1236,274	3337,941	15	108,57	38,52

Chainage	Geological formations	Distance of the roof from the surface (m)	J1	J2	J3	J4	J5	Type of failure	Position of the wedge	F.S.	Volume (m ³)	Weight (tns)	z-length (m)	Appar-ent face (m ²)	Height (m)
35792,5 - 35802,9	Gneiss and marble	22	161/77	204/65	247/31	5/30 S		Collapse	Upper left wedge	0	1596,816	4311,403	31,37	212,72	26,18
35908,4 - 35934,626	Marble	85	155/64	204/62 F	258/19 S	35908,4 - 35934,626		Collapse	Roof wedge	0	109,254	294,986	26,56	69,1	5,41
35934,626 - 35948,349	Gneiss, marble, pegmatite, quartzite	105	55/62	198/72	250/70	283/12 S		Collapse	Upper left wedge	0	1539,353	4156,252	59,53	422,28	14,27
35948,349 - 35955,63	Marble	105	100/68	66/56	288/8 S			Collapse	Upper right wedge	0	1449,127	3912,462	17,44	118,23	41,21
36144,19 - 36188,494	Marble	158	224/60	140/68	33/68	348/13 F		Collapse	Upper right wedge	0	786,449	2123,411	49,36	269,86	9,69
36215,595 - 36240,379	Gneiss	170	233/66	332/68	43/78	310/11 S		Collapse	Roof wedge	0	243,995	658,786	40,22	91,62	9,02
36350,746 - 36425,28	Gneiss	130	227/78	137/52 S	238/39	19/27 S		Collapse	Upper right wedge	0	4390,322	11853,87	34,02	262,22	57,48
36481,783 - 36529,937	Chloritic schist and gneiss	99	221/72	26/74	137/16 S	147/60		Collapse	Roof wedge	0	370,929	1001,508	71,82	178,32	7,11
36359,4 - 36717,5	Gneiss and chloritic schist	32	246/74	155/20 S	149/74	28/75		Collapse	Roof wedge	0	704,133	1901,158	41,42	214,13	11,69
36717,5-36740,9	Gneiss and granite	26	135/37	220/63	49/75	267/6 S		Collapse	Upper left wedge	0	280,457	757,235	15,51	86,46	11,72
36749 - 36763,1	Granite and kaolinite	20	48/16 S	117/70 F	210/19	26/84		Collapse	Lower right wedge	0	435,204	1175,05	32,9	129,55	12,59
36765,73 - 36766,7	Gneiss	15	45/84	348/38 S	108/46 S	158/60 F		Collapse	Upper left wedge	0	467,882	1263,282	105,6	295,25	4,95
36777,5 - 36781,9	Gneiss and marble	8	188/70 F	287/63	35/63	120/70 F		Collapse	Roof wedge	0	362,944	980,039	38,51	207,03	6,21
36+781,9 - 36789	Gneiss	7	36/83	81/89	153/68 S	171/36		Collapse	Roof wedge	0	451,866	1220,39	14,83	57,62	26,9
								Collapse	Roof wedge	0	506,556	1367,7	20,86	124,35	13,8
								Collapse	Upper right wedge	0	659,163	1779,739	8,3	31,97	67,29
								Collapse		0	1057,986	2856,561	21,09	182,01	28,21

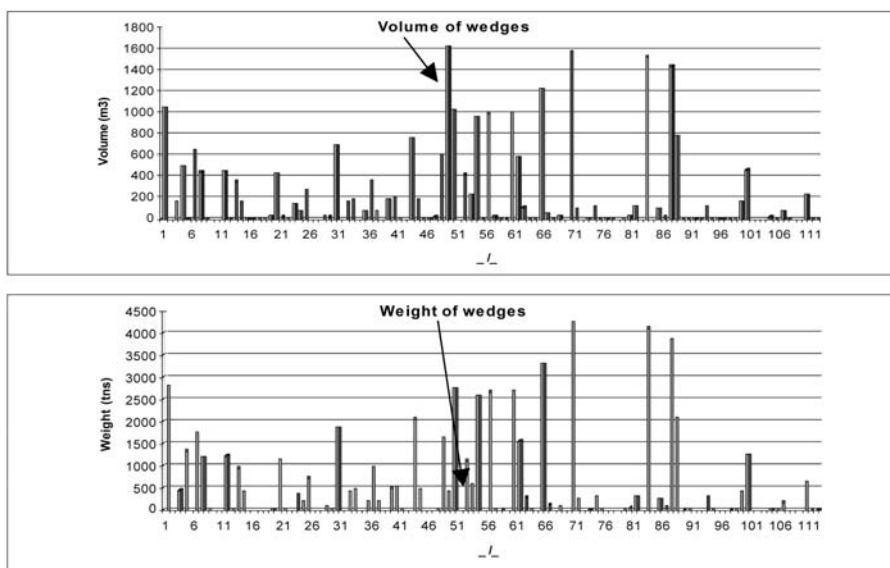


Fig. 2: Comparison between volume and weight of wedges. The arrow shows the position of wedge with volume of 1646,741m³, and weight of 446,2 tns.

3. Excavation methods

The rock mass along the tunnel differs from one place to another. Hard gneiss rock fair qualified of marble of granite was alternated with fractured and deformed rock mass of gneiss and marble. Furthermore, the presence of chloritic schist and the shear zone, minimize the safety of the excavation using the simple mechanical means. So, in order to excavate the tunnel safety, we ought to apply different excavated methods, taking into account rock mass behaviour (Marinos et al, 2005).

Near the outlets and where the rock mass was very poor, the tunnel was excavated mechanically, using the NATM method of excavation. The use of explosive measures was preferred on poor and fair quality of hard rock mass. The excavation of chloritic schist and the shear zone was very dangerous. Although the chloritic schist was very hard and it was very difficult to be excavated with mechanical means, it was deformed very quickly, when it was in conduct with the atmosphere. So, before the removal of excavation material to be completed, pieces of chloritic schist were felled down. The SCL method of excavation was preferred on that case in order to support small parts of the face before the excavation be completed. Furthermore, light explosion used in order to crack the hard rock mass helping the excavation. The sudden change of rock mass quality created the necessity of fore polling.

4. Tunnel stability

The sliding along a plane, the décollement from the roof and the fall of wedges (Chatziangelou et al, 2001) were the common failure causes. Sliding took place along a tectonic surface from the walls of the tunnel. On the other hand, the décollement of a plate is due to its smooth surface in addition with the influence of gravity (Table 1).

One hundred and eleven wedges were measured along the tunnel (Table 2). All the wedges were to be collapsed, so the calculated safety factor, before the application of support was zero. From ch.36+139,41 to ch.36+176,222 a wedge with volume of 19244,17 m³ had been observed on the

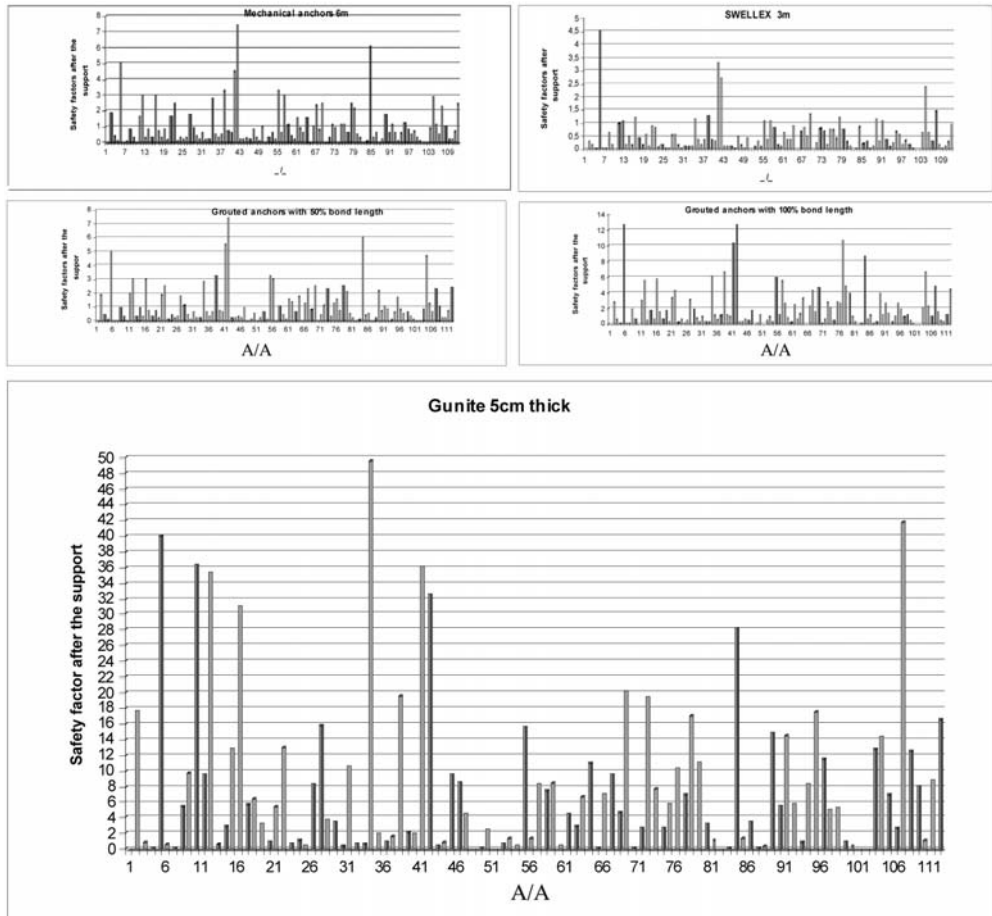


Fig. 3: Safety factors of the wedges after the support of different measures.

upper right part of the tunnel. The failure of that wedge could cause the collapse or all the overlying formations up to the surface. That wedge didn't take into account on our estimations. Another one big wedge, with volume of 4390,22 m³ (from ch.36+215,595 to ch.36+240,379), which was also formed on the upper right part of the tunnel didn't take into account on our estimations.

Usually, there is a relation between the weight and the volume of the wedges. It is common place, the wedges with big volume to be also heavy. But an exception of the above, was observed between ch.35+710 and ch.35+716,5, where there is a wedge with the one of the biggest volumes (1646,741m³), but one of the slightest ones (weighted 446,2 tns) (Fig.2) That is due to the very poor quality of the rock mass, in addition to fracture and deformation. The deformation reduced the apparent weight of the rock mass. Also, the numerous of discontinuities, as they are crossed, they cause empty space at the cross point, so the weight of the wedge does not increase so much as the volume increase.

5. Comparing different support measures

The rock mass quality methods, RMR and GSI, were used for determining the efficacious support measures of the slopes and the tunnels in the area (Christaras et al, 2002). According to the geotechnical

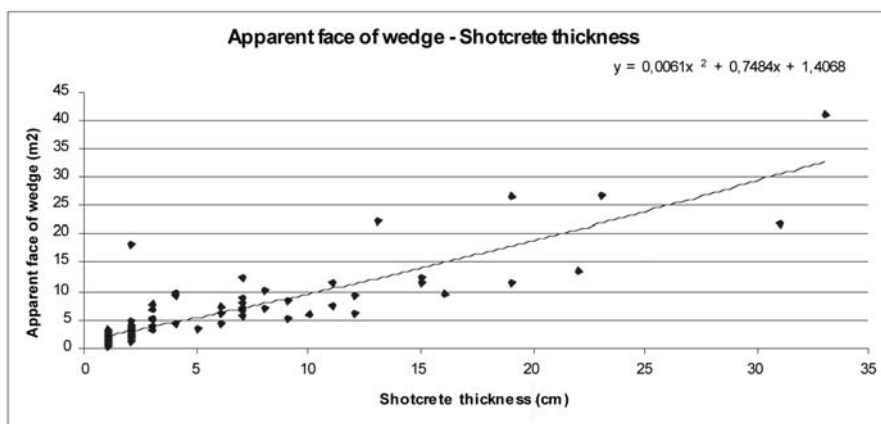


Fig. 4: Relationship between apparent face of wedge and shotcrete thickness.

characteristics of the rock mass, the proposed support measures are completed with different types. The present paper examines the effectiveness of different types of anchors and shotcrete on the rock mass of Symbol Unit. For this purpose, the support of the tunnel was tested using mechanical anchors 6m long, swellex 3m long, grouted anchors 3m long with 50% bond length, grouted anchors 3m long with 100% bond length and shotcrete with thickness of 5cm (Fig.3). Actually, the wedges tested to be supported with one of the above measures, without using combination of them. The required safety factor which was used for the comparisons was 1,5.

Twenty five wedges were observed to be supported with mechanical anchors with length of 6m. Five wedges were supported with swellex bolts. So, the mechanical anchors can support more wedges than the swellex bolts can. Also, there is no difference when the bolts are grouted at 50% of their length and are totally not grouted. The safety becomes bigger when the bolts are totally grouted. Forty seven wedges are supported sufficiently. Also, the grouted anchors with 100% bond length give bigger safety factors than the grouted anchors with 50% bond length. The percent of safety increases two times with the use of grouted anchors with 100% bond length. As far as shotcrete concern, seventy four wedges are supported effectively with shotcrete 5cm thick.

6. Calculation of shotcrete thickness using the apparent face of wedge

As the excavation of tunnels and the application of the support measures are dangerous, the quick calculation of shotcrete thickness during the excavation is useful. Comparing the apparent face of the wedges (the surface which is appeared at the inner surface of the tunnel) with the demanded shotcrete thickness (thinner than 40cm), in order the unstable wedges to be supported, a relationship was resulted (Fig.4);

$$F \text{ (m}^2\text{)} = 0,0061 * [h \text{ (cm)}]^2 + 0,7484 * h \text{ (cm)} + 1,4068 \quad (1)$$

where h = shotcrete thickness (cm)

F = apparent face of the wedge (m²)

The coefficient of the above relationship was calculated 0,877.

The above relationship has the same form with the relationship, which has calculated from the data of Asprovalta tunnels of Egnatia Highway (Chatziangelou, 2008);

$$F \text{ (m}^2\text{)} = 0,3489 * [h \text{ (cm)}]^2 + 16,654 * h \text{ (cm)} + 14,049 \quad (2)$$

Asprovalta tunnels are located at Serbomakedonian mass and the tunnels are passed through gneiss with pegmatitic intercalations, marble and amphibolite. The coefficient of that relationship was calculated 0,082.

7. Conclusions-Results

The tunnel which crosses the Symbol Mountain was excavated dangerously because of the difficult geological status with unexpected failure conditions. The sliding along a plane, the décollement from the roof and the fall of wedges were the common failure causes.

Different methods were used in order to excavate the tunnel safely. The NATM method of excavation was used near the outlets and where the rock mass was very poor. On poor and fair quality of hard rock mass the explosive measures were the most effective. Also, light explosion was used in order to crack the hard rock mass helping the excavation. Chloritic schist formation and the places, where the loose deformed material flowed from the walls and the face, were excavated by the SCL method.

Studying the geometrical characteristics of wedges, we concluded that the weight reduce of the wedges with big volume is due to i) deformation which reduces the apparent weight of the rock mass and ii) the cross of the numerous discontinuities, that they cause empty space at the cross point.

Examining the effectiveness of different types of anchors and shotcrete, we concluded that the mechanical anchors can support more wedges than the swellex bolts can. Also, there is no difference when the bolts are grouted at 50% of their length and are totally not grouted. The safety becomes bigger when the bolts are totally grouted. As far as shotcrete concern, more than 50% of wedges are supported effectively with shotcrete 5cm thick.

Finally, comparing the apparent face of the wedges with the demanded shotcrete thickness (thinner than 40 cm), in order the unsteady wedges be supported, a relationship (1) was resulted. The above relationship has the same form with the relationship (2), which has calculated from the data of Asprovalta tunnels of Egnatia Highway;

Consequently, there is a relation between apparent face of the wedges and the demanded shotcrete thickness being formed;

$$y = a * x^2 + b * x + c \quad (3)$$

8. References

- Bieniawski, Z.T., 1989. Engineering rock mass classifications. New York: Wiley.
- Chatziangelou M., Christaras B., Dimopoulos G., Soulios G., Kiliyas A., 2001. Support of unstable wedges along the Platamon railway tunnel under construction, in northern Greece. *Journ. Eng. Geology, Elsevier*, Amsterdam, Ed.nr.1060.
- Chatziangelou M., 2008. Estimation of failure conditions that appears on poor quality rock mass of Asprovalta tunnels and support measures, P.H.D. Thesis, *Aristotle University of Thessaloniki*.
- Christaras, B., Chatziangelou, M., Malliaroudakis, Em. & Merkos, S., 2002. Support Capacity of wedges and RMR classification along the Asprovalta tunnel of Egnatia Highway, in n. Greece, 9th Congress of the International Association for Engineering Geology and the Environment, *J.L. van Rooy and C.A. Jermey*, ISBN No.0-620-28559-1.
- Hoek, E., 2004. Rockmass classification. Hoek's Corner < www.rockscience.com > (accessed December 2004)
- Marinos, P., Hoek, E., Kazilis, N., Agistalis, G. & Marinos, V., 2005. The tunnels of Egnatia highway, Greece. Design and construction in a variety of rock masses under difficult geological conditions. Geology and linear in fractures. *Proceedings of Int. Symposium*, Lion, 2005.

PRELIMINARY RESULTS REGARDING THE ROCK FALLS OF DECEMBER 17, 2009 AT TEMPI, GREECE

Christaras B.¹, Papathanassiou G.¹, Vouvalidis K.², Pavlides S.¹

¹ Aristotle University of Thessaloniki, Department of Geology, 54124 Thessaloniki, Greece,
christar@geo.auth.gr, gpapatha@auth.gr, pavlides@geo.auth.gr

² Aristotle University of Thessaloniki, Department of Physical and Environmental Geography, 54124
Thessaloniki, Greece, vouval@geo.auth.gr

Abstract

On December 17, 2009, a large size rock fall generated at the area of Tempi, Central Greece causing one casualty. In particular, a large block was detached from a high of 70 meters and started to roll downslope and gradually became a rock slide. About 120 tones of rock material moved downward to the road resulting to the close of the national road. Few days after the slope failure, a field survey organized by the Department of Geology, AUTH took place in order to evaluate the rock fall hazard in the area and to define the triggering causal factors. As an outcome, we concluded that the heavily broken rock mass and the heavy rain-falls, of the previous days, contribute significantly to the generation of the slope failure. The rocky slope was limited stable and the high joint water pressure caused the failure of the slope.

Key words: rock fall, Tempi, engineering geology, hazard, Greece

1. Introduction

A rock fall is a fragment of rock detached by sliding, toppling or falling that falls along a vertical or sub-vertical cliff, proceeds down slope by bouncing and flying along ballistic trajectories or by rolling on talus or debris slopes (Varnes, 1978). Very occasionally, rock fall initiates catastrophic debris streams, which are even more dangerous (Hsu, 1975). Rock falls range from small cobbles to large boulders hundreds of cubic meters in size and travel at speeds ranging from few to tens of meters per second (Guzzetti et al., 2002). Minor rock falls affect most of the rock slopes, whereas large size ones such as cliff falls and rock avalanches, affect only great rock slopes with geological conditions favourable to instability (Rouiller et al., 1998).

After the rock has been detached it descends the slope in different modes of motion mainly depending the mean slope gradient. The three most important modes of motion (Fig.1) are freefall through the air, bouncing on the slope surface and rolling over the slope surface (Dorren, 2003).

The detachment of rock from bedrock slope is triggered by several factors such as weathering, earthquake and human activities while the fall of a rock is determined by factors like the slope morphology and the direct surrounding of the potential falling rock (Dorren, 2003). The generation of rock fall is a rapid phenomenon and represents a continuous hazard in mountain areas worldwide. There are numerous examples of infrastructure destroyed or people killed by rock fall. To protect endangered residential areas and infrastructure, it is necessary to assess the risk posed by rock fall (Dorren, 2003).

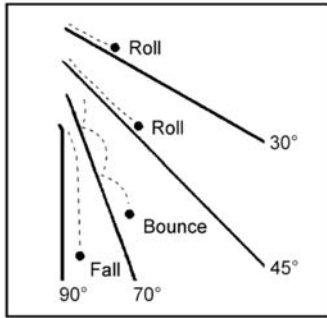


Fig. 1: The three most important modes of motion (from Dorren 2003).

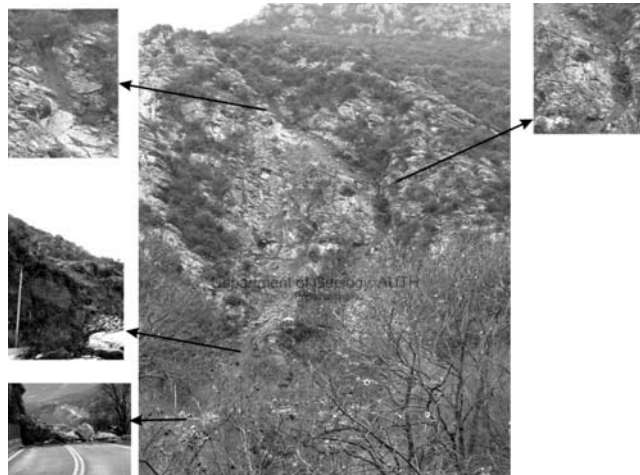


Fig. 2: Source area and path of the of rock falls.

On December 17, 2009 large size slope instability took place at the area of Tempi, central Greece resulting to one casualty and the permanent close of the national road Athens-Thessaloniki. In particular a large block was detached from a high up to 70 meters and moved downward (figure 2). During its fall the initial boulder triggered the detachment of smaller rocks, creating a combination of rock falls and rock slides. As it is shown in figure 3, the fall track of this failure is separated into two paths.

The basic aim of this study is the evaluation of rock fall hazard in the area of Tempi and the definition of the main triggering causal factor of the large size rock fall of December 17, 2009.

2. Geology and geomorphology of the area

The area of study is located in the inner part of Pinios straits (Tempi valley) between the Mounts of Olympus and Ossa. It is located within the Pelagonian zone (Aubuin 1959, Mountrakis 1984) between the geological masses of the Olympus and Ossa Mounts. The structural sequence in the Mt. Olympus region of the Pelagonian zone, from top to bottom, comprises (Schmitt 1983, Schermer 1993): (A) the *ophiolite unit*, consisting of ophiolitic igneous rocks, in coherent thrust sheets and serpentinite-matrix melange, overlain by limestone; (B) the *Infrapierien unit*, gneiss and schist overlain by metasedimentary and metavolcanic rocks and Triassic-Jurassic neritic carbonate rocks; (C) the *Pierien unit*, Paleozoic granitic gneiss overlain by a thin metaclastic sequence and Triassic- Jurassic neritic carbonate rocks; (D) the *Ambelakia unit*, continental margin carbonate and quartzofeldspathic sedimentary rocks, and basic to intermediate volcanic rocks of uncertain age; and (E) the *Olympos unit*, Triassic and Lower Cretaceous to Eocene neritic carbonate rocks overlain by Eocene flysch (Godfriaux 1968, Schmitt 1983). The rock falls area is placed in Ambelakia Unit (Fig. 4).

The study area is located on the steep slopes of the foothills of Ossa Mt. shaped by the erosional processes of the Pinios River. These erosional processes formed the steep-walled inner gorge of the Tempi valley. The gradual changes of the base level in combination with the tectonic uplift of the area (Gonnoi Horst) are the main causes for the lowering of the river's profile and the creation of several pairs of degradational terraces (Psilovikos, 1991). Between these terraces



Fig. 3: Fall track of the boulders (red circles indicate the source area and green lines show the path).

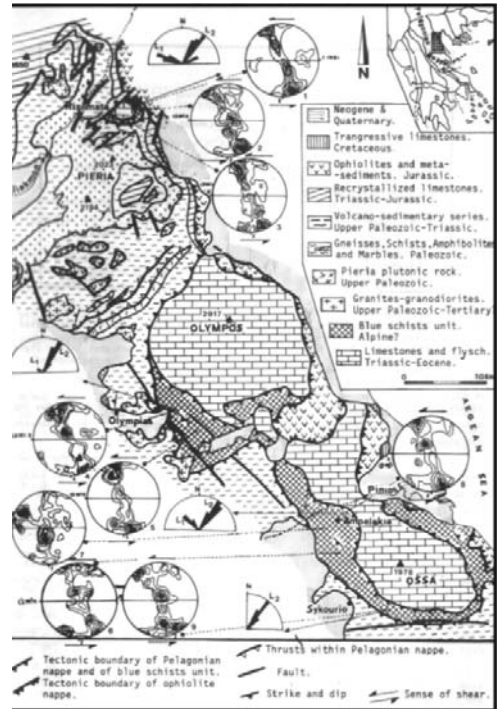


Fig. 4: Geological map of the Olympos Ossa window (from Kiliias et al., 1991). The rock falls area is located in Ambelakia – Ossa unit.

steep walls were formed by the action of running water. Finally, the landscape of the valley is shaped by the intense karstification of the carbonated rocks of the slopes due to the elevated water table and the dissolution – erosion caused by the surficial and underground water runoff.

3. Seismotectonic settings of the area

During the second half of the 20th century, Thessaly and the broader area of northern Greece experienced a series of strong earthquakes (M_s 6.3 to 6.9), which caused damage to a large number of localities and to all its major towns. It is therefore characterized an area of moderate-to-high seismicity. In fact, low-to-moderate seismic activity was also observed in the 19th century and there are a few sources reporting earthquakes in the area even in the previous centuries (Ambraseys & Jackson, 1990).

The last moderate size earthquake occurred on June 9, 2003 ($M_S=5.5$; NOA), when Northern Thessaly (central Greece) was shaken and dozens of buildings in the area of southern (or lower) Mt Olympus and western Tempi were shocked. The macro-seismic intensity was assessed at 6/7EMS-98. The magnitude of the earthquake using the Quick RCMT solution was computed at $M_W=5.2$ (NOA). Spectral analysis of the mainshock records provided a moment magnitude of $M_W=5.3$. The epicentre was originally located SW of Mt Olympus and NE of the city Larisa, between the villages Gonnoi and Karya, both of which suffered considerable damage. The focal mechanism solution of the main shock was obtained from P-waves first motion polarities (Pavlidis

et al., 2004). The two nodal planes gave strike, dip and rake values of $299^{\circ}/44^{\circ}/-67^{\circ}$ for NP1 and $90^{\circ}/50^{\circ}/-110^{\circ}$ for NP2, respectively. The spatial distribution of the aftershocks showed a WNW-ESE orientation of the fault plane, in agreement with the focal mechanism of the main-shock. The first survey aimed at the identification of the seismogenic zone and correlation of geological evidence with damage distribution. Geological and tectonic information of the region point out the occurrence of a major active fault (Omolio Fault, eastern Tempi), as well as the Kallipefki segment and the Gonnoi smaller structures, all directed WNW-ESE. These dip-slip normal faults show evidence of Late Quaternary activity. The WNW-ESE trending structures dominate the area. Accordingly, from the two nodal planes of the focal mechanism, NP1 is likely the seismogenic plane, therefore confirming the N-S regional direction of crustal extension.

The area is dominated by normal faults, which began forming during the Middle Pleistocene, as a consequence of the N-S extension, which affected the whole Aegean region (Caputo & Pavlides 1993). Geological and tectonic information of the broader study area (Caputo & Pavlides 1993), point out the occurrence of many small to moderate length faults and a major active fault (or series of faults) affecting this region of Thessaly, the so-called “Omolio Fault” (Caputo, 1990) and the ESE-WNW ($\sim 100\text{-}110^{\circ}$) Tempi valley normal faults. The Omolio tectonic structure is a WNW-ESE trending northward-dipping dip-slip normal fault showing evidences of Late Quaternary activity.

Regarding the relation between seismotectonic parameters within an area and the occurrence of slope instabilities, Keefer (1984) stated that the most susceptible to initiation under seismic conditions landslides are rock falls and rock slides. The characteristics of the rock falls, described by Keefer (1984), are movement of bounding, rolling or free fall of high velocity with shallow depth (less than 3m). In particular, he concluded that earthquakes with $M < 6.5$ triggered proportionally more these type of failures and proportionally fewer landslides of all other types. Furthermore, the lower magnitude that could be defined as a threshold of earthquake-induced rock falls is equal to $M=4$.

Therefore, historical seismicity information of the area was collected regarding the instrumental period in order to examine the occurrence of earthquakes capable to generate rockfalls within the area of Tempi. As it can be seen on Table 1, many events of magnitude $M > 4$ occurred in the vicinity of study area (fig. 5), thus the parameter of active tectonic should be taken into account during the construction of remedial measures.

4. Engineering geological investigation

Three main tectonic systems are found in the area, given in Table 2. In the area where the failure was generated most unstable conditions of rock slopes are related to planar weaknesses. Wedge failures most likely where line of intersection of two fracture planes dips $< \phi$ and daylights in slope. The studied failure started by the sliding of a big block along the joint 350/47 (Fig. 6) which activated and drifted smaller geomaterials, down slope, toward the road (Fig. 7). The bedding of the crystalline limestone is $110/10$ (Fig. 8). The related stability analysis of the slope is given in Fig. 9.

According to Fig. 9, joint 350/47, corresponded to the field observed sliding surface, is limited included in the sliding area of stability analysis diagram, confirming the limited stability of the slope. This block was retaining in situ, for long time, as joint surfaces are not, usually, totally open, but some small retaining “bridges”, remain inside the rock-mass and keep the stone parts together. Another joint, with data: 15/48, also gives limited safety conditions, even for dry con-

Table 1. Parameters of the earthquakes that occurred in the area after 1941

Year	Mm/dd	Lat	long	Depth (km)	Magnitude (M)
1941	0301	39.670	22.540	00.0	6.3
1941	0301	39.600	22.500	00.0	5.1
1941	0301	39.600	22.500	00.0	4.9
1964	0921	39.650	22.680	33.0	4.8
1981	1229	40.050	22.660	04.0	4.0
1990	0313	40.000	22.490	08.0	4.5
1990	1115	39.880	22.510	05.0	4.3
1993	1003	39.920	22.440	07.0	4.0
1997	0725	39.960	22.540	09.0	4.1
2003	0609	39.940	22.420	16.0	5.1

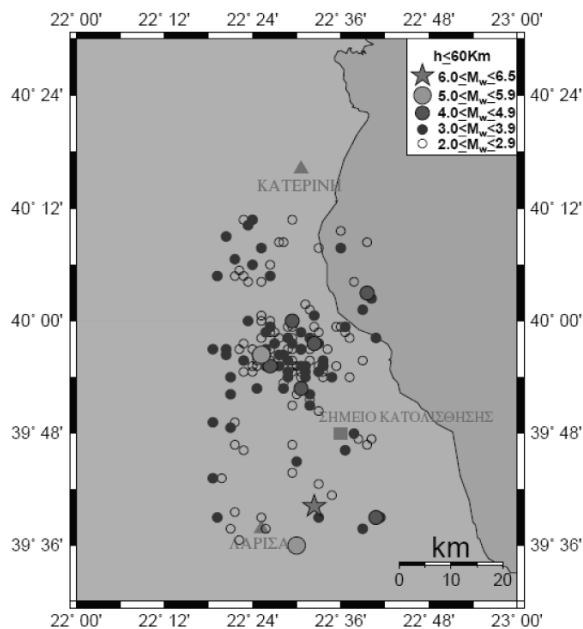


Fig. 5: Map showing the distribution of earthquake epicenters.

dition, found on the boundary line of the sliding area. Furthermore, another joint, with data: 202/83, is found, on the boundary line of the toppling area of the diagram of Fig. 9. The above data give the impression of a slope with limited general stability, which could decrease in heavy rain conditions, as happened in the studied case.

In Table 3, daily rainfall data, from Meteorological Stations found at both sides of Tempi area (Volos, Larissa, Makrinitza, Zagora, and Dion), are given for the former period of that event. According to these data, on Dec 10, 09 and Dec 12, 09, heavy rainfalls occurred at both sides



Fig. 6: The initiation of the slope failure originated as sliding along the joint 350/47.



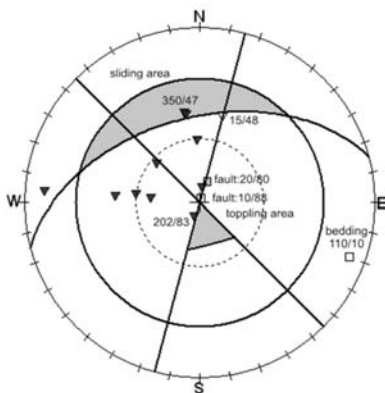
Fig. 7: Boulders on the road.



Fig. 8: Bedding 110/10 and fault 20/80.

Table 2. Bedding and tectonic systems of the limestone, at the southeastern slope of Tempi ravine, at the site of the failure.

Bedding	110°/10°
Joint system 1	350°/47°
Joint system 2	277°/60°
Joint system 3	20°/80°
Road direction	70°-80° (mean: 75°)
South eastern slope (mean)	345°/50°



Tempi discontinuities at the slope of failure			
Discontinuity	Structure	Dip direction	Dip
1	large joint	350	47
2	large joint	277	60
3	fault	20	80
4	large joint	351	48
5	fault	10	88
6	bedding	110	10
7	large joint	357	61
8	large joint	8	83
9	large joint	15	48
10	large joint	311	63
11	large joint	274	12
12	large joint	275	67
13	large joint	202	83
14	large joint	274	50

Fig. 9: Stereographic projection of the planes mapped on the rock slope in order to estimate the sliding potential.

Table 3. Daily rainfalls in the studied area.

	Larissa	Volos	Makrinitza	Zagora	Dion (Pieria)
Date	EMY	Nat.Observatory	Amateurish	Amateurish	Nat.Observatory
1/12/2009	0,0	0,2	0,0	0,0	0,0
2/12/2009	5,0	4,4	6,6	14,5	24,8
3/12/2009	10,0	8,2	16,6	25,3	16,2
4/12/2009	0,0	0,0	0,0	0,0	0,0
5/12/2009	3,0	17,2	47,2	66,3	8,6
6/12/2009	0,1	2,2	8,4	15,6	0,0
7/12/2009	0,0	0,0	0,0	0,0	0,0
8/12/2009	0,0	0,0	0,0	0,0	0,0
9/12/2009	2,0	3,8	5,4	6,5	24,8
10/12/2009	27,0	126,4	417,2	208,3	70,2
11/12/2009	1,0	8,6	45,4	52,7	0,4
12/12/2009	11,0	8,0	23,6	100,8	22,0
13/12/2009	2,0	0,2	2,0	4,4	0,4
14/12/2009	0,0	0,0	0,0	0,3	3,0
15/12/2009	7,0	10,0	10,0	12,6	10,2
16/12/2009	0,0	0,4	0,0	0,0	0,2
17/12/2009	0,0	0,2	0,2	0,5	0,2
18/12/2009	7,0	5,2	4,4	20,1	3,2
19/12/2009	1,0	0,2	0,0	0,9	1,0
Total	76,1	195,2	587,0	528,7	185,2
Mean	50,8	47,1	29,35	26,44	9,26

of the studied slope failure. Groundwater is the most important single factor in triggering landslide events. High rainfalls cause numerous shallow slides where high water pressure can rapidly reach slip surfaces. The increase of joint water pressure reduces significantly rock mass strength, by increasing the driving forces along the joints. Joint water becomes more active in cases where the rock mass is highly broken, as result of the combination of the tectonic systems which firstly contribute to the loosening of the rock mass but also contributes to higher joint water pressure which increases the driving forces and decreases the slope stability.

5. Conclusions-Results

Based on the above analysis, the following conclusions are derived:

- Three joint sets were determined, which are presented in Table 2. These joint sets limit the created rock blocs and involve in their sliding.
- The heavily broken rock mass and the heavy rain-falls, of the previous days, contribute significantly to the generation of the slope failure. The rocky slope was limited stable and the high joint water pressure caused the failure of the slope.
- According to our stability analysis, the failure activated by the sliding of the rock block along the joint: 350/47. Also other joints with relative data could also be activated, under favorable conditions.
- According to the above results, we propose the engineering site investigation of the area for better knowledge of sliding conditions.

6. References

- Ambraseys N.N. & Jackson J.A. (1990): Seismicity and associated strain of central Greece between 1890 and 1988, *Geophys. J. Int.*, 101, 663-708.
- Aubouin, J. 1959. Contribution a l'etude geologique de la Grece septentrionale: les confins de l'Epire et de la Thessalia. *Annls geol. Pays Hell.* 10, 1-483.
- Caputo R. 1990. Geological and structural study of the recent and active brittle deformation of the Neogene-Quaternary basins of Thessaly (Greece), *Scientific Annals*, 12, Aris-totle University of Thessaloniki, 2 vol., 5 encl., 252 p., Thessaloniki.
- Caputo R., Pavlides S. 1993. Late Cainozoic geodynamic evolution of Thessaly and surroundings (central-northern Greece), *Tectonophys.*, 223, 339-362.
- Dorren L., 2003. A review of rockfall mechanics and modelling approaches, *Progress in Physical Geography*, 27, 69-87
- Godfriaux, I. 1968. Etude geologique de la region de l'Olympe (Grece). *Annls geol. Pays Hell.* 19, 1-271.
- Guzzetti F., Crosta G., Detti R., Agliardi F., 2002. STONE: a computer program for the three-dimensional simulation of rock-falls. *Computers and Geosciences*, 28, 1079-1093
- Hsu K.J., 1975. Catastrophic debris streams generated by rockfalls, *Geological Society of America*, 86, 129-140
- Keefer, D.K. 1984, Landslides caused by earthquake, *Bull Geol Soc of Amer* **95**, 406-421
- Kilias, A., Frisch, W., Ratschbacher, L., Sfeikos, A. 1991. Structural evolution and metamorphism of blueschist, Ambelakia nappe, eastern Thessaly, Greece, *Bul Geol Soc of Greece*, 25, 1, 81-99
- Mountrakis, D., 1984. *Geology of Greece*. University Studio Press, Thessaloniki.
- Pavlides S.I, Kouskouna V.2, Ganas A.3, Caputo R.4, Karastathis V.3 & Sokos E. 2004. The Gonnoi (NE Thessaly - Greece) earthquake (June 2003, Ms=5.5) and the neotectonic regime of Lower Olympus, 5th International Symposium on Eastern Mediterranean Geology Thessaloniki, Greece, 14-20 April 2004
- Psilovikos, A., 1991. The evolution of Pinios River in Thessaly. *Proceedings of the 2nd Symposium of Trikala area studies*.
- Rouiller J.D., Jaboyedoff M., Marro Ch., Philipposian F., Mamin M., 1998. Pentes instables dans le Pennique valaisan. *Rapport final du programme national de Recherche PNR 31/CREALP*, 98,

239p

- Schmitt, A. 1983. Nouvelles contributions a l'etude geologique des Pieria, de l'Olympe, et de l'Ossa (Grece du Nord). Unpublished these d'etat, Faculte Polytechnique de Mons.
- Varnes D.J., 1978. Slope movements types and processes. In: Landslide analysis and control, Schuster R.L. and Krizek R.J. (eds), Transportation Research Board, Special Report, Washington, DC, 176, 11-33

EVALUATING THE TRIGGERING FACTORS OF THE ROCK FALLS OF 16TH AND 21ST DECEMBER 2009 IN NEA FOKEA, CHALKIDIKI, NORTHERN GREECE

Christaras B.¹, Syrides G.¹, Papathanassiou G.¹, Chatzipetros A.¹,
Mavromatis T. ¹. Pavlides Sp.¹

¹ Aristotle University of Thessaloniki, Department of Geology, 54124 Thessaloniki, Greece,
christar@auth.gr, syrides@auth.gr, gpapatha@auth.gr, ac@auth.gr, pavlides@geo.auth.gr

Abstract

This paper aims to present the characteristics of the rock falls generated on the 16th and 21st of December 2009 at the Nea Moudania – Kassandria country road in Kassandria Peninsula, Chalkidiki, Greece. Both of those events induced damages to the asphalt road and forced the local authorities to close the road to traffic until the construction of protective measures. In order to evaluate the rock fall hazard and analyze the slope instability in the area, the present study focuses on three main triggering factors: rainfall, stratigraphy and tectonic setting.

Key words: rock fall, stratigraphy, rainfall, Chalkidiki, Greece

1. Introduction

The detachment of rock from bedrock slope is triggered by several factors such as weathering, earthquake and human activities while the fall of a rock is determined by factors like the slope morphology and the direct surrounding of the potential falling rock (Dorren, 2003).

In the study area, several rock-falls occurred and some small creeps appeared, according to historical reports, on the asphalt pavement; they were usually rapidly repaired and the road opened for traffic in a short time. The event of 16th of December 2009 occurred during a heavy rainfall, at approximately 21:30, while few days later, on Monday 21st, a second larger rock fall close to the previous one caused the permanent closure of Nea Moudania – Kassandria road.

A few hours after the second event a field survey took place, in order to report and evaluate the rock fall hazard in the area. In this paper the triggering factors of the rock falls are analyzed and the outcome of this research is presented.

2. Geomorphological setting

Kassandria is the westernmost peninsula of Chalkidiki (fig. 1), forming an elongated strip of land. A smooth landscape consisting of very wide dry valleys and low (mean altitude 30-60 m asl) hilly terrain dominates the northern part, between Potidaea and Kassandria villages. On the contrary, the southern part of the peninsula reveals a higher (up to 333 m asl) hilly terrain, highly affected by erosion. From a tectonic point of view Kassandria peninsula can be considered as a horst (Marinos et al., 1970; Psilovikos et al., 1988; Syrides 1990).

The northern part of Kassandria reveals characteristics inherited from an older mature relief that was probably affected by a younger tectonic phase (Psilovikos et al., 1988; Syrides 1990). Criteria for

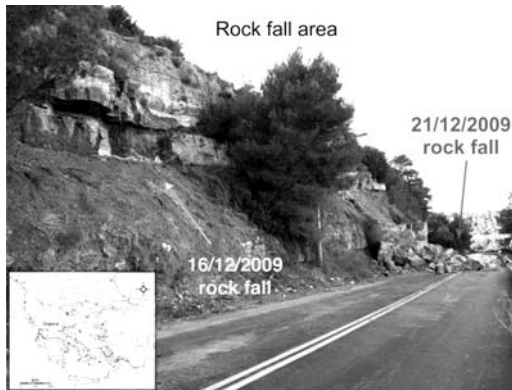


Fig. 1: Rock falling phenomena along the Nea Moudania – Kassandria road on 16th and 21st December, 2009.

identifying the tectonic effect on the relief are:

- Very steep linear coasts bordering a raised block of land with flat mature relief.
- Formation of coastal terraces in soft sediments.
- Cutoff of the mature valleys along the coast line and formation of “hanging valleys”.
- A new erosional cycle with formation of younger valleys starting from the coast.
- It is remarkable also that in northern Kassandra these mature valleys, trending from NE towards SW are also cut off along the eastern coast; as a result the watershed practically coincides with the eastern coast.

The present coastal morphology results also from the subsequent coastal processes of erosion-deposition, as well as the intensive human intervention becoming enduringly active during at least the past 3 decades (Psilovikos et al., 1988).

3. Geological setting

Kassandra peninsula is almost entirely covered by Neogene – Quaternary sediments. Only in the southern part older rocks appear (Mesozoic limestones, ophiolites & Paleogene sandstones), forming the pre-Neogene basement.

According to Syrides (1990) Kassandra peninsula is situated along the eastern side of the extensive Axios – Thermaikos basin that was formed during early Miocene and gradually filled up by mainly clastic Neogene and Quaternary sediments. Total thickness of these sediments exceeds 5 km in the centre of the basin, gradually diminishing towards the margins. In the area of western Chalkidiki and Kassandra peninsula these sediments are classified into six (6) sedimentary formations:

1. Antonios Fm (?Lower - Middle up to Upper Miocene). Fluviolacustrine sediments, alternating lenses of loose Sands, cobbles and gravel.
2. Triglia Fm (Upper Miocene, Vallesian – Early Turolian). Continental sediments, Red beds.
3. Trilophos Fm (Uppermost Miocene, “Pontian”, Turolian). Well stratified beds of fossiliferous sands, sandstones, clays, limestones, containing a brackish mollusc fauna of Paratethyan origin.
4. Gonia Fm (Pliocene, Ruscinian). Fluviolacustrine sediments consisting of lenses and beds of sand, clay, sandstone, marl and massive marly limestone.

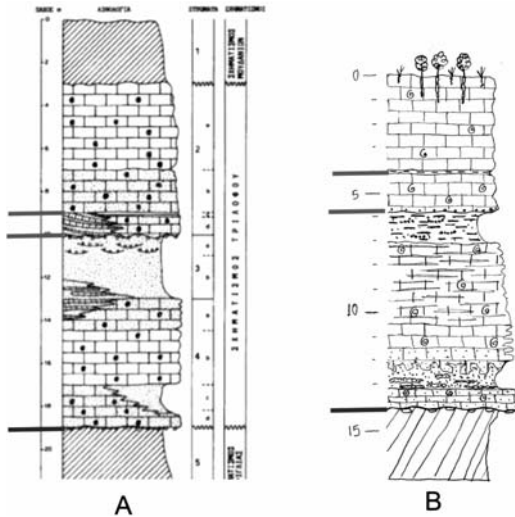


Fig. 2: A) Stratigraphic column of the sediments in Nea Fokea – Athytos area (Syrides 1990) and b) stratigraphic column of the study area.

5. Moudania Fm (Villafranchian and later). Continental sediments, Red beds.

6. Eleochoxia Fm (Pleistocene – Holocene). Tuffaceous limestones and travertines deposited by the action of carstic or thermal springs, with a restricted occurrence south of Katsika mt.

The above sediments dip ~2-3° towards SSE in the area of West Chalkidiki, but in Kassandra the dip direction is generally opposite, towards NNW. In northern Kassandra 4 of the above sedimentary formations appear:

- Moudania Fm covers the area from Nea Potidea up to Kallithea and Kassandria villages.
- Gonias Fm appears only in the west side of the peninsula at Sani area.
- Trilophos Fm appears as a hard fossiliferous limestone along the east coast while at the west coast (Sani) it outcrops as sands, clays and sandstones.
- Triglia Fm is exposed just below the Trilophos Fm which actually covers and protects the softer red beds.

The steep coastal terrace along the east coast, from Nea Potidaea up to Kallithea villages, forms a natural section ~ 15 km long that allows a good view of these sediments. Red beds of both Triglia & Moudania Fms dominate the whole section. The limestone of Trilophos Fm is interbedded between them, allowing the distinction between each other. Due to the slight NNW dipdirection, this limestone firstly appears at sea level in Nea Fokea village but southwards gradually rises up the top of the terrace.

Coastal erosion undercuts the terrace, favouring rock fall of large blocks of limestone; the latter is very characteristic south of Nea Fokea.

A stratigraphic column (Fig 2a) for the sediments exposed in the area of Nea Fokea – Athytos villages is given by Syrides (1990),

1. Red beds of Moudania Fm
2. Fossiliferous limestone consisting of numerous badly preserved shells of Limnocardiids and Dreissenids. 2a is oolitic with sparitic cement, 2b contains sand, 2c is a thin (~20cm) bed of cohesive grey-white clay, 2d contains more sand that increases towards the base and contains also small pebbles and gravel the last well visible embedded at the base of this layer.



Fig. 3: Source area of the rock falls occurred on December 16, 2009.



Fig. 4: Source area of the December 21, 2009 rock falls.

3. Reddish brown sandy loam. 3a is more sandy with thin lenses of gravel, 3b is more fine grained with thin bedding.
4. Fossiliferous sandy limestone contains also numerous badly preserved shells of *Limnocardii*s and *Dreissenids*. 4a reddish-brownish sandy limestone, 4b grey-whitish limestone more sandy at the base, 4c loose sand with sandstone concretions, 4d yellowish-grey to reddish yellow sandy limestone with *Limnocardii*s and *Melanopsidae* with more sand and embedded large cobbles at the base.
5. Red beds of Triglia Fm.

4. Evaluating the triggering factors of the rock falls

On Wednesday 16th and Monday 21st of December 2009, rock falling took place on the Nea Moudania – Kassandria country road, between the 20th and 21st kms. Both of these slope instabilities fortunately caused only structural damages and no casualties.

More specifically, on Wednesday, December 16 at 21:30, two large size boulders of 6-8 m³ detached from a height of 8 m and fell onto the road. This rock fall event forced the local authorities to temporarily close the road for few hours in order to remove the fallen blocks and construct a new protective metal barrier along the steep slope of the road cut.

However, few days later, on Monday morning of December 21st, a larger scale slope failure happened. As shown in figure 4, boulders with volume ranging from 2 to 15m³ fell on the road from a height of 10 meters, causing the permanent closure of the country road. A few hours after the second slope failure, a field survey took place in order to examine the rock falls and evaluate the triggering factors.

The present study focuses on the heavy rainfall activity that took place on 15th and 16th of December, a few hours before the first event, as well as on the rainfall that was recorded during Sunday, 20th of December. Furthermore, the stratigraphy of the site was studied, since a soil layer (sandy loam) is present beneath the source area of rock falls and finally, the structural status of the area and the discontinuities that created the blocks of limestone are analyzed.

5. Rainfall activity

Initially, the monitored precipitation at the Kassandra weather station was examined. The weather

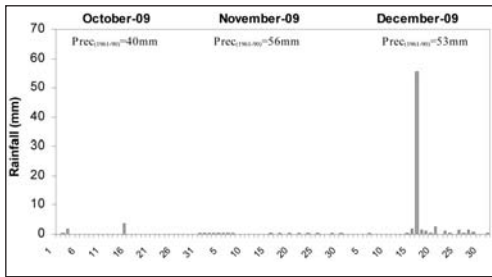


Fig. 5: The daily precipitation in Kassandra from October 1st to December 31st 2009. The normal precipitation values (1961-90) of the weather station in AUTH are also presented.

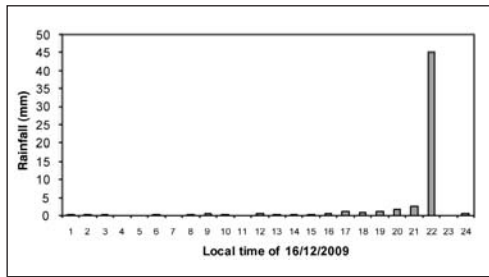


Fig. 6. The hourly precipitation in Kassandra at 16/12/2009.

station of Kassandra (40°03'N, 23° 25'E, altitude = 37 m) was established by the Aristotle University of Thessaloniki (AUTH) only very recently (since 2007), thus the precipitation records of the period under investigation in Kassandra were compared with the normal values of the same parameter for the period 1961-1990 of AUTH (40°37'N, 22°57'E, altitude = 32 m). In particular, the monthly total rainfall in Kassandra in December 2009 was 68 mm (distributed in 15 days) (Fig. 5), 28% more than the normal amount (53 mm) AUTH received for this month during 1961-1990. The relatively wet December followed the severely dry months of October (6 mm vs. the normal value of 40 mm) and November (3 mm vs. the normal value of 56 mm) of 2009. However, from the above mentioned total amount Kassandra received in December, more than 81% (or 56 mm) dropped in one single day (16/12/2009). Although this specific rain episode lasted all day (Fig. 6), more than 80% (45mm) of rain was measured from 21:00 to 22:00 local time.

6. Stratigraphy

The stratigraphy (fig 2b) of the sediments along the rock falls is very similar with that (fig 2a) of Syrides (1990) for the wider area, while differences are observed due to the lateral changes of the various beds.

From a stratigraphic point of view, three “weak horizons” of low strength are defined in this column (fig 2b); a thin layer of grey-whitish cohesive clay (bed 2c) pointed as grey line, a second layer of reddish-brown sandy loam (bed 3) (red line depicts the contact between 2 and c beds) and a third layer defined as the contact (violet line) between the base of the Trilophos Fm limestone and the Triglia Fm red beds.

It is remarkable that within the limestone numerous vertical cracks allow the percolating water to pass downwards, but the intercalation of reddish-brown sandy layer (bed 3) between the limestone beds causes the drying up of the water from the superimposed limestone along this contact. As a result, thick reed vegetation appears along and below the contact. It is also remarkable that this bed of reddish sandy loam prevents water from percolating in the lower strata, resulting to the dryness of contact between the base of the limestone (Trilophos Fm.) and the top of the red beds (Triglia Fm.).

Regarding the influence of stratigraphy to the triggering of rock falls, Kotze (2007) stated that any soil stratum that intercalates between or appears below a thick hard rock bed can be considered as a “weak horizon” that is subject to preferential weathering and erosion with ongoing exposure to the elements. Thus, the overlying more resistant limestone beds become undercut. As undercutting advances, the overlying limestone eventually collapses, due to sudden brittle failures occurring along prevalent rock mass defects that act as release planes.

In our cases, the above conclusion precisely describes one of the triggering factors (stratigraphy) and



Fig. 7. The layer of reddish-brown sandy loam is slowly washed out by the percolating water from the overlying limestone (note the beginning of undercutting). The water favors thick reed vegetation. It is a matter of time this slow process to undercut the limestone causing a rockfall in this place in the future.

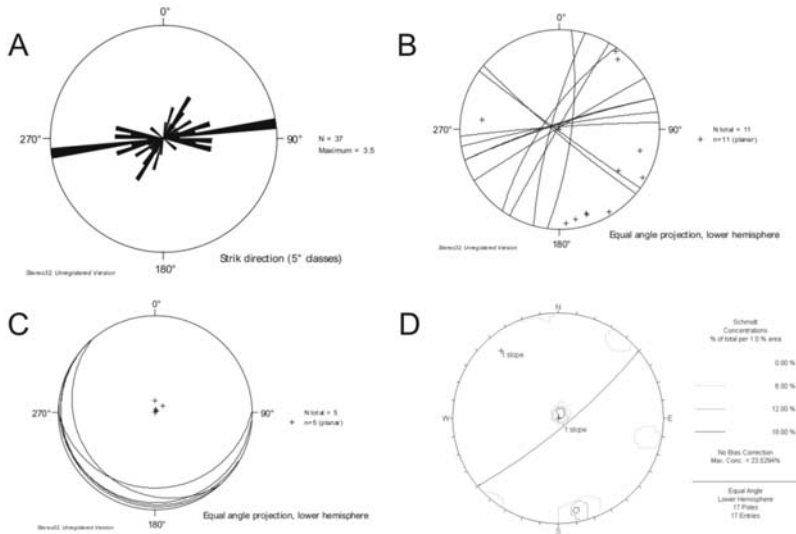


Fig. 8. a) Rose diagram, b) joints stereoplot, c) bedding stereoplot and d) contour plot in the source area of the rock falls. The **bold line** in the contour plot represents the general orientation of the slope.

the unstable conditions that were created these specific two days (16th and 21st of December 2009), thus concluding that in both cases the rock falls were generated by the undercut of the reddish brown sandy loam bed.

7. Structural setting

The main structure of the study area is a WSW – ENE trending normal fault, which causes the displacement of the strata by about 12-15 metres. The amount of displacement is not clear, because of the lack of outcrops. The fault dips towards the NNW and the visible fault zone has a width of about 20 m. The actual fault zone however is much wider, as is indicated by the intense relief just on the north of the site: a transverse valley of the same WSW – ENE trend is formed due to the erosion of

the main fault zone, which is probably located along this valley. The observed normal fault is therefore a synthetic footwall secondary fault, and it is characterized as possibly active since its strike is perpendicular to the extensional axis of the local stress field.

The strata appear to have a gentle dip towards the SSW (fig. 8), while their strike is similar to the road cut direction; dip direction however is opposite to the road cut's one, reducing the possibility of water saturation to the road cut. The dip direction of the strata can be associated to footwall rebound backtilting, which is typical in areas adjacent to a fault zone.

The dominant joint system has a strike of 075° - 080° , parallel to the above mentioned normal fault, while a conjugate secondary system of much less importance trends at about 030° . All joints are of high angle ($>75^{\circ}$) and most of them almost vertical (fig. 8). They are open joints, typically filled with fine-grained material and calcite, while at their uppermost part they sometimes appear eroded and have a heave of up to 3 cm.

The joints appear to affect the pavement of the connecting road to the nearby hotel. A set of cracks is aligned in deformation zones in *en échelon* and overlapping pattern. These zones are parallel to the main fault and they have formed as a result of both the pre-existence of joints, as well as the soil creep towards the road cut (hence their "strike-slip" appearance).

8. Conclusions-Results

On the 16th and 21st December 2009, rock falls occurred at the eastern coastal area of Kassandra peninsula in northern Greece. This study aims to describe the characteristics of the slope failures and evaluate their triggering factors. In particular, we examined the rainfall activity, the stratigraphy and the tectonic regime in the area. According to data from the weather station in Kassandra, more than 81% of rainfall (or 56 mm) of the total amount for December, dropped in one single day (16/12/2009). Moreover, the dense system of discontinuities in combination with the subhorizontal bedding plane, under the effects of weathering, divided the limestone bed into a series of contiguous blocks or slabs. All the fallen blocks of rocks originate from the layers above a layer of reddish sandy loam. The outcome provided by this study is that the rock falling phenomena in Nea Fokea were generated due to the undercut of a specific layer of reddish brown sandy loam bed, as consequence of extremely high precipitation.

9. References

- Dorren L., 2003. A review of rockfall mechanics and modelling approaches, *Progress in Physical Geography*, 27, 69-87
- Kotze G., 2007. An assessment of rockfall frequency for the coastal cliff-lines of Pittwater local government area, Sydney. *Australian Geomechanics* 42, 1, 213-219.
- Marinos G., Sakelariou – Mane E., Sotiriadis L., Sapountzis H., 1970. On the palaeogeography of Northern Aegeis in the area of Chalkidiki. *Ann. Geol. de Pays Hell.* 22, 1-27, Athens (in Greek).
- Mountrakis D., Syrides G., Polymenakos L., Pavlides S., 1993. The neotectonic structure of the eastern margin of Axios – Thermaikos basin in the area of west Chalkidiki (central Macedonia), Greece. *Bull. Geol. Soc. Greece*, v. XXVIII/1, 379-395, Athens (in Greek).
- Psilovikos A., Syrides G. & Chachamidou E. 1988. Coastal Phenomena in Kassandra peninsula, Chalkidiki. *Bull. Geol. Soc. Greece*, v. XX, 325-339, Athens (in Greek).
- Syrides, G., 1990. Lithostratigraphic, Biostratigraphic and Palaeogeographic Study of the Neogene Quaternary Sedimentary Deposits of Chalkidiki Peninsula, Macedonia, Greece. Ph D Thesis. *Scientific Annals School of Geology*. I, 11, 243 p. Thessaloniki (in Greek).

ENGINEERING GEOLOGICAL AND GEOTECHNICAL INVESTIGATION OF LANDSLIDE EVENTS IN WILDFIRE AFFECTED AREAS OF ILIA PREFECTURE, WESTERN GREECE

Depountis N.¹, Lainas S.², Pyrgakis D.², Sabatakakis N.², and Koukis G.²

¹ Region of Western Greece, Directorate of Public Works, 26110 Patras, Greece,
nikosdepountis@hotmail.com

² University of Patras, Department of Geology, Laboratory of Engineering Geology, 26500 Patras, Greece,
splainas@upatras.gr

Abstract

In August 2007 Ilia Prefecture suffered one of the most devastating wildfires that have ever happened on European level. Approximately 870km², mainly forest and agricultural land, were lost, more than 60 people were killed, hundreds were injured and many villages suffered extensive damage. Heavy rainfall and human activities, favoured by the loss of vegetation and the overall susceptibility of geological formations in landsliding, induced the manifestation or re-activation of various scale landslide phenomena. In order to investigate and mitigate the problem University of Patras was commissioned by the Region of Western Greece to undertake an Engineering Geological and Geotechnical investigation. Site investigation accomplished in seven municipalities focusing on several landslide events with serious socio-economic impact and as a result many small scale cases were identified. In each one of these cases large scale engineering geological mapping was conducted and remedial and protection measures were designed.

Key words: Wildfires, Landslides, Geotechnical Investigation, Ilia Prefecture, Western Greece

1. Introduction

Few months after the devastating wildfires of August 2007 that affected Ilia Prefecture the University of Patras was commissioned by the Region of Western Greece to undertake an Engineering Geological and Geotechnical investigation, aiming at the treatment of landslide phenomena particularly in seven municipalities that had suffered extensive damage.

The inquiring project titled “*Engineering Geological and Geotechnical investigation in wildfire affected Municipalities of the Ilia Prefecture for the identification and treatment of landslide phenomena – Design of landslide hazard mitigation measures*” and was supervised by the Department of Transport Works/Directorate of Public Works/Region of Western Greece.

The project was completed in September 2008 and comprised the followings:

- a) Identification of all landslide phenomena and failures that occurred in the seven municipalities of the project: Amaliada, Andritsaina, Iardanos, Skillountos Oleni, Pineia, and Foloji.

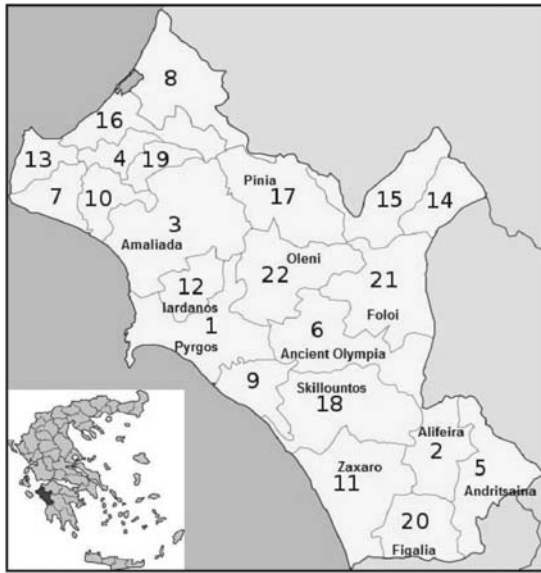


Fig. 1: Investigation area – Municipalities of the Ilia Prefecture.

- b) Evaluation of landslide hazard and selection of the most serious cases for further investigation.
- c) Engineering geological and geotechnical investigation of forty six (46) landslide cases that seriously affected the human environment.
- d) Identification of landslide causes and trigger.
- e) Production of technical reports and geotechnical maps as well as design of landslide hazard mitigation measures.
- f) Submission of proposals for further investigation.

2. Investigation area

The investigation area comprised the Municipalities of Amaliada, Andritsaina, Iardanos, Pinia, Skillountos, Oleni, and Foloï (Fig. 1), occupying a total area of approximately 1115km². The total area of the Ilia Prefecture is 2618km² and the burnt land estimated to be 870km² (approximately 33% of the total area). The most affected Municipalities were those of the project as well as the Municipalities of Zaxaro, Alifeira, Figalia, and Ancient Olympia (Fig. 1). From the burnt land the bigger percentage included forest and agricultural land as well as residential districts. Further investigation is needed in the Municipalities of Zaxaro, Alifeira, Figaleia, and Arxaia Olympia that were not included in the inquiring project.

3. Identification of landslide phenomena in the investigation area

3.1. Landslide types and causes of movement

Zaruba and Mencl (1969, 1976) and Varnes (1978) have developed the most well known landslide classification Tables. Table 1, was adopted for landslide identification and classification during the project, illustrates a schematic landslide classification (Varnes, 1978) taking into account the modifications made by Cruden and Varnes (1996). Some integration has also been made by using the definitions of Hutchinson (1988), Coates (1977), and Hungr et al. (2001).

According to up to today studies in the Ilia Prefecture have been identified (from 1950 until

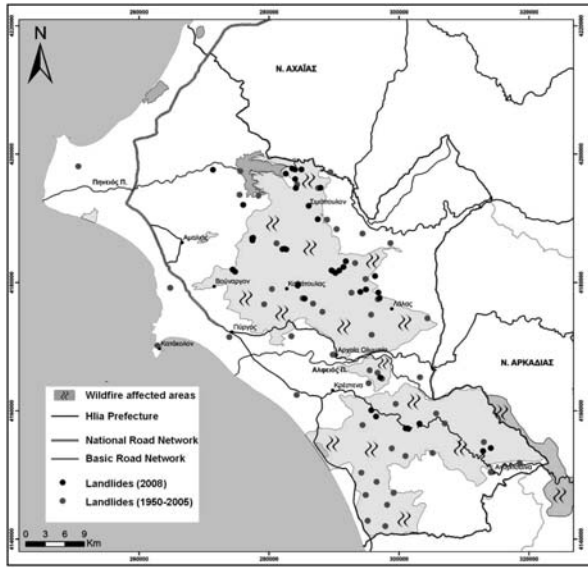


Fig. 2: Landslides identified in the Ilia Prefecture (1950-2005) & (2008).

Table 1.

<i>Type of movement</i>		<i>Type of material</i>			
		<i>Bedroc</i>	<i>Engineering soils</i>		
			<i>Predominantly fineg</i>	<i>Predominantly coarse</i>	
<i>Falls</i>		Rockfall	Earth fall	Debris fall	
<i>Topples</i>		Rock topple	Earth topple	Debris topple	
<i>Slides</i>	<i>Rotationa</i>	Rock slump	Earth slump	Debris slump	
	<i>Transla-tional</i>	<i>Few units</i>	Rock block slide	Earth block slide	Debris block slide
		<i>Many units</i>	Rock slide	Earth slide	Debris slide
<i>Lateral spreads</i>		Rock spread	Earth spread	Debris spread	
<i>Flows</i>		Rock flow	Earth flow	Debris flow	
		Rock avalanche		Debris avalanche	
		(Deep creep)	(Soil creep)		
<i>Complex and compound</i>		Combination in time or space of two or more principal types of movement			

2005) fifty eight (58) landslides (Fig. 2) of intermediate and high vulnerability. Thirty seven (37) of them (percentage 64%) are located in the investigation area, affected by the wildfires of August 2007. Therefore, many of them were expected to be reactivated with bigger intensity, because of the unfavourable conditions that prevailed after the wildfires.

During the current investigation forty six (46) landslide cases (Fig. 2) that seriously affected the human environment, of intermediate and high vulnerability, most of them existed before, were thoroughly investigated and an identification of the main types and causes of movement was made (Table 2) by using the previous landslide classification of Table 1.

Table 2.

<i>No</i>	<i>Location</i>	<i>Main types of movement</i>	<i>Main causes of movement</i>
	<i>Amaliada</i>		
1	Keramidia village	Road embankment failure/ Earth Slump and Flow	Weathering of soils/ Undercutting
2	Peristeri village road entrance	Earth Slump - Soil Creep	Weathering of soils
3	Peristeri village	Road embankment failure/ Earth Slump and Flow	Weathering of soils/ Loading
4	Peristeri Elementary school	Soil Creep	Weathering of soils
5	Provincial road Peristeri-Inoi	Road embankment failure/ Earth Slump and Flow	Weathering of soils/ Undercutting & Loading
6	North of Pinios Lake - Earth dam	Earth Slump	Undercutting & Excavation
	<i>Andritsaina</i>		
7	Miloi village	Rock Falls and Flow	Weathering of jointed rocks
8	Sikies village	Earth Slump	Fluvial erosion
9	Provincial road Andritsaina-Sekoulas	Debris Flow	Fluvial erosion
	<i>Iardanos</i>		
10	Mun. road Vounargo-Fragkopidima	Rock Falls/Earth Slides	Weathering of soft rocks/ Steep slopes & Excavation
11	Provincial road Vroxitsa-Korifi	Earth Flow	Weathering of soils
12	Provincial road Vroxitsa-Korifi	Road embankment failure	Weathering of soils
	<i>Pinia</i>		
13	Latta village	Earth Slump and Flow	Weathering of soils
14	Valmi village	Earth Slump	Weathering of soils
15	Municipal road Valmi-Apidoula	Earth Slides and Falls Debris Slides and Falls	Weathering of soils/ Undercutting
16	Provincial road Valmi-Xenies	Debris Slides and Falls	Weathering of soft rocks/ Steep slopes & Excavation
17	Provincial road Valmi-Agrapidoxori	Earth Falls	Weathering of soils/ Fluvial erosion
18	Agrapidoxori village road entrance	Road embankment failure/ Earth Flow	Weathering of soils/ Undercutting
19	Simopoulo village road entrance	Earth Flow	Undercutting
20	Agnanta village	Earth Slides and Flow	Weathering of soils/ Steep slopes
21	Kotrona hamlet	Soil Creep	Undercutting
22	Mazaraki village	Earth Slides and Flow	Weathering of soils
23	Kalo Paidi village	Earth Slumps and Flow Debris Slides and Flow	Weathering of soils/ Undercutting & Loading

<i>No</i>	<i>Location</i>	<i>Main types of movement</i>	<i>Main causes of movement</i>
	<i>Skillountos</i>		
24	Graika village	Earth and Debris Flow	Weathering of soils
25	Grillos cillage	Soil Creep	Weathering of soils
26	Platiana village	Rock Slides and Falls Earth and Debris Slides	Weathering of jointed rocks/Steep slopes
27	Municipal road Platiana - Archaeological site	Rock Slides and Falls Earth Slumps - Debris Falls	Weathering of jointed rocks/Steep slopes & Excavation
28	Municipal road to Tripiti	Road embankment failure/ Earth Slump and Flow	Weathering of soils/ Undercutting
29	Provincial road Krestena-Graika	Road embankment failure/ Earth Slump	Fluvial erosion/ Undercutting
30	Frixa village	Earth Slumps and Flow Earth Slides	Weathering of soils/ Fluvial erosion & Loading
31	Frixa village road entrance	Road embankment failure/ Earth Slide	Weathering of soils/ Excavation
	<i>Oleni</i>		
32	Rural road Goumero-Askitis	Rock Falls Earth Slides and Flow	Weathering of soft rocks/ Steep slopes & Excavation
33	Municipal road Goumero-Agia Anna (Vrisi)	Road embankment failure/ Earth Slump and Flow	Weathering of soils/ Excavation
34	Municipal road Goumero-Agia Anna (Koukos)	Road embankment failure/ Debris Slump	Weathering of soils/ Excavation
35	Goumero village road entance	Earth Slide	Weathering of soils
36	Agia Anna village	Debris Slide	Weathering of soils
37	Agios Georgios village	Earth Slide	Weathering of soft rocks/ Loading
38	Municipal road Koutsoxera-Mouzaki	Road embankment failure/ Earth Flow	Weathering of soils
39	Koutsoxera church	Earth Slide	Weathering of soft rocks/ Loading
40	Koutsoxera Primary school	Earth Flow - Soil Creep	Weathering of soils/ Loading
41	Provincial road Oleni-Magoula	Earth Slide and Flow	Weathering of soils/ Excavation
	<i>Foloi</i>		
42	Doukas village	Earth Slump and Flow	Weathering of soils
43	Milies village	Earth and Debris Flow	Weathering of soils/ Excavation
44	Provincial road in Avra springs	Rock and Debris Falls	Fluvial erosion/Undercutting
45	Neraida village	Rock Slides & Falls	Weathering of jointed rocks
46	Nea Persaina village	Earth Flow - Soil Creep	Weathering of soils

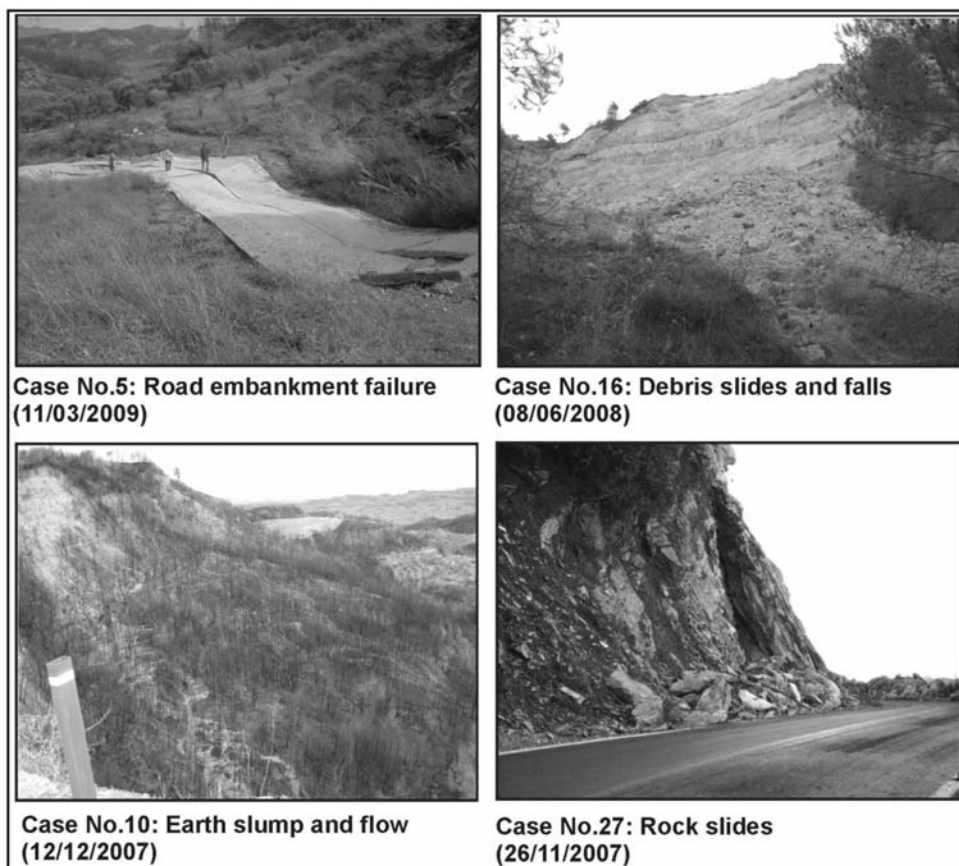


Fig. 3: Landslides identified in the Ilia Prefecture (1950-2005) & (2008).

The primary cause of movement in most of the cases of Table 2 was the loss of vertical vegetative and forestry structure after the wildfires. In shallow and poor soils the removal of deep-rooted vegetation was crucial and destabilized the already fragile slopes and as a result many landslides that existed before reactivated. The main trigger of landslide reactivation was either the intense rainfall or in some cases (7, 15, 16) a combination of rainfall and seismic activity.

Concerning the main causes of movement, according to Table 2, was the intense weathering of soils, soft rocks and hard rocks as well as:

- Excavation created by human activities mainly for the construction of roads and houses.
- Undercutting created either by human activities or physical processes.
- Loading created by human activities or excess pore water pressure after an intense rainfall
- Fluvial erosion created by rivers and streams causing loss of support on the toe of generally steep slopes or along the river/stream banks.

All landslide cases were located with precise coordinates in maps of suitable scale and the forty six (46) of them are presented in Fig. 2 along with those occurred during the period 1950-2005.

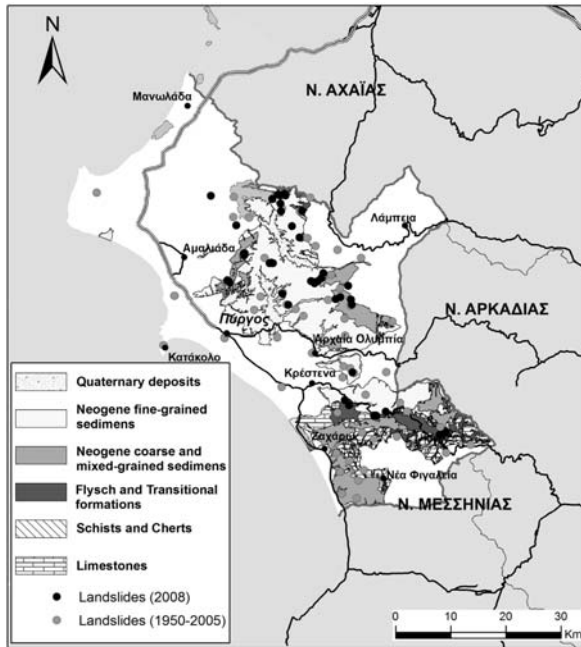


Fig. 4: Engineering Geological conditions and landslides in the Iliia Prefecture.

3.2. Effect of Engineering Geological conditions on landslide movement

The identified 46 landslide cases were occurred mainly with a complex type of movement (falls, slides, and flow) and affected by the prevailed geological formations. Earth flow, slumps, slides, and soil creeps were occurred mainly in the fine Neogenic sediments which dominate in the area. Debris slides and flow were occurred mainly in the coarse Neogenic sediments, whereas rock falls and slides as well as debris falls were activated in limestones and sandstones (Fig. 3).

All these landslides were triggered by heavy rainfall and/or seismic activity favoured by the loss of vegetation after the wildfires and the overall susceptibility of the prevailed geological formations in landsliding (Fig. 4). The geological formations of the Neogenic sediments constituted by weathered soft rocks of sandy-silt constitution, friable sandstones, and poor soils of sandy-silt constitution are prone in earth flow, slumps and slides as well as rock and debris falls and slides. In addition the jointed rocks of the limestone bedrock produce heavy rock falls and slides.

The prevailed engineering geological conditions combined with the loss of vegetation, the deforestation and the intense rainfalls contributed in the deterioration of landslide problem. However, in many cases the horizontal stratigraphy combined with the prevailed low relief produced landslides in such a scale that can be treated with protection measures economically and technically feasible provided that they will be faced in time.

4. Proposed remedial and protection measures

The proposed remedial and protection measures aiming at the treatment of landslide phenomena in the Iliia Prefecture can be summarized in the following paragraphs and Table 3:

a) Surface drainage works with the construction of surface or shallow drains, as well as diversion ditches of rain-storm waters along the road network. Surface drains includes concrete

Table 3.

<i>No</i>	<i>Location</i>	<i>Main types of movement</i>	<i>Main causes of movement</i>
	<i>Amaliada</i>		
1	Keramidia village	Road embankment failure/ Earth Slump and Flow	Drainage works/Gabion wall/ Ground improvement
2	Peristeri village road entrance	Earth Slump - Soil Creep	Surface drainage
3	Peristeri village	Road embankment failure/ Earth Slump and Flow	Drainage works/Driven-pile wall/Ground improvement
4	Peristeri Elementary school	Soil Creep	Surface drainage/Gravity wall
5	Provincial road Peristeri-Inoi	Road embankment failure/ Earth Slump and Flow	Drainage/Gabion wall/ Ground improvement/Un- loading
6	North of Pinios Lake - Earth dam	Earth Slump	Surface drainage/Gabion wall/Driven-pile wall/ Rescaling
	<i>Andritsaina</i>		
7	Miloi village	Rock Falls and Flow	Surface drainage/Rockfall barrier/Rock scaling
8	Sikies village	Earth Slump	Drainage works/Gabion wall
9	Provincial road Andritsaina-Sekoulas	Debris Flow	Surface drainage/Gravity wall
	<i>Iardanos</i>		
10	Mun. road Vounargo-Fragkopidima	Rock Falls/Earth Slides	Surface drainage/Geogrids
11	Provincial road Vroxitsa-Korifi	Earth Flow	Surface drainage/Vegetation
12	Provincial road Vroxitsa-Korifi	Road embankment failure	Drainage works
	<i>Pinia</i>		
13	Latta village	Earth Slump and Flow	Drainage works
14	Valmi village	Earth Slump	Surface drainage
15	Municipal road Valmi-Apidoula	Earth Slides and Falls Debris Slides and Falls	Surface drainage/Gravity walls/Driven-pile wall
16	Provincial road Valmi-Xenies	Debris Slides and Falls	Surface drainage/ Gravity wall/Geogrids
17	Provincial road Valmi-Agrapidoxori	Earth Falls	Surface drainage/Geogrids
18	Agrapidoxori village road entrance	Road embankment failure/ Earth Flow	Surface drainage/ Gabion wall
19	Simopoulo village road entrance	Earth Flow	Surface drainage/Gabion wall
20	Agnanta village	Earth Slides and Flow	Surface drainage/Vegetation
21	Kotrona hamlet	Soil Creep	Surface drainage
22	Mazaraki village	Earth Slides and Flow	Surface drainage
23	Kalo Paidi village	Earth Slumps and Flow Debris Slides and Flow	Drainage works/Gabion walls/Gravity walls/Dri- ven-pile wall

<i>No</i>	<i>Location</i>	<i>Main types of movement</i>	<i>Main causes of movement</i>
	<i>Skilloountos</i>		
24	Graika village	Earth and Debris Flow	Surface drainage
25	Grillos cillage	Soil Creep	Surface drainage
26	Platiana village	Rock Slides and Falls Earth and Debris Slides	Surface drainage/Gabion wall/Rockfall barrier/Rock scaling
27	Municipal road Platiana - Archaeological site	Rock Slides and Falls Earth Slumps - Debris Falls	Surface drainage/Gabion wall Gravity walls/Unloading
28	Municipal road to Tripiti	Road embankment failure/ Earth Slump and Flow	Surface drainage/ Gabion wall
29	Provincial road Krestena-Graika	Road embankment failure/ Earth Slump	Surface drainage/ Gabion wall
30	Frixa village	Earth Slumps and Flow Earth Slides	Moving of population
31	Frixa village road entrance	Road embankment failure/ Earth Slide	Surface drainage/Gabion wall/ Ground improvement
	<i>Oleni</i>		
32	Rural road Goumero-Askitis	Rock Falls Earth Slides and Flow	Surface drainage/Unloading/Rock scaling
33	Municipal road Goumero-Agia Anna (Vrisi)	Road embankment failure/ Earth Slump and Flow	Drainage works/Gabion wall
34	Municipal road Goumero-Agia Anna (Koukos)	Road embankment failure/ Debris Slump	Surface drainage
35	Goumero village road entance	Earth Slide	Surface drainage
36	Agia Anna village	Debris Slide	Rescaling
37	Agios Georgios village	Earth Slide	Surface drainage/Ground improvement
38	Municipal road Koutsoxera-Mouzaki	Road embankment failure/ Earth Flow	Surface drainage/Ground improvement
39	Koutsoxera church	Earth Slide	Gravity wall
40	Koutsoxera Primary school	Earth Flow - Soil Creep	Drainage works/Gabion walls
41	Provincial road Oleni-Magoula	Earth Slide and Flow	Surface drainage/Gabion wall
	<i>Foloi</i>		
42	Doukas village	Earth Slump and Flow	Surface drainage
43	Milies village	Earth and Debris Flow	Surface drainage/Vegetation
44	Provincial road in Avra springs	Rock and Debris Falls	Rock scaling/Gabion wall/ Suspended netting
45	Neraida village	Rock Slides & Falls	Rockfall barrier
46	Nea Persaina village	Earth Flow - Soil Creep	Surface drainage

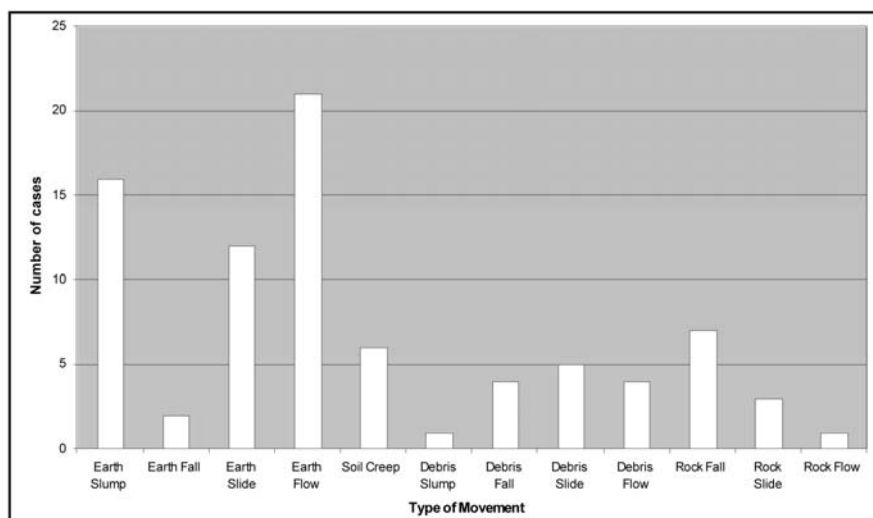


Fig. 5: Main types of landslide movement.

diversion ditches, whereas shallow-interception drains includes perforated tubes covered by granular material in trenches up to 2m deep lined with geotextiles.

b) Subsurface drainage works with the construction of drainage trenches up to 3m deep and 1m wide, as well as drainage blankets up to 1m thick on top of the base of road embankments in order to reduce water infiltration and divert quickly subsurface water away of the problem.

c) Construction of retaining walls, usually concrete gravity walls and gabion walls. Gravity walls were proposed to be constructed on small slopes or small parts of large slopes in cases of solid ground. Gabion walls were proposed in cases of small slopes and road embankments as toe weight. **Driven pile-walls** were proposed to be constructed in cases of deep slide problems.

d) Rockfall barriers were proposed for construction in cases 7, 25, 45, where steep rocky slopes of a great height prone to rock falls and slides were existed, in order to protect residential areas.

e) Ground improvement which includes development of vegetation, geotextiles, geogrids in soil slopes or road embankments that have failed due to poor substratum conditions. Vegetation cover was proposed to reduce water infiltration and provide tensile strength in surface layers. Anchored geotextiles or geogrids were proposed in cases to fix fragile surface slopes and allow plant growth.

f) Slope modification by unloading or rescaling soil slopes and scaling rock slopes.

5. Conclusions

All landslide cases activated or reactivated mainly with a complex type of movement (Fig. 5). Earth flow, slumps, slides, and soil creeps were occurred in the fine Neogenic sediments. Debris slides and flow were occurred in the coarse Neogenic sediments, whereas rock falls and slides as well as debris falls were activated in limestones and sandstones.

All landslides were triggered by heavy rainfall and/or seismic activity. The prevailed engineering geological conditions combined with the loss of vegetation, the deforestation, the in-

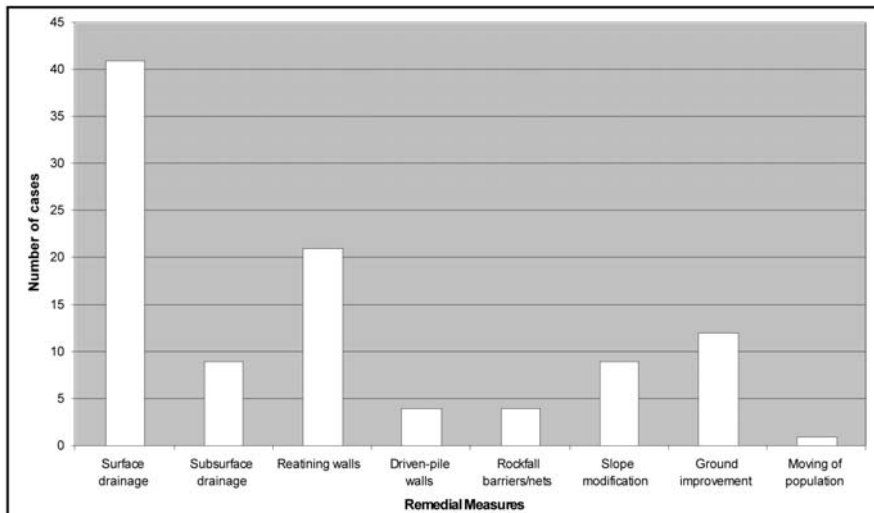


Fig. 6: Remedial and protection measures of landslide cases.

creased weathering and the intense rainfalls contributed in the deterioration of landslide problem. Human activities and fluvial erosion in some cases increased the landslide problem.

All remedial and protection measures proposed for landslide treatment are illustrated in Fig. 6 and mainly include surface and subsurface drainage works combined in many cases with the construction of retaining walls. The other main type of remedial works includes ground improvement and rockfall barriers for the protection of residential areas.

6. Acknowledgments

The work was carried out under the support of the Region of Western Greece. The authors wish to express their sincere appreciation to its generous support.

7. References

- Coates, D.R. 1977. Landslide prospectives. *In: Landslides, Geological Society of America*, p.3–38.
- Cruden D.M., and Varnes, D.J. 1996. Landslide Types and Processes. *In: Turner, A.K., and Schuster, R. L., Eds. Landslides: Investigation and Mitigation*. Transportation Research Board, Special Report 247, National Research Council, Washington D.C., pp. 36-75.
- Hungr, O, Evans, S.G., Bovis, M, and Hutchinson, J.N. 2001. Review of the classification of landslides of the flow type. *Environmental and Engineering Geoscience*, VII, pp. 221-238.
- Hutchinson, J.N. 1988. General Report: Morphological and Geotechnical Parameters of Landslides in Relation to Geology and Hydrogeology. *In: Proc. Fifth International Symposium on Landslides (C. Bonnard, ed.)*, A.A. Balkema, Rotterdam. Netherlands, Vol. 1, pp. 3-35.
- Varnes, D.J. 1978. Slope movement types and processes. *In: Schuster, R. L., and Krizek, R. J., Eds. Landslides: Analysis and Control*. Transportation Research Board, Special Report 176, National Research Council, Washington D.C., pp. 12–33.
- Zaruba, Q., and Mencl, V. 1969. Landslides and their control. Elsevier, Amsterdam, 205 pp.
- Zaruba, Q. and Mencl, V. 1976. Engineering Geology. Elsevier, Amsterdam, 504 pp.

TUNNEL EXCAVATION IN CLAYEY-MARLY FORMATIONS: THE CASE OF KALLIDROMO TUNNEL

Diasakos Nikolaos¹, Amerikanos Panagiotis¹, Tryfonas Georgios¹,
Vagioutou Eleni¹, Baltzois Vassilios¹, Bloukas Stavros¹, Tagkas Theodoros²,
Malandrakis Eleftherios², Poulakis Nikolaos², Kalogerogiannis Georgios²,
Tsirigotis Nikolaos²

¹ ERGOSE S.A., supervision team, paamerikan@ergose.gr, gitryfonas@ergose.gr

² TERNA S.A., tunnel section construction, ternakallidromo@tee.gr

Abstract

This paper presents the excavation of Kallidromo railway tunnel in clay and clay-marl formations. During the past years various approaches were considered both at the design and construction level, for the completion of this difficult part of the tunnel. Finally a method has been selected and successfully applied which combines the principles of yielding and double support.

Key words: Kallidromo tunnel, clay formations, yielding support, double support.

1. Introduction

The paper presents the excavation of Kallidromo twin-tube single-track tunnel in clay – clay-marl formations. The excavation was based on a method which combines the yielding and double support principles, modified according to the approved designs, instrumentation measurements and the tunnel conditions that were encountered.

2. Project description

The twin-tube single-track tunnel of Kallidromo is part of the New High-Speed Railway Line Tithorea – Lianokladi, in the section from Tithorea Railway Station Ch. 0+000 to Ch. 19+000. The said line is a subsection of the railway line connecting Athens to Thessaloniki (Fig. 1). The railway tunnel has two tubes 9.034m long each, a net cross-section of 58m², a design speed of 250km/hour, cross-cuts every 500m, elevation approx. 200m and a longitudinal decrescent gradient of 6‰ towards north. It runs in a general North– South direction and it is going to be the longest tunnel in Greece. The proj-



Fig. 1: Greek railway net.
Location of the Kallidromo tunnel.

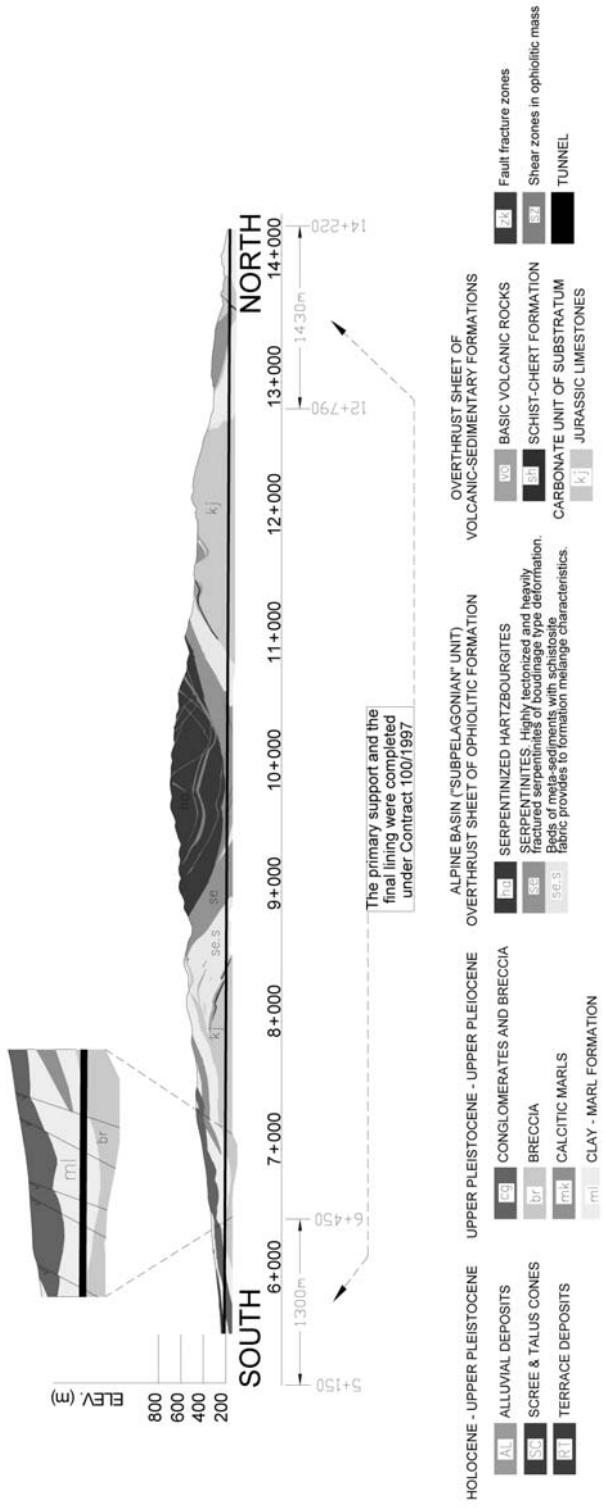


Fig. 2: Geological Longitudinal Section of The Kallidromo Tunnel.

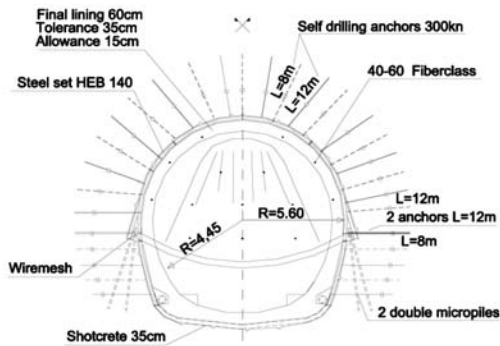


Fig. 3: Cross section of initial design S6.1c.

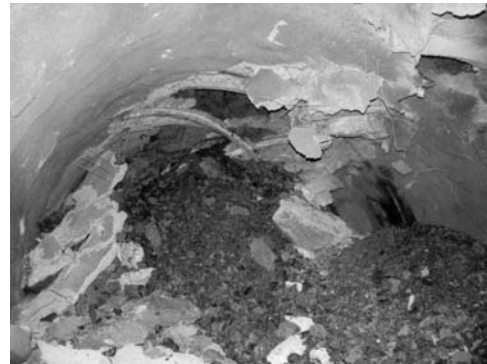


Fig. 4: Collapsed area in the right tube.

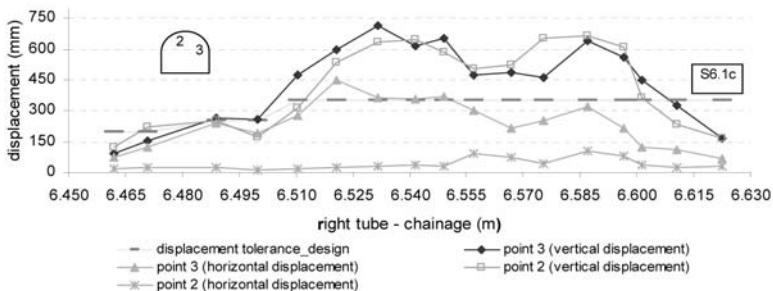


Fig. 5: Displacements close to collapsed area.

ect is a continuation of a previous contract (No 100/1997) under which 1.300m were excavated from the South drive and 1.430m from the North drive in each tube and final lining was installed in 1.300m of each drive respectively.

3. Geology of the tunnel area

The area of interest (Fig. 2) mostly consists of Alpine formations of the Pelagonian zone, which also constitute the bedrock of the area, and the overlying Post-Alpine formations and deposits. Maximum overburden is 540m, approximately in the middle of the tunnel. Alpine formations are divided as follows, from bottom to top:

- Carbonate bedrock unit: Bituminous limestone dating back to the Upper Triassic – Upper Jurassic (kj)
- Tectonic cover of volcano-sedimentary formations: Shale, chert, sandstone, marly limestone and basaltic pillow lavas (vo)
- Ophiolitic tectonic cover from bottom to top:
 - Schistose serpentinite (se.s)
 - Serpentinite (se)
 - Serpentinized hartzburgite (ha)

Based on their structure and composition, schistose serpentinites are described as ophiolitic mélange.

Post-Alpine formations are divided as follows, from bottom to top:

- Upper Pliocene – Upper Pleistocene formations

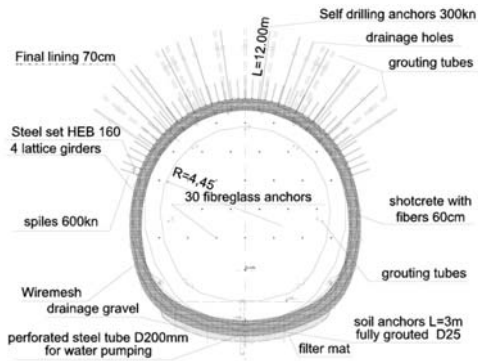


Fig. 6: Rehabilitation cross section S3.A.



Fig. 7: Old collapsed tunnel during re-excavation.

- Conglomerate-breccia (br)
- Clay-marl formation (ml)
- Calcitic marl (mk)
- Limestone conglomerate (cg)
- Formations and deposits of the Upper Pleistocene – Holocene
 - Terrace Deposits (RT)
 - Scree & Talus Cones (SC)
 - Alluvial Deposits (AL)

The area referred to below is the area of the clay-marl formations (ml) of the south drive from Ch. 6+470 to Ch. 7+115 (645m long, see Fig. 2), where the height of the overlying formations starts from 120m and reaches about 230m. This formation is very heterogeneous and mainly consists of alternating intercalations of tenacious blue-grey schistose clay, locally containing grey-white calcitic concretions, and intercalations of tenacious dark brown clay. There are also encountered lenses and intercalations of medium to coarse-grained sand with an average thickness ranging approximately from 0,20m – 2,00m. More rarely the formation contains lenticular intercalations of conglomerates. At its base there are interbeds of organic material.

In terms of grading, the formation is mostly classified as lean (CL) and fat (CH) clay, whereas the sandy intercalations as silty (SM) and clayey (SC) sand. Locally there are intercalations characterized as clayey-sandy silt (ML). The formation has a medium to high plasticity and a high swelling potential.

4. Description of temporary support measures implemented in the past

The tunnel excavation from the South drive started under an older contract (No 100/1997) and about 1.400m in total were excavated from each drive. In the “ml” formation (from Ch. 6+470 to Ch. 6+665 in the right tube) support measures (category S6.1c) included 30cm thick shotcrete, steel sets HEB 140, wiremesh and self-drilling anchors with a bearing capacity of 300kn and 600kn. Excavation was performed in three phases. Phase A (top heading) included the enlargement of the steel set foundation (elephant foot), foot micropiles and primary reinforcement of the tunnel face with fibreglass anchors (see Fig. 3). In addition, in order to minimize displacements during Phase A the working floor was closed with a temporary invert, reinforced with double wiremesh. The convergences measured were in the order of 70cm (see Fig. 5), which lead to repeated reconstructions of the cross-section. However, approximately at Ch. 6+625 in the right tube the tunnel collapsed (Fig. 4) over about 40m and as a result excavation works were stopped.

We note the following issues in order to show the extent of adverse conditions affecting this par-

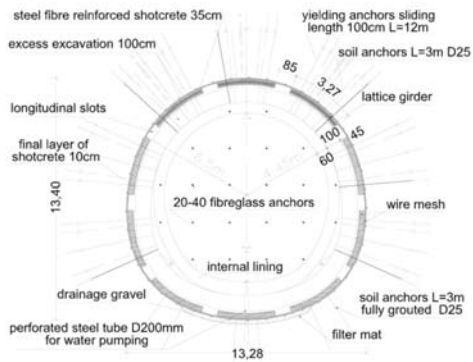


Fig. 8: Yielding cross section Y45.g



Fig. 9: Yielding cross section Y45.g – primary support.

tical part of the project:

- The area is characterized by recent lacustrine deposits with inherently unfavourable technical-geological characteristics.
- Formations have a clayey, clayey-marly composition with slickensides and local intercalations of sandy lenses.
- Clays mainly consist of minerals such as montmorillonite, and in general they are highly swelling.
- Formations have low strength in relation to the stresses imposed by the overburden, thus creating squeezing conditions.
- The layout of the tunnels (twin tunnels) provides for a small axial distance between the two tubes (35m) and creates negative interactions during the excavation and support phases.
- The tunnel overburden is high for this type of geological formations.

In addition to the above, the following unexpected disavouring factors were also identified, and are summarized below:

- Wandering flows were observed and the groundwater table was not easily detectable due to the low primary water permeability of the formations.
- Clay strength reached extremely low levels (residual – ultimate strength) under continuous loading and slow deformation (strain-softening behaviour).
- Water influx was facilitated by increased permeability zones (sandy intercalations) as well as by the loosening caused by the tunnel excavation on surrounding formations.
- The strength of the formations was further degraded due to the impact of the water mainly on the slickensides as well as on the main clay mass (softening).

The creep effect of the clay, which preserves the squeezing - compression on the shell (25th Report of Prof. P. Marinos 1/07/2002). After some balance was temporarily restored in the shell, the continuous deformation (secondary creep) lead to uncontrolled deformations.

“The combination of the aforementioned conditions which exist in Kallidromo tunnel makes this case particularly interesting and unique. Even at the international level there is limited experience in construction and especially in dealing with emergency situations when all the above conditions are present” (Technical Site Report of Dr. Evert Hoek 3/06/2002).

The area was successfully restored with the stiff cross-section S3.A (Fig. 6, 7) which provided for 1m full-face boring, 0,6m thick steel fibre reinforced shotcrete, spiles 600Kn 12m long/ 6m of tunnel length, fibreglass anchors in the tunnel face, self-drilling anchors 12m (300-600)Kn, 1 steel

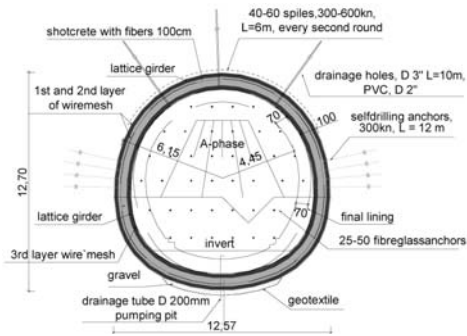


Fig. 10: Yielding - double support cross section.



Fig. 11: Yielding - double support.

set HEB 160/m of tunnel length, 4 lattice girders/ m of tunnel length, and two rows of wiremesh. The retendering of the project provided the opportunity to conduct a wide-range geological – geotechnical plan, and a new final design was performed, which provided that in the “ml” formation the tunnel would be constructed with the yielding support method (Fig. 8, 9). The philosophy of this method is to allow the “soil mass” to converge in a radial direction up to 1m by using ten longitudinal gaps in the shotcrete shell (support class Y45g) and special design yielding anchors, before applying a uniform closed ring for the temporary support of the tunnel. This method was applied in two parts of the tunnel, 10m long each. The main problems that occurred during construction with the yielding support method are as follows:

- extended face collapses,
- less than anticipated convergence,
- difficulty in placing the yielding anchors,
- fractures in shotcrete segments,
- insecurity of personnel due to unsafe working conditions.

5. Description of the yielding – double support method

Based on the experience gained in the previous period, recording and interpreting the behaviour of the “ml” formation and the support class cross-sections, after a series of modifications we have arrived at a new cross-section, combining the principles of the yielding & the stiff support (double support). The tunnel is excavated in two phases (Fig. 10, 11), the distance between them being over 6,00m. During the A phase (top heading) the advance step is (0,70 - 1,00)m, a coating of category C30/37 35cm thick shotcrete is applied, 3 steel lattice girders type Pantex 100/20 /m of tunnel length are placed, as well as 2 sets of wiremesh and 8pc 12,00m long /m of tunnel length, self-drilling anchors, with a bearing capacity of 300Kn. The tunnel face is reinforced with fibreglass anchors with a capacity of 200Kn every 5,00m of tunnel length or five days advance, and the roof is secured with spiles {6,00m long self-drilling anchors with a bearing capacity of (300 or 600)Kn every second round}. The behaviour of the support is closely monitored with closely-spaced sets of instruments consisting of convergence points every (5-15)m, anchor load cells, shotcrete load cells every (20-30)m and extensometers every about 100m. Based on all the information gathered it was decided that the excavation bench would follow the top heading at a distance of about 18 m or a time-distance of about 5 days, in order to allow for the partial unloading of the soil mass with displacements of up to approximately 15 cm. It is noted that anchors are only placed in the tunnel sides (4 items per tunnel side) in order to minimize convergences and facilitate settlements, since no prevention measure was taken (elephant

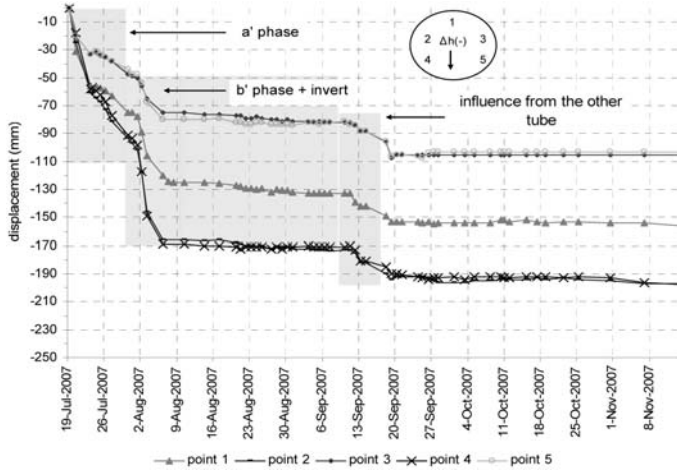


Fig. 12: Vertical Displacements during excavation and primary support.

foot, micropiles, temporary invert etc).

Once the allowable settlements and convergences are completed, we proceed with the excavation of B phase (bench & invert with an advance step of 3m), during which the same support measures are applied as in the top heading, except for the placement of anchors. Then a second support ring is constructed, made of strong wiremesh, one steel lattice girder type Pantex 100/20 per running meter and 65 cm thick steel fibre reinforced shotcrete of category C30/37, thus fully completing the temporary support of the tunnel.

Moreover, after the completion of the internal ring, an allowance of 0,2m is taken into account, in case additional support measures need to be applied. However, such measures have not been necessary.

With this method the progress rate achieved is (30 – 35)m of excavation and temporary support per tunnel tube per month, working 24 hours a day 7 days a week.

6. Instrumentation monitoring

Instrumentation monitoring both during construction and after completion of the temporary support has revealed interesting information about clay behaviour.

First of all, during top heading construction the rate of lateral displacements (convergences) was relatively low, namely 1 cm per day, as opposed to vertical displacements, which reached up to 3cm per day. When the temporary support was completed displacements practically disappeared, as shown in the displacement diagram (Fig. 12). It is also worth noting in the diagram the impact on the cross-section caused by the excavation bench and the invert, as well as by the adjacent tube. Extensometers indicated a loosening zone extending over 15,0m, which loosened within 3-4 days from the excavation of the face. Anchor load cell measurements have shown that initially the load of anchors placed at the vertical benches exceeded their strength (over 300Kn), where as anchors placed higher were barely or not loaded. For this reason it was decided not to install anchors higher than 3m of the A phase working level. Instead the cross-section was reinforced at the vertical benches by installing four anchors per running meter in each side, placed in triangular grid configuration. As a result, anchors were evenly loaded and the load did not exceed anchor limits. Following the completion of the internal support ring, anchors were quickly unloaded until the load almost reached zero. This behaviour is compatible with the indications taken from the extensometers.

7. Problems in the application of the method

During the application of the support method described above, the following problems have occurred:

Problems caused by “ml” behaviour uncertainty both during excavation and after the completion of the support. Before the sequence of works could be stabilized, the excavation procedure was modified both in terms of timing and with respect to the type of support used, and as a result progress rate was very low. Moreover, it was deemed necessary to open an additional cross-cut and install the final lining, in order to secure the first 270m of the 645m that were driven in total in each tube inside the clay-marl formation.

Problems caused by the instability of the excavation faces. Frequent collapses of the excavation faces due to circular or plane slips that caused overexcavations and delays in the progress of works. This problem was adequately addressed through partial excavation, face buttress, and installation of spiles and fibreglass face anchors.

Another major challenge was the presence of large quantities of water (70m³/hour) in the sand layers that were inside the “ml” mass, resulting in the creation of instable conditions in the excavation face, combined with the presence of abundant mud on the work floor, which made construction works difficult.

The difficulty of placing large quantities of very thick shotcrete (in the order of 65cm) was overcome through the use of appropriate concrete compositions.

Finally, construction costs were rather high due to the large quantities of shotcrete; however, it is noted that this cost is lower than the cost of the tunnel sections that needed to be repaired or reconstructed.

8. Conclusions

It can be concluded that the yielding support – double ring method has been proven successful. During the tunnel excavation and support, as well as after the completion of the primary lining, the ring behaviour was predictable and showed minimum deviations, mainly at the excavation face.

With this method approximately 1100m of the tunnel have been completed, admittedly under very difficult geological conditions, and the project’s technical staff is optimistic regarding the completion of the biggest tunnel in Greece.

9. References

- Office Malios S.A.. Final design study of the Kallidromo tunnel for the constructive joint venture, 1998.
- E. Hoek, unpublished site report, 3/6/2002.
- P. Marinos, Professor of National Technical University of Athens, unpublished site report, 1/7/2002.
- M. H. Aleksiadou, Geological design study of the Kallidromo tunnel for Ergose Company, 2003.
- W. Wittke Professor Dr. Engineer, NAMA S.A, Final design study of the Kallidromo tunnel for Ergose Company, 2003.
- K. Mitsugi, Y. Kajiwara, Construction of the 3rd longest mountain tunnel in the world – Excavation of swollen and soft mudstone layers, AITES – ITA 2001 World Tunnel Congress, Volume III.

ENVIRONMENTAL PLANNING OF ABANDONED QUARRIES REHABILITATION – A METHODOLOGY

Hagiou Eleonora¹, Konstantopoulou Garyfalia²

¹ Institute of Geology and Mineral Exploration (I.G.M.E.), Olympic Village, Thrakomacedones
GR 136 77 Acharnes, Athens, GREECE, Mining Engineer, Dpt of Mineral Exploration
and Techno-economical Studies, e-mail: norahagiou@igme.gr

² Institute of Geology and Mineral Exploration (I.G.M.E.), Olympic Village, Thrakomacedones
GR 136 77 Acharnes, Athens, GREECE, Dpt of Engineering Geology, e-mail: kongar@igme.gr

Abstract

Restoration of abandoned quarry sites has been for quite a few years practiced in various places in Greece, mainly in the broader district of Athens, a wide range of rehabilitation solutions has been used by the local authorities in order to cover basic needs of the population (cultural and athletic centres, municipal storage and parking facilities for heavy vehicles, open theatres, municipal waste facilities, cemeteries etc.). Still restoration of abandoned quarries (aggregate material, marble, industrial minerals etc) remains a major problem for almost every prefecture and has to be solved gradually due to lack of the necessary funds, solving the most acute environmental problems and covering basic needs of the population for municipal facilities.

In this paper the development of a methodology is presented for the elaboration of a priority list for the restoration/rehabilitation of numerous abandoned quarries comprised in a geographical or administrative entity. Using multi-criteria analysis and geographical information system we have concluded in a quick and cost effective method for the hierarchical classification of restoration sites. The establishment of an adequate set of criteria for the priority list is of main importance for the successful application of the method.

Key words: *Restoration, abandoned quarry, rehabilitation, multi-criteria analysis, hierarchical classification.*

1. Introduction

Restoration of abandoned quarry sites has been for quite a few years practiced in various places in Greece, mainly in the broader district of Athens, a wide range of rehabilitation solutions has been used by the local authorities in order to cover basic needs of the population (cultural and athletic centres, municipal storage and parking facilities for heavy vehicles, open theatres, municipal waste facilities, cemeteries etc.). Still restoration of abandoned quarries (aggregate material, marble, industrial minerals etc) remains a major problem (Figs 1 & 2) for almost every prefecture and has to be solved gradually due to lack of the necessary funds, solving the most acute environmental problems and covering basic needs of the population for municipal facilities (Fig. 3.).

In this paper the development of a methodology is presented for the elaboration of a priority list for the restoration/ rehabilitation of numerous abandoned quarries comprised in a geographical or ad-



Fig. 1: Uncontrolled waste dump in an abandoned quarry (Kozani).



Fig. 2: Visual disturbance from abandoned quarry excavation (Ioannina).



Fig. 3: Alternative plans for abandoned quarry rehabilitation (a. theatre, b. reforestation/recreation park, c. litter transhipment station, d. athletic centre).

ministrative entity. Using multi-criteria analysis and geographical information system we have concluded in a quick and cost effective method for the hierarchical classification of restoration sites. The establishment of an adequate set of criteria for the priority list is of main importance for the successful application of the method.

2. Scope

Taking into consideration all the aforementioned, a project was formulated, within the Third Community Support Framework, aiming to provide a methodological tool for use by the local administration authorities, at any level, in order to acquire a priority intervention list and select the most appropriate rehabilitation solution for abandoned quarries located in their region, taking into account environmental, social and economic criteria based on their priorities and their economic and technical potential.

3. Methodology

It is well known that there is no systematic recording of the quarrying activity at central level and for the granting of operating concessions a number of public authorities are involved (Prefectures, Mining inspectorate Agencies, Dpts of Industry and Mineral Wealth of the Regional Administration), varying according to the ownership status of the land (public or private) and the commodity produced (Marble, aggregates etc.). Thus, abandoned quarries, especially if they are more than a decade old, are often of “unknown identity”, that is to say it is almost impossible to find concrete elements for the period of operation, the exploiter or their property arrangement. That made necessary a first phase for the survey of abandoned quarries and the localization of the quarry sites.

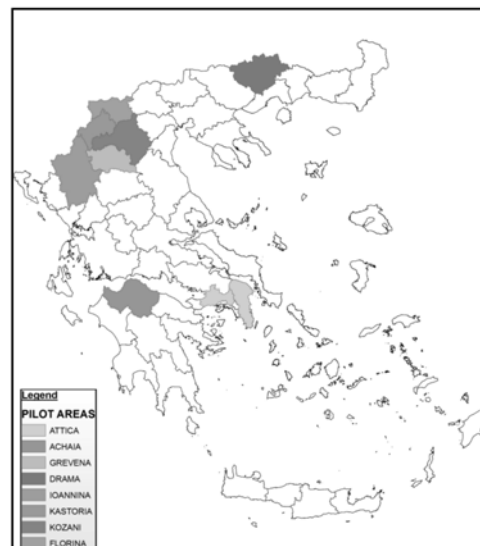
4. Selection of pilot areas

The following five representative districts were selected taking into account, besides the former extensive quarrying activity, the size of the urban centres, namely the following:

- Prefecture of Achaia
- Prefecture of Ioannina
- Prefecture of Drama
- Region of Western Macedonia
- Prefecture of Attica

Phase I: Survey of abandoned quarries - Creation of a Data Base

In the selected regions, with the assistance of the Regional Administration, the Prefectures and local Municipalities, a survey of abandoned public quarries was carried out. A questionnaire was drawn up with data related to the geographic site, the area, the access and the orientation of each quarry, its morphology, as well as data on the soil,



the climate, the fauna and flora of the region. Furthermore, geological, mineral, hydro geological, hydrological, geotechnical and ground characteristics, land uses in the direct and wider environment of the quarry were also recorded, as well as the population (size, economic activity etc) and the deficiencies in communal facilities.

Phase II: Hierarchical classification of abandoned quarries for restoration

The application of, well established or most up to date, rehabilitation solutions for quarry sites, can not be carried out simultaneously, due mainly to lack of the necessary funds. Therefore the selection of specific criteria is necessitated for the compilation of a priority list concerning the most urgent intervention for quarry sites rehabilitation.

Using multi-criteria analysis and GIS we concluded in a quick and cost effective method for the hierarchical classification of restoration sites. The establishment of an adequate set of criteria for the priority list is of main importance for the successful application of the method.

The application of criteria, with determined factors of importance, can set the quarries of a district in order of precedence and consequently lead to the rational planning of feasible rehabilitation solutions.

The following criteria were set for the establishment of a priority list (Table 1., Figure 6.) of inert quarry sites restoration/ rehabilitation, at any administration level, with the corresponding measurement index:

A. The intensity of the pollution problem

Three criteria were used, ground water pollution hazard, safety hazard and visual disturbance, for the calculation of the environmental problem caused by abandoned quarries:

Ground water pollution /Health hazard

- The use of the site as a waste dump and the sort of the deposited waste (inert, municipal or industrial/dangerous)
- The permeability of the quarry rocks

Safety hazard

- Quarry site hazard (slope and face stability etc.)
- Accessibility of the site (protective fencing, distance from roads and populated areas)

Visual disturbance (Figure 4)

- Extent of visibility

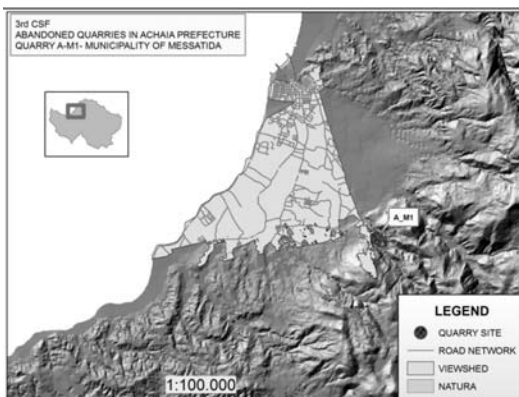


Fig. 4: Calculation of the visual disturbance indicator with the use of Geographical Information System.

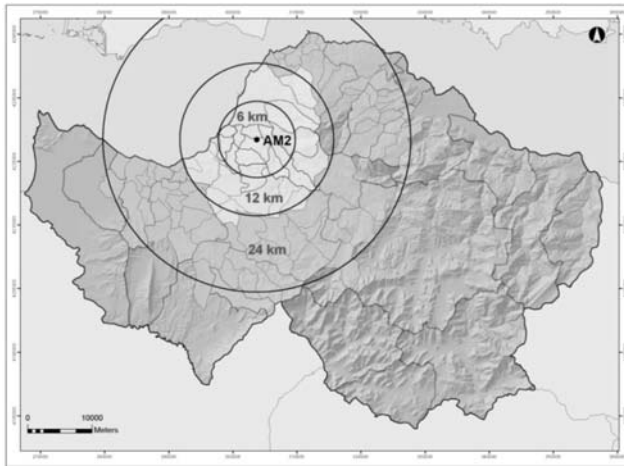


Fig. 5. Calculation of the population indicator with the use of Geographical Information System.

- The population included in this extent
- The length of national roads network included in this extent
- The presence of special protection areas (NATURA, archaeological sites etc)

B. The adequacy of the quarry site for communal facilities

Two criteria were considered adequate for the evaluation of quarry sites as far as their competence for communal facilities is concerned:

- The area of the quarry site
- The distance and the accessibility from neighbouring settlements as well as the population size that could be possibly serviced (figure 5.)

PHASE III: Selection of the optimal rehabilitation solution for specific quarry sites

For this purpose a methodology of gradual approach was followed, including the following 5 steps:

1. Detailed examination of the quarry site, legal status, ownership status, topographic chart, geometrical characteristics, geological, hydro geological, geotechnical and environmental data.
2. Recording of deficiencies in infrastructure and communal facilities at local and peripheral level. Initial approach of feasible alternative solutions, based on permissible land use
3. Limitation of the number of alternative solutions based on restrictive/prohibitive conditions, for every solution under consideration, and the specific conditions of the quarry site under examination.
4. Modulation of distinct alternative rehabilitation plans and their detailed description.
5. Assessment of the alternative plans with Multi-criteria Analysis. Consultation with the directly involved parts (citizens, municipality, local organizations and associations). Formulation of the final list of alternative plans and their scores.

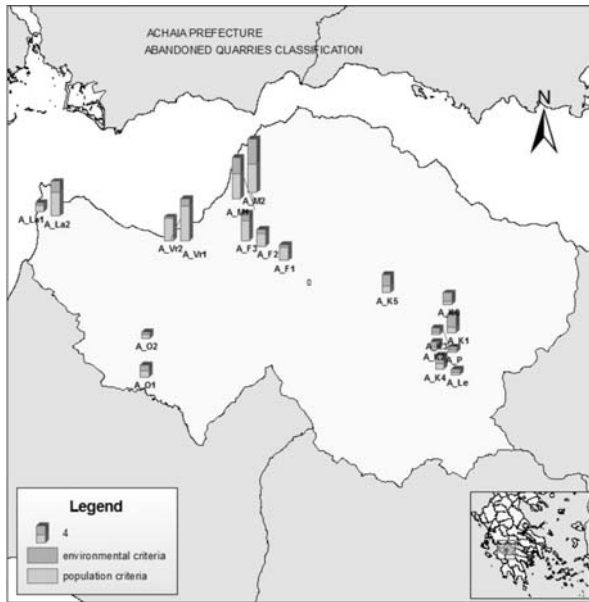


Fig. 6. Abandoned quarry sites in Achaia prefecture and their ranking with environmental and population criteria.

Table 1. Quarry site scoring according to environmental and population indicators

QUARRY	GR.WATER HAZARD	SAFETY HAZARD	VISUAL DISTURBANCE	TOTAL 1	AREA	POPULA- TION	TOTAL 2	TOTAL	RANK
A_Vr1	0	6	0,002	1,80	10	5,94	7,97	4,27	3
A_Vr2	0	1	0,002	0,30	4,5	5,94	5,22	2,27	7
A_K1	0	10	0,492	3,10	1,5	0,96	1,23	2,35	6
A_K2	0	2	2,762	1,15	0,3	0,88	0,59	0,93	15
A_K3	0	2	2,542	0,96	0,2	0,92	0,56	0,80	16
A_K4	0	6	0,225	1,85	2	0,86	1,43	1,68	10
A_K5	1	6	1,834	2,67	1,5	1,51	1,50	2,20	8
A_K6	0	6	0,416	1,88	0,2	1,52	0,86	1,47	12
A_La1	0	2	0,168	0,63	2	1,00	1,50	0,98	14
A_La2	0	6	3,428	2,49	10	1,02	5,51	3,70	4
A_Le	0	2	0,368	0,67	0,4	0,63	0,52	0,61	19
A_M1	0	10	3,684	3,74	2,4	9,25	5,83	4,57	2
A_M2	4	10	4,185	5,84	3,5	9,80	6,65	6,16	1
A_P	0	2	0,464	0,69	0,5	0,61	0,55	0,64	18
A_F1	0	2	0,187	0,64	1	5,03	3,01	1,59	11
A_F2	0	2	1,591	0,92	0,6	5,59	3,10	1,79	9
A_F3	0	2	5,486	1,70	3,2	6,16	4,68	2,89	5
A_O1	0	2	3,301	1,26	2	1,00	1,50	1,36	13
A_O2	0	2	0,321	0,66	0,3	1,30	0,80	0,72	17

Table 2. Selection criteria for optimal quarry rehabilitation planning.

Local/ peripheral needs
Requirements of each solution in space and infrastructure
Operating cost/ Maintenance cost
Investment cost/economic limitations of the operator
Technical requirements/ capabilities
Environmental impacts
Legal framework limitations
Possibility of combination of different solutions
Compatibility with the development plan of the district

The selection criteria for the optimal rehabilitation plan for each quarry site under examination are presented in Table 2.

4. Conclusions-Results

A great number of abandoned quarries (aggregates, decorative rocks and industrial minerals) are located, more or less, throughout the country. Some renters continue their suspended operation under the pretext of site restoration. Other quarries have been abandoned in the restoration capabilities of the nature. Quite a few have been used as uncontrolled waste dumps, thus becoming a major focal point for severe environmental pollution.

During the last 30 years, a growing interest for the rational management of the quarrying activity, as well as the restoration of the abandoned quarries, appears by the local authorities. It became at last common belief that the operation of a quarry has severe impact on the natural environment and can damage the environmental balance (natural relief, water resources, soil, flora and fauna). The legislation for quarry exploitation takes into account the protection of the natural environment and becomes stricter all over Europe, establishing more environmental restrictions for the quarrying activity.

The gradual restoration/ exploitation of abandoned quarry sites with local intervention can contribute to the amelioration of the environmental quality into and in the surroundings of the cities and towns and can be included in the regional development planning.

The abandoned quarry excavations indicate recent irrational quarry exploitation. Very high and steep slopes and irregular levels are a very common image leading in safety hazards (rock falls mass movement). The adverse impact on the environment is obvious, while the problem is enlarged in the vicinity of large urban centres, in the boundaries of which many aggregate quarries are often found.

Apart from the excavation activity a major aesthetic violence of the landscape is caused by the residues of the processing plants, especially the fines, as well as during the construction of the roads networks.

The proposed methodology on adequate quarry sites selection and determination of the most suitable rehabilitation solution proposed in the present study can constitute a useful tool for the local administration at any level. The compiled database can be enriched with new data, concluding from the materialization of the proposed solutions.

5. Acknowledgments

This study was conducted within the Third Community Support Framework of IGME and was financed 50% from the E.E.C and 50% from the Hellenic State.

6. References

- Beinat, E. (Editor), Nijkamp, P. 1998. *Multicriteria Analysis for Land-Use Management*, Springer.
- Belton, V., Stewart, T., 2002. Multiple criteria decision analysis: an integrated approach. *Dordrecht: Kluwer Academic Publications*.
- Damigos, D., Kaliampakos, D., 1999. Using Environmental Economics to Evaluate Quarry Rehabilitation Alternatives. *Proceedings of the 6th International Conference on Environmental Science and Technology*, Vol. B, pp. 514-521, Pythagorion, Samos, Greece.
- Diakoulaki, D., 2006. System Analysis and Decision Making, *National Technical University, Dpt of Chemical Engineers, Laboratory of Industrial and Energy Economics*, September 2006.
- Hatzistathis A., Spikoudis I., 1992. Protection of Nature and Architecture of Landscape. *Book Edition*, Thessaloniki.
- Hinloopen, E., Nijkamp, P., Rietveld, P., 1983. Qualitative Discrete Multiple Criteria Choice Models, *Regional Planning, Regional Science and Urban Economics 13*.
- Kaliampakos, D., Damigos, D., 1998. Quarry Rehabilitation in Attica. *Mining Environmental Management*, Vol. 6, No 1, pp. 13-14.
- Kaliampakos, D.C., Panou, D.G., Damigos, D.G, 1999. Integrated Multicriteria and Cost – Benefit Analysis Methodology for Appraisal of After – use Plans for Quarries in Urban Areas. *International Mining and Minerals*, Vol. 2, No 15, pp. 67-74, March 1999..
- Kaliampakos, D., Damigos, D., 2006. Developing fuzzy AHP system to evaluate rehabilitation alternatives of asbestos industrial complex
- Menegaki, M.,Kaliampakos, D., 2005. Surface Mining Design: a systematic Approach to the evaluation of Visual Impacts, *Proceedings of the International Conference on Mining and the Environment, Metals and Energy Recovery, securing the Future*, Vol.2, pp.716-725, Skelleftea, Sweden, 27 june-1 july 2005.
- Menegaki, M.,Kaliampakos, D., 2006. Lanscape Analysis as a tool for Surface Mining Design, *Environment and Planning B:Planning and Design, 2006, volume 33, pp 185-196*
- Nijkamp, P., Rietveld, P., Voogd, H., 1990. Multicriteria Evaluation in Physical Planning, *Contributions to Economic Analysis*; 185, North-Holland, Amsterdam.
- Saaty, T.L., 1980. *The Analytic Hierarchy Process*, New York : *McGraw-Hill*, 1980.
- Saaty T. L., 1990. *Multicriteria Decision Making. The Analytic Hierarchy Process*, *RWS Publications*, Pittsburgh PA, USA, Second Edition.

ELASTIC PROPERTIES OF ROCKS

**Karagianni A.¹, Karoutzos G.¹, Ktena S.¹, Vagenas N.¹, Vlachopoulos I.¹,
Sabatakakis N.¹ and Koukis G.¹**

¹ *University of Patras, Department of Geology, Section of Applied Geology and Geophysics, Laboratory of Engineering Geology, 26500 Patras, Greece*

Abstract

The aim of this paper is to determine the elastic parameters of some rocks and especially limestones, schist, sandstones, conglomerates, peridotites and granites using a large number of laboratory tests performed on intact rock samples. The range of values for Young's modulus and uniaxial compressive strength is evaluated, while the relationship between elastic and strength parameters is defined. Regression analyses were applied to define relations among these parameters and the range of values of modulus ratio (MR) is estimated for each rock type.

Key words: *Young's modulus, uniaxial compressive strength, modulus ratio, deformability, laboratory testing.*

1. Introduction

Deere and Miller (1966) proposed the classification of intact rock based on the ratio of tangent modulus of elasticity, E_t , to unconfined compressive strength (σ_c) in five classes, from A (very high modulus ratio, $E_t/\sigma_c > 500$) to E (very low modulus ratio, $E_t/\sigma_c < 50$) respectively.

Hoek and Diederichs (2006) used this modulus ratio, calling this MR, along with the GSI value of the rock mass classification in order to estimate the rock mass deformation modulus, E_{tm} , giving general guidelines for the selection of MR values in the case of lack of experimental data.

In this paper the range of MR values for some representative Greek rocks is estimated and the obtained values are compared with those proposed by Hoek and Diederichs (2006) regarding GSI application.

2. Test procedure

A number of block samples were obtained from different outcrops of rocks formations. The sampling locations were widely distributed around the Greek territory. Laboratory core drill and saw machines were used to cut the samples and end faces in order to provide cylindrical specimens in size, shape and ends geometries according to testing requirements. The specimen size was 54 mm (NX) to 80 mm in diameter with a length to diameter ratio of 2.0 to 2.5. The execution of laboratory tests on intact rock material was in accordance with I.S.R.M. suggested methods (1981) and A.S.T.M. standards (D 3148-93). More specifically, the parameters of rocks specimens determined by tests carried out in laboratory, in dry conditions for a better comparison of the results, were uniaxial compressive strength (UCS- σ_c), and E_t (elastic Young's modulus). Finally, laboratory tests were conducted in more than 200 intact rock specimens.

Table 1. Results of intact rock elastic parameters

Results and statistical parameters	σ_c (MPa)	E_t (MPa)	$MR = E_t / \sigma_c$
schist			
Minimum value (Min)	5.2	2000	134
Maximum value (Max)	94.0	44000	920
Mean value (Mean)	32.5	12690	445
Standard deviation (Std dev)	20.2	10286	230
Number of samples (n)	31	31	31
peridotite			
Minimum value (Min)	1.9	2050	152
Maximum value (Max)	100.0	66600	2235
Mean value (Mean)	31.2	21926	1082
Standard deviation (Std dev)	34.5	21361	676
Number of samples (n)	7	7	7
conglomerate			
Minimum value (Min)	5.2	1700	124
Maximum value (Max)	76.0	41800	962
Mean value (Mean)	25.5	13043	473
Standard deviation (Std dev)	13.9	11117	264
Number of samples (n)	21	21	21
sandstone			
Minimum value (Min)	13.5	3420	120
Maximum value (Max)	205.7	71750	727
Mean value (Mean)	80.9	26364	371
Standard deviation (Std dev)	56.4	17481	164
Number of samples (n)	36	36	36
limestone			
Minimum value (Min)	11.8	4700	160
Maximum value (Max)	243.9	254470	1445
Mean value (Mean)	89.7	71868	766
Standard deviation (Std dev)	56.8	59194	323
Number of samples (n)	101	101	101
granite – gneiss			
Minimum value (Min)	15.9	2590	147
Maximum value (Max)	116.6	88790	865
Mean value (Mean)	64.8	31874	455
Standard deviation (Std dev)	37.8	27410	285
Number of samples (n)	13	13	13

3. Test results – correlations between rock properties

The values of the determined elastic and strength rock material properties are summarized in Table 1. As it shown in Table 1, the MR values for tested rock specimens range as follows: 134 to 920 for

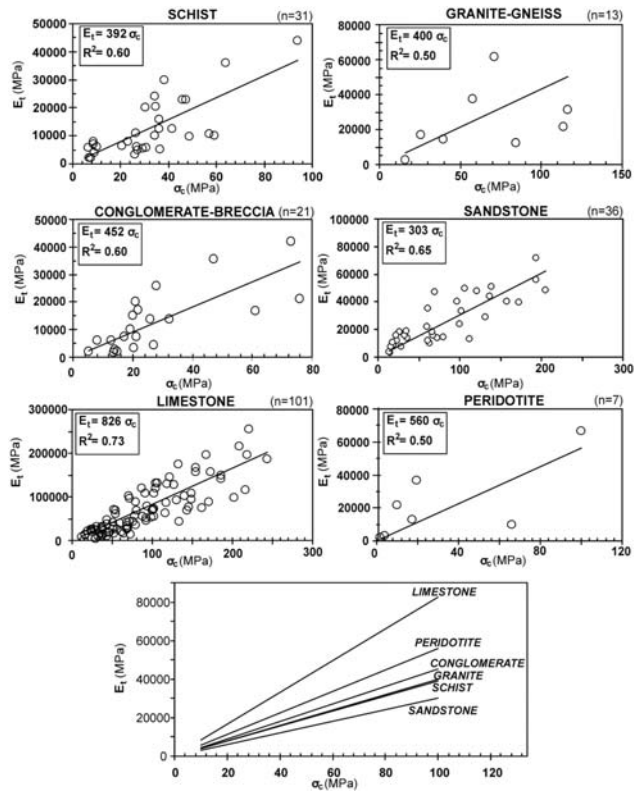


Fig. 1: Correlation between elastic Young's modulus E_t and uniaxial compressive strength σ_c for various rock material.

schist (loading perpendicular to weakness plane), 152 to 2235 for peridotites, 124 to 962 for conglomerate, 120 to 727 for sandstone, 160 to 1445 for limestones, and 147 to 865 for granite.

Regression analysis was applied to define the relation among elastic rock properties. The regression procedure was to fit a line through the points, which is computed so that the squared deviations of the measured points from that line are minimized. The line in a two-variable space was defined by the relevant equation, whereas the value of coefficient of determination or R-square value was also determined. The R-square value is an indicator of how well the model fits the data.

Comparing the determined MR values with those suggested by Hoek and Diederichs (2006), it is concluded that the MR values of the specimens tested and especially peridotite present a greater range.

Moreover, the relationships between E_t and UCS for rock specimens tested are expressed by the equations (Fig. 1):

$$E_t = 392 \cdot \sigma_c \text{ for schist } (E_t: \text{MPa}, \sigma_c: \text{MPa}), R^2 = 0.60 \quad (1)$$

$$E_t = 400 \cdot \sigma_c \text{ for granites - gneiss } (E_t: \text{MPa}, \sigma_c: \text{MPa}), R^2 = 0.50 \quad (2)$$

$$E_t = 452 \cdot \sigma_c \text{ for conglomerate - breccia } (E_t: \text{MPa}, \sigma_c: \text{MPa}), R^2 = 0.60 \quad (3)$$

$$E_t = 303 \cdot \sigma_c \text{ for sandstones } (E_t: \text{MPa}, \sigma_c: \text{MPa}), R^2 = 0.65 \quad (4)$$

$$E_t = 826 \cdot \sigma_c \text{ for limestones } (E_t: \text{MPa}, \sigma_c: \text{MPa}), R^2 = 0.73 \quad (5)$$

$$E_t = 560 \cdot \sigma_c \text{ for peridotites } (E_t: \text{MPa}, \sigma_c: \text{MPa}), R^2 = 0.50 \quad (6)$$

The above estimated relations for limestone and sandstone (eq. 4 and 5) are quite similar to those previously suggested by Sabatakakis et al (2009). It is noted that the eq. 5 in this study include a complementary number of about fifteen data pairs.

Tuğrul and Zarif (2000) suggested similar linear function for limestones, while power functions have been reported by Duncan and Dunne (1967), Dearman and Irfan (1978), Irfan and Powell (1985), Turk et al. (1994), Gupta and Rao (2000) for igneous, metamorphic and sedimentary rocks having different degree of weathering.

4. Conclusions-Results

The evaluation of strength and deformability parameters of rocks obtained by laboratory test results led to the establishment of regression equations among elastic rock properties. A linear function exists between Young's modulus and unconfined compressive strength with RM values ranging a lot. The mean MR values for tested rock specimens are as follows: 392 for schist (loading perpendicular to weakness plane), 560 for peridotites, 452 for conglomerate, 303 for sandstone, 826 for limestones, and 400 for granite. The variability of deformability parameters is mainly related to the textural characteristics and composition changes of the rock material.

5. References

- American Society for Testing and Materials, 1993. Standard test method for elastic moduli of intact rock core specimens in uniaxial compression, *Annual Book of Standards*. vol. 04.08, D3148-93.
- Dearman, W.R., Irfan, T.Y., 1978. Assessment of the degree of the weathering in granite using petrographic and physical index tests. *Proc. of the International Symposium on Deterioration and Protection of Stone Monuments*, Unesco, Paris, pp 1-35, paper 2.3.
- Deere, D.U., Miller, R.P., 1967. *Engineering classification and index properties for intact rocks*. Tech. Rep. No. AFWL-TR-65-116. University of Illinois, Urbana. 229p.
- Duncan, N., Dunne, M.H., 1967. A regional study of the development of residual soils. *Proc. of the 4th African Regional Conference on Soil Mechanics Found. Engineering*, Cape Town, pp. 109-119.
- Gupta, A.S., Seshagiri Rao, K., 2000. Weathering effects on the strength and deformational behaviour of crystalline rocks under uniaxial compression state. *Engineering Geology*, 56, pp. 257-274.
- Hoek, E., Diederichs, M.S., 2006. Empirical estimation of rock mass modulus. *International Journal of Rock Mechanics and Mining Sciences*, 43, pp. 203-215.
- Irfan, T.Y., Powell, G.E., 1985. Engineering geological investigations for pile foundation on a deeply weathering granitic rock in Hong Kong. *Bulletin of the association of Engineering Geology*, 32, pp. 67-80.
- ISRM Suggested Methods, 1981. Suggested methods. Rock characterization, testing and monitoring, ed. E.T. Brown, Pergamon Press, Oxford.
- Sabatakakis, N., Koukis, G., Tsiambaos, G., Papanakli, S., 2008. Index properties and strength variation controlled by microstructure for sedimentary rocks. *Engineering Geology*, 11.
- Tugrul, A., Zarif, I.H., 2000. Engineering aspects of limestone weathering in Istanbul, Turkey. *Bulletin of Engineering Geology and the Environment*, 58 (3), pp. 191-206.
- Turk, N. Koca, M.Y., Yuzer, E., Qztas, T., Erdogan, M., 1994. Engineering geological problems of the first phase of the Izmir Metro. *Proc. of the 7th International IAEG Congress*. Lisbon. Balkema. Rotterdam. pp. 4259-4264.

MINERALOGICAL COMPOSITION AND FABRIC AS RELATED TO THE MECHANICAL BEHAVIOR OF THE FINE – GRAINED PLIO-PLEISTOCENE SEDIMENTS OF ACHAIA, GREECE

Kouki A.¹

¹ Ministry of Public Works, EYDE – Motorway PATHE, Alexandras Av. 205, Athens, Greece,
kouki.nassia@gmail.com

Abstract

The fine grained sediments of the Plio-Pleistocene deposits of Achaia have been distinguished into two geotechnical units, stratigraphically successive, the Upper and the Lower one. A number of tests were performed in samples from both units in order to determine their mineralogical composition and fabric, as well as their CaCO₃ content. From these it is shown that the two units present main differences in mineralogical composition, type and percentage of clay minerals, concretion ratio and calcium carbonate content, which directly affect their mechanical behavior in construction of technical works.

Key words: *Upper Geotechnical unit, Lower Geotechnical unit, Mineralogical composition and fabric, Calcium carbonate content.*

1. Introduction

The fine-grained facies of the Achaia Plio-pleistocene sediments (Kouki, 2006; Kouki and Rozos, 2010), which can be generally termed as “Marls” and belong to Neogene sediments, were distinguished into two separate units, the Upper and Lower one, based at first on engineering geological – geotechnical criteria. However, there was the need to further confirm this distinction, concerning their structure criteria. To this direction, detailed microscopic-mineralogical analysis was performed, as well as determination of CaCO₃ content, while laboratory tests (soil classification and mechanical parameters tests) had already been performed in all samples.

The above analyses led to the determination of the mineralogical composition (semi-quantitative analysis) and structure of both units, as well as to the identification of the type and percentage of clay minerals, CaCO₃ distribution and the role of aggregations.

It has to be mentioned that in Greece, marls are mainly of Miocene to Pliocene age, marine or lacustrine origin and in many cases they contain macro and micro-fossils, as well as leaves and coal beds, while their degree of diagenesis differs from site to site.

Many researchers have studied the structure and engineering behaviour of marls in Greece (Kavounidis, 1980; Lupini et al, 1980; Sotiropoulos, 1982; Dounias et al., 1985; Kavounidis, 1985; Theofanopoulos and Theofanopoulos, 1985; Gasios and Christodoulis, 1988; Kavounidis, 1988; Kavounidis et al., 1988; Tsiambaos and Christoulas, 1988; Rozos, 1989; Tsiambaos, 1988; Tsifoutidis, 1993; Christodoulou, 2000).

2. Petrographical - mineralogic analyses and physico-mechanical properties of the formations

2.1 Research - Results

The first attempt to determine the mineralogical composition of these formations was made along with the construction of Bozaitika Tunnel. Fifteen (15) soil samples (D1-D6 and D108 – D116) were collected from two sites (ch. 2+380 and ch. 2+640) and tested. Soil classification tests were performed in all these samples, along with some mechanical tests to estimate shear strength parameters. Mineralogical analysis was applied in three of these samples, while CaCO₃ content was determined in all of them. The results are shown in Table 1.

From the evaluation of these laboratory test results the following conclusions can be drawn:

- According to their texture (grain size distribution) and the Atterberg Limits the formations can be classified in the following categories (Table 2).
- Based to the results shown in Tables 1 and 2 it can be concluded that there is correlation between CaCO₃ and clay minerals content, as well as sand content. It was observed that CaCO₃ content is reduced as we go from marls – clayey marls (CH, CL) to more sandy – silty formations (CL-ML, ML) and even more to sandy horizons (SC, SM)
- By correlating CaCO₃ content and cohesiveness it can be shown that more cohesive soils present

Table 1. Laboratory tests results for all samples.

Sample No	w (%)	Wet unit weight (gr/cm ³)	Grain size distribution			Atterberg Limits			Triaxial test UU		UCS (KPa)	CaCO ₃ %	AUSCS Classification
			Sand (%)	Silt (%)	Clay (%)	LL (%)	PL (%)	PI (%)	c (KPα)	φ°			
D1	23.2	2.16	47.0	25.0	28.0	NP			-	-	78	9.7	ML
D2	-	-	47.0	24.0	29.0	NP	-	-	-	9.0			ML
D3	11.7	-	12.0	79.0	9.0	25.0	18.0	7.0	150	39	-	20.5	CL
D4	18.0	2.25	3.0	78.0	19.0	38.0	21.0	17.0	370	16	634	21.5	CL
D5	18.1	2.32	10.0	70.0	20.0	36.0	20.0	16.0	410	13	870	13.0	CL
D6	25.0	2.14	12.0	72.0	16.0	NP			80	22	133	7.5	CL
D108	29.8	-	7.0	93.0		50.0	25.0	25.0	400	26	-	37.5	CL
D109	-	-	7.0	93.0		24.3	2.09		-	-	1358	35.0	CL
D110	23.0	2.22	3.0	67.0	30.0	35.0	18.0	17.0	350	14	579	6.5	CL
D111	-	-	6.0	72.0	22.0	55.0	28.0	27.0	-	-	-	37.5	CH
D112	-	-	6.0	57.0	37.0	56.0	26.0	30.0	-	-	-	25.0	CH
D113	-	-	4.0	60.0	36.0	51.0	27.0	24.0	-	-	-	21.0	CH
D114	-	-	4.0	66.0	30.0	50.0	27.0	23.0	-	-	-	25.0	CL
D115	-	-	4.0	67.0	29.0	55.0	27.0	28.0	-	-	-	38.0	CH
D116	-	-	5.0	64.0	31.0	59.0	28.0	31.0	-	-	-	29.0	CH

Table 2. Laboratory tests results of Table 1 samples, summarized in three soil classification categories (CH, CL, ML).

	Sand %	Silt %	Clay %	LL	PL	PI	CaCO ₃ %
CH	4-6	57-72	22-37	51-59	26-28	24-31	21-38
CL	3-12	67-79	9-30	25-50	18-27	7-23	7.5-37.5
ML	47	24-25	28-29	NP	NP	NP	9-9.7

higher contents of carbonate minerals. In this case, shear strength parameters (c and ϕ), as well as uniaxial compressive strength are relatively higher.

- As far as their mineralogical composition is concerned, samples classified as clayey marls or argillaceous marls - marls mainly consisted of calcite, clay minerals and quartz. On the contrary, in more sandy or silty samples (sandy silts to sands) quartz dominates, where it is found in the form of small grains of equal size to very small grains in sand material. In the so called clayey marls, rarely relatively bigger grains of quartz can also be found, arbitrarily dispersed in the soil mass.
- Calcite's content decreases as sand's increases, but is also relatively high in the clayey materials.
- The dominant clay minerals are illite and in a smaller percentage montmorillonite. These minerals along with calcite constitute the main matrix of the formations. The clay minerals content decreases as sand's portion increases.
- Finally, chlorite, micas (moschovite, serikite and less often biotite) and albite are also present in small quantities, while in more sandy samples Fe-hydroxides can also be found, due to increased permeability and easier therefore infiltration of water.

After the distinction of these sediments into two separate geotechnical units, the Upper and the Lower one, there was the need to repeat the mineralogical analyses in samples from both units. For that purpose seven (7) samples were used, two (2) from the Upper unit (D24, D27), one from the Intermediate unit (D17) and four from the Lower unit (D121, D125, D130 and D134). In all samples More specifically, mineralogical and petrographic analyses were performed in the Mineralogy – Petrography Laboratory of IGME and the Laboratory of Minerals and Rocks of Patras University, by using: a) the optical method under polotic and stereoscopic microscope and b) the X-ray perithlasimetry method (XRD). Semi-quantitative analysis was done by using EVA 6.0 software and ICPDS database. Calcite's content was measured after removing content of carbonates, while montmorillonite content with the method of methylene blue.

In Table 3 the results of mineralogical analyses are presented, while in Table 4 the physical and mechanical properties of the tested samples.

From all the above analyses and the tests performed the following can be recorded for each sample:

Sample D17

According to soil-classification tests this sample is classified as CL, while from the mineralogical analysis as marly clay. It belongs to the Intermediate unit (from the Lower to the Upper unit) and according to CaCO₃ content, it is classified as a clay-marl (Photo 1).

Sample D24

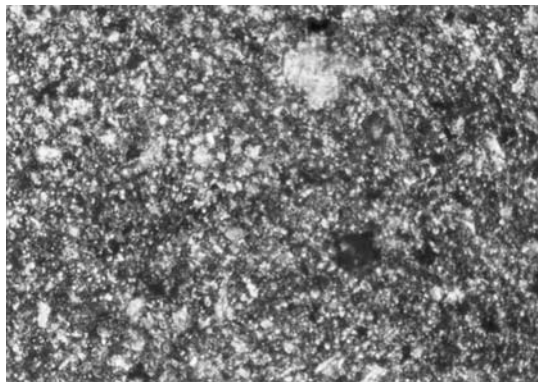
It is classified as ML, while from the mineralogical analysis as siliceous micro-sandstone. It be-

Table 3. Mineralogical composition of the samples (semi-quantitative analysis)

Sample	Quartz	Calcite	Albite	Illite	Kaolinite	Chlorite	Montmorillonite
D17	23	20	6	26	13	4	8
D24	39	11,6	14	16	7	5	6,8
D27	37	15	12	16	8	6	5,2
D121	18	35	5	10	18	3	10,8
D125	22	30	6	15	14	3	9,6
D130	32	22,6	6	14	13	4	8,4
D134	31	21,6	13	15	9	5	5,2

Table 4. Results of soil materials laboratory tests.

Sample	w (%)	Spec. weigh	Unit weight		Grain size distribution			Atterberg Limits			Triaxial test UU		AUSCS
			Wet (gr/cm ³)	Dry (gr/cm ³)	Sand (%)	Silt (%)	Clay (%)	LL (%)	PL (%)	PI (%)	c (KPα)	φ	
D17	17,73	2,68	21,50	18,26	1,76	73,13	25,11	32,83	20,95	11,88	648,7	4,74	CL
D24	14,76	2,64	20,90	18,21	1,90	83,22	14,88	31,82	20,69	11,13	207,3	23,54	CL
D27	10,78	2,63	20,20	18,23	34,22	58,04	7,74	20,09	16,43	3,66	182,6	13,77	ML
D121	17,82	2,72	1,89	1,6	1,4	63,46	35,14	33,89	15,87	18,02	141,6	16,6	CL
D125	15,17	2,72	2,11	1,83	1,21	58,55	40,24	32,97	15,43	17,54	106,1	31,2	CL
D130	14,87	2,71	2,22	1,93	1,77	76,78	21,25	28,6	18,77	9,83	182,9	28,45	CL
D134	8,58	2,67	2,05	1,89	10,55	71,4	18,05	23,1	17,56	5,54	42,61	22,97	CL-ML

**Photo 1:** Sample D17. Quartz and zircon in calcite (Nicol+, length 250μ).

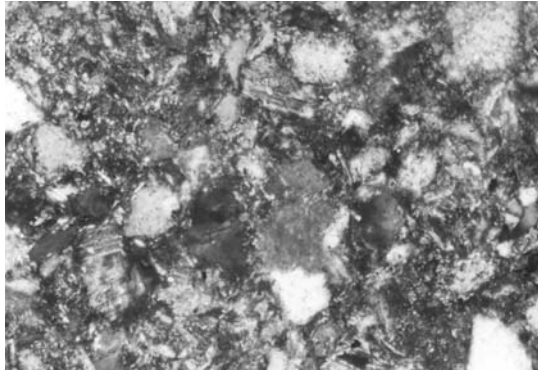


Photo 2: Sample D24. Quartz, moschovite, calcite and feldspar. Matrix material is calcite (Nicols+, length 250 μ).

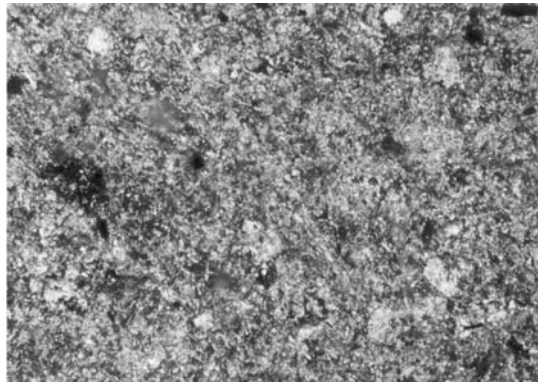


Photo 3: Sample D121. Micrite, chlorite, moschobite, clastic quartz, calcite grains (Nicols+, length 250 μ).

longs to the Upper Geotechnical unit and according to CaCO_3 content, it is classified as a marly clay (Photo 2).

Sample D27

It is classified as ML, while from the mineralogical analysis as siliceous micro-sandstone. It belongs to the Upper Geotechnical unit and can not be classified according to CaCO_3 content as a non argillaceous sediment.

Sample D121

It is classified as CL, while from the mineralogical analysis as marly clay. It belongs to the Lower Geotechnical unit and according to CaCO_3 content, it is in the limit between clayey marls and marls (Photo 3).

Sample D125

It is classified as CL, while from the mineralogical analysis as marly clay. It belongs to the Lower Geotechnical unit and according to CaCO_3 content, it is classified as a clayey marl.

Sample D130

According to soil-classification tests this sample is classified as CL, while from the mineralogical analysis it is classified as siliceous mudstone. It belongs to the Lower Geotechnical unit and according to CaCO_3 content, as a clayey marl.

Sample D134

It is classified as CL-ML, while from the mineralogical analysis as siliceous micro-sandstone with thin mudstone sub-layers. It belongs to the Lower Geotechnical unit and according to CaCO₃ content, it is classified as a clayey marl.

By assessing all the above it can be concluded that:

- All samples tested are cohesive, with small to medium porosity and with few small fissures.
- Samples D24 and D27 of the Upper Geotechnical unit have a light yellow color, fine -sandy texture and increased content of quartz (37-39%), which is also illustrated in the grain-size analysis, where the total contents of sand and silt are 85% and 92% respectively, while the clay percentage is 15% and 8%. On the contrary, according to the mineralogical analysis (semi-quantitative analysis) the clay minerals content for each sample is approximately 35%, which confirms the presence of aggregations. It is noted that sample D27, with higher sand content and lower silt content than sample D24, presents greater aggregation. More specifically, the Aggregation ratio (Ar) is 2.62 and 4.52 for the two samples respectively.

As far as the clay minerals are concerned, illite is the dominant one (16%), while kaolinite (7-8%), montmorillonite (5-7%) and chlorite (5-6%) are also present. Calcite's content is between 11.5% and 15%. In general, these samples contain more quartz and albite and less calcite and clay minerals than the rest of the samples.

- Sample D17 belongs to the Intermediate Geotechnical unit and therefore has properties from both units, Upper and Lower. It has light yellow color, smooth, non-brittle texture and leptocrystallic-pelitic structure. It doesn't have clear bedding, while it contains fossils and shell fragments and presents signs of bio-disturbance. Quartz percentage is less (23%) in comparison to the previous samples, which in the grain-size analysis corresponds to high silt content (73%), when sand is only 1.76%. Clay content is also high (25%), while from the mineralogical analysis the clay minerals content is 51% and the aggregation ratio Ar=2.0. Calcite's content is also high (20%). The dominant clay mineral is illite (26%), kaolinite is 13%, monmorillonite is 8% and chlorite 4%.
- Samples D121, D125, D130 and D135 of the Lower Geotechnical unit not only have significant differences comparing to the samples of the Upper Unit, but also present differences among them, which clearly shows that in marls, clay-marls and clayey marls that belong to the Lower unit there can also be found intermediate types at places, mainly of silty composition or with silty intercalations. The existence of these intermediate types does not in any case alter the clayey marly nature of the Lower unit formations

Thus, samples D121 and D125 are of light gray color and belong to the typical clayey marls, with small sand percentages (1,4 and 1,2%), reduced silt content (63,5% and 58,5%) and higher clay one (35% and 40% respectively). Quartz percentage is only 18% and 22% for the two samples, while calcite is 35% and 30% respectively. Kaolinite is the dominant clay mineral (18 and 14%), followed by illite (10 and 15%), montmorillonite, which presents greater values than the rest of the samples (10,8 and 9,6% respectively) and at last chlorite with around 3%. The total clay minerals content for both samples is approximately 42% and thus the aggregation ratio is 1.20 and 1.05 respectively. It has to be mentioned that these samples differ from sample D17 of the Intermediate unit, as far as Ar and clay minerals content are concerned, even though they have the same structure (klastic) and texture (solid).

Samples D130 and D134, of the Lower also unit, differ from the typical clayey marls (D121 and D125) and are characterized as clay-marls, mainly due to the increased silt content (77% and 71.5%

respectively) and the smaller clay one (21% and 18%) and therefore the increased quartz content (32% and 31%) and decreased clay minerals content (32% and 31%), as shown from the mineralogical analyses. The Aggregation ratio is 1.84 and 1.88 respectively. Calcite content is also low (21.6% and 22%). The dominant clay mineral is illite, followed by kaolinite and montmorillonite according to their relative contents. The above declare that samples D130 and D134 belong basically to the intermediate types in the Lower unit mentioned above.

From the above it is concluded that the clear division of these fine-grained sediments into separate geotechnical units, of distinct composition, structure and mechanical behavior can only be done by the correlation of field observation, microscopic - mineralogical analyses and laboratory soil materials tests.

3. Conclusions

There is a correlation in the percentage of calcium carbonate content with the clay and sand content, as this decreases from marls-clayey marls (CH, CL) to sandy-silts (CL-ML, ML), and further more in the sandy layers SC, SM.

From the correlation of the percentage of calcium carbonate content with the cohesiveness of the samples it can be seen that the most cohesive samples present increased contents of carbonic minerals.

As far as the mineralogical composition is concerned, samples which are classified as clayey marls-marls mainly contain calcite, clay minerals and quartz. On the contrary, samples that contain high percentage of sand and silt (from sandy silts to sands) present increased quartz percentages, in a way that quartz can constitute their main component.

As far as the clayey minerals are concerned, mainly illite and in a smaller content montmorillonite are recorded, which compose, along with calcite, the conjunctive material of these sediments. The percentage of these minerals decreases with the increase of sand content.

Upper Geotechnical unit samples have light-yellow color and fine grained sandy texture, increased quartz content, and clay fraction from mineralogical analysis roughly around 35%, indicative of the existence of concretion (the concretion ratio ranges among 2.62 to 4.58).

Lower Geotechnical Unit samples are noticeably differentiated both from those of the Upper Unit, as well as from those of their own unit, since intermediary types of silt composition or silt layers prevail at places. Thus, the common clayey marls appear with decreased sand contents and increased clay contents. Samples from Lower unit that comprise intermediate types and are characterized as clayey marls have higher percentages of silt, lower percentages of clayey fraction, while from mineralogical analysis quartz percentage was found higher, clayey mineral percentage lower, and the concretion ratio ranges from 1.84 to 1.88.

4. References

- Gasios, E. & Christodoulis, I., 1988. Investigations for the damages of the National Route Athens – Salonika, Km 70+000 – Km 90+000 due to expansive soil. *Bulletin of Geological Society of Greece*, Vol. XX/3, p.133-145.
- Gasios, E., Christodoulis, I., 1988. Mechanical behavior of expansive marls in Thiva's field. *Proceedings of the 1st Hellenic Congress of Geotechnical Engineering*, TEE – HSSMGE, T-1, Athens, p. 33-36.
- Theophanopoulos, P. και Theophanopoulos, N., 1985. Mechanical behaviour of marly formations under

- Electronic Microscope “Scanning”. *Proceedings of the 2nd Hellenic Conference of Geotechnical Engineering “Foundation design parameters”*, HSSMGE, Athens, p. 321-330.
- Kavounidis, S., 1980. Some remarks from the investigation of marls. *Technical Chronicles*, 2, p. 24-27.
- Kavounidis, S., 1985. Geotechnical consideration of marly formations. *Proceedings of Conference “Geotechnical problems of Piraeus marls”*, TEE, Athens, p. 23-64.
- Kavounidis, S., 1988. A proposal for common approach of the mechanical behavior of marls. *Proceedings of the 1st Hellenic Congress of Geotechnical Engineering*, TEE, T.3, Athens, p. 191-192.
- Kavounidis, S., Tika, Th., Dounias, G.Th., 1988. Greek marls under the microscope. *Proceedings of the 1st Hellenic Congress of Geotechnical Engineering*, TEE, T.1, Athens, p. 59-62.
- Kostopoulos, S., 1988. Geotechnical consideration of marly formations in Greece. *Proceedings of the 1st Hellenic Congress of Geotechnical Engineering*, TEE – HSSMGE, T-1, Athens, p. 63-68.
- Kouki A., 2006. Engineering geological – geotechnical parameters and mechanical behavior of hard soils and soft rocks in the design of underground works. *PhD Thesis*, University of Patras.
- Kouki, A. and Rozos, D., 2010a. Engineering geological – geotechnical conditions in the wider area of Patras ring – road. Compilation of the relevant map at a scale of 1:5000. *Proceedings of the 12th International Congress of Geological Society of Greece*, Patras, May, 2010.
- Kouki, A. and Rozos, D., 2010b. The fine-grained Plio-pleistocene deposits in Achaia – Greece and their distinction in characteristic geotechnical unities. *Proceedings of the 12th International Congress of Geological Society of Greece*, Patras, May, 2010.
- Lupini, J.F. Hight, D.W., Kavounidis, S., 1980. Some observations of microfabric and their role in understanding soil behavior. *Rivista Italiana di Geotecnica*, Anno XIV-N.2
- Dounias, G., Tika, Th., Kavounidis, S., 1985. Some observations of microfabric of marls of Piraeus. *Proceedings of Conference “Geotechnical problems of Piraeus marls”*, TEE, Athens, p. 171-184.
- Rozos, D., 1998. Engineering Geological conditions in Achaia County. Geomechanical characteristics of Plio-pleistocene sediments. *PhD Thesis*, University of Patras, 453p.
- Sotiropoulos, I., 1982. Marls. *Proceedings of the 1st Hellenic Geotechnical Conference*, HSSMGE, Athens, p. 243-266.
- Tsiambaos, G., Christoulas, S., 1988. Mechanical behavior of marls in Iraklion, Crete. *Proceedings of the 1st Hellenic Congress of Geotechnical Engineering*, TEE – HSSMGE, T-1, Athens, p. 109-112.
- Tsiambaos, G., 1988. Engineering geological characteristics of marls in Iraklion, Crete. *PhD Thesis*, University of Patras.
- Tsifoutidis, G., 1993. Intrinsic properties of Hellenic marls. *Ph.D Thesis*. University of Durham. United Kingdom.
- Christodouloupoulou, T., 2000. Microstructure of the fine grained Neogene – Pliopleistocene sediments of North Peloponnese, in relation to their physical and mechanical properties. *PhD Thesis*, University of Patras.

THE FINE-GRAINED PLIO-PLEISTOCENE DEPOSITS IN ACHAIA – GREECE AND THEIR DISTINCTION IN CHARACTERISTIC GEOTECHNICAL UNITS

Kouki A.¹, Rozos D.²

¹ Ministry of Public Works, EYDE – Motorway PATHE, Alexandras Av. 205, Athens, Greece,
kouki.nassia@gmail.com

² National Technical University of Athens, School of Mining and Metallurgical Engineering, Laboratory of
Engineering Geology and Hydrogeology, 9, Heroon Polytechniou Str 157 80, Zografou (Athens) Greece,
rozos@metal.ntua.gr

Abstract

The fine grained Plio-Pleistocene sediments encountered along the Patras Ring Road project (PRR) were distinguished into two lithological units, the Upper Geotechnical and the Lower Geotechnical Unit, based on the detailed engineering geological – geotechnical mapping, at a scale of 1:5000, on fieldwork, as well as on data gained from the boreholes drilled during the design and construction of the project. These units are distinguishable, stratigraphically successive and present basic differences in lithological composition, consistency and permeability and therefore different mechanical behaviour during construction.

Key words: Patras ring road, Pliopleistocene sediments, fine grained, Upper Geotechnical unit, Lower Geotechnical unit.

1. Introduction

By taking into account site investigation data for Patras Ring Road (RPP) the findings from the construction of the project (Efpalinos Techniki, 1996, 1997, Edafomechaniki 1995, 1997 & 1998, Kastor, 1998, 1999, OMETE 1998 and Pangea, 1998, 1999 & 2001), other studies (Attewell, 1993, Rozos, 1989, Koukis & Rozos, 1990, Tsiambaos & Koukis 1990, Koukis et al., 2005), and the results of our research, an inceptive suspicion was confirmed. This was that the fine-grained facies of the Pliopleistocene sediments, in which the project was mainly hospitalized, are formulated in two distinguishable and successive units: (a) the Upper Geotechnical unit and (b) the Lower Geotechnical unit (Kouki, 2006). An intermediate Transitional zone of small thickness can be separated at places, between these two units.

It is pointed out that the Lower unit is not easily recognized on the surface, since it is stratigraphically covered by the Upper one. Its presence was firstly acquainted during the excavation of the underground works, when its different geotechnical behavior was realized. Thus, it was mainly sought in deep gorges of the wider area, during the field work. It has to be mentioned here that the presence of these distinguishable geotechnical units was not evaluated during the geological - geotechnical investigations for the design of the PRR.

The field characteristics of these units are described in detail in the engineering geological - geotechnical map at a scale of 1:5000, that was compiled for the study area (Kouki, 2006, Kouki and Rozos, 2010), while in *Photos 1, 2 and 3*, their presence is documented.



Photo 1: Southern portal of tunnel SB (left branch). The two units (Upper and Lower ones) are distinguished, due to color and structure. Their continuity is interrupted by faults that considerably change dipping.



Photo 2: Northern portal of tunnel SA (left branch). The Pliopleistocene sediments are characterized by almost horizontal dipping. The Lower unit, grayish blue in color, is progressively changing, through the transitional zone, into the light gray Upper unit. In the centre of the Figure a normal fault is presented, that has substantially change the previous sequence and thus the slope (in the left hand site of the figure) is only occupied by sediments of the Upper unit.

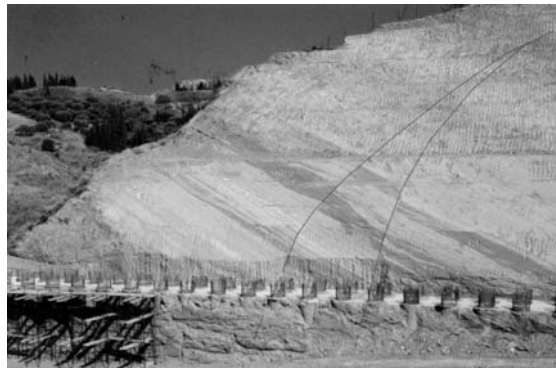


Photo 3: Characteristic stratigraphic sequence of the fine-grained facies of Pliopleistocene sediments, with the grayish blue deeper horizons (Lower unit), that progressively is developing in the grayish brown transition zone and the light gray horizons of the Upper unit.

2. Evaluation of the data from the geotechnical study

Beyond the field work findings, further investigation regarding the segregation of the above units in the fine grained Pliopleistocene sediments, was also facilitated, by the data from boreholes drilled for the design of Patras Ring Road (Kastor, 1998, Edafomechaniki, 1995, 1997 & 1998, Pangea 1998, 1999). In every log of the 169 boreholes examined, there was an effort to group the various litho-facies that were recorded, in order to find out whether these distinguishable Upper and Lower units do exist in the wider study area or whether this is a unified formation with small differentiations. For that reason, the field observations and description of borehole logs, such as color, composition, cohesiveness, were basically examined along with in situ tests, such as SPT, and laboratory tests (i.e. grain size distribution and Atterberg limits). Characteristic logging of a geotechnical borehole is given in *Figure 1*.

3. The compilation of the geotechnical cross sections along the two branches of Patras ring road

For better understanding of the Upper and Lower units, the geotechnical cross sections for both branches (right and left) of Patras ring road were drawn (Figures 2 and 3). For the compilation of these, the topographic sections from the design of Patras Ring Road were used, supplemented with both the surface mapping, engineering geological and tectonic data, as well as those derived from borehole logs.

Thus, the segregation of the units was achieved with accuracy and the thickness was estimated ranging for the Upper unit from 2 to 37m, for the Transitional zone up to 8m, while the Lower unit has quite a significant thickness of over 60m.

Additionally, from the above sections it is shown that in the region of the Archaeological site of the area (Tunnel S1- Cut and Cover - Tunnel SG) and southwards, clayey marly horizons with coarse-grained materials of Pliopleistocene sediments were mapped, overlying the Upper unit, with a thickness fluctuating from 10 to 40m. Also, the Cut and Cover in Mpozaitika site, was opened in Dilluvial conglomerates.

Concerning the problems related to the Upper unit during construction, these are mainly due to the frequent alternation of beds with different lithological composition, such as brownish yellow to brownish gray clayey marls, sandy marls, sandy silts - sands, sandstones and conglomerates. The sandstones and conglomerates present differences in cohesiveness, fracturing and weathering, as well as in permeability. Thus, the sandy layers – sandstones are usually saturated and can create confined aquifers of small capacity, which can cause serious problems during the construction of technical works. Moreover, the formations of the Upper unit usually create thick weathering and fracturing zones, which lead to instability problems, especially in the case of tunnels with overburden of small thickness.

On the contrary, the Lower unit (usually stiff marls to clayey marls with thin coarse grained intercalations) is practically considered as impermeable and cohesive formation, which generally demonstrates uniform and very good geomechanical behaviour during the construction of underground works. It is pointed out that, this formation is distinguished for its dense bedding, which at places becomes foliar. This positively acts in conditions of regular moisture content (increased cohesion) and negatively when this formation is saturated, where the absorbed water in their structure leads progressively to collapse. This is mainly observed when the Lower unit formations are constantly watered in depth from overlying permeable layers of the Upper unit, as well as along structural discontinuities (faults and fractures).

4. Conclusions-Results

Based on the evaluation of all collected data, the following conclusions can be made:

- The discrimination of individual units was achieved in all borehole logs examined. Moreover, in some of the logs the limits between the units are not clear, due to the presence of an intermediate transitional zone of small thickness.
- The formations of Lower unit, as well as those of the transitional zone present high cohesiveness and characteristic bedding with frequent alternations of layers, which makes the discontinuities intersecting the formation visible. So, normal and reversed faults were observed due to tensile and compressive stresses on these sediments. On the contrary, these characteristics do not exist in the

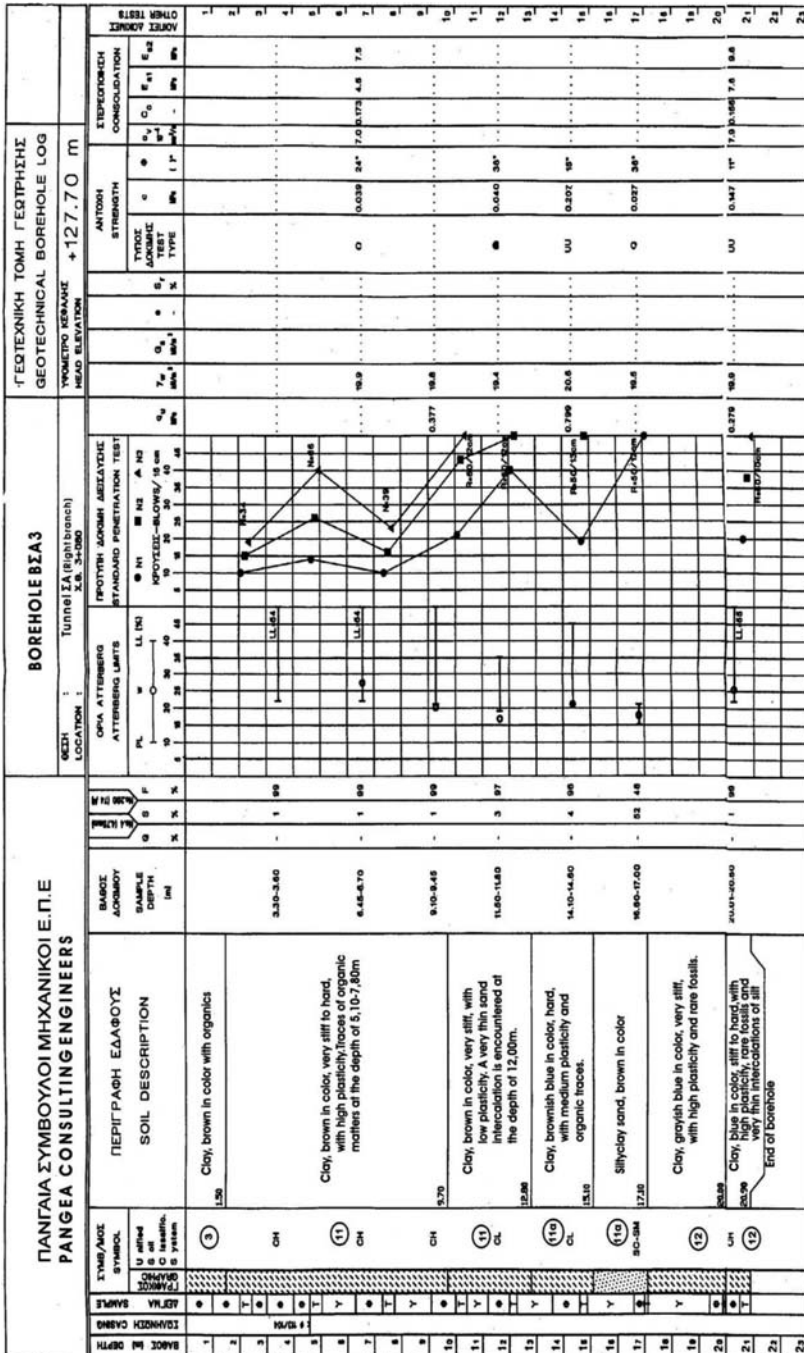


Fig. 1: Indicative record of a geotechnical borehole log, in which the geotechnical units, based on the relevant map, were separated.

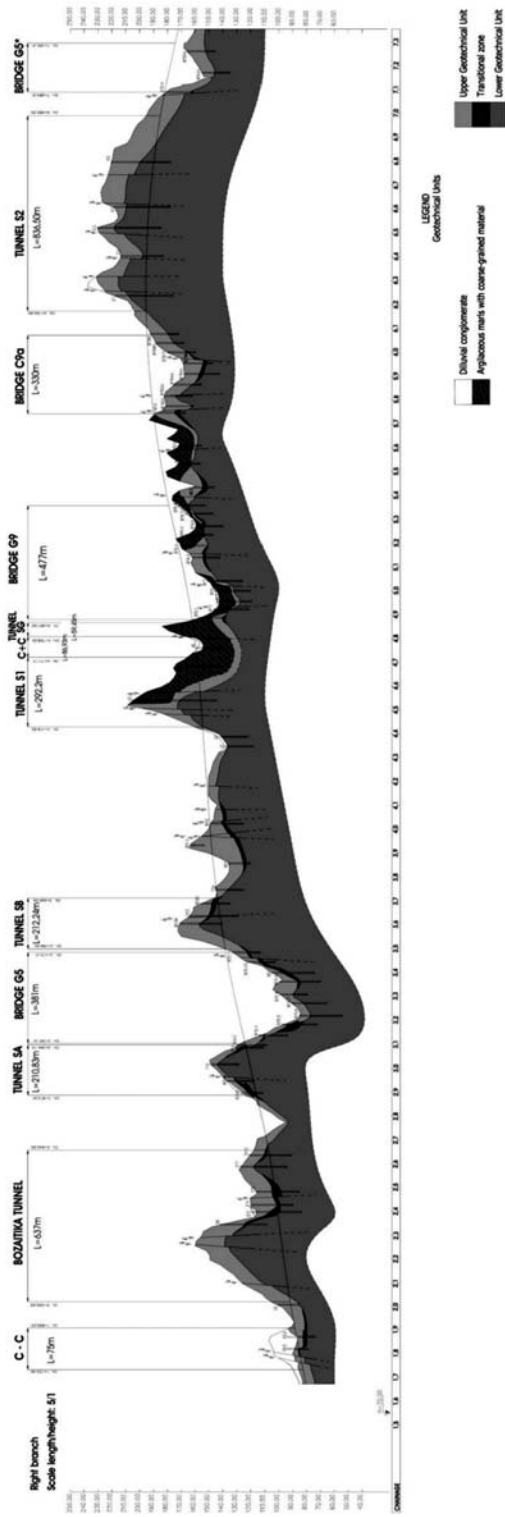


Fig. 2: Geotechnical cross section of the right branch of Patras Ring Road with the various underground works (Ch. 1+500 to Ch. 7+300).

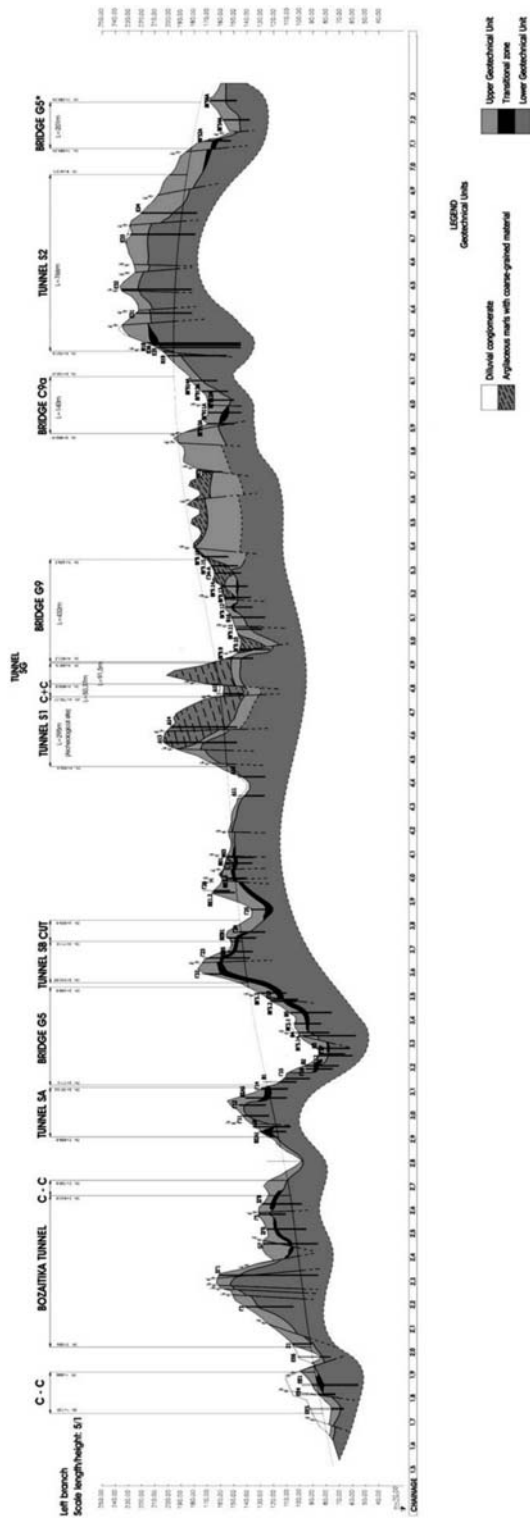


Fig. 3: Geotechnical cross section of the left branch of Patras Ring Road with the various underground works (Ch. 1+500 to Ch. 7+300).

Upper unit, due to its lithology and cohesiveness.

- There was an absolute match of the surface mapping observations with data from boreholes, which confirmed the presence and the segregation of the two units. Thus, this discrimination reflects both the surficial and the in-depth growth of the units, facilitating the confrontation of the geotechnical problems, which can arise during construction of technical works.

Based on all the above peculiarities, it is obvious that every further research for technical works under design should be focused on a detailed imprinting of these formations, both surficially and in-depth. This will also enable the evaluation of their individual characteristics. With the confirmation and acceptance of this consideration and based on the fact that the Pliopleistocene sediments and in general the Neogene sediments in many regions of the Greek territory present an equivalent structure (in terms of lithology and stratigraphic sequence), it would be useful the geological and geotechnical research to be conducted towards this direction from the initial stages of the design. In this way the potential geotechnical problems will be pointed out at the early stage of the design, resulting to most optimal planning of technical works.

5. References

- Attewell, P.B. 1993. Tunnelling and site investigation. Proc. of Int. Symposium on Geotechnical Engineering of Hard Soils – Soft Rocks, Athens. Balkema Rotterdam.
- EFPALINOS TECHNIKI, (1996). Patras Ring Road (RPP). Final design of Mpozaitika tunnel. *Unpublished reports, Athens.*
- EDAFOMECHANIKI (1995, 1997, 1998). Patras Ring Road (RPP). Geotechnical investigations for the twin tunnels in Mpozaitika site “Agia Barbara”. *Unpublished reports, Athens.*
- KASTOR (1998, 1999). Patras Ring Road (RPP). Geotechnical investigation and design of twin tunnels in Archaeological and Girokomion sites. *Unpublished reports, Athens.*
- Koukis, G., Rozos, D., 1990. Geotechnical properties of Neogene sediments of the NW Peloponnesus Greece. Proc 6th Int. IAEG Congress, Amsterdam p405-412. Balkema, Rotterdam.
- Koukis, G., Sadatakakis, N., Tsiambaos, G. and Katrivesis, N., 2005. Engineering Geological approach to the evaluation of seismic risk in metropolitan regions: case study of Patras, Greece. *Bull. of Eng. Geol. and Environment*, 64:p219-235.
- Kouki A. 2006. Engineering geological – geotechnical parameters and mechanical behavior of hard soils and soft rocks in the design of underground works. Unpublished PhD Thesis (in Greek, with extensive summary in English). *University of Patras, p.414.*
- Kouki, A. and Rozos, D. 2010. Engineering geological – geotechnical conditions in the wider area of Patras Ring – Road. Compilation of the relevant map at a scale of 1:5000. Bulletin of the Geological Society of Greece - 12th International Congress, Patras, Greece (in press).
- OMETE (1998). Patras Ring Road (RPP). Primary support design of the twin tunnels in Archaeological and Girokomion sites. *Unpublished reports, Athens.*
- PANGEA (1998,1999, 2001). Patras Ring Road (RPP). Primary support design of the twin tunnels SA, SB and SG. *Unpublished reports, Athens.*
- Rozos, D. 1998. Engineering Geological conditions in Achaia County. Geomechanical characteristics of Plio-pleistocene sediments. PhD Thesis (in Greek, with extensive summary in English)., University of Patras, 453p. Rio Patras.
- Tsiambaos, G., Koukis, G., 1990. Geotechnical conditions of the Iraklion city, Crete. Proc 6th Int. IAEG Congress, Amsterdam V3, p2037-2042. Balkema, Rotterdam.

ENGINEERING GEOLOGICAL – GEOTECHNICAL CONDITIONS IN PATRAS RING ROAD WIDER AREA, GREECE. COMPILATION OF THE RELEVANT MAP AT SCALE OF 1:5000

Kouki A.¹, Rozos D.²

¹ Ministry of Public Works, EYDE – Motorway PATHE, Alexandras Av. 205, Athens, Greece,
kouki.nassia@gmail.com

² National Technical University of Athens, School of Mining and Metallurgical Engineering, Laboratory of
Engineering Geology and Hydrogeology, 9, Heroon Polytechniou Str 157 80, Zografou (Athens) Greece,
rozos@metal.ntua.gr

Abstract

In order to evaluate the geotechnical parameters and the mechanical behavior of the Plio-Pleistocene sediments encountered along the Patras Ring Road, the lithology, the structure, the hydrogeological regime, the hydro meteorological data and the seismicity of the wider area were firstly examined.

More specifically, the morphological relief map and the map of slope inclination were compiled on the digitized topographic map, along with the engineering geological – geotechnical map of the area, at a scale of 1:5000, where the distinction of the Plio-Pleistocene deposits is shown. This distinction was based on geological criteria, as far as lithology and stratigraphic sequence are concerned, as well as on engineering geological – geotechnical criteria.

Key words: Patras Ring Road, Pliopleistocene sediments, Geotechnical units, Eng. Geological – Geotechnical mapping.

1. Introduction

Regarding the mechanical behavior of the geological formations that belong to the category of “Hard Soils – Soft Rocks”, the Plio-Pleistocene sediments of Achaia were studied, focusing on the area of Patras Ring Road (Kouki, 2006). The above formations have also been studied in the past, respecting their geological, engineering geological and hydrogeological features, (Doutsos et al, 1987, 1988; Rozos, 1989; Kontopoulos & Zelilidis, 1992, 1997; Voudouris, 1995; Tsiambaos et al, 1997; Koukis et al, 2005, 2007).

The investigation of these formations is of great importance, as there was no previous experience on tunneling through them. Therefore, data from the geological and geotechnical reports for the project were used, along with field investigation and the detailed engineering geological and geotechnical mapping. All data helped to have a general view and a good approach of these formations and led to the division of their fine grained facies into two separate Geotechnical Units, the Upper and the Lower one. These Units are characterized by their different lithology, mineralogical composition, physicommechanical features and mechanical behavior.



Photo 1: General view of the Plio-Pleistocene sediments in the hilly area behind the bridge Γ5. The Alpine formations are visible in the upper part of the photo (Panahaikon Mountain).

2. Location and geomorphologic setting of the study area

The wider study area is located at the NW part of Achaia County, with an average elevation of 600m and an average slope inclination between 6.0 and 15.5%. The morphological relief is a result of combined action of lithology, tectonism, weathering and erosion processes. Especially, the present morphology of the area has been formed by post-Alpine tectonic movements, as well as the evolution of the various morphological cycles, that continue to the present time.

Geologically, the wider area consists, from the west to the east, of formations of Gavrobo-Tripoli and Pindos Geotectonic zones. The hilly areas that surround the high mountains consist of post-alpine sediments. The summits of these hills are usually round-shaped and not sharp-shaped, indicating intense erosion processes (Photo 1).

Hydrographic network has been developed as a result of combination of lithological features, tectonics and morphology, as well as climate. It is mainly oriented along main faults zones.

The engineering geological map of Figure 1 shows, in more detail, the geological conditions along the alignment. It can be concluded that the Ring Road is mainly founded on Plio-pleistocene sediments, coarse and fine – grained and less on Quaternary deposits. The later can be divided into mixed-phase loose, loose mainly coarse-grained, coherent coarse-grained and mixed-phase coherent formations.

After revising and processing of aerial photos and field investigation it was concluded that the main faulting directions are NE-SW and NW-SE.

Due to the tectonic activity, the area is characterized by intense seismicity. The most recent earthquakes of the broader region are the earthquake of Alkyonides in 1981 ($M_s=6.7$) and of Aigion in 1995 ($M_s=6.2$). These magnitudes are relatively high and since they are close to the study area, it is possible that future earthquakes can cause there damages (Sokos, 1998). It is noted that Achaia belongs, according to the Greek Seismic Code (NEAK, 2004) to the zone of seismic hazard II ($a=0.24g$)

3. Hydro meteorological data – Hydrogeological regime

For the investigation of distribution and fluctuation of climatic parameters, meteorological data from the National Meteorological Service were used and especially data from Patra's station, covering the period 1931-2004.

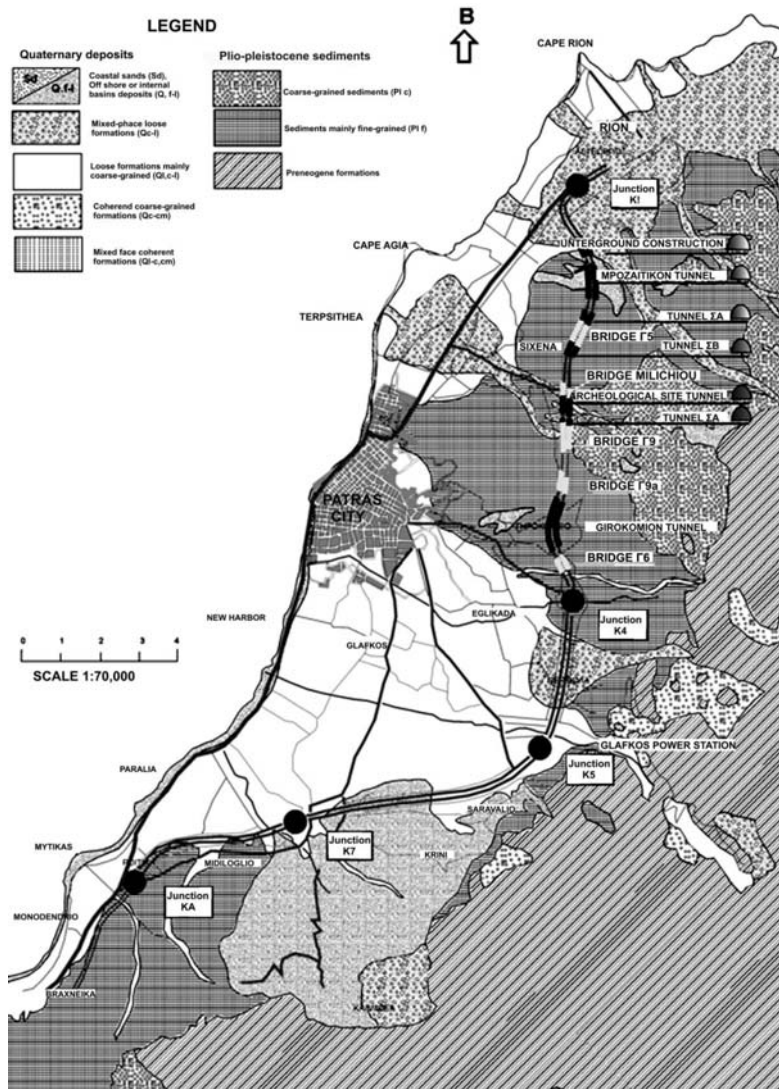


Fig. 1: Engineering geological map of Patras Ring Road wider area.

The lower temperatures dominate during the winter (10,6°C) and the higher during the summer (25.8°C), while autumn temperatures are about three degrees higher than those of spring period.

Annual rainfall heights show large fluctuation from 350mm in dry periods (e.g. 2000) to 1350mm during wet periods, such as 1993 or 2003. Based on these data and the fact that these geological formations are susceptible to erosion, it is concluded that it is the combined effect of thermal weathering and mechanical erosion that causes further loosening and strength reduction. This leads to locally unstable conditions and the manifestation of landslides.

From the hydrogeological point of view, the geological formations were divided into different categories, according to their estimated permeability. They were classified as pervious (e.g. loose Qua-

ternary deposits), permeable with secondary porosity (Karstic limestones), semi-pervious (Plio-pleistocene sediments, coarse-grained, Plc and fine-grained, Plf), and impervious (Flysch and Cherts).

According to the above and by taking into account the possible effects on the Ring Road construction, special attention was given to the Plio-Pleistocene sediments, because the majority of underground excavations took place in these formations. In Plc formations the lithology and stratigraphy result to the creation of aquifers and springs of medium to high discharge, located along the contacts of pervious and impervious beds. In Plf sediments, successive confined or perched aquifers are formed, usually inside coarse lenses. These conditions caused, in some cases, water flow during underground excavations, but the typical clayey and marly facies of these sediments are considered as impervious formations.

Furthermore, after analysis of piezometric curves in the lowland areas it was concluded that even in the most permeable alluvial deposits the water table was very low, so groundwater could not affect the Ring Road.

4. Engineering Geological – Geotechnical mapping at 1:5000 scale

After scanning of the hardcopy map, digitizing was performed in GIS environment. Digital data, such as elevation contours every 20m, rivers, inhabited areas, as well as Ring Road alignment was classified in thematic layers. All data were projected to the Greek Grid (ΕΓΣΑ 87).

Based on the alignment final design drawings two cross-sections along the road axis were drawn at a scale of 1:5000 (length) and 1:1000 (height) that correspond to the left and right branch (Kouki, 2006; Kouki & Rozos, 2010).

By using the digitized maps, Digital Elevation Models and slope maps were created. These maps show that the Road crosses areas with fully developed hydrographic network, with main directions perpendicular to the alignment. The elevation ranges from 20 to 240m. The greater part of the road crosses relatively plain areas (inclined up to 10°), while the underground works are located in areas of intense relief (inclination from 10° up to more than 30°).

From geological point of view, these Plio-pleistocene sediments have been so far presented in the IGME Geological Sheets of Nafpaktos, Patras and Chalandritsa at a scale of 1:50,000 (IGME, 1971, 1980, 1984), while their engineering geological properties are described by Rozos (1989) and Kouki (2006). The geological and geotechnical studies that were conducted before and during the project of Patras Ring Road did not further divide these sediments. Their geotechnical assessment was based on the results of soil classification tests and data from numerous boreholes, drilled for this purpose.

The present study was focused on the Ring Road wider area, first of all through the engineering geological mapping, using topographical maps at a scale of 1:5000. Previous data was taken under consideration (Rozos, 1989, Koukis and Rozos, 1990; Rozos et al, 2006), as well as data from the 169 boreholes drilled along the project (Kouki, 2006). Mapping was assisted by aerial-photo interpretation, using recent (2002) large-scale aerial photos (at a scale of 1:5000).

The legend of the map provides a rather comprehensive description of the geological formations (Kouki, 2006), as far as lithology, sedimentation type, distribution of different soil facies, degree of diagenesis and cohesiveness, type of soil matrix, color, permeability, as well as fracturing and weathering degree are concerned. Based on the above geological and geotechnical criteria. and the experience gained from the construction of the project, there was a distinction of the fine-grained facies

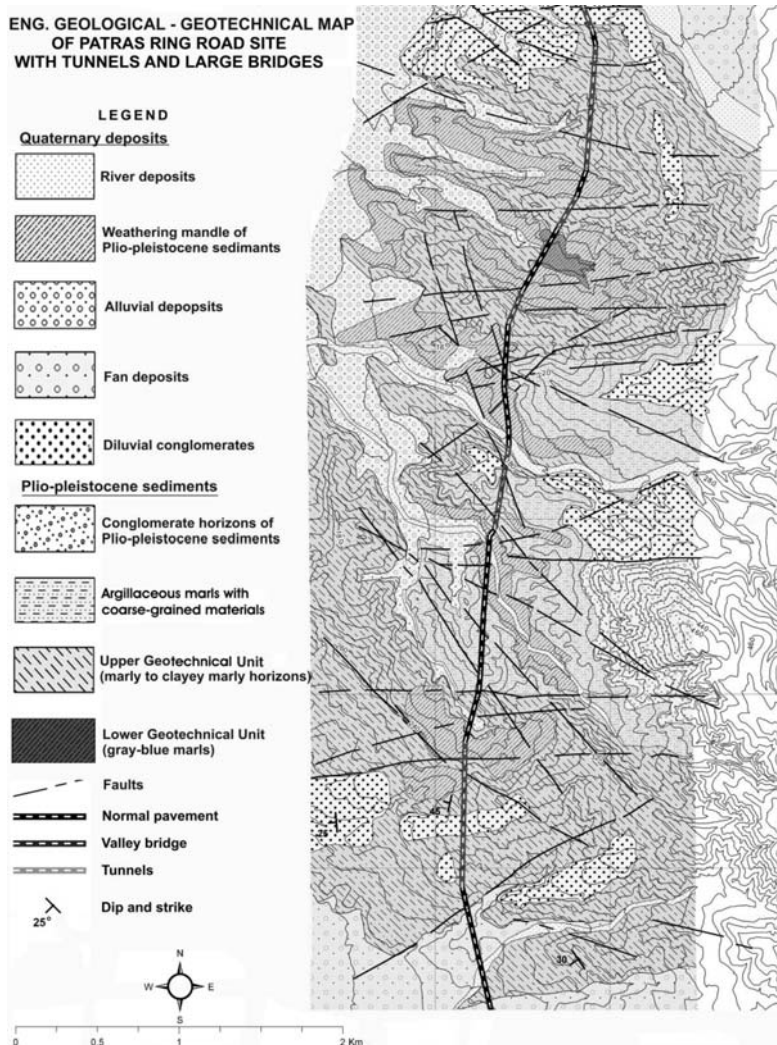


Fig. 2. Engineering Geological - Geotechnical map of Patras Ring Road site.



Photo 2: South part of Girokomion tunnel ($\Sigma 2$), right branch. The Diluvial conglomerates cover with unconformity the Upper Geotechnical unit.



Photo 3: Exit of SG tunnel. Stratigraphic column of the Upper Geotechnical Unit at the base, overlaid by conglomerates with distinct bedding (Unit of Argillaceous marls with coarse-grained material).

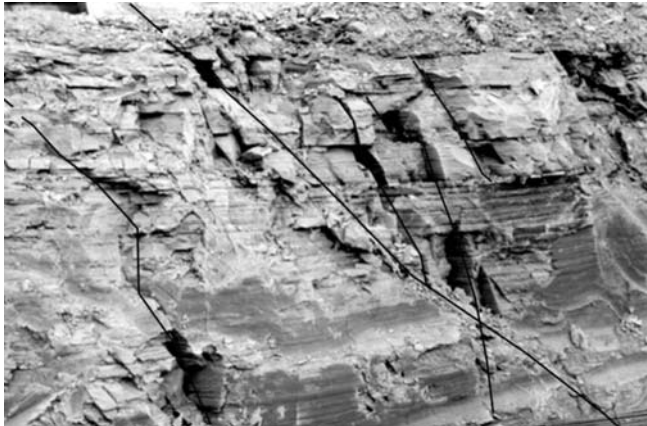


Photo 4: Gray-blue marls horizons of the Lower Geotechnical unit at a slope near a Cut & Cover at the exit of Bozaitika tunnel. The almost horizontal layers and the high fracturing of these weak rocks are shown. The fracturing is due to joint sets almost vertical to the bedding.

of the Plio-pleistocene sediments into two geotechnical units, the Upper and Lower one. In Figure 2, a simplified version of the engineering geological - geotechnical map is given.

It is concluded that the project is mainly hosted in the fine-grained Plio-Pleistocene sediments (Upper and Lower Geotechnical units). Also, a part of it was constructed in the argillaceous marls with coarse grained materials, while the first Cut and Cover of the project in the diluvial conglomerates (Photos 2, 3 and 4).

It is pointed out that the Lower Geotechnical unit appears only in a few places and it would not have been recorded unless it was met during underground excavations. It should be mentioned, that dur-

ing the geological and geotechnical investigations prior to construction, the Plio-Pleistocene sediments were studied geotechnically as a whole, without any further subdivision.

More specifically, the Upper Geotechnical unit is characterized by frequent alternations of brown-yellow to brown-gray clayey marls, sandy marls, sandy silts, sands and sandstones. The Lower unit consists of beds of gray-blue marls, usually stiff, clayey marls with some sparse coarser phases, mainly sands or sandy silts. Problems that are connected to the Upper unit can be attributed to this alternation of horizons with different lithology, cohesiveness, fracturing and weathering degree, as well as permeability. On the contrary, the Lower unit is considered to be an impervious and very cohesive formation, with homogenous and generally very good mechanical behavior during underground excavations.

5. Conclusions – Results

This paper studies the Plio-Pleistocene sediments in the area of Patras Ring Road in Achaia, Greece. It aims to a better knowledge of their mechanical behavior and response during the construction of engineering works of large scale and particularly underground ones.

The area that these formations cover is generally hilly, while the mountainous areas that surround them consist of Alpine bedrock rocks, (i.e. formations of Olonos - Pindos and Gavrobo –Tripoli Geotectonic Zones).

The investigation of these Plio-Pleistocene sediments, which are geomechanically classified as “Hard Soils-Soft Rocks”, was based on their surface appearance and on samples from numerous boreholes. This resulted to the division of their fine-grained facies into two separate Geotechnical units, the Upper and the Lower one, with a Transitional zone between them at places. Both units are characterized by their different lithology, mineralogical composition and physicommechanical properties. It is noted that for the design of Patras Ring Road, the two units, Upper and Lower one, were not dealt as distinct formations with different geotechnical behavior, but were considered as a uniform one.

Aiming to a better understanding of the extent of both units and the importance of their distinction for the design of underground works, engineering geological mapping at a 1:5000 scale was performed. Their vertical extent was presented in two geotechnical cross-sections along the alignment of each branch, including faults and the Transitional zone. The Upper unit formations can cause problems during construction, due to their frequent alternation of different lithological types, fracturing, weathering, as well as due to their locally increased permeability. On the contrary, the Lower unit is an impervious and very cohesive formation, with very good behavior during tunnel excavation and construction. The problems related to this unit are basically located in areas where the formations are saturated (mainly along fault zones), which leads progressively to the loosening of their structure.

6. References

- Doutsos, T., Kontopoulos, N., Frydas, D. 1987. Neotectonic evolution of the north-western continental Greece. *Geol. Rundsch.*, 76/2, Stuttgart. pp. 433-450.
- Doutsos, T., Kontopoulos, N., Poulimenos, G. 1988. The Corinth – Patras rift as the initial stage of continental fragmentation behind an active island arc (Greece). *Basin Research*, 1, pp.177-190.
- IGME, 1971. Geological map of Greece at a scale of 1:50,000, “Nafpactos sheet”.Athens.
- IGME, 1980. Geological map of Greece at a scale of 1:50,000, “Patras sheet”.Athens.

- IGME, 1984. Geological map of Greece at a scale of 1:50,000, "Chalandritsa sheet". Athens.
- Kontopoulos, N., Zelilidis, A. 1992. Upper Pliocene lacustrine environments in the intramontane Rio graben basin, NW Peloponnesus, Greece. *N.Jb.Geol.Paläont.Mh., H.2, Stuttgart*, pp.102-114.
- Kontopoulos, N., Zelilidis, A. 1997. Depositional environments of the coarse-grained lower Pleistocene deposits in the Rio – Antirio basin, Greece. *Proc. Int. Symposium on Engineering Geology and the Environment, IAEG, Athens. vol.1, Balkema, Rotterdam*.
- Kouki A. 2006. Engineering geological – geotechnical parameters and mechanical behavior of hard soils and soft rocks in the design of underground works. PhD Thesis. In Greek, with extensive summary in English. University of Patras, p.414.
- Koukis, G., Rozos, D., 1990. Geotechnical properties of Neogene sediments of the NW Peloponnesus Greece. *Proc 6th Int. IAEG Congress, Amsterdam p405-412. Balkema, Rotterdam*.
- Koukis, G., Sabatakakis, N., Tsiambaos, G. and Katrivesis, N., 2005. Engineering geological approach to the evaluation of seismic risk in metropolitan regions: case study of Patras, Greece. *Bulletin of Eng. Geol. and Environment*, 64: p 219-235.
- Koukis, G., Sabatakakis, N., Lainas, S., 2007. Soil suitability estimation for housing purposes in landslide – prone areas. The case of Karya village, Patras, W. Greece. *Bulletin of the Geological Society of Greece, Proc. 11th Int. Congr., vol. xxx, 1683-1694*.
- National Meteorological Service, 2004. Climate data from Patra's station for the period of 1931-2004, Athens.
- NEAK, 2004. New Hellenic Anti-Seismic Code, Athens.
- Rozos, D. 1998. Engineering Geological conditions in Achaia County. Geomechanical characteristics of Plio-Pleistocene sediments. PhD Thesis (in Greek, with extensive summary in English). University of Patras, 453p. Rio Patras.
- Rozos, D., Koukis, G., Sabatakakis, N., 2006. Large scale engineering geological map of the Patras city wider area, Greece. *The Geological Society of London, IAEG 2006, paper no 241*.
- Sokos, E. 1998. Strong ground motion synthesis at the city of Patras. PhD Thesis, University of Patras.
- Tsiambaos, G., Sabatakakis, N., Koukis, G., 1997. Engineering geological environment and urban planning of the city of Patras, Greece. *Proceedings of the Int. Symp. of Eng. Geology and the Environment, Athens, 23-27 June, vol. 3:1527-1534*.
- Voudouris, K. 1995. Hydrogeological conditions of the NW part of Achaia Province. PhD Thesis, University of Patras.

THE ANTHROPOGENIC CHANGES IN THE GEOLOGICAL ENVIRONMENT IN THE SOUTH OF EAST SIBERIA

Kozyreva E.A., Khak V.A.

Institute of the Earth's Crust Russian Academy of Sciences Siberian Branch, Laboratory of engineering geology and geoecology, Lermontov Street 128, 664033 Irkutsk, Russia, kozyreva@crust.irk.ru, khak@crust.irk.ru

Abstract

The investigation results of the geological environment's condition in an areas marked by high anthropogenic load are described in this paper. In the southern East Siberia the strategy of key sites monitoring is used for this purpose. The selection of key sites is determined by the specific character of geological environment, as well as by the intensity and relationships of developing geological processes. In the studied territory the great variety of exogenic processes can be observed, the majority of them being activated by technogenic factors. To the inherited processes the gravitation, cryogenic and those induced by surface and subsurface water activity belong. In order to estimate the actual condition of the territories and to ensure the undisturbed exploitation of engineering structures, the specific features of lithosphere, the development of exogenic geological processes and the evolution of the anthropogenesis should be taken under consideration.

Key words: *geodynamical territory conditions, engineering structure influence area, inherited exogenic geological processes, karst landslide deformation, abrasion-accumulation process, processes interaction*

1. Introduction

Over the last 100-year period the role of human activity in the detrimental influence on the environment substantially increased, that is expressed as transformation of the natural conditions. The development and use of new technologies and engineering structures presents the definite intrusion into the laws of nature. The complicated relationships between the technical objects and the natural conditions manifest themselves in the form of radical changes in the geological environment, influencing the character of development of exogenic geological processes.

The southern area of East Siberia has experienced a series of growing anthropogenic activities during the history of the economic development of the region. Growing population, big cities with diverse infrastructure, exploitation of the Angara cascade hydro-electric stations with large artificial water reservoirs are the considerable contributors to activation of and origination of additional processes in the territory. The inherited geological processes are processes which were engendered in different geological environment and currently are labilized in connection with change of conditions (including anthropogenesis) (Trzhtsinsky et al., 1999).

Big industrial cities of the region such as Irkutsk, Angarsk, Bratsk, Ust-Ilimsk and Usolie-Sibirskoye are located primarily in the south of the territory (Fig. 1). The biggest part of population (~88%) ag-

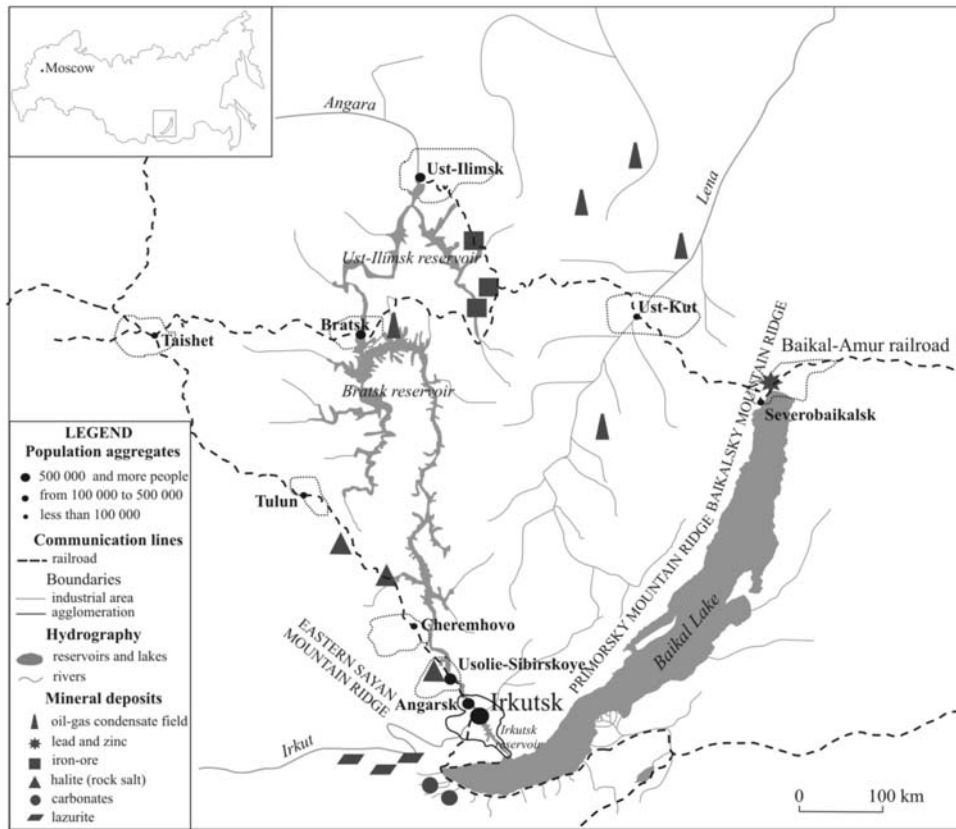


Fig. 1: Location of the study area, showing the basic elements of anthropogenic load.

glomerates in this area, with the residents numbering about 0.6 mln. in Irkutsk, 0.25 mln. in Angarsk, 0.25 mln. in Bratsk, 0.1 mln. in Ust-Ilimsk and 0.1 mln. in Usolie-Sibirskoye; according to the census conducted in January 1, 2005. The industrial development of cities tends to concentrate near the transport ways such as the Trans-Siberian railway and the western part of the Baikal-Amur railway which bind the described region with the European territory of Russia (The general characteristic..., 2005).

In the territory of East Siberia the mining industry (coal, native gold, iron, salt, building materials etc.) develops over the long time; its detrimental effect on the geological environment manifests itself primarily in the form of damage to the morphometric characteristics of the land surface and the tension of soil.

The construction and exploitation of hydro-electric power plants (HPP) on the Angara-river such as the Irkutsk HPP (since 1962), Bratsk HPP (1967) and Ust-Ilimsk HPP (1977) with their water storage reservoirs have radically changed the geological environment of southern East Siberia. The changes occurred in the form of activation of inherited exogenic geological processes, and the origination of a new phenomenon (formerly not typical of the area), i.e. the change of shores. Abrasion of reservoir shores accompanied by other genetic group of processes benefits to the formation of various shore types (Kozyreva et al., 2004).

2. Brief historical view of the southern East Siberia; the geological setting of the territory

The evolution of the anthropogenic load on the environment of Siberia is to a large extent associated with the history of its colonization by Russian people. The troops of Russian Cossacks fought their way to Siberia, being often attacked by Siberian nomadic tribes. After the defeat of the Siberian Khanate (the Tatar Principality that existed in West Siberia in 16th century), the territory of Siberia became a part of Russia. Within the history of Siberia, the territory of southern East Siberia belongs to the regions of large economical and administrative importance. In 1620, the first settlement of Irkutsk was founded on the left shore of the Irkut-river. The period of 1625-1650 was marked by the intensive economic development and the population of the territory was stimulated by the search for minerals (silver, gold etc.). In the course of time, the temporary Siberian settlements became the large towns. Irkutsk was built at first as a stockaded town (1652), since 1661 Irkutsk has the statute of the city. The growing population, intensive commercial development of mineral deposits benefited to increasing of the importance of Irkutsk and other Siberian towns (Brief Siberian chronicle, 2003).

The southern area of East Siberia occupies the considerable part of Siberian platform and the Baikal rift zone. The region is marked by continental climate, composite geological structure, specific geomorphologic features, permafrost and high seismicity (up to M9); all these features attribute to specific engineering-geological conditions of the region. The Siberian platform's base has the two-stage structure, the lower stage being presented by metamorphic and igneous rocks of Archean and Early Proterozoic. The sedimentary cover of the platform is marked by three structural stages of sedimentation: 1) Lower Middle –Paleozoic, 2) Upper Paleozoic-Mesozoic, and 3) Cenozoic. During Perm and Triassic periods, the active volcanic and magmatic processes stimulated the development of extensive trappean formations in the platform area (Trzhtsinsky et al., 2007). The south-eastern area of Siberian platform abut on the Lake Baikal is marked by high seismicity, whose age ranges from Archean to Quaternary, with dominating occurrence of granitoides.

3. Methods

The estimation of geodynamical condition of the territory is based on both the qualitative and quantitative analysis of the dynamics of most typical exogenic geological processes. The quantitative characteristics (such as degree of land damage by exogenic processes, depth of effects and intensity of processes etc.), identify the changes that occur within the rock massif and the ecological-geodynamical trends in the development of investigated territory. Our investigations revealed the most important factors that influence the dynamics of exogenic geological processes with the purpose to determine the access to their monitoring.

The strategy of comprehensive survey and standard computer programs were used for the first time for investigation of shore areas of artificial reservoirs; currently this strategy is used also in other key sites of investigations in East Siberia.

The methodology of investigation comprises 3 procedures: 1) selection of the key site for investigation using the data on the general trends of development and activation of geological processes in the areas of influence of engineering structures in different periods of time; the analysis of conditions and factors responsible for development of sub-systems prior and after the construction of engineering structures, and the interpretation of airphotos; 2) monitoring and topographic survey in the observation sites; 3) the analysis of investigation data and construction of 3-dimensional cartographic models to define the qualitative and quantitative relationships within the geo-system.

The comparative analysis of models provides the estimation of the character of processes, compar-

ison of their dynamics in the context with the natural and anthropogenic factors, and the definition of relationships between the system elements and influence of the factors upon the development of the whole system and each particular element.

Currently, the GPS-technology of survey is used in kinematic regime in key sites of shore areas of reservoirs. This provides the efficient processing of field data for the estimation of quantitative characteristics of exogenic geological processes. In the laboratory, the digital 3-dimensional cartographic models of particular sites, the composite index maps and the maps of engineering-geological zoning of the territory are prepared.

4. Exogenic geological processes as the indication of development of the territory

In the territory of southern East Siberia, a great variety of exogenic processes can be observed; the majority of them are labilized naturally, or have the anthropogenic analogs. To the inherited processes belong the gravitational, cryogenic and those induced by the action of surface and subsurface waters.

The areas of developing exogenic processes are marked by different potentials of geodynamical hazard and social-economical risk. This is determined primarily by quantitative and qualitative characteristics of process development, as well as by the extents of economical development and population of the territory. This paper deals with the processes of wide occurrence, and particularly those marked by grave consequences.

In the course of construction of the Baikal-Amur railroad, the friable frozen rocks such as component moraines were stripped on a number of hillsides due to the slope undercutting and construction of embankments. Deposition of warm soil during the construction of the railroad embankment initiated the defrosting and degradation of frozen layer, which entailed the origination of landslide distortions ranging from typical solifluction to fluid soil creep and formation of rotational slides.

The degradation of permafrost is accompanied by formation of the water bearing stratum confined to permafrost, which drains in the area of embankment base as numerous springs scattered over the slope area. In some slopes with steep benches, the inundation of the friable sandy-argillaceous rock formations underlying the water-bearing stratum, initiates the fluid soil creep, in places together with shrub and small trees, resulting in formation of typical hummocky land with sliding forest.

The occurrence of permafrost is the determining factor of the peculiar character of the territory. In the context of economical development of the region, the varying conditions of heat exchange on the land surface stimulated the degradation of permafrost and activation of cryogenic processes (such as icing, thermokarst, thermoerosion, solifluction, frost heave etc.). Besides, the presence of hydrophilic argillaceous rocks within the terrigene deposits benefited to the origination of landslide. The cutting of slopes or deep steep-sided excavation present the real cause of considerable technogenic deformations. As the case, the Kazankan landslide area can be cited, where a definite part of the railroad was laid on the sand and sandy-loam moraine deposits at the south-eastward slope (12-17°), of the North-Muya ridge; in the case of inundation the deposits assume the features of plasticity and thixotropy (Geology and seismicity of Baikal-Amur railroad zone, 1985). At the 15-20% moisture, the slopes creep even at a small load or shake (Fig. 2).

In the territories of negative relief the construction and exploitation of the railroad bridges induced the intensive development of deformations that entailed the displacement of the roadbed towards the valley of the Muiyakan-river. To improve the situation, the whole bridge structure was shifted for 15-

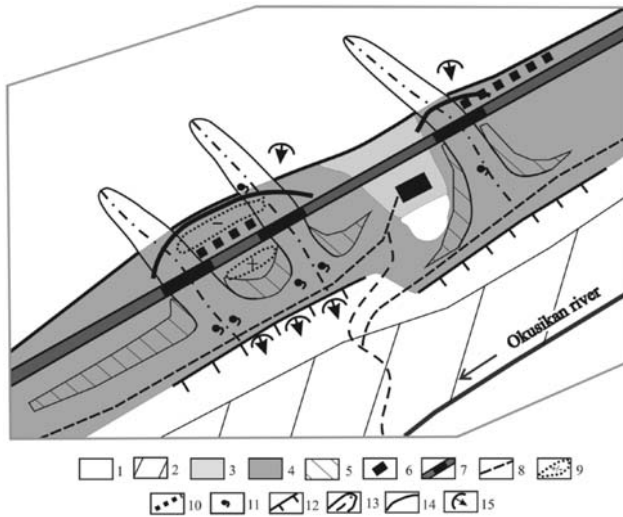


Fig. 2: Diagrammatic plan of Kazankan site: 1 – natural slope; 2 – accumulative terrace of Okusikan river; 3 – outlier of moraine; 4 – zone of railroad construction; 5 – steep slopes; 6 – station; 7 – railroad bed with bridges; 8 – roads; 9 – zone with positive (negative) amplitudes of horizontal deformations; 10 – culvert; 11 – spring; 12 – steep benches; 13 – ravines with steep thalwegs; 14 – rotational slides; 15 – small landslide body.

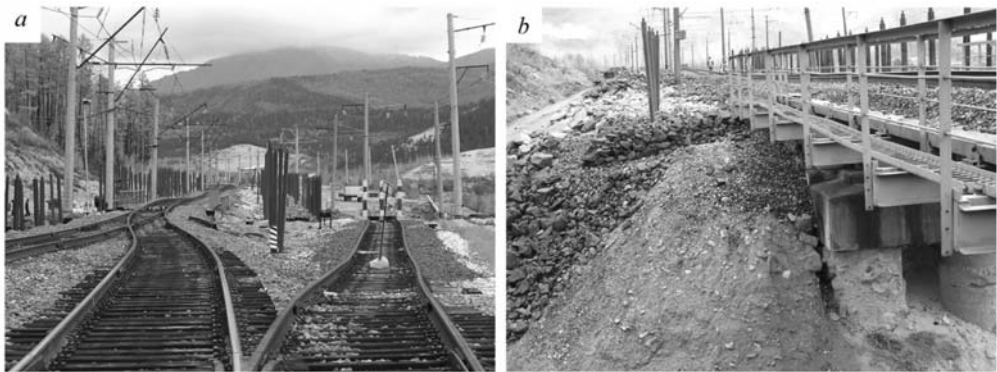


Fig. 3: (a): The railroad section displaced along the lines of the river valley, as a result of the slope deformations; (b): The open fissure in the abutment of the bridge.

20 meters towards the mountain slope (Fig. 3a). This measure, however, did not solve the problem as the displacement of the bridge structure proceeded. This was evidenced by the manifestation of fractures 15-18 m in length, up to 6 cm in width and with up to 20 cm visible depth in the mountain slope along the roadbed. Besides, the open fissures appeared in the abutment of the middle and the eastern bridges; in the base of abutment of the middle bridge the cavities appeared as the consequence of soil subsidence (Fig. 3b).

The thickness of sliding body is determined by the thickness of the defrosted zone. The upper border of the permafrost layer lying in a depth of 6-8 m, serves as the impermeable bed of the aquifer, confined to sandy-loam intercalations whose inundation benefits to formation of the slide zones.

In the case described, the relationships between two engineering-geological phenomena are discussed: 1) the degradation of frozen rocks, and 2) the landslide dislocations. The permafrost degradation was concerned as the primary phenomenon, and the landslide dislocation as the secondary. At present, however, the main hazard of the roadbed deformation and shifting of bridges is menaced by landslide, i.e. there is a direct evidence of the synergetic effect of both phenomena.

The karst process in the described territory is due to the occurrence of carbonate and sulphate deposits in ~40% of its area. Development of karst occurs both in the sedimentary deposits of carbonate and gypsiferous rocks of Cambrian and Ordovician, and in the deeply metamorphosed carbonate layers of Archean and Proterozoic. According to the lithologic features of karsting rocks, the occurrence of carbonate, sulphate and sulphate-carbonate karst is recorded, with domination of carbonate karst bound up with limestones and dolomites of Cambrian and Ordovician. However, the largest technogenic effects are attributed to the activation of sulphate karst process which is typical of the Angara-Lena region and is bound up with gypsum anhydrite rocks of Middle-Lower Cambrian and the lows of Verkholsk Suite of Upper Cambrian.

The anthropogenic changes in the character of process development manifest in larger extent within the influence zone of southern area of Bratsk reservoir, where the sulphate-carbonate deposits occur at absolute elevation marks of 380-400 m. For example, these changes occur in the zones of variable water saturation, and in the top area of the zone of complete water saturation, which provides the high rate leaching and karst activation in the reservoir's backing zone. Below the 10 m-thick layer of Quaternary deposits, the presence of karst forms was plotted. With the aid of symmetrical electro-profiling (SEP) the occurrence of inherited karst was revealed. By drilling, the karst cavities of different depth (up to 63 m) filled with wet loose material of high capacity were found.

The comparison of karsting gypsa and dolomites in laboratory and in situ revealed that the annual rate of gypsum bleaching in the studied region is 0.02-0.08 mm, which is by 2-3 orders of magnitude higher than that of dolomite (Filippov, 1988). So, the sulphate rocks are most susceptible to variations of hydrodynamical conditions, typical of the backing zone of Bratsk reservoir, whose amplitude of water level fluctuation is 10 m, as recorded during the 40-year period of reservoir exploitation.

In the course of exploitation of the reservoirs, the rates of karst development rose by one order of magnitude. So, the territories defined as formerly stable and low-stable (marked by formation of 0.01-0.1 karst hole/km² annually) are actually defined as unstable (with annual caving 0.1-1.0 karst hole/km²) and greatly unstable (with annual caving of 1.0-10.0 karst hole/km²). The zone of eventual activation of the gypsum karst incremented up to 6 km width; the territory covered by karst forms also increased (Fig. 4). Due to the deformation of land surface within the Khadakhan-Melkhitui karst massif more than 550 hectares of the territory of agricultural land use were lost, and a number of buildings were damaged (Trzhtsinsky et al., 2005).

The activation of karst landslide deformation in the shore area is evidenced by the origination of additional caverns, suffosional karst funnels, as well as the well-defined landslide elements, such as cracks, joints, trenches, etc. In the zones of variable water level, the horizontal solution caverns filled with friable material (dolomite meal) develop at the base of shore slopes. The laboratory analysis of this material (dolomite meal) has shown its low mechanical strength: under the inundation conditions it acquires the plasticity and fluidity features. The slackened state of filling material is the

cause of the plastic deformation, stimulating the displacement of overlying rock layers towards the erosional channels. The dynamics of development of karst landslide areas depends upon the leaching rates of carbonate rocks in the slope base. One of the sites in the cape area of the Shaloty bay of the Bratsk reservoir can be considered as the typical case of intensive development of the karst landslide deformation. Within this area, the evident karst and landslide relationships regulated by the reservoir's water regime can be observed. In this area, the shore slopes are affected by two rotational slides; actually this is the technogenic landslide of blockglide type. The interpretation of aerial photos made in 1953 shows, that this was formerly a stable area located on the steep slope over the Angara-river's water level, and separated from the river channel by the low terrace with faint relief. The aerial photos made after the reservoir impounding show the well-defined landslide forms close to the brink. The systematic yearly investigation of the deformation-affected slopes and the analysis of field materials revealed the occurrence of landslide trenches and the starting formation of additional fissure zone aslope; this demonstrates the high dynamics of landslide process ascertained by the annual land surface grading. The washout of deluvial deposits at higher water level in the reservoir (recorded during the period of 2003–2004) leads to the 3 m-deep retreat of the slope base. Within fissure zones the subsidence of land surface (15 cm/year) occurs. The mechanism of this block-type landslide is the slow depth creep of slope. The permanent high rate of karst development exists within the massif, and the intense landslide deformation in the influence zone of the reservoir occurs.

The origination and intense development of the abrasion-accumulative processes (which are new for the discussed territory) were induced principally by anthropogenic factors. The construction of reser-

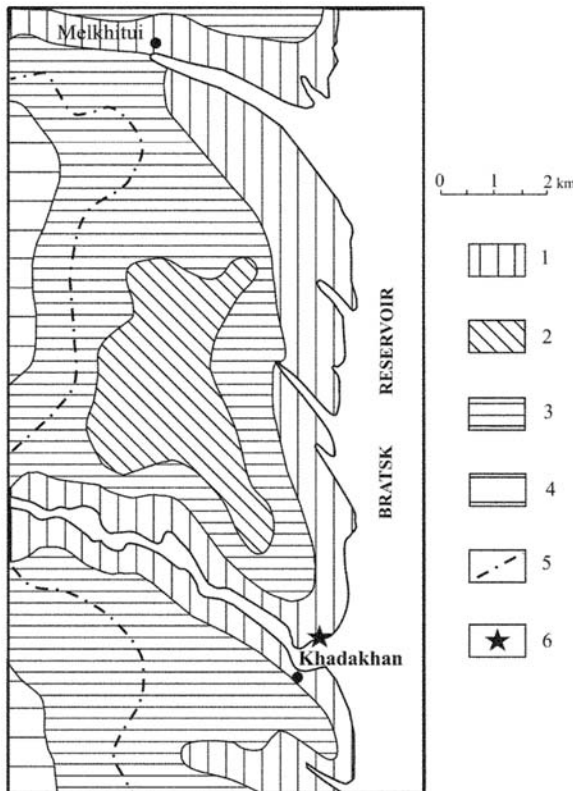


Fig. 4: Zoning of the area of Bratsk reservoir (Khadakhan-Melkhitui karst massif) by the stability against karst processes; areas: 1 – greatly unstable (1 to 10 karst holes/km² annually); 2 – unstable (0.1 to 1 karst hole/km² annually); 3 – low-stable (0.01 to 0.1 karst hole/km² annually); 4 – stable (<0.01 karst hole/km² annually); 5 – the zone of prognostic activation of the karst; 6 – the site of intensive development of the karst landslide deformation in the cape area of the Shaloty bay.

voirs of the Angara cascade hydroelectric stations entailed the radical change in the environment of the territory, particularly the morphometric conditions of the slopes and interfluvial areas. In the course of exploitation of reservoirs, many river terraces got entirely submerged; the changed water table caused the extensive decrease of stability of steep slopes. The abrasion process spread over the large area of shore zone: ~3000 km in length and 200 m in width (Ovchinnikov et al., 1999).

One of the basic factors that influence the dynamics of abrasion-accumulation processes is the water level regime, whose instability and large-amplitude variations determine the active stage of the shore slope failure, the initial stage of formation of shoals and along-shore banks. The actual regimes of reservoir exploitation benefits to formation of accumulative and abrasion-accumulative banks that serve as wave dampers and impede the shore abrasion, particularly in the Bratsk reservoir.

The original character of shore zones of artificial reservoirs is attributed to close interaction of definite processes within shore slopes. In the Rassvet-site of the Bratsk reservoir's shore area, the erosion process intensely develops aslope from the shore edge. The rate of erosion development is currently (after the 40-year exploitation of the reservoir) is 8 m/year at maximum water level. High intensity of erosion development is evidenced by increasing number of erosion cuts and the total volume of gully forms. At present, development of 36 erosion forms with the total volume of 1959 m³ within the 2 km-long shore area is recorded. The current observations reveal that the gullies have increased in number (by 20 gully forms) and volume (by 916 m³) against the data of 2004.

The current development of gully forms is attributed to the influence of recurrent water level fluctuations in the reservoir, as well as the abrasion process. These are the basic factors of the modern gully activity. The shore cliff undercutting at high water level entails its upslope displacement and the destruction of major gentle mouth parts of gully forms that decreases their length and impedes the formation of longitudinal profile of equilibrium (Fig. 5a). Lowering of the water level stimulates the vertical erosion in gully bottoms and the activation of backward erosion (Fig. 5b,c). Destruction of gully mouth parts at higher water level, and intensification of the vertical and backward erosion at low water level induce the formation of the stepped profile of gully thalwegs (Mazaeva et al., 2006).

This is the consequence of recurrent prevalence of the high rate shore abrasion over the vertical erosion. The seasonal variations of the reservoir water level also influence the cyclic changing of the ground moisture irrespective of the climate conditions. It should be noted that the lithological variability of deposits presented by the underconsolidated loess-like sandy loams, overlying the sand layers, as well as their properties (such as dusty condition, sulphate salinization of sandy loams and sands) make the grounds erosion-pliable. In the condition of high humidity the ground acquires the characteristics of fast water soaking, instability and shrinkage-strain (Khak et al., 2008).

The gully forms of complex genesis developing currently in shore areas of the Bratsk reservoir, display the diverse relationships between the natural environment and the human activity (construction of reservoirs and the manner of their exploitation). The formation of longitudinal profile of equilibrium for the above mentioned forms is impossible at the actual regime of exploitation of the Bratsk reservoir and the incessant process of shore abrasion.

5. Conclusion

Development of exogenic geological processes in the territory of East Siberia is determined by the general historical factors, the inherited condition of the region and a group of external factors, particularly by human made actions. In the context of current engineering-geological investigations, the



Fig. 5: Dynamics of gully form conditional by activation of the vertical erosion; (a): The data of July 2, 2007; (b, c): The data of July 7, 2007.

principal trends in the development of different genetic groups of exogenic processes, and the invariable mechanisms and forms of their occurrence have been determined. The variations concern the dynamics of processes, the extents of damage to the territory, and the activity and intensity of developing processes. In connection with increasing anthropogenic load some territories of East Siberia achieve status of bad social-economical risk area.

For estimation of the present-day conditions in the described territory, and ensuring of the undisturbed exploitation of engineering structures, the natural peculiarities of lithosphere, development of exogenic geological processes and the evolution of anthropogenesis should be taken into consideration.

6. Acknowledgments

The work has been done with financial support of Russian Federation President's Grants Council.

7. References

- Brief Siberian chronicle (Kungurskaya), 2003. *Making, forewarning and notes by K.G. Levi and N.V. Zadonina*, Irkutsk, Publ. «Vremia stranstviy», 184pp. (in Russian)
- Geology and seismicity of Baikal-Amur railroad zone, 1985. *Engineering geology, engineering seismology*, Novosibirsk, Publ. SB RAS, 192pp. (in Russian)
- Filippov, V.M, 1988. Dynamics of karst processes in the area of Angara reservoirs. *Abstract of thesis for Cand. Geol. Sci.*, Leningrad, 17pp. (in Russian)

- Khak, V.A., Grobelska, H., Mazaeva, O., and Brykala D, 2008. Conditions of the gully origin in the coastal area of the Bratsk reservoir. In A. Jankovski and E. Kozyreva (eds), *The exogenic processes in the geological environment. Estimation of natural hazards*, 46-53, Institute of Earth Crust SB RAS; University of Silesia – Faculty of Earth Sciences; Irkutsk-Sosnowiec. 107pp. (in Russian)
- Kozyreva, E., Mazaeva, O., Molenda, T., Rzetala, M.A., Rzetala, M., and Trzhtsiniski, Yu.B., 2004. *Geomorphological processes in conditions of human impact – Lake Baikal, southern part of the Angara valley, Silesian Upland*, Sosnowiec, University of Silesia – Faculty of Earth Sciences, 102pp.
- Mazaeva, O., Grobelska, H., and Hak, V., 2006. Rozwoj dolinek erozyjnych w strefie brzegowej sztucznego zbiornika wodnego (zbiornik Bracki, Rosja) – Development of erosional furrows in shore zone of the man-made reservoirs (Bratsk reservoir, Russia), *Dokumentacja geograficzna. Geografia fizyczna*, nr. 32, 195-199. (in Polish)
- Ovchinnikov, G.I., Pavlov, S.Kh., and Trzhtsiniski, Yu.B., 1999. *Change of geological environment in the Angaro-Yenisei reservoir-affected areas.* – Nauka, Novosibirsk, 254 pp. (in Russian)
- The general characteristic of Irkutsk region, 2005. *The State Report about the environmental conditions in Irkutsk region*, Irkutsk, 327pp. (in Russian)
- Trzhtsiniski, Yu., Kozyreva, E., and Mazayeva, O., 1999. Evolution of the geological environment under the influence of Angara reservoirs. In O. Kashmenskaya (ed), *Shores of seas and inland reservoirs. Topical problems of geology, geomorphology and dynamics*, 101-114, Novosibirsk, Publ. SB RAS, 272pp. (in Russian)
- Trzhtsiniski, Yu.B., Kozyreva, E.A., Mazayeva, O.A., and Khak, V.A., 2007. *The modern exo-geodynamics of southern territory of Siberian region*, Irkutsk, Institute of Earth Crust SB RAS, 155pp. (in Russian)
- Trzhtsiniski, Yu.B., Kozyreva, E.A., and Verkhosin, I.I., 2005 *Engineering-geological characteristics of the Irkutsk amphitheatre*, Irkutsk, Publ. Irkutsk State Technical University, 124pp. (in Russian)

BUILDINGS' DAMAGE AT HOREMI VILLAGE, ARKADIA, GREECE: EVALUATION OF THE GEOTECHNICAL CONDITIONS AT SHALLOW DEPTHS

Kynigalaki M., Kanaris D., Nikolaou N., Kontogianni V.

IGME / Engineering Geology Dpt., Entrance C, 1, Sp. Louis St, Olympic Village, 136 77 Acharnae, Athens, Greece, nikolaou@igme.gr

Abstract

Horemi village is located in Central Peloponnesus, at the western margins of Megalopoli basin. For several years failure phenomena on the village buildings have been reported, causing problems related both to the safety of the inhabitants, as well as to the development of the area.

For the above reasons a geotechnical investigation program was carried out, to study the origin of the failures and lead to certain conclusions for the mitigation of the phenomena.

In situ exploratory works, with reference to the investigation of litho-stratigraphy, ground foundation conditions, as well as laboratory testing, provided the necessary data for further research testing of the soil physical and mechanical parameters.

Building failure recording, trial pits description, sample collection and laboratory testing, pointed out that failure phenomena are due to geotechnical rather than geological effects.

The detection of a clayey horizon, presenting high to very high plasticity and swelling behavior, related to the significant montmorillonite proportion in the surface or shallow geological formations, showed good correlation to building damages. The aforementioned observations are considered to clarify the case presented in this paper.

Key words: *swelling, montmorillonite, damage on buildings, Horemi, Greece*

1. Introduction

Damage of common buildings founded on sediments, resting by the margins of Post-alpine basins, occurs frequently in the Greek territory. This leads to long-lasting problems, social rather than technical, related to citizens' and property's safety, finally affecting the urban development.

The specific location of these areas, in terms of morphological characteristics, lithological setting, geodynamic regime, hydrogeological conditions, particular geotechnical properties and construction details of the buildings, should be studied in order to evaluate the significance of each factor to the damage observed.

Nevertheless, various other causes (human activity etc), could be involved in buildings' damage and must be encountered according to the in situ evidence.

The present paper is a contribution to cases, where local geotechnical conditions, is believed to rule the phenomena, while tectonics play also a role. This is judged to occur, due to lack of any field data, indicating broader movement effects.

Thus this study focuses on the examination of the geotechnical behavior of the soil formations, bearing the constructions.

2. The study area

2.1 Location and morphology

Horemi village is situated, at roughly 5km straight line distance, SW of Megalopolis town in central Peloponnesus (Fig.1). It is found at the western margins of Megalopolis basin at an approximate mean altitude of 380 metres. The basin is surrounded by four mountains, namely Mainalo to the north, Lykaio to the west, Taygetos to the south, Parnonas to the east and occupies the western part, of the in between the aforementioned mountains, formed low area.

At this section of the basin's margins, westwards to Alfios river, low hills are observed, separated to each other by streams. The streams present a SW to NE direction of flow and create ravines of various depths and almost vertical slopes. This low relief configuration, is related to the low, generally, dips of the geological formations and the predominance of soft horizons, in the geological structure.

The residential area of Horemi (Fig.1, is developed, at the top, almost flat part of the hill, while slopes with generally smooth morphological dips ($5-10^\circ$), are formed mainly at the eastern section. Locally only, medium dipping slopes are observed.

Regarding the hydrographical network, Megalopolis basin is drained by Alfios river, his tributary Elissonas and several streams. The position of Alfios river is asymmetrical as for the long axis of the basin and this axis coincides with the general flow direction of the river that is from the SSE to the NNW. Alfios enters the basin at the south-eastern part of the basin, at an altitude of 410 metres, and further on, joins Koutifarina stream. It exits the basin of Megalopolis at the north-western edge, near Karitaina village at an altitude of 350 metres. Westwards from Koutifarina, Xerilas stream enters the basin following the SE to NW fault zone direction of Falaisia (Taygetos) region.

2.2 Geological structure – lithological composition

Megalopolis basin is a tectonic graben, with long axis having an approximate length of 15km and direction from NNW to SSE, whereas short axis presenting a length of about 10km. The basin is occupied by Pleistocene formations, of lacustrine and fluvial origin. Neogene sediments outcrop mainly at the eastern margins of the basin and at places in the northern, while the basin's borders are occupied by the Alpine formations of Pindos Zone, Tripolis Zone and the Phyllite – Quartzite series, which is tectonically underlying Tripolis Zone and / or Pindos Zone.

More specifically in the north-eastern, eastern and southern sections of the basin, geological formations of Tripolis Zone prevail, while limestone tectonic segments of Pindos Zone and parts of the Phyllite – Quartzite series appear at places. Furthermore, on the western and north-western boundaries of the basin, layers of Pindos Zone are present.

Below are given, the horizons that constitute the abovementioned geotectonical Zones, according to the Geological Map of IGME of 1:50.000 scale ("Megalopolis" sheet, Papadopoulos et al., 1997). The formations are listed from the oldest to the newest and are as follows:

- Phyllite – Quartzite series
- Tripolis Zone carbonate sediments and flysch.
- Pindos Zone tectonized materials, members of the ophiolitic series, cherts, first flysch, limestones and flysch transition beds.

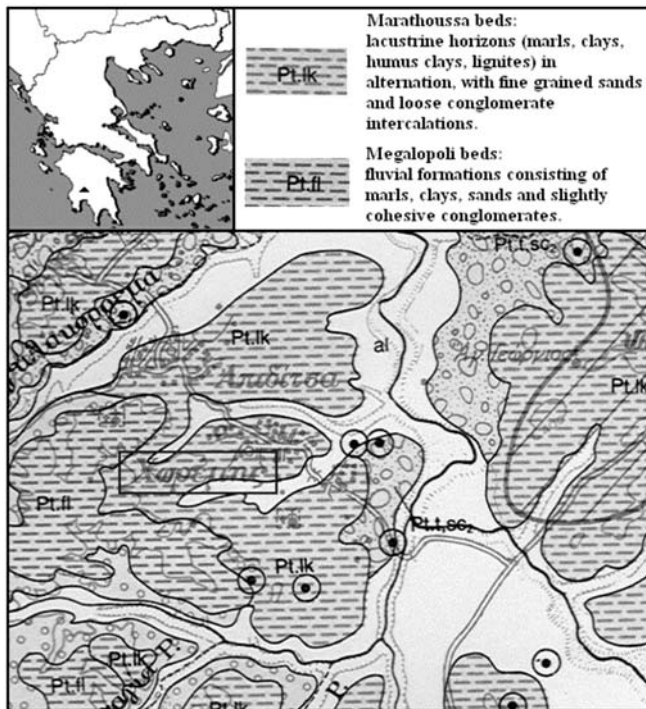


Fig. 1: Geological Map of Horemi (“Megalopolis” sheet, 1:50.000 scale, I.G.M.E., 1997). Inset: Map of Greece, triangle indicates the Horemi area.

As regards the Post-alpine formations, sediments of Pliocene, Pleistocene as well as Holocene deposits can be encountered. Analytically:

Pliocene formations: Two units of lacustrine as well as fluvial phases are met, with total thickness 60 to 120m, namely from base to top:

Makryssion formation: marls, clays with lignites and conglomerates.

Trilofo formation: marls, clays, loose conglomerates

Pleistocene sediments:

Apiditsa formation: terrestrial phases, consisting of red clayey sands with slightly cohesive conglomerates and scree with red clays. Thickness 50 to 100m.

Horemi formation: sediments of lacustrine and fluvial phases, deposited during hot and cold period of Pleistocene, respectively. They have total thickness of 200m and include the following:

—Marathoussa beds: lacustrine horizons (marls, clays, lignites) in alternation, with fine grained sands and loose conglomerate intercalations (Fig.1).

—Megalopoli beds: fluvial formations consisting of marls, clays, sands and slightly cohesive conglomerates laterally passing to Marathoussa beds (Fig.1).

Thoknia – Potamia formation: they constitute the two basin’s terraces and consist of silts, clays, sands, gravel, loose conglomerates and mixed phases in the form of scree. Total thickness of 10 to 40m.

Holocene deposits:

Recent and old talus cones and scree: silts, loam and loose conglomerates.

Alluvial deposits: Loose clayey-sands with gravel and cobbles in the river and stream beds, as well as terraces of small extent.

Referring to the strict Horemi village area, according to the Geological Map of Figure 1, the urban area is founded on the Pleistocene aged Horemi formation and to be exact in Marathoussa beds.

2.3 Geodynamic regime

2.3.1. Tectonics

Megalopolis basin was created as a tectonic graben, between Oligocene and Upper Pliocene age. It was formed after the overthrust movement of Pindos Zone over Tripolis Zone, during the en echelon faulting phase that followed.

The basin was initially filled with lacustrine sediments, while deposition of lacustrine, and river materials in alternations, followed. This was the result of the continuing sinking of the basin, the uplift of its margins, the circles of erosion and deposition, as well as of the alternation of hot and cold periods. It is also related to the speed of rise of the water level in the interior of the basin. The continual sinking of Megalopolis basin and uplift of its marginal zones, is connected to the earthquake potential of the region.

Regarding the structure of the Alpine basement, at the marginal zone and at the interior of Megalopolis basin also, geophysical researches (Papadopoulos, 1985) showed the following: starting from the eastern part of the basin, the basement gradually passes from higher to deeper horizons until Perivolia village to the west. Afterwards it falls abruptly to the west, up to a depth of about 500m. In the western part of the basin, the basement falls rapidly to the east and sketches out a fault zone, with direction NW/SE, almost parallel to the flow of Alfios river. This fault zone along the west margins of the basin is crossed by E-W directing faults. Finally in the central part of the basin, no features of particular tectonic interest are observed.

2.3.2. Seismicity

The region of Central Peloponnesus presents intense seismic activity since the antiquity (Galanopoulos, 1955). Earthquakes which occurred during the historical years and are reported as catastrophic for the region of Megalopolis, are the following:

- 1783, earthquake felt in Gortynia region caused failure in churches, as well as collapse of houses in Stemnitsa village.
- 1897 and 1898 two earthquakes sensed in all Southern Greece and Italy caused damage in Tripoli.

Afterwards, during the modern period, the following earthquakes are characterized as the most disastrous for the region of Megalopolis:

- 1952, 13 June, a strong earthquake caused damage in Horemi.
- 1965, 5 April, a severe earthquake occurred in Central Peloponnesus and caused deaths and injuries, created ground failure and destroyed completely 1.426 houses. Among the most damaged villages are Horemi, Apiditsa, and Tripotamo (intensity X Mercalli).
- 1966, 1 September, a disastrous earthquake took place in the region of Megalopolis, where injuries and building collapses were recorded (intensities VII-VIII Mercalli). The most serious building damages were well correlated with the foundation conditions, morphology and tectonics of the site.

In the bibliography (Papadopoulos, 1985), is pointed out that the seismic activity of Megalopolis basin seems to be mainly expressed at the margins, along or near tectonic lines, with directions NNW-SSE and E-W respectively.

Also in conclusion, the above researcher marks out that high seismic intensities in the basin of Megalopolis, are owed mainly to the physical and mechanical properties of the Pleistocene formations, as well as to the geometry of the geological basement. Thus, despite the significant thickness of these sediments (up to 500m) at the western margin, the severe destructions caused by the earthquakes are related to the intense slope of the geological basement, as a result of faulting.

3. Site investigation

For the needs of the present research, in Horemi village, one (1) geotechnical borehole, up to 40.50m in depth and in situ testing (SPT, permeability) have been carried out, while seven (7) trial pits have also been excavated. According to the (N) value of blows, the fine grained soils met are characterized as *stiff* and the coarse grained as *dense*. In addition, the permeability of the formations, was found to be *low*, in general.

4. Laboratory testing

Soil mechanics laboratory tests (Soil Mechanics Lab of IGME) were implemented in selected samples, for the measurement of their physical and mechanical parameters. Also, mineralogical studies (Dept. of Mineralogy and Petrology, IGME), for the quantitative and qualitative determination of their mineralogical composition, were also conducted. Below, the results of the as above laboratory analyses are specified:

4.1 Soil mechanics

Fifteen samples, chosen from the borehole cores, as well as the trial pits' materials, were tested, for the determination of their grain size distribution, consolidation, shear strength and unconfined compression strength parameters.

In the samples taken from the shallow horizons, the existence of a fractured, stiff clay, was found out. It presents high to very high plasticity, smooth slickenslide surfaces covered by Mn oxides, mean thickness of 2.00m and was observed in a depth varying from 0.40m to 3.60m. The swelling pressure measured, ranges from 50 up to 400kPa.

4.2 Mineralogical studies

Given that the clayey formations met during the investigations at Horemi, present expansion, four samples from the borehole drilled and three samples from the trial pits, were chosen for mineralogical analyses. These analyses revealed high percentages of quartz and (Na, Ca) montmorillonite in all the samples examined, as well as absence of calcite in the mineralogical composition of the samples taken from the trial pits.

Montmorillonite belongs to smectites, which constitute one of the chief swelling clay minerals group, while Na-montmorillonite presents the greatest potential for expansion, of all the clay minerals. It forms crystals very small in size, characterized by intense moisture uptake (Gillot, 1987).

5. Geotechnical evaluation

The activity of clays has a direct relationship with plasticity index and clay fraction of whole sample ($\% < 2 \mu\text{m}$). Activity ranges between 0.50 and 0.80 for all samples corresponding to normal clays, with only one sample being no active (activity 0.20).

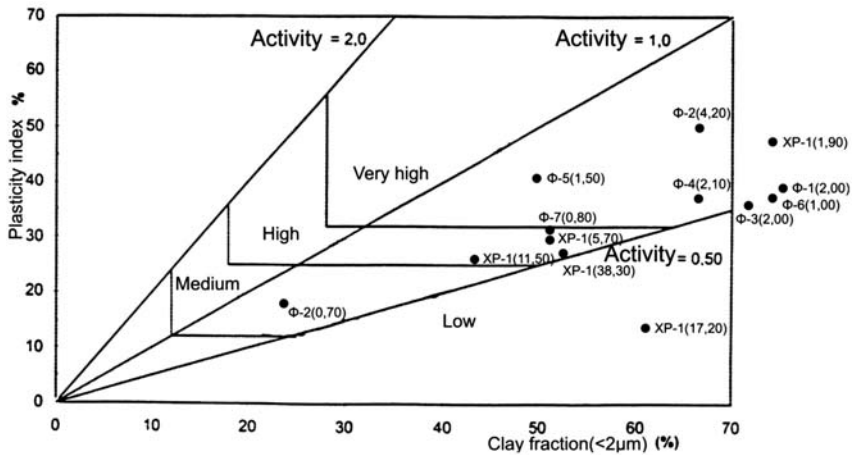


Fig. 2: Activity and swell potential of examined soils, Van der Merwe (1964) modified by Grabowska - Olszewska (1998).

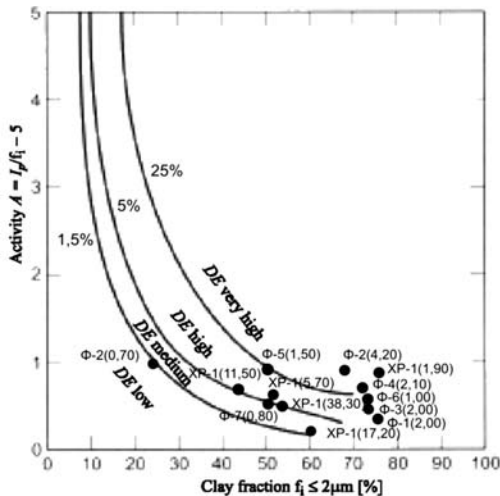


Fig. 3: Degree of expansion (DE) classification chart according to Seed et al. (1962).

Concerning the swell seven samples have very high, five samples high – medium and one sample low swell potential (Van der Merwe, 1964, chart modified by Grabowska – Olszewska 1998 for the evaluation of potential expansiveness, Fig.2).

For quantitative evaluation of the swell according to Seed et al (1962) it was estimated that five (5) samples have very high (>25%), six (6) samples have high (5 – 25%) and only two (2) samples have low degree of expansion (1.5%, Fig.3).

6. Buildings' failure assessment.

Three in situ investigations at Horemi village between May 2007 and April 2008 aimed to record damage on buildings and other structures. Recorded damage involved fractures on the walls of several houses and yards located at areas indicated on the map of figure 4. All fractures share the following characteristics: they are either diagonal, breaking the house walls (Fig.5), or horizontal and



Fig. 4: Aerial photo of Horemi village. Areas with damaged buildings are drawn. The dot indicates the house with most important damage and the triangle indicates the church of Horemi (see also Fig. 5).

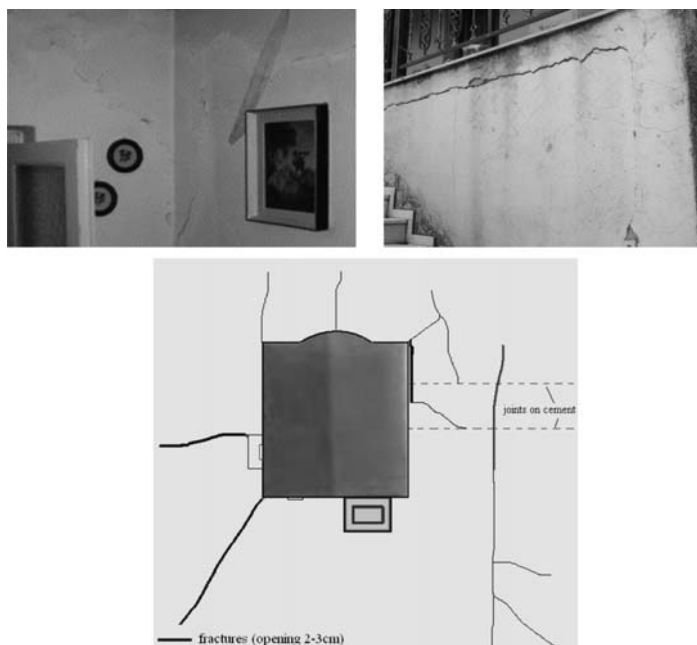


Fig. 5: Top: Photos from the house with most important damage (dot on map of Fig. 4), showing extensive fractures (diagonal, vertical and horizontal) on the walls. Bottom: A sketch showing allocation of fractures on the cement yard of the church (triangle on map of Fig. 4).

vertical unjoining the walls from the structure skeleton (Fig.5). Both types of fractures reveal shear stresses due to differential settlement of the building.

Besides damage on buildings, extensive failure was found at cement yards, as for instance around the church of the village (Fig.5). Those fractures, locally showing vertical dislocation, are obviously due to ground settlement.

7. Discussion

Laboratory tests revealed that clays at Horemi undergo significant swelling when water content increases. Inevitably, when water is removed, i.e. due to seasonal changes of the ground water, shrinking phenomena take place. Swelling and shrinking occur at successive circles generating small fractures in the clay and locally, at relatively higher loadings - for instance beneath two-store buildings as shown above (Fig. 5) - sliding along these fractures is triggered. This seems to be the most likely reason for damage observed at heavier, though newer, houses founded on the clay.

The mechanism of swelling and shrinkage seems to be responsible also for detachment and breaking of cement yards around the church (Fig. 5) and houses at Horemi village.

8. Conclusions

Horemi village is founded on Pleistocene aged lacustrine, thick formations, situated at the western part of Megalopolis basin, where the geological basement falls rapidly to the east, as a result of the NW/SE fault zone, crossed by E-W directing faults. The seismic history of the area, mainly expressed at the margins of the basin, is characterized by high seismic intensities due to the physical and mechanical properties of the Pleistocene formations, as well as to tectonics.

Site investigation and lab testing revealed, at shallow depths, the existence of a fractured, stiff clay, presenting high to very high plasticity. Slikenslide surfaces were observed while a significant high percentage of montmorillonite was determined. Thus, high swelling potential and degree of expansion were detected.

The above engineering geological characteristics, in relation to the mineralogical composition, seem to indicate the mechanism causing the buildings' damage: swelling and shrinking successive circles, generating small fractures in the clay and locally sliding along these fractures.

9. References

- Carter, M. 1983. Geotechnical Engineering Handbook. London, 226pp.
- Gillot, J. 1987. Clay in Engineering Geology. Amsterdam, Elsevier Publications.
- Kaperonis, N., Athanassiou, A., Agelopoulos, G., 1974. Geological research of "Marathousa - Northern Horemi" lignite-bearing field of Megalopolis Basin. Athens, Public Power Corporation Publications.
- Papadopoulos, P., Luettig, G., Vinken, R. 1997. Geological Map, scale 1:50.000, "Megalopolis" sheet, Athens (IGME).
- Papadopoulos, T., 1985. Geophysical researches in the region of Megalopolis Basin. PhD Thesis. Athens, University Publications.
- Papazachos, V., Papazachou, K., 1989. The earthquakes of Greece. Thessaloniki, Ziti Publications.
- Spyropoulos P., 1997. Chronicle of earthquakes in Greece, from the antiquity up to today. Athens – Giannena, Dodoni Publications.
- Tzitziras, A., 2001. Geotechnical reconnaissance in Tripotamos and Horemis villages, Municipality of Megalopolis, Athens (IGME unpublished report in greek).
- Vetoulis, D., 1965. Geological report on the review of seismically affected settlements of Tripotamia Gortynias and Tripotamos Megalopolis, in Arkadia Prefecture Athens (IGEY unpublished report in greek).

EARTHQUAKE-INDUCED ROCKFALLS IN SANTOMERI VILLAGE, WESTERN GREECE

Lainas S.¹, Koulouris S.¹, Vagenas S.¹, Depountis N.²,
Sabatakakis N.¹ and Koukis G.¹

¹ University of Patras, Department of Geology, Laboratory of Engineering Geology, 26500 Patras, Greece, splainas@upatras.gr

² Region of Western Greece, Directorate of Public Works, nikosdepountis@hotmail.com

Abstract

On the 8th of June 2008 an earthquake of magnitude $M_s=6.5$ occurred in Western Greece, affecting Achaia and Ilia Prefectures. According to state reports 2 casualties occurred, 214 people were injured and more than 15 villages and towns suffered extensive damages in properties and infrastructures. Among the secondary phenomena that were reported were extensive rockfalls that affected Santomeri village; a small village located on the western slope of the Skolis mountain. Large-sized limestone boulders, some reaching a volume up to $10m^3$ stroke houses and blocked roads, fortunately without casualties. The village was temporarily evacuated and the Laboratory of Engineering Geology was commissioned to undertake an Engineering Geological appraisal in order to investigate the extent of the rockfall events, assess the rockfall hazard and propose retention and protective measures so the area to be soon re-inhabited. After conducting a detailed engineering geological and geotechnical survey which included large scale engineering geological mapping, rockmass characterization and laboratory tests the inhabited area was initially divided in two zones of different rock fall risk level. By performing rockfall analyses in critical traverses a rock fall retention system, 325m long in total, comprising rock fall barrier was finally proposed.

Key words: Earthquake-induced rock fall, rock fall analysis, Achaia, Western Greece

1. Introduction

On the 8th of June 2008, 15:25 local time, a strong earthquake of magnitude $M_s=6.5$ stroke Western Greece, affecting mainly Achaia and Ilia Prefectures. According to state reports two people were killed, 214 were injured and more than 15 villages and towns suffered extensive damages in properties and infrastructures. Among the earthquake's secondary phenomena, apart from surface ruptures, some liquefaction phenomena, slope failures etc there were large scale rock falls. In particular, extensive rock falls manifested at "Skolis" mountain. Some roads were blocked by the rockfalls, houses were destroyed, fortunately without casualties. As a result, three villages were temporarily evacuated ("Haraygi", "Portes" and "Santomeri") as a measure to protect inhabitants from probable reactivation during an after-shock. After field reconnaissance from the Department of Geology it was decided that only Santomeri village faces serious rockfall risk and so the Department of Geology was commissioned to undertake an engineering geological appraisal in order to assess rockfall hazard and to propose retention-protective measures so the area to be soon re-inhabited.

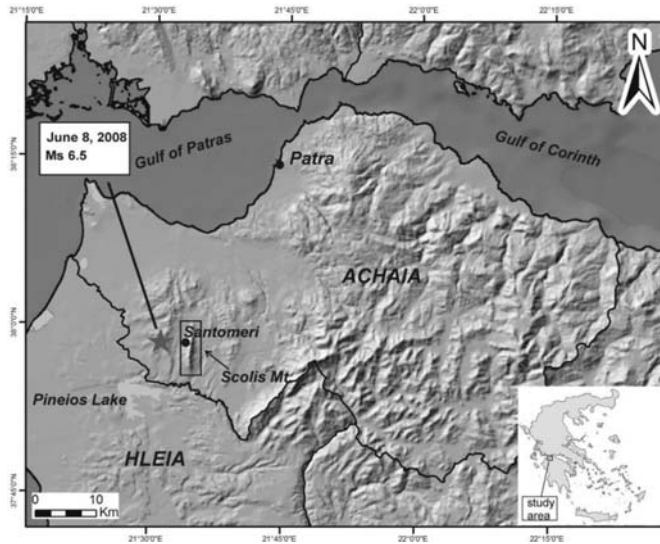


Fig. 1: Simplified map showing the location of the study area and the epicentre of the 8th of June 2008 earthquake.

This paper focuses on estimating the critical rockfall parameters such as kinetic energy, bouncing height, rock endpoints and coefficients of restitution, in order to propose the appropriate design specifications of the required retention measures.

2. Geological setting

Santomeri village is founded on the western slope of “Skolis” mountain (Fig. 1) at an elevation of 400-500m. This mountain is a long morphological feature with N-S orientation with maximum elevation of about 970m. It is characterized by steep slopes, especially at its western part. Steepness is closely related to the geological and tectonic features. At higher elevations Cretaceous and Eocene limestones of Gabrovo-Tripolis Geotectonic Zone (Dercourt, 1964, Fleury, 1980) form slopes inclined up to 90 degrees and up to 80 meters high, while the eastern and western slopes which are composed by Flysch of the same Zone and scree, form gentler slopes that incline at about 45-50 degrees.

The main tectonic feature of this area is the overthrusting of Cretaceous limestones on the Flysch (Fleury, 1980). This has caused intense deformation and fracturing of the rockmass making it more susceptible to slope instability phenomena.

3. Methods

3.1 General

The research included engineering geological mapping at a 1:1000 scale, rockmass characterization and classification, recording and classification of fallen rocks according to their estimated volume and finally rock fall statistical analyses in seven (7) selected traverses. Along each traverse rockfall statistical analyses were done, in order to compute kinetic energy, bounce height and maximum travel distance. The coefficients of normal and tangential restitution were estimated from back calculation of known rock paths and rock endpoints according to field observations of the rockfall events.

3.2 Engineering geological conditions

In order to investigate the engineering geological conditions and the factors that control slope stability, engineering geological mapping at 1:1000 scale was conducted. Due to the absence of recent topographic data mapping was based on the existing maps of 1:5000 scale and on satellite images. These maps were georeferenced to the Greek Geodetic Referencing System (GGRS 87) and digitized. The map's data, concerning newly constructed houses and road network was updated after field work.

Three engineering geological units were mapped, as shown in the corresponding engineering geological map (Fig. 2). From the most recent to the older these are:

Recent rockfall debris

They are loose deposits of rockfall debris consisted of grey and white limestone blocks of various size. They were deposited on the slope's surface after weathering of the limestones and during previous earthquakes. The area that they cover was extended during the 2008 earthquake.

Scree

They are loose to semi-cemented Quaternary deposits which consist of white and gray limestone fragments of various size mixed with brown sandy or clayey matrix derived from the weathering of limestone and flysch basement rocks.

Flysch

It has Oligocenic age and belongs to the Gavrovo-Tripoli Geotectonic Zone. It consists of successive medium-bedded fine-grained sandstones and mudstones of brown or gray colour. They are susceptible to weathering processes and, as a result, they are characterized by up to 1-meter thick weathering mantle. Besides, along the thrust zone with the limestones, flysch is intensely deformed, fractured and folded.

Limestones

Grey and white gray limestones interbedded with marly limestones of Cretaceous and Eocene age that belong to the Gavrovo-Tripolitsa Geotectonic Zone. They are formations of high strength with continuous bedding, inclined opposite to the slope.

The engineering geological map also depicts the main rockfall path that destroyed a house and the traces of the seven rockfall analysis traverses.

3.3 Rock fall recording

In order to estimate the most "possible" rock fall traces fallen rock boulders were recorded, mainly inside and near the inhabited area, even if scarce rock boulders of various size were also found in the broader area as a result of older rock fall events. Recording was done by locating each boulder by GPS and classifying each one according to its source material, origin, and estimated volume. Recording focused on boulders of estimated volume more than 2m³ which were divided into four (4) volume classes. As shown in Fig 3, the most recordings belong to the volume classes between 2 and 5m³. It must be noted that many of the recorded volumes may not represent the original volumes of the detached blocks, because many of them could have been broken during falling and crashing on the slope.

3.4 Rockmass classification – slope stability conditions

In order to estimate rockmass quality and assess slope stability conditions geomechanical descrip-

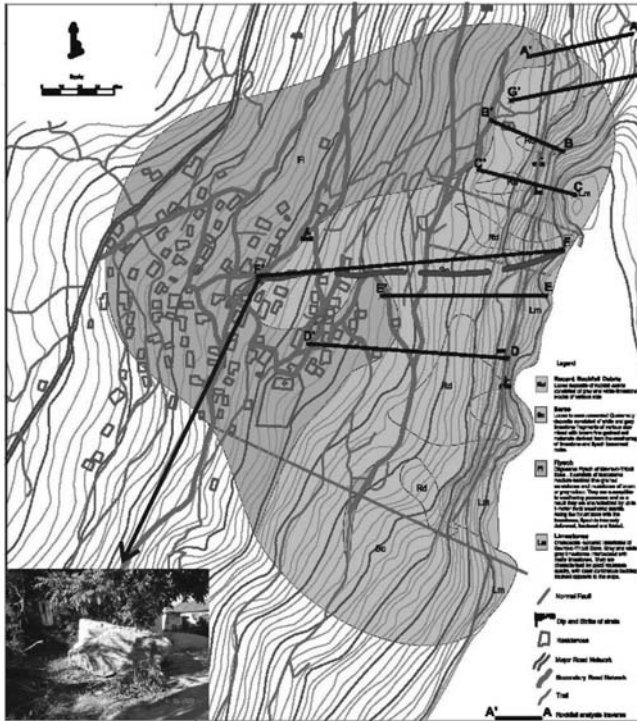


Fig. 2: Engineering Geological map of Santomeri area also showing the seven rock fall traverses and the course-endpoint of a large limestone boulder.

Table 1.

<i>Disc. Type/Set</i>	<i>Orientation</i>	<i>Aperture</i>	<i>Spacing</i>	<i>Persistence</i>	<i>Roughness</i>	<i>JRC</i>	<i>JCS (MPa)</i>	<i>Filling Material</i>
Bedding Plane/B	89/16	2,5-10 mm	200-600 mm	10-20m	Rough undulating	10 - 12	130 ± 50	Clean - Sandy
Fault/F	265/85	10-100 cm	600-2000 mm	>20m	Smooth undulating	8 - 10	110 ± 40	Clean - Sandy
Joint/J1	266/54	10-100 cm	600-2000 mm	>20m	Smooth undulating	8 - 10	125 ± 50	Clean - Sandy
Joint/J2	182/82	1-10 cm	200-600 mm	10-20m	Smooth undulating	8 - 10	115 ± 45	Clean - Sandy

tion of discontinuities according to ISRM (1981) was performed. The joint-wall compression strength was estimated in the field by using Schmidt Hammer Test, while the limestone uniaxial compression strength and shear strength parameters were measured with laboratory tests in rock samples. It was found that rockmass is jointed by four (4) main discontinuity sets with mean dip/dip directions as shown in Table 1.

Rockmass quality was estimated according to GSI (Hoek and Marinos, 2000) and RMR (Beniawski, 1989) classification systems. Based on the discontinuities' properties and the bedding orientation RMR was estimated in the range of 55-65, classifying limestones as rockmass of "Good" to

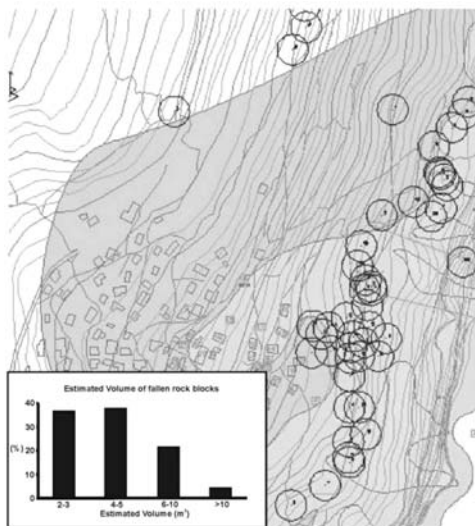


Fig. 3: Distribution of rock blocks around Santomeri village and corresponding graph, showing their estimated volume range.

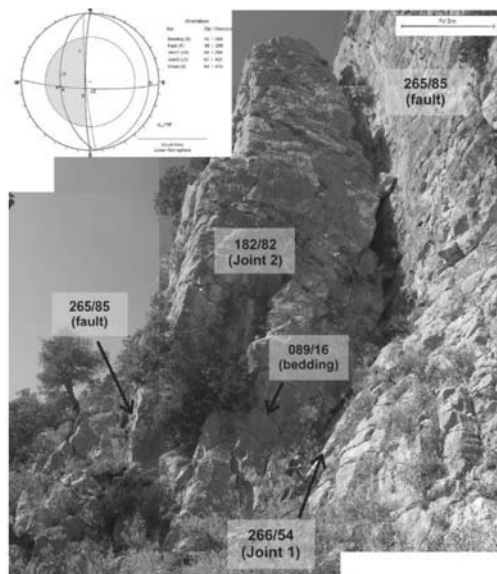


Fig. 4: Major discontinuity sets and corresponding Major Planes Plot in Limestone.

“Medium” quality. GSI was estimated in the field in the range of 50-60.

Slope stability conditions were estimated by performing preliminary kinematic analysis after plotting the discontinuity sets in Schmidt’s stereographs. As shown in the following Major Planes Plot (Fig. 4) instability can potentially occur in the following cases

- a. Planar slide along set J_1 .
- b. Wedge failure along the wedge formed by sets J_1 and J_2 (wedge A).

It was finally concluded that stability is mainly governed by Joint set “ J_1 ” which is oriented almost

Table 2.

<i>Traverse</i>	<i>Length (m)</i>	<i>Slope height(m)</i>	<i>Average slope gradient (deg)</i>
A-A'	120	60	26.6
B-B'	80	65	38.7
C-C'	100	90	43.5
D-D'	210	110	27.5
E-E'	150	110	36.1
F-F'	340	190	29.2
G-G'	120	50	22.8



Fig. 5: Locations of the analysed Rockfall traverses. The location of a house destroyed by the rockfall is also shown.

parallel to the slope, by major fault surface (Fault “F”) which has very high persistence and by Joint set “J₂” which is oriented perpendicularly to J₁ and forms with it potentially unstable wedges.

Rock fall statistical analyses were performed in seven (7) traverses. The selection of the traverses was based on field observations concerning the traces of the major rockfall events and on the fallen rock recordings. Table 2 gives information about traverse length, average slope gradient and slope height. The location of each traverse correlated with the observed rockfall rock fall courses are also shown in Fig.5.

Rock fall analyses were performed by using *Rocfall 4.0* (Rocscience Inc.). By using this software it was possible to determine Kinetic Energy, Velocity, “Bounce Height” and location of Rock Endpoints for the entire slope along each traverse. It also assisted to determine the most effective retaining measures to protect the village from possible future rock fall events. By performing these rock fall analyses coefficients or restitution (R_N and R_T) were also estimated for the specific site conditions.

For the design of each slope elevation data from the available maps was used with some modifications, if necessary. Because rockfall is strongly influenced by slope material (vegetation, soil cover etc), different slope surface materials were assigned in every traverse, according to field observations about vegetation type, scree cover, areas with clean bedrock etc.

Each rock fall analysis included 2000 throws of a single rock. Initiation points (data seeders) were assigned in each analysis, according to field observations and estimations regarding the most pos-

Table 3.

<i>Slope material</i>	R_N (mean values)	R_T (mean values)
Limestone Bedrock	0.550	0.920
Soil with little vegetation	0.290	0.550
Soil with tree vegetation	0.300	0.800
Talus cover	0.320	0.820
Talus with vegetation	0.320	0.800
Asphalt	0.400	0.900

sible sites for rock falling. Each slope was further divided in different segments in order to assign different slope materials. In every analysis rockfall parameters were calculated in 100 points along each slope making possible to graphically view calculations along the slope.

Because R_N and R_T coefficients can not be directly measured, they were estimated by performing back analysis calculations. Every analysis started by putting as input values suggested values of R_N and R_T for every material, according to the literature. As a second step, each analysis was calibrated in order to match the results with known rock paths and endpoints according to field observations, estimating, finally, R_N and R_T coefficients for the specific site conditions. For slope friction angle default values were used, while slope roughness values were based on the topographical accuracy with a standard deviation of 2 degrees.

Data collectors were finally put in selected points along the slope in order to get information about the necessary absorption capacity of the required retaining measures.

4. Conclusions - Results

Rock fall analyses mainly aimed to assess rockfall hazard in Santomeri village and to propose retention-protective measures so the area to be soon re-inhabited after the earthquake. Besides, with this research it was possible to estimate critical rockfall parameters such as Kinetic Energy, Bouncing Height, Rock Endpoints and Coefficients of Restitution.

Coefficients of normal and tangential Restitution were estimated for every material that covers the slope surface along the traverses. Proposed values for similar conditions were initially used and then the model was calibrated so that the results match to field observations regarding fall traces and rock endpoints. The mean values of the finally estimated coefficients are shown in Table 3.

After performing the analyses in all traverses it was possible to estimate the distribution of every computed parameter (Table 4). Computed results were collected by assigning in each analysis “data collector” points located at sites where the construction of retentions measures had been initially proposed. It was found that Kinetic Energy varies between 3000 and 8000kJ with the lower values at north and the higher at south. Travel velocity and Energy were mostly affected by slope steepness and slope surface material, especially in areas of clean limestone bedrock or by the presence of tall trees. Very steep segments along the slopes favour free falling instead of bouncing or rolling, while the crushing of rocks on tall trees results to sudden modifications of Kinetic Energy and rockfall course.

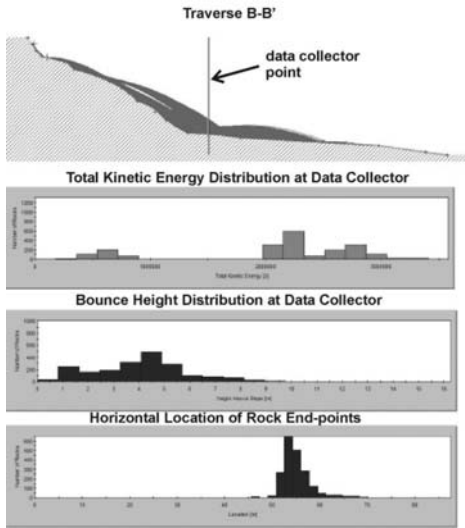


Fig. 6: Rock fall analysis results along traverse B-B'.

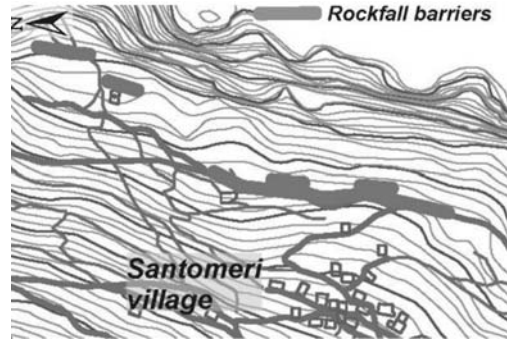


Fig. 7: Plan of the proposed Rockfall protection barriers.

Table 4.

<i>Traverse</i>	<i>mass (kgr)</i>	<i>Estimated Volume (m³)</i>	<i>Total Kinetic Energy (kJ)</i>	<i>Bounce height (m)</i>	<i>Maximum endpoints (m)</i>
A-A'	5200	2	≤350 (90% of throws) Maximum: 390	≤0.8 (80% of throws) Maximum: 3	120
B-B'	7000	3	≤3000 (95% of throws) Maximum: 3350	≤4 (80% of throws) Maximum: 5	50-60
C-C'	65000	25	≤13000 (85% of throws) Maximum: 16500	≤1.5	80-90
D-D'	5000	3	≤4000 (80% of throws) Maximum: 7500	≤0.6	70-90
E-E'	5000	2.5	≤2300 (80% of throws) Maximum: 2800	≤3 (90% of throws) Maximum: 5	190
F-F'	16000	6-7	≤8000 (95% of throws) Maximum: 10000	≤2	300
G-G'	10000	3.5-4	≤2500 (90% of throws) Maximum: 3200	≤1.5	130

Bounce heights were generally found up to 4 meters. They were strongly influenced by the slope surface materials and by intense changes in topography. Higher Bounce heights were calculated in sites of exposed limestone bedrock.

Rock endpoints are generally between 100-300 meters from the start point of each traverse. The final endpoint was strongly influenced by topography and steep modifications of slope gradient. Sudden changes from steep to gentle slope segments and energy reduction due to crushing force sometimes

rocks to stop moving and rest on the slope, before reaching the maximum possible endpoint. The village is within the above endpoint range since it is located within a distance less than 250m from rock-fall affected zones. Fig. 6 shows an example of the analysis results, as calculated along traverse B-B'.

Rockfall protection barriers with absorption capacity of 3000 kJ, 5 meters high and having a total length of 325 meters were initially proposed in selected places along the slope, as shown in Fig. 7.

5. Acknowledgments

The work was carried out under the support of the Region of Western Greece. The authors wish to express their sincere appreciation to its generous support.

6. References

- Bieniawski, Z.T., 1989. "Engineering rock mass classifications." *Published by John Wiley & Sons*, New York, 251 pp.
- Decourt, J., 1964. Contribution à l' étude géologique d'un secteur du Péloponnèse septentrional. *Ann géol. Pays. Hellen.*, 15, pp. 1-418, Athènes.
- Fleury, J.J., 1980. Les zones de Gavrovo-Tripolitza et du Pinde-Olonos (Grèce continentale et Peloponnèse du Nord). Evolution d'une plateforme et d'un bassin dans leur cadre alpin. *Soc. Géol. Nord. Publ. no 4*, 651 pp., Lille.
- I.S.R.M. Suggested Methods, 1981. «Rock Characterization Testing and Monitoring», *Editor E. Brown, Pergamon Press*.
- Hoek, E. and Brown, E.T., 1997. "Practical estimates of rock mass strength". *Intl. J. Rock Mech. & Mining Sci. & Geomechanics Abstracts*. 34(8), pp. 1165-1186
- Hoek, E., Brown, P. and Bennis, M., 1998. "Applicability of the Geological Strength Index (GSI) classification for very weak and sheared rock masses. The case of the Athens Schist Formation". *Bull. Engg. Env.* 57(2), pp. 151 – 160.
- Hoek, E. and Marinos, P., 2000. Predicting Tunnel Squeezing. *Tunnels and Tunneling International*, Part 1 – November Issue 2000, pp. 45 – 51, Part 2 – December 2000, pp. 34 – 36.
- ITSAK, 2008. The Achaia-Hleia earthquake. 4th Technical Report, Institute of Engineering Seismology and Antiseismic Constructions, 67pp, Thessaloniki. Available online at: <http://www.itsak.gr>.
- Koukis, G. et al, 2008. Engineering Geological - Geotechnical conditions and retention measures after the 8th June 2008 earthquake in Santomeri Village, W. Greece. *Technical Report, University of Patras, Department of Geology*, 52 pp, Patra
- Palmstrom, A., 1982. The volumetric joint count – a useful and simple measure of the degree of rock jointing", *Proc. 4th Congr. Int. Assn. Engng. Geol.*, Delhi 5, pp. 221 – 228.
- RocScience Inc, 2003. RocFall Advanced Tutorial. Rocscience Inc, 8pp.
- RocScience Inc, 2004. RocFall V.4, Rocscience Inc, Canada.
- Tsiambaos, G. and Sabatakakis, N. (2000). "Considerations on RMR classification system concerning limestone slope stability", *Proceedings of the International Conference on Geotechnical and Geological Engineering (GeoEng2000)*, Melbourne, pp.19 – 24.
- Vagenas, N., 2009. Rockfall analyses of Rockfall events induced by the 8th June 2008 earthquake in Santomeri Village, W. Greece. *Master Thesis, University of Patras, Department of Geology*, 304 pp, Patra

LAND SUBSIDENCE INDUCED BY THE OVEREXPLOITATION OF THE AQUIFERS IN KALOCHORI VILLAGE – NEW APPROACH BY MEANS OF THE COMPUTATIONAL GEOTECHNICAL ENGINEERING

Loupasakis C.¹ and Rozos D.²

¹ National Technical University of Athens, School of Mining and Metallurgical Engineering, Laboratory of Engineering Geology and Hydrogeology, 9, Heroon Polytechniou Str 157 80, Zografou (Athens) Greece, cloupasakis@metal.ntua.gr

² National Technical University of Athens, School of Mining and Metallurgical Engineering, Laboratory of Engineering Geology and Hydrogeology, 9, Heroon Polytechniou Str 157 80, Zografou (Athens) Greece, rozos@metal.ntua.gr

Abstract

Land subsidence induced by the overexploitation of the aquifers in Kalochori village has been occurring since 1965. The excessive water pumping led to the development of surface subsidence reaching, in several areas, the maximum values of 3 to 4m. The evaluation of the geological, geotechnical and hydrogeological setting of the wider Kalochori region as well as the historical background of the subsidence phenomena provided variable data, which were finally used for the study of the phenomenon by means of a finite element method simulation. The availability of the various geodetic records allowed the cross-checking of the results and the conduction of all necessary back analyses. Also, the knowledge of the land use distribution and the activities taking place in the wider Kalochori region helped the rational interpretation of the phenomenon and the detection of its causal factors.

Key words: *land subsidence, FEM simulation, aquifers' overexploitation, geo- hazards.*

1. Introduction

The increasing need for water, during the last decades, led to the overexploitation of aquifers in several regions in Greece. The overexploitation of aquifers susceptible to compaction led to the manifestation of land subsidence, in areas like Thessaly plain, Kalochori village, Megalopolis, Anargiri region (on the southwest of Florina) and Messara valley.

One of the first noticed land subsidence phenomenon in Greece is that in Kalochori region. Kalochori village occupy the lowlands between the delta of Gallikos river and the west side of Thessaloniki (Fig. 1). In the 1960's the wider Kalochori region became the main industrial centre of the area, leading to the increasing need of water, covered by productive wells. The overexploitation of the aquifers was also enchased by the excessive water pumping conducted by the Water Company of Thessaloniki (Fig. 1). The subsidence phenomena in Kalochori region were first noticed in the early 1960's. Since then, the morphological and the environmental setting of the region changed violently.

The land subsidence phenomena in Kalochori region have been studied during the last 25 years by many researchers. The majority of the researchers credit the subsidence mainly to the compaction

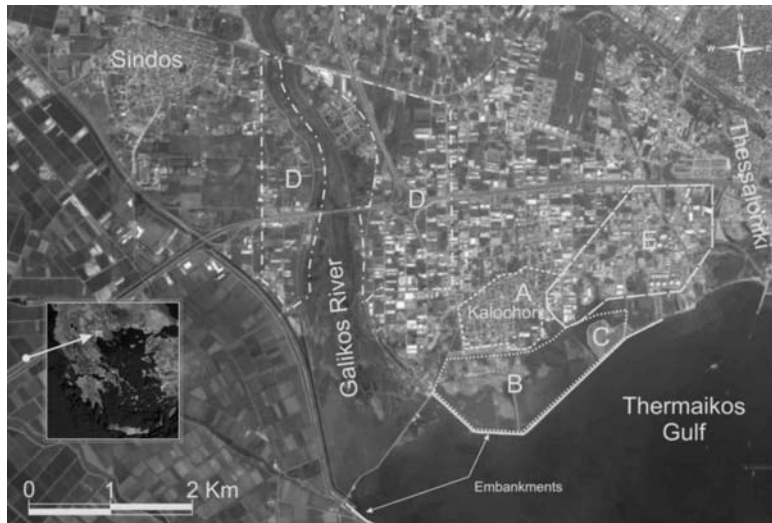


Fig. 1: Satellite picture (Google Earth) presenting the Kalochori Village in relation to Thessaloniki as well as the land use distribution in the wider region. The outlines enclose the following areas: A: Kalochori village, B: lagoon, C: waste dumping site, D: Water Company's productive wells areas, E: industrial area until the 1980's. Today the industries occupy almost all the wider Kalochori area.

of the reservoirs (Andronopoulos et al., 1990 & 1991, Hatzinakos et al., 1990, Rozos et al., 1993), although many other interpretations have also been expressed. Psimoulis et al. (2006) attributed the subsidence phenomenon to a large scale natural effect on which smaller scale anthropogenic effects, like water pumping induced compaction, are superimposed. Doukakis (2005) expressed the opinion that the rapid sea intrusion, beside the land subsidence, is amplified by the coastline erosion and by the sea level rising caused by the climate changes. Dimopoulos (2005) claimed that the subsidence phenomena in Kalochori region are caused by the consolidation of the loose silty-clay deposits and by the flowing sand phenomenon taking place close to the coastline. Stiros (2001) expressed that apart from the reservoirs' compaction, possible additional causes of the ground subsidence are: a) the consolidation of near-surface sediments, b) the oxidation of peat soils in the vadose zone, c) the syndimentary deformation of the delta, and d) the sub-surface instability of the delta front mud. The variety of the interpretations reveals the confusion that has been caused by the complexity of the phenomenon.

This study aims to coevaluate all available data provided by the numerous studies conducted in the area, in order to examine the land subsidence by means of a computational geotechnical engineering methods. The various geodetic records allow the cross-checking of the results and the conduction of all necessary back analyses, in order to calibrate and evaluate the geotechnical parameters as well as the Finite element simulation model.

2. Subsidence phenomena history

In 1965 a progressive marine invasion was noticed and finally, in 1969, during a period of intensive rainfall, the seawater reached the village. For the protection of the village an embankment was constructed along the entire coastline. This construction collapsed in 1973 due to continuous deforma-



Fig. 2: (Left) Submerged remnants of the old electricity network constructed along the side of a road, SW of Kalochori, in 1975. (Right) Emerged well's pipes at a 100 m deep well located in the Institute of Wheat Cultivation (SW of Kalochori). The pipes have been extracted 0.8 m over the ground surface. The photos were taken in 2008.

tions. In 1976 a new barrier was constructed in a forwarded position. Unfortunately three years later in 1979, after a storm, the embankment failed causing the re-flooding of the village. Finally, in 1980 a new larger dam was constructed. Since then several damages and extensions of the embankment were recorded, but the main construction managed to resist the subsidence deformations and the dynamic loading of the waves. This barrier is combined with an extensive surface draining network and several pumping-stations in order to prevent the inland from flooding.

Through the years several signs referring to the total amount of the subsidence were reported. Andronopoulos et al. (1990, 1991) reported that between 1964 and 1990 several basements were filled with gravels in order to prevent them from flooding, also the main square of Kalochori was reconstructed about 1.2m higher for the same purpose. Further more, it was reported that in many wells the pipes were extracted up to 2m over the surface. Some signs are still visible today (Fig 2).

Many researchers estimated subsidence deformations to exceed 3m in several locations (Andronopoulos et al., 1990 & 1991, Hatzinakos et al., 1990, Rozos et al., 2004). This estimation was finally supported by Stiros (2001), who compared the 1:5000 topographic diagrams for the period 1955 – 1980 (Fig. 3A). By means of that process, besides the total deformations values, Stiros proved that, until the 1980's, the maximum subsidence regions (subsidence >3m) were coinciding with the areas containing the pumping wells of the Water Company of Thessaloniki (Fig. 1) and with the south-western section of the industrial area containing the most water-consuming industries. According to geodetic measurements conducted during the last 20 years the rate of subsidence in the wider study area varies from 2,8 to 13 cm/yr. particularly, based on measurements conducted by the laboratory of geodesy of the A.U.Th. (Badelas et al., 1996), from September 1992 to July 1995, the subsidence rate in Kalochori region ranged from -3 to -13 cm/yr (Fig. 3b). Also, Doukas et al. (2004), by measuring a leveling network consisting of 37 stations, for a period of ten years, 1992 – 2002, estimated that the subsidence speed varied from -2,8 to -5 cm/yr. Note that, in both case studies the greatest subsidence occurred in the SE area of Kalochori. So, during the last decade, due to the in-activation of the Water Company's wells, the deformed areas have moved to the SW section of the old industrial area (Fig. 1).

Concluding, taking into account the various studies conducted for Kalochori region, the total amount

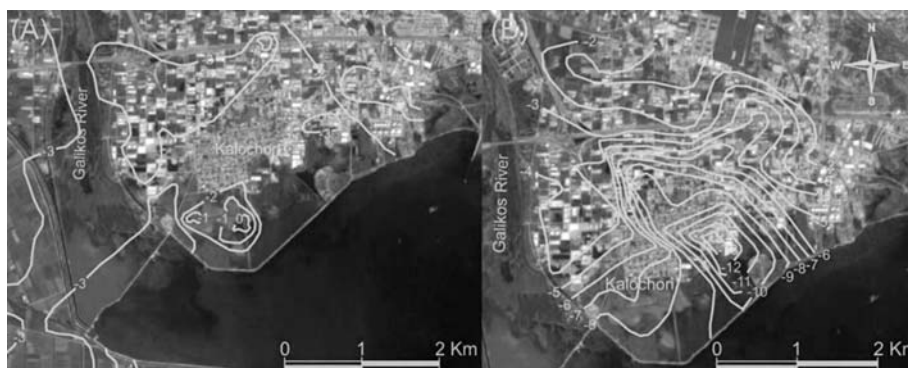


Fig. 3: (A) Equal subsidence contours, in meters, for the period 1955 – 1980 (Stiros, 2001). The 4 m contour, at the North of Kalochori, indicates an excavation. The -2, -1 and 0 contours, the south of Kalochori, indicates waste infill or earth-fill deposition. (B) Equal rate of subsidence contours (in cm/yr), from September 1992 to July 1995 (Badelas et al., 1996). The contours were plotted on Satellite images taken from Google Earth.



Fig. 4: View of the main embankment constructed in the South of Kalochori. On the right side of the embankment the sea level is about 0.5m below the road level. On the left (interior) side, the lagoon water level is 4 to 5m below the road level. Concluding, the inland is at least 4m below the sea level.

of subsidence in the past 45 years must be reaching, in several areas, the maximum values of 3 to 4m. Furthermore, based on the same studies, the subsidence phenomenon keeps on developing at a mean rate of -5 cm/yr. At the present time, extended areas along the coastline are located below the sea level (Fig. 4)

3. Geological, Hydrogeological and geotechnical setting

The upper formation of the study area (Hatzinakos et al., 1990, Rozos et al., 2000, 2004) is occupied by loose quaternary deposits. According to the geophysical investigation conducted by Nikolaou and Nikolaidis in 1987, those deposits extend down to a depth varying from 150 to 400m. Furthermore, based on additional data coming from the profiles of petroleum investigation drills (Demiris, 1988), carried out in the wider study area during 1962, the deeper strata are occupied by neogene deposits reaching down to a maximum depth of 600-700m. The neogene formations consist of silty sands and sands with silt, clay and infrequent fine gravel intercalations.

According to the profiles of eight (8) geotechnical boreholes drilled in the Kalochori region (Andronopoulos, 1979, Andronopoulos et al., 1990), reaching down to depths varying from 20 to 90m, the quaternary deposits consist of clays, silty clays, sands and silty sands including organic material. The various in-situ and laboratory tests conducted on the core samples have given sufficient information about the physical and the mechanical properties of the above mentioned formations extended in the narrow study area

The lithostratigraphy of the sediments up to the depth of 90m consists of the following formations: the top horizons, from the surface to a depth of 4.5 to 15m, are occupied by yellow-brown fine to medium grain sands and silty sands. Under the sands and down to a varying depth of 26.5 to 35.3 m extends a black-gray silty sands horizon including organic materials. These impermeable silty sands constitute a barrier between the deep artesian aquifers and the unconfined shallow aquifer extending in the overlying sands. The deeper horizons consist of brown sands and black-gray silty sands in alternations. The thickness of the interchanging layers varies from 5 to 50 m increasing proportionally to the depth. The brown sands are medium to coarse grain and in several depths thin silty sand intercalations are located. The diagenesis and the compaction degree of the above described sediments increase proportionally to the depth. Although there is not any available geotechnical information for depths over 90m, the geophysical investigation results and data coming from water drilling profiles showed that the above mentioned alteration routine continues down to the Neocene basement. A simplified typical cross section is presented in Fig. 9.

In agreement with the above described geological setting the formations of the wide study area contain one unconfined shallow aquifer extending in the overlying sands and a system of successive confined - artesian aquifers developing below the impermeable black-gray silty sand layer, located under the top sand. At the deep confined, the aquiferous units are the brown sands, interrupted by thick black-gray silty sands intercalations.

The water table depth of the unconfined shallow aquifer fluctuates from 1.5 to 3m and the quality of the water is very poor (Loupasakis et al., 1997; Soulios, 1999). This aquifer reaches down to a depth of 10 to 15 m and is widely used for meeting the needs of the farmers for irrigation water or occasionally as drinking water for cattle breeding purposes.

The first wells discharging the deep aquifers were constructed by the industries and by the Water Supply Company of Thessaloniki in 1955. Since then, the Water Company has constructed about 30 productive wells and the Kalochori village authorities 7 more, some of them reaching down to depths more than 200m. Further more, It is estimated that in the wider Kalochori area, during the last 50 years, more than 250 industrial wells have been operating. Most of these wells were drilled without the proper state permits. The great number of deep drills, points out the excessive discharge that has been taking place during the last decades in the wider area.

The piezometric surface of the aquifers, in the majority of drills constructed in Kalochori region during the 50s, was over the ground and the drills were artesian. Despite that, the overexploitation of the aquifers over the years caused the intensive drawdown of the piezometric surface and finally in 1981, it fell 37m (Andronopoulos et al., 1990). In the early 1980`s the water company abandoned the majority of the drills. Unfortunately, the authorities could not control the industrial drills, which were kept operating. Nevertheless, the reduction of the pumping wells led to the partial recovery of the piezometric surface level. According to measurements conducted during the period of 1997 – 2000 for a study commissioned by the Water Company (Soulios, 1999), the piezometric surface's level in the Kalochori region varied from 20 to 30m. The extreme variation points out the dynamic character of the aquifer caused by the continuous pumping.

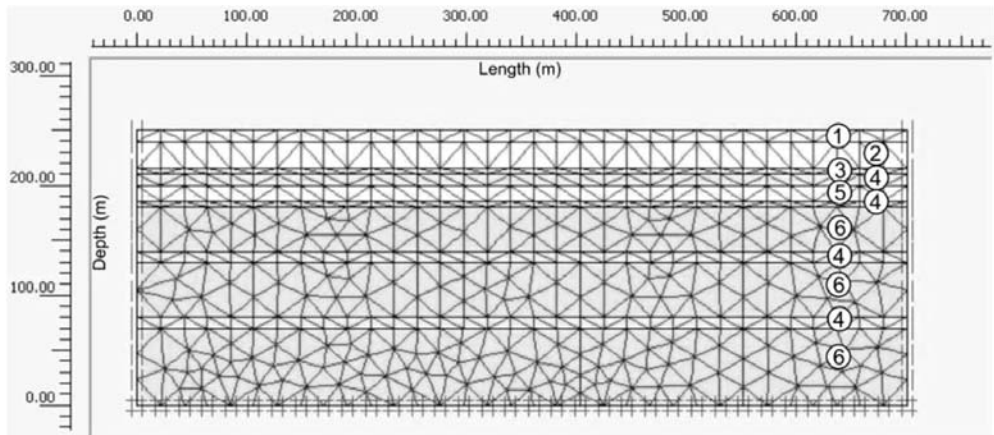


Fig. 5: Cross section of the simulated 250m deep profile. The numbers correlate the soil data set parameters presented in table 1 with the horizons.

4. Simulation procedure of the subsidence phenomenon

The gradual drawdown of the piezometric surface for about 40m definitely affected the pore pressure distribution in the overexploited confined aquifer formations. The pore pressure reduction could be considered responsible for the subsidence phenomenon. So, the simulation of the gradual piezometric surface drawdown in a typical profile, by means of finite or discrete element methods, could define the influence of the pore pressure reduction and could clarify the mechanism of the subsidence phenomenon. The numerous studies conducted for the Kalochori region provided plenty of data concerning the geological, the geotechnical, the hydrogeological setting as well as the historical background of the subsidence phenomena. These data covered all the requirements for setting up the polyparametric finite element simulation model applied in the present study. Furthermore, the availability of the various geodetic records allowed the crosschecking of the results and the conduction of all necessary back analyses, in order to calibrate the simulation model. These data appeared to be necessary and the model could not be applied without knowing them. Correspondingly, all these data could not be valuable without using a sophisticated polyparametric numerical analysis method as the one applied in this study. Practically, this case study was considered as the perfect chance of applying this FE method for the analysis of a water pumping induced subsidence phenomenon.

The simulation was conducted by using the PLAXIS (V 8.6) two – dimensional finite element code (Brinkgreve et al., 2002). This two – dimensional code could be considered sufficient as the present study practically deals with the simulation of a typical cross section with no horizontal transitions. The simulation procedure was applied in two characteristic profiles (Loupasakis & Rozos, 2009). Combining the geological and hydrogeological setting, the maximum depth of the overexploited confined aquifers ranges between 150 and 250m. Therefore, the two typical profiles of 150 and 250m were considered for the simulation of the subsidence phenomenon. The alteration and the thickness of the simulated geological formations is clearly presented in figure 5 and in table 1 and it is identical in both profiles. The only difference is that in the 150m deep profile the bottom layers are missing. The width of the typical profiles was selected to be approximately three times bigger than their depth. Standard horizontal and vertical fixities were applied. The coarseness of the mesh was also selected to be fine in order to fit the narrow geological layers (Fig. 5).

The reevaluation of the available geotechnical data (Andronopoulos, 1979, Andronopoulos et al.,

Table 1. Soil data sets parameters.

Parameter	Yellow-brown sands (1)	Black-gray silty sands (2)	Brown sands and silty sands (3)	Black-gray silty sands (4)	Brown sands and silty sands (5)	Brown sands and silty sands (6)
Depth (m)	0-10	10-35	35-40	40-50, 65-70, 110-120, 170-180	50-65	70-110, 120-170, 180-250
Type	Drained	Drained	Drained	Drained	Drained	Drained
γ (kN/m ³)	18,50	16,00	19,50	17,50	18,50	19,50
γ_{sat} (kN/m ³)	20,60	17,50	22,00	19,80	20,60	22,00
k_x (m/day)	8,93	0,638	8,93	0,638	8,93	8,93
k_y (m/day)	8,93	0,638	8,93	0,638	8,93	8,93
E_{ref} (kN/m ²)	16668	5400	19164	11250	16665	18570
ν (-)	0,25	0,20	0,25	0,25	0,25	0,30
G_{ref} (kN/m ²)	6666	2250	7667	4500	6668	7142
E_{oed} (kN/m ²)	20010	6000	22995	13501	19989	25005
c_{ref} (kN/m ²)	10,00	60,00	35,00	80,00	10,00	40,00
ϕ (°)	38,50	7,00	40,00	15,00	38,50	40,00
Ψ (°)	3,00	0,00	5,00	0,00	3,00	5,00

1990) proved that the appropriate model for the simulation procedure was the elastic – perfect plastic model based on the Mohr – Coulomb failure criterion (Mohr – Coulomb model). The final values of the mechanical parameters selected for the simulation of the geological formations are presented in Table 1.

As mentioned, the piezometric level in the majority of the deep wells constructed in Kalochori region in 1955 was over the surface. Therefore, for the configuration of the models' initial pore pressure the confined aquifers' piezometric surfaces were set 5m over the ground surface. On the contrary, the water table depth of the unconfined shallow aquifer was set 5m below the ground surface and it was kept stable during the entire calculation procedure. Furthermore, a close flow boundary was applied at the base of the profiles.

The simulation procedure was divided in five calculation phases. During the first calculation phase, the piezometric level was reduced from +5m to -10m and during the next phases the level was increasingly reduced 10m reaching down to the maximum depth of -50m. The maximum piezometric level drawdown recorded during the years was 37m. In addition, the models were set to calculate the effect of an extra 10m piezometric level drawdown, from -40 to -50m, in order to study the effect of a hypothetical future development of the phenomenon. The calculations were carried out using the "plastic analysis" procedure – a typical elastic-plastic deformation analysis defined by the selected calculations model. Because of the slow deformation rates, it was considered that no excess pore pressure conditions were generated so the "drained behavior" setting was selected. The gradual reduction of the piezometric surface was applied by means of the "stage construction" routine.

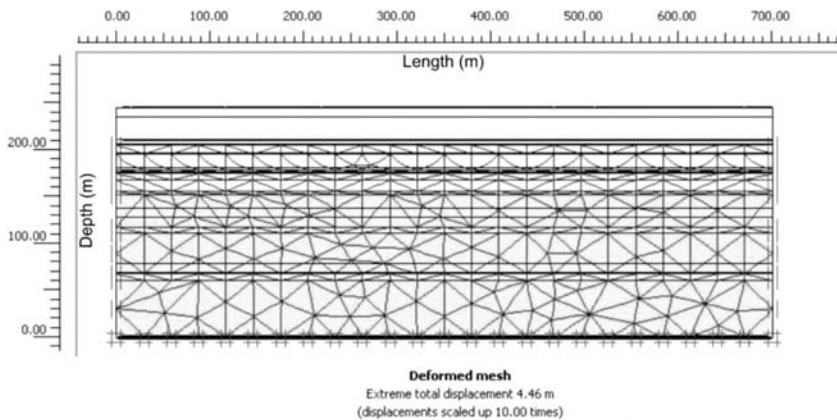


Fig. 6: Deformed mesh of the 250m deep profile after the drawdown of the piezometric level 40m under the ground surface.

5. Simulation results

The simulation results indicated that piezometric surface downgrading to the depth of -40m caused total deformations of -3.05 and -4.46m (Fig. 6) to the 150 and 250m profiles, respectively. The deformations are in good agreement with those observed in the wider Kalochori region.

Except for the total displacements, the simulation procedure allowed the evaluation of the gradual piezometric surface downgrading effect and provided a complete set of displacement, strain, stress and pore pressure values for the various calculation steps (table 2). Regarding to the stress and the pore pressure values, the gradual reduction of the piezometric level causes a proportional reduction of the pore pressures and an increase of the effective principal stress. The preserved balance between the pore pressures and the effective stresses keeps the total principal stress stable. This helps understand the difference between the subsidence and the consolidation mechanism; the subsidence could occur without the application of additional external loads and it appears to be the result of the balance kept between the effective stresses and the pore pressure, when the water level drops.

Although the gradual reduction of the pore pressure led to an expected increase of the displacements (table 2), the rate of those deformations decreases in respect to the piezometric level redraw. As a result, although the deformations keep on developing, they gradually slow down as the formations reach to their maximum compaction level.

Despite the gradual decrease of the deformation rate, it was estimated that a 10m additional reduction of the piezometric level, from -40 to -50m, could cause extra deformations of -0.46 to -0.79m to the wider Kalochori region. Those deformations will cause problems to the embankments as in several sections they exceed the sea level less than 1m.

The step – vertical displacement graphs (Fig. 7) drawn for the various depths of the profiles, point out the expected gradual reduction of the displacements in respect to the depth. The differences occurred between the displacements in the various depths and through the same calculation steps, can be related to the emersion of the wells` pipes occurred in the wider Kalochori area. Therefore, as presented in the 250m deep profile (Fig.7), the deferential vertical displacements between the points located at the -10 and at -110m are 2.2m. This displacement could definitely justify the 0.9m emersion of the 100m deep well`s pipes presented in Fig. 2. Note that the differences between the estimated deferen-

Table 2. Maximum (Extreme) displacement, strain, stress and pore pressure values for the various piezometric level drawdown calculation steps in both simulation profiles.

Piezometric surface level (m)	Maximum total vertical displacement (m)	Total phase vertical displacement (m)	Maximum effective principal stress (kN/m ²) *	Maximum total principal stress (kN/m ²) *	Maximum active pore pressure (kN/m ²) * Simulation
Simulation profile reaching down 150m					
-10	-0.735	-0.736	-1.68 10 ³	-3.07 10 ³	-1.40 10 ³
-20	-1.55	-0.825	-1.77 10 ³	-3.07 10 ³	-1.30 10 ³
-30	-2.36	-0.820	-1.86 10 ³	-3.06 10 ³	-1.20 10 ³
-40	-3.05	-0.705	-1.95 10 ³	-3.05 10 ³	-1.10 10 ³
-50	-3.50	-0.458	-2.04 10 ³	-3.04 10 ³	-0.996 10 ³
Simulation profile reaching down 250m					
-10	-1.08	-1.08	-2.85 10 ³	-5.24 10 ³	-2.39 10 ³
-20	-2.25	-1.18	-2.94 10 ³	-5.23 10 ³	-2.29 10 ³
-30	-3.40	-1.16	-3.03 10 ³	-5.22 10 ³	-2.19 10 ³
-40	-4.46	-1.07	-3.12 10 ³	-5.21 10 ³	-2.09 10 ³
-50	-5.24	-0.7845	-3.20 10 ³	-5.19 10 ³	-1.99 10 ³

* Compression = Negative

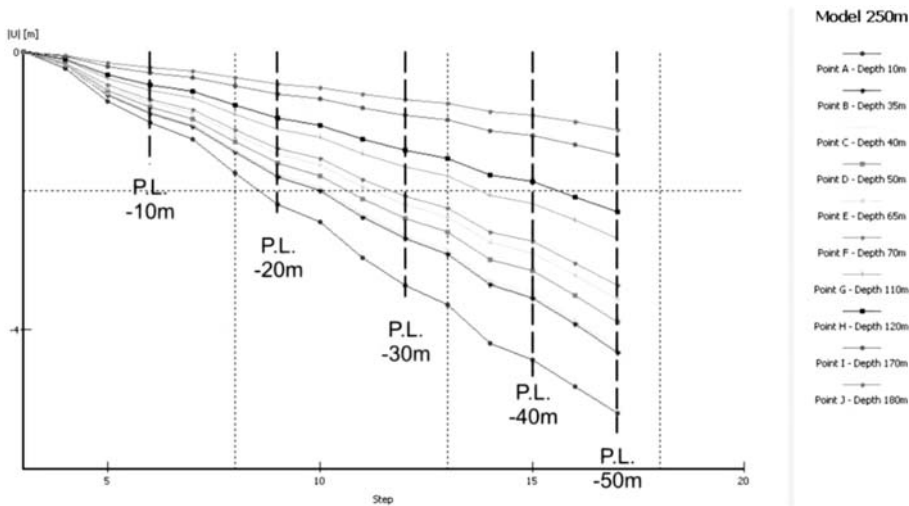


Fig. 7: Vertical strain – calculation steps curves presenting the development of the deformations in critical points appointed at the bases of the layers forming the 250m deep profile. The vertical dashed lines point out the final calculation steps of the various piezometric level (P.L.) drawdown steps.

tial displacements and the occurred emersion of the pipes could be explained by the fact that, before the extraction of the pipes and because of their considerable weight, they should have statically penetrated the underlying formations maybe for more than one metre before they started emerging.

6. Concluding remarks

Taking into consideration the results of the simulation the occurred excessive deformations can be attributed mainly to the overexploitation of the confined aquifers. Besides the encouraging results of the simulation, there are many other indications weakening the main theories of the, claimed by many researchers, near-surface deformations. The lack of differential settlements, even in the oldest and the heaviest residential and industrial buildings, the development of the deformations in areas completely unloaded by manmade surface structures, the unchanged hydrological conditions of the shallow unconfined aquifer through the years, are some of the most important indications or facts weakening the above mentioned theories. If the near – surface sands or organic silty sands were susceptible to intensive settlements, this could have affected the surface constructions and the deformations could had been more intensive in areas occupied by residential or even more by heavy industrial buildings.

Concluding, the only way to reduce the deformation rate of the subsidence phenomena and protect the Kalochoi region from further deformations, is to decrease and control the quantities of the extracted ground water.

7. References

- Andronopoulos V. 1979. Geological and geotechnical study in the Kalochoi (Thessaloniki) area. Institute of Geology and Mineral Exploration Report, Athens, p. 90.
- Andronopoulos V., Rozos D., Hatzinakos I. 1990. Geotechnical study of ground settlement in the Kalochoi area, Thessaloniki District. Institute of Geology and Mineral Exploration Report, Athens, p. 45.
- Andronopoulos V., Rozos, D., Hatzinakos, I. 1991. Subsidence phenomena in the industrial area of Thessaloniki, Greece. In: Johnson, A. (Ed.). Land Subsidence, vol. 200. IAHS Publishers, pp. 59-69.
- Badelas A., Savvaidis P., Ifadis I., Doukas I. (1996). Monitoring of ground subsidence in the area of Kalochoi by using a high precision leveling control network. *Technical Report No. 2853*, Research Committee, Aristotle University of Thessaloniki, p. 157.
- Brinkgreve, R.B.J., Broere, W., Waterman, D. (2006) Plaxis, Fine Element Code for Soil and Rock Analyses, 2D - Version 8, A.A. Balkema, Rotterdam Brookfield.
- Demiris K. 1988. Geological settings and their influence on the development of the areas on the west of Thessaloniki. Proceedings of the symposium on the technical problems affecting the areas on the west of Thessaloniki, Technical Chamber of Greece, Thessaloniki.
- Dimopoulos G. 2005. Investigation of the conditions generating soil settlements in Sindos – Kalochoi area of Thessaloniki. In: Stournaras G., Pavlopoulos K., Bellos Th. (Eds.), Proceedings of the 7th Hellenic Hydrogeological Conference and 2nd MEM Workshop on Fissured Rocks Hydrogeology, Vol. 1, pp. 135-146.
- Doukakis E. 2005. Coastal red spots along the western Thermaikos gulf. Proceedings of the 9th International Conference on Environmental Science and Technology, Rhodes island, Greece, pp. A334 - A339.
- Doukas I., Ifadis I., Savvaidis P. 2004. Monitoring and analysis of ground subsidence due to water pumping in the area of Thessaloniki, Hellas. Proceedings of FIG Working Week, Athens, Greece. p. 14
- Hatzinakos I., Rozos, D., Apostolidis, E. 1990. Engineering geological mapping and related geotechnical problems in the wider industrial area of Thessaloniki, Greece. In: Price, D. (Ed.), Proceedings of Sixth International IAEG Congress, Amsterdam, Balkema, pp. 127-134.
- Loupasakis C., Sotiriadis M., Soulios G. 1997, Hydrochemical characteristics of the underground water of the plain area located between Thessaloniki and N. Halkidona, Proceedings of the 4th Hydrogeological Congress of the Hellenic Hydrogeological Committee and the Association of Geologists and

- Mineralogists of Cyprus, Thessaloniki, pp. 194 – 212.
- Loupasakis C., Rozos D., 2009, Land Subsidence Induced by Water Pumping in Kalochori Village (North Greece) - Simulation of the Phenomenon by Means of the Finite Element Method, Quarterly Journal of Engineering Geology and Hydrogeology, Geological Society of London, v. 42, No. 3; pp. 369-382.
- Nicolaou, S., Nicolaidis, M. 1987. Geoelectric study in Kalochori village of Thessaloniki, Institute of Geology and Mineral Exploration Report, Athens, p. 10.
- Rozos D., Apostolidis E., Christaras B., (2000) Engineering – geological map of Thessaloniki wider area. Proceedings of national meeting on protection of Thessaloniki from natural hazards, 46-53.
- Rozos D., Apostolidis E., Hatzinakos I. (2004) Engineering – geological map of Thessaloniki wider area, Greece. Bull. Eng. Geol. Env., 63. 103-108.
- Rozos D., Hatzinakos I. 1993. Geological conditions and geomechanical behaviour of the neogene sediments in the area west of Thessaloniki (Greece). Proceedings of International Symposium on Geotechnical Engineering of Hard Soils – Soft Rocks, Greece. In: Anagnostopoulos et al (Eds.) Balkema, Rotterdam, Vol. 1 pp. 269-274.
- Psimoulis, P., Ghilardi, M., Fouache, E., Stiros, S. 2007. Subsidence and evolution of the Thessaloniki Plain, Greece, based on historical leveling and GPS data. Engineering Geology, 90, 55-70.
- Soulios, G. 1999. Research for the development of the aquifers in the low lands on the west of Thessaloniki for the interests of the Water Company of Thessaloniki. Research Committee *Technical Report*, Aristotle University of Thessaloniki, p. 99.
- Stiros, S. 2001. Rapid subsidence of the Thessaloniki (Northern Greece) coastal plain, 1960-1999. Engineering Geology, 61, 243-256.

GEOTECHNICAL INVESTIGATION OF THE ROCK SLOPE STABILITY PROBLEMS OCCURRED AT THE FOUNDATIONS OF THE COASTAL BYZANTINE WALL OF KAVALA CITY, GREECE

Loupasakis C.¹, Spanou N.², Kanaris D.³, Exioglou D. ⁴, Georgakopoulos A.⁵

¹ Institute of Geology and Mineral Exploration, Engineering Geology Department, Olympic Village, 13677, Acharnae, Greece, cloupas@igme.gr

² Institute of Geology and Mineral Exploration, Engineering Geology Department, Olympic Village, 13677, Acharnae, Greece, spanou@igme.gr

³ Institute of Geology and Mineral Exploration, Engineering Geology Department, Olympic Village, 13677, Acharnae, Greece, dkanaris@igme.gr

⁴ Institute of Geology and Mineral Exploration, East Macedonia-Thrace Regional Branch, Brokoumi 30, 67100, Xanthi, Greece, dimitrisexioglou@yahoo.gr

⁵ Aristotle University of Thessaloniki, School of Geology, Department of Mineralogy-Petrology-Economic Geology, Laboratory of Economic Geology, 54124, Thessaloniki, Greece, ageorgak@geo.auth.gr

Abstract

The coastal Byzantine wall of Kavala is located at the Panagia peninsula and it is founded on the Simvolou granite. The granite rock mass appears to be fractured by joint sets with very high persistence (>20m) and very wide spacing (60cm – 2m), forming large rock blocks. Further more, the Panagia peninsula is intersected by numerous parallel normal faults, forming extended zones of intensively fractured rock mass. Along the coastline the granite appear to be eroded by the sea waves, forming small gulfs around the faults.

The Byzantine wall is founded along the edge of the fractured slopes forming the coast line of the peninsula, arising issues about the safety of the historical construction. The joint sets form numerous rock wedges with unfavourable orientation, many sections of the slopes are undercut by the wave erosion and in the majority of the fault zones the rock mass presents intensive fragmentation.

The above described condition of the rock mass was recorded in detail along the entire coast line and all unstable sections were located. A full set of support measures was proposed for all unfavourable sections aiming to the improvement of the geotechnical behaviour of the rock mass, constituting the foundation formation of the Byzantine wall.

Key words: *Rock slope stability, rock wedges, Panagia coastal Byzantine wall, Kavala*

1. Introduction

Castles were constructed for ages in morphologically isolated locations providing the necessary additional natural defence. These locations besides their defensive advantage they leave these constructions exposed to the destructive powers of the nature. Rock slope stability problems, earth

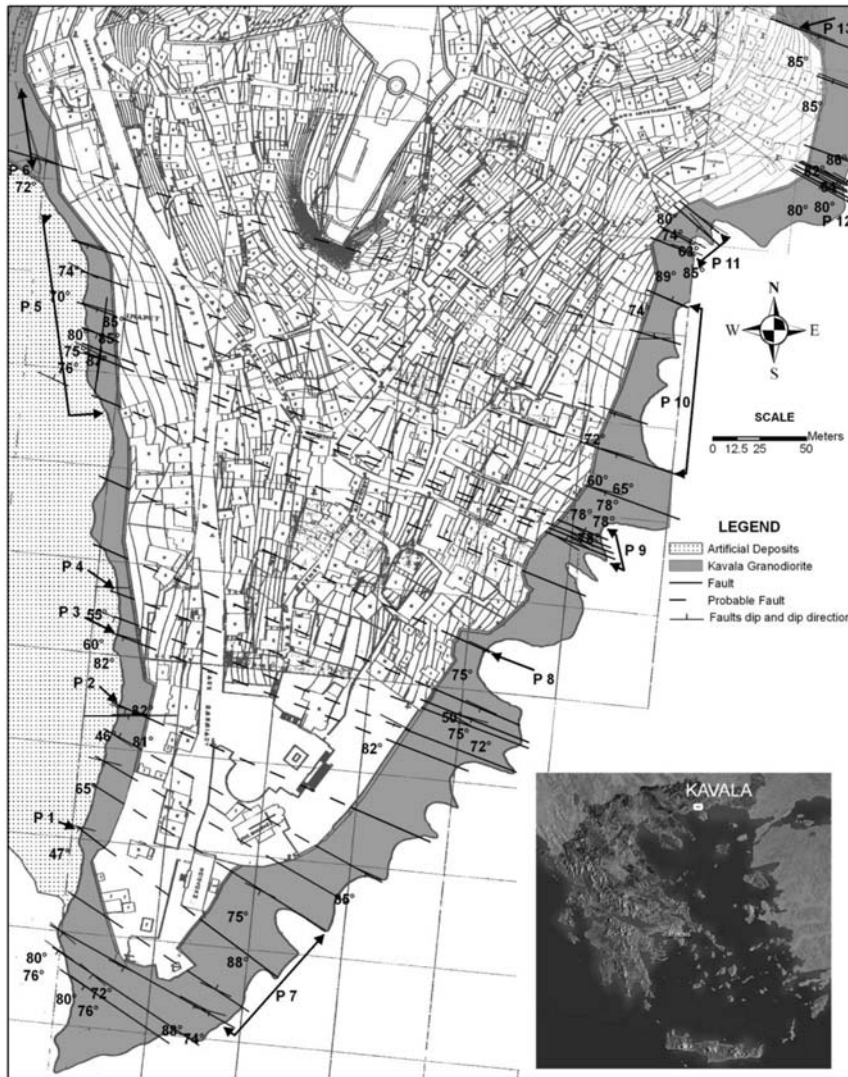


Fig. 1: Geological map of the peninsula presenting the location of the numerous normal faults recorded along the slopes. The gulfs excavated, by the wave erosion, along the faults' zones are clearly presented. The locations indicated by the P1 to P13 signs refer to parts where slope stability problems occur.

sliding problems, wave erosion, wind erosion are some of the most common phenomena damaging these historical monuments (Loupasakis & Georgakopoulos, 2009; Topal et al., 2007; Greif, 2006; Donnelly et al, 2005; Kamh, 2005; Vlcko, 2004; Kolait & Koumantakis, 1991; Ghosh, 1990).

Intense public interest for safeguarding such historical structures, requires the application of remedial measures. Several cases prove that these measures are usually focused on the preservation of the architectural character of the monuments, underestimating or overlooking the before mentioned geological – geotechnical problems. The destructions manifesting in some of these monuments prove that, comprehensive and detailed engineering geological and geotechnical investigations should be

conducted before remedial and corrective measures are proposed and applied.

The coastal Byzantine wall of Kavala is a typical example of monument that, besides the controversial static sufficiency of the structure, several geotechnical issues arise concerning the stability of the rock slopes bearing the wall. The Byzantine wall of Kavala encloses Panagia's settlement which is sited at the homonymous triangular peninsula (Fig. 1). The settlement is located 60m over the sea level and its boundaries are clearly distinguished by natural and artificial structures, such as the coastal wall, the slopes, the terrestrial wall and the byzantine aqueduct.

The main factor affecting the morphology of the peninsula and as a result the slope stability is the wave erosion. These erosive procedures combined with the tectonic fragmentation formed the vertical slopes bearing the wall. In several parts the slopes are intensively undercut, especially along the major tectonic faults intersecting the peninsula vertically (Fig. 1). The erosion along the coastline led to the formulation of repeated gulfs, reaching the base of the wall. Along the west side of the peninsula the erosive procedures are suspended because of the construction of an extended pier.

This paper is based on the results of an extended study conducted in Kavala, aiming to locate unstable slopes into the urban environment of the city and to propose measures for the improvement of the geotechnical behaviour of the rock mass. During the study the slopes surrounding the Panagia peninsula were analysed in details, providing substantial data for the condition of the rock mass and for its effect on the integrity of the overlay monument.

2. Geological setting

The wider study area is formed by Simvolou granite, part of the Rodopi plutonic mass. Simvolou granite is a big plutonic body sited to the SW part of Kavala prefecture, occupying an area of about 150 km². The plutonic rock has been transformed under greenschist metamorphic phase. It is a granite – granodiorite, medium granuled and penetrated by a dense system of pegmatite and aplite veins. At places it shows a porphyritic texture with phenocrysts of K-feldspar (orthoclase) bigger than 5 centimeters. Two mineral phases can be noticed in the rock, one igneous and another metamorphic (IGME, 1973).

The main systems of faults of the Rodopic mass have SW – NE and NW – SE direction. Panagia peninsula is intersected by numerous parallel normal faults (Fig. 1), forming extended zones of intensively fractured rock mass. The sub-horizontal shearing, the dense systems of joints and the perpendicular faults intersect the rock mass forming numerous wedges along the slopes of the peninsula.

3. Rock slope stability problems

The stability of the rock slopes surrounding Panagia peninsula was examined taking under consideration the joint sets and the faults intersecting the rock mass, the morphology and the orientation of the slopes as well as the wave erosion effect and the location of the wall in relation to the slopes. Based on these data the slopes were divided in two major categories a) the slopes along the west - southwest part of the peninsula, protected from the wave erosion by the pier and b) the slopes along the southeast part exposed to the sea action.

The western – south western slopes present dip ranging between 45° and 90° and height extending 10 to 20m over the pier level. The Byzantine wall along several sections was founded close to the edge of the slopes and as a result slope failures can effect directly the integrity of the monument (Figs 2 & 4). The stability problems are more intensive along the faults. The rock mass is fractured and



Fig. 2: Location P1. A fault intersects the slope forming a huge rock wedge and a wide fractured zone. The Wall fills the gap between the two sections of the fault.



Fig. 3: Location P4. An intensively fractured zone caused by a fault. The wave erosion caused intensive underexcavation to the slope.

the wall was constructed in direct continuity with the slope. Even worse, in some places the wall was constructed forming a bridge across the two sections of the fault (Fig 3 & 5B,C,D). Figures 2 to 5 present typical examples of sections appearing slope stability problems capable of effecting the Byzantine monument.

The statistical analysis of joint sets measurements, conducted along the slopes, proved that the rock mass was intersected by 3 major joint sets: a) J1: 305/72, b) J2: 203/86 and c) J3:240/8. J1 and J2 are almost vertical, forming the slopes, while J3 is almost horizontal rising to the slopes. As expected, the joint sets are parallel to the main fault direction, 200/77 & 283/81, intersecting the peninsula (Fig. 1). Referring to the slopes, they are distributed in two main directions 272-302/65-90 and 202-216/45-85.

Stability analyses conducted for the slopes with a dip direction 272°-302°, revealed that joints sets J1 and J2 form rock wedges rising along the slopes. These wedges tend to slide along the axis formed by the intersection of the before mentioned joints, with an angle of 73°. The slopes appearing a dip angle smaller than 73° are safe, as the rock wedges are self supported. On the contrary, the slopes with a larger dip angle are unstable. These wedge slides can threaten the Byzantine Wall only in cases where the foundation of the wall was constructed close to the slope edge. Precisely, in parts where the foundations were constructed in a distance smaller than half the height of the slope (Fig. 5E). Signs of oversized wedges that have already failed are visible in several parts of the slopes (Figs. 2, 4 and 6).

The corresponding analyses conducted for the slopes with a dip direction 202°-216° proved that those slopes are stable; no oversized rock wedges are formed (Fig. 5A). The only stability problems can be expected by the falls of small rock blocks sited along the slope face.



Fig. 4: Location P2. An oversized rock wedge that probably failed during the excavation of the small tunnel appearing at the base of the slope, on the left side of the picture. The extension of the failure could very easily damage the Byzantine wall.

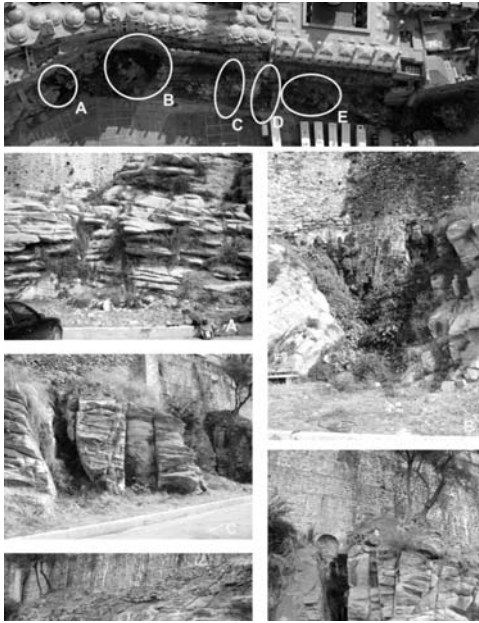


Fig. 5: Part P5. View of the slopes below Imaret monument intersected by the faults presented in the map of Fig. 1. The deterioration of the rock mass along the major tectonic lines cause serious rock slope stability problems threatening the monument. The letters pointing the various unstable locations correspond to the homonymous pictures (5A to 5E).

The South-eastern slopes present dip ranging between 45° and 90° and height extending 20 to 30m over the sea level. The lower parts of the slopes are found into the sea, effected by the marine erosion. The longest parts of the Byzantine wall are protected from the marine erosion and from the rock wedge failures as they are founded far from the edge of the slopes. However, along parts where the slopes are intersected by numerous faults, erosion processes have formed small gulfs and the sea has approached the historical construction, putting its foundation in danger (Fig. 7).

The statistical analysis of joint sets measurements, conducted along the slopes, proved that the rock mass along the SE slopes was also intersected by the 3, before mentioned, major joint sets. Their slightly changed orientation data are: a) J1: 294/87, b) J2: 205/79 and c) J3: 112/15. Referring to the slopes, they are distributed in two main directions 102-122/75-90 and 205-216/30-55 and they are also effected by the orientation of the major tectonic structures and the joints sets.



Fig. 6: Part P6. Several rock wedges are formed, to prevent them from sliding the underexcavated rock blocks were sub founded by the use of masonry walls – fills (lower right corner of the picture).

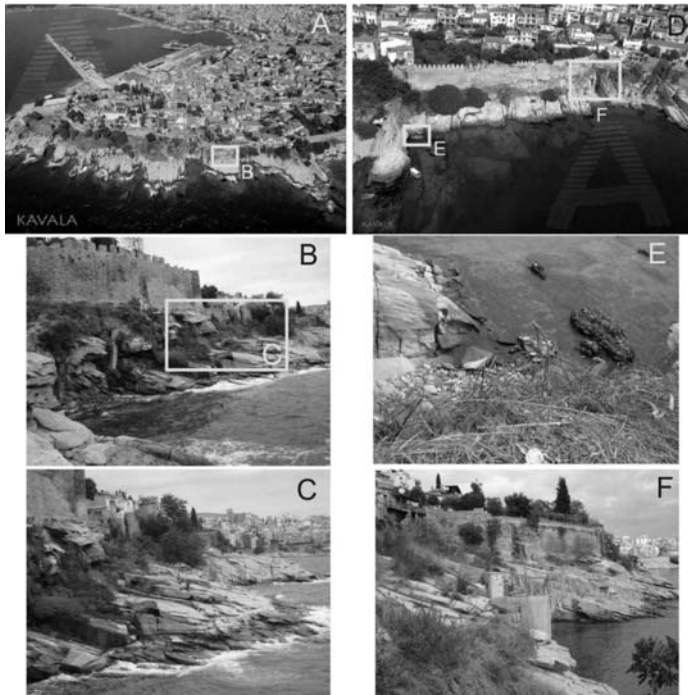


Fig. 7: Parts P9 and P10. View of the slopes along the SE part of the peninsula. Along the parts where the slopes are intersected by numerous faults the marine erosion processes have formed small gulfs and the sea has approached the historical construction, putting its foundation in danger. E: A collapsed section of the wall is presented.

Slope stability analyses applied to 205° - 216° inclined slopes proved that there is no danger for rock wedges sliding. On the contrary, J2 combined with the other joint sets, form rock fragments prone to toppling. Therefore, the Byzantine wall's stability is in danger only at the sites where it is founded close to the slope edge. Correspondingly, slope stability analyses to the slopes presenting 102° - 122° dip direction verified that there is no prospect for plain or wedge failure occurrence. However, despite J3 joint set's low dip angle and J2 perpendicular development to the slope, J1 joint set orientation appoint the slopes unstable to toppling.



Fig. 8: Part P13. Underexcavated slope along a fault scarp. The wall was founded close to the edge. The toppling or the rupturing of the rock mass could cause extensive damages to the monument.

Concluding, the slopes sited at the SE part of Panagia peninsula are not prone to rock sliding. On the contrary, toppling is likely to occur. Rock fragments of 2-3meters maximum height could topple, especially in parts where their foot is undercut (Figs. 7, 8). These phenomena could damage the historical monument at those areas where marine erosion has excavated rupture zones reaching to Byzantine wall's foundation.

4. Proposed support measures

Along the slopes were located thirteen (13) parts with serious stability problems, able to effect the Byzantine wall (Fig. 1 Parts P1 to P13). These problems are a) wedge or plain failures (Varnes, 1978; Koukis & Sabatakakis, 2007), especially along the W-SW slopes and the fault zones, b) toppling failures (Goodman & Bray, 1976), along the SE slopes and c) extensive underexcavation problems, especially along the unprotected by the pier SE slopes. Further more, random rockfalls were recorded all around the peninsula, even along the stable parts of the slopes, because of the rock blocks sited along the slopes. Those blocks were formed by the joints intersecting the rock mass and they were displaced by the marine erosion and/or by the human activities.

The proposed support measures aim to efface the rock fall danger and to protect the Byzantine wall, by taking under consideration the monumental character of the site and the request for its minimum aesthetic destruction (Loupasakis et al., 2009).

In order to avoid the wedge, plane and toppling failures spot bolting and sub-foundation constructions were proposed. To be more precise, the overhanging blocks could be supported by grouted rock bolts installed in selected locations. The underexcavated parts could be supported by filling the void with reinforced concrete constructions (buttresses, gravity walls etc.) camouflaged by stone coating. As presented in fig. 6, sub-foundation constructions were also applied in the past.

The marine erosion of the slopes can be effaced by the installation of seawalls. These breakwater structures can be constructed by granite boulders, fitting to the surrounding bedrock and causing the minimum aesthetic distortion to the site. As presented in figure 7, the shallow sea, close to the coastline, allows the installation of the boulders by using barges. Unfortunately, these structures are going to block the small beaches formed along the gulfs. Small piers or narrow passages through the breakwater structures can provide solution to the problem.

The random rockfalls recorded especially along W-SW slopes can be encountered by installing a safety fence or a wide hedgerow along the base of the slopes. This conventional solution does not obstruct the activities taking place along the pier because a small flowerbed has already been constructed and it only has to be upgraded.

5. Conclusions – discussion

This case study clearly presents that the geotechnical problems occurring at slopes used as foundation formations of castles could cause serious damages to the monuments. So, it is essential these problems to be effaced before applying any other reconstruction projects.

The modern techniques for improving the geotechnical behaviour of the geological formations and of the rock mass, in particular, can provide solutions without causing serious aesthetic distraction to the sites.

The general conclusion that, the geotechnical problems should be effaced according to priority, could be proposed to all monuments appearing geotechnical problems of all kinds (slope stability, landslides, settlement, subsidence etc.).

6. References

- Donnelly, L. J., Culshaw, M. G., Hobbs, P. R. N., Flint, R. C., Jackson, P. D. , 2005. Engineering geological and geophysical investigations of a slope failure at Edinburgh Castle, Scotland. *Bulletin of Engineering Geology and the Environment*, 64: 119–137.
- Ghosh, D. K., 1990. Geological evaluation of foundations of ancient monuments and stability of rockcut caves in central India. *Environmental Geology*, 16:15–22 .
- Goodman, R.E., Bray, J.W., 1976. Toppling of rock slopes. In *Proc. Specialty Conference on Rock Engineering for Foundations and Slopes*, American Society of Civil Engineers, New York, Vol. 2, pp. 201- 234.
- Greif, V., Sassa, K., Fukuoka, H., 2006. Failure mechanism in an extremely slow rock slide at Bitchu-Matsuyama castle site (Japan). *Landslides*, 3: 22–38.
- I.G.M.E., 1973. Geological map of Greece, Kavala Sheet (scale 1:50.000), Athens, I.G.M.E. Publications.
- Kamh, G. M. E., 2005. The impact of landslides and salt weathering on Roman structures at high latitudes – Conway Castle, Great Britain: a case study. *Environmental Geology*, 48: 238–254.
- Kolaiti, E. and Koumantakis, J., 1991. Engineering – Geological study of St. George castle of Cephalonia (Ionian Islands, Greece). *Bulletin of the International Association of Engineering Geology*, No 43, Paris.
- Koukis, G., Sabatakakis, N., 2007. *Geology of engineering constructions*. Papatotiriou Publications, Athens, pp. 575.
- Loupasakis, C., Georgakopoulos A., 2009. Geotechnical problems occurred at the costal wall of Kavala, at the Lighthouse location, and the proposed protection measures. *Proceedings of the 2nd Pan-Hellenic conference of the Society for research and promotion of scientific reconstruction of monuments*, pp. 189 – 191.
- Loupasakis C., Spanou N., Kanaris D., Exioglou D., 2009. Geotechnical investigation of the stability of rock slopes located at the Kavala municipality. Unpublished report, IGME, Athens pp. 111.
- Topal, T., Akin, M., Ozden, U. A., 2007. Assessment of rockfall hazard around Afyon Castle, Turkey. *Environmental Geology*, 53:191–200.
- Varnes, D.J., 1978. Slope movement types and processes. In *Special Report 176: Landslides: Analysis and Control*, Eds.: Schuster R.L., Krizek R.J., TRB, National Research Council, Washington D.C., pp. 12-33.
- Vlcko, J., 2004. Extremely slow slope movements influencing the stability of Spis Castle, UNESCO site. *Landslides*, 1:67–71.

GEOLOGICAL BEHAVIOUR OF ROCK MASSES IN UNDERGROUND EXCAVATIONS

Marinos P. V.¹

¹ *Geotechnical Engineering Department, National Technical University of Athens, 15780 Athens - Greece, vmarinos@central.ntua.gr*

Abstract

The paper deals with the engineering geological behaviour of rock masses in underground excavations. In general, the application of the well-known classification systems has the drawback of not displaying necessary information concerning the behaviour of rock masses, especially the weak ones, in tunnelling. Consequently, there are many cases in which the geological “identity” of the geomaterial is lost since it is not involved in the analysis. In that way it is possible that its special characteristics are mislaid. Within this framework, a system for assessing the failure type mechanisms of the rockmass (i.e. deformation due to overstressing, overbrakes or wedge failure, “chimney” type failure, ravelling ground) for unsupported tunnel-section is presented. These parameters, used for this system, are the structure of the rockmass, the intact rock strength and the overburden thickness. The experience gained by the recent tunnelling construction in the Greek territory, under particularly difficult geological conditions, provided excellent and numerous data for this study.

Key words: *rock mass classification, tunnelling, weak rock mass, failure type*

1. Introduction

A sound and economical design of an underground excavation is based on the compilation of a realistic geological model, the engineering geological characterization of the rock mass and the appraisal of the in situ stresses and the hydrogeological conditions. Tunnelling in rock masses requires instinct knowledge of the geomaterial since the features of mineralogical composition, lithology, structure, fracturing, tectonic disturbance, weathering, and groundwater presence, vary and change frequently with tunnel depth and makes the design a procedure with great particularities.

Tunnel design is a complex procedure and is composed of several stages. In the last decades, there has been a rapid growth on the computational analysis of tunnels. Regardless to these present calculative tools and friendly software the results must be carefully reviewed due to possible lack of precision and parameter uncertainties. Hence, a clear understanding of the rock mass tunnel behaviour followed by the proper parameter specification should be a basic concern before final tunnel design analysis.

There are no clear solutions on this approach. Nowadays, the role of the geological material in the design is improved with the progress of the investigation methods, the advancement of the geotechnical classification systems and the consequent quantification of the rock masses. All these are crucial to the tunnel design. On the other hand, the wide use of the well known classifications (GSI, RMR, Q or others) may guide to reverse or misleading results, namely the by-pass of basic geolog-

ical and mechanical principles, which consist the fundamental background for the geotechnical design. The use of the geotechnical classification systems, as proper as it may be done, is confined to the quantification of the rock mass without any consideration on the behaviour that the geomaterial “prefers” when excavated. The behaviour in tunnelling may differ from rock mass to rock mass, even if they have the same characterization value, under the same stress field and hydrogeological conditions. An example of two equally classified rock masses with the GSI and RMR systems but with completely different behaviour after their excavation, is shown in figure 1.

What is highlighted in this paper is that the classification “numbers” must be also supported, in an engineering friendly way, by the engineering geological behaviour, namely the type and the mechanism of failure that “fits” best to the rock mass under consideration. Otherwise, the geological identity of the geomaterial is lost, while any in situ particularities which can be crucial to the tunnel instability may be disregarded.

Rock mass behaviour appraisal in tunnelling and its connection to the design has been the subject of significant research interest. Goricki et al. (2004), Schubert (2004), Poschl and Kleberger (2004) and Potsch et al. (2004) study the rock mass behaviour from the design and construction experience of the Alpine tunnels and Palmstrom and Stille (2007) of other tunnels.

In this context, a database named “Tunnel Information and Analysis System” (TIAS), was designed and created (Marinos et al., 2006) for Greek tunnels. A huge number of geological, engineering geological and geotechnical data from the site investigation, design and the construction of 62 tunnels of Egnatia Highway in Northern Greece were considered. The data from this information, together with relevant field work, were processed and evaluated by numerous correlations. This work resulted to a classification and a tunnel behaviour system is proposed. The results of this research intend to assist to the selection of the appropriate design parameters and the conceptual choice of the support measures.

2. Engineering Geological Behaviour in Tunnelling

2.1 General

Failures or instabilities are certainly an undesirable phenomenon to tunnel construction. Nevertheless, they express the most accurate “method” to confirm or re-evaluate the geotechnical model and thus use the appropriate design tools. The term instability mechanism-behaviour as referred here involves all the mechanisms that endanger the tunnel section either when the rock mass has not been yet supported after its excavation or temporarily supported behaving together with the support shell. In this paper, the reaction of the rock mass immediately after its underground excavation and before the support implementation is examined. Thus, the engineering geological characteristics – keys to the tunnel stability are of great importance.

2.2 Design methodology

A design methodology for this approach is proposed by Goricki et al. (2004) and Schubert (2004), a section of which is studied here. The first step of this methodology involves the definition of rock mass types, the second the evaluation of rock mass tunnel behaviour, the third step suggests the setting of the tunnel excavation-support system based on the previous behaviour with the inclusion of the geotechnical parameters, the fourth the detection of unified characteristics-sections of equal support requirements along the tunnel and final the fifth step the determination of the excavation and support categories qualified to cost and time terms (organization of the tender documents). This paper focuses on the second and third step.

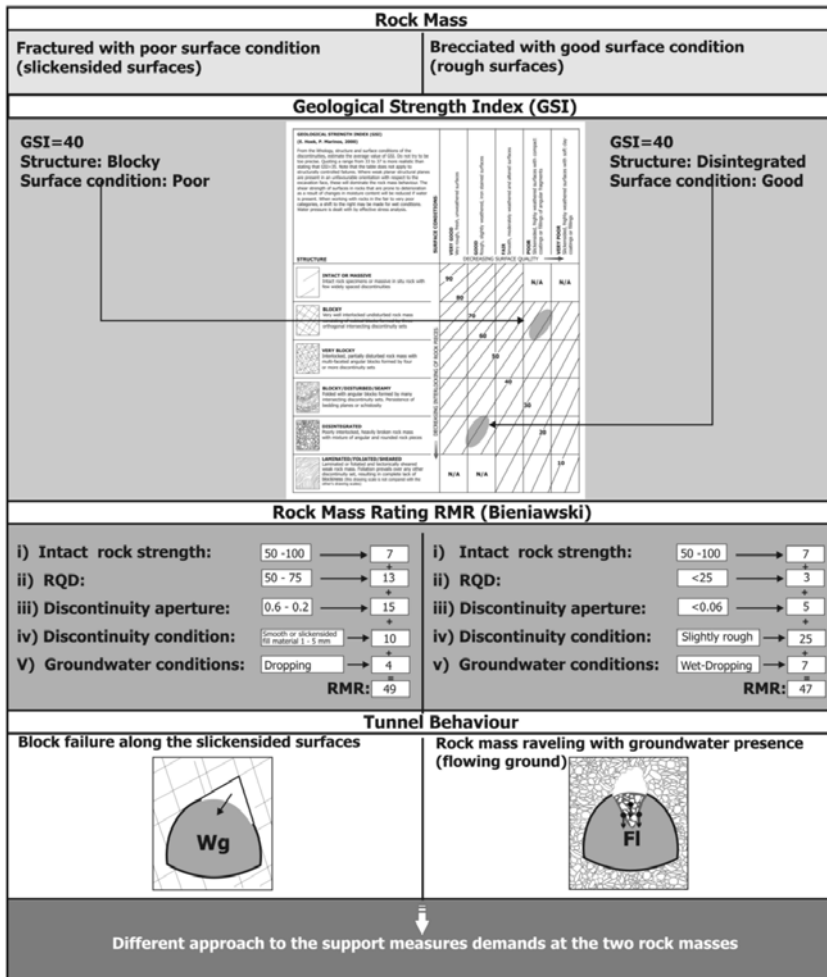


Fig. 1: Example of two equally rated rock masses with the GSI and RMR system but with completely different behaviour in tunnelling and supporting measures.

The rock mass behaviour, in a non urban environment, from the excavation of 62 tunnels in northern Greece, was examined for the purpose of this research.

2.3 Tunnel Behaviour Types

A tunnel behaviour assessment in order to assist to the design parameter selection and the support elements selection is presented hereafter. The behaviour type must be precise and solid. This can be achieved initially by the recognition of the general failure category, referred mainly as gravity and stress controlled and then by a more specific inspection in each category. Normally, there are cases when both general categories may be applied. Tunnel behaviour types are presented and briefly described in figure 2. It should be noted that deformation problems are estimated by the ratio of the uniaxial rock mass strength to insitu stresses, σ_{cm}/p_0 (Hoek and Marinos, 2000).



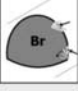








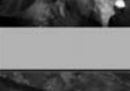






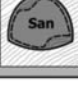

ENGINEERING GEOLOGICAL BEHAVIOUR TYPES OF AN UNSUPPORTED TUNNEL		EQUIVALENT BEHAVIOUR TYPE OF A SUPPORTED TUNNEL	
St	Stable tunnel section with local gravity failures. Rock mass is compact with limited and isolated discontinuities		
Br	Brittle failure or rock bursting in great depths		
Wg	Wedge sliding or gravity driven failures. Inconsiderable deformations. The rock mass is blocky to very blocky, defining blocks possible to fail or slide. The stability is controlled by the geometrical and mechanical characteristics of the discontinuities. The ratio of rock mass strength to the in situ stress (α_{in}/p_0) is high (>0.6-0.7) and there are no deformations ($\epsilon < 1\%$)		
Ch	Chimney type failure. Rock mass is highly fractured, maintaining in most of the times its structure (or at least the surrounded rock mass). Rock mass does not have good interlocking (open structure) and in combination with low confinement (lateral stress) can drive to block falls which develop to larger overbrakes of chimney type. The overbrakes may be stopped and "bridged" by better quality rock masses, depending on the in situ conditions. In this type may be applied cases of brecciated and disintegrated rock mass but in ground of high confinement (high lateral stress)		
Rv	Raveling ground. The rock mass is brecciated and disintegrated or foliated with practically zero cohesion and depending on the intact rock interlocking (Rv1 case) but also possible secondary hosted geomaterial, e.g. clay (Rv2 case), can generate immediate rock mass raveling in face and tunnel perimeter. The difference with Ch type lies in the block size, which is very small here, the self support timing, which is very limited here and the failure extension, where it is difficult to be restricted due to the lack of better rock mass quality in the surrounding zone		
FI	Flowing ground. The rock mass is disintegrated with practically zero cohesion and intense groundwater presence along the discontinuities and the rock mass fragments are flowing with water inside the tunnel		
Sh	Minor to medium deformations, with the development of shear failures in a close perimeter around the tunnel. Rock mass is consisted by low strength ($\alpha_c < 15\text{MPa}$) intact rocks while the rock mass structure, through classification systems, reduces in overall the rock mass strength. Deformations develop either at a small to medium tunnel cover (around 50m) in case of poor sheared rock masses, either in larger cover in case of better quality rock masses. The ratio of rock mass strength to the in situ stress (α_{in}/p_0) is low ($0.3 < \alpha_{in}/p_0 < 0.6$) and deformations are measured or expected to be medium (1-2.5 %)		
Sq	Large deformations, due to overstraining with the development of shear failures in an extended perimeter around the tunnel. Rock mass is consisted by low strength ($\alpha_c < 15\text{MPa}$) intact rocks while the rock mass structure, through classification systems, reduces in overall the rock mass strength. The ratio of rock mass strength to the in situ stress (α_{in}/p_0) is very low ($\alpha_{in}/p_0 < 0.3$) and deformations are measured or expected to be $> 2.5\%$, while these can be also taken place at the face		
Sw	Swelling ground. Rock mass is consisted of a significant amount of swelling minerals (montmorillonite, smectite, anhydrite) which swell and deform under groundwater presence. It is often developed on tunnel floor when the support ring is not fully closed		
San	Anisotropic deformations. The rock mass is heterogeneous (stratified or consists specific weak zones) and develop deformational characteristics along a certain direction		

Fig. 2: Brief description and schematic presentation of the tunnel behaviour types (based on data from Potsch et. al., 2004 and from the author)

3. Tunnel Behaviour System

3.1 Methodology

The assessment of the engineering geological behaviour of the rock mass was done with a certain method-philosophy. The first step involves the understanding of the possible tunnel failures-behaviour, as far the mechanism is concerned. The next step was to define all the possible rock mass types for several formations which were identified by specific engineering geological characteristics affecting their behaviour. These types were recognized along the 62 tunnels which were investigated, together with their design parameters. The following stage involved the grouping of the support cat-

egories for a number of rock mass models and a variety of insitu conditions. At the same time, a comparison of the rock mass behaviour after its excavation was done, in order to compare it with the design. In the next step, the effort was focused on handling the construction records. The data were justified by field work and in situ inspections and the behaviour was classified for every rock mass type. Finally, the temporary support measures philosophy and principles for a certain behaviour type was assessed.

3.2 Rock mass behaviour assessment













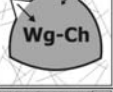




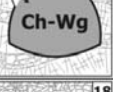

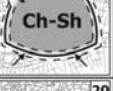


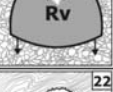
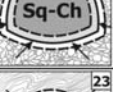

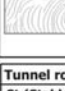
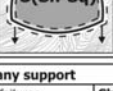

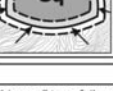
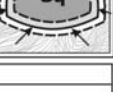
The demand for classified geological information, directly linked to the design and tunnel support measures to be applied, guided to a system for the assessment of the failure type mechanisms and behaviour of the rock mass for unsupported tunnel-section, based on the structure of the rock mass, the intact rock strength and the thickness of the overburden.

The suggested system, called Tunnel Behaviour Chart (TBC), is shown in figure 3. The scope of this diagram is to provide the logic and failure mechanism of several rock mass types often met in nature. It is noted that in the chart there are no quantified limits-ranges of the uniaxial compressive strength of the intact rock (σ_{ci}) and the overburden thickness (H), but only qualitative of high and low values. However, some general quantified limits for σ_{ci} and H for each GSI structure column are presented in table 1. These values although, based on reasonable trends, should only be considered as purely indicative.

The data of this assessment were based on the excavation of tunnels with the conventional method with top heading and bench in a non-urban environment with an overburden, less than 600m. The philosophy of the Tunnel Behaviour chart becomes more comprehensible if we acknowledge the following:

- The rock mass structure is a basic parameter to estimate its immediate response in underground excavation. The pattern of structures of the GSI system was selected.
- Overburden thickness H is an other principle parameter to access the behaviour type, since it is in conjunction to the insitu stresses and the general confinement conditions. The behaviour types that were examined are referred to tunnel construction under a cover of 30m to 300m (a case around 600m was also included). For the gravity driven failures, tunnel depth can determine the extent or restrain of a failure, since the degree of interlocking between the rock blocks changes and the confinement pressure is different. For example, a ground may ravel (Rv) close to the ground surface but under higher cover a chimney type (Ch) failure may be observed. As far as the stress controlled behaviour is concerned, overburden thickness H defines when shear failures and deformations are generated.
- Intact rock strength σ_{ci} values that were involved in the design of those tunnels, ranged between 5 to 40 Mpa. The selected extreme values that nominate the rock mass behaviour are based in two criteria: i) the value when shear failures and deformations initiate and ii) the value which accords best with the present deformational characteristics of the rock mass structure (e.g. fractured, brecciated, sheared).

The surface condition of the discontinuities, the second composite of GSI system, mainly affects the intensity of the failure phenomenon and is not accounted to the behaviour type definition. Only few are the cases where surface quality can accommodate a behaviour type. For example, high clay presence along the discontinuities or as a zone in the rock mass may shift the gravity driven behaviour types to the vertical axis of the chart (e.g. from Wg [9] to Ch [13]). Groundwater presence does not affect the behaviour type but affects the factor of safety. However, in some cases, like in “Disintegrated” rock mass, the groundwater presence may “shift” from a Chimney (Ch) or Raveling (Rv) behaviour type to Flowing ground (Fl) type.

TUNNEL BEHAVIOUR CHART (TBC)	OVERBURDEN			
	Low thickness ($H \ll$)		High thickness ($H \gg$)	
	INTACT ROCK STRENGTH (σ_{ci})			
ROCK MASS STRUCTURE (BASED TO GSI)	$\sigma_{ci} \ll$	$\sigma_{ci} \gg$	$\sigma_{ci} \ll$	$\sigma_{ci} \gg$
 INTACT OR MASSIVE Intact rock specimens or massive in situ rock with few widely spaced discontinuities	1 	2 	3 	4 
 BLOCKY Very well interlocked undisturbed rock mass consisting of cubical blocks formed by three orthogonal intersecting discontinuity sets	5 	6 	7 	8 
 VERY BLOCKY Interlocked, partially disturbed rock mass with multi-faceted angular blocks formed by four or more discontinuity sets	9 	10 	11 	12 
 BLOCKY/DISTURBED/SEAMY Folded with angular blocks formed by many intersecting discontinuity sets. Persistence of bedding planes or schistosity	13 	14 	15 	16 
 DISINTEGRATED Poorly interlocked, heavily broken rock mass with mixture of angular and rounded rock pieces	17 	18 	19 	20 
 LAMINATED/FOLIATED/SHEARED Laminated or foliated and tectonically sheared weak rock mass. Foliation prevails over any other discontinuity set, resulting in complete lack of blockiness (this drawing scale is not compared with the other's drawing scales)	21 	22 	23 	24 
Tunnel rock mass behaviour types without any support				
St (Stable): Stable tunnel section with local gravity failures		Ch (Chimney failure): "Chimney" type failure		
Wg (Wedge failure): Wedge sliding or gravity driven failures		Rv (Raveling ground): Raveling ground		
Sq (Squeezing ground): Large deformations, due to overstraining with the development of shear failures in an extended perimeter around the tunnel		Sh (Shearing failures in shallow zone around the tunnel perimeter): Minor to medium deformations, with the development of shear failures in a close perimeter around the tunnel		
The engineering geological behaviour may be also controlled by two or three different mechanisms (e.g. Sh-Ch)				

Notes:

- There are no quantified limits-ranges of the uniaxial compressive strength (σ_{ci}) of the intact rock and overburden thickness (H), but only qualitative high and low values. This is done to avoid standardization from a non-experienced user. The scope of this diagram is to provide the logic and failure mechanism of several rock mass types often met in nature. However, an indicative initial value of σ_{ci} can be 15 MPa.
- The overburden limits, where deformations develop, are not the same for every rock mass type and change according to the structure. These limits are 150m for the "good" structures ("Intact" and "Blocky"), 100m for the medium ("Very Blocky") and around 70m for the poor to very poor structures ("Blocky Disturbed", "Disintegrated" and "Sheared").
- The discontinuity surface conditions, the second composite of the GSI system, mainly affect the intensity of the failure phenomenon.
- High clay presence along the discontinuities or as a zone in the rock mass may shift the gravity-driven behaviour types to the vertical axis of the chart (e.g. from Wg[9] to Ch [13]).
- Groundwater presence mainly affects the factor of safety and not the behaviour type. Though, in some cases, like in "Blocky-Disturbed" & "Disintegrated" rock mass, the groundwater presence may "shift" a Chimney (Ch) or Raveling (Rv) behaviour type to Flowing Ground (FG).
- The chart is not referred to very large H (e.g. lot of hundreds or >1000m).

Fig. 3: Tunnel Behaviour Chart (TBC): A system for rock mass behaviour assessment.

Stress controlled failures: The development of remarkable deformations around a non-urban tunnel is characterized by a ratio of $\sigma_{cm}/p_0 < 0.6-0.7$ (Hoek and Marinos, 2001). In particular, when σ_{cm}/p_0 is among 0.3 and 0.7, shear failures can propagate in a shallow zone around the tunnel perimeter (Sh behaviour). Such cases concern rock masses with poor to very poor structures and low intact rock strength (<10-15 MPa) under medium overburden or with good structures and low intact rock strength under high cover. Squeezing conditions (behaviour Sq) with severe tunnel deformations may develop when $\sigma_{cm}/p_0 < 0.3$.

Table 1. General indicative quantified ranges for σ_{ci} and overburden thickness (H) and GSI values for every tunnel behaviour type (1-24) from the Tunnel Behaviour Chart of figure 3.

<i>TBC Case</i>	<i>GSI value range</i>	<i>GSI Structure</i>	<i>σ_{ci} (MPa)</i>	<i>Overburden thickness H (m) limit</i>
1, 3	70–80	Intact	<15	150
2, 4	70–90		>15	
5	50–60	Blocky	10–15	20–150
6	50–80		>15	<150
7	50–60		<15	>150
8	50–80		>15	>150
9, 11	35–55	Very Blocky	10–15	100
10 – 12	40–60		>15	
13, 15	25–45	Blocky – Disturbed/Seamy	<15	70
14, 16	30–50		>15	
17 – 19	15–35	Disintegrated	<15	70
18 – 20	35–45		>15	
21, 23	15–25	Disintegrated	<10	70
22, 24	15–35	Laminated/Foliated/Sheared	>10	

Gravity controlled failures: Gravity driven failures can take place when a rock mass is fractured in planes and is formed by blocks. When these blocks are revealed after the excavation they may fall or slide, according to the tunnel geometry and the shear strength characteristics of the discontinuity planes. Chimney (Ch) and raveling (Rv) types can take place in rock masses with low interlocking of blocks. The rock mass cannot “bridge” immediately after the fall and the overbreak may be irregular and significant. Volume and frequency of these behaviour types depend on the structure of the rock mass (“Blocky-Disturbed” and “Disintegrated”), its relaxation (“open structure”) and the tunnel depth, since it will improve the rock mass quality and the confinement pressure which may tighten the structure of the rock blocks.

4. Tunnel support measures – Design philosophy

The design of the temporary support categories consists of two stages: the selection of the proper support elements and their analysis. The general concept and the selection of the elements lie on the uncertainty of the engineering geological behaviour of the rock mass. This procedure is very important, since there are cases where a specific behaviour cannot still be accurately. That is why the decision is frequently based on the experience and the geotechnical appreciation and less on analytical solutions.

Thus, in conjunction with the tunnel behaviour system, presented in the previous paragraph, this study concluded also to a step-by step procedure towards the design. This approach initiates after the definition of the rock mass types along the tunnel and the evaluation of the geological and insitu conditions. The rock characteristic – “keys”, which dictates the stability or instability of the tunnel, are then assessed. The behaviour of the rock mass after its excavation in an unsupported section is then investigated and the design philosophy is defined. After the identification of the failure mechanism, the suitable design parameters can be selected. Finally, the tunnel support philosophy and the re-

ENGINEERING GEOLOGICAL CHARACTERIZATION FOR TUNNELING (1/2)

Classification phase (primary, evaluation, construction):	
Location:	
Date:	
I. GEOLOGICAL CONDITIONS	
a) Lithology ☐ Geotectonic unit: ☐ General formation it may belongs (e.g. Flysch): ☐ Rock mass name:	☐ Pindos ophiolitic complex ☐ Serpentinised Peridotite with foliated-clayey serpentinite zones Note: Information concerning significant alteration of the rock mass, intact rock or surface weathering, presence of hosted - clayey geomaterial and bedding thickness if it is stratified
b) Tectonism ☐ Tectonic zones: = Major thrust zones which affect the project in great scale: = Localized fault or disturbed zones: ☐ Fracturing or Shearing: = Fracturing degree: = Continuation- persistence of fracturing with depth: = Shearing or foliation across the rock mass or along the discontinuities: ☐ Folding: = Type: = Geometry:	The big thrust of Pindos ophiolites over the geotectonic unit of flysch is extended in the wide tunnel area but does not crossed. = Several foliated zones across the peridotite blocks = Slightly fractured <input type="checkbox"/> Fractured <input type="checkbox"/> Very fractured <input type="checkbox"/> Brecciated <input checked="" type="checkbox"/> = Preserves the same structure characteristics to tunnel depth (~90m) = Foliation met mainly along the joints, only sometimes has "intruded" to the rock mass
c) Weathering ☐ Discontinuities: ☐ Intact rock: ☐ Persistence with depth:	☐ Serpentinised discontinuities (slickensided) ☐ Only locally affected ☐ It does not follow any pattern, Irregular geometry and extent also in depth
d) Permeability ☐ Qualitative appraisal: ☐ Quantitative appraisal:	☐ High ($k > 10^{-3}$ m/sec) <input type="checkbox"/> Low ($k: 10^{-5} - 10^{-6}$ m/sec) <input checked="" type="checkbox"/> Practically impermeable ($k < 10^{-6}$ m/sec) <input type="checkbox"/> ☐ Medium ($k: 10^{-4} - 10^{-5}$ m/sec) <input type="checkbox"/> Very low ($k: 10^{-7} - 10^{-8}$ m/sec) <input type="checkbox"/> Localized groundwater, presence in the peridotite rock trapped behind clayey zones. ☐ k: _____ m/sec
II. INSITU CONDITIONS	
a) Overburden ☐ Overburden range with similar behaviour: ☐ Insitu stresses ($P_v = \gamma H_{min} - \gamma H_{max}$):	☐ H: 30 - 100 m / H: _____ m / H: _____ m ☐ P_v : 0.75 - 2.5 MPa / P_v : _____ MPa / P_v : _____ MPa
b) Surrounded zone close to tunnel perimeter ☐ Competent zone around one tunnel diameter distance: ☐ Low strength zone around one tunnel diameter distance:	☐ Competent zone <input type="checkbox"/> Incompetent zone <input checked="" type="checkbox"/> Dip: _____ / _____ Dip Direction Thickness: _____ m Geological characteristics: Possible foliated-clayey serpentinite in 2m zones
c) Hydrogeological conditions ☐ Aquifer according to the tunnel axis:	☐ Unknown
d) Stress field ☐ Particular presence or absence of lateral pressures	☐ Foliated-clayey zones may specify irregular blocks
e) Other boundaries	☐
III. CHARACTERISTIC "KEYS" FOR TUNNEL STABILITY OR INSTABILITY	
☐ Intact rock strength: ☐ Rock mass strength to insitu stress ratio (σ_{int}/P_v): ☐ Structure "interlocking": ☐ Presence of low strength minerals: ☐ Intact rock weathering, clay filling: ☐ Groundwater presence: ☐ Block geometry - bed thickness: ☐ Rock mass structure (based to GSI): ☐ Discontinuity geometry: ☐ Discontinuity persistence: ☐ Discontinuity quality (based to GSI): ☐ Rock Quality Index (RQD): ☐ Other characteristic:	☐ > 30 MPa ☐ $\sigma_{int}/P_v > 1$ <input checked="" type="checkbox"/> $0.3 < \sigma_{int}/P_v < 1$ <input type="checkbox"/> $\sigma_{int}/P_v < 0.3$ <input type="checkbox"/> ☐ Due to the serpentinisation it does not have good interlocking ☐ Serpentine at discontinuities. Clay typically at discontinuities ☐ Foliated-clayey zones may specify irregular blocks ☐ Possibility of trapped permeable small aquifers behind impermeable clayey zones which may be unfavorable to the tunnel stability due to excessive pressures. May act as a "lubricant" in the serpentinised discontinuities decreasing its strength characteristics. ☐ 0.2-0.5m x 0.2-0.5m ☐ Blocky <input type="checkbox"/> Very blocky <input checked="" type="checkbox"/> Blocky/Disturbed/Seamy <input type="checkbox"/> ☐ Disintegrated <input type="checkbox"/> Laminated/Sheared <input type="checkbox"/> ☐ It poses significant role in wedge failures ☐ They present persistence but is reduced due to the serpentinised zones ☐ Very good <input type="checkbox"/> Good <input type="checkbox"/> Fair <input type="checkbox"/> Poor <input checked="" type="checkbox"/> Very poor <input checked="" type="checkbox"/> ☐ RQD: _____ ☐
Basic-"Keys" characteristics: The behaviour is controlled by the rock mass: Yes <input type="checkbox"/> No <input type="checkbox"/> The behaviour is controlled by the discontinuities: Yes <input checked="" type="checkbox"/> No <input type="checkbox"/> Fill the relevant rock mass parameters in field "Va" Fill the relevant parameters of the discontinuities shear strength in field "Vb"	

Fig. 4: Rock mass characterization method in tunnelling towards the design (Sheet 1/2).

ENGINEERING GEOLOGICAL CHARACTERIZATION FOR TUNNELING (2/2)

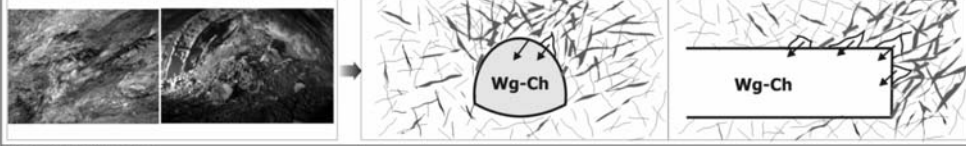

IV. ROCK MASS BEHAVIOUR IN TUNNEL EXCAVATION																																																																																											
<p>a) Isotropy:</p> <ul style="list-style-type: none"> <input type="radio"/> Isotropical: <input type="radio"/> Anisotropical: <p>b) Behaviour type of unsupported tunnel section:</p> <ul style="list-style-type: none"> <input type="radio"/> Qualitative: 	<p><input type="radio"/> Yes <input type="checkbox"/> No <input type="checkbox"/> Gravity driven failures</p> <p><input type="radio"/> Yes <input checked="" type="checkbox"/> No <input type="checkbox"/> Gravity driven failures</p> <p><input type="radio"/> Wedge slidings (Wg) or gravity driven failures. Possibility for greater-more extended chimney type failures (Ch) containing blocks which are surrounded by clayey foliated zones. Face stability problems may also occur from the same mechanism. Special attention should be given in possible "lubrication" of the serpentinised zones if water is present. If these zones appear in critical tunnel section areas, as the foundation area, vertical displacements (settlements) of the whole section may be developed</p>																																																																																										
																																																																																											
<p>c) Design philosophy:</p> <ul style="list-style-type: none"> <input type="radio"/> Wedge analysis (e.g. Unwedge Analysis) <input type="radio"/> Wedge and shear failure deformation analysis (Wedge and Numerical Analysis) <input type="radio"/> Shear failure -Deformation analysis (Numerical Analysis) <input type="radio"/> Empirical design 	<p><input checked="" type="checkbox"/> The use of the classifications are recommended only for the design parameters selection and not for categorization and selection of the support section</p> <p><input type="checkbox"/> Stress problems should also be analyzed but will not govern the support selection</p>																																																																																										
V. DETAIL CHARACTERISTICS AND DESIGN PARAMETERS																																																																																											
<p>a) Rock mass parameters (Hoek & Brown):</p> <p>GSi value: <input type="text" value="30 - 35"/></p> <div style="border: 1px solid black; padding: 2px; font-size: 8px;"> <p>NUMERICAL STRONGNESS INDEX (GSI) An empirical strength index (GSI) is defined as the sum of the rock mass quality (RMR) and the rock mass structure (RMS) indices. The GSI index is a measure of the rock mass strength and is used to estimate the rock mass strength parameters for the Hoek-Brown failure criterion. The GSI index is a function of the rock mass quality (RMR) and the rock mass structure (RMS) indices. The GSI index is a function of the rock mass quality (RMR) and the rock mass structure (RMS) indices.</p> </div>  <p style="text-align: center; font-size: 8px;">GSI chart (2000)</p> <p>Intact rock strength: σ_{ci}: <input type="text" value="30"/> MPa</p> <p>Constant m: <input type="text" value="22"/></p> <p>Y: <input type="text" value="0.026"/> MN/m²</p> <p>Modulus Ratio (MR) or (EI): <input type="text" value="MR=550"/></p> <p>Disturbance factor (D): <input type="text" value="0"/></p> <p>Classification RMR, Q: <input type="text" value="-"/></p>	<p>b) Discontinuity parameters:</p> <p>Number of discontinuities: <input type="text" value="4"/></p> <p>Geometry (Dip/dip direction): J_1: <input type="text"/> / <input type="text"/> J_2: <input type="text"/> / <input type="text"/> J_3: <input type="text"/> / <input type="text"/></p> <p>Persistence: <input type="text" value="1 - 3"/> m <input type="text"/> m <input type="text"/> m</p> <p>Distance: <input type="text" value="0.2 - 0.5"/> m <input type="text"/> m <input type="text"/> m</p> <p>Aperture: <input type="text" value="1 - 3"/> mm <input type="text"/> mm <input type="text"/> mm</p> <p>Filling material:</p> <table style="width: 100%; border-collapse: collapse;"> <tr> <td>Hard < 5mm</td><td><input type="checkbox"/></td> <td>Hard < 5mm</td><td><input type="checkbox"/></td> <td>Hard < 5mm</td><td><input type="checkbox"/></td> </tr> <tr> <td>Hard > 5mm</td><td><input type="checkbox"/></td> <td>Hard > 5mm</td><td><input type="checkbox"/></td> <td>Hard > 5mm</td><td><input type="checkbox"/></td> </tr> <tr> <td>Soft < 5mm</td><td><input type="checkbox"/></td> <td>Soft < 5mm</td><td><input checked="" type="checkbox"/></td> <td>Soft < 5mm</td><td><input type="checkbox"/></td> </tr> <tr> <td>Soft > 5mm</td><td><input checked="" type="checkbox"/></td> <td>Soft > 5mm</td><td><input type="checkbox"/></td> <td>Soft > 5mm</td><td><input type="checkbox"/></td> </tr> <tr> <td>None</td><td><input type="checkbox"/></td> <td>None</td><td><input type="checkbox"/></td> <td>None</td><td><input type="checkbox"/></td> </tr> </table> <p>Weathering:</p> <table style="width: 100%; border-collapse: collapse;"> <tr> <td>Unweathered</td><td><input type="checkbox"/></td> <td>Unweathered</td><td><input type="checkbox"/></td> <td>Unweathered</td><td><input type="checkbox"/></td> </tr> <tr> <td>Slightly</td><td><input type="checkbox"/></td> <td>Slightly</td><td><input type="checkbox"/></td> <td>Slightly</td><td><input type="checkbox"/></td> </tr> <tr> <td>Moderately</td><td><input type="checkbox"/></td> <td>Moderately</td><td><input checked="" type="checkbox"/></td> <td>Moderately</td><td><input checked="" type="checkbox"/></td> </tr> <tr> <td>Highly</td><td><input checked="" type="checkbox"/></td> <td>Highly</td><td><input type="checkbox"/></td> <td>Highly</td><td><input type="checkbox"/></td> </tr> <tr> <td>Decomposed</td><td><input type="checkbox"/></td> <td>Decomposed</td><td><input type="checkbox"/></td> <td>Decomposed</td><td><input type="checkbox"/></td> </tr> </table> <p>Ground water conditions:</p> <table style="width: 100%; border-collapse: collapse;"> <tr> <td>Dry</td><td><input type="checkbox"/></td> <td>Dry</td><td><input type="checkbox"/></td> <td>Dry</td><td><input type="checkbox"/></td> </tr> <tr> <td>Sub-wet</td><td><input type="checkbox"/></td> <td>Sub-wet</td><td><input type="checkbox"/></td> <td>Sub-wet</td><td><input type="checkbox"/></td> </tr> <tr> <td>Wet</td><td><input checked="" type="checkbox"/></td> <td>Wet</td><td><input checked="" type="checkbox"/></td> <td>Wet</td><td><input checked="" type="checkbox"/></td> </tr> <tr> <td>In drops</td><td><input type="checkbox"/></td> <td>In drops</td><td><input type="checkbox"/></td> <td>In drops</td><td><input type="checkbox"/></td> </tr> <tr> <td>Flow</td><td><input type="checkbox"/></td> <td>Flow</td><td><input type="checkbox"/></td> <td>Flow</td><td><input type="checkbox"/></td> </tr> </table> <p>Joint Roughness Condition (JRC): <input type="text" value="4 - 6"/></p> <p>Joint Compression Strength (JCS): <input type="text" value="25"/> MPa <input type="text"/> MPa <input type="text"/> MPa</p> <p>Discontinuities:</p> <p>Friction angle (ϕ): J_1: <input type="text" value="25 - 30"/> * J_2: <input type="text"/> * J_3: <input type="text"/> *</p> <p>Cohesion (c): J_1: <input type="text" value="0"/> KPa J_2: <input type="text"/> KPa J_3: <input type="text"/> KPa</p>	Hard < 5mm	<input type="checkbox"/>	Hard < 5mm	<input type="checkbox"/>	Hard < 5mm	<input type="checkbox"/>	Hard > 5mm	<input type="checkbox"/>	Hard > 5mm	<input type="checkbox"/>	Hard > 5mm	<input type="checkbox"/>	Soft < 5mm	<input type="checkbox"/>	Soft < 5mm	<input checked="" type="checkbox"/>	Soft < 5mm	<input type="checkbox"/>	Soft > 5mm	<input checked="" type="checkbox"/>	Soft > 5mm	<input type="checkbox"/>	Soft > 5mm	<input type="checkbox"/>	None	<input type="checkbox"/>	None	<input type="checkbox"/>	None	<input type="checkbox"/>	Unweathered	<input type="checkbox"/>	Unweathered	<input type="checkbox"/>	Unweathered	<input type="checkbox"/>	Slightly	<input type="checkbox"/>	Slightly	<input type="checkbox"/>	Slightly	<input type="checkbox"/>	Moderately	<input type="checkbox"/>	Moderately	<input checked="" type="checkbox"/>	Moderately	<input checked="" type="checkbox"/>	Highly	<input checked="" type="checkbox"/>	Highly	<input type="checkbox"/>	Highly	<input type="checkbox"/>	Decomposed	<input type="checkbox"/>	Decomposed	<input type="checkbox"/>	Decomposed	<input type="checkbox"/>	Dry	<input type="checkbox"/>	Dry	<input type="checkbox"/>	Dry	<input type="checkbox"/>	Sub-wet	<input type="checkbox"/>	Sub-wet	<input type="checkbox"/>	Sub-wet	<input type="checkbox"/>	Wet	<input checked="" type="checkbox"/>	Wet	<input checked="" type="checkbox"/>	Wet	<input checked="" type="checkbox"/>	In drops	<input type="checkbox"/>	In drops	<input type="checkbox"/>	In drops	<input type="checkbox"/>	Flow	<input type="checkbox"/>	Flow	<input type="checkbox"/>	Flow	<input type="checkbox"/>
Hard < 5mm	<input type="checkbox"/>	Hard < 5mm	<input type="checkbox"/>	Hard < 5mm	<input type="checkbox"/>																																																																																						
Hard > 5mm	<input type="checkbox"/>	Hard > 5mm	<input type="checkbox"/>	Hard > 5mm	<input type="checkbox"/>																																																																																						
Soft < 5mm	<input type="checkbox"/>	Soft < 5mm	<input checked="" type="checkbox"/>	Soft < 5mm	<input type="checkbox"/>																																																																																						
Soft > 5mm	<input checked="" type="checkbox"/>	Soft > 5mm	<input type="checkbox"/>	Soft > 5mm	<input type="checkbox"/>																																																																																						
None	<input type="checkbox"/>	None	<input type="checkbox"/>	None	<input type="checkbox"/>																																																																																						
Unweathered	<input type="checkbox"/>	Unweathered	<input type="checkbox"/>	Unweathered	<input type="checkbox"/>																																																																																						
Slightly	<input type="checkbox"/>	Slightly	<input type="checkbox"/>	Slightly	<input type="checkbox"/>																																																																																						
Moderately	<input type="checkbox"/>	Moderately	<input checked="" type="checkbox"/>	Moderately	<input checked="" type="checkbox"/>																																																																																						
Highly	<input checked="" type="checkbox"/>	Highly	<input type="checkbox"/>	Highly	<input type="checkbox"/>																																																																																						
Decomposed	<input type="checkbox"/>	Decomposed	<input type="checkbox"/>	Decomposed	<input type="checkbox"/>																																																																																						
Dry	<input type="checkbox"/>	Dry	<input type="checkbox"/>	Dry	<input type="checkbox"/>																																																																																						
Sub-wet	<input type="checkbox"/>	Sub-wet	<input type="checkbox"/>	Sub-wet	<input type="checkbox"/>																																																																																						
Wet	<input checked="" type="checkbox"/>	Wet	<input checked="" type="checkbox"/>	Wet	<input checked="" type="checkbox"/>																																																																																						
In drops	<input type="checkbox"/>	In drops	<input type="checkbox"/>	In drops	<input type="checkbox"/>																																																																																						
Flow	<input type="checkbox"/>	Flow	<input type="checkbox"/>	Flow	<input type="checkbox"/>																																																																																						
VI. TUNNEL SUPPORT PHILOSOPHY																																																																																											
<p>Qualitative:</p> <ul style="list-style-type: none"> -Excavation phases: -Excavation step: -Shotcrete bolts: -Steel sets: -Not heavy face support (e.g. spiles): -Face support (e.g. fibreglass, forepolling, invert): -Water drainage: -Other (e.g. grouting): 	<p><input type="checkbox"/> Two phases (Top Heading and Bench)</p> <p><input type="checkbox"/> Small tunnel advance (~1.5m) in order to confine the rock mass and avoid the revealing of the foliated zones. Shotcrete should be applied to control the gravity controlled failures and not the deformations (depends with depth). Bolts should have a significant length to contain greater overbrake.</p> <p><input type="checkbox"/> Should be closely implemented (1-1.5m) to confine some blocks often marked by the weak clayey zones.</p> <p><input type="checkbox"/> It may be required to apply spiles and face buttress in case of continuous appearance of the clayey zones.</p> <p><input type="checkbox"/> In higher overburden (>200m) heavier support measures may be applied.</p> <p><input type="checkbox"/> Long drainage holes to avoid water pressure behind the support shell and the face. Protected drainage canals on the tunnel floor to avoid the "lubrication" of serpentinised zones.</p>																																																																																										
VII. REMAINING RISK																																																																																											
<p><input type="checkbox"/> Possible rock strength reduction due to "lubrication" by water circulation when the trenches along the tunnel are poorly constructed. In this case significant vertical convergence due to the settlement of the support shell may developed</p>																																																																																											

Fig. 5. Rock mass characterization method in tunnelling towards the design (Sheet 2/2)

maining risk are reported. This method of rock mass characterization in tunnelling is presented in two sheets with a given example in figure 4 and 5.

5. Conclusions

The use of rock mass classification systems and the resulting quantitative characterization of rock masses cannot directly correspond to their behaviour in underground excavations. Great care should be given to the assessment and sound understanding of the engineering geological behaviour types, prior to tunnel design and analysis. That is to identify the possible failure modes and nature of problems which is expected for the particular rock mass type. In that order, the selection of the tunnel support elements and characteristics together with the evaluation of the geotechnical properties can be soundly assessed from the beginning. Hence a more realistic design along the tunnel can be performed.

A methodology where the rock mass behaviour integrates to the tunnel design procedure is suggested. For this methodology, the basic step is to identify the “key” engineering geological characteristics, which control instability potential of the rock mass. Towards this direction a system for the tunnel behaviour assessment is presented based on the rock mass structure, the intact rock strength and the overburden thickness.

6. Acknowledgments

The author acknowledges the support and encouragement of G. Tsiambaos, Assistant Professor of the Geotechnical department of NTUA, which supervised this research. He would like to thank Egnatia Odos S.A. for its support and the assignment of the relevant research program. Special thanks should be offered to the geologist D. Papouli for her assistant to the preparation of the figures.

7. References

- Goricki, W., Schubert, G., Riedmueller, G., 2004. New Developments for the design and construction of tunnels in complex rock masses. *International Journal of Rock Mechanics and Mining Sciences*, 41(3), CD-ROM.
- Hoek, E., Marinos, P., 2000. Predicting tunnel squeezing in weak heterogeneous masses. *Tunnels and Tunnelling International*, Part 1—November Issue 2000, pp. 45-51; Part 2—December 2000, pp. 34-36.
- Marinos, V., Korkaris, K., Prountzopoulos, G., Romosiou A, Fortsakis, P., Mirmiris, K., Petroutsatou, K., Koumoutsakos, D., Kiamos, K., Lazaridou, S., Pitsas, G., Rigopoulou, M., Marinos, P., Lampropoulos, S., 2006. The construction of a geotechnical database for the Egnatia Highway S.A. *Proceedings of the 5th Hellenic Geotechnical*, Xanthi 2006, 3, pp. 525-531. (in Greek).
- Marinos P. V. (2007). “Geotechnical classification and engineering geological behaviour of weak and complex rock masses in tunneling”, Doctoral thesis, School of Civil Engineering, Geotechnical Engineering Department, National Technical University of Athens (NTUA), Athens, July (in greek).
- Palmstrom, A., Stille, H., 2007. Ground behaviour and rock engineering tools for underground excavations. *Tunnelling and Underground Space Technology*, 27, pp. 363-376.
- Poschl, I., Kleberger, J., 2004. Geotechnical risks in rock mass characterisation - Part 1. *Tunnels and Tunnelling International*, May issue, pp. 37-39. Part 2., October issue, pp. 36-38.
- Potsch, M., Schubert, W., Goricki, A., Steidl, A., 2004. Determination of Rock Mass Behaviour Types - a Case Study. *EUROCK 2004 and 53th Geomechanics Colloquium*, Schubert ed., VGE publ.
- Schubert, W., 2004. Basics and Application of the Austrian Guideline for the Geomechanical Design of Underground Structures. *EUROCK 2004 and 53th Geomechanics Colloquium*, Schubert ed., VGE publ.

NEW PROPOSED GSI CLASSIFICATION CHARTS FOR WEAK OR COMPLEX ROCK MASSES

Marinos P. V.¹

¹ *Geotechnical Engineering Department, National Technical University of Athens, 15780 Athens - Greece, vmarinos@central.ntua.gr*

Abstract

The paper deals with the geotechnical classification of weak and complex rock masses. The complexity of these geological material demands a more specialized research and geological characterization due to the special features of their rock mass types regarding both their structure and their lithological characteristics. The weak and complex rock masses under consideration, often heterogeneous and containing rocks of extremely low strength, have in most cases undergone highly tectonised disturbance resulting in the destruction of their initial structure, while weathering can be another particular feature. The geotechnical types and their characterization of rock masses that can be developed in flysch, molasse, brecciated limestone, ophiolites and disturbed or weathered gneiss are studied here. In order to describe these masses in a quantitative way and provide numerical values to engineering design, new or revised rock mass classification diagrams are introduced within the general concept of the GSI system, or specific projections inside the existing GSI diagram are proposed. The fundamental source for this research was data from the design and construction of 62 tunnels of Egnatia Highway appropriately assessed, processed, correlated and associated with field work.

Key words: *rock mass classification, GSI, weak rock mass, flysch-molasse, ophiolites, gneiss*

1. Introduction

The last decades there has been a rapid development on almost all the stages of a geotechnical design in engineering construction. Analysis and computational methods are the fields where great advance has been made. However, regardless the great capabilities offered by the present computational tools, the results are still encountering uncertainties due to the difficulties in defining design parameters. Hence, the basic attention should be focused on the definition of the geotechnical parameters and on the engineering geological behaviour of the rock mass.

Estimation of rock mass properties can be achieved by one of the following methods: a) laboratory testing, b) in situ testing, c) use of rock mass classifications (GSI, RMR, Q, etc.) and d) back analysis. However, in laboratory, samples are not representative of the rock mass due to the disturbance, jointing and the heterogeneity of most formations. Additionally, it is often not realistic or always feasible to carry out in situ tests. Back analysis, is the best way to estimate the geotechnical parameters, but only when construction has started, by evaluation of the deformation measurements and it can be used to validate or modify the parameters used. To estimate reasonable geotechnical parameters for the design before engineering construction, where

back analysis is not possible, there is no option but to rely upon the use of a rock mass classification scheme - system of rock mass quantification that is correlated with the basic parameters needed for the design. These systems must cover a wide range of geological conditions, including the weak and complex ones which have more particularities. Though, in order to avoid the by-pass of basic geological and mechanical principles, these “numbers” must be also supported by the engineering geological behaviour, namely the type and mechanism of failure that “fits” best to the rock mass according to the engineering project.

The base of this research was a database named “Tunnel Information and Analysis System” (TIAS) established in the frame of the PhD research of the author (Marinos, 2007). Through this data base, a great number of geological, engineering geological and geotechnical data from the design and the construction of 62 tunnels of Egnatia Highway in Northern Greece were processed. These data, in conjunction with relevant field work, was evaluated by numerous correlations and observations and a result of this research was the extension or re-evaluation of the geotechnical classifications in the field of weak and complex rock masses. The rock masses presented in this paper are those of flysch, molasse, particular cases of limestones, ophiolites and disturbed – weathered gneiss.

2. Geotechnical classifications

The demand for rock mass classification becomes perceptible when laboratory testing was not adequate to cover the geotechnical perspectives of a rock mass. After Terzaghi’s 1946 classification for loads on tunnels, in the middle of 70’s the RMR (Bieniawski, 1973) and Q (Barton et al., 1974) classification systems were introduced. These systems were developed in order to provide tunnel support requirements for simple failure mechanisms controlled by sliding and rotation of intact rock blocks, through a rating of rock masses. Though, with the rapid growth of calculation and design tools, where progressive failures and temporary support measures can be analysed, the need for solid rock mass parameters became more than ever required. The failure criterion created by Hoek and Brown in 1980 to estimate the rock mass strength parameters is thus strongly connected to the Geological Strength Index (GSI), covering a wide range of geological conditions, including some weak rock masses like foliated and sheared (Hoek et al., 1998). The system was also extended to heterogeneous rock masses, such as flysch by Marinos and Hoek (2001).

3. Geotechnical classification of weak and complex rock masses

The weak rock masses that are examined in this study are generated by tectonical compression or weathering. Cases, where the decreasing of the quality is expressed on the rock mass scale and not necessarily on the primary low intact rock strength is thus presented. The initial intact rock strength before any disturbance can be either low or high. A complex rock mass is referred here as the one that displays evident lithological, structural and geotechnical heterogeneities and non-uniformities in macroscopic scale (scale of meters). The great number of geotechnical investigations and the experiences gained from tunnelling in Greece offered plenty of data concerning the engineering geological conditions of several formations and thus enabled their distinction in rock mass types and their quantification. As a result, new or revised GSI charts for weak and complex rock masses are presented in this paper based on PhD results (PhD, Marinos, 2007). In particular, these diagrams are for heterogeneous rock masses such as flysch, molassic formations, disturbed and weathered gneiss and projections for ophiolites and limestones.

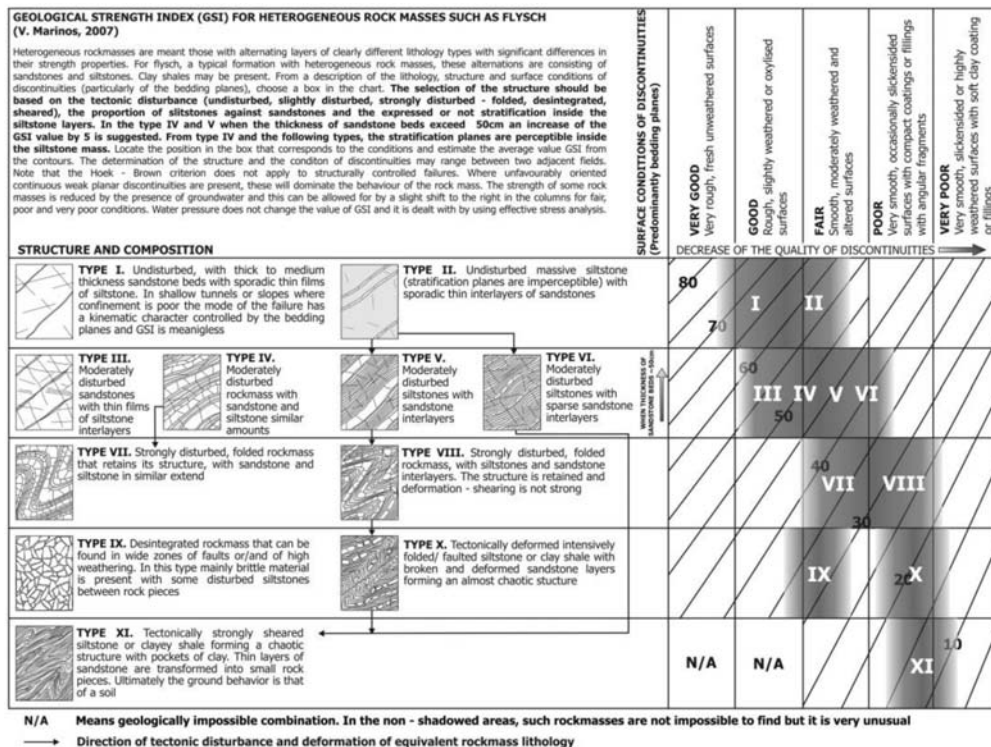


Fig. 1: A new GSI classification chart for heterogeneous rock masses such as flysch.

3.1. Geotechnical classification of heterogeneous rock masses such as flysch

Flysch formations are generally characterized by diverse heterogeneity, presence of members with low strength geomaterial and tectonically disturbed structures. In order to investigate the rock mass properties of flysch, 12 tunnels driven in various geological environments were examined. Flysch formations are classified here to 11 rock mass types (I to XI) according to the siltstone-sandstone participation and their tectonic disturbance.

A new GSI diagram for heterogeneous rock masses such as flysch is presented, where a certain range of GSI values for every rock mass type is proposed (figure 1). The 2001 chart (Marinos and Hoek, 2001) is been revised here with modifications in values and with additions of new types often met in nature. In the new diagram, GSI values are increased from 10 to 35 units for the “Blocky” to “Undisturbed” structures, respectively, particularly for the siltstone type. The high presence of siltstone beds does not decrease the GSI value, but only in the highly disturbed forms. When rock mass is undisturbed or slightly disturbed, independently of siltstone or sandstone predominance, GSI ratings have to be considered much higher. This was confirmed in tunnel construction, where lighter temporary support categories (correlated with high GSI values) were implemented and experienced marginal measured deformations. Hence, the selection of the structure should be initially based on the tectonic disturbance (from undisturbed to sheared rock masses), then on the proportion of siltstones against sandstones and finally on the expressed or not bedding stratification inside the siltstone layers. One more addition in the GSI chart is the

Table 1. Suggested proportions of values for each flysch rock type to be considered for the “intact rock” property determination (σ_{ci} and m_i) (based on Marinós and Hoek, 2001)

Flysch type	Proportions of values for each member of rock type to be considered for the weighted “intact rock” property determination
I, III	Use values for sandstone beds
II	Use values for siltstone or shale
IV	Thin beds: Reduce sandstone values by 10% and use full values for siltstone Thick beds: Use equivalent values for siltstone and sandstone beds
V	Reduce sandstone values by 20% and use full values for siltstone
VI	Use values for siltstone or shale
VII	Reduce sandstone values by 20% and use full values for siltstone
VIII	Reduce sandstone values by 20% and use full values for siltstone
IX	Use equivalent values for siltstone and sandstone beds according to their participation
X	Reduce sandstone values by 40% and use full values for siltstone
XI	Use values for siltstone or shale

bedding thickness consideration of the competent sandstone beds. In the type IV and V (slightly disturbed structures) when the thickness of sandstone beds exceeds 50cm, an increase of the GSI value by 5 is suggested. It is noticed that for the non disturbed types anisotropy is present due to the bedding planes and in analysis this fact should be taken into consideration.

In addition to the GSI values, it is necessary to consider the selection of the “intact” rock properties σ_{ci} , m_i and E_i for the heterogeneous rock masses considered as a unit. A ‘weighted average’ of the intact strength properties of the strong and weak layers is proposed in Table 1.

3.2. Geotechnical classification of molassic rock masses

Molasse is quite different from flysch, although both are consisting of same lithological types, since molasse is formed after the orogenesis, and did not suffer from compressional tectonics. The proposed GSI chart for molasses can be of general application to all formations consisting from alternations of sedimentary rocks not associated with significant tectonic disturbance, though this chart was based on the observations from the excavation of 12 tunnels along the Egnatia highway in molassic formation. The GSI chart for molasses has already been published (Hoek et. al. 2004) but is included in this paper in order to be compared and distinguished from the flysch chart.

As the molasse strata were formed after the main orogenesis, the deterioration of the quality of their rock mass is limited. Only in few cases the molassic formations may be deformed and present thrusts due to the final advance of tectonic napes but such a decrease of their quality is localized.

The siltstone (or marly) members are very vulnerable to weathering and a development of fissility parallel to the bedding when these rocks are exposed or are close to the surface may be developed. Thus in outcrops they appear thinly layered and when they alternate with sand-

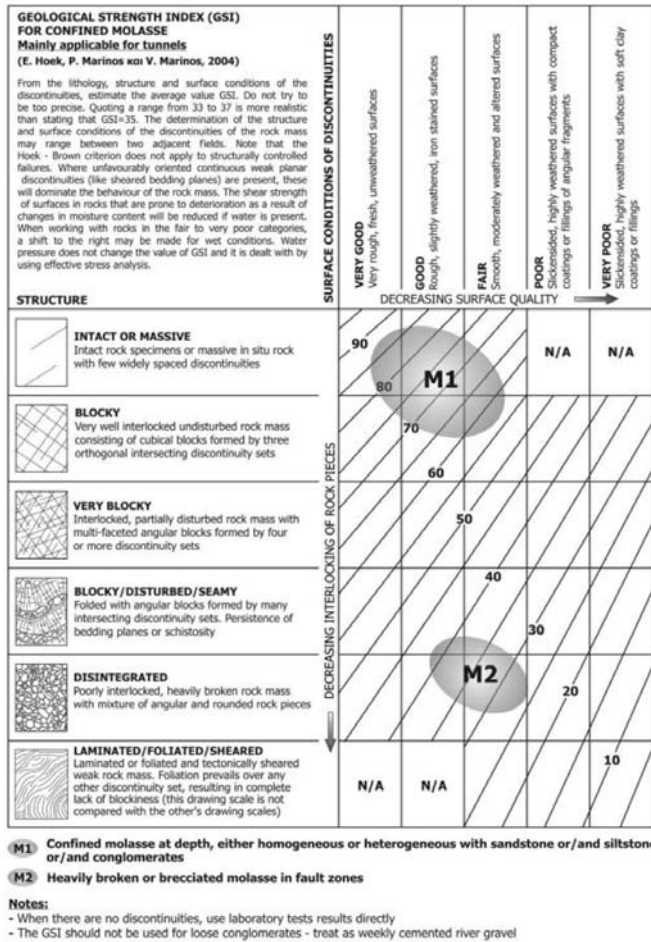


Fig. 2: GSI classification chart for molassic rock masses in depth (applicable for tunnels)

stones, their appearance resemblances to flysch. This appearance in outcrops can be misleading when considering the behaviour of these molassic rocks in a confined underground environment in which the process of air slaking is restricted and the rock mass is continuous and massive without any sign of stratification or schistosity inside the siltstone beds.

As a result, molassic rock masses have dramatically different structure when they outcrop or are close to the surface as compared to those confined in depth, where bedding planes, especially the siltstone ones, do not appear as clearly defined discontinuity surfaces. In such cases the use of the fundamental GSI chart reproduced in Fig. 2, is recommended and the zone designated M1 of a value of 50–60 or more is to be applied. If no discontinuities are present, GSI values are very high and the rock mass can be treated as intact with engineering parameters given by direct laboratory testing. When fault zones are encountered in depth, the rock mass may be highly broken but it will not have been subjected to air slaking. Hence the fundamental rock GSI chart given in Fig. 2 can be used but the GSI value will lie in the range of 25–40 as shown by the selected area M2.

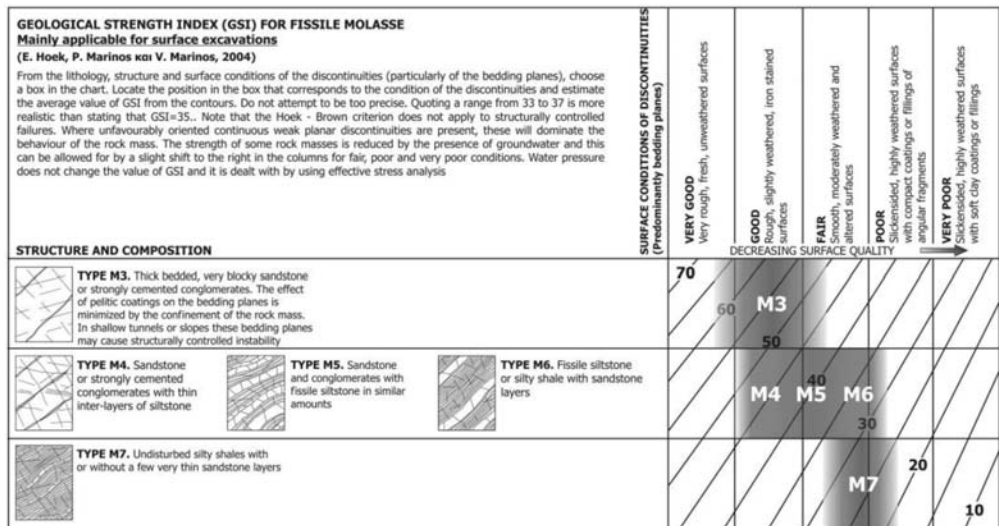


Fig. 3: GSI classification chart for molassic rock masses in surface (applicable for surface excavations)

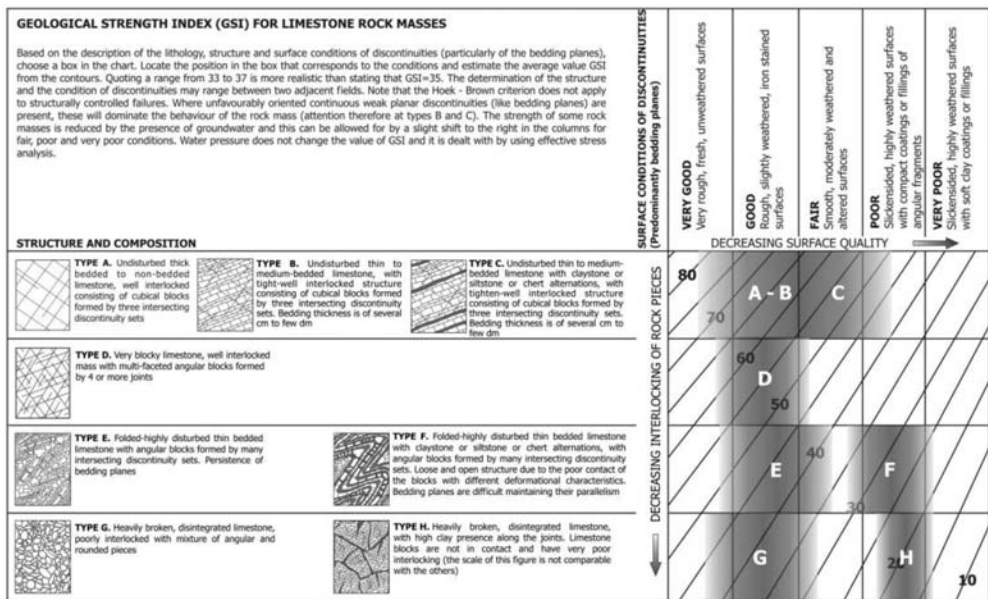


Fig. 4: GSI classification chart for limestone rock masses, including tectonically disturbed rock masses, with or without claystone, siltstone or chert intercalations.

In surface, the heterogeneity of the formation is discernible and similarities exist with the structure of some types of flysch. Hence the GSI chart for heterogeneous rock masses such as flysch can be used with the exclusion of sheared and disturbed types and with a slight shifting to the left of the flysch chart categories, as the molasse is always less disturbed. This version of the chart, for fissile molassic rocks (M3–M7 designations), is presented in Fig. 3.

3.3. Geotechnical classification of brecciated limestone formations

Limestones, in general, are neither weak nor complex formations. Though, if they are depressed in great areas by thrusting and tectonic rucks, poor rock masses can be produced. The rock mass is disintegrated with no remains of the initial structure due to the brittle behaviour of the limestone blocks. Two tunnels in heavily fractured limestones and three others in normal geotechnical conditions were examined in this study.

The rock mass quality may thus be poor to very poor because of the disintegrated structure which is characterized as heavily broken with a mixture of angular and rounded pieces (type G in fig.4). The RQD of such rock mass is zero ($RQD=0$) although a good frictional strength may be present. Cohesion is absent except if cemented material is present. In these cases the GSI value ranges from 30-45. In case of heavily broken limestone, with high clay presence along the joints (type H), where the pieces are not in contact and have very poor interlocking, the friction properties of the rock mass is significantly reduced. The rock mass is characterized as disintegrated with very poor surface condition with GSI values between 15 and 25.

Thin to medium bedded limestones, when are tectonically undisturbed (unfolded-slightly fractured) they present highly tight structure (type B) with “sewed” bedding planes. In such cases, rock mass is characterized as “Blocky” with “Good” to “Fair” surface conditions and is thus rated from 55 to 70. These values were confirmed after tunnel excavation where very light support measures were applied (GSI design value >55). In design analysis in low stress environment structural instability will be the failure process and the GSI is not applicable. In high stress GSI can be approximately used taking into account however the anisotropy provoked by the bedding planes.

In case of claystone or siltstone intercalations in a folded-highly disturbed rock mass, the structure is less tight due to the poor contact of the blocks with different deformational characteristics (the plastic members are sheared and the limestone beds are broken and cannot follow the same deformation pattern) and the parallelism between the bedding planes is limited.

3.4 Geotechnical classification of ophiolitic rock masses

Ophiolites often associated with subsequent overthrusts, contain a variety of rock types with geotechnical qualities varying from excellent to fair, becoming poor to very poor when serpentinisation is extensive and/or shearing present. The main included types are peridotites, gabbros, peridotites more or less serpentinised, serpentinites, schisto-serpentinites, sheared serpentinites, pillow lavas and chaotic masses in ophiolitic melanges. A high degree of serpentinisation together with the intensity of shearing may result to a mass where is difficult to identify any initial texture or fabric. This study is based on field data from outcrops, cuts in slopes, borehole cores and tunnel excavations (7 from Egnatia Highway) and from various significant ophiolitic complexes and melanges in northern and central Greece. A GSI chart is already published (Marinos et al 2005), but it is reproduced here together with the other new charts in order to include all charts of complex rock masses in the same paper, but also since an other type of rock mass is added.

Peridotites are strong and behave as typical brittle materials. Their tectonic disturbance is expressed in terms of intersecting joint sets. The range of GSI for peridotitic types of rock masses in an ophiolitic complex is shown in Fig. 5 (areas I and II). Serpentinisation can be present on the surface of discontinuities and the conditions of the joints are dramatically reduced to poor

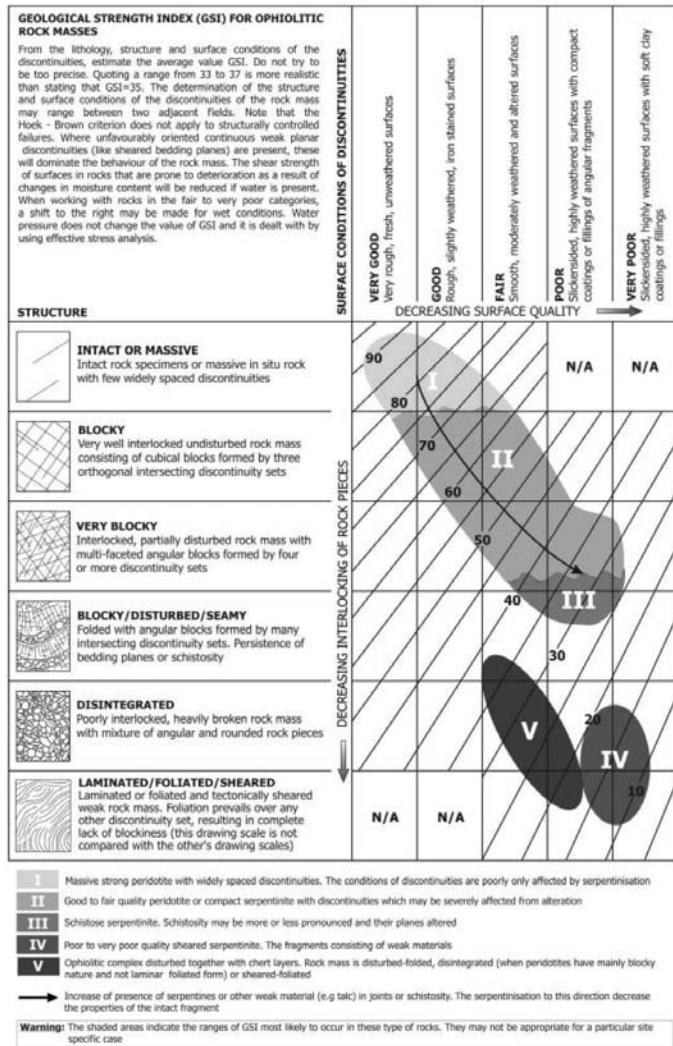


Fig. 5. GSI classification chart for ophiolitic rock masses

or very poor with coatings of “slippery” minerals such as serpentine or even talc. When the rock mass is jointed or fractured the GSI values drop as low as 35, not only due to a disturbed structure but also because of the conditions of the discontinuities, which become smooth and slippery due to serpentinisation. In a disturbed peridotitic mass, the serpentinisation process often loosens and disintegrates parts of the rock itself, not only contributing to lower GSI values but also reducing the intact strength values. Such disturbed peridotites fall in the lower bound of area II of the GSI diagram of Fig. 5.

If the process of serpentinisation is due to autometamorphism and/or associated with tectonic thrust, the rock mass is poor, with a schistose disturbed structure which may reduce the GSI to values to 30 or less (area III in the GSI diagram of Fig. 5). In the sheared zones of serpentinites there is a lack of blockiness, which allows the rock to disintegrate into slippery laminar pieces

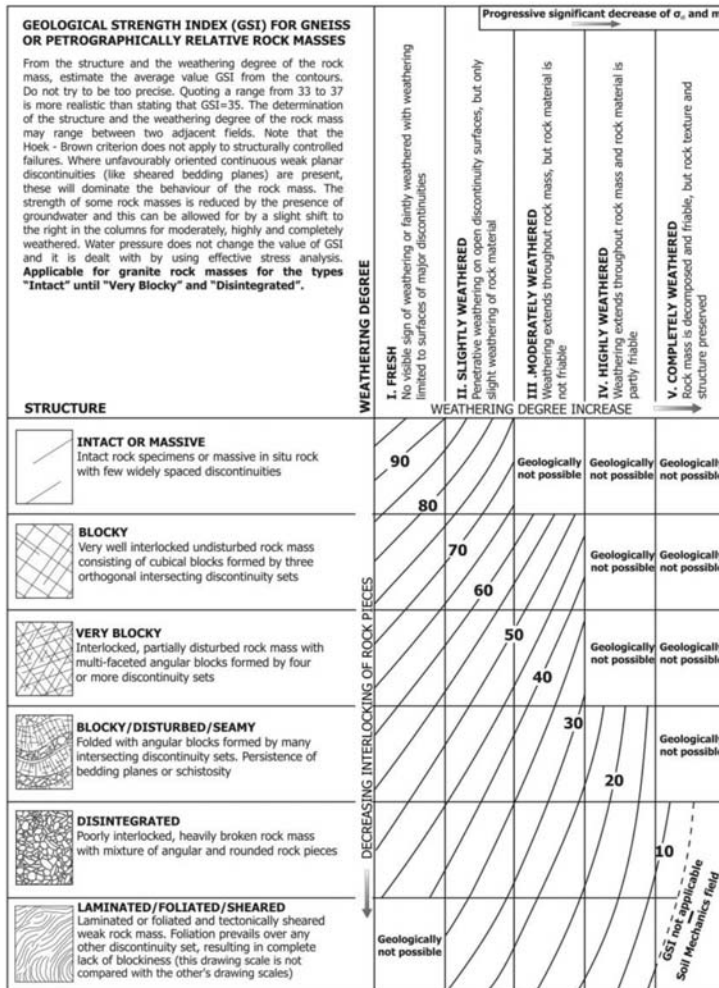


Fig. 6. GSI classification chart for gneiss or petrographically similar rock masses

and small flakes of millimeters in size. GSI values can drop to less than 20 (Fig. 5, area IV).

When the serpentinisation, due to weathering, has affected all the mass, in addition to the reduction of the intact strength there is a dramatic disintegration of the structure of the rock mass too.

In ophiolitic melanges, where rocks of the ophiolitic sequences are mixed in complete disorder with other rocks of various origins (flysch formations, chert and other), the rock mass is disturbed-folded or disintegrated (when peridotites have mainly blocky nature and not laminar – foliated form) or sheared-foliated and, thus, low to very low GSI values are assigned (area V in Fig.5).

3.5 Geotechnical classification of tectonically disturbed and weathered gneiss rock masses

Fresh gneiss forms evidently very competent rock masses with minor problems in geotechnical works. However, in certain geological conditions gneiss can produce poor to very poor rock

masses. This environment is produced by intensive and sequent tectonic disturbance and thus weathering and alteration is favored in various degrees and depths.

In such conditions, the intact rock and rock mass strength present a wide range in values and the behaviour in ground works can be from simple to extremely problematic. Six tunnels along the Egnatia highway were investigated in a gneissic environment. In a disturbed tectonically environment, the complexity in gneiss rock mass, due to intense weathering (alteration of feldspars to clayey minerals) and fracturing, is characterized by erratic geometry to all directions. Here, the simple common case that the fracturing and weathering is gradually reduced with depth does not exist.

Thrust zones with brittle deformation encounter highly broken and weathering geomaterial, which can have significant thickness (up to 10m) consisting of remains of friable pieces in a texture governed mainly by clayey-sandy weathered product. On the other hand, gneiss rock masses can also be deformed in a ductile like manner when the initial structure is schistosed under high stresses (structures recognized along the base tunnels in Alps).

A decrease in the GSI value is proposed for the gneissic rock masses in order to consider more appropriately the weathering effect. By the comparison of the classifications and the temporary support categories between the design and the construction records, it was shown that this decrease lies to around 10 units. However, the use of this numerical difference must be carefully done due to construction issues, like for example the procedure to connect a classification value with the support category selection. Of course, this difference could also be due to the application of heavier support demand due to frequent over-brakes, like chimney type failures and not due to stress controlled problems. Nevertheless, the wide application of heavier support systems between similar geotechnical conditions, corresponding to a difference of 10 units, in all the tunnels and the geological concept described before, agreed to this diversity.

The new GSI chart is thus proposed for gneiss or rock masses with similarities in weathering, as the granite. This chart maintains the basic structures but the surface conditions of joints are replaced by the weathering grades (from Fresh-grade I to Completely Weathered- grade V, Brown, 1981). This is associated with a new calibration and the substitution of the straight lines of the fundamental chart with curved lines, bended to the left side of the chart.. As the weathering degree increases to the right, bending is increased as well. In the first column, where the rock mass is not weathered (category I), the calibration lines remains the same and GSI values do not change. The Decrease in GSI values starts from "Slightly weathered" (category II) rock masses and becomes higher (around 10 units) in "Completely weathered" rock masses (category V) with a "Blocky-Disturbed" or "Disintegrated" structure. However, a number of unfeasible geologically conditions (e.g. "Very Blocky" and "Highly weathered" rock mass) must be excluded from the GSI chart.

4. Conclusions

This paper deals with the geotechnical classification of weak and complex rock masses such as flysch, molasse, gneiss (in its disturbed form), ophiolites and particular cases of limestones. The complexity of these geological material imposed a more specialized research for their geological characterization due to the special features of their rock masses regarding both their structure and their lithological characteristics. The weak and complex rock masses analysed had either undergone highly tectonised disturbance resulting in the destruction of their initial

structure or/and weathering. They include in many cases an inherent heterogeneity with members of low strength.. The experience gained by the recent excavation of 62 tunnels in the Greek territory, under particularly difficult geological conditions, provided a great number of data, which were processed in a geotechnical database. From their assessment and analysis a number of new charts of the Geological Strength Index (GSI) are proposed, extending its application in the quantitative description of the geological material for engineering purposes.

5. Acknowledgments

The author acknowledges the support and encouragement of G. Tsiambaos, Associate Professor of NTUA. The author would like also to thanks Egnatia Odos S.A. for its support for the assignment of the relevant research program. Special thanks should be offered to the geologist D. Papouli for her assistant to the preparation of the figures.

6. References

- Barton, N.R., Lien, R., Lunde, J., 1974. Engineering classification of rock masses for the design of tunnel support. *Rock Mechanics*, 6(4), pp. 189-239.
- Bieniawski, Z.T., 1973. Engineering classification of jointed rock masses. *Trans South Afr. Inst. Civ. Eng.* 15, pp. 335-344.
- Brown, E.T., 1981. Rock characterization, testing and monitoring—ISRM suggested methods. Pergamon, Oxford, pp.171-183.
- Hoek, E., Marinos, P. and Benissi, M., 1998. Applicability of the Geological Strength Index (GSI) classification for very weak and sheared rock masses. The case of the Athens Schist Formation. *Bulletin of Engineering Geology and the Environment*, 57(2), pp. 151-160.
- Hoek, E., Carranza-Torres, C., Corkum, B., 2002. Hoek - Brown failure criterion - 2002 edition. In: Bawden H.R.W., Curran, J., Telesnicki, M. (eds). *Proceedings of NARMS-TAC 2002*, Toronto, pp. 267-273.
- Hoek, E., Marinos, P., and Marinos, V., 2004. Characterization and engineering properties of tectonically undisturbed but lithologically varied sedimentary rock masses. *International Journal of Rock Mechanics and Mining Sciences*, 42(2), pp. 277-285.
- Marinos, P., Hoek, E., 2000. GSI: a geologically friendly tool for rock mass strength estimation. In: *Proceedings of the GeoEng2000 at the international conference on geotechnical and geological engineering*, Melbourne, Technomic publishers, Lancaster, pp. 1422-1446.
- Marinos, P., Hoek, E., 2001. Estimating the geotechnical properties of heterogeneous rock masses such as flysch. *Bulletin of Engineering Geology and the Environment*, 60, pp. 82-92.
- Marinos, P., Hoek, E., Marinos, V., 2005. Variability of the engineering properties of rock masses quantified by the geological strength index: the case of ophiolites with special emphasis on tunnelling. *Bulletin of Engineering Geology and the Environment*, 65(2), pp. 129-142.
- Marinos P. V. (2007). "Geotechnical classification and engineering geological behaviour of weak and complex rock masses in tunneling", Doctoral thesis, School of Civil Engineering, Geotechnical Engineering Department, National Technical University of Athens (NTUA), Athens, July (in greek).
- Stille, H., Palmstroem, A., 2003. Classification as a tool in rock engineering. *Tunnelling and Underground Space Technology*, 18, pp. 331-345.

STRENGTH AND DEFORMABILITY OF SPECIFIC SEDIMENTARY AND OPHIOLITHIC ROCKS

Marinos P. V.¹, Tsiambaos G¹

¹Geotechnical Engineering Department, National Technical University of Athens, 15780 Athens - Greece,
vmarinos@central.ntua.gr

Abstract

The paper deals with the evaluation of strength and deformability of sedimentary rocks and ophiolites based on the processing of laboratory testing results. Characteristic values and their typical range for the parameters σ_{ci} , E_i , as well as the Modulus Ratio (MR) are presented. These parameters are significant for the estimation of the strength and deformability of the rock mass since σ_{ci} is basic component for the solution of Hoek-Brown failure criterion and E_i and MR are important components of the latest rock mass deformability expression (Hoek-Diederichs, 2006). The recent site investigation and laboratory work undergone for the design of numerous tunnels in the Greek territory provided very good and sufficient data, derived from a specifically established database, for the estimation of strength and deformability of specific rocks. These rocks are sandstones and siltstones of flysch and molassic formations, as well as limestones and ophiolites.

Key words: rock strength, deformability, Modulus Ratio (MR), sedimentary rocks, ophiolite

1. Introduction

Geotechnical engineering works such as surface and underground excavations requires strength and deformability rock parameters for a detailed design analysis. Most of the cases these parameters concerns the rock mass properties. However, the estimation of the rock mass properties, through certain relations, requires the intact rock strength and deformability values. Indeed the uniaxial compressive strength (UCS) of the intact rock is a basic component on the Hoek and Brown failure criterion (Hoek et al., 2002), which is used for the rock mass strength estimation. In addition, the deformation modulus of the intact rock (E_i) or the Modulus Ratio (MR) is often comprehended in several empirical relations for the calculation of the rock mass deformation modulus (E_{rm}). Such relations are suggested by Hoek and Diederichs (2006), Ramamurthy (2004), Sonmez et al. (2004) and Zhang and Einstein (2004). Some other important application of uniaxial compressive strength includes rock mass characterization and excavation method selection. Nevertheless, estimation or selection of an appropriate value of UCS or E_i can be difficult, since it can vary for the same rock.

A tool of this research was a database named “Tunnel Information and Analysis System” (TIAS) established in the frame of the PhD research of the author (Marinos, 2007). Through this database, a great number of geological, engineering geological and geotechnical data from the design and the construction of 62 tunnels of Egnatia Highway in Northern Greece were processed. A significant part of the input information in the database is the laboratory test results of several rocks. These data were evaluated and a result of this research is the definition of characteristic values for the Uniax-

ial Compressive Strength (UCS), intact rock deformation modulus (E_i) and Modulus Ratio (MR) for several rocks. The rocks that are examined in this paper are those of sandstone, siltstone, conglomerate, marly limestones and peridotites. It is noted that the properties of the clastic rocks (sandstone, siltstone and conglomerate) are examined for both flysch and molassic environments, since they present particular differences in their nature.

2. Strength and deformability parameters

2.1 Characteristic values of sedimentary rocks

The study for the uniaxial compressive strength (UCS) and the deformation modulus (E_i) of the sandstone, siltstone and the conglomerate intact rocks was done, based on numerous lab test results from the TIAS database. The great number of lab testing in these rocks enabled this process, reducing the possibility of error or confused values. These data were derived from the design of 13 tunnels in a flysch and 12 tunnels in molassic environment and are examined separately due to their different nature.

Both formations are characterized mainly by rhythmic alternations of sandstone and pelitic rocks (siltstones, silty or clayey shales). Conglomerate beds may also be included. Flysch is associated with orogenesis, since it ends the cycle of sedimentation of a basin before the paroxysm folding process. Molassic deposits were deposited during a quiescent period after the main orogenesis and have not suffered from compression. Naturally, flysch and molassic rock strength and deformability vary from place to place but their diverse sedimentation environment and compression history creates notable differences in their values.

The mean, minimum and maximum value of the uniaxial compressive strength (UCS) and deformation modulus (E_i) of these intact rock materials for flysch and molassic formations are presented in Table 1. The higher UCS values are presented in flysch sandstone with a mean value of 43MPa, a minimum of 10 MPa and a maximum of 120 MPa. Similar range is noted in molassic sandstone but with a mean value of 35 MPa. As far as the E_i is concerned, a mean value of around 13000MPa is observed for a flysch sandstone and 8700MPa for a molassic one. In siltstones a mean UCS value of around 16-17MPa is evaluated for both flysch and molassic formations, while E_i is estimated 4600MPa in a flysch environment and 3000MPa in molassic series. Conglomerates present UCS values between 16MPa (flysch) and 23MPa (molasse) and E_i values between 4600MPa (flysch) and 7400MPa (molasse).

It should be highlighted here, that siltstones and silty sandstones are susceptible to slaking, thus the rock after its atmospheric exposure can be rapidly altered, schistosed or even disintegrated. Thus, it is very important to test the specimen immediately in site if possible after their recovery, in order not to obtain very low results. In addition, point load may not be adequate to measure the strength, since the pressure point may "invade" within the weak rock. Anyhow, testing must be applied vertical to the direction of the rock fissility.

Accordingly, the mean, minimum and maximum UCS and E_i values for marly limestones are presented in Table 1. These values are generally low, because of their marly nature, with a mean UCS value of 21MPa and a maximum close to 50MPa.

2.2 Characteristic values of ophiolitic rocks

Measuring the strength of the intact rock, from such rock masses is always a problem because of the

Table 1. Characteristic UCS and Ei values, their typical range and standard deviation (STD) for sedimentary rocks and peridotites

Rock material	Rock material properties	Number of tests	Min	Max	Mean	STD
Sandstone (flysch)	UCS (MPa)	238	10.00	119.60	46.07	28.85
	Ei (MPa)	130	2019	56000	13354	12892
Sandstone (molasse)	UCS (MPa)	258	10.76	116.73	35.06	21.05
	Ei (MPa)	132	2000	31300	8763	7373
Siltstone (flysch)	UCS (MPa)	107	2.43	62.00	17.36	12.68
	Ei (MPa)	76	698	17000	4628	4116
Siltstone (molasse)	UCS (MPa)	152	1.92	51.11	16.91	10.77
	Ei (MPa)	58	650	9070	2984	1845
Conglomerate (flysch)	UCS (MPa)	61	5.18	54.00	16.16	2.37
	Ei (MPa)	48	669	14400	4588	3321
Conglomerate (molasse)	UCS (MPa)	165	5.00	68.19	23.05	13.86
	Ei (MPa)	82	1140	19400	7432	5096
Marly Limestone	UCS (MPa)	35	5.71	49.00	20.64	10.93
	Ei (MPa)	30	725.93	15980	3844	2072
Peridotite	UCS (MPa)	118	12.20	131.60	43.34	24.62
	Ei (MPa)	33	5000	44554	19924	11874

influence of “schistosity” which reduces the strength. A number of lab test results of the uniaxial strength (UCS) and deformation modulus (Ei) of peridotites were processed and the values are presented in Table 1.

A great range in both UCS and Ei values is presented. The mean value of the uniaxial compressive strength is 43MPa ranging from 12MPa to 130MPa. When peridotites are not serpentised they have a range of UCS from 50 MPa to more than 100 MPa. On the other hand, UCS is considered 40 MPa for the serpentinite and 30 MPa for the schisto-serpentinite (Marinos et. al., 2005).

3. Modulus Ratio (MR)

3.1 General

Hoek and Diederichs (2006) proposed a new equation for the estimation of the rock mass deformation modulus E_{rm} (1).

$$E_{rm} = Ei \left[0.02 + \frac{1 - D/2}{1 + e^{((60+15D-GSI)/11)}} \right] \quad (1)$$

, where, E_i the intact rock deformation modulus, GSI is the Geological Strength Index and D the Disturbance factor due to the excavation method.

Table 2. Suggestions of MR values by Deere (1968) and Palmstrom and Singh (2001).

Rock material	MR value range
Sandstone	200-350
Siltstone	350-400
Conglomerate	300-400
Crystalline Limestone	400-600
Sparitic Limestone	600-800
Micritic Limestone	800-1000
Peridotite	250-300

This relation resulted after the evaluation of insitu tests on the deformability of the rock mass, together with information on the uniaxial compressive strength (UCS) and geological description of the rock mass. These information, allowed an analysis where the ration E_{mm}/E_i could be used. For this approach the Modulus Ratio (MR) after Deere (1968) is used for several rock types. The Modulus Ratio (MR) for the intact rocks is calculated from the equation (2):

$$E_i = MR\sigma_{ci} \quad (2)$$

, where, σ_{ci} is the uniaxial compressive strength (UCS) of the intact rock.

Hoek and Diedrichs (2006) note that the MR values are difficult to be calculated in precise, since a slight disturbance in rock state and structure (especially for weak rocks) can be crucial to the σ_{ci} measure. A certain range of MR values are suggested by Deere (1968) and Palmstrom and Singh (2001) (Table 2.)

Previous research on sedimentary rocks in Greece provided MR value ranges for sandstone specimens from 120 to 727, with a mean value of 303 and for limestone specimens from 160 to 1380, with a mean value of 810 (Sabatakakis et al., 2008). Moreover, Tziallas et al. (2009) proposed a typical range of MR values for sandstones between 200 and 400 and for limestones between 300 and 500.

MR values for several sedimentary rocks and ophiolites are proposed in this paper after the evaluation of numerous lab tests processed from TIAS database.

3.2 Modulus Ratio (MR) characteristic values

Modulus Ratio (MR) is calculated from the correlation of the uniaxial compressive strength (UCS) and deformation modulus of the intact rock (E_i). The MR (E_i/UCS) correlation diagrams of sandstone, siltstone and conglomerate are separately presented for flysch (first column) and molassic (second column) formations in Fig. 1. MR value is estimated by a best fitted curve (confident limits 95%), where a range of possible values is also noted (grey area). Similarly, the UCS- E_i correlation diagram that provides the MR value for the limestone and peridotitic rocks is shown in Fig. 2.

The mean MR values (best fitted curve) and their typical range were calculated from the correlation of UCS and E_i lab tests and the results are presented in Table 2.

Table 3. Characteristic MR values and their typical range for sedimentary and ophiolitic rocks

Rock material	Number of tests	MR value	
		Range	Mean*
Sandstone (flysch)	72	80-300	140
Sandstone (molasse)	123	100-260	170
Siltstone (flysch)	65	100-400	245
Siltstone (molasse)	58	120-220	160
Conglomerate (flysch)	45	110-400	230
Conglomerate (molasse)	79	180-670	375
Marly Limestone	25	100-300	170
Peridotite	34	230-760	420

*Mean value is estimated by best fitted curve (confident limits 95%)

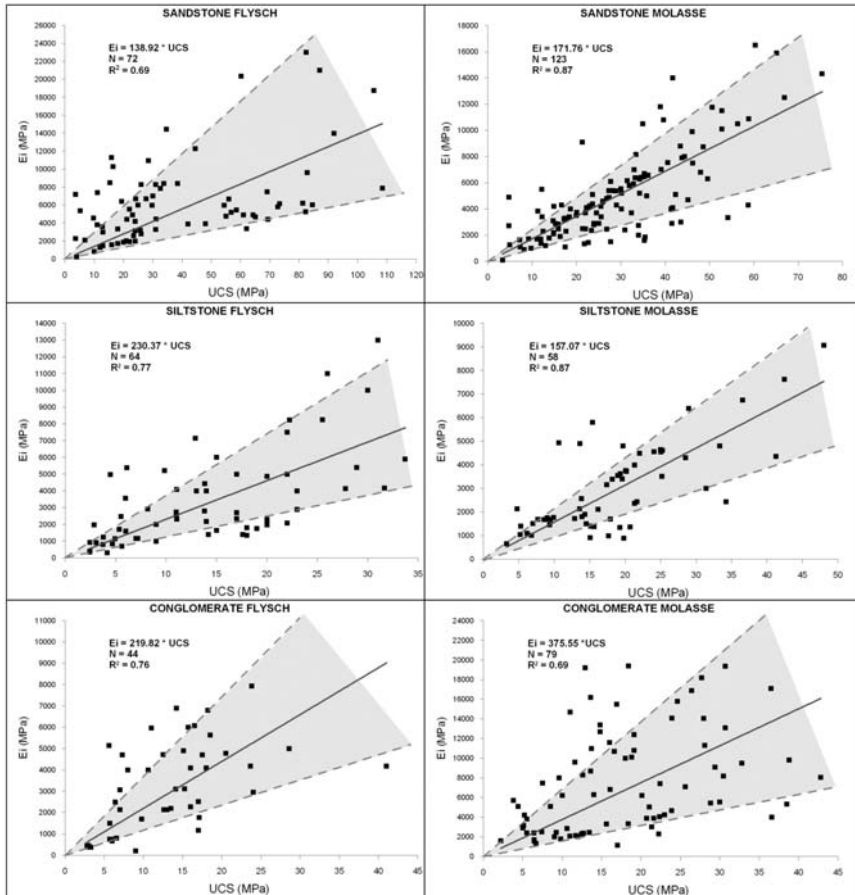


Fig. 1: UCS-Ei correlation diagram that provides the MR value of sandstone, siltstone and conglomerate for flysch (left column) and molassic (right column) formations

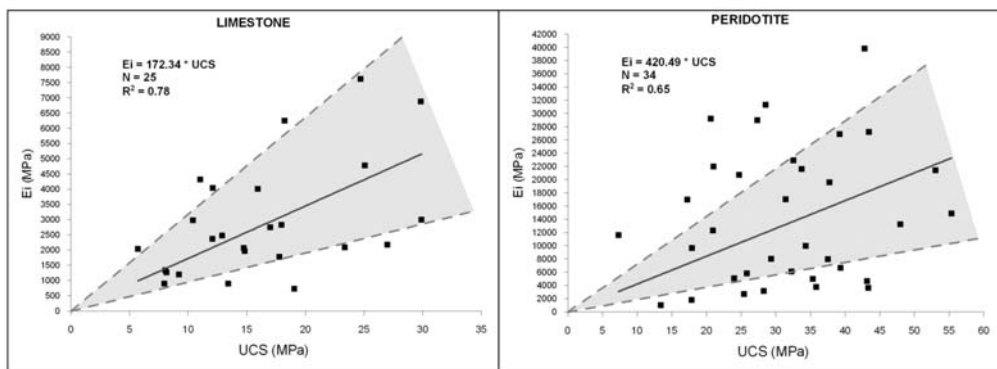


Fig. 2: UUCS-Ei correlation diagram that provides the MR value for the marly limestones and peridotites.

4. Discussion

4.1 Discussion on strength and deformability results

The uniaxial compressive strength of a sandstone in flysch formations is around 40-45MPa which is higher than the molassic one. Sandstone composite in molasses are often silty or marly and present lower strength values. The uniaxial compression strength may be around 10MPa when it is silty or marly and it can be over 50MPa in its typical granular form. A typical value that best describes the sandstone intact rock strength in molassic formations, in Northern Greece is 30-35MPa. On the other hand, typical intact rock strength of siltstones in flysch and molasses is around 15MPa. Nevertheless, when siltstones have high presence of clayey minerals the uniaxial compressive strength ranges between 5MPa to 10MPa. In conglomerates, the uniaxial compressive strength of the molassic formations is around 20-25MPa, while lower values (~15-17MPa) are met in flysch formations due to the poorer cement.

Similar differences are also met in the Ei values, as far as the sandstone is concerned. The deformation modulus (Ei) of the sandstone in a flysch environment is much higher than the molassic one. This is caused mainly due to the low compression during the sedimentation of the molassic formations. Smaller difference is also observed in the siltstone rocks. On the other hand, the Ei value of a conglomerate in molassic sediments is much higher than the flysch one. Here, the compression and sedimentation history does not define so the deformability of the material as much as the cementation does. The cementation in molassic conglomerates is calcarenitic, while in flysch formations is mainly clayey.

As far as the strength and deformability of the limestone is concerned, the observed low values are in agreement with the marly nature of the rock.

The UCS and Ei values of peridotitic rocks present a significant range. The evaluation of the results in peridotites shows that this great range of values corresponds to the variable peridotitic nature, namely of a fresh and a serpentinised peridotite. Serpentinisation (transformation of ferromagnesian minerals, olivine in particular, to serpentine - a lattice mineral of either fibrous or laminar form) changes the strength and deformation characteristics of peridotitic rocks, since the laminar-schistosed new minerals alter the rock texture.

4.2 Discussion on Modulus Ratio (MR) results

The suggested MR values from Deere (1968) and Palmstom and Singh (2001) are 275 ± 75 for sandstone, 375 ± 25 for siltstone and 350 ± 50 for conglomerate. These values present notable differences with the ones of this study (Table 2), since the mean values are generally lower. Similar values are only presented in molassic conglomerates. Significant differences are also noted in limestones given that the same references propose MR values from 400 to 1000 according to the texture and in this research a value from 100 to 300 is suggested for the marly limestones.

As far as the peridotites are concerned, the proposed MR values from Deere (1968) and Palmstom and Singh (2001) are 250-300. Comparing these with the ones presented in this research it is evident that there is a significant difference in values. On the other hand, the same authors suggest an MR value for a gabbro around 450 (± 50), which is approximate with the one resulted here (Table 3). This difference between these references and the ones processed here, highlight again the problematic nature of ophiolitic rocks because of the serpentinitisation, in order to obtain representative E_i or MR values.

5. Conclusions

The unconfined compressive strength (UCS), deformation modulus (E_i) and the Modulus Ratio (MR) of the intact rock are basic components in certain relations, used to estimate the rock mass properties in whole. The evaluation of strength and deformability of sedimentary rocks and ophiolites based on the processing of laboratory testing results was done in this paper and the characteristic values and their typical range for the parameters σ_{ci} , E_i , as well as the Modulus Ratio (MR) are presented. The rocks that were examined are those of sandstone, siltstone, conglomerate, marly limestones and peridotites. The properties of the clastic rocks were examined for both flysch and molassic environments and their differences were highlighted. The processed and evaluated data derived from a specifically established database from the design of 62 tunnels of Egnatia Highway in Northern Greece.

6. Acknowledgments

The authors would like to thank Egnatia Odos S.A. for its support and the assignment of a research program concerning a geotechnical database construction.

7. References

- Deere, D.U., 1964. Technical description of rock cores for engineering purposes. *Rock Mechanics and Engineering Geology*, 1(1), pp. 17-22.
- Hoek, E., Diederichs, M.S., 2006. Empirical estimation of rock mass modulus. *International Journal of Rock Mechanics and Mining Sciences*, 43, pp. 203-215.
- Hoek, E., Carranza-Torres, C., Corkum, B., 2002. Hoek - Brown failure criterion - 2002 edition. In: Bawden H.R.W., Curran, J., Telesnicki, M. (eds). *Proceedings of NARMS-TAC 2002*, Toronto, pp. 267-273.
- Marinos, P., Hoek, E., Marinos, V., 2005. Variability of the engineering properties of rock masses quantified by the geological strength index: the case of ophiolites with special emphasis on tunnelling. *Bulletin of Engineering Geology and the Environment*, 65(2), pp. 129-142.
- Marinos P. V., 2007. "Geotechnical classification and engineering geological behaviour of weak and complex rock masses in tunneling", Doctoral thesis, School of Civil Engineering, Geotechnical Engi-

- neering Department, National Technical University of Athens (NTUA), Athens, July (in greek).
- Palmstrom, A., Singh, R., 2001. The deformation modulus of rock masses: comparisons between in situ tests and indirect estimates. *Tunnelling and Underground Space Technology*, 16, pp. 115-131.
- Ramamurthy T., 2004. A geo-engineering classification for rocks and rock masses. *Int J Rock Mech Min Sci* 41:89–101.
- Sabatakakis, N., Koukis, G., Tsiambaos, G., Papanakli, S., 2008. “Index properties and strength variation controlled by microstructure for sedimentary rocks”, *Engineering Geology*, Elsevier, 97, 80-90.
- Sonmez H, Gokceoglu C, Ulusay R., 2004. Indirect determination of the modulus of deformation of rock masses based on the GSI system. *Int J Rock Mech Min Sci* 41(5):849–857.
- Tziallas, G.P., Tsiambaos, G., Saroglou, H., 2009. “Determination of rock strength and deformability of intact rocks”, *Electronic Journal of Geotechnical Engineering*, 14 G, 1-12.
- Zhang L, Einstein HH., 2004. Using RQD to estimate the deformation modulus of rock masses. *Int J Rock Mech Min Sci* 41(2):337–341.

LANDSLIDE IN NACHTERSTEDT OF GERMANY

Moraiti E.¹, Christaras B.² and Brauer R.³

¹ IGME, Athens, GR, e-mail: moraiti@igme.gr

² Aristotle University of Thessaloniki School of Geology, Lab. of Engineering Geology & Hydrogeology, Lab, GR, e-mail: christar@geo.auth.gr

³ Saxon State Office for the Environment, Agriculture and Geology, e-mail: Rainer.Brauer@smul.sachsen.de

Abstract

On July 18, 2009, an important landslide occurred in Nachterstedt City toward to the artificial Concordia Lake, which was created, in 1994, at the place of an old coal mine, at the edge of the city. The area is located to North-East of Harz, between the cities of Aschersleben and Quedlingburg. An underground coal mine is responsible for this damage which caused the damage of a privet house and a big building. Three people were also died. The mine apparently closed in 1991 whereupon it was converted into a recreation area. The landslide was caused by the increase of the groundwater level, in the coal mine, after a heavy rain, in relation to the water level of the lake.

Key words: *Nachterstedt, landslides, halocinetic movements.*

1 Introduction

On July, 18, 2009, an important landslide created at coastal part of Nachterstedt City toward to Concordia Lake. Three people were died and a privet two-floor house was destroyed together with a big building (Fig.1). The sliding was related to existence of a coal mine under the city. On Feb. 2, 1959, a similar landslide, of 5.8 million m³, had also activated by the coal mine works. One min worker died and many reactions were activated, in the East Germany of that period, regarding to the coal mine exploitation method used.

Nachterstedt was offered, in 961, to Baron Gero. Many historians refer that people leave in this city, from 500 AD. The coal started to be exploited, in 19th c. AD. The first boreholes were performed in 1842/43 and in 1957, the Concordia coal mine, a field of 600 hectares, started to be exploited. It is the area of the present lake, which was responsible for the occurred landslides. The exploitation of the 30 m thick coal layer was started at a depth of 15 m. tunnel).

2. Geologic Overview

During the Eocene in the area of the Ascherslebener saddle tectonic movements caused an up-rise of the deep lying Zechsteinsaltlayers. The salt moved away from the rims of the saddle into its core. Hereby sinks were created into which from NW marine Sediments could transgress. During phases of reduced sink movements moors or swamps developed from which the exploited brown coal has been mined. The general geological structure of the Paleogene at



Fig. 1: The landslide of July 19, 2009, in Nachterstedt (Petley, 2009, <http://daveslandslideblog.blogspot.com/>).



Fig. 2: Location of Nachterstedt City (<http://earth.google.com/download-earth.html/>).

Nachterstedt is characterized by rhythmic and cyclic sedimentary sequences (Balaske, 1992, 1998). These cycles begin with sands, partly transgressive conglomerates, followed by silty sand and silt. The final members of such cycles form the coal seams. Reasons for the cyclic structure were interactions between global-eustatic and more local modifying factors (Salt tectonics halocinetic movements). In particular, during the middle Eocene in the descending part of the basin area of Nachterstedt three workable coal beds could develop. The age of these autochthonous coals, supported by tree stumps and root horizons, is clearly determined on the fossil content of the intermediate marine sediments and on pollen dating. By invasion of humic acids previously existing micro- and macro-fossils (foraminifera, bivalves and gastropods) had been dissolved. For stratigraphic classifications therefore mainly siliceous dinoflagellates have been used. These species characterise mainly a coastal habitat. Shallow marine sedimentary structures as well as local sand dunes in the profile series support such an interpretation (Woldstedt, 1926, Voigt, 1963, Ahrendt et al., 1995).

The section of Nachterstedt (Balaske, 1998) begins with about 35m of a so called basic clay in which Intercalations of silts and sand might occur. This lowermost sequence is followed by 15-20m of sand- and siltbeds locally with browncoalseams. The completion of this cycle is seam

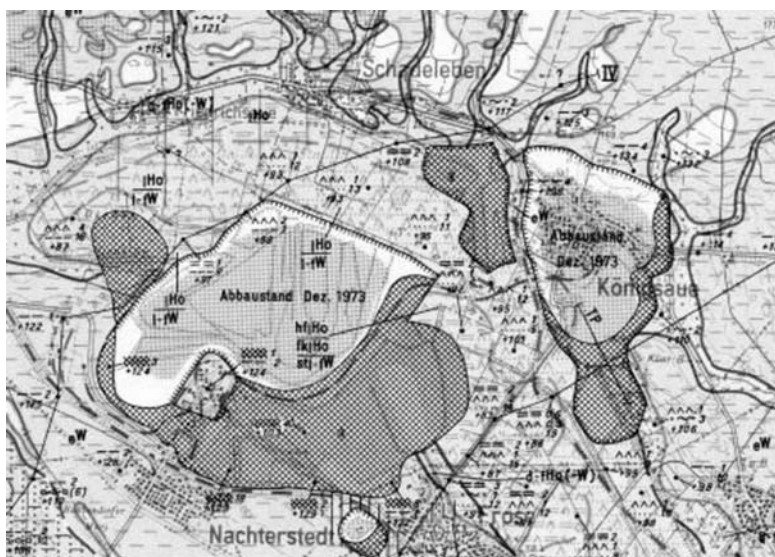


Fig. 3: Geological map 1:50.000 of Nachterstedt area, sheet 2363 Quedlinburg, horizon card IE Ho, editorship conclusion January 1975 (Karpe, 1975, 1986a, 1986b).

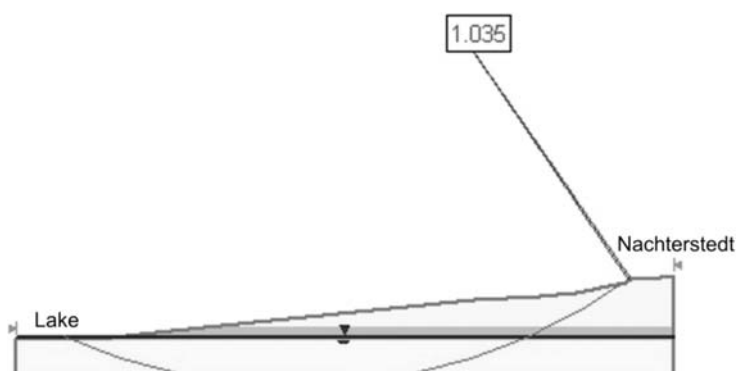


Fig. 4: The damaged area together with a schematic slope stability analysis, showing the limited stability conditions of the area in rain conditions.

Nr. I, also called Lower seem. On top follow about 30m of silts and sands with two further coal horizons, the so called seem II and seem III, respectively middle and upper seem. . The final part of the middle Eocene is characterised by several meters thick, transgressive coarse sand. The so called Latdorf-Formation of the Upper Eocene then starts with few meters of glauconitic fine sands (Lehmann, 1933, Knochenhauer, 1950, Waltemate, 1956, Seichter, 1958).

The entire sequence of Nachterstedt was marked by climate changes and fluctuations in sea level and modified by the local halocinetic development of underlying salt structures. In particular, the halocinetic lowering of the marginal basins had an influence on the geometry of the coalbeds: While the areas far from the Ascherslebener saddle had already been flooded, the areas more near to the central saddle structure came into lofty positions and so into the influ-

ence of groundwater. This allowed an ongoing growth of the different swamps during the embankment of marine sediments in the areas of the adjacent coasts and seas.

3. The landside

The area, in study, covers the Northern coastal part of Nachterstedt City, in the eastern part of Germany, located to North-East of Harz, between the cities of Aschersleben and Quedlingburg. An artificial lake was created, in 1994, at the open pit of a coal mine, which stopped to be exploited in 1991. In the geological map, 1:25000, of 1926, the displacement of the railway line, to the south, out of the coal outcrop, is referred (Petley, 2009). The southern coast of this lake is unstable because of the change of the water level, during the time (Eberhardt, 1969, Karpe, 1986a, 1986b, Blumenstengel & Unger, 1993, Blumenstengel & Volland, 1995, Blumenstengel et al., 1996).

According to the geological map, 1:50.000 of Fig. 3, the area, where the sliding occurred, above the coal layer, consists, of a) 1 m man made deposits, b) 2m, gW: löss, c) 11m, ρ SI medium to coarse grained sand, d) 3m, ρ H: gravel and sand, e) 6 m, ρ EV: medium to coarse grained sand, f) 2 m, ρ EV sand g) 4 m, ρ EV: medium to coarse grained sand, f) 3 m, ρ EV: fine to medium sand.

The landside refers to a subsidence of approximately one million cubic meters (1.31 million cy) of soil. There were no reports of cracking or settlement of soils in the vicinity prior to the failure. Nevertheless, a quick slope stability calculation, for rain conditions, showed a limited safety factor which easily could explain the occurrence of that sliding, which wasn't the first during the last 50 years. The landslide wasn't, probably, due to the presence of the old mine, itself, but its presence probably contributed to the activation of the sliding. The sliding caused a massive wake on the Concordia Lake, which flooded the surrounding shores and flushed boats onto the banks. As it was mentioned previously, the lake is a result of brown coal surface mining operations and was generated in 1991. Currently, Concordia Lake covers approximately 350 Hectares (865 acres) and is up to 30 meters (100 ft) deep.

According to the analysis of Fig. 4, the slope had a limited stability, of SF=1.035, which negatively changed after a very strong rainfall. The damage was very important and for this reason a further investigation is needed, for determining the stability frame, which doesn't only depends on the rain but also on the existence of underground openings which remained after coal exploitation and influence on the stability of the coastal zone of the living area of the village.

4. Conclusion

The living area of Nachterstedt is located over a coal mine, which is not active any more but important underground opening decrease the stability of the ground at the surface.

The stability analysis gave a safety factor 1, which very easily can be changed, under specific weather conditions. The recent landslide is the result of this limited stability conditions of the area.

The last landslide showed that a completed ground stability investigation is necessary to be performed, at the coastal zone, for avoiding any further sliding, in the future.

5. References

Ahrendt, H., Köthe, A., Lietzow, A., Martheine, D. & Ritzkowski, S. (1995): Lithostratigraphie, Biostratigraphie und radiometrische Datierung des Unter-Eozäns von Helmstedt (SE-Nieder-

- sachsen). Z. dt. geol. Ges., 146 (H2): S. 450-457; Hannover
- Balaska, P. (1992): Nachweis mariner und marin beeinflusster Sedimente in den Zwischenmittel der eozänen Braunkohlen bei Aschersleben in der östlichen subherzynen Senke. Zbl. Geol. Paläont., Teil I, 12: 2953-2962; Stuttgart
- Balaska, P. 1998. Die marin beeinflussten Sande im Tertiär von Nachterstedt-Schadeleben in der östlichen Subherzynen Senke – Sedimentologie, Fazies und stratigraphische Bewertung; 58p. (*unpublished. Dis., Durham Univ*)
- Blumenstengel, H. & Unger, K.-P. (1993): Zur Stratigraphie des flözführenden Tertiärs der Egelner Mulden. (Sachsen-Anhalt) Geol. Jb., A 142.: 113-129; Hannover
- Blumenstengel, H. & Volland, L. (1995): Geologische Abschlußdokumentation stillgelegter Braunkohlentagebaue am Beispiel des Referenzprofils im Tagebau Merseburg-Ost. Mitt. Geol. LA Sachsen-Anhalt, 1: 55-67; Halle
- Blumenstengel, H., Krutzsch, W., Volland, L. (1996): Revidierte Stratigraphie tertiärer Ablagerungen im südlichen Sachsen-Anhalt, Teil 1: Raum Halle-Merseburg. Hall. Jb. f. Geowiss., Reihe B, Beih. 1:
- Eberhardt, F. (1969): Geologischer Bau und Erdgasführung des Subherzynen Beckens. □unveröff. Diss. BA Freiberg: 161 S.; Freiberg.
- <http://earth.google.com/download-earth.html/> : Nachterstedt City, in Google Earth. 2009.
- Karpe, W. (1986a): Teilerkundung der Lagerstätte Nachterstedt, TF Schadeleben. unveröff. Bericht: 216 S.; BKW -Nachterstedt [MIBRAG-Archiv]
- Karpe, W. (1986b): Die Beziehungen zwischen der Versalzung von Braunkohle und den prätertiären Strukturen im Raum Nachterstedt, Subherzyne Senke. Z. angew. Geol. 32 (3): 70-73; Berlin.
- Karpe, W. (1975): Geologische Karte des Ascherslebener Sattels (Maßstab 1 : 50. 000). unveröffentlichte Karte, Manuskript; Halle [Archiv GLA LSA]
- Knochenhauer, G. (1950) : Das Braunkohlenvorkommen von Nachterstedt in seiner geologischen Lage nach den neusten Aufschlüssen. unveröff. Meldearbeit Bergakademie Freiberg: 86. S., Freiberg
- Lehman, R. (1933): Die Braunkohlenlagerstätte von Nachterstedt. In: Franke, P. [Hrsg.]:
- Petley, D. 2009. Intriguing landslide at Nachterstedt in Germany, in *Dave's landslide block*: <http://daveslandslideblog.blogspot.com/>
- Seichter, A. (1958): Feinstratigraphische Untersuchungen mittels Sporen- und Pollenanalysen an Braunkohlen aus Nachterstedt und Königsau unter Berücksichtigung der Anwendungsmöglichkeiten von Remissionsmessungen. unveröff. Diss. BA Freiberg: 108 S.; Freiberg.
- Voigt, E. (1963): Über Randtröge vor Schollenrändern und ihre Bedeutung im Gebiet der Mitteleuropäischen Senke und angrenzender Gebiete. Z. dt. geol. Ges., 114 (1962): 378–418, Hannover
- von der HOCHT, F. (1992) : Bestimmung der Evertebraten aus dem Unteroligozän von Nachterstedt. unveröff. Bericht: 4 S.; Kerpen-Balkhausen [Archiv GLA LSA]
- Waltemate, G. (1956): Feinstratigraphische Untersuchungen der Braunkohle in den Tagebauen Nachterstedt und Königsau. unveröff. Diplomarbeit. MLU Halle: 84 S.; Halle
- Woldstedt, P. (1926): Zur Tektonik des subherzynen Beckens. Z. dt. geol. Ges., 76: 183 – 201; Berlin.

TUNNELING IN OPHIOLITHIC SERIES FORMATIONS: TUNNELS OF THE NEW HIGH-SPEED RAILWAY DOUBLE TRACK LINE - SECTION LIANOKLADI - DOMOKOS

Mourtzas N.¹ and Gkiolas A.²

¹ Geologist PhD, Gaiaergon Geotechnical Firm., Kefallinias 16-18, 15231 Athens, Greece, gaiaergon@gmail.com

² Civil Engineer, PhD, Geomechaniki S.A, Ethnikis Antistaseos 91, 15351 Pallini, Greece geomsot@gmail.com.

Abstract

For the project “3rd phase of design of the new high speed double track line - section Lianokladi – Domokos (subsection: Ch. 0+000 - Ch. 13+500)” geological and geotechnical investigations and designs were implemented for tunnels and cut & cover of the subsection Ch. 9+685 - Ch. 12+254. The above subsection, a significant part of which is already constructed, includes three tunnels (SS1, SS2 and SS4) and one Cut & Cover (SS3). Tunnels SS1, SS2 and SS4 are of lengths 860m, 477m and 495m, with overburden 58m, 50m and 60m respectively and are driven in mountainous area consisting of ophiolitic series formations, mainly massive basalts with varying fragmentation, dolerites, spilitic intrusions and serpentinites. The above formations are characterised by variable fragmentation, weathering and degree of alteration. At places metamorphic basalt (amphibolite) is also encountered. Schist-chert intrusions and ophiolitic material with intense schistification, are considered of tectonic origin and are connected with the major and secondary compressive fault zone in the area. Limestone blocks inside the ophiolitic mass are also considered of tectonic origin. The narrow area of the alignment is characterized by the presence of normal and transverse faults, along with major joints crossing the rockmass. The formations along the tunnels, according to their engineering – geological behaviour, were separated to seven geotechnical units. Representative values for the geotechnical parameters of each unit were determined and analyses for the corresponding primary support categories were performed, using code UNWEDGE (RocScience) for rock-classes where behaviour of underground excavation is determined mainly due to orientation of joints and using code PHASE² version 6.011 (RocScience) for formations where behaviour of underground excavation is determined mainly by their strength and deformability.

Key words: ophiolites, compressive fault zone, high speed double track line, tunnel, Central Greece.

1. Introduction – Project Description – Tunnel Excavation Geometry

For the project “3rd phase of design of the new high speed double track line - section Lianokladi – Domokos (subsection: Ch. 0+000 - Ch. 13+500)” geological and geotechnical investigations and designs were implemented for tunnels and cut & cover of the subsection Ch. 9+685 - Ch. 12+254. The above subsection, a significant part of which is already constructed, includes three tunnels SS1, SS2 and SS4 (Fig. 1).

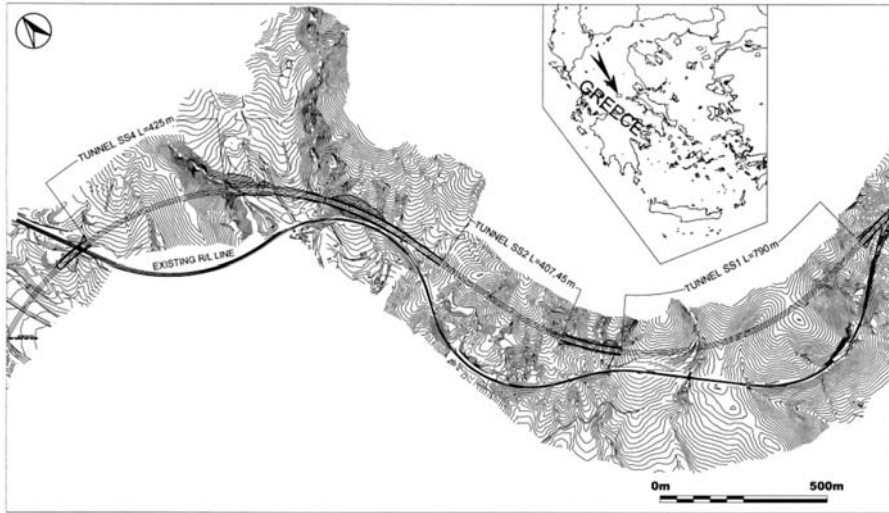


Fig. 1: Location map of the project area.

Tunnel SS1 is of length 860m, with maximum overburden of 58m. The alignment passes with a high radius curve. The tunnel axis trend is E-SE to W-NW, with a longitudinal slope of 2%. Tunnel SS2 is of length 477m, with maximum overburden of 50m. The alignment passes with a high radius curve. The tunnel axis trend is NW to SE, with a longitudinal slope of 1.84%. Tunnel SS4 is of length 495m, with maximum overburden of 60m. The alignment passes with a high radius curve. The tunnel axis trend is E-SE to W-NW, with a longitudinal slope of 1.84%

Geometry of the tunnels is horseshoe shaped and excavation takes place in two phases: upper and lower bench. In adverse ground conditions, upper bench (temporary) and lower bench inverters are also constructed. The excavated section width is of approximately 14m.

2. Geological setting

The project area extends on the southern margin of the Othrys Mountain chain where the geological structure is characterized by a series of nappes, placed on top the Pelagonic platform during Upper Jurassic – Lower Cretaceous (Hynes 1974).

The higher nappe includes typical ophiolitic rocks (peridotites, gabbros, dolerites, pillow lavas), while the lower one is constituted by Volcano-Sedimentary formations. On top of the nappes an Upper Cretaceous transgression cover has been deposited (Smith et al., 1975), while the whole sequence is found overthrust along a westward-direction over flysch of the Upper Cretaceous – Tertiary (Faulp et al., 1996).

The geological structure of the broader area includes three tectonic nappes which constitute the rocks of the substratum and of which the lower one includes the schist-chert formation, the following includes basalts (dolerites) and the higher one peridotites. The overthrust front of the peridotitic nappe is found inside the strict area of the project.

The intense topographic relief at the tunnels area is shaped on rocks of the Ophiolitic Sequence, mainly by basalts, dolerites, spilitic intrusions and serpentinites. These formations are characterized

by varying degrees of fragmentation, weathering and alteration.

The schist-chert intercalations and the schistified ophiolitic material are considered to be of tectonic origin and they are linked mainly to the primary and secondary tangential compressional structures of the area and to fault tectonics.

Extended limestone bodies which are locally found inside the ophiolitic masses are also considered of tectonic origin. This complex lithologic and tectonic structure of the area was mapped in detail on a 1:200 scale at the extended in length, high slopes of the existing railroad track, which stretch 20m to 300m downhill the new railroad axis.

In particular, the tunnels are expected to be drilled through:

Basalts (Dolerites), medium-grained, greenish-grey to grey, comprised mainly by pyroxenes and plagioclasts on a semi-crystalline porphyritic texture, with a varying degree of fragmentation and locally intense alterations, while inside the formation pillow lavas locally occur.

Altered Spilites: with compact fabric, characteristic intermediate texture and spherulites, intruded inside the original serpentinite rock, which in turn is fragmented and locally re-cemented mainly with clay minerals, serpentine and feldspars and secondary with quartz, chlorite and calcite.

The formation is found intensely altered, with abundance of calcite, part of which came from the alteration of plagioclasts while another is found in veinlets. The distribution of the calcite inside the rock is anisomeric. The main minerals of this occurrence are calcite, quartz and plagioclast, while secondary minerals are chlorite and iron oxides.

Limestone: with granular texture and compact fabric. The main mineral is calcite and the secondary ones are chlorite, quartz and iron oxides.

Spilite: with intermediate texture and compact fabric. It is lava of spilitic constitution, which seems to cross through and locally enclave the serpentinite. Calcite observed in veinlets and amygdules.

The rock is crossed by quartz microveins (stockwork) of heterogeneous origin, whose percentage of participation varies locally within the rock mass. The main minerals of the rock are feldspars, chlorite, serpentine and calcite, while the secondary minerals are quartz and clay minerals.

Serpentinite: with symplectic texture and compact fabric, main minerals are serpentine, talc, chlorite and plagioclasts and secondary minerals calcite and iron oxides.

The **foliaceous** friable formations are distinguished in

Schists-cherts with intensely **foliaceous to shaly** structure, brown to purple.

Cleaved, breccious and altered ophiolitic material: with breccias, fragments and bodies of ophiolites and limestones in its mass, intensely folded and locally with chaotic structure.

In boreholes it appears in the form of silty-clayey gravels, of ophiolitic origin, with sand or intensely fractured cherts in the form of pebbles of 0.05x0.04x0.03m size. Locally chert layers, of 2m maximum thickness, intervene, intensely to very intensely fractured.

Altered ophiolitic materials: in the form of coherent calc-clay material; whitish to yellowish.

Intensely weathered and loosened surface zones of the rocky substratum. It involves sandy clays to clayey sands, brown to brownish-grey, which include fragments and breccias of ophiolites. In boreholes they appear in the form of ophiolite fragments and pebbles, of 0.02x0.01m to 0.05x0.3m

sizes, with locally occurring sandy clays.

The strict area of the axis is characterized by small to medium scale up-thrusting events, normal and reverse structures, as well as by major joints crossing the rock-mass.

3. Groundwater regime

The bedrock in the area is considered as permeable formation especially when it is intensely fragmented, fractured or intensely fractured. On the other hand schistified, friable formations are considered as impermeable formations and only in zones of intense shearing may develop a weak water table.

For tunnel SS1, based on the water level measurements from boreholes, in the initial region of the tunnel (Ch. 9+685 ÷ Ch. 9+753) the groundwater level is expected between 6.5m to 14m above the tunnel redline, in the region from Ch. 9+753 to Ch. 10+040, between 14m to 31m above the tunnel redline, in the region from Ch. 10+040 to Ch. 10+227 between 3m to 14m, in the region from Ch. 10+227 to Ch. 10+433 between 1m to 1,5m and in the final region of the tunnel from Ch. Ch. 10+433 to Ch. 10+475, groundwater level is expected below the level of the tunnel.

For tunnel SS2, based on the water level measurements from boreholes in the initial region of the tunnel (Ch. 10+681 to Ch. 10+735), the groundwater level is expected between 1m to 9,5m above the tunnel redline. In the region of the tunnel from Ch. 10+735 to Ch. 11+055 groundwater level is expected between 10m to 23m above the tunnel redline and in the final region of the tunnel from Ch. 11+055 to Ch. 11+089 between 5m to 11m above the tunnel redline.

For tunnel SS4, based on the water level measurements from boreholes in the initial region of the tunnel (Ch. 11+800 to Ch. 11+976) the groundwater level is expected between 18m to 24m above the tunnel redline, in the region of the tunnel from Ch. 11+976 to Ch. 12+022 at 24m and in the final region of the tunnel from Ch. 12+022 to Ch. 12+225 between 11m and 23m.

4. Geotechnical Units

The formations along the tunnels, according to their engineering – geological behavior, were separated to seven geotechnical units, as follows:

Geotechnical Unit TE-1: This unit includes massive to slightly fragmented ophiolites, of low strength, with RQD greater than 60%, rock mass rating (RMR) between 45 and 65 (category II to III according to Bieniawski 1989) and estimated GSI ranging between 45 and 55 (according to Hoek-Brown, 2002)

Geotechnical Unit TE-2: This unit includes intensely fragmented ophiolites, of low strength, with RQD between 30% and 60%, rock mass rating (RMR) between 35 and 45 (category III to IV according to Bieniawski 1989) and estimated GSI ranging between 35 and 45.

Geotechnical Unit TE-3: This unit includes intensely fragmented to fractured ophiolites, of low strength, with RQD between 0% and 30%, rock mass rating (RMR) between 10 and 35 (category IV to V according to Bieniawski 1989) and estimated GSI ranging between 25 and 35.

Geotechnical Unit TE-4: This unit includes intensely fractured ophiolites, in the form of gravel and cobbles with sizes from 0.03x0.01m to 0.07x0.05m and rock mass rating (RMR) less than 10%. Estimated GSI ranging between 20 and 25.

Geotechnical Unit TE-5: This unit includes schistified, heavily broken and altered ophiolitic material with angular and rounded rock pieces of ophiolites and limestone, intensely folded, with a chaotic structure at places and brown to crimson almost soil-like material of the schist-chert formation with intense schistification, in 0.05m to 0.02m thick layers. In borehole samples, the above material appears in the form of silty-clayey gravel of ophiolitic origin, with sand, or intensely fragmented chert, in the form of gravel and cobbles with approx. size of 0.05x0.04x0.03m. At places intensely fragmented to heavily broken chert interlayers of up to 2m thickness, are encountered. Estimated GSI ranging between 15 and 20.

Geotechnical Unit TE-6: This unit includes altered, mylonitized material, associated with zones of tectonic deformation. It appears in the form of sub-white to sub-yellow sand, with low cohesion. Estimated GSI ranging between 15 and 20

Geotechnical Unit TE-7: This unit includes limestone blocks, of intermediate strength, intensely folded and fractured and up to at places intensely fractured. Estimated GSI ranging between 35 and 40. The Geotechnical unit TE-7 is merely encountered in tunnel SS1.

5. Geological- Geotechnical conditions along tunnels

The ophiolitic mass along tunnel SS1 is separated in six regions, in tunnel SS2 in four regions and in tunnel SS4 in three regions. In the area of tunnel SS1, a total of eight continuous sampling boreholes have been executed, five in the area of tunnel SS2 and four in the area of tunnel SS4. The Geological- Geotechnical long section of tunnel SS1 is presented in Figure 2, of tunnel SS2 in Figure 3 and of tunnel SS4 in Figure 4.

Tunneling conditions along tunnels area extremely variable, ranging from favorable to adverse. The estimated percentages of Geotechnical units for the three tunnels are presented in table 1:

Table 1 Estimated percentages of Geotechnical units for the tunnels

Tunnel	Region		Geotechnical Units Percentages (%)						
	Start Ch.	End Ch.	TE-1	TE-2	TE-3	TE-4	TE-5	TE-6	TE-7
SS1	9+685	9+753	32%	35	25%	3%	4%	1%	-
	9+753	10+040	-	-	25%	8%	64%	2%	1%
	10+040	10+227	-	22%	35%	7%	5%	-	31%
	10+227	10+251	-	5%	10%	12%	72%	-	1%
	10+251	10+433	-	1%	2%	6%	55%	28%	8%
	10+433	10+457	24%	26%	36%	7%	7%	-	-
SS2	10+681	10+735	1%	-	4%	70%	25%	-	-
	10+735	10+922	27%	15%	28%	26%	-	4%	-
	10+922	11+062	19%	30%	42%	3%	6%	-	-
	11+062	11+089	-	5%	-	35%	60%	-	-
SS4	11+800	11+976	50%	10%	37%	-	2%	1	-
	11+976	12+022	-	-	20%	25%	55%	-	-
	12+022	12+225	18%	35%	36%	5%	1%	5%	-

6. Rockmass classes. Association with Geotechnical units

Based on the available geological and geotechnical data and the expected behavior of the rockmass during excavation the following five rockmass classes were implemented

Rockmass class A – Massive to slightly fragmented rockmass. Rockmass class A includes massive to slightly fragmented ophiolites (TE-1) and limestone blocks, of intermediate strength, intensely folded and fractured and up to at places intensely fractured (TE-7). Stable behavior during excavation. No systematic relaxation of rock blocks and depending on the geometry of the discontinuities, possible formation of wedges. Systematic support against wedges is required. No practical impact of underground water in rockmass strength. Excavation with explosives. Representative GSI values:

TE-1: GSI = 45 – 55 & TE-7: GSI = 35 – 45

Rockmass class B1 - Intensely fragmented rockmass: Rockmass class B1 includes intensely fragmented ophiolites, of low strength (TE-2). Relaxation of rock blocks and formation of wedges. Systematic support against wedges is required. Small impact of underground water in rockmass strength. Excavation with explosives. Representative GSI values:

TE-2: GSI = 35 - 45

Rockmass class B2 - Intensely fragmented to fractured rockmass: Rockmass class B2 includes intensely fragmented to fractured ophiolites, of low strength. Increased risk of failure without installation of immediate support measures. Medium impact of underground water in rockmass strength. Excavation with mechanical means. Representative GSI values:

TE-3: GSI = 25 – 35

Rockmass class C1 - Intensely fractured rockmass: Rockmass class C1 includes intensely fractured ophiolites, in the form of gravel and cobbles (TE-4). Systematically and intensely tectonised and sheared rockmass, of very low strength and intense weathering. At places soil-like material with possibility of appearance of rock boulders. Immediate deformation. Development of failure zones of reduced thickness in the sidewalls. High impact of underground water in rockmass strength. Excavation with mechanical means. Representative GSI values:

TE-4: GSI = 20 – 25

Rockmass class C2 - Schistified, friable formations: Rockmass class C2 includes schistified, heavily broken and altered ophiolitic material with angular and rounded rock pieces of ophiolites and limestone, intensely folded, with a chaotic structure and soil-like material of the schist-chert formation with intense schistification, (TE-5) altered, mylonitized material, associated with zones of tectonic deformation appearing in the form of sand with low cohesion (TE-6). Systematically and intensely tectonised and sheared rockmass, of very low strength and very intense weathering. Soil-like material with possibility of appearance of rock boulders. Immediate deformation. Development of failure zones of reduced thickness in the sidewalls. High impact of underground water in the rockmass strength. Excavation with mechanical means. Representative GSI values:

TE-5, TE-6: GSI = 15 - 20

For the above rockmass classes representative values of geotechnical parameters were estimated by means of Hoek-Brown criterion (2002), and are presented in table 2.

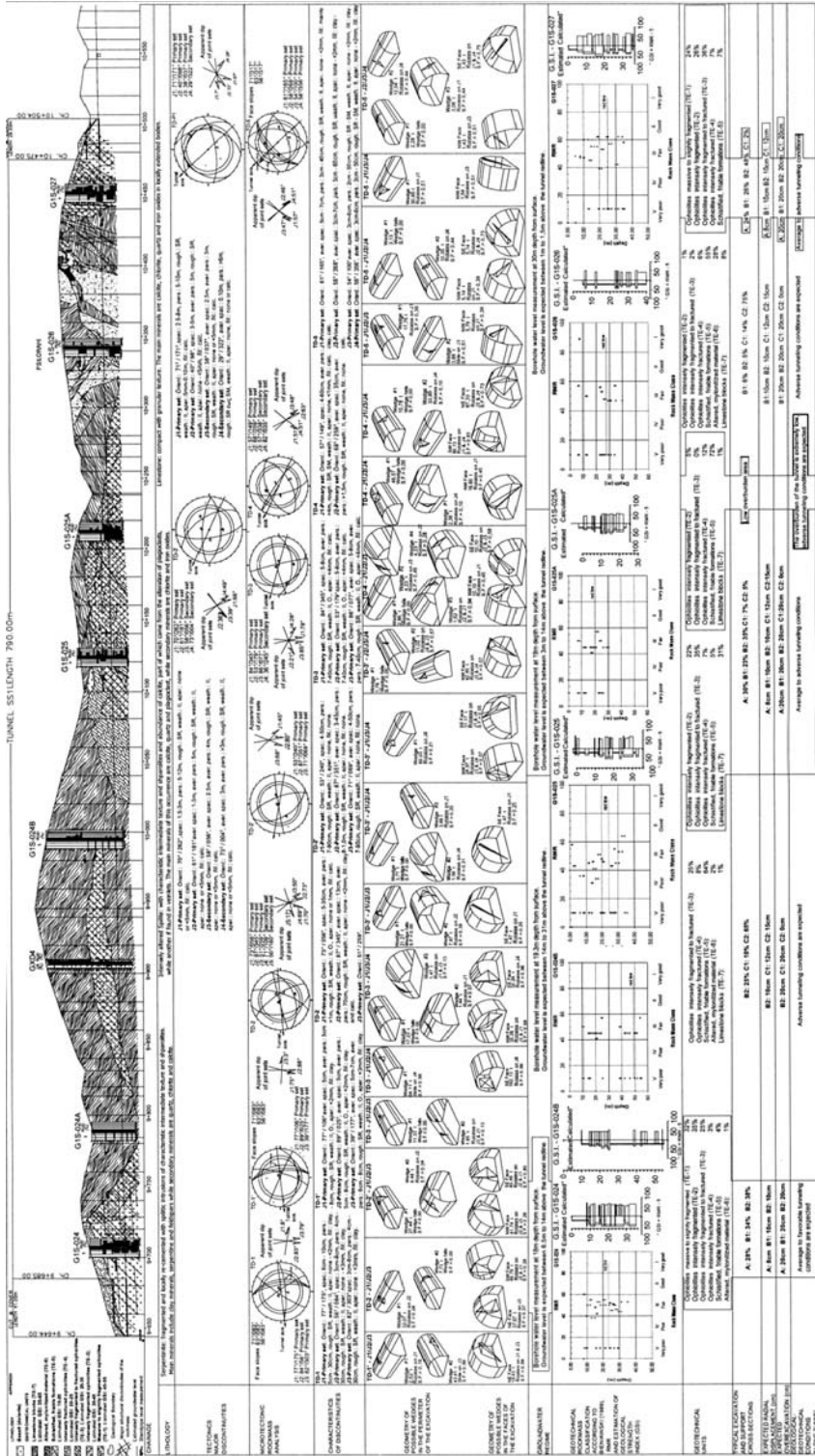


Fig. 2: Geological – Geotechnical longitudinal section of SS1 tunnel

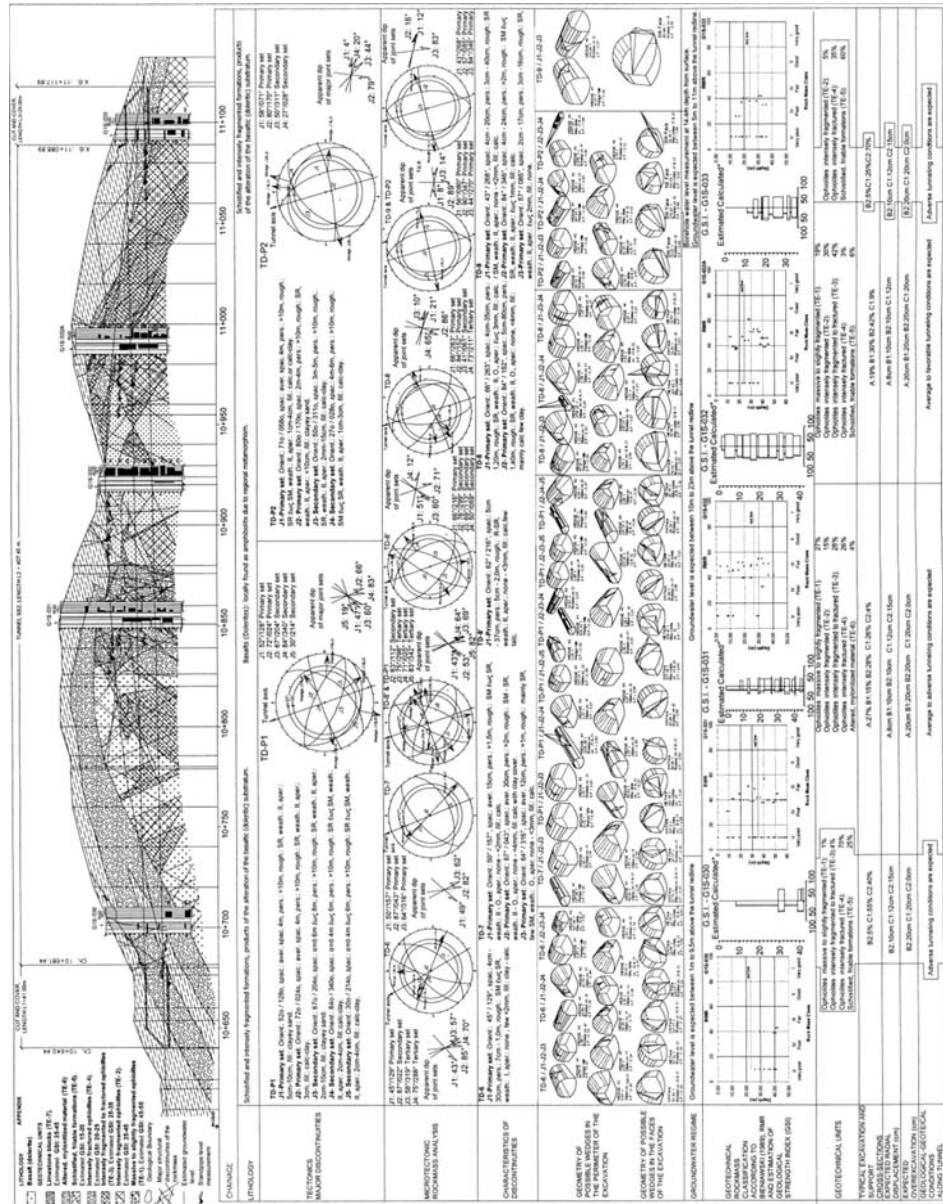


Fig. 3: Geological – Geotechnical longitudinal section of SS2 tunnel

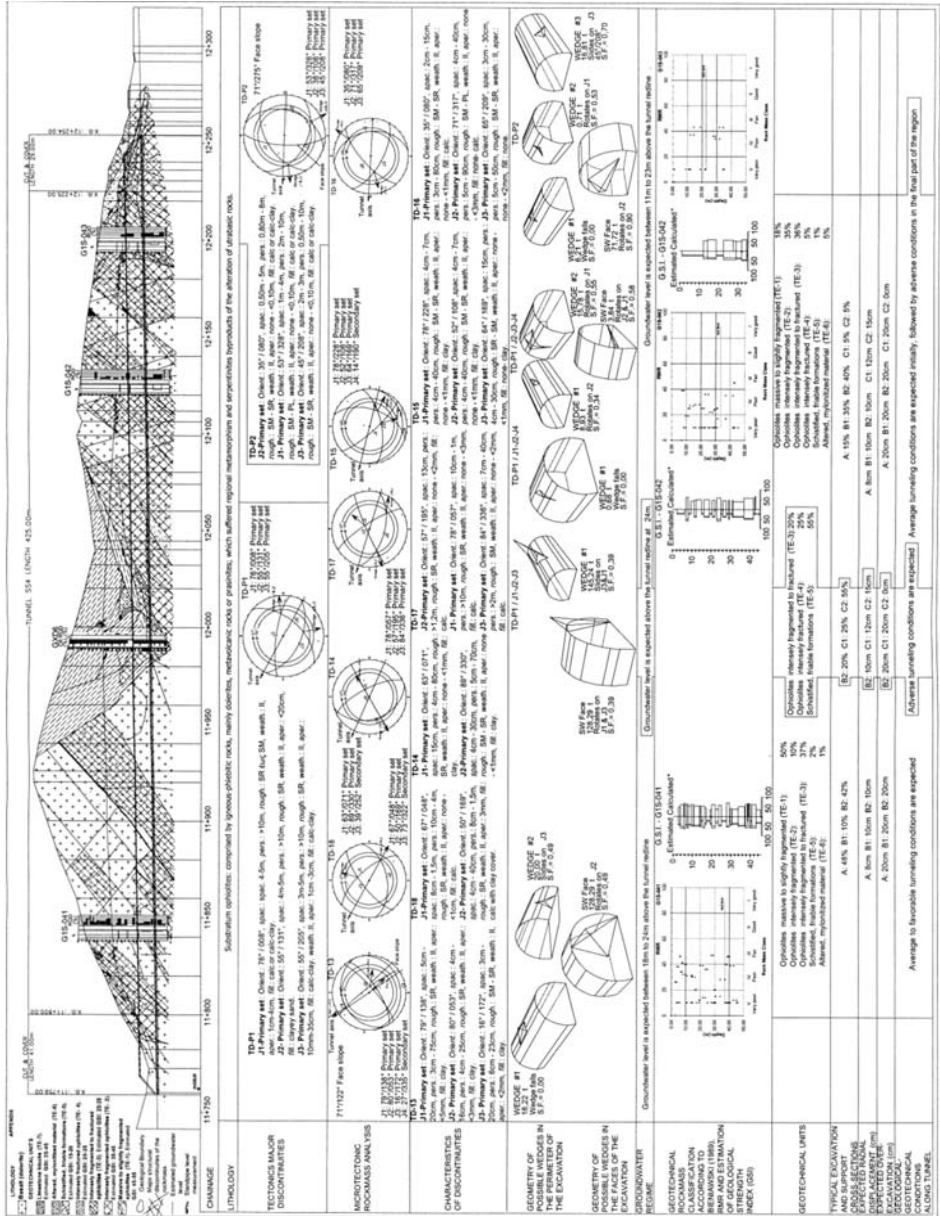


Fig. 4: Geotechnical longitudinal section of SS4 tunnel

Table 2. Geotechnical design parameters

Rockmass class	Geotechnical unit	GSI	GSI (design)	σ_{ci} (MPa)	m_i	Overburden up to H (m)	γ (kN/m ³)
A	TE-1	45-55	45	20	25	48~60	28
	TE-7	35-45	35	40	10	48~60	27
B1	TE-2	35-45	35	15	20	48~60	26
B2	TE-3	25-35	25	12	20	48~60	26
C1	TE-4	20-25	20	7	15	48~60	22
C2	TE-5, TE-6	15-20	15	5	15	48~60	22

Table 3. Typical excavation and support cross-sections – Association with rockmass classes and geotechnical units

Rockmass class	Geotechnical unit	Typical excavation and support cross-sections
A	TE-1, TE-7	A
B1	TE-2	B1
B2	TE-3	B2
C1	TE-4	C1
C2	TE-5, TE-6	C2

Based on the above design parameters, analyses for the dimensioning of the typical excavation and support cross-sections were performed.

7. Typical excavation and support cross-sections

For the five rockmass classes, five corresponding typical excavation and support cross-sections were implemented for the tunnels. The typical excavation and support cross-sections are presented in figures 5 and 6.

Their association with rockmass classes and geotechnical units is presented in table 3.

The predominant factor affecting the behavior of the underground excavation for rockmass class A, is the orientation of intersecting structural discontinuities and on the other hand for rockmass classes C1 and C2 is the structural behavior of the rockmass for the expected range of values of in-situ stress, rockmass strength and deformability parameters. For rockmass classes B1 and B2, both factors are important.

For rockmass classes B1, B2, C1, C2, finite element stress analyses were performed for the developed excavation and support models. For the calculation of induced stress on the immediate support elements and for the estimation of tunnel wall convergence and thickness of yield zone in the rockmass, computer code PHASE² ver 6.011 (developed by RocScience) was used.

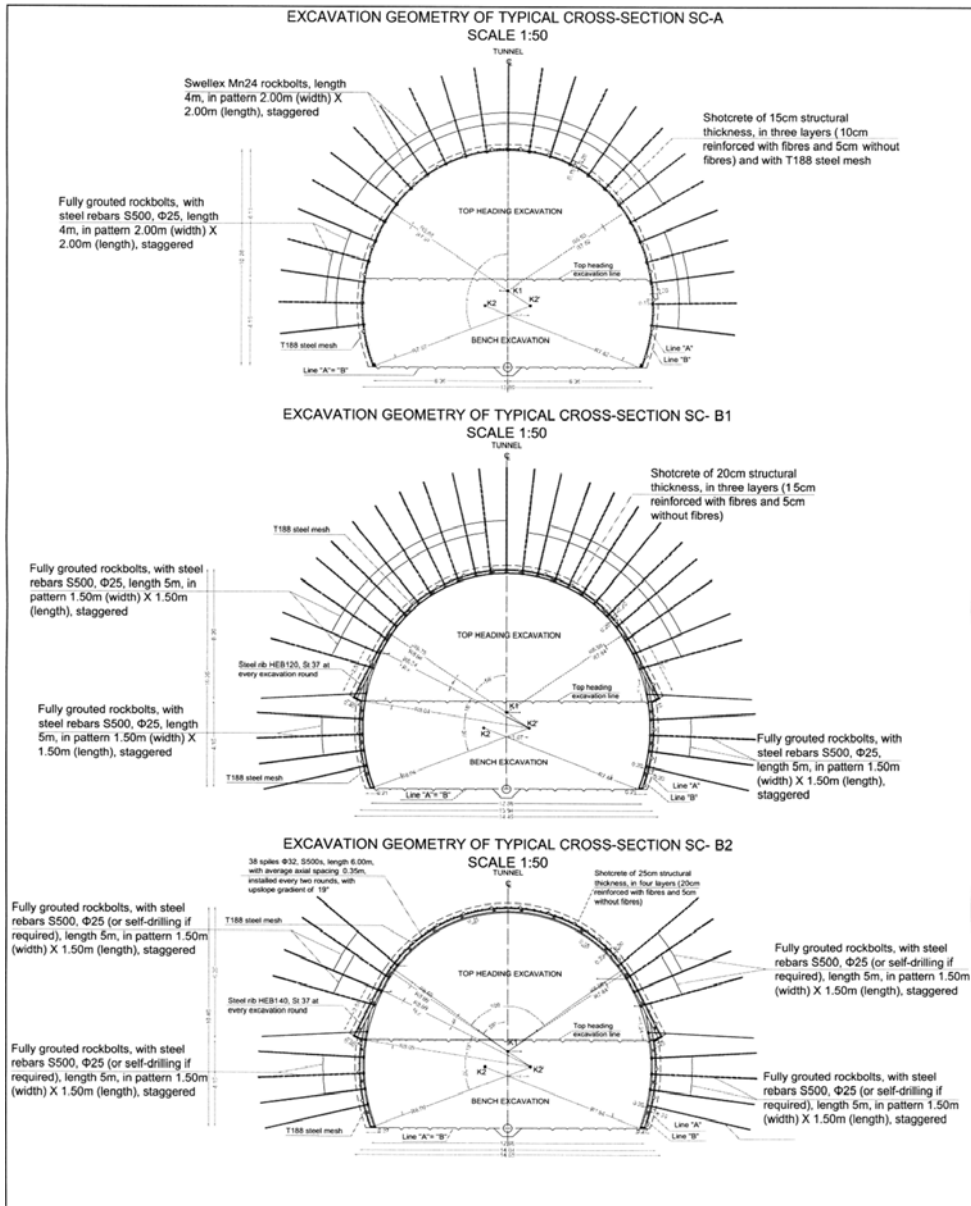


Fig. 5: Typical cross-section SC-A, SC-B1 and SC-B2

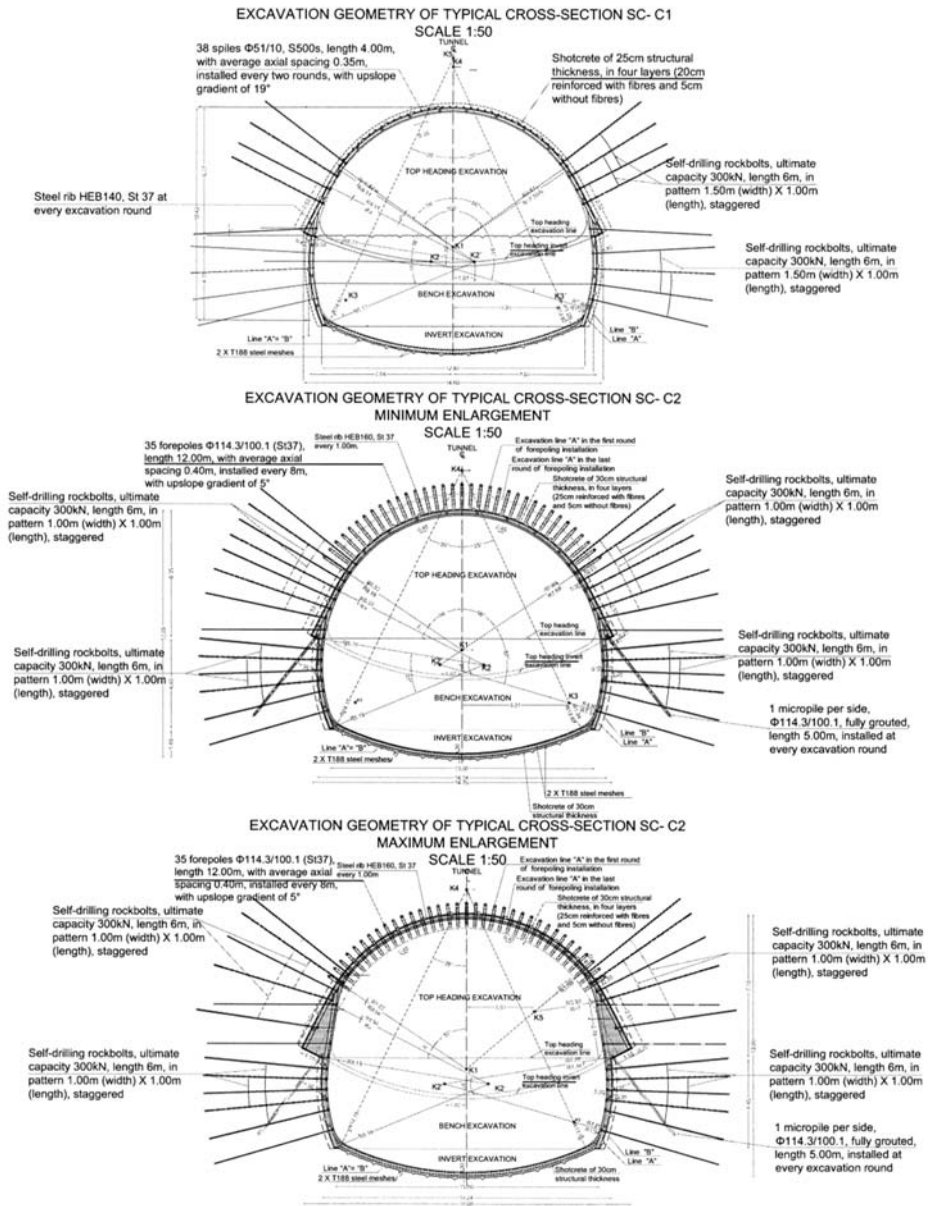


Fig. 6: Typical cross-section SC-C1 and SC-C2

Table 4. Support measures of typical excavation and support cross-sections

Typical excavation and support cross-sections	A	B1	B2	C1	C2
Shotcrete (thickness in cm)	15 cm	20 cm	25 cm	25 cm	30 cm
Rockbolts (type – length in m)	Swellex MN24 - Ø25/S500 (L=4m)	Ø25/S500 (L=5m)	Ø25/S500 or Self-drilling (L=5m)	Self-drilling (L=6m)	Self-drilling (L=6m)
Steel rib	No	HEB 120	HEB 140	HEB 140	HEB 160
Elephant foot (thickness in cm)	No	40 cm	40 cm	40 cm	40 έως 115 cm
Face Shotcrete (thickness in cm)	No	No	0-5cm	5cm	5cm/10cm
Face core	No	No	No	No	Yes
Face dowels Fiberglass (pieces)	No	No	0-9	9	16
Spiles or forepoles	No	No	Spiles (38 steel bars Ø32-St37)	Spiles (38 steel tubes Φ51/10-St37)	forepoles (35 steel tubes Φ114/100-St37)
Temporary (top-heading) invert	No	No	No	Yes	Yes
Final invert	No	No	No	Yes	Yes

The results of the above analyses were used for the assessment of the adequacy of the immediate support measures of each one of the five typical excavation and support cross-sections. The support measures of each one of the five typical excavation and support cross-sections are presented in Table 4.

Based on the results of the elasto-plastic, finite element stress analyses of the excavation and support models, for the examined combinations of typical excavation and support cross-sections, rockmass classes and overburden, the following conclusions were drawn

- The magnitude of expected convergence, as calculated for each one of the excavation stages, is limited for most cases within generally accepted levels. In particular for typical excavation and support cross-sections A, B1 and B2, the estimated axial deformation is in the order of 1 to 2.5cm, for C1 in the order of 4 to 5cm and for C2 in the order of 4.5 to 6.5cm
- The thickness of yield zone in the rockmass is relatively small (in the order of 1 to 3.5m) for typical excavation and support cross-sections A, B1 and B2 and intermediate to high (in the order of 4 to 41m) for typical excavation and support cross-sections C1 and C2.

- Induced stresses in shotcrete are generally lower than its capacity, with rare exceptions, mainly at the joining area of top heading and temporary invert and the joining area of bench and final invert. Furthermore the percentage of yielded liner elements (used to model shotcrete) does not exceed 2%.
- The induced forces on rockbolts installed at the perimeter of the excavation, are generally lower than the rockbolts' capacities. However, in some rare cases, the capacities of rockbolts are exceeded, but this does not affect the total stability of the underground excavation.

8. Conclusions

The heterogeneity of the ophiolites in the area is expressed by variable behaviour of the rockmass, from competent rock to very weak soil-like material, which in turn is responsible for the rapidly changing tunnelling conditions even in short distances. Furthermore, the groundwater level also varies significantly, from below the redline, up to 31m above it.

In order to cope with such rapidly changing tunnelling conditions, appropriate rockmass classes and corresponding support classes were adopted. The support classes utilise support measures ranging from light, for relatively good rockmass classes (e.g. A), to very heavy, for very poor rockmass classes (e.g. C1 and C2).

Finally, a relatively accurate estimation of the percentages of the Geotechnical units along the tunnels, as the one presented above, is of crucial importance for a successful tunnelling operation.

9. References

- Bieniawski, Z.T. 1989. Engineering rock mass classifications. New York: Wiley.
- Faulp P., Pavlopoulos A., Wagneich M. and Migiros G. 1996. Pre-Tertiary blueschist terrains in the Hellenides: evidence from detrital mineral of flysch successions. *Terra Nova* 9, 186-190.
- Hoek, E., Carranza-Torres, C.T., and Corkum, B. 2002, Hoek-Brown failure criterion – 2002 edition. Proc. North American Rock Mechanics Society meeting in Toronto in July 2002
- Hynes A.J, 1974. Igneous activity at the birth of ocean basin in eastern Greece. *Canadian Journal of Earth Science* 11, 842-853.
- Smith A.G., Hynes A.J, Menzies M, Nisbet E.G., Price I., Welland M.J. and Ferriere J., 1975. The stratigraphy of the Orthis mountains, eastern central Greece: a deformed Mesozoic margin sequence. *Ecllogae.geol.Helv.*, 68/3, 463-481.

SLOPE STABILIZATION ON CHALKOUTSI – DILESI ROAD, AT PIGADAKIA LOCATION, ATTICA PREFECTURE

Mourtzas N. D.¹, Symeonidis K.², Passas N.³, Alkalais E.⁴, Kolaiti E.⁵

¹ *Geologist PhD, Gaiaergon Geotechnical Firm., Kefallinias 16-18, 15231 Athens, Greece, gaiaergon@gmail.com*

² *Geologist MSc, Gaiaergon Geotechnical Firm., Kefallinias 16-18, 15231 Athens, Greece, gaiaergon@gmail.com*

³ *Geologist PhD, Public Works Administration of the Prefecture of Attica*

^{4,5} *Geotechnical Engineer, Gaiaergon Geotechnical Firm., Kefallinias 16-18, 15231 Athens, Greece, gaiaergon@gmail.com*

Abstract

A series of ongoing landslides occurred at the steep coastal slopes at Pigadakia location, on the road connecting Chalkoutsi and Dilesi towns, at NE Attica. These landslides caused severe disruption on local traffic.

Engineering geological study revealed the local geological conditions and the complex mechanism of the landslides. Site is located on the Neogene deposits composed mainly by layers of sandy or silty clays, marly clays with thin layers of conglomerates. Multiple landslides occurred on the steep costal slopes at a length of 280m parallel to the coast line. On the upper slopes which are composed by loose clayey materials typical circular failures occurred while on the lower ones, composed by hard clays and marls, discontinuities delineate failures under the weathering influence of sea waves. Six boreholes were drilled with piezometers and inclinometers installed in order to investigate the progress of the failures. The stabilization of the upper slopes included the use of soil nails covered with geocells. The lower slopes stabilization included the protection from sea wave erosion by covering slopes with a rock fill embankment.

1. Introduction – Project description

This paper aims at the presentation of the consecutive slides that have been developed in the slopes of the road from Chalkoutsi to Dilesi at the location “Pigadakia”, causing the reduction of the active cross-section of road and in some cases the complete interruption of the traffic. An engineering geological approach of the problem is presented along with the results of the geotechnical investigation, an analysis of the mechanism of landslides and finally the two alternative solutions for the remedial measures needed. It is noted that the final geological design, the geotechnical investigation and the preliminary and final geotechnical design of slope stabilization measures, were carried out during the period from May 2005 to October 2008 under a contract assigned by the Directorate of Public Works of Attica Prefecture.

2. Morphological setting

The sheer coastal slope, along which the failures develop (Fig. 1), is the ending of the broader area's upstream hill morphology. This hill morphology has the form of an elongated ridge with gradually declining altitudes and it is directed from NE at Kamari with a peak altitude of +76.5 and terminates, at a peak of +29.9, in the area of the study.

The drainage system, on the west side of the ridge is incomplete with lengths limited below 100m, of 2nd stream order and with limited branching but with substantial in-depth erosion, while on the east side of the ridge a stream of 3rd order is developed on a NNE direction with a high branching coefficient, a total length of some 300m, low dipping along the stream and with substantial in-depth erosion.

The extended, under study, failures develop into a plugging cliff, about 280m length, which extend in a WNW direction, parallel to the coastline. The coastal slope, which is 38 m in height, to the upper part with altitude of +35 to +38 presents mild morphological slopes about 15%. To the part with altitude of +29 to +35, slopes are about 85%, whereas to the rest part dip becomes extremely steep, about 100%. At an average altitude of +18 to +20 the under study part of Halkoutsi – Dileisi road, about 7 m width, intervenes.

At the areas where the failures are occurred, steep decollement morphology appears in the upper disintegration parts. At the lower parts, where materials accumulate, exist milder and soil creep morphologies.

3. Geological setting

The geological substratum at the failures area is formed by the Neogene deposits of Halkoutsi-Dileisi (Mettos 1992, Koumantakis 1971) while the younger deposits include the eluvial cover, littoral deposits, landslide materials and slope erosion products.

The Neogene substratum consists of brown-red colored rotations of clay, sandy, marly and clayey clay (c-cl) beddings, with thin conglomerate and breccia (c.gr) intercalations (Fig.1, Fig.2 and Fig.3). The lower horizons at sea level seem hard and cohesive, while the upper horizons are semi-cohesive to loose with cohesive beddings insertions. The persistence of the discontinuities crossing the formation is greater than 3m, with planar, slightly rough surfaces, closed or with apertures up to 5mm, walls slightly weathered, void or with reddish clayey material and dipping at N, NW and SW directions with dips of 40°, 85° and 80° respectively, forming planar and wedge failures (Fig. 1). Within the fine material appear sparse pebbles, small-sized breccias and fossil bones from mammals.

The conglomerate and breccia intercalations are continuous, planar or slightly undulating, parallel or sub-parallel, with distinct bed boundaries. They comprise of gray, brown and whitish gravels with an average size of 0.036x0.022x0.018m and limestone pebbles, strongly cemented with light brownish to red brownish clayey-sand material. Coarse materials are poorly to very poorly sorted, with gravel shapes being spherical to tabular with subangular to subrounded roundness, while sand granules, of quartz origin, are also being spherical to tabular with angular to subrounded roundness. The conglomerate and breccia intercalations exhibit depositional structures of normal graded to composite bed sequences (Fig. 2 and Fig.3).

The, 200m total thickness, formation is the lateral and upwards transition of the Oropos fluvial-terrestrial formation and presents depositional dip, about 20°, towards SSW. Slopes are covered on their bases by landslide materials and slope erosion products and exhibit characteristic erosional

structures formed by the surface water runoff. The Neogene substratum appearing along the natural and man-made slopes is presented in detail at the lithostratigraphic logs of figure 2.

The clayey nature of the Neogene deposits doesn't allow the development of aquifer zones in their masses and only at its coarse or sandy intrusions seasonal, perched, low yield aquifers can be developed, which their discharge can cause pore pressure to increase and the underlying clay layers impregnation. This impregnation, as wells as, the water infiltration can also cause the development of pore pressure and creeping at the loose landslide materials.

4. Description of failures

For descriptive purposes the failures that occur along the coastal forehead are divided into the upper part and the lower part in relation to the road (Fig. 1).

4.1 Upper slope

In this part two main and three secondary failures can be found.

The first main failure (L1) pertains to soil material fracture and sliding with head scarp altitudes from +28 to +30 and toe at the road level at +16. The range of fracture is 18m while the accumulation of sliding material, at the road level, has 21m range. The second main failure (L2), which is the most important, is located about 7m to the west from the previous one, with head scarp altitudes from +31 to +35 and toe at the road level at +19, has 32m range and analogical accumulation range at the toe.

However, fractures and small movements are located in the slope part upstream of the main landslides to +35.50 altitudes, thus pointing the fact that the phenomenon is developing towards upstream. The secondary failures, as well as smaller ones, are events of limited fractures and sliding-erosions of the slope and materials accumulations at the slope base. The first of those (Ls1) took place east of (L1) failure with a range of 11m at an altitude of +26 while the second one (Ls2) west of (L2) failure with a range of 9m at an altitude of 30.

4.2 Lower slope

This part exhibit the most extended failures of the area, with five main landslides and three of minor importance and numerous small sliding-erosions along the steep coastal slope.

The first main landslide (L3) presents the most significant fracture range of 75m, with head scarp altitude of +16 while the range of the slope base, where the sliding material accumulates, is 50m. The landslide materials have an estimated thickness of 3m, while their morphology, with repeated fractures and slides refers to an evolutionary process of the phenomenon, due to the loss of support at their base from the erosive action of sea waves. The second main landslide (L4), which is considerably smaller than the first one with a fracture range of 46m and head scarp altitudes ranging from +6 to +10, has an estimated landslide materials thickness of 1.5m to 2,0m. The third main landslide (L5) has low fracture range about 15m, at an altitude of +20, while the thick soil material of the failure presents wavy morphology -with repeated fractures and slides- which refers to an evolutionary process because of the erosive action of sea waves. The fourth main landslide (L6) has fracture range 50m and head scarp altitude of +21 and reaches the sea level with range of the accumulated soil material about 60m. The thickness of the landslide materials is estimated some 4m and their morphology reveal the evolutionary process of the failure. The fifth main landslide (L7) at the west part of the study area concern the whole slope lower the road which is subjected to continues soil material creeping due to the

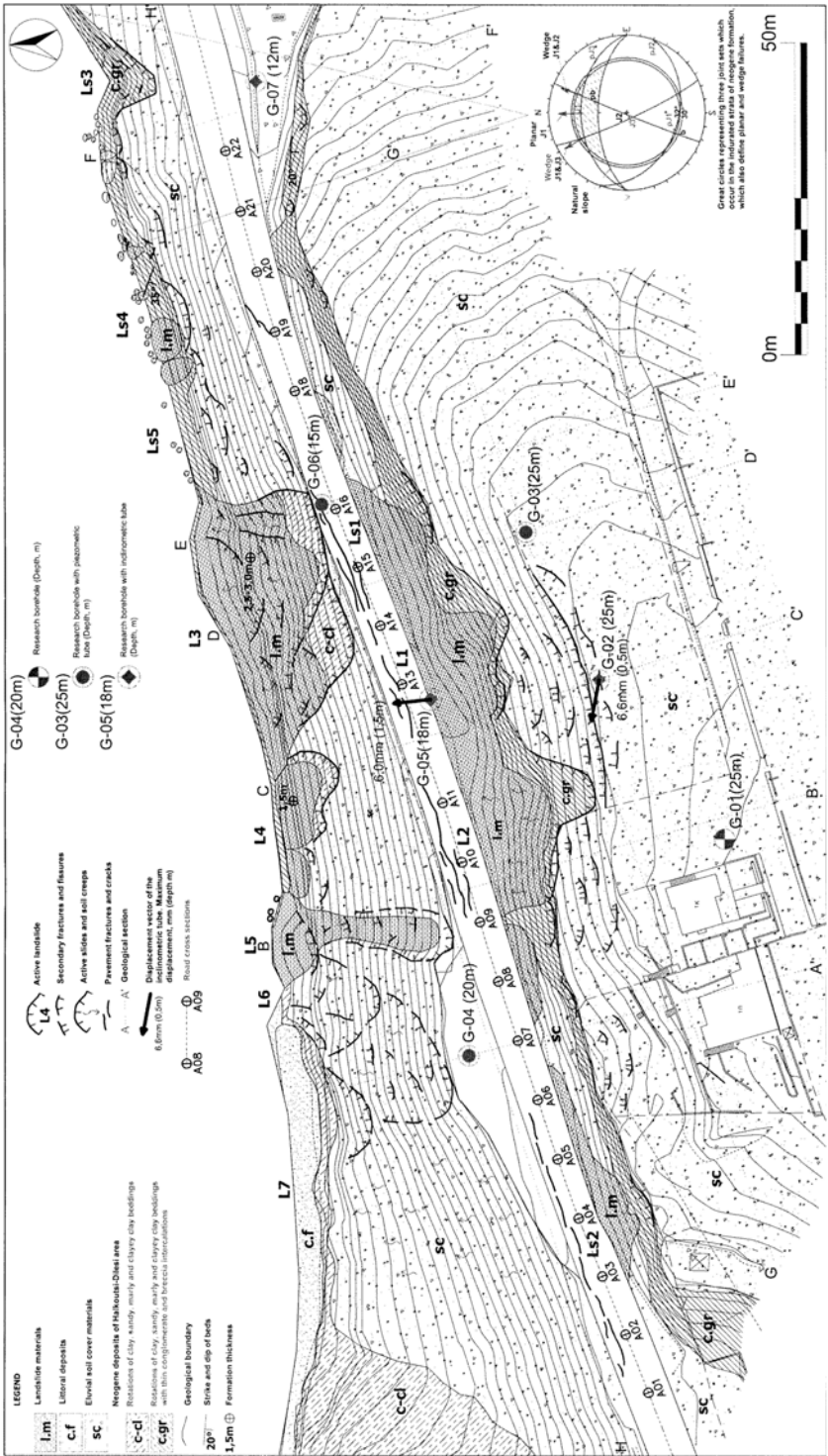


Fig. 1: Geological map of the project area.

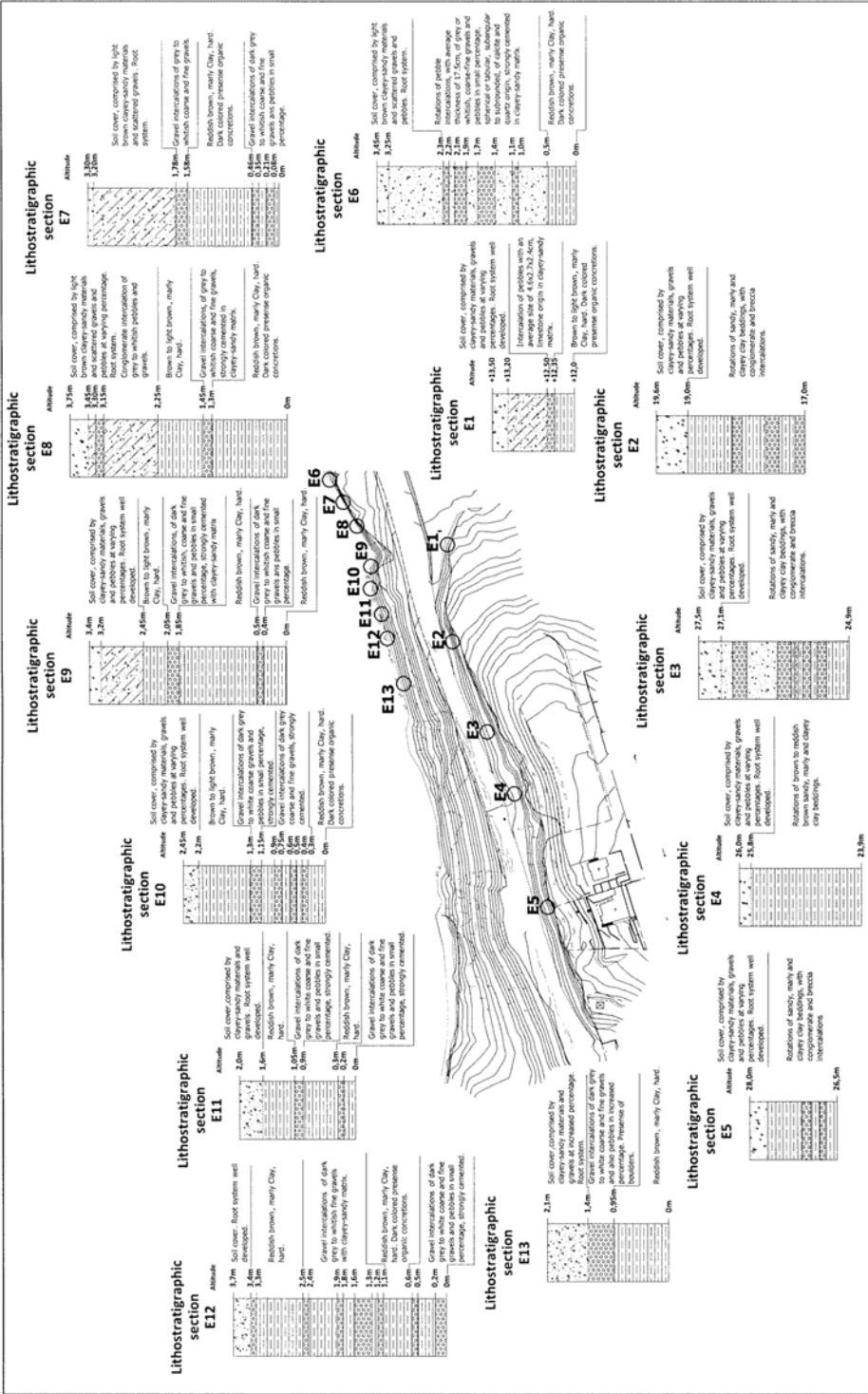


Fig.2: Lithostratigraphic sections of the natural slopes.

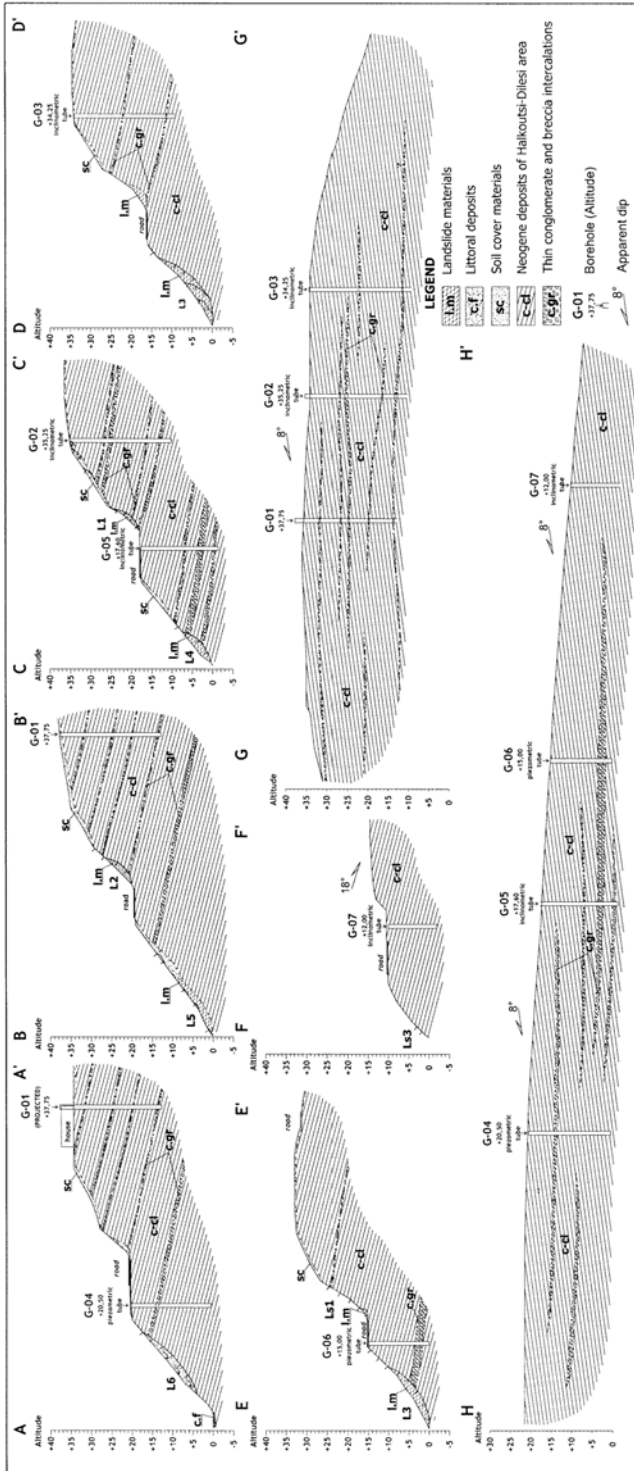


Fig. 3: Geological cross sections.

Table 1

Preparatory causal factors : 1.6, 1.9, 4.1
Triggering causal factors : 2.5, 3.1

loss of support at their base. The range of this slope part is about 70m and the maximum altitude of the phenomena origination is on the road where there are continuous cracks and recessions.

The three secondary failures Ls3, Ls4 and Ls5 pertain to the east part of coastal slope which extend about 150m length with a maximum altitude of +8. These failures concern part of the slopes that are delimited by discontinuities and due to the lack of support detach and accumulate at their toe as rock blocks of a maximum diameter of 1.0m. The total landslides at the lower part of the road cause support deletion of the road, so the north half of the pavement present fractures, cracks and downstream movements. The main causes of the failures events according to macroscopic observation and experience from similar engineering geological behavior of other formations recapitulate as follows:

- Modification of stability conditions, provoked by the excavation for the road construction. Steep to extremely steep gradient, where the failures occur.
- High overconsolidation of the neogene deposits.
- Extensive erosion because of slope exposure to the superficial water (e.g. intense rainfalls).
- Support loss at the slope toe by the continuous erosion of the sea waves.
- Impregnation of clay layers and increase of pore pressure from water which percolates through coarse layers and relieve to the slope front.
- Presence of discontinuities in the clayey formation, which in combination with the support loss at the slope toe result in the detachment of large clayey blocks.

Based on the above, from the physical point of view, the slope can considered as “marginally stable” (Crozier, 1986 and WP/WLI (1994)). The Landslide Report after WP/WLI (1994) is presented in Table 1.

5. Geotechnical investigation - Results

In order to investigate the geotechnical conditions in the slides areas, seven (7) exploratory boreholes with labeling G-01÷G-07 and continuous sampling were carried out. The three boreholes (with labeling G-01÷G-03) were carried out in the upper slope of the existing road. The remaining four boreholes (with labeling G-04÷G-07) were carried out in the lower part of the slope. The places of implementation of drillings are presented in Fig. 1 and the geotechnical borehole logs are presented in Fig. 4. In all the boreholes, during the drilling works Standard Penetration Tests were carried out (SPT) every 2,0-3,0m, in order to estimate the in situ consistency of clayey formations and in situ density of the granular formations. In boreholes G-03, G-04 and G-06 stand pipe piezometers were placed in order to measure the short and long term fluctuation of the water level inside the boreholes. In Table 2, measurements of the water level are presented during drilling as well as the measurements taken after the completion of the geotechnical investigation works.

In boreholes G-02, G-05 and G-07 inclinometer casings were placed, in order to monitor the size and direction of movement of the slopes. The first inclinometer measurement (reference) was taken after the completion of the investigation works (8/4/2006). Another two measurements were taken in

Table 2

Borehole	Date	Borehole casing (m)	Water Level depth (m)	
			Morning	Evening
G-01	17/3/2006	6,0	Drilling start	Dry
	20/3/2006		dry	3,00
	21/3/2006		9,50	3,00
	23/3/2006		13,00	
	24/3/2006		13,70	
G-02	23/3/2006	15,0	Drilling start	2,30
	24/3/2006		6,30	
G-03	21/3/2006	2,40	Drilling start	Dry
	22/3/2006		dry	13,50
	23/3/2006		19,0	
	24/3/2006		22,80	
	15/7/2006*		dry	
G-04	13/3/2006	7,00	Drilling start	Dry
	14/3/2006		dry	dry
	15/3/2006		dry	dry
	21/3/2006		dry	
	15/7/2006*		dry	
G-05	31/3/2006	-	Drilling start	Dry
G-06	1/4/2006	-	Drilling start	0,80
	15/7/2006*		14,50	
G-07	16/3/2006	-	Drilling start	dry

* level in piezometer

25/5/2006 and in 29/6/2006. The displacement vectors measured in the above time interval (approx. 3 months) along with the maximum recorded displacement (in mm) and the depth, in which it was observed, are presented in Fig. 1. During that period, the recorded displacements were small (~5-6mm) inside the error limits of the instrument and were presented in small depths G-02: 0,5m, G-05: 1,5m, G-07: 0,5m).

After the completion of the in situ works, laboratory tests were carried out in selected borehole samples including index tests (grain size, hydrometer tests and Atterberg limits, moisture content, unit weight, degree of saturation, specific gravity and void ratio) and tests for the determination of mechanical characteristics of the samples (triaxial compression UU, CUPP, direct shear CU and unconfined compression).

According to the results of the investigation works the area is covered by formations of very hard clays of high plasticity that in their majority are unsaturated and include preexisting discontinuities, fissure planes and slickensides. In the clayey formations in various depths, dense sand-gravel layers are present, constituted mainly from clayey gravel with sand to clayey sands with gravel.

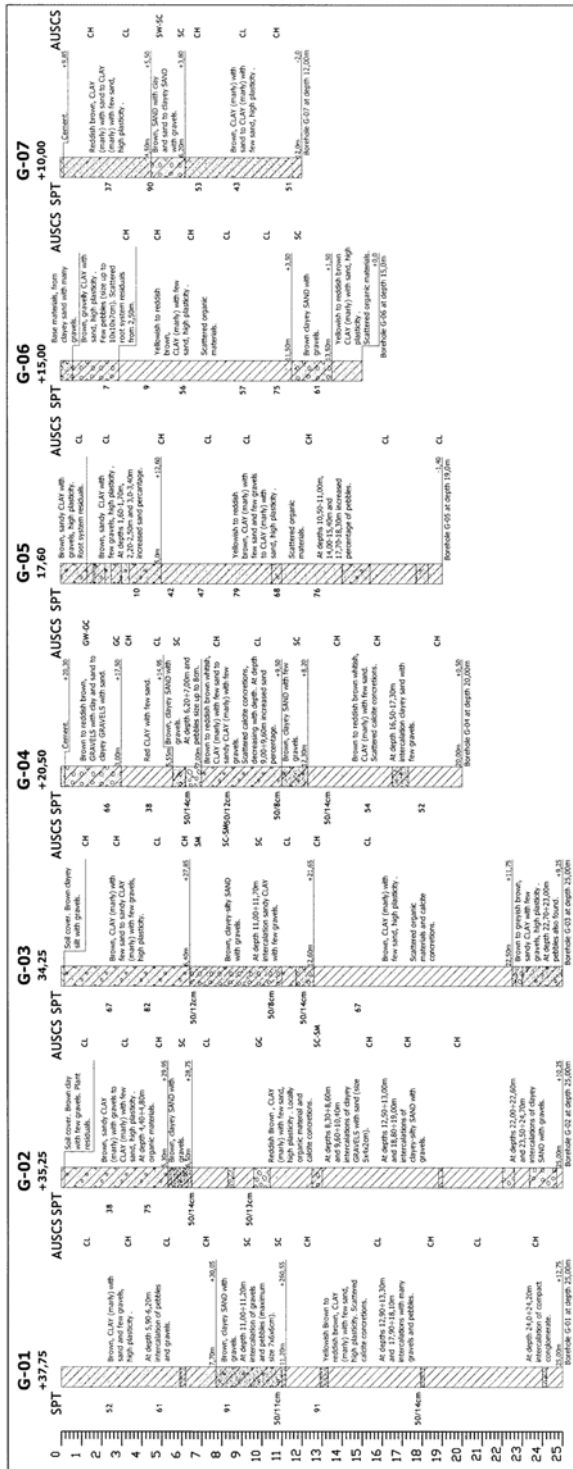


Fig.4: Boreholes logs

The observed slides in lower and upper slopes of the road are caused by the gradual diminishing of the shear resistance of hard clayey formations due to the progressive loss of the cohesion component of the shear strength, caused by the combined action of increased moisture content and displacements. The increase of the moisture content is caused by the infiltration of surface waters to the interior of their mass and is facilitated by the presence of the preexisting discontinuities into the body of the clay. The steep excavation slopes ($45^{\circ} - 55^{\circ}$) applied and the gradual loss of the shear strength from peak values to the fully softened values (Skempton, A.W., 1948, 1964, 1967, 1977; Terzaghi, K., Peck, R.B., Gholamreza, M., 1996) led to an increased tendency for slope displacements. In order to ensure the long term stability of the slopes an excavation with milder slopes ($\sim 25^{\circ} - 30^{\circ}$) was necessary. Regarding the lower slopes, their instability is influenced by the additional continuous erosion of the slope toe by the sea waves causing a continuous loss of their support.

6. Soil profile - Mechanical characteristics of soil formations

For the estimation of mechanical characteristics of soil formations presented in the upper slopes, boreholes G-01, G-02 and G-03 were carried out. According to the results of these boreholes the following soil formations were distinguished:

- a. CH 1: Brown fat CLAYS, of high plasticity, with sand to sandy with a varying percentage of gravel, hard to very hard. The formation was found at depths 0.0 to 7.7 at G-01, 0.0-5.3 at G-02 and 0.0-6.4 at G-03.
- b. CH 2: Yellowish brown to Yellowish red fat marly CLAYS, of high plasticity, with sand to sandy with a varying percentage of gravel, very hard. The formation was found at depths 11.2 to 25.0 (end) at G-01, 6.5-25.0 (end) at G-02 and 10.0-25.0 (end) at G-03.
- c. SC 1: Brown clayey SANDS with gravel to clayey Gravel with sand, very dense. The formation was found at depths 7.7 to 11.2 at G-01, 5.3-6.5 at G-02 and 6.4-10.0 at G-03.

The mechanical parameters of the aforementioned formation assumed in the calculations, are presented Table 3:

Table 3

	CH 1		CH 2		SC1	
	Measured (Peak values)	Design Value	Measured (Peak values)	Design Value	Measured	Design Value
Unit weight, γ_b (kN/m ³)	18,5-21,2	20	17,9-21,7	20,5	20,5-21,0	20,5
Undrained shear resistance, S_u (kPa)	292,5-442	250	229,7-697,2	300	-	-
Effective parameters (* : Long term design values for clays - <u>fully softened</u> with a loss of cohesion due to fissuring)						
Cohesion, C' (kPa)	0,0-5,0	2,0*	0,0-97,2	2,0*	0,0-5,0	1,0
Friction Angle, ϕ' (peak), ($^{\circ}$)	31,5-43,5	28*	14,3-41,5	27*	35-37	35

7. Brief description of remedial measures for upper slope

The proposed remedial measures for stabilization concern only the slides observed in the slopes extending over the road. Remedial measures for the lower slopes were not examined, because prior to any geotechnical study for remedial actions needed, a marine design (which was not in the object of the design at hand) should identify the sea defense works to prevent the sea erosion at the slope toe (e.g. the height, thickness and blanketing material needed for the protection of slope toe due the sea waves and currents expected in the area).

For the stabilization of the upper slopes two alternative solutions of stabilization were examined. In order to choose between the two, apart from economic criteria or criteria of construction speed, legal and economic issues have also to be considered due to the need of exceeding at certain locations the limits of expropriation at the upper slope crest area.

7.1 Solution A: Stabilization with milder excavations and soil nails

Solution A presupposes the possibility of limited surpassing the existing limits of expropriation. Firstly a cleaning of the slope surface is carried out removing the loose failed material involved in the slides. Afterwards an excavation of the slopes with milder slopes, minimizing as much as possible the surpassing of the existing limits of expropriation of the upper slope and more specifically in the Eastern part of the slope where houses exist. For the reinforcement of the newly formed slopes and in order to achieve the required factors of safety in static and seismic loading, the placement of passive soil nails is anticipated. Finally, for the protection of clay from the surface erosion and water infiltration and for the minimization of the probability of future loss of resistance of the surficial clay layers, a cover of “soft” type (soft cover) is placed on the slope surface comprising a needle punched geotextile and a geocell cover in filled and planted with vegetation. At the crest and the slope berms a suitable collection and dewatering system (eg. ditches) of the surface water is anticipated, for the fastest possible removal of the water from the slopes (Fig. 5, left).

7.2 Solution B: Stabilization with concrete wall founded on piles

For the case where it is not possible to exceed the existing limits of expropriation of the upper slopes, a continuous retaining wall with a variable height is constructed at the upper slope toe. The wall will be founded on piles. The piles on one side contribute on the total stability and in the same time help in the significant reduction of required excavations in slope toe for the construction of the wall shoe, which can trigger new slides. The area between the wall and slope surface will be backfilled with granular material (eg. rock fill). The backfill slope will be 1:2 (h:b). In the crest of the backfill embankment a suitable water collection system will be constructed (eg. ditches) in order to lead all surface waters outside the wall region (Fig. 5, right).

It is pointed out that in the case of Solution A, when remedial and stabilization works will be specified for the lower slopes, due to the additional excavations needed for the removal of failed materials, in order to ensure the stability of the road and upper slopes additional temporary retaining works may have to be constructed. In such an event, a construction of a pile wall at the crest of the lower slope maybe necessary along with the placement of prestressed anchors. In the event that Solution B will be applied, due to the presence of the wall foundation piles, it is not necessary to construct a temporary retaining pile wall (Fig. 5, left).

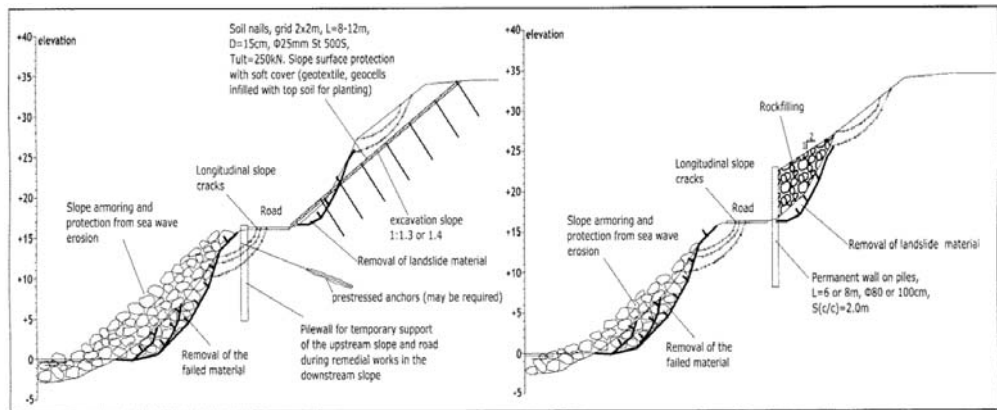


Fig. 5: Schematic reconstruction of solutions A (left) and B (right)

8. Detailed description of Solution A – Calculations

8.1 Description – methodology – assumptions

The stabilization measures of the upper slopes according to alternative solution A (Fig. 6), in more details comprises:

- a) Cleaning and removal of loose failed material from the slope surface.
- b) In the eastern part of the slope, between sections A03 ÷ A09, where houses exist near the slope crest, excavation with slopes 1:1,3 (37,6°) and placement permanent passive soil nails, in a grid 1,8x1,8m and length $L_a = 12m$.
In the remainder part of the slope from section A10 ÷ A22, where no houses exist near the crest, excavation with slopes 1:1,4 (35,5°) and placement permanent passive soil nails, in a grid 2x2m. Due the big height of the slopes that are created in this section of the slope (up to $H \sim 18m$), for slopes over 9m a berm is constructed having a width of 4m. Reinforcing soil nails at lower slope section ($H \leq 9m$) have length $L_a = 8m$, while in the upper section ($H > 9m$) will have length $L_a = 10m$.
- c) Protection of the clayey surface with placement of a cover of “soft” type which includes a layer of a non woven needle punched geotextile and a layer of geocells in filled with soil for vegetation.
- d) In the intermediary berms and the slope crest, a suitable water collection and drainage system (e.g ditches with appropriate sloping) will be constructed for the surface waters (e.g from rainfalls or other causes), in order to avoid the water concentration for large time intervals and that will probably infiltrate in the interior of the hard clay formations.

The reinforcing action of the soil nails will be required for the long term stability of the slope and for this reason should be considered as permanent. Soil nail has a diameter $D_a = 15cm$ and a reinforcing bar $\Phi 25mm$ from steel S500s. Due the permanent nature of the nails, all metallic parts (reinf. bar, anchor plate, nut, protective cover e.t.c), shall be constructed from stainless steel.

For the calculations concerning the slope stability in the present study, the PC software “SLIDE” ver. the 5.27 of Rocscience was used. All calculations were carried out for the most unfavorable cross-sections from the point of geometry (cross-section A09 and cross-section A14) and for the long-term stability (permanent situation) assuming the corresponding parameters for long-term conditions

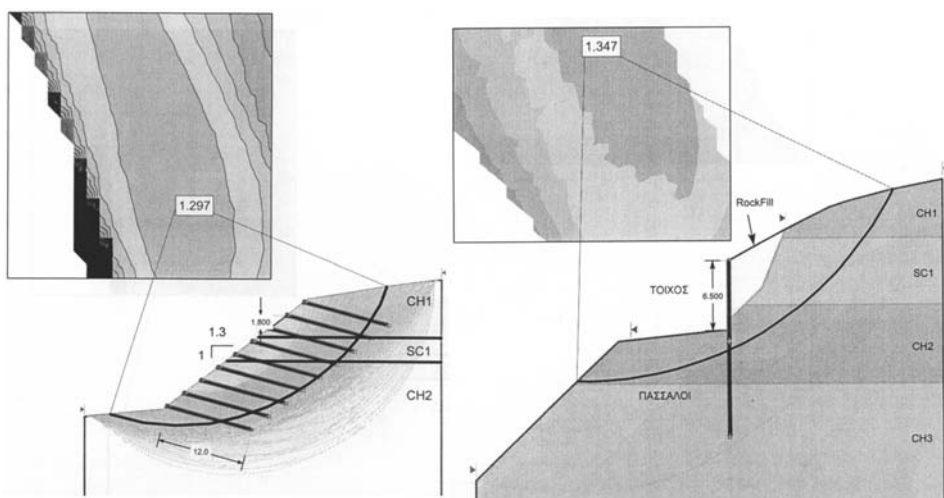


Fig. 6: Circular surfaces examined using the modified Bishop method of slices at the A09 section for remedial measures according to solution A (left) and at section A18 for remedial measures according to solution B (right).

of fully softened conditions for the clay formations and not the peak effective parameters. The calculations were carried out for static and seismic case with required factors of safety (F.S.) = 1,30 and 1,00, respectively

The ultimate side shear capacity of the nails was estimated using the expression $\tau(ult) = \alpha * Su$, α : cohesion coefficient = 0,4, Su : undrained shear resistance of clay = 250 – 300 kPa. And for a factor of safety (FS = 2,0) the allowable nail shear resistance (per linear meter), is : $Tal.(/l.m) = \pi * 0,15 \times 0,4 * (250-300) / 2,0 = 23 \div 28$ kN/m

The anchor plate at the nail head has minimum dimensions of 25x25cm and a minimum thickness $t=12$ mm.

8.2 Calculation results

For the determination of the slip surface with the smaller factor of safety, a large number of circular surfaces (as observed and in the actual slides) were examined covering the entire slope (the upper with the proposed measures and the lower at its present state), using the modified Bishop method of slices. The minimum factors of safety (F.S) calculated with application of the stabilizing measures of Solution A, are 1.30 and 1.02 for static and seismic loads respectively at section A09 and 1.34 and 1.04 for static and seismic loads respectively at section A14.

9. Detailed description of Solution B – Calculations

9.1 Description – methodology – assumptions

The stabilization measures of the upper slopes according to alternative solution B, in more details comprises:

a) Construction of wall foundation piles which at the same time increase the stability of the upper slope against deep sited (passing below the toe of upper slope) failure surfaces during temporary ex-

cavations needed for the stabilization of the lower slope.

b) Construction of a reinforced concrete continuous wall and filling of the space behind the wall and the existing upper slope surface. The fill material will be granular (e.g. rockfill, ballast material) exhibiting high mechanical characteristics without requiring intensive compaction. Due to the high hydraulic conductivity of these materials, any water accumulated behind the wall can be easily removed not creating hydrostatic pressures on the wall. The slope of the granular fill behind the wall, will be 1: 2 (h:b).

c) In front of the wall and in the crest of the fill of embankment a suitable water collection and drainage system (eg. ditches with appropriate sloping) should be constructed for the surface waters as well as for the water that circulate behind the wall.

The wall height varies from $H=6,5\text{m}$ (between cross sections A16, A17 and A18) to $H = 2\text{m}$, at the ends of the wall (cross-sections A02 and A21). Calculations concerning the general stability of the existing slopes with the proposed remedial measures (fill, wall and piles) were carried out. For the calculations of the available factor of safety, the PC software "SLIDE" ver. the 5.27 was used. All calculations were carried for the long term stability using the effective parameters for fully softened conditions for the clay formations and not the peak effective parameters. The calculations were carried out for static and seismic case with required factors of safety (F.S.) =1,30 and 1,00, respectively.

Calculations were performed for various wall heights (H) and more precisely for $H=4\text{m}$ (cross-section A7), for $H= 5\text{m}$ (cross-section A13) and for $H = 6,5\text{m}$ (cross-section A18). Due to the fact that the clayey materials of the slopes are covered by the fill placed behind the wall, mechanisms leading to the loss of the fissured clay strength due to loss of overburden, changes of water content and temperature variations are somewhat suppressed. For this reason, for the clayey materials encountered at larger depths from the slope surface a smaller loss of cohesion is anticipated. For this reason slightly bigger values of cohesion (by 2-3kPa) were used in the stability calculations in solution B in contrast of fully softened values used in the calculations for solution A.

For the fill material placed behind the wall (e.g rockfill, ballast) the assumed parameters for the calculations were: $\gamma = 19 - 20 \text{ kN/m}^3$, $c = 0 \text{ kPa}$, $\phi' = 34 - 35^\circ$.

9.2 Calculation Results

The minimum factors of safety calculated for solution B, by examining a large number of potential circular slip surfaces covering the entire slope (the upper with the proposed measures and the lower at its present state), using the modified Bishop method of slices, are 1.57 and 1.09 for static and seismic loads respectively at section A07, 1.29 and 1.00 for static and seismic loads respectively at section A13, 1.34 and 1.04 for static and seismic loads respectively at section A14 and 1.35 and 1.00 for static and seismic loads respectively at section A18.

9.3 Wall foundation piles

For wall heights exceeding $H \geq 5,5\text{m}$, foundation piles having a length $L_p=8\text{m}$ and diameter $\Phi 100\text{cm}$ are anticipated. The spacing (c/c) of piles below the wall is $s=2\text{m}$.

For wall heights smaller than $H < 5,5\text{m}$, foundation piles having a length $L_p=6\text{m}$ and diameter $\Phi 80\text{cm}$ are anticipated. The spacing (c/c) of piles below the wall is $s=2\text{m}$.

For the dimensioning of the wall and the foundation piles, calculations were carried for static and seismic conditions. In order to estimate the bearing capacity of the piles, the methodology of DIN 4014 (03/90) was used. The response of the piles to lateral loads was calculated using equivalent elastoplastic soil springs for short term and long term conditions.

10. Conclusions

The observed slope failures in the upper slopes were triggered by the heavy rainfall in combination with the steep excavation slopes applied for the road construction. The observed failures in the lower slopes are mainly triggered by the continuous wave erosion at the slope toe.

Two alternative solutions of stabilization were examined for the upper slopes which offer the required safety for the whole slope (upper and lower) assuming the conditions of the lower slope remain at the present state. Since changes at the lower slope toe due to sea wave erosion cannot be excluded sometime in the future, a marine design should be carried out to determine the appropriate armoring works.

The stabilization solution which will be adopted, apart to cost effectiveness and construction speed has to take into account legal and economic issues due to liabilities to property owners at the upper slope crest area.

11. References

- Crozier, M.J., 1986. Landslides – Causes, consequences and environment, Croom Helm, London, 252 p.
- Mettos, A., 1992. Geological and Palaeogeographic study of the neogene and quaternary continental formation of NE Attiki and SE Boeotia. PhD Thesis Dept. of Geology Univ. of Athens.
- Koumantakis, I., 1971. Chalkoutsi Pontian formations, S. Attica. *Ann. Geol. Pays Hellen.*, 27, 274-284.
- Popescu, M.E., 1994. A suggested method for reporting landslide causes, *Bulletin of the International Association of Engineering Geology*, Paris, 50, 71-74.
- The rate of softening in stiff fissured clays, with special reference to London Clay. *Proc. 2nd Int. Conf. Soil Mech. Rotterdam*, 2, pp. 50-53.
- Skempton, A.W., 1948. The rate of softening in stiff fissured clays, with special reference to London Clay. *Proc. 2nd Int. Conf. Soil Mech. Rotterdam*, 2, pp. 50-53.
- Skempton, A.W., 1964. Long term stability of clay slopes. *Geotechnique* 14, No. 2, pp. 77-101.
- Skempton, A.W., & Petley, D.J., 1967. The strength along structural discontinuities in stiff clays. *Proc. Geotech. Conf. Oslo* 2, pp. 29-46.
- Skempton, A.W., 1977. Slope stability of cuttings in Brown London Clay. *Special Lectures Section, Proc. of the 9th Int. Conf. on Soil Mech. and Found. Eng.*, Tokyo, Vol. 3, pp. 261-270.
- Terzaghi, K., Peck, R.B., Gholamreza, M., 1996, *Soil mechanics in engineering practice*, John Wiley & Sons Inc.

SLOPE INSTABILITY MONITORING BY SPACE-BORNE SAR INTERFEROMETRY: PRELIMINARY RESULTS FROM PANACHAICO MOUNTAIN (WESTERN GREECE)

Parcharidis I. ¹, Foumelis M. ¹ and Kourkouli P. ¹

¹Harokopio University of Athens, Department of Geography, El. Venizelou 70, 176 71, Athens, Greece,
parchar@hua.gr, mfoum@hua.gr, pkourkouli@hua.gr

Abstract

Space borne differential synthetic aperture radar interferometry (DInSAR) has already proven its potential for mapping ground deformation phenomena, e.g. earthquakes, volcano dynamics, etc covering in continuity large areas.

The innovative Persistent Scatterers Interferometry (PSI) technique, which overcomes several limitations of conventional SAR differential interferometry especially for applications in landslide studies, is suitable for monitoring slope deformations with millimetric precision. With PSI technique we detect the deformation, for long periods, that occur in an area as average annual deformation (mm/y) and is not spatially continuous but in terms of points (point targets).

The aim of this study is to present preliminary results on the monitoring of slope instability in Panachaiko Mountain and particularly of the slopes facing the city of Patras. For this purpose we processed and analysed 42 ERS 1 and ERS 2 SAR scenes acquired in the time span 1992 and 2001, by applying the Interferometric Point Target Analysis algorithm.

Point target reflectors with stable radar response over time were selected. In this case most of the point targets correspond to buildings of the local settlements or to rock outcrops. Additionally, millimetric target displacements along the line of sight direction were detected allowing measurements of slow terrain motion.

Key words: SAR Interferometry, Persistent Scatterers, IPTA algorithm, slope instability, Panachaiko Mountain, Patras City.

1. Introduction

Numerous phenomena can induce displacements of the earth surface and thus cause disorders in structures and infrastructures particularly in urban areas. Landslides affect many areas of Greece and are characterized by low probability of evolution into a catastrophic event but can have very large direct and indirect impacts on man-made structures. Methodologies for the risk assessment and mitigation are therefore a major issue.

Conventional methods of ground deformation monitoring present many disadvantages such as high costs and time consuming. The space based Differential Interferometry SAR (DInSAR) techniques could present a valuable tool for detecting, monitoring, quantifying the deformation and with field-

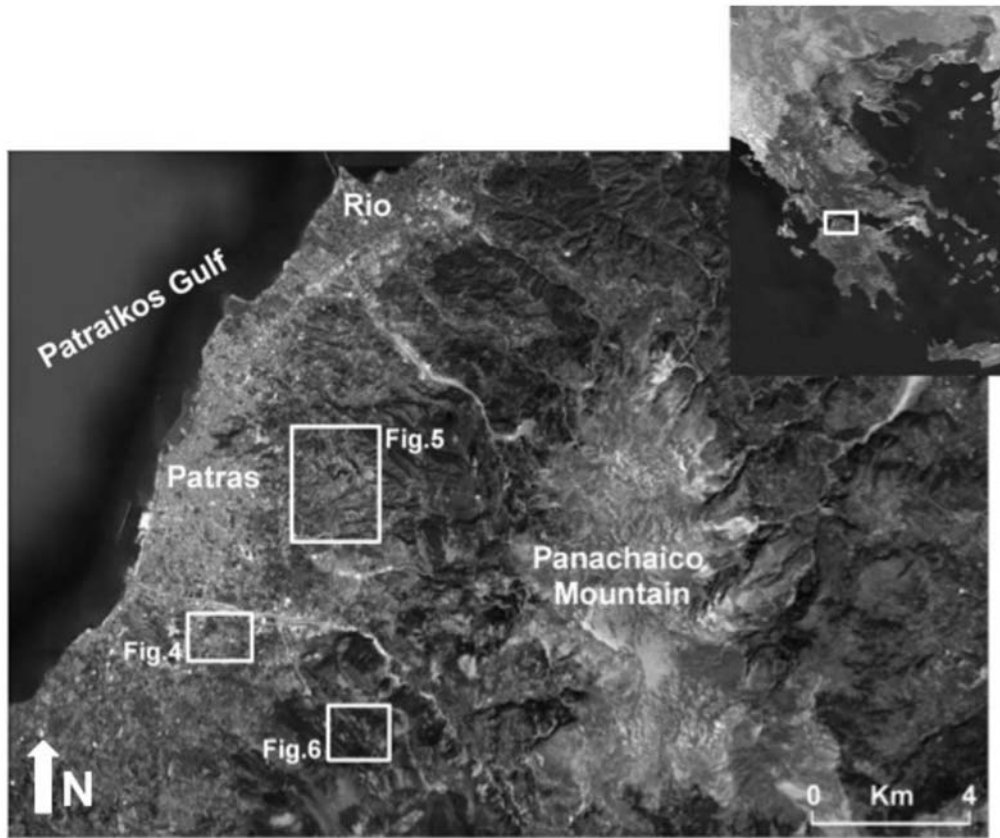


Fig. 1: Location map of the area (the frames are referred to the corresponding Figures).

work contribution can identify causes which may induce deformation.

DInSAR has already proven its potential for mapping ground deformation phenomena, e.g. earthquakes, volcano dynamics, etc and to cover in continuity large areas.

In recent years the innovative Persistent or Permanent Scatterers Interferometry (PSI) technique, which overcomes several limitations of repeat-pass interferometry, has been widely applied for monitoring of slope instability with millimetric precision (Delacourt 2003, Strozzi et al. 2005, Colesanti & Wasowski 2006, Rott & Nagler 2006, Corsini et al. 2006, Bovenga et al. 2006, Peyret et al. 2008, Meisina et al. 2008, Castaneda et al. 2009).

Significant difficulties are found when using this technique as an operational tool. These difficulties are related to the large variability of slope instabilities in terms of mechanisms of movement, failure geometries, size of unstable areas and deformation rates (Strozzi et al. 2005). Some other limitations are connected to the acquisition parameters of the SAR platforms.

The aim of this study is to present preliminary results of an application of PS interferometry for detecting and monitoring of slope instability at regional and local scale, quantify the spatial distribution of surface deformation and analyze the time evolution of displacement, in Panachaiko Mountain

and particularly of the slopes facing the city of Patras (Fig. 1). This site was chosen for the presence of a number of mass movements as it is mentioned from many authors (Sabatakakis et al. 2005, Koukis et al. 2007, Koukis et al 2009). For this purpose we processed and analysed a rich data set of ERS 1, ERS 2 SAR scenes, acquired in the time span 1992 and 2001, by applying the IPTA (Interferometric Point Target Analysis) method of the GAMMA s/w.

2. Principles of Persistent Scatterers Interferometry (PSI)

“Traditional” ground motion monitoring methods are based on field surveys. These methods include optical levelling, Global Position Systems, extensometers etc. During the last sixteen years the SAR Interferometric technique based on radar satellite data have become a useful tool for ground deformation detection and monitoring. Radar is an active sensor that alternatively sends out radio waves in form of pulses and records the echoes scattered back by objects (targets) hit by the waves along their travelling path. Each echo (backscattered signal) is a modified version of the transmitted pulse through the reflectivity function of the target(s) seen on the ground. Since the transmitted signal is a complex quantity, also the signal received by the radar is complex. It is composed by the magnitude, which is related to the power scattered back toward the sensor by the target, and the phase, which is expressed by the two-way path distance between the sensor and the target. Both amplitude of the radar signal and phase carry valuable information for the interferometric applications.

The magnitude and the phase of the complex interferograms are generally referred to as the degree of coherence (or simply coherence) and the interferometric (InSAR) phase respectively. The coherence measures the degree of correlation between two SAR images. The interferometric phase image has values between 0 and 2π (or between $-\pi$ and π depending on the representation used) and therefore appears as a series of fringes. The interferometric phase is a sensitive measure of the change in slant range.

Two consecutive fringes represent a phase difference of 2π . Areas of low coherence are characterized by noisy interferometric phase. Coherence is a measure of the phase noise or fringe visibility.

Since 1992, conventional 2-pass Differential InSAR (DinSAR) has been used by the scientific community to further study and understand specific ground deformation hazards. Normally this interferometric method is used to map ground deformation caused by a natural event like earthquake or landslide etc. What we need is the minimum of two SAR images one before and one after the event and also a Digital Elevation Model (DEM) of the area under study. The basic idea of differential interferometric processing is to separate the topography and displacement related phase terms allowing, in particular, the retrieval of a differential displacement map. This goal is achieved by subtracting the topography related phase using the DEM.

Repeat-pass Differential Interferometric techniques show limitations related to land-cover dependent temporal signal decorrelation and atmospheric propagation effects. Furthermore, the applicability of this interferometric technique depends also on the magnitude of the deformation. Recent developments (end of 90's) in differential interferometry have demonstrated some potential to overcome some of the above limitations of the conventional interferometry and also for more accurate and temporally dependent results. To maximize the precision with which displacement signals are detected, and to minimise effects like atmospheric the so-called Permanent or Persistent Scatterers Interferometry has been developed (Ferretti et al. 2001, Werner et al. 2003). This recent technique allows the calculation of fine motions of individual ground and structure points over wide areas (Fig. 2). By examining interferometric phase from stable, point-like targets, it is possible to moni-

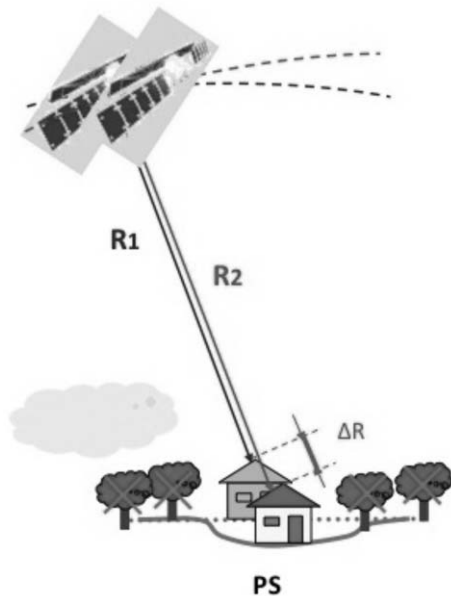


Fig. 2: The basic concept of the Persistent Scatterers Interferometry methodology.

tor stability over areas that normally are characterized as “low coherence”. Additionally, millimetric target displacements along the line of sight direction can be detected allowing measurement of slow terrain motion.

Interferometric Point Target Analysis (IPTA) is a specific method of PSI to exploit temporal and spatial characteristics of the interferometric signatures collected from point targets to map scatterer deformation history.

3. Data used and processing

As input data Single-Look Complex SAR images, from European remote sensing satellites ERS-1 and 2 operating at C-band, have been used.

After an accurate searching at EOLI database ERS 1 & 2 scenes covering the area of interest have been ordered. A total number of 42 ERS archive scenes, track: 279 and frame: 2835, covering the period 1992-2001 (Table 1) were acquired. The acquisitions have descending orbit that means with line of sight (LOS) approximately ESE-WNW.

Persistent Scatterers Interferometry (PSI) is a technique used to calculate fine motions of individual ground and structures points over wide areas. These reflectors should remain stable (interferometric phase stability over time). Interferometric Point Target Analysis (IPTA) is a specific method of PSI, developed by GAMMA Remote Sensing (Switzerland) to exploit temporal and spatial characteristics of interferometric signatures collected from point targets to map scatterer deformation history (Werner et al., 2003).

Interferometric processing for the selected study area was performed using 42 ERS-1 and 2 SAR scenes acquired between 1992 and 2001 along descending track 279. Initial estimates of the interferometric baselines were calculated from available precise orbit state vectors from Delft Institute

Table 1.

Count	Satellite	Slave (date)	Orbits	Bp (meters)	dT (days)
1	ERS 1	11/12/1992	6937	73.913	-933
2	ERS 1	06/10/1993	9943	-477.395	-723
3	ERS 1	08/19/1993	10945	-323.744	-653
4	ERS 1	10/28/1993	11947	569.7341	-583
5	ERS 1	03/25/1995	19305	-1169.985	-70
6	ERS 1	04/29/1995	19806	-518.4969	-35
7	ERS 1	06/03/1995	20307	0	0
8	ERS 1	07/08/1995	20808	-583.3577	35
9	ERS 2	08/13/1995	1636	82.8884	71
10	ERS 2	09/17/1995	2137	-360.0171	106
11	ERS 1	10/21/1995	22311	761.2519	140
12	ERS 2	12/31/1995	3640	186.241	211
13	ERS 2	05/19/1996	5644	71.012	351
14	ERS 2	06/23/1996	6145	-83.809	386
15	ERS 2	09/01/1996	7147	-514.627	456
16	ERS 2	10/06/1996	7648	-392.684	491
17	ERS 2	11/10/1996	8149	1064.863	526
18	ERS 2	12/15/1996	8650	-309.172	561
19	ERS 2	01/19/1997	9151	-28.695	596
20	ERS 2	02/23/1997	9652	-182.299	631
21	ERS 2	05/04/1997	10654	-360.3074	701
22	ERS 2	06/08/1997	11155	-166.9323	736
23	ERS 2	07/13/1997	11656	-124.871	771
24	ERS 2	08/17/1997	12157	111.4587	806
25	ERS 2	09/21/1997	12658	-263.2312	841
26	ERS 2	11/30/1997	13660	177.4578	911
27	ERS 2	01/04/1998	14161	116.4249	946
28	ERS 2	04/19/1998	15664	193.0535	1051
29	ERS 2	05/24/1998	16165	-160.6964	1086
30	ERS 2	06/28/1998	16666	-834.8781	1121
31	ERS 2	08/02/1998	17167	56.7021	1156
32	ERS 2	09/06/1998	17668	47.0451	1191
33	ERS 2	02/28/1999	20173	302.9872	1366
34	ERS 2	06/13/1999	21676	-559.7601	106
35	ERS 2	07/18/1999	22177	455.9664	1506
36	ERS 2	08/22/1999	22678	1012.1175	1541
37	ERS 2	09/26/1999	23179	448.5963	1576
38	ERS 2	10/31/1999	23680	357.309	1611
39	ERS 2	12/05/1999	24181	-121.9885	1646
40	ERS 2	01/09/2000	24682	-140.144	1681
41	ERS 2	04/23/2000	26185	953.687	1786
42	ERS 2	05/28/2000	26686	806.600	1821

(NL) for Earth-Oriented Space Research (DEOS) (Scharoo and Visser, 1998). The topographic phase was simulated based on SRTM v2 DEM of approximate spatial resolution of 90 m.

Starting from a stack of co-registered SLC images, the selection of the reference scene was based primarily on the baseline minimization criteria. In addition, the selection of a reference scene acquired near the temporal average of the available SAR acquisitions is also of interest. For the specific project the ERS scene acquired on 3 June-1995 with orbit number 20307 was selected as reference scene.

The first step of the analysis involves the identification of candidate point targets for which the time-series analysis will be performed. In this case two different approaches were applied. The first approach is based on the spectral properties of each individual SLC image. This is done by identifying point targets of low spectral phase diversity. The second approach involves the identification of candidate point targets based on low intensity variability, since by definition point targets do not show speckle behaviour as simple coherent scatterer dominates the echo. Finally, point targets determined previously were combined into a single preliminary point list containing a total number of 78,647 records. At this stage of the analysis the distribution of point targets seems not to be restricted over flat areas, but also show significant presence over mountainous regions.

The analysis of the differential interferometric phases in the temporal direction is an important element of an interferometric point target analysis. Point data stack of differential interferograms was generated and analyzed by means of phase regression analysis in the temporal domain using two dimensional bi-linear regression model.

Two dimensional regression analysis is done with the dimensions corresponding to the perpendicular baseline of the interferometric pairs and to the time difference between the two SLC of the interferometric pairs according to:

$$a_0 + a_1 * b_{perp} [i] + a_2 * \Delta t [i]$$

a_0 : phase offset, a_1 : slope in baseline dimension (can be converted into point height correction), a_2 : slope in time dimension (can be converted into linear deformation rate), b_{perp} : perpendicular baseline component of interferograms, and Δt : time interval of interferograms.

The model examines linear dependence of the topographic phase on the perpendicular baseline component as well as linear phase dependence with time, solving respectively for both height correction and constant deformation rate of the point target relative to the reference. The regression analysis of the entire stack of observations was first conducted using multiple patches, within each patch one reference is determined, and then using the selected single reference point as a global reference. This procedure was followed in order to minimize the effect of distance between the two pairs phase components, as the atmospheric distortion, baseline error (residual orbital phase trends) and higher relative deformation rates result in higher deviations of the individual points from the regression plain.

The quality of the preliminary candidate points were then carefully evaluated based on the estimated standard deviation of the differential interferometric phase from the 2-D regression model. Points with a phase standard deviation larger than the indicated threshold (in this case 1.0) were rejected reducing significantly the number of scatterers to 3353 over the study area. The majority of the rejected points were located over mountainous areas non build-up zones.

The general phase model for IPTA that used is the same as the conventional interferometry. The unwrapped interferometric phase Φ_{unw} is expressed as the sum of topographic phase Φ_{topo} , deformation phase Φ_{def} , path delay (atmospheric phase) Φ_{atm} and the phase noise Φ_{noise} .

$$\Phi_{unw} = \Phi_{topo} + \Phi_{def} + \Phi_{atm} + \Phi_{noise} \text{ (Werner et al., 2003)}$$

Phase terms related to the atmosphere, non-linear deformation, baseline errors and noise could be discriminated within the residual phases based on their differing spatial and temporal dependencies (Werner et al., 2003).

Unwrapped phases calculated from the regression analysis described above and the corresponding topographic phases were then used in a least-squares approach for baseline refinement. The analysis was limited over areas exhibiting no deformation as dictated by the linear deformation estimates. Introducing the refined baselines and taking into consideration the early estimated height corrections and linear deformation rates, the interferometric phase model was updated in a second iteration.

Additional processing includes temporal and spatial filtering of newly estimated residual phases to compensate for atmosphere and noise. Atmospheric screen was attributed to large scale non-linear residuals and subtracted from the model by applying low-pass spatial filtering on the residual phases. Phase noise was treated by spatially filtering of phases around the reference, assuming stability of the area considered.

Further iteration applying the additional corrections results in the final regression model. Results consist of point heights, linear deformation rates, atmospheric phase, refined baselines, quality information (temporal coherence) and non-linear deformation histories for each point. It is important to mention that the final deformation model, as a consequence of the assumptions made during the estimation.

4. Analysis-Interpretation

After transformation of the interferometric results from range–Doppler coordinates into map geometry (geographic coordinates), point targets were imported in a GIS environment and plotted on a panchromatic Landsat-7 ETM+ image and in Google Earth environment for point targets identification (Fig. 3). The majority of the targets correspond to the buildings forming villages.

In this location slopes face west and north-west making the descending scenes suitable for the interferometric application. Phenomena like layover and foreshortening are not recognised in the average multi-look reflectivity image.

The displacement rates, along the line of sight (LOS), vary from -4.6 to 7 mm/year for the entire area of processing. In total 1073 persistent scatterers were identified. Negative values indicate displacement away from the radar sensor, towards down slope in this case. Examining the scatterers and their rates of displacement on a more detail scale we noticed groups of targets presenting negative values. A typical case is the Demenika village where the values of the targets vary between -3.1 and 0.7 mm/year (Fig. 4). Additionally, targets with negative values are observed over the tunnel of the new suburban national road with rates between -4.0 and 0.2 mm/year (Fig. 5).

A distinct case in our results concerns a group of point targets over a slope, one kilometre towards NE of Moni Omplou. These targets have negative values and correspond not to human structures but to rocks outcrops (Fig. 6).

Finally the historic deformation diagrams for specific point targets from the above sites were created (Fig. 7) showing the tendency of the displacement during the time span (1992-2001).

5. Results-Discussion

In this study a dataset of Envisat scenes were processed using the IPTA algorithm in order to create

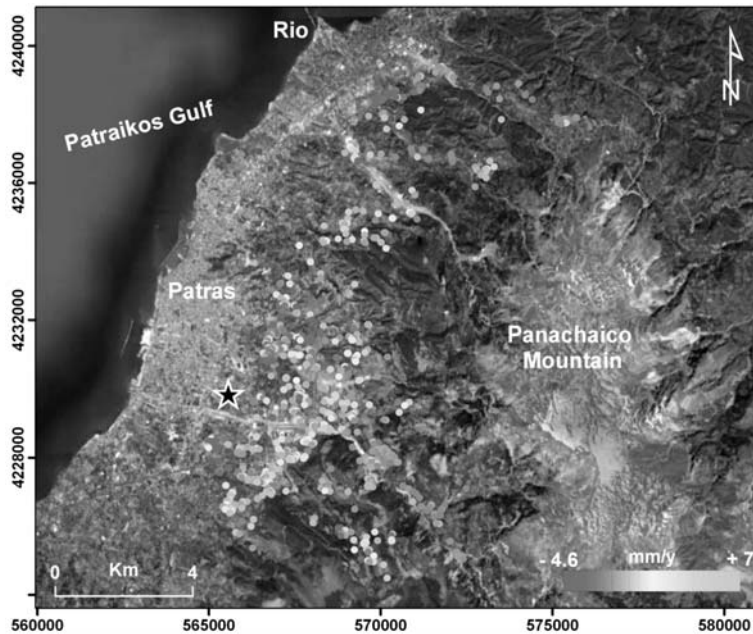


Fig. 3: Linear deformation rates for point targets estimated over the study area and plotted on a QuickBird satellite image

a persistent scatterers deformation map in order to detect soil instability over the Panachaiko slopes facing Patras city. Produced results show areas with negative values that means a displacement away from the satellite. These areas could correspond with areas of ground instability. For specific targets the historical deformation diagrams were created. Interferometric results should be accompanied by detailed field work verify the interferometric results. Based on the observation that even over villages the point targets are few a new processing with the selected reference point much close at the areas of interest probably will increase the number of targets and thus the points of measurements. Generally speaking, the persistent scatterers interferometry approach offers an alternative in respect to the “conventional” or repeat-pass interferometry. With this technique the corresponding stable point targets can be identified and analyzed their displacement in time. The main limitations (Colesanti and Wasowski 2006, Rott and Nagler 2006) of PSI to identify landslides are related to:

- One dimensional deformation data provision along the line of sight.
- A limited range of detectable displacements (up to 10 cm/yr) focusing only on very slow slope deformation.
- Limited rock outcrops and buildings in the area so the detectable persistent scatterers are very few.

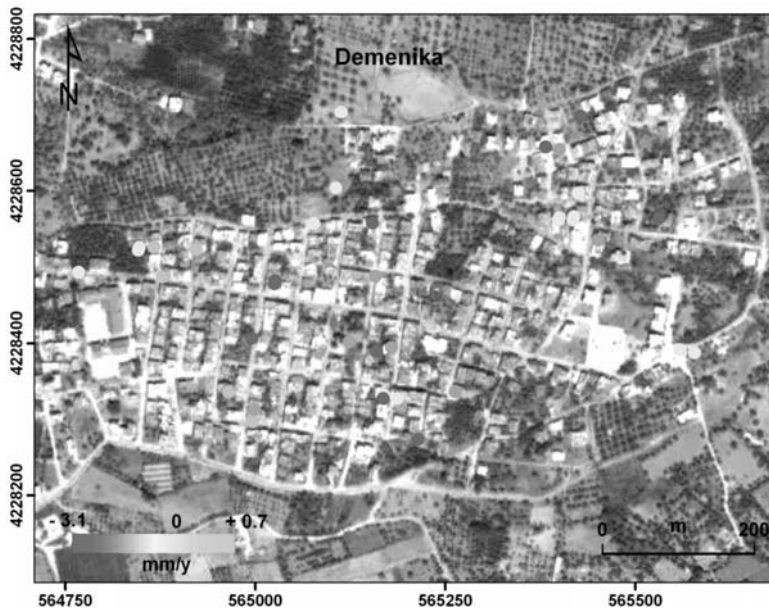


Fig. 4: Linear deformation rates for point targets estimated over Demeniko village

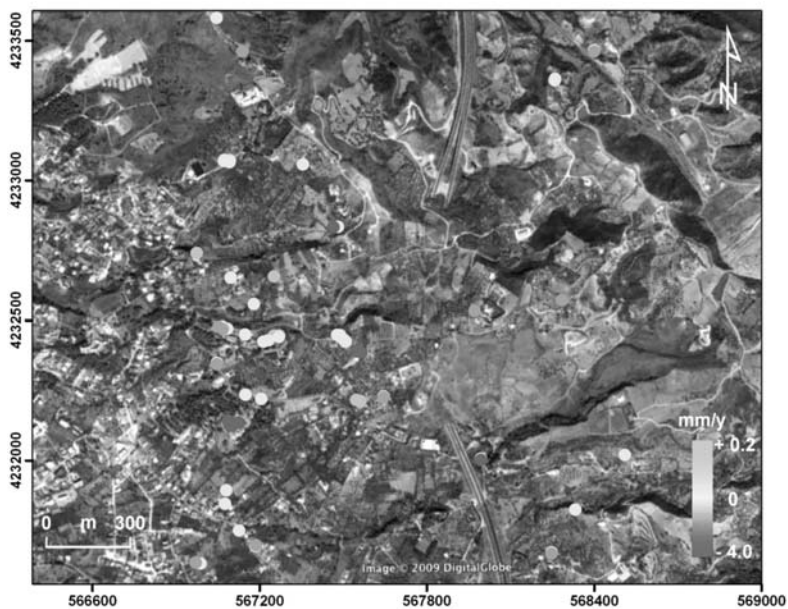


Fig. 5: Linear deformation rates for point targets estimated over the tunnelling area

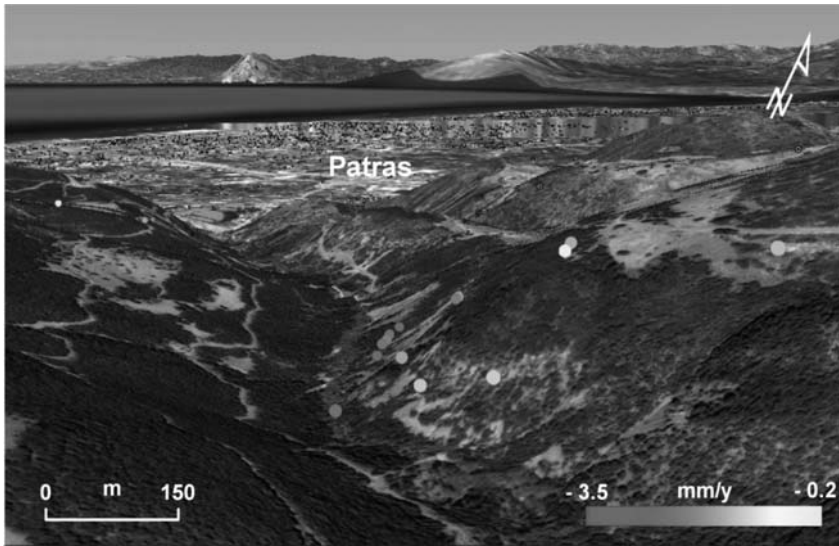


Fig. 6: Linear deformation rates for point targets estimated over the Moni Omlou slope

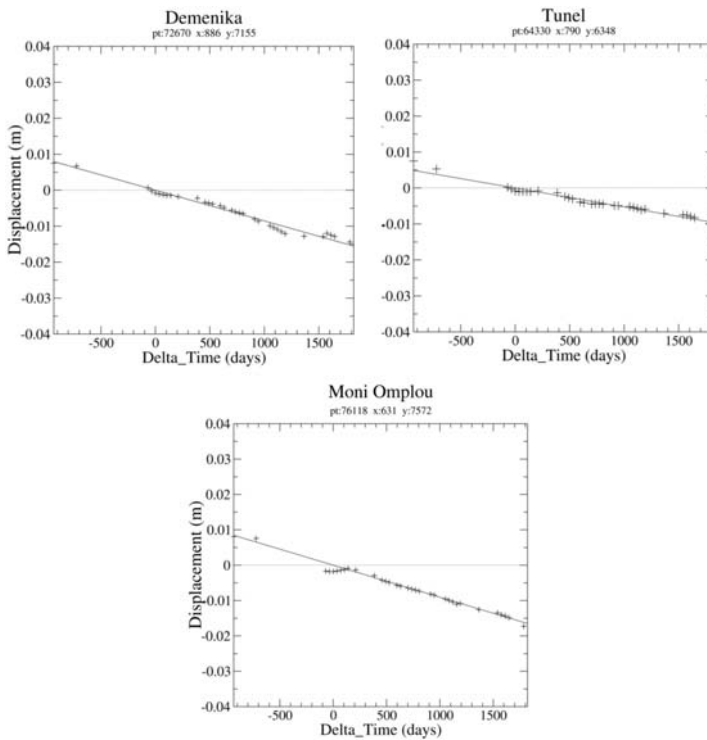


Fig. 7: Typical displacement histories (1992–2001) for specific point targets in the three areas showing a displacement away from the sensor. Values lie within about 0.2 cm of the linear rate with a standard deviation significantly below 1 rad.

References

- Bovenga F., Nutricato R., Refice A. and Wasowski J., 2006. Application of multi-temporal differential interferometry to slope instability detection in urban/peri-urban areas. *Engineering Geology* 88, 218-239.
- Castaneda C., Gutierrez F., Manunta M. and Galve J., 2009. DInSAR measurements of ground deformation by sinkholes, mining subsidence and landslides, Ebro River, Spain. *Earth Surface Processes and Landforms* 34, 1562-1574.
- Colesanti C. and Wasowski J., 2006. Investigating landslides with space-borne Synthetic Aperture Radar (SAR) interferometry. *Engineering Geology* 88, 173-199.
- Corsini A., Farina P., Antonello G., Barbieri M., Casagli N., Coren F., Guerri L., Ronchetti F., Sterzai P., Tarchi D., 2006. Space-borne and ground-based SAR interferometry as tools for landslide hazard management in civil protection. *International Journal of Remote Sensing* 27(12), 2351-2369.
- Delacourt C., Allemand P., Squarzonni C., Picard F., Raucoules D., Carnec C., 2003. Potential and limitation of ERS-Differential SAR Interferometry for landslide studies in the French Alps and Pyrenees. *In proceedings of FRINGE 2003*.
- Ferretti, A.; Prati, C.; Rocca, F., 2001. Permanent scatterers in SAR interferometry. *IEEE T. Geosci. Remote*, 39, 8-20.
- Koukis G., Sabatakakis N., Lainas S., 2007. Soil suitability estimation for housing purposes in landslide-prone areas. The case of Karya Village, Patras, W, Greece. *Bulletin of the Geological Society of Greece*, vol. XXXVII,
- Koukis G., Sabatakakis N., Ferentinou M., Lainas S., Alexiadou X., Panagopoulos A., 2009. Landslide phenomena related to major fault tectonics: rift zone of Corinth Gulf, Greece. *Bull. Eng. Geol. Environ.* DOI 10.1007/s10064-008-0184-8.
- Meisina C., Zucca F., Notti D. Colombo A., Cucchi A., Savio G., Giannico C. and Bianchi M., 2008. *Sensors* 8, 7469-7492.
- Peyret M., Djamour Y., Rizza M., Ritz J.-F., Hurtrez J.-E., Goudarzi M, Nankali H., Chery J., Le Dortz K., Uri F., 2008. Monitoring of the large slow Kahrod landslide in Alborz mountain range (Iran) by GPS and SAR interferometry. *Engineering Geology* 100, 131-141.
- Rott H. and Nagler T., 2006. The contribution of radar interferometry to the assessment of landslide hazards. *Advances in Space Research*, 37, 710-719.
- Sabatakakis N., Koukis G., Mourtas D., 2005. Composite landslides induced by heavy rainfalls in suburban areas: city of Patras and surrounding area, western Greece. *Landslides* 2, 202-211.
- Scharoo R. and Visser P.N.A.M., 1998. Precise orbit determination and gravity field improvement for the ERS satellites. *Journal Geophysical Research*, vol. 103, 8113-8127.
- Strozzi T., Farina P., Corsini A., Ambrosi C., Thüring M., Zilger J., Wiesmann A., Wegmüller U., Werner C., 2005. Survey and monitoring of landslide displacements by means of L-band satellite SAR interferometry. *Landslides* 2 (3), 193-201.
- Werner, C.; Wegmüller, U.; Strozzi, T.; Wiesmann, A. (2003). Interferometric point target analysis for deformation mapping. *In Proceedings of the IEEE International Geoscience and Remote Sensing Symposium*, Toulouse, France, July 2003, 7, 4362-4364.

12ο ΔΙΕΘΝΕΣ ΣΥΝΕΔΡΙΟ ΤΗΣ ΕΛΛΗΝΙΚΗΣ ΓΕΩΛΟΓΙΚΗΣ ΕΤΑΙΡΙΑΣ
ΠΛΑΝΗΤΗΣ ΓΗ: Γεωλογικές Διεργασίες και Βιώσιμη Ανάπτυξη

12th INTERNATIONAL CONGRESS OF THE GEOLOGICAL SOCIETY OF GREECE
PLANET EARTH: Geological Processes and Sustainable Development



ΦΥΣΙΚΕΣ ΚΑΤΑΣΤΡΟΦΕΣ / NATURAL HAZARDS

ASSESSMENT OF THE VULNERABILITY DEGREE OF DIFFERENT LITHOLOGICAL FORMATIONS IN THE CATCHMENT AREA OF AGIA EIRINI GORGE, WESTERN CRETE

Bizoura A.¹, Lykoudi E.², Spyridonos E.³, and Manoutsoglou E.⁴

¹ Technical University of Crete, Department of Mineral Resources Engineering, 73100 Chania, Greece, katbizou@diamond.mred.tuc.gr

² National Technical University of Athens, School of Mining Engineering and Metallurgy, Department of Geological Sciences, 15780 Athens, Greece, elykoudi@metal.ntua.gr

³ National and Kapodistrian University of Athens, Faculty of Geology and Geoenvironment, Department of Dynamic, Tectonic & Applied Geology, 15784 Athens, Greece, vangelis@zedat.fu-berlin.de

⁴ Technical University of Crete, Department of Mineral Resources Engineering, 73100 Chania, Greece, emanout@diamond.mred.tuc.gr

Abstract

This paper presents a methodology for assessing the degree of vulnerability of different lithology formations constituting the drainage basin of the gorge of Agia Eirini. The methodology is based on the processing of spatial aspects parameters of lithology, hydrography, geomorphology and the vegetation cover, which are related with the weathering impact on formations either directly or indirectly.

Initially a series of primary spatial data on geology, topography, the river network and the land use in the region, were used to produce thematic maps. These maps include the geological map, the digital terrain model (DTM), the map of the land use, and hydrographic maps of density and frequency. By processing the data according to their role in enhancing the vulnerability of formations, the data were determined and the following thematic maps: "Map of geological formations susceptible to weathering", "Map of hydrographic texture", "Map of morphological inclinations" and "land use map protecting against the loss of disintegrated material were produced. By appropriate combination of these secondary data, areas of vulnerability of formations were recorded which are shown on a final thematic map. This information is particularly valuable in the management planning and gives the opportunity to evaluate and predict the impact of various proposed projects or future scenarios. They can also be used to identify positions to take necessary measures to protect areas at high risk of loss of material.

Key words: *vulnerability, drainage basin, weathering, Agia Eirini gorge, West Crete*

1. Introduction

Management planning of natural resources is a necessity nowadays. In this context with the possibilities offered by modern information systems, a methodology for assessing the vulnerability of the formations constituting the drainage basin of the gorge of Agia Eirini was implemented.

In recent years, the increasing development of Geographical Information Systems (GIS) has provided powerful tools for the collection, storage, analysis and presentation of geographically oriented data. The possibility of management of such georeferenced data has made the GIS a powerful decision support tool.

We set up a database for the drainage basin of the gorge of Agia Eirini. By processing spatial aspects of lithology, hydrography, geomorphology and the vegetation cover, we assessed the vulnerability of the formations constituting the catchment area of the gorge. Lithology, hydrography, geomorphology and the vegetation cover are different parameters related to weathering. The analysis of their significance and the appropriate combination of those parameters provided a thematic map of the vulnerability degree of the formations.

The gorge of Agia Eirini is located on the west side of the White Mountains (Fig. 1). It belongs to the Selino province of the Chania Prefecture. The gorge is one of the most famous gorges of Crete and is a multiply protected area (part of the “White Mountains” National Park, “Natura 2000 Area”, “Important Bird Area” and “Special Protection Area”). It consists of metamorphic carbonate rocks of the Trypali unit, a formation of Triassic age, and the Phyllite unit formations.

2. Geological setting

Today, the island of Crete is located north of the Hellenic trench. The geological framework consists largely of nappes of contrasting lithologies and metamorphism that were stacked southwards during an Oligocene to early Miocene N-S compression. Most of the whole nappe stack of continental Greece is recognized in Crete. It has however a reduced thickness and more important shortening. The nappes are stacked from top to bottom, i.e. from the most internal to external units in the following order: Asterousia nappe, Miamou nappe, Arvi nappe, Pindos-Ethia nappe, Tripolitza nappe, Phyllite nappe and Trypali nappe. The Plattenkalk Group represents the lowermost known tectonic unit beneath the nappe pile of Crete and their formation has been involved in the tectonometamorphic process during the Oligocene-Miocene.

The complexity of the geological structure and access difficulties, due to the high topographical relief and thin infrastructure, are the main reasons that in Western Crete, the existing geological maps are dated back in the 1960's; whilst for some parts, as the area of Palaiochora the basic geological map has just been published. Although a number of geoscientists have worked and published papers regarding the wider area (e.g. Manutsoglu et al. 1999; 2001; 2003), the gorge in particular has recently become subject of systematic studies (Bizoura et al. 2004; 2006).

According to these researchers, on the map region, apart from the Quaternary and Neogene sequences, parts of the Tripolis series are found, consisting of Jurassic and Cretaceous limestone, eastern of the southern end of the gorge. On the northern and western part of the region, grey and white dolomitic marbles appear, containing a characteristic bituminous horizon of 2-3 m thickness, which are tectonically positioned over the underlying formations. The marbles are locally similar to the crystalline Plattenkalk limestones, but without flints. These are the Trypali unit limestones (Creutzburg & Seidel, 1975), of no later than Middle Triassic age, the tectonological position of which is known (always thrust over the Plattenkalk group) but their paleogeographical position is unknown and has been subject of long scientific controversies.

The underlying unit is build by rocks of the Plattenkalk-Group. The first detailed lithostratigraphical description, which revised the dating on the geological map (Carboniferous-Perm), was prepared by Fytrolakis (1980) and was supplemented by Soujon et al. (1998).

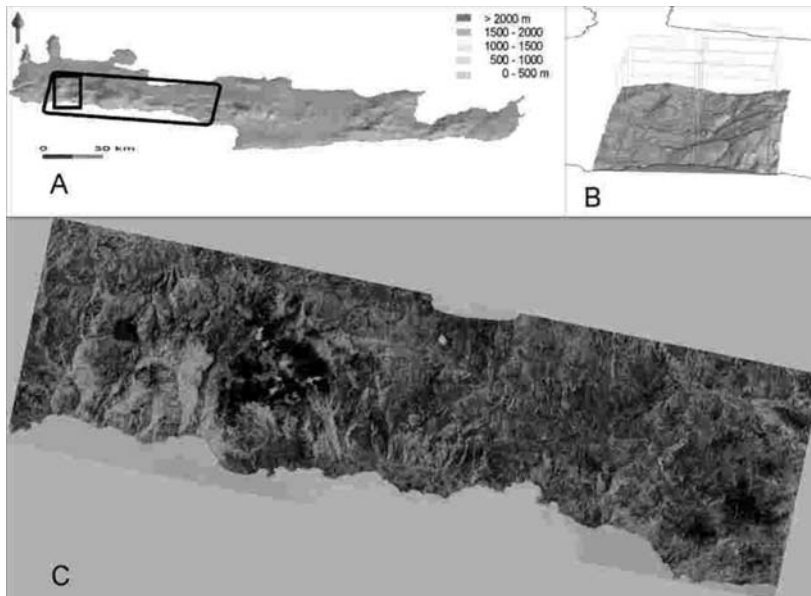


Fig. 1: A: Geographical position of the study area. B: Projected orthophoto maps of the study area & C: Landsat - TM (Scene 182-35, UTM Zone 35, Zones 742 RGB).

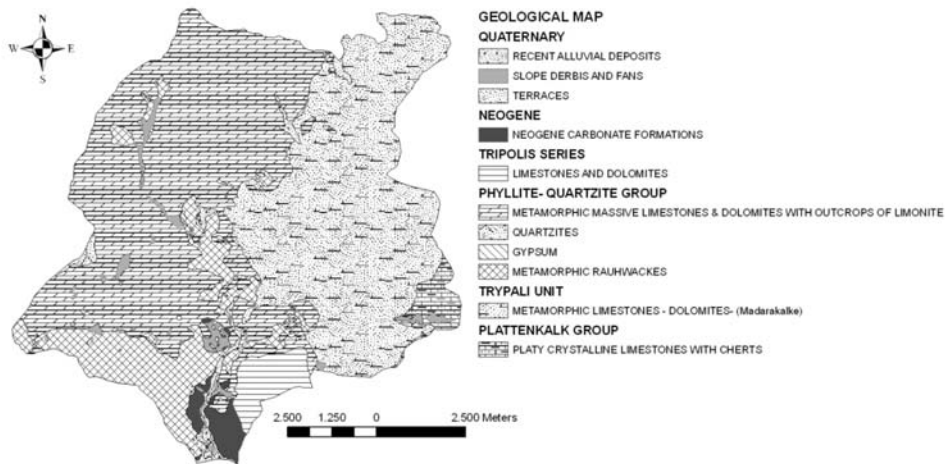


Fig. 2: Digitized geological map after Tataris et al., (1969) of Agia Eirini drainage basin.

The wider research area is part of a mega-structure, that determined the morphotectonical evolution of the region during the Neogene and the Quaternary. The visible core of this structure is the Gigilos mountain peak, on the northern part of the Samaria gorge, which is build by the older rocks of the Plattenkalk series (Manutsoglu et al, 2003). On both sides of this peak the strata dipping is changed, for the overlying formations, for the Plattenkalk group and for the rocks of the overthrust Trypali unit, while maintaining a similar direction of NNE-SSW. On the NW side of the Samaria gorge, the overlying formations have undergone intense tectonic movement, forming a tectonic breccia of considerable thickness. This mega-structure dips towards NE.

As a result of this dipping, at the SW part of the Samaria Gorge the formations of the underlying Plattenkalk unit are not present; instead the metamorphic carbonate rocks of the Trypali unit appear. The contact is tectonic and is characterized by the existence of tectonic breccia, which locally exceeds 2 m thickness. The nappe thickness at this location is no more than 50 m, but to the west it is more than 200 m. The Agia Eirini gorge evolved in this fractured metamorphic carbonate sequence of large thickness. In the I.G.M.E. geological map (Tataris et al., 1969), the gorge is shown to evolve entirely in the Trypali unit metamorphic rocks. However, field work revealed that also metamorphic rocks of the Plattenkalk group appear in the gorge, which are not shown in the map, probably due to its scale (1:50000). The appearance of the tectonically lower unit is of significant importance for the explanation of the formation of the gorge, which simply evolved along a fault zone. To exhibit all these data, a three dimensional morphotectonical - geological model has been constructed (Manutsoglu et al., 1999).

3. Data and results

3.1 Data

The basic aim of this work was the assessment of the vulnerability degree of different lithological formations in the drainage basin of Agia Eirini gorge. The gorge comprises the Quaternary and Neogene formations, the carbonate rocks of the Tripolis series, the Plattenkalk Group, the rock of the Trypali unit and the Phyllite –Quartzite group (Fig 2).

For the attainment of this aim, the following data were used:

- geological map, 1:50.000 scale (Alikianos sheet), by the Institute of Geology and Mineral Exploration (I.G.M.E.),
- topographical map, 1:50.000 scale (Vatolakkos sheet), by the Hellenic Military Geographical Service (H.M.G.S.),
- digital map of the Cretan region with 20 -meter elevation contours,
- land use map, 1:100.000 scale of the European program CORINE land cover,
- data and records acquired from field work conducted in the study area.

For the storage, processing and analysis of the primary data, the ArcGis program of ESRI was used. With this software we set up a database for the study area. Besides primary data, the database includes secondary data as well, which were derived by the analysis and processing of the raw data and by all studies conducted in the area. The secondary data include the digitized geological map (which is supplemented with details from field work), the digitized river network, the digital terrain model, the map of morphological gradients, maps of the hydrographic frequency and density etc.

The vulnerability degree of the geological formations in the basin of Agia Eirini resulted from a combination of four variables. These variables are related with the weathering impact on formations either directly or indirectly and they can be displayed spatially (Marinos et al. 1998, Alexouli – Livaditi et al. 2002, Lycoudi & Scarpeli 2006), with the production of the following thematic maps:

- map of geological formations susceptible to weathering,
- map of morphological inclinations,
- map of hydrographic texture,
- land use map protecting against the loss of disintegrated material.

The combination of the above maps (based on their impact to weathering) produced maps dis-

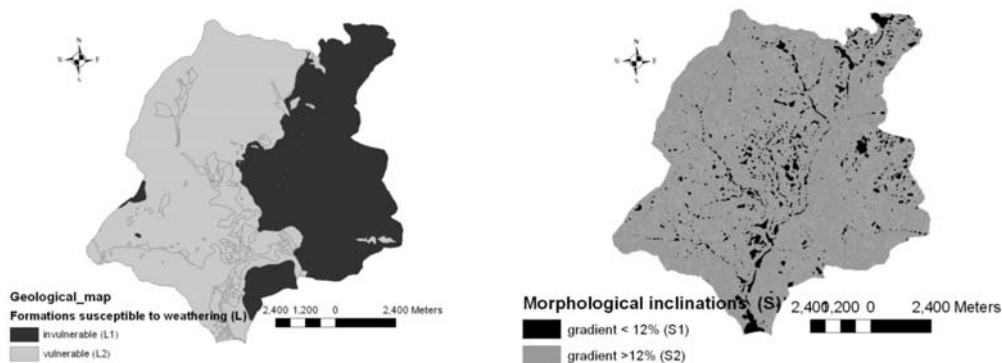


Fig. 3: a) Map of geological formations susceptible to weathering (L). b) Map of morphological inclinations (S).

playing the vulnerability degree of the formations and, thus, the risk of material loss. With this method we constructed two applications: with and without the vegetation cover factor.

3.2 Data analysis and results

Based on geological, hydrogeological and hydrolithological (permeability) information, the digitized geological map was converted into the map of geological formations susceptible to weathering (L) (Fig 3a). In especial this conversion was based on the stone composition, the degree of transformation, and qualitative data from field work related to the weathering mantle observed.

The formations were classified into two categories. The first one comprises formations rather invulnerable with little disintegrated mantle thickness (L1). The second one contains the vulnerable formations with thick disintegrated mantle (L2). The first group (L1) comprised the carbonate rocks of the Tripolis series, the Plattenkalk Group, the rock of the Trypali unit and quartzite parts of the group of Phyllite -Quartzite. Group (L2) consisted of almost all the Phyllite -Quartzite series and the Quaternary and Neogene formations.

From the digitized topographic map of the region we created the digital terrain model (DTM) by using the ArcGis software. With further processing the DTM model, the morphological inclination map was produced. This map was classified depending on the gradient of slopes and two categories were distinguished. The first category (S1) includes areas with slopes of less than 12% and the second group (S2) areas with slope greater than 12% (Fig 3b).

The watershed and the drainage network of the study area were digitized and sorted according to Strahler (1964) classification. The drainage network and, therefore the basin of the gorge of Agia Eirini are of the fifth class. Then, the lower order basins of the 4th and the 3rd class were digitized and the values of the hydrological frequency and density were calculated for all the basins. The drainage density (D_u) of an order u drainage network is “the ratio of the total length of all branches of the river network of a u order basin to the area of this basin” (Horton 1945). Drainage frequency (F_u) of an order u drainage network is “the ratio of the total number of branches of an order u basin to the area of this basin” (Horton 1945). In a river network, the tex-

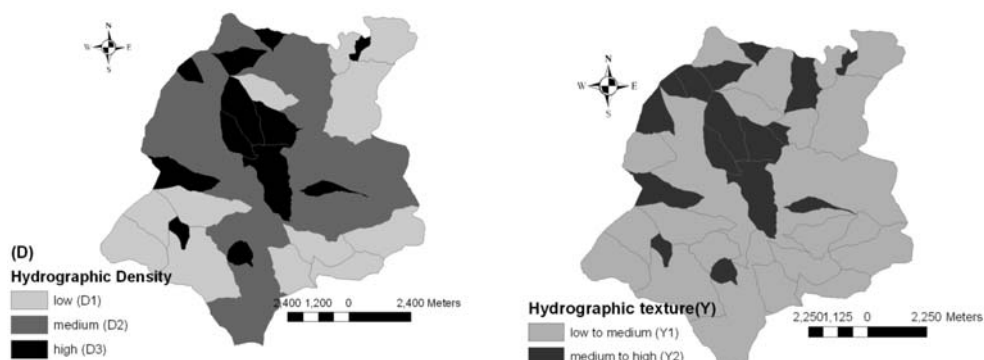


Fig. 4: a) Map of hydrographic density (D). b) Map of hydrographic texture(Y).

Table 1. Categorisation of vulnerability factors

1) Geological formations susceptible to weathering (L)	invulnerable L1: limestones, dolomites, quartzites etc.	vulnerable L2: contemporary silting, colluvial deposits, phyllites etc.	
2) Morphological inclinations (S)	S1: <12%	S2: >12%	
3) Hydrographic texture (Y)	Low to medium Y1: Combination of F1, F2 and D1, D2	Medium to high Y2: Combination of F2, F3 and D2, D3	
3a) Hydrographic frequency (F)	low F1: $F \leq 6,81$	medium F2: $6,81 < F \leq 9,32$	high F3: $9,32 < F$
3b) Hydrographic density (D)	low D1: $D \leq 2,82$	medium D2: $2,82 < D \leq 3,44$	high D3: $3,44 < D$
4) Land use/vegetation cover (C)	C1: sparse shrubs, grasslands and areas with little or no vegetation	C2: olives and agricultural areas	C3: forests

ture is determined by the growth sectors of the drainage basin and depends on the parameters of the drainage density and of frequency. The drainage basin area of the gorge is 100 km².

We created the map of hydrographic texture from the maps of hydrographic frequency (F) and hydrographic density (D) (Fig. 4a). According to Table 1, the study area was divided into three categories of hydrographic density and frequency: high, medium and low, D1, D2, D3 and F1, F2, F3, respectively. The combination of these categories provided the “hydrographic texture map”, which comprised two categories of areas: a) with low to moderate texture (Y1) and b) with moderate to high texture (Y2) (Fig. 4b).

The first category includes areas with medium and low values of frequency and density and the second category areas with high and medium values of frequency and density.

Table 2. Classification of vulnerability provided by the combination of the first three thematic maps (without the vegetation cover factor)

VULNERABILITY WITHOUT THE VEGETATION COVER FACTOR				
Vulnerability	(Low) T1	(Low to medium) T2	(Medium to high) T3	(Very high) T4
	L1,S1,Y1	L1,S1,Y2 & L1,S2,Y1 & L2,S1,Y1	L1,S2,Y2 & L2,S1,Y2 & L2,S2,Y1	L2,S2,Y2
Area (km ²)	4,21	36,49	44,71	14,59
Percentage (%)	4,21	36,49	44,71	14,59

Taking into account the three final maps of the first three thematic sections, described above, -map of geological formations susceptible to weathering (L), map of morphological inclinations (S) and map of hydrographic texture (Y)- a new map was produced. This was the map of formations vulnerability and risk of material loss (T), based on lithological and geomorphological criteria but without taking into account the factor of vegetation cover (Fig. 5a). The combination of those three thematic maps, led to determination of the study area into four zones of vulnerability (table 2).

Extending the investigation of the influence of various factors on the vulnerability of the formations and creating a simulation model of vulnerability led to taking another factor into consideration. The vegetation cover factor was categorized according to “Corine” land use map and field observations. Three groups of vegetation cover were distinguished: a) sparse shrubs, natural grasslands and areas with little or no vegetation (C1), b) olive groves and other agricultural areas (C2) and, c) forests (C3) (Alexouli-Livaditi & Livaditis 1997, Alexouli-Livaditi et al. 2002).

The protection offered by vegetation, is clearly dependent on the type of vegetation. The greatest protection is provided by thick forests and dense bushes. Less protection is offered by sparse woods and various crops. Areas with no vegetation are totally unprotected (Kotoulas 1985).

Combining information of the vulnerability and vegetation cover maps produced the “vulnerability map of the lithological formations and of risk of material loss considering the vegetation factor“ (ST). (Fig. 5b), It also produced the determination of the research area into four zones of vulnerability (table 3).

Table 3. Classification of vulnerability provided by combination of the four thematic maps (with the vegetation cover factor).

VULNERABILITY WITH THE VEGETATION COVER FACTOR				
Vulnerability	(Low) ST1	(Low to medium) ST2	(Medium to high) ST3	(Very high) ST4
	Combination of T1 & C1,C2,C3 T2 & C3	Combination of T2 & C1,C2 T3 & C3	Combination of T3 & C1,C2 T4 & C3	Combination of T4&C1,C2
Area (km ²)	15,96	27,95	41,85	14,24
Percentage (%)	15,96	27,95	41,85	14,24

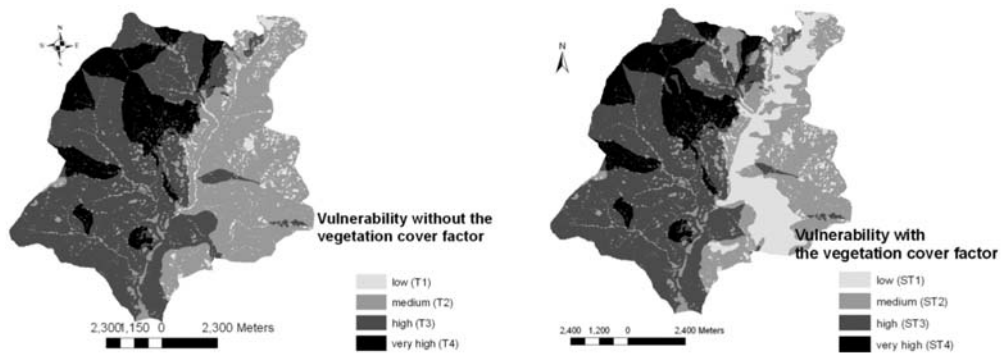


Fig. 5: Map of vulnerability without the vegetation cover factor. b) Map of vulnerability with the vegetation cover factor

4. Conclusions

Sustainable management of protected areas requires good knowledge of the entire system and effective tools. Setting up a GIS with the possibility of spatial and qualitative assessment of the potential loss of disintegrated material is a powerful tool essential for the management and protection of natural ecosystem of Agia Eirini gorge.

In this work the appropriate combination of a series of maps produced thematic maps presenting the vulnerability of the basin formations of the gorge of Agia Eirini and the risk of losing the disintegrated material. The results of this process can be a guide to monitoring and sustainable environmental management of the basin of the gorge of Agia Eirini.

The existence of this information in a GIS has a lot of advantages. Besides the possibility of future adjustments and all the advantages of a digital database, the proposed method of spatial estimation of material loss could be used to predict the impact of future changes (e.g. land use changes) or in disaster scenarios (e.g. destruction of plant cover due to fire) and define the effects of those changes on the natural environment.

Identifying high risk positions gives the opportunity to take protecting measures and prevent the environmental impact. Moreover this method is necessary for the application of the Water Framework Directive 2000/60 and for the spatial planning of land use.

5. References

- Alexouli-Livaditi, A. & Livaditis, G. 1997. Investigation and delineation of the areas where intense erosion and mass wasting may occur at Tinos Island, Greece, *International Symposium Engineering Geology and Environment*, pp. 25-29, Balkema, Rotterdam.
- Alexouli-Livaditi, A., Livaditis, G. & Lykoudi, E. 2002. Evaluation of geological formation erodibility and sediment production in Lesvos island, *6th Panhellenic Geographical Conference*, Thessaloniki.
- Bizoura K., Manutsoglu E. & Spyridonos E. 2004. Visualization with GIS of Agia Eirini gorge at the southern margins of the White Mountains, *Bulletin of the Geological Society of Greece vol. XXXVI/2, Proceedings of the 10th International Congress*, Thessaloniki, 1018-1025
- Bizoura K., Manutsoglu E. & Spyridonos E. 2006. Analogical and digital geological map of Agia

- Eirini gorge at the southern margins of the White Mountains, SW Crete *Proceedings of the 8th national Congress of Cartography*, Thessaloniki, pp. 459-468
- Creutzburg N. and Seidel E. 1975. Zum Stand der Geologie des Preaneogens auf Kreta. *Neues Jahrbuch Geologie und Palaeontologie Abhandlung*. Vol. 198, pp. 363-383.
- Fytrolakis N. 1980. The geological structure of Crete. *NTU Athens*. pp. 146.
- Horton, R., 1945. Erosional development of streams and their drainage basins: hypsographical approach to quantitative morphology”. *Geol. Soc. Amer. Bul.* 54, pp. 275-370.
- Kotoulas D, 1985. Control of torrential currents, *University press*, Thessaloniki, pp267-293.
- Lykoudi, E., Scarpeli S. 2006. The map as a tool of analysis in soil erosion. Application to Evrotas basin, *Proceedings of the 9th national Congress of Cartography*, Crete Chania.
- Manutsoglu E., Jacobshagen V., Spyridonos E. and Skala W. 1999. Geologische 3D-Modellierung der Plattenkalk-Gruppe West-Kretas (Erste Ergebnisse). *Mathematische Geologie*, Vol. 4, pp 73-79.
- Manutsoglu E., Spyridonos E., Soujon A. and Jacobshagen V. 2001. Revision of the geological map and 3D modelling of the geological structure of the Samaria gorge region, W. Crete, *Bulletin of the geological Society of Greece*, Vol. XXXIV/1, pp. 29-36.
- Manutsoglu E., Soujon A. & Jacobshagen V., 2003. “Tectonic structure and fabric developmant of the Plattenkalk unit around the Samaria gorge”, Western Crete, Greece. *Z. dt. geol. Ges.*, 154/1, pp. 85-100.
- Marinos P., Plessas S., & Baladaki-Plessa K. 1998. Thematic maps on the risk evaluation against erosion, and sediments production in Attica, *Bulletin of the 4th National Geographical Symposium*, pp. 584-616, Athens.
- Strahler, A., 1964. Quantitative geomorphology of drainage basins and channel networks. In: Chow, V. (ed.) *Handbook of applied hydrology*, Section 4-II, pp. 39-76, McGraw-Hill Book Co., New York.
- Soujon A., Jacobshagen V. and Manutsoglu E. 1998. A lithostratigraphic correlation of the Plattenkalk occurrences of Crete (Greece). *Bulletin of the geological Society of Greece*, Vol. XXXII/1, pp. 41-48.
- Tataris A. and Christodoulou G. 1969. Geological map of Greece, 1:50.000, Vatolakkos sheet”, *I.G.M.E.*, Athens.

FLOOD HISTORY ANALYSIS AND ITS CONTRIBUTION TO FLOOD HAZARD ASSESSMENT. THE CASE OF MARATHONAS, GREECE

Diakakis M.¹

¹Department of Geology and Geoenvironment, National and Kapodistrian University of Athens 15784 Athens, Greece, diakakism@geol.uoa.gr

Abstract

Flood history analysis contributes decisively to a more realistic assessment of flood hazard. In this work, systematic data collection on past flood events in Marathonas area (Attica, Greece) together with the development of a database, allowed the thorough study of flooding phenomena and their evolution over time. The study area consists of three dominant catchments with rich flooding history, namely Rapentosa, Charadros and Kato Souli. Information gathered from governmental and insurance organizations, emergency agencies, the press, field interviews and other documentary sources, along with geomorphologic and geologic evidence, were stored, structured and analyzed in a GIS platform and were used to reconstruct flood events with detail. Valuable results were produced concerning the causes, the characteristics, the spatial distribution of damages and the extent of inundation for each event. Moreover, the rate of recurrence of flooding phenomena was calculated across the floodplain, so that the areas of higher risk were identified and delineated. The active part of the floodplain was outlined and its migration overtime was studied. Furthermore, the methodology underlined the imperfections of the existing risk mitigation strategy and the past emergency experiences were appraised in a way that they highlight the priorities and will help improve management of future situations of risk.

Key words: flood hazard, flood history, Marathonas, flood frequency, Marathon, Attica, Greece.

1. Introduction

In many parts of Greece flooding occurs in small, flash flood prone watersheds drained by ephemeral water courses with little or no water at all for most of the year. In this context and given the scarcity of instrumental hydrological records, classic hydraulic modeling may not be adequate in assessing flood hazard. Thus, the use of alternate methods becomes necessary for a better understanding of the flooding processes and the mitigation of the associated risk. Analysis of flooding history is a technique that can produce results within these limitations. Historical flood records have been used in the past in the Mediterranean region (e.g. Garcia & Garcia 2003) and around the world (Benito et al 2004, Hergert & Meurs 2007) to improve the knowledge in the field of hydrological extremes. Historical flood analysis focuses on identifying hazard areas based on careful reconstruction and examination of past flood events. The objective of this work is to outline a methodology that contributes to an in depth appraisal of the flooding problem in a specific area, in this case Marathonas in Greece, regardless the availability of instrumental records.

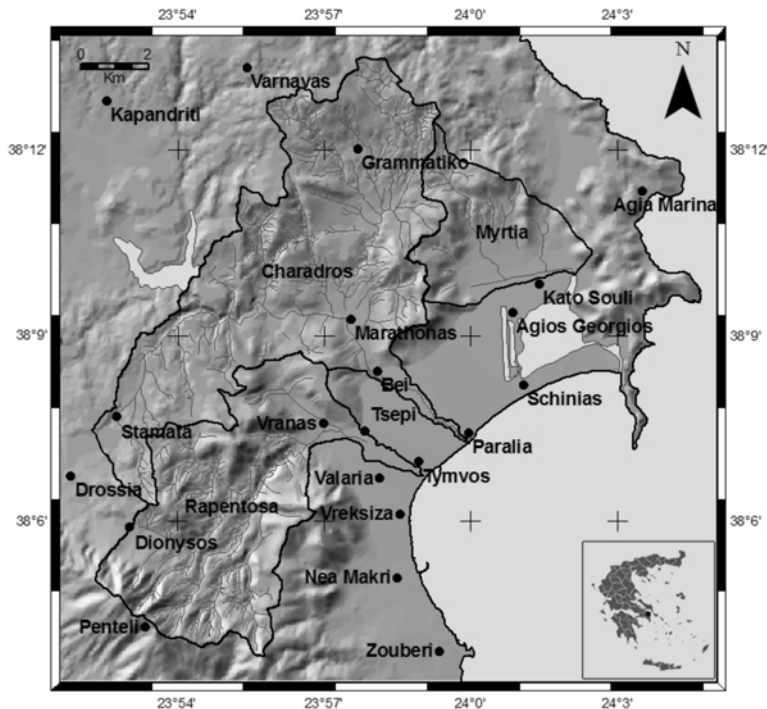


Fig. 1: Map showing the three catchments, the drainage network and the main settlements and landmarks. At the north east part of the map Myrtia borders with Charadros, which in turn borders with Rapentosa catchment from the south.

2. Background

2.1 Setting

The study area lies in the north-east part of Attica in Greece and consists of three relatively small catchments, namely Rapentosa, Charadros and Myrtia (Kato Souli). In terms of geomorphology, it comprises of a hilly area, with steep slopes and the famous for its battle plain of Marathonas, through which the drainage networks flow into the sea. The area is inhabited by approximately 8000 people with Marathonas and Kato Souli being the most important settlements.

The southernmost catchment (37,5 km²) is drained by Rapentosa torrent and borders with Nea Makri from the south and with Charadros catchment from the north. The drainage network reaches the north side of Penteli and Dionysos and runs off, forming a steep gorge, into Marathonas plain and through Vranas settlement. At present the torrent is drained at the last part of its course by an artificial underground waterway. Bordering from the north with Rapentosa, Charadros is the largest of the 3 catchments, even though its drainage area was reduced to 60,2 km² after the construction of Marathonas' dam in 1929. It reaches the sea at the central part of the plain, passing between Kotroni and Stavrokoraki hills and through the modern village of Marathonas. The third and smallest catchment (15,2 km²) is drained by Myrtia torrent, a poorly developed drainage network which flows into a marsh, lying on the north-east part of the plain. The water, leaving the hilly area drains into artificial channels until it reaches the swamp and subsequently the sea through a manmade canal. All three catchments are dry for most of the year.

In terms of geology, the study area consists of a series of Mesozoic formations, accompanied by postalpine Cenozoic sediments. From base to top, one can distinguish lower-middle Triassic marbles followed by Northeastern Attiki Schist formations with marbles intercalations of Jurassic age and Northeastern Attiki Marbles of Cretaceous age. Upper Miocene breccioconglomerates and fluviolacustrine formations can be found on top of the Mesozoic series. Fine grained fluvial deposits of Pleistocene age are abundant Charadros banks. The plain is dominated by Holocene alluvial deposits accompanied by some talus cones.

2.2 Previous works

Historical flood records have been used in the past for the study of flood risk. Potter (1978) first suggested that the past behaviour of a river is a very important ingredient in all hydrological investigations and can be exploited thoroughly with the use of information contained in historical records. Bayliss and Reed (2001) proposed flood history study as an alternative practice to improve our knowledge on hydrologic extremes. Glaser and Stangl (2003) suggest that historical records are an important source for the evaluation of frequency of such events. Both Potter (1978) and Bayliss and Reed (2001) recommended periodical journals, newspapers, chronicles, specialists reports, government databases, pictures, the world wide web and other various sources as a basis for information mining. Barriandos et al (2003) suggested local and central government, church and private collections and notarial archives as good sources of information.

Previous works exploited documentary data to provide further understanding on the flooding problem of several places. Glaser and Stangl (2003) studied extreme inundation events in central Europe since 1300 using documents dating back to the middle ages and other anecdotal evidence. In their study they connected flood occurrence with historic climate and atmospheric patterns. Macdonald et al (2003) used documentary data, newspapers, epigraphic records and eyewitness observations along with instrumental records in order to examine the flood-generating mechanisms of river Ouse in UK. In their study they reconstructed flooding history since 1600AD and suggested that its analysis can improve understanding of flood risk considerably. Herget and Meurs (2007) studied past extreme events in the city of Cologne in Germany with the help of written descriptions, paintings and other evidence and recreated peak river discharges for historical floods. Past flood data were also utilized to project the evolution of flooding in time and space. Conesa Garcia and Garcia Garcia (2003) used anecdotal evidence to reconstruct flooding history of Cartagena, in Spain, identifying high and low risk locations.

Documentary hydrological data have been correlated in the past with flood event frequencies to improve risk prevention and readiness. Bayliss and Reed (2001) studied the case of river Avon at Worcestershire and suggested that it is essential in flood risk studies to review flood frequency curves by augmenting existing data with the use of historical records. Agasse (2003) collected data from the press, official telegrams, unpublished reports and interviews with local people and reconstructed Normandy's flooding record during 17th to 20th centuries. In this study Agasse examined the trends of flood frequency and intensity. Williams and Archer (2002) collected data from unpublished reports, meteorological magazines and websites to reconstruct floods in the English Midlands. In their study, they demonstrated how flood history improves risk assessment as it is carried out through the use of conventional hydrometric record. Benito et al (2004) suggested that systematic and non-systematic data can be combined to improve flood frequency analysis with direct impact on flood risk assessment.

3. Data

The basic concept of examining flooding history is the collection of information about every single event recorded, followed by data structuring and analysis with specific techniques. Therefore, the starting point of this investigation was the identification of data sources.

3.1. Data types and sources

As far as local government organizations are concerned, the Prefectural Administration of East Attica provided detailed reports about flood damages on infrastructure, including damaged property owners' accounts, description of locations, of water height and extent. The municipality of Marathonas provided documents and verbal descriptions of past events. Information was also gathered from central government organizations, i.e. the General Secretariat of Civil Protection and the Earthquake Rehabilitation Service, in the form of maps demarcating flood zones and districts that were hit in the past. Greek Fire Department provided a database of emergency incidents concerning flooding in the area, reporting locations, time and type of event. Data on damages on agriculture were collected from the Hellenic National Agricultural Insurance Organization along with damage type and time specifications. National and local newspapers and were researched in depth for articles describing flood damages and conditions. Their archive was easily accessible and of very good quality and coverage through the years. World Wide Web was proved an excellent guide to locate information sources and damage compensation mandates. Pictures and videos obtained from national channels, newspapers, websites and local residents were exceptionally revealing of the conditions of flooding. Details on damages and observation on water stage and extent were collected by interviewing local people. Data were also collected from the Archaeological Society at Athens which contained a considerable amount of information in the form of diaries and written descriptions due to the continuous presence of researchers since the 19th century.

3.2. Data compilation

Since the ancient years the plain was notorious for its floods. Charadros became proverbial for its fierce floodwaters in ancient local societies (Hammond 1968). Locally, the river god was worshiped as the lord of the violent force of Charadros (Sekunda 2002), showing a form of primitive knowledge concerning the local flooding phenomena. However, the first detailed description of a flood event comes from Leake (1841). In his work, he describes a violent flood that washed away many houses in the settlements of Marathonas and Bei in the autumn of 1805, changing the landscape completely. The events occurred after Rapentosa and Charadros torrents inundated large areas of the plain. Leake (1841) also mentions that Charadros and Rapentosa are noted for their 'occasional impetuosity' and that the plain is usually subject to inundations from the two torrents ('particularly Charadros'). Davidson (1880) describes a flash flood in 1879 that carried away a lot of material from the banks of Charadros from the inner parts of the plain to the sea. Hughes (1901) also notes the strong effect that flooding from Rapentosa and Charadros has on the plain morphology and the amount of material deposited there during extreme events. The first captured picture of a flood in Marathonas comes from Charadros (in 1926) showing high velocity waters, damaging structures and equipment that were used at the time for the preparations of the construction of Marathonas dam (EYDAP 2003). Sotiriadis during his archaeological investigations (1925-1937) noted that although the two main torrents are dry even in the winter, the plain is "occasionally inundated" (Sotiriadis 1933). In 1959 (July the 3rd) overflowing of Rapentosa torrent hit the plain damaging crops and drowning animals (Empros 1959). Almost a decade later Hammond (1968) notices that Charadros and Vranas overflow occasionally transporting large amounts of materials on the plain and to the sea.

In 21st of October 1979, Kato Souli and Agios Georgios flooded after a high intensity rainfall, leading to approximately 1600m² of damaged crops. The event was accredited then to a debris-clogged canal in the Kato Souli area. In 1980 (October 27th) Rapentosa inundated its banks, leading to one casualty, two injured people, many damaged cars, houses and crops in Vranas village. Unfortunately, although these two events were covered extensively by the press at the time and are very well known to the local community there are no official government documents survive today. However, numerous detailed reports can be found in 1979 and 1980 newspapers articles database (Nea 1979, Apogevmatini 1980).

After 1987 the data and the descriptions become more detailed. The archive of the Prefectural Administration of East Attica (2007) contained ten floods events accompanied by detailed descriptions of damages and locations. The database of the Hellenic National Agricultural Insurance Organization (2007) for the study area, contained eight flood events that damaged agricultural land or equipment and detailed information on extent, location, cost and time of damages recorded. The events

Table 1. Flood events in the area of study based on the records of the Prefectural Administration of East Attica (2007) and the Hellenic National Agricultural Insurance Organization (2007).

<i>Recorded flood events</i>			
<i>Event Date</i>	<i>Locations that suffered damages (shown in fig. 1)</i>	<i>Damages in buildings and infrastructure</i>	<i>Damages in agriculture</i>
12th Nov. 1987	Patitiria, Tsepi, Vranas, Tymvos, Valaria and Paralia	No detailed record	No record
26t Feb. 1988	Vranas, Patitiria, Tsepi, Valaria, Paralia and Tymvos	No detailed record. Approximately 30 houses, 20 vehicles	No record
27th Jan. 1996	Paralia, Valaria and Patitira	2 businesses, fencing in some houses, road network, public utilities	No record
12th Nov. 1998	Patitira, Tsepi and Valaria	10 buildings and the road network	No record
20th Nov. 1998	Patitiria, Tsepi, Tymvos and Valaria	2 buildings and the road network	No detailed record
27th Mar. 1999	Patitiria, Vreksiza, Tymvos and Valaria	No record	11 businesses, truck farms
14th Jan. 2001	Patitiria, Vranas, Tsepi, Paralia, Bei, Kato Souli, Rizari, Tymvos	9 buildings (household utensils and parts of the structure), many vehicles	42 businesses greenhouses, olive groves, truck farms
3rd Nov. 2001	Vranas, Tsepi, Valaria, Bei, Paralia, Marathonas and Tymvos	18 buildings, some vehicles and the road network	33 businesses, greenhouses, olive groves, truck farms
14th Dec. 2002	Valaria, Tsepi and Patitiria	No record	9 businesses, mainly greenhouses
26th Jan. 2003	Vranas, Tsepi, Rizari, Bei, Patitiria, Agios Georgios	6 buildings, road network and the sewerage system	21 businesses, mainly truck farms
16 Sep. 2005	Kato Souli, Agios Georgios, Marathonas village, Patitiria, Tsepi, Paralia, Rizari and Bei	Only minor damages to some buildings and fencing	21 businesses, mainly greenhouses
23 Nov. 2005	Patitiria, Tymvos, Tsepi, Valaria, Marathonas village, Plasi, Paralia, Kato Souli and Agios Georgios	10 buildings (houses and businesses), road network, public utilities	29 businesses, greenhouses and fields, truck farms

from these two sources are summarized in table 1.

These twelve flood events in total were confirmed by cross-referencing with the record of the Greek Fire Department (2007), the archive of the General Secretariat of Civil Protection (GSCP 2006), the record of Earthquake Rehabilitation Service (2006), articles from the Greek Parliament Newspaper Archive and television broadcasts obtained from the archive of national television stations. In some cases complementary information was collected from these sources.

4. Methods

4.1 Data analysis

Initially, upon collection exploitable and good quality information was selected from raw data and stored in a database, based on categorizing different types of evidence like water stage, extent, speed, severity and type of damage, time and duration of flooding. This step was followed by the compilation of an overall list of past flood events in the area. In a second phase, damages on structures and agriculture were plotted in a GIS environment along with evidence provided from pictures and videos to form an accurate reconstruction of every flood event between 1979 and 2008. Each one of these polygon shapes symbolizing reconstructed inundated areas, were converted to raster data with cell value of 1 for inundated locations and 0 for non-inundated locations. These raster data were subsequently mathematically added with the use of Weighted Sum tool of computer software ArcMAP 9.2 (ESRI 2008). Thus, raster cells were added with same-location cells of each flood event. In this way, the resulting raster symbolized the spatial extent of all the flood events and each cell contained information on how many times it was inundated. This very attribute provided a clear view of the flood recurrence rate for each location for the last 30 years, which was the time period with adequate data. It also allowed interesting observations on the evolution of flooding. Finally descriptions, reports and other evidence were examined to determine the main causes of the flooding problem in the area.

4.2 Geologic and geomorphologic observations

Assessment of the influence of geologic and geomorphologic features in extreme hydrological events was considered important. Therefore, factors of geology and geomorphology of the three basins were calculated in an effort to estimate in what extent they are linked to flooding phenomena. Namely mean slope and basin elongation ratio were computed due to their influence on the hydrograph form (Sith & Ward 1998), whereas basin area and geologic formations permeability due to their importance in water volume drained. In this work, geologic formations were classified in three groups based on their hydrogeological behaviour. The first group consisted of higher permeability carbonate rocks, the second of impermeable formations, like schist, and the third from post alpine porous sediments of intermediate permeability. Additionally, the channel morphometry of the three torrents was studied in order to examine the degree to which the flooding phenomena are enhanced by parameters of the drainage network like channel's morphomology and dimensions. This was carried out by field observations and by studying geologic, topographic and historical maps of the area.

5. Results

5.1 Flood history summary

Examination of the collected evidence showed a rich history of flooding in the plain of Marathonas. From ancient years until modern days the area suffered numerous incidents. Apart from the one known

Table 2. Table showing recorded flood events in the study area

<i>Flood events in Marathonas area</i>									
<i>Year</i>	<i>Date</i>	<i>Basin</i>			<i>Year</i>	<i>Date</i>	<i>Basin</i>		
		Charadros	Rapentosa	Myrtia			Charadros	Rapentosa	Myrtia
1805	Autumn	×	×		1998	November 12th		×	
1879	Autumn	×			1998	November 20th		×	
1926	Unknown	×			1999	March 27th		×	
1959	July 3rd		×		2001	January 14th	×	×	×
1979	October 21st			×	2001	November 4th	×	×	
1980	October 27th		×		2002	December 14th		×	×
1987	November 12th	×	×		2003	January 29th	×	×	×
1988	February 26th		×		2005	September 16th	×	×	×
1996	January 26th	×	×		2005	November 23rd	×	×	×

casualty and some injuries, damages included buildings (houses and businesses), agricultural land and equipment, vehicles, the road network and important infrastructure. Flooding continued through the years even though significant flood defenses were developed. Based on the compiled data, one can identify 18 distinct flood events (shown in table 2) extending back to 1805. The record is considered to be complete only after 1979, in contrast with period before this year when data coverage was not adequate. Table 2 shows all the recorded flooding incidents separately for each torrent.

5.2 Characteristics and evolution of flooding

Careful study of the events' descriptions showed a series of common characteristics like the abrupt rise of flood waters and the relatively short duration of inundation. It also showed higher water velocities around Rapentosa torrent (Vranas and Patitiria) than at Charadros (Bei and Paralia) and even lower speeds at Vreksiza, Valaria, Agios Georgios and Kato Souli. In some cases, vegetation debris and sediment content was abundant in floodwaters (Prefectural Administration of East Attica 2007), a phenomenon that can be attributed to the forest fires of 1995 and 1998 in the area. Concerning the evolution of affected areas, it is evident that before the construction of Marathonas Dam, flooding in Charadros was more frequent. Thus, after 1929 flood areas around Charadros were considerably reduced along with associated damages. It is also apparent that flooding problems in Myrtia torrent have been intensified in the last six years in the record, most probably due to the recent development of housing, road networks and other public works without appropriate sewerage.

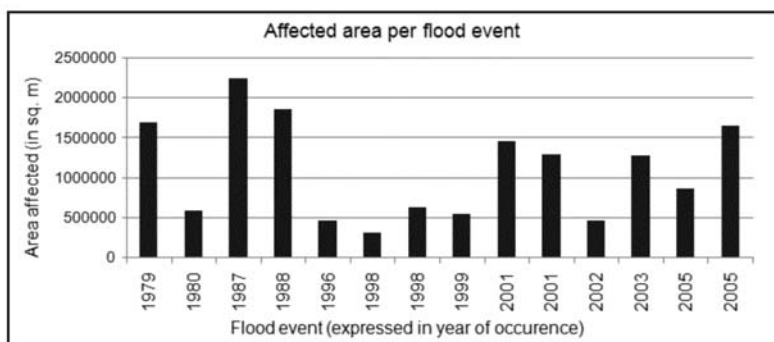


Fig. 2: Chart showing the fluctuation of affected areas in square metres through the years, for each flood event. In horizontal axis, events are expressed in year of occurrence.

Table 3. Recorded damages for compensation purposes (Prefectural Administration of East Attica 2007, Hellenic National Agricultural Insurance Organization 2007).

<i>Officially recorded damages</i>	<i>Rapentosa</i>	<i>Charadros</i>	<i>Myrtia</i>
Buildings damaged (1996-2009)	38	9	10
Damaged agricultural land (1999-2009)	802.000 m ²	78.000 m ²	287.000 m ²

Human interference with hydrologic processes is considered to have intensified flooding phenomena through blocking drainage routes towards the sea and reducing the flow capacity of channels. Such effects are evident at Patitiria and Tymvos, Paralia and Agios Georgios. Changes due to the recent development of flood defenses have to be evaluated in the long term.

5.3. Damage type and distribution

Analysis of the spatial distribution of damages, illustrates that Rapentosa (mainly Tsepi and Patitiria) are the most affected areas. In most cases damages included agricultural land and equipment, greenhouses, vehicles, buildings fencing and masonry, household utensils and loss of some domestic and livestock animals.

5.4 Flood recurrence rate

Flooding has a higher repetition rate in Rapentosa torrent (13 events in 30 years) than in Charadros (7 events in 30 years) and Myrtia catchment (6 events in 30 years). Data analysis, as described in 4.1, showed explicitly the areas with higher recurrence rate. Figure 3 illustrates these areas with a ranking based on the number of events suffered in 30 years. Thus, high recurrence rate represents areas that flooded 10 to 14 times during this period, whereas medium recurrence rate locations that flooded 5 to 9 times and low recurrence rate areas 1 to 4 times. According to this process high recurrence rate locations can be identified at Patitiria and Tymvos and medium rate areas at Valaria and Agios Georgios.

5.5 Correlation with geologic and geomorphologic data

Examination of calculated basin properties showed that higher recurrence flood rate in Rapentosa in comparison with the other two torrents is partly connected to its increased percentage of imper-

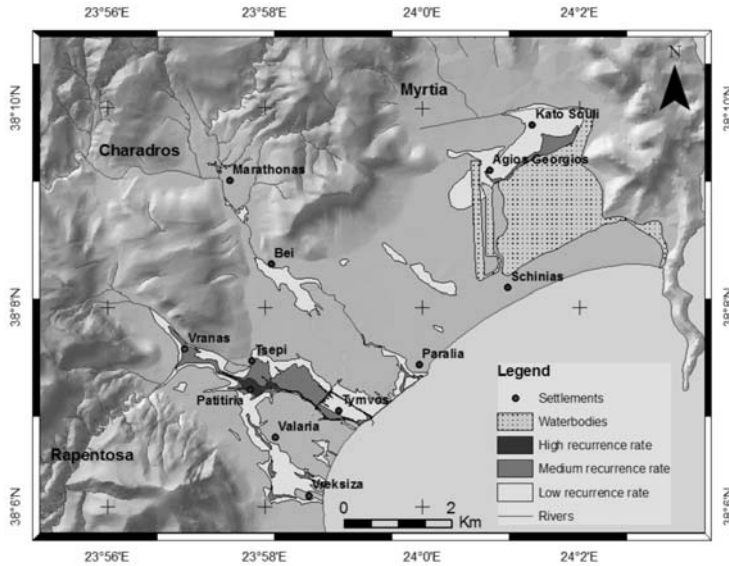


Fig. 3: Map showing the areas that flooded during last 30 years. High recurrence rate represents areas that flooded 10 to 14 times in 30 years. Medium recurrence rate stand for locations that flooded 5 to 9 times and low recurrence rate areas that flooded 1 to 4 times in the same period.

Table 4. Table showing calculated properties for the three drainage basins.

<i>Calculated basin properties</i>			
<i>Properties</i>	<i>Rapentosa</i>	<i>Charadros</i>	<i>Myrtia</i>
Mean Slope (%)	33.3	21.3	22
Area (Km ²)	37.5	60.2	11.7
Elongation Ratio	0.46	0.56	0.70
High permeability formations (% of total area)	45.4%	50.3%	58.4%
Medium permeability formations (% of total area)	13.2%	19.8%	29.3%
Impermeable formations (% of total area)	41.4%	29.9%	12.3%

meable formations and its higher mean slope value. The first attribute augments the total volume of runoff and the second increases peak flow rates, reduces the watershed's time of concentration and raises the stream power of storm runoff as it enters the plain. On the other hand, basin area and elongation ratio do not show good correlation with historical analysis results, denoting a less critical role for these parameters.

Field and map observations on the torrents' morphology suggest channel morphometry plays a very important role. As far as Rapentosa is concerned, the torrent's morphological characteristics degenerate and it eventually disappears morphologically at about 2km before reaching the sea. A careful study of older published maps and sketches shows the same regime for the last 180 years. Namely, the same setting as today appears in 1829 Leake's sketch-map (in Hammond 1968), in 1880 Kauper's map (Kauper 1889), in Hughes' sketch of 1901 (Hughes 1901), in Caspari's (1911) map, in Hellenic Military Geographical Service's (HMGS) sketch-map of 1928 (in Hammond 1968), in

Vanderpool's 1966 sketch-map (Vanderpool 1966), and in HMGS topographical maps of 1970's. This shows a natural diffusion of the channel in its last section. The point where the torrents characteristics disappear in all the maps, coincides with the higher flood recurrence rate areas (i.e. Patitiria). This regime together with the high percentage of impermeable formations and its high mean slope increases Rapentosa's natural potential for flooding in comparison with the other two watersheds. In relation with channel dimensions, field observations show that human activities have greatly affected the torrents' flow capacity. In case of Rapentosa in Vranas and Patitiria and in case of Charadros in Bei and along the coast.

6. Conclusions

Past flooding in Marathonas is a well known phenomenon in an anecdotal sense, but it has not been studied systematically. This analysis proves that Rapentosa is the most hazardous between the three torrents studied. It also shows that Kato Souli (Myrtia torrent) suffered more damages in the last decade compared to the past. The locations where more damages are concentrated are Patitiria, Tsepi, Tymvos and Agios Georgios. These areas show higher possibility to be also affected by flooding in the future. In the case of Rapentosa, human development in the course of the river, mainly in Patitira and Tsepi, augments exposure and vulnerability and obstructs local hydrologic processes in a degree to which the possibility of overflowing is increased. Hazard is further augmented due to natural basin characteristics and the drainage network's natural diffusion. Extensive development along the coast and around the marsh interferes also with drainage processes obstructing surface runoff in Charadros and Myrtia.

In this context and taking into account that high flow rates are part of a river's natural process, a significant step towards the problem's solution would be a long term policy of reducing intervention to hydrological processes. This involves of course gradual removal of human activities from the active floodplain. Meanwhile, developing flood defenses is valuable but in many cases, including the event of November 2005 in Marathonas is proved to be inadequate.

It should be also kept in mind that the methodology has a number of limitations. For example flooding phenomena are subject to natural and human induced change and therefore the method's results must not be perceived as stationary and have to be reviewed every time new knowledge is available. Moreover, quiet periods in the flood record, in some cases, may not correspond to periods lacking flood events.

This method can be used either as a standalone process or to verify results of other methodologies. Generally, examining high temporal extent historical records are a special benefit when studying rare natural disasters, especially when hydrological data are scarce. The use of such methods for reconstruction of flood history has a great potential in Greece due to the early and continuous habitation. In this work, past flooding is perceived as the result of an evolving natural experiment. In this context, flooding history analysis offers and in depth appreciation of the flooding problem and its evolution over time.

7. References

Agasse, E., 2003, Flooding from the 17th to 20th centuries in Normandy (western France) methodology and use of historical data. In *Thorndycraft, V.R., Benito G., Barriendos M. and Llasat M.C., (eds.): Palaeofloods, Historical Floods & Climatic Variability: Applications in Flood Risk Assessment*, Proceedings of the PHEFRA Workshop, Barcelona, Spain, 16-19th October, 2002, CSIC, Madrid, pp. 99-106.

- Apogevmantini 1980. *Ghild drowned in Marathonas* (in Greek). Newspaper “Apogevmatini”, October 29 1980, p.1, Greek Parliament Newspaper Archive, Athens, Greece.
- Barriendos, M., Llasat, C., Barrera, A., Rigo, T. 2003. The study of flood events from documentary sources: Methodological guidelines for historical source identification and flood characterization in the Iberian Peninsula. In *Thorndycraft, V.R., Benito G., Barriendos M. and Llasat M.C., (eds.): Palaeofloods, Historical Floods & Climatic Variability: Applications in Flood Risk Assessment*, Proceedings of the PHEFRA Workshop, Barcelona, Spain, 16-19th October, 2002, CSIC, Madrid, pp. 87-92.
- Bayliss, A.C., Reed, D.W. 2001. *The use of historical data in flood frequency estimation, Report to MAFF*, Centre of Ecology and Hydrology, Wallingford.
- Benito, G., Lang, M., Barriendos, M., Llasat M.C., Frances, F., Ouarda, T., Thorndycraft, V.R., Enzel Y., Bardossy A., Coeur, D., Bobee B. 2004. Use of Systematic, Palaeoflood and Historical Data for the Improvement of Flood Risk Estimation. Review of Scientific Methods. *Natural Hazards* 31: 623–643.
- Caspari, M. O. B., 1911. Stray notes on the Persian Wars, *The Journal of Hellenic Studies*, Vol. 31, pp. 100-109.
- Conesa-García C., García-García E. 2003. Historical evolution of the flood areas in Cartagena (South-East Spain). In *Thorndycraft, V.R., Benito G., Barriendos M. and Llasat M.C., (eds.): Palaeofloods, Historical Floods & Climatic Variability: Applications in Flood Risk Assessment*, Proceedings of the PHEFRA Workshop, Barcelona, Spain, 16-19th October, 2002, CSIC, Madrid, pp. 149-154.
- Davidson, T. 1880. The Dionysion at Marathon, *The American Journal of Philology*, Vol. 1, pp. 58-59.
- Earthquake Rehabilitation Service 2006. *Statistics: Emergency incidents and correlation with YAS archive*. Earthquake Rehabilitation Service (YAS), Ministry of Ministry of the Environment, Physical Planning and Public Works, Athens, Greece.
- Empros 1959. ‘Damages caused by the storm in Attica region’ (in Greek). Newspaper Empros, 4th July 1959, p.10, Digital Newspapers Collection, Greek National Library, Athens, Greece.
- ESRI 2008. *ArcGIS 9.2 Geographical Information System Software*. Economic and Social Research Institute. Geographic Information System, Redlands, California.
- EYDAP 2003. *Water cycle in Attica*, Athens Water Supply and Sewerage Company (EYDAP SA). [Online], <http://www.eydap.gr/media/stagonoulis/KuklosNerou/gr/024.htm> [Last Accessed: 3/9/08].
- Glaser, R., Stangl, H., 2003. Floods in Central Europe since 1300. In *Thorndycraft, V.R., Benito G., Barriendos M. and Llasat M.C., (eds.): Palaeofloods, Historical Floods & Climatic Variability: Applications in Flood Risk Assessment*, Proceedings of the PHEFRA Workshop, Barcelona, Spain, 16-19th October, 2002, CSIC, Madrid, pp. 93-98.
- Greek Fire Department 2007. *Emergency incidents in the Municipality of Marathonas, Greece*. Department of Informatics and Communication, Greek Fire Department, Athens, Greece.
- GSCP 2006. *Flooding in East Attica Prefecture*. General Secretariat of Civil Protection, Ministry of the Interior, Public Administration & Decentralization, Athens, Greece.
- Hammond, N. G. L., 1968. The Campaign and the Battle of Marathon, *The Journal of Hellenic Studies*, 88, pp. 13-57.
- Hellenic National Agricultural Insurance Organization 2007. *Flood damages in municipality of Marathonas, Greece (1999-2008)*, Hellenic National Agricultural Insurance Organization (ELGA), Ministry of Rural Development and Food.
- Hergert J., Meurs H., 2007. Reconstructing peak discharges of historic flood levels in the city of Cologne, Germany, *4th International Palaeoflood Workshop*, Crete, Greece, 24th-30th June 2007
- Hughes, M. 1901 Marathon. *The Classical Review*, 15 (2), pp. 131-136.
- Kauper J. A. 1889. *Karten Von Attika (Marathon)*. Berlin, Deitrich Reimer

- Leake W. M. (1841). *The topography of Athens and the Demi, Volume 2, The Demi of Attica*. [online] <http://books.google.co.uk/books?id=sB0GAAAAQAAJ&printsec=titlepage> [Last accessed: 3/9/08]
- Macdonald, N., Black, A.R., Werritty, A., 2003. Historical and pooled flood frequency analysis for the River Ouse, York, UK. In *Thorndycraft, V.R., Benito G., Barriendos M. and Llasat M.C., (eds.): Palaeofloods, Historical Floods & Climatic Variability: Applications in Flood Risk Assessment*, Proceedings of the PHEFRA Workshop, Barcelona, Spain, 16-19th October, 2002, CSIC, Madrid, pp. 217-222.
- Nea 1979. 'Woman in peril in Kato Souli' (in Greek). Newspaper "Ta Nea" 22 October 1979, p.1, Greek Parliament Newspaper Archive, Athens, Greece
- Potter, H. R. 1978. *The use of historic records for the augmentation of hydrological data*. Wallingford, Institute of Hydrology, (IH Report No.46).
- Prefectural Administration of East Attica 2007. *Technical Services Archive, Natural Disaster Damages (1987-2005)*. Technical Services Department, Prefectural Administration of East Attica.
- Robinson, D. M., Blegen, E. P., 1936. Archaeological News and Discussions. *American Journal of Archaeology*, Vol. 40, No. 2, (Apr. - Jun., 1936), pp. 247-270.
- Sekunda, N., 2002. *Marathon 490 BC: The first Persian War*. Oxford: Osprey Publishing
- Sith, K., Ward, R., 1998. *Floods : physical processes and human impacts*. Chichester : John Willey & Sons
- Sotiriadis, G., 1933. *Excavations at Marathon*. Proceedings of the Archaeological Society (Praktika) pp. 31-46.
- Vanderpool E., 1966. The Deme of Marathon and the Herakleion. *American Journal of Archaeology*, Vol. 70, No. 4, (Oct., 1966), pp. 319-323
- Williams, A., Archer, D., 2002. The use of historical flood information in the English Midlands to improve risk assessment. *Hydrological Sciences Journal*, Vol. 47(1), pp. 67-76.

LANDSLIDE MOVEMENTS RELATED TO PRECIPITATION. ANALYSIS OF A STATISTICAL SAMPLE FROM THE GREEK AREA

Gournelos T.¹, Nastos P. T.¹, Chalkias D.², Tsagas D.², Theodorou D.¹

¹ *University of Athens, Faculty of Geology and Geoenvironment, Department of Geography and Climatology, 157 84 Athens, Greece*

² *Harokopio University, Kallithea Athens, Greece*

Abstract

It is known that the Greek area the majority of landslides have been triggered by heavy precipitation. This paper examines the statistical properties of precipitation directly related to the landslides in the Greek area. A database was constructed for the period 1980-1988, where for each landslide the daily maximum, the monthly and the annual precipitation totals were recorded. All these data were introduced in a GIS environment. Finally, a statistical analysis was carried out to study the relation between precipitation and landslide movement.

Key words: *Landslides, precipitation, Greece*

1. Introduction

The landslide movements are relatively intense in the Greek area and are directly related to the relief, lithology and vegetation. The principal mechanisms for triggering a landslide are the heavy precipitation events, earthquakes and human intervention. The precipitation variability and the distribution of precipitation frequency in the Mediterranean and Greece have been studied by many researchers (Repapis 1986, Nastos 1993, Metaxas et al. 1999, Maheras and Anagnostopoulou 2003, Nastos and Zerefos 2007, 2008). In Greece, 92% of the precipitation during the wet season (October-March) is produced by cyclonic circulation types (Maheras and Anagnostopoulou 2003), while during the summer the intense precipitation and hail events are associated with the geostrophic vorticity advection (Spanos 2004). The winter is characterized by cyclonic variability and low mean pressure in the Mediterranean. The highest values of pressure appear in the east area and are associated with the Siberian anticyclone. In March and April, as the main characteristics of the upper air flow (e.g. Jet stream) start moving to the north from their southern winter positions. The rainy season continues until May, when a dry summer regime is established. The precipitation over Greece, is rarely affected by Atlantic cyclones, but is linked to cyclogenesis in the Mediterranean region (Luterbacher et al. 2006). According to the results of climate models projection (A1B scenario) precipitation will shift to the north and during 2080-2099 the precipitation will decrease over 20% with respect to the period 1980-1999 (IPCC 2007) at the southeast areas of the Mediterranean. Besides, the frequency of intense cyclones in the Mediterranean will significantly decrease, but the future cyclones will be more intense (Anagnostopoulou et al. 2006). In a more recent study, Nastos & Zerefos (2008) showed that extreme precipitation events appear during winter months in the western and eastern sub regions of Greece, and mainly during autumn in the rest of the country. Moreover, the fitted Gamma distributions to the daily precipitation totals with respect to the 45-year period

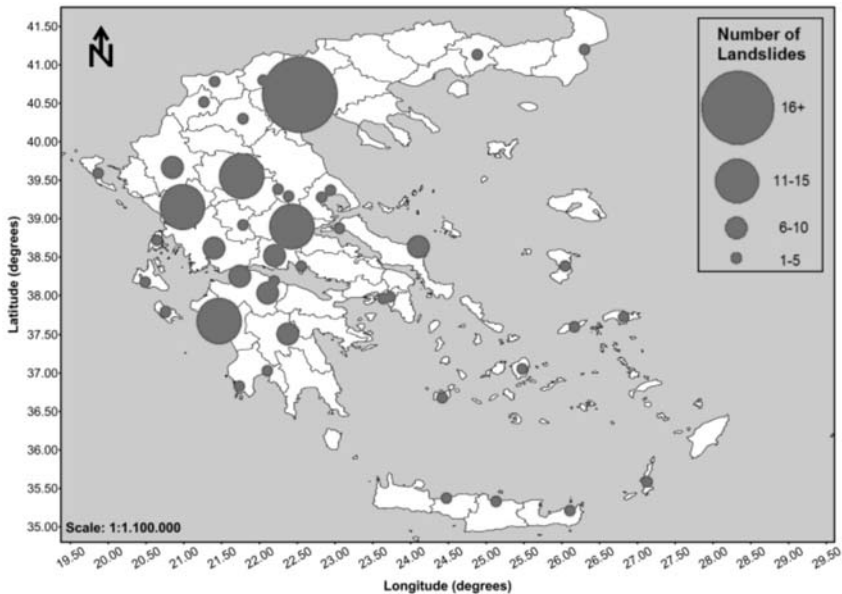


Fig. 1: Spatial distribution of the landslides in relation to the nearest sites with precipitation observations.

(1957-2001) revealed that high values of variance and scale parameter of the fitted Gamma distributions appear in the western, eastern and southeastern Greece, especially during the period 1991-2000, pointing out the appearance of the extreme daily precipitation.

There are several works in the international literature related to the spatial distribution and characteristics of landslides in the Greek area (Koukis 1982, Koukis & Ziourkas 1991, Lekkas 2001, Gournelos et al. 2006). Nevertheless, studies which focus on the relationship of landslide movements and precipitation are limited and only of local character (Anagnostopoulos & Georgiadis 1997, Koukis et al. 1997, Nikolaou et al. 1997). In the present study, an effort is made to examine the relationship between landslide movements and precipitation in the wider Greek area.

2. Data and Analysis

The study of the correlation of precipitation and landslides requires the collection of many variables in spatial and temporal distribution. For this reason, firstly, a database of landslide phenomena was constructed (Gournelos et al. 2006) for the period 1970-1988 and in the process all the factors causing these phenomena were analyzed.

It is absolutely certain that the majority of landslides happen due to precipitation events. In order to examine the relationship between precipitation and landslides, a second database concerning daily maximum, monthly and annual precipitation totals was constructed. The precipitation data were derived from the Hellenic National Meteorological Service (HNMS) and concern meteorological stations, which are representative to the areas, where sustained landslides occurred. The spatial distribution of the sites (HNMS meteorological stations) with precipitation data in close distance to the area of recorded landslides is depicted in Figure 1. The proportional circles appeared in Figure 1 show only the number of landslides in the neighboring area of the meteorological stations.

Finally, after entering the data into a G.I.S. environment, and the development of various thematic maps, statistical analysis of the rainfall data was carried out.

3. Results and discussion

The correlation of the precipitation and landslide events was initiated mainly by Gaine (1980) and continued later by other researchers (Keffer et al. 1987, Grozier 1999, Wilson and Wieczorek 1995, Guzzetti et al. 2004, Aleotti 2004, Glade et al. 2005). The aforementioned authors studied either empirical relationships between precipitation and landslides by constructing intensity duration curves, or physical processing models.

The statistics of the annual, monthly and maximum daily precipitation totals associated with the recorded landslides in the wider area of Greece are presented in Table 1. It is crystal clear that in most of the cases, extreme precipitation events are associated with landslides development.

In order to examine the precipitation impact on the development of landslides, the monthly precipitation recorded in the specific months when landslides happened in the wider Greek area are depicted in Figure 2. It is remarkable that, in some cases the monthly precipitation totals exceed 250mm, which corresponds over 30% of the annual precipitation in several areas. Figure 3 presents the monthly precipitation totals as a percentage (%) of the respective annual precipitation totals with respect to landslides dates, for different sites of Greece. Another significant parameter which is closely related to the onset of landslides is the maximum daily precipitation totals. The recorded daily maximum precipitation totals (mm) with respect to landslides dates, for different sites of Greece, appear in Figure 4.

Extreme daily precipitation events, that in many cases exceed 30mm, which is a threshold of heavy precipitation events (Nastos and Zerefos 2008), seem to be typical for the development of landslides in areas that are also vulnerable to other physical factors. In this point it is worthy to point out that,

Table 1. Statistics of the precipitation totals triggering landslide movements

	Annual Precipitation (mm)	Monthly Precipitation (mm)	Maximum daily precipitation (mm)
Number of sites	184	184	184
Mean	775.2	111.1	33.5
Standard deviation	261.5	81.3	23.4
Maximum	1509.9	390.3	135.5
Skew	2.7	4.5	7.2
Kurtosis	-0.1	0.9	7.5

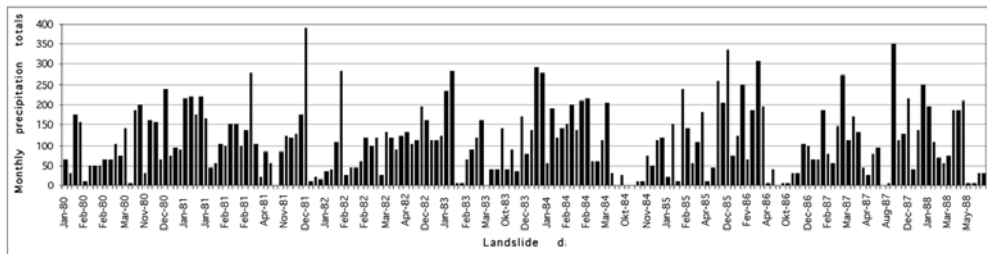


Fig. 2: Monthly precipitation totals (mm) with respect to landslides dates, for different sites of Greece.

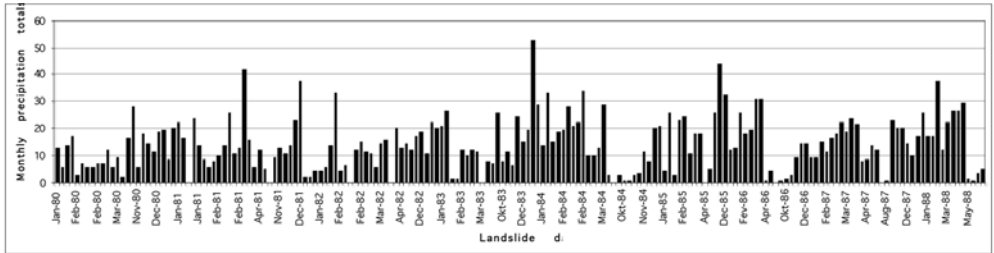


Fig. 3: Monthly precipitation totals as a percentage (%) of the respective annual precipitation totals with respect to landslides dates, for different sites of Greece.

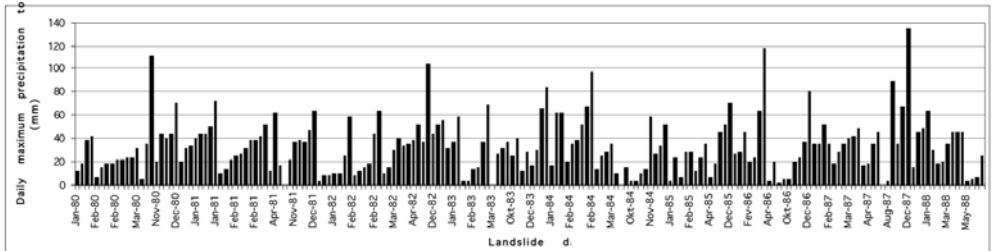


Fig. 4: Daily maximum precipitation totals (mm) with respect to landslides dates, for different sites of Greece.

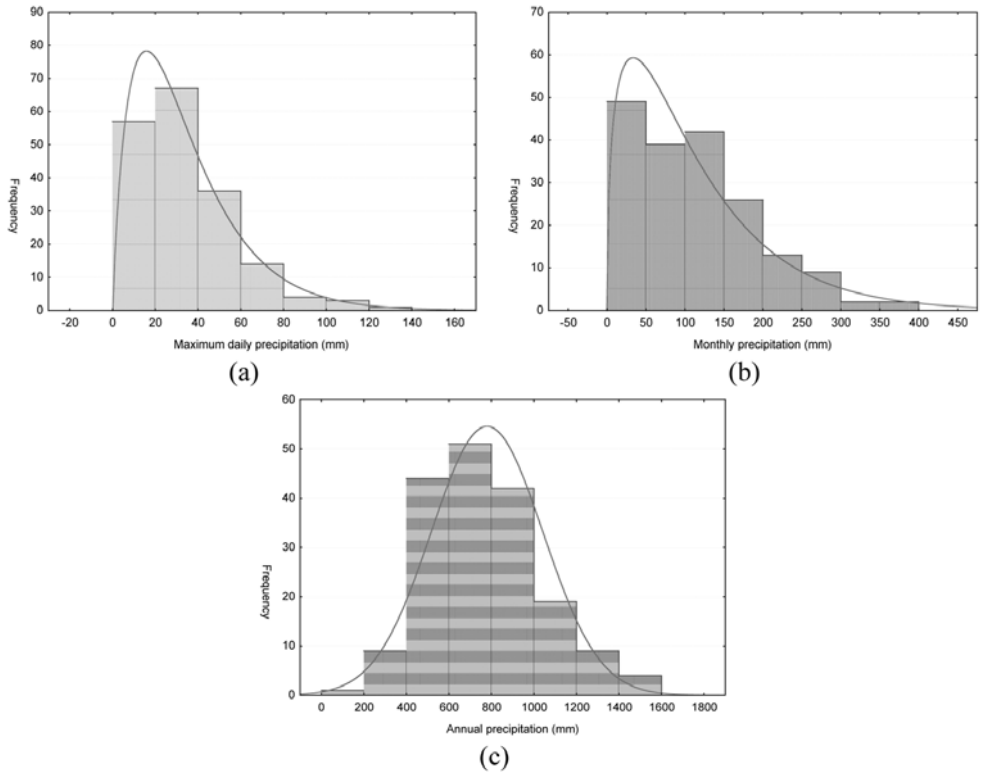


Fig. 5: Histograms of daily maximum (a), monthly (b) and annual (c) precipitation totals.

the database used concerns landslides that occurred throughout the country, for the specific time period 1980-1988.

In the process, histogram analysis was carried out in order to find out the prevailed classes of daily maximum, monthly and annual precipitation totals corresponding to landslide movements. Besides, appropriate distributions, such as Gamma distribution for daily maximum and monthly precipitation totals and Normal distribution for the annual precipitation totals, were fitted to the histograms. Regarding daily maximum precipitation, the class 20-40mm seems to be the prevailed one, while the class 0-50mm and the class 600-800mm correspond to the more frequent monthly and annual precipitation totals, respectively, for landslides phenomena.

4. Conclusions

The performed analysis, in order to show the relationship between landslide events and precipitation totals, for the whole Greek territory, during the period 1980-1988, revealed the following conclusions: The majority of the landslides were due to intense and short-term precipitation events. The mean daily maximum precipitation related to the outbreaks of landslides phenomena was found 33.5 ± 23.4 mm, the mean monthly precipitation 111.1 ± 81.3 mm, while the mean annual precipitation 775.2 ± 261.5 mm. The temporal distribution of landslides revealed that, their frequency, as expected, was greater within the period December–February, followed by spring and even less by summer months.

5. References

- Aleotti, P., 2004. A warning system of rainfall – induced shallow failure. *Engineering Geology* 73, 247–265
- Anagnostopoulos, C., Georgiadis, M., 1997. Analysis of rainfall data and correlation to landslides: The case of Sykia-Pieria, Greece. *Engin. Geol. and the Environment*, Marinou, Koukis, Tsiambaos and Stournaras (eds), Balkema, Rotterdam.
- Anagnostopoulou, Chr., Tolika, K., Flocas, H., Maheras, P., 2006. Cyclones in the Mediterranean region: Present and future climate scenarios derived from a general circulation model (HadAM3P). *Advances in Geosciences* 7:9-14.
- Crozier, M.J., 1999. Prediction of rainfall–triggered landslides: a test of the antecedent water status model. *Earth Surface Processes and Landforms* 24, 825-833
- Glade, T., Dikau R., Bell R., 2003. National landslide susceptibility map for Germany. *Geophysical Research Abstracts* Vol. 5.
- Gournelos, T., Chalkias, Ch., Tsagas, D., 2006. Landslide Susceptibility Zonation of Greece Using Fuzzy Logic Rules and Geographical Information Systems. *Geography* 12, 114-126
- Guzzetti, F., Carrara, A., Cardinali, M., Reichenbach, P., 1999. Landslide hazard evaluation: a review of current techniques and their application in a multi-scale study, Central Italy. *Geomorphology* 31, 181-216.
- Guzzetti, F., Cardinali, M., Reichenbach, P., Cipolla, F., Sebastiani, C., Galli, M., Salvati, P., 2004. Landslides triggered by the 23 November 2000 rainfall event in the Imperia Province, Western Liguria, Italy. *Engineering Geology* 73, 229-245.
- IPCC, 2007. Summary for policymakers. In: S. Solomon, D. Qin, M. Manning, Z. Chen, M. Marquis, K.B. Averyt, M. Tignor and H.L. Miller, Editors, *Climate Change 2007: The Physical Science Basis*. Contribution of Working Group I to the Fourth Assessment Report of the Intergovernmental Panel on Climate Change, Cambridge University Press, Cambridge, United Kingdom/New York, NY, USA.
- Keefer, D.K., Wilson, R. C., Mark, R.K., Brabb, E.E., Brown, W.M., Ellen, S.D., Harp, E.L., Wieczorek, G.F., Alger, C.S., Zarkin, R.S., 1987. Real–time landslide warning during heavy rainfall. *Science*,

- Koukis, G., Pyrgiotis, L., Rozos, D., 1997. Landslide phenomena and stability analysis related with the construction of the Ano Diakopto road deviation, Achaia country, Greece. *Engin.Geol. and the Environment*, Marinos, Koukis, Tsiambaos & Stournaras (EDS) Balkema, Rotterdam.
- Koukis, G., Ziourkas, C., 1991. Slope instability phenomena in Greece: a statistical analysis. *Bulletin of the IAEG* 43, 47-60.
- Koukis, G., 1982. Mass movements in the Greek territory. A critical factor for environment evaluation and development. IV Cong. Int.Ass. Eng. Geology. Vol. III. New Delhi.
- Lekkas, E., 2001. Landslide Hazards in Greece. EUG XI, European Union of Geosciences, Cambridge Publications, Abstract Volume, Vol.6, p.508, Strasbourg.
- Luterbacher, J. et al., 2006. Mediterranean climate variability over the last centuries: a review. In: P. Lionello, P. Malanotte-Rizzoli and R. Boscolo (Eds), *Mediterranean Climate Variability*, Amsterdam. Elsevier, pp. 27-148.
- Maheras, P., Anagnostopoulou, Chr., 2003. Circulation Types and their Influence on the interannual variability and precipitation changes in Greece, Mediterranean Climate-Variability and Trends. Springer Verlag, Berlin, Heidelberg, 215-239.
- Metaxas, D.A., Philandras, C.M., Nastos, P.T., Repapis, C.C., 1999. Variability of precipitation pattern in Greece during the year. *Fresenius Environmental Bulletin* 8, 1-6.
- Nastos, P.T., 1993. Changements de la pluviosite en region Hellenique pendant la periode 1858 - 1992. Proceedings of the 6th Colloque International de Climatologie, 22-25 Septembre, 1993, Thessaloniki, Grece, Vol. 6, pp. 183-190.
- Nastos, P.T., Zerefos, C.S., 2007. On extreme daily precipitation totals at Athens, Greece. *Advances in Geosciences* 10, 59-66.
- Nastos, P.T., Zerefos, C.S., 2008. Decadal changes in extreme daily precipitation in Greece. *Advances in Geosciences* 16, 55-62.
- Nikolaou, N., Koukis, G., Lambrakis, N., 1997. Rainfall and Landslide manifestation corellation in Korinthos county, Greece, in proceedings of Inernational Symposium on Engineering Geology and the Environment, Marinos P., Koukis G., Tsiampaos G., Stournaras G. (eds.), Vol. 1, pp. 919-925.
- Repapis, C.C., 1986. Temporal fluctuations of precipitation in Greece. *Rivista di Meteorologia and Aeronomia* XLVI, 1-2, 19-25.
- Spanos, S., 2004. Climatology of cyclones during the warm-dry period in south Balkan Peninsula and eastern Mediterranean. PhD. Thesis 199 pp. (in Greek)
- Wilson, R.C., Wiczorek, G.F., 1995. Rainfall thresholds for the initiation of debris flows at La Honda, California. *Environmental and Engineering Geoscience* 1(1), 11-27.

THE POTENTIAL NATURAL HAZARDS TO BE CONSIDERED IN THE DESIGN AND EXPLOITATION OF THE AERIAL ROPE-WAY IN THE “GORA SOBOLINAYA” MOUNTAIN-SKIING RESORT (SOUTHERN PRIBAIKALIA, RUSSIA)

Alena V. Kadetova, Elena A. Kozireva

Institute of the Earth's Crust Academy of Sciences Siberian Branch, Laboratory of engineering geology and geocology, Lermontov Street 128, 664033 Irkutsk, Russia, alena-kadetova@yandex.ru, kozireva@crust.irk.ru

Abstract

The paper deals with investigation of potential geological hazards to be taken into consideration in designing of the aerial rope-way, as well as problems of development of the recreation infrastructure in mountain lands with the complicated building conditions.

Key words: *exogenous geological processes.*

1. Introduction

The paper deals with the study of exogenic geological processes that develop in the influence area of the “Gora Sobolinaya” mountain-skiing complex. The complex was founded in late 1970s within the watershed area of rivers Kharlahta and Babkha in the south-western shore of Lake Baikal. The region is marked by attractive conditions for the active winter holiday: a lot of sunny days within the year, abundance of snow and diversity of ski-tracks. The mountain-skiing resort is situated at the elevation of 1001 m a.s.l., the maximum slope is 48.8°, the total length of ski-tracks > 12 km. The popularity of mountain-skiing and growing accommodation capacity of the resort complex require the expansion of its infrastructure: building of new structures, widening of ski-tracks etc.; all these factors will provide the large technogenic load on the geological environment of the territory.

The paper aims to study the general engineering-geological situation in the site of the aerial rope-way construction, and to investigate the hazardous exogenic processes to prevent the eventual accidents. The planned aerial rope-way system belongs to the 1st class of amenability level according to the GOST 27751-88; it presents the linear feature with bearing poles resting on the solid reinforced concrete basement (buried 0.1 m deeper of the frozen rocks stratum), and two rope-driving stations: 1) the lower station serving as drive-tension mechanism (Station I), and 2) the return motion mechanism atop of the mountain (900-910 m a.s.l.) (Station II). This structure belongs to the objects of high social amenability. The natural condition of the region such as considerable seasonal variations of temperature, seasonal freezing and thawing of soil, undulating relief and high seismicity, produce definite troubles to construction and exploitation of the lifting systems.

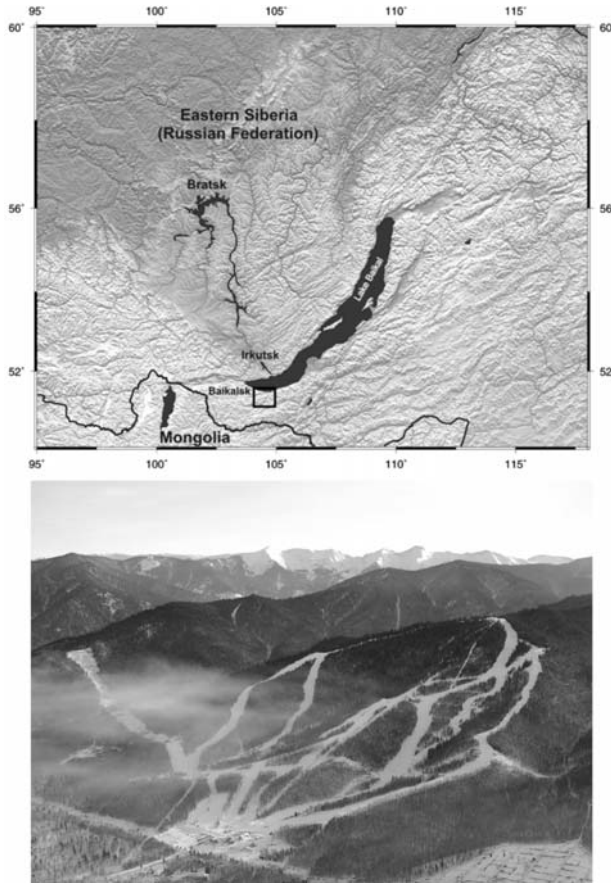


Fig. 1: (upper): location map. Squares symbolize the investigation area; (lower): general view of the “Gora Sobolinaya” mountain skiing complex (Photo by Alexander Sizov).

2. Geological and geographical setting

2.1. Geomorphology and relief

The discussed area occupies the territory of the Baikal rift zone within the central part of Euro-Asian mainland. In the context of the specific geological structure, history of development, kinematics of tectonical movement in the upper area of lithosphere, the territory is marked by complicated engineering-geological conditions: the mountainous relief formed by recent tectonical movements. The engineering works of the “Gora Sobolinaya” complex are located in the piedmont area of Khमार-Daban mountain ridge marked by the occurrence of paleo-peneplane elements, sharp crests, peaks, the elevation ranging from 500 m to 1001 m a.s.l. (Fig. 1). The piedmont territory composed of coarse clastics is gently dipped towards the lake; the width of piedmont plain ranges from 1 km to 2 km.

The discussed territory is of the erosion-tectonical type, with dissected middle-height relief (Fig. 2). The elevation ranges from 700 m to 1758 m a.s.l., with the relative elevations of the valley floors 500-1000 m a.s.l.

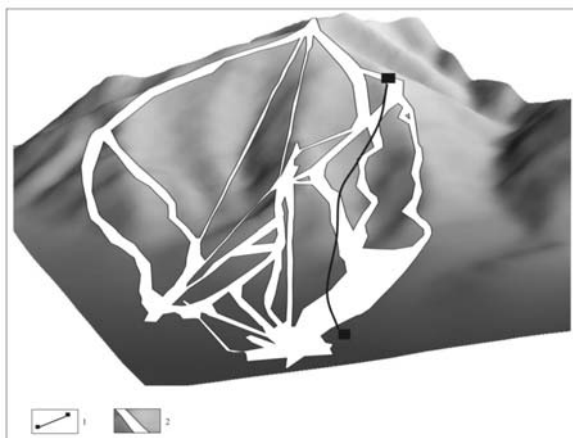


Fig. 2: The 3-D model of the Sobolinaya Mountain (1-the planned aerial rope-way; 2- skiing tracks).

2.2. Climate

The territory of Pribaikalia belongs to the region of continental climate: long and cold winter, short warm summer; the amplitude of temperature variations averages to 60°, the no-frosting periods lasting for 130 days.

The first autumn frosts occur in mid-September, the cases of late frosts are documented in May; the cases of zero crossing occur within the periods of 150-180 days. This is one of the most important factors of frost weathering of solid rocks. The continental climate is the cause of deep seasonal freezing and long-lasting periods of ground thawing. The atmospheric precipitation occurs primarily in the periods June–August; the monthly precipitation maximum being observed in July. Within the year, the precipitation amounts to 80-90% as rains, and 5-30% as solid precipitation. Thus, the most important climate factors are: frequent temperature drops, abundant atmospheric precipitation and deep seasonal ground freezing.

2.3. Geological structure

According to the Geological Map (1:200000) (1973), the main area of the discussed slope is presented by the Archeic-Lower Proterozoic formation of white marbles (in places by graphitic and phlogopite-containing ones), with lenticular intercalations of calciphyres, ophicalcites, pink diopsidic marbles, skarn and gneiss deposits (Fig. 3).

The foot area of the slope, and a definite part of its upper area are composed of non-segmented Early-Proterozoic rocks of compound structure, belonging to the Babkha massif. Here the basic rocks alternate with the enclosing rock mass. The petrographic composition of intrusions is presented by pyroxene-amphibole and olivine gabbro, gabbro-diabases, gabbro-diorites and diorites. Occasional dike formations are presented by diabases and diabasic porphyrites. The part of northern slope (the site of planned lifting system) is presented by Late-Proterozoic intrusions of the Sayan complex (third phase) composed of granitoid deposits and confined to slackened areas of deep faults. Granitoides are of pink, pinky-grey, reddish-pink and light-grey (almost white) color.

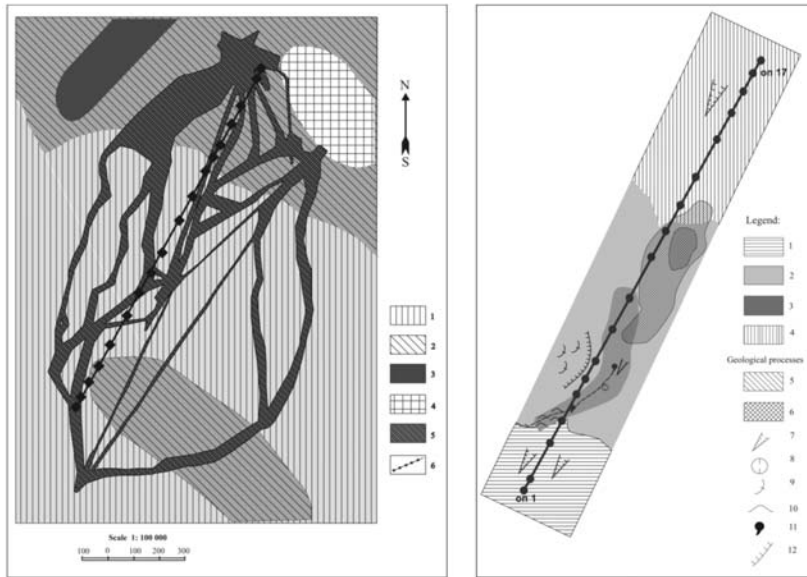


Fig. 3: (left): Geological index-map of the mountain-skiing complex's territory: 1 – Archeir-Lower Proterozoic formation of white marbles with lenticular intercalations of calciphyres, opicalcites, pink diopsidic marbles, skarn and gneisses; 2 – Late-Proterozoic intrusion of Sayan complex (3-rd phase) granitoides; 3 – river bed alluvial deposits of Holocene (cobble roundstone, gravel, semigravel); 4 – non-segmented intrusions of Early-Proterozoic rocks (gabbroides and diorites); 5 – skiing tracks; 6 – lifting system; (right): Index-map of engineering-geological zonation of lifting system route: 1 – slope of up to 15° steepness; 2 – slope of up to 40° steepness; 3 – creek valley; 4 – slope of > 40 ° steepness; 5 – borders of overgrown old stone stream; 7 – erosion; 8 – suffosional subsidence; 9 – solifluction; 10 – swamping; 11 – groundwater discharge; 12 – cut slope.

2.4. Geological processes

The described territory belongs to the regions of high seismicity (~M9), as evidenced by the Seismo-Zoning Map-97. High seismicity in combination with typical geo-cryological conditions, specific hydro-meteorological and geologic-geomorphological conditions are the determining factors of exogenous geological processes such as weathering, mudstream, soil creep, rockfall, landslide etc.

Weathering. The processes of physical weathering intensely develop in mountainous areas marked by considerable temperature variations and frequent cases of zero crossing. Considerable disintegration of outcropped solid rocks is caused by thermal weathering. The amplitude of diurnal and annual temperature variations in the upper rock layer reach 40-50° at the elevation mark 900 m a.s.l., and 70-80° at 1700 m a.s.l. The variations of soil temperature at these elevations occur in the following manner: 320-350 cases of zero crossing within the year in the slopes of south-exposed slopes, and up to 200 cases in the north-exposed slopes. The repeating cases of heating and cooling produce the destructive effect upon physical characteristics of denudated rocks that turn into breakstone and gruss. Within the year, the influence of seasonal factors upon the rock weathering is observed. The winter time (December-March) is the period of the relative rest (Solonenko 1962). Along with the thermal weathering, the destruction and crushing of solid rocks occur due to frost wedging and chemical weathering as the consequence of dissolution of carbonates and other elements.

Gravitation processes. Wide occurrence of gravitation processes in the territory is attributed to a

number of factors such as the rugged mountainous relief, extensive outcrop of solid rocks and their disintegration, high rate of physical weathering, abundant atmospheric precipitation, active tectonics and high seismicity. The phenomenon of rockfall is typical of the rocky slopes of valleys, dissected by narrow denudation rills of relatively small depth and length (Engineering geology of Pribaikalia 1968). In many cases, the rockfall masses contribute to formation of the mudstream solid phase. The rock debris of the size 0.2-0.4 m across are easily transported by water streams of 2-3 m/s rate. The rock debris particles of size >1.0 m across are typical only of the rockfall areas with intrusive formations. The detrital slopes (sometimes of large size) are present in the areas of outcropped solid rocks. The major amounts of loose rock debris accumulate in the detrital cone in late spring, summer and early autumn, i.e. during the periods of snow thawing, frequent cases of zero crossing and abundant atmospheric precipitation. This time is marked by the maximum stream of clastic material due to the water action, avalanche denudation, etc. The fluid soil creep is more typical of the northern offspur of Khamar-Daban mountain ridge. In the morphological aspects, the fluid soil creep from steep slopes occur in the form of stripping of the 3-5 m-wide (in places 10-12 m-wide) and 0.2-0.3 m-thick bands of the earth mass. The triggering factors of the soil creep are generally the lateral erosion and cutting of slopes.

Permafrost processes. In the described territory the permafrost is of the sparse occurrence. In high mountain areas, the 80 m-thick layers of frozen rocks occur in all elements of the relief (Leshchikov 1978). In the piedmont area with ~1300 m a.s.l. elevation, the permafrost is of insular occurrence, typical of sodded and forested lowlands. The seasonal thawing of permafrost reaches 1.0-1.3 m depth in early summer and up to 2.0-2.5 m in late summer. The average of seasonal ground freezing depth reaches 1.8-2.3 m.

3. Methods

The investigation of natural hazards from exogenic geological processes, and the evaluation of engineering-geological potential of the geological environment are based on the following factors:

1. The preliminary works comprise:
 - accumulation and analysis of the archive and published data concerning the area of planned works;
 - interpretation of the space- and aerial photographs;
 - analysis of engineering-geological data on the bore pits, stripping of overburden.
2. Field investigations:
 - reconnaissance survey of slopes;
 - geographical siting of skiing paths and location of the aerial rope-way bearing poles;
 - the GPS survey of the rope-way profile;
 - the route survey and description of the reference points (the sites for bearing poles) and the areas of developing geological processes.
3. The office works:
 - the analysis of engineering-geological conditions of the building ground, using the archive and field materials;
 - evaluation of natural and technogenic conditions in the building site;
 - drawing of index maps of engineering-geological conditions in the aerial rope-way site;
 - forecast of qualitative changes of the engineering-geological conditions in the region of planned work.

During the preliminary works, the definite archive materials concerning the area of investigation were studied, including the scientific reports on the geological structure, seismotectonics and engineering-geological conditions of the territory. Interpretation of the space- and aerial photographs of different years, analysis of cartographic materials, as well as the materials from core drilling.

The reconnaissance survey was carried out to reveal the hazard of exogenic processes, degree of the rock weathering and rock strength properties in the context of construction of the bearing poles, the places of groundwater discharge, swamped areas and other natural phenomena.

The route survey for the aerial rope-way spreads over the existing mountain-skiing tracks with the rope-tow lifting systems up to the elevation marks of 899 m a.s.l., and the actually used lifting systems to check their serviceability. One of the survey routes runs in the evened part of the piedmont area to note the main water streams, as well as in the sites bearing poles foundation; the total amount of the survey points is 17.

The geographical siting of observation points and the planned route of lifting system was based on the GPS methods. The total of noted and sited points amounted to 54: in the places of foundation of bearing poles located in the areas of groundwater discharge; in the areas of developing exogenic processes. For the analysis of cartographic materials and zonation of the course of the aerial rope-way, the geo-informational systems (GIS) were used. The GIS-systems are widely used in the engineering-geological practice for a number of purposes such as investigation and simulation of landslide hazard (Carrara and Pike 2008), estimation of the rockfall (Charalambous and Sakeliariou 2007), and mapping of erosional risks (Bathrellos and Skilodimou 2007). The maps of natural geodynamical conditions in the mountain-skiing complex, and the technogenic load, were prepared. The maps show the relief, the geological structure, the skiing-tracks and the lifting systems, the foundation of the rope-way poles, and record the exogenic geological processes. For the automation of the data analysis, the GIS methods were used. For solving of simple problems in the analysis of one or two layers, the thematic maps were drawn, which represent the general trends in the development of exogenic processes in different areas, and the natural conditions in the discussed territory. The thematic maps based on the methods of ranges and point density determines the scatter or concentration of the objects in different areas. This method can be used primarily for the group of layers, representing the exogenic processes, and particularly the relationships between the definite negative processes and the geological environment.

4. Conclusions-Results

The studied area is marked by the complicated climate, geological and seismic conditions. The planned lifting system (aerial rope-way) belongs to the category of high responsibility, and its exploitation will increase the load upon the geological environment. The comprehensive geo-ecological evaluation of the area was carried out to reduce the detrimental impacts of hazardous geological processes.

The area of the lifting system route is located on the north-exposed slope of north-western strike. The snow cover remains since early November till mid-May. The route will cross the following geomorphological elements: creek valley floors, slopes of two opposite watersheds, as well as the north-exposed slope of the Sobolinaya Mountain (Fig2.). In the definite area of native slope, the spot cutting, surface grading (partially up to the horizontal level at 535-540 m level marks) were made. Uphill of these level marks, the slope was cut and stripped for laying of the mountain ski-runs. Due to the lack of sod and soil cover, the slope massif becomes subject to deep weathering that acceler-

ates the rock destruction and increases the thickness of weathered zone. Besides, the technogenically disturbed slopes are subject to the intensive ground ablation, contributing to formation of new eluvial-deluvial deposits

The onslope deposits are presented by argillaceous rock debris of talus (Fig.1). The thickness of eluvial-deluvial deposits increases downhill. This distribution of the sedimentary cover depends on the intensity of ground ablation. The 100 m-long hillside cut for poling (poles N6 and N7) stripped the following soil column: the 0.2-0.3 m-thick sod layer, the 20 m-thick layer of heavily-eroded bedrocks and the non-uniform folded-fold massif of solid rocks such as granitoides, marbles, gneisses. The eroded rocks present the sandy loam-filled platy formations, easily crumbling to dust. In the lower part of soil column there are the seamy metamorphic rocks with high strength properties.

The poles N1, N2 and N3 are located in sites of 1-15° inclination. The mountain slope is marked by the removed relief with small erosion forms and scours caused by the intensive ground ablation; the slope basement is composed of talus material (Fig.3).

The poles N4 and N5 are located on stable opposite slopes of creek valley; between them there is the swamped area with low-yield groundwater discharge. The geological map and material of field investigations show that the groundwater discharge is situated in the area of contact between the marbles of the Pereval-series and the intrusive gneisses. Besides, another low-yield groundwater discharge is located upslope, surrounded by the small-size swamp area. The melt and discharged waters fuse at the bottom of creek valley, forming the surface water stream "Stream" with well-defined channel of the U-shape profile, the 2.5 m width and up to 1.5 m-high vertical edges. The valley bottom is covered by coarse pebble of local rocks (marble, granite).

Below the 545 m elevation mark, the "Stream" water stream was piped and conducted away from the territory of ski-depot. In autumn periods the water stream becomes poor in water, and freezes in winter. In May 2008, the inspection carried out in the resort territory with the snow cover still remaining in some places, did not find any sign of icing in the areas of the "Stream" water stream and groundwater discharge.

The hillside cutting and stripping were made for poles N6 and N7. In the places upslope, small solifluction deformations of ~4 m length with 5 m-high steps were found. The foundations of bearing poles were sited in stable slopes.

The pole N8 is located on the technogenically disturbed slope with graded surface, removed sod cover and stripped deluvial deposits and intensive ground ablation. The foundations for poles N9, N10 and N11 are located on the 40° slope. The poles N10 and N11 are located within the area of stone river with outcropping coarse rock debris of relatively equal size (~1.5-2.0 m across) in the centre of stone field, and grassed and bushy perimeter area (Fig.4). The stone field is stable, without any sign of movement (rock walls, fractures, zones of bleaching). The coarse rock debris insulate the bedrock surface from the solar radiation, saving the low temperature in the area of stone field and hindering the ground defrosting rate. High permeability of rock and the near-surface location of frozen rocks promote the intense downhill runoff of thawing water across the stone field body. Besides, the bushy surface of the stone field's lower edge is the evidence of its stability.

In the area of pole N12 (above the 700-710 m a.s.l. elevation marks) the slope steepness exceeds 40°, reaching in places 47°. The lack of sod cover is the cause of intensive downhill ground ablation that starts with the snow thawing; the intensity of ground ablation depends upon the thickness of snow cover and slope steepness. In the case of simultaneous snow thawing and excess raining, the rates of defrosting and intensity of ground ablation increase, entailing the erosion and dissection of the re-



Fig. 4: Geological processes developing within the area of lifting system route: stone stream (left); ground ablation (right).

lief. Great amounts of fine- and medium-disperse material are transported downhill by ephemeral water streams. The intense ground ablation occurs also in the area of graded site of the Station II placed atop of the mountain at the elevation of 900-910 m a.s.l.

After the comprehensive investigation of the lifting system course, the engineering-geological zoning of the territory according to the slope steepness was made: 1) zone of up to 15° slope; 2) zone of 40° slope; and 3) zone of $> 40^\circ$ slope (Fig.3).

Each zone is marked by the occurrence of definite exogenic processes. The zone number 1 is marked by erosion development, here the poles NN 1-4 are sited; the zone number 2 (poles NN 5-11) is marked by seasonal (ephemeral) water streams, groundwater discharge, swamp areas, solifluction in the area of poles NN 5-7; the poles N 10 and N 11 are sited in the channel of the overgrown old stone stream; the zone number 3 is marked by the intense ground ablation; here the poles NN 12-17 are sited.

The study of geologic-geomorphological conditions, climate and other features of the territory, as well as the engineering-geological characteristics of the area of lifting system, revealed the occurrence of solid rocks covered by a thin layer of loose eluvial-deluvial deposits in the place of contact of poles with the geological environment. The course of the planned aerial rope-way will cross several geomorphological elements of similar genesis. The territory is marked by sloping surface and simple hydrogeological conditions scarcely affected by technogenic factors. According to these factors as well as to the Manual Building Code CII 11-105-97, the site for construction of the aerial rope-way can be referred to the category II of complexity of engineering-geological conditions.

The depth of foundation bury rules out the risks of deformation from the decrease of the soil's bearing power: in accordance with the engineering design, the foundation should be buried deeper of the seasonally frozen rock stratum. All foundations rest on either the solid rocks or the non-contracting eluvial-deluvial grounds.

In the area of the planned lifting system's foundation, no hazardous geological processes were found; this means that the poles rest on the stable ground, not subject to the influence of exogenic geological processes. The technogenic load within the discussed area is bound up with the construction of mountain-skiing tracks: the selective slope cutting, surface grading, removing of sod cover and snow retention on the slopes entail the increase of weathering rate, surface runoff and formation of the eluvial-deluvial layer. The interference in the geological environment is confined to the near-surface

area and does not affect the mechanisms and components of the geosystem. All exogenic geological processes developing in the vicinity of the mountain-skiing tracks remain undisturbed, their dynamics obeying to natural climate factors.

In the context of the actual geologic-geomorphological conditions in the site and the invariable technogenic factors, no changes in the engineering-geological conditions and the safe exploitation of the aerial rope-way can be expected. Major part of its exploitation period is designed for winter months (since November till May); the maximum technogenic load will therefore fall on frozen slopes. It should be noted that the territory is marked by high degree of natural risk; in the course of exploitation of the aerial rope-way the yearly monitoring of the skiing-track and the bearing poles will be required to avoid the unreasonable load on the geological environment

5. Acknowledgments

The authors thank the management of the “Gora Sobolinaya” resort for their kind help in the investigations. The index-map for Fig.1 was drawn with the use of GMT program pack (Wessel et al. 2007). The work has been done with financial support of Russian Federation President’s Grants Council.

6. References

- Bathrellos G.D., Skilodimou H.D., 2007. *Using the analytic hierarchy process to create an erosion risk map. A case study in Malakasiotiko stream, Trikala prefecture*. Bulletin of the Geological Society of Greece, vol. XXXVII, 1904-1915.
- Carrara A., Pike R. J., 2008. *GIS technology and models for assessing landslide hazard and risk*. Geomorphology 94, 257-260.
- Charalambous S., Sakeliariou M., 2007. *Estimation of rockfall hazard using a GIS-based three-dimensional; rockfall simulation model*. Bulletin of the Geological Society of Greece, vol. XXXVII, 1934-1946.
- Engineering geology of USSR. Vol. III. East-Siberia, 1977, Moscow, 643 pp. (in Russian).
- General seismic zoning of the territory of Russian Federation. OCP-97. Complete set of maps and materials for the Guide of Building Rules - “Building in seismic regions”, 1998, Moscow (in Russian).
- Geological Map of USSR (1:200000). The East-Sayan series, sheet M-48-III.Explanatory note, 1973, Moscow. (in Russian)
- Guide for Building Rules 11-02-96. Engineering survey for building purposes. (in Russian).
- Guide for Building Rules 22-01-95. Geophysical factors of hazardous natural impacts. (in Russian).
- Leshchikov F.N., 1978. *Frozen rocks of Priangaria and Pribaikalia*. Nauka, Novosibirsk, 139 pp. (in Russian).
- Solonenko V.P., 1960. *Essays of the engineering geology of East Siberia*. Irkutsk, 86 pp. (in Russian).
- Wessel P., W.H.F Smith, 2007. *The Generic Mapping Tools. Technical Reference and Cookbook* Version 4.2.

HISTORICAL LANDSLIDES IN THE PREFECTURE OF IOANNINA – COLLECTION AND ANALYSIS OF DATA

Kalantzi F.¹, Doutsou I.², Koukouvelas I.¹

¹ *University of Patras, Department of Geology, 26500 Patras, Greece, feikal8@yahoo.gr
iannis@upatras.gr*

² *Ioanna.doutsou@Kcl.ac.uk*

Abstract

The present study assessed landslide events over a time span of fifty years in the prefecture of Ioannina. Historical data analysis commonly provides valuable data for understanding distribution of landslides. The methodology included collection and analysis of articles about landslides events found in the local newspapers between 1960 and 2008, also in the national newspapers (1960-1967) and in the contemporary national newspapers (1995-2008). The time interval selected in this study is representative of the entire time period of systematic newspapers publication. During this time span, eighty nine historical landslides were identified. Newspaper articles annotate the time and the location of the landslides as well as primarily the role of weather conditions in triggering the landslides. In addition, published articles provide information on the damages caused by the landslides. The study shows that these events occurred due to extremely high precipitation, snowstorms or prolonged rainfall. The monthly distribution of the recorded phenomena shows an increase of landslide events during January-March and November-December, as these are the months with the highest precipitation and snowing in the prefecture. Although time clustering of the landslides within the Ioannina Prefecture in the time interval 1960 to 2006 was found to be repeated every forty years, their spatial clustering appears to change.

Key words: *landslides, historical data, newspapers, Ioannina*

1. Introduction

With a direct impact on humans and a number of indirect consequences, landslide events have nowadays been one of the international scientific community's hazards research interests. Landslides in Greece, their triggering mechanisms, their characteristics and restoration projects have been widely assessed and described with the use of statistical analysis by a number of scholars (Koukis 1988, Κούκης και Ρόζος 1982, Ζιούρκας και Κούκης 1989, Κούκης και Ζιούρκας 1989, Koukis and Ziourkas 1991, Koukis et al. 1994, Koukis et al 1996, Koukis et al 1997). In this study, we consider the collection of historical data as a necessary process in order to approach landslides phenomena and the vulnerability of the human environment. A wealth of international literature (Dominguez Cuesta et al.1999, Guzzetti et al. 1994, 2002, Calcaterra et al.2003, Carrara et al. 2003, Tropeano and Turconi 2004, Tarhule 2005, Sawyer and Butler 2006, Devoli et al. 2007a and b, Wrathall 2007) has used effectively press reports, databases and articles about landslide events and other natural disasters as valuable sources of information when

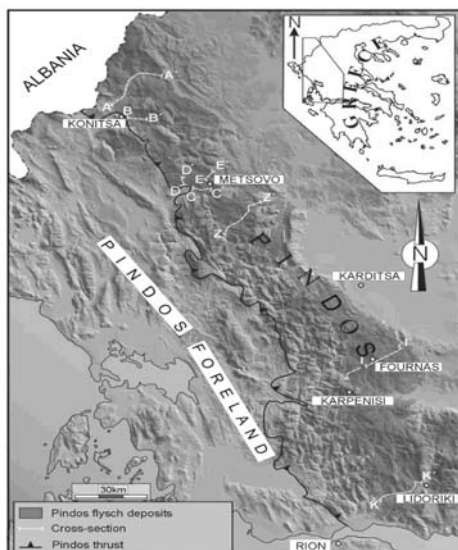


Fig. 1: Digital model of the ground of the Epirus region (http://www.ntua.gr/MIRC/db/epirus_db/ GEOLOGIA_HPEIROY/Geologia_Hpeirou.htm).

compiling scientific accounts of landslides events. In line with this method, this study collects valuable information about the landslides events from a variety of sources such as technical reports, historical monographs, scientific documents, public libraries, internet and newspapers.

Due to a lack of database of recorded landslides events in the prefecture of Ioannina, newspapers represent a valuable source of information not only for the assessment of landslide events but also for the creation of a landslides inventory. Press industry in Greece which firstly appears at the end of the 19th century, is regarded as the first mean for the transmission of news concerning natural hazards and disasters (e.g. landslides, or earthquakes). The present study focuses on landslide events recorded between 1960 and 2008. Relevant information on landslide events has been obtained using newspapers as main sources to investigate temporal and spatial distribution, types of landslides, and their triggering mechanisms in the prefecture of Ioannina.

2. Study Region

The prefecture of Ioannina belongs in the region of Epirus (Fig.1) with an estimated population of 175,000. With an area of 4,990 km² (<http://medlab.cs.uoi.gr>), the prefecture of Ioannina is one of the largest and mountainous prefecture in Greece (www.epirus.gov.gr). In Easterly, the prefecture's natural border constitutes of the mountain range of Pindos, while centrally are found the mountainous groups of Zagori and Mitsikeli. Mountain ranges of the prefecture include Kasidiaris, Kourenton, Douskos and Mourgana in the western and Souli and Tomaros in the south. The climate of Ioannina is continental with an average temperature of around 6,1 °C. The annual rainfalls vary, ranging between 1.000 and 2.000 mm (www.hnms.gr).

The Ioannina Prefecture is geologically extended from the Mesohellenic Trough in the east to the frontal parts of the Ionian zone in the west (Doutsos et al. 2006). Three major structural provinces can be distinguished in this section: (1) the Mesohellenic Trough; (2) the Pindos fold-and-thrust belt; and (3) a broadly spaced array of thrusts within the Ionian zone in the west (Fig. 2). The Mesohellenic Trough is primarily floored by the Pindos ocean ophiolitic rocks and is filled by the Middle Eocene flysch and Oligocene to Lower Miocene molasse sediments (Fig.

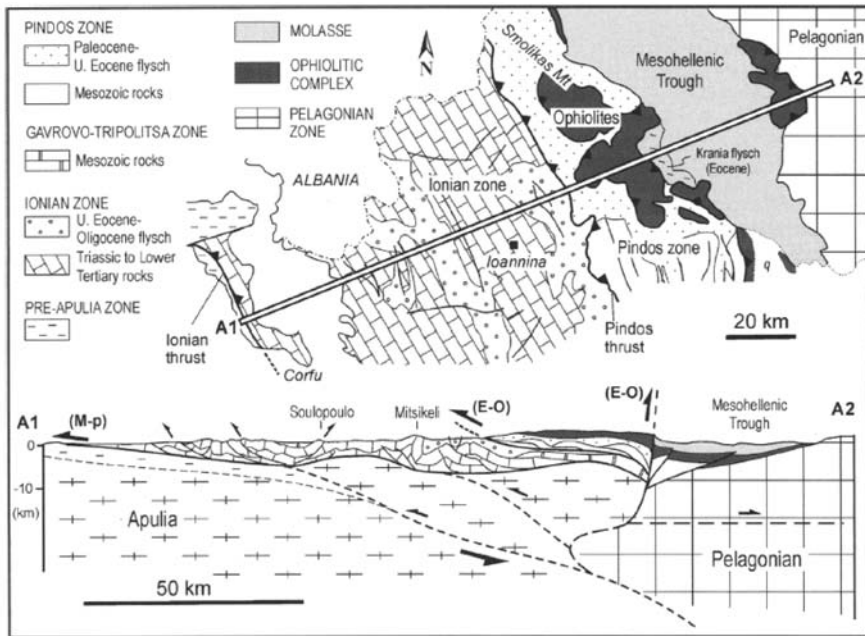


Fig. 2: Tectonic map of Ioannina area and their surroundings (adapted from Doutsos et al. 2006).

2) (Doutsos et al. 1994, 2006). At the western border of the Mesohellenic Trough a high-angle reverse fault carries the ophiolitic rocks over the Pindos zone flysch (Fig. 2). The area west of the Mesohellenic Trough to the west border of the Ioannina prefecture is mainly occupied by calcareous rocks of the Ionian zone and two main flysch basins, the Pindos and Ionian (Xypoliass and Koukouvelas 2005). The deformation in this area appears to be significant, involving flysch-filled piggyback basins in the east and a system of thrust faults to the west that caused steep slopes and intense fracturing of the rocks in the area under study.

3. Methodology

The present study relies on a database of all possible documents describing landslides events which occurred between 1960- 2008. Firstly, we collected information from public archives, historical monographs and technical reports. As the amount of data collected from these sources regarding the initial research period was insufficient, there was a follow up research in newspaper texts. More specifically, all newspapers were manually read and searched chronologically starting from 1960. The information was collected by copying the originals texts or copying only the most important sentences regarding landslides (i.e., title of the news or the text below photos). Subsequently, the landslide events were categorized according to their spatial and temporal distribution as well as their triggering mechanisms. Internet sources were used as well. Technical reports referring to landslide events helped us to cross-check the newspaper reports.

The local newspapers “Proinos Logos” and “Hpeirotikos Agonas” were the main newspaper used as sources of information for this study. Occasionally, the newspaper articles included photos. A total of 89 articles that recorded landslides were found, mainly in the Zosimaia Public Central Historical Library. Additional sources used for the study were the digital online

archive of the national newspaper “Eleftheria” referring to 1960-1967 and other contemporary national newspapers (“Ethnos” 2005-2008, “Eleftherotipia” 2001-2008, “Kathimerini” 2001-2008, “Rizospastis” 1995-2008, “To Vima” 2001-2008 and “Ta Nea” 2001-2008). Sources from local authorities such as the Greek Institute of Geology and Mineral Exploration (Preveza Branch) and the Director’s Office of Technical Services of the Ioannina’s prefecture have also been used but not thoroughly investigated.

4. Types of data and limitations

From the 89 historical landslide events found in different sources, 91% was obtained from newspapers, 9% from technical reports scientific papers and other sources (monographs, books, or web pages). Nine different newspapers were consulted and 98 articles were found describing landslide processes. “Proinos Logos” newspaper provided the largest number of records followed by “Hpirotikos Agonas”.

Based mainly on data extracted from the newspapers, landslides’ descriptions in the press appear to have some common characteristics. How do these stories describe the landslide events and in what features of their occurrence do they rely on? To this end, textual analysis based on newspaper stories produced the following coding categories which reflect the characteristics of the press coverage and at the same time provide valuable information about the landslides occurrence: a) temporal information b) spatial information c) descriptions of the event and implications d) triggering mechanisms e) estimations about future activities f) sources of information and their reliability.

However, there were certain considerations about the obtained data that affect the study’s results. Newspapers usually reported the date of the event although occasionally without specifying the exact temporal information (e.g. “last week”). Spatial information about landslide events was variable. The newspaper sources usually provided information on the locality affected, but do not provide information on the source area. In some cases, places reported – names of streets, roads, villages and mountains- could not be located in current topographic maps as they have changed throughout time. For this reason, it was difficult in these particular cases to locate the exact place of landslide events in the topographic map. In cases that the places reported were not recognizable, landslides’ locations were assigned based on interviews with aged people or our own knowledge of the area.

Temporal information and data on the location of the landslide events are also variable, being extremely detailed in some cases –especially in contemporary descriptions- and rather uncertain in others. The size of the landslide is usually not recorded, but sometimes it is given in a qualitative way. Here are some examples (Figs. 3 and 4): “Strong Earthquake Shaking was felt in Konitsa” during the shaking individual boulders fall down slopes in the Aaos Gorge and “Landslides triggered in an area of approximately 2,500 sq. m. However, what cause fear are wet sliding masses (probably the reporter is referred to debris flows during the earthquake) that devastated everything down the slope from Profitis Ilias summit covering vegetated areas too. In addition it is remarkable and horrible the dense array of scars on the slope”.

Also, the reliability of available data had to be carefully considered as it was not possible to evaluate the validity and accuracy of information presented in the articles. The ability of the press to reconstruct an event and mislead public opinion has always been a concern for media scholars. In this study, inaccuracies regard landslide’s dimension and their threat evaluation. In



Fig. 3: Headline of newspaper “Proinos Logos”, Auguts 19, 1960 recording earthquake triggered landslides.

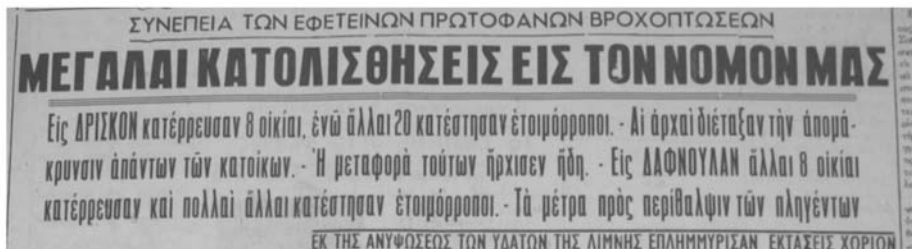


Fig. 4: Head line news from Proinos Logos 22 January 1963.

some cases, stories lack scientific resources and as a result reproduce misleading estimations of the hazards, rumours and overestimations of the situation. Such journalistic practices are particularly evident in contemporary reporting.

Nevertheless, newspapers through publishing technical reports and scientific information written from specialists and adapted to public knowledge help people understand the landslide hazards and the possible solutions of the problems revealed and in this case newspapers offer significant data (e.g. the newspaper article by Koukis, Eleftherotipia 04/01/2006).

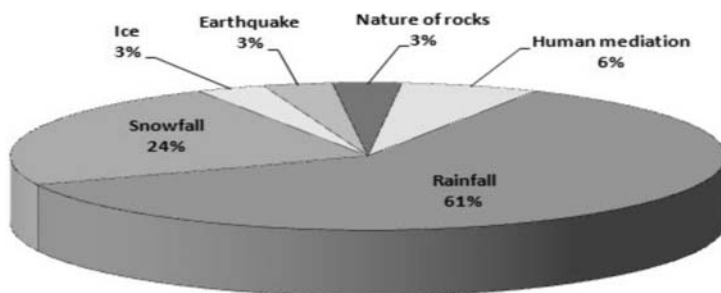


Fig. 5. Most common triggering mechanisms for recorded historical landslides.

When more than one source was available for the same landslide event, the data were extracted from those sources that were judged to be the best documented or most reliable. In case of multiple sources, we selected the cross-examination of the sources adopting the most conservative descriptions.

5. Results

Landslide events occurring in the region of Ioannina are mostly a topic of the local press and it is only the major landslides events that they appear in the national press. After having obtained a large database of the articles corresponding to a large time span of 60 years, articles were analyzed both quantitatively and in qualitative terms and provided useful information about landslides events and the way they gain publicity.

5.1 Landslides' triggering mechanisms

The major percentage (88%) of the landslide events in the prefecture takes place after extreme physical phenomena (heavy rainfall, snowfall and ice)(Figs. 4 and 5). According to the statistic analysis of 800 cases of landslide events in Greece, the mean annual rainfall height corresponding to the landslide areas is 1164,8 mm while for 50% of the cases 1090 mm (Koukis 1988; Koukis and Ziourkas 1991). Also the relative frequency of landslides and the mean annual rainfall height is connected through an exponential relationship (Koukis, 1988). Our results are in accordance with these studies as the landslide events under study occur due to extreme physical phenomena such as heavy and continuous rain, snowfall, ice and strong wind. Specifically according to the press reports landslides triggered by rainfall correspond to 62%, these related with snowfall to 23% and ice 3% (Fig. 5). Rainfalls are the most frequent triggering mechanism of the historical landslides recorded. Although landslides have occurred throughout the year, their monthly distribution clearly shows an increment in the number of events during the period from January-March and November-December (Fig. 6). These time periods seem to be the months with the major rainfall percentage in the prefecture.

The time period between the rainfall and the landslide event was about 2 – 3 days. In minor percentages the landslide events were due to other causes (e.g. earthquakes). Still, someone could consider the human factor, which can act upon the site or the extent of the landslide event.

5.2 Landslides' temporal and spatial distribution

Newspaper sources provided a rich database of spatial information about the occurrence of land-

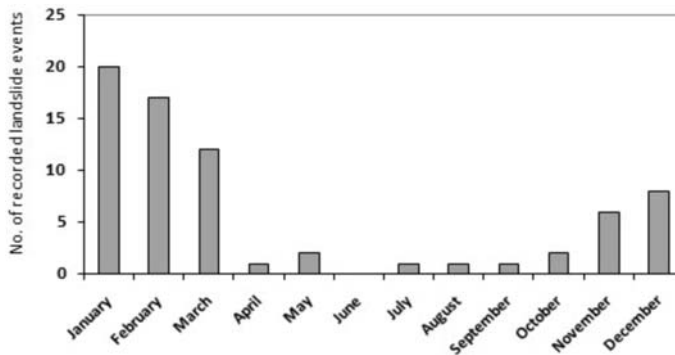


Fig. 6. Monthly distribution of recorded landslides in the period investigated.



Fig. s. 7 and 8. Landslide events in regions of the Ioannina Prefecture during 1963-1966 (on the left) and 2003-2008 (on the right).

slides events in the prefecture. This information could best be presented in topographic maps.

Major landslide activity was observed during 1963-1966 (Fig.7) and 2003-2006 (Fig.8). The figure (9) represents the frequency of the landslide events related with its temporal distribution between 1963- 2008. Observations of the landslides activity during 1913-1923 are also referred by the elderly witnesses but their location and the triggering reasons remain unknown and thus any further analysis is difficult. However, overall the existence of three periods of concentration of landslides suggests repeatability of their clustering every forty years.

5.3 Landslides’ implications on the human

The major type of infrastructure and services affected by landslides events in the prefecture of Ioannina was national roads followed by buildings. There are two recorded life losses in 1964

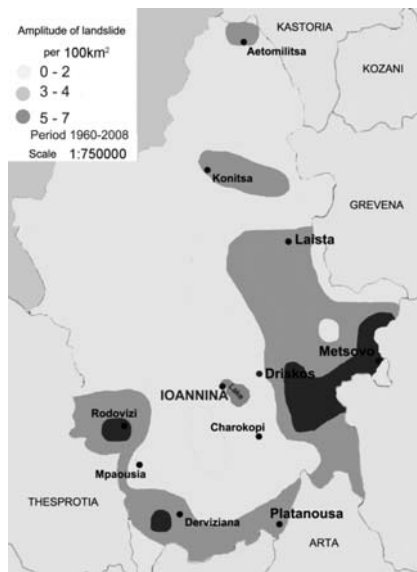


Fig. 9. The frequency of the landslide events related with its temporal distribution from between 1963-2008.

and 1996. Early press stories (1960-1970) present the landslide events with an emphasis on people's emotions rather than describing the actual event. The majority of the articles present the government's plans and actions in response to the destructive effects of the landslides, stress the amount of government subsidies to the families affected, while a great number of articles are edited by locals who are appealing to the government for help. In this early season, (1960-1970) reports also emphasize the causes of landslides (rain, snowfall, wind, ice, lack of trees to hold the soil) and their consequences.

The extent of press coverage of a landslide event was found to be analogous to the implications of the event for humans in the area. It was found that newspapers usually record landslides that affected people's infrastructure, and other human resources, emphasizing those large-magnitude events that occurred in urban areas or affecting roads and in those areas with press correspondents nearby. Whenever landslide events resulted in major disasters, newspapers presented reports of the events for 3-4 subsequent days in the first page. Usually, the newspaper returned to the landslide event after 8-10 days to comment on the government's actions and record the damages on properties and infrastructures due to the landslide event.

Landslides' consequences in the area's infrastructure and in the life of the locals are numerous. Articles report the accurate numbers of the families that suffered economic losses, cars destroyed, farms and places that flooded. Interestingly, there is plenty of numerical information concerning economic damages and government compensation schemes. As the majority of the landslides occurred nearby national roads, a very common consequence reported are damages in the national road infrastructure that cause delays and severe circulatory troubles.

It was also observed that between 1960 – 1970 - where the majority of landslide events occurred -, there is a considerable limited criticism to the government's measures. On the contrary, the press presents the government's response to the situation, emphasizing the compensation schemes and grants for the affected families. Gradually, the press coverage displays greater criticism to the government which appears to be inactive and neglect the situation in the area. So, while early stories rely heavily on official evaluations of the damages caused by landslides

and reporters' sources are government representatives who arrive in the area to estimate the damage, later on reporters rely mostly on personal experiences and witnesses' stories to present the extent of the damage.

While old newspaper articles were carefully written, offering precise descriptions of the events recent story writing displays some characteristics which undermine its credibility. According to contemporary reporting trends (2000-2008) stories present vivid descriptions of the landslides events. In general, recent stories give more accurate information regarding the place and the time of the landslides, include quotes from officials, are illustrated with photos and in some cases they provide estimations about future activity or warn citizens how to cope with possible future disasters. However, in an effort to emotionalize the disaster, reporters write their stories using long sentences with a plethora of adjectives, unrealistic metaphors and active verbs. Recent articles show a lack of experience and academic background of the reporters in the description of natural hazards. Such unrealistic accounts of the situation, may lead to an overestimation of the hazard or impede our understanding of landslides phenomena.

6. Summary and conclusion

For the first time indexing of local and national newspapers was performed and historical data was collected about landslide events in the prefecture of Ioannina. Newspapers represented the most important source of landslide information for the period between 1963-1990 in the absence of inventories and specific technical reports.

For the period 1963-2008 eighty nine landslide events were recorded. Information on the date of the event, location, triggering mechanisms, numbers of casualties, and damages on infrastructures was obtained.

The duration of newspapers' landslide reports through time was proportional with the size of the event or its consequences on people's infrastructure and properties. Occasionally, in the newspaper articles analysis of the landslide events from geologists are included.

The collected data can be used in the construction of an inventory of historical landslide events showing their type, temporal and spatial distribution. That will provide the basis for a more comprehensive landslide hazard assessment in the prefecture of Ioannina.

As it was recorded the major disasters on properties, roads and the greatest appeal on newspapers were during 1963-1966 and 2003-2006. Furthermore, after discussion with local elderly people it was revealed that major landslide events took place from between 1913-1923. This shows a repeatability of major landslide events in the Prefecture every forty years.

7. References

- Calcaterra, D., Parise, M., and Palma, B., 2003. Combining historical and geological data for the assessment of the landslide hazard: a case study from Campania, Italy. *Nat Hazards Earth Syst Sci*, 3, 3-16.
- Carrara, A., Crosta, G., and Frattini, P., 2003. Geomorphological and historical data in assessing landslide hazard, *Earth Surf Process Landforms*, 28, 1125-1142.
- Devoli, G., Morales, A., and Høeg, K. 2007a. Historical landslides in Nicaragua—collection and analysis of data. *Landslides*, 4, 5-18.
- Devoli, G., Strauch, W., Chávez, G., and Høeg, K., 2007b. A landslide database for Nicaragua: a tool

- for landslide-hazard management, *Landslides*, 4, 163-176.
- Dominguez Cuesta, M.J., Jimenez Sanchez, M., Rodriguez, G.A., 1999. Press archives as temporal records of landslides in the North of Spain: relationships between rainfall and instability slope events. *Geomorphology*, 30, 125-132.
- Doutsos, T., Koukouvelas, I.K., and Xypolias, P., 2006. A new orogenic model for the External Hellenides. In: Robertson, A.H.F. & Mountrakis, D. (eds) *Tectonic Development of the Eastern Mediterranean Region*, *Geol Soc Spec Publ* 260, 507-520.
- Doutsos, T., Koukouvelas, I., Zelilidis, A., and Kontoloulos N. 1994. Intracontinental wedging and postorogenic collapse in the Mesohellenic Trough. *Geol Rund*, 83, 257-275.
- Guzzetti, F., Cardinali, M., Reichenbach, P. 1994. The AVI project- A bibliographical and archive inventory of landslides and floods in Italy. *Environ Management*, 18, 623-633.
- Guzzetti, F., Cipolla, F., Lolli, O., Pagliacci, S., Sebastiani, C., Tonelli, G., 2002. Information system on historical landslides and floods in Italy. *Urban Hazards Forum*. John Jay College, CUNY, New York.
- Κούκης Γ., και Ρόζος, Δ., 1982. Γεωτεχνικές συνθήκες και κατολισθητικές κινήσεις στον Ελληνικό χώρο, σε σχέση με τη γεωλογική δομή και γεωτεχνική εξέλιξη. *Ορυκτός Πλούτος*, τεύχος 16, Αθήνα
- Κούκης, Γ., και Ζίουρκας, Κ., 1989. Κατολισθητικές κινήσεις στον Ελληνικό χώρο - Στατιστική θεώρηση. *Ορυκτός πλούτος*, 58, 39-58.
- Koukis, G., 1988. Slope deformation phenomena related to the engineering geological conditions in Greece. *Proceedings 5th Inter. Symp. on Landslides*, 2, 1187-1192.
- Koukis, G., Ziourkas, K., 1991. Slope instability phenomena in Greece. A statistical analysis. *Bulletin of the Int. Assoc. of Engineering Geology*, 43, 47-60.
- Koukis, G., Tsiambaos, G., Sabatakakis, N., 1994. Slope movements in the Greek territory: A statistical approach. *Proceedings 7th International Congress, IAEG*, 4621-4628, Lisboa-Portugal.
- Koukis, G., Tsiambaos, G., Sabatakakis, N., 1996. Landslides in Greece: Research, evolution and quantitative analysis. *Proceedings 7th International Symposium on Landslides, 1935-1940*, Trondheim, Norway.
- Koukis, G., Rozos, D., Hatzinakos, I., 1996. Rainfall induced landslides in Achaia county, Greece. *Proc. of International Congress of I.A.E.G.*, A. A. Balkema, Vol. III, pp 1929-1934, Norway.
- Koukis, G., Rozos, D., Hatzinakos, I., 1997. Relationship between rainfall and landslides in the formations of Achaia county, Greece. *Proc. of International Symposium of I.A.E.G. in Engineering Geology and the Environment*, A.A. Balkema, Vol.1, pp.793-798, Ιούνιος 1997. Rotterdam.
- Sawyer, C., Butler, D., 2006. A chronology of high-magnitude snow avalanches reconstructed from archived newspapers. *Disaster Prevention and Management*, 15, 313-324.
- Tarhule, A., 2005. Damaging rainfall and flooding: The other Sahel hazards. *Climatic change*, 72, 355-377.
- Tropeano, D., Turconi, L., 2004. Using Historical Documents for Landslide, Debris Flow and Stream Flood Prevention. *Applications in Northern Italy*, *Natural Hazards*, 31, 663-679.
- Wrathall, J., 2007. *Natural Hazard Reporting in the UK*. Press. *Disasters*, 12, 177-182.
- Xypolias, P., and Koukouvelas, I.K., 2005. Paleostress magnitude in a Fold-Thrust Belt (External Hellenides, Greece): evidence from twinning in calcareous rocks. *Episodes*, 28, 245-251.
- Ζίουρκας, Κ., και Κούκης, Γ., 1989. Κατολισθητικά φαινόμενα στο Νομό Ευρυτανίας. Πολυμεταβλητή ανάλυση δεδομένων. *Δελτίο Κ.Ε.Δ.Ε.*, 1-2, 15-30.

Internet

www.epirus.gov.gr

www.hnms.gr

<http://medlab.cs.uoi.gr>

[http://www.ntua.gr/MIRC/db /epirus_db/ GEOLOGIA_HPEIROY/Geologia_Hpeirou.htm](http://www.ntua.gr/MIRC/db/epirus_db/ GEOLOGIA_HPEIROY/Geologia_Hpeirou.htm)

Newspapers

Eleftheria

Eleftherotipia

Ethnos

Hpeirotikos Agonas

Kathimerini

Proinos Logos

Rizospastis

Ta Nea

To Vima

MACROSEISMICITY AND GEOLOGICAL EFFECTS OF THE WENCHUAN EARTHQUAKE (Ms 8.0R - 12 MAY 2008), SICHUAN, CHINA: MACRO-DISTRIBUTION AND COMPARISON OF EMS₁₉₉₈ AND ESI₂₀₀₇ INTENSITIES

Lekkas, E.

¹ *National & Kapodistrian University of Athens, Department of Geology & Geoenvironment, Sector of Dynamic Tectonic Applied Geology, Panepistimioupoli Zografou, Athens 15784, Greece, elekkas@geol.uoa.gr, www.elekkas.gr*

Abstract

The Wenchuan earthquake of the 12th of May 2008, in Sichuan county of China can be classified as a large scale event based on the tectonic structures that triggered the earthquake and the effects caused on the human, structural and natural environment. The aim of this paper is to present the geotectonic and seismotectonic regime of the earthquake affected region based on field data along the seismic fault zone and an attempt is made towards the: (i) estimation of the intensity values according to EMS₁₉₉₈ (European Microseismic Scale, 1998) and ESI₂₀₀₇ (Environmental Seismic Intensity Scale, 2007) and the determination of their geographical distribution in a macroscale, (ii) interpretation of the intensity values data and their distribution according to the seismotectonic, geodynamic and geotechnical regime, and (iii) conduction of a comparative evaluation review on the application of both EMS₁₉₉₈ and ESI₂₀₀₇. The application of both EMS₁₉₉₈ and ESI₂₀₀₇ and the comparative evaluation of the results indicate that the estimated values of EMS₁₉₉₈ and ESI₂₀₀₇ were almost in agreement, despite the fact that the geographical locations of assessment data were different suggesting that the application and use of both scales appears to represent a useful and reliable tool for seismic hazard estimation.

Key words: Wenchuan earthquake, China, macroseismicity, geological effects, EMS₁₉₉₈, ESI₂₀₀₇.

1. Introduction

On May 12, 2008, a great earthquake of Ms 8.0 (Mw 7.9) struck south China. This catastrophic event caused many human casualties and heavy engineering damages in a wide area along the Longmenshan fault zone. Numerous buildings collapsed or were damaged to various levels due to the fault displacement extending over 220 km and the many earthquake related phenomena, such as landslides, rock falls mudslides and liquefactions. The basic lifeline systems such as transportation, electricity, communications, water supply and drainage, gas and hydraulic structures etc, were heavily damaged at a level not previously encountered in Chinese history. The heavily damaged roads, bridges, power lines and other systems obstacolated significantly the earthquake relief work, contributing to the human and economic loss.

As reported by the Chinese Ministry of Civil Affairs (September 4), the death toll reached 69,226 casualties and the number of missing was 17,923. Moreover, 374,200 injuries were recorded. The

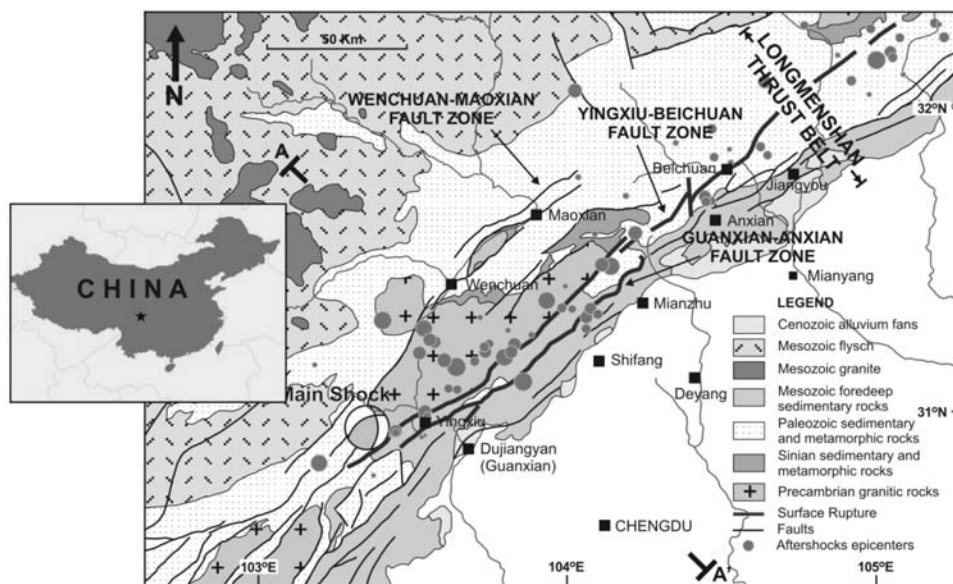


Fig. 1: Geological map of the greater earthquake affected region (12th May 2008) exhibiting the activated faults, the main shock location and the epicenters of the main aftershocks (modified, from Burchfiel et al. 1995, Densmore et al. 2007). For section AA' see Figure 2.

number of homeless people amounted to over 15 million. The percentage of homeless people exceeded 90% in the inflicted areas of Beichuan and Qingchuan. The estimated direct economic property loss (including infrastructure) is about 845 billion RMB (82 billion €).

The epicenter of the earthquake was located in Yingxiu town (31.0°N, 103.4°E) in the southwest side of Wenchuan County, with a focal depth of 14 km according to the Chinese Earthquake Administration (CEA), 21 km from Dujiangyan (Guanxian), and 75 km from the capital of Sichuan province, Chengdu (Fig. 1).

The aims of this paper are: (i) to briefly present the geotectonic and seismotectonic regime of the region affected by the earthquake based on field data along the causative fault, (ii) to estimate the intensity values according to the EMS₁₉₉₈ (Grünthal, 1998) and ESI₂₀₀₇ (Michetti et al., 2007) and to determine their geographical distribution in a mapscale, (iii) to interpret the intensity values data and their evolution according to the seismotectonic, geodynamic and geotechnical regime, (iv) to conduct a comparative evaluation review on the application of both EMS₁₉₉₈ and ESI₂₀₀₇.

2.1 Geodynamic – Seismotectonic Framework

This epicentre of this great earthquake was located on the Longmenshan thrust belt, which is a well studied reverse fault zone in the northwest of Sichuan Province (Burchfiel et al. 2008, Chen et al. 2008). This fault zone starts from Luding and Tianquan in the south, extends north-eastwards through Baoxing, Dujiangyan (Guanxian), Beichuan, Jiangyou, and Guangyuan, up to Mianxian of Shanxi Province. The total length is about 500 km, and the width is 40-50 km. The fault zone comprises 3 splays (Figs 1, 2). The southern segments of these fault splays are the Guanxian-Anxian Fault, Yingxiu-Beichuan Fault and Wenchuan-Maoxian Fault respectively (Burchfiel et al. 1995, Densmore et al. 2007).

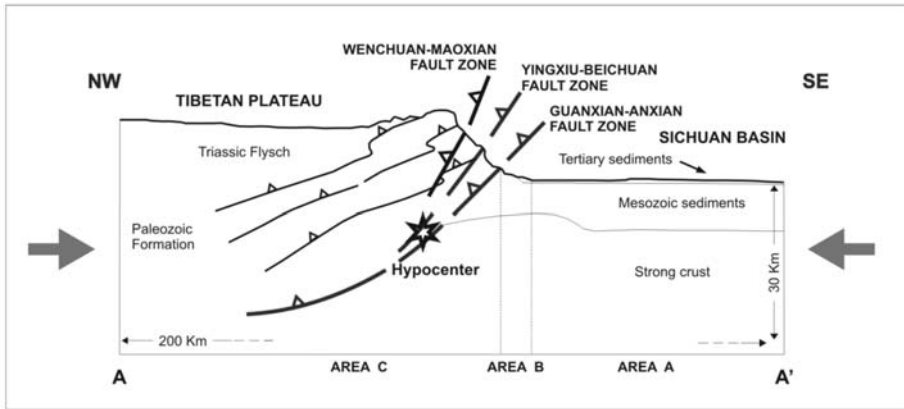


Fig. 2: Geological section trending NW-SE across the tectonic structure of the affected region with the activated faults and the epicenter location. The areas A, B and C are noted to exhibit variations of the intensities values (Burchfiel et al. 1995, Densmore et al. 2007).

The earthquake generated 220 km of surface rupture along the Yingxiu-Beinchuan fault, characterized by right-lateral oblique slip and 72 km of surface rupture along the Guanxian-Anxian fault, characterized by reverse slip (Fig. 1). Maximum vertical and horizontal displacements of 6.2 m and 4.9 m, respectively, were recorded along the Yingxiu-Beinchuan fault, whereas maximum vertical and horizontal displacements of 3.5 m and 1.0 m, respectively were recorded along the Guanxian-Anxian fault (Hao et al. 2008, Chen et al. 2008). The overall strike of the fault zone is N45°E, dip angle 50-70° towards the NW. This large scale fault zone is not only the boundary between Ganqing Block and South China Block, but also the boundary between the mountainous area and the basin of Sichuan. It separates: (i) the extended region of Tibetan Plateau towards the west – northwest with high altitudes exceeding 5,000 m and (ii) the Sichuan Basin towards the SE representing extended lowland with altitudes that do not exceed 1,000 m.

In conclusion, the distribution of this seismic fault as well as its kinematics and dynamic characteristics are attributed to the geodynamic frame of the greater region, characterized by large scale thrusting of the Tibetan Plateau towards the east on the rigid block of Sichuan Basin. This geodynamic frame is a result of the prevailing compressional regime along the Himalayan Mountain belt attributed to the progression of the Indian plate towards the north. (Burchfiel 2004, Burchfiel et al. 2008, Densmore et al. 2007, Gan et al. 2007, Hubbard & Shaw 2009, Royden et al. 2008, Tectonics Observatory of Caltech 2008, Zhang et al 2004, USGS 2008).

3. Intensity Estimation According to EMS₁₉₉₈

Based on field work and recordings of damages on infrastructure and constructions conducted in an extended region of the order of 50,000 km² and based on recent publications (Houssam et al. 2008, Sun et al. 2008, Lekkas 2008a, Kabeyasawa et al. 2008), the following values and geographical distribution of intensities according to EMS₁₉₉₈ (Grünthal 1998) were observed.

AREA A

It mainly corresponds to the extended lowland region of Sichuan Basin (Figs 1, 2) with altitudes that do not exceed 1000 m.

A1. Shifang Region: The Shifang town and the greater surrounding area are located on the morphologically flat area, approximately 15 km towards the SE of the Guanxian-Anxian fault. It is estimated that 10% of the buildings collapsed or suffered severe damages, while more than 20% of the constructions underwent structural damages. These were multistory constructions usually from 2 to 6 floors which probably presented structural imperfections, while there was no systematic geographical differentiation of the collapses within the urban centre. It should be pointed out that the founding substratum corresponds to cohesive Quaternary formations which unconformably lay on the rocky basement of the Sichuan Basin and are not more than 200 m thick. The estimated intensity value for this region is $VII_{EMS-1998}$.

A2. Mianyang Region: The Mianyang region is located on the morphologically lowland section 20-30 km towards the SE of the fault trace. The recorded damages mainly included fractures on the walls of first floors of modern constructions, while only a small number of multistory buildings collapsed or suffered serious structural damages. These were constructions with up to 6 floors that probably presented structural imperfections and did not follow the modern anti-seismic design regulations. The geological – geotechnical conditions are uniform and do not differentiate from site to site within the urban centre. In the greater area, cohesive Quaternary formations occur that cover older Sichuan Basin formations. The estimated intensity value for this area is on the order of $VI_{EMS-1998}$.

A3. Deyang Region: The Deyang Town and the surrounding area is located on the morphologically lowland section, approximately 25-40 km SE of the seismic fault. The observed damages in the region mainly include cracks on the walls of the first floors of modern constructions, while a small number of multistory buildings collapsed or suffered severe structural damages. These were constructions, usually up to 5-6 floors, that probably presented structural imperfections and did not follow modern anti-seismic design regulations. In addition, it should be mentioned that the collapses and damages presented random distribution within the urban area. It is estimated that the intensity value in this region is on the order of $VI_{EMS-1998}$.

AREA B

Essentially, this area, 10-20 km wide and 250 km long (Figs 1, 2), corresponds to the elongated region of NE-SW direction that includes the foothills of the Tibetan Plateau and more specifically it is bounded by the flat lowland region towards the southeast of Sichuan Basin and by the trace of the coseismic fault rupture to the northwest.

B1. Dujiangyan Region: The town of Dujiangyan (Guanxian) is located 20 km east of the epicenter, 50 km west of the capital city Chengdu, in the zone defined by the boundary between the lowland and the high relief regions. It is located only 5 km towards the SE of the seismic fault trace. The town develops in its greater extent on a large scale alluvial fan, formed by the Min River that drains a wide mountainous region, while some of its branches run through the town. In the town, approximately 300 constructions totally or partially collapsed while 20% of the buildings suffered serious construction damages. Mainly multistory buildings collapsed, modern and older, constructed of reinforced concrete. Most collapses were located on the foothills of the mountainous region towards the west and the morphologically higher areas and less on the lowlands. Especially interesting are the new buildings under construction that follow modern anti-seismic design regulation at the higher elevations of the town that collapsed or underwent serious structural damages. In these areas, it seems that the nature of the founding ground which is composed of remnants of river deposits and debris of limited thickness on the rocky background played a determinant role. It is estimated that 30% of the building collapses observed in this town were located on similar deposits (Fig. 3). Finally it should be mentioned that schools, hospitals and tenths of factories and industrial constructions collapsed in the



Fig. 3: View of a recently constructed building at the suburbs of Dujiangyan (Guanxian) with serious structural damages on the ground floor props. (type of construction D, damage degree 4) (a) and view of a hospital unit in the same town that totally collapsed (type of construction D, damage degree 5) (b).

greater urban area while all sort of infrastructure suffered serious damage. The estimated general intensity value in the area is on the order of $VIII_{EMS-1998}$, while locally it approached $IX_{EMS-1998}$.

B2. Mianzhu Town: The town of Mianzhu is located 50 km NE of the Dujiangyan (Guanxian) town and only 5 km SE of the seismic fault. It is estimated that 20% of the buildings totally or partially collapsed, while 60% of the buildings suffered considerable damages. The damages are mainly on multistory buildings, modern or older, while constructions with 1 or 2 floors suffered fewer damages. Dominant causes for the damages in many constructions were the architectural mannerism and features, especially in cases of constructions with frames without high level of earthquake resistant design. Moreover, many schools, hospitals and industrial units collapsed causing thousands of casualties while the infrastructure was either destroyed or seriously damaged. The estimated intensity in the area exceeded $VIII_{EMS-1998}$ and locally approached $IX_{EMS-1998}$.

AREA C

This region characterized by widespread damage represents the mountainous section of the Tibetan Plateau that includes towards the southeast the outcrop of the seismic fault extending northwest for at least 100 km (Figs 1, 2).

C1. The Beinchuan Regions: The Beinchuan, Hongbai, Hanwaug, Yingxiu, Guanxian, Jiangyou towns as well as smaller settlements, are scattered in the mountainous western section of the affected region. They develop mainly on the morphologically flat areas and especially on older and modern river terraces and on slopes on both sides of the river terraces. Both slopes and river terraces are composed of unconsolidated formations and more specifically by river – stream deposits that are characterized by a dominant presence of pebbles, breccia, and graded material and by recent and older debris as well as fans of variable thickness. The above formations cover in a great extent the Tibetan Plateau formations.

Impressive was the trace of the main branch of the seismic fault (Yingxiu-Beinchuan Fault) from the suburbs of the Beinchuan and Yingxiu towns, while the same branch trace was recorded through the region including the smaller towns of Hongbai and Hanwaug. In those regions and at a zone 150 m wide around the trace, total collapses of constructions were recorded, even in recent constructions that followed anti – seismic design regulations

The damage suffered by old and new constructions was a result of this above described morpho-



Fig. 4: Oblique aerial view of residential constructions in the Wenchuan and Beinchuan towns that suffered total destruction. These towns were founded on river terraces in the mountainous region. Large scale landslides on the surrounding slopes contributed to the destruction of the residential constructions (Xinhua News Agency China 2008, Reuters 2008).

logical, geological, tectonic and geotechnical framework. In the Wenchuan region, 85% of the constructions collapsed partially or totally, while the rest suffered significant structural damages. It is indicative that only a few buildings (<15%) did not suffer partial or total collapse. The estimated intensity for this region is $XI_{EMS-1998}$ while in some locations approached $XII_{EMS-1998}$.

C2. Wenchuan Town – Maoxian Town: The Wenchuan and Maoxian towns are located 30 km west of the activated Yingxiu-Beinchuan fault branch, along the Wenchuan-Maoxian fault branch that was not activated during the earthquake.

In all settlements, the constructions collapsed or suffered considerable structural damage to an extent that exceeded 50% (Fig. 4). It is indicative that only a small percentage of the constructions, that did not exceed 20%, was left intact. In addition, infrastructures such as bridges, tunnels and dams either collapsed or suffered considerable damage. Finally, in the greater region, landslides and rock falls were recorded due to the high energy relief and the unconsolidated lithologies, that caused additional damage in settlements and infrastructure. The general estimated intensity for this region is $X_{EMS-1998}$ and locally approaches $XI_{EMS-1998}$.

4. Intensity Estimation according to ESI_{2007}

Extended observations and recordings were carried out in the study area investigating the primary and secondary effects based on the ESI_{2007} guidelines (Michetti et al., 2007). Observations of the primary and secondary effects were carried out in a region exceeding 50,000 Km^2 and are presented for each area from west to east in the following paragraphs. Recent publication data were taken into account (Hao et al. 2008, Lekkas 2008a, Lekkas 2008b, Chen et al. 2008, Zhao et al. 2008). The main results are summarized in Table 1.



Fig 5: Views of the Yingxiu-Beinchuan seismic fault at the outskirts of Yingxiu town.

AREA A

A1. Significant variations of the water level in wells and of the flow-rate of springs were locally recorded, as well as small variations of the physical properties of water; turbidity in lakes, springs and wells were also observed.

A2. Fractures up to 5-10 cm wide and up to hundred meters long were observed, commonly in loose alluvial deposits and saturated soils. Centimeter-wide cracks were common in asphalt roads.

A3. Liquefaction was frequently recorded in the area, depending on local conditions; the most typical effects were: sand boils up to ca. 1 m in diameter; apparent water fountains in still waters; localized lateral spreading and settlements (subsidence up to ca. 30 cm), with fissuring parallel to waterfront areas (river banks, lakes, canals) (Chen et al. 2008).

The overall estimated intensity value for Area A is VII – VIII_{ESI-2007}.

AREA B

B1. Ground ruptures were recorded, up to a few km long, with offsets generally in the order of several cm.

B2. Springs changed, generally temporarily, their flow-rate. Some modest springs even run dry. Temporary variations of water level were also observed in wells. Variations of chemical-physical properties of water, most commonly temperature, were observed in springs.

B3. Fractures up to 100 cm wide and up to hundreds meters long were observed in loose alluvial deposits and saturated soils. Cracks were common in paved asphalt roads, as well as small pressure undulations.

B4. Landslides were widespread in prone areas, also on gentle slopes; as well as rock falls on steep gorges, their size being frequently large (10^5 m³). Landslides dammed many valleys causing temporary or even permanent small lakes. Many riverbanks, artificial embankments and excavations collapsed.

B5. Liquefaction and water upsurges were frequent; sand boiled up to 3 m in diameter; the most typical effects being: apparent water fountains in still waters; frequent lateral spreading and settlements (subsidence of more than ca. 30 cm), with fissuring parallel to waterfront areas.

B6. Small boulders and tree trunks were thrown in the air and carried away from their site for meters depending on slope angle and roundness, leaving typical imprints in soft soil.

Table 1.

		PRIMARY EFFECTS					SECONDARY EFFECTS		
		Surface faulting and deformations	Hydrological anomalies	Anomalous waves / tsunamis	Ground cracks	Slope movement	Liquefactions	Jumping Stones	Total Area
From I to III		There are no environmental effects that can be used as diagnostic							
VI	SLIGHTLY DAMAGING Modest effects in the environment								
VII	DAMAGING Appreciable effects in the environment		A1		A2				
VIII	HEAVILY DAMAGING Extensive effects in the environment						A3		10 km ²
IX	DESTRUCTIVE Effects in the environment are a widespread source of considerable hazard and become important for intensity assessment	B1	B2		B3	B4	B5	B6	1 000 km ²
X	VERY DESTRUCTIVE Effects in the environment become a leading source of hazards and are critical for intensity assessment						C6		5 000 km ²
XI	DEVASTATING Effects in the environment become decisive for intensity assessment, due to saturation of structural damage		C2	C3	C4	C5		C7	10 000 km ²
XII	COMPLETELY DEVASTATING Effects in the environment are the only tool for intensity assessment	C1							50 000 km ²

The estimated intensity value for Area B is $IX_{ESI-2007}$.

AREA C

C1. As reported above, this earthquake generated a 220 km surface rupture along the Yingxiu-Beinchuan fault and a 72 km surface rupture along the Guanxian-Anxian fault (Figs 1, 5). Maximum vertical and horizontal displacements of 6.2 m and 4.9 m, respectively, were observed along the Yingxiu-Beinchuan fault, whereas a maximum vertical displacement of 3.5 m occurred along the Guanxian-Anxian fault (Hao et al., 2008).

C2. Many springs significantly changed their flow-rate and elevation of outcrop. Additionally, many springs run temporarily or even permanently dry. Temporary or permanent variations of water level were observed in wells. Strong variations of physical properties of water, most commonly temperature, was observed in springs. Water became very muddy in large basins, rivers, wells and springs.

C3. Intense water undulations were recorded in the lakes of the area either due to the earthquake tremor or due to landslides triggered at the banks. It is worth mentioning that at the artificial lake of the Zipingpu dam the waves caused by the extensive landslides in the surrounding mountains exceeded 10 meters in height causing the death of about 100 fishermen.

C4. Open ground cracks up to several meters wide were very frequently recorded, mainly in loose alluvial deposits. In competent rocks they did not exceed 1 m.

C5. Large landslides and rock-falls ($>10^5-10^6$ m³) were frequently recorded, practically regardless of equilibrium state of slopes (Figs 6, 7), causing many temporary or permanent barrier lakes. River banks, artificial embankments, and sides of excavations collapsed. Levees and earth dams incurred serious damages (Lekkas 2008b, Zhao et al. 2008, Xu et al. 2009).

C6. Liquefaction, with water upsurge and soil compaction was recorded, that changed the aspect of wide zones; sand volcanoes more than 8 m in diameter, vertical subsidence > 3 m, large and long fissures due to lateral spreading were common.

C7. Big boulders with diameter of several meters were thrown in the air and moved away from their site for long distances down even gentle slopes.

The estimated intensity values for Area C range from X to $XII_{ESI-2007}$ (Fig. 7).

5. Discussion and Conclusions

The earthquake of the 12th of May 2008 in Sichuan county of China can be classified as a large scale event based on the size of the tectonic structures that triggered the earthquake and the effects caused on the human and natural environment.

Intensity values could be estimated for a broad area around the epicentre based on EMS_{1998} and ESI_{2007} (Figs 7, 8).

Area A is characterized by intensities VI-VII $_{EMS1998}$ as a result of its relative distance from the seismic fault, the flat relief and relatively favorable geotechnical conditions and of course the development of the area on the footwall that Sichuan basin represents. As a result of the above, the damages in constructions were restricted and in general were decreasing towards the east – southeast, as the horizontal distance from the seismic fault and the epicenter was increasing. In the area values of VII-VIII $_{ESI2007}$ were recorded that, compared to the VI – VII values of the EMS_{1998} , are locally higher by one degree mainly as a result of the widespread liquefactions, hydrological changes and

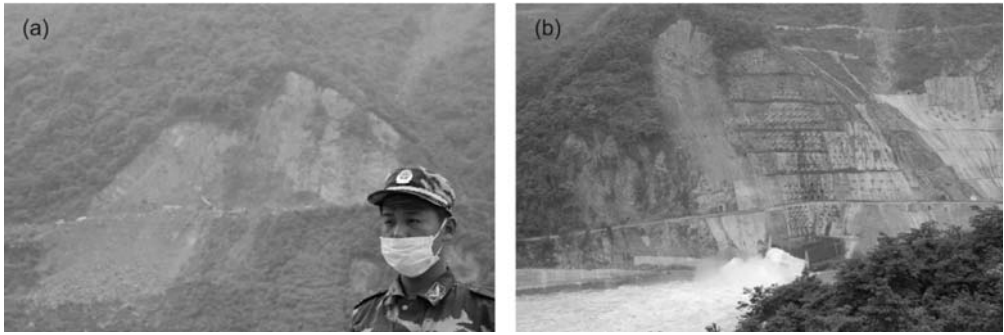


Fig. 6: View of large-scale landslides that were triggered in the mountainous region along river Min (a) and view of the Zipingpu Dam (b).



Fig. 7: Views of Beinchuan town which was almost totally destroyed ($ESI_{2007} = XI, XII$) due to the combined action of the seismic fault Yingxiu-Beinchuan (arrows) and the huge landslides.

ground failures. Nevertheless, in general, there is an agreement in the intensity values of both EMS_{1998} and ESI_{2007} for Area A.

Area B corresponds to the intermediate morphological zone between the high relief of Tibetan Plateau to the northwest and the Sichuan Basin to the southeast bounded towards the northwest by the trace of the seismic fault. It is characterized by a complex relief with characteristics corresponding mainly to rivers, alluvial deposits and debris fans. Here, the values according to EMS_{1998} reached VIII and only locally approached IX, while the values according to the ESI_{2007} reached IX. The highly developed hydrographic network, the high water table, the unconsolidated, partly cohesive material of the alluvial deposits and the intense phenomena of erosion and deposition of unconsolidated material created an adverse geotechnical setting for the development of urban centres. As well, these factors favored the triggering of secondary phenomena and intense morphological changes that affected directly the values of ESI_{2007} .

Area C corresponds to the portion of Tibetan Plateau characterized by high relief, steep slopes, dense river network, deep erosion and intense phenomena of erosion. It includes the tectonic structure activated during the earthquake and develops towards the west corresponding essentially to the causative fault hanging wall. In area C, the EMS_{1998} and ESI_{2007} intensity values are generally in agreement. The values $X-XII_{EMS-1998}$ represent extended collapses of constructions due to the un-

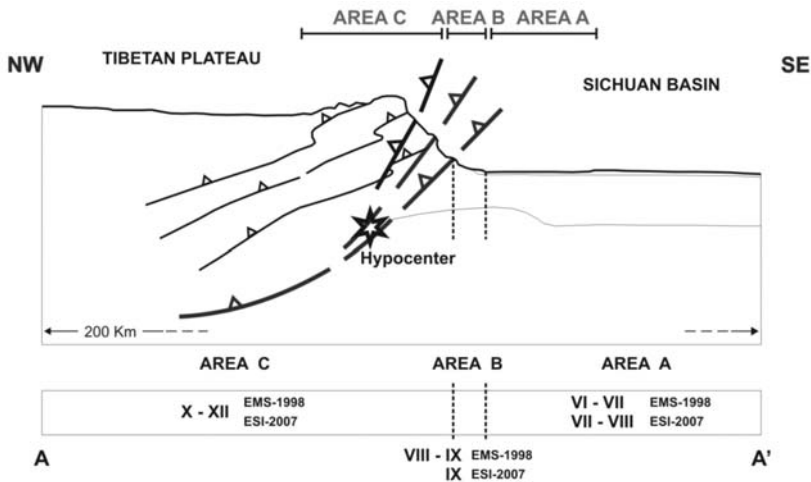


Fig. 8: Schematic cross-section NW-SE trending with the location of areas A, B and C and the estimated values according to EMS₁₉₉₈ and ESI₂₀₀₇ intensity scales.

favorable geotechnical and geomorphological conditions and to diffuse landslides. The values of X-XII_{ESI-2007} derive from the presence of the fault trace at surface and the secondary effects that developed in numerous places such as ground ruptures, large-scale landslides and tsunamis in lakes as a result of the geomorphological conditions, the negative geotechnical conditions and the complex geological setting.

Summarizing, by the application of both EMS₁₉₉₈ and ESI₂₀₀₇ and the comparison of the results based on the geodynamic, seismotectonic, geomorphological and geotechnical frame of the region affected by the 12th of May, 2008 earthquake, the following conclusions can be drawn (Fig. 8):

No significant variations on the values of both intensity scales were recorded during their application for the areas A, B and C, that correspond to three clearly distinct areas: (i) the flat lowland area of Sichuan Basin, located southeast of the trace of the seismic fault, (ii) the elongated area of a general northeast – southwest direction with special morphological characteristics, located to the southeast of the seismic fault trace and (iii) the region that includes the occurrence of extensive surface faulting to the west and corresponds to the Tibetan Plateau.

The value variations in both scales that were estimated between the footwall (area A) and the hanging wall (area C) are of the order of 2 to 4 degrees. At the elongated zone (area B) to the southeast of the activated fault zone intermediate values were estimated.

So the application and use of both EMS₁₉₉₈ and ESI₂₀₀₇ represent a fundamental tool for the estimation of seismic hazard in a region and should be encouraged. In particular, the ESI₂₀₀₇ could be applied to past, even prehistorical events time frames since it is based on geological effects not biased by cultural/technical differences either in time and space.

6. References

- Burchfiel, B.C. (2004). New Technology, New Geological Challenges. *GSA Today*, 14, No.2, 4-7.
- Burchfiel, B.C., Chen, Z., Liu, Y. and Royden, L.H. (1995). Tectonics of the Longmen Shan and adjacent regions, central China. *International Geological Review*: 37 661-738.

- Burchfiel, B.C., Royden, L.H., Van der Hilst, R.D. and Hager, B.H. (2008). A geological and geophysical context for the Wenchuan earthquake of 12 May 2008, Sichuan, People's Republic of China. *GSA Today*, 18, No.7. 4-11.
- Chen, L., Hou, L., Cao, Z., Yuan, X., Sun, R., Wang, W., Mang, F., Chen, H., and Dong, L. (2008). Liq-uefaction Investigation of Wenchuan Earthquake. 14th WCEE, Beijing, China, S31-049.
- Densmore A.L., Ellis, M.A., Li, Y., Zhou, R., Hancock, G.S., and Richardson, N. (2007). Active tectonics of the Beinchuan and Pengguan faults at the eastern margin of the Tibetan Plateau. *Tectonics*. 26 TC4005, doi:10.1029/2006TC001987.
- Gan, W.J., Zhang, P.Z., Shen, Z.K., Niu, Z.J., Wang, M., Wan, Y.G., Zhou, D.M., and Cheng, J. (2007). Present-day crustal motion within the Tibetan Plateau inferred from GPS measurements. *J. Geophys. Res. - Solid Earth*. 112 B08416, doi:10.1029/2005JB004120.
- Grünthal, G. ed. (1998). *European Macroseismic Scale 1998*. Conseil de l' Europe, 15 99.
- Hao, K.X.S., Si, H. and Fujiwara, H. (2008). A Preliminary Investigation of the Coseismic Surface-Ruptures for Wenchuan Earthquake of 12 May 2008, Sichuan, China. 14th WCEE, Beijing, China, S31-007.
- Houssam, M.A., Li, Y., Oday, A.S., A'ssim, A. and Wang, L. (2008). A Comprehensive Analysis Of The Devastating Wenchuan Earthquake Of May 12th 2008. 14th WCEE, Beijing, China, S31-014.
- Hubbard, J., and Shaw, J. (2009). Uplift of the Longmen Shan and Tibetan plateau, and the 2008 Wenchuan (M=7.9). *Nature*, 458 194-197.
- Kabeyasawa, T., Kabeyasawa, T., Kusunoki, K. and Li, K. (2008). An Outline of Damages to School Buildings in Dujiangyan by the Wenchuan Earthquake on May 12, 2008. 14th WCEE, Beijing, China, S31-002
- Lekkas, E. (2008a). Wenchuan Earthquake (Mw 7.9, 12 May 2008) Sichuan, China. Geotectonic Regime and Damage Macro-Distribution. 14th WCEE, Beijing, China, S31-015.
- Lekkas, E. (2008b). Zipingpu Dam Failures (Sichuan Prefecture, China) caused by the 7.9R Earthquake on the 12th May 2008. ESC 2008, 31st General Assembly, Crete Island, Greece, 238-239.
- Michetti A.M., Esposito, E., Guerrieri, L., Porfido, S., Serva, L., Tatevossian, R., Vittori, E., Audemard, F., Azuma, T., Clague, J., Comerci, V., Gürpınar, A., Mccalpin, J., Mohammadioun, B., Möerner, N.A., Ota, Y., Roghazin, E. (2007). Environmental Seismic Intensity Scale 2007 - ESI 2007. In: Guerrieri L. and Vittori E. (Eds.), *Memorie Descrittive della Carta Geologica d'Italia*, 74, 7-54, Servizio Geologico d'Italia – Dipartimento Difesa del Suolo, APAT, Roma, Italy.
- Royden, L.H., Burchfiel, B.C. and Van der Hilst, R.D. (2008). The geological evolution of the Tibetan Plateau. *Science*, 321. no. 5892, 1054 - 1058.
- Sun, J., Q. Meng, Ma, Q., Shi, H. and Sun, Z. (2008). Outline introduction of building damage in high intensity areas of Wenchuan M8.0 earthquake. 14th WCEE, Beijing, China, S31-020.
- Tectonics Observatory of Caltech (2008) The science behind China's 2008 Sichuan earthquake. <http://www.tectonics.caltech.edu/outreach/highlights/2008MayChinaEQ/index.html>.
- USGS (2008). Magnitude 7.9 - Eastern Sichuan, China <http://earthquake.usgs.gov/eqcenter/eqinthe-news/2008/us2008ryan/>.
- Xu, Q., Fan, X.M., and Westen, C.V. (2009). Landslide dams triggered by the Wenchuan Earthquake, Sichuan Province, South West China. *Bull Eng Geol Environ*, 68, No. 3, 373-386.
- Zhang, P.Z., Shen, Z., Wang, M., Gan, W.J., Burgmann, R. and Molnar, P. (2004). Continuous deformation of the Tibetan Plateau from global positioning system data, *Geology*, 32 809-812.
- Zhao, J., Zhou, Z. and Wu, J. (2008). Investigation of landslide and rockfall caused by Wenchuan earthquake of Ms8.0. 14th WCEE, Beijing, China, S31-050.

PROBABILISTIC EVALUATION OF LIQUEFACTION-INDUCED GROUND FAILURES TRIGGERED BY SEISMIC LOADING IN URBAN ENVIRONMENT; CASE STUDIES FROM GREECE

Papathanassiou G.¹, Pavlides S.¹

¹ Aristotle University of Thessaloniki, Department of Geology, 54124 Thessaloniki, Greece,
gpapatha@auth.gr

Abstract

An issue that should be taken into account by urban planners in Greece, for the extension of urban areas, is the likelihood of earthquake-induced ground deformations. In this paper, information is provided regarding the methodology that is applied for the prediction of liquefaction manifestations in urban environment. In particular, a review of our research concerning the evaluation of the probability of liquefaction-induced ground disruption in three towns, Larissa, Edessa and Lefkada, is presented. The evaluation of probability was achieved using the Liquefaction Potential Index methodology and the relatively classification, introduced in late 80's and modified by Papathanassiou (2008).

Key words: liquefaction, urban geology, hazard, Greece

1. Introduction

Studies regarding the probabilistic evaluation of liquefaction potential of the geological units in Greece started in the beginning of this decade at the Department of Geology of Aristotle University of Thessaloniki. The occurrence of liquefaction phenomena and the generation of relative failures are crucial issues that should be taken into account regarding the safety of structures within an urban environment due to the seismotectonic regimen and the historical seismicity of the broader Aegean Region. In particular, Greece shows the highest seismicity in Europe and is considered as one of the most prone to earthquakes countries globally. According to the new Greek Seismic Code (EAK 2000), Greece is subdivided into three seismic hazard zones where the design accelerations on seismic bedrock are assigned as 0.16g, 0.24g and 0.36g for the first, the second, and the third zone, respectively. However, regarding the local scale studies, the influence of site-effects should be taken into account for the estimation of the surface acceleration instead of the provided by EAK parameters of the design acceleration, a , which should be mainly employed in regional scale maps.

Furthermore, the susceptibility to liquefaction of several areas in Greece is shown by Papathanassiou et al. (2005), where a map of historical liquefaction occurrences in broader Aegean region, including Greece, is compiled based on descriptions included in seismic catalogues and primary sources. The outcome provided by this study is that these types of secondary effects reoccur within specific areas in Greece particularly in Thessaly, Ionian Islands and the Gulf of Corinth including the urban environments of the town of Larissa, Aeghio and Corinth.

Liquefaction is the transformation of saturated granular material from a solid state to a liquid state

as a consequence of increased pore pressures that reduce the effective strength of the material (Youd 1973). The liquefaction of a subsoil layer may induced surface disruption such as ground settlements, sand boils and lateral spreading and leads to structural damages at buildings, pipelines, bridges etc. Areas susceptible to liquefaction can be identified through detailed geologic, geomorphic and hydrologic mapping (Witter et al. 2006) while the liquefaction potential is evaluated based on data regarding the susceptibility to liquefaction of the soil layer and the expected value of ground motion triggered by the earthquake.

In order to evaluate the liquefaction potential of a subsoil layer, the procedure proposed by Youd et al. (2001) is usually applied. According to this procedure, the ability of a soil element to resist liquefaction is defined as factor of safety against liquefaction, F_s , and two variables are required for its calculation: the cyclic resistance ratio CRR and the earthquake induced cyclic stress ratio CSR at a specific depth for a given design earthquake. This deterministic approach has been modified the last decade by several researchers who proposed probabilistic-based approaches for the assessment of the liquefaction potential of a soil layer. Among them, the procedures proposed by Seed et al (2003) and Boulanger and Idriss (2004) were the most known methodologies that are applied by engineers and geologists.

In addition, Iwasaki et al. (1978), proposed an index (LPI) for the evaluation of liquefaction potential of a site instead of a soil layer. The advantage of LPI is that it quantifies the likely of liquefaction of the site, by providing a unique value for the entire soil column instead of several factors of safety per layer. Therefore, the values of LPI were used for the compilation of liquefaction hazard maps. These maps comprise a preliminary assessing tool of the liquefaction potential and can be used by decision makers for urban planning purposes.

In this study, a review of liquefaction studies performed in Greece is presented, regarding the evaluation of liquefaction potential in three towns; Lefkada, Larissa and Edessa. The goal of our research was twofold; a. evaluation of the surficial acceleration using different methodologies and b. focus on the role of the site conditions in comparison to the proposed by EAK values of ground motion and computation of the probability of liquefaction surface occurrence at these towns. The employed values of surface acceleration in our analysis were either recorded by accelerometers or estimated using 1-D site response analysis and geology-based proposed amplification factors. The liquefaction potential and the probability of liquefaction-induced ground disruption phenomena were evaluated using the approaches proposed by Iwasaki et al. (1978) and Papathanassiou (2008), respectively.

2. Liquefaction-induced failures in urban environment

Reports describing liquefaction related phenomena within the Aegean broader region can be found in seismic catalogues and primary sources from 1509 A.C. (Papathanassiou et al. 2005). Large scale manifestations were reported and mapped by Schmidt (1867) regarding the Aeghio 1861 earthquake while the first event that occurred close to an urban environment and studied in detail was the 1906 San Francisco earthquake. However, the most severe liquefaction-induced damages to civil infrastructure were observed after the Niigata and Anchorage earthquakes in 1964 which helped to identify liquefaction as a major problem within an urban area (Idriss and Boulanger 2008). Other major events that provided data regarding the occurrence of liquefaction were the 1989 Loma Prieta and the 1995 Kobe earthquakes. The latter event caused pervasive liquefaction throughout the reclaimed lands and the manmade islands in the Kobe region, causing extensive structural damages to quay walls around the port facilities and associated damage to the cranes and other supporting facilities (Idriss and Boulanger 2008).

Moreover, during the last decade of the 20th century two large earthquakes occurred in Turkey and Taiwan in 1999 that induced severe damages to the cities of Adapazari, Izmit, Golcuk and Nantou, Yuanlin, Wufeng, respectively. Data provided by post earthquake reconnaissance reports, performed in these urban areas, became the base layer for the modification of existing methodologies and for the introduction of new probabilistic approaches regarding the liquefaction hazard in urban environments.

In particular, sand boiling and lateral spreading were reported in association with coastal failures and the permanent displacements in horizontal and vertical directions due to lateral spreading ranged between 60 and 480 cm and 28 and 110 cm, respectively (Aydan and Ulusay 2000). The incidents of liquefaction phenomena were mainly observed in inland alluvial areas and along coastal areas inducing damage to ports and industrial facilities but some occurred in the free field away from the structures (Sonmez et al. 2008). The Chi-Chi earthquake (Taiwan) occurred in 1999 and induced the damages and collapses of bridges, port facilities and buildings. According to Yuan et al. (2003) among the 39 districts of the city of Yuanlin the 17 were found to have suffered significant settlement and 8 were found to have obvious liquefaction evidence such as sand boils (Sonmez et al. 2008).

Regarding Greece, the most severe liquefaction-induced structures damages within an urban area were reported at the waterfront area of the town of Lefkada. According to Papathanassiou et al. (2005) liquefaction occurrences (sand boils and vent fractures) were observed mainly in the waterfront area, and caused damages to pavements and sidewalks behind seawalls. In addition, severe damages to port facilities, probably due to liquefaction of the subsoil layers, were observed at the towns of Argostoli, Lixouri and Zakynthos after the devastating 1953 earthquake.

3. Methods for estimating the liquefaction potential

3.1 Evaluating the liquefaction susceptibility and the potential of the soil layers

The evaluation of liquefaction susceptibility used to be realized by applying the “Chinese” criteria (Wang, 1979) or the guidelines proposed by Andrews and Martin (2000). Both of these criteria taken into account the appearance of fine grain sized material in the soil element and particularly the percent of clay size. However, published papers by Seed et al. (2003) and Bray and Sancio (2006) stated that the plasticity behavior of fine size particles of soils is more important than the percent of clay-size fines. Thus, they proposed new criteria where soils with fines content more than 35% are considered as potentially liquefiable when its liquid limit is less than 37% and the plasticity index is less than 12% while the water content is high relative to their liquid limit (Seed et al. 2003).

Having evaluated the liquefaction susceptibility of the soil layers, the computation of the factor of safety should be performed. According to Youd et al. (2001) the factor of safety, F_s , is the ratio between the cyclic resistance ratio CRR and the earthquake induced cyclic stress ratio CSR.

The CSR is expressed as:

$$CSR = 0.65 \times \left(\frac{a_{\max}}{g} \right) \times \left(\frac{\sigma_{vo}}{\sigma'_{vo}} \right) \times r_d \quad (1)$$

Where σ_{vo} : total vertical stress at depth z , σ'_{vo} : effective vertical stress at the same depth, a_{\max} : peak horizontal ground acceleration, g : acceleration due to gravity and r_d : stress reduction factor. In this study, the term r_d was estimated using the Liao and Whitman (1986) equation:

$$r_d = 1.0 - 0.00765 \times z \quad \text{for } z < 9.15 \text{ m} \quad (2)$$

$$r_d = 1.174 - 0.0267 \times z \quad \text{for } 9.15 \text{ m} < z < 23 \text{ m} \quad (3)$$

Finally, the CSR values have been divided by the magnitude scaling factor, MSF, which is calculated by the following equation, Youd et al. (2001):

$$MSF = \left(\frac{Mw}{7.5} \right)^{2.56} \quad (4)$$

Afterwards, the CRR, is computed using the following equation (Youd et al. 2001)

$$CRR = \frac{1}{34 - N_{1(60)}} + \frac{N_{1(60)}}{135} + \frac{50}{[10 \times N_{1(60)} + 45]^2} - \frac{1}{200} \quad (5)$$

The calculation of $N_{1(60)}$ is influenced by the measured standard penetration resistance N , the overburden pressure factor C_n , the correction for hammer energy ratio (ER) C_e , the correction for borehole diameter, C_b the correction factor for rod length C_r and the correction for samplers with or without liners. The C_n was calculated according to the equation proposed by Liao and Whitman (1986), $C_n = (Pa/\sigma_{vo})^{0.5}$, while the others factors were estimated using the parameters suggested by Youd et al. (2001). Additionally, a “fine content” correction was applied to the calculated $N_{1(60)}$ value in order to obtain an equivalent clean sand value $N_{1(60)_{cs}}$ given by the equations proposed by Youd et al. (2001).

3.2 Estimating the surface acceleration value

A critical issue regarding the compilation of hazard maps in urban environment is to evaluate the earthquake parameters at the ground surface since the proposed by Greek Seismic code values should only be used for regional scale maps. In particular, the employed a_{max} should be estimated based either on ground motion recorded close to the study area or using geology-based amplification factors or performing 1-D site response analysis. Regarding the case studies that are presented in this review, the estimation of a_{max} was achieved based on these three options.

In order to account for amplification effect due to surface geology, the regression proposed by Stewart et al. (2003) can be used. In particular, the amplification factor, f , and the surface acceleration a_{max} are computed using the equations proposed by Stewart et al. (2003):

$$\ln(f) = a + b \ln(PGA) \quad (6)$$

$$a_{max} = PGA * f \quad (7)$$

where f is the amplification factor; a , b are parameters depending on the age and the material texture of soil; and PGA is the value of design acceleration on rock outcrop conditions; a_{max} is the value of surface acceleration which is employed on the evaluation of liquefaction potential.

A more sophisticated method, for the estimation of surface acceleration value is achieved by performing site response analyses. In particular, 1D analysis are based on shear wave velocities V_s values of the subsoil layers and real acceleration time histories that are selected with respect to the type of causative fault, the magnitude of the earthquake and the geological conditions at the recorded

station. A web site where time histories can be downloaded is the European Strong motion Database (ESD) www.isesd.cv.ic.ac.uk/ESD. Afterwards, a scaling based on the value of the design acceleration of Greek Seismic code is suggested and the scaled PGA time histories can be used as input motion in order to estimate the value of acceleration on ground surface.

3.3 Liquefaction Potential Index

The evaluation of liquefaction potential in urban areas can be finally achieved based on the Liquefaction Potential Index approach proposed by Iwasaki et al. (1978; 1982). The index is proportional to the thickness of the liquefiable layer, the thickness of the non-liquefiable (cap) layer and the value of the factor of safety against liquefaction and is defined as:

$$LPI = \int_0^z F(z)W(z)dz \quad (8)$$

Where z is the depth below the ground surface in meters; $F(z)$ is a function of the factor of safety against liquefaction, F_s , where $F(z) = 1 - F_s$ when $F_s < 0.95$, $F(z) = 2.106 e^{-18.427F_s}$ if $0.95 < F_s < 1.2$ and if $F_s > 1.2$, $F(z) = 0$ (Sonmez, 2003). Equation (1) gives the values of LPI ranging from 0 to 100.

Iwasaki et al. (1982) calibrated the severity of liquefaction-induced damages with the LPI values using data provided by 87 SPT borings in liquefied and non-liquefied sites in Japan. According to this calibration, liquefaction failure potential has been characterized as high where LPI ranges between 5 and 15 and low at sites where $0 < LPI < 5$. The liquefaction potential is extremely low where LPI is equal to 0, and extremely high at sites where $LPI > 15$. The LPI methodology was modified by Sonmez (2003), by adding a threshold value of 1.2 instead of 1 of the factor of safety and by introducing two new categories of potential, “non-liquefiable” and “moderate”. At sites where LPI values range between 2 and 5 the potential was defined as moderate, while where LPI ranges between 0 and 2 the site was characterized as low liquefaction potential area. Finally, sites where the LPI value is equal to zero were characterized as non liquefiable (Sonmez 2003).

Furthermore, Toprak and Holzer (2003) attempted to relate LPI with the severity of the surface manifestations of liquefaction, using CPT's from the 1989 Loma Prieta, California earthquake. They observed that the median values of LPI were 5 and 12, respectively, in areas with sand boils and lateral spreads. Lower and upper quartiles were 3 and 10 for sand boils and 5 and 17 for lateral spreads. Recently, Papathanassiou (2008) proposed a new calibration that resulted from the application of the box-whisker plot method to data provided by borings with SPT. According to this study, at sites where $LPI > 32$ liquefaction-induced failures of “high” degree, such as lateral spreading phenomena, are likely to occur, while at sites where $LPI < 19$ no liquefaction manifestations should be expected. At sites where the LPI value ranges between 19 and 29, “medium” degree of severity liquefaction surface evidence, such as sand boils and ejection of material is likely to occur. As it is stated by Papathanassiou (2008), a reason for the differences among the threshold LPI proposed by Iwasaki et al. (1982), Toprak and Holzer (2003) and Papathanassiou (2008) is that in the latter study the evaluation of liquefaction susceptibility of soil layers was based on the modified criteria proposed by Seed et al. (2003) in lieu of “Chinese criteria”.

Moreover, Lee et al. (2003) re calibrated the scale, based on CPT data conducted in liquefied sites in Taiwan after the 1999 Chi-Chi earthquake, proposing that liquefaction potential of a site is very high and low where LPI is greater than 30 and less than 20 respectively, while where LPI values range between 20 and 30 the potential is characterized as medium. Sonmez and Gokceoglu (2005)

used the probability of liquefaction PL in lieu of factor of safety in order to compute the LPI or Liquefaction Severity Index L_s , as they named it in their paper, and they proposed a new classification. Furthermore, Li et al. (2006) also defined the LPI or IL as a function of probability of liquefaction and they proposed mathematical formula for the evaluation of the probability of liquefaction-induced ground failure. Finally, Papathanassiou (2008) using a logistic regression analyses, proposed a LPI-based approach for the calculation of the probability of liquefaction manifestations. For a comprehensive description of these procedures, the reader is referred to Holzer (2008).

The advantage of LPI is that it quantifies the likely of liquefaction of the site, by providing a unique value for the entire soil column instead of several factors of safety per layer. Therefore, the values of LPI were used for the compilation of liquefaction hazard maps. These maps comprise a preliminary assessing tool of the liquefaction potential and can be used by decision makers for urban planning purposes. Such thematic maps were published for Busehr, Iran (Hosseini 1998), for the state of California, USA (Holzer et al. 2002), for the town of Inegol, Turkey (Sonmez 2003; Sonmez and Gokceoglu (2005), for the town of Ceyhan, Turkey (Ulusay and Kuru 2004), and for the city of Lefkada, Greece (Papathanassiou et al. 2005), California, U.S.A by Lenz and Baise (2007) and Memphis, U.S.A (Cramer et al. 2008)

4. Evaluating the probability of surface liquefaction occurrence in urban environments: case studies in Greece

As it is mentioned in previous section, the assessment of liquefaction hazard within urban areas is a crucial issue in order to avoid possible structural damages triggered by earthquakes. This can be achieved by applying the methodology of Liquefaction Potential Index and afterwards, by correlating the estimating LPI values with the liquefaction potential as it is described in published classifications (Iwasaki et al. 1978; Sonmez 2003). Another approach for showing the hazard due to liquefaction is the compilation of a probability-based map, using suggested probabilistic regressions provided by statistical analysis (logistic regression, discriminant, Bayesian method).

In this article, cases studies from Greece are going to be presented where liquefaction hazard maps were compiled based on either the classification of LPI values with liquefaction potential proposed by Iwasaki et al. (1978) or based on the probability of liquefaction surface occurrences that was computed using the regression proposed by Papathanassiou (2008). These case studies were selected due to the fact that are located at different seismic hazard zones according to EAK (2000), thus including a variety in the earthquake magnitude. Regarding the estimation of the value of surface acceleration, three different approaches were applied and resulted to different acceleration values than the proposed by EAK (2000) ones, indicating the importance of performing site-specific analyses within an urban environment. In particular, in the first case (Lefkada) the employed value of a_{max} , for the calculation of LPI, was recorded within the urban area during the Lefkada 2003 earthquake, in the second case study, the town of Edessa, the surface acceleration was estimated based on 1-D site response analysis and finally, in the third case, the town of Larissa, the a_{max} was estimated using geology-based amplification factors.

4.1 Lefkada

Within the urban area of the town of Lefkada, liquefaction phenomena have been reported more than one time according to the historical catalogue of liquefaction manifestations published by Papathanassiou et al. (2005). The latest event occurred in 2003 and triggered soil liquefaction and related damages mainly to port facilities. As it was reported by Papathanassiou et al. (2005) in the

town of Lefkada, liquefaction of the subsoil layers caused damages to pavements and sidewalks behind seawalls. According to eyewitnesses, muddy water was ejected at a height of 50 cm from cracks in a pavement surface near the waterfront, indicating high excess pore pressure generating during earthquake shaking. Furthermore, we observed that the asphalt pavement was covered by a thin sandy-silty layer which was ejected from the ground fissures. The length of the fissures varied from few meters to tens of m and their width from a few mm to 8 cm.

In order to evaluate the liquefaction potential of the subsoil at the urban area of Lefkada, data provided by boreholes that were performed during post reconnaissance field surveys, were collected. Using this information, the liquefaction susceptibility and the factor of safety of the soil layers were estimated. The employed earthquake characteristics were equal to $a_{max}=0.4g$, recorded by the permanent network of ITSAK (Institute of Engineering Seismology and Earthquake Engineering) during the main shock at the center of the city, while the M_s value corresponds to the one of the 2003 earthquake ($M_s=6.4$), and is similar to the maximum earthquake magnitude that occurred in Lefkada island (after 1911) according to historical seismicity of the area.

Afterwards, the LPI value per borehole was computed based on Iwasaki et al. (1978) methodology and a map of liquefaction potential was compiled using the proposed classification. The predicted areas of high liquefaction potential are in agreement with the sites where liquefaction-induced ground failures were triggered by the 2003 Lefkada earthquake, indicating that LPI may be a useful tool for future seismic hazards studies.

4.2 Edessa

The case study of the town of Edessa was more complicated due to the fact that the geology and the topography of the area indicate that an amplification of the ground motion is possible. Thus, we concluded that the proposed value of PGA, 0.16g, by the EAK (2000) is not representative for a “microzonation” study and we decided to perform 1-D site response analysis using data provided by seven borings with SPT. In order to achieve this, several real acceleration time histories were selected with respect to the type of causative fault, the magnitude of the earthquake and the geological conditions at the recorded station, and were downloaded by the web site of European Strong motion Database (ESD) www.isesd.cv.ic.ac.uk/ESD (Papathanassiou and Valkaniotis, 2009).

Afterwards, the input acceleration time histories have been chosen for scaling based on the value of the design acceleration of Greek Seismic code and the scaled time histories were used as input motion in order to estimate the value of acceleration on ground surface for each one of the seven site. The computed a_{max} values at the sites that were estimated using the EERA software proposed by Bardet et al. (2000).

Having estimated the a_{max} , we proceeded to the computation of LPI values based on seven geotechnical profiles that were provided by the boreholes. In addition, the probability of liquefaction surface evidence per site was computed using the proposed by Papathanassiou (2008) LPI-based equation:

$$Pr ob(liquefaction) = \left(\frac{1}{1 + e^{-(-3.092+0.218 \times LPI)}} \right) \quad (9)$$

The outcome of this study indicates that when the a_{max} is equal to the proposed by the EAK (2000) no liquefaction-induced surface disruption is expected. However, liquefaction phenomena, such as

sand boils, are expected to be triggered when the amplification of the ground motion due to local geology is taken into account. This result is in agreement with the secondary effects triggered by the 1395 event that occurred close to the town of Edessa.

4.3 Larissa

The third case study that is presented in this article deals with the assessment of liquefaction hazard at the urban area of Larissa. This area was selected due to the fact that is classified as a liquefaction-prone zone since historical reports exist describing earthquake-induced ground failures, including liquefaction manifestations, triggered by the March 1st 1941 earthquake and due to the fact that the town is situated upon sediments deposited by the river of Pinios which traverses the town that are considered as potentially liquefiable.

The estimation of liquefaction potential and the computation of the probability of liquefaction surface evidence were achieved using data provided by geotechnical profiles of borings with SPT and based on the LPI methodology and the LPI-based regressions proposed by Iwasaki et al. (1978) and Papathanassiou (2008), respectively. In addition, in order to estimate the surface acceleration values of the ground motion, the provided design acceleration value of EAK (2000) was used as a baseline layer and afterwards, for every site an a_{max} value was estimated using geology-based amplification factors, as they were proposed by Stewart et al. (2003).

The outcome of this research shows that the occurrence of liquefaction surface evidences is likely only at two areas close to river Pinios, although the fact that it was expected to be triggered in more places. This result could be explained by the fact that the majority of susceptible to liquefaction layers are not loose enough ($SPT-N > 25$) to be liquefied under this seismic scenario and that the average depth of the groundwater table is more than 4 meters.

5. Conclusions-Results

The basic aim of this article is to present the methodologies that are applied for the evaluation of liquefaction potential of subsoil layers and for the compilation of liquefaction hazard maps in urban environments. Furthermore, a brief presentation regarding the importance of the site-specific conditions is given and three different approaches for the estimation of the surface acceleration that are used for the computation of factor of safety against liquefaction are proposed.

This goal is achieved by analyzing the most-known methods and their applications in urban areas, presenting examples from Greece. In particular, three case studies are presented, representing the towns of Lefkada, Larissa and Edessa, where liquefaction hazard maps were already compiled. Regarding the town of Lefkada, the validation of the LPI-based liquefaction potential map was realized by comparing it with the earthquake-induced liquefaction phenomena distribution while the provided probability map of liquefaction surface occurrence of the town of Edessa was validated using the information regarding the 1395 earthquake secondary effects. Finally, the areas where liquefaction phenomena are expected to be triggered within the urban area of Larissa are in agreement with the distribution of land sliding and liquefaction manifestations triggered by the March, 1st 1941 Larissa earthquake. As an outcome of these studies, we concluded that within urban areas in earthquake prone countries it is important to evaluate the liquefaction hazard since by this way it is possible to delineate areas where structural damages due to liquefaction of the subsoil layers are expected to occur.

6. References

- Andrews, D.C. and Martin, G.R., 2000. Criteria for liquefaction of silty sands, in: 12th World Conference on Earthquake Engineering, Auckland, New Zealand
- Aydan, O. and Ulusay, R., 2000. A preliminary investigation report for a collaborative research on the liquefaction and faulting-induced ground deformations and associated damages in 1999 Kocaeli earthquake region, Ankara (unpublished)
- Bardet, J, Ichii, K. and Lin, C., 2000. EERA, a computer program for equivalent linear earthquake site response analysis of layered soil deposits. WWW document URL, University of Southern California, 38 pp
- Boulanger, R.W., and Idriss, I.M., 2004. Evaluating the potential for liquefaction or cyclic failure of silts and clays, Report No UCD/CGM-04/01, Center for geotechnical modeling, University of California, Davis.
- Bray, J.D. and Sancio, R.B., 2006. Assessment of the Liquefaction Susceptibility of Fine-Grained Soils, *Journal of Geotechnical and Geoenvironmental Engineering*, ASCE, 132(9): 1165-1177
- Cramer, C.H., Rix, G.J. and Tucker, K. 2008. Probabilistic liquefaction hazard maps for Memphis, Tennessee. *Seismological Research Letters*, 78 (in press).
- EAK, 2000. Greek Seismic Code, OASP, Athens, 72 pp and 7 Appendixes
- Hosseini, S.M.M.M. 1998. Microzonation for liquefaction in Busehr, Iran. Proc. 11th European Conference on Earthquake Engineering (CD-ROM), A.A. Balkema, Rotterdam
- Holzer T.L., Bennett M.J., Noce T.E., Padovani A.C. and Tinsley J.C., III 2002. Liquefaction hazard and shaking amplification maps of Alameda, Berkeley, Emeryville, Oakland, and Piedmont: A digital database. Open-file Report 02-296, U.S. Geological Survey, Menlo Park, CA.
- Idriss, I.M. and Boulanger, R.W. 2008. Soil liquefaction during earthquakes, EERI publication, 235 pp
- Iwasaki, T., Tatsuoaka, F., Tokida, K. and Yasuda, S., 1978. A practical method for assessing soil liquefaction potential based on case studies at various sites in Japan. Proc. 2nd International Conference on Microzonation: 885-896.
- Iwasaki, T, Tokida, K, Tatsuoaka, F, Watanabe, S, Yasuda, S. and Sato, H. 1982. Microzonation for soil liquefaction potential using simplified methods. In: Proceedings of the 3rd International Conference on microzonation. 3: 1310-1330.
- Lenz, J.A. and Baise, L.G. 2007. Spatial variability of liquefaction potential in regional mapping using CPT and SPT data, *Soil Dynamics and Earthquake Engineering*, 27(7): 690-702
- Liao, S. and Whitman, R.V. 1986. Overburden correction factor for SPT in sand, *Journal of Geotechnical Engineering*, ASCE. 112 (3): 373-377.
- Papathanassiou, G. Pavlides, S. Christaras, B. and Pitilakis, K., 2005a. Liquefaction case histories and empirical relations of earthquake magnitude versus distance from the broader Aegean Region, *Journal of Geodynamics*, 40: 257-278
- Papathanassiou G., Pavlides S. and Ganas A. 2005b. The 2003 Lefkada earthquake: Field observations and preliminary microzonation map based on liquefaction potential index for the town of Lefkada. *Engineering Geology*, 82 (1): 12-31.
- Papathanassiou, G. 2008. LPI-based approach for calibrating the severity of liquefaction-induced failures and for assessing the probability of liquefaction surface evidence, *Engineering Geology*, 96: 94-104
- Papathanassiou, G. and Valkaniotis, S. 2009. Liquefaction hazard mapping at the town of Edessa, Northern Greece, *Natural Hazards*, DOI 10.1007/s11069-009-9412-1
- Schmidt, J., 1867. Information regarding the 26th of December 1861 earthquake, 52 pp. Athens
- Seed, R.B., Cetin, O.K., Moss, R.E.S., Kammerer, A.M., Wu, J., Pestana, J.M., Riemer, M.F., Sancio,

- R.B., Bray, J.D., Kayen, R.E. and Faris, A. 2003. Recent advances in soil liquefaction engineering: a unified and consistent framework, 26th annual ASCE L.A. Geot. Spring Sem., Long Beach, California, April 30, 71 pp
- Sonmez, H. 2003. Modification of the liquefaction potential index and liquefaction susceptibility mapping for a liquefaction-prone area (Inegol, Turkey). *Environmental Geology* 44(7): 862-871.
- Sonmez, H. and Gokceoglu, C. 2005. A liquefaction severity index suggested for engineering practice. *Environmental Geology* 48(1): 81-91.
- Sonmez, B., Ulusay, R. and Sonmez H. 2008. A study on the identification of liquefaction-induced failures on ground surface based on the data from the 1999 Kocaeli and Chi-Chi earthquakes, *Engineering Geology*, 97: 112-125
- Stewart, JP., Liu, AH. and Choi, Y. 2003. Amplification Factors for Spectral Acceleration in Tectonically Active Regions. *Bulletin of Seismological Society of America*; 93(1): 332-352; DOI: 10.1785/0120020049
- Toprak, S. and Holzer, T.L. 2003. Liquefaction potential index: Field assessment.” *Journal of Geotechnical Geoenvironmental Engineering* 129(4): 315-322.
- Wang, W. 1979. Some findings in soil liquefaction, Research report, water conservancy and hydroelectric power scientific research institute, Beijing, August.
- Witter, C.R., Knudsen, L.K., Sowers, M.J., Wentworth, M.C., Koehler, D.R. and Randolph, C.E. 2006. Maps of Quaternary Deposits and liquefaction susceptibility in the Central San Francisco Bay Region, California, Open file report 2006-1037, USGS, 43 pp.
- Youd, T.L. 1973. Liquefaction, flow and associated ground failure: U.S. Geological Survey Circular 688, 12 pp.
- Youd, T.L., Idriss, I.M., Andrus, R.D., Arango, I., Castro, G., Christian, J.T., Dobry, R., Finn, W.D.L., Harder, L.F., Hynes, M.E., Ishihara, K., Koester, J.P., Liao, S.S.C., Marcursion, III WF, Marti, G.R., Mitchell, J.K., Moriwaki, Y., Power, M.S., Robertson, P.K., Seed, R.B., and Stokoe II K.H. 2001. Liquefaction resistance of soils: summary report from the 1996 NCEER and 1998 NCEER/NSF workshops on evaluation of liquefaction resistance of soils, *Journal of Geotechnical Geoenvironmental Engineering*, 817-833
- Yuan, H., Yang, S.H., Andrus, R.D. and Juang, H. 2003. Liquefaction-induced ground failure: a study of the Chi-Chi earthquake cases. *Engineering Geology*, 71: 141-155

LIQUEFACTION SUSCEPTIBILITY MAP OF GREECE

Papathanassiou G.¹, Valkaniotis S.¹, Chaztipetros A.I.¹, Pavlides S.¹

¹ *Aristotle University of Thessaloniki, Department of Geology, 54124 Thessaloniki, Greece, gpapatha@auth.gr*

Abstract

The basic goal of this study is the delineation of liquefaction susceptibility zones by correlating geological, geomorphological, seismological and past liquefaction occurrences information. A liquefaction susceptibility map should be used as a screening guide by decision makers for avoiding in advance prone to liquefaction areas. In order to compile this map, we took into consideration published data regarding the surficial distribution of geological units (IGME), the seismic hazard zonation in Greece as it is defined by the Earthquake Palling and Protection Organization and the distribution of historical liquefaction occurrences provided by the relatively database DALO v1.0 (<http://users.auth.gr/gpapatha/dalo.htm>). Initially, Quaternary age deposits were classified into categories of susceptibility based on their age and depositional process, having considered the designed value of acceleration. Afterwards, areas where past liquefaction occurrences were reported have been upgraded one level. The result obtained by this study is that as very high susceptibility zones are considered the coastal areas at the Ionian Islands and at the Gulf of Corinth

Key words: liquefaction, hazard, susceptibility, Greece

1. Introduction

Greece shows the highest seismicity in Europe and is considered as one of the most prone to earthquake countries globally. Thus, it is obvious that earthquake-induced ground failures (landslides, liquefaction etc.) and their effects on the man made environment should be taken into consideration.

Liquefaction is the transformation of saturated, unconsolidated granular material from a solid state to a liquid state as a consequence of increased pore pressures that reduce the effective strength of the material (Youd 1973). The loss of shear strength can cause permanent ground deformations and damage to man-made structures. Therefore, a map showing the prone to liquefaction areas could be used by decision makers and urban planners in order to avoid areas likely to ground failures.

In order to prevent the occurrence of soil liquefaction and to minimize its effects to the man made environment, studies regarding the susceptibility of the geological units should initially take place. Areas susceptible to liquefaction can be identified through detailed geologic, geomorphic and hydrologic mapping (Witter et al. 2006). Afterwards, a prone to liquefaction area should be further investigated in detail in order to evaluate the liquefaction potential and the degree of ground and/or structural failure.

Liquefaction susceptibility maps delineate zones estimated to be liquefiable under given earthquake parameters and have been compiled for several regions and countries including USA, Greece, Japan,

Iran, Turkey etc. In particular, maps were developed for the San Francisco Bay region (Youd and Perkins 1987; Knudsen and others 1997; Knudsen et al. 2000; Holzer et al. 2002), for Los Angeles urban area (Tinsley et al. 1985), for the region of Thrace, Greece (Papathanassiou et al. 2008) etc. These maps do not predict liquefaction-related ground failures, although ground failures may accompany liquefaction and are more likely to occur in areas with higher liquefaction susceptibility (Tinsley et al. 1985). Moreover, large scale maps, regarding the liquefaction-induced ground disruption, were published for urban areas using data provided by in-situ tests (mainly SPT and CPT). These “micro-zonation” maps were compiled based on the LPI methodology, suggested by Iwasaki et al. (1978).

The basic goal of this study was the evaluation of the liquefaction susceptibility of geologic units in Greece and a compilation of a map of 1:500.000 scale, using information provided by geologic, geomorphologic and seismic hazard investigations. The information provided by this map should be used only as a screening guide for planning purposes

2. Geo-engineering evaluation of liquefaction susceptibility

Several researchers and scientific groups of civil engineers and engineering geologists have studied the liquefaction susceptibility of soil units and proposed criteria for their classification. Brief descriptions of the most used guidelines are presented in this section including the procedures that should be followed for the evaluation of liquefaction susceptibility.

In general, the susceptibility to liquefaction of a geological unit can be evaluated based on its depositional environment; the depositional process affect the liquefaction susceptibility of sediments since fine and coarse grained soils sorted by fluvial or wave actions are more susceptible than unsorted sediments (Youd 1998). In particular, liquefaction susceptibility can be defined based on small scale information and/or data provided by in-situ tests. The former assessment is achieved by collecting data regarding the depositional environment, the age of sediments, the value of peak ground acceleration and the depth of ground water table and the latter based on detailed information of a soil formation such as the grain-size characteristics and the values of Atterberg limits.

In particular, regarding the regional scale approach, Wakamatsu (1992) classified sedimentary deposits using geomorphological criteria in 3 categories of liquefaction susceptibility under the ground motion at the MMS intensity VIII: likely, possible and not likely. Areas classified as “not likely” liquefaction susceptibility define zones where liquefaction-induced failures are not expected. On the contrary, zones where geomorphological units such as natural levee, former river channel, sandy dry river channel and artificial fill were classified as the highest level of liquefaction potential, i.e. liquefaction likely (TC4 1999). At these areas, further investigation using in-situ test and quantitative parameters of subsoil layers must be performed.

Moreover, another well known procedure for the characterisation of an area as liquefiable was proposed by the California Department of Conservation, Division of Mines and Geology (CDMG 1999). According to these guidelines, a zone is considered as prone to liquefaction when is meeting the following criteria:

- evidence of historical liquefaction occurrences,
- data from in-situ tests and analyses indicate that the soils are likely to liquefy,

in case of lacking of the above data, a site is considered as susceptible to liquefaction when:

- area containing soils of late Holocene age, the groundwater is less 13 meters deep and the peak ground acceleration (PGA) having a 10% probability of being exceeded in 50 years is greater than 0.1g,

- soils of Holocene age where the depth of groundwater table is less than 10 meters and the PGA (10% in 50 years) is greater than 0.2g,
- areas containing soil deposits of latest Pleistocene age, where the PGA has a 10% probability of being exceeded in 50 years is greater or equal to 0.3g and the depth of the groundwater table is less than 6 meters

A second approach that is followed for the evaluation of liquefaction susceptibility of a soil unit is based on results obtained by laboratory tests, regarding the grain-size characteristics and the values of Atterberg limits of the soil element. In general, sands was believed that were more susceptible than silts or gravel, but laboratory test to fine-grained soils from liquefied soils collected after the earthquakes of Kocaeli and Chi-Chi in 1999, showed that cohesive soils could also liquefied under specific conditions.

In particular, Tsuchida (1971), defined boundaries curves for potentially liquefiable soils based on their grain size distribution curves. Few years later, Wang (1979) and Seed & Idriss (1982) suggested that the classification of a soil element depends on the Atterberg limits and the percentage of clay-size material. Andrews and Martin (2000) re-evaluated the liquefaction field case histories and transported the “Modified Chinese Criteria” to US conventions. However, recent data (Seed et al. 2003), provided by post-earthquake in-situ tests at liquefied sites triggered by the last two devastating earthquakes of Kocaeli and Taiwan in 1999, indicated that the “modified Chinese criteria” and the liquefaction susceptibility criteria proposed by are considered conservative. Seed et al. (2003) concluded that the plasticity behaviour of fine size particles of soils is more important than the percent clay size, and there are numerous cases of liquefaction with more than 10% clay-size fines. According to these recommendations, soils with fines content more than 35% are characterized potentially liquefiable when its liquid limit is less than 37 and the plasticity index is less than 12 ($LL \leq 37$ and $PI \leq 12$), and the water content is high relative to their Liquid Limit ($w_c > 0.8 LL$). Consequently, fine-grained soils, previous characterized as non-liquefiable based on liquefaction susceptibility criteria proposed by and Andrews and Martin (2000), are now considered potentially liquefiable according to the recommendations of Seed et al. (2003).

3. Methods

3.1 Surficial Geology

Geologic criteria such as age, depositional environment, relative density, depth to free ground water affect the liquefaction susceptibility of a geologic unit. Understanding the depositional environment and the ages of the geologic units allows the assessment of liquefaction susceptibility. According to Youd (1998) the younger, looser and more segregated the deposit the greater the susceptibility to liquefaction. Older (Pre-Pleistocene) or cemented deposits are almost universally resistant to liquefaction.

In our study, using as a baseline data the geological map of Greece (IGME 1989), we proceed to the digitization of the geological units. Afterwards, the geological units were classified into two categories based on their ages; pre-quaternary and quaternary. This separation was made in order to further analyze and evaluate the liquefaction susceptibility of the deposits of Quaternary sediments since pre-Pleistocene deposits are classified as very low susceptibility units (Youd 1998). The characterization of these sediments had been realized by the Institute of Geological and Mineral Exploration of Greece (IGME 1989) and was adopted in this study.

In particular, as Holocene _1 (latest Holocene age) sediments were grouped the coastal, fluvial, deltaic, marsh deposits: sands, clays, loams, clayely sands usually fine-grained and loose. The presence of a surficial water table (with small seasonal fluctuation of the water-level is one of their char-

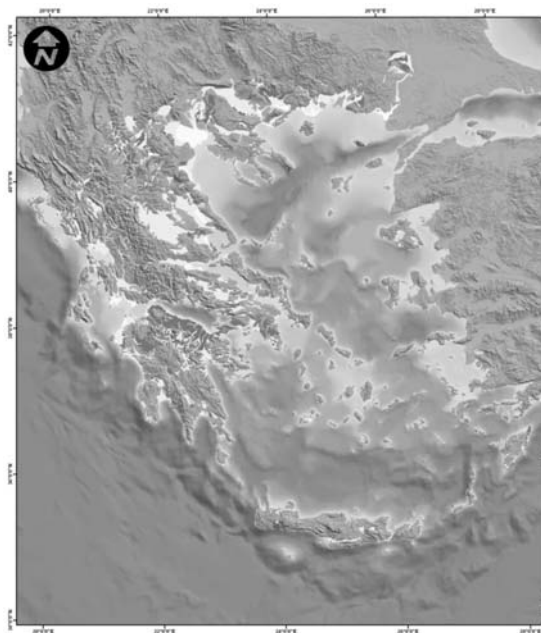


Fig. 1: Geological map of Greece showing the distribution of quaternary sediments (modified from IGME, 1989).

acteristics. Their thickness is about 60m approximately.

As Holocene (Holocene age) sediments were characterized recent to present formations mainly consisted of alluvial deposits, fluvial deposits, dunes: sands, clays, sandy or silty clays usually without a surficial water layer. Loose formations and locally slightly cohesive, fine to coarse grained. Their thickness ranges from a few tens of meters, locally exceeding 100m.

Finally, the Pt (Pleistocene age) sediments include old alluvial deposits, scree, talus cones mainly of Pleistocene age. No surficial water is observed while the thickness is usually around 20m.

3.2 Historical liquefaction occurrences in Greece

Liquefaction is known to occur repeatedly in the same site, thus maps showing the localities of past liquefaction may be considered as potential area of liquefaction in future earthquakes (Youd, 1984). However, lack of evidence does not provide adequate proof that a site is immune to liquefaction (Youd 1988).

In order to identify a detailed map of the distribution of past liquefaction occurrences in Greece, we used the information provided by the published database of DALO v1.0. The Database of historical Liquefaction Occurrences DALO v1.0 (Papathanassiou and Pavlides, 2009) is an open-access file where information regarding liquefaction-induced ground and/or structural deformations is provided. The database was constructed under Ms-Access software and is consisted of six tables and six relative forms. The constructed six tables, used for the introduction of data, are cross-linked by key using elements that are common to several tables, such as the earthquake ID, the failure ID, site ID and reference ID. The independent tables include information regarding the earthquake, the liquefied site, the causative fault, the type of failure, the recorded ground motion and the historical source where the liquefaction-induced failures were described. The presentation of the collected data is accomplished using forms that were decided to be grouped in two main categories. The first

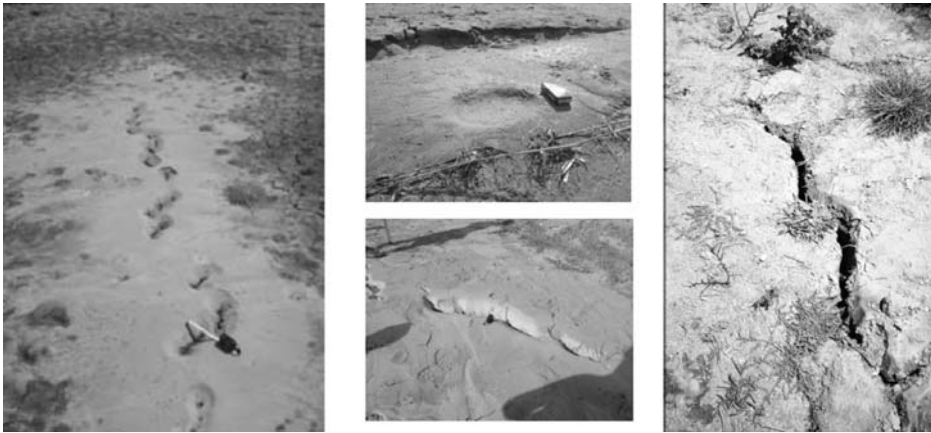


Fig. 2: Liquefaction manifestations in Roupakia, Nidri, Kato Achaia and Alikes, triggered by the events of 8th June, 2008 and 14th August, 2003 in Peloponnesus and Lefkada, respectively.

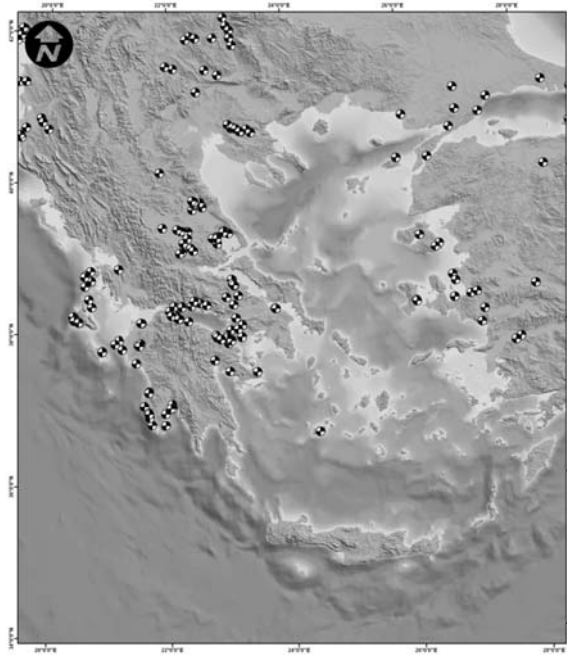


Fig. 3: Map of historical liquefaction occurrences in the broader Aegean region from 1509 AD to 2008 AD (Papanastasiou et al., 2005).

group provides information of earthquake-induced liquefaction characteristics while the second one includes data regarding the liquefied site. The navigation into the database is accomplished by an introductory form which gives to the researcher the opportunity to select one of these two groups for browsing through its contents. Moreover, searching for a specific liquefied site or an earthquake that triggered liquefaction phenomena is now possible and can be achieved by selecting the relative

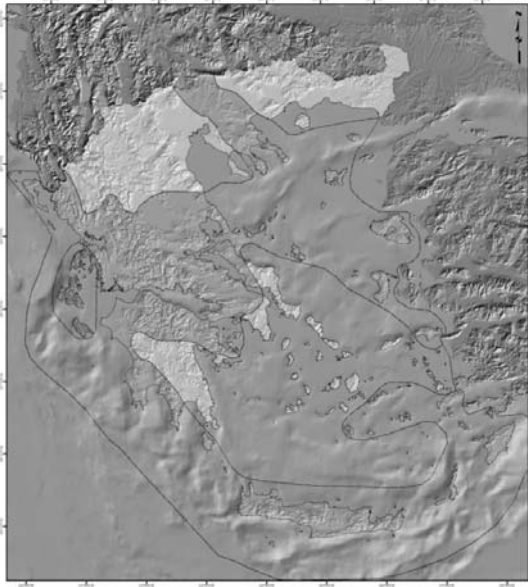


Fig. 4: Seismic hazard zonation of Greece (modified from EAK, 2000)

options, appeared in the menu at the right side of the introductory form. The search is realized using the primary keys of EqID and siteID, respectively and the user can select an earthquake based on the date of occurrence or a liquefied site based on its location.

The first entry in the dataset is in the 16th century AD (Papathanassiou et al., 2005) while the cut-off data for this project is provided by the earthquake-induced liquefaction of June 8th, 2008 in NW Peloponnesus, Greece. However, the oldest event that is mentioned in the seismic catalogues and was correlated to liquefaction-induced failures is the event of 373 B.C. in Elikei (Gulf of Corinth).

A total of 55 earthquakes-induced liquefaction phenomena were introduced into the dataset providing information about 321 cases of liquefaction manifestations. Regarding the areas that were re-liquefied during that period, this study resulted (fig. 3) that they are located mainly at the Gulf of Corinth, the islands of the Ionian Sea and the region of Thessaly (Central Greece).

3.3 Seismic hazard zonation

The third criterion that should be examined for the classification of an area as liquefiable is the seismic input. In case of regional scale projects, it is proposed to take into account national hazard maps showing contours of PGA with various probabilities of exceedance (Youd, 1998). In our study, we took into consideration the map provided by the Earthquake Planning and Protection Organisation (EAK, 2000). According to this project, Greece has been divided in three subareas regarding the seismic hazard, where the expected value of PGA, having a 10% probability of being exceeded in 50 years.

In particular, the first zone delineates areas of low seismicity, mainly in Northern Greece, where the expected PGA is evaluated as 0.16g and within the second one the PGA is assigned as 0.24g. Areas located within the third zone, the Ionian islands and a smaller area in the mainland, were characterized as high seismicity zones where the expected value of PGA is equal to 0.36g (fig. 4).

4. Defining the liquefaction susceptibility classes

Taking into account the data describing in the previous section, we proceed to the compilation of the liquefaction susceptibility map of Greece which delineates the areas where liquefaction materials are most likely to exist.

Initially, the categories of susceptibility were assigned based on the geologic (age and depositional environment) characteristics of the sediments and the value of peak ground acceleration that is expected within an area according to Greek Seismic Code. In particular, geologic units characterized as Holocene_1 (latest Holocene age) deposits are classified as Very high, high and moderate susceptibility sediments when they are located in zones where the expected PGA was evaluated as 0.36, 0.24 and 0.16g respectively. Geologic units described as Holocene sediments are characterized as high and moderate susceptibility in seismic zones of 0.36, and 0.24, 0.16g, respectively while the Pt (Pleistocene age) sediments were introduced into the groups of low and very low susceptibility, in areas where the PGA was evaluated as 0.36 and 0.24g for the former group and 0.16g for the latter one.

Afterwards, we examined the occurrence of historical liquefaction phenomena within an area and we re-evaluated the susceptibility of the soil units. In particular, the susceptibility of geologic units where liquefaction phenomena were reported more than once, were upgraded one level. For example, the coastal area at the Gulf of Corinth and the Ionian Islands were upgraded from high to very high susceptibility. Applying the same criterion, areas in Thessaly (Central Greece) were upgraded from moderate to high due to the occurrence of liquefaction manifestations, generated by the events of 1941 and 1954.

Finally, a total of 5 liquefaction susceptibility categories were assigned to the mapped geologic units based on their geological, seismological and past liquefaction occurrences information and a liquefaction susceptibility map was developed as it is shown in figure 5. These groups consisted of Very high, high, moderate, low and very low susceptibility classes.

4.1 Categories of liquefaction susceptibility

In this section are described the classes of liquefaction susceptibility that are proposed by our study. Applying these criteria, the characterization of a geological unit as susceptible to liquefaction or not can be achieved. In particular:

- As **Very high** susceptibility units are defined the geological units describing sediments of latest Holocene age that are located within areas where the expected PGA is 0.36g. In addition, latest Holocene and Holocene age deposits located within areas of 0.24 and 0.36g, respectively and within areas where past liquefaction occurrences were reported are also classified as Very high susceptibility zones,
- As **High** susceptibility are grouped the geological units included describing sediments of latest Holocene age and Holocene age located within areas where, in some cases, past liquefaction occurrences were reported and where the expected PGA is evaluated as 0.24 and 0.36g, respectively,
- As **Moderate** susceptibility the sediments of latest Holocene age and Holocene age located within areas where the expected PGA is evaluated as 0.16 and 0.24g, respectively,
- As **Low** susceptibility, the geological units of Pleistocene age within areas where the expected PGA is high (0.36g and 0.24g) and the occurrence of liquefaction is possible under specific conditions,

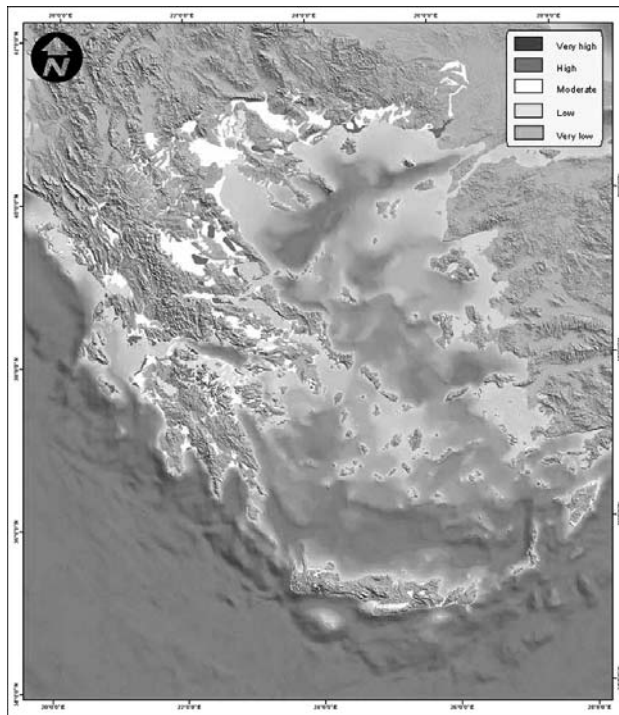


Fig. 5: Liquefaction susceptibility map of Greece.

- And as **Very low** susceptibility, the sediments of Pleistocene age, located within areas of low seismicity (0.16g) where liquefaction isn't expected to be triggered.

5. Conclusions-Results

Greece is considered as the most prone to earthquake country in Europe. Therefore, the evaluation of primary and secondary effects triggered by an earthquake is crucial for the avoidance of structural damages. In this study, the procedure that was followed for the compilation of the liquefaction susceptibility map of Greece in scale 1:500.000 is presented. In order to develop this map several criteria were taken into consideration. Initially, data regarding the distribution of geological units and the seismic hazard zonation were collected by published maps and reports. Furthermore, the occurrence of historical liquefaction phenomena was evaluated using the published database of DALO v1.0 and the sites where past liquefaction was reported were plotted as a separate layer and correlated afterwards with the layers of geology and seismic hazard zonation. As a result, the geological units were classified into 5 categories of susceptibility; very high, high, moderate, low and very low. The outcome provided by this study delineates the areas that are susceptible to liquefy. However, in order to evaluate the liquefaction potential of an area detailed investigations are required.

6. References

Andrews, D.C., and Martin, G.R., 2000. Criteria for liquefaction of silty sands, In: 12th World Conference on Earthquake Engineering, Auckland, New Zealand

- EAK, 2000. Greek Seismic Code, OASP, Athens, 72 pp and 7 Appendixes
- CDMG, 1999. Guidelines for analyzing and mitigating liquefaction hazards in California, California Department of Conservation, Division of Mines and Geology, Special Publication 117, p. 63
- Holzer, T.L. Bennett, M.J., Noce, T.E., Padovani, A.C., Tinsley, J. C. III., 2002. Liquefaction hazard and shaking amplification maps of Alameda, Berkeley, Emeryville, Oakland, and Piedmont, California: A digital database. U.S. Geological Survey Open File Rep. 02-296 (version 1.0), U.S. Geological Survey, Menlo Park, Calif., (<http://geopubs.wr.usgs.gov/open-file/of02-296>)
- IGME. 1989. Seismotectonic map of Greece, 1:500000 scale
- Iwasaki, T., Tatsuoaka, F., Tokida, K., Yasuda, S., 1978. A practical method for assessing soil liquefaction potential based on case studies at various sites in Japan. *Proceedings. 2nd Int. Conf. on Microzonation, San Francisco*, 2, 885-896
- Knudsen, K.L., Lettis, W.R., 1997. Preliminary maps showing Quaternary geology of twenty 7.5-minute quadrangles, eastern Stockton, California, 1:100,000 quadrangle: National Earthquake Hazards Reduction Program, U.S. Geological Survey, Final Technical Report, Award #1434-94-G-2499.
- Knudsen, K.L., J.M. Sowers, R.C. Witter, C.M. Wentworth, E.J. Helley, 2000, Preliminary Maps of Quaternary Deposits and Liquefaction Susceptibility, Nine-County San Francisco Bay Region, California: A Digital Database, U.S. Geological Survey Open-File Report 00- 444. Digital Database by Wentworth, C.M., Nicholson, R.S., Wright, H.M., and Brown, K.H. Online Version 1.0.
- Papathanassiou G, Pavlides S, Christaras B, Pitilakis K (2005) "Liquefaction case histories and empirical relations of earthquake magnitude versus distance from the broader Aegean Region, *Journal of Geodynamics*, 40, 257-278
- Papathanassiou G., Valkaniotis S., Pavlides Sp, 2008. Geo-engineering mapping with respect to liquefaction susceptibility of the region of Thrace, North-eastern Greece, *Proceedings of the 31st General Assembly of the European Seismological Commission ESC 2008 Hersonissos, Crete, Greece, 7-12 September 2008*
- Papathanassiou G., and Pavlides Sp., 2009. GIS-based Database of historical Liquefaction Occurrences in broader Aegean region, DALO v1.0, *Proceedings of the Earthquake Geotechnical Engineering Satellite Conference XVIIth International Conference on Soil Mechanics & Geotechnical Engineering 2-3. 10. 2009, Alexandria, Egypt*
- Seed H.B., and Idriss, I.M., 1982. Ground motion and soil liquefaction during earthquakes, monograph, EERI, Oakland, Ca, 134 pp.
- Seed, R.B., Cetin, O.K., Moss, R.E.S., Kammerer, A.M., Wu, J., Pestana, J.M., Riemer, M.F., Sancio, R.B., Bray, J.D., Kayen, R.E., Faris, A., 2003. Recent advances in soil liquefaction engineering: a unified and consistent framework, 26th annual ASCE L.A. Geot. Spring Sem., Long Beach, California, April 30, 71 pp
- TC4, 1999. Manual for zonation on seismic geotechnical hazards (revised version), Technical Committee of Earthquake geotechnical engineering ISSMGE, pp. 219
- Tinsley, J.C., Youd, T.L., Perkins, D.M., Chen, A.T.F, 1985, Evaluating Liquefaction Potential, in Ziony, J.I., ed., Evaluating earthquake hazards in the Los Angeles Region - an earth science perspective: U.S. Geological Survey Professional Paper 1360, 263-316.
- Tsuchida, H., 1971. Estimation of liquefaction potential of sandy soils, *Proceedings of the 3rd Joint Meeting, US-Japan, UNJR*
- Youd, T.L., 1973. Liquefaction, flow and associated ground failure: U.S. Geological Survey Circular 688, 12 pp.
- Youd T.L (1984) Recurrence of liquefaction at the same site, *Proceedings of the 8th World Conference*

on Earthquake Engineering, 3, 231-238

- Youd, T.L., 1998. Screening guide for rapid assessment of liquefaction hazard at highway bridge site, Technical report MCEER-98-0005, 58 pp.
- Youd, T.L., Idriss, I.M., 1978. Mapping of liquefaction induced ground failure potential, *J. Geotech Eng Div.*, ASCE, 117, 1, 35-50
- Youd, T.L., Perkins, D.M., 1987. Mapping of Liquefaction Severity Index, *J. Geotech Eng Div.*, ASCE, 113, 11, 1374-1392
- Youd, T.L., Idriss, I.M., Andrus, R.D., Arango, I., Castro, G., Christian, J.T., Dobry, R., Finn, W.D.L., Harder, L.F., Hynes, M.E., Ishihara, K., Koester, J.P., Liao, S.S.C., Marcursion, III WF, Marti, G.R., Mitchell, J.K., Moriwaki, Y., Power, M.S., Robertson, P.K., Seed, R.B., Stokoe II K.H. 2001. Liquefaction resistance of soils: summary report from the 1996 NCEER and 1998 NCEER/NSF workshops on evaluation of liquefaction resistance of soils, *J. Geotec. Geoenv. Eng.*, 817-833
- Wang, W., 1979. Some findings in soil liquefaction, Research report, water conservancy and hydroelectric power scientific research institute, Beijing, August.
- Wakamatsu, K., 1992. Evaluation of liquefaction susceptibility based on detailed geomorphological classification, *Proceedings of the Technical Papers of Annual Meeting Architectural Institute of Japan*, B, 1443-1444 (in Japanese)
- Wakamatsu K., 1993. History of Soil liquefaction in Japan and Assessment of Liquefaction Potential based on Geomorphology, PhD Thesis, Waseda University Tokyo, Japan, 245pp.
- Witter, C.R., Knudsen, L.K., Sowers, M.J., Wentworth, M.C., Koehler, D.R., Randolph, C.E., 2006. Maps of Quaternary Deposits and liquefaction susceptibility in the Central San Francisco Bay Regio, California, Open file report 2006-1037, USGS, pp. 43

GROUND FAILURE DUE TO GYPSUM DISSOLUTION

Eleftheria Poyiadji ¹, Nikolaos Nikolaou ¹, Petros Karmis ²

¹ Division of Engineering Geology, Institute of Geology and Mineral Exploration

² Division of Geophysics, Institute of Geology and Mineral Exploration

Abstract

Gypsum in Hellas and Cyprus occurs in three different types: (a) bedded (mainly of Messinian age in Cyprus and Crete), (b) domes (mainly western Hellas and Crete), and (c) as bodies, fragments and cementing material in Triassic conglomerate formations (western Hellas). Ground failure caused by void migration to the surface, resulting from gypsum dissolution, is a common phenomenon in such areas, which are also found in other European countries (e.g., Italy, Spain, Switzerland, U.K., Lithuania, Latvia, Poland, Romania, Turkey, Ukraine and Russia). In this paper three different case studies of ground failure are presented: Cyprus, Crete (Viannos) and Corfu. Engineering geological, stratigraphical, geophysical, hydrogeological and hydrogeochemical studies of these areas, revealed the direct relationship between surface runoff, and ground water circulation with the rate of gypsum dissolution, the subsequent development of karst hollows, and the associated ground failure in urban and suburban environments. Two main models were defined, according to different mechanisms of gypsum dissolution. The first model is associated with the erosion activity of surface runoff, the second with the dissolving capacity of ground water. Risks to the urban and suburban environments were assessed, and guidelines as well as mitigation measures were proposed.

Key words: ground failure, gypsum, Cyprus, Crete, Corfu

1. Introduction

Gypsum in Hellas and Cyprus occurs in three different types: (a) bedded (mainly of Messinian age in Cyprus and Crete), (b) domes (mainly western Hellas and Crete), and (c) as bodies, fragments and cementing material in Triassic conglomerate formations (western Hellas).

Gypsum affects many parts of Europe including Italy, Spain, Switzerland, U.K., Lithuania, Latvia, Poland, Romania, Turkey, Ukraine and Russia. Subsidence caused by gypsum dissolution has been recorded in Texas (Olive 1957), Canada (Wigley et al. 1973), Germany (Hundt 1950; Herrmann 1964; Strobel 1973), the Alps (Nicod 1977), Russia (Gorbunova 1977) and Newfoundland (Sweet 1977).

The presence of gypsum many times causes serious ground failure problems, especially when occurring in urban areas. Some of the towns and cities worldwide that are affected by gypsum geohazards are: Ripon and Darlington in the U.K. (Cooper 1995), the city of Zaragoza (Benito et al. 1995) and the town of Calatayud (Gutierrez et al. 2002) in Spain, the outskirts of Paris (Toulemont 1984) in France, Stuttgart and many towns peripheral to the Hartz Mountains in Germany (Pfeiffer and Hahn 1972; Strobel 1973), and the towns of Birzai and Pasvalys in Lithuania (Paukstys 1996).

Gypsum can also cause severe problems when it is situated beneath large engineering structures: at

least 14 examples of dams losing water or failing (James 1992) have been recorded in the USA, and at least two dams in China have been affected (Lu Yaoru and Cooper 1997). In the UK, at Ratcliffe, south-west of Nottingham, power station foundations have been affected by water leakage and dissolution of thin Triassic gypsum beds (Seedhouse and Sanders 1993).

There is a need for detailed site investigation and common methodology approaches for the mitigation of gypsum geohazards. In Hellas and Cyprus, several urban areas, mainly villages, are being affected by sinkholes due to gypsum dissolution. In the following, three distinctive case studies are presented.

2. Gypsum dissolution rates

Gypsum ($\text{CaSO}_4 \cdot 2\text{H}_2\text{O}$) dissolves in flowing water about one hundred times more rapidly than limestone, but at only about one thousandth the rate of halite. At Ripon Parks where Permian gypsum abuts the River Ure a large block (3m^3) of gypsum fell into the river and dissolved in 14 months. This occurrence was reported by James et al. (1981) who presented formulae from which the gypsum dissolution rates can be calculated (dissolution rates were estimated between 0.1 and 1.7 m per annum).

The rate of gypsum dissolution increases with temperature and the speed at which water passes the gypsum surface. The gypsum dissolution rates observed in the field agreed closely with those obtained from laboratory experiments by James and Kirkpatrick (1980), James and Lupton (1978) and by Kemper et al. (1975). These observations considered the dissolution of gypsum by pure water. In subsurface conditions where calcium carbonate is dissolved in the groundwater (waters rich in CaCO_3) the solubility of gypsum is increased; gypsum solubility may also be increased by the presence of other ions in solution such as chloride (Deer et al. 1962; Kempe 1972).

Water abstraction could affect gypsum-water systems. Calculations for a major water abstractor pumping from the Permian gypsum and limestone beds in Northern England show some alarming results. The water contains approximately 1200 ppm of SO_4 mainly as dissolved CaSO_4 ; the abstractor pumps 212 Ml of water per annum. This is equivalent to removing approximately 200 m^3 of gypsum a year from the area. It is likely that much of the dissolution represents the enlargement of joints over a wide area. (Cooper 1988). In places, such as at Ripon in North Yorkshire, the dissolution is so active that a new subsidence feature appears every year or two (Jones et al. 2005).

3. Case studies

3.1 Cyprus

Gypsum in Cyprus occurs in the form of strata layers created during Messinian Salinity Crisis in the Mediterranean. These Messinian evaporates (“Kalavassos formation”) were deposited usually in fault controlled basins. (Koutsouveli et al. 2008). Gypsum layers are found between the Lower and the Upper Gypsiferous Marls.

Several ground failure problems were encountered in urban areas, mostly during the last decade, that resulted mainly by an increase of water abstraction (over-pumping). A two-year (2005-2006) project has been carried out by the Geological Survey Department of Cyprus in collaboration with the Institute of Geology and Mineral Exploration (IGME-Greece), and its external partners (Geoinvest-Cyprus, cbs - C. Stergiopoulos), for the study of sinkholes due to gypsum dissolution in Cyprus.

The target of the project was, a) the study of areas with known problems affecting urban environment and b) the definition of sinkhole prone areas and recommendation of appropriate mitigation measures.

The following works were conducted by a multi scientific team:

- Interpretation of airphotos and satellite images,
- Engineering Geological Studies,
- Geophysical Investigations,
- Hydrogeological – Geochemical studies,
- Underground stability analysis of cavities,
- Geotechnical Evaluation – Geological “Suitability” (using GIS).

Interpretation of airphotos and satellite images

The contribution of the interpretation-analysis of airphotos and satellite images to the current study was the definition of faults and its relation to karst structures and phenomena. Several geo-forms, such as sinkholes, lowlands, and cracks, were recognised and recorded.

Engineering Geological Studies

Detailed site investigation was carried out in areas formed by Kalavassos formations, with emphasis on two pilot areas (Pera Chorio – Nisou and Aradipou), leading to the following works:

- Engineering geological mapping,
- Palynological analysis,
- Surveillance – evaluation of geotechnical boreholes,
- Laboratory tests (soil and rock mechanics),
- GIS database,
- Correlation and interpretation of all data – design of engineering geological cross sections.

In the areas of Cyprus gypsum outcrops, engineering geological maps were produced in a scale of 1:5,000, using field data, palynological analysis, data from the interpretation of satellite images and airphotos, as well data from the boreholes.

In seven areas, twenty eight (28) geotechnical boreholes were drilled with total length 1,537.50 m.

Soil and Rock mechanic tests were carried out for the determination of natural and mechanical characteristics of the formations. Several specimens, representative of the various types of gypsum (marble, selenite, brecciated), were tested in uniaxial compression and then slake durability tests were performed on the “broken” samples.

The slake durability test examines mainly the mechanical corrosion of the rocks trying to simulate the climatic changes of dryness and wetness. The initial water used for the test was pure (distilled) water, while the used water at the end of the test was chemically analysed.

The following results were deduced from the correlation and interpretation of chemical analyses, slake durability index and the uniaxial compressive strength of the gypsum specimens:

- Gypsum of “marble” type present greater strength,
- Mechanical corrosion is not influenced by sample strength nor by the type of gypsum,
- Chemical analysis of the used water shows that all types of gypsum are soluble. The used water was found rich in Ca^{2+} and SO_4^{2-} , consequently the samples were supersaturated in gypsum,
- The values of the proportion $\text{Na}:\text{Cl} < 1.0$ show that gypsum samples present low relevant concentrations of Na explained by the way of gypsum genesis,
- The values of the slake durability index, which corresponds to the percentage of dry mass of the fragments retained by a drum of 2.0 mm (No 10) square-mesh after two cycles of oven drying and 10 min of mixing in water, vary between 76.2 and 95.6.

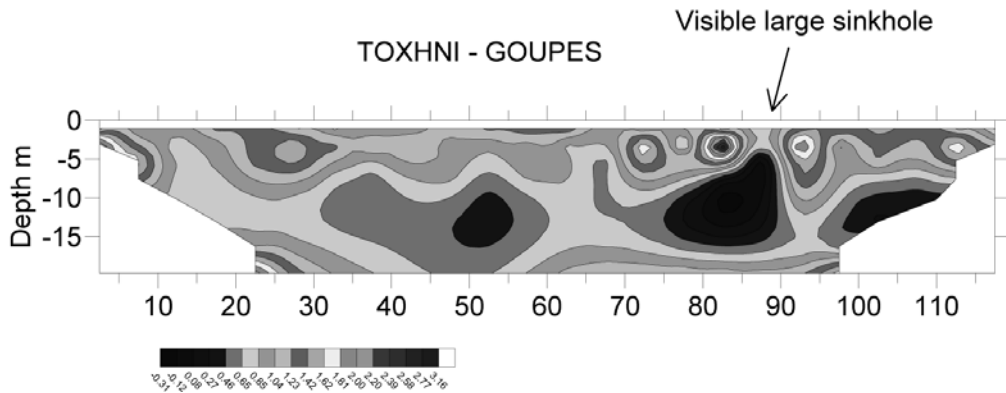


Fig. 1: Example of resistivity anomaly obtained over visible large sinkhole.

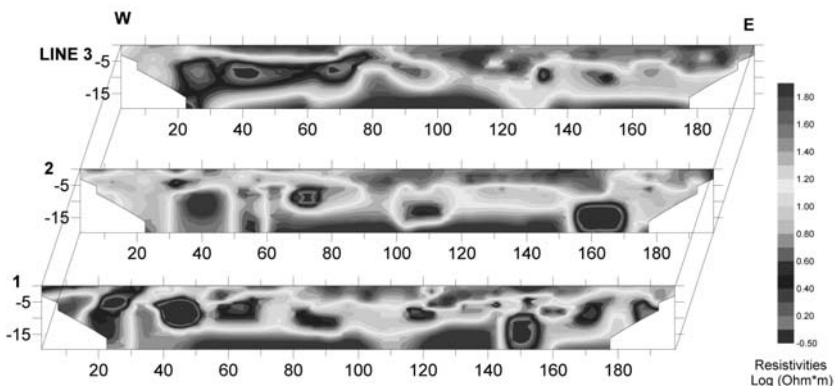


Fig. 2: Inverted resistivity sections of lines 1 to 3 at Pera Chorio, Cyprus.

Engineering geological cross sections were designed in all selected sites, which helped the better understanding of the geological structure. The data used for the design of engineering geological cross sections derived from morphological relief, field mapping, geophysical investigations and boreholes (195 boreholes with total length 6,132.60m were decoded and evaluated).

Geophysical Investigations

The Electrical Resistivity Tomography technique was utilized in the Cyprus study with good results. Targets tend to appear as conductive anomalies when filled with clay material and resistive anomalies when they are empty. The work was carried out using a 24-electrode system with a Pole Dipole array and an electrode spacing of 3 and 5 m.

In Figure 1 an example is presented of the typical anomaly pattern of ERT obtained over an open sinkhole. The cavity is filled with clayey material with resistivity values smaller than 2 Ohm*m.

The method was applied on grids with parallel lines at a distance of 10 m. In Figure 2 the results of 3 parallel lines are presented. The lines were located within the banks of a river and this resulted to a large number of anomalies possibly associated with sinkholes.

A layer of coarse grained sediments is shown near surface to a depth of 3 to 5 m with resistivity val-

ues between 20 and 60 Ohm*m (1.25 to 1.8 in log scale). The layer of gypsum marl is detected at that depth, with resistivity values in the range of 5 to 12 Ohm*m (0.6 – 1.2 log scale). The presence of possible sinkholes is identified by the characteristic circular or funnel shale conductive anomalies with values between 1 to 3 Ohm*m.

In certain cases, the presence of a sinkhole is been evidenced by a conductive lineament migrating and reaching the surface.

“Anomalies” with characteristics of cavities were detected in all sites except Aradippou because the cavities there are found in great depths, greater that the max depth where geophysical investigation can reach.

Hydrogeological – Geochemical studies

In the frame of the hydrogeological, hydrochemical and geochemical investigations, a network of hydro-points was established in two reference sites (Aradippou and Pera Chorio Nisou) and water table measurements and sampling of underground water were carried out. The frequency of measurements for year 2005 was every six months and for year 2006 every month. Moreover, hydrochemical and geochemical analyses were carried out on selected soil and rock samples from the drill cores.

The physicochemical parameters evaluated were pH, Ca, SO_4^{2-} , HCO_3^- and electrical conductivity (E.C.). The physicochemical “trends” were correlated to the hydraulic characteristics of the underground water flow.

The karst forms observed in the drill cores allowed the introduction of the reference sites into the following four categories of karst types:

“young”,
“active”,
“mature” and
“inactive”.

The main conclusions referring to genetic mechanism of gypsum karst were the following:

- An important factor of gypsiferous formations solubility is the groundwater. This is confirmed by the tracing of “active” or “young” karst cavities in great depths under impermeable overburden formations with thickness ≥ 60 m. Within these conditions, surface water cannot act mechanically.
- Karst processes are natural phenomena that are under development. The progress of karst formation depends on the local engineering geological conditions. Consequently, the time occurrence and magnitude of sinkholes varies in every location.
- Finally, “saturation” conditions, namely equilibrium state and pausing of solution processes, cannot be reached as both groundwater systems, Aradippou and Pera Chorio – Nisou, are not “closed”. Thus, the whole process of karst development is a natural phenomenon in progress and cannot be stopped.

Underground stability analysis of cavities

Underground stability analysis was performed for the determination of the geological suitability of a village called Maroni (Poyiadji et al. 2009). The stability analysis was carried out for karst cavities under the central area of the village with a hypothetical geometry. According to the results of the stability analysis and the calculations of safety factors for the examined wedges it was concluded that there is a stability problem of a tetrahedral wedge falling from the roof, but the expected ground failure on the surface should be very small.

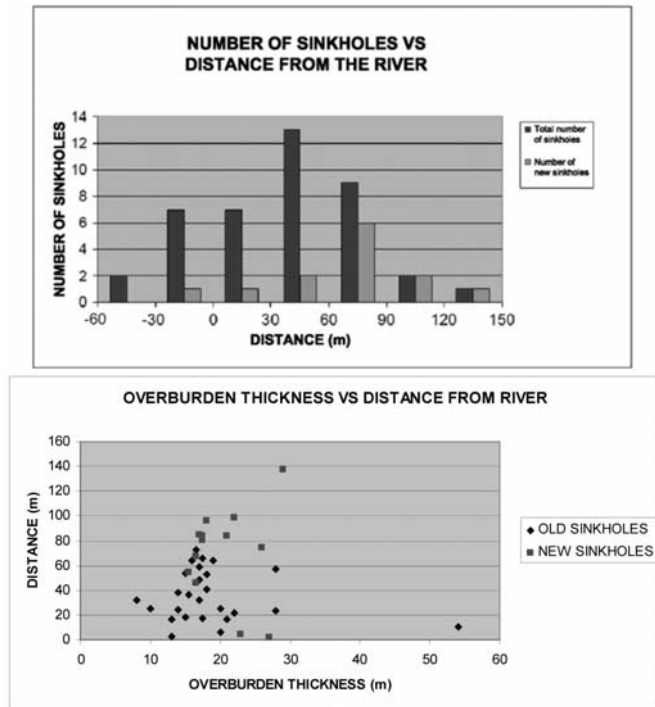


Fig. 3: a) left – Number of sinkholes versus distance from the river, b) right – Overburden thickness versus distance from the river

Geotechnical Evaluation – Geological “Suitability” (using GIS)

In the frame of the geotechnical evaluation, the distribution and magnitude of sinkholes in a selected area were statistically evaluated. Every sinkhole was numbered and for each one several characteristics were recorded (time of occurrence, distance from the river, thickness of overburden loose materials, thickness of cohesive overburden material, max diameter and surface area).

The greater number of sinkholes occurs in the zone of 30-60 m, an area that coincides with the riverbed (Fig. 3a). The distance from the river of younger sinkholes, tend to increase (Fig. 3b). This can be explained by the theory that the mechanical action of the water washes out filling materials and progressively can reach more remote areas.

The distance from the river is determinative factor while the overburden thickness also affects the development of sinkholes. Another controlling factor for the development of sinkholes is the depth of groundwater table as the mechanical action of river water decreases when entering in the regional water table because of the reduction of its velocity.

The greater recorded distance of a sinkhole from the river was 137 m (Fig. 3a) and the greater overburden thickness 54m (Fig. 4a).

The study of sinkholes due to gypsum dissolution revealed that in Cyprus two are the most significant genetic models (Table 1).

One of the main targets of the study was the estimation of ground failure consequences on urban en-

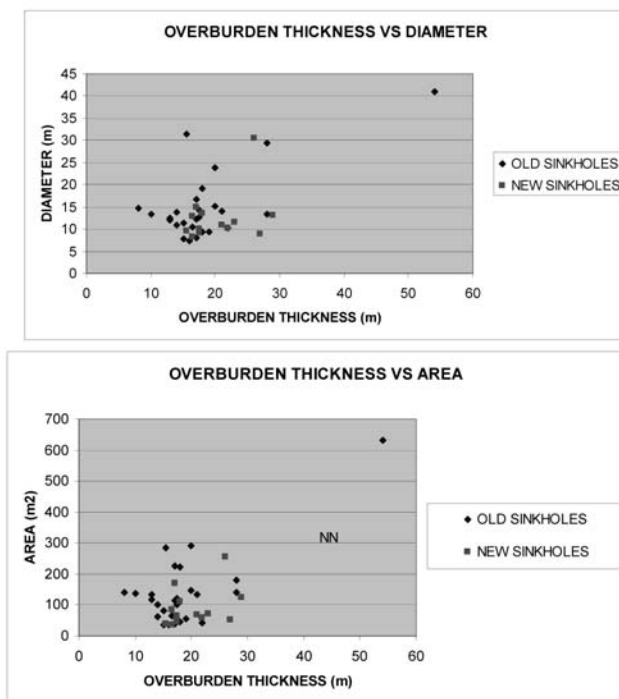


Fig. 4: a) left – Overburden thickness versus diameter of sinkholes, b) right – Overburden thickness versus area of the sinkholes

Table 1.

<i>MAIN CHARACTERISTICS</i>	<i>MAIN INFLUENCING FACTORS</i>
TYPE I (Pera Chorio – Nisou) the dissolution of gypsum and associated problems occur in the vicinity of rivers	
<ul style="list-style-type: none"> • Mature karst environment • Direct inflow of runoff water • Washout of filled karst • Low dissolving capacity of groundwater 	<ul style="list-style-type: none"> • Distance from watercourse • Thickness and lithological overburden type • Groundwater table depth
TYPE II (Aradippou), the dissolving capacity of groundwater is high, there is no direct flow of runoff water and the associated problems at the surface are controlled mainly by the fault systems.	
<ul style="list-style-type: none"> • Young karst • Overburden formations of low permeability • Widening of underground voids • High dissolving capacity of groundwater 	<ul style="list-style-type: none"> • Thickness and lithological overburden type • Overburden formations of low permeability • Dissolving capacity of groundwater • Fault systems

vironment and the design of geological housing “suitability” maps for the selected areas. The main target of a geological “suitability” study is to define zones with same characteristics in respect to safe



Fig. 5: a) left – An old sinkhole in a riverbed , b) right – Linear ground cracks.

housing. The term “safe” refers to any kind of geo-problem and its consequences; thus any geological condition that can affect people, buildings and infrastructure. In the case of this study, the main geo-problem is the development of sinkholes and so the zones correspond to different degree of sinkhole prone areas but also are related to the set of respective measures or directives that can be applied for every zone.

Geological “suitability” can be determined provided that the genetic model is defined together with the determination of the local engineering geological conditions. Geotechnical maps of 1:2,000 scale were designed for this purpose in six (6) areas mostly effected by gypsum geo-problems.

The general criteria that were used for the determination suitability zones were the following:

- Gypsum thickness,
- Presence or not of karst forms, type, magnitude, distribution and depth,
- Gypsum depth (overburden thickness),
- Lithological type and geomechanical characteristics of overburden formations,
- Type of groundwater and fluctuations of water table,
- Solubility,
- General engineering geological conditions.

3.2 Crete - Viannos

In May 2000 a large sinkhole developed in an agriculture area south of Ano Viannos village in Crete, causing the collapse of a local road. The sinkhole had a conical shape with 50m diameter and depth (Fig. 6).

IGME conducted a preliminary site investigation, which included engineering geological mapping in 1:5,000 scale, hydrogeological and geophysical works.

The sinkhole occurred in the edge of a small internal basin consisting by alluvial and Neogene deposits. The surrounding cliffs are formed by alpine formations (mainly limestones and flysch) belonging to two geotectonic zones: Olonos – Pindos and Gavrovo – Tripolis. Oligocene gypsum domes were also recorded as intrusions in flysch and limestone of Pindos zone.

The site investigation revealed that there were several old sinkholes in the greater area. The possible formations that could be connected with such phenomena were limestones and gypsum. Gypsum

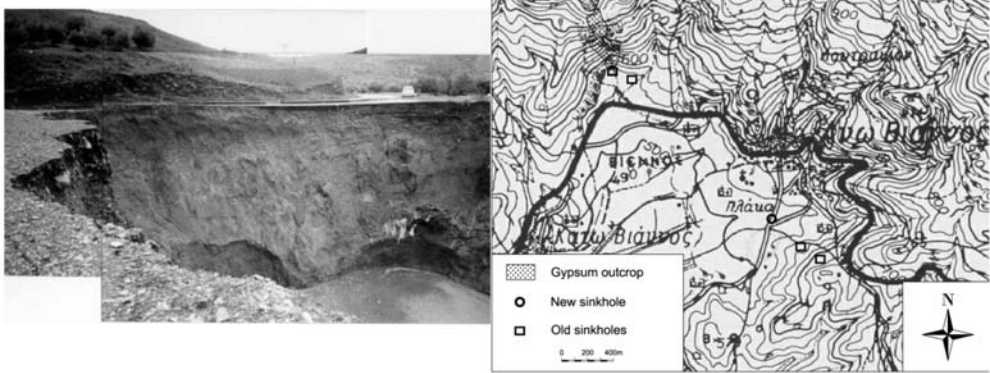


Fig. 6: a) left – A sinkhole in Viannos village (May 2000), Crete , b) Topographical map of Viannos village area.

outcrops were mapped in the greater area and two old sinkholes were directly related to them (Fig. 6b). The geophysical investigation in the vicinity of the sinkhole confirmed the existence of gypsum in the form of dome, exactly under the sinkhole. The estimated depth of the gypsum dome roof was about 130 m. The projection of the gypsum dome on the surface had an elongated shape with max diameter of approximately 180 m in a NNE-SSW direction and min, which fluctuated between 30 and 90 m.

This preliminary study suggested that the investigations (mainly geophysical surveys and geotechnical drillings) should expand in a wider area to cover the whole region where old sinkholes were recorded.

The local road should be abandoned and a diversion constructed, away from the sinkhole. Moreover, instructions were given for the filling of the sinkhole under examination:

- The filling must consist of large rocks at the base of the sinkhole, fragmented and earth materials on top of them,
- After a logical time when any settlements should be eliminated by adding more earth materials, concrete should be introduced in the hole,
- The final stage should be the construction of a reinforced concrete plate, which will cover the hole plus a ring with 15m thickness.

According to information received from the local authorities the road was diverted but the sinkhole is still open, gradually filling from river materials.

3.3 Corfu

Near the town of Corfu (Temploni area) a large sinkhole was developed in May 2008 (Fig. 7). IGME conducted a hydrogeological, engineering geological and geophysical survey for the study of the phenomenon. The region is a typical karstic area from the dissolution of gypsum with characteristic morphological features like dolines, karstic shafts and generally karstic geo-forms. Geologically the area consists of Triassic breccia (limestone fragments with gypsum as cemented material) and Triassic gypsum.

The tectonic structure of the area affects the geographical distribution of failures as the circulation of water and its dissolving action act much easier along the faults and discontinuities in general.



Fig. 7: The sinkhole in Temploni are.

The sinkhole under study has a symmetrical cylindrical form, inclined towards North, with 11m diameter. The depth of it was estimated 40m, using stratigraphic and hydrogeological data. The area of this ground failure geologically consists from Triassic breccia covered by clayey marly material with thickness at least 7m.

The Electrical Resistivity Tomography technique was also utilized in Corfu study with excellent results. A number of 15 lines were surveyed at 2 orthogonal orientations and spacing of 5 and 10m. As can be seen in Figure 8 a large resistivity anomaly is recorded over the void, with a characteristic funnel shape. The gypsum is easily distinguished from the overlying breccias sediments, with high resistivity values in the range of 500 to 700 Ohm*m. The effect of 3D geometry is evident in the interpreted 2D sections. The void which is easily detected on line SV1 is not seen on lines S10 and S11. A large resistive layer is seen instead and the resolution is lost. The large number of available data enabled the 3D processing and interpretation of the surveys. This was effected with the use of the program DC_3Dpro by Junh-Ho Kim and Mywong-Jong Yi of the Korean Institute of Geosciences and Mineral resources. In conclusion the application of ERT has proved the effectiveness of the method and the relative merits of using 3D interpretation schemes. Sinkholes are 3D targets and they require 3D processing and interpretation approach.

The under study phenomenon of ground failure and the development of the sinkhole was studied in detail and the geophysical achieved to determine the geometry of the underground cavity, while the hydro-geological and engineering geological findings clarify completely the genetic mechanism.

As it was described in the aforementioned paragraphs the geophysical investigations revealed the existence of an underground cavity under the sinkhole. The cavity is unfilled and was formed in gypsum formations. The elevation of upper part of cavity is estimated at absolute altitude +55 with overburden thickness 10m of rock formations (gypsum and Triassic breccias) and 13m of soil materials (clayey marly materials). The creation of the sinkhole derived from the partial failure of the roof of the cavity, which created a passage for the overburden loose soil materials.

The existence of the underground unfilled cavity complicates the rehabilitation of the sinkhole by filling it, while there is a risk of total collapse of the cavity which would result in the creation of a larger ground failure. Dissolution of gypsum is a continuous and relatively rapid process leading to the widening of cavities and the induced seismicity of the region increases the probability of a total collapse.

The study focused on the consequences of a total collapse. The best approach to the specific problem was the delimitation of a high risk zone, where it was proposed that building should be prohib-

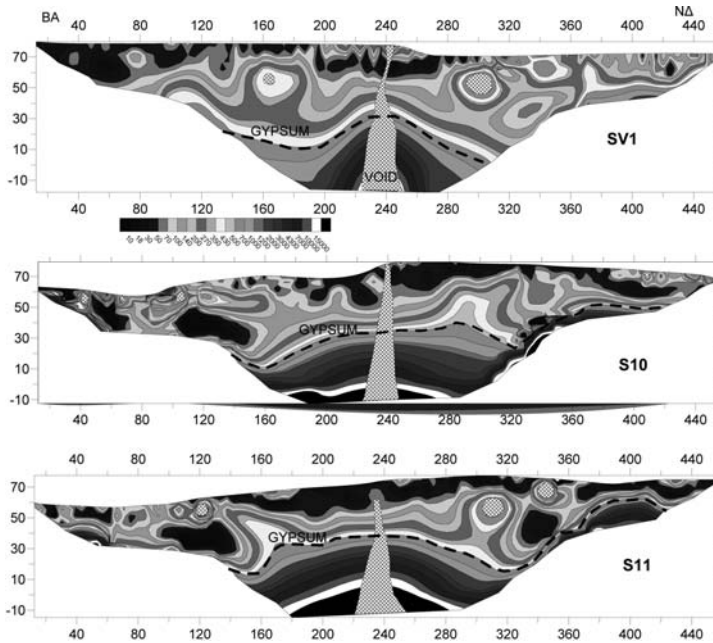


Fig. 8: 2D Inversion results of lines SV, S10, S11. Line SV1 is running over the sinkhole.

ited and the existing buildings should be abandoned. The determination of high risk zone resulted from the greater diameter of the cavity, the average thickness and the angle of friction of overburden loose soil materials ($13\text{m} - 45^\circ$). The resulted zone outside the sinkhole had a width of 13m.

The whole area is at a stage of development and as it was already mentioned similar engineering geological and hydro-geological conditions exist. The possible impacts on built environment as well as on humans should be investigated. For this reason the following were proposed:

- Determination of investigation zones according to engineering geological and urban planning criteria,
- Detailed engineering geological and hydro-geological investigations,
- Geophysical surveys,
- Geotechnical evaluation and determination of hazard zones.

In addition to aforementioned and until their implementation, geological, geophysical and geotechnical investigations should be conducted locally prior to any new construction of buildings or any other structures.

4. Conclusions - Discussion

The presence of gypsum and associated karst formation many times cause serious ground failure problems, especially when occurring in urban areas. Karst processes are natural phenomena that are continuous and the rate and type of karst development depend on the local geological conditions (tectonism, type of gypsum, overall geological structure).

Experience gained through aforementioned studies shows that there is a need for detailed site investigations (engineering geological, hydrogeological, geophysical and geotechnical surveys) with

target the good understanding of the genetic mechanism and local conditions, before applying any mitigation measures.

For large areas geological suitability maps help the determination of “safe” zones. A first logical approach would be to avoid the problematic areas by relocating structures to an area not affected. In the case that this is not possible mitigation measures depend mainly on the size of ground failures and the importance of structures under risk.

5. Acknowledgments

The authors thank all contributors of the three case studies coming from Institute of Geology and Mineral Exploration (IGME-Greece), Geological Survey Department of Cyprus, Geoinvest-Cyprus, cbs - C. Stergiopoulos.

6. References

- Benito, G, Perez del Campo, P., Gutierrez-Elorza, M, Sancho, C., 1995. Natural and human-induced sinkholes in gypsum terrain and associated environmental problems in NE Spain. *Environmental Geology*, Vol. 25, 156-164.
- Cooper, A.H., 1988. Subsidence resulting from the dissolution of Permian gypsum in the Ripon area; its relevance to mining and water abstraction. In: Bell FG, Culshaw MG, Cripps JC, Lovell MA (eds) Engineering geology of underground movements. *Geological Society of London, Engineering Geology Special Publication*, vol 5, pp 387–390.
- Cooper, A.H., 1995. Subsidence hazards due to the dissolution of Permian gypsum in England: investigation and remediation. In: Beck FB (ed) Karst Geohazards: engineering and environmental problems in karst terrane. *Proceedings of the 5th multidisciplinary conference on sinkholes and the engineering and environmental impacts of karst Gatlinburg/ Tennessee/2–5 April 1995, AA Balkema, Rotterdam*. pp 23–29.
- Deer, W.A., Howie, R.A., Zussman, J., 1962. Gypsum. In: *Rock Forming Minerals*, Vol. 5, 201-18. Longmans, London.
- Gorbunova, K.A., 1977. Morphology of gypsum karst. In: *FORD, T.D. (ed.), (q.v.)*, 221-2.
- Gutierrez, F., Cooper, A.H., 2002. Evaporite dissolution subsidence in the historical city of Calatayud, Spain: damage appraisal, mitigation and prevention. *Natural Hazards*, 25, 259-288.
- Herrmann, A., 1964. Gips- und Anhydritvorkommen in Nordwestdeutschland. *Silikat JI*, 3, 442 66.
- Hundt, R., 1950. Erdfalltektonik. W. Knapp, Halle (Saale).
- James, A.N., Lupton, A.R.R., 1978. Gypsum and anhydrite in foundations of hydraulic structures. *Geotechnique*. London, 28, 249-72.
- James, A.N, Cooper, A.H., Holliday, D.W., 1981. Solution of the gypsum cliff (Permian Middle Marl) by the River Ure at Ripon Parks, North Yorkshire. *Proceedings of the Yorkshire Geological Society*, 43, 433-450.
- James, A.N., 1992. Soluble materials in civil engineering. Ellis Horwood Ltd, England. 433pp.
- James, A.N., Kirkpatrick, I.M.. 1980. Design of foundations of dams containing soluble rocks and soils. *Q. J/ eng. Geol. Lond.* 13, 189 98.
- Jones, C.J.F.P., Cooper, A.H., 2005. Road construction over voids caused by active gypsum dissolution, with an example from Ripon, North Yorkshire, England. *Environmental Geology*. Vol 48, pt.3 384-394.
- Kemmerly, P.R., 1980. A time-distribution study of doline collapse: framework for prediction. *Environ. Geol.* 3, 123-30.

- Kempe, S., 1972. Cave genesis in gypsum with particular reference to underwater conditions. *Cave Sci. No. 49*, 1-6.
- Kemper, W.D., Olsen, J., De Mooy, C.J., 1975. Dissolution rate of gypsum in flowing water. *Proc. Soil Sci. Soc. Am.* 39, 458-63.
- Kim J-H., Tsourlos, P., Karmis, P., 2009. ERT inversion with a priori information. In : *Proceedings of the Near Surface EAGE conference*, Sept. 2009, Dublin, Ireland
- Koutsouveli, A., Poyiadji, E., Nikolaou, N., Kyriakou, E., 2008. Geological-Geotechnical investigations of “karst” phenomena in gypsiferous Messinian sediments in Cyprus, *33rd IGC, Oslo, GTE-01, abstract CD*
- Lu Yaoru, Cooper, A.H., 1997. Gypsum karst geohazards in China. 117-126 in Beck, F.B. and Stephenson, J.B (eds) *The Engineering Geology and Hydrogeology of Karst Terranes. Proceedings of the Sixth Multidisciplinary Conference on Sinkholes and the Engineering and Environmental Impacts of Karst Springfield/Missouri/6-9 April 1997. A.A.Balkema, Rotterdam.*
- Nicod, J., 1977. Deux karst du gypse remarquables des Alpes occidentales. In: *Ford, T.D. (ed.) (q.v.)*, 321-5.
- Olive, W.W., 1957. Solution-subsidence troughs, Castile Formation of Gypsum Plain, Texas and New Mexico. *Bull. geol. Soc. Am.* 68, 351-8.
- Paukstys, B., 1996. Hydrogeology and Groundwater Protection Problems in Karst Region of Lithuania. *Geological Society of Lithuania, Vilnius, vol. 6, pp. 1-72.*
- Pfeiffer, D., Hahn, J., 1972. Karst of Germany. In: Herak, M., Stringfield, V.T. (Eds.), *Karst: Important Karst Regions of the Northern Hemisphere. Elsevier, Amsterdam, pp. 187-223.*
- Poyiadji, El. Hadjicharalambous, Kl. Sampatakakis, P. Karmis, P. Demetriadis, Al. Nikolaou N. and Stergiopoulos, C. 2009: “Sinkholes due to gypsum dissolution genetic mechanism – definition of sink-hole prone areas - a case study in Cyprus”, *2nd International Workshop on sinkholes, Rome, 3-4 December.*
- Seedhouse, R.L., Sanders, R.L., 1993. Investigations for cooling tower foundations in Mercia Mudstone at Ratcliffe-on- Soar, Nottinghamshire. 465-471 in Cripps, J.C., Coulthard, J.C., Culshaw, M.G., Forster, A., Hencher, S.R. & Moon, C. (Eds). *The Engineering Geology of Weak Rock. Proceedings of the 26th annual conference of the Engineering Group of the Geological Society, Leeds, September, 1990. A.A..Balkema, Rotterdam.*
- Strobel, W., 1973. Der Grundgips im Raum Stuttgart als Modell für Gipsauslaugung und Bildung von Erd-fallen. In: *Proceedings of a symposium on sinkholes and subsidence, Hannover, [T1-G] 1-8. Deutsche Gessellschaft für Erd- und Grundbau. Essen.*
- Sweet, G.A., 1977. Hydrogeology of gypsum karst in Newfoundland. In: *Ford, T.D. (ed.) (q.v.)*, 390-1.
- Toulemont, M., 1984. Le karst gypseux du Lutétien supérieur de la région parisienne. Caractéristiques et impact sur le milieu urbain. *Revue de Géologie Dynamique et de Géographie Physique.* 25, 213-228.
- Wigley, T.M.L., Drake, J.J., Quinlan, J.F., Ford, D.C., 1973. Geomorphology and geochemistry of a gypsum karst near Canal Flats, British Columbia. *Can. J. Earth Sci.* 10, 113-29.
- Yi M.-J., Kim J.-H., Chung K.-L. (2003). Enhancing the resolving power of least-squares inversion with active constraint balancing. *Geophysics*, 68, 931-941

EVALUATION OF SOIL EROSION AND SUSCEPTIBILITY TO LANDSLIDE MANIFESTATION AS A CONSEQUENCE OF WILDFIRE EVENTS AFFECTED THE ZACHARO MUNICIPALITY, PELOPONNESUS, GREECE

**Rozos D. , Lykoudi E. , Tsangaratos P., Markantonis K., Georgiadis P.,
Rondoyanni Th., Leivaditi A., Kyrousis I.**

National Technical University of Athens, School of Mining and Metallurgical Engineering, Department of Geological Sciences, 9 Iroon Polytechniou, 15780, Zografou, Greece, rozos@metal.ntua.gr, mmgpel@central.ntua.gr, ptsag@metal.ntua.gr, markantonis@metal.ntua.gr, pangeor@central.ntua.gr, rondo@central.ntua.gr, alexouli@metal.ntua.gr, kyrousis@metal.ntua.gr

Abstract

In August 2007, a wildfire affected an area of approximately 135.000m² in the Municipality of Zacharo, located in Southern Greece at the Peloponnesus peninsula, causing the loss of 41 human lives, and having a dramatic impact on both ecology and economic-social welfare.

The present study applies a simplified model for the evaluation of soil erosion and the susceptibility to landslide manifestation on the hydrological basins of the Zacharo Municipality, as consequence of wildfire. The methodology was based on the evaluation and analysis of territorial parameters such as lithology, geomorphology, hydrography and land cover, which are thought to be directly or indirectly related to soil erosion.

The final product was a series of hazardous maps showing pre and post-fire soil erosion. An almost double increase in the post-fire area of high vulnerability was identified, covering 48% of the total area, and affecting dramatically the nearby communities. The outcome of this study helped the local and prefectural authorities to address certain mitigating measures in order to face the disastrous consequences of post-fire soil erosion.

Key words: *wildfire, soil erosion, landslide manifestation, modelling vulnerability to soil erosion, post-fire management plan, Municipality of Zacharo.*

1. Introduction

In August 2007, a wildfire affected an area of approximately 135.000m² in the Municipality of Zacharo (75% of the total land area), located in Southern Greece at the Peloponnesus peninsula. It was considered as one of the greatest natural disasters in the history of modern Greece, followed by the loss of 41 human lives and the dramatic impact on both ecology and economic-social welfare. About 70 % of the total cultivated area has been severely burned. According to the Greek office of World Wildlife Fund, the 22.5% of the Kaiafa Lake and forest, an area of exceptional ecological value, was severely burned. Its unique biodiversity has been harmed to a great degree, while endemic species of both flora and fauna suffered severe damage.

As a response to that disastrous event a research team from the National Technical University of Athens was formed to help the local Authorities to confront the disastrous effects of wildfire on the environment and the economic and social welfare of the nearby communities, associated with the geological environment and the natural processes that followed the wildfire.

It is well documented that areas affected by wildfire are frequently prone to flooding, landslide manifestation, debris and sediment flows (Gartner et al. 2004), events that are found to be accelerated during the wet season immediately after the wildfire. The parameters that influence the degree in which such events will be triggered are namely: topography, geology, soil characteristics, type of flora, precipitation (amount, intensity and duration) and finally fire severity (Swanson 1981). In general, such extreme events have as a result the removal of plant cover and litter layer, two matters that play an important role in the prevention of soil erosion caused by rainfall impact and overland flow. The consequence of this process is the significant increase in soil vulnerability to erosion processes, while soil alteration in physical and chemical properties is also observed (DeBano et al. 1998). The reactivation of landslide phenomena, mainly destructive debris flows, is also to be expected as a result of high intensity rainfall events, and this will result in blocking drainage pathways, damaging residential structures and network and most importantly endangering human life.

The extend of soil cover and weak rocks that appears along with the recorded high rainfall intensity in the Zacharo area indicate that the manifestation of adverse affects, such as flooding, landslide, debris, and sediment flows, are expected to be very significant and therefore mitigation measures should be implied as soon as possible.

Consequently, the effort of this work was aimed towards identifying, through modelling, the areas of high soil vulnerability to erosion processes and areas prone to landslide manifestation, in order to apply the necessary mitigating measures presenting a valuable post fire erosion control treatment.

2. Methodology

The procedure followed during the preparation of a post-fire management plan can be grouped into the following three (3) phases:

- a) Collection and process of all available bibliographical data concerning the research area. Mapping and classifying the burned areas according to the burn severity and also verifying and accomplishing a geological map at a scale of 1:25.000, were necessary. Determination and inspection of areas prone to flooding, and areas prone to landsliding.
- b) Construction of a valuable database, by processing and digitizing the available data. The data were introduced into a GIS system, in order to construct a variety of thematic maps that would assist the study of the geomorphologic characteristics of the area. Also, a quantitative analysis of the hydrological networks was done and the development of a simplified model for estimating the vulnerability of the formations against soil erosion was established during this phase.
- c) Suggestions of mitigating measures in areas of concern and validation of the outcomes of the study will be the aim of this phase.

3. Geomorphology and Geological settings

Based on the geotechnical survey carried out (Rozos et al. 2008) the study area morphologically is placed among the basin fold of Zacharo, characterized by a multifold evolution on the account of the

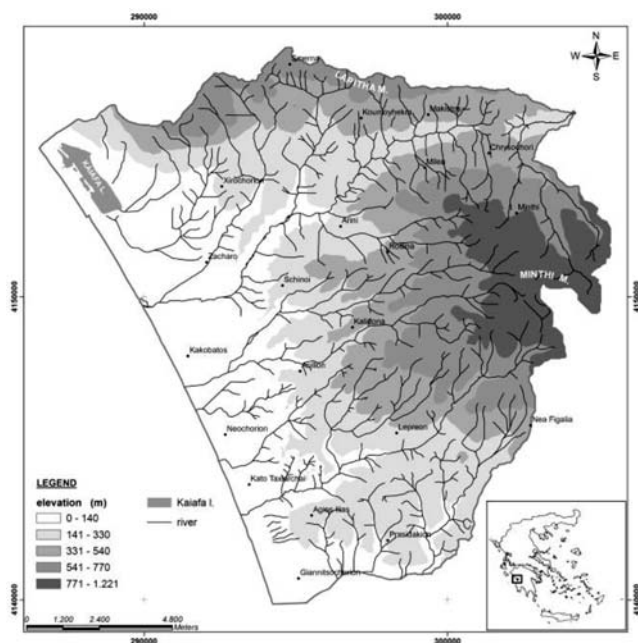


Fig. 1: Morphological Map of the study area.

adjacency with the Ionian trench. Lapithas Mountain to the north and Minthis Mountain to the east are dominant, while a lowland area is observed to the west with small morphological elevation variance, due to the presence of sand-dunes along the coastline. Lake Kaiafa, north to the city of Zacharo, is considered as another dominant morphological element (Fig. 1).

The hydrographic network of the area is relatively dense mainly to the south and west presenting a more complex form, while its type is considered as dendritic and rectangular, with asymmetry within the hydrological basins. It typically reaches the 4th and 5th class according to Strahler scale while the Kallidonic River reaches the 6th class. The area has a mean annual precipitation of 900mm at the hilly and lowland areas, while in the highlands it is higher than 1000mm. Also, the mean annual temperature is 17.4°C, and the mean annual moisture reaches 69%. Finally, the dominant wind direction is southwest.

Geologically the study area consists of alpine and post-alpine formations, which belong to the Ionian, Gavrovo and Pindos Geotectonic zones (IGME 1972; 1974; 1979) (Fig. 2). The formations are limestones Triassic, Jurassic and Cretaceous in age, Schist – Chert formations, transition sediments to flysch and flysch formations. Concerning the post-alpine deposits, Neogene sediments and Quaternary deposits, which appear mainly in the basin of Nedas and Zacharos Rivers, dominate in the hilly and lowland areas. Regarding the permeability of the above formations, they are classified into three categories, namely: a) high permeable, b) low to medium permeable and c) practically impermeable, while a shallow water table is observed within the intense weathering zones.

4. The Soil Erosion Vulnerability model

The estimation of the spatial soil vulnerability index and the identification of the prone to landslide manifestation areas was the main objective of the second phase. The spatial soil vulnerability index

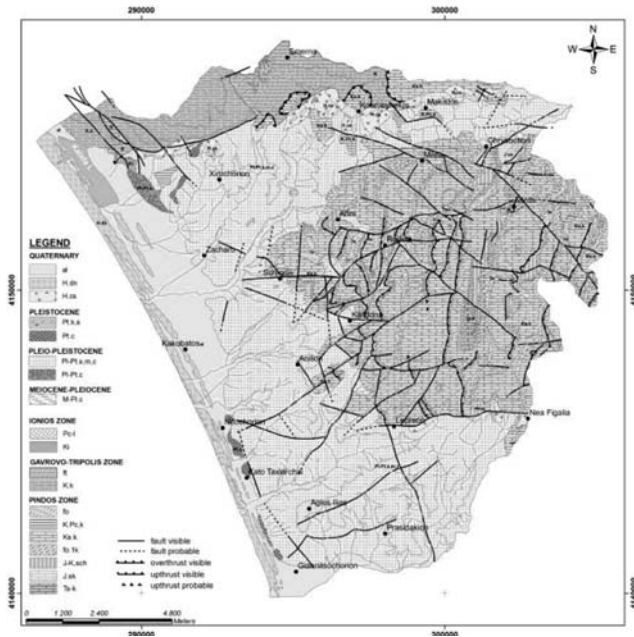


Fig. 2: The geological map of the study area.

was evaluated by applying a simplified model (Alexoudi et al. 2002; Lykoudi et al. 2004) while lithological type, slope gradient, hydrographic texture and vegetation cover were considered as input variables.

A few modifications to the original model were necessary to be done. Specifically, the precipitation parameter was not included in the developed model as it was indirectly calculated by the drainage texture, drainage density and drainage frequency, and also it appeared to have insignificant spatial variation.

However, the most important modification was the input in the original model of a thematic map of “burn severity”, which showed the relative amount of damage attributed to an area, as a consequence of wildfire (Key and Benson 2006). It has been observed that in high burn severity areas the probabilities of instability and soil erosion problems are more likely to occur (Benavides-Solorio and MacDonald 2001). The resulting classified map was conducted after field inspection and was coded into three (3) classes of fire severity, namely (a) unburned, (b) moderate burned, and (c) highly burned (Fig. 3).

The classification of the formations into three (3) lithological categories was made according to their likelihood to erode, taking into account the knowledge gained after the field inspection, but also the combined estimation of the lithological texture, the infiltration ability and permeability of the formations in question. In the first category, unweathered intact formations with high permeability, but also those with a weathering mantle of small thickness were classified; In the second category formations which exhibit medium to high infiltration and medium to low permeability value, but also those which are covered by a weathering mantle of medium to big thickness were grouped; In the third category formations that are characterized by high infiltration values and low permeability, and also those which are covered by weathering mantle of great thickness were included.



Fig. 4: Vulnerability map of Soil Erosion

5. Landslide spatial distribution and characteristics

As already mentioned, areas with high burn severity values would be more likely to exhibit instability problems. Such behaviour could be influenced by several factors that have as a result the reduction of the strength parameters of the formations and the manifestation of landslide or debris flows. The main primary parameters responsible for landslide manifestation throughout the studied area could be grouped as follows:

- The presence of geological formations that are characterized by low geomechanical properties,
- The sequence of geological formations with different geomechanical properties both to the horizontal and vertical extent,
- The intense tectonic action, and seismic activity,

while the main secondary ones are:

- The weathering and erosion process,
- The amount, intensity and duration of precipitation,
- The human intervention, concerning road infrastructure, and cultivation,

The last two are the main triggering factors to slope failures manifestation.

The instability problems were mainly connected with the neogene sediments, the flysch formations and the schist-chert series of Pindos zone. They were also observed in highly weathered zones of carbonate formations and in sites where the main discontinuity systems of the rock formations had the same direction to the natural or artificial slopes. They appear in large cultivated areas and on the main road network (Fig.5a & 5b).

Significant landslides have also been reported to influence populated areas, with main examples the landslides in Kalidona and Lepreo villages.



Fig. 5: Significant Landslide phenomena in (a) the road of Koumouthekla – Makistos and (b) outside the Koumouthekla village.

6. Defining areas of high risk

By using the developed model, areas characterized by high risk were identified by taking into consideration the susceptibility of soil erosion and landslide manifestation. The area that showed an increase in vulnerability, as a consequence of the August 2007 wildfire, was about 55km², i.e. 27% of the total area, while the 73% has remained the same. From the area that shows vulnerability increase, about 10.1km² (5% of the total area) changed from low to medium vulnerability, about 16.0km² (8% of the total area) from low to high vulnerability, and 29.0km² (14% of the total area) from medium to high vulnerability class. The areas that are located mainly at the Northern part of Zacharo municipality (Lapithas mount.), at the central (between Kalidona and Chrisochori village) and the southern part (north of the valley of river Neda) were considered as the most vulnerable ones (Figure 6). Therefore, the suggested mitigation measures should be mainly applied in those areas.

During the study another problem was revealed to the research team. The volumes of water at the exit of the final drain channel downwards the residual area of Zacharo town, compared with the volumes entering the drain channel before the residential area, show a considerable increase. This indicates that the pluvial water of the residential area is added to that of drainage through the sewer channel network. To avoid the flood risk in such cases, the construction of a parallel to the main drain channel or a parametrical one to the town of Zacharo could be the solution.

7. Mitigation measures – Post fire erosion control treatment

The implementation of a post-fire erosion control treatment was the main objective of the third phase. The goal of this treatment is to cost-effectively protect the onsite and downstream areas, until the native vegetation germinates, by reducing and delaying the volume of accelerated sediment yield that typically follows a wildfire. The effort was focused in the direction of providing actions that could be followed by the local authorities. The proposed remedial measures were mainly directed towards mitigating the effects of wildfire by taking into consideration the combined evaluation of soil vulnerability index and the zones of landslide instability. Many types of mitigation measures, both on the hillslopes and stream channels were utilized, taking the form of mechanical barriers that retain debris or thick soil covers in place, and reduce the erosive processes caused by rain splash and overland flow, or the form of specific actions that had to be applied before the beginning of the wet season. Those actions included:

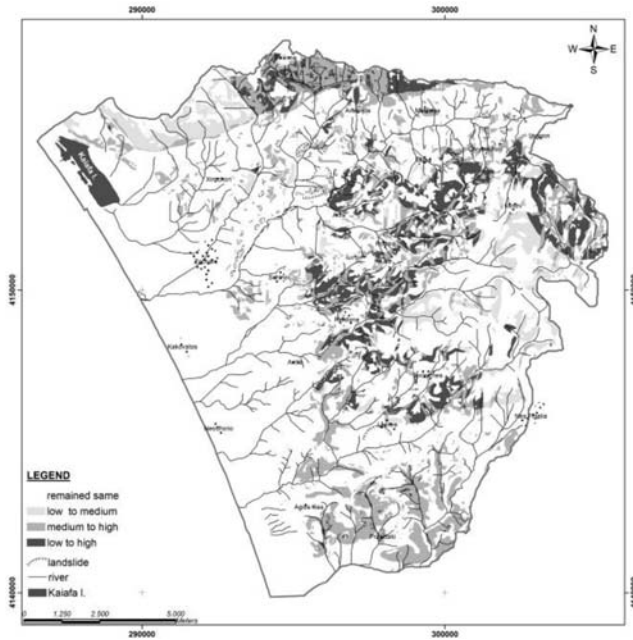


Fig. 6: High risk areas showing the spatial distribution (of what?)

- Immediate installation of an emergency alarm system, that could warn the local authorities in the case of intensive precipitation events, in order to evacuate if necessary the populated areas.
- Construction of log-barriers, and small wooden dams, which retain the material of the eroded soil cover on slopes; thus contributing to the increase of the infiltration rate and reduce of the water runoff velocity.
- Installation of “fences” from steel panels of certain diameter in certain sites along the river path, in order to capture objects that would otherwise block the drainage pathways and act as obstacles forcing the water to flow outside its path.
- Clearance and in some cases widening the main hydrographic network axes.
- Continuous inspection and clearance of the sewer network within the residential area of the Zacharo municipality.

Regarding the construction of log-barriers on slopes, the burned trees should have been cut down, trimmed, and their branches and/or logs should have been placed on the ground along certain contour lines (Figure 7). As a result, water runoff is not permitted to follow a straight down-slope path. The water is forced to meander back and forth between logs; thus is reducing its velocity and allow water with sufficient time to percolate into the soil. Log-barriers of 3 to 9m long and 40 to 60cm in diameter should be used in areas of high vulnerability indicated by the model (Fig. 6).

The debris racks (metallic fences) have to be installed in the main drainage pathways and for working effectively, the local authorities are obligated to continuously inspect and when necessary remove the captured material (Fig. 8a & 8b).

8. Discussion and Results

In general, the behavior of geological formations, in response to the natural processes that followed the



Fig. 7: Log or brunch barriers (a) and small wooden dams (b) for soil erosion protection.



Fig. 8: Debris Rack (metallic fence) (a), widening and clearance of river network (b).

wildfire, depends on their lithological composition, their tectonic history, the susceptibility to the processes of weathering and erosion, along with the geo-mechanical action of ground and surface water.

Furthermore in the examined burned areas, the strength properties of the formations are reduced as a consequence of both, the geo-mechanical action of water (ground and surface) and the changes on the surface layer of the burned area. Specifically the carbonate rocks present a relatively good geo-mechanical behavior; with rare instability problems (mainly rock falls). The frequent instability problems manifested in flysch, schist-chert and other clastic formations, are creep and various types of slides. In general, landslide manifestation increases in frequency and density in areas where slopes (natural or man-made), have high gradient and in zones of intense weathering. In plio-pleistocene formations altering behaviour could be found, as a consequence of the differences in lithological composition and tectonic distress. In those formations the gradient between the slopes and the dip of the strata is also a parameter that influences their behaviour. Finally the alluvial deposits that cover the lowland area of the municipality of Zacharo (gentle slope gradient) do not exhibit any instability problems.

The implementation of the developed methodology has been helpful in the evaluation of the vulnerability degree of the formations concerning soil erosion. By using GIS system, i) a map of lithological formations prone to erosion, ii) a map of slope gradient (S), iii) a map of hydrographic texture (Y), iv) a map of land use / land cover, and v) a map of burn severity area, were produced. Furthermore, by applying spatial analysis techniques, the vulnerability of formations to soil erosion was calculated in order to produce the final vulnerability map. In particular, severely burned areas with over 35% of slope gradient, with high hydrographic texture value covered by formations of high infiltration and low permeability values are considered as high vulnerability soil erosion areas. Also



Fig. 9: Failure of log-barrier (a), and effective implementation (b).

those which are covered by weathering mantle of great thickness and are severely burned are considered as high risk areas.

After a wildfire the severity and amount of the disastrous events which affect landscape evolution typically decline in subsequent years as the environment becomes stable. The recovery rate varies and is influenced mainly by the magnitude of the wildfire, the climate, and the soil characteristics of the region in question. These features probably persist longer in arid and semi-arid climates than in humid ones. In the region of Zacharo a medium to high recovery rate was observed. As already mentioned, the area receives a significant amount of precipitation, while the mean annual moisture content reaches 69%, enhancing the vegetation recovery in great parts of the burned area. Parallel to that, the proposed mitigation measures seemed to work well in most of the implemented areas. Their success was also supported by the mild climatic conditions during the first wet season after the wildfire, as well as the relative coordination and efficient actions performed by the local authorities.

Evaluating the applied measures, it was revealed that the grain size of the material produced by soil erosion processes is a significant factor for the effectiveness of the log-barriers. Indeed, large amount of fine-grained material makes the effectiveness of the log-barriers insufficient. The consequences of the present high or low amount of fine-grained soils are shown in Figure 9. Finally, the construction of log-barriers in carbonate formations was found to be inappropriate having in most cases negative influence.

9. References

- Alexoudi-Livaditi A., Livaditis G., Lykoudi E., 2002. Evaluating the vulnerability to erosion of geological formations and the sediment yield in Lesvos. 6th Hellenic Geographical Conference, Thessaloniki.
- Benavides-Solorio, J.; MacDonald, L.H. 2001. Post-fire runoff and erosion from simulated rainfall on small plots, Colorado Front Range. *Hydrological Processes*. 15:2931-2952.
- DeBano, L.F., Neary, D.G., Ffolliott, P.F., 1998. *Fire's Effects on Ecosystems*. Wiley, New York.
- Gartner, J.E., Bigio, E.R., Cannon, S.H., 2004. *Compilation of postwildfire runoff-event data from the western United States*. Open- File Report (United States Geological Survey) 04-1085 (<http://pubs.usgs.gov/of/2004/1085.html>).
- IGME publications, *Geological map of Greece*, scale 1:50.000, (Kyparissia 1979, Kato Figaleia 1974,

Olympia 1972, and Tropaia 1979 sheets).

- Key H., Benson C., 2006. Landscape assessment (LA). In: D.C. Lutes, R.E. Keanne, J.F. Caratti, C.H. Key, N.C. Benson and L.J. Gangi, Editors, *FIREMON: Fire Effects Monitoring and Inventory System General Technical Report RMRS-GTR-164-CD*. USDA Forestry Service, Fort Collins, Colorado.
- Lykoudi E., Zarris D., 2004. The influence of drainage network formation and characteristics over a catchment's sediment yield. 2nd International Conference on Fluvial Hydraulic and Environmental Engineering Girolamo Ippolito, University of Napoli Federico II, Naples, Italy, June 23-25.
- Rozos D., Georgiadis P., Alexoudi A., Kyrousis G., Marinos P., Rondogianni T., Tsiambaos G., Lykoudi E., Markantonis K., Tsangaratos P., 2008. Evaluating soil erosion in the basin of the municipality of Zacharo, Research Team "A" for the fire-stricken areas, NTUA, Athens, Greece.
- Swanson J., 1981. Fire and geomorphic processes. in: Mooney, H.A., Bonnicksen, T.M., Christiansen, N.L., Lotan, J.E., Reiners, W.A. (Eds.), *Fire Regime and Ecosystem Properties*, United States Department of Agriculture, Forest Service, General Technical Report WO vol. 26. United States Government Planning Office, Washington, DC, pp. 401–421.

12ο ΔΙΕΘΝΕΣ ΣΥΝΕΔΡΙΟ ΤΗΣ ΕΛΛΗΝΙΚΗΣ ΓΕΩΛΟΓΙΚΗΣ ΕΤΑΙΡΙΑΣ
ΠΛΑΝΗΤΗΣ ΓΗ: Γεωλογικές Διεργασίες και Βιώσιμη Ανάπτυξη

12th INTERNATIONAL CONGRESS OF THE GEOLOGICAL SOCIETY OF GREECE
PLANET EARTH: Geological Processes and Sustainable Development



ΑΣΤΙΚΗ ΓΕΩΛΟΓΙΑ / URBAN GEOLOGY

ENGINEERING GEOLOGICAL MAPPING IN THE URBAN AND SUBURBAN REGION OF NAFPLION CITY (ARGOLIS, GREECE)

Em. Apostolidis and An. Koutsouveli

Institute of Geology & Mineral Exploration, Department of Engineering Geology, Olympic Village, Entrance C, 136 77 Acharnae, Greece, emmapost@ath.forthnet.gr

Abstract

In our days the strategy of an integrated planning approach in dealing with urban development matters, is a reality and engineering geology plays a primary role. In the present study an approach of the engineering geological conditions of Nafplion city and the wider area are given.

In the region of interest, four (4) sampling boreholes were drilled by IGME, up to the depth of 40m. During the boring procedure in situ SPT and permeability tests were carried out, as well as the lithology of obtained material has been described. Samples, undisturbed and disturbed, have also collected for further laboratory tests. After the completion of each borehole, piezometric tubes were installed, for the monitoring of the underground water table. Laboratory tests for the determination of physical and mechanical characteristics of all drilled formations were executed.

The geotechnical distinction and unification of the geological formations was made on a 1:5,000 topographical map, in accordance with the up to date international practice. The engineering geological map in the urban and suburban region of Nafplion city is presented and the geotechnical characteristics of the formations structuring the area are evaluated. The combination of the results of the drilling programme as well as on the engineering geological approach and the geological structure of the studied area, resulted the compilation of the engineering geological map (scale 1:5,000) of Nafplion city wide area, where 18 engineering geological types are distinguished. The boreholes data of other public bodies have been also taken into account for this compilation. As the task of this project was the contribution to the urban development of Nafplion city, this engineering geological map will be a useful tool for engineers, planners, civil authorities, etc.

Key words: *engineering geological mapping, urban development, Nafplion, Argolis, Greece.*

1. Introduction

The region of study is extended north the city of Nafplion up to Tiryntha, southern up to the Stefaniotiko hill and eastern up to Exoni region. The morphology of studied area is characterized by the mountainous landscape that prevails in southern and the soft flat landscape that dominates to the north, with the exception of certain small hills. The drainage pattern in the mountainous part has a short length, as well as in the flat part small streams and torrents are seasonal developed. In the coastal region, according bibliographic references, the aquifer is found about the sea level, while in the plain is found in depth 1-4 meters. This happens because of the in-

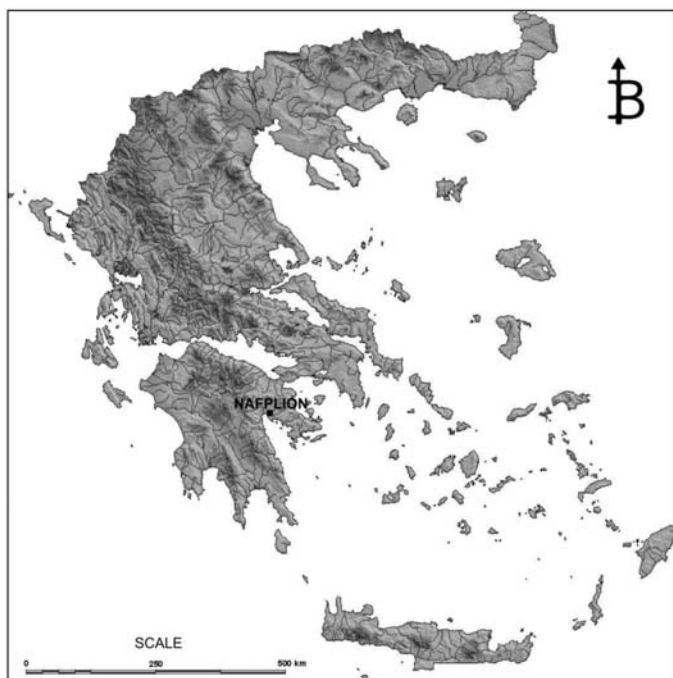


Fig. 1: Location of the wider Nafplion area, Argolis, Greece.

tensive exploitation of the wells and boreholes of the area, resulting to the subsidence of the aquifer and the salinity of waters.

2. Seismicity and seismic hazard

The wider area of Nafplion is characterized by low seismic hazard, as far as it has not been affected by very big earthquakes, but is influenced by neighbouring centres of seismic activity. Relating to the seismic action planning, according to the last modification of Greek Antiseismic Regulation (EPPO, 2001), the wider area is classified in the category I of seismic hazard, with seismic acceleration of territory $A=a \cdot g$, where $a=0,16$ and g the acceleration of gravity ($=981 \text{ cm/sec}^2$).

3. Geological structure

According to the IGME Geological map of Greece in scale 1:50.000 (sheet NAFPLION, by Tataris et al.) the dominated geological formations in the wide studied area from the older to younger are:

- Limestones of Middle Triassic age: They occur southern of Palamidi and eastern of Nafplion city. It concerns a carbonate rock group in which the lower members consist usually of reddish, hard limestones with cherts and thin intercalations of marls, they are followed by white-yellow slabby limestones with thin intercalations and cherts and thick-bedded ones with coarse clastic material.
- Limestones of Lower Cretaceous age: They are well bedded to massive, usually gray, and

in places with intercalations of marls. They occur at Palamidi, Akronafplia, Exostis and Profitis Elias regions.

- Limestones of Upper Cretaceous age: They occur in small outcrops at Akronafplia region and consist of thin bedded to thin slabbed limestones of white-pink colour, in places with intercalations and nodules of cherts.
- Idivided flysch of Maestrichtian age: It dominates in eastern and southeastern of Nafplion city and consists of calcite shales, sandy marls, sandstones and conglomerates with intercalations of clastic limestones. In the lower layers and towards the transition sediments to the underlying limestones serpentines are presents.
- Quaternary deposits: They occur mainly in the plain area, which is extended north of Nafplion city. They consist of thin-grains to gross-grains loose materials of coastal and terrestrial origin. On the mountainsides and hillsides of the area, old and recent screes and talus cones are developed

The tectonic activity in the studied area is quite complicated with faults, folds and upthrusts jn large scale. The folds and the large scale upthrusts appear to the preneogene formations, while the faults usually normals are responsible for the morphology of the recent landscape and the creation of seashores, such as the trench of Argive plain. The main faulting directions are E-W, NW-SE, and NE-SW.

4. Engineering geological mapping and structure of the wider Nafplion area

Engineering geology developed in response to the increasing demands of various technical works, which required a better understanding of the interaction between the ground, foundations and constructions, in order to build more economically and on a safer base.

In the Hellenic territory, engineering geological maps have been progressively developed and as far as practical have incorporated information from various technical works. Even a few years ago, there was lack of regional maps giving basic engineering geological information, such as for planning land use and technical works, the selection of the most appropriate types and methods of construction and the better protection of the environment. To this end, the engineering geological map of Greece, at a scale of 1:500,000 (IGME, 1993), constituted one of the first important efforts. In addition, the 1:10,000 engineering geological map of the wider Thessaloniki area is considered to be a basic infrastructure tool for more detailed investigations, as well as a useful aid for responsible civil authorities and technical personnel, during the preliminary stage of various technical works (Hadzinakos et. al, 1990; Rozos et. al, 1990; Rozos et. al, 2004).

The engineering geological distinction and unification of the geological formations was made on a 1:5,000 topographical map, in accordance with the up to date international practice. Necessary adjustments for the peculiarities of the Greek territory (Koukis, 1980; Koukis, 1988) and especially of the area under study were also taken into account. According to the international views and recommendations (Anon, 1972; Anon, 1979; Anon, 1981; Bell, 1981; Carter, 1983; Dearman and Matoula, 1976; Matoula et. al, 1986; UNESCO/IAEG, 1976), the above map is characterised as a multi purpose, synoptic and large scale engineering geological map, and is shown with a simplified legend in Figure 3. In the above map (Figure 2) the surface development of all lithological types is given, while their geotechnical description is presented below.

The data used in the description of the lithological types were obtained from many boreholes executed by a number of investigators from both the public and private sectors. Also, in the re-

gion of interest, four (4) sampling boreholes were drilled by IGME, up to the depth of 40m. During the boring procedure in situ SPT and permeability tests were carried out, as well as the lithology of obtained material has been described. Samples, undisturbed and disturbed, have also collected for further laboratory tests. After the completion of each borehole, piezometric tubes were installed, for the monitoring of the underground water table. Laboratory tests for the determination of physical and mechanical characteristics of all drilled formations were executed (Apostolidis and Koutsouveli, 2007).

The engineering geological map of the wider Nafplion area, at a scale of 1:5,000, contributes significantly to the optimization of land use and better planning of technical works. However, such maps cannot be considered a substitute for in situ geotechnical investigations at the microscale for every individual construction. This map distinguishes eighteen (18) engineering geological types, ET (Figures 2 and 3). Many geotechnical boreholes as well as in situ observations and sampling were used in the preparation of this map. Special emphasis was given to those units, which are present in inhabited/industrial areas. The brief descriptions of the engineering rocks and soils follow those prepared for Engineering Geological Mapping. The engineering geological type (ET) has the highest degree of physical homogeneity. It should be uniform in lithological character and physical state. These units can be characterized by statistically determined values derived from individual determinations of physical and mechanical properties and are generally shown only on large-scale maps (UNESCO/IAEG, 1976).

A little lower are given in details the descriptions of eighteen (18) engineering geological types (ET) that were divided in the region of interest, from the younger to the older one (Apostolidis and Koutsouveli, 2008):

- Type Ia: Loose materials of embankments of historical and younger age, small thickness (less than 1 m). These materials consist of structural stones, tiles, coats and other constructive materials mixed with soil deposits, which mainly have a silty-sandy composition, with some grits and gravels.
- Type Ib: Loose materials of embankments and recent deposits of sandy clays, sands and gravels in places. The thickness of this formation usually varies between 1- 4 m.

The formations of type Ia and Ib appear in a great section to the down town of Nafplion. Their geomechanical behaviour is unsatisfactory imposing the improvement of the soil to the safety of the various constructions.

- Type IIa and IIb: Deposits in river-beds. They are incohesive materials of small thickness, from cobbles of various size and origin, sands and locally silty-clays. They have divided in two types, type IIa (mainly coarse-grained materials) and type IIb (mainly fine-grained materials and sand). In general, their geomechanical behaviour is controlled by the characteristics and percentage of the fine material.
- Type III: Clays, silts and locally sandy-silts, soft, mainly grey or grizzled colour. At places, it contains organics, shells and plant remains. They are characterized, usually, by high plasticity, while locally, under certain conditions, are expected phenomena of subsidences and liquefactions.

Physical and mechanical properties (usual range of values):

$$w_L = 22.0 - 67.0 \% \quad c = 6 - 122 \text{ KPa}$$

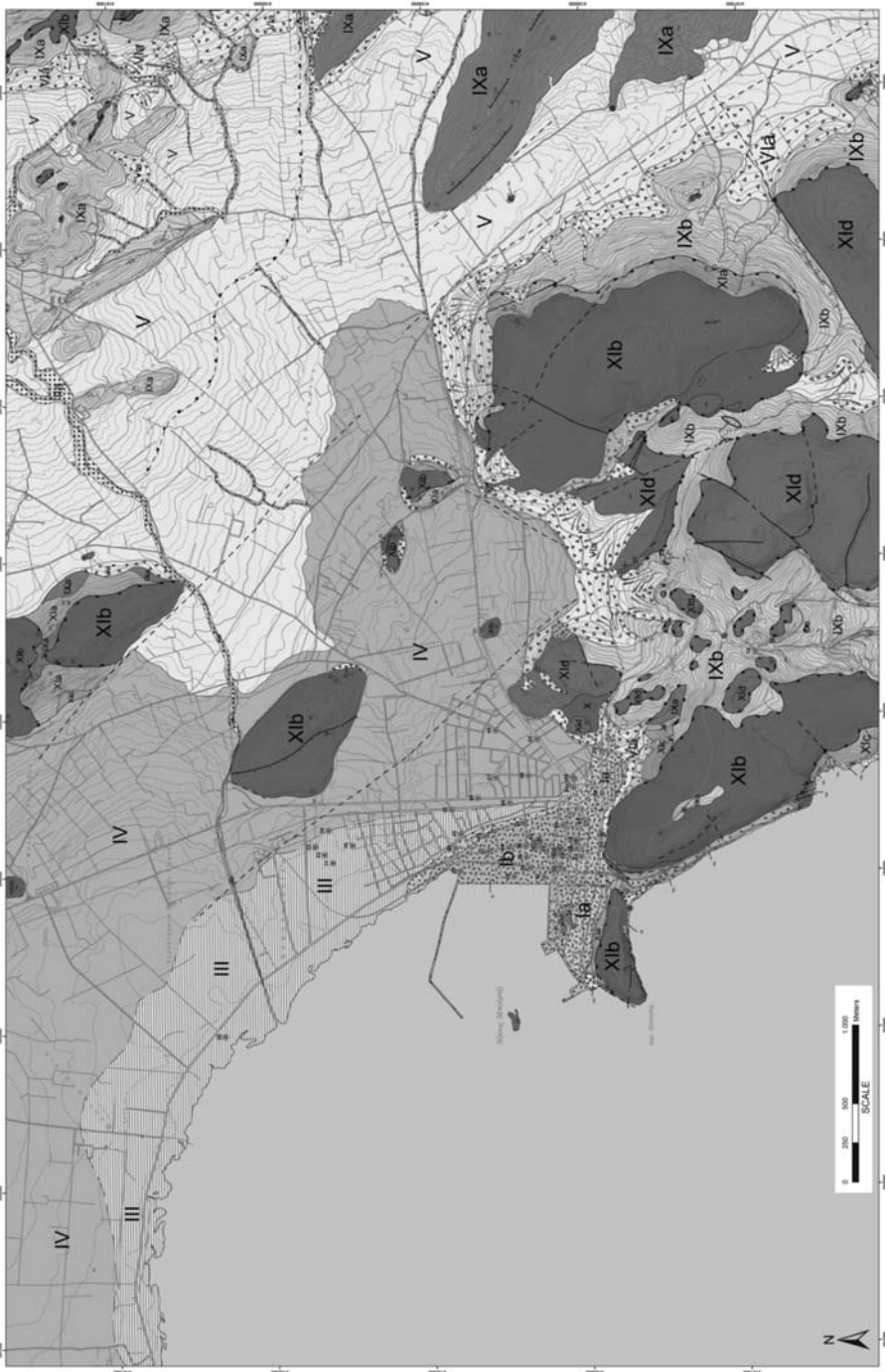


Fig. 2: Engineering geological map of the wider urban and suburban region of Nafplion city, Argolis, Greece.

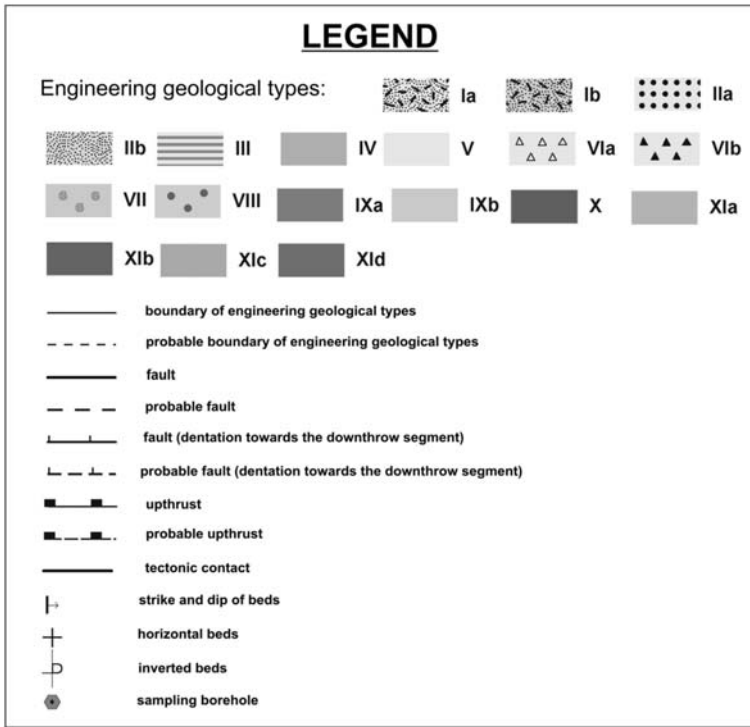


Fig. 3: Legend of engineering geological map (Figure 2).

$$I_p = 11.0 - 43.0 \% \quad q_u = 10 - 201 \text{ KPa}$$

$$w = 17.8 - 65.3 \% \quad c_c = 0.041 - 0.46$$

$$\gamma_b = 16.7 - 20.3 \text{ kN/m}^3 \quad e_o = 0.728 - 1.348$$

$$e = 0.62 - 0.74$$

- Type IV: Clays and silts, brown or red-brown or yellow-brown colour, with small variations in the percentage of sand and small gravels at places. They are characterized by middle to high plasticity and middle to big coherence.

Physical and mechanical properties (usual range of values):

$$w_L = 20.0 - 65.0 \% \quad c = 8 - 155 \text{ KPa}$$

$$I_p = 10.5 - 50.0 \% \quad q_u = 26 - 598 \text{ KPa}$$

$$w = 13.0 - 41.4 \% \quad c_c = 0.08 - 0.33$$

$$\gamma_b = 18.1 - 21.6 \text{ kN/m}^3 \quad e_o = 0.499 - 1.045$$

$$e = 0.50 - 0.94$$

- Type V: Loose deposits of mixed phases, brown or red-brown colour. They are composed of silty-clays, sandy-clays, sands, grids, gravels and cobbles of various size and



Photo 1: The formation of engineering-geological type VII, with the characteristic fossils *Strombus bubonius*.

origin. They are characterized by frequent and rapid changes in their lithological composition and grain size distribution towards their horizontal and vertical development. Their behaviour is controlled by their thickness, their lithological anisotropy and the inclination of the ground (especially in the case of dynamic loading). The strong heterogeneity of these formations results in high anisotropy of their mechanical behaviour, but they usually show satisfactory shear strength parameters, especially in areas with gentle morphology. In general, their geomechanical behaviour is usually controlled by the characteristics and percentage of the fine material.

- Type VIa: Screens and talus cones. Pebbles, cobbles and small fragments of limestones, with sandy-clay materials, constitute them. Usually, they present poor coherence, with decreased geomechanical characteristics.
- Type VIb: Cohesive (usually) to semi-cohesive screens and breccias. They are composed of coarse-grained elements of different origin (mainly from limestones) and various sizes with reddish colour cement (usually red calc-clays). At places, olistholiths of various dimensions are presented. In its entirety, this formation behaves as weak-rock, with decreased geomechanical characteristics.
- Type VII: Cohesive conglomerates in banks, with red clayey cement. At places, the formation has the look of pebbly and encloses the characteristic fossils *Strombus bubonius* (Photograph 1). In its entirety, this formation behaves as powerful weak-rock, with satisfactory geomechanical behaviour.
- Type VIII: Cohesive conglomerates-microconglomerates, from cobbles of various origin and size and red calc-clay cement, in layers 10-15cm. In its entirety, this formation behaves as weak-rock, with satisfactory geomechanical behaviour.
- Type IXa: Flysch consisted of sandstones, quartzitic sandstones, sandy-marls, siltstones

and conglomerates with intercalations of limestones. They are usually thin-bedded, but often with sandstone layers, 0,50-1,00m thick. The layers present strong traces of horizontal tectonic deformation (folds, wrinkles, inversions, fractures and fragmentations). In macroscale, flysch is considered as an impermeable formation, allowing the occurrence of small springs (usually between the fragmentation zone and/or weathering mantle and bedrock). Surface beds usually show a medium to strong weathering and a dense net of discontinuities (bedding planes and joints) causing intense secondary looseness. Flysch, usually, gives a weathering mantle of varying thickness. This formation characterized by an obvious instability, which is usually connected with the numerous heterogeneous layer contacts and the steep bed inclinations, in conjunction with the strong relief and the action of water. Therefore, problems connected with foundation of technical works are very often, usually shown as shear strength problems of the formation. In general, geotechnical behaviour presents a clear anisotropy and rapid changes, controlled by the degree of looseness (weathering-fragmentation), the orientation of discontinuities, the dip of slopes and the action of water. The landslide phenomena usually affecting weathering mantle and upper fragmentation zone.

- Type IXb: Flysch consisted of calcareous schists, sandstones, quartzitic sandstones, conglomerates, reddish marls, sandy-marls, siltstones, with intercalations of limestones in thin layers. At places, usually near upthrusts, flysch is semi-metamorphic with olistholiths of various dimensions (limestones, dolomites, ophiolites, etc). This formation is intensely fractured and multifolded and gives a weathering mantle of varying thickness. They present downgrading geomechanical characteristics and strength parameters, but unfavourable factors such as the intense-multiple fracturing and weathering of the cement, in conjunction with steep slopes and possible base erosion often cause loosening of the rockmass.
- Type X: Formation intensely fractured and multifolded, which is constituted from serpentines, ophiolites, serpentinized peridotites, siltstones, sandstones, conglomerates, limestones, cherts, etc. It is presented as one completely fractionally rockmass with decreased geomechanical characteristics, which at places, due to erosion, is changed in remaining soil.

Physical and mechanical properties (usual range) of values for soil materials of altered mantle of serpentines:

$$\begin{array}{ll}
 w_L = 30,3 \% & c = 67 \text{ KPa} \\
 I_p = 14,6 \% & q_u = 35 \text{ KPa} \\
 w = 20,5 \% & c_c = 0,145 \\
 \gamma_b = 20,0 \text{ kN/m}^3 & e_o = 0,612
 \end{array}$$

Physical and mechanical properties (usual range) of values for soil materials of decomposed serpentine:

$$\begin{array}{ll}
 w_L = 29,3 - 46,2 \% & c = 219 \text{ KPa} \\
 I_p = 9,4 - 31,1 \% & q_u = 321 - 477 \text{ KPa} \\
 w = 12,2 - 15,2 \% & c_c = 0,040 \\
 \gamma_b = 21,4 - 24,5 \text{ kN/m}^3 & e_o = 0,266
 \end{array}$$

- **Type XIa:** Limestones, white or pinkish or reddish in colour, thin-bedded to thin-slabbed, hard, with nodules or lenticular silica layers at places. The intact rock is characterized by high values of strength parameters, while the rockmass shows medium to high permeability and good geomechanical behaviour for the foundation of technical works.
- **Type XIb:** Limestones, white-gray or grayish in colour, medium - thick-bedded or unbedded, usually fractured and strongly karstified in the upper beds. In certain cases and in a local scale, limestone rockmass breaks in fragments. Failures are usually observed as rockfalls on steep slopes, where an increased secondary loosening of the rockmass occurs or in cases where disturbances of the natural stability state and dynamic loading have taken place. In its entirety, this formation is characterized by good geomechanical behaviour.
- **Type XIc:** Cherts, in intercalations with thin-bedded limestones, conglomerates or breccias and few ophiolites in places. Reddish formation, with satisfactory geomechanical behaviour.
- **Type Xid:** Limestones and dolomites, white-gray or grayish in colour, medium to thick-bedded, compact, fractured and faulted. Underground water is restricted in the fractured zone of limestones, while dolomites are considered practically impermeable or semi-permeable. At places, usually on steep slopes, failures are observed as rockfalls. In its entirety, this formation is characterized by good geomechanical behaviour.

5. Conclusions

From the above analysis, regarding the compilation of the engineering geological map of Nafplion wider area at a scale of 1:5,000, the following remarks can be made:

- For the preparation of the above-mentioned map, which is thought to be a very useful tool for the better land use and planning, both an extended fieldwork and the evaluation of many geotechnical boreholes were used.
- Thus, eighteen (18) engineering geological types (ET) have been distinguished. Special attention was given to those units which structure inhabited zones as well as industrial areas, to avoid problems to the future development of the wider area.
- For every type, the ranges of the values of some main physical and mechanical properties examined, as well as a general description of their geomechanical behaviour, are given.
- As the task of this project was the contribution to the urban development of Nafplion city, this engineering geological map will be a useful tool for engineers, planners, civil authorities, etc.

6. References

- Anon., 1972. The preparation of maps and plans in terms of Engineering Geology. Q. Jl. Eng. Geol., Vol. 5, pp 293-381.
- Anon., 1979. Report of the Commission of Eng. Geological mapping of the IAEG, Part I.: Rock and Soil materials. Classification of rocks and soils for engineering geological mapping. Bulletin of IAEG, No19, Krefeld, pp 364-371.
- Anon., 1981. Rock and Soil description for engineering geological mapping. Report of the Com-

- mission of Engineering Geological Mapping. Bulletin of IAEG, No24, Krefeld.
- Apostolidis, E. and Koutsouveli An., 2007. Geotechnical study of the wider urban and suburban region of Nafplion city, Argolis. Unpublished study of IGME (T-2587), Athens.
- Apostolidis, E. and Koutsouveli An., 2008. Engineering geological map of the wider urban and suburban region of Nafplion city, Argolis. Unpublished study of IGME (T-2588), Athens.
- Bell, F.G., 1981. Engineering properties of soils and rocks. Butterworth Co., Ltd., London, 149 pp.
- Carter, M., 1983. Geotechnical Engineering Handbook, London, 226pp.
- Dearman, W. R. and Matula, M., 1976. Environmental aspects of Engineering Geological Mapping. Bulletin of I.A.E.G., Vol.14, pp 141-146.
- E.P.P.O., 2001. Greek Antiseismic Rules 2000 (in Greek), Athens, Greece, pp 257.
- Hadzinakos I., Rozos D. and Apostolidis E., 1990: Engineering geological mapping and related geotechnical problems in the wider industrial area of Thessaloniki, Greece. Proceedings of 6th International IAEG Congress, Balkema, Rotterdam, pp. 127-134.
- IGME, 1993. Engineering geological map of Greece, scale of 1:500,000, Athens.
- Koukis, G., 1980. Geological - Geotechnical maps and their use in technical works. Mining and Metallurgical Annals, Vol. 44, Athens, pp 29-40.
- Koukis, G., 1988. Slope deformation phenomena related to the engineering geological conditions in Greece. Proceedings of the 5th International symposium on Landslides, Vol. 2, Lausanne, Balkema Publ, Rotterdam, pp 1187-1192.
- Matoula, M., Hrasna, H., Vleko, J., 1986. Regional Engineering geological maps for land use planning documents. Proceedings of 5th International I.A.E.G. Congress, Buenos Aires, Balkema, Rotterdam, pp 1821-1827.
- Rozos D., Xatzinakos I and Apostolidis E, 1990. Engineering geological mapping and related geotechnical problems in the wider industrial area of Thessaloniki, Greece. Proc. of the 6th International Congress of Engineering Geology (IAEG), Vol.1, Amsterdam, pp 127-134.
- Rozos D., Apostolidis E. and Xatzinakos I.†, 2004. Engineering-geological map of the wider Thessaloniki area, Greece. Bulletin of Engineering Geology and the Environment, Volume 63, Number 2, June 2004, pp. 103-108.
- Tataris A., Kallergis G.Kounis G., 1970. Geological map of Greece at a scale of 1:50,000, Nafplion sheet, IGME, Athens.
- UNESCO/IAEG, 1976. Engineering geological maps. A guide to their preparation. The Unesco Press, Paris, 79p.

Notation

The following symbols were used in this paper:

w_L : liquid limit

c : cohesion (from direct shear test or triaxial shear test – Unconsolidated Undrained)

I_p : plastic index

q_u : uniaxial compressive strength

W : moisture content

c_c : compression index (from consolidation test)

γ_b : bulk density

e_o : initial void ratio (from consolidation test)

e : void ratio

NEOTECTONIC STUDY OF URBAN AND SUBURBAN NAFPLIO AREA (ARGOLIDA-GREECE)

Georgiou Ch., Galanakis D.

*Institute of Geology & Mineral Exploration (IGME), 1 Sp. Loui, Acharnae 136.77
Athens, Greece, chgeorgiou@igme.gr & galanakis@igme.gr*

Abstract

The wider studied area does not present strong seismic activity, and is characterized however by the existence of active and potentially active faults that were estimated by the fieldwork and the air photographs and satellite images. These faults are located mainly in the boundaries of basins. Some faults are potentially active and have been activated in the Pliocene-Pleistocene under a NE-SW stress field, while some other faults have been activated in the Quaternary under NW-SE stress field, as show the results from the neotectonic analysis. According to the usual seismic magnitudes that were observed in the broader area, they are roughly about 6 Richter maximum vertical displacement expected in the 65 cm and as calculated by the theoretical magnitude. This observed maximum displacement is near the active or seismic fault and is decreasing or increasing depending on the distance from the fault trace.

Particular attention needs in the cases, where the Nauplio urban area, is found in the passage of solid geological formations of the Alpine basement to the unconsolidated Neogene or Quaternary formations.

In this case, a different distribution of seismic waves is observed between the solid rocks and the unconsolidated Neogene or Quaternary formations. In this region the magnitude of vertical displacement is maximum because the strengthened considerably and the dynamic condensation of not cohesive materials.

An also important element is the determination of width zone of both sides of the fault, where surface changes are observed (faults, subsidences etc) during the earthquake activity. The width of this area depends on the geological and tectonic structure.

Key words: *neotectonic fault, slip-vector, fault scarp, Argolikos gulf, Peloponnesus.*

1. Geological setting

The Hellenides consist of NW-SE-trending parallel tectonic belts or “isopic zones” (Aubouin 1959). The Pelagonian zone forms the boundary between the internal and external Hellenides. This zone where includes also the Argolis Peninsula, is represented by Palaeozoic metamorphic basement, with cover of Permo-Triassic clastic sediments bearing rift volcanics, with Triassic-Jurassic metamorphosed and non-metamorphosed platform carbonates (Fotiadis, 2008, Gaitanakis P. & Photiades, 1992, Photiades & Skourtsis – Coroneou, 1994a). This zone upwards is overthrust by ophiolites and melanges (Aubouin et al. 1970, Jacobshagen 1986), and is transgressed by Late Jurassic to Late

Cretaceous carbonate cover sequences and flysch.

The main orogenic phase of Greek territory was expressed in the late Mesozoic- Eocene (Jacobshagen 1986, Bortolotti et al 2003), when was realized the microplate conflict with movement to the north. The final orogenic phase was completed in Oligocene and followed by geodynamic movements under an extension stress field in neogene as a result of the creation of many neotectonic basins.

Three main Alpine tectonic phases have affected the Argolida region and present the following characteristics

- 1st** Compression phase: The upper Tithonian characterized by overfolding axes to have a N-S direction and internal overthrusts of the same direction.
- 2nd** Extension phase: The NE-SW direction had affected as mentioned before the N-S tectonic structures. It caused interruption in the sedimentation from NW and led to the deposition of autochthonous limestones of Albian age, which were followed by flysch formation of Ypresian age.
- 3rd** Compression phase: The Eocene age flysch is of an important geodynamic regime (is connected also with the blueschist phase of Cyclades). This compressional phase that reactivated old NE-SW tectonic structures and caused shear zones and the compressional movement to NW.

Two newer extensional phases that followed, from Miocene-Pliocene until upper Quaternary, affected the older geological structures and formed the Argolida peninsula.

Argolikos Gulf is one of the east Peloponnesus neotectonic grabens, that extended south of Nafplio region (fig 1) with a maximum depth of 700 m and is also linked with the Aegean sea. The western coast of Argolikos gulf delimited by a mountainous chain, that is interrupted locally from alluvial fans and in these sites the maximum sea depths are decreased abruptly.

In north Argolikos Gulf a wide submarine horst 8-10 km length characterizes the creation a wedge of sediments of plio-pleistocene age, due to the river depositions and these horst is delimited by the presence of neotectonic faults, (Van Andel et al 1993).

2. Neotectonic regime of Argolikos gulf

The more important neotectonic structure of Argolikos gulf is the system of faults of western margin with NNW-SSE direction and subsidence in the Eastern part (fig. 1). The Eastern margin towards the Nafplio area is affected by smaller faults and a system of joints which are connected with the margins.

In central Argolida territory in the Karnezaiika region is affected by a shear faults system with sinistral component (Fig. 1). In southern Argolida, the neotectonic fault system affect, the Alpine basement of the region.

The action of this fault system has influenced the Pleistocene sediments of the total region, which subsidies in the Argolikos gulf area in 300-400 m isobaths with a dip of 3° to the south-west.

Along of western side of Argolikos gulf, during Holocene the rate of is of 50cm/kyr (Finke 1988) while to the southern is of 100cm/kyr and tends to zero in the Eastern side near Nauplio city. In the Spetses area the subsidence is approximately 150 cm. /kyr (Flemming & Webb 1986).

According to these data, the Argolikos gulf constitutes a neotectonic structure with half-graben char-

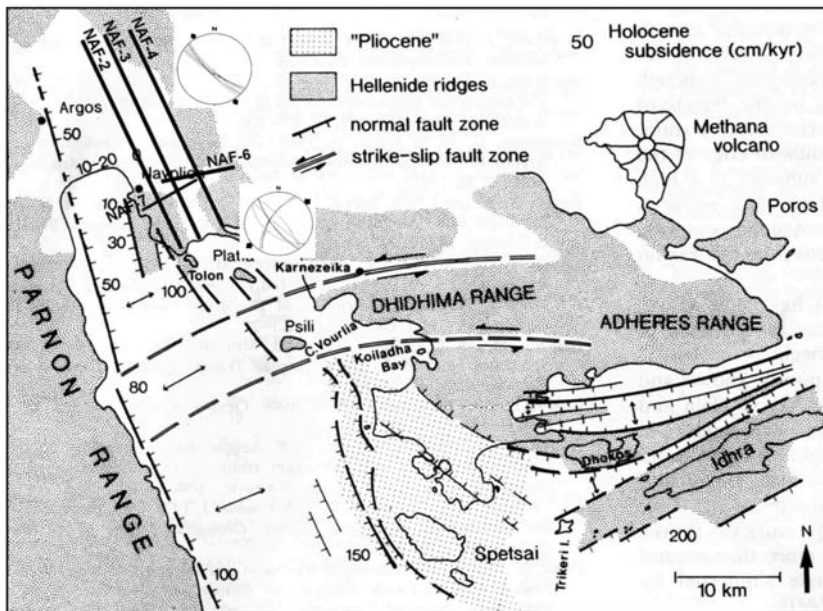


Fig. 1: Neotectonic map of the wider studied area and the rate of subsidence in various places of Argolikos gulf (Van Andel et al 1993) This map is modified with new tectonic data from the Nauplio region which are connected with submarine data.

acteristics. Even though the Argolida region shows very low seismic activity, characteristics features of active tectonics regime are observed.

The Karnezaiika region and the broader are affected by transtensional system faults in a roughly E-W direction which gives an explicit morphology of the active faults, thus creating the narrow and steep Karnezaiika valley. The surfaces of the faults present various generations of tectonic slickensides due to the different reactivations.

According to the seismological and bibliographic data, (Drakopoulos & Makropoulos 1982, Ambraseys, N.N. 1988 and Greek Antiseismic Regulation G.A.R. 2003) as well as from the evaluation of seismotectonic data of Greek territory, the studied area is classified in the (I) category zone of seismic hazard, with seismic territory acceleration $A = a \times g$, where $a = 0,16$ typical feature of category I.

2.1 Study of Faults

During the fieldwork, seven neotectonic faults were recognized, mapped and measured close to the Nauplio city.

The faults that described below, are normal and are activated under an extensional stress field, that prevailed during the creation of Argolikos gulf, or in a later stage at the duration of Quaternary-Holocene and they are characterized as active or potential active faults.

The stress field analysis of faults and the analysis of tendencies, gave the places and the position of axes σ_1 , σ_2 , σ_3 . The latter (σ_3), determines the direction of extension stress field in different geological time.

NAF-1: The NAF-1 fault in the geological map (fig. 2) of the present study, is a normal fault and



LEGEND

Post Alpine Deposits:

Holocene: 1. Swamp deposits, 2. Alluvial deposits, 3. Fluvial terrestrial deposits, 4. Talus scree and cones,
Pleistocene : 5. Cohesive talus scree,

Alpine Deposits (Pelagonian Zone):

6. Limestone with cherts (Upper Cretaceous), 7. Limestone (Lower-Upper Cretaceous), 8. Tectonic mélange (Jurassic), 9. Tectonic nape of flyschoid mélange (Upper Cretaceous-Eocene), 10. Flysch, 11. Limestone with cherts (Upper Cretaceous-Paleocene), 12. Conglomerate and Breccias carbonate serie (Cretaceous) 13. Limestone and Dolomite (Triassic – Lower Jurassic)

Fig. 2: Geological map of Nafplio area present normal faults

has a NNW-SSE direction and dip 75° - 80° W. The main surface fracture of this fault is located in the submarine region in the west of Nafplio.

This fault has influenced also the early Tyrrhenian sediments, which are found up to 10 meters above the current sea level. Inside these sediments, exist characteristic marine fauna with *Strombus Bobonius* (Zötl et al 1999) which characterize the Tyrrhenian age (fig. 3). This uplift movement appears clear along the Arvanitia coast south of Nauplio city (fig. 4).

The tectonic and stratigraphic data mean that the fault NAF-1 is an active fault with length that exceeds the 15 kilometres. The expected movement uplift, in the case of a future seismic activity of this fault, can exceed the 40 cm (Bonilla et al 1984, Wells & Coppersmith 1994, Ambraseys & Jackson 1998).

NAF-2: The NAF-2 fault in the geological map (fig.2) is normal and has also a NNW-SSE direction and dips 80° to the west.

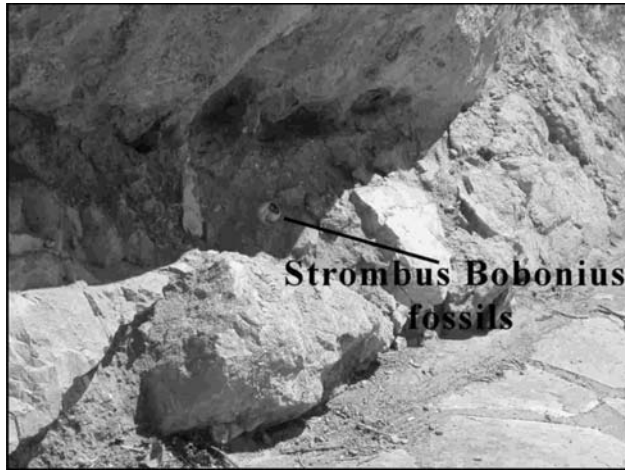


Fig. 3: Marine and terrestrial sediments with characteristic Tyrrhenian fossils with *Strombus Bobonius* characteristic Tyrrhenian age.



Fig. 4: Characteristic form of uplifting movement of Arvanitia coast (1,5m) from the sea level (a) and 4 m. from the fossil site of the previous picture (b).

This fault has affected the Alpine basement and the Quaternary depositions (Fig. 5). Based on the neotectonic study of the wider area it can be said that the fault NAF-2 is an active fault with length that exceeds the 4,5 kilometres. The expected uplift in an event of seismic activity of this fault, can exceed the 15 cm. (Wells & Coppersmith 1994, Ambraseys & Jackson 1998, Pavlides et al 2000).

The fault planes that are located in the Triassic-Jourassic marbles of the region have oxide depositions and tectonic slickensides. The analysis of measurements show that this system of faults is activated under extension stress field with NW-SE direction that is the same with the present extension stress field, (fig. 6).



Fig. 5: Active fault plane NAF-2 in the marbles with oxides depositions and tectonic slickensides.

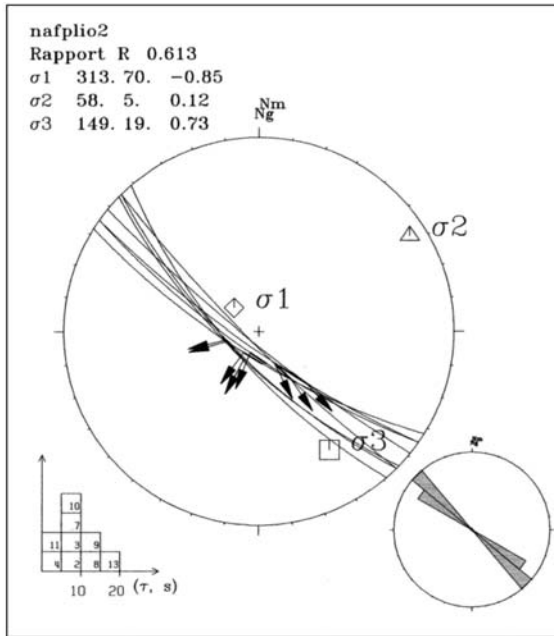


Fig. 6: Tectonic analysis of measurements on the Alpine basement in the region, where the fault plane of NAF-2 are located. In the rosedigram network Schmidt (southern hemisphere) the faults planes, the slickensides, as well as the positions and directions of axes σ_1 , σ_2 , σ_3 are shown.

NAF-3: The NAF-3 fault in the geological map is normal and it has also a NNW-SSE direction and dips to the East.

This fault has affected the Neogene and Quaternary deposits of the region, as shown by the morpho-tectonic, satellite and cartographic data because it deforms small streams and form small graben and horst. The tectonic study of the wider region shows that fault NAF-3, is an active with length that exceeds the 21 kilometres. The expected surface displacement in a future seismic activity of this fault can exceed the 48 cm (Wells & Coppersmith 1994, Ambraseys & Jackson 1998, Pavlides et al 2000).



Fig. 7: Fault NAF-7 of ENE-WNW direction affects the marbles and Quaternary sediments, East of Nafplio area.

NAF-4: The NAF-4 fault (fig. 2), is normal and has also a NNW-SSE direction and dips to the West.

This fault affected the Neogene and Quaternary deposits of the region based on morfoctectonic, satellite and cartographic data. The tectonic study of the wider region shows, that fault NAF-4 is potentially active, with a length that exceeds the 21 kilometres. The expected displacement in an event of seismic activity of this fault, can exceed 48 cm.

NAF-5: This fault (fig. 2) has also the same NNW-SSE direction and dips to the East. This fault affected the Neogene and Quaternary deposits of the region us shown by morfoctectonic data. The neotectonic study of the broader area shows that the NAF-5 fault is potentially active with a length that exceeds the 15 km. The expected displacement during seismic activity can exceed the 41 cm.

NAF-6: This normal fault has an E-W direction and dips to the Noth. This fault affected the Alpine basement and the Neogene sediments of the region. The tectonic study of the wider region reveals that the NAF-6 fault is potentially active with a length that exceeds the 5,6 kilometres. The expected shift in an event of seismic excitation of this fault, can exceed the 16 cm (Wells & Coppersmith 1994, Ambraseys & Jackson 1998).

NAF-7: The normal NAF-7 fault (Fig. 2) has an ENE-WNW direction and dips to the North. The main fault plane is located East of Nafplio city (fig. 7). This fault has influenced the Alpine basement and the neogene sediments. Based on the tectonic study of the wider study area, it can be said that fault NAF-7 is potentially active with a length that exceeds the 2,6 kilometres. The expected shift, in case of seismic activity, can exceed the 10 cm.

The fault affected the Triassic-Jourassic marbles of the region and on the fault plane iron oxides depositions, with slickensides, are observed. The analysis of measurements (fig. 8) shows that this system of faults of this specific direction, is activated under extension stress field with a NE-SW direction which is identified also in the older stress field as shown by the position of axis σ_3 .

3. CONCLUSIONS

The broader studied area does not present intense seismic activity, however is characterized by the

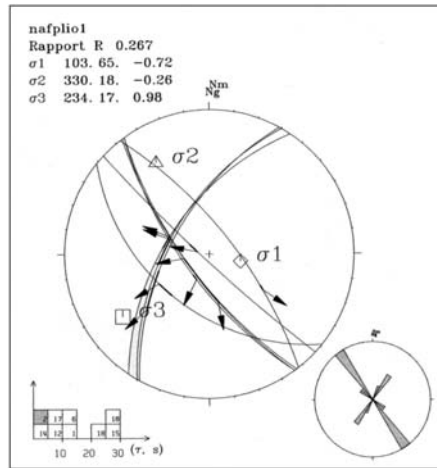


Fig. 8: Stereonet Schmidt, showing slickenside, slip vectors, as measured in the field, with the three principal σ_1 , σ_2 , σ_3 stress axes and the NE-SW direction of extension stress field (σ_3). Data from the area West of Nafplio (NAF-2 fault).

presence of active or potentially active faults where mapped during the fieldwork. These faults are connected with boundaries various basins. The faults show that, the older NAF-4, NAF-5, NAF-6, NAF-7 (table I), are potentially active and have activated during Pliocene-Pleistocene and characterized by extension stress field of NE-SW direction. The newer ones, NAF1, NAF2, NAF3 (table I) have been activated at Quaternary and are controlled by the new extension stress field of NW-SE direction.

Because the usual maximum seismic magnitudes that are observed in the wider region, are around 6 Richter, it is calculated, that the theoretical magnitude of maximum vertical surface displacement, is in the order of 65cm. This maximum displacement is observed near the surface of the active or seismic fault and decreases as the distance from the fault is increasing.

Particular attention must be shown in cases where the urban area of Nauplio extends over the compact Alpine geological formations to the unconsolidated Neogene and Quaternary ones.

In this case, different behaviour of seismic waves that crosses the compact rocks and the unconsolidated geological sediments is observed. In those sites we observe the maximum vertical displacement, due to the dynamic condensation of no cohesive materials caused by seismic vibrations.

An also important element is the determination of the width of the area at both sides of the fault trace, in which surface changes (ruptures, subsidences, liquidations etc) are expected during a future seismic activity. The width of this area depends mainly on the geological and tectonic structure and on the degree of seismic risk of the region, which is crossed by the fault.

For the calculation of the maximum displacement during seismic activity, the existing empiric relations can be used correlating the magnitude of earthquake (M_s) and length of fault (L) and the surface displacement (D). The most recent results that concern Greek territory and Eastern Mediterranean give more reliable magnitudes (Wells & Coppersmith 1994, Ambraseys & Jackson 1998).

With regard to these characteristics, the surface fault plane, the length of the fault and the earthquake magnitude, the maximum seismic surface displacement in the Nafplio area can reach the 48 cm.

Table 1.

FAULT	LENGTH (Km)	EXPECTED SURFACE SHIFT (cm) (Wells D. & Coppersmith 1994)	TYPE OF FAULT
NAF 1	21	48	Normal - Active
NAF 2	4,6	15	Normal - Active
NAF 3	21	48	Normal - Active
NAF 4	21	48	Normal - Potentially Active
NAF 5	15	41	Normal - Potentially Active
NAF 6	5,6	16	Normal - Potentially Active
NAF 7	2,6	10	Normal - Potentially Active

Contrary, the usual seismic magnitudes that were observed in the broader area, are roughly 6 Richter, and the theoretical sizes of maximum vertical displacement is calculated to be around 65 cm.

4. References

- Ambraseys, N.N., Jackson, J.A., (1990). Seismicity and associated strain of central Greece between 1890 and 1988. *Geophysical Journal International* 101, 663-708.
- Ambraseys, N.N. (1988): Data for investigation of the long-term seismicity of Central Greece. "Proc. European School on the Seismic Hazard Assessment, Athens, 9-16 May 1988"1-7.
- Bonilla, M.G., Mark, R.K., & Lienkaemper (1984): Statistical relations among earthquake magnitude, surface rupture length, and surface fault displacement. *Bull. Seism. Soc. Am.*, vol. 74m., No 6, p. 2379-2411.
- Bortolotti, V., Carras, N, Chiari, M., Fazzuoli, M., Marcucci, M., Photiades, A. & Principi, G. (2003). The Argolis Peninsula in the palaeogeographic and geodynamic frame of the Hellenides. *Ofioliti*, 28/2, 79-94.
- Drakopoulos, J., & Makropoulos, C., (1982): Seismology, seismotectonics, seismic hazard and earthquake prediction. National report of Greece. Working Group. A Final report, Unesco, A-65, A-98.
- Finke E. A. (1988): Landscape evolution and the Argive Plain Greece: Paleocology, Holocene Depositional History and Coastline Changes. PhD thesis. Stanfodt University. Univ. Microfilms Ann. Arbor, Michigan.
- Flemming N.C. & Webb, C. O., (1986): Tectonic and eostatic coastal changes during the last 10.000 years derived from archaeological data *Zeitschrift fur Geomorphologie. Neue Folge. Supplement Bahd*, 62, 1-29
- Fotiadis Ad., (2008): Geological study of the urban and the wider Nafplio area, Argolida Prefecture. *Institute of Geology and Mineral Exploration, Athens*.
- Gaitanakis P. & Photiades A.D. (1992): New data on the geology of Southern Argolis (Peloponnesus, Greece). 6th Congress of the Geol. Soc. Greece, Athens, May 1992, Greece, Abstract vol. p. 42-43.
- Jacobshagen, V. (1986): *Geologie von Grieechenland*, 363 s., Berlin, Stuttgart (Gebruder Borntraeger).
- Οργανισμός Αντισεισμικού Σχεδιασμού και Προστασίας (ΟΑΣΠ, 2000 & 2004): *Ελληνικός Αντισεισμικός Κανονισμός (ΕΑΚ)*, Αθήνα.
- Pavlidis, S., Caputo, R., Chatzipetros, A., (2000). Empirical relationships among earthquake magnitude, surface ruptures and maximum displacement in the broader Aegean Region. *Proceedings of the Third*

International Conference on the Geology of the Eastern Mediterranean.

- Photiades A.D. (1998). Tectonic evolution of Northern Argolis Peninsula (Greece). The "Third International Conference on the Geology of the Eastern Mediterranean", Nicosia, Cyprus, Sept. 23-26, 1998. Abstracts vol., p.53.
- Photiades A.D. & Skourtsis - Coroneou V. (1994a). Stratigraphic and paleogeographic evolution of the Northern Argolis (Greece) during the Cretaceous-Paleogene. 7th Congress of the Geol. Soc. Greece, Thessaloniki, May 1994, Greece. Abstracts vol., p. 65-66.
- Tataris, A., Kalergis, A., Kounis, D., (1970): Geological map of Greece – Nafplio Sheet (Scale 1:50.000). *Institute of Geology and Mineral Exploration I.G.M.E , Athens.*
- Van Andel t. H., Perissoratis C., Rondoyanni T., (1993): Quaternary tectonics of the Argolikos Gulf and adjacent basins, Greece. *Journal of the Geological Society, London, Vol 150, pp. 529-539*
- Wells D. & Coppersmith, (1994): New empirical relationships among magnitude, rupture length, rupture area and surface displacement. *Bull. Seism. Soc. Amer., vol. 84, No 4, pp.974-1002.*
- Zötl, J. G., Geyh, M. A., Riepler, F., Mettos, A., & Ch. Georgiou (1999): Klimaepochen, eustatische Meeresspiegelschwankungen und Strandterrassen im östlichen Mittelmeer (Griechenland). *Beiträge zur Hydrogeologie/ 49/50, seiten 5-66, Graz .*

LIQUEFACTION RISK ASSESSMENT BY THE USE OF GEOPHYSICAL TECHNIQUES: THE TEST AREA OF NAFPLION CITY, GREECE

**Karastathis V.K.,¹ Karmis P.,² Novikova T.,¹ Roumelioti Z.,³ Gerolymatou E.,¹,
Papanastassiou D.,¹ Liakopoulos S.,¹ Giannouloupoulos P.,² Tsombos P.,²
G. A. Papadopoulos¹**

¹ National Observatory of Athens, Geodynamics Institute, PO Box 20048, GR 118 10 Athens Greece,
Karastathis@gein.noa.gr

² Institute of Geology and Mineral Exploration (IGME), S. Loui 1, 3rd Entrance Olympic Village,
Acharnae 136 77, Greece

³ Department of Geophysics, Aristotle University of Thessaloniki, P.O. Box 352-1, 54124 Thessaloniki,
Greece,

Abstract

An efficient and cost effective site characterization, with regard to the seismic hazard and liquefaction risk assessment, was accomplished with the aid of geophysics in the area, where the Nafplion city of Greece is expanding. The methodology adopted includes the recognition of the possible earthquake sources of the wider region, their modelling, in order to stochastically simulate the strong ground motion at the investigation area, and finally the calculation of the liquefaction risk. The investigation area was suspected of high liquefaction potential since the foundation ground consists of loose sandy silt with very shallow aquifer. The geophysical techniques considerably contributed to the detection and characterization of possible local seismic faults with the implementation of gravity and seismic methods. Special emphasis was given to the seismic depth migration and particularly to the construction of valid velocity models, in order to precisely calculate the dips of the possible faults. Additionally the geophysical techniques provided the near surface velocity structure for the calculation of the amplification of the seismic motion up to the surface, also required for the final estimation of the liquefaction risk. The seismic methods (seismic reflection, seismic refraction, seismic modelling, MASW, multichannel analysis of microtremors and crosshole investigations), if combined with geo-technical borehole testing, enhance their reliability and cover large areas in a cost-effective way in comparison with the standard borehole tests. In Nafplion area, evidence was found for a low factor of safety against liquefaction at specific sites within the study area. The results show that liquefaction probability can reach 80% at some sites depending on selected earthquake scenario, mainly at depths between 5 and 10 meters. This should be considered as highly important information for making risk-based design decision in this region.

Key words: seismic techniques, faults detection, liquefaction.

1. Introduction

The urban planning of many cities is usually based on economic and social factors, without taking always into account the local geology and the active geodynamic processes. The problems emerg-

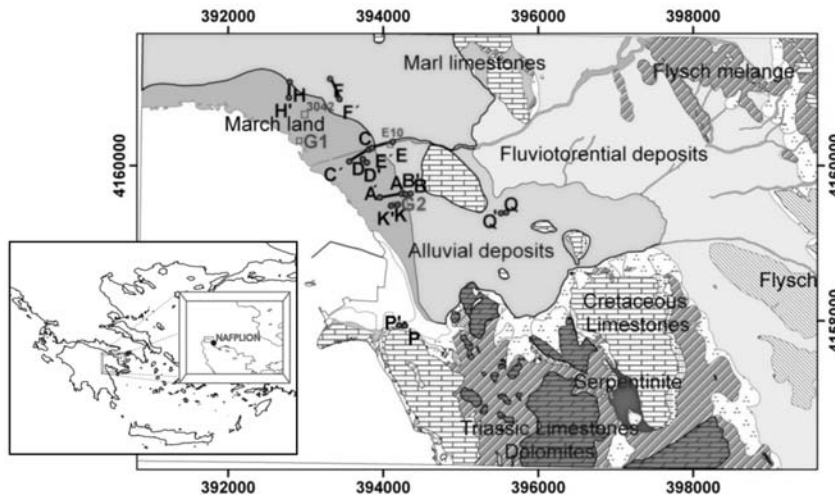


Fig. 1: Geological map of the investigated area. The seismic lines are presented with black colour. The boreholes are indicated with red coloured points. The embedded map shows the survey area (small box) close to Nafplion city.

ing due to this constraint are accentuated with the increase of the population, the industrialization and the seismic impact during the last decades. Nafplion is one of these cities (see Fig. 1), originally founded on safe ground, but it is expanding in recent years along the coastline on ground of questionable safety factor with reference to seismic and liquefaction risk.

The need to set up and test a methodology, able to give reliable evaluation of the seismic and liquefaction risk for extensive areas, is considerable, especially for the countries with high seismicity, like Greece.

The methodology followed, combined the usual borehole testing measurements of the standard regulation for the seismic and liquefaction risk with geophysical measurements, in order to spread out high credibility information to wider areas. The geophysical techniques also aided to the detection and study of the local active faults. According to the legal framework of many countries, the regular building is hindered in the adjacent to active faults areas. Similar restrictions apply to soils liable to liquefaction during a strong earthquake, to areas with slope stability problems, or to unconsolidated embankments etc. (EAK, 2000 - Greek Earthquake Design Code). Therefore, building can be allowed only if these factors are excluded. However exceptions are also possible, in special cases, after conducting special studies on the assessment and dealing with these particular risks. The gravity survey, as a reconnaissance method, is suitable to locate possible deformations of the bedrock, which can be attributed to faults. As a follow-up survey, seismic depth imaging can delineate the structure if this is related to an active or inactive fault. In the case of active faults, the dip and the total throw are usually examined.

The procedure for liquefaction assessment included the calculation of the Factor of Safety (FS) against liquefaction and the potential of liquefaction in terms of probability, (where $FS = \text{cyclic shear stress required to cause liquefaction} / \text{equivalent cyclic shear stress induced by earthquake}$), the evaluation of liquefaction time history for specific historical earthquakes scenarios and the analysis of site response in region of Nafplion taking into account the liquefaction susceptibility of the stratum.

2. Geological setting

The regional geology of the Argos plain is composed of: Coastal deposits, made of loose, fine silty sands and silty-clayey soils, alluvial fans and fluvio-torrential deposits. The sediments' bedrock includes alpine and post-alpine sediments, such as flysch, limestone and Neogene marl conglomerates. The investigation area (see the geological map of Figure 1) is formed by alluvial, mainly lagoonal deposits, overlying flysch and limestone formations.

With regards to groundwater regime, within the Quaternary deposits, successive groundwater aquifers are developed, being under intensive exploitation by well boring. This resulted to a considerable sea water intrusion in recent years. Within some parts of the investigation area, at an altitude lying of a few meters above sea level, a weak unconfined coastal aquifer is developed at a small depth near surface, which is underlain by deeper confined aquifers. This shallow unconfined aquifer belongs to a local marshland. The sand-silty, clayey-silty nature of soils and the presence of the ground water table near the surface, constitute a particularly unfavourable regime concerning the foundations. Within this regime an attentive control of the liquefaction potential is pertinent.

In the Argos plain, where Nafplion is situated, a liquefaction has been recorded in the past, happened on 2/6/1898 and caused from an earthquake of $M=7$ with epicentre (37.6° , 22.5°) only 27 km far (NNW) from Nafplion (Ambraseys and Jackson, 1990, Papathanassiou et al., 2005). Three important seismic zones in the wider region of Nafplion have given strong earthquakes in the historic era (Iria fault, Epidaurus fault and Xylokastro fault) (Papazachos and Papazachou, 2003).

3. Geophysical investigations

The geophysical techniques were carried out in the area aiming at: a) the detection of possible local seismic faults and b) the determination of the velocity models in order to contribute to the estimation of the amplification of the possible peak ground acceleration (PGA) in the study area and the evaluation of the Factor of Safety against Liquefaction.

3.1. Geophysical investigations for mapping the bedrock relief and detection of possible faults

Gravity survey

The gravity survey covered an area of 35 km² with 270 stations, conducted with a Scintrex CG-5 gravity meter. From the Bouguer map a residual map was extracted (Fig. 2). Two major lineaments (see Fig. 2) can be seen possibly attributed to faults: The first one lies at the eastern side of the area with NW-SE direction. This is a known fault that has been mapped in the past from geologists as an inactive one. The second one, at the western part of the map, runs through the investigation area. Further investigation work with seismic methods was considered necessary.

Seismic Survey

A seismic survey was conducted to delineate the suspected fault as pointed out from the gravity survey. Each of the seismic profiles (see Fig. 1) AA', CC', EE', FF' was about 300 m long. The line HH' was 180 m long. The main target of the seismic profiles was the determination of the dip of the bedrock surface and whether this could be associated to an active fault plane.

The survey layout for the shallow reflection seismics mostly used, was the "fixed spread" instead of the usual "roll-along". The "fixed spread" layout was not only easier in acquisition, in the case

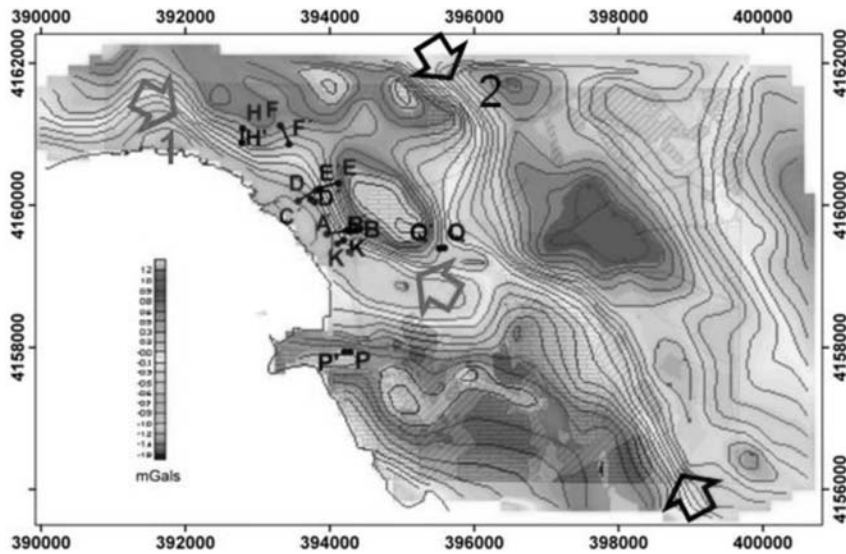


Fig. 2: The residual gravity anomaly map indicates the existence of two possible faults at the investigation area.

of urban environment, but was also very valuable since permitted the acquisition of data usable for refraction – wide angle reflection velocity modelling. A reliable velocity model is needed for depth migrating seismic data. We must bear in mind that if a fault is present in a seismic profile, then migration is a prerequisite.

The seismic source utilized, was an accelerated dropping weight and provided us with high quality records in all the seismic lines.

The joined lines EE' and CC' run perpendicular to the strike of the gravity lineament.

The first arrivals of the refracted waves in both profiles after tomographic processing, did not succeed to reach the bedrock. However the arrivals of reflected waves were processed by Zelt and Smith (1992) code, and produced velocity models with excellent fitting between calculated and observed arrival times (Fig. 3a). The resulted velocity models (Fig. 3b) indicate a fairly smooth layering to the bedrock. The bedrock is detected at 90 m depth at the beginning of the line EE', reaching the 200 m at the end of CC'. The results are in agreement with an old water-wall at the starting edge of EE', which intersected the limestone bedrock at 93 m depth.

Two layers can be distinguished above the bedrock at line CC'. The second layer, probably flysh, pinches out within the line EE', but this cannot be resolved due to the limitation of vertical resolution.

Figure 4a shows the joined time migrated profile with simple depth conversion. Figures 4b,c show the resulted profiles after Kirchhoff depth migration with the use of the velocity model of the Figure 3b. The slope of the bedrock surface is steeper at the depth migrated profile.

The results of the depth migration (Fig. 4b,c) of the EE' and CC' lines suggest that the gravity lineament is caused by two smooth subsidence features of the bedrock at the starting parts of CC' and EE'. Both dip values are at about 25° and cannot suggest an active seismic fault. It is noted that apparent dips are measured and probably at a direction different of the bedrock gradient. Assuming that the strike of the gravity contour lines follow that of the slopping bedrock, the EE' profile is at an

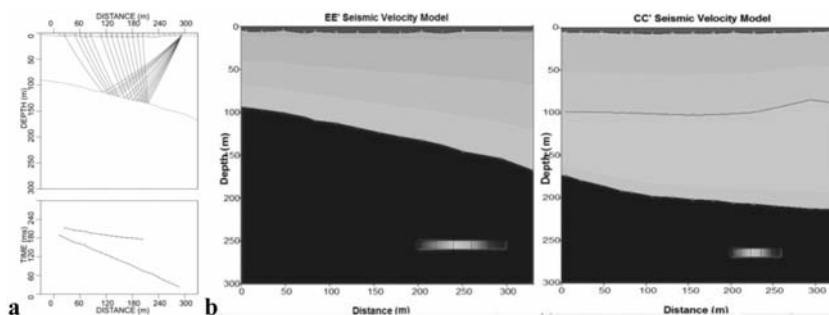


Fig. 3: Velocity modelling of the profiles EE' and CC' .

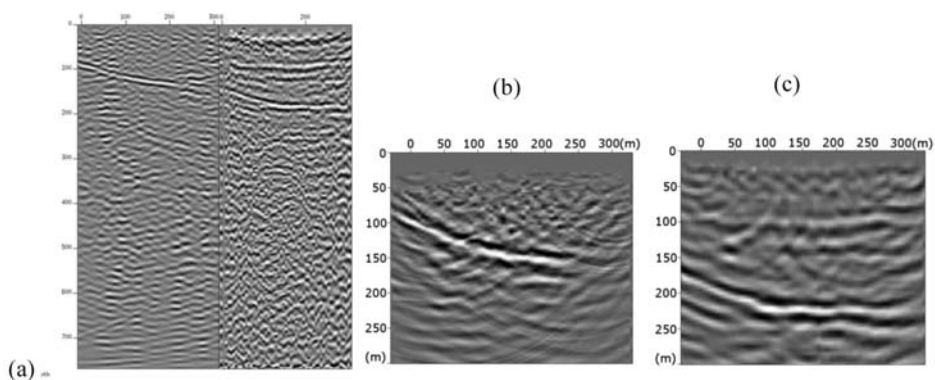


Fig. 4: a) Time migrated and depth converted jointed seismic section of the profiles EE'and CC' (b) and (c) Kirchhoff depth migrated profiles EE' and CC' respectively.

angle of 8° - 17° with this. The line CC' is almost vertical to the gravity contour lines. Therefore after simple geometric calculations the real value of the dip up to 26° , can be estimated.

Similar dip values were also obtained in the AA' profile after similar processing and calculations. The profile FF' confirmed also the pinch out of flysh layer. Figure 5 shows also the results of HH' processing in different stages. The results of HH' are also in full accordance with these of the other profiles.

In conclusion, the linear features of the Bouguer map cannot be attributed to active seismic faults but only to small and low dip inactive faults.

3.2 Geophysical investigations to the characterization of foundation ground

Aiming to the assessment of the foundation ground, crosshole seismic tests were conducted at two sites within the study area, along with SPT testing and laboratory tests on borehole core samples.

In addition seismic surveys were jointly carried out between the boreholes in such a way to fill in with the adequate information. Figure 2 shows all the sites where the seismic surveys were conducted. At BB', DD', KK', PP', QQ', the methods of seismic refraction of P and S waves, MASW (Xia et al. 1999) as well as microtremors analysis were applied. Additionally at the sites AA', CC',

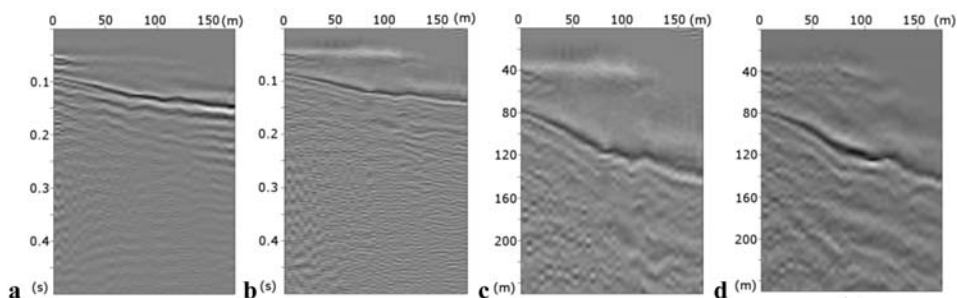


Fig. 5: a. Unmagranted stack section of the profile HH' b. A section after deconvolution c. A deconvolved section after depth conversion d. Time migrated and depth converted section.

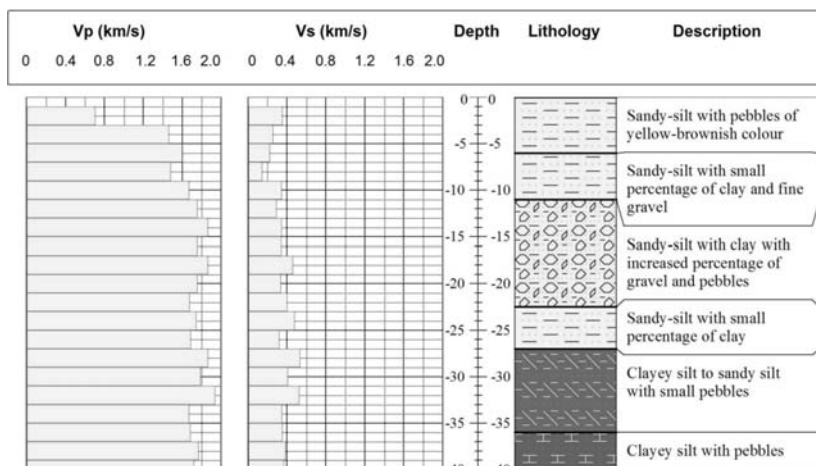


Fig. 6: Crosshole test results with the geological log.

EE' and FF' where seismic reflection and refraction data were acquired, MASW was also applied. The seismic crosshole tests were conducted according to the ASTM D4428/D4428M-07 standard. At each site a pair of boreholes was drilled at 5 meters distance, at the depth of 40 meters. The results showed that the shear wave seismic velocity values in the loose sandy-silt and clayey silt intercalating formations did not exceed 0.4 km/s, but moreover there are parts with values lower than even 0.2 km/s. The P-wave velocity is high due to the saturation from the sea intrusion at the area. The results of the crosshole testing G2 and borehole log (Fig. 1) are presented in Fig. 6.

At the site of borehole G2 (Fig. 2) Reverse VSP (RVSP) modelling was also conducted with the seismic source in the borehole and the receivers at the surface. The results of tomographic algorithm (Hayashi and Takahashi, 2001) were excellent and it was found that the drilling of second hole could be spared.

Figure 7 shows the result of the RVSP modelling and a comparison diagram with the crosshole test. The crosshole testing and RVSP were also used to calibrate and validate the results of MASW.

The application of MASW gave satisfactory results and detected low S-wave velocity zones. In a

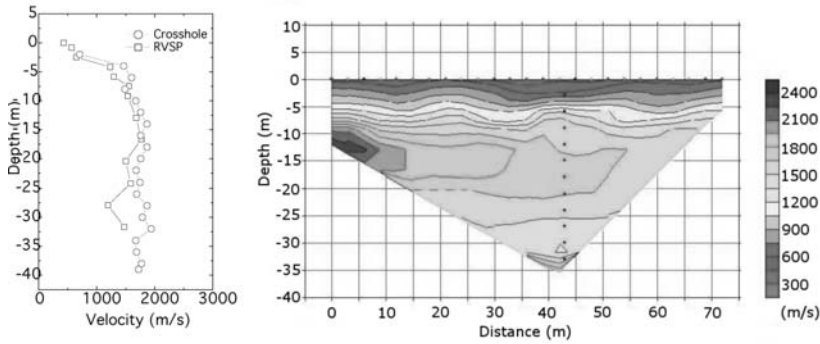


Fig. 7: Left: Comparison of RVSP (circles) with crosshole testing (squares). Right: The velocity model of RVSP at the site K.

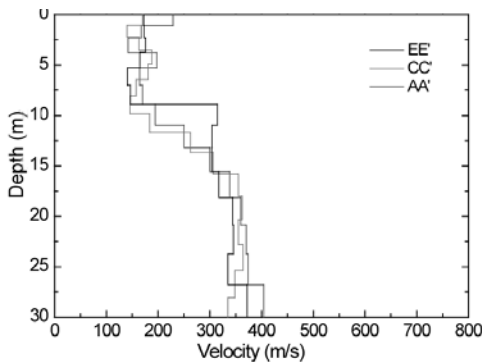


Fig. 8: MASW results systematically showed low S-wave velocity values at the first 10 m depth.

close distance to G2 borehole MASW was applied and the results were in full accordance to the crosshole test.

As shown in Figure 8 the S-wave velocity presents low velocities in the first 10 m in all investigated area. This is also found from S-wave seismic refraction profiles. Microtremors analysis also assisted to the description of the deeper S-wave velocity variation.

From information derived from the local boreholes the layer corresponding to the low S-wave velocity values is sandy-silt to silty-sand, soft formation without plasticity. The laboratory analysis found sand concentration of 29% and 66% at 4.90- 5.55 m and 7.90 - 8.55 m depth respectively. This evidence supports the high liquefaction risk.

4. Liquefaction analysis

The assessment of the liquefaction risk was based on the results of the seismic surveys, the geotechnical borehole testing and the stochastic simulation of strong ground motion for specific earthquake scenarios (Beresnev and Atkinson, 1997), selected based on the historical seismicity of this region.

The procedure consisted of the following steps:

1. Calculation of the Factor of Safety (FS) against liquefaction, and estimation of the potential for liquefaction in terms of probability (PL), based on factors of safety.
2. Evaluation of liquefaction time histories at the potentially liquefiable sites, using nonlinear,

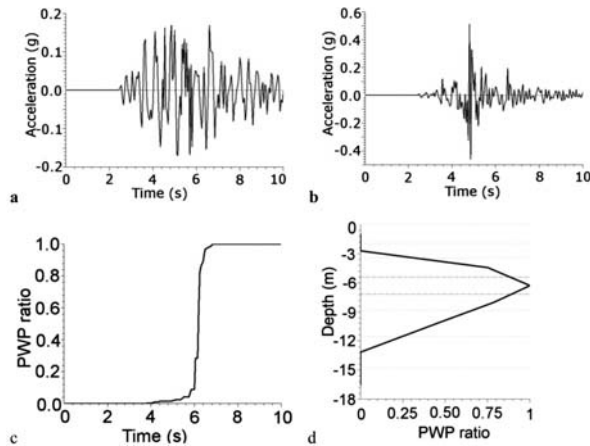


Fig. 9: Results of the liquefaction analysis for the AA' test site of Nafplion: (a) surface acceleration time history; (b) the acceleration time history at the potentially liquefiable layer; (c) the time history and (d) the depth distribution of pore water pressure ratio.

effective stress site response analysis (Matasovic, 2006), capable of modelling pore water pressure generation and dissipation.

3. Analysis of seismic site response in the Nafplion area taking into account the liquefaction susceptibility of the ground depending on the earthquake scenarios.

The results of our analyses indicated the scenario of the activation of the Iria fault (Argos fault in Papazachos and Papazachou, 2003) as the worst one in terms of the liquefaction potential. The Epidaurus fault also showed similar characteristics in contrast to the Xylokastro fault that did not give high probability of liquefaction.

In the cases where high liquefaction potential was predicted, low values of PGA at the surface and seismic motion enriched in longer periods were observed. This was due to the fact that some layers, at depth, liquefied.

An example of this analysis is given for an $M=6.4$ hypothetical earthquake on the Iria fault in Fig. 9. Figure 9 shows (a) the surface acceleration time history (b) the acceleration time history at the potentially liquefiable layer, (c) the time history and (d) the depth distribution of pore water pressure ratio for the test site AA'. In the case of this earthquake scenario, liquefaction effect will prevent the effect of soil amplification. The ground acceleration at the surface level (Fig. 9a) has lower amplitudes and longer periods than the respective one below the liquefiable layer (Fig. 9b). This can be attributed, to the soil liquefaction occurrence to some extent at this site (Fig. 9c, d). For this earthquake scenario, the occurrence of liquefaction, in terms of probability, was high, reaching 86 % at depths between 6 to 10 m.

The discussion of the results of the site response analysis is not a subject of our present paper; however, the reader can find such detailed analysis in the paper of Karastathis et al. (2010).

5. Conclusions

The area where the Nafplion city is expanding, after its examination with realistic earthquake scenarios based on known earthquake sources associated with strong and catastrophic events in the recent past, can be considered as liable for liquefaction phenomena under certain conditions of seismic loading. The problem was mainly found at the depths of 8 to 10 meters, where a loose sand-silty layer is present with particularly low S-wave velocity values. The liquefaction potential was calculated,

based on the results of the geotechnical investigations, laboratory tests and the results of the seismic surveys. A high liquefaction risk is anticipated mostly for strong earthquake scenarios at Iria and Epidaurus faults.

The study area was also examined for possible unexposed faults by a combined application of gravity and seismic methods but the results cannot support the presence of active faults.

The techniques utilized in Nafplion case, can also be applied with low cost in any other site with similar conditions as far as the liquefaction phenomenon is concerned. The view, that the geophysical techniques have already reached the required reliability to be included in the standard liquefaction risk studies, is well supported by the results.

6. Acknowledgments

This study was implemented in the frame of the project “Collection and Documentation of Geothematic Information for Urban Areas in Greece”. Funded by Competiveness Priority Axis 7: Measure 7.3 and ERDF.

We would like to thank Dr S. Chiotis for his contribution on the design and the materialization of the project. We also thank Dr A. Koutsouveli, who supervised the drilling and the geotechnical laboratory study; and A. Fodiadis who provided us with the geological map of the study area.

Thanks are also due to Dr K. Dimitropoulos, geophysicist in Hellenic Petroleum for his comments and to Mr. G. Michaletos, engineer of our team for his support in fieldwork.

7. References

- Ambraseys, N. N., Jackson, J. A., 1990. Seismicity and associated strain of central Greece between 1890 and 1988. *Geophysical Journal International*, 101, 663-708.
- Beresnev, I. A., Atkinson, G. M., 1997. Modeling finite-fault radiation from the ω spectrum. *Bulletin of the Seismological Society of America*, 87, 67 – 84.
- EAK 2000. Greek Earthquake Design Code, Earthquake Planning and Protection Organisation - Association of Civil Engineers of Greece. Athens 2001, (in Greek).
- Hayashi K., Takahashi T., 2001. High resolution seismic refraction method using surface and borehole data for site characterization of rocks. *International Journal of Rock Mechanics and Mining Sciences*, 38, 807-813.
- Karastathis V. K., Papadopoulos G. A., Novikova T., Roumelioti Z., Karmis P., Tsombos P., 2010. Prediction and evaluation of nonlinear site response with potentially liquefiable layers in the area of Nafplion (Peloponnesus, Greece) for a repeat of historical earthquakes. Submitted to *Natural Hazards and Earth System Sciences*.
- Matasovic, N., 2006. D-MOD_2-A computer program for seismic response analysis of horizontally layered soil deposits, earthfill dams, and solid waste landfills. *Users's manual. GeoMotions, LLC*.
- Papazachos, B.C. and Papazachou, C. B., 2003. Οι Σεισμοί της Ελλάδας, Θεσσαλονίκη, Εκδ. ΖΗΤΗ, 286pp. (Οι σεισμοί της Ελλάδος, Thessaloniki, Ziti Edit., 286pp.) Spector and Grant (1970)
- Papathanassiou G., Pavlides, S., Charitaras B., Pitilakis, K., 2005. Liquefaction case histories and empirical relations of earthquake magnitude versus distance from the broader Aegean region. *Journal of Geodynamics*, 40, 257-278.
- Zelt, C. A., Smith R. B., 1992. Seismic travelttime inversion for 2-D crustal velocity structure. *Geophysical Journal International*, 108, 16-34.

GEOPHYSICAL INVESTIGATIONS AT NAFPLION CITY, GREECE. HYDROGEOLOGICAL IMPLICATION

Karmis P., D., Giannouloupoulos P., Tsombos P.

*Institute of Geology and Mineral Exploration (IGME), S. Loui 1, 3rd Entrance Olympic Village, Acharnae
136 77, Greece*

Abstract

The application of selected geophysical methods within the framework of an Urban Geology investigation program performed by IGME at Nafplion city, contributed to the overall geo-scientific characterization of the study area. The methodology adopted included the application of Time Domain Electromagnetic, Electrical resistivity tomography, Gravity and Seismic Crosshole surveys. The results of the geophysical investigation provided quantitative information regarding the distribution of seawater intrusion in the area and determined factors controlling its extent within the investigated region. The intrusion may occur in three distinct horizons. The first within the shallow unconfined aquifer within the top 12 meters of fluvial deposits showing values of electrical conductivity in the range of 1 and 4 Siemens/m, corresponding to TDS values between 5000 and 20000 mg/L, as determined by the TEM surveys. Lower conductivity values between 0.3 and 1 Siemens/m are found within the second aquifer occurring between 15 and 45 meters. Similar order of conductivity values are found within the deeper horizon, lying below 45 meters depth, attributed also to seawater intrusion mainly in carbonate formations. Areas of fresh groundwater, were delineated by a combination of TEM, ERT and gravity methods. These areas are structurally controlled by faults and the presence of impermeable flysch overlying the limestone formation.

Key words: *Geophysical techniques, salinization, electrical conductivity.*

1. Introduction

The present paper deals with the results of the geophysical surveys carried out in 2007-2008 within the urban area of Nafplio, within the framework of the project Urban Geology undertaken by IGME. The program of geophysical surveys included Gravity, Electrical resistivity tomography (ERT), Transient Electromagnetic soundings (TEM) and seismic crosshole tests. Information derived by Gravity data is complimentary to TEM and ERT

The results of the geophysical investigations provided quantitative information regarding the geological structure and the distribution of saline water intrusion in the area and determined factors controlling its lateral extent. The Argos plain has suffered serious groundwater degradation in recent years, due to the seawater intrusion which mainly occurred during the second half of the last century. The application of TEM and ERT techniques can supply information regarding the extent of this phenomenon and to delineate aquifers with respect to their salinization.

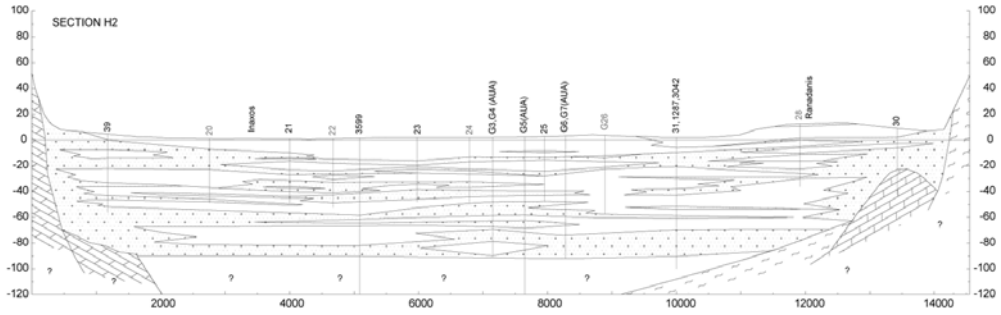


Fig. 1: A representative hydrostratigraphic section (west – east) of the alluvial deposits of Argos plain (Giannouloupoulos, 2000, 2001).

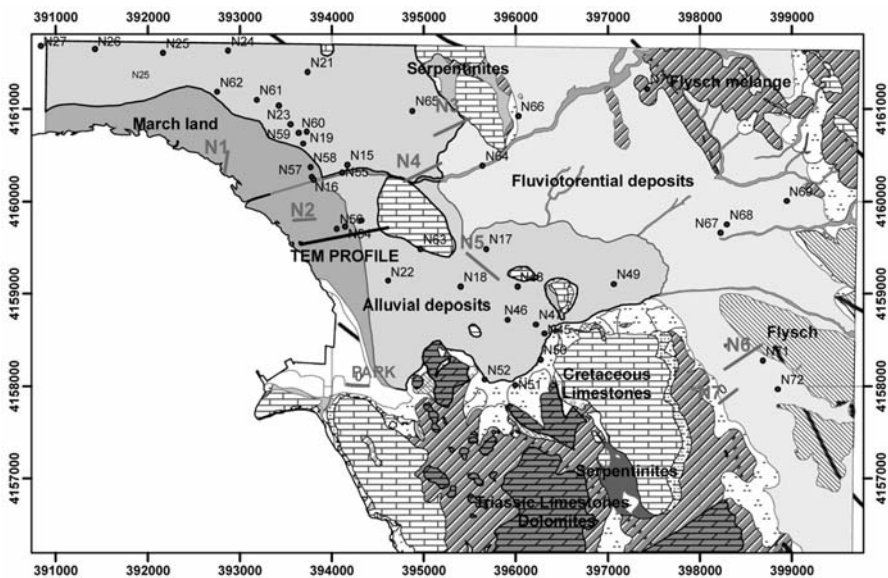


Fig. 2: Geological map of the investigated area (A.Fotiades, D.Metropoulos, 2008) . The resistivity tomography lines are coloured red. The numbered dots indicate the location of TEM soundings.

2. Geological and hydrostratigraphic setting

The regional geology of the Argos plain is composed of Quaternary alluvial deposits, composed by alternations of fine and coarse sediments such as clays, marls, silty sands and silty-clayey layers and fluvial deposits while at the outskirts of the plain those sediments are transitionally surrounded by alluvial fans constituting a “piedmont” type of deposition. The underlying bedrock of the plain is made up by alpine and post-alpine sediments, such as flysch, limestone and Neogene marl conglomerates (Giannouloupoulos, 2000,2001). The investigation area (see Fig. 2, 3) is formed by alluvial, mainly lagoonal deposits, overlying flysch and limestone formations, locally outcropped and historically attracting well known Mycenaean settlements such as Tyrins

With regards to groundwater regime, within the Quaternary deposits, successive groundwater

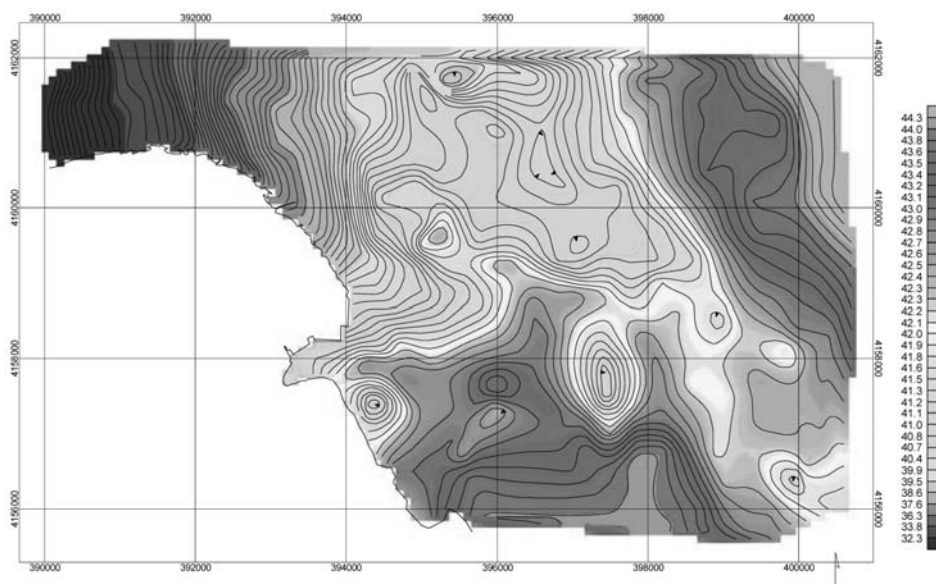


Fig. 3: Bouguer map of Nafplio area

aquifers are developed, being regionally overexploited through numerous dug wells and boreholes. This resulted to a considerable seawater encroachment in recent years. Within some parts of the investigation area, a weak and shallow unconfined coastal aquifer prevails, which is underlain by a succession of deeper confined aquifers separated by layers of fine sediments.

3. Geophysical investigations

The geophysical techniques aimed to the detection of the bedrock relief, the major structural and hydrostratigraphic elements and also to assess the extent of the sea intrusion in the area.

Gravity survey

The gravity survey covered an area of 35 km² with 270 stations, conducted with a Scintrex CG-5 gravity meter.

From the Bouguer map of Fig. 3 a residual gravity map is extracted (Fig. 4) and overlain on the geological map. The positive anomalies GP1, GP2, GP3 are associated with the Cretaceous Limestone outcrops in the area. The anomalies GP4 and GP5 are associated with Triassic Limestones belonging to the basement. The negative anomalies GN1, GN2 and GN3 form a tectonic graben, bounded to the SW by a well known fault. Another NW-SE striking lineament is observed to the further south of the positive anomaly GP1, possibly associated with a second fault.

Electrical resistivity tomography (ERT)

The ERT method is the most commonly used 2D resistivity imaging method in recent years. This powerful method nowadays is being employed on a routine basis in various configurations with multielectrode arrays (48 electrodes), with spacings up to 20 m, reaching investigation depths of 200 m.

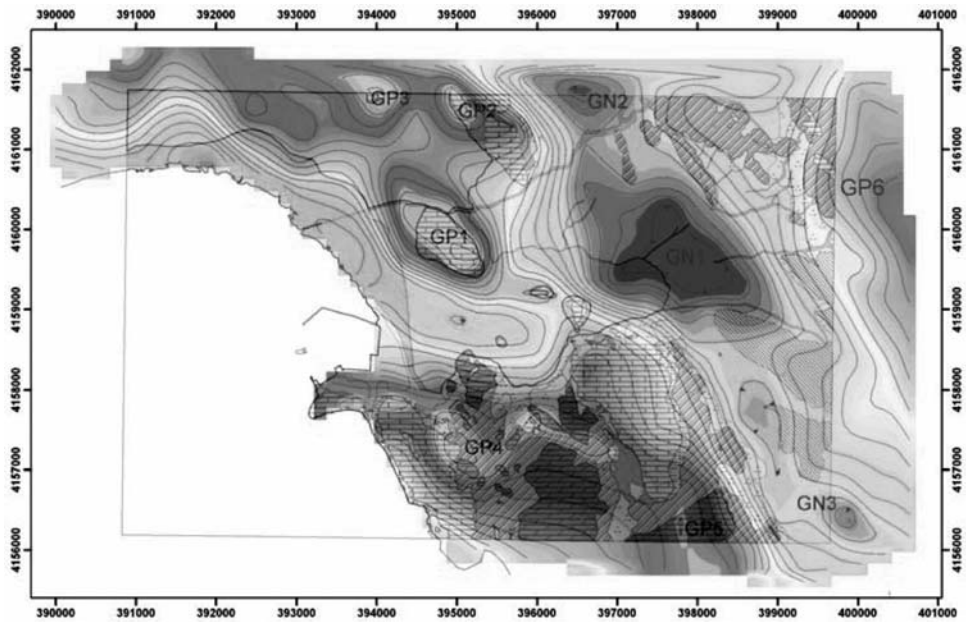


Fig. 4: Residual gravity map overlain on the geological map.

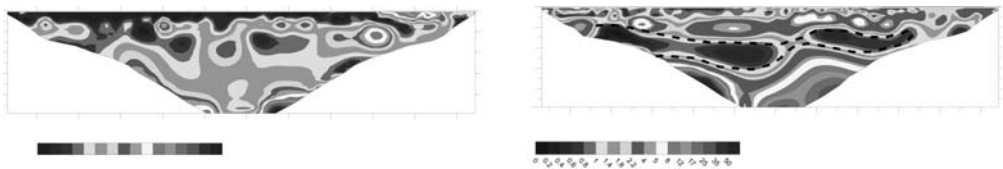


Fig. 5: Modeled resistivity sections of profiles N1 and N2.

Profiles N1 and N2 (Figure 5) were cited on the marsh land close to the coastline and were surveyed in order to evaluate the effect of salinization structure.

The results show the presence of sand-silty and clayey-silty sediments, saturated with solutions, of relatively high salinity. In fact, resistivity values even lower than 1 Ω .m are recorded from the land surface to the depth of 5 m (Profile N1). The presence of another low resistivity layer reaching depths of 30 m is evident on both profiles N1 and N2. The higher resistivity values, of 20-40 Ω .m, occurring deeper than 30 and 40 m are probably attributed to the underlying flysch bedrock (Fig. 5).

Bulk electrical resistivity values are generally dependent both of the rock - soil type and the pore fluid properties. Allowing for the very high conductivity of saline water with respect to the relatively moderate conductivity of prevailing sediments, it can be inferred that the recorded resistivity values reflect the order of salinity of pore water. This methodology calibrated on site specific data can be used as tool for the quantification and mapping of seawater intrusion in coastal areas.

Fishman and Friedman (1989) proposed an empirical relationship relating the electrical conductivity of aqueous solutions to the Total Dissolved Solids (TDS).

$$\sigma(\text{S/m}) \approx \alpha \text{ TDS (mg/L)}$$

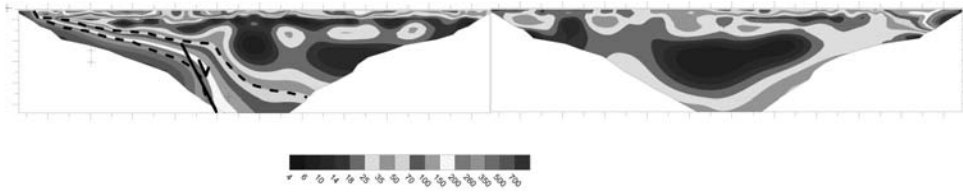


Fig. 6: Modeled resistivity sections of profiles N3 and N4

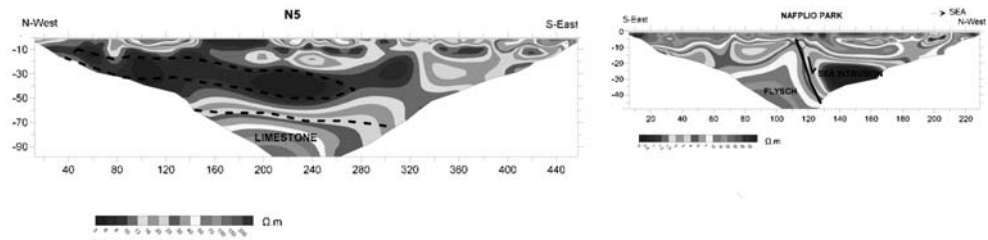


Fig. 7: Modeled resistivity sections of profiles N5 and Nafplio park.

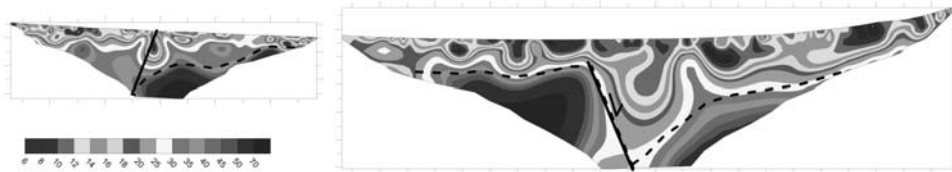


Fig. 8: Modeled resistivity sections of profiles N6 and N7.

where σ is the electrical conductivity and α a constant ranging from 1.2×10^{-4} to 2×10^{-4} . Making use of more than 250 chemical analyses data (Giannouloupolous 2000) of major ions and calculating the corresponding TDS (Lloyd and Heathcote, 1985) it was found that α factor in the Aplain of Argos is 2×10^{-4} .

Assuming that the bulk electrical resistivity (or conductivity) is dominated by the pore fluid resistivity we use the above formula to calculate the groundwater salinity. An average value of $0.5 \Omega \cdot m$ was used, and a value of $\alpha = 2 \times 10^{-4}$ resulting to an average TDS value of 10.000 mg/L .

In figure 6 profiles N3 and N4 were surveyed to test the possible occurrence of sea water intrusion in the valley formed between the two limestone hills. Resistivity values higher than $4 \Omega \cdot m$ are recorded, and attributed to the confining marl and clayey sediments. There is no evidence of sea intrusion in this area. The geometry of the limestone constraining fault is clearly seen at the SW end of profile N4.

The modeled resistivity section of profile N5 (Fig.7) shows the occurrence of a conductive layer expanding mainly from 30 to 50 m depth being overlain by shallow layers of varying resistivity. Low resistivity values of $3-5 \Omega \cdot m$ are attributed to clayey deposits. A resistive bedrock (Limestone) can be seen at a depth of 60 m.

ERT was also conducted close to the centre of Nafplio city along the railway park and the resistivity section is shown in figure 7. The presence of the seawater intrusion can be recognized with low

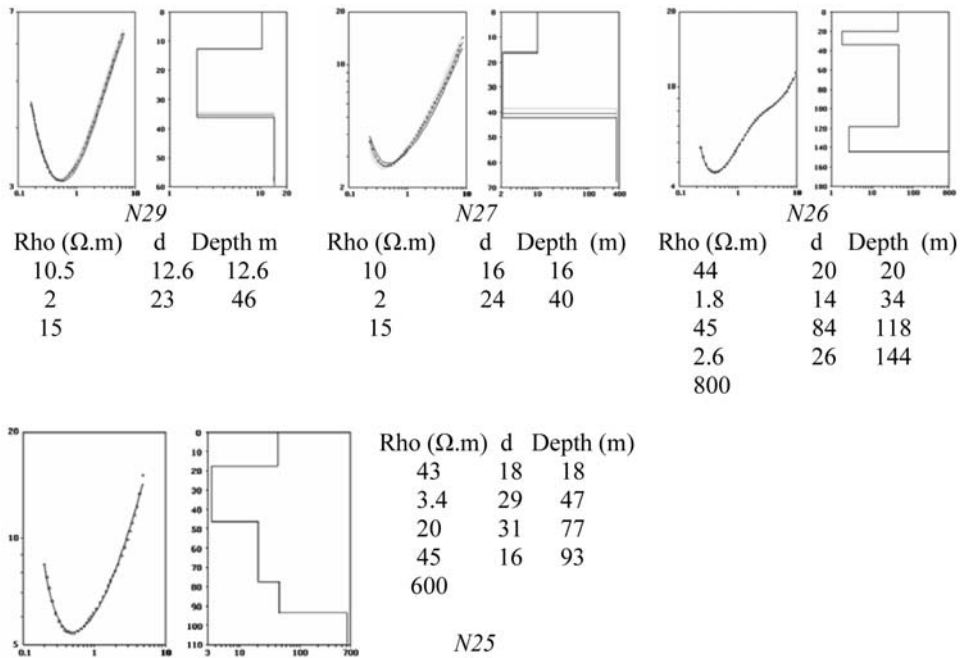


Fig. 9: Examples of TEM soundings with interpretation models. Salinization affects only the shallow unconfined aquifer.

resistivity values of 0.3 to 1 $\Omega.m$. The seawater intrusion is bounded to the South-East by a fault zone. The presence of flysch bedrock to the SE limits the extent of the salinization.

The interpreted sections of figure 8 show the ERT results of profiles N6 and N7, sited at the tectonic graben shown on the gravity map of figure 4. The occurrence of a fault can be clearly seen at the middle of profile N6. There is no indication of seawater intrusion in this area.

4. Transient Electromagnetic Method (TEM)

The TEM method has been developed mainly since the mid-1980's and tutorial articles specifically concerned with the method can be found in McNeill (1980), West and Macnae (1991), Ward and Hohmann(1987) and Zhdanov and Keller (1994). The method was originally developed for use in the mining industry to image electrical contrasts to depths of hundreds of meters. Compared with other mapping methods TEM is relatively cheap, has a large penetration depth and it gives both structural and lithological information. Its strength lies on its ability to resolve and quantify low-resistivity layers, while resistivity values exceeding 80-120 Ωm are not precisely determined.

TEM has a decreasing capability in resolving individual layers with depth, due to the diffusive nature of the method, meaning that succession of individual thin layers will commonly be averaged into one model layer. Due to difficulties in recording data at very early decay times the upper 10-20 m of the geoelectrical model are averaged into one layer. Recent improvements in transmitter turn-off time and sampling rate has improved resolution of the top 20 metres below surface making fast-sampling TEM a useful tool in salinity surveys. It has been used as an airborne tool covering large areas in the search of paleochannels, hidden valleys and mapping salinity.

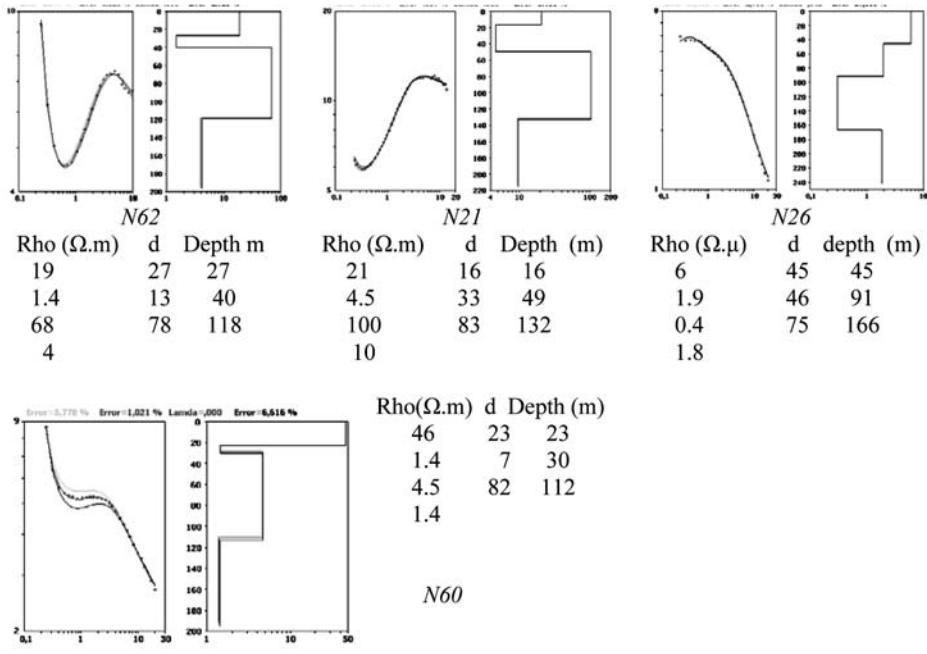


Fig. 10: Sea intrusion occurs both near surface and at the porous basement.

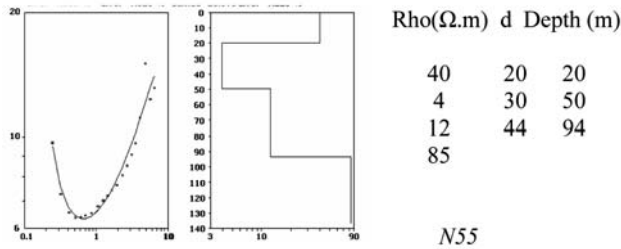


Fig. 10 Limestone detected as basement with no salinization. Results are calibrated with borehole G10 which intersected limestone at 92 m depth.

A number of 70 TEM soundings was conducted in the project area using single loop configuration of 100x100 m or 50x50 m used simultaneously as transmitter and receiver.

All soundings have been processed and inverted using 1D modelling code (Karmis 2003).

The results are classified according to the degree of the saline intrusion and the nature of the basement.

In the following figures characteristic examples of TEM soundings are presented. In figure 9 the apparent resistivity versus time is plotted on the left part of each graph, along with the interpretation model on the right side. The sea intrusion is evident at all soundings in depths between 12 and 40 m. The limited penetration depth, due to cultural noise, on N27 and N29 limits the interpretation depth of stratigraphy to the depth of flysch, whereas at soundings N25 and N26 limestone was detected as bedrock below flysch. A second category of TEM soundings show the salinization effect both on the surface layers (top 40 m) and within the basement. By combining available drilling information, the porous formation of the basement is assigned to limestone which is also vulnerable to salinization.

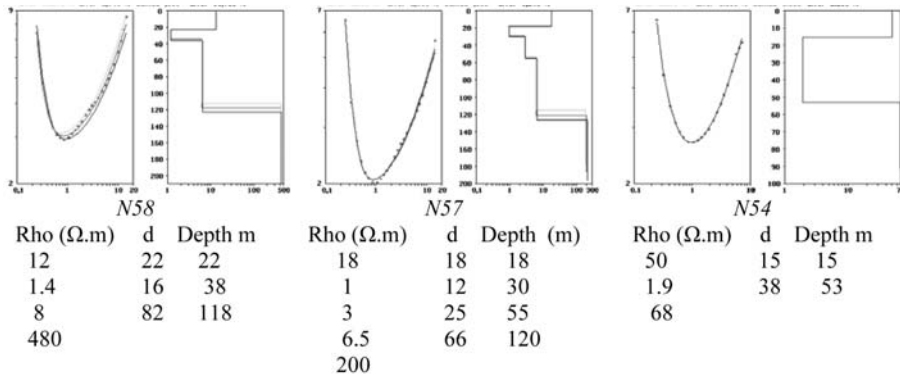


Fig. 11: TEM soundings N58 and N57 located limestone not affected by salinization.

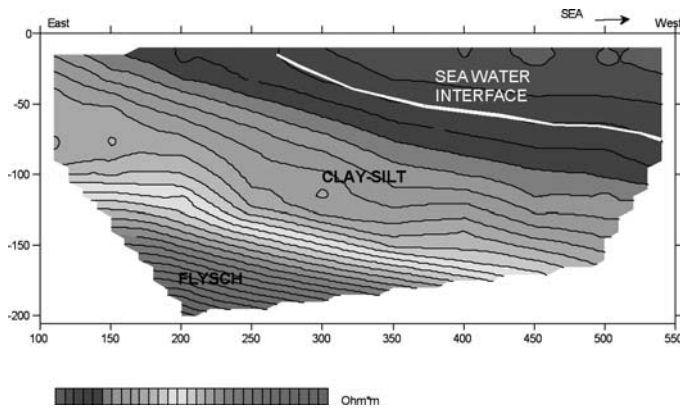


Fig. 12: TEM 2D resistivity section of TEM profile.

Sounding N62 (figure 10) shows the effect of seawater intrusion at depths between 27 and 40 m. Below this depth a relatively resistive layer is detected, interpreted as sand layer. The salinization is also evident at the depth of 118 m, which probably marks the top of the limestone. This interpretation is verified by the drilling results of borehole 3042, to the SE of N62, which intersected this limestone at the depth of 110 m. Similar results are shown at N21, where the limestone can be seen at 132 m depth. The results of N26 indicate that seawater intrusion comes into effect at 45 m depth. The results of N60 are typical patterns of responses obtained over porous carbonate formation polluted by seawater intrusion. The presence of an aquifer affected by seawater intrusion is detected at 23 m depth. This aquifer is followed by a succession of fine clayey sediments, with the limestone at 112 m with resistivity of 1.4 $\Omega.m$, due to the saline water. The results of figure 11 show the presence of fresh - water carbonate layer. This is probably due to the presence of a flysch layer on top of the limestone which acts as a protecting barrier.

The N57 and N58 soundings show also the presence of limestone bedrock at depths of 120 m. However, the penetration depth of N54 does not allow the detection of the limestone bedrock.

5. TEM Profile

The TEM profile was surveyed with a dense spacing of 50 m and a 50x50 m loop. The results are shown in figure 12. The interpretation model is a pseudo-2D section with resistivity and depth values are calculated per each decay channel, resulting to a dense and closely spaced dataset.

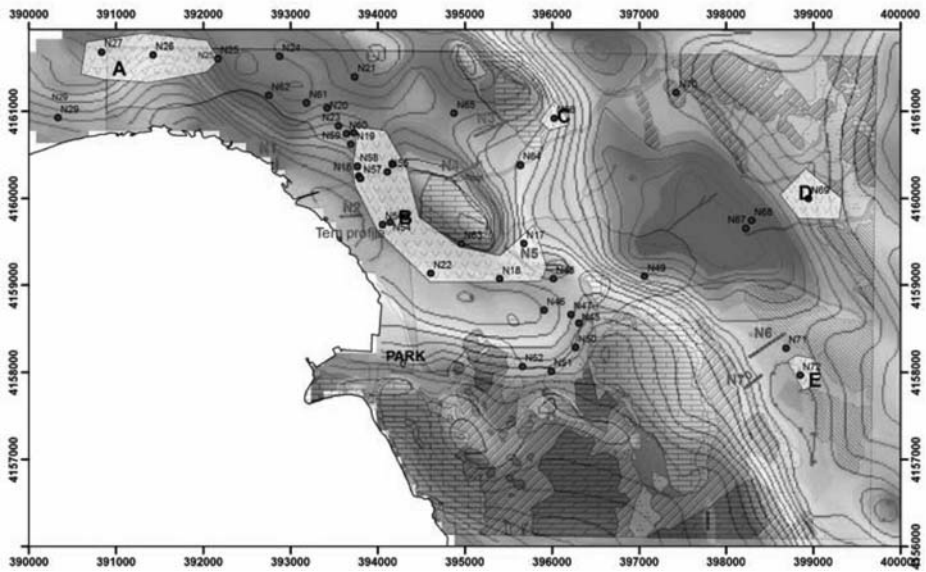


Fig. 13: Areas A, B, C, D and E with limited salinization pollution due to existence of impermeable cap layers above the carbonate basement.

The section shows the geologic succession gently dipping to the SouthWest at small angle. There is no indication of a fault in this line. The seawater intrusion is clearly recognized with resistivity values lower than 2 Ω .m. Below the shallow silty-clayey sediments the flysch layer is detected.

6. Conclusions

The application of the geophysical surveys added important new and detailed information to the construction of hydrostratigraphic models in coastal areas, giving a more comprehensive understanding of the formation of the subsurface layers and structures. Gravity survey provided general information on the subsurface structures, whereas the results of the ERT and TEM surveys show the importance of these methods in environmental and groundwater investigations in coastal areas. They constitute an effective tool for mapping the fresh -seawater interface in the alluvium and carbonate aquifer. They are particularly suitable for determining the resistivity and thickness of highly conductive targets such as clays and saline aquifers. Accordingly they can be used to map potential aquifer layers, recognized as sediments with relatively high resistivity.

The low resistivity sediments are indicative of low permeability deposits such as clays. These low permeability clayey layers may serve as protection against groundwater contamination caused by seepage of pollutants and seawater.

With regards to the particular results of the aforementioned geophysical surveys the effect of the sea water contamination is mainly identified within three horizons. The first is a shallow layer from surface to approximately 12 meters close to the coastline of the march land, with very low values of electrical resistivity below 1 Ω .m. These values, according to an empiric formula, correspond to TDS values in the range of 5000 and 10000 mg/L. The second horizon corresponds to saturated sediments made of sand and gravel (confined aquifer) with resistivity values between 1 and 3 Ω .m located in relatively shallow depths between 15 and 40 m. The third horizon has similar resistivity values at

depths larger than 40 meters and corresponds to the porous formation (limestone) which is heavily polluted by the sea intrusion.

As a rule of thumb it can be stated that bulk resistivity values lower than 2 Ω .m correspond to saline water, where higher values between 2 and 4 Ω .m may be attributed either to various combinations between brackish water or to the lithology.

Occurrence of low-permeable layers such as flysch above the carbonate aquifers was detected in certain areas delineated in the map of figure 12. In areas A and B the seawater intrusion is limited only within the second horizon due to the presence of flysch overlying the deeper limestone. The flysch is gently dipping towards the sea and limits the effect of the sea intrusion to the limestone.

In areas C, D and E sea intrusion is not observed. In this region fault discovered seen by gravity method, control the encroachment of seawater intrusion. The rest of the area is heavily polluted by the sea intrusion. The region between areas A and B and between B and Palamidi hill act as conduits for the salinization of the mainland.

The combined application of high resolution TEM and ERT surveys can be an effective tool for studying the effect of the sea-intrusion and map salinity changes.

7. Acknowledgments

This study was implemented in the frame of the project “Collection and Documentation of Geothematic Information for Urban Areas in Greece”. Funded by Competitiveness Priority Axis 7: Measure 7.3 and ERDF.

8. References

- Giannouloupolous P. *Groundwater flow and mathematical models in the plain of Argos*. Agricultural University of Athens, Department of Natural resources Development and Agr. Engineering. Unpublished Ph.D. Thesis. 362 p, 2000
- Giannouloupolous P. *Hydrostratigraphic conditions of the alluvial sediments of Argos Plain – Aquifer formations*. Proceedings of the 9th Int. Congress of Greek Geol. Society, Vol 5, pp.1793-1800, 2001
- Karmis P. *Automatic interpretation of TEM data*, PhD Thesis, University of Athens, p. 248, 2003
- Lloyd J. and A. Heathcote. *Natural Inorganic Hydrochemistry in Relation to Groundwater*. Oxford University Press. 296 p., 1985
- McNeill J.D. *Applications of transient electromagnetic techniques*, Geonics Ltd. Technical Note TN-17, 1980
- McNeill J.D. *Use of electromagnetic methods for groundwater studies*. In Ward S.H.(Ed). *Geotechnical and environmental problems 01*. Society of Exploration Geophysicists, pp. 91-218, 1990
- Rubin Y., Hubbard S. *Hydrogeophysics* Springer, p. 523, 2005
- Ward S.H., Hohmann G.H. *Electromagnetic theory for geophysical applications*. In Nabighian, M.N. (Ed) *Electromagnetic methods in Applied Geophysics*, vol 2a, Society of Exploration Geophysicists, pp. 131-311, 1987
- Zhadanov M.S., Keller G.V., *The Geoelectrical Methods in Geophysical Exploration*, Elsevier, 884 pp., 1994.

RADON: GEOINFORMATION FOR THE PLANNING OF URBAN – SUBURBAN REGIONS. THE CASE OF NAFPLION CITY, GREECE

A. Koukoulis¹ and D.E. Karageorgiou¹

¹ *Institute of Geology and Mineral Exploration, Olympic Village, Entrance C, 136 77 Acharnae, Greece, dek@igme.gr*

Abstract

Radon is trapped in the terrestrial cover as a transmutation product of natural radioactive elements. It is directly related to the geotectonic environment and the atmosphere contains traces of radon near the ground, as a result of emanations from soil and rocks, both of which contain minute quantities of radium; it also infiltrates into the ground and circulates in groundwater. Because naturally occurring radon gas has come to be recognised as a potentially serious health hazard, especially in the built environment, a radon and radiometric (α - and γ -radiation) survey was carried out in the urban and suburban region of Nafplion, using the same grid of 500 x 500 m that was used by other methods, i.e., urban geochemical and geophysical surveys. Radon was measured down to a soil depth of 50 cm, and at each site α - and γ -radiation measurements were taken. The survey results have shown that these concentrations are low compared to other regions of Greece. However, potential accumulations of radon in closed underground spaces cannot be excluded. The isoradon contours of these concentrations form anisotropy axes of main NW to NE and N-S direction related to geological-tectonic structures.

Key words: *Radon, γ -radiation, α -radiation, urban, Nafplion, Peloponnese, Greece*

1. Introduction

It is well known that radon gas is widespread in the environment at low levels, however it can easily accumulate in closed underground spaces and with passive escape it can reach houses and endanger human health. Its short half-life allows radon to travel long distances, before its radioactivity decreases by half, rendering it a good indicator-tracer of deeper causes of the background, invisible from the surface (Vougioukalakis, et al., 2000), due to the fact that as a noble gas it does not participate in reactions.

The current study is performed in the context of a more integrated design involving the geological, geotechnical, hydrogeological, geochemical and geophysical research and study of urban and suburban pilot area of Nafplion in Argolida Prefecture. The measurement of radon at the depth of 50 cm is followed by the measurement of γ -radiation in the same position on the surface, in order to correlate the radioactivity of rocks with radon.

The radon concentrated in the soil depends on its high or not high production, on the rock background, or on its escape or not escape to the atmosphere. These mechanisms can change from one rock to another, or even in the same rock, therefore the study of radon in soil requires special attention to the geological - tectonic environment, as well as the general mechanisms of permeability, porosity, solubility in water, etc.

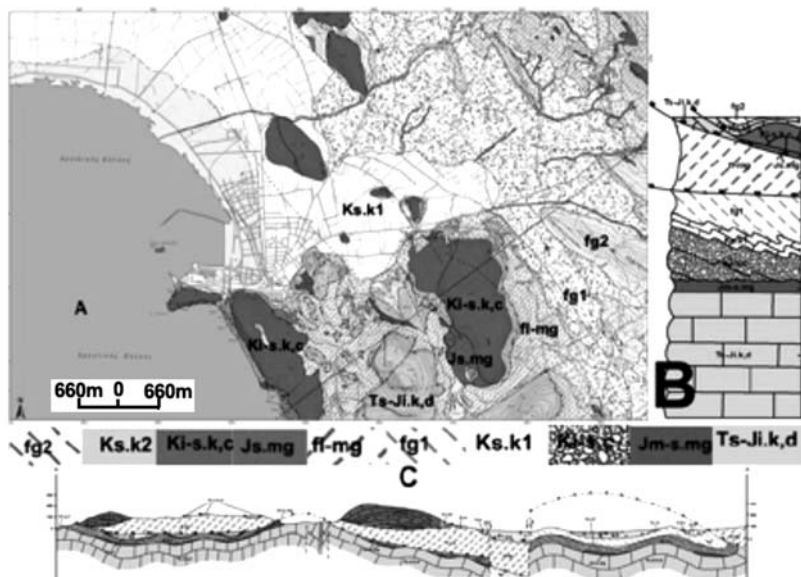


Fig. 1: Geological map (A), tectono-stratigraphic column (B) and geological section (C) of the greater Nafplion area. Lower Unit, Triassic-Jurassic shallow-water carbonate (Ts-Ji.k,d), tectono-sedimentary ophiolitic melange (Jm-s.mg), Meso-autochthonous series with Cretaceous carbonates (Ki-s.c & Ks.k1), post-Ypresian flysch (fg1); Middle Unit, flyschoidal melange complex (fl-mg); Upper Unit, serpentinite sole (Js.mg), Triassic-Jurassic carbonate outlier (Ts-Ji.k,d), Cretaceous carbonate outlier (Ki-s.k.c & Ks.k2) with flysch (fg2) and late Eocene tectonic phase. (Photiadis, 2010).

Upon processing the first data, specific distribution structures were already revealed, which demonstrate the sensitive behaviour of the method applied for the correlation of radon in soil with geotectonic structures in research area. A first interpretation of the sensitive variations is given with the geological map of research area on scale 1: 5,000.

2. Geological Environment

The geological structure of research area came from the tectonic accumulation of three units, after a series of compression and tensile events, which occurred generally in the Pelagonic zone from Jurassic until the post-Eocene period. It is distinguished (Photiadis, 2008) as follows:

The para-autochthonous or lower unit, of middle Triassic-Lias age consisting of a carbonate, neritic sequence with pelagic, nodular limestones, pelagic sediments of red cherts, siliceous silts and a tectonic-sedimentary mixture of Malm age. The carbonate conglomerate sequence of Cretaceous and the post-Ypresian flysch of Argolida follow unconformably after several erosion and emersion events.

The intermediate unit, of post-Eocene occurring through a flyschoid tectonic mixture of continental and oceanic tectonic bodies into a flyschoid cementing material due to the collapse, destruction, detachment and tectonic accumulation of the internal pelagonian - continental margin during the collision of the Hellenides.

The upper section, which is tectonically drifted with (or without) intercalation of the previous unit,

consisting of limestone flakes of Cretaceous age with accompanying tectonic foot of serpentinites, as well as mega-blocks of carbonate rocks of middle Triassic-Lias age, detached from the underlying lower unit.

3. Methods

3.1 Measurement Instruments

Measurements of radon in soil of urban and suburban areas Nafplion, initially started with the use of two instruments: RAD 7 by Durrigde (USA) and EPP 10 by Saphymo - Stel company (France). Both are portable units designed to measure radon in air sample in soil. RAD 7 is a monitoring, sensitive and automated instrument, but has a significant turnaround time, of about 1 h. The instruments' measurement is taken in automatically controlled humidity, which must be less than 5%. The electronic detector of moisture blocks often rendering the instrument difficult to handle for systematic research. The instrument has a silicon detector. The measurements are repeated in 4 equal time intervals and are given in pci/l with a deviation of a few tens of units. Printed histograms of the radioactive element that emits radiation are given too. EPP 10 is not a recording – automatic instrument, but it is suitable for systematic work and, more importantly, it does not block outside. For the above reasons, after a series of double measurements and due to the fact that significant problems were encountered with the electronic instrument, the measurements were limited to EPP 10.

The scintillation- meter consists of a 150 AVP photomultiplier, which transforms into electricity the sparks emitted by ray alpha upon hitting the inner walls of glass vial coated with zinc sulphide and activated with silver (ZnS [Ag]). These electrical impulses then determine the electronic circuits of information processing, from which finally a micro amber meter gives results expressed in beats per second, c / s, (Dumoulin, 1978).

The measurement of γ -radiation at ground level is fast becoming a routine using the Saphymo – Stel company (France), SPP2N meter of scintillation for small, intermediate and large scales of measurements, 50, 150, 500, 1,500, 5,000 and 15,000 c / s. A NaI crystal is built into the portable device and the measurement refers primarily to the γ -radiation emitted by radio with the farther degradations elements lead and bismuth 214 with a small half period of 26.8 and 19.7 minutes, but with the relevant energy being at the highest level of 0.188 - (0.250-0.294-0.350) and 0.606 MeV respectively.

The measurement of gamma radiation is proportional to the quantity of the parent uranium, as long as there was enough time to reach radioactive equilibrium, 1 million years for the group of uranium and 70 years for that of thorium. Usually the radioactive equilibrium exists in nature, but sometimes

Table 1. Average calculated correspondence for different units in four (4) representative radon value groups in Nafplion area.

Class c/s EPP 10	pci/lt	Bq/m3	% Prices
0,0-1,0	0,0-27,4	0,0-1.015	47,47
1,0-3,0	27,4-82,2	1.015-3.045	27,85
3,0-4,5	82,2-123,4	3.045-4.570	9,49
>4,5	>123,4	>4.570	15,19
Total			100

there is movement, solubility, leaching or precipitation of one element and as a result some already existing elements, for example in water, are found in abundance and other insoluble elements will be deposited because of their nature. In this case, a full analysis of radioisotopes, which can be identified, such as uranium, thorium, radium, radon, etc. (CREGU, 1981) is necessary.

3.2 Field research measurements

Based on the research needs of the project, the measurements in the field were carried out using grid of 500 m. The identification of the location spots in the countryside was determined with GPS of a few meters' accuracy, in relation to fixed points such as roads' intersections, canals, streams, etc., as well as morphological data of the area. The approach of the desired point was achieved either by car or on foot, while in case this was difficult or impossible; the closest accessible spot to the location was selected, in order to increase productive work time.

Before air sampling, from a depth of about 50cm in the ground, the instrument was prepared, vacuum was created inside, the indications were controlled etc. In the first five minutes of operation of the instrument, which is the accepted constant of integration, the average price represents the best measurement of the position.

For a total research area of about 36Km², 158 measurements were taken, which are, prima facie, satisfactory for the identification of sensitive variations of radon, i.e. approximately 5 measurements per Km².

4. Results - Assessment

The summary of data measurements is presented in Tab. 2 and Table 3, expressed in c / s, SPP2N and EPP 10, for the γ and α radiations of stations of the research field.

In an ideal case, the values of radon in soil should remain at stable levels. However, in most cases radon prices often vary, due to various factors, such as changes in the uranium-thorium contents in different background rocks, or even in one and the same rock, variations to thickness, porosity, per-

Table 2. Data of γ radiation in the urban and suburban area of Nafplion.

Serial Number	Class	Mean class	Frequency	Cumulative Frequency	% Prices
1	0,0-5,0	2,5	0	0	
2	5,0-10,0	7,5	9	9	25,95
3	10,0-15,0	12,5	23	32	
4	15,0-20,0	17,5	24	56	
5	20,0-25,0	22,5	37	93	46,20
6	25,0-30,0	27,5	12	105	
7	30,0-35,0	32,5	16	121	
8	35,0-40,0	37,5	20	141	22,78
9	40,0-45,0	42,5	5	146	
10	45,0-50,0	47,5	11	157	10,76
11	50,0-55,0	52,5	1	158	

Table 3. Radon subsoil in urban and suburban area of Nafplion.

Serial Number	Class	Mean class	Frequency	Cumulative Frequency	% Prices
1	0-0.5	0.25	63	63	47.47
2	0.5-1.0	0.75	12	75	
3	1.0-1.5.	1.25	9	84	
4	1.5-2.0	1.75	12	96	
5	2.0-2.5	2.25	12	108	27.85
6	2.5-3.0	2.75	11	119	
7	3.0-3.5	3.25	10	129	
8	3.5-4.0	3.75	4	133	9.49
9	4.0-4.5	4.25	1	134	
10	4.5-5.0	4.75	6	140	
11	5.0-5.5	5.25	5	145	
12	5.5-6.0	5.75	5	150	
13	6.0-6.5	6.25	4	154	
14	6.5-7.0	6.75	2	156	15.19
15	7.0-7.5	7.25	0	156	
16	7.5-8.0	7.75	0	156	
17	8.0-8.5	8.25	1	157	
18	8.5-9.0	8.75	0	157	
19	9.0-9.5	9.25	0	157	
20	9.5-10.0	9.75	1	158	
TOTAL					100

meability, the circulation of hot or cold water, or some changes from cracks, joints, etc., allowing dissolution in water or passive removal - release of radon into the atmosphere.

According to the measurements from all plants (Table 3):

- 47% of the data indicates very low values of 0,0 - 1,0 c / s EPP 10, namely 0, 0 - 27,4 pci / lt or 0,0 - 1.000Bq/m³,
- 28% of the values also remains lower than 1, 0 - 3.0 ERP 10, namely 27,4 -82,2 pci / lt or 1.000 - 3.050 Bq/m³,
- 25% of the values is higher than 3.050 Bq/m³, although they are still lower than the values of radon in other regions of Greece.

As a measure of comparison it should be mentioned that in France, 200 - 500 Bq/m³ are accumulated in closed spaces, when values greater than 10.000 Bq / m³ are measured in the underground (Lempereur, 1988). Also in the urban area of Kalamata, in all 370 radiotracer open- type LR 115 in schools and underground spaces, almost all values of radon were below the level of 200 Bq/m³ (Geranios et al., 2001).

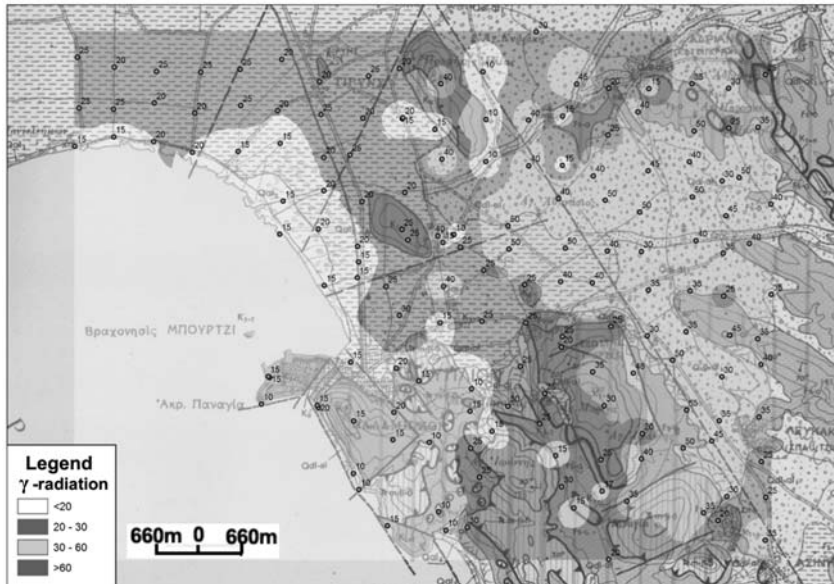


Fig.2: Distribution of γ -radiation in urban and suburban area of Nafplion.

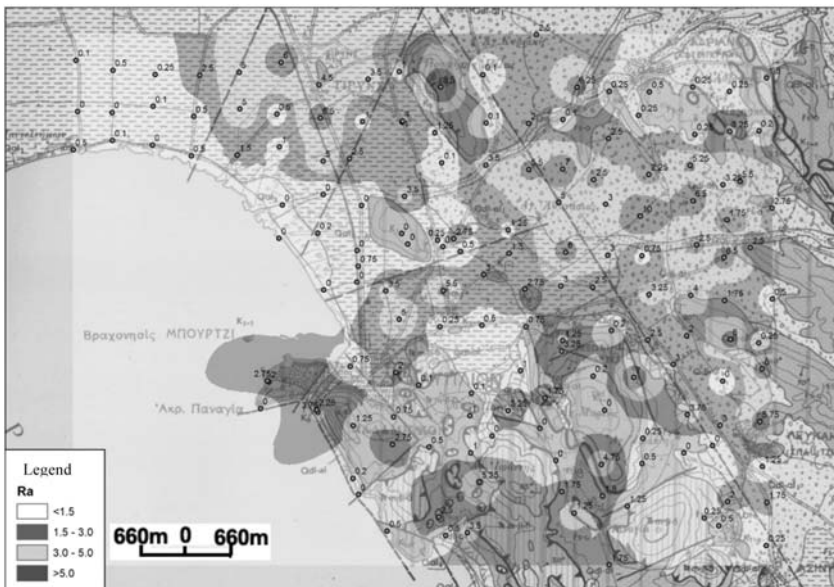


Fig 3: Points of measurements of radon and uranium in the urban and suburban area of Nafplion.

For the overall assessment of risk from radon in the human environment three key parameters are necessary to evaluate: the contents produced by the background rock, the selective-passive escape of radon in the air and the potential accumulation in enclosed and thus habitable spaces. Therefore, the measurement of radon in soil expresses the result of the first two factors.

The level of measurement of radon is affected significantly by water, since radon has a large solubility in water depending also on its physiochemical characteristics such as pH, temperature, pressure, concentrations of various ions, metals, non-metals compounds, etc. It is soluble in certain circumstances and less in others, for example at 0° C exhibits the double rate of solubility in comparison with the 25o C (Ball et al., 1991).

Given the above, the values of radon stand out in the old and new deposits of streams, north-east of the outskirts of Nafplion, which exhibit a high background with most of the highest rates of radon above the $X + 2 \sigma$.

Low concentrations are present in the Cretaceous limestones, in contrast to those of Senonion, where two stations measured amongst the highest concentrations.

Interim radon values, with the greater range, from very low values to well above $X+\sigma$ are present in the flysch. The same prices are presented in alluvial deposits in the area of St. Panteleimon.

Tirynta and Nafplion. In these cases, however, the values form North – East axes anisotropy near the town of Nafplion and in North – South direction close to Tirynta, associated with non-visible from the surface geotectonic structures.

However, the main anisotropy in the distribution of radon, which is almost parallel to the coastline and is about 3 Km from this, found at the level of the town of Nafplion up to 1Km of the level of Tirynta, appears to have a northwest direction. It extends across virtually all geological formations with a thickness exceeding the 2Km and is associated with deeper tectonic structures invisible on the surface, but also on the geological occurrences under study.

The average Triassic limestone for example, or those of the lower Cretaceous and flysch appear to eliminate the impression of these deep structures, southeastern of Nafplion town, in relation to existing deposits in North -East .

An interruption or also cover of the mega-structure in North – West appears at the area of Prophet Elias of Nafplion and Tiryns, having a North –East direction and a smaller North-South direction respectively with reduced radon values, which could be interpreted as a possible definition of the entry area of the sea to the well horizon.

5. Conclusions

The concentrations of radon in urban and suburban area of Nafplion, which are measured on the ground, do not represent a source of additional radioactive burden for the population. These values, like the values of γ -radiation at ground level are low compared with other regions of Greece. As low as they may be, potentially, one cannot exclude the possibility of radon accumulation in enclosed underground spaces to levels that require check of the house for the existence of radon.

The isoradon curves show anisotropy axes, which vary according to the geological formation and the underlying deeper or not tectonic structures, prevailing in the area of research. Three issues can be identified:

- 1) Separation of rocks with the lowest, intermediate and above the level $X+2\sigma$ concentrations.
- 2) A dominant anisotropy Northwest, almost parallel to the coastline, which is associated with underlying tectonic structures and shows a slight growth of her conjugate at North- East direction, at the level of Nafplion town.

- 3) Smaller North- East and North - South anisotropies at the height of Prophet Elias Nafplion area and Tiryntha respectively, may designate the possible range of sea entrance shaft to the well horizon.

6. Acknowledgments

For the integration of Radon research to the project “Geological research of urban and suburban areas of Greece”, and the excellent cooperation, we would like to thank sincerely all the staff of the project and principally the Project Leader Mr. P. Tsompos. Also sincere thanks to our colleague M. Xenakis for his assistance on mapping system with GIS and finally to Barbara Pefani for her remarks in the presentation of this study.

7. References

- Ball, T. K., Cameron, D. C., Colman, T. B., Roberts, P. D., 1991. Behaviour of radon in the geological environment; a review. *Quart. J. Engin. Geol.*, 24, 169-182.
- CREGU, (Center for Research on the geology of uranium), 1981. Uranium and oxido-reduction, Nancy, CREGU, 316 pp.
- Dumoulin, C, J., 1978. Methods of detection of uranium, Razes, Center for Information and specificity, CEA, 141 p.
- Geranios, A., Kakoulidou, M., Mavroidis, F., Moschou, M., Fischer, S., Burian, I. and Holecek, J., 2001. Measurements of radon in Kalamata, Greece, NCSR Demokritos “ ”, 1st Congress of Environmental Radioactivity “ ”, 41 - 44 p.
- Lempereur, J, D., 1988. A deadly gas blowing from the subsoil, France, *Science and Life*, no 846,11 pp.
- Photiadis, A., 2008. Geological study of urban and suburban pilot area Nafplion, IGME, 15 p.
- Photiadis, A., 2010 Geological survey in scale 1:5.000 of the greater Nafplion area (NW Argolis, Greece)
- Vougioukalakis, G., Vlachos, M., and Kaliozizis, G., 2000. Soil gas measurements in Attica during the earthquake of September 1999, Athens, IGME, 8 p.

ROCK SLOPE STABILITY PROBLEMS IN NATURAL SIGHTSEEING AREAS - AN EXAMPLE FROM ARVANITIA, NAFPLIO, GREECE

Loupasakis C.¹, Galanakis D.² and Rozos D.³

¹*Institute of Geology and Mineral Exploration, Engineering Geology Department, Olympic Village, 13677, Acharnae, Greece, cloupas@igme.gr*

²*Institute of Geology and Mineral Exploration, General Geology and Geological Mapping Department, Olympic Village, 13677, Acharnae, Greece, galanakis@igme.gr*

³*National Technical University of Athens, School of Mining & Metallurgical Engineering, Laboratory of Engineering Geology and Hydrogeology, 9 Heroon Polytechniou str., 157 80, Athens, rozos@metal.ntua.gr*

Abstract

The morphological and geological setting of Greece, the active tectonics and the irrational human activities results to the fact that several natural sightseeing areas or even more, archaeological sites and monuments are located in areas with unfavourable geotechnical conditions. The selection of the proper support and protection measures in most of the cases appear to be very difficult because the applied measures must reassure the minimum aesthetic destruction of the sites.

The natural sightseeing area of the Arvanitia walkway, in Nafplio city, is a typical example of site, with extensive human activities, manifesting serious rockfall stability problems. The applied stability analysis pointed out the geotechnical problems and allowed the suggestion of measures for the improvement of the geotechnical behaviour of the rock mass. The measures were planned with respect to the natural beauty and the historical character of the site. Further more, the stability problems located at the slopes of the Kastoria lake walkway are briefly presented. The differences between the two sites revealed the geotechnical problems arising when the landplaning engineers do not take under consideration the engineering geological conditions during the construction of infrastructures.

Key words: *rockfall, natural sightseeing areas, Arvanitia walkway, Nafplio city.*

1. Introduction

Within the limits of Greece Territory several natural sightseeing areas or even more archaeological sites and monuments are located in areas with unfavourable geological conditions. Areas subjected to sliding, creeping or settlement phenomena have been used as foundation formations. Also several sites are founded on the base of unstable slopes arising issues for their safety and stability.

The natural sightseeing areas of Porto Katsiki beach in Lefkada and Navagio beach in Zakynthos Island are located along the base of extremely high and unstable slopes. Several sections of the walkway along the Kastoria Lake are constructed at the base of steep slopes. The slopes of the Acropolis` hill in Athens contain numerous rock wedges threatening the safety of the surrounding monuments (Andronopoulos & Koukis, 1976). Delphi archaeological site is located on the base of an extremely high limestone slope appearing numerous rockfalls. These examples clearly present the variety of the sites affected by geological – geotechnical causal factors causing slope instability.

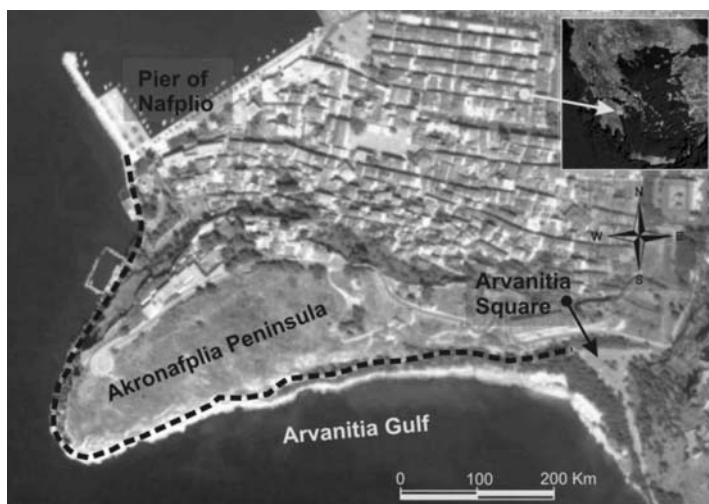


Fig. 1: Satellite pictures - taken from Google Earth - pointing the location of Arvanitia walkway in relation to Nafplio city.

The selection of the proper support and protection measures in those cases appear to be very difficult. No matter how intensive the problems are the applied measures must avoid or even restore, in a certain extent, the aesthetic alteration of the sites.

The natural sightseeing area of the Arvanitia walkway is a typical example of a site appearing rock fall stability problems. Arvanitia walkway connects the pier of the city with Arvanitia square, extending to a total length of 1100m (fig.1). The southern part of the street, along the Akronafplia gulf (650m), was constructed by means of extensive excavations along the base of the peninsula. These artificial slopes appear serious stability problems because the excavation was done using mass of explosives and without taking any measures for the removal of the overhanging rocks. Furthermore, in several sections the road was constructed attached to the base of the slopes or even worse under overhanging parts (negative inclinations). The occurred stability problems beside the numerous walkers threat the life of the climbers exercising on these slopes.

The objective of this study was to reveal and analyse the stability problems of the slopes and to propose the proper remedial measures by taking under consideration the sightseeing character of the site and the request for its minimum aesthetic destruction. Apart from Arvanitia walkway, the stability problems encountered at the slopes of the Kastoria lake walkway are briefly presented. The differences between the two sites presented the geotechnical problems arising when the landplaning engineers do not take under consideration the engineering geological setting during the construction of infrastructures.

2. Morphological - Geological setting

The old city of Nafplio was built at the north foot of Acronafplia peninsula. Arvanitia walkway encircle the peninsula connecting the pier, from the west, with the Arvanitia square, to the east (Fig. 1).

The inclination of the slopes surrounding the peninsula vary, affected mainly by the tectonics. The slopes along the north side of Acronafplia present relatively smooth inclination and therefore the city

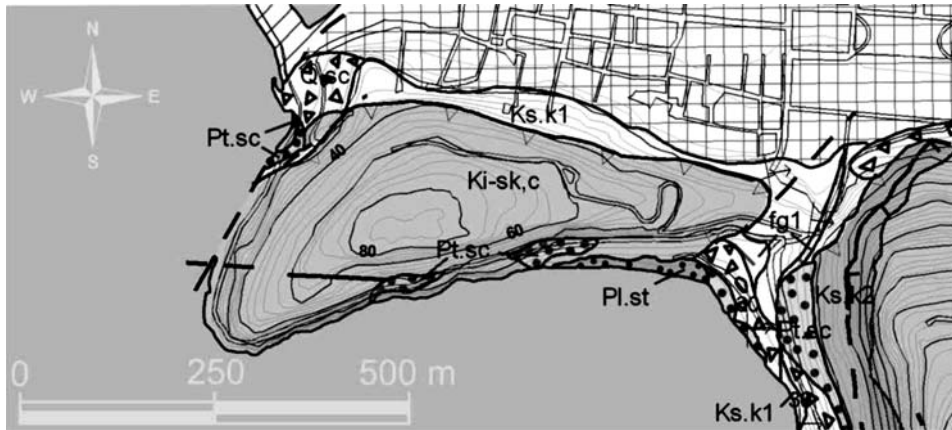


Fig. 2: Geological map of the Akronafplia peninsula. Geological formations: Ki-sk,c: Cretaceous Neritic Limestone and Base Conglomerate, Pt.sc: Pleistocene cohesive Debris, Pl.st: Pliocene Limestone Breccias with, Qsc: Quaternary alluvial fans (Fotiadis, 2008).

extends towards the hill. On the contrary, the north-western and the southern slopes are effected by normal faults and fractures presenting steep to very steep inclination, respectively.

This status affects proportionally the safety of Arvanitia walkway. Along the southern side of Acronafplia peninsula, with the very steep slopes, the walkway is constructed attached to the base of the slopes. Also because of the limited space, in several sections extensive excavations with negative inclination, or even more a small tunnel were conducted in order to open up the walkway. On the contrary, along the north-western part of the pedestrianized street with the smoother slopes, the excavations were reduced to the minimum and the walkway was constructed on a safe distance from any steep slope.

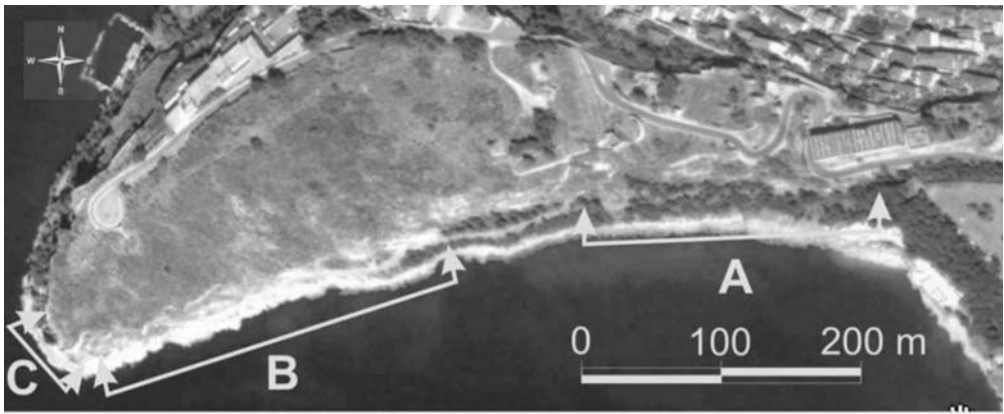
The Arvanitia walkway was constructed intersecting mainly the Cretaceous neritic limestones and the base conglomerates (Ki-sk,c) consisting of the peninsula. Some parts of the walkways also cross Pleistocene cohesive debris (Pt.sc) and Quaternary alluvial fans (Qsc), as shown in the geological map of figure 2 (Fotiadis, 2008; IGME, 1982).

The limestone appears to be massive with limited karstic erosion mainly along the faults. The rock mass of limestones is fractured by multiple joint sets forming numerous wedges along the natural and artificial slopes. The Pleistocene debris and the alluvial fans appear to be cohesive with favourable mechanical characteristics, classifying them as soft rocks.

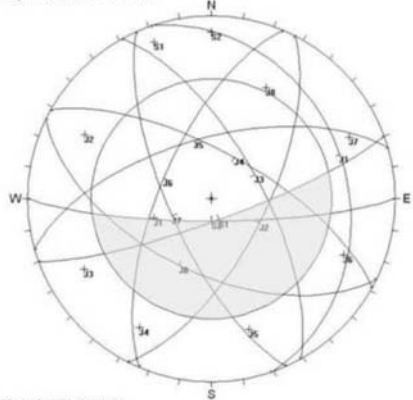
During the field work numerous normal faults were recorded. The projection of the tectonic data on the Schmidt net reveals that their orientations are NE-SW, NNW-SSE and NW-SE determinately affecting the geomorphologic structure of the peninsula.

3. Geotechnical setting- safety assessment

The slopes along the Arvanitia walkway can be distinguished in two categories, taking into account both the location of the road in relation to the base of the slope and the available space for the installation of the support and protection measures. As presented in figures 3, 4 and 5 sections A, B



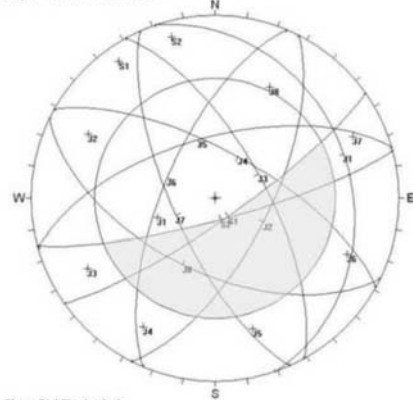
Nafplio - Arvanitia - Section A



Slope Stability Analysis

A

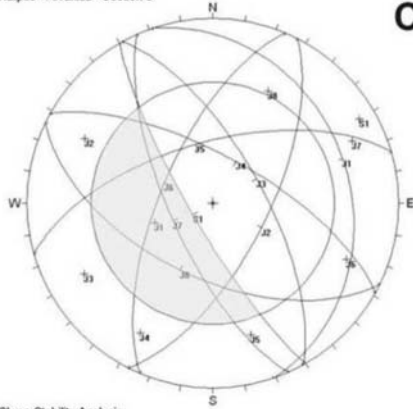
Nafplio - Arvanitia - Section B



Slope Stability Analysis

B

Nafplio - Arvanitia - Section 3



Slope Stability Analysis

C

Fig 3. Satellite picture (Google Earth) pointing the parts of Arvanitia walkway (A, B and C) constructed along the base of the slopes. The Schmidt stereo diagrams presenting the numerous joint sets intersecting the A, B and C parts of the slopes. The numerous unstable wedges are clearly presented by checking the intersected major planes in the "zone of potential instability" (grey area) (Hocking, 1976; Hoek & Bray, 1981).

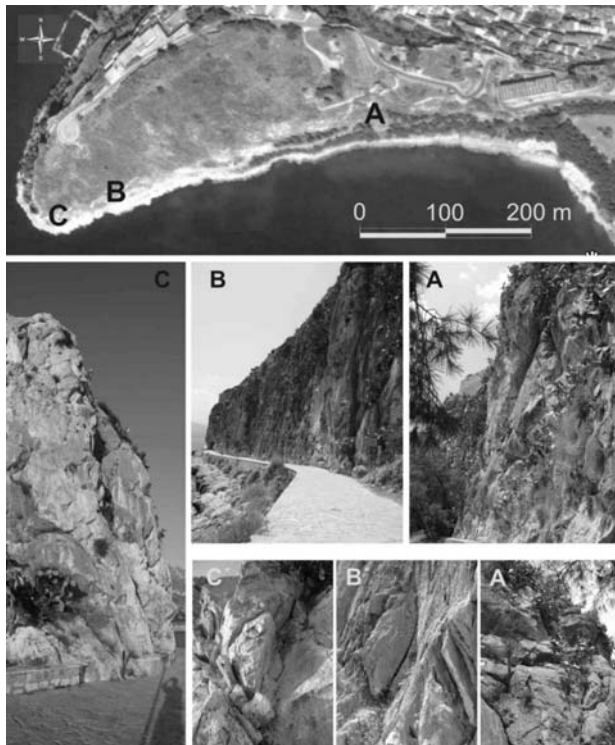


Fig 4. Photos presenting the condition of the rock mass in the before mentioned parts A, B and C of the walkway. Pictures A', B' and C' present focus on main wedges in the corresponding slopes.

and C are constructed attached to the base of the slopes without leaving any space for the installation of any protection measure. Those sections appear serious stability problems, due to the rock mass fracturing, and the disturbance caused by the excavation procedure.

The Schmidt stereo-diagrams presented in figure 3 prove that the A, B and C parts of the slopes are intersected by multiple joint sets. Most of the joints appear very high persistence (>20 m), wide spacing (1-2 m), no separation (< 0.1 mm) and lack of weathering. Those parameters explain the high RQD values (reaching up to 80-90%) and justify the also high RMR ratings (75-80) that classify the limestones in the “good” rock mass category (Kolligri, 2008). Based on the before mentioned characteristics of the joints, the wedges formed along the slopes are common and almost always oversized.

Beside the tectonics, the rock mass condition was affected by unadvised excavation procedure. The lack of any pre-splitting technique during the cutting of the artificial slopes (figure 5c), led to the intensive cracking of their rock mass. The abundance of the overhanging blocks, the height of the slopes (reaching up to 40 m) and the installation of the road on the base of the slopes without keeping any safety distance, cause serious safety issues.

All these problems are even more intensive along section C. Several meters of the walkway are constructed not only attached at the base of the slope, but along overhanging parts. Even a small tunnel was constructed in order to cross a ledge of the rocky slope (fig. 5).

The slopes along the rest of the walkway (except parts A, B and C) manifest the same tectonic fragmentation but they are not disturbed by any excavation procedure. Further more the available space along the base of these slopes, as well as the tree cover, allow the installation of all necessary protection measures without causing any aesthetic destruction to the site (fig. 6).

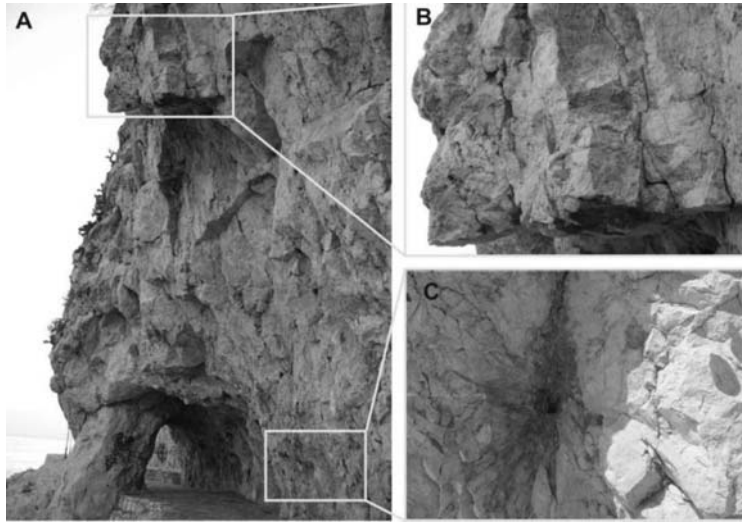


Fig 5.: A) A small tunnel constructed along section C. B) Wedges hanged over the entrance of the tunnel. C) the intense artificial fracturing around a drill used for the installation of explosives.



Fig 6.: Photos taken from the slopes extending between section A and B. The available space allows the installation of camouflaged protection measures.

4. Proposed support and protection measures

For the selection of the proper support measures of sections A, B and C, besides the stability analyses, rockfall propagation analyses were conducted (Fig. 7A), using the *RocFall* statistical analysis program. These analyses revealed that the spreading of the falling rocks covers the entire road width.

Unfortunately, the above mentioned stability problems require the application of remedial measures causing disturbance to the natural sightseeing character of the site. Indeed, the actions needed to be applied are: a) removal of all overhanging detached rock blocks, using controlled quarrying b) ap-

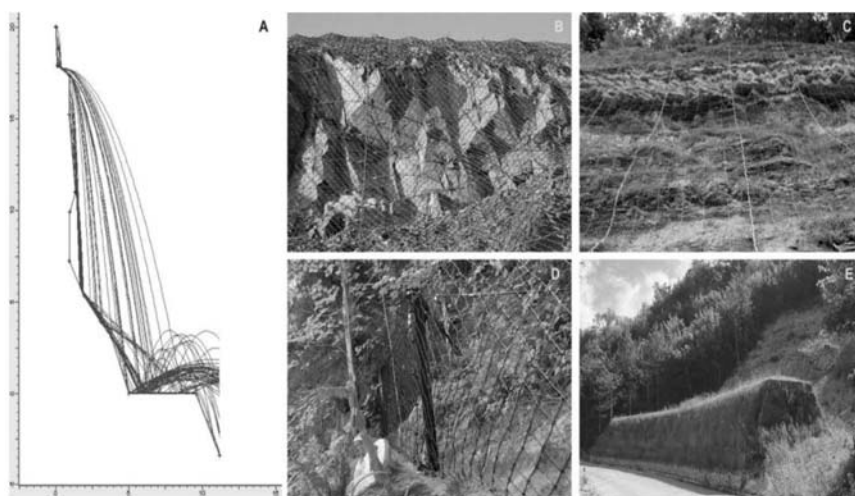


Fig 7.: A) Analysis for the estimation of the rock fall propagation in a typical cross section of the slope, B, C, D and E) typical support and protection measures. Wire nets (B and C), fences (D) and gabion boxes embankments (E).

plication of spot bolting in order to stabilize all the big rock wedges and c) installation of a high strength rockfall protection uniaxial netting along the entire slope (Fig. 7B, C).

Alternatively, as the net, causes a visible aesthetic demission, it could be substituted by the installation of a metallic frames shelter, covered on top with wavy sheet iron. Metallic frame constructions could be designed to take over the impact of a rock fall and at the same time their architectural design could make them fit the natural sightseeing setting.

The selection of the proper protection measures for the slope parts being at a distance longer than ten meters from the walkway can be easily confronted. The available modern protection fences systems (Fig. 7D) could be very effective without causing any aesthetic distraction to the sightseeing site. These fences could be installed along the base of the slopes within the limits of the declivity extending between the slope base and the walkway, and can be camouflaged by planting trees or bushes. Along the western part of the walkway, with the larger available base declivity space, gabion boxes embankments (Fig. 7E) can be installed instead of fences. The installation of these embankments is cheap and they require no maintenance expenses, unless they are damaged.

5. Rock slope stability problems in Kastoria lake sightseeing walkway

Unfortunately, the ignorance of the engineering geological characteristics and the underestimation of the stability problems led to the inappropriate land planning design of many other natural sightseeing areas all over Greece (Rozos & Nikolaou, 1996; Koukis et al. 1997; Koukis & Rozos, 1997; Koukis et al., 2005; Loupasakis & Karfakis, 2007). Figure 8 presents as an example, the sightseeing site of Kastoria lake walkway exhibiting similar geotechnical problems. The Kastoria lake walkway is a, 8,5 km long, narrow road surrounding the peninsula. The stability problems vary from section to section, but generally they are not so intensive as these reported in Arvanitia walkway. The slopes are sorter and gentler and the distance between the base of the slope and the road is sufficient

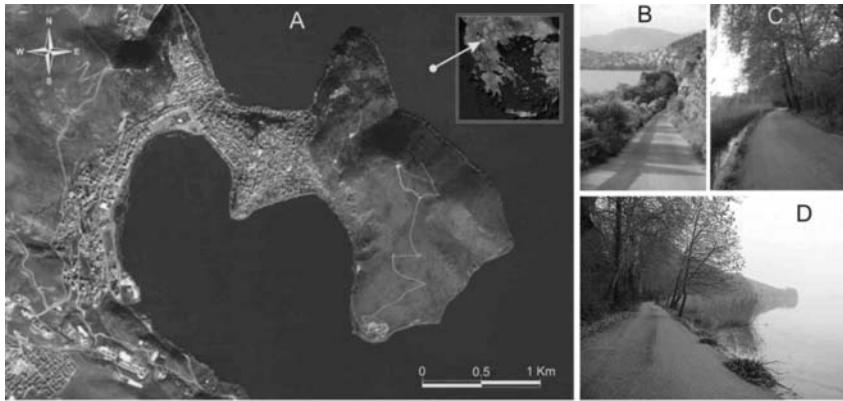


Fig 8.: A) Satellite pictures - taken from Google Earth - pointing the Kastoria peninsula surrounded by the, 8,5 km long, lake walkway, B, C and D) variant views of the walkway sections.

for the installation of proper protection measures, such as metallic fences, sort concrete walls or excavated trapping ditches (Fig. 8C & D). Limited sections with steep slopes (Fig. 8B) can be protected with wire nets, without causing serious aesthetic alteration to the site because of their reduced contribution to the total length of the road. Most of the before mentioned geotechnical problems could have been avoided if during the construction of the road the condition of the rockmass was taken under consideration. For example the road could have been constructed 1m higher in order to give space for a trapping ditch. Also, due to the shallow depth of the lake, limited section could have been constructed over the lake, avoiding the excavations.

6. Conclusions – discussion

The stability analysis of the slopes at Arvanitia practically prove that with the present conditions, the examined walkway can be considered as an extremely dangerous sight seeing location. The numerous rock blocks hanging all over the slopes can very easily harm the citizens using the road. A strong earthquake motion or even an intensive rainfall could become the triggering effect of a rockfall (WP/WLI, 1994). Moreover, the climber athletes using the slopes as a practise field could trigger a rockfall by unlocking a wedge with their own bodyweight. As it can be easily understood an incident like that could be fatal for their lives.

The proposed measures are unavoidable going to cause an aesthetic destruction to the site. The installation of netting along the entire slope faces of sections A, B and C is going to cover the natural wildness of the rockmass but also to abolish the numerous birds nesting along the slopes.

Although the morphology of the peninsula, especially along the south side, is steep, the stability problems could have been reduced or even avoided if the walkway was constructed closer to the sea over embankments without disturbing or approaching the slopes, leaving space for the installation of proper protection measures. Obviously, the walkway was designed without taking under consideration the stability problems of the slopes.

As a result, the engineering geological characteristics of the slopes should be taken into consideration when natural sightseeing areas are upgraded for public use. The proper engineering geological study helps land planning of sightseeing sites, to the direction of their correct development. Further

more, proper land planning of the facilities can reduce the hazards and, consequently, can reduce the cost of any slope support measures. It is imperative that the study of engineering geological conditions must precede the land planning and development of these sites .

7. Acknowledgments

This study was conducted in the frame of the Third Community Support Framework of IGME and was financed from the E.E.C. and from the Hellenic State.

8. References

- Andronopoulos B. & Koukis G., 1976. Engineering geology study in the Acropolis area – Athens. *Institute of Geology and Mineral Exploration, Athens*.
- Fotiadis Ad., 2008. Geological study of the urban and the wider Nafplio area, Argolida Prefecture. *Institute of Geology and Mineral Exploration, Athens*.
- Hocking G., 1976. A method of distinguishing between single and double plane sliding of tetrahedral wedges. *Intern. J. Rock Mechanics and Mining Sciences*, 13: 225-226.
- Hoek E., Bray J.W. 1981. Rock Slope Engineering. *Revised 3rd edition, Institution of Mining and Metallurgy, London*.
- Institute of Geology and Mineral Exploration – I.G.M.E., 1982. Geological map of Greece – Nafplio Sheet (Scale 1:50.000). *Institute of Geology and Mineral Exploration , Athens*.
- Loupasakis C., Karfakis J., 2007. Abandoned Quarries in Urban Areas - Safety Assessment and Rational Land Planning Design. *Quarterly Journal of Engineering Geology and Hydrogeology, Geological Society of London , Volume 41: 109-117*.
- Koukis G., Sabatakakis N., Nikolaou N., Loupasakis C. 2005. Landslide hazard zonation in Greece. In: Sassa k, Fukuoka H, Wang F, Wang G (eds) *Proceedings of open symposium on landslide risk analysis and sustainable disaster management in the First General Assembly of International Consortium on Landslides, Springer-Verlag, Berlin*, pp 291-296.
- Rozos D., Nikolaou N., 1997. Geotechnical investigation for the preservation of Chania Venetian Fortress site, Crete-Greece. *Proc. of Arrigo Croce Memorial Symposium (Naples, Oct. 3/4, 1996), A.A. Balkema, Vol.1, pp.287-292. Rotterdam*.
- WP/WLI (International Geotechnical Societies' UNESCO Working Party on World Landslide Inventory). 1994. A suggested method for reporting landslides causes. *Bulletin of the International Association of Engineering Geology*. 50, 71-74.
- Koligri E., 2008. Engineering geological – hydrogeological conditions and stability problems at the Nafplio castle. *Diploma Thesis of the School of Mining and Metallurgical Engineering, NTUA*. Supervisor professor: Rozos D., pp. 115. Athens.

UPPER QUATERNARY EVOLUTION OF THE NORTHERN ARGOLIS GULF, NAFPLIO AREA

Mitropoulos D.¹ and Zananiri I.¹

¹ Institute of Geology and Mineral Exploration (I.G.M.E.), Spirou Loui 1, Olympic Village, 3rd Entrance, 136 77 Acharnae, Greece, dmitropoulos@igme.gr, izanan@igme.gr

Abstract

The recent palaeogeographic history of the Gulf of Argolis was studied by means of marine geophysical surveys and sediment sampling for subsequent laboratory analyses. Data interpretation suggests a relatively smooth seafloor gradient, characterized by an amphitheatrical pattern of the sea bottom. Prominent beetling features comprise the Bourtzi islet near Nafplio coast, small ridges in the southern margin of the studied area, and several conical ridges in the central part of the gulf. Four unconformities were identified, defining four different sedimentary units. Granulometry measurements allowed the mapping of present-day seafloor sediment distribution, where fine sediments prevail; the only exception was observed at the eastern coastal areas, where sand content reaches 70%. Contouring of granulometry statistical parameters highlights a NW towards SE transfer of fine-grain sediments. Finally, taking into account the results of the present study and all available information for the broader area, a model for the Upper Quaternary palaeogeographic evolution of the Argolis Gulf was constructed.

Key words: Upper Quaternary, marine geophysics, seismic profiles, bathymetry, stratigraphy, Aegean Sea, Argolis Gulf

1. Introduction

The Institute of Geology and Mineral Exploration (I.G.M.E.) of Greece, in the frame of “Community Support Framework 2000 – 2006”, Operational Program “Competitiveness”, implemented the project called “Collection, codification and documentation of geothematic information for urban and suburban areas in Greece. Pilot studies”. In the framework of sub-project 3 “Integrated geological, geotechnical, hydrogeological, geochemical, geophysical and marine studies of the urban and suburban pilot area of Nafplio, Argolis municipality”, marine geology research was carried out at the Gulf around the broader Nafplio area (Andrinopoulos et al., 2008). This paper presents the Upper Quaternary stratigraphy and paleogeographic evolution during the same period of the northern Argolis Gulf (Fig. 1) using high-resolution seismic-reflection profiles and surface sediment sampling.

2. Geological setting

The Argolis Gulf is located off the east coast of Peloponnese, opening into the Aegean Sea. It is surrounded by two prefectures, Arcadia and Argolis. At the head of the gulf we find its principal port, Nafplio, and the mouth of the Inakhos River. Just north of the head of the gulf is the

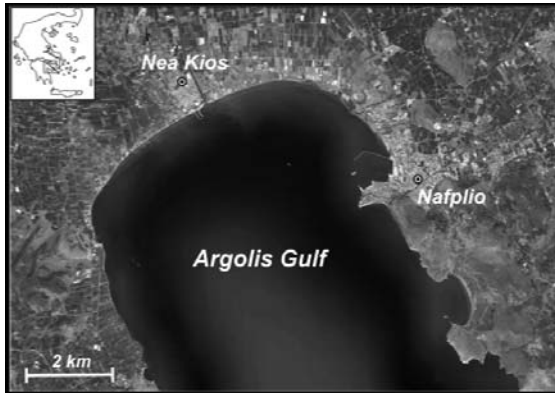


Fig. 1: Satellite image – taken from Google Earth – showing the location of the Argolis Gulf and main topographic features of the broader Nafplio area.

city of Argos, an important Mycenaean and Dorian centre. The prominent topographic features of the gulf are: Bourtzi, a small island in shallow waters with the homonymous castle, and Akronafplia peninsula, bounding from the north Nafplio seaport. The inclination of the slopes surrounding the gulf vary, affected mainly by tectonics, while the wider studied area is characterized by the existence of active and potentially active faults (Georgiou & Galanakis, 2009).

The Argolis peninsula geotectonically belongs to the Pelagonian isopic zone of the Internal Hellenides. It comprises a composite nappe pile (Bortolotti et al., 2003 and references therein) of several imbricated pre-Neogene tectonic units, tectonically assembled in two major distinct tectonic phases, one in the late Jurassic and the other in the late Eocene (Photiades & Skourtsis-Coroneou, 1994). A detailed geological survey in scale 1:5.000 of the greater Nafplio area was carried out by Photiades (2008).

3. Data acquisition

Geophysical data from the Argolis Gulf were collected during a single cruise by the vessel *Agni 3*, in September 2006. The acquisition area covers a rectangular area of 3 km×4.5 km (Fig. 2), with 22 parallel lines in E–W direction, track spacing of 200m, and 4 profiles in N–S direction, track spacing of 500m (for a total of 100 km).

A Geoacoustics 3.5 kHz 10KW high-resolution shallow seismic system (Fig. 3) was used with a resolution of 20-50 cm and an average penetration of 30-40 m. Data were recorded in analogue format with a EPC 9800 graphic recorder. Recording sweep rate and triggering of acoustic waves was set to \square and $\frac{1}{4}$ of a sec respectively. An assumed sound velocity of 1500 m/s was used to derive the water depths and the thickness of subbottom layers (Houtz, 1973). Bathymetric data were collected with a KNUDSEN LED 320M precision depth recorder (12 and 200 kHz), with increased resolution, 10-20 cm, and satisfactory penetration, 30m.

The recognition of seismic sequences and their interpretation are based on the seismic stratigraphic analysis methods outlined by Mitchum and Vail (1977), Sangree and Widmier (1979) and Brown and Fisher (1980). Processing and plotting of the seismic data was carried out at IGME using Surfer software (Golden Software); kriging interpolation was applied. Our knowledge of the oceans from geophysics depends heavily on positioning observations accurately. In the present study a GPS Magellan sportrak map system was used for navigation giving an accuracy of about 5m, which is adequate for sea geophysical studies. To avoid interpretation er-

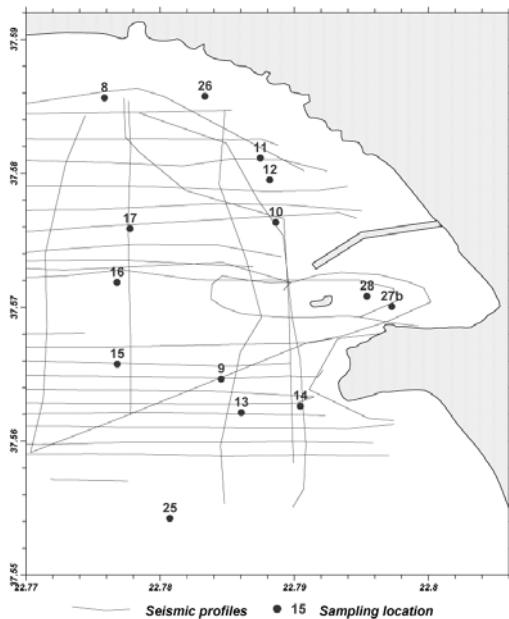


Fig. 2: Index map showing the location of seismic-reflection profiles and numbered surface samples collected from the Argolis Gulf.

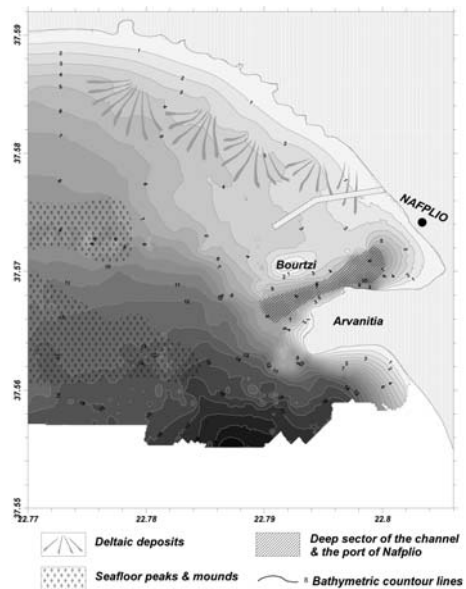


Fig. 3: Present-day bathymetry of the study area, obtained from marine geophysical data. Bathymetric contour lines every 1m.

rors, acoustic response data should be complemented with sedimentological data from surface samples. Thus, 14 samples (Fig. 2), of both fine- and coarse-grained material, from the sea-bottom surface were gathered, using a Dietz la Font and a Van Veen bottom grab samplers.

4. Results

4.1 Bathymetry

Seismic data is generally of good quality and allowed the elaboration of a high resolution, scale 1:5.000, bathymetric map of the northern Argolis Gulf. Bathymetric contour lines are drawn every 1m (Fig. 3). The Argolis gulf is characterized by regular seafloor morphology with an amphitheatric pattern. A maximum depth of 22m, below sea level, is measured, while the steeper inclinations are observed in the southeastern sector of the study area. Prominent feature of the gulf is the mound forming Bourtzi islet, off the coast of Nafplio; it is a ENE-WSW trending elliptically shaped mound, defined by the 2m bathymetric contour line. In the central part of the gulf small underwater conical peaks, of 20-50m diameter and 2m height, are present (Figs. 3 and 4). Another element, worth noting, is the morphology observed throughout the channel between Bourtzi island and Cape Arvanitia, at Akronafplia peninsula. It constitutes a deepening corridor of the channel and the port of Nafplio, with approximately 1200m length, 200m width and 8m depth.

4.2 Sub-bottom structure

Seismic reflection data comprise the most obvious and directly analysed seismic parameter and show the gross stratification patterns from which depositional processes, erosion and palaeo-

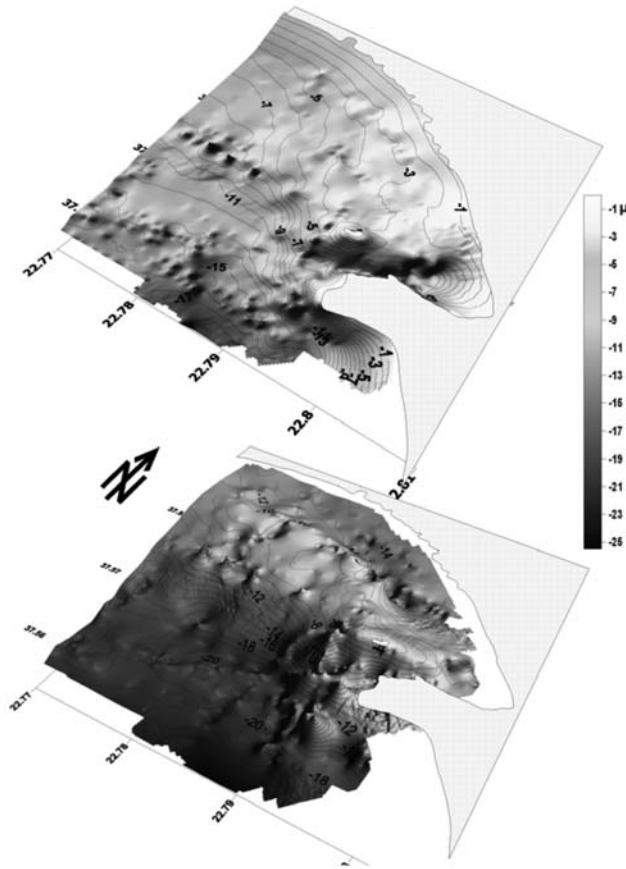


Fig. 4: 3D view of the present-day seafloor morphology (top) and horizon B (bottom).

pography can be determined (Mitchum et al., 1977). Three main seismic reflectors, that define three unconformities (horizons a-c), bounding four seismic units (A-D), are observed in the study area (Figs. 5 & 6). Two examples of seismic profiles are shown in Figures 5 and 6, where the interpreted profiles illustrate the primary seismic stratigraphic and geomorphic elements discussed in the text. The unconformities observed are, from top to bottom the following: Horizon a: The upper unconformity appears as a strong reflector, extending almost everywhere in the study area. It is found at depths varying from 1-6m below present-day sea bottom level, while in places it is wedge-shaped towards the seafloor. This horizon is regular, in general, with erosional features, e.g. old channels, only locally present. Horizon b: A second unconformity is detected in the seismic profiles as a very strong reflector, irregularly shaped, spanning all over the studied area. It is found at varying depths, 1-10m, below the present-day sea bottom surface. This horizon is a very irregular surface, characterized by the presence of old channels and stream beds, dipping 1-8m. The morphological differences between unconformity *b* and the present-day seafloor can be seen in Figure 4. Seismic horizons a and b converge and wedge into the seafloor around the Bourtzi mound. Horizon c: The lower unconformity is detected only around the Bourtzi islet; as we move away from this mound it is steeply dipping, soon exceeding depth penetration of our equipment.

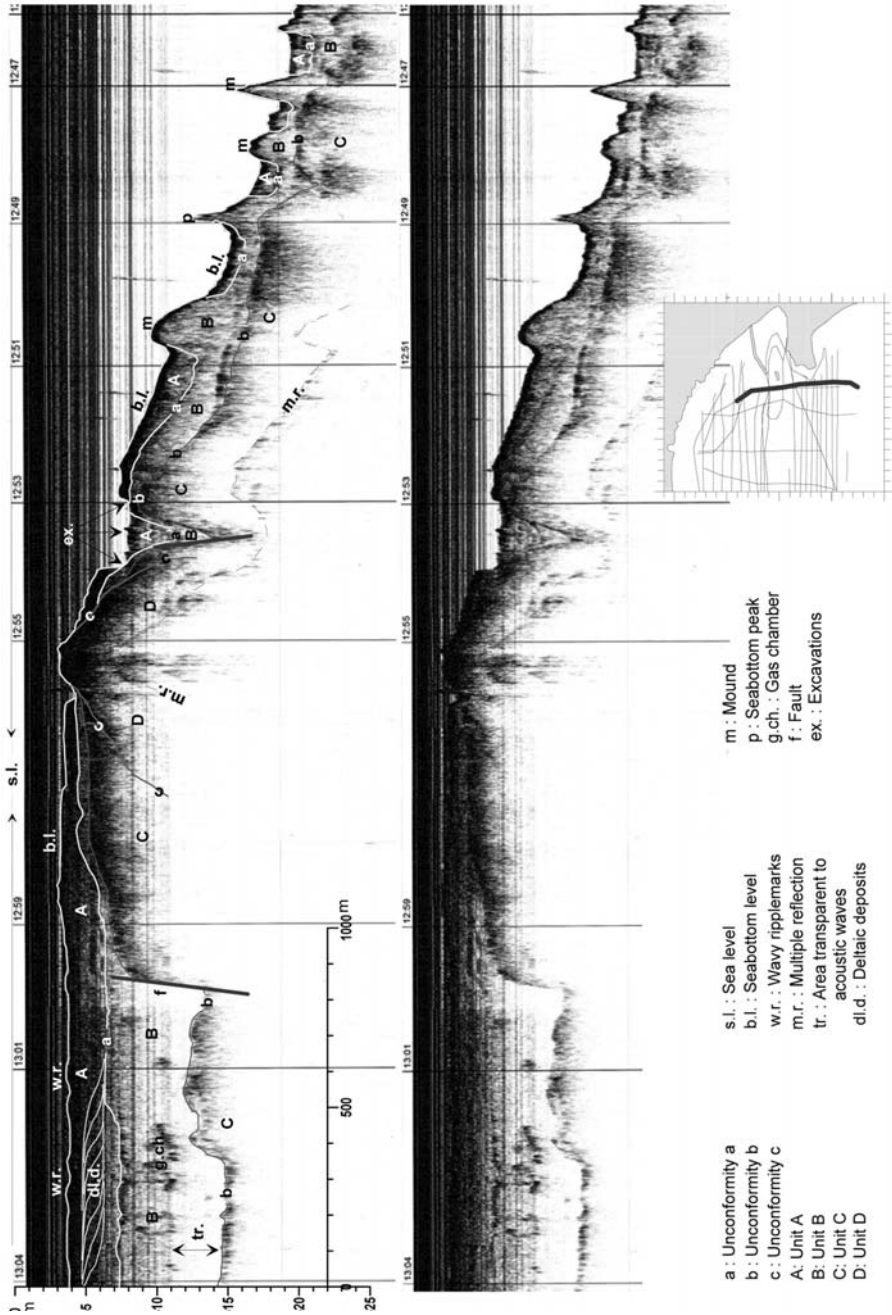


Fig. 5: Interpreted (top) and uninterpreted (bottom) 3,5 kHz seismic reflection profile (SN-12).

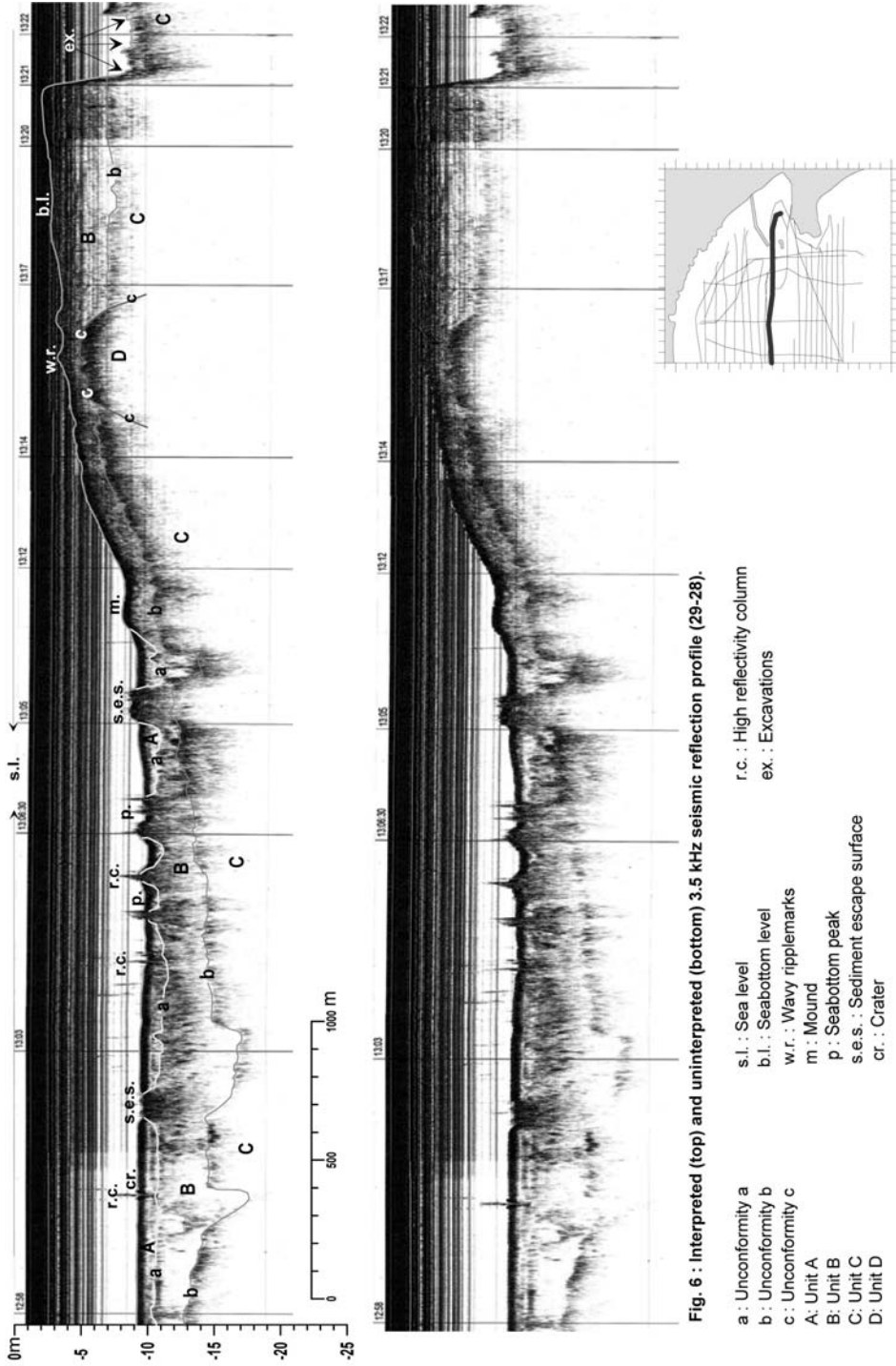


Fig. 6: Interpreted (top) and uninterpreted (bottom) 3,5 kHz seismic reflection profile (29-28).

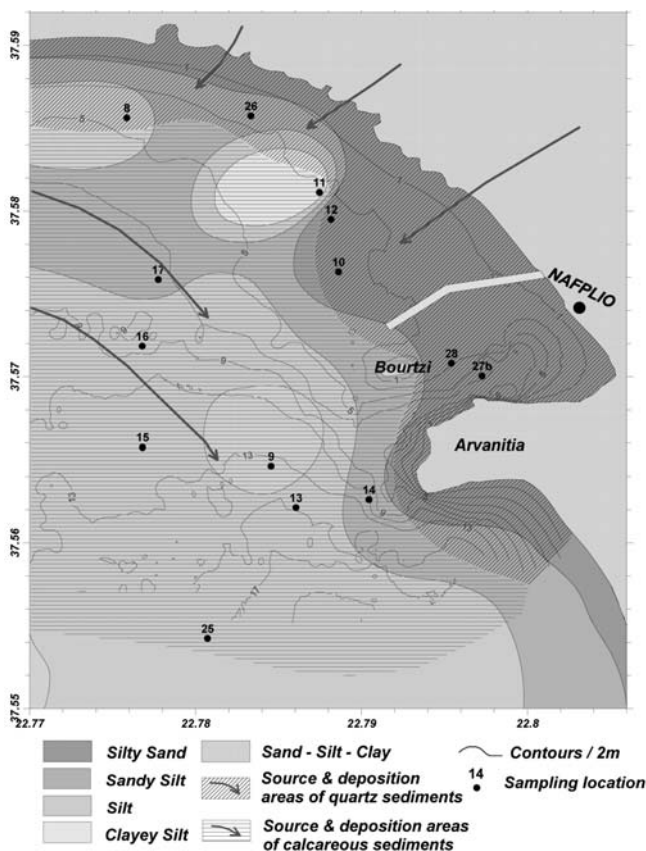


Fig. 7: Sediment distribution over the seafloor surface.

The sedimentary units determined from seismic data are, from top to bottom, the following: **Unit A**: The upper unit comprises mostly fine-grained sediments (silt and clay), while in the coastal areas a gradual transition to more coarse-grained materials is observed. This unit extends over the whole study area, with thickness varying from 0-6m. Its upper limit, which constitutes the present-day seafloor, exhibits locally at 4-7m depth, wavy ripplemarks formed during rough sea periods. At the northeastern part of the gulf, over the base of unit A, well-developed deltaic deposits are observed, with prograding delta characteristics. **Unit B**: Reflectors a and b define a sequence of intercalating coarse- and fine-grained sedimentary layers. This unit, spanning all over the study area, varies in thickness from 0-13m; the smaller values are observed along a zone northwest of Bourtzi mound, while at both sides of this area the thickness is increased abruptly, reaching 12m. In the interior of unit B seismic data indicate the presence of numerous secondary unconformities, old channels and watercourses of rivers filled by younger sediments that are often re-eroded and refilled. In the central and southern regions the emersion of this unit creates small elevations at the seafloor; from the top of these peaks an escape of fluid material into the sea water is observed, while at the regions where this unit is overlain by thin sedimentary layers perforation of unit A and creation of small craters on the sea bottom takes place. The nature of these fluids was not possible to be precisely determined from the existing data. However, from the seismic characteristics it can be deduced that they are probably due to the escape of freshwater that circulates within unit B. Finally, in the interior of this unit there

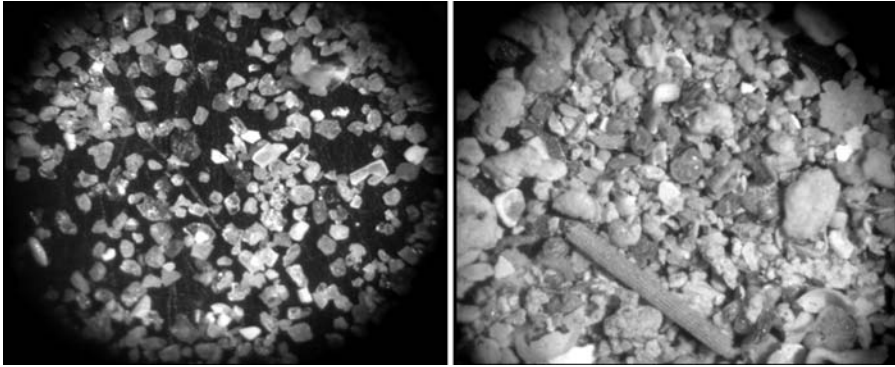


Fig. 8: Representative sediment samples with predominance of quartz crystalloclasts (left) and calcareous rocks lithoclasts (right). Photos from stereoscopic microscope (x20).

are obvious signs of sapropelic deposits and biogenic gases. Unit C: This seismic layer extends almost throughout the gulf, with intense characteristics of erosion over its surface. The thickness was not possible to be thoroughly mapped because it appears opaque to acoustic waves. This unit comprises a cohesive sandstone formation, rich in marine shells. At the eastern part it appears affected by a NW-SE directed fault system, which caused the development of a horst and a graben, both NW-SE trending. Unit D: This seismic unit is only locally detected, around the Bourtzi mound and the Arvanitia coastline, up to 18m depth. It constitutes an extension of the Mesozoic limestones from these regions beneath Unit C.

4.3 . Sediment texture

Granulometry analyses allowed the compilation of a distribution map for sediments of the seafloor (Fig. 7). In this map we can observe the predominance of fine-grain sediments (silts, sandy silts, clayey silts), with the exception of the coastal – and mainly the eastern – areas where sand content increases up to 70%. Examining the statistical parameters (Table 1) derived, using the formulas of Folk (1974), from the granulometry analyses data it is obvious that for the majority of sediments the mean size is less than 4Φ (0.0625mm). The values of skewness, which for all samples exceeds 1Φ , characterizes poorly sorted sediments. Finally, the spatial distribution of statistical parameters indicates a trend for transportation of fine-grained sediments from NW towards SE.

From the microscopic examination of the sand fraction of each sample it is evident that the sediments of the gulf can be divided in two categories, based on their qualitative and quantitative composition. The first group includes coastal sediments, which comprise quartz crystalloclasts and biogenic components in a fraction up to 95% of the total sand content; the second is made up by sediments from the central and southern areas that are characterized by the presence of calcareous rocks lithoclasts and biogenic components up to 95% (Fig. 8). This fact leads to the conclusion that sediments of the first category emanate mainly from erosion of flysch formations from the east and northeastern areas of the Argolis gulf, while the second are mostly products of erosion from calcareous rocks around the northwestern coasts of the gulf. In both cases biogenic material consists of shells and fragments of benthic foraminifera, lamelibranchii, bryozoa, porifera, gastropods, brachiopods, biogenic structures and aggregates.

Table 1. Statistics derived from granulometry analyses, using the formulas of Folk (1974). Depth (in meters) measured from sea level; Mean size $Mz=(\Phi16+\Phi50+\Phi84)/3$; Standard deviation $\sigma I=(\Phi84-\Phi16)/4+(\Phi95-\Phi5)/66$; Skewness $SK1=(\Phi16+\Phi84-2\Phi50)/2(\Phi84-\Phi16)$; Kurtosis $KG=(\Phi95-\Phi5)/2.44(\Phi75-\Phi25)$

Sample	Depth (m)	Mean Size (Φ)	Standard Deviation (Φ)	Skewness (Φ)	Kurtosis (Φ)
08	3.5	5.47	3.08	-0.05	0.95
09	10.5	5.84	3.46	-0.29	0.76
10	3.0	4.08	1.75	0.40	1.97
11	3.0	6.80	2.80	-0.27	1.53
12	4.5	2.88	1.00	0.36	0.69
13	11.1	6.64	1.86	-0.23	1.68
14	9.2	5.20	2.45	-0.12	0.95
15	15.0	7.12	1.05	-0.15	1.49
16	6.5	6.60	2.04	-0.38	1.92
17	6.8	5.24	3.18	-0.53	1.44
25	2.5	5.68	2.73	0.17	1.13
26	2.9	5.17	2.27	0.35	1.21
28	3.3	3.88	3.29	0.15	0.73
27b	6.5	0.76	2.75	0.93	1.20

5. Conclusions - Palaeogeographic evolution

Based on all data and published information (Finke, 1988; Perissoratis & Van Anel, 1988; Perissoratis et al., 2000; Stanley & Vitaliano, 1987; Stanley et al. 1990; Van Anel & Perissoratis, 2006) the palaeogeographic evolution of the Argolis gulf during the Upper Quaternary can be determined:

During the last glacial period, that took place 18,000 years ago, sea level reached a minimum of 120m below the present datum (Fig.9) and thus dry land extended down to this depth. Subsequent melting of ice and important growth of the local hydrographic network resulted in intense erosion of the area and collection of significant amount of sediment from the same area; thus, the sandstones of Unit C were revealed, through a much eroded surface, namely unconformity b.

The presence of a horst, NW-SE directed and dipping towards the NW, played a decisive role in the palaeogeography of the Argolis gulf. After sea regression this horst acted as a barrier and did not allow the total drainage of the adjacent tectonic ditch, resulting in the creation of lakes at the level of -13m down to -15m approximately. These lakes most probably extended northern from the present-day coastline (Fig.10) and linked at the time the northeastern hydrographic network to the northwestern one. The fine-grained sediments deposited by both networks constitute Unit B.

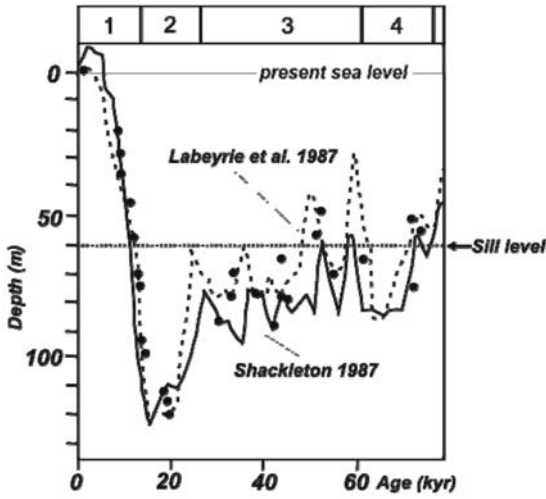


Fig. 9: Global eustatic sea level change during the last 80,000 years (Van Andel & Perissoratis, 2006).

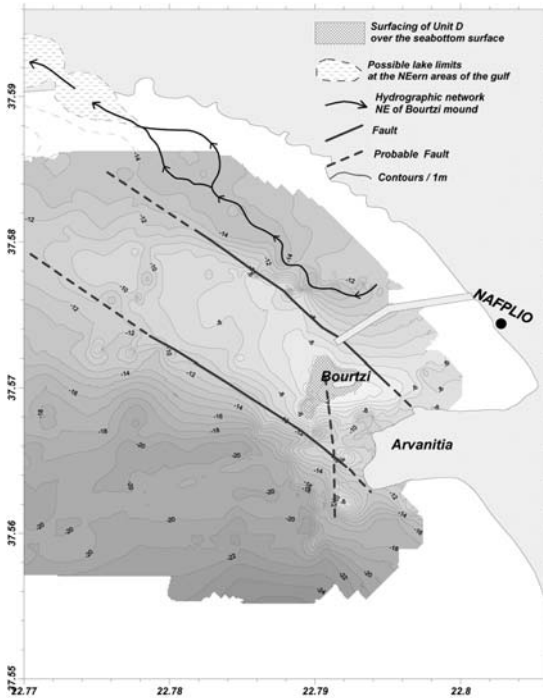


Fig. 10: Topographic and morphologic map of unconformity b.

The continuing melt of glaciers resulted in a rapid rise of the sea level that gradually covered Unit B, which was unconformably overlain – originally at the deeper regions and successively at the shallower ones – by the more recent marine sediments of Unit A.

When the sea level reached the level of the lakes, the latter had been completely filled by the ultrafine-grain material of Unit B. The continuous sea transgression caused a rise in the sea

level up to -5m, covering the whole region of the lakes, creating a lagoon area. In this new environment sediments, transported by the hydrographic network, were deposited as deltaic thrusts over a long period.

Finally, 6,000 years ago the level of the sea reached its present-day status, submerging the lower dry land up to the fringes of the ancient Tiryns mounds. At that time the growth of delta deposits ceases and they are covered by the more recent Holocene marine sediments of Unit A. The constant infill of material resulted in the repletion of shallow lagoons, moving thus the coastline to its current position.

The uninterrupted sedimentation, on-going even today, will result in the continuous expansion of land against the sea. However, at present this phenomenon appears to have slowed down considerably, due to a decrease in rainfalls over the last years and to anthropogenic intervention (e.g. overpumping of the aquifers, interventions in the hydrographic network).

6. Acknowledgements

This study was funded by the Community Support Framework 2000 – 2006 (Operational Program “Competitiveness”). A. Andrinopoulos, E. Zimianitis, P. Zacharaki, S. Maroulakis and G. Efthimiou participated in the geophysical field work. Dr. P. Tsombos, scientific responsible of the project, is warmly thanked for his encouragement and support during the realization of this study.

7. References

- Andrinopoulos, A., Zacharaki, P., Zimianitis, E., Maroulakis, S., Mitropoulos, D. & Efthimiou, G., 2008. Marine geology research in the northern Argolis gulf – Nafplio area, Argolis prefecture. *Institute of Geology & Mineral Exploration, Athens.*
- Bortolotti, V., Carras, N., Chiari, M., Fazzuoli, M., Marcucci, M., Photiades, A. & Principi, G., 2003. The Argolis Peninsula in the palaeogeographic and geodynamic frame of the Hellenides. *Ofioliti*, 28/2, 79-94.
- Brown, L.F.Jr. & Fisher, W.L., 1980. Seismic Stratigraphic Interpretation and Petroleum Exploration. *AAPG Contin. Educ. Course Note*, Ser. 16, 125 pp.
- Folk, R.L., 1974. The petrology of sedimentary rocks, Austin, Hemphill Publishing Co., 182 pp.
- Finke, E.A.W., 1988. Landscape Evolution and the Argive Plain, Greece: Paleoecology, holocene Depositional History and Coastline Changes. *PhD thesis*, Stanford University, University Microfilms, Ann Arbor, Michigan.
- Georgiou, Ch. & Galanakis, D., 2009. Neotectonic and seismotectonic study in the urban and sub-urban regions of Nafplio city (Argolida), *This volume.*
- Houtz, R.E., 1973. *Physics of Sound in Marine Sediments*. Plenum Press, New York.
- Labeyrie, L.D., Duplessy, J.C. & Blanc, P.L., 1987. Variations in the mode of formation and temperature of oceanic deep waters over the past 125,000 years. *Nature* 327, 477–482.
- Mitchum, R.M.Jr. & Vail, P.R., 1977. Seismic stratigraphy and global changes of sea level, part 7: seismic stratigraphic interpretation procedure. In: C.E. Payton (Editor), *Seismic Stratigraphy – Applications to Hydrocarbon Exploration. AAPG Mem.*, 26, 135-143.
- Mitchum, R.M.Jr., Vail, P.R. & Sangree, J.B., 1977. Seismic stratigraphy and global changes of sea level, part 6: stratigraphic interpretation of seismic reflection patterns in depositional sequences. In: C.E. Payton (Editor), *Seismic Stratigraphy – Applications to Hydrocarbon Exploration. AAPG*

- Mem.*, 26, 117-133.
- Perissoratis, C., & Van Andel, T.H., 1988. Late Quaternary alluviation and soil formation and soil formation in the southern Argolid: In history, causes and archaeological implications. *Journal of Archaeological Science* 11, 281-306.
- Perissoratis, C., Piper, D.J.W. & Lykousis V., 2000. Alternating marine and lacustrine sedimentation during Late Quaternary in the gulf of Corinth rift basin, central Greece. *Marine Geology* 167, 391 – 411.
- Photiades, A. & Skourtsis-Coroneou, V., 1994. Stratigraphic and paleogeographic evolution of the Northern Argolis (Greece) during the Cretaceous - Paleogene. *Bull. Geol. Soc. Greece*, vol. XXX/2, 135-146.
- Photiadis A., 2008. Geological study of the urban and the wider Nafplio area. Argolida Prefecture. *Institute of Geology and Mineral Exploration*, Athens.
- Sangree, J.B. & Widmier, J.M., 1979. Interpretation of depositional facies from seismic data. *Geophysics*, 44, 131-160.
- Shackleton, N.J., 1987. Oxygen isotopes, ice volume and sea level. *Quat. Sci. Rev.* 6, 183–190.
- Stanley, D.J. & Vitaliano, C.J., 1987. The landscape of the southern Argolid. In: Van Andel, T.H. & Sutton, S.B. (eds) *Landscape and People of the Franchthi Region. Excavations at Franchthi Cave*, Greece, 2, Indiana University Press, Bloomington, 1- 62.
- Stanley, D.J., Zangger, E., & Perissoratis C., 1990. Quaternary transgressive/regressive cycles in the gulf of Argos, Greece. *Quaternary Research*, 34, 317-329.
- Van Andel, T.H. & Perissoratis, C., 2006. Late Quaternary depositional history of the North Evvoikos Gulf, Aegean Sea, Greece. *Marine Geology*, 232, 157-172.

REMOTE SENSING APPLICATIONS IN THE FRAME OF “URBAN GEOLOGY” PROJECT

Nikolakopoulos K.¹, Tsombos P.¹

¹ *Institute of Geology and Mineral Exploration, Olympic Village Entrance C, 13677 Acharnae Athens, Greece knikolakopoulos@igme.gr, ptsombos@igme.gr*

Abstract

In the frame of the “Urban Geology” project of IGME a lot of remote sensing applications were carried out: DSMs creation and accuracy verification, orthorectification of very high resolution satellite data, data fusion, multitemporal and multisensor image analysis, land cover and land use change detection e.t.c. The applications that took place in the pilot case of Nafplio are presented in this study.

Key words: *DSM, orthorectification, fusion, multitemporal data, Corine Land Cover.*

1. Introduction

One of the major projects of the Institute of Geology & Mineral Exploration (IGME) regard a modern issue of geology called “Urban Geology”. In the frame of that project there was a need for a high accuracy Digital Surface Model “DSM” covering the whole country and update high resolution satellite data for the prefectures capital cities. Thus, many remote sensing applications were carried out: DSMs were created from different satellite data and accuracy control was done. The DSMs and the derived products were compared with respective data from topographic maps and airphoto stereopairs. The DSMs were used for the orthorectification of high resolution images and other applications such as slope and aspect map creation, environmental planning et.c. High resolution (Ikonos and Quickbird) data was also orthorectified. Those data is used for the land use classification, land cover change detection and the urban area mapping. Land cover change detection was done using multi-temporal and multisensor satellite data covering the last thirty years. For the broader area of Nafplio all the changes that occurred in the urban and suburban area were detected and mapped. The urban expansion rate was estimated and the human interferences in the natural landscape were recorded. Land use classification and change detection was also done. The scope of this study was to briefly describe all the remote sensing applications carried out in the frame of “Urban Geology” project.

2. DSM creation from satellite data and accuracy control

For the purposes of “Urban Geology” project there is need for a high accuracy DSM. The DSM should be used for the orthorectification of high resolution images and other applications such as slope map creation, environmental planning et.c. Thus, there is a huge pressure for very accurate elevation data covering the entire country surface.

The official sources of elevation data with a Pan-Hellenic coverage are only two: the topographic maps of the Greek Military Service and DSMs created from airphoto stereopairs provided by the Ministry of Agriculture in ASCII format.

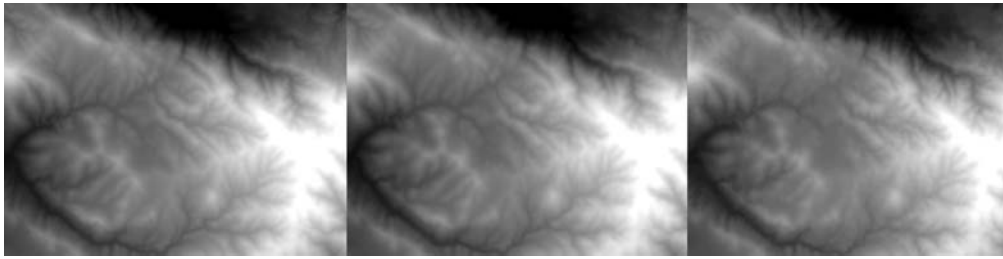


Fig.1: (left): Part of Cartosat DSM with a pixel size of 20m; (middle): Part of Airphoto DSM with a pixel size of 20m; (right): Part of DEM created from the 1/5000 topographic maps with the same pixel size.

The most popular data sources for the creation of DTM are the digitized contours of the topographic maps. The 1:50.000 topographic maps, with a contour interval of twenty meters, present a nominal horizontal accuracy of 20 meters and a nominal vertical accuracy of 10 meters with 90% confidence. The data were in most cases extracted with photogrammetric techniques from aerial stereo-photographs during the 80's. The usual update rate for these maps ranges from ten to twenty years. As a result in many cases a lot of changes have been done during this period and there is a need for updating. The 1:5.000 topographic maps present better nominal horizontal and vertical accuracy as the contour interval is 4m but in many areas there are also intermediate contours of 2 or 1m but the update rate is even worse and most of the maps have been created during the seventies.

The Ministry of Agriculture provide DSMs in ASCII format created from airphoto stereopairs. The pixel size of that DSM is twenty meters and the nominal vertical accuracy ranges between 2 and 3 meters. The data is distributed in tiles of 12 km².

Image stereopairs from satellite sensors seem to provide a quite accurate and cost affordable source of elevation data. Thus we had to assess the accuracy of DSMs created from different satellite stereopairs. DSMs from ASTER, Cartosat and ALOS data were created and compared with the DEM from the 1/5000 topographic maps and the DSMs of the Ministry of Agriculture. Different accuracy controls pointed out that the DSMs created from the Cartosat (Fig. 1) and the ALOS stereopair are suitable for the needs of the Urban Geology project (Tsombos et al. 2008; Tsombos and Nikolakopoulos 2008; Nikolakopoulos et al. 2009). In general, it was proved that the accuracy of the DSMs from ALOS and Cartosat data ranges between 2.5 and 5m and it is comparable with the nominal vertical accuracy of the DSMs of the Ministry of Agriculture.

3. Data fusion

In the frame of "Urban Geology" project of IGME there is need for very accurate remote sensing multispectral data with the maximum spatial resolution context. This data is used for the updating of the existing topographic maps, for land use classification, land cover change detection and the urban area mapping.

Six different fusion algorithms Modified HIS (Siddiqui Y., 2003), Local Mean Method (LMM) (De Béthune et al. 1998), Local Mean and Variance Method (LMVM) presented by (De Béthune et al. 1998), Wavelet (King et al. 2001; Lemeshefsky G., 1999; Lemeshefsky G., 2002), Ehlers (Ehlers M., 2004; Ling et al. 2007; Ehlers et al. 2008) and Pansharp (Zhang Y., 1999) were applied to Quickbird data set in order to assess the quality of the fused products.

The data set covering Nafplio area corresponds to a Quickbird panchromatic image (0.6 m) and its

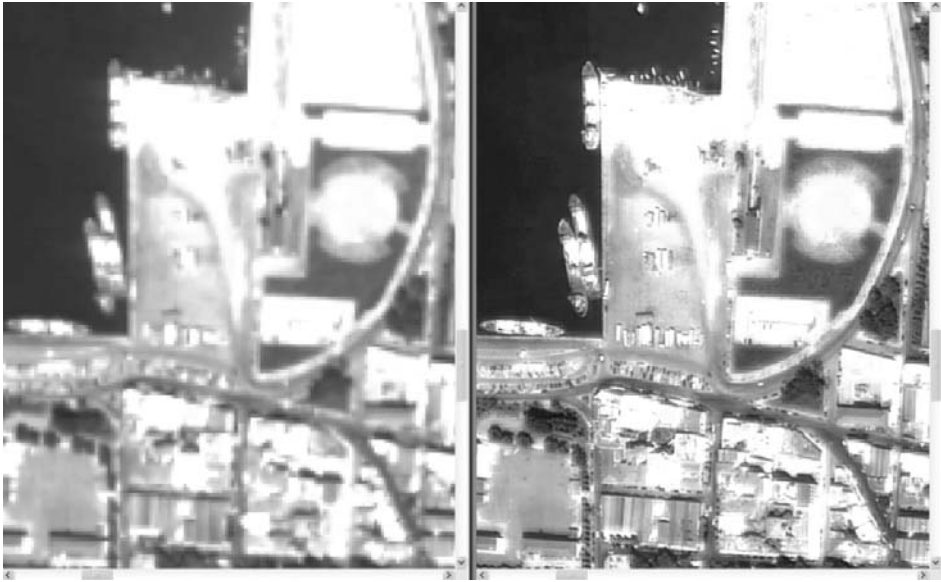


Fig. 2: (left): Part of the original Quickbird image of Nafplio with 0,6m pixel resolution; (right): the fused image with the Ehlers algorithm with the same resolution.

synchronous acquired multispectral channels (2.4 m). The panchromatic band and the multispectral bands have been fused in images that combine the spectral characteristics of the multispectral data with the relatively high spatial resolution of the panchromatic band. In all cases, the nearest neighborhood resampling method was applied. For each fused image the following issues have been examined: a) the visual qualitative result (Fig. 2), b) the statistical parameters of the histograms of the various frequency bands and c) the correlation coefficient. Those criteria are in accordance with the general quality assessment criteria that were described in previous studies (Wald et al. 1997, Chavez et al. 1991). It was proved (Nikolakopoulos and Tsombos, 2009) that all the above mentioned algorithms are suitable for the fusion of Quickbird data.

4. Multitemporal and multisensor image processing

In this contribution, the potential and the restrictions of combined optical air and spaceborne imagery for digitally measuring the urban expansion of Nafplio city in the last thirty years was assessed. For this work, the spatial resolution of the available images is, besides the time period between the acquisitions, the most crucial parameter. Minor or major changes have to be identified from the available images with predefined resolution. So there was a necessity to use images that cover the broader area with a similar spatial resolution.

4.1 Data sets used

In order to locate and map the urban expansion we have used satellite data and topographic maps of the Hellenic Army Geographical Service (1/5:000 scale). The remote sensing data used are the following:

- A quickbird multispectral image with a spatial resolution of 0.6m acquired on 3/9/2003.



Fig. 3: Airphoto mosaic from the Ministry of Agriculture.



Fig. 4: The declassified aerial image.

- An airphoto mosaic from the Ministry of Agriculture (Fig. 3). The data is distributed in tiles of 12 km² with a spatial resolution of 1m. The mosaic was created from airphotos acquired on 2000.
- An orthorectified Landsat 2 MSS image acquired on 21 /8 /1977 with a spatial resolution of sixty meters.
- A declassified aerial image acquired at 12/7/1975. Declassified Satellite Imagery consists of approximately 50,000 images that were taken from 1963 to 1980. These photographic images were collected by the KH-7 Surveillance System and the KH-9 Mapping System. The images have variable scales and the image quality can be variable. Cloud cover is common. The film and print products are produced from a duplicate negative source. The specific image was acquired from the KH-9 Mapping System and it has a nominal resolution that ranges between 20 and 30 feet (6-9 meters). The film was scanned at 7 microns and its final size overpassed 1.3GB (Fig. 4).



Fig. 5: The orthorectified aerial image of Nafplio at 1/25.000 scale.

4.2 Digital image processing

The Quickbird have been orthorectified using ground control points (gcp's) collected with a DGPS. A DEM from the digitized contours from the 1/5000 topographic maps was used for the orthorectification.

The declassified aerial photo was orthorectified taking into account more than 200 gcp's distributed in whole image. The gcp's were collected from an orthorectified Landsat 7 panchromatic image with 15m pixel size. A SRTM DEM has been used for the orthorectification of the image. The resampling method for warping the data was nearest neighborhood interpolation and the new pixel size of 4 meters.

Then the pansharp fusion algorithm was used in order to merge the declassified aerial photo (Fig. 5) with the Landsat 2 MSS image (Fig. 6). The result images (Fig. 7) have an improved spatial resolution of 4m and the spectral characteristics of the original landsat 2 MSS image.

4.3 Urban expansion

In order to map and estimate the intensity and the spatial pattern of urban expansion in Nafplio we digitized the urban boundaries based on two period satellite data obtained in 1977 and 2003 respectively. The urban area was divided into two major categories:

- The urban zone characterized as a dense build – up area.
- The suburban area, surrounding the urban zone and directly connected with it, characterized as a less dense build – up area, compared to urban area.

For the better understanding of the urban expansion spatial pattern, we considered necessary to digitize additionally the transportation network of the covering study area. Digitized roads were grouped into two categories:

- Main roads including primary roads such as national roads, national rural roads, urban streets, etc.
- Local roads including secondary roads such as not connected streets, unpaved roads, tracks, etc.

The following maps represent, in different colors, the urban - suburban zones and the main - local roads located in the broader study area at 1977 (Fig. 8) and at 2003 (Fig.9). Finally, the new constructions during the period 2000 - 2003 were digitized from the Quickbird image (Fig. 10).



Fig. 6: The Landsat2 MSS image of Nafplio at 1/25.000 scale.



Fig. 7: The fused image of Nafplio at 1/25.000 scale.

5. Results

From the GIS analysis of the remote sensing data, the following results were carried out:

The total surface growth of the city is approximately 77% (Zervakou et al. 2008). The urban area growth is almost double (98%, mainly observed north of the city of 1977), while suburban area increased at 61% (mainly observed east of the city of 1977). The results are presented in Table 1.

From 1977 up to 2003, according to satellite data and derived maps, we observe that the clear urban area expanded covering the preexisting suburban area, while the suburban area expanded covering the rural area. The urban area extended to north in parallel with coastal zone which is characterized by beautiful landscapes. This means that urban growth is clearly connected with local morphology and other economic – tourist factors. The suburban area expanded easterly, following the preexisting main road network and becoming at the same time better connected with the vital economic – tourist area of Nafplio city. Since 1977, the road network within the urban and suburban area has become denser and better connected (Zervakou et al. 2008).

During the same period the population of Nafplio city was continuously increasing (30% more residents in 20 years) according to the official inventories (Table 2). The annual rate of the population



Fig. 8: The road network in Nafplio city in 1977. With red colour the Urban zone and with yellow the Suburban zone.



Fig. 9: The road network in Nafplio city in 2003. With red colour the Urban zone and with yellow the Suburban zone.

Table 1. Urban and Suburban area in Nafplio and total difference during the period 1977 -2003.

<i>1977</i>		<i>2003</i>	
Type	Area (km2)	Type	Area (km2)
Urban area	1,031	Urban area	2,038
Suburban area	1,391	Suburban area	2,247
Total area	2,422	Total area	4,285
Total Difference 1977- 2003			1,863 Km2

increase is 1.6%. The rate of new buildings construction during the period 2000 - 2003 was only 0.05%. The total number of the new constructions was 202 (Table 3). From the new buildings 124 were classified as new houses, 5 as pools and 72 as other constructions (Table 4).

The road network for the 1977 was digitized from the 1/5.000 topographic maps. The major road network was increased by 30Km during the period 1977-2003. The local area network was increased by 77km. The total increase of 107 km (Table 5) gives an annual rate of 1.21%.

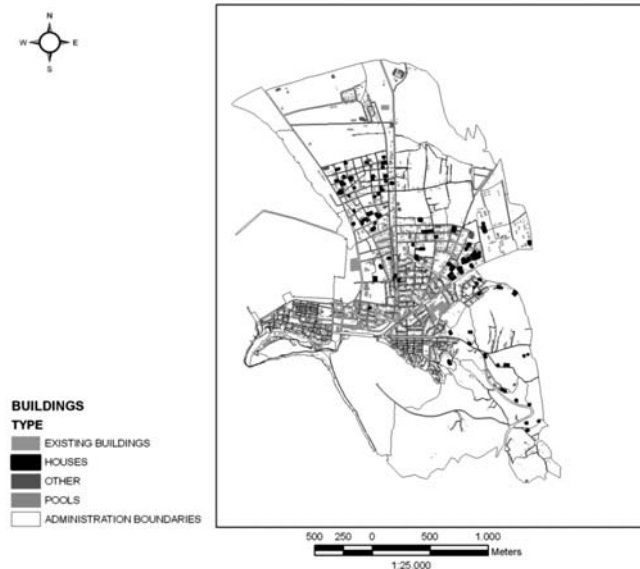


Fig. 10: New buildings in the city of Nafplio from 2000 to 2003.

Table 2. Population of Nafplio city in 1981, 1991, 2001.(source: National Statistical Service).

Year	Population	Difference
1981	10.611	-
1991	11.897	1.286
2001	13.822	1.925

Table 3. Number of constructions in the city of Nafplio.

Year	2000	2003
No of Constructions	3574	3776
Difference		202

Table 4. Type of the new constructions in the city of Nafplio.

<i>Houses</i>	124
<i>Pools</i>	5
<i>Other constructions</i>	72
<i>Total</i>	202

Table 5. Road network in the broader area of Nafplio (length in km).

	1977 (from the topographic maps)	2003
<i>Major road network</i>	215,889	245,720
<i>Local road network</i>	124,456	201,764
<i>Total</i>	340,344	447,484

6. References

- Chavez, P.S. Jr., Sides, S.C., Anderson, J.A., 1991. Comparison of three different methods to merge multi-resolution and multispectral data : Landsat TM and SPOT Panchromatic, *Photogrammetric Engineering and Remote Sensing*, Vol. 57, N° 3, pp. 295-303.
- De Béthune Stanislas, Fabrice Muller, Jean-Paul Donnay, 1998. Fusion Of Multispectral And Panchromatic Images By Local Mean And Variance Matching Filtering Techniques, *Fusion of Earth Data*, Sophia Antipolis, France, 28-30 January 1998.
- Ehlers Manfred, 2004. Spectral characteristics preserving image fusion based on Fourier domain filtering, *Proc. of SPIE* Vol. 5574 p. 1-13.
- Ehlers M., Klonus S., and Astrand P.J., 2008. Quality assessment for multi-sensor multi-date image fusion, *Proc. XXIIth Int. Congr. ISPRS*, Beijing, China p. 499-506.
- King, Roger and Wang, Jianwen, 2001. A Wavelet Based Algorithm for Pan Sharpening Landsat 7 Imagery, 2001. *Erdas Field Guide* 2008. Vol. II pp. 358.
- Lemeshewsky, George P, 1999. Multispectral multisensor image fusion using wavelet transforms, *Proc of SPIE* Vol. 3716, p. 214-222.
- Lemeshewsky, George P, 2002b. Multispectral Image sharpening Using a Shift-Invariant Wavelet Transform and Adaptive Processing of Multiresolution Edges, *Proc of SPIE*, vol. 4736, p. 189-200.
- Ling Y., Ehlers M., Usery L., and Madden M., 2007. FFT-enhanced IHS transform method for fusing high resolution satellite images, *ISPRS Journal of Photogrammetry & Remote Sensing* 61, 381-392.
- Nikolakopoulos Konstantinos G. & Panagiotis I. Tsombos, 2009. "Ameliorating the spatial resolution of high resolution satellite data for use in urban areas". *Urban and Regional Data Management*, CRC Press, Editors A. Krek, M. Rumor, S. Zlatanova & E.M. Fendel, 2009, p.399-408.
- Nikolakopoulos Konstantinos G., Panagiotis I. Tsombos & Lathourakis George, 2009. "Comparison of different along the track satellite stereo-pair for DEM Extraction", *29th EARSeL Symposium*, 14 έως 21 Ιουνίου 2009, Μεσογειακό Αγρονομικό Ινστιτούτο Χανίων. ΠΡΚ υπό Δημοσίευση.
- Siddiqui Yusuf, 2003. The Modified Ihs Method For Fusing Satellite Imagery, *ASPRS 2003 Annual Conference Proceedings*, May 2003 Anchorage, Alaska, In Press.
- Tsombos Panagiotis I., Konstantinos G. Nikolakopoulos & Lathourakis George, 2008. "DEM creation from Cartosat data and comparison to DEM from other sources". 15th International Symposium on Remote Sensing of the International Society for Optical Engineering, 15-19 September 2008 Cardiff, Wales, UK. *Proc. of SPIE*, Vol. 7106 p. 71061C1-12.
- Tsombos Panagiotis I. & Konstantinos G. Nikolakopoulos, 2008. "DEM creation from ALOS data and comparison to DEM from other sources. A case study from Greece". *Proceedings of ALOS 2008 Primary Investigators Symposium*. Unpaginated CDROM
- Wald, L., Ranchin, Th., Mangolini, M., 1997. Fusion of satellite images of different spatial resolutions: Assessing the quality of resulting images, *Photogrammetric Engineering and Remote Sensing*, Vol. 63, N° 6, pp. 691-699.
- Zervakou D Alexandra, Konstantinos G. Nikolakopoulos, Panagiotis I. Tsombos & George P. Papanikolaou, 2008. Monitoring the urban expansion of Sparta and Nafplio cities using remote sensing and GIS techniques, *Proc. of SPIE*, Vol. 7104 p.7104071-12.
- Zhang Y., A new merging method and its spectral and spatial effects, *International Journal of Remote Sensing*, vol. 20, 1999, pp. 2003-2014.

GEOLOGICAL CONTRIBUTION TO THE TECTONO- STRATIGRA- PHY OF THE NAFPLION AREA (NW ARGOLIS, GREECE)

Photiades A.

*Institute of Geology and Mineral Exploration, Olympic Village, 13677 Acharnae, Attica, Greece,
fotiadis@igme.gr,*

Abstract

The geological mapping in scale 1:5.000 in the greater Nafplion area indicated a Tertiary nappe stack of different Pelagonian-originated tectonic units structurally overlying the Subpelagonian series of Argolis Peninsula.

The Subpelagonian series as lower unit is characterized by a shallow-water carbonate platform of Middle Triassic to Early Jurassic age, locally deep-water ammonitico-rosso facies and red cherts and is overlain by a tectono-sedimentary ophiolitic melange of Malm age. After the compressive tectonic phase of late Jurassic, the Nafplion area at that time records a severe extensional intra-Cretaceous syn-rift phase leading to the deposition of diachronous Meso-autochthonous Cretaceous limestone deposits rich in faulted-derived limestone breccias series, topped by deep-water limestone of Campanian-Maastrichtian and then from Lower Tertiary pelagic limestone facies passes upwards into post-Ypresian flysch.

The different Pelagonian telescoped tectonic units were contemporaneously overthrusting north-westward, over the Subpelagonian post-Ypresian flysch sequence, during the Late Eocene compressive phase, are successively characterized by: (a) a middle tectonic unit of a flyschoidal melange of Late Cretaceous-Early Tertiary age, like the Adheres Melange surfaces in Southern Argolis, associated with various carbonate and ophiolite tectonosomes trapped and carried within this highly disrupted terrigenous flyschoidal melange and, (b) an upper unit consists of Cretaceous carbonate slivers bearing serpentinite sole (Palamidi, Akronafplia, Profitis Ilias, Aria) and/or of Middle Triassic-Early Jurassic carbonate platform slices.

The above nappe stacking may be connected with the Eocene continental collision of the Hellenides.

Key words: *extensional intra-Cretaceous syn-rift phase, meso-autochthonous series, flyschoidal melange, carbonate outlier, Nafplion, Argolis Greece.*

1. Introduction

The Argolis peninsula geotectonically belongs to the Pelagonian isopic zone of the Internal Hellenides and forms a composite nappe pile (Bortolotti et al. 2003 and references therein) of several imbricated pre-Neogene tectonic units (Fig.1). However, the transitional paleogeographic environment between the Pindos and the Pelagonian isopic zones, as revealed by the presence of Trapezona and Epidavros Series (Vrielynck, 1978, 1980), places the Argolis peninsula in the Subpelagonian isopic zone (Photiades & Skourtsis-Coroneou, 1994 and reference therein) and only

the thick Cretaceous outliers with serpentinite sole, as an Upper tectonic unit, belong to the Pelagonian isopic zone (Photiades, 1986; Mermighis, 1989).

Particularly, the Mesozoic carbonate sequences and the flysch successions in the Nafplion area (Fig. 2a) were interpreted by Tataris et al. (1970) as being continuous stratigraphic sequence successions. However, recognition of various Mesozoic carbonate sequences with flysch differences lead to the realization that the continental collision in this part of the internal Hellenides was a more complex tectono-sedimentary series of events than originally suspected.

The work undertaken was based on large scale (1:5.000) geological mapping covers 50 km² of the broad area of Nafplion city (Fig. 3), with a view to elucidate the previous geological ambiguities, to reexamine critical contacts of small areas heaving complex boundary conditions, and to establish of its comprehensive tectono-stratigraphy.

2. Previous investigations and structural setting

Dercourt (1964) viewed the entire Triassic-Jurassic carbonate formation (Serie de Trapezona) of Argolis as being allochthonous and separated from the Gavrovo-Tripolis zone by high-angle faults. Süsskoch, (1967), Bannert & Bender (1968) and Bachmann & Risch (1979) considered the Triassic-Jurassic carbonate facies differences to reflect basinal and platformal areas within an autochthonous heterogeneous carbonate platform. This kind of carbonate facies differences is being interpreted by Tataris et al. (1970) as a transitional paleogeographic domain between Subpelagonian and Pindos isopic zones. However, Aubouin et al. (1970) placed the Argolis area in Subpelagonian zone.

The Triassic-Liassic deep-water limestones (calcaires d'Epidaure) have been considered by Vrielynck (1978, 1980) and Baumgartner (1985) as being allochthonous, tectonically overlying a homogeneous carbonate platform. Moreover, the last author considered these strata to represent the eastern continental margin of the Pelagonian platform and proposed a subsequent emplacement of these deep-water limestones into the platform during Late Jurassic orogenesis. Baumgartner (1985) subdivided further the neritic platform sequences into two units, an external Adhami Basal Sequence and an internal Dhidhymi-Trapezona Basal Sequence distinguished on the basis of overlying ophiolite-derived clastics and an allochthonous ophiolite thrust sheet, which is not found over the external Adhami Basal Sequence, surfaced around Nafplion area and interpreted the above two juxtaposed units as being the result of strike-slip faulting.

The nature of sedimentation changed abruptly in Early Jurassic times with hemipelagic deposition of ammonitico-rosso limestone, interpreted as regional collapse of the platform and continued subsidence giving rise to the accumulation of radiolarian cherts in Middle-Upper Jurassic times (Baumgartner, 1985; Bortolotti et al., 2003).

The obduction of Argolis ophiolitic nappe would originated from Pindos zone (Robertson & Dixon, 1984; Clift, 1996) or from Vardar zone (Dercourt et al., 1993; Bortolotti et al., 2003; Bortolotti & Principi, 2005) in late Upper Jurassic time and was manifested by the deposition of ophiolite-derived debris flows and turbidites generated by the advancing thrust sheet of pillow lavas nappe (Baumgartner, 1985; Photiades, 1986; Photiades, 1989; Dostal et al., 1991; Capedri et al., 1996) with T-MOR and N-MOR basalts affinities of Triassic to Jurassic ages (Bortolotti et al., 2002, 2003; Saccani et al., 2004).

A hiatus in sedimentation after obduction was succeeded by a diachronous carbonate transgression, over a formerly tectonized sub-marine palaeorelief where the Meso-autochthonous sedimentary se-



Fig. 1: Geological simplified map of Argolis. Modified from Bortolotti et al. (2003). 1: Triassic-Jurassic shallow-water limestone (a), Triassic-Jurassic hemipelagic limestone (b), 2: pillow-lava ophiolite nappe, 3: Mesozoic autochthonous series with Cretaceous - Lower Eocene carbonate, 4: post-Ypresian flysch, 5: flyschoidal melange (a) with hemipelagic limestone (b), 6: Cretaceous limestone (b) with serpentinite (a), 7: Upper Miocene to Pliocene sediments (a) and Quaternary sediments (b), Φ_1 : late Jurassic tectonic phase and Φ_2 : late Eocene tectonic phase.

quence of Argolis has been deposited giving rise to the Ligourio, Stamateika, Agios Dimitrios, Midhea-Manesi, Kandhia, Karnazeika, Stavropodi and Mataranga members, which began in the Upper Jurassic age and continued into the Lower Eocene age (Tataris et al., 1970; Vrielynck, 1978, 1982; Bannert et al., 1984; Baumgartner 1985; Photiades & Skourtsis-Coroneou, 1994; Bortolotti et al., 2003). The beginning of the deposition was diachronous. The sequence in its maximum development includes Albian to Cenomanian neritic limestone. The subsidence of the platform is recorded from Turonian times when rapid deepening of the carbonate facies and intra-platform faulting occurred which is characterized by faulted-derived breccias rich in basaltic and red chert clasts, cemented by Campanian-Maastrichtian pink hemipelagic limestone, deposited during this episode, and then from Paleocene up to the Lower-Middle Eocene pelagic to reefal limestone facies passes upwards into post-Ypresian flysch. Events of emergence associated with intensive erosion- with several hiatus- took place during the Late Cenomanian-Early Senonian and the Late Maastrichtian-Palaeocene (Photiades and Skourtsis-Coroneou 1994).

Tectonically upwards in south, central and northwestern parts of Argolis Peninsula several thrust sheets are dominated and structured, from the base to the top, by a prominent flyschoidal melange or Adheres melange after Bortolotti et al. (2003), which is not organised formation and is developed as an intensively deformed arenaceous flysch including blocks of several lithologies. This flyschoidal melange is described as Ermioni Complex after Robertson et al. (1987) and contains various tectonosomes of Mid-Upper Jurassic granodiorite associated with Upper Jurassic limestone (Photiades & Keay, 2000), andesitic volcanic to pyroclastic rocks (Sideris et al., 1987), bearing tectonic slivers of MOR basalts (Robertson et al., 1987; Clift, 1996) of Upper Jurassic age (Bortolotti et al., 2003), ser-

pentinite and pelagic limestone of Campanian-Maastrichtian. Moreover, the flyschoidal melange is locally associated with a deep-water limestone of Aptian-Maastrichtian age (Clift and Robertson, 1990b), and passes conformably upwards into calcareous and terrigenous turbiditic flysch deposits of Maastrichtian – Paleogene age (Susskoch et al., 1984), Paleocene and Paleocene-Eocene ages (Christodoulou, 1972; Bachmann & Risch, 1979). However, Clift (1996) agrees with the data of Bachmann & Risch (1979) and Bortolotti et al. (2003) found a Late Cretaceous age (probably Campanian).

Finally, the flyschoidal melange is tectonically overlain by an Upper tectonic Unit (Photiades, 1986; Mermighis, 1989) or Faniskos Unit (Bortolotti et al., 2003), which consists of schistose serpentized harzburgite tectonic “melange” including various boninitic and metamorphic rocks (Photiades 1986, Dostal et al., 1991; Saccani & Photiades, 2005), and is overlain upwards by several transgressed shallow-water carbonate sequences of (a) Kimmeridgian-Portlandian age (Decrouez et al., 1983; Tsaila-Monopolis et al., 1992), (b) via a conglomeratic and/or a lateritic episode by a thick neritic Cretaceous limestone sequences, range from Barremian to Turonian, topped by reddish hemipelagic limestone of Middle Maastrichtian age (Akros formation, Palamidi formation and Faniskos formation; Fourni formation; Decrouez 1976, 1977 a, b; Charvet et al., 1976; Philip et al. 1989; Gaitanakis and Photiades, 1993; Photiades and Skourtsis-Coroneou 1994; Gaitanakis et al. 2007) and, also (c) of deep-water limestones of Aptian-Maastrichtian age (Decrouez 1976, 1977c; Clift & Robertson, 1990b; Gaitanakis et al. 2007) pass up rapidly into terrigenous flysch of Middle-Upper Maastrichtian age (Mermighis, 1989).

On the other hand, Clift & Robertson (1990a, b) affirm that all the Mesozoic platform carbonate units and their overriding thrust sheets form part of a single tectonostratigraphic succession of Pelagonian zone. Later, Clift (1996) modified the previous scheme as regards to the Adheres area where Triassic-Jurassic carbonate unit with its ophiolitic Upper Jurassic melange are “conformably and uncomformably” overlain by the Akros Formation platform and basin carbonate facies and then by the “turbiditic flysch of the Ermioni Complex” (also the Cretaceous slope limestones of the Poros Formation would be the base of the Ermioni Complex).

3. Tectono-stratigraphy

Observations

In the study area, Tataris et al. (1970) show that over a unique and undifferentiated Tertiary siliceous turbiditic flysch sequence (Fig. 2a), which is floored by a single continuous Cretaceous sequence (Palamidi, Akronafplia, Aria, Karathonas), is consistently thrust by sheets of Triassic-Jurassic limestones and assigned them as cherty deep-water carbonates originated from the para-autochthonous Triassic-Jurassic limestones sequence.

Remapping of this area shows (Fig. 2b and 3), however that this Tertiary siliceous turbiditic flysch sequence (coded as fg1 in Fig. 3) appears to a great extent in the NE part of Lefkakia area. At this outcrop the flysch is highly cemented, thin-medium bedded, coarse-fine grained sandstone turbidites, dominated by polycrystalline quartz debris. The source terrain of the flysch is obviously to be the metamorphic basement of the Pelagonian zone, lying to the northeast, as the only known source for the abundant polycrystalline quartz. The total thickness of the flysch around Nafplion is given by proposed cross-section (Fig. 3, C) where must be an underlying concealed sequence of Karathonas limestone (coded as Ki-s.c and Ks.k1 in Fig. 3), the ophiolitic-derived clastic formation (coded as Jm-s.mg) and the basement with Triassic-Liassic Trapezona platform (coded as Ts-Ji.k.d).

The widespread ophiolite-derived clastics of Malm age (Baumgrtner, 1985; Bortolotti et al., 2003

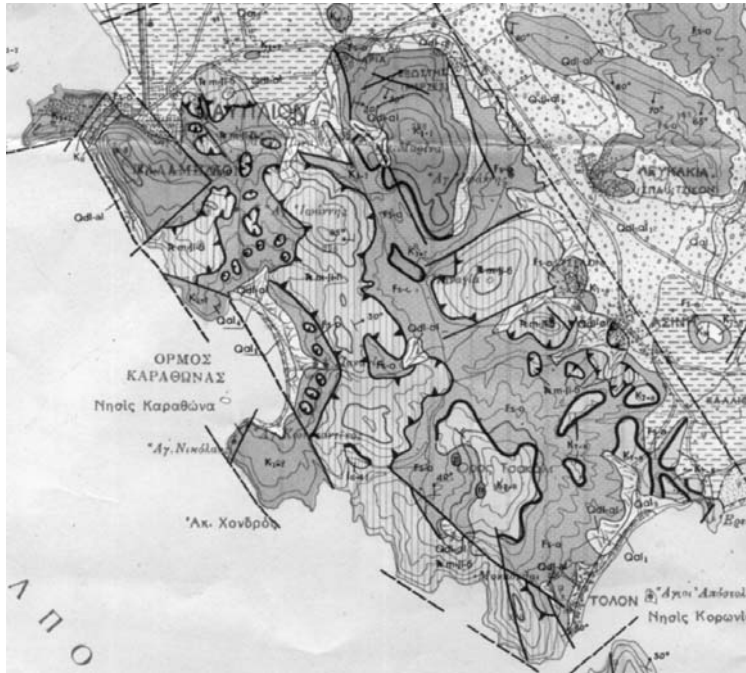


Fig. 2a: Extracted geological part from geological map of Nafplion sheet in scale 1:50.000 (Tataris et al., 1970). Undivided Tertiary siliceous turbiditic flysch (fs-o), Cretaceous sequence (K1-7, K7-8), serpentinite (π) and Middle Triassic-Liassic bearing chert limestone (Tm-Ji-6).

and references therein), outcrop as tectono-sedimentary ophiolitic melange succession, lie above the drowned platform sequence of the Trapezona, which appears at the western and northern parts (between Palamidi and Aria mountains) of the study area (Fig. 2b, sections a, c).

The Karathonas limestone sequence (northern and southern parts of Karathonas bay) of Cretaceous-lower Eocene age is unconformably developed over the ophiolitic-derived clastic formation and the basement of Triassic-Liassic Trapezona platform (Fig. 2b, sections c, d). The Karathonas limestone sequence is a coarse calcareous dominated conglomerate, cemented in a matrix of reddish micritic limestone, provided by shallow-water fault limestone breccias, whilst more thickly bedded, redeposited limestones replace shallow-water packstones. They show evidence of a sharp increase subsidence and intra-platform faulting in Turonian time marked by interval of breccias and can be related of regional extension at this time. Above this level the facies deepen markedly so that pink to reddish hemipelagic limestones of Campanian-Maastrichtian to Paleocene age and flysch (coded as fg1 in Fig. 3) sequences are found (at the northward contact-base of the Akronafplia peninsular hill leading to the Nafplion city and at the contact-base between Akronafplia and Palamidi mountains).

Locally, the previous breccias are also developed up to Lower Eocene shallow-water limestone (like Agios Dimitrios and Midea-Manesi formations by Tataris et al., 1970; Vrielynck 1982; or at Anas-tassopouleika area (Ligourio) and then pass up to a post-Ypresian flysch sequence (Photiades & Skourtsis-Coroneou, 1994). Bachmann & Risch (1979) have been documented Paleocene to Eocene ages within the clastics and Bortolotti et al. (2003) have been assigned an Upper Paleocene age within reddish marls at the basal part of the flysch sequence.

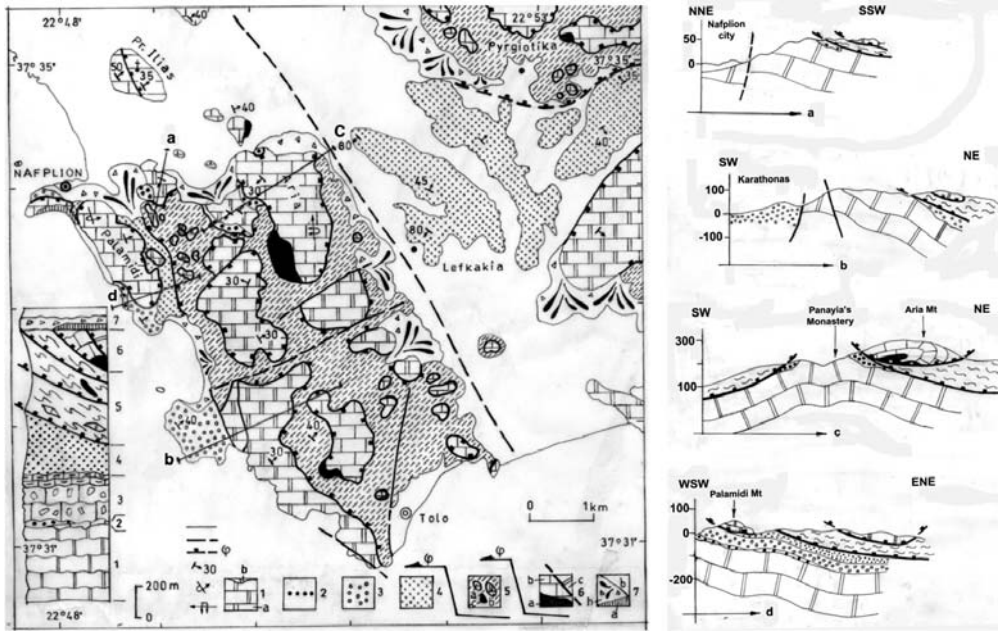


Fig. 2b: Geological simplified map (Photiadis & Mitropoulos, in press), tectono-stratigraphic column and schematic cross-sections (a, b, c and d) of the greater Nafplion area. Lower Unit, 1: Triassic-Jurassic shallow-water limestone (a) with ammonitico-rosso (b), 2: tectono-sedimentary ophiolitic melange, 3: Meso-autochthonous series with Upper Cretaceous - Lower Eocene carbonates, 4: post-Ypresian flysch; Middle Unit, 5: flyschoidal melange complex with Cretaceous carbonate (a), Triassic carbonate (b) and serpentinite (c) tectonosomes, Upper Unit, 6: Cretaceous (b) and Triassic (c) carbonate outliers with serpentinite (a) sole, 7: Tyrrhenian deposits (a), Quaternary sediments (b) and ϕ : late Eocene tectonic phase.

The Triassic-Liassic Trapezona platform, the ophiolitic-derived clastic formation, the unconformably Karathonas limestone sequence with flysch succession belong to the Subpelagonian domain of Argolis (Photiadis & Skourtsis-Coroneou, 1994 and references therein).

On the other hand, the SW and NE (Pyrgiotika) areas (Fig. 2b, 3A) are exclusively composed by a tectonically highly disrupted flysch bearing ophiolitic blocks that may represent a remnant of flyschoidal melange (coded as fl-mg in Fig. 3). More precisely, the flyschoidal melange is composed as marly terrigenous poorly cemented turbiditic flysch, which is mostly composed of sheared debris flow rich of ophiolitic debris, like red chert, basalt and serpentinite, of reworked sandstone debris flow and of various Cretaceous limestone breccias. Bortolotti et al. (2003) found a Late Cretaceous age (probably Campanian) for the Adheres melange surfaces in southeast Argolis.

The Tertiary overriding thrust plane, of the flyschoidal melange above the siliceous turbiditic flysch sequence, has cut strongly down sequence into the Trapezona sequence and could be also represented as out of sequence thrusting, due to the already complicate uplifting of the Subpelagonian Meso-autochthonous series of Argolis, before this Tertiary folding and thrusting of the Pelagonian-derived flyschoidal melange associated with Upper tectonic unit.

Furthermore, the flyschoidal melange of Nafplion area is tectonically overlain by Cretaceous limestone klippens and Triassic-Jurassic limestone slivers.

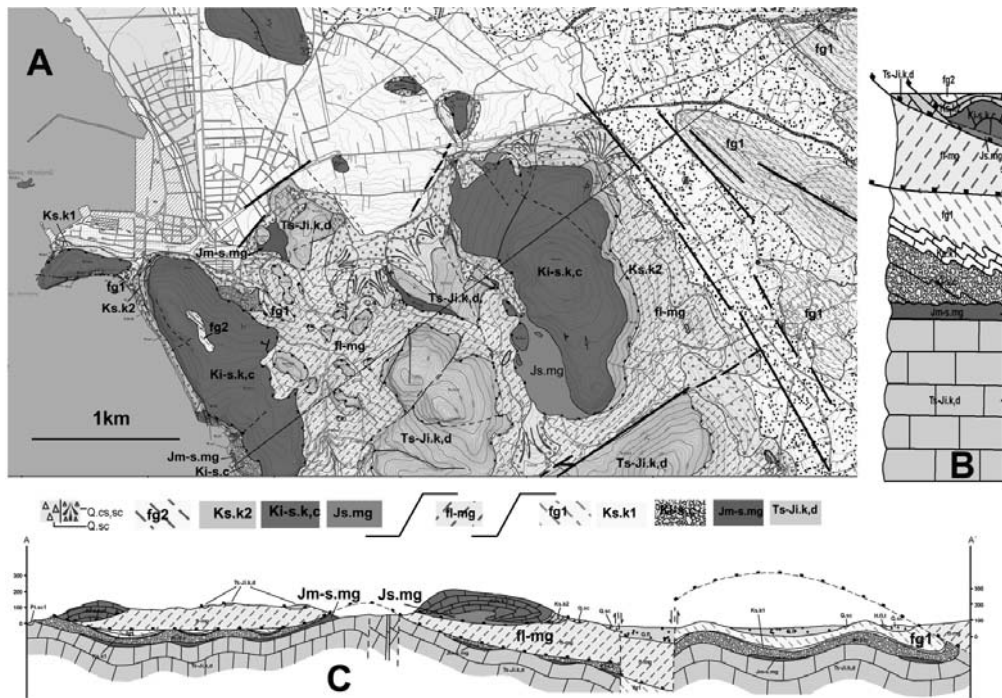


Fig. 3: Geological map (A), tectono-stratigraphic column (B) and geological section (C) of the greater Nafplion area. Lower Unit, Triassic-Jurassic shallow-water carbonate (Ts-Ji.k,d), tectono-sedimentary ophiolitic melange (Jm-s.mg), Meso-autochthonous series with Cretaceous carbonates (Ki-s.c & Ks.k1), post-Ypresian flysch (fg1); Middle Unit, flyschoidal melange complex (fl-mg), probably of Upper Cretaceous age; Upper Unit, serpentinite sole (Js.mg), Triassic-Jurassic carbonate outlier (Ts-Ji.k,d), Cretaceous carbonate outlier (Ki-s.k.c & Ks.k2) with post-Upper Cretaceous flysch (fg2) and late Eocene tectonic phase.

The outcrops of various tectonic sized slices are composed of shallow-water limestone of Triassic-Jurassic age (coded as Ts-Ji.k,d in Fig. 3) that also crops out as basement too and of several tectono-somes of Cretaceous limestone (coded as Ki-s.k,c and Ks.k2 in Fig. 3) bearing serpentinite sole (coded as Js.mg) (Akronafplia, Palamidi and Aria mountains) and confirm that their thrusting was obviously from southeast to northwest and overthrusting also the Pindos flysch in the Argos Castle area that consists of Cretaceous outlier with serpentinite sole too.

The carbonate Cretaceous sequence exposures of the Akronafplia, Palamidi, and Aria Mountains and of several hillocks around Nafplion, such as Profitis Ilias, are clearly thrust sheets or klippen, which lie over the flyschoidal melange. At the base of western part contact-base of Aria massif, a several m-thick conglomeratic formation, including abundant serpentinite and Kimmeridgian neritic clasts, is clearly exposed over serpentinites. Analogous transgressional event is also signalized by Cayeux (1904). Clasts of ophiolitic material are well-rounded in upwards carbonate Barremian sequences. These carbonate Cretaceous sequences are typically massive, thick-bedded bioclastic rocks, suggesting accumulation in a quiet shelf environment from Barremian to pre-Turonian, until a rapid transition to pelagic micrites of Campanian-Maastrichtian age (Dercourt, 1964; Decrouez 1977a, b) towards the top of the section and then pass to post-Maastrichtian calcarenites to marly terrigenous poorly cemented turbiditic flysch, as remnant at the top of Palamidi mountain (coded as fg2 in Fig. 3).

These slices are considered as an Upper tectonic unit originated from the Pelagonian domain (Photiades, 1986; Mermighis, 1989) and are structurally overlying the flyschoidal melange (Bortolotti et al., 2003). Apparently, the flyschoidal melange reached the Nafplion area, shedding debris onto this frontal thrust area, extending from Nafplion to Ligourio depression, but also northward to Tyrintha depression plain outlined in its central part by several Cretaceous age hillocks such as the Prophitis Ilias.

Synthesis

The resulted tectono-stratigraphy of Nafplion area is schematically illustrated in Figures 2b and 3 and comprises the para- and meso-autochthonous Mesozoic series and post-Ypresian flysch of Argolis that belong to the Subpelagonian domain (Aubouin et al., 1970; Photiades et Skourtsis-Coroneou, 1994 and references therein), which is overlapping by a tectonic flyschoidal melange of probably Late Cretaceous age, like Adheres melange (Bortolotti et al., 2003), as Middle tectonic Unit, and finally at top by Cretaceous and/or Triassic limestone outliers with serpentinite sole as Upper Unit originated from Pelagonian domain (Photiades, 1986; Mermighis, 1989). These units were tectonically piled up during the late Eocene or post-flysch compressive period that challenged the whole Pelagonian and Subpelagonian domains (Vrielynck, 1982; Photiades, 1986; Photiades & Karfakis, 1998; Bortolotti et al., 2003).

The three pre-Neogene tectonic units (Fig.3) are from the base to the top as follow:

3.1. Lower Unit

The Lower Unit (Fig. 3A-B) comprises a Middle Triassic to Early Jurassic massively bedded, shallow-water carbonate (Trapezona or Didyma-Trapezona) platform, which is locally followed upwards by condensed reddish nodular pelagic limestones of Toarcian-Bathonian age (Bachmann & Risch, 1979) and is pursued with reddish brown thin-bedded ribbon siliceous mudstones and radiolarian cherts (20-50m thick) of Oxfordian-Kimmeridgian age (Baumgartner 1985; Bortolotti et al. 2003). These deep-sea sediments are generally interpreted to be a reflection of drowning of the platform, and the siliceous sediments are successively developed upwards by a tectono-sedimentary ophiolitic melange succession of Malm age. The ophiolitic melange consists of turbiditic sorted layers of fine-grained distal detritic ophiolitic sediments (5-50m thick) alternating with sorted layers rich in ophiolitic clasts, in addition to thin layers of Kimmeridgian-Tithonian radiolarites. This sequence is followed upward by ophiolitic olistostromes (5-50m in thickness) containing rounded fragments (up to 50 cm in diameter) of boninitic lavas and coarse-grained boninitic-type rocks set in arenitic matrix of various ophiolitic clasts and fragments originated from the underlying limestones and radiolarian cherts. The boninitic lavas and coarse-grained boninitic-type considered to be generated in supra-subduction setting (Photiades 1986; Dostal et al. 1991; Capedri et al. 1996). The presence of such deposit records the paroxysmal tectono-sedimentary events due to early compressional late Jurassic tectonic phase, affecting synchronously the oceanic basin and the Subpelagonian continental margin (Photiades, 1986; Dostal et al. 1991; Capedri et al. 1996; Bortolotti et al., 2003).

The above para-autochthonous succession, in Nafplion area, has undergone during the Cretaceous time important erosion episodes, following by unconformably transgressive deposition of the Cretaceous-Lower Tertiary carbonate sequences (Meso-autochthonous Series), which pass up to a typical post-Ypresian flysch of Argolis (Vrielynck 1981; Photiades 1986; Photiades & Skourtsis-Coroneou 1994; Bortolotti et al., 2003).

A roughly up to 100 m thick Cretaceous to lower Eocene sequence, at Karathonas bay and around

Palamidi and Arvanitia (Akronafplia) foothills, consists of interbedded pelagic limestones, cherts and coarse polymict carbonate breccias sequence including ophiolitic fragments (mainly basalt and serpentinite) and shallow water limestones derived from the below deeply altered and fractured Early Jurassic shallow-water carbonate platform. This coarse ophiolite-carbonate breccias sequence succession evolving progressively into pink and red pelagic limestone rich in Globotruncanidae of Upper Cretaceous – Paleocene age, follows up with the red mudstones of Upper Paleocene age (Bachmann & Risch, 1979; Bortolotti et al., 2003) and then from marly-sandstone to quartz-rich sandstone flysch sequences of post-Ypresian age (Photiades & Skourtsis-Coroneou, 1994).

Furthermore, the coarse polymict carbonate breccias of the Mesoautochthonous Series is interpreted as a channel or canyon fill in a pelagic environment and attests the fact that the ophiolite nappe in the greater area of Nafplion has been completely eroded due to the Cretaceous syn-tectonic events activated by Mesozoic extensional faults (see Fig. 2, like NE-SW Lefkakia graben faulted area). On the contrary, in the eastern and central Argolis areas, the pillow-lavas-bearing ophiolite nappe surfaces and is also unconformably overlain by several heterogeneous Cretaceous series, as well as by post-Ypresian flysch (Photiades 1986; Photiades & Skourtsis-Coroneou 1994).

3.2. The Middle Unit with a tectonic flyschoidal mélange

The Middle Unit (Fig. 3A-B) consists of a tectonic flyschoidal mélange (see Fig. 2b, Pyrgiotika area), which tectonically emplaced above the Meso-autochthonous Series of greater Nafplion area and drifted slices and/or tectonosomes, originated both from continental and oceanic environment, within a flyschoidal matrix. The flyschoidal mélange originated by the tectonic accretion of the innermost exposed Pelagonian continental margin during the late Eocene continental collision of the Hellenides (Bortolotti et al., 2003 and references therein).

Nevertheless, the flyschoidal mélange that developed during the Eocene ensialic tectonic phase tectonically overlies the Meso-autochthonous Series (Bachmann & Risch, 1979; Bortolotti *et al.*, 2003) in central-east Argolis and mainly surfaces in southern Argolis, known as Adheres melanges (see Fig.1), which is characterized by a disrupted turbiditic succession of siltstones, sandstones and marls affected by strong pervasive deformations. Bortolotti *et al.* (2003) suggest an Upper Cretaceous (Campanian) age for this mélange, and Bachmann & Risch (1979) propose an Eocene age formation. However, Clift & Robertson (1990b) and Clift (1996) named the above mélange as Ermioni Complex and consider that is deposited over the ophiolite.

Besides, this mélange incorporates blocks of various natures, including Triassic volcanics, Middle–Late Jurassic radiolarites, Jurassic and Cretaceous limestones, andesites, Jurassic granodiorite, serpentinites and various basalts, originated from the Pelagonian continental margin and the Vardar Ocean (Bortolotti *et al.*, 2003 and references therein).

3.3 Upper Unit with Cretaceous and/or Triassic limestone outliers

An Upper Unit (Fig. 3A-B) emplaced tectonically over the previous ones and synchronously thrust over the flyschoidal mélange, and is composed, at the base, by a schistose serpentinite tectonic sole (up to 100m thick) bearing meter-sized, lens-shaped blocks of basalts, boninitic rocks (Capedri *et al.*, 1996) and various exotic blocks (Photiades, 1986) and, at the top, by an unconformably Cretaceous carbonate sequence cover (up to 350m thick). Furthermore, several Cretaceous limestone (Dercourt, 1964; Decrouez, 1977a, b) outliers such as Palamidi, covered with apparently post-Upper Cretaceous flysch, Akronafplia, Profitis Ilias and Aria with serpentinite tectonic sole, as well as

tectonosomes and/or megablocks of Triassic- Liassic carbonates detached from the shallow-water carbonate sequence of the Subpelagonian Lower Unit and are overthrust the flyschoidal melange (Fig. 3C).

The Upper unit tectonically overlies the post-Ypresian flysch of the Meso-autochthonous series in eastern and central Argolis, as well as the Adheres mélange in south Argolis, where is also tectonically overlain by Kimmeridgian–Maastrichtian carbonate slices of the Upper unit, which are covered, in turn, by a post-Upper Cretaceous flysch.

4. Discussion-Conclusion

The Nafplion area is built by Upper Triassic to Lower Jurassic platform limestone and this series overthrust during the late Jurassic by pillow-lava ophiolite nappe and then the area turned into deeply eroded during Cretaceous times. Upper Cretaceous pelagic and coarse clastic sediments breccias rich in basalts, serpentinites and shallow-water limestones record the important extensional intra-Cretaceous syn-rift phase which affects the Argolis peninsula. These sediments unconformably overlie the Upper Triassic to Lower Jurassic platform limestone and certify the ongoing erosion of the pillow-lavas ophiolite nappe in a high-relief, deeper marine environment.

These Meso-autochthonous series with detrital levels are evolved progressively into pink and red pelagic limestone of Upper Cretaceous. Up section follow of Paleocene limestone interbeds, which are in turn conformably covered by post-Ypresian flysch.

However, the imbricated pre-Neogene stacking units of greater Nafplion area have been caused by the northwestward post-flysch overthrusting of the flyschoidal melange and of the Upper unit over the previous para- and meso-autochthonous Subpelagonian series.

The flyschoidal melange and the overriding Upper tectonic unit could be interpreted as thrust sheet units that record the collapse of the Pelagonian continental margin and Vardar Ocean (Bortolotti et al., 2003), and were contemporaneously thrusting northwestward over the post-Ypresian flysch of the meso-autochthonous Subpelagonian series of Argolis Peninsula (Photiades & Skourtsis-Corneou, 1994; Photiades & Karfakis, 1998).

This post-flysch tectonic phase, of significant geodynamic importance may be connected to the continental collision between Internal and External Hellenides and to the associated Cycladic blueschist belt formation, during the Eocene (Jolivet & Brun, 2010) and leading during the late Eocene to the tectonic accretion of the Subpelagonian and Pelagonian isopic zones in Argolis Peninsula.

Flyschoidal melange and Upper tectonic unit could be interpreted as thrust sheet units, telescoped from Vardar and Pelagonian Zones, towards the northwestern onto the Subpelagonian Meso-autochthonous series of Argolis.

5. References

- Aubouin J., Bonneau M., Celet P., Charvet J., Clement B., Degardin J.M., Dercourt J., Ferrière J., Fleury J.J., Guernet C., Maillot H., Mania J.H., Mansy J.L., Terry J., Thiebault P., Tsoflias P. and Verrioux J.J., 1970. Contribution à la géologie des Hellénides: le Gavrovo, le Pinde et la zone ophiolitique subpélagonienne. *Ann. Soc. Géol. Nord*, 90: 277-306.
- Bachmann, G.H. and Risch, H., 1979. Die geologische Entwicklung der Argolis-Halbinsel (Peloponnes, Griechenland). *Geol. Jb.*, B32: 3-177.
- Bannert, D. and Bender, H., 1968. Zur Geologie der Argolis-Halbinsel (Peloponnes, Griechenland). *Ge-*

- ological et Palaeontologica*, 2, 151-162.
- Bannert, D., Kalkreuth, W., Wallner, P., Risch, H. and Bachmann, G.H., 1984. Ligourion sheet in scale 1:50.000, Geological map of Greece. *Institute of Geology and Mineral Exploration, Athens 1984, Greece*.
- Baumgartner, P.O., 1985. Jurassic sedimentary evolution and nappe emplacement in the Argolis Peninsula (Peloponnesus, Greece). *Mém. Soc. Helv. Sci. Nat.* 99: 1-111.
- Bortolotti, V., Carras, N., Chiari, M., Fazzuoli, M., Marcucci, M., Photiades, A. and Principi, G., 2002. New geological observations and biostratigraphic data on the Argolis Peninsula: palaeogeographic and geodynamic. *Ofioliti*, 2002, 27 (1), 43-46 43.
- Bortolotti, V., Carras, N., Chiari, M., Fazzuoli, M., Marcucci, M., Photiades, A. and Principi, G., 2003. The Argolis Peninsula in the palaeogeographic and geodynamic frame of the Hellenides. *Ofioliti*, 28/2, 79-94.
- Bortolotti, V. and Principi, G., 2005. Tethyan ophiolites and Pangea break-up. *The Island Arc* 14, 442-470.
- Capedri, S., Grandi, R., Photiades, A. and Toscani, L., 1996. "Boninitic" clasts from the Mesozoic olistostrome and turbidites of Angelokastron (Argolis, Greece). *Geological Journal*, vol. 31, 301-322.
- Cayeux, L., 1904. Géologie des environs de Nauplie. Existence du Jurassique supérieur et de l'Infracrétacé en Argolide (Grèce). *Bull. Soc. Geol. France*, (4), 4, 87-105.
- Charvet J., Décrouez D. and Polsak A., 1976. Le Crétacé du Faniskos (Argolide, Grèce). Examen paléontologique, répercussions stratigraphiques, paléogéographiques et tectoniques. *Arch. Sci. Genève*, 29 (3): 247-258.
- Christodoulou G., 1972. The age of some formations of the Poros Island (Argolis, E. Peloponnesos), and their tectonical relation. *Bull. Geol. Soc. Greece*, 8 (2): 163-180.
- Clift, P.D., 1996. Accretion tectonics of the Neotethyan Ermioni Complex, Peloponnesos, Greece. *J. Geol. Soc. London*, 153, 745-757.
- Clift, P.D. and Robertson, A.H.F., 1990a. Deep-water basins within the Mesozoic carbonate platform of Argolis, Greece. *J. Geol. Soc. London*, 147, 825-836.
- Clift, P.D. and Robertson, A.H.F., 1990b. A Cretaceous Neo-Tethyan carbonate margin in Argolis, southern Greece. *Geol. Mag.*, 127: 299-308.
- Decrouez, D., 1976. Étude stratigraphique et micropaléontologique du Crétacé d'Argolide (Péloponnèse, Grèce). *Thèse Univ. de Genève, Suisse*, 157pp.
- Decrouez, D., 1977a. Etude stratigraphique du Crétacé d'Argolide (Péloponnèse septentrional, Grèce). 1- Introduction générale et la formation de l'Akros (domaine ophiolitique externe). *Notes Lab. Paleont. Univ. Geneve*, (3): 1-8.
- Decrouez, D., 1977b. Etude stratigraphique du Crétacé d'Argolide (Péloponnèse septentrional, Grèce). La formation de la Palamede, Sous zone de Trapezona. *Notes Lab. Paleont. Univ. Geneve*, (4): 1-6.
- Decrouez, D., 1977c. Étude stratigraphique du Crétacé d'Argolide (Péloponnèse septentrional, Grèce). 3- La Série du Cap Kastri en Argolide méridionale et conclusions générales. *Note du Laboratoire de Paléontologie de l'Université de Genève, Fascicule, N° 5*, 1-4.
- Decrouez, D., Conrad, M.A. and Vrielynck, B., 1983. Sur la présence de calcaires d'âge jurassique supérieur en Argolide méridionale (Péloponnèse, Grèce). *Eclogae Geologicae Helvetiae*, 76/2, p. 317-325.
- Dercourt, J., 1964. Contribution à l'étude géologique d'un secteur du Péloponnèse septentrional. *Annales Géologiques des Pays Helléniques*, 15, 1-417.
- Dercourt, J., Ricou, L.E. and Vrielynck, B., 1993 (Eds.), Atlas Tethys palaeoenvironmental maps. *Gau-*

thier-Villars, Paris, 307 pp.

- Dostal, J., Toscani, L., Photiades, A. and Capedri, S., 1991. Geochemistry and petrogenesis of Tethyan ophiolites from Northern Argolis (Peloponnesus, Greece). *European Journal of Mineralogy*, vol. 3, 105-121.
- Philip, J., Mermighis, A. & Tronchetti, G., 1989. Nouvelles données stratigraphique et paléogéographiques sur le Crétacé supérieur de domaine Hellénique interne. Le Massif de l' Akros (Argolide, Grèce). *C. R. Acad. Sci. Paris*, 308, 1379-1384.
- Gaitanakis, P. and Photiades, A., 1993. New data on the geology of Southern Argolis (Peloponnesus, Greece). *Bull. Geol. Soc. Greece*, 28 (1): 247-267.
- Gaitanakis, P., Photiades, A., Tsaila-Monopolis, S. and Tsapralis, V., 2007. Geological map of Greece in scale 1:50.000 "KRANIDI-SPETSES sheet". *Athens Institute of Geology and Mineral Exploration*.
- Jolivet, L. and Brun, J-P., 2010. Cenozoic geodynamic evolution of the Aegean. *Int J Earth Sci (Geol. Rundsch.)* 99:109–138.
- Mermighis, A., 1989. Plats-formes carbonatées et récifs à rudistes du Crétacé supérieur de l'Argolide septentrionale (Péloponnèse NE, Grèce). *Thèse Université de Provence*, 171p.
- Photiades, A.D., 1986. Contribution à l'étude géologique et métallogénique des unités ophiolitiques de l'Argolide septentrionale (Grèce). *Thèse de Doctorat de 3^e cycle, Université de Franche - Comte (Besançon)*, n^o 499, 261p.
- Photiades, A., 1989. The diversity of Jurassic volcanism in the inner parts of the Hellenides: The Northern Argolis ophiolitic units (Peloponnesus, Greece). *Bull. Geol. Soc. Greece*, 23/2, 515-530.
- Photiades, A., in press. Revised geological map of Lygourio sheet in scale 1:50.000, Geological map of Greece, B' Edition. *Institute of Geology and Mineral Exploration, Athens, Greece*.
- Photiades, A. and Karfakis, J., 1998. Tectonic evolution of Northern Argolis Peninsula (Greece). *Third Intern. Conf. "Geology of the Eastern Mediterranean"*, Nicosia, Cyprus, September 1998. *Abstr.*, p. 53.
- Photiades, A. and Keay, S., 2000. Mid-Late Jurassic granodiorite basement in southern Argolis Peninsula (Greece): tectonostratigraphic implications. In: *Panayides, I., Xenophontos, C. & Malpas, J. (eds), 2000, Proceedings of the Third International Conference on the Geology of the Eastern Mediterranean. Geol. Surv. Dpt. Cyprus*, 233-239.
- Photiades, A., Mitropoulos, D., in press. Revised geological map of Nafplion sheet in scale 1:50.000 , B' Edition. *Institute of Geology and Mineral Exploration, Athens, Greece*.
- Photiades, A., Skourtsis-Coroneou, V., 1994. Stratigraphic and paleogeographic evolution of the Northern Argolis (Greece) during the Cretaceous - Paleogene. *Bull. Geol. Soc. Greece*, vol. XXX/2, 135-146.
- Robertson, A.H.F. and Dixon, J.E., 1984. Introduction: aspects of the geological evolution of the Eastern Mediterranean. In: *J.E. Dixon and A.H.F. Robertson (Eds.), The geological evolution of the Eastern Mediterranean. Geol. Soc. London Spec. Publ.*, 17: 1-74.
- Robertson, A.H.F., Varnavas, S. and Panagos, A., 1987. Ocean ridge origin and tectonic setting of Mesozoic sulphide and oxide deposits of the Argolis Peninsula of the Peloponnesus, Greece. *Sed. Geol.*, 53, 1-32.
- Saccani, E., Padoa, E. and Photiades, A., 2004. Triassic mid-ocean ridge basalts from the Argolis Peninsula (Greece): new constraints for the early oceanization phases of the Neo-Tethyan Pindos basin. In *Dilek Y. & Robinson P. T. (eds). Ophiolites in Earth History, Geological Society of London Special Publication*, vol. 218, pp. 109–27.
- Saccani, E. and Photiades, A., 2005. Petrogenesis and tectonomagmatic significance of volcanic and sub-volcanic rocks in the Albanide–Hellenide ophiolitic mélanges. *The Island Arc (2005) 14*, 494–516.

- Sideris, C., Skounakis, St. and Simantov, J., 1987. Trace and REE geochemistry of a basic lava series from the Ermioni area (Argolis Peninsula, Greece). *Ofioliti*, 12/1, 107-112.
- Süsskoch, H., 1967. Die Geologie der südöstlichen Argolis (Peloponnes, Griechenland). Diss. Univ. Marburg, Marburg.
- Süsskoch, H., Bannert, D., Kalkreuth, W., Strauss, M., Jacobshagen, V., Fytikas, M., Innocenti, F. and Mazzuoli, R., 1984. Geological map of Greece in scale 1:50.000 "Methana sheet". *Institute of Geology and Mineral Exploration, Athens, Greece*.
- Tataris, A., Kallergis, G., Kounis, G., Bizon, G. and Christodoulou, G., 1970. Nafplion sheet in scale 1:50.000, Geological map of Greece. *Institute for Geology and Subsurface Research, Athens 1970, Greece*.
- Tsaila-Monopolis, S., Csaszar, G., Gaitanakis, P., Bodnar, E., Gorog, A. and Turnsek, D., 1992. Stratigraphy and sedimentary patterns of the Frachti hill, Argolis, Greece. *In: Abstracts of 6th Congress of the Geol. Soc. Greece, IGCP 262-Tethyan Cretaceous platform correlation, Athens, May 25-27, 1992, p.24*.
- Vrielynck, B., 1978. Données nouvelles sur les zones internes du Péloponnèse (Grèce). *Thèse de 3^e cycle, Univ. de Lille, 137pp*.
- Vrielynck, B., 1980. Précisions sur la stratigraphie du Trias d'Argolide (Péloponnèse, Grèce) et conséquences structurales. *Bull. Soc. géol. France, 22, 3, 345-352*.
- Vrielynck, B., 1982. Evolution paleogeographique et structurale de la presqu'île d'Argolide (Grèce). *Revue de geologie dynamique et de geographie physique, 23(4), 277-288*.

AQUEOUS ENVIRONMENT AND EFFECTS ON THE CIVIL AREAS: THE CASE OF NAFPLIO

Sabatakakis P.¹, Koukis G.²

*1 Institute of Geological and Mineral Research, Department of Hydrogeology
sabataki@otenet.gr*

*2 Institute of Geological and Mineral Research, Department of Hydrogeology
koukis@igme.gr*

Abstract

This paper made an effort through the data and conclusions drawn to highlight the impact of the water element, surface and groundwater in urban and suburban area of Nafplio. Through exploratory wells constructed for this reason, water - measurements and water - chemical analysis carried out, made a series of thematic maps which are dimensioned Spatiotemporal rain water flocking to urban and suburban area in case of extreme rainfall events, illustrating the depth, the direction of groundwater flow and the corrosivity of groundwater in relation to the foundations. The accuracy of the figures obtained for surface water and groundwater is a function of time series and the density of the network, and certainly is indicative and could be much more detailed if the network was denser. In any case, this work tries to highlight the value that may have similar operations on urban planning and foundations.

Key words: water points, corrosivity, Langelier indicator.

1. Introduction

This paper was prepared on the basis of hydrogeological work carried out under the project ‘‘Geo - thematic Information of urban and suburban areas of Greece - Pilot Applications’’ and the 6920/005 project which was implemented by the Directorate of Geological Mapping of IGME. The field work included water - measurements, groundwater sampling and research drilling. The laboratory work involved laboratory tests of water samples such as chemical analysis and measurements of underground water from urban and suburban area of Nafplio, all made in the chemical laboratories of IGME.

The final processing of hydrogeological data gathered and taken into account ‘‘other’’ parallel research conducted under this program (Geological mapping, geophysical prospection, geochemical work).

2. Topography – Hydrology Line

The area included in the topographic sheet ‘‘NAFPLIO 1:50.000’’ Edition GMS. The total area examined and directly affecting the rain water to urban and suburban area of Nafplio is 3,32 km². While urban and suburban area was estimated at 0,45 km². The altitude in urban and suburban area varies from 0.50 m to 62 m on slopes Palamidi. The geomorphologic relief has two settings. Bold



Fig. 1: hydrologic map of urban and suburban areas of Nafplio.

rocky and steep south and southeast and flat alluvial origin main new urban and suburban part of Nafplio. Basis of rainfall data of meteorological station Nafplio, which provides the largest time series measurements from 1900, the average amount of annual precipitation is estimated at 525, 3 mm. The direct nearest station of “Pyrgelas” is operating since 1981 and has annual average amount of precipitation 481 mm. Both stations have recorded rainfall of the same region. Their locations are sufficiently different in terms of conditions that could affect rainfall.

From the daily rainfall cards found that in the Argolic field are not unusual, highly events with intensity $i = 60-70 \text{ mm / h}$. The most common duration was around $20' - 40'$. The region which affects rain water to urban and suburban area, divided into five (5) sub areas (Figure 1).

Location “A” that extends in the north - north slope Palamidiou with surface drainage section $0,19 \text{ km}^2$ region of interest and is the most extensive $2,7 \text{ km}^2$. Location “C” with surface drainage $0,4 \text{ km}^2$.

Location “W” with drainage surface $0,4 \text{ km}^2$. Location “R” in the northern slope of Acronafplia with limited drainage area $0,01 \text{ km}^2$. In the following areas is not taken into account the extent of built areas (urban and sub-urban area). Based on the topography formed within the urban and sub-urban area are concentrated around the storm water drainage. The first pillar is powered by Sub’ ‘A’ in which three small basins developed water streams. All the thirty streams form a total area of $0,19 \text{ km}^2$ drainage area of a common influx, the triangle of roads Nafplion - Nafplion and Argos - Aria. The second major rainwater drainage is important that primarily affects the new urban part of Nafplio. Powered by high hydro geological and surface storm water Sub’ ‘B’”. The catchment area is that many blind streams plains leading to sub-urban lowland Bampafonou area (north of the urban area). In sub - urban area Polygon the appropriate topographical conditions for convergence of all these sub-catchment with the main axis “exit” to the beach in place just north of the Municipal Parking. The catchment area “B” sub-surface accepts external inputs. A raw estimate in case of an incident rainfall intensity (i) = 70 mm / h and a $30'$ is that in the catchment area of the sub region “B”, not including external inputs can be collected on the 980.000 m^3 rain water which would seek “exit” to the sea in position between the Municipal Parking and the breakwater. Because water is not near

a particular river, but the sum of all small basins of different streams was not easy to calculate the concentration of "years" (tc) of rain water at a given location as the entrance of the urban area. A raw estimate was based on the type "Snyders" (modified) $tc = Ct + (L + I) n / \sqrt{s}$ (in hours). In this assessment the water surface is perceived as a single basin. As the main watercourse flood line in the urban area, that extends up to the entrance of the urban area (near the road Nafplio-Argos). The "Time" tc concentration greater supply of rain water at the height of the road was estimated to be 20 since starting an intense rainfall episode features mentioned above. The third line of rain water drainage affecting the urban-sub-urban area located north of the polygon is fuelled by the Sub "C". A small catchment area compared with the previous two. The other two sub "D" and "R" are not creating targeted drainage lines within the urban-sub-urban area and rain are very dispersed.

3. Geological Structures

The region has been geologically mapped in the past the period 1964-68 and included in the geological map sheet "Nafplio" climate. 1:50.000 IGME ed. Fotiadis and Mitropoulos (2006) further improved the existing geological mapping and illustrate the new elements on a scale 1:5000. In analyzing the structure divided into three (3) modules (fig.2): a) Low unit (Paraftochthoni) neritic carbonate sequence of Middle Triassic-Liasic from pelagic nodular limestones, pelagic sediments and siliceous hornstone siltstones and a tectonic-sedimentary mélange of Malmo. b) Intermediate Unit, Flysch tectonic mélange of the Post-eocenic period (?) Upper section of the Cretaceous calcareous flakes along with a tectonic mesh of serpentine flakes and large pieces of Mid-Triassic – Liasic carbonates, detached from the underlying carbonate unit. These formations domain the mountains in the region of interest (Palamidi, Exostis, Lefkania, Prophet Elijah). The thicknesses of the modules based on both the drilling and stratigraphic data that is estimated to Low E. 160-180 m, the Intermediate E. \leq 60m. and Upper E. 180-220m. The flat part of the urban-suburban area of Nafplion is part of the tectonic draft of the Argolis area. Based on drilling performed, that the thickness of the granular sediment in some places is $>$ 280m. Previously in various research projects have been drilling throughout the Argolic Field which is a detailed analysis of drilled granular layers (Galeos 1967, Poulavasilis, Mimidis, Giannouloupoulos 1996).

In the flat part of the region of interest based on data from two research carried out drilling for water at shallower depths (48m) is interesting to note that the puncture was near the foot of the massif Palamidiou ($<$ 60m) Granular materials are thick $>$ 50m. The same pattern and at the foot Welfare and Prophet Elias with input from private drilling for water. This suggests that at least in this eastern margin of the sedimentary basin Argolic Field is determined by fluctuations in several large jumps.

4. Hydrogeological Conditions

The hydrogeology of the "Argolic Field" is been repeatedly studied and researched because of the great interest presented by the region since the early 1960s. Continued over-exploitation of groundwater in granular through the large number of private drilling have caused widespread salinization problems that exist today in length. Since many of these research work has been recovered enough (Zervas1965, Galeos1967, Theodoropoulos, Zaman 1970, Poulavasiliki, Mimidis, Giannouloupoulos 2000, Sampatakakis Fotiadis Kallergis 1995, Giannouloupoulos 2001, Maravegias 2000). Apart from studies and surveys on the water potential of Argolic Field, was developed and a significant number of individual studies.

The area of lowland part of the urban - sub-urban area of Nafplio is like the rest of the field from successive Argolic granular aquifer. The mountain section is structured by independent water geo-

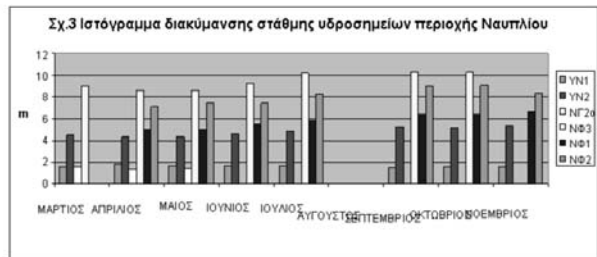


Fig. 2: (left): water level curves map; (right): water level histogram.

logical chambers but have hydraulic contact with the lowland aquifers. The work of water-measurements were level measurements of groundwater developed in eight (8) time series for March - April - May - June - July - September - October - November 2006. The water-measurements network is based on two research wells, a private drilling well and three private wells. It is estimated that the results would be better if there were more available water points. And the program under which it was given economic margins. Based on measurements made relative histogram was drawn (fig. 2) a reading which yields the following: All levels of the network show the same trends of diversification in the same series. The exception is the water point YN1 corresponding exploratory drilling in the park "position." This can be explained by the fact that the well in this location in close vicinity to the sea and as will be presented below will be confirmed by its chemicals.

The range of modulation level is different in water point water point. This is probably due to different local conditions of hydraulic conductivity of materials in which the aquifer is developed. It must be noted that this regarded to the shallow aquifer hydrostatic "free" level and not to deeper "pressure" aquifers which are developed in the area of Field Argolic basis of literature.

Based on the average level of each water points resulting from all the time series of measurements, prepared the map water level "curves" on a scale 1:5.000 (Fig. 2). An analysis of the features of this map is concluded that: The hydraulic gradient (i) the aquifer is very small indeed expect such a hydrogeological environment in close proximity to the sea and horizontal - sub horizontal layer development fine grain materials. The estimated values are between $i = 0,05\%$ and $i = 0,03\%$. Based on the overall slope of the aquifer shows that groundwater traffic of "exit" in the waters around the median volume of limestone Acronauplia. This movement regards the underground waters of eastern and north-eastern part of the urban and sub-urban area of Nafplio, while the north-west part is almost in static conditions compared to the adjacent sea. The hydraulic gradients are elusive because of their small values.

5. Sampling – Chemical Analysis

Simultaneously with the level measurements, groundwater sampling was performed at the same points of the network, in no-pumping conditions, as well as pH and temperature measurements. The water samples were analyzed at the chemical laboratories of IGME. There were an equal number of samples and time series water chemical analysis.

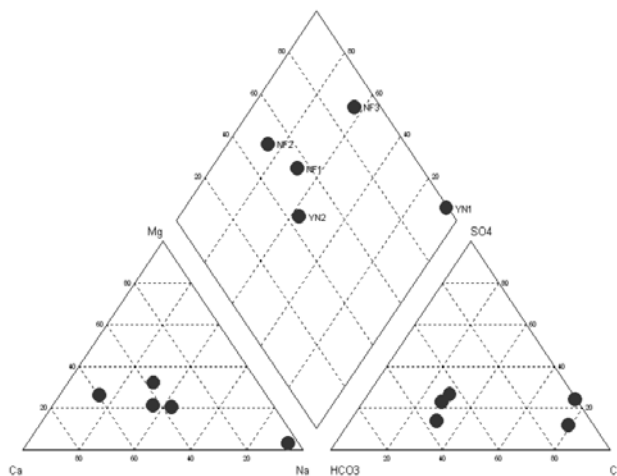


Fig. 3: Piper diagram.

Based on water chemical analysis and physic-chemical measurements were classification of water samples in Figure Piper, made histograms basic ion water chemical maps and estimated the ratio Langelier.

5a. Piper diagram

Shows the ‘average’ prices of water chemical analysis carried out in water points the ‘network’. From this diagram shows that:

- Samples from the water points NF1 and NF2 are classified in the field of “slightly chloridic and sulphate – calcareous and magnesium” water.
- Samples from water point YN1 are classified in the field of “super-chlorate-sodium” waters.
- Samples from water point YN2 are classified in the field of bicarbonate and magnesium.
- Samples from water point NF3 are classified in the field of strongly “chloride and sulphate-magnesium and calcareous” water. These water chemical data are in agreement with the isochlorion curves maps data and the effect of the shallow aquifer from sea intrusion.

5b. Histograms

Prepared total seven (7) histograms of which two related to pH and temperature outdoors and the other ions NO₃, NO₂, NH₄, Na and Cl.

Histogram pH

Prices of water point’s network showed different price trends during the time series and irregular fluctuations. This can be interpreted as the effect of price which is not due to physical water chemical factors (e.g. wet - dry season) but likely to exogenous factors.

In several cases there was a combination of increased prices with little prices NO₃ pH. The higher values observed in almost all time series in water point YN1.

Histogram of rural temperature

The temperature measurements were rural in 2006 by month March to November. Besides a sharp temperature difference must be attributed to a malfunction of the body or exogenous cause of the

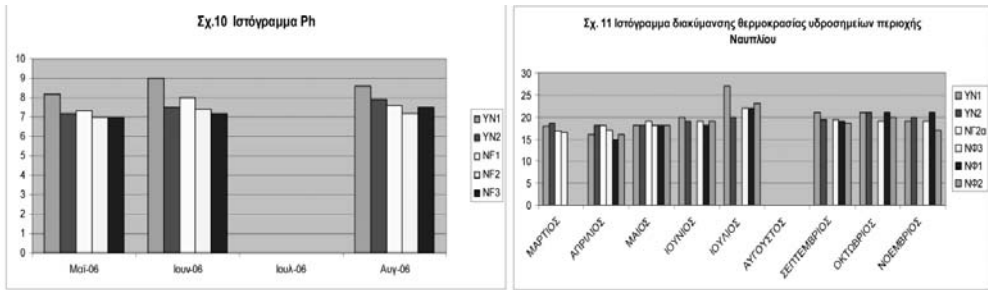


Fig. 4 (left): Ph histogram; (right): temperature histogram.

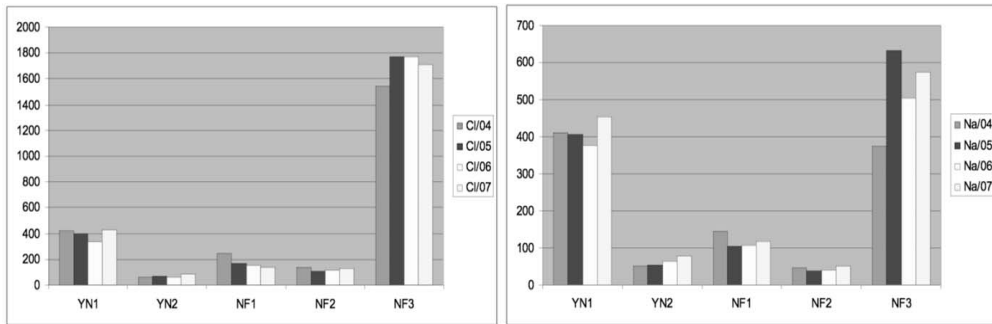


Fig. 5 (left): Cl histogram; (right): Na histogram.

price 27° C in July 2006 in water point YN1, the other two values are “trends.” Lower prices seen in the months March - April - May and peak in June to October (fig.4). The first three months represent a time period and supply the months June to October the dry season.

Na and Cl histograms

The water points YN1 and NF3 present consistently the largest values compared to the other all the time series samples. The high prices of Na and Cl are due to natural water penetration which is quite intense and widespread in the whole region of Argolida Field.

Water point YN1 (in the “Park”) is directly affected by the water penetration that occurs through the high permeable limestone volume of Acronafplia. The water point NF3 presents the highest rates in Na and Cl due to salinization that characterize generally the “granular” aquifers of Argolic Field. In the other water points, the effect of the sea seems to be very limited. In water point YN2 the three variations to prices well above the period 1 / 2007, 2 / 2007 8 / 2007 in comparison with other time series should be attributed to external factors as pollution since are being shown similar increases in the prices of NO₃-and SO₄ -.

NO₂, NH₄, NO₃ histograms

From the histogram of NO₂ ion (fig.6) is shown that there are no effects of pollution in the same period at all water points. In what water points recorded values higher than the limit, there is no correlation between time and is a local phenomenon.

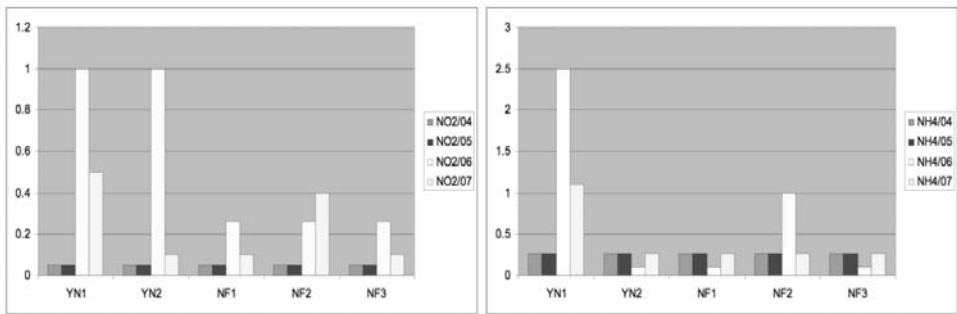


Fig.6: (left): NO₂ histogram; (right): NH₄ histogram.

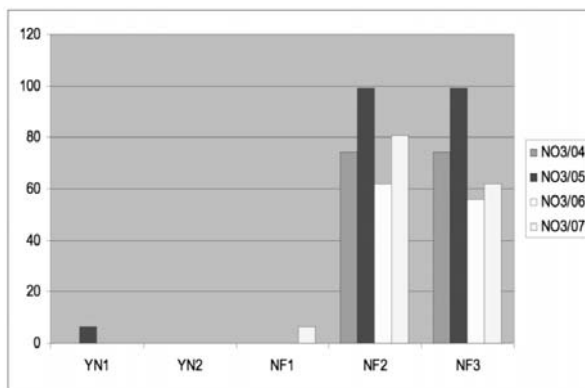


Fig. 7: NO₃ histogram.

The water point YN1 presents the most intense and frequent aggravating prices in the NO₂. Here are water points NF3 and NF2.

The water point YN1 terms of location is within the urban area of Nafplio. While water points NF3 and NF2 facing the suburban area with rural areas. Looking at the histogram of NH₄ ion (fig.6) found that only water point which shows prices beyond the limits of even a single episode, is in water point NF2. From the histogram of NO₃ (fig.7) shows that the highest frequency to pollution by nitrates occurs primarily within water point NF3 and secondly in water point NF2. Also charge very high prices but a limited number of time series, the water point YN2.

Analyzing the spatial and temporal distribution of these values in NO₃ concluded that the effects of this pollution would be caused by agricultural activities (fertilization) after both water point NF3 and NF2 are within the farms are cultivated and fertilized regularly (citrus).

5c. Water chemical Na and Cl maps

The equivalent curves of Cl⁻ was around 200 ppm while the Na²⁺ of 40 ppm (fig.8). Both maps show that the increase in both Cl⁻ and the Na²⁺ occurs from two different geographical "fronts", the SSE and N (Akronafplia - Skipjack). Based on the equivalent curves in the urban area the average values of Cl⁻ and Na²⁺ range ≥ 320 ppm, respectively. In the "sub - urban area" the average values of these ions have greater range (100 - 1100ppm for Cl⁻ and 80 - 400 ppm for Na²⁺. This is certainly a water chemical environment with highly saline ground water whose NaCl's source is the sea-water.

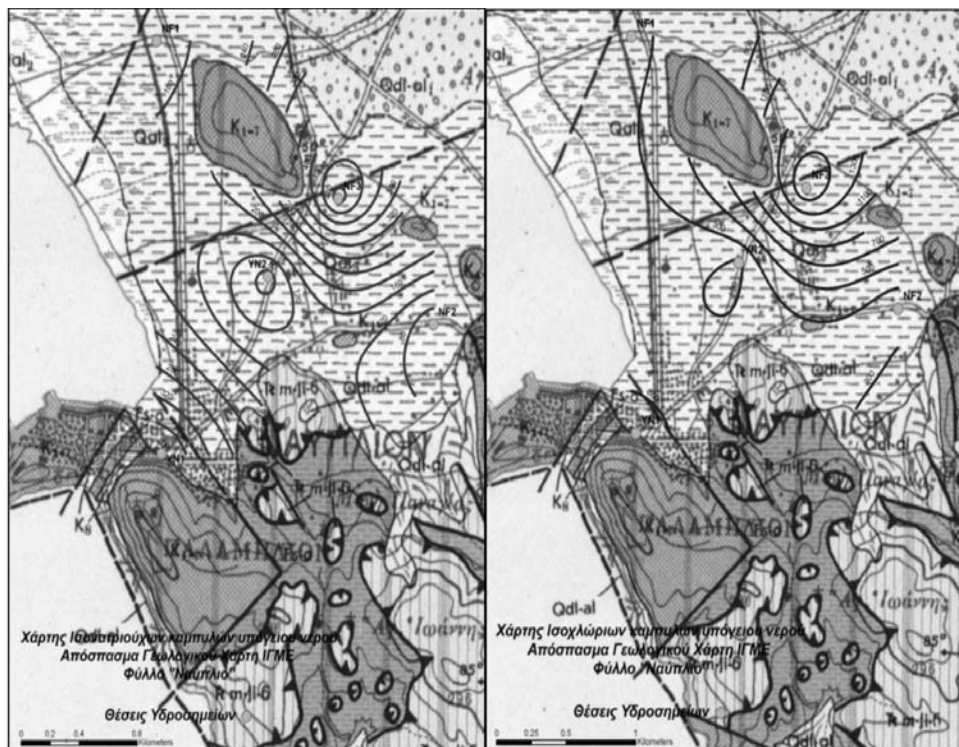


Fig. 8: (left): Water chemical Na map; (right): Water chemical Cl map

5d. Ion relationship $Ca + Mg / K + Na$

The above ion relationship is known that is used to detect areas of enrichment of water, combined of course with other physicochemical parameters. In this case sought only in general terms to provide some interpretations on the spatial and temporal conditions of enrichment of survey because of the time series data are not sufficient. Based on Table III price for each and every water point time series reveal that:

- All prices in water point YN1 are <1 . This means that the groundwater in the location of this water point not directly but are enriched downstream part of the wider aquifer. This certainly confirms the prevailing conditions of urbanization widely round the water point which certainly does not allow direct effects of percolation and enrichment in this part of the groundwater.
- Prices in water point YN2 for March and April 2006 indicate that groundwater is enriched directly in this region. In all other time series of prices show that enrichment is weakened and represents underground water aquifer downstream part.
- In NF1, NF2 and NF3 water points, the values suggest that groundwater in their regions enriched directly by percolation. Summary can be argued that the two drilling for water that are paving to a depth of 40 meters underground water is not directly enhanced by direct water penetration phenomena (in particular this is the area YN1) but by lateral loads. Unlike in the areas of water points NF1, NF2 and NF3 groundwater has a local origin, representing that the shallow aquifer due to the shallow wells, as opposed to two drilling for water supplies that have identified other than water

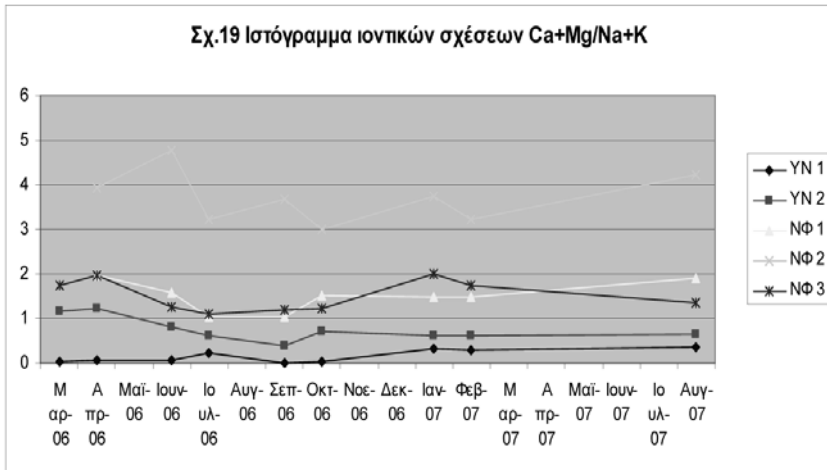


Fig. 9: Ion relationship Ca + Mg / K +Na histogram .

TABLE I - CA + MG / NA + K					
Date of Sampling	YN1	YN2	NΦ1	NΦ2	NΦ3
Mar/06	0,031	1,168	-	-	1,739
Apr/06	0,075	1,225	1,964	3,94	1,957
Jun/06	0,057	0,820	1,575	4,768	1,271
Jul/06	0,227	0,606	1,026	3,241	1,100
Sep/06	0,016	0,393	1,041	3,680	1,188
Okt/06	0,033	0,701	1,513	2,985	1,222
Jan/07	0,307	0,628	1,484	3,744	1,989
Feb/07	0,275	0,617	1,487	3,234	1,740
Aug/07	0,346	0,637	1,890	4,218	1,340
Average Values	0,152	0,755	1,497	3,726	1,505

and shallow aquifer water from a deeper aquifer. Most documents this situation is the relevant figure (Fig. 9).

5e. Corrosivity of groundwater

The indicators used to monitor the corrosivity of water and the case of groundwater near Nafplio, are two:

- The index Ryznar: used to determine deposition of CaCO₃ in water at any temperature up to 93 ° C and prognosis of erosive capacity of water.
- The index Langelier: to control the erosive capacity of water or salt deposition. Proposed a "saturation index" (saturation index, Si). The definition requires knowledge of the alkalinity

of the Ca ions concentration, of pH, temperature, TDS. Positive values mean Si deposition CaCO_3 or other salts, dissolving negative values and the values $\text{Si} = 1$ neutral state. The determination of the Index results from $\text{Si} = \text{pH} - \text{pH}_s$ (where the actual pH and pH_s where the saturation).

Much of the foundations of buildings in urban low (coastal) area of Nafplion located throughout the year or periodically within the saturated zone of the aquifer by changes of the hydrostatic level.

From Table I we suggest that in locations where there are two water points YN1 and YN2 several building foundations may be located permanently or periodically within the saturated zone of the aquifer. The boundaries of this residential area, which is susceptible to this phenomenon, can be identified through the preparation of maps of equal-level curves relate to different periods.

The map which is presented in this report (fig. 8) refers to “average” values for each water point network. The diagram of the variations in levels for each water point (Fig. 8) shows that variations in level are not equivalent (downward or upward) to all water points and at the same time series. But in the same direction except water point YN1 which is directly affected by the upward and downward movements of the sea.

The study was considered useful to determine the saturation index (Langelier).

YN1	YN2	NΦ1	NΦ2	NΦ3
2,4	1,8	1,5	1,3	1,2

Based on the average values of physicochemical parameters of the samples taken outdoors and workshops identified the following indicators for each water point.

The above values show that all sites are represented by water points network is important to heavy deposition of salts and corrosion on all metal construction, reinforced concrete, etc. contact for a long time in the underground water.

6. Conclusions-Results

6a. Hydrologic Conditions

The area of investigation because of geomorphological terrain is separated into two physiographic units: mountain and plain. This differentiates physiography and conditions in rain water in the urban area of Nafplio.

The flat section formed by two lines on rain water drainage that may affect the urban area of Nafplio. The first pillar is powered by a drainage catchment area of 0,17 km^2 small size and quantities of rain water can be generated by a strong global rainfall is negligible.

The second line of drainage is important and affects mainly the new urban part of Nafplio. The surface drainage area is 2,7 km^2 . But the volume of rain water and contribute to “external” basins through two entrances, which identified the site Bampafono. In an episode of rainfall intensity (i) = 70 mm / h and for 30 minutes, which occur in Argolic Field can create a rain water volume equal to about 980.000 m^3 . These quantities are based on the topography of the urban and peri-urban area will cross the new part of the city of Nafplion which is defined between the City Parking and the new breakwater and will end at sea (Fig. 2). The above amounts did not take into account the rain water that would enter from the two entrances at the region of Bampafono, and which is estimated to be clearly higher.

Because surface water is not considered a specific area but is the sum of small basins different streams was not easy to calculate the concentration of “years” (tc) of rain water as described above in a given topographic position (e.g.; the “entrance” of the urban area). An approximate estimate is based on the type of Snyder's (modified) $tc = Ct + (L + l) n / \bar{O} S$ (in hours). Considering as a single basin of this water surface with the main watercourse flood line in the urban area “B” and that extend up to the entrance of the urban area (near the road Nafplion - Argos), the “concentration time” (tc) of the largest providers of rain water at the rate of road Nafplion - Argos was estimated to be 20’ from the moment you start an episode of intense rainfall.

Of course all the above references to surface water and flood their impact on urban and suburban area of Nafplio are conceptual in nature as the primary data available for these estimates were made were few. The aim, however this report is to demonstrate that these hydrologic sizes in urban areas can be identified and exploited to the course of an urban planning area.

6b. Groundwater

The groundwater grows shallow in most of the urban area of Nafplio. Evaluating the average values of all time - series (measured from the five (5) water points “network”) we conclude that the level of groundwater varies on average between measurements to 0.27 m at the low sites (coastal) and 2.25 m in high. Also according to the depth of the aquifer large number of building foundations of the urban area is always in the saturated part of the aquifer throughout the year.

A number of foundations are also building in magazines saturated part of the aquifer (wet season). And finally to higher places and especially in the slopes of the urban and suburban area, the foundations of buildings are in the “ventilation zone” of the aquifer. As a result they are only affected by the percolation of surface waters to the “saturated” zone.

The demarcation of the three (3) these subregions the area of research in which the foundations accept a varying degree the influence of underground water could be achieved if there was a utilitarian scale water points denser network monitoring. The network water points which were used, we provide only an indicative list of conditions on the water level fluctuation during the hydrological year and spatial variations in urban and suburban area of Nafplio.

Regarding the groundwater chemicals based on the calculation of the index Ryznar, the groundwater has throughout the period of measurements such a quality characterized by pH values ranging between 7 and 9 in all water points and all time series sampling.

This is interpreted that at the foundations of reinforced concrete and steel stockades only salt deposition occurs and not erosion.

In conclusion these findings, the overall assessment is that by ensuring a monitoring network denser and longer time series of measurements, at least three (3) hydrological years can provide a reliable and use-based data on the structure of the aquifer and the quality characteristics they affect the foundations. Also while in the present investigation there were no measurements of water run-off and their impact on urban and suburban environment of Nafplion is estimated that in a multi-level research on the Geoenvironment should not be missing references to floods but a downstream part of the wider aquifer. This certainly confirms the prevailing conditions of urbanization beyond.

7. References

- Fotiadis, Mitropoulos, D., (2006): "Geologic Map 1:5.000 region of "Nafplion", Ed IGME.
- Galeos, A., (1967): "Study on the alluvial deposits of the Argolic Field to estimate the behavior and the capacity of the aquifers. Ministry of Agriculture (YEV), Athens.
- Giannouloupoulos, P., (2000): "Underground hydraulic and mathematical models in Argolic Field. Instructive Thesis, Agricultural. University of Athens.
- Maravegias D., (2002): "balance studies and control quality of Peloponnesian groundwater - Argolis.
- Melamed, A., and Mandel, (1962): "Preliminary Report on possible Remedial Measures and Additional Irrigation Development in the Argow plain. Kingdom of Greece, Ministry of Agriculture. TAHAL (Water Planning) Ltd. Zopp.
- Poulovasilis, Mimidis, T., Giannouloupoulos P., (1966): "Research Project to use the dam for irrigation water Kiveri Andhra Pradesh and monitoring and management of the salinization groundwater of Argolic Field." Laboratory of Agricultural Hydraulics
- Sabatakakis, P., Fotiadis, A., Kallergis, C., (1995): "3rd Hydro geological Congress"- Heraklion, Crete.
- Tataris, A., Kallergis, G., Swings, G., (1965): Geological map "Nafplion" sheet, scale 1:50.000, IGME ed.
- Zervas S., (1965): "Hydrogeological study of Argolic Field's water resources » Ministry of Agriculture (YEV), Athens.

GEOCHEMICAL STUDY OF THE URBAN AND SUBURBAN AREA OF NAFPLION CITY, ARGOLIDHA PREFECTURE, HELLAS

Tassiou, S.¹, and Vassiliades, E.¹

*Institute of Geology and Mineral Exploration, 1 Spirou Louis Street, Olympic Village, Entrance C, 136 77
Acharnae, Attiki, Hellas, stassiou@igme.gr, evassiliades@igme.gr*

Abstract

Soil, as the primary receptor of anthropogenic urban contamination acts as a sink for a variety of toxic and other hazardous substances. It constitutes, therefore, an indicator of contamination and may be utilised geochemically to assess environmental quality of urban and suburban areas.

In Nafplion, an urban and suburban area of 50 km², was investigated using for the first time in Hellas an integrated approach with all available geoscientific techniques to make an in-depth environmental impact assessment. One of these techniques was applied geochemistry, which mapped the geochemistry of surface soil (0-10 cm) with 144 samples, collected on a regular grid of 500 x 500 m. The following fifty determinands were measured on the soil samples: Ag, Al, As, B, Ba, Be, Bi, Ca, Cd, Ce, Co, Cr, Cu, Fe, Ga, Ge, Hg, K, La, Li, Mg, Mn, Mo, Na, Nb, Ni, P, Pb, Rb, Re, S, Sb, Sc, Se, Sn, Sr, Ta, Te, Th, Ti, Tl, U, V, W, Y, Zn, Zr, pH, electrical conductivity and grain-size distribution.

The aim of the geochemical study was to distinguish, as far as possible, the origin of chemical elements, and (i) to classify them as geogenic or anthropogenic; (ii) to delineate contaminated areas, and (iii) to assess potential future impacts of human activities on soil.

Interpretation of the resulting geochemical patterns has shown that those of Al, Fe, Be, Ce, Cr, Co, Ga, Ge, K, La, Li, Mg, Nb, Ni, Rb, Sc, Sr, Tl, V, Y, W and Zr are of geogenic origin, since they are directly related to parent rocks, whereas patterns of As, B, Ba, Bi, Ca, Cd, Cu, Mn, Mo, Na, P, Pb, S, Sb, Sn, Th, U and Zn are interpreted as being of dual origin, geogenic and anthropogenic. In this paper, the geochemical distribution of only five elements shall be described, i.e., Pb, Zn, Cu, Ni and Na. This case study was indeed very interesting, since for the interpretation of some patterns, even the military history of the area had to be unravelled.

Key words: *soil, urban geochemistry, Nafplion, Hellas.*

1. Introduction

As more population is moving to towns, seeking better working and living conditions, there is a greater pressure on finding suitable land for industrial, residential and recreational use. Urban and suburban soil, because of past and current polluting activities, is considered to be of potentially high health risk with respect to toxic elements and organic compounds. Surface soil is the main receptor of urban contaminating activities, since it acts as a collector and a reservoir of toxic elements and other substances. It is, therefore, a good indicator of anthropogenic contamination, thus, allowing the geochemical assessment of the quality of the urban and suburban environment. Since, the qual-



Fig. 1: Map of Hellas showing the location of the city of Nafplion in relation to Athens.

ity of our living environment affects our health and overall well being, it is necessary to map the distribution of toxic elements and other substances in soil, and to locate and delineate precisely hazardous areas, which must be rehabilitated before their reuse for residential, recreational, or even industrial, purposes.

The present work is part of an integrated geo-environmental study and refers to the results of the geochemical survey carried out in the urban-suburban area of the city of Nafplion (Tassiou, 2009; Vasiliades, 2009), which is situated in the north-eastern part of Peloponnese, Hellas (Fig. 1). The integrated geo-environmental study covers an area of 50 km², and is delimited to the south by the Palamidi hill, to the east by Aria hill and the Exostis-Lefkakia depression, to the north by the Argos-Tirinta-Nafplion plain and to the west by the Akronafplia (Arvanitia) peninsula (Fig. 2).

2. Objectives of urban geochemical survey

The aims of the soil geochemical study, carried out in the urban-suburban area of the city of Nafplion, were to distinguish, as far as possible, the origin of inorganic chemical elements, and (i) to classify them as geogenic or anthropogenic; (ii) to delineate contaminated areas, and (iii) to assess potential future impacts of human activities on surface soil.

3. Lithology and morphology

In summary, the geological formations on which the residual soil was developed are the following (Photiades, 2008, 2010):

- neritic limestone of Lower to Upper Cretaceous age with its base rich in serpentinite breccio-conglomerate;
- limestone and dolomite of Upper Triassic to Lower Jurassic age, locally with Fe-Mn encrustations;
- serpentinite tectonic mélange;
- flysch mélange;
- tectono-sedimentary mélange (clastic ophiolitic formation),
- Quaternary alluvial deposits with swampy and brackish soil, and
- Recent fluvial deposits comprising heterogeneous coarse materials, derived from the erosion of the pre-Neogene basement.

Morphologically, the area constitutes an old weathered surface. The limestone outcrops are strongly weathered, and the collected soil samples are mostly residual (*terra rossa*).

4. Methods

4.1 Sampling and sample preparation

The routine soil samples (0-10 cm) were collected from a regular grid of 500 x 500 m that covered an area of 50 km². Duplicate field samples were collected from 10% of the sites for quality control purposes, and the estimation of sampling, analytical and geochemical variance. In total, 144 soil samples were collected, weighing about one kilogram each. The soil samples were dried at 30°C and then sieved through a <2 mm nylon screen.

4.2 Chemical analysis

The following chemical elements were determined by an ICP-AES Spectrometer after a hot aqua regia leach: Ag, Al, As, B, Ba, Be, Bi, Ca, Cd, Ce, Co, Cr, Cu, Fe, Ga, Ge, Hg, K, La, Li, Mg, Mn, Mo, Na, Nb, Ni, P, Pb, Rb, Re, S, Sb, Sc, Se, Sn, Sr, Ta, Te, Th, Ti, Tl, U, V, W, Y, Zn and Zr. Aqua regia dissolution is effective for base metals and associated elements in sulphides, oxides and carbonates. Rock forming elements and refractories are only partially attacked. It is noted that the aqua regia leach is partial for B, Ba, Be, Ca, Ce, Cr, Fe, Ga, Ge, La, Li, Mg, Nb, Rb, Re, Sb, Sc, Sn, Sr, Ta, Te, Th, Ti, Tl, W and Zr, and limited for Al, K and Na. In addition, the soil pH, conductivity and the grain-size distribution were also determined.

The quality of analytical results was monitored by laboratory internal control samples, blanks and subsamples of the routine soil and field duplicates. Overall analytical precision was better than 5% at the 95% confidence level for almost all elements determined.

4.3 Data processing

A geostatistical spatial structural analysis study was performed on the geochemical data of each element by plotting semi-variograms in different directions, and testing the extracted parameters by point kriging before plotting its distribution map by ordinary kriging with Golden Software's Surfer program (Tassiou, 2009; Vassiliades, 2009). A ten grade colour scale was used for map plotting, which is based on the following percentiles: 2.5, 5, 10, 15, 25, 50, 75, 90, 95 and 97.5.

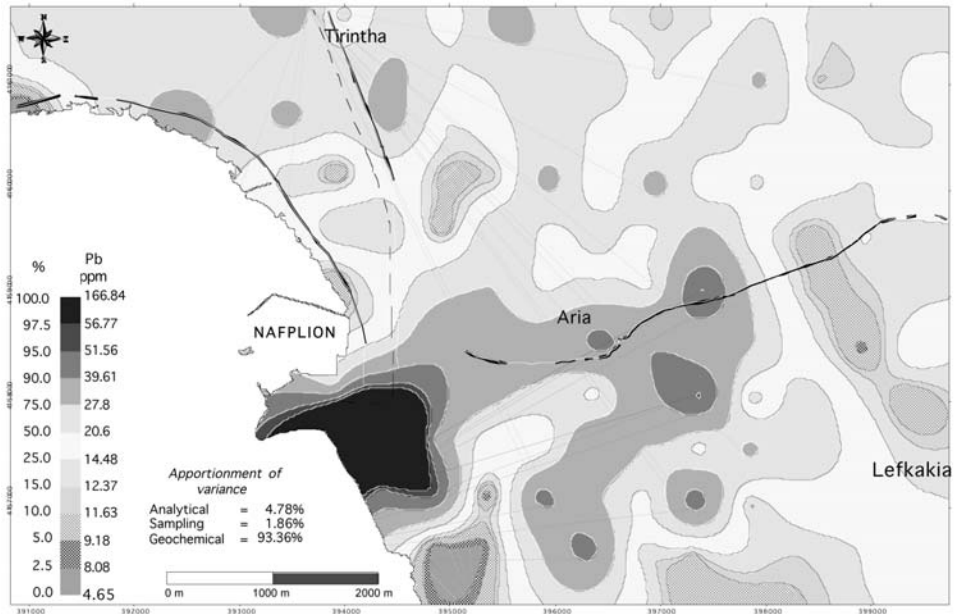


Fig. 2: Geochemical distribution of aqua regia extractable Pb in the <2 mm fraction of soil (0-10 cm), Nafplion, Peloponnese, Hellas.

5. Results

In this paper, the geochemical distribution of only a few elements is described, *e.g.*, Pb, Sn, Cu, Ni, and Na. For a full description of results the reports by Tassiou (2009) and Vassiliades (2009) should be consulted.

5.1 Lead (Pb) distribution

Lead varies in surface soil (0-10 cm) from 4.65 to 166.8 ppm, with a mean and median of 30.0 and 20.6 ppm, respectively (Fig. 2). One sample had a value of 882 ppm Pb, and was removed for the data processing, because it distorted the patterns. Levels of Pb > 51.56 ppm characterise the city of Nafplion, and especially the area of Palamidio castle, with the source of polluting activities going back to the Hellenic war of independence against Turkey in the early nineteenth century. Elevated Pb values are also observed near to major roads.

5.2 Tin (Sn) distribution

The Sn variation in surface soil (0-10 cm) is from 0.1 to 17.6 ppm, with a mean and median of 1.69 and 0.97 ppm, respectively (Fig. 3). Given that 11 ppm Sn is the maximum total value for uncontaminated soil (Chapman, 1972; Kabata-Pendias and Pendias 1984), values > 9 ppm Sn, specifically in the city of Nafplion, and around Palamidi hill, appear to be related to anthropogenic activities. Similar to Pb, elevated Sn values are observed near to major roads.

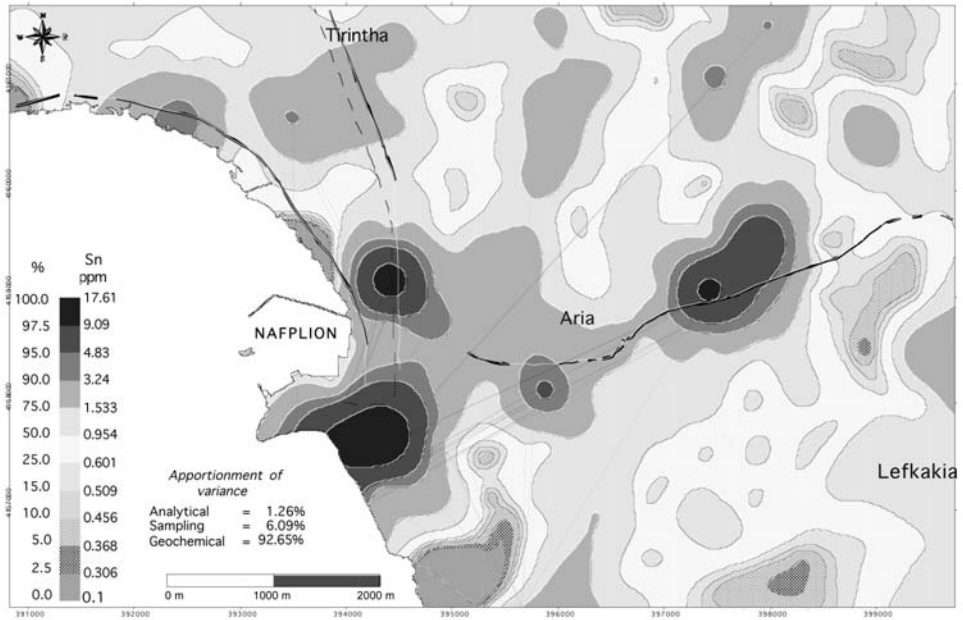


Fig. 3: Geochemical distribution of aqua regia extractable Sn in the <2 mm fraction of soil (0-10 cm), Nafplion, Peloponnese, Hellas.

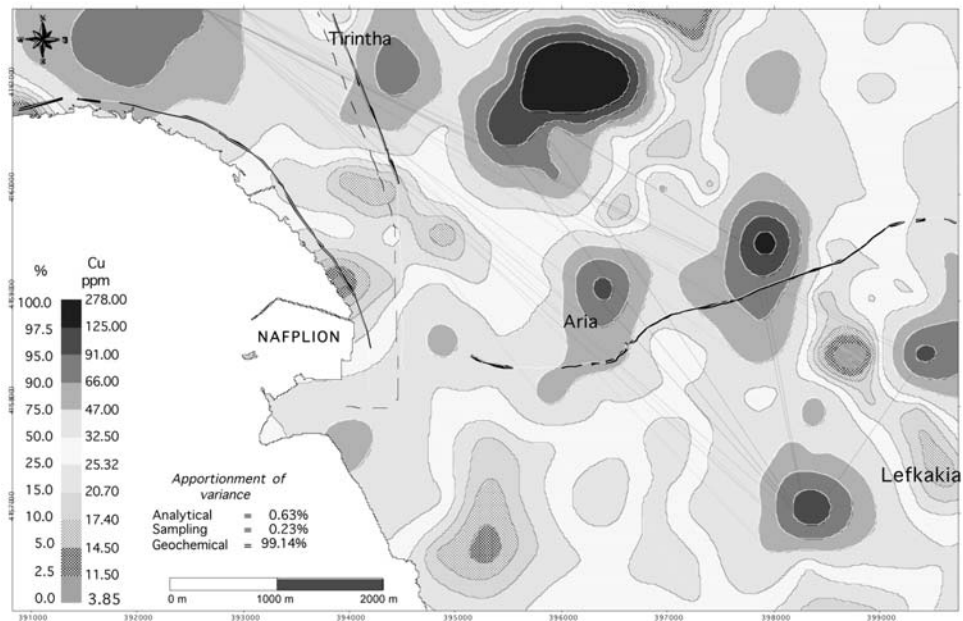


Fig. 4: Geochemical distribution of aqua regia extractable Cu in the <2 mm fraction of soil (0-10 cm), Nafplion, Peloponnese, Hellas.

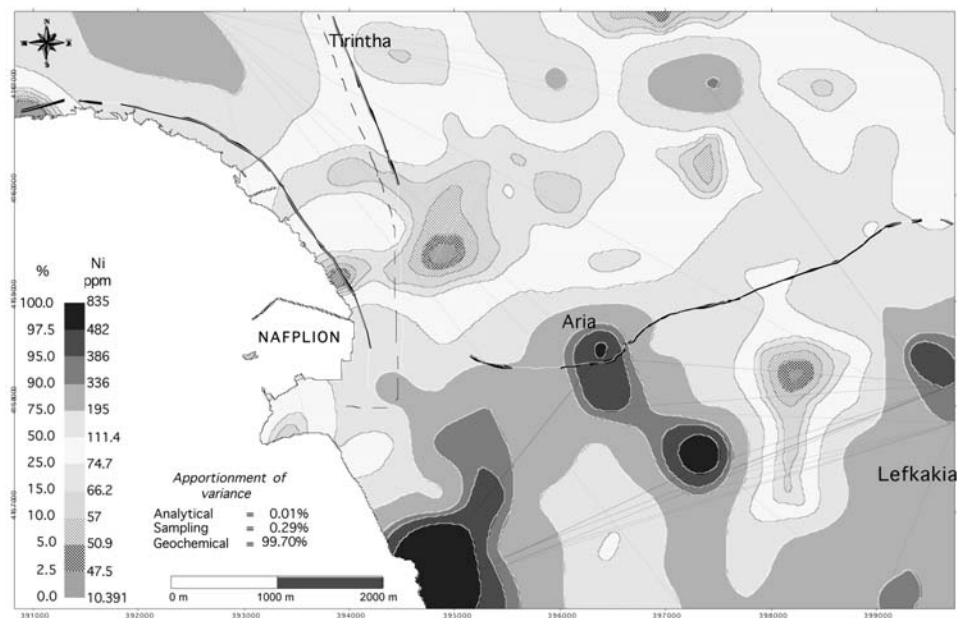


Fig. 5: Geochemical distribution of aqua regia extractable Ni in the <2 mm fraction of soil (0-10 cm), Nafplion, Peloponnese, Hellas.

5.3 Copper (Cu) distribution

Copper varies in surface soil (0-10 cm) from 3.85 to 278 ppm, with a mean and median of 41.6 and 32.7 ppm, respectively (Fig. 4). The elevated Cu values (>47 ppm) in the north part of the study area, to the north-east of Aria and to the south-west of Lefkadia are considered to be due to agricultural activities, *i.e.*, copper sulphate is used as a herbicide, fungicide and pesticide.

5.4 Nickel (Ni) distribution

The Ni distribution in surface soil (0-10 cm) varies from 10.4 to 835.6 ppm, with a mean and median of 158.3 and 112.0 ppm, respectively (Fig. 5). The high Ni values characterise the flysch tectonic mélangé, which locally includes olistoliths of mafic lava, serpentinite and ophiolitic rocks, as well as the tectono-sedimentary mélangé of Upper Jurassic and the serpentinite tectonic mélangé. The geochemical patterns of Ni are almost identical to those of Cr and partly of Co, suggesting, therefore, that the anomalous patterns are of geogenic origin.

5.5 Sodium (Na) distribution

Sodium varies in surface soil (0-10 cm) from 0.005 to 0.864%, with a mean and median of 0.033 and 0.015%, respectively (Fig. 5). High Na concentrations are observed in the western part of the area along the coast, and mainly to the north of Nafplion. The reasons for these elevated Na values in surface soil are probably sea spray, and irrigation with saline water due to marine water intrusion caused by over pumping of shallow aquifers. This area is also characterised by high values of B, S and Sr, supporting, therefore, the marine influence interpretation.

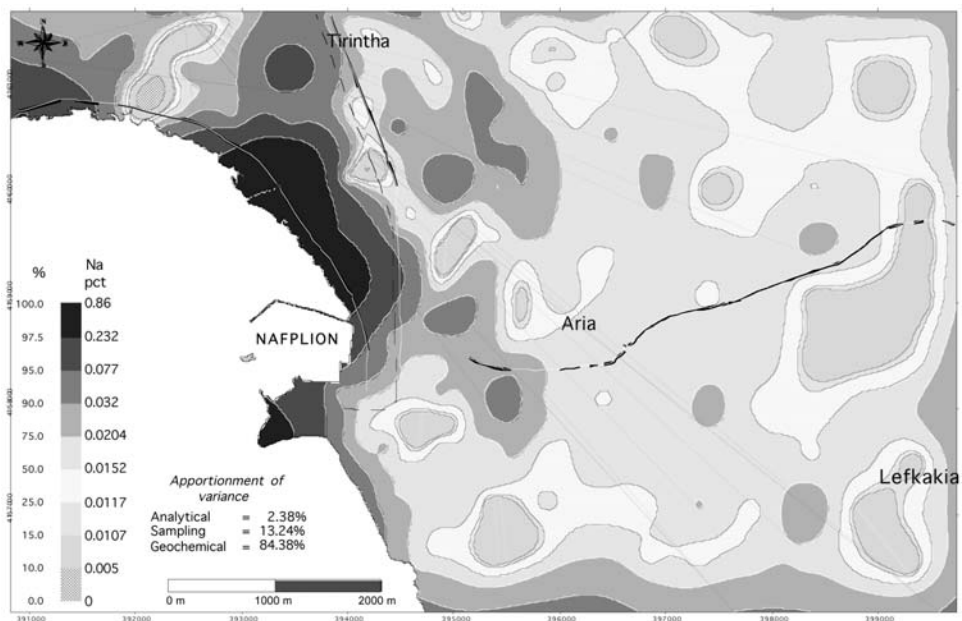


Fig. 6: Geochemical distribution of aqua regia extractable Na in the <2 mm fraction of soil (0-10 cm), Nafplion, Peloponnese, Hellas.

6. Conclusions

Interpretation of geochemical patterns of elements, presented on maps, is a complex, and difficult task, because it requires an integrated evaluation of all available information. It involves the study of raw data, their statistical parameters, including linear correlation coefficients, as well as pH, electrical conductivity, particle size distribution, geology and geomorphology of the area, and finally *in-situ* observations with respect to land use.

Elevated geochemical patterns of Cr, Ni, Co, Mg and pH describe geological structures, such as the tectono-sedimentary mélange and serpentinite mélange. Areas with intense chemical weathering of limestone (occurrence of terra rossa) are indicated by elevated geochemical patterns of Al and low Ca. In the terra rossa there is an accumulation of many elements (*e.g.*, Al, As, Ba, Be, Cd, Ce, La, Ga, Ge, Fe, Mn, Pb, Sb, Sc, V, Zn), and the resulting patterns are considered to be of geogenic origin. Other elements with values, exceeding the natural geochemical background, such as Pb, Sn, Sb, Zn, Mo, \pm As, \pm Bi, are associated with urban development. Whereas, locally elevated values of Cu, P, U, Zn, \pm Cd and \pm Th occur in agricultural areas, and are ascribed, therefore, to be caused mainly by anthropogenic activities (Tassiou, 2009).

It is concluded that overall, the distribution patterns of chemical elements in the Nafplion urban and suburban area are mainly of geogenic origin, and that anthropogenic contamination is of local significance.

Finally, urban geochemical studies are important, because they provide fundamental data about the chemical state of our living and working environment, and they also establish the geochemical baseline against which comparisons can be made in the future by either monitoring programmes or accidents of any type.

7. Acknowledgments

This paper is published by permission of the I.G.M.E. General Director. The project “Collection and Documentation of Geothematic Information of Urban and Suburban areas of Hellas – Pilot Applications” (Subproject 3: “Integrated geological, engineering geological, hydrogeological, geochemical and geophysical study of the urban and suburban pilot area of Nafplion, Argolidha Prefecture”) was co-financed by the third EU Community Support Framework Programme and the Hellenic State (2000-2006), Operational programme “Competitiveness”, Priority Axis 7 “Energy and Sustainable Development”, Measure 7.3 “Exploitation of natural resources and support in meeting environmental commitments”. The Director of the I.G.M.E. Division of Geochemistry and Environment, EurGeol Alecos Demetriades, is thanked for his support and constructive comments for the improvement of this concise paper.

8. References

- Chapman, H.D. (Editor), 1972. *Diagnostic criteria for plants and soils*. University of California, Riverside, California, 793 pp.
- Kabata Pendias, A. & Pendias, H., 1984. *Trace elements in soils and plants*. CRC Press, Inc., Boca Raton, Florida, 315 pp.
- Photiades, A., 2008. *Geological study of the urban and suburban pilot area of Nafplion (Argolidha Prefecture)*. Report of Subproject 6920/003: Integrated geological, engineering geological, hydrogeological, geochemical and geophysical study of the urban and suburban pilot area of Nafplion Argolidha. Institute of Geology and Mineral Exploration, Athens, Hellas, 15 pp. (text in Greek).
- Photiades, A., 2010. *Geological survey at a scale of 1:5000 of the greater Nafplion area (NW Argolis, Greece)*. This volume.
- Tassiou, S., 2009. *Geochemical environmental study of the urban-suburban area of Nafplion, Volume 2: Interpretation text*. Report of Subproject 6920/003: Integrated geological, engineering geological, hydrogeological, geochemical and geophysical study of the urban and suburban pilot area of Nafplion Argolidha. Institute of Geology and Mineral Exploration, Acharnae, Attiki, Hellas, 132 pp. (text in Greek).
- Vassiliades, E., 2009. *Geochemical environmental study of the urban-suburban area of Nafplion, Volume 2: Geochemical maps*. Report of Subproject 6920/003: Integrated geological, engineering geological, hydrogeological, geochemical and geophysical study of the urban and suburban pilot area of Nafplion Argolidha. Institute of Geology and Mineral Exploration, Acharnae, Attiki, Hellas, 48 pp. (text in Greek).

THE “URBAN GEOLOGY” PROJECT OF IGME: THE CASE STUDY OF NAFPLIO, ARGOLIS PREFECTURE, GREECE

Tsombos P. I.¹ and Zervakou A. D.¹

¹*Institute of Geology and Mineral Exploration (I.G.M.E.), Olympic Village, 3rd Entrance, 13677 Acharnae, Athens, Greece, ptsombos@igme.gr, zervakou@igme.gr*

Abstract

The Institute of Geology and Mineral Exploration of Greece (I.G.M.E.), in the framework of CSF 2000 – 2006 (Community Support Framework 2000-2006), implemented the pilot project “Collection, Codification and Documentation of geothematic information for urban and suburban areas in Greece - pilot applications”. Geological, geochemical, geophysical, geotechnical, hydrogeological and other geothematic data concerning the urban and surrounding areas of Drama (North Greece), Nafplio & Sparti (Peloponnese) and Thrakomakedones (Attica) were collected. Drillings, geological and neotectonic mapping and other “in situ” measurements and field work took place. All initial and derived analogical and digital data were compiled and processed in specially designed geo-databases in GIS Environment. The final results are presented in geothematic maps and other digital products (DEMs, 2D – 3D surfaces, geodatabases). Such data constitute the essential knowledge base for land use planning and environmental protection in specific urban areas. Through this pilot project, new scientific approaches, methodologies and standards were developed and improved in order to apply to other future projects concerning the major cities of the whole country.

Key words: *Urban Geology, geothematic mapping, GIS, pilot areas, Nafplio.*

1. Introduction

The Institute of Geology and Mineral Exploration of Greece (I.G.M.E), in the framework of CSF 2000 – 2006 (Community Support Framework 2000-2006, Operational Program Competitiveness, Priority axis 7: Energy and Sustainable Development, Measure 7.3: Exploitation of natural resources and support in meeting environmental commitments, Action 7.3.1) implemented the project titled “Collection, codification and documentation of geothematic information for urban and suburban areas in Greece - pilot applications”.

Through the implementation of this project, existing geothematic information concerning geological, hydrogeological, geotechnical, geochemical and geophysical reports for urban and suburban areas over the whole country was compiled into a database. Data recording and management was achieved through the use of GIS technology.

Additionally, the geoscientific information was enriched with data derived from “in situ” survey at four pilot areas of different geological structure (Nafplio, Drama, Sparti and Thrakomakedones). All geoinformation from geological mapping, geotechnical – geochemical – geophysical research and measurements was stored and processed in specially designed geodatabases in GIS environment.

Through the compilation of geological data, this Urban Geology project aimed to the understanding of the surface and subsurface geology of the specific area. Thus, the knowledge of the geological conditions will constitute an essential base for the identification and evaluation of geohazards relating to natural processes and human activities at the wider study area.

All derivative project results and digital data (geodatabases, thematic maps, 3D models - surfaces) are available to:

- State's services in charge of the protection and enhancement of natural and human made environment
- State authorities and engineers whose activities concern infrastructure development and big public works
- Authorities dealing with the confrontation of major natural disasters
- Archaeological services

This project should be the starting point for future relative studies concerning any big city of the whole country or individually where it is required.

2. Historical overview of Urban Geology studies

Only a hundred years ago, there were no cities on earth with a population of 5 million residents. Nowadays, the urban enlargement and overpopulation of the western areas is an increasing tendency. It is estimated that there are over 60 such cities. Half of the world's population lives in urbanized areas which cover only 0.7% of the total earth surface (according to IWGUG).

The aggregation of population leads to the concentration of human activities and economic wealth, over consumption of natural resources and urban growth without planning and sustainable management. As a result, urban societies are exposed to various dangers and threats with economic, social, ecological – environmental impacts on the urban surroundings.

Problems associated with urban development are addressed by the International Working Group on Urban Geology. These problems are related with geological and hydrological conditions of urban areas and those of their surroundings, e.g. flooding, land subsidence, groundwater pollution, soil contamination, earthquakes, volcanic eruptions, coastal and river erosion, landslides, sinkholes, soft and expansive soils causing foundation instability, etc.

For all these reasons, no sustainable urban planning can be done without geological information support. The field of *Urban Geology* is working towards inducing decision makers and planers to take into account all geological factors in order to predict and minimize natural hazard, protect and harmonize natural environment.

Urban Geology studies rely on diverse branches of earth sciences such as hydrology, engineering geology, geochemistry, stratigraphy and geomorphology in order to build a three-dimensional model of the character of the land and to explain the geological processes involved in the dynamic equilibrium of the local environment (Giroux and Bélanger, 2003).

In the past, traditional approaches on Urban Geology were mostly focused on the mechanical behavior of different geological materials under the cities and the identification of infrastructures stability (roads, buildings). Today the environmental - geological researches, focused on urban areas, cover a wide variety of queries, such as potable water supply, waste disposal, soil vulnerability etc.

The necessity for Urban Geology in the United States was born as settlement spread into the haz-

ard-prone lands of the West. Prior to about 1950, few maps presented engineering geology data and, if they did, it was intended for the use of engineers, not planners (Rau, 2005).

The need for maps of Urban Geology was recognized publicly in Canada at the turn of the century and probably well before by individual practitioners. In a paper presented to the Royal Society of Canada in 1900, Dr. H. M. Ami said “The larger cities of our Dominion, as well as those of other countries, are the centers of work and research in the pathways of science and commerce. . . What the drill has to penetrate in any one of our larger centers of activity in Canada is a question not only of interest but also of economic value.” He proceeded to give summary accounts of the Urban Geology of Saint John, Montreal, Ottawa, Quebec, and Toronto, and this, almost seventy years ago (Legget, 1969).

The concern over the urban development and its environmental impacts promotes the collaboration and close interaction between geoscientists, environmental scientists, engineers, planners, decision makers. This multidisciplinary approach has led to the increase of relevant scientific publications such as “Environmental Geology” (Springer), “Environmental & Engineering Geosciences” (Geological Society of America and Engineering Geologists), “Environmental Modeling and Assessment” (Baltzer Science Publishers), “Journal of Environmental Planning and Management” (Carfax Publishing) and “Environment and Urbanization” (International Institute for Environment and Development).

In 1991, International Working Group on Urban Geology (IWGUG) was established to provide an international platform in which geoscientists and non-geoscientists can discuss issues of mutual interest concerning urban development. Both the International Association of Engineering Geology (IAEG) and the International Association of Hydrogeologists (IAH) supported this initiative to form a Working Group and joined as founding members.

3. Case study: Pilot area of Nafplio, Argolis prefecture, Peloponnese, Greece

3.1 Work tasks outline

The third subproject of the Urban Geology Project of I.G.M.E. titled “Integrated geological, geotechnical, hydrogeological, geochemical, geophysical and marine studies of urban and suburban area of Nafplio, Argolis Prefecture” realized at the broader area of Nafplio. The total study area covered a surface of 50 Km² (Fig.1).

The project focused on the collection of field work data and other geological information generated from previous studies of the urban and surrounding area of the city. Fieldwork comprised (Zervakou A. et al., 2007):

- Geological mapping at 1:5.000 scale for the identification and evaluation of geological settings in the study area.
- Neotectonic mapping at 1:5.000 scale for the identification and evaluation of active faults in the study area.
- Geotechnical mapping at 1:5.000 scale for the identification and evaluation of physical, mechanical and geotechnical properties of geological formations in the study area.
- Water and soil field sampling for geochemical analyses.
- Radon measurements.
- Surface geophysical measurements.
- Deep geophysical measurements.



Fig. 1: Reference map of Nafplio's broader area. The black line outlines the study area (Zervakou A. et al, 2007).

- Marine geological survey
- Fieldwork survey for the verification of remote sensing data interpretation
- Geoarchaeological survey

After the field survey and data acquisition, the following work tasks were implemented (Zervakou A. et al., 2007):

- Soil and water laboratory tests and geochemical analyses.
- Soilmechanics, rockmechanics laboratory tests for the determination of physical and mechanical properties of the penetrated formations.
- Test shallow drillings ("in situ" SPT and permeability tests).
- Data elaboration.
- Data evaluation.
- Data input, management and analysis in GIS environment.
- Digital thematic maps compilation in GIS environment.
- Technical reports, publications.

3.2 Accomplished tasks

During the project the following work tasks were carried out:

1. Geological mapping at 1:5.000 scale.
2. Neotectonic mapping at 1:5.000 scale (Fig. 2).
3. Test Drillings (Fig. 3).
4. Geotechnical mapping at 1:5.000 scale.
5. Geotechnical survey and sampling in 22 locations – Geotechnical rock mass classification in 22 locations (according to Bieniawski).



Fig. 2: Neotectonic faults occurring at the broader area of Nafplio (Galanakis and Georgiou, 2008).



Fig. 3: Test drilling core samples taken from the broader area of Nafplio (Pantelias, 2009).

6. Hydrogeological survey, piezometric measurements, water sampling in 5 locations and chemical analyses (Ca, C, Na, NH₄, NO₂, NO₃, SO₄).
7. Soil sampling in 144 locations and geochemical analyses for the determination of 44 chemical elements such as Ag, As, B, Cr, Cu, Fe, etc.
8. Radon measurements.
9. Marine geological survey (Bathymetry, morphology, sampling) (Fig.4).
10. Geophysical survey (Fig. 5):
 - a. Cross – hole Seismic measurements.
 - b. Diffraction seismic measurements.
 - c. Topographic – gravity measurements.
 - d, Electromagnetical measurements.
 - e. Electrical tomography.

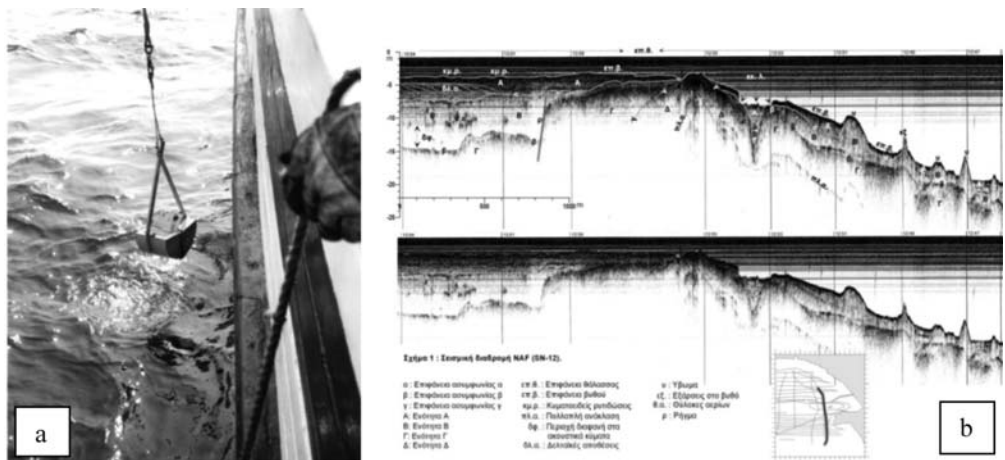


Fig. 4: a) Surface sediment sample collected from the sea floor in the marine area near the city of Nafplio, b) Seismic profile taken from the broader marine area near the city of Nafplio (Andrinopoulos et al., 2008).

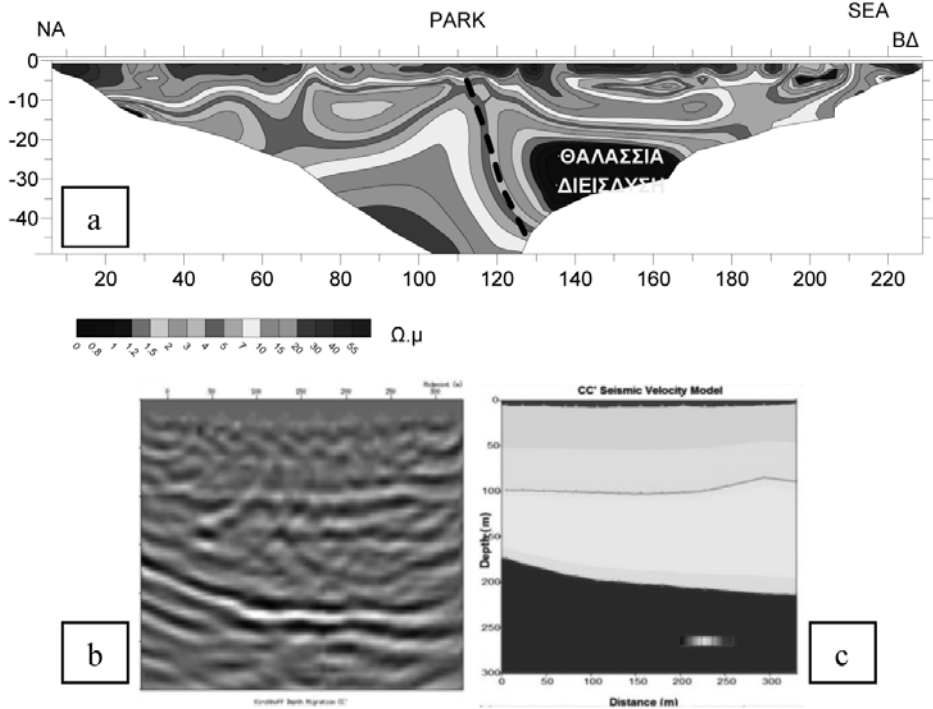


Fig. 5: a) Electric Resistivity Tomography inversion, b) and c) Seismic survey for the detection of possible faults (Karmis, 2008).

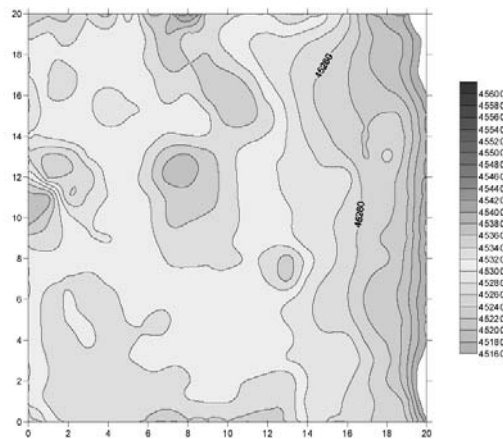


Fig. 6: Magnetic survey near the ancient Agora at the city of Argos (Zanani, 2009; Zanani et al., 2010).

11. Geoarchaeological survey at the broader area of Nafplio (Fig. 6).
12. Geodatabase design, creation and data input.
13. Data management, data analysis.
14. Thematic maps compilation.
15. DEMs and other digital 2D and 3D surfaces creation.

3.3 Urban Geology Geodatabase

The complexity of Urban Geology geoinformation can be well stored, described and processed within the frame of a Geographic Information System (GIS).

All geoscientific information derived from field work and data elaboration was stored and processed into a geographic database specially designed for such data. For this specific application an ArcGIS Personal Geodatabase was created (Fig.7).



Fig. 7: “Nafplio” Geodatabase structure and content (Zervakou and Tsombos, 2010).

3.4 Thematic maps and other digital products

Maps are the best tool to represent, describe, interpret and understand the real world. A map provides information on the existence, the location, the distance and the relation between spatial features. Therefore, any spatial planning, like urban planning, requires a supply of maps.

All processed fieldwork data and results derived from this particular project are presented in geothematic maps and 2D – 3D digital models - surfaces. Two samples of the produced geothematic digital products are displayed bellow (Fig. 8 & 9).

4. Conclusions

Natural hazards are geological and environmental phenomena occurring at irregular intervals and at varying intensity. Urban areas are more at risk than others, depending on natural factors such as ge-

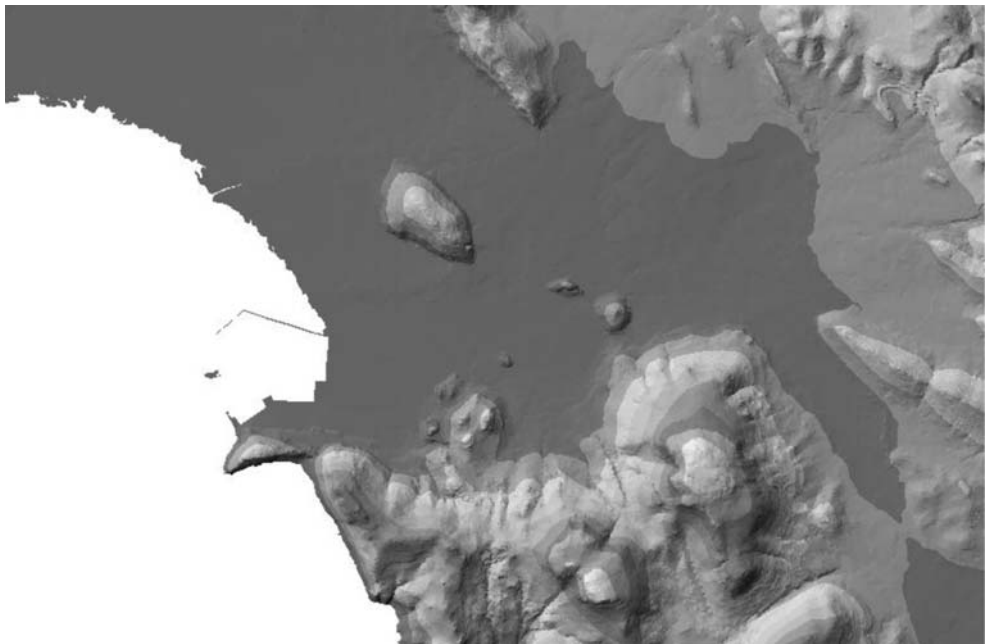


Fig. 8: High detailed TIN representing the surface morphology of the study area (Zervakou et al., 2007).

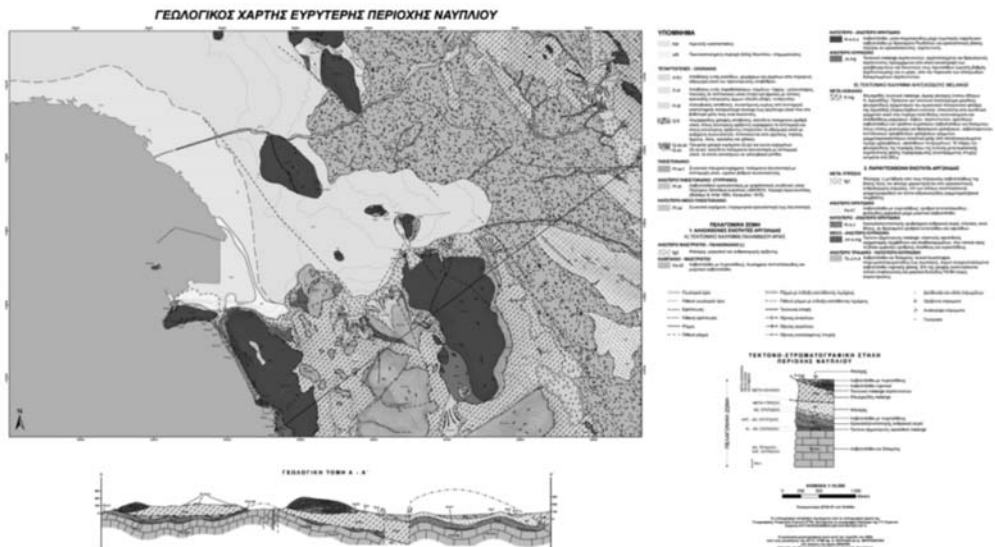


Fig. 9: Geological map of the study area (Photiades, 2008).

ology, topography and intensive human activities. Today, scientific knowledge and advanced technologies are applied for hazard evaluation and risk reduction, sustainable land use and urban planning.

Urban Geology is working towards inducing decision makers and planners to take into account all geological factors in order to predict and minimize natural hazard, protect and harmonize natural environment in urbanized areas.

Urban Geology project of I.G.M.E., accomplished within the framework of CSF 2000 – 2006, focused on the collection and management of geothematic information concerning urban and suburban areas. Specialized and dedicated studies took place at four pilot urban areas. Nafplio, the capital city of Argolis prefecture, was one of them.

Geographic Information Systems provided the best environment for the collection, storage, management, processing, analysis and cartographic representation of complex geoscientific information. All compiled data were stored, processed in geodatabase and presented in a set of thematic maps and other 2D and 3D digital products.

Geological information constitutes the essential knowledge base for a country development. Thus, the concentration of a big volume of data (maps, technical reports, laboratory analyses etc) in the Institute of Geology and Mineral Exploration will facilitate the geoinformation dissemination to public sector, companies and individuals.

To conclude, through this pilot project new scientific approaches, methodologies and standards were developed and improved in order to apply to other future projects concerning capital centers of the whole country.

5. Acknowledgements

This study was accomplished within the framework of the project “Collection and Documentation of Geothematic Information for Urban and Suburban areas in Greece – Pilot Applications”. The program was funded by the Operational Program “Competitiveness” Priority Axis 7: Energy and Sustainable Development, Measure 7.3: Exploitation of natural resources and support in meeting environmental commitments. The Operational Program “Competitiveness” was co-funded by the European Regional Development Fund (ERDF).

We would like to thank all colleagues who participated in this multidisciplinary project: Andrinopoulos A., Apostolidis E., Chiotis E., Chiras S., Demetriades A., Efthimiou G., Filos G., Galanakis D., Ganotis G., Georgiou Ch., Iordanidis S., Karageorgiou D., Karmis P., Karpetas Th., Kokkalis Th., Kostopoulos A., Koukis G., Koukoulis A., Kousoulas F., Koutsouveli A., Kyriakopoulos Th., Lappas I., Letsios K., Loupasakis C., Manazis St., Mastrogiannis F., Michalopoulos N., Mitropoulos D., Moraiti E., Nikolaides M., Nikolakopoulos K., Nikolaou N., Panagopoulos A., Pantelias E., Paraschakis Th., Photiades A., Pisinis K., Polyizou L., Sampatakakis P., Spyropoulos I., Tassiou S., Tsiounis E., Tzoumas S., Vassiliades E., Vertsiotis V., Zacharaki P., Zagouroglou C., Zananiri I. and Zimianitis E. Special acknowledgment is granted to the team of the Geodynamics Institute of the National Observatory of Athens (scientific responsible: Karastathis V.) and the geologists Hademenos V., Maroulakis Sp. for their systematic work and support.

6. References

Andrinopoulos, A., Zacharaki, E., Zimianitis, E., Maroulakis, S., Mitropoulos, D. and Efthimiou, G.,

2008. Marine geological study of the Northern Argolic gulf. Technical report, IGME, Athens, Greece.
- Galanakis, D. and Georgiou, Ch., 2008. Neotectonic study of the urban and suburban area of Nafplio (pilot application). Technical report, IGME, Athens, Greece.
- Giroux, D., Bélanger, J.R., 2003. An interactive map viewer for the Urban Geology of Ottawa (Canada): an example of web publishing. *European Geophysical Society, Geophysical Research Abstracts*, Vol. 5, 00842. Available online at: <http://www.cosis.net/abstracts/EAE03/00842/EAE03-J-00842.pdf>
- Karmis, P., 2008. Electrical – electromagnetical survey at the urban area of Nafplio, Argolis prefecture. Technical report, IGME, Athens, Greece.
- Legget, R.F., 1969. Urban Geology. *Canadian Building Digest*, CBD – 113, National Research Council Canada. Available online at: <http://irc.web-t.cisti.nrc.ca/cbd/cbd113e.html>
- Pantelias, E., Zervakou, A., Tsombos, P. and Nikolakopoulos, K., 2008. Spatial database for the management of Urban Geology geothematic information: the case of Drama City, Greece. *Proceedings, 15th International Symposium on Remote Sensing of the International Society for Optical Engineering, September 15-19, Cardiff, Wales, United Kingdom*, Proc. SPIE, Vol. 7110.
- Pantelias, E., 2009. Test drillings at the urban and suburban pilot area of Nafplio, Argolis prefecture. Technical report, IGME, Athens, Greece.
- Photiades, A., 2008. Geological study of the urban and suburban pilot area of Nafplio, Argolis prefecture. Technical report, IGME, Athens, Greece.
- Rau, J., 2005. Teaching Urban Geology from the Bottom Up. *Geotimes*. Available online at: <http://www.agiweb.org/geotimes/oct05/comment.html>
- Zananiri, I., 2009. Geomagnetic survey at the city of Argos, Argolis Prefecture. Technical report, IGME, Athens, Greece.
- Zananiri, I., Hademenos, V. and Piteros, Ch., 2010. Geophysical investigations near the ancient Agora at the city of Argos, Greece. *Journal of Geophysics and Engineering*, Vol. 7.
- Zervakou, A., Tsombos, P. and Nikolakopoulos, K., 2007. Urban Geology: Documentation of geo-thematic information for urban areas in Greece: the case of Nafplion. *Proceedings, 14th International Symposium on Remote Sensing of the International Society for Optical Engineering, September 17-20, Palazzo degli Affari Conference Ctr., Florence, Italy*, Proc. SPIE, Vol. 6749 p. 67491G1-12.
- Zervakou, A., Tsombos, P. and Nikolakopoulos, K., 2008. Urban Geology and GIS: The example of IGME. *5th Greek Conference HellasGIs: «GIS and Environment», December 4-5, Athens, Greece*.
- Zervakou, A.D. and Tsombos, P.I., 2010. GIS in Urban Geology: the case study of Nafplio, Argolis prefecture, Greece. *Bulletin of the Geological Society of Greece, Proceedings of the 12th International Congress* (this volume).

GEOARCHAEOLOGICAL STUDIES IN URBAN AND SUBURBAN AREAS OF THE ARGOLIS PREFECTURE.

Zananiri I.¹, Chiotis E.¹, Tsombos P.¹, Hademenos V.¹ and Zervakou A.¹

¹ Institute of Geology and Mineral Exploration (I.G.M.E.), Division of General Geology and Geological Mapping, I Spirou Loui str., Olympic Village, 3rd Entrance, 13677 Acharnae, Greece, izanan@igme.gr, echiotis@otenet.gr, ptsombos@igme.gr, bashadem@hotmail.com, zervakou@igme.gr

Abstract

The application of earth science principles and techniques to the understanding of the archaeological record has become a common practice, while reducing the archaeological risk is possible by clarifying areas of archaeological potential at an early stage. Towards this scope non-invasive geophysical magnetometry surveys were carried out at the city of Argos, successfully locating areas of interest for future excavations. Geoarchaeology studies in the Argolis Prefecture also involved the spatial location of the archaeological protection zones in the city of Nafplio, by combining data from the Official Government Gazettes, aerial photographs and high-resolution satellite images. Another study dealt with the palaeogeographic evolution of the broader Palea Epidavros area; field-work comprised electric resistivity soundings, total field magnetic measurements and two research boreholes at different altitudes. Finally, geoarchaeological research was employed to locate rocks suitable for the restoration of the Grave Circle A of Mycenae. The data management and cartographic representation was performed, in all cases, using Geographic Information Systems, where a geographic database was created, including all available information: local geology, topographic features, satellite images and archaeological data.

Key words: *geoarchaeology, magnetometry, electric resistivity, GIS, Argolis prefecture.*

1. Introduction

Geoarchaeology is an approach to the study of archaeological issues using the methods and concepts of the earth sciences. Attention is focused on the physical context of archaeological remains, especially in relation to geomorphological processes, site formation, post-depositional transformations, and the relationships between cultural and natural processes [Geoarchaeology (n.d.), 2010]. Modern geoarchaeological research makes use of a vast number of sophisticated techniques that either have been used in geology and pedology or have been developed or refined for geoarchaeological purposes.

Towards this scope, advanced geophysical techniques have been widely employed over the past decades to assist archaeologists during excavation planning (e.g. Patella and Hesse, 1999; Sarris and Jones, 2000; Gaffney and Gater 2003, Vafidis et al., 2005; English Heritage, 2008). Their application is based on the detection of inhomogeneities of the geophysical parameters of the ground, caused by the presence of buried archaeological structures and artefacts. Detailed magnetometry is a rapid, effective and non-invasive tool for the localization of buried structures (e.g. Tsokas et al., 1986, 1994) and constitutes the basis of archaeological surveying, complemented where necessary



Fig. 1: Satellite image – taken from Google Earth – showing the location of the studied sites in the Argolis prefecture.

by ground penetrating radar, electric and electromagnetic methods (e.g. Sambuelli et al., 1999; Kvamme, 2001; Diamanti et al., 2005; Drahor, 2006; Papadopoulos et al., 2009).

The Institute of Geology and Mineral Exploration (I.G.M.E.) of Greece, in the frame of “Community Support Framework 2000 – 2006”, Operational Program “Competitiveness”, implemented the project called “Collection, codification and documentation of geothematic information for urban and suburban areas in Greece. Pilot studies”. In the framework of subproject 3 “Integrated geological, geotechnical, hydrogeological, geochemical, geophysical and marine studies of the urban and suburban pilot area of Nafplio, Argolis municipality”, geoarchaeological investigations were carried out in urban archaeological locations. This paper presents the preliminary results from the application of archaeological geophysics at the city of Argos and the town of Palea Epidavros, as well as data from two geoarchaeology studies that involve the city of Nafplio and the 1st Grave Circle in the acropolis of Mycenae (Fig. 1).

2. Geological setting

The Argolis Peninsula consists of a stack of tectonic units, comprising ophiolites as well as deep water and platform sediments deposited at the Pelagonian margin (Pomoni-Papaioannou and Photiades, 2007). It comprises a composite nappe pile (Bortolotti et al., 2003 and references therein) of several imbricated pre-Neogene tectonic units, tectonically assembled in two major distinct tectonic phases, one in the late Jurassic and the other in the late Eocene (Photiades and Skourtsis-Coroneou, 1994). The study area is covered by three adjacent geological map sheets of 1:50.000 scale, namely the Argos (Papastamatiou et al., 1970), Ligourion (Tataris et al., 1970) and Nafplion (Bannert et al., 1984), the latter two recently updated by Photiades (pers. communication). A detailed analysis of the local geology can be found in Photiades (2008, 2010).



Fig. 2: (a) Remains of occupation structures revealed during excavation by the 4th Ephoria of Prehistoric and Classical Antiquities (E.P.C.A.) nearby the study area. The remnants were buried at about 0.5 m depth. Site 1 of the present study is seen in the background; (b) General view of site 2, where the layout of the measuring grid is shown.

3. Argos

The city of Argos, today an agricultural and industrial centre of the Argolis Prefecture, was one of the most prominent city-states from the beginning of Archaic Times (c. 800 B.C.) and through to Classical Times. The modern city is mainly built on a 1.5-5.0m elevated surface of alluvial deposits (Pitéros, 1998), that overlay ancient habitation ruins.

In order to reduce risk in archaeological excavations by identifying areas of high potential at an early stage a non-invasive geophysical survey was carried (Zananiri and Zervakou, 2008; Zananiri, 2009, Zananiri et al. 2010). Based on historical and archaeological evidence three sites were chosen near the ancient Agora of Argos (Fig. 2) and at the outskirts of the city. Total field and gradient magnetic measurements were collected over several grids, with 1m spacing between measurement points. Representative samples from the top-soil and possible construction materials were taken for laboratory measurements of the low-field magnetic susceptibility, enabling a qualitative estimation of the nature of the expected magnetic anomalies. For example, positive magnetic anomalies may represent the remains of brick walls, while negative anomalies can correspond to limestone constructions in a relatively high susceptibility environment. Mapping, filtering and inversion procedures of the magnetic data have been used in tandem (Fig. 3). The data management and cartographic representation was performed using Geographic Information Systems, where a geographic database was created, including all available information for the broader Argos area. The results of the geophysical survey were able to highlight the presence of linear and geometric structures possibly representing inhabitation ruins, namely small building remnants and road foundations according to observations from neighbouring excavations. As can be seen in Figure 4 the general anomaly directions of a 20 × 20 grid, located near the ancient Agora of Argos are trending NW-SE parallel to the suggested positions of the main ancient roads at the city of Argos (Pausanias II, 19.3). Thus, the authors were able to suggest to the archaeologists excavation tests on the basis of the residual magnetic map.

4. Nafplio

Geoarchaeology studies in the Argolis Prefecture also involved the spatial location of the archaeo-

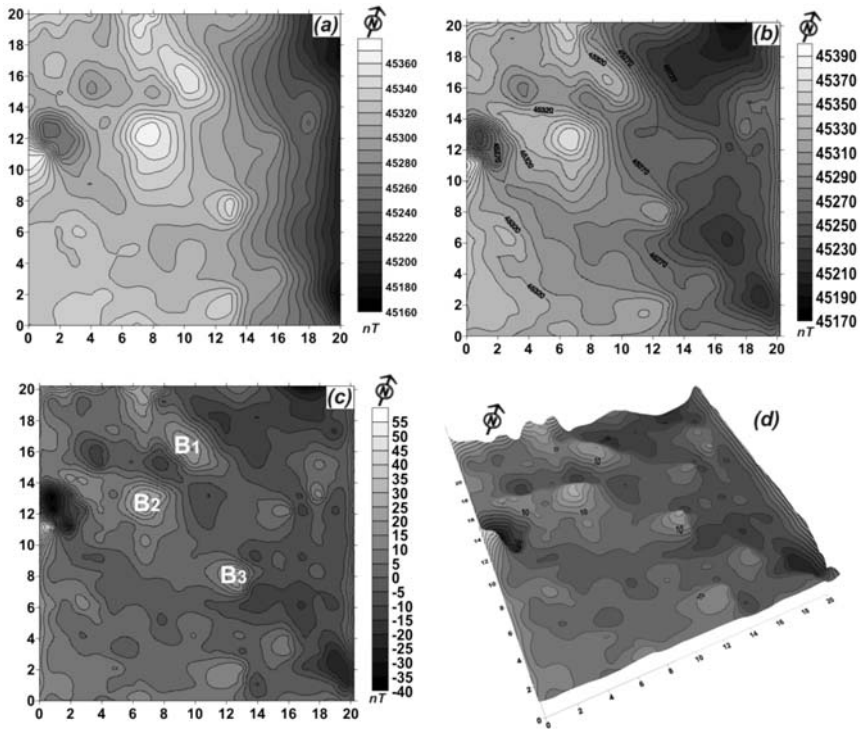


Fig. 3: Magnetic survey results from a 20×20 grid, located near the ancient Agora of Argos: (a) Raw data of the total magnetic field (after diurnal correction and despiking); (b) reduction to pole; (c) residual field and (d) 3-D mapping of the residual magnetic field. The letters B₁, B₂ and B₃ denote areas having high positive anomalies, which may correspond to foundation remnants, e.g. pillars from the corners of buildings.

logical protection zones in the city of Nafplio. These zones were defined by the Hellenic State and published in the Official Government Gazettes, however their location was not easily accessible to the general public and a need for an intelligible visual representation was imminent. This task was carried out by combining data from the Official Government Gazettes, aerial photographs and high-resolution satellite images in a GIS environment. Thus, a detailed mapping of the limits of zone A – totally protected, no construction allowed – and zone B – partially protected, conditional construction allowed – was performed (Fig. 4).

In this way that information is easily accessible by the local authorities, the scientific community and the general public, providing a handy tool for monitoring the current situation and effectively planning urban development of the city of Nafplio.

5. Palea Epidavros

The ancient town of Palea Epidavros, inhabited since the 3rd millennium B.C., has not been systematically excavated; however, numerous ruins, from different eras, outcrop all over the so-called “Nisi”, which is the Greek term for island, peninsula. The ancient theatre, t.i. the Small Theater of Ancient Epidavros, is found on the western side of the peninsula, near the slope of the strait connecting the Nisi peninsula with the mainland. Noteworthy is the fact that Pausanias, when during his travels visited the area in the middle of 2nd century A.D. refers to the temples, the agora and the sea-

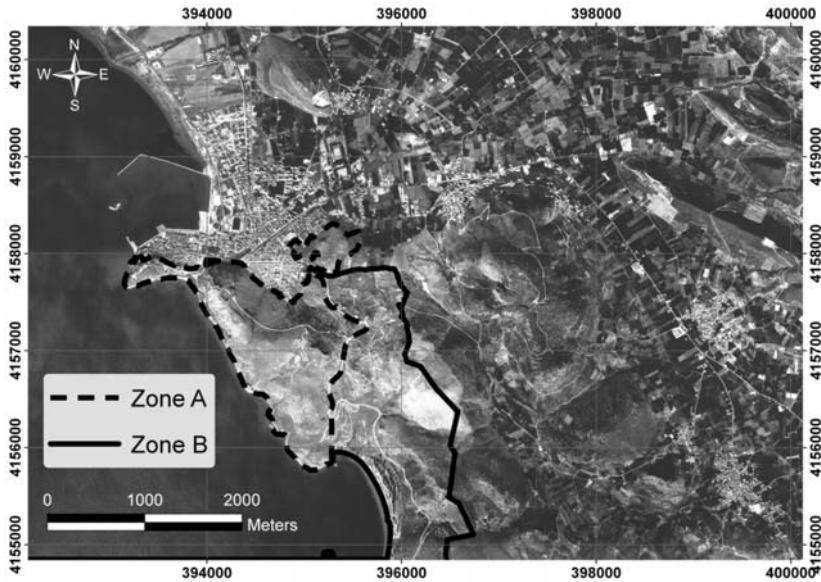


Fig. 4: Orthophoto mosaic from the broader Nafplio area, where the archaeological protection zones for the city of Nafplio are shown.

port, but does not mention the theatre. Thus, several questions arise concerning the palaeogeographic evolution of the area and especially the strait of Nisi.

Towards this scope a geophysical and stratigraphy study was carried out (Zananiri, 2009) in the broader area of Palea Epidavros, in order to investigate the possible presence of a marine channel between the Nisi peninsula and the main coast. The fieldwork comprised 17 vertical electric soundings (Figs. 5 & 6) and measurements of the total magnetic field at a total of 90 stations; finally in May 2008 two exploratory boreholes were drilled, reaching 12.16m and 14.40m respectively. The locations of the fieldwork activities were determined in collaboration with archaeologists from the 4th Ephoria of Prehistoric and Classical Antiquities (E.P.C.A.). A preliminary examination of the drilled cores has been carried out, while detailed textural examination is in progress. Finally, laboratory magnetic measurements (Fig. 7) were performed on samples from both cores, taken every 10-15cm: low and high field magnetic susceptibility, frequency dependence calculation, isothermal remanence acquisition and thermomagnetic analyses. The data management and cartographic representation was performed using Geographic Information Systems and Google Earth platform.

6. Grave Circle A of Mycenae

The Grave Circle A of Mycenae (Fig. 8), excavated in the 1876 by Schliemann, is among the most important prehistoric monuments of Greece, very well known for the rich findings and the gold masks of the royal burials dated to the 16th century B.C. Later, in the 13th century B.C., the graves were enclosed by upright slabs of stone, forming two concentric circles.

The target of the survey (Chiotis et al., 2006), assigned to I.G.M.E. by the Committee for the restoration of Mycenae, was to localize similar rocks, proper for the restoration of these concentric circles.

The slabs of the monument consist by 84% of bioclastic limestone; they are frequently rich in siz-

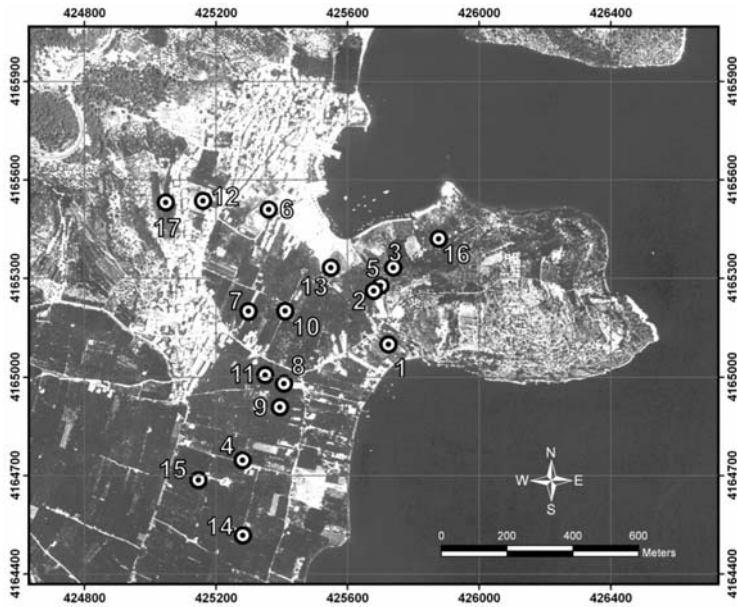


Fig. 5: Satellite image of the broader Palea Epidavros area where the location of the VESs is shown.

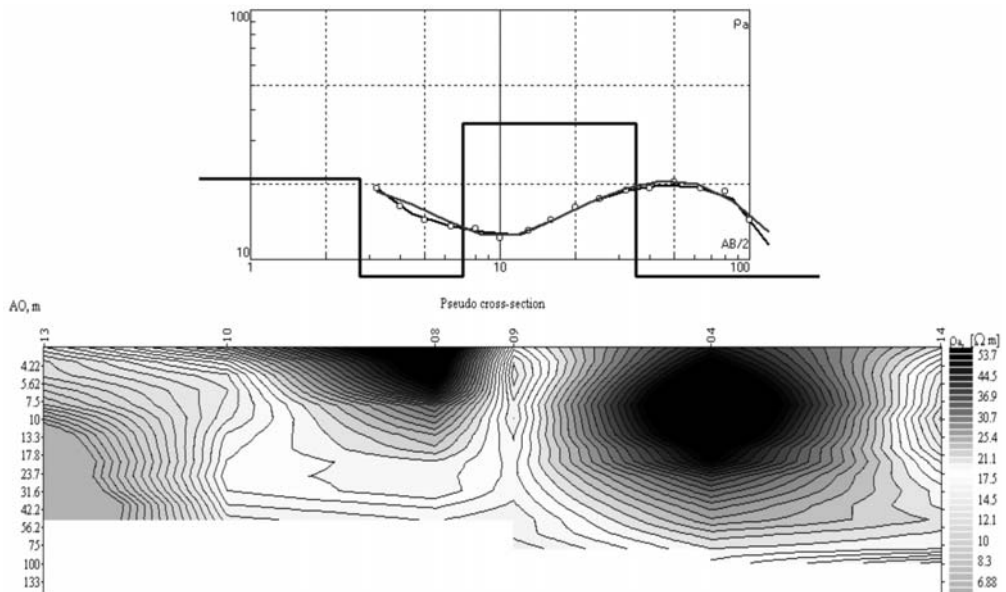


Fig. 6: An example of a vertical electric sounding (top) and the corresponding pseudo cross-section of apparent resistivity (bottom).

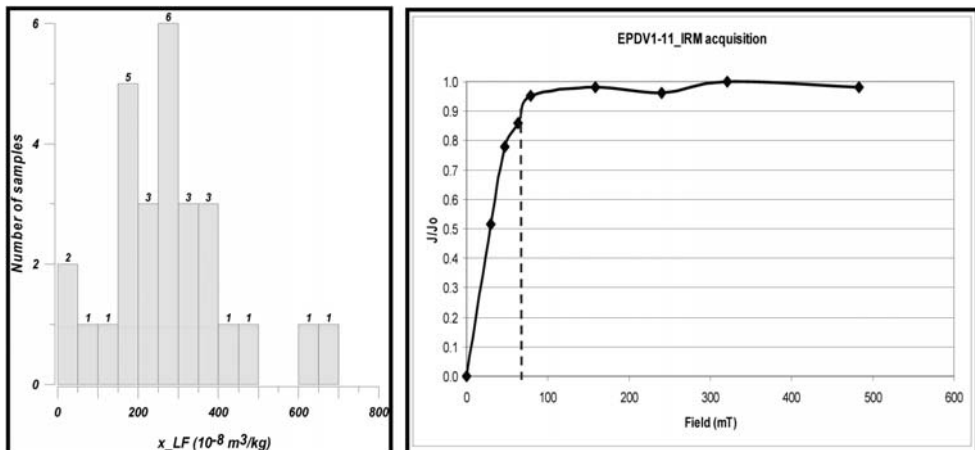


Fig. 7: Low field magnetic susceptibility histogram (left) and isothermal remanent magnetization acquisition curves (right) from samples extracted from the Epidavros boreholes.

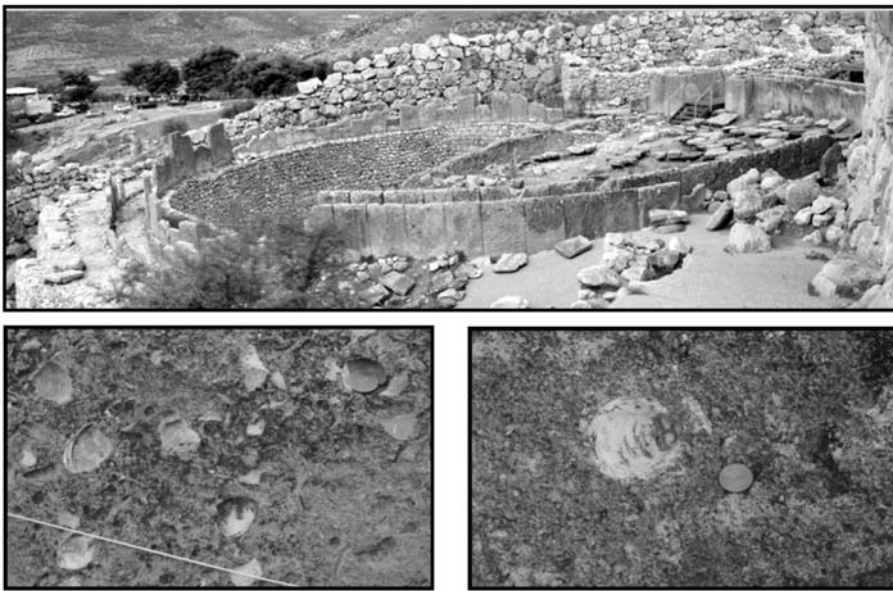


Fig. 8: Grave Circle A of Mycenae: view from SE (top) and typical images of fossiliferous rocks from the Grave Circle columns (bottom).

able fossils indicating a littoral marine environment of sedimentation. The rest participating rock types are sandstone, occasionally fossiliferous, fine conglomerate and oolitic limestone. Palaeontological and lithofacial criteria were suggestive of a Pleistocene age; taking into account the geological setting of the broader area, located near the Gulf of Corinth – an active extensional basin, the search for similar rocks was focused on the Tyrrhenian formations, starting from the outcrops in Nafplion and shifting successively to Corinth, Loutraki and Perachora areas (Zananiri et al., 2008 and references therein). The requirement of the restoration team for compact slabs, (1×1.5×0.15m)

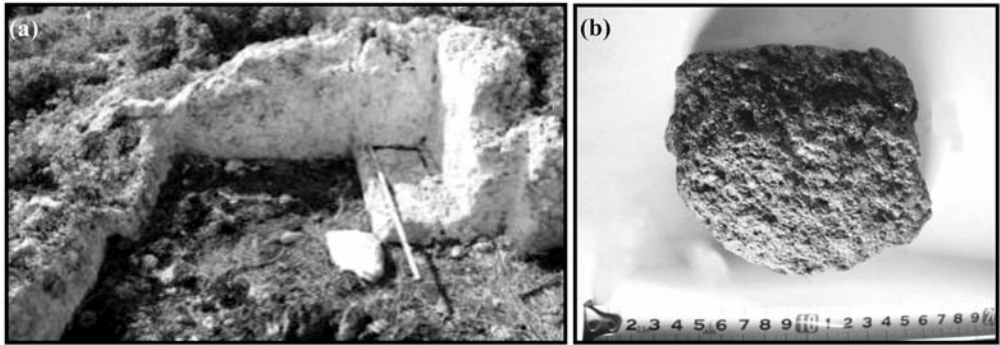


Fig. 9: (a) Ancient quarry of fossiliferous limestone in a Tyrrhenean marine terrace at Perachora peninsula; (b) Volcanic grinder.

large, was a serious restriction that excluded many of the already mapped geological outcrops. Proper formations with sufficient reserves were localized in the area of Perachora, near the Vouliagmeni Lake. The Tyrrhenian outcrops in Perachora occur in terraces which are tectonically uplifted up to an elevation of 160m. The prehistoric quarries (Fig. 9a) used for the excavation of the slabs of the Grave Circle A were also found in Perachora, very close to Mycenaean chamber tombs. The excavated blocks were surrounded by trenches, 12cm wide, partly opened by rock abrasion through the use of volcanic rocks (Fig. 9b). A similar grinder of volcanic rock was also found in the monument, apparently used for smoothing the slabs.

7. Conclusions

The discipline of geoarchaeology, where geology sides with archaeology towards the study and preservation of our cultural heritage, is highly prominent worldwide and during the past few decades is being developed in Greece as well. The Institute of Geology & Mineral Exploration, in the framework of C.S.F. 2000 – 2006 implemented geoarchaeological research in the broader area of Argolis Prefecture, one of the most active regions in Greece in terms of archaeological excavations that have taken place during the past decades. The studies presented here constitute a joint initiative by the I.G.M.E. and the archaeologists of the 4th Ephoria of Prehistorical and Classical Antiquities towards the development of a systematic geoarchaeological survey in the Argolis Prefecture.

From the realization of these projects, and a preliminary interpretation of the results, several conclusions were drawn and important information was provided:

- The magnetic survey, at the city of Argos, provided indications for the location and burial depth of occupational remnants.
- A detailed mapping of the archaeological protection zones around the city of Nafplio was accomplished.
- There are indications that a marine channel used to separate the Nisi peninsula from the main land at Palea Epidavros
- Ancient quarries of fossiliferous limestones, suitable for the restoration of the Grave Circle A columns, were found in Tyrrhenean marine terraces at Perachora peninsula.

However, it is important to point out that geophysical surveys and other applied geological techniques do not substitute archaeological excavations but can contribute significantly to an optimum excavation planning by defining areas of increased interest and thus cut down excavation cost and time.

8. Acknowledgements

This work was funded by the Community Support Framework 2000 – 2006 (Operational Program “Competitiveness”). We would like to thank A. Banaka, Director of the 4th Ephoria of Prehistoric and Classical Antiquities at Nafplio, and Ch. Pitero, Assistant Director, for their support and encouragement in the application of earth sciences towards the rescue of cultural heritage. G. Papatanasopoulos, Ch. Antoniadis, E. Paleologou, G. Biniaris, S. Spiropoulou and G. Tzavalis are gratefully acknowledged for providing invaluable information and assistance during the conception and realization of this project. We thank all colleagues who participated in this multidisciplinary research and especially Dr. A. Photiadis, Dr. E. Dimou, G. Efthimiou, and D. Mitropoulos. P. Tsailas kindly provided geomagnetic data from the Magnetic Observatory of I.G.M.E. Prof. D. Kondopoulou is warmly thanked for allowing the use of the facilities at the Palaeomagnetic Laboratory of the Aristotle University of Thessaloniki. Finally, we are especially grateful to Prof. A. Georgakopoulos, former General Director of I.G.M.E., for his encouragement and support towards the development of geoarchaeological research.

9. References

- Bannert, D., Kalkreuth, W. and Wallner, 1984. Geological map scale 1:50.000. Sheet of Nafplion. *Institute of Geology and Mineral Exploration*, Athens, Greece.
- Bortolotti, V., Carras, N., Chiari, M., Fazzuoli, M., Marcucci, M., Photiades, A. and Principi, G., 2003. The Argolis Peninsula in the palaeogeographic and geodynamic frame of the Hellenides. *Ofioliti*, 28/2, 79-94.
- Chiotis, E., Tsombos, P. and Photiades, A., 2006. Report of the results from a geological survey for the recommendation of proper rocks for the restoration of the Grave Circle A in Mycenae. *Institute of Geology & Mineral Exploration*, Athens, pp.31.
- Diamanti, N.G., Tsokas, G.N., Tsourlos, P.I. and Vafidis, A., 2005. Integrated interpretation of geophysical data in the archaeological site of Europos (Northern Greece). *Archaeological Prospection* 12, 79-91.
- Drahor, M.G., 2006. Integrated geophysical studies in the upper part of Sardis archaeological site, Turkey. *Journal of Applied Geophysics* 59, 205-223.
- English Heritage, 2008. *Geophysical Survey in Archaeological Field Evaluation*. English Heritage, Swindon, pp. 60.
- Gaffney, C. and Gater, J., 2003. *Revealing the buried past: geophysics for archaeologists*. Stroud, Tempus.
- Geoarchaeology (n.d.), 2010. *The Concise Oxford Dictionary of Archaeology*. Retrieved January 21, 2010, from Answers.com Web site: <http://www.answers.com/topic/geoarchaeology-1>
- Kvamme, K.L., 2001. Current practices in archaeogeophysics. In: *Earth Sciences and Archaeology* (Eds. Goldberg, P., Holliday, V.T. & Ferring, C.R.), Kluwer Academic/Plenum New York, pp.353-384.
- Papadopoulos, N., Sarris, A., Yi, M.J. and Kim, J.H., 2009. Urban archaeological investigations using surface 3D Ground Penetrating Radar and Electrical Resistivity Tomography methods. *Exploration Geophysics* 40(1), 56-68.
- Patella, D. and Hesse, D.A., 1999. Electric, Magnetic and Electromagnetic methods applied to cultural heritage. *Journal of Applied Geophysics*, Special Issue 41, 135-311.
- Πανσανίου, 1903. *Ελλάδος Περιήγησις*, Βιβλίο ΙΙ: Κορινθιακά ed. F. Spiro, Leipzig, Teubner (M. l'abbé Gedoy, 1731, *Pausanias: Voyage historique de la Grèce* / traduit en François. Tome douzième chez Didot Paris).

- Papastamatiou, I., Vetoulis, D., Tataris, A., Christodoulou, G., Bornovas, I., Lalechos, N. and Kounis, G., 1970. Geological map scale 1:50.000. Sheet of Argos. *Institute of Geology and Mineral Exploration*, Athens Greece.
- Photiades, A. and Skourtsis-Coroneou, V., 1994. Stratigraphic and paleogeographic evolution of the Northern Argolis (Greece) during the Cretaceous - Paleogene. *Bull. Geol. Soc. Greece*, vol. XXX/2, 135-146.
- Photiadis A., 2008. Geological study of the urban and the wider Nafplio area. Argolida Prefecture. *Institute of Geology and Mineral Exploration*, Athens.
- Photiadis A., 2010. Geological survey in scale 1:5.000 of the greater Nafplion area (NW Argolis, Greece). *Bulletin of the Geological Society of Greece, Proceedings of the 12th International Congress* (this volume).
- Pitéros, Ch., 1998. Contribution a la topographie Argienne. Le site, les remparts et quelques problèmes topographiques. *Recherches Franco-Helléniques* III, 179-210.
- Pomoni-Papaioannou, F. and Photiades, A., 2007. Stacked loferite cycles and paleosoils (Upper Triassic, Argolis Peninsula, Greece), *Proc. 25th IAS Meeting, Patras, Greece*, p. 141.
- Renfrew, C., 1976. Archaeology and the earth sciences. In: *Geoarchaeology: Earth Science and the Past* (Eds D.A. Davidson & M.L. Shackley), Duckworth, London, pp. 1-5.
- Sambuelli, L., Socco, L.V. and Brecciaroli, L., 1999. Acquisition and processing of electric, magnetic and GPR data on a Roman site (Victimulae, Salussola, Biella). *Journal of Applied Geophysics* 41, 189-204.
- Sarris, A. and Jones, R., 2000. Geophysical and related techniques applied to archaeological survey in the Mediterranean: A Review. *Journal of Mediterranean Archaeology*, 13(1), 3-75.
- Tataris, A., Kallergis, G. and Kounis, G., 1970. Geological map scale 1:50.000. Sheet of Ligourion. *Institute of Geology and Mineral Exploration*, Athens, Greece.
- Tsokas, G.N., Rocca, A.Ch. and Papazachos, B.C., 1986. Magnetic prospecting at the Prehistoric site of the village Mandalo in Northern Greece. *P.A.C.T.* 15, 143-152.
- Tsokas, G.N., Giannopoulos, A., Tsourlos, P., Vargemezis, G., Tealby, J.M., Sarris, A., Papazachos, C.B. and Savopoulou, T., 1994. A large scale geophysical survey in the archaeological site of Europos (northern Greece). *Journal of Applied Geophysics* 32, 85-98.
- Vafidis, A., Economou, N., Ganiatsos, Y., Manakou, M., Poulioudis, G., Sourlas, G., Vrontaki, E., Sarris, A., Guy, M. and Kalpaxis, Th., 2005. Integrated geophysical studies at ancient Itanos (Greece). *Journal of Archaeological Science* 32, 1023-1036.
- Zananiri, I. and Zervakou, A., 2008. Geoarchaeological survey at the broader Argos area, Argolis Prefecture. *Institute of Geology & Mineral Exploration*, Athens, pp. 32.
- Zananiri, I., Tsombos, P., Photiades, A. and Chiotis, E., 2008. The Gulf of Corinth as an international geological laboratory. The case of Perachora peninsula. *Bull. Geol. Soc. Greece*, Proceedings of the Conference "Land and Sea of Korinthos", XXXVI, 53-64.
- Zananiri, I., 2009. Geomagnetic survey at the city of Argos, Argolis Prefecture. *Institute of Geology & Mineral Exploration*, Athens, pp. 26.
- Zananiri, I., Hademenos, V. and Piteros, Ch., 2010. Geophysical investigations near the ancient Agora at the city of Argos, Greece. *Journal of Geophysics and Engineering*, Vol. 7.

VISUALIZATION OF DATASETS FROM URBAN GEOLOGY STUDIES USING GOOGLE EARTH: THE CASE STUDY OF NAFPLIO, ARGOLIS PREFECTURE.

Zananiri I.¹, Zervakou A.¹, Tsombos P.¹ and Chiotis E.¹

¹ *Institute of Geology and Mineral Exploration (I.G.M.E.), Olympic Village, 3rd Entrance, 13677 Acharnae, Greece, izanan@igme.gr, zervakou@igme.gr, ptsombos@igme.gr, echiotis@otenet.gr*

Abstract

The systematic use of tools provided in Geographic Information Systems in data mapping makes easy the management of the data acquired from urban geology studies. However, the information derived concern not only the scientific society but also the local authorities and the general public. Thus, a simple way of data dissemination had to be adopted. Online tools, such as those pioneered by Google Earth™ (GE), are changing the way in which scientists and the general public interact with geospatial data in a virtual environment. In the past years since its 2005 introduction, GE has introduced numerous applications, in geosciences as well as in many socio-economic disciplines. I.G.M.E., in the framework of CSF 2000 – 2006 (Operational Program “Competitiveness”), implemented the project called “Collection, codification and documentation of geothematic information for urban and suburban areas in Greece. Pilot studies”. Data management and cartographic representation was performed using G.I.S., where a geographic database was created, including all available information for the studied areas: geology, topography, satellite images, geophysical, geochemical, geotechnical, hydrogeological and geoarchaeological data. Critical information from the geodatabase concerning the study area of the city of Nafplio, Argolis Prefecture, were imported in Google Earth and stored as a Keyhole Markup Language Zipped file, rendering a 2-D layer in GE directly, to facilitate dissemination.

Key words: *Google Earth, GIS database, urban geology, Nafplio.*

1. Introduction

Sustainable urban planning and development depends on the access to high quality geological data; therefore urban geology has emerged as an important research area worldwide (e.g. Legget, 1969; de Mulder, 1993; Fuchu et al., 1994; Karrow and White, 1998; Nott, 2003). Urban geology studies rely on diverse branches of earth sciences, such as geological mapping, satellite remote sensing, hydrology, engineering geology, geochemistry, geophysics, environmental geology and geoarchaeology, in order to build a three-dimensional model of the character of the land and to explain the geological processes involved in the dynamic equilibrium of the local environment. The acquired geothematic information contributes to the design and implementation of prevention and protection measures against natural hazards, the realization of rational urban planning, the protection and enhancement of the urban and suburban environment and the setting of qualitative and quantitative targets for environmental goods. They constitute a constant source of information for the compilation



Fig. 1: Satellite image from Google Earth showing the location of the city of Nafplio and main topographic features of the broader area.

of studies, as well as reference point for possible future changes, ensuring the spatial and geological coherency of the entire data set (maps, borehole logs, geophysical measurements, etc). Furthermore, the interoperability of data banks at urban and national levels is a stake of prime importance for all providers of referenced geological data.

Geographic Information Systems (GIS) is a powerful tool for many aspects of geospatial analyses (Longley et al., 2001), but while used routinely to map data and solve complex problems, its adoption in data sharing has been lagging. Part of the problem is that desktop GIS software is commercial and complex in use and the required geospatial data are in most cases inaccessible for non-professional users. Open source solutions for Web mapping, such as the UMN MapServer (MapServer, 2009) or Deegree (Deegree, 2007) are often available for free, but require knowledge of digital maps, encoding and transfer protocols. The recent development of Google Earth (GE; Google Inc., 2009), a free web-based geographical information service that provides satellite imagery and three-dimensional (3D) data depicting the entire planet, has changed the way in which scientists and the general public interact with geospatial data in a virtual environment.

In this paper we demonstrate how geospatial data can be easily displayed and communicated by combining GE and GIS, using data from an urban geology study, carried out by the Institute of Geology and Mineral Exploration (I.G.M.E.) of Greece.

2. The case study of Nafplio

The first systematic recording, codification and documentation of “Urban geology” geothematic information in Greece was implemented by the I.G.M.E. with the participation of 70 specialized scientists and 30 technical employees, in the frame of the project “Collection, codification and documentation of geothematic information for urban and suburban areas in Greece - pilot applications” (Operational Program “Competitiveness“, Community Support Framework 2000-2006) (Tsombos and Zervakou, 2010). Subproject 3, called “Integrated geological, geotechnical, hydrogeological, geochemical, geophysical and marine studies of the urban and suburban pilot area of Nafplio, Argolis prefecture” (Zervakou et al., 2007), focused in the broader area of Nafplio (Fig. 1), in north eastern Peloponnese.

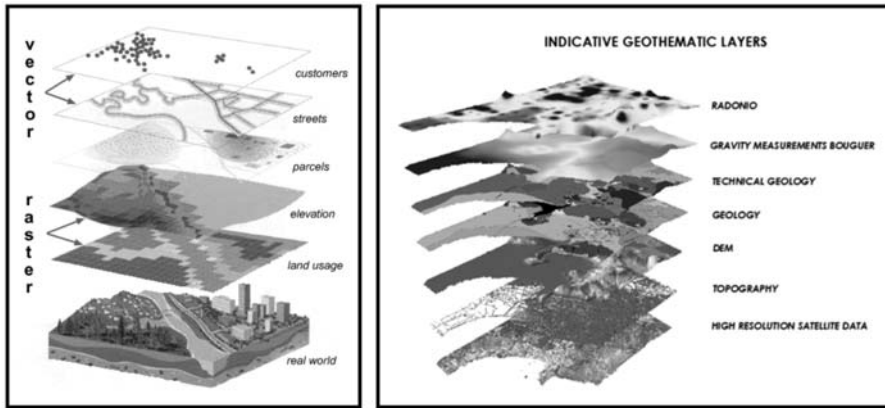


Fig. 2: The concept of geothematic layers (ESRI) in a general example for urban development (left) and the case of Nafplio from the urban geology project of IGME (right).

During the elaboration of this project “in situ” studies and measurements took place; all geoscience information derived from various sources such as borehole logs, geological mapping, geotechnical, geochemical, geophysical research and measurements, hydrological reports and digital elevation models were compiled, stored and processed in specially designed georeferenced databases in GIS environment.

2.1. General information of the study area

Nafplio (146 km southwest of Athens) is a seaport city that has been expanded up to the hillsides near the north end of the Argolic Gulf (Argolikos Bay). Most of the old city is on a peninsula jutting into the gulf. This peninsula forms a naturally protected bay that is enhanced by the addition of man-made moles.

The city was the First capital of the liberated, from the Turks, Greece from 1829 to 1834. Its buildings, renowned castles and generally the whole layout of the city makes Nafplio an important tourist centre. The fortress complex of Nafplio is extensive and imposing. The oldest fortress of all is Akro-nafplia, in the homonymous peninsula. On the opposite rocky hill rises the famous Palamidi. Bourtzi is found in front of the harbour, in the shallow waters. All three castles are remarkable not only for their archaeological importance but also for their incredible location.

Nafplio city is connected with the national road Corinth - Tripoli through main provincial transportation network via Argos (SW of Nafplio). Also there is now a railway station with daily trains from/to Corinth and Athens and there is a connection with Ermioni, Porto Heli, Tolo, and the Argosaronic Gulf Islands by flying dolphins or boats from Piraeus. As a result, Nafplio is a well-connected city with the mainland Peloponnese and the near ports.

3. Applied methodology

3.1. GIS applications

GIS are used by a heterogeneous group of individuals and organizations for an incredibly wide variety of applications. A Geographic Information System is best described as an integrated collection of hardware, software, data and computer users, which operates in an institutional context. The key features that differentiate GIS from other information systems are the general focus on spatial entities and relationship, together with specific attention to spatial analytical and modelling operations.

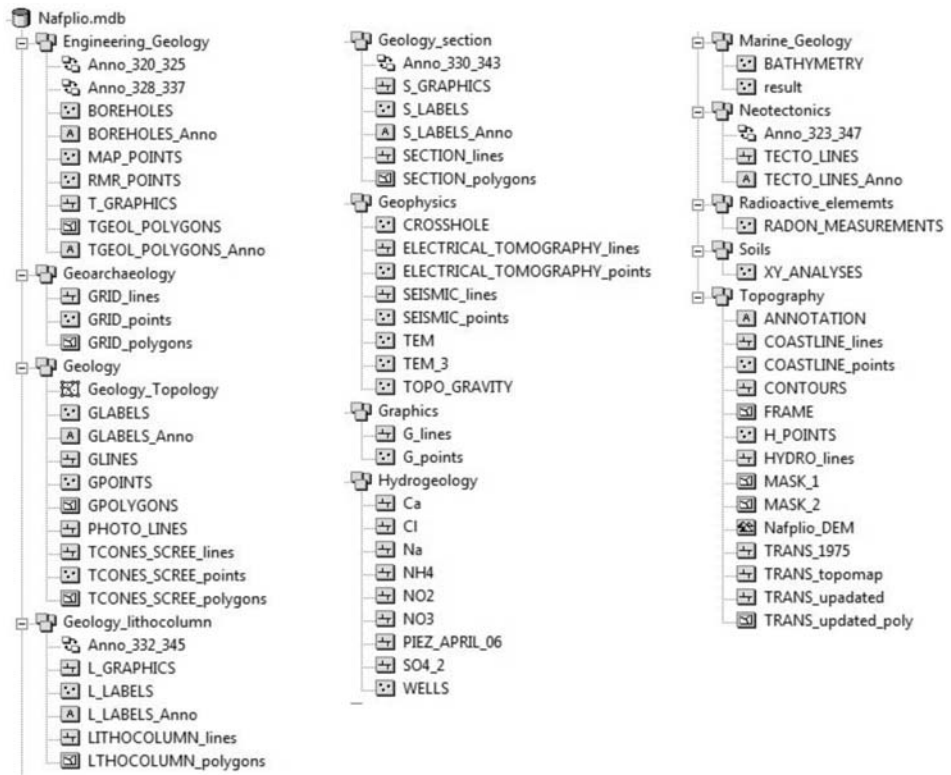


Fig. 3: Nafplio Urban geology geodatabase contents.

In a technical sense, it is the ability to organize and integrate apparently disparate data sets together which makes GIS so powerful (Maguire, 1991).

The spatial searching and overlay operations are a key functional feature of GIS (Maguire, 1991). A more comprehensive and easy way to define GIS is the one that looks at the disposition, in layers (Fig. 2), of its data sets.

Geographic information systems have emerged in the last decade as an essential tool for urban and resource planning and management. Their capacity to store, retrieve, analyse, model and map large areas with huge volumes of spatial data has led to an extraordinary proliferation of applications. Geographic information systems are now used for land use planning, utilities management, ecosystems modelling, landscape assessment and planning, transportation and infrastructure planning, market analysis, visual impact analysis, facilities management, tax assessment, real estate analysis and many other applications.

Within a Geographic Information System a spatial database or so called “Geodatabase” is a crucial component that can be used to store, manipulate and process such complex data derived from urban survey and study. Geodatabases enable efficient state management and archiving of geodata. Actually, the geodatabase is the core geographic information model to organize GIS data into thematic layers and spatial representations. It supports both vector and raster data, while entities are represented as objects with properties, behaviour, and relationships.

For the specific urban geology project of IGME a geodatabase called “Nafplion” (Fig. 3) was built in GIS Environment (software ArcGIS 9x, ArcInfo version, ESRI). The used format for editing and data management was ArcGIS Geodatabase, a native data structure for ArcGIS software. It is a collection of geographic datasets of various types held in a common file system folder, a Microsoft Access database, or a multi-user relational database, such as Oracle, Microsoft SQL Server, or IBM DB2.

All geoinformation is compiled in feature classes and grouped in the following thematically organized feature datasets (a detailed description of dataset contents is given by Zervakou & Tsombos, 2010):

- Feature dataset Topography
- Feature dataset Geology
- Feature dataset Engineering Geology
- Feature dataset Neotectonics
- Feature dataset Marine Geology:
- Feature dataset Hydrogeology
- Feature dataset Geophysics
- Feature dataset Soils
- Feature dataset Radioactive elements
- Feature dataset Geoarchaeology

3.2. Web-based application

Access to spatial data as well as advanced mapping and spatial analysis over the Internet is becoming more common (e.g. Beaudette and O’Green, 2009; Montesano et al., 2009). Recent attention has focused on developing GIS functionality in the Internet, Worldwide Web and private intranets, termed as WebGIS.

WebGIS holds the potential to make *distributed geographic information* available to a very large worldwide audience. In order to access the spatial information, the user needs only to have a Web browser and access to the Internet. This way, internet users are able to access GIS applications from their browsers without purchasing proprietary GIS software.

Web 2.0 applications such as Google Maps, Yahoo Maps, or Microsoft Live Maps provide free access to easy-to-use functionality as well as high-quality map data. With the success of Google Earth (2007) and Microsoft Virtual Earth (2007), the broader community has found an interest in visualising scenarios, city-centres and entire maps interactively in 3D (e.g. Pearce et al., 2007; Conroy et al., 2008).

More specifically, Google Earth combines satellite imagery, geographic data and Google’s search capabilities to create a virtual globe application that you can download to your desktop to access on-line spatial data. GE is a virtual globe, currently freely available for personal use on PC running on Windows, Macintosh and Linux operating system. For commercial and professional use many, affordable, solutions are available. The original project was developed by Keyhole Inc. (2001), which was bought by Google in 2004.

Data organized in layers can be exported to the Keyhole Mark-up Language (KML/KMZ) native to GE, transmitted to colleagues, members of the local authorities or even the general public as an email attachment, and then simply “dragged and dropped” by the recipient onto their own desktop GE display, where the map layers appear “draped” over the GE landscape. The recipient has access to all the graphics and attributes of each map layer that has been exported from GIS as well as to all GE tools, e.g. ability to adjust map layer transparencies, labelling, longitude/latitude (or UTM determinations),



Fig. 4: Google Earth representation of topographic linear spatial features (contours, hydrological network, transportation network) from the broader area of Nafplio.

spatial measurements, and “tilting” of landscapes for enhanced 3D views. These tools are often sufficient to allow the non-GIS user to obtain specific information of interest from the data.

4. Examples of dataset visualization in the study area

One of the challenges met during the elaboration of the urban geology project was the dissemination of the results to users of different access levels. In this paper, we present how GIS data derived from the “Urban geology” project of IGME can be freely and easily transmitted to anyone with Internet access and familiarity with Google Earth. Thematic layers, created in ArcGIS, were converted from EGSA’87 (Greek Geodetic Reference System of 1987) to WGS84 Geographic Coordinate System to ensure compatibility with GE and then exported to a KMZ data file.

4.1. Topography

Detailed topography is a key feature for every study concerning spatial information. Thus, all available topographic data for the broader Nafplio area were digitized and imported in the “Nafplio” database. A graphic representation of the most important topographic linear features is given in Figure 4.

4.2. Geology

A detailed geological mapping in a 1:5.000 scale was performed by Photiades (2008). According to this survey the broader Nafplio area is covered by alluvial deposits, mainly lagoonal, overlying flysch and limestone formations (Fig. 5).

4.3. Neotectonics

According to a thorough neotectonic study, carried out by Galanakis and Georgiou (2008), the



Fig. 5: Google Earth representation of geological formations from the broader area of Nafplio (Photiades, 2008).



Fig. 6: Google Earth representation of neotectonic linear features from the broader area of Nafplio (Galanakis and Georgiou, 2008).

broader area of Nafplio is characterized by the existence of active and potentially active faults mainly found in the boundaries of basins (Fig. 6).

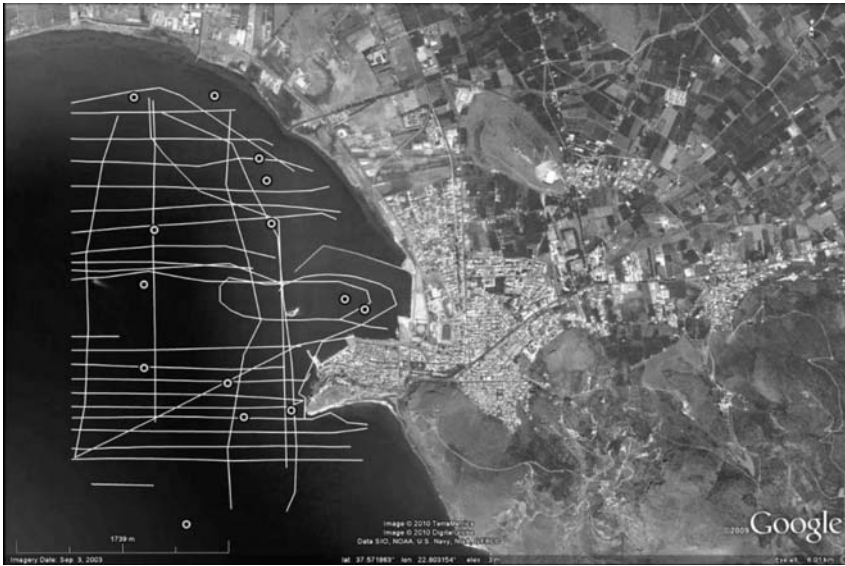


Fig. 7: Google Earth representation showing the location of seismic-reflection profiles and surface samples collected from the Argolic Gulf (Andrinopoulos et al., 2008).

4.4 Marine Geology

In the framework of the urban geology project, marine geology research was carried out in the Gulf surrounding the city of Nafplio (Andrinopoulos et al., 2008). The survey included 26 high-resolution seismic-reflection profiles and the collection of 14 sea-bottom surface samples (Fig. 7).

4.5. Geoarchaeology

A significant characteristic of urban and suburban areas, that has to be taken into account during urban development, is the presence of archaeological remains. Thus, during the elaboration of the urban geology project of I.G.M.E., an approach to the study of archaeological issues was attempted, using the methods and concepts of the earth sciences (Zananiri et al., 2010). An example is presented in Figure 8, where the archaeological protection zones of the broader area of Nafplio were mapped in detail.

5. Conclusions

In this paper we dealt with the crucial issue of data dissemination from urban geology studies to various recipients. We demonstrated how map layers, originally created in ArcGIS, can be shared with users having no experience with or access to GIS by sending an email attachment. All that is required is access to the Web and Google Earth, a powerful and freely downloadable geographic visualization tool. This opens up enormous possibilities for the free and easy dissemination of geospatial information in a visually meaningful and stimulating way to colleagues, local authorities and the interested general public around the world. Furthermore, this well-organized and easily accessible dataset can constitute a valuable tool in the hands of public authorities towards decision making and control, e.g. of building activities outside the defined urban development areas.



Fig. 8: Google earth representation of archaeological protection zones for the Nafplio area. Zone A corresponds to totally protected areas where no construction is allowed; Zone B encloses partially protected areas where conditional construction is allowed.

Through the Google Earth platform the derivative maps (geological, geotechnical, geochemical, geophysical etc.) and other digital data such as sampling points, elevation models, 2D – 3D digital surfaces are available and accessible to all, public or private sector or even general public, managing issues concerning the protection and enhancement of the urban and suburban environment.

A KMZ file with the geospatial data from the pilot area of Nafplio, for level C users (general public), can be requested via e-mail from the authors or downloaded from the IGME website: <http://www.igme.gr>. It is intended that the results from subsequent studies will be incorporated into the Nafplio “urban geology” database, and consequently the GE file, keeping users up-to-date. Moreover, following the example of Compieta et al. (2007), we plan to create a Google Earth-based tool for data mining and spatial analysis. This application will incorporate widgets designed to select the information to deal with, which will be rendered in 3D over a map and other layers provided by GE.

6. Acknowledgements

This work was funded by the Community Support Framework 2000 – 2006 (Operational Program “Competitiveness”). We thank all colleagues who participated in this multidisciplinary project, the first integrated urban geology study in Greece.

7. References

- Andrinopoulos, A., Zacharaki, P., Zimianitis, E., Maroulakis, S., Mitropoulos, D. and Efthimiou, G., 2008. Marine geology research in the northern Argolic gulf – Nafplio area, Argolis prefecture. Technical Report I.G.M.E., Athens, Greece.
- Beaudette, D.E. and O’Geen, A.T., 2009. Soil-Web: An online soil survey for California, Arizona, and Nevada. *Computers & Geosciences*, 35, 2119-2128.

- Compieta, P., Di Martino, S., Bertolotto, M., Ferrucci, F. and Kechadi, T., 2007. Exploratory spatio-temporal data mining and visualization. *Journal of Visual Languages & Computing*, 18, 255-279.
- Conroy, G.C., Anemone, R.L., Van Regenmorter, J. and Addison, A., 2008. Google Earth, GIS, and the Great Divide: A new and simple method for sharing paleontological data. *Journal of Human Evolution*, 55, 751-755.
- Deegree, 2007 (accessed 02/12/2009). Deegree – Free software for spatial data infrastructures. URL: <http://www.deegree.org>
- Fuchu, D., Yuhai, L. and Sijing, W., 1994. Urban geology: a case study of Tongchuan city, Shaanxi Province, China. *Engineering Geology*, 38 (1-2), 165-175.
- Galanakis, D. and Georgiou, Ch., 2008. Neotectonic study at the urban and suburban area of Nafplio city (pilot application). *Technical report, I.G.M.E.*, Athens, Greece.
- Google Inc., 2009 (accessed 15/06/2009). Google Earth: A 3D interface to the planet. URL: <http://earth.google.com/>
- Karrow, P.F. and White, O.L., 1998. Urban Geology of Canadian cities. *Geological Association of Canada, special paper 42*, p.p. 500, Canada.
- Legget, R.F., 1969. Urban Geology. *Canadian Building Digest*, CBD – 113, National Research Council Canada, URL: <http://irc.web-t.cisti.nrc.ca/cbd/cbd113e.html>
- Longley, P.A., Goodchild, M.F., Maguire, D.J. and Rhind, D.W., 2001. *Geographic Information Systems and Science*. John Wiley & Sons, 472 pp.
- Maguire, D.J., 1991. An overview and definition of GIS. In: D.J. Maguire, M.F. Goodchild and D.W. Rhind (eds), *Geographical Information Systems Principles and Applications*. Longman Scientific and Technical, John Wiley and Sons, Inc., New York, 9-20.
- MapServer, 2009 (accessed 02/12/2009). Mapserver – Open source development environment for building spatially enabled internet applications. URL: <http://mapserver.gis.umn.edu/>
- Montesano, P.M., Nelson, R., Sun, G., Margolis, H., Kerber, A. and Ranson, K.J., 2009. MODIS tree cover validation for the circumpolar taiga-tundra transition zone. *Remote Sensing of Environment*, 113, 2130-2141.
- De Mulder, E.F.J., 1993. Urban geology in Europe: overview. *Quaternary International*, 20, 5-11.
- Nott, J.F., 2003. The urban geology of Darwin, Australia. *Quaternary International*, 103, 83-90.
- Pearce, J.M., Johnson, S.J. and Grant, G.B., 2007. 3D-mapping optimization of embodied energy of transportation. *Resources, Conservation & Recycling*, 51, 435-453.
- Photiadis A., 2008. Geological study of the urban and the wider Nafplio area. Argolida Prefecture. *Technical Report I.G.M.E.*, Athens, Greece.
- Tsombos, P.I. and Zervakou, A.D., 2010. The “Urban Geology” project of IGME. *Bulletin of the Geological Society of Greece, Proc. of the 12th International Congress* (this volume).
- Zanariri, I., Chiotis, E., Tsombos, P., Hademenos, V. and Zervakou, A., 2010. Geoarchaeological research in urban and suburban areas of the Argolis Prefecture. *Bulletin of the Geological Society of Greece, Proceedings of the 12th International Congress* (this volume).
- Zervakou, A.D., Tsombos, P.I. and Nikolakopoulos, K.G., 2007. Urban Geology: Documentation of geothematic information for urban areas in Greece, the case of Nafplio Greece. *14th International Symposium on Remote Sensing of the International Society for Optical Engineering, Florence, Italy*, Vol. 6749, 67491G1-12.
- Zervakou, A.D. and Tsombos, P.I., 2010. GIS in Urban Geology. The case of Nafplio city, Greece. *Bulletin of the Geological Society of Greece, Proceedings of the 12th International Congress* (this volume).

GIS IN URBAN GEOLOGY: THE CASE STUDY OF NAFPLIO, ARGOLIS PREFECTURE, GREECE

Zervakou A.D.¹ and Tsombos P.I.¹

¹ Institute of Geology and Mineral Exploration (I.G.M.E.), Olympic Village, 3rd Entrance, 13677 Acharnae, Greece, zervakou@igme.gr, ptsombos@igme.gr

Abstract

The aggregation of population in big cities leads to the concentration of human activities, overconsumption of natural resources and urban growth without spatial planning and sustainable management. As a result, urban societies are exposed to various dangers and threats with economic, social, ecological, and environmental impacts on the urban surroundings. Problems associated with urban development are related to the existing geological conditions. Therefore, the provision of appropriate geological information about the urban environment is essential for every sustainable urban planning. The first systematic recording, codification and documentation of "Urban Geology" geothematic information in Greece was implemented by the Institute of Geology and Mineral Exploration (I.G.M.E.) in the framework of the project called "Collection, codification and documentation of geothematic information for urban and suburban areas in Greece - pilot applications". Through the implementation of this project, geological mapping, geotechnical, geochemical, geophysical research and measurements took place at four pilot cities of Greece. Nafplio, the capital city of Argolis prefecture, was one of them. During the project, all compiled data were stored and processed in specially designed geodatabases in GIS environment in order to produce multifunctional geothematic maps and other digital products (DEMs, 2D - 3D surfaces).

Key words: Urban Geology, geothematic information, GIS, Nafplio.

1. Introduction

According to current estimates, cities occupy 4% or less of the world's terrestrial surface, yet they are home to almost half of the global population, consume close to three-quarters of the world's natural resources and generate three-quarters of its pollution and wastes.

Urban areas expanding dramatically quickly, often without sustainable planning, are more at risk than other areas. Their dependence on natural factors such as geology, topography, proximity to hazard sources and intensive human activities arise the disaster risk. Hence, the urbanization process in developing countries is indicative of a process that needs considerable attention.

Given that the Earth's population will in future be concentrated into 'mega-cities', with the attendant problems associated with the concentration of the human race into a small part of the Earth's land surface, an increasing focus for geologists is the urban environment.

The basic role of the Institute of Geology and Mineral Exploration of Greece (I.G.M.E.) regarding urban geological information is to increase the utilization and facilitate the dissemination of geo-

logical data for urban planning and risk management. I.G.M.E. can provide the planners and other interested parties with geological data easily understood by non-geologist users.

In this paper we demonstrate how the multifunctional technology of Geographic Information Systems (GIS) was used in order to collect, store, manage, process, analyze and cartographically represent the complex geoscientific information derived from Urban Geology studies, carried out by IGME, with an emphasis given in Nafplio.

2. Urban Geology

Essential to effective urban planning is the availability of accurate, understandable, and pertinent data on *Urban Geology* that decision-makers can use in making informed choices. Unfortunately, geological information is an underused resource in planning, despite the fact that the majority of cities owe their historical development to geological factors.

Urban Geology is a relatively new branch of the earth sciences that came into life in the past fifty years. It is the study or application of geology to urban centers, urban development and planning. The importance of geology as applied to cities has been stressed repeatedly by Legget (1973) and Legget and Karrow (1983).

Urban Geology is not only important for every urban centre or city, it is also site specific. Each city with its unique set of geological settings and geological constraints poses different or unique sets of problems for the engineers and developers. Since all construction and development works are sited on/in earth materials, it is geology that will indicate the types of problems that are encountered at each site/city (Tan et al., 1990).

Urban geologists have actually three broad tasks (Hancock and Skinner, 2000):

- to manage the provision of mineral, construction, water, and conservation resources,
- to provide appropriate geological information for construction, engineering, and waste-management projects and
- to manage and mitigate the natural and human-induced hazards that threaten an increasingly concentrated and therefore vulnerable urban population.

An Urban Geology project provides the opportunity to compile all the geoscience information available for capital cities and release the information in a standard format that could be accessible to all users including the private sector, the various levels of governments, universities and the general public (Bélanger and Moore, 1999).

The last decades, globally, many geological surveys and other institutes have operated “Urban Geology” programs aiming to provide up-to-date information on ground-related issues for the towns and cities. Through the collection and compilation of geological data, Urban Geology projects contribute:

- to the identification and evaluation of geohazards,
- to the development of countermeasures to reduce them,
- to the preservation of urban and surrounding environment.

3. The case study of Nafplio, Argolis prefecture

The first systematic recording, codification and documentation of Urban Geology geothematic information in Greece was implemented by the Institute of Geology and Mineral Exploration (I.G.M.E.) in the framework of the project called “Collection, codification and documentation of geothematic information for urban and suburban areas in Greece - pilot applications”.

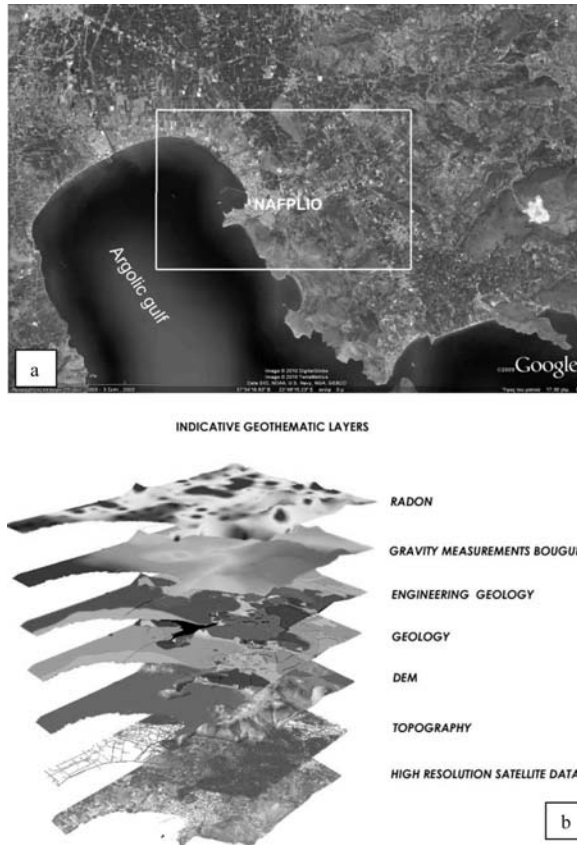


Fig. 1: (a) Satellite image from Google Earth showing the study area (included within the white box), (b) Indicative diagram of Urban Geology geothematic layers produced through “Urban Geology” project of I.G.M.E. (Pantelias et al., 2008).

The third subproject called “Integrated geological, geotechnical, hydrogeological, geochemical, geophysical and marine studies in urban and suburban area of Nafplio, Argolis Prefecture” took place at the broader area of Nafplio (Fig. 1a).

The aim of the project was the compilation of existing geoinformation concerning geological, hydrogeological, geotechnical, geochemical and geophysical reports for urban and suburban areas over the whole country in databases. At the same time, desk and field survey was carried out. All information derived from geological mapping, geotechnical – geochemical – geophysical – marine research and measurements was stored and processed in spatial databases, specially designed for the demands of the specific project, in GIS environment. The project’s results are presented in geothematic maps and other digital products.

3.1. Project outline

An Urban Geology project should compile and release all the available information for the specific area. This includes all properties of the bedrock and surficial materials, aquifers, geochemistry, geotechnical characteristics and other parameters. There is a need for site-specific information such as

geological maps at a large scale (1:5.000, 1:1.000), stratigraphic cross-sections, topographic maps (1:5.000 scale), logs from boreholes, soil and water sampling, etc. Users, including public and private sector, demand information as detailed and specific as possible and at a scale as large as possible.

As mentioned above, the specific Urban Geology project focused on the collection and integration of field work – laboratorial - processed data derived from various sources, summarized to the following (Zervakou et al., 2007):

- Geological mapping at 1:5.000 scale for the identification and evaluation of geological settings in the study area.
- Neotectonic mapping at 1:5.000 scale for the identification and evaluation of active faults in the study area.
- Geotechnical mapping at 1:5.000 scale for the identification and evaluation of physical, mechanical and geotechnical properties of geological formations in the study area.
- Geotechnical survey and sampling in 22 locations.
- Geotechnical rock mass classification in 22 locations (according to Bieniawski).
- Hydrogeological survey.
- Geochemical survey.
- Water and soil field sampling for geochemical analyses.
- Radon measurements.
- Surface Geophysical survey.
- Deep Geophysical survey.
- Marine geological survey.
- Geoarchaeological survey.

3.2. Geographic Information System

To store, describe and process the complex information derived from field work and laboratory processing, GIS technology was chosen as the best solution for the input, storage, management, analysis and cartographic representation of such geographic information. The software used for the development of the specific GIS application was ArcGIS 9x, ArcInfo version, ESRI.

GIS elaboration comprised the following stages (Zervakou et al., 2007):

- Design and building of the geographic database.
- Data import (Digitizing, GPS points, etc.).
- Descriptive information and hyperlink input.
- Data management (transformations, topology, editing, etc).
- DEMs and other surfaces generation.
- Thematic maps compilation.

3.3. Geodatabase schema and contents

The real world is too complex for our immediate and direct understanding. For this reason we create “models” of reality that are intended to have some similarity with selected aspects of the real world. Databases are created from these “models” as a fundamental step in coming to know the nature and status of that reality. A spatial database is a collection of spatially referenced data that acts as a model of reality in the sense that the database represents a selected set or approximation of phenomena (Goodchild and Kemp, 1990).



Fig. 2: “Nafplio” Geodatabase schema and contents.

A spatial database is designed to store, query, and manipulate geographic information and spatial data. It is also known as a *geodatabase*. Within a spatial database, spatial data is treated as any other data type. Vector data can be stored as point, line or polygon data types, and may have an associated spatial reference system. Some geodatabases also include support for storing raster data.

For the specific GIS application an ArcGIS Personal Geodatabase was built. Personal geodatabases are much like file-based workspaces. Microsoft Access is used to work with attribute tables in such geodatabases. They support single user editing and no versioning support is provided. All geographic data are stored in feature classes, classified in different Feature Datasets and single tables containing additional information. The used projected coordinate system is the Greek Geodetic Reference System EGSA'87 (Datum: D_GGRS_1987, Spheroid: GRS_1980).

In particular, the “Nafplio” Geodatabase (Fig. 2) contains the following feature datasets which comprise thematically related feature classes (Zervakou et al., 2008):

- *Feature dataset Topography:* Topographic data derived from four topographic maps of the Geographic Military Service at 1:5000 scale, covering the study area.

Topology Rules				
Name	Origin (<i>FeatureClass::Subtype</i>)	Rule Type	Destination (<i>FeatureClass::Subtype</i>)	Trigger Events
	Glines:: 'Opia	Must be covered by boundary of	Gpolygons:: All Subtypes	No
	Glines:: 'Opia	Must not have dangles	Glines:: 'Opia	No
	Gpolygons:: All Subtypes	Must not have overlaps	Gpolygons:: All Subtypes	No
	Gpolygons:: All Subtypes	Boundary must be covered by	Glines:: 'Opia	No
	Gpolygons:: All Subtypes	Must not have gaps	Gpolygons:: All Subtypes	No
	Glabels:: All Subtypes	Must be properly inside polygons	Gpolygons:: All Subtypes	No
	Glines:: All Subtypes	Must not overlap	Glines:: All Subtypes	No
	Glines:: 'Opia	Must not intersect	Glines:: 'Opia	No
	Glines:: All Subtypes	Must not self overlap	Glines:: All Subtypes	No
	Glines:: All Subtypes	Must not self intersect	Glines:: All Subtypes	No

Fig. 3: Topology rules for the geology dataset (Pantelias et al., 2008).

- *Feature dataset Geology:* Geological data derived from four geological maps of 1:5.000 scale covering the study area. This feature dataset contains also linear features generated from airphotos interpretation.
- *Feature dataset Engineering Geology:* Geotechnical data derived from four geotechnical maps of 1:5.000 scale covering the study area. This dataset contains also data coming from specific survey, observations and soil mechanics, rock mechanics laboratory tests for the determination of physical and mechanical properties of the penetrated formations.
- *Feature dataset Neotectonics:* Neotectonic data derived from detailed field mapping and observations.
- *Feature dataset Hydrogeology:* Hydrogeological data concerning water chemical analyses and piezometric contours.
- *Feature dataset Geophysics:* Geophysical data comprising gravity – seismic – electrical – electromagnetical measurements
- *Feature dataset Soils:* Soil geochemical data derived from field sampling and laboratory analyses.
- *Feature dataset Marine Geology:* Data coming from marine geology survey (Bathymetry, morphology, sampling).
- *Feature dataset Radioactive elements:* Data concerning radon measurements
- *Feature dataset Geoarchaeology:* Data derived from geoarchaeological survey in the broader area of Nafplio.

As mentioned above, the customized geodatabase contains also special elements that contribute to the best data management and integrity. These elements are topology¹, domains², subtypes³ and re-

¹ In geodatabases Topology constitutes the arrangement that constrains how point, line, and polygon features share geometry (ArcGIS Desktop help).

² Attribute domains are used to constrain the values allowed in any particular attribute for a table or feature class. A domain is a declaration of acceptable attribute values (ArcGIS Desktop help).

³ Subtypes are records in a table or feature class that have been grouped based on an attribute field. Subtypes are implemented by creating coded values and, therefore, must be associated with fields of the data type short or long integer (ArcGIS Desktop help).

⁴ An item in the geodatabase that stores information about a relationship. Relationship classes define relationships between objects in the geodatabase. These relationships can be simple one-to-one relationships or more complex one-to-many (or many-to-many) relationships between features and table rows. (ArcGIS Desktop help).

GEOLOGICAL LINEAR FEATURES (SUBTYPES)	BOUNDARIES
	FAULTS
	OTHER TECTONIC LINES (e.g. overthrusts, upthrusts, tectonic contacts)
	SPECIAL GEOLOGICAL LINES (e.g. landslide lines)

Fig. 4: Subtypes for the geology dataset (Pantelias et al., 2008).



Fig. 5: Topographic map of the study area.

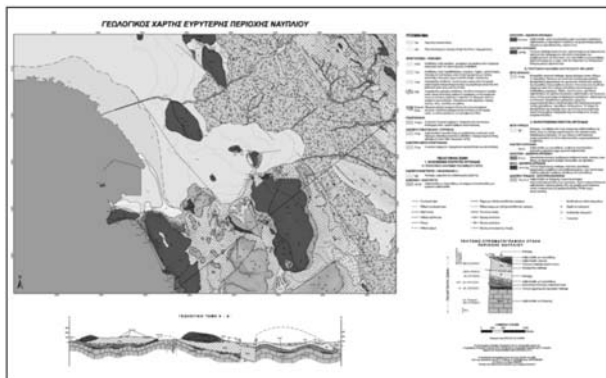


Fig. 6: Geological map of the study area (Pothiades, 2008).

relationship classes⁴. In summary, they:

- provide a strong mechanism to perform integrity checks on data.
- help to validate and maintain better feature representations in the geodatabase.
- enable richer and more efficient analytical functions in Geographic Information System.

Subtypes and topology rules for the geology dataset are presented below (Fig. 3 and 4).

3.4. Derived digital cartographic products

Urban planning process is complex, but an effective urban strategy involves land-use planning to guide development and appropriate use of land areas.

Geothematic cartographic products and especially maps are used effectively towards this scope.

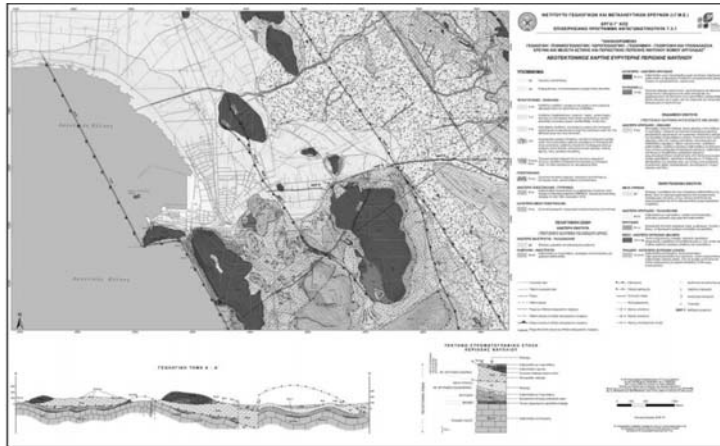


Fig. 7: Neotectonic map of the study area (Galanakis and Georgiou, 2008).

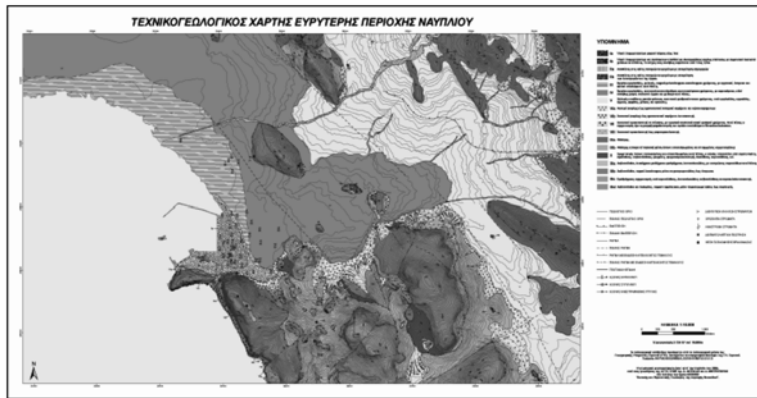


Fig. 8: Engineering geological map of the study area (Apostolidis and Koutsouveli, 2008).



Fig. 9: Hydrological map of the study area (Sampatakakis et al., 2009).

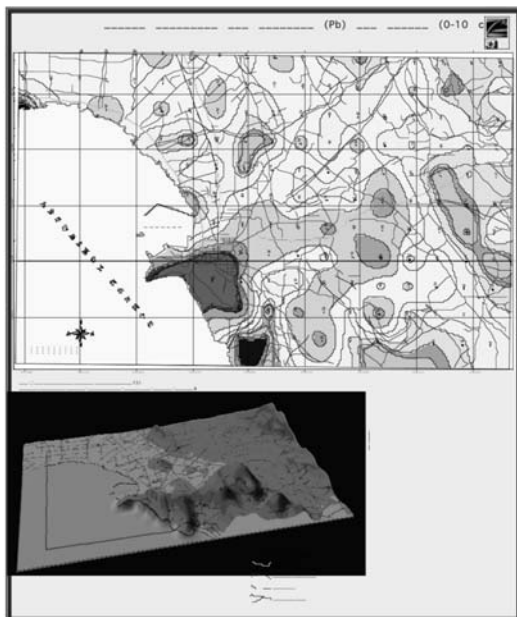


Fig. 10: Geochemical map displaying the Pb spatial distribution in soil in the study area (Tassiou, 2008; Vassiliades, 2008).

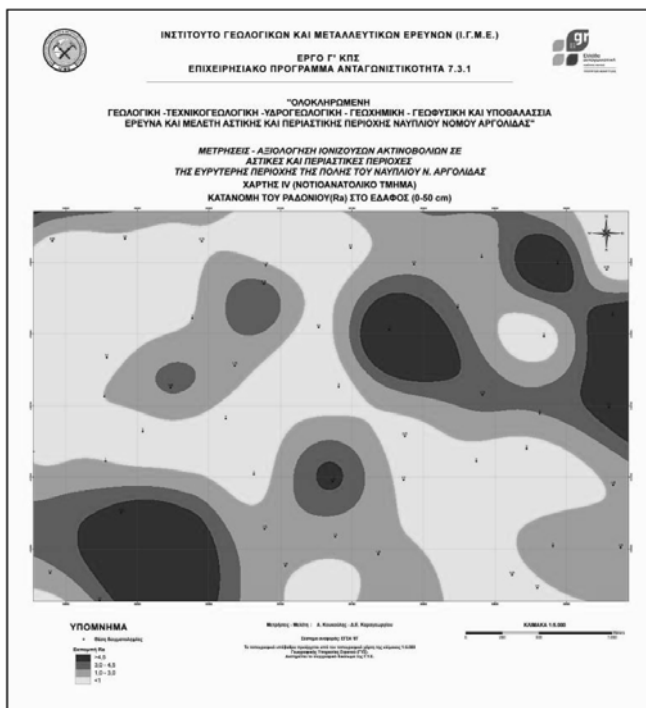


Fig. 11: Map displaying the Radon concentration in soil in the study area (Koukoulis and Karageorgiou, 2008).

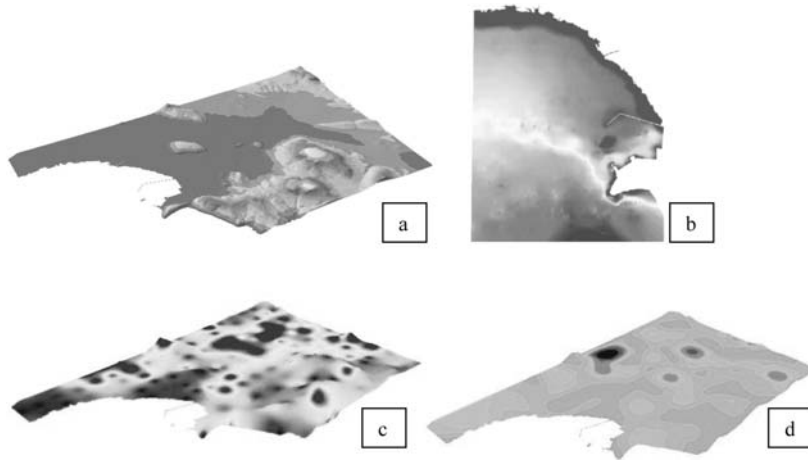


Fig. 12: (a) High detailed TIN displaying the surface morphology of the study area, (b) raster representing the seafloor morphology of the marine area near the city of Nafplio (Argolic Gulf) (Andrinopoulos et al., 2008), (c) raster representing the radon concentration in soil in the study area (Koukoulis and Karageorgiou, 2008), (d) raster representing the Cu spatial distribution in soil in the study area (Tassiou, 2008; Vassiliades, 2008).

Specifically, they constitute a powerful tool for urban planning by:

- providing specific geoinformation about particular locations.
- providing general information about geospatial patterns.
- giving the opportunity to compare patterns on two or more maps.
- providing identification of specific uses for designated sites.
- providing identification of suitable areas for urban or regional development.

In the framework of Urban Geology Project of IGME, all collected and processed data from field surveys, desk surveys, monitoring, terrain and laboratory analysis are presented in a form that is accessible to all, in a set of thematic maps and other digital 2D and 3D data representing the morphology, geology, hydrogeology, ground conditions, tectonics, hazards, and so on of the study area of Nafplio (Fig. 5 - 12).

4. Conclusions

Urban Geology studies rely on diverse branches of earth sciences such as hydrology, engineering geology, geochemistry, stratigraphy, geomorphology etc. The geoscience information derived from various sources is compiled in a digital format and stored in georeferenced databases in the form of point, linear, and polygon data. This information constitutes the geoscience knowledge base which is then processed by Geographic Information Systems (GIS) to integrate the various sources of information and produce derived graphics, maps and models describing the geological infrastructure and response of the geological environment to human activities.

Urban Geology project of I.G.M.E. accomplished in the framework of CSF 2000 – 2006, focused on the compilation and integration of such data. Specialized and dedicated studies took place at four

pilot urban areas. Nafplio, the capital city of Argolis prefecture, was one of them.

Geographic Information Systems provided the best environment for the collection, storage, management, processing, analysis and cartographic representation of complex geoscientific information. All compiled data, stored in specially customized geodatabase, were classified in geothematic layers (feature classes), grouped in geothematic datasets (feature datasets) and processed in order to produce multifunctional surfaces and geothematic maps. Special geodatabase elements such as topology, domains, subtypes and relationship classes were used for the best data management and integrity.

All collected and processed data from field surveys, desk surveys, monitoring and laboratory analysis are presented in a form that is accessible to all, in a set of thematic maps and other digital 2D and 3D data, representing the morphology, geology, hydrogeology, ground conditions, tectonics, hazards etc. in the specific study area.

5. Acknowledgements

This study was accomplished within the framework of the project “Collection and Documentation of Geothematic Information for Urban and Suburban areas in Greece – Pilot Applications”. The program was funded by the Operational Program “Competitiveness” Priority Axis 7: Energy and Sustainable Development, Measure 7.3: Exploitation of natural resources and support in meeting environmental commitments. The Operational Program “Competitiveness” was co-funded by the European Regional Development Fund (ERDF).

We would like to thank all colleagues who participated in this multidisciplinary project: Andrinopoulos A., Apostolidis E., Chiotis E., Chiras S., Demetriades A., Efthimiou G., Filos G., Galanakis D., Ganotis G., Georgiou Ch., Iordanidis S., Karageorgiou D., Karmis P., Karpetas Th., Kokkalis Th., Kostopoulos A., Koukis G., Koukoulis A., Kousoulas F., Koutsouveli A., Kyriakopoulos Th., Lappas I., Letsios K., Loupasakis C., Manazis St., Mastrogiannis F., Michalopoulos N., Mitropoulos D., Moraiti E., Nikolaides M., Nikolakopoulos K., Nikolaou N., Panagopoulos A., Pantelias E., Paraschakis Th., Photiades A., Pisinis K., Polyzou L., Sampatakakis P., Spyropoulos I., Tassiou S., Tsiounis E., Tzoumas S., Vassiliades E., Vertsiotis V., Zacharaki P., Zagourogrou C., Zananiri I. and Zimianitis E. Special acknowledgment is granted to the team of the Geodynamics Institute of the National Observatory of Athens (scientific responsible: Karastathis V.) and the geologists Hademenos V., Maroulakis Sp. for their systematic work and support.

6. References

- Andrinopoulos, A., Zacharaki, E., Zimianitis, E., Maroulakis, S., Mitropoulos, D. and Efthimiou, G., 2008. Marine geological study of the Northern Argolic gulf. Technical report, IGME, Athens, Greece.
- Apostolidis, E. and Koutsouveli, A., 2008. Engineering geological map of the urban and suburban area of Nafplio city. Technical report, IGME, Athens, Greece.
- ArcGIS Desktop Help, 1999-2008, ESRI.
- Bélangier, J.R. and Moore, C.W., 1999. The use and value of Urban Geology in Canada: A case study in the National Capital Region. *Geoscience Canada*, Vol. 26, N° 3. Available online at: <http://gsc.nrcan.gc.ca/urbgeo/natcap/pdf/urbangeologypub.pdf>
- Galanakis, D. and Georgiou, Ch., 2008. Neotectonic study of the urban and suburban area of Nafplio city (pilot application). Technical report, IGME, Athens, Greece.
- Goodchild, M.F. and Kemp, K.K. (eds.), 1990. Spatial databases as models of reality, *NCGIA Core Curriculum in GIS*, Unit 10, National Center for Geographic Information Analysis, University of Cali-

- ifornia, Santa Barbara CA. Available online at: <http://www.geog.ubc.ca/courses/klink/gis.notes/ncgia/u10.html>
- Hancock, P. and Skinner, B.J., 2000. Urban Geology. *The Oxford Companion to the Earth*. Oxford University Press. Available online at: <http://www.encyclopedia.com/doc/1O112-urbangeology.html>
- Koukoulis, A. and Karegeorgiou, D.E., 2008. Measurements – evaluation of ionizing radiation in urban and suburban areas of Nafplio city. Technical report, IGME, Athens, Greece.
- Legget, R.F., 1973. *Cities and Geology*. McGraw Hill, New York. p. p. 624.
- Legget, R.F. and Karrow, P.F., 1983. *Handbook of Geology in Civil Engineering*. McGraw- Hill, New York.
- Pantelias, E., Zervakou, A., Tsombos, P. and Nikolakopoulos, K., 2008. Spatial database for the management of Urban Geology geothematic information: the case of Drama City, Greece. Proceedings, *15th International Symposium on Remote Sensing of the International Society for Optical Engineering, September 15-19, Cardiff, Wales, United Kingdom*, Proc. SPIE, Vol. 7110.
- Photiades, A., 2008. Geological study of the urban and suburban pilot area of Nafplio city, Argolis prefecture. Technical report, IGME, Athens, Greece.
- Sampatakakis, P., Koukis, G. and Lappas, I., 2009. Hydrogeological and Hydrological study of the urban and suburban area of Nafplio. Technical report, IGME, Athens, Greece.
- Tan, B.K. and Komoo I., 1990. Urban Geology: Case study of Kuala Lumpur, Malaysia. *Engineering Geology*. Elsevier Science Publishers, B.V 28, 71-94.
- Tassiou, S., 2008. Geochemical environmental study of the urban and suburban area of Nafplio, Argolis prefecture - Vol. 1 Interpretation. Technical report, IGME, Athens, Greece.
- Vassiliades, E., 2008. Geochemical environmental study of the urban and suburban area of Nafplio, Argolis prefecture – Vol. 2 Geochemical maps. IGME, Athens, Greece.
- Zervakou, A., Tsombos, P. and Nikolakopoulos, K., 2007. Urban Geology: Documentation of geo-thematic information for urban areas in Greece: the case of Nafplio. Proceedings, *14th International Symposium on Remote Sensing of the International Society for Optical Engineering, September 17-20, Palazzo degli Affari Conference Ctr., Florence, Italy*, Proc. SPIE, Vol. 6749 p. 67491G1-12.
- Zervakou, A., Tsombos, P. and Nikolakopoulos, K., 2008. Urban Geology and GIS: The example of IGME. *5th Greek Conference HellasGIS: «GIS and Environment»*, December 4-5, Athens, Greece.

12ο ΔΙΕΘΝΕΣ ΣΥΝΕΔΡΙΟ ΤΗΣ ΕΛΛΗΝΙΚΗΣ ΓΕΩΛΟΓΙΚΗΣ ΕΤΑΙΡΙΑΣ
ΠΛΑΝΗΤΗΣ ΓΗ: Γεωλογικές Διεργασίες και Βιώσιμη Ανάπτυξη

12th INTERNATIONAL CONGRESS OF THE GEOLOGICAL SOCIETY OF GREECE
PLANET EARTH: Geological Processes and Sustainable Development



Γ.Σ.Π. ΣΤΙΣ ΓΕΩΕΠΙΣΤΗΜΕΣ / GIS IN EARTH SCIENCES

SOIL EROSION ASSESMENT IN SOUTHERN EVIA ISLAND USING USLE AND GIS

Bathrellos. G.D.¹, Skilodimou H.D.¹, and Chousianitis K.G.²

¹ Department of Geography & Climatology, Faculty of Geology & Geoenvironment, National & Kapodistrian University of Athens, University Campus, Zografou, 15784 Athens, Greece, gbathellos@geol.uoa.gr

² Department of Geography & Climatology, Faculty of Geology & Geoenvironment, National & Kapodistrian University of Athens, University Campus, Zografou, 15784 Athens, Greece, hskilodimou@geol.uoa.gr

² Space Applications Research Unit in Geosciences, Department of Geophysics - Geothermics, Faculty of Geology and Geoenvironment, National and Kapodistrian University of Athens, 15784 Zografou, Athens - Greece, chousia@geol.uoa.gr.

Abstract

In the present study the evaluation of soil erosion in Southern Evia Island was carried out. Data related with precipitation, morphology, land cover and lithology were collected. A spatial database was created and the further processing of the collected data was prepared using GIS. The Universal Soil Loss Equation (USLE) was used to predict the spatial distribution of the average annual rate of erosion. Five major factors were used to calculate the soil loss. These are rainfall erosivity (R), soil erodibility (K), slope length and steepness (LS), cropping management (C) and conservation supporting practice (P). Each factor is the numerical estimate of a specific condition that affects the severity of soil erosion. The obtained soil loss values were used to create the erosion risk map. The applied methodology provides a cost effected and rapid estimation of areas that are vulnerable to soil erosion and need immediate attention from soil conservation point of view. Moreover these results can be used to assist land use planning.

Key words: Soil erosion risk, USLE, Southern Evia Island, GIS

1. Introduction

Soil erosion is one form of soil degradation and is a naturally occurring process on all land, whose agents are water and wind. Soil erosion may be a slow process that continues relatively unnoticed, or it may occur at an alarming rate causing serious soil loss. Soil loss and its associated impacts are important and widespread environmental problems today, which have far-reaching economic, political, social and environmental implications due to both on-site and off-site damages (Thampapillai and Anderson, 1994). The main on-site impact is the reduction of soil quality which caused by the loss of the nutrient-rich upper layers of the soil and the reduced water-holding capacity of many eroded soils. In addition, the soil that is detached by accelerated water or wind erosion may be transported at considerable distances. This gives rise to the off-site problems. Water erosion's main off-site effect is the movement of sediment and agricultural pollutants into watercourses. This can lead to the disruption of the ecosystems of lakes, and contamination of drinking water. Another major off-site impact results from the agricultural chemicals that often move with eroded sediment (Dregne, 2002; Descroix and Mathys, 2003).

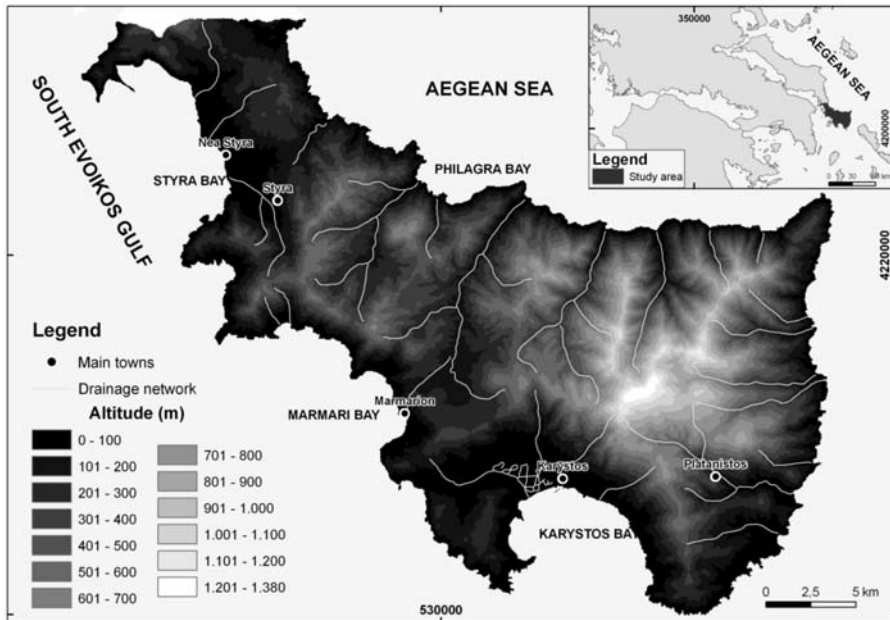


Fig. 1: The digital elevation model (DEM) of the study area superimposed by drainage network and main towns. The inset at upper right shows the location of the study area within the Greek territory.

The object of this study is to determine the areas most threatened by soil erosion by implementing the widely applied Universal Soil Loss Equation (USLE) of Wischmeier and Smith (1978) in Geographical Information System (GIS). GIS permits effective and accurate application of the USLE model in grid environment, which would allow us to analyse soil erosion in great detail. Precipitation, morphology, lithology and land cover spatial databases were constructed in the analysis and maps relevant to soil erosion were created using the GIS capabilities. The case study of the present paper is Southern Evia Island, Central Greece, which covers an area of about 602km² with altitudes varying between 0 and 1380m (Fig.1).

2. Methods

2.1 USLE equation

The Universal Loss Equation (USLE) is an equation that predicts the amount of soil lost per acre per year due to soil erosion. The USLE equation has been developed by Wischmeier and Smith (1978). This equation was the first empirical erosion equation that was not tied to a specific region, thus the title “Universal” Soil Loss Equation, and has been used in more than 100 countries. Five major factors are used to calculate the soil loss for a given site. Each factor is the numerical estimate of a specific condition that affects the severity of soil erosion at a particular location. The values reflected by these factors can vary considerably due to varying weather conditions. Therefore, the values obtained from the USLE more accurately represent long-term averages and the soil erosion is estimated as follows:

$$A = R \times K \times LS \times C \times P$$

Where A is the average annual soil loss rate (t ha⁻¹ year⁻¹), R is the rainfall erosivity factor (MJ mm ha⁻¹ h⁻¹ year⁻¹), K is the soil erodibility factor (t ha h ha⁻¹ MJ⁻¹ mm⁻¹), LS is the topographic factor (unitless), C is the cropping management factor (unitless) and P is the erosion control practice factor (unitless). The units of average annual soil loss rate (A) are carried by the R and K factors. These two factors represent the cause and effect of soil erosion. The R factor represents the erosive power of rainfall on the soil regardless of what type of soil it is, while the K factor represents the extent that the specific soil type resists erosive forces. The remaining USLE factors (LS, C and P) may be thought of as adjustment factors. In the present study the soil loss in Southern Evia Island was estimated on a 20x20 m cell basis resolution by overlaying the five digital parameter layers (R, K, LS, C and P) in raster format after some modifications in the calculation of the K factor.

2.2 Development of model database for USLE

To apply the USLE, a spatial database including precipitation, morphology, land cover and lithology was constructed using ArcGIS software (ESRI, 2005). The factors for the USLE equation were calculated and extracted from the spatial databases. Individual GIS files were built for each factor in the USLE and combined by cell-grid procedures in GIS to predict soil loss in the spatial domain. The dataset that was available consisted of the following:

- A Digital Elevation Model (DEM), which is a representation in raster format of the surface of the study area. The Digital Elevation Model was created at 20 m resolution by digitizing the contours of “Karistos” and “Platanistos” topographic map-sheets on a scale of 1:50.000, published by the Hellenic Military Geographical Service.
- The IGME “Karistos-Platanistos” (1991) and “Rafina” (1977) geological maps scanned from the corresponding paper map-sheets.
- The land cover in vector format (polygon layer) from CORINE database on a scale of 1:100.000.
- Meteorological tabular data (temperature and rainfall) from Karistos, Marathonas and Rafina meteorological stations of the Hellenic National Meteorological Service.

The R, K, LS and C factors which are required in calculating soil erosion from USLE were extracted from the spatial database. In the following sections we describe these factors respectively.

RAINFALL EROSIVITY FACTOR

The R-factor represents the erosivity of the climate at a particular location and evaluates the erosive potential of the rainfall. It is the average yearly sum of the products of the kinetic energy of each storm with the maximum 30 minute rainfall intensity of the storm. The energy of a given storm depends upon all the intensities at which the rain occurred and the amount of precipitation that is associated with each particular intensity value. However, in this application the lack of a dense meteorological network in the broader study area made us use the linear equation of Van der Knijff et al. (2000) which calculates the R-factor as a function of the mean annual rainfall (mm):

$$R = \alpha \cdot P_j$$

where P_j is the mean annual rainfall (mm) and the coefficient $\alpha = 1.3$. Monthly meteorological tabular rainfall data of 11-14 years was used to calculate the R-factor for the weather stations Karystos, Marathonas and Rafina, whose mean annual rainfall calculated to be 700.4 mm, 397.0 mm and 357.6 mm respectively. Finally, the Inverse distance weighting (IDW) interpolation method was applied to produce the spatial layer of the R-factor.

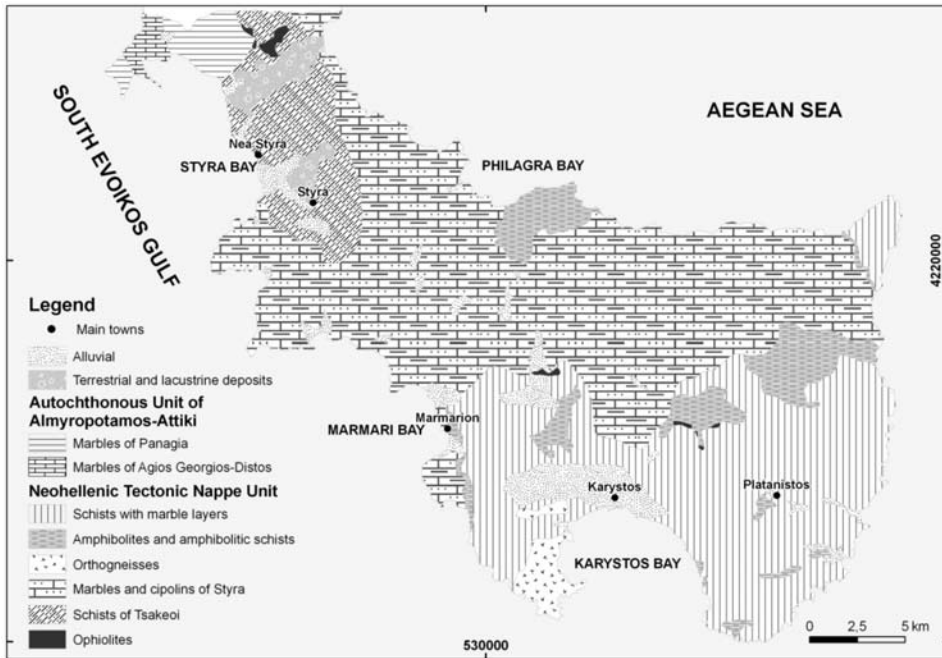


Fig. 2: Simplified geological map of Southern Evia Island (based on the Geological Maps of IGME 1:50.000, Karistos-Platanistos and Rafina sheets).

SOIL ERODIBILITY FACTOR

The K-factor is an empirical measure of soil erodibility and is a function of intrinsic soil properties. Erodibility varies with soil texture, aggregate stability, infiltration capacity and organic and chemical content (Karydas et al., 2009). This factor is influenced by the detachability of the soil, by the infiltration and runoff and the transportability of the sediment eroded from the soil. The main soil properties affecting the K-factor are soil texture, including the amount of fine sand in addition to the usual sand, silt and clay percentages used to describe soil texture, organic matter, soil structure and the permeability (Wischmeier et al. 1971; Mitchell and Bubenzer 1980; Dabral et al. 2001). Foster et al. (1991) proposed the following equation for the calculation of the K-factor:

$$K=2.8 \cdot 10^{-7} M^{1.14} (12-a) + 4.3 \cdot 10^{-3} (b-2) + 3.3 (c-3)$$

Where M is the particle size parameter (% silt + % very fine sand) x (100 - % clay), a is the organic matter content (%), b is the soil structure code (very fine granular = 1, fine granular = 2, coarse granular = 3, lattice or massive = 4) and c is the soil permeability class (fast = 1, fast to moderately fast = 2, moderately fast = 3, moderately fast to slow = 4, slow = 5, very slow = 6). These values are applied for soil erodibility factor when a soil map is available.

However, in this work the K-factor was calculated from the geological maps, due to unavailability of precise and reliable soil datasets for the study area. The geological formations were derived from the geological map sheets of Karistos-Platanistos (IGME, 1991) and Rafina (IGME, 1977). Formations from the Autochthonous unit of Almyropotamos-Attiki and the Neohellenic tectonic nappe unit participate in the geological structure of the study area. More specifically, the geological for-

Table 1. Classification of the geological formations and estimated soil erodibility factor values.

<i>Lithology</i>	<i>K Factor</i>
Marbles	0,0005
Marbles and cipolins with schists intercalations	0,001
Ophiolites	0,007
Orthogneisses	0,0003
Schists	0,009
Schists with marble layers	0,006
Alluvial and near shore deposits	0,02
Terrestrial and lacustrine deposits	0,02

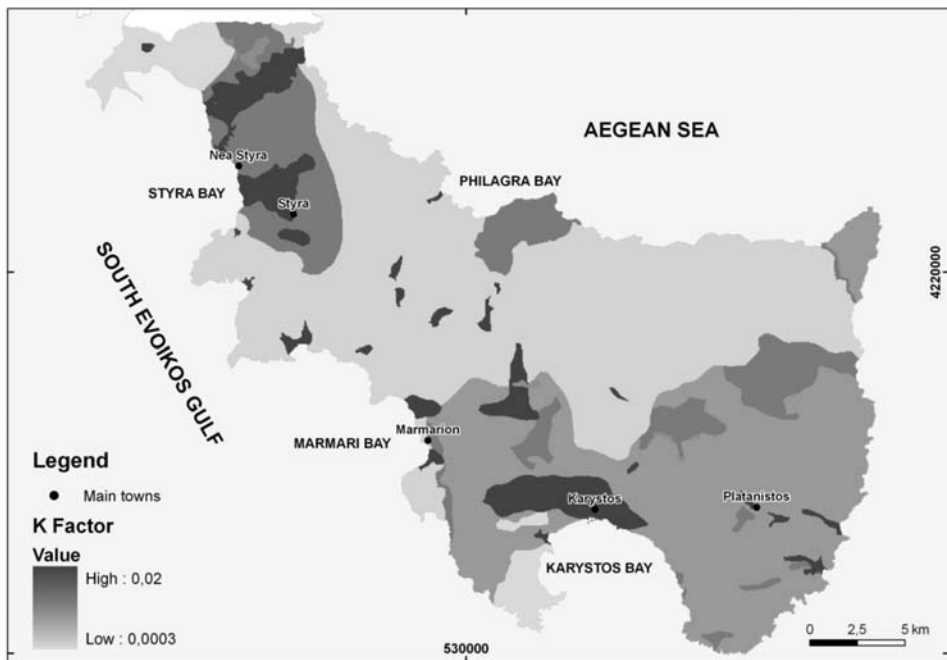


Fig. 3: Spatial distribution map of the soil erodibility factor in the study area.

mations that were identified are alluvial, terrestrial and lacustrine deposits, marbles of Panagia and Agios Georgios-Distos (Autochthonous unit of Almyropotamos-Attiki), schists with marble layers, amphibolites and amphibolitic schists, orthogneisses, marbles and cipolins of Styra, schists of Tsakeoi and ophiolites (Neohellenic tectonic nappe unit). The simplified geological map of the study area are shown in Fig.2.

The formations were classified according to parent material and depending on their sensitivity to erosion, their infiltration capacity, their aggregate stability and their organic and chemical content. Val-

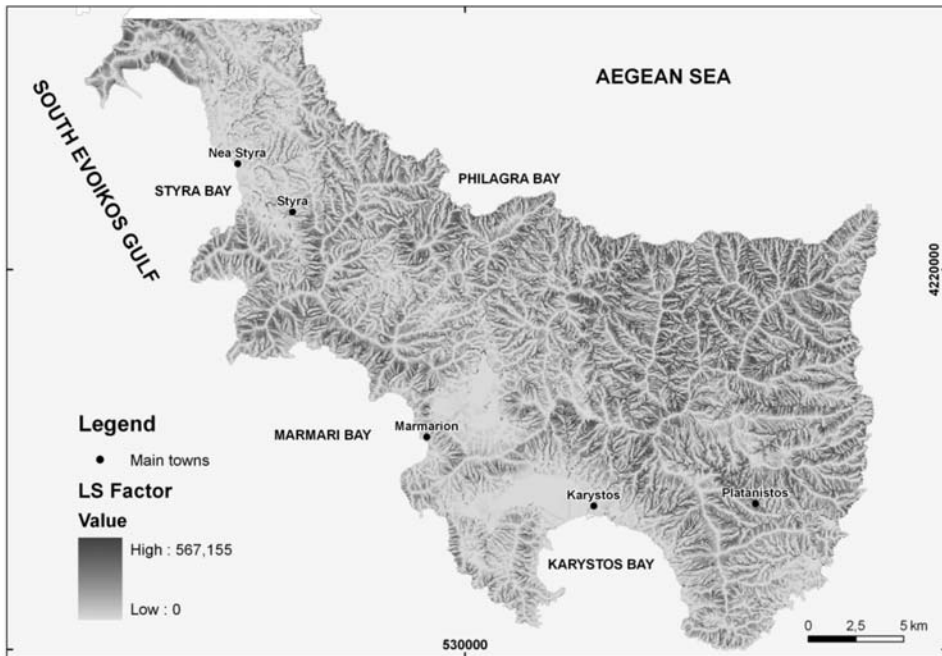


Fig. 4: Spatial distribution map of the topographic factor in the study area.

uses of K-factor were assigned in every formation, computed for every grid cell and producing the K-factor map. Soil erodibility factor was found to be in the range between 0.0003 – 0.02 (Table 1). The spatial distribution of the K- factor is presented in Fig. 3.

TOPOGRAPHIC FACTOR

This factor can be divided into L and S factors that respectively account for slope length and slope steepness and jointly they refer to the topographic (or relief) influence on erosion intensity. Naturally, the steeper the slope of a field, the greater the amount of soil loss from erosion (Desmet & Govers 1996). Soil erosion also increases as the slope length, which is defined as the distance from the origin of overland flow to the point where deposition begins to occur, increases due to the greater accumulation of runoff. The topographic factor can be determined by multiplying the L and S factors. The technique for estimating the LS-factor was proposed by Moore and Burch (1986 a and b) using equations such as

$$LS = (\text{Flow Accumulation} \times \text{Cell Size} / 22.13)^{0.4} \times [\sin(\text{Slope} \times 0.01745 / 0.0896)]^{1.3}$$

In this study, both the flow accumulation and the slope steepness were estimated from the Digital Elevation Model (resolution 20 m) of the study area, after the required processing. Finally, the LS-factor was found to be in the range of 0.1 to 567.155 and its spatial distribution is shown in Fig. 4.

CROPPING MANAGEMENT FACTOR

The C factor reflects the effect of cropping and management practices on the soil erosion rate and it is mainly related to the vegetation's cover percentage. Undisturbed forests and dense grass provide the best soil protection and are about equal in their effectiveness. Forage crops are next in ef-

Table 2. Cropping management factor for different land cover classes.

<i>Land cover.</i>	<i>C Factor</i>
Non-irrigated arable land	0,250
Permanently irrigated land	0,300
Vineyards	0,350
Olive groves	0,400
Pastures	0,010
Complex cultivation patterns	0,170
Land principally occupied by agriculture, with significant areas of natural vegetation	0,200
Broad-leaved forest	0,001
Coniferous forest	0,001
Mixed forest	0,001
Natural grassland	0,010
Sclerophyllous vegetation	0,009
Transitional woodland-shrub	0,009
Bare rock	0,450
Sparsely vegetated areas	0,350
Burned areas	0,550

fectiveness, because of their relatively dense cover. Small grains, such as wheat, provide intermediate cover and offer considerable obstruction to surface wash. Row crops, such as corn, offer relatively little living cover during the early growth stages and thereby leave the soil susceptible to erosion, unless residues from previous crops cover the soil surface (Brady and Weil 1999). In the present study, the C-factor values were derived from the CORINE land cover database on a scale of 1:100.000. The study area was classified into 17 land cover classes (Table 2). For each land cover class a corresponding C-factor value was given by utilising the values given in the literature (Wischmeier and Smith 1978, Cebecauer et al. 2000), adjusted for the present study area. Urbanized areas were excluded from the evaluation, while attention was given at the areas that were affected by the wildfires of 2007 and 2009. The largest value was assigned at these areas, which were determined by photo-interpretation using MODIS Terra satellite images of the study area. Finally, the map and the distribution of land cover C-factor values are shown in Fig. 5.

EROSION CONTROL PRACTICE FACTOR

P-factor reflects the effects of practices such as construction of terraces or contour strips that will reduce the amount and rate of the water runoff and thus reduce the amount of erosion. Wischmeier and Smith (1978) defined the P-factor as the ratio of soil loss with a specific support practice to the corresponding soil loss with up and down cultivation. The lower the P-value, the more effective the conservation practice is considered to be at reducing soil erosion. However, in the present study, the P value 1.0 was assigned, because on a scale of 1:50.000 it was not possible to obtain data regarding support practices.

3. Results

SOIL EROSION POTENTIAL

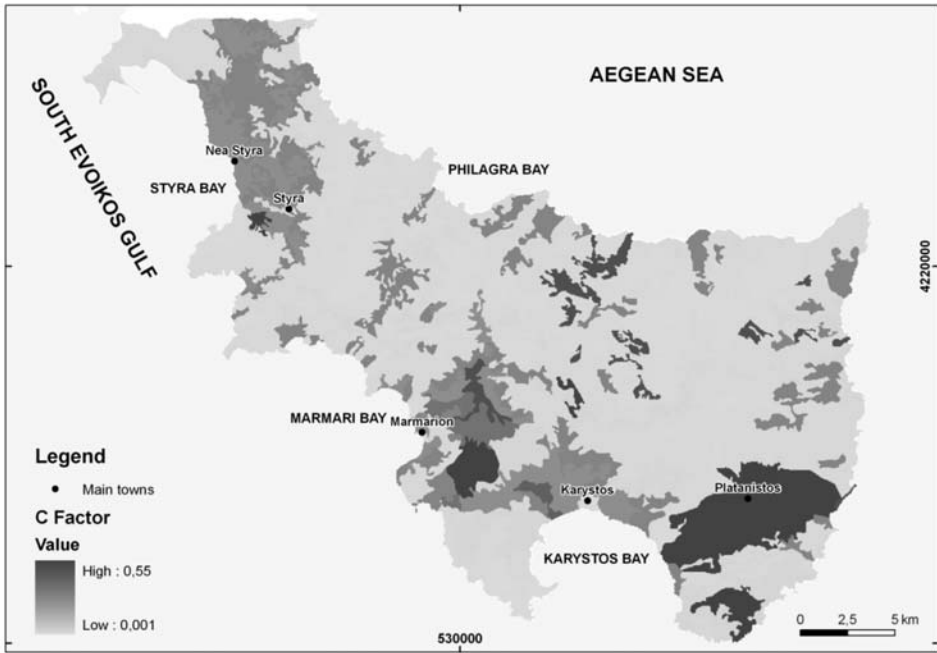


Fig. 5: Spatial distribution map of the cropping management factor in the study area.

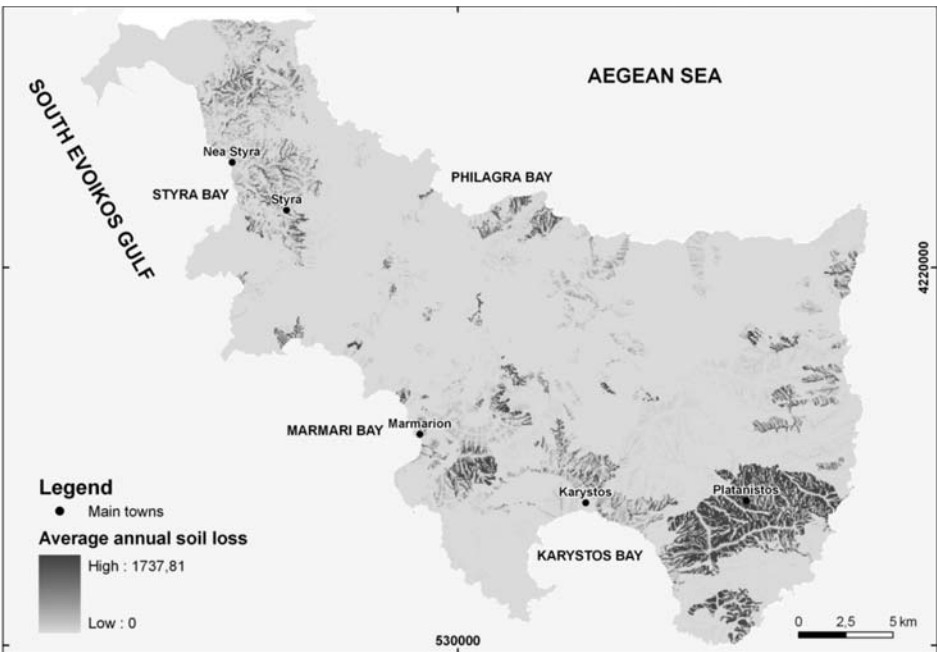


Fig. 6: Spatial distribution map of the average annual soil loss in the study area.

Finally, the implementation of Universal Loss Equation in GIS by multiplying the above described raster files that corresponds to the five factors of the USLE equation, gave the spatial distribution map of the average annual soil loss potential (A) in tons per acre per year in Southern Evia Island (Fig. 6). This was accomplished in ArcGIS by using the raster calculator tool. The highest computed rate of soil erosion potential is 1,737 tons per acre per year. Generally, the highest rates are in the affected areas by the wildfires of 2007 and 2009 and in the areas where the slope exceeds approximately 30 degrees. The final map should be interpreted as the maximum possible extent of erosion.

4. Conclusions

The purpose of this study was the identification of the soil erosion-prone areas in Southern Evia Island using the well-known Universal Soil Loss Equation (USLE) and GIS, as it has become increasingly apparent that computer based GIS can provide the means to model soil erosion effectively. A set of factors as identified in the USLE were studied and reviewed. These include the rainfall erosivity factor (R-factor), the soil erodibility factor (K-factor), the slope and slope length factor (LS-factor), the cropping management factor (C-factor) and the erosion control practice factor (P-factor). These factors which consist of a set of logically related geographic features and attributes were used as data input.

Analysis of monthly rainfall data of the past fourteen years gave the R-factor. The K-factor was calculated based on the geological maps, while it is originally based on soil analysis data, because of the lack of precise and reliable soil datasets for the study area. Digital elevation model (DEM), interpolated from elevation contours, was used to generate the LS-factor. Spatial land cover, extracted from CORINE database on a scale of 1:100.000, was used to determine the spatial C-factor, while photo-interpretation led to the identification of the areas that severely affected by the 2007 and 2009 wildfires in Southern Evia Island. Each of the above mentioned USLE factors, with associated attribute data, was digitally encoded in a GIS database to eventually create the corresponding thematic layers. Then, these layers were spatially overlaid to produce the resultant layer, which yielded the spatial distribution map of the average annual soil loss in the study area.

From the analysis it is evident that severe soil loss covers an area (150 tons/hectares/year) of about 14%. The highest average soil loss was occurred in areas that were affected by the wildfires of 2007 and 2009, while the lowest soil loss rate was found in forest areas. These results proved that soil erosion rates can reach alarming levels in rugged terrain after wildfires and measures to reduce the amount of soil erosion need to be taken at these areas, where plant material and the litter layer that break up the intensity of severe rainstorms is destroyed. The severe soil loss from areas with high erosion rates will cause potential flood risk mainly in lowlands and coastal areas of Karystos Bay. This is caused because eroded soil has decreased capacity to absorb water and the increased runoff can lead to downstream flooding and local damage to property near these areas. In addition, the increased accumulation of eroded materials from watercourses and their deposition in these areas can result in extra damages after flood events. Moreover, vegetation cover strongly influence the erosion process, as due to high vegetation cover such as in forest areas annual soil loss rate seems to be low, in contrast to the burned areas, where little vegetation cover results in high erosion rates.

5. References

- Brady, NC., Weil RR 1999. The nature and properties of soils. Prentice Hall, Upper Saddle River, New Jersey, 881 pp
- Cebecauer, T., Suri, M., Hofierka, J., Fulajaitar E 2000. Corine land cover in the context of soil erosion

- assessment at regional scale. http://www.corine.dfd.dlr.de/media/download/ws-clc_celecauer_et-al.pdf
- Dabral, PP., Murry, RL., Lollen, P., 2001. Erodibility status under different land uses in Dikrong river basin of Arunachal Pradesh. *Indian. Soil Conserv.*, 29(3), 280-282.
- Descroix, L., Mathys, N. 2003. Processes, spatio-temporal factors and measurements of current erosion in the French Southern Alps: a review. *Earth Surface Processes and Landforms*, 28, 993 – 1011.
- Desmet, PJ, Govers, G 1996. A GIS-procedure for the automated calculation of the USLE LS-factor on topographically complex landscape units. *Soil Water Conserv* 51(5), 427–433
- Dregne, H. E. 2002. Land Degradation in the Drylands. *Arid Land Research and Management*, 16, 99 – 132.
- ESRI, 2005. ArcDoc for ArcGIS, version 9 Help on CDROM.
- Foster, GR., Mc Cool, DK., Renard, KG., Moldenhauer, WC., 1991. Conversion of the Universal Soil Loss Equation to SI metric units. *Soil Water Conserv.*, 36, 356-359.
- IGME, 1977. Geological Map of Greece (Rafina sheet), scale 1:50.000.
- IGME, 1991. Geological Map of Greece (Karistos-Platanistos sheet), scale 1:50.000.
- Karydas, C., Sekuloska, T., Silleos, G. 2009. 'Quantification and site-specification of the support practice factor when mapping soil erosion risk associated with olive plantations in the Mediterranean island of Crete. *Environmental Monitoring and Assessment* 149, 19-28.
- Mitchell, J., & Bubenzer, G. D. (1980) Soil loss estimation. In Kirkby, M. J., & Morgan, R. P. C. (Eds.) *Soil erosion*, John Wiley & Sons: Chichester.
- Moore I, Burch G 1986a. Physical basis of the length-slope factor in the universal soil loss equation. *Soil Sci Soc Am* 50,1294–1298.
- Moore I, Burch G 1986b. Modeling erosion and deposition: topographic effects. *Trans Am Soc Agr Eng* 29(6),1624–1630, 1640
- Thampapillai, DA., Anderson, JR., 1994. A review of the socio-economic analysis of soil degradation problem for developed and developing countries. *Rev. Mark Agric. Econ.*, 62, 291-315.
- Van Der Knijff, J.M., Jones, R.J.A. and Montanarella, L., 2000. Soil Erosion Risk Assessment in Europe, EUR 19044 EN, 34pp.
- Wischmeier WH, Johnson CB, Cross BV (1971) A soil erodibility nomograph for farmland and construction sites. *Soil Water Conserv* 26 (5),189–193
- Wischmeier, W.H. and Smith, D.D. 1978. Predicting Rainfall Erosion Losses. USDA Agriculture Handbook No.537.

KARSTIC LANDSCAPE STUDY BASED ON REMOTE SENSING DATA: THE CASE OF KSIROMERO REGION, AITOLOAKARNANIA - WESTERN GREECE

Golubović Deliganni M.¹, Parcharidis I.¹, Pavlopoulos K.¹

¹ Harokopio University, Faculty of Geography, 70 El. Venizelou Str., 17671 Athens, Greece
miljanamakis@yahoo.com, parchar@hua.gr, kpavlop@hua.gr

Abstract

The aim of this study is to investigate and recognize karst landforms in the area of Ksiromero (Aitoloakarnania, Western Greece) based on medium resolution remote sensing data. In order to highlight karstic structures appropriate and innovative methodologies of image analysis have been developed, applied and compared. In particular, the original Landsat 5 TM bands have been, first, ad-hoc stretched and then processed to obtain the so-called Tasseled Cap Features and the Principal Component images. Finally, a comparative study between the two methods has been carried out.

Key words: Karst landscape, Landsat TM, Principal Component Analysis, Tasseled Cap, Ksiromero, Western Greece

1. Introduction

The characteristics of drainage networks, morphology, soil cover and other diagnostic parameters such as vegetation and moisture can be studied using multispectral satellite images. Various lithologies reflect radiation in different ways, depending on surface properties (soil, vegetation, morphology etc); consequently, evaluating such properties and their cumulative effects can lead to conclusions regarding the type and state of the lithology. Because all physical or non physical surfaces reflect the electromagnetic radiation according to their physical-chemical properties Landsat TM multispectral bands are considered particularly suitable to detect and study common features in karst areas.

This study highlights karst features in the area of Ksiromero, Aitoloakarnania, Western Greece using different image processing methods, based on spectral and spatial image enhancement.

2. Regional and local geological setting

Ksiromero is a region in the northern section of the Prefecture of Aitoloakarnania in western Greece (Fig.1). The region has a total area extent of 106,76 km² and ranges in elevation from 178 m to 1.314 m above sea level. The area is within the Ionian Geotectonic Zone, part of the External Hellenides Platform that extends west from mainland Greece and appears on the western edge of Peloponnesus.

Long thrust faults that trend east-west and northeast-southwest and long reversed and normal faults that trend northwest-southeast are characteristics of the Ionian Zone.

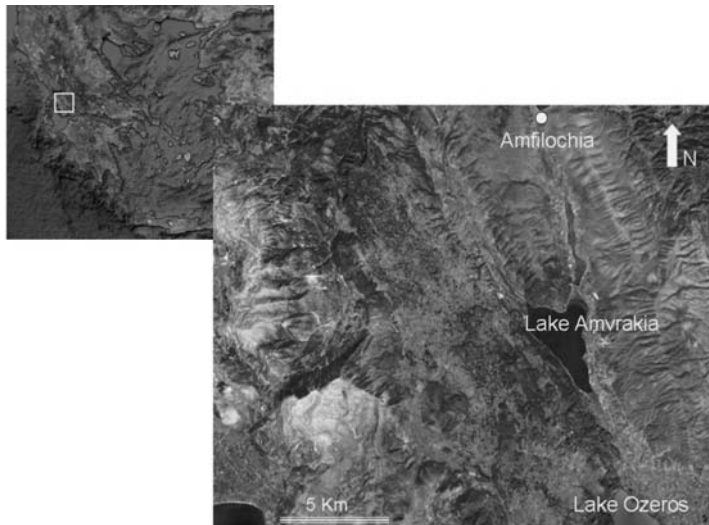


Fig.1: Location of Ksiromero area (Aitolokarnania, Western Greece) on a very high resolution satellite image QuickBird (source: Google Earth).

During Permo-Triassic time, the Ionian Zone was a shallow, restricted, marine basin which accumulated over 150 m of evaporites (Karakitsios, 1992), of which gypsum is notably exposed. Their episodic deposition may have allowed the development of a paleointrastratal karst, as described in other regions by Bosak et al. (1989), although no direct evidence has been found. Triassic Tryphos Formation carbonate breccia conglomerates were deposited over the evaporites, followed by up to 200 m of dolomite and as much as 300 m of the Pantocrator Limestone into the Early Jurassic. At that time, the shallow Tethys Sea covered a continental platform which extended throughout nearly all of western Greece. The carbonate breccia conglomerates are epigenetic, formed during the Triassic from major tectonic activity, diapiric deformation and dissolution of underlying evaporites. These conditions continued with small modifications up to the end of the Jurassic. From the Pliocene to the Quaternary, more recent gypsum deformation occurred at the surface due to underlying diapiric movement along prominent faults (Underhill, 1988). The Tryphos carbonate breccias are the main karstified rocks of the region. They range from 10-200 m thick and cover 70% of the area. Geologic information of the region are provided by the Institute of Geology and Mineral Exploration (1986, 1987).

From a geographic perspective, the region internally drains water to where it is not exploitable for use. Hydrogeologically, it is a system of closed karst watersheds whose recharge characteristics are poorly defined and where the downgradient destination of its groundwater is unknown. While recharge occurs through the higher elevation limestones and dolomites, most of it is transmitted through the Tryphos breccia and the underlying gypsum. The highly soluble gypsum matrix of the conglomerate produces a relatively uniform high-permeability surface that minimizes surface runoff. While most karst features of the region are developed in the Tryphos formation, their density may have been greater if the matrix had been carbonate. Additionally, the few open caves and conduits in the region likely result from the high production of a residual terra rossa soils, talus and debris cones from gypsum, limestones breccia and conglomerates. The soils are accumulated on all surfaces, especially in dolines and poljes, and runoff is insufficient to transport them through the karst to create more open caves.

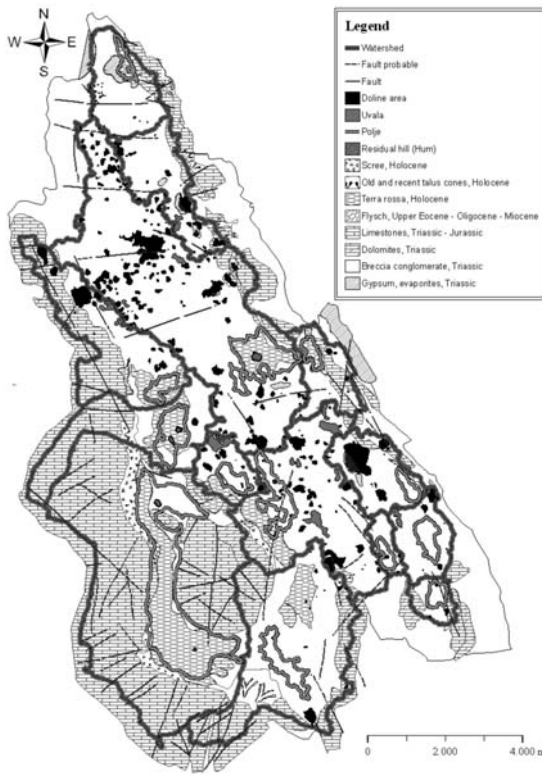


Fig.2: Karst geomorphological map Ksiromero, Aitolokarnania, Western Greece.

3. Karst geomorphology and and geographic information system (GIS) analysis

To better evaluate the karst geomorphologic characteristics of Ksiromero region, this study is based on comparing of results of field research, digitalized geodatabase of karst landforms and Landsat Satellite images. As results of karst geodatabase and geological information of the region of research we created karst geomorphologic map of Ksiromero, Aitolokarnania, Western Greece (Fig.2: geological maps of IGME, 1986, 1987).

With use of ArcGIS Info 9.3 we created a detailed geodatabase of karst landforms and developed a mechanism for symbolically identifying the ephemeral, temporal, or inferred features common for karst in this region. All 1:5000 topographic sheets of the region were digitized at 4-m contour intervals and interpolated at 2m above mean sea level to allow detailed visualization and analysis. We created a database with all existing karst forms and their sub-groups in different layers.

We identified 14 poljes in the region. Through watershed delineation, we identified one large compound karst basin, which includes nine smaller polje watersheds, and five smaller separate watersheds for poljes. We found 17 residual hills in the poljes, comprised predominantly of limestone intercalated with gypsum and likely the result of lesser solubility than tectonic factors. We identified a total of 278 dolines with funnel, shallow, and a few collapse morphologies. We also identified 12 uvalas. Ponors are rare but exist at the contact of the limestone with the breccia conglomerates and follow faults. Using Čar's (2001) classification scheme, Ksiromero primarily has broken, broken collapse, near-fault, and fault dolines.

4. Methodology, data used and processing

The present study aims at enhancing the understanding of karst morphology at Ksiromero as recorded in a Landsat TM scene acquired on September 9th 1992 at 9:25 UTC time. To highlight these features, different image processing methods based on suitable statistical (spectral) and filtering (spatial) procedures were applied to the Landsat TM multispectral data. Finally a computer-aided visual comparison of the two methods of processing was used to determine which is most suitable for such application.

At first, a subset of the full scene was created covering the study area. Next, two methods of spectral enhancement were applied (i) Principal Component Analysis and (ii) Tasseled Cap Transformation.

4.1 . Principal Component Analysis

Principal Component Analysis (PCA) is a statistical method to produce uncorrelated output bands that segregate noise components and reduce the dimensionality of the data set (Richards, 1999). Because multispectral data bands are often highly correlated, the PCA transformation is used to produce uncorrelated output bands. This is achieved by creating a new set (principal component bands) of orthogonal axes that have their origin at the data mean and are rotated so the data variance is maximized.

The principle component bands are linear combinations of the original spectral bands and are uncorrelated. The first component coincides with the direction and length of the widest transect of the ellipse and therefore it measures the highest variation within the data. The respective image appears panchromatic with no spectral input. The second principal component is the widest transect of the ellipse perpendicular to the first component and describes the largest amount of variance not contained in the first component. The remaining principal components are similarly determined (Taylor, 1977).

We adapted Landsat satellite imaging of Ksiromero, using ERDAS Imagine 9.1 software, for PCA. Standardized principle component transformations were conducted using the six bands of the Landsat image, excluding the thermal band. We determined: PC1 = 90%, PC2 = 6.5%, PC3 = 2.3%, PC4 = 0.5%, PC5 = 0.3% and PC6 = 0.01%. using the first three components we created a color image (Fig.3).

4.2 . Data analysis of Tasseled Cap Transformation

The Tasseled Cap (TCs) features, also known as Kauth-Thomas Transforms, are utilized for enhancing spectral information content of satellite data (Kauth and Thomas, 1976). The different bands in a multispectral image can be visualized as defining an N-dimensional space where N is the number of bands. Each pixel, positioned according to its DN value in each band, lies within the N-dimensional space. This pixel distribution is determined by the absorption/reflection spectra of the imaged material. This clustering of the pixels is termed the data structure (Crist and Kauth, 1986). The data structure can be considered a multidimensional hyperellipsoid. The principal axes of this data structure are not necessarily aligned with the axes of the data space (defined as the bands of the input image). They are more directly related to the absorption spectra. For viewing purposes, it is advantageous to rotate the N-dimensional space such that one or two of the data structure axes are aligned with the Viewer X and Y axes. In particular, we could view the axes that are largest for the data structure produced by the absorption peaks of special interest for the application.

Table 1. TC coefficients for Thematic Mapper sensor (source: ERDAS, Imagine).

	Layer 1	Layer 2	Layer 3	Layer 4	Layer 5	Layer 6
1	0.3037	0.2793	0.4743	0.5585	0.5082	0.1863
2	-0.2848	-0.2435	-0.5436	0.7243	0.084	-0.18
3	0.1509	0.1973	0.3279	0.3406	-0.7112	-0.4572
4	0.8832	-0.0819	-0.458	-0.0032	-0.0563	0.013
5	0.0573	0.026	0.0335	-0.1943	0.4766	-0.8545
6	0.1238	-0.9038	0.4042	0.4041	-0.0261	0.024

The TCs are calculated by applying a linear affine transformation, substantially based on the conversion of given input band data set in a new data set of composite values. The transformation depends on the sensor, in this case Landsat TM. The original TCs were first derived for the four bands of the Landsat MSS sensor. Later, the TC transformation was extended to the Landsat TM/ETM (Crist and Cicone, 1984) and IKONOS sensors (Horne, 2003). As for Landsat 5 TM data the coefficients to achieve the TCs are given in Table 1.

Research has produced three data structure axes (Crist et al, 1986; Crist and Kauth, 1986):

- Brightness — a weighted sum of all bands, defined in the direction of the principal variation in soil reflectance.
- Greenness — orthogonal to brightness, a contrast between the near-infrared and visible bands; strongly related to the amount of green vegetation in the scene.
- Wetness — relates to soil moisture (Lillesand and Kiefer, 1987).

The resulting TCs covering the study area are shown in Figure 4 as false color composite image where brightness, greenness and wetness are respectively displayed as red, green and blue.

Finally, a high-pass filter was applied to make the image sharper and to highlight linear features.

5. Conclusions-Results

Ksiromero is a region of carbonate breccia conglomerate karst, with morphologic and hydrologic characteristics complicated by underlying evaporites and preferential dissolution of the gypsum matrix.

Karst in the carbonate breccia conglomerates has dramatic features, including richly developed fields of dolines, uvalas, and poljes but its features cannot be adequately understood based on carbonate karst conditions alone. Figure 5 and 6 overlays the karst landforms shown in with Figure 2 with the PCA and TC imagery to provide comparison of how well each delineates those landforms.

With PCA method the borders of karst forms cannot be clearly recognized, but only inferred.

We can recognize large karst features, such as the largest polje's watershed but limestone pavement and smaller karst features like dolines or uvalas are otherwise difficult or impossible to remotely discern by this method. Also some of hums are recognizable and that probably depends on the wealthier of vegetative covering, or of different geological composition of their rocks from the geological base of their poljes. We came to this conclusion because to the change of color scheme in places that corresponds to positions of hum. This is partially controlled by the spatial resolution of the satellite system used.



Fig. 3: PCA color image using the first three components as RGB.



Fig. 4: Tasseled Cap color image (Brightness=Red, Greenness=Green, Wetness=Blue).

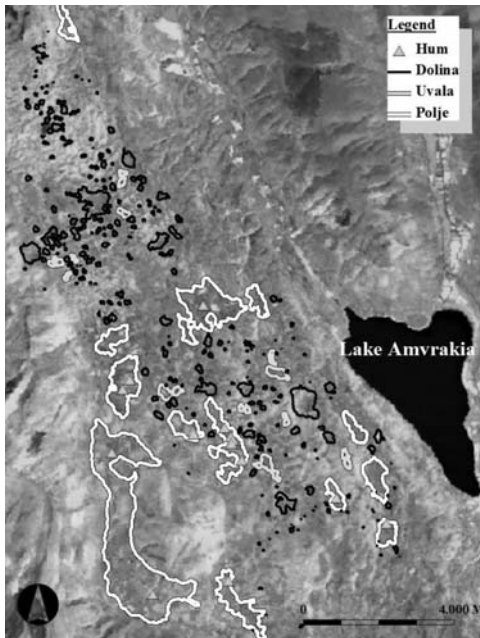


Fig. 5: PCA color image with Kast landscape features.

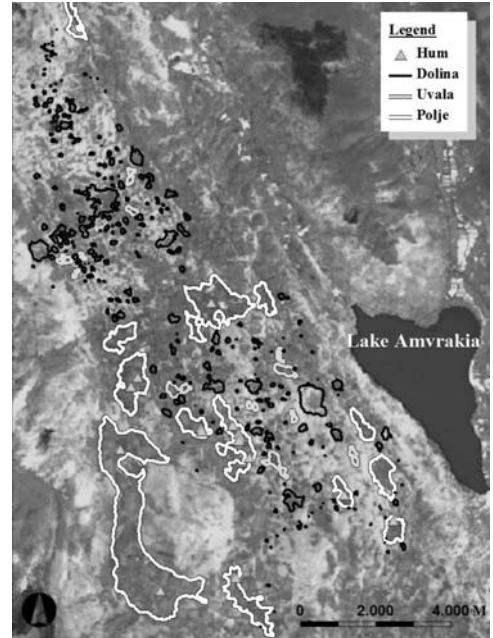


Fig. 6: TC color image with Kast landscape.

With TCs methods the boundaries of some karst forms are more easily mapped and some are even sharply defined.

Also, if we compare the geological map of the study area with the TCs satellite image, the difference is more clearly pronounced. From comparative analysis of TCs satellite images with geological maps and karst morphological maps we conclude that some of bottoms of big karst forms are almost clearly defined with the brightness color scheme like limestones breccia-conglomerates or terra rossa bottoms of big poljes and big dolines between greenness – wetness color scheme of slopes especially those of limestones or dolomites as well in contact with those developed along the faults.

Ksiromero is not a classic limestone bedrock karstic area. The breccia - conglomerate carbonate geology background makes this area unusual due to the size of its karst landforms, type of vegetative cover, lack of a significant surface hydrological network, which make it difficult to remotely image karst features. In contrast, classical karst regions have limestone and dolomites bedrock where the variation in soil reflectance, green vegetation, and soil moisture more clearly expresses karst landforms with the TCs method.

6. References

- Bosák P., Ford D.C., Glazek J., Horacek I. (Eds.) (1989) Paleokarst—a systematic and regional view, *Academia Prague, Czechoslovakia*, 725 p.
- Crist E.P., Laurin R., Cicone R.C. (1986) Vegetation and Soils Information Contained in Transformed Thematic Mapper Data. Paper presented at International Geosciences and Remote Sensing Symposium (IGARSS)' 86 Symposium, *ESA Publications Division, ESA SP-254*.
- Crist E.P., Kauth R.J. (1986) The Tasseled Cap De-Mystified. *Photogrammetric Engineering & Remote Sensing* 52 (1): 81-86.
- Crist E.P.; Cicone R.C., (1984) A Physically-Based Transformation of Thematic Mapper Data – The TM Tasseled Cap. *IEEE Transactions of Geoscience and Remote Sensing* 22(3), 256-263.
- Čar J. (2001) Structural bases for shaping of dolines. *Acta Carsologica*, 30(2), 239-256.
- Ford D., Williams P. (2007) *Karst Hydrology and Geomorphology. John Wiley & Sons, LTD, West Sussex, England*
- Horne J.H. (2003) A tasseled cap transformation for IKONOS images. ASPRS Annual Conference Proceedings. American Society of Photogrammetry and Remote Sensing, *Anchorage, Alaska -USA*, 2003; pp. 1-7
- Institute of Geology and Mineral Exploration, IGME (1986) Geological map of Greece: Astrakos Sheet. *Institute of Geology and Mineral Exploration*, 1 sheet.
- Institute of Geology and Mineral Exploration, IGME (1987) Geological map of Greece: Amphilochia Sheet. *Institute of Geology and Mineral Exploration*, 1 sheet.
- Karakitsos V. (1992) Ouverture et Inversion Tectonique du Bassin Ionien (Epire, Grece). *Annales Geologiques des pays Helleniques*, 35, 185-318.
- Kauth R.J., Thomas G.S. (1976) The tasseled cap: A graphic description of the spectral-temporal development of agricultural crops as seen by Landsat, Final proceedings: Second international symposium on machine processing of remotely sensed data, *Purdue University, West Lafayette*, pp. 41–51.
- Klimchouk A. (2000) Speleogenesis - Evolution of Karst Aquifers. *National Speleological Society, Alabama U.S.A.*
- Lavreau J. (1991) De-Hazing Landsat Thematic Mapper Images. *Photogrammetric Engineering & Remote Sensing* 57 (10): 1297-1302.

- Lillesand T.M., Kiefer R.W. (1987) Remote Sensing and Image Interpretation. New York: *John Wiley & Sons, Inc.*
- Richards A. (1999) Remote Sensing digital image analysis: An introduction, *Springer-Verlag*, Berlin, p. 240.
- Sabins F.F. (1996) Remote Sensing: Principles and Interpretation, *W. H. Freeman and Company*, New York, 3rd ed., 494 p.
- Taylor P.J. (1977) Quantitative Methods in Geography: An Introduction to Spatial Analysis. Boston, Massachusetts: *Houghton Mifflin Company*.
- Underhill J.R. (1988) Triassic evaporates and Plio-Quaternary diapirism in western Greece. *Journal of the Geological Society*, 145(2), 269-282.
- Veni G. (1999) A geomorphological strategy for conducting environmental impact assessments in karst areas. *Geomorphology*, 31, 151-180.

APPLICATION OF A BAYESIAN APPROACH IN GIS BASED MODEL FOR EVALUATING LANDSLIDE SUSCEPTIBILITY. CASE STUDY KIMI AREA, EUBOEA, GREECE

Ilia I.¹, Tsangaratos P.², Koumantakis I.³, Rozos D.⁴

¹National University of Athens, School of Mining and Metallurgical Engineering, Department of Geology, Laboratory of Engineering Geology and Hydrogeology, Iroon Polytechniou, 15780, Zografou, Greece, gilia@metal.ntua.gr

²National University of Athens, School of Mining and Metallurgical Engineering, Department of Geology, Laboratory of Engineering Geology and Hydrogeology, Iroon Polytechniou, 15780, Zografou, Greece, ptsag@metal.ntua.gr

³National University of Athens, School of Mining and Metallurgical Engineering, Department of Geology, Laboratory of Engineering Geology and Hydrogeology, Iroon Polytechniou, 15780, Zografou, Greece, mmgski@central.ntua.gr

⁴National University of Athens, School of Mining and Metallurgical Engineering, Department of Geology, Laboratory of Engineering Geology and Hydrogeology, Iroon Polytechniou, 15780, Zografou, Greece, rozos@metal.ntua.gr

Abstract

The purpose of this study is to present a Bayesian approach (weight-of-evidence method) that utilizes GIS and employs statistical analysis in defining the main factors contributing to the occurrence of landslides in Kimi, Euboea, Greece and to calculate the probability for future landslide manifestation. Landslide locations were identified from field surveys and interpretation of aerial photographs. Additional data were collected from various sources (topographic, geological, land cover maps etc.) and introduced into a spatial database using GIS technology. The above data sources have been used to generate various thematic data layers that have been resampled to 20x20 m² grid size. Applying the developed methodology it was possible to generate appropriate susceptibility maps and thus to predict areas of instability. The results of the analysis were verified using the landslide location data, showing a satisfactory agreement between expected and existing data on landslide location. The outcomes could be used to reduce associated hazards, and to plan land use construction.

Key words: Weight of evidence, Bayesian approach, landslide susceptibility, GIS.

1. Introduction

The prediction and mitigation of geological hazards are considered the most critical part for urban development, as they represent a threat, the direct and indirect results of which affect the economic and social issues of any community. Among geological hazards, landslide phenomena constitute the most frequent one and pose a serious problem especially when manifested in populated areas.

However, due to the complexity and variability of the causative and triggering factors, the evaluation of landslide phenomena often produces outcomes characterized by high uncertainty.

In recent years the development of numerous methods, which employs the use of Geographic Information Systems (GIS), have been able to express the hazard and susceptibility of landslide manifestation, providing cost and time effective tools for evaluating the most critical slope sites (Carrara et al, 1991, Guzzetti et al. 1999, Dai et al, 2002, Chung and Fabbri 2003, Lee et al, 2004, Rozos et al. 2008), producing less uncertain results. GIS-based models are capable to capture, store, manipulate, analyze and display diverse sets of spatial and non-spatial data, but also to integrate appropriate engineering models (Babu & Mukesh, 2002) during evaluation of related engineering problems, such as landslide.

The Weight of Evidence methodology presented in this study follows a similar approach in order to evaluate landslide phenomena. It's a quantitative method which has been adapted to GIS applications in the 1980's to map mineral potential, combining evidence in support of a hypothesis (Kemp et al., 1999, Raines et al., 2000). Although originally designed for non-spatial application, the method can be also used for spatial predictions when the target is the probability of point occurrences (Kemp et al., 1999). The method has been recently used in evaluating landslide susceptibility using GIS techniques (Lee et al, 2002, Mathew et al, 2007, Bettian et al, 2007).

In this paper, the effectiveness of the method has been tested in Kimi, an area experienced substantial landslide events, where a well documented and formulated database exists (Ilia et al, 2008). The database allowed the utilization of GIS technology and probability analysis in defining the main factors contributing to the occurrence of landslides events, and also calculating the probability for future landslide manifestation. Thus the produced landslide susceptibility map will identify zones of varying degree of instability based on the estimated significance of the causative factors, regardless of the time factor. Moreover, this map will be an efficient supporting tool used by decision makers in urban planning and regional land development.

2. Study area

2.1 Geological settings

Euboea, is the second largest island of Greece (after Crete) and the third largest island of the Eastern Mediterranean. Geographically, it is located eastern of Attica and extends along the eastern coast of Greece. Geologically, in Euboea Island outcrop three tectonic units (Katsikatos et al. 1986).

In Euboea, the 'Pelagonian Unit', the northern part of the island is occupied by non-metamorphic rocks. The southern part of the Island is covered by high-pressure/low-temperature rocks named 'South Euboea Blueschist Belt', the northern extension of the intermediate level Cycladic Blueschist Unit. Under these rocks in central Euboea, the para-autochthonous 'Almyropotamos Unit' outcrops in a tectonic window. This unit, which is composed of Mesozoic–Eocene sediments, pertains to the external part of the Hellenides (Dürr et al. 1978) and is considered to have experienced only low-pressure metamorphism (Shaked et al. 2000).

The Kimi-Aliveri basin, which has been selected as the study area, was formed in the Early Miocene. This basin was filled by conglomerates and marls of 500m thick, with lignite intercalations, which was later intruded by volcanic rocks (Katsikatos 1976, Pe-Piper & Piper 1994). In the southern margin of this basin, conglomerates, with a thickness of 1000m, of late Miocene in age (Katsikatos et al. 1981) were accumulated.

More analytically as presented by a previous study (Koumantakis et al, 2008, Ilia et al, 2008) we can find (Figure 1):

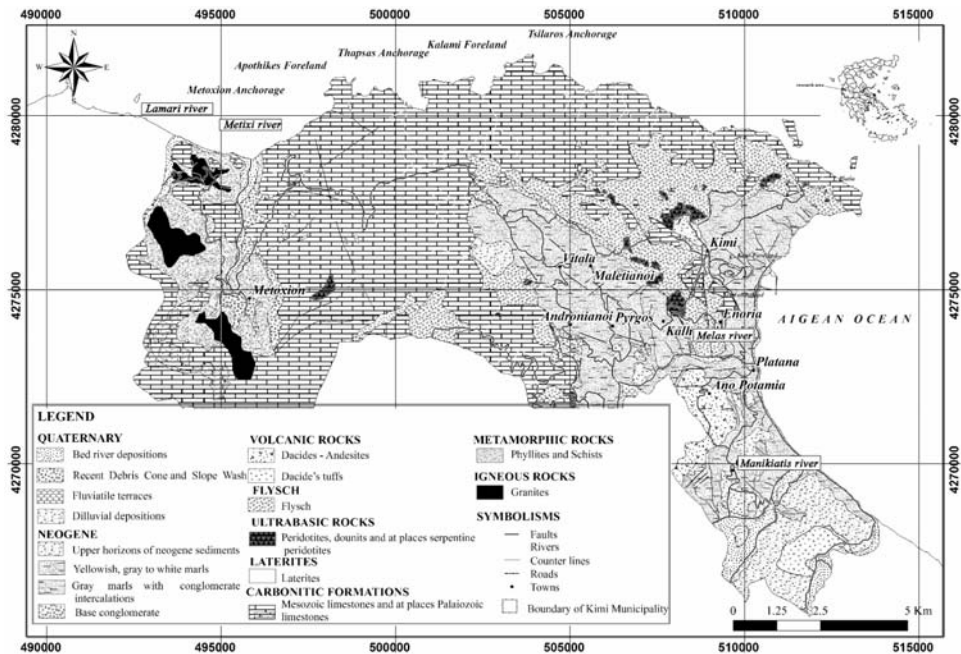


Fig. 1: Geological Map of Kimi Municipality.

- The Quaternary deposits presented in the study area, consist of bed river deposits, debris and slope wash, as well as of fluvial terraces and alluvial depositions.
- The Upper horizons of neogene sediments are constituted by conglomerate alternations and clayey marls. Grits, gravels and pebbles are of volcanic origin and their size varies from 2 - 4 cm.
- The Base conglomerate presents medium to low cohesiveness. Volcanic rocks are presented in the south - eastern department of the Municipality of Kimi with dacites - andesites.
- Flysch formation is constituted by alternations of clayey schists, sandstones, conglomerates and limestones.
- Ultrabasic rocks consist of peridotites, dounits and at places serpentine peridotites. Lateritic are plotted in the western part of Kimi basin.
- Carbonitic formations are presented with Mesozoic, and at places, Palaeozoic limestones. Palaeozoic phyllites and schists, occur usually high cracked and weathered with high weathering.
- Granites are presented in the Western part of Kimi basin, in Carboniferous age.

2.2 Climatic features

The climatic features in a region, in relation with the nature of the rock and the slope inclinations, are thought to be crucial factors, with regard to all kinds of failures in the geological formations. The infiltrated water, in conjunction with the seasonal and daily temperature fluctuations, produces a relaxation of the coherence of the rock formations that often leads to landslide manifestation. For the assessment of the climatic features, all monthly rainfall, temperature and humidity data taken from the Kimi station of the Meteorological Service (221m. altitude), have been exploited. The analysis

showed that the mean annual temperature for the period 1956 – 1989 is 16°C, while January is the coldest month with an average monthly temperature of 8,6°C, February with 8,5°C, December and March with 10°C. July is the warmer month, with an average monthly temperature of 24,9°C. The average annual humidity in the station of Kimi, is 61.7%. The monthly average during the dry season is close to 50%, while during the period from October to February the humidity range from 66 to 70%. The predominant wind direction is north. Finally, the average annual amount of rainfall is 1071mm, but in highland zones of the region, the annual amount of rainfall is expected to be higher.

3. Data and Methodology

The applied methodology uses the Weight of Evidence probabilistic model, based on the Bayes theorem and on the concepts of prior and posterior probability, to determine if the given specifications (a set of independent variables) results in unstable or stable slopes (dependent variable). The main objective is assessing the spatial relationship between the distribution of the areas affected by landslides, known landslide locations, and the distribution of the analyzed landslide susceptibility variables, evidential themes. It is therefore possible to calculate the degree of influence that each variable had, but also the degree of influence it will have in the future, regarding the manifestation of landslide events.

As it is obvious this approach implies that future landslides occur under conditions and factors similar to those acted in the past, and such behaviour will remain constant over time. It also implies that the factors should be conditionally independent from each other regarding the occurrence of landslide events, an assumption that should be checked excluding depended factors from subsequent analysis.

In an area which contains a number of instability sites (L), the prior probability of slide occurrence per unit area, is calculated as the total number of slides observed in the past, under similar conditions over the total area (A).

$$P\{L\} = \frac{N\{L\}}{N\{A\}}$$

Having a set of evidence data, which could be thought as landslide-influenced factors, the prior probability could be modified and addressed as conditional or posterior probability $P\{L | B\}$, expressing the probability that an event (L) will occur under the presence or the absence of an evidence B,

$$P\{L | B\} = \frac{P\{L \cap B\}}{P\{B\}} = P\{L\} \times \frac{P\{B | L\}}{P\{B\}}$$

and

$$P\{L | \bar{B}\} = \frac{P\{L \cap \bar{B}\}}{P\{\bar{B}\}} = P\{L\} \times \frac{P\{\bar{B} | L\}}{P\{\bar{B}\}}$$

For mathematical reasons, the conditional probabilities can be expressed more conveniently as odds:

$$O = P / 1 - P$$

Therefore, the above equations are modified as:

$$O\{L | B\} = O\{L\} \times \frac{P\{B | L\}}{P\{B | \bar{L}\}}$$

and

$$O\{L | \bar{B}\} = O\{L | B\} \times \frac{P\{\bar{B} | L\}}{P\{\bar{B} | \bar{L}\}}$$

, where $O\{L | B\}$ and $O\{L | \bar{B}\}$ are the posterior odds of a landslide event (L), given the presence or the absence of an evidence (B).

Bonham-Carter (1994) defined positive and negative weights for the evidence (B) (W^+ and W^-) giving information about whether there is a positive or a negative correlation between the evidence and the landslide locations that combine those conditional probabilities as:

$$W^+ = \ln \frac{P\{B | L\}}{P\{B | \bar{L}\}}, \text{ when the evidence (B) is present and}$$

$$W^- = \ln \frac{P\{\bar{B} | L\}}{P\{\bar{B} | \bar{L}\}}, \text{ when the evidence } (\bar{B}) \text{ is absent}$$

If there are N evidence factors, then the weights can be summed up to find the natural logarithm of the posterior odds of the potential slide sites as given by:

$$\ln O_{\text{posterior}}\{L\} = \sum_{i=1}^n W_i + \ln O_{\text{prior}}\{L\}$$

Another measure of the spatial association between the landslide event (L) and the evidence (B) is provided through the magnitude of contrast C, which is determined by the difference, W^+ , W^- . When C is positive it implies positive correlation and when it is negative it implies negative spatial association. This means that if more events (landslides) occur within an evidence layer that would be expected by chance, the W^+ is positive and the W^- is negative. Conversely, W^+ is negative and W^- is positive where fewer events occur within an evidence layer than would be expected by chance (Bonham-Carter et al. 1989).

The studentized value of C is calculated as the ratio of C to its standard deviation $S(C)$, $C / S(C)$, and serves as a guide to the significance of the spatial association, acting as a measure of the relative certainty of the posterior probability (Bonham-Carter 1994).

To run successfully the proposed methodology, a well structured spatial database which contains data, concerning landslide locations, in digital format, such as geological maps, topographic characteristics, infrastructure networks and many more features, are required. All the landslide-related factors which are to be used in the analysis were rasterized, converted to cells, and introduced in the GIS system. Slope failures were presented as points, so each set of variables could be presented on a simple thematic map, with binary pattern, showing stable and unstable cells. As a first step, the probability that a landslide would occur if evidence is present or absent was calculated for each of the above evidence layers. For each cell the final probability was the sum of contrasts of each variable, as above mentioned.

The model was built up using a Training Data set, consisting of about 85% of the entire landslide events and a landslide susceptibility map was produced. The remainder 15%, Testing set of data, was

used in order to validate the model. The distinction of the database into training and test data has been done randomly, in order to guarantee that both are random samples from the same distribution.

4. Generating evidence layers

There are no specific criteria or guidelines for selecting the parameters to include in the developed model. However, the general idea is a) the independent variables should have a certain relation to the dependent variable, b) to vary spatially, c) to be expressed in a measurable scale, and d) its effect should not account for double consequences in the final result (Ayalew & Yamagishi, 2004). In the study area, the main triggering factor is the high amount of precipitation and in some extent tectonic activity. However those two factors have been excluded from the model since the objective was to produce landslide susceptibility map and to identify zones of varying degree of instability based on the estimated significance of the causative factors have, regardless of the time factor and any triggering factor.

Having in mind the above mentioned, lithology, altitude, slope inclination, slope orientation and road network proximity, are include in the model as causative factors responsible for landslide manifestation. These factors form the necessary evidence layers that the method needs. A brief description of each of the evidence layers and the spatial distribution of landslide events are given below:

The model requires landslide location data introduced in the GIS system as a point shapefile. A total of 72 landslides locations of various dimensions were identified and mapped in the whole area of the Municipality of Kimi. A detailed examination of the affected area with field observations along with the interpretation of aerial photographs was helpful in order to construct a landslide database contain data from various sources of information.

Lithology is considered as one of the most causative parameter regarding the landslide manifestation throughout Greece. The large surface development of formations appearing in cyclothematic sequences, such as schist-chert formations, flysch sediments, Molassic and Neogene deposits with anisotropic geomechanical behaviour facilitate the manifestation of abundant slope failures (Koukis and Rozos, 1982, Koukis, 1988). In the studied area landslide events mainly took place at the upper horizons of the Neogene marls and flysh formations, which were mainly covered by thick weathering mantle.

The altitude of a site is a combined result of the tectonic activity and the erosion – weathering processes and is related to climatic conditions through an interactive influence. Thus, altitude is indirectly contributing to the slope failure manifestation.

The inclination of a slope along with the orientation plays a significant role in the concept of landslide manifestation as a causative factor (Rozos et al, 2008). It seems that such behaviour is controlled by the combined influence of many variables, such as the intensity and severity of climatic conditions, the weathering processes, the type and density of vegetation cover, as well as the discontinuity pattern and internal geometry of the geological formations (Huma and Radulescu, 1978, Carrara 1983, 1984, Maharaja, 1993). In addition certain orientations are associated by increased snow concentration, higher erosion and intense wreathing process as the climatic agents facilitate the cyclic alteration of dry and wet periods. In the study area, those orientations were the NNW-NNE (315° - 45°) and SE-SW (135° - 225°).

Finally it has been observed that many landslides occur close to the road network. The slope instability could be caused either by the uncontrolled or controlled blasting and widening of the roads, or by the loss of support due to removal of material from the lower portion of the slopes during road widening. The continuous data have been converted to a binary pattern, using buffer zones in order

to identify a statistical correlation between road proximity and landslide locations.

Each one of the above mentioned factors was introduced in GIS system providing the necessary evidence thematic layers in digital format, producing grid files with cell size 20x20m, appropriate for statistical and probabilistic analysis. The classification followed for each factor was based on expert knowledge and bibliographical reference (Rozos et al, 2008, Ilia et al, 2008).

4.1 Checking for conditional independency

As already mentioned the Weight of Evidence method in order to be applied successfully assumes conditional independency among the landslide-influenced factors and that the population of each factor has a normal distribution. To calculate such independency, χ^2 (chi-square) method was used. The first step in computing the Chi-squared statistic is the computation of the contingency table, which is set up for each pair using as reference points the landslide locations. The number of observed landslide locations in each cell of the table is compared with the expected. The assumption of conditional independency is tested by determine if the measured χ^2 value exceeds or not a theoretical χ^2 value, given by the number of degrees of freedom and the level of significance. In Table 3 the results of Chi-squared statistic are showed, implying that each of the analyzed variables should be included in the model since the assumption of conditional independency among them is true. For example it can be seen that the pairs of slope inclination and slope orientation shows a conditional independency, since the theoretical χ^2 value, shown in the table in brackets, is 26.217 at the 99% significance level (degree of freedom = 8) and the calculated χ^2 value was 20.226. This implies that those predictor variables could be used together for the calculation of landslide susceptibility map, since the null hypothesis of independence is true.

5. Results and discussion

The accuracy of the outcomes depends mostly on the amount and quality of available data, the working scale and the selection of the appropriate analysis and modelling. The process of creating those thematic layers, involves several qualitative or quantitative approaches (Soeters and van Westen, 1996, Aleotti and Chowdhury, 1999; Guzzetti et al., 1999). As mentioned by Bonham-Carter (1994), the results of the Weight of Evidence method, are strongly dependent on the number of events in-

Table 1. Chi-square statistics.

Parameters	Lithology	Slope orientation	Slope inclination	Altitude	Road Proximity
Lithology	-	27,903 (32,00)	11,55 (26,217)	11,152 (37,566)	5,297 (20,090)
Slope orientation		-	20,226(26,217)	6,085 (37,566)	6,215 (20,090)
Slope inclination			-	6,357 (30,578)	10,235 (16,812)
Altitude				-	5,5767 (23,209)
Road Proximity					-

Table 2. Weight of Evidence analysis between landslide-events and factors.

No	Road Proximity	W ⁺	s-W ⁺	W ⁻	s-W ⁻	C	s-c	c/s-c
1	0-100m	1.309	0.2858	-0.666	0.037	1.976	0.256	7.713
2	100m-200m	0.6789	0.0666	-0.146	0.021	0.852	0.297	2.782
3	200m-300m	0.64827	0.0833	-0.108	0.02	0.7566	0.321	2.354
4	>300m	0	3.71E-06	0.978	0.016	-0.9775	0.127	-7.695
No	Lithology	W ⁺	s-W ⁺	W ⁻	s-W ⁻	C	s-c	s-c
1	Class 1	-2,367	0,333	0,677	0,016	-3,045	0,591	-5,144
2	Class 2	0	0	0,010	0,016	-0,010	0,127	-0,079
3	Class 3	-1,287	0,500	0,091	0,016	-1,379	0,718	-1,919
4	Class 4	1,224	0,032	-0,534	0,032	1,759	0,254	6,924
5	Class 5	0,692	0,038	-0,308	0,027	1,001	0,257	3,890
No	Slope inclination	W ⁺	s-W ⁺	W ⁻	s-W ⁻	C	s-c	s-c
1	0-17°	0,127	0,023	-0,224	0,050	0,352	0,271	1,297
2	17° - 36°	-0,154	0,052	0,076	0,023	-0,231	0,275	-0,838
3	36°-50°	-0,994	1,00	0,028	0,016	-1,023	1,008	-1,015
4	> 50°	0	0	0,002	0,016	-0,003	0,127	-0,021
No	Slope aspect	W ⁺	s-W ⁺	W ⁻	s-W ⁻	C	s-c	c/s-c
1	225° - 275°	-1,382	1,000	0,050	0,016	-1,433	1,008	-1,421
2	45° - 90°	-0,168	0,100	0,035	0,019	-0,204	0,345	-0,592
3	90°-135°, 275°-315°	-0,240	0,090	0,060	0,019	-0,301	0,332	-0,904
4	315° - 450°, 135°-225°	0,217	0,025	-0,303	0,045	0,521	0,265	1,962
No	Altitude	W ⁺	s-W ⁺	W ⁻	s-W ⁻	C	s-c	c/s-c
1	0-220m	0,672	0,023	-0,707	0,050	1,380	0,271	5,079
2	220-440m	0,024	0,062	-0,008	0,021	0,033	0,290	0,114
3	440-660m	-1,002	0,250	0,126	0,017	-1,130	0,516	-2,185
4	660-880m	0	0	0,163	0,016	-0,164	0,127	-1,287
5	880-1100m	0	0	0,069	0,016	-0,069	0,127	-0,546
6	>1100m	0	0	0,008	0,016	-0,009	0,127	-0,070

roduced in the model (e.g., on the estimation of probabilities) and on the quality of the landslide inventory map. Therefore, probabilities are very low if the area is characterized by rare events, and the results have to be cautiously interpreted. Applying the Weight of Evidence method, the spatial rela-

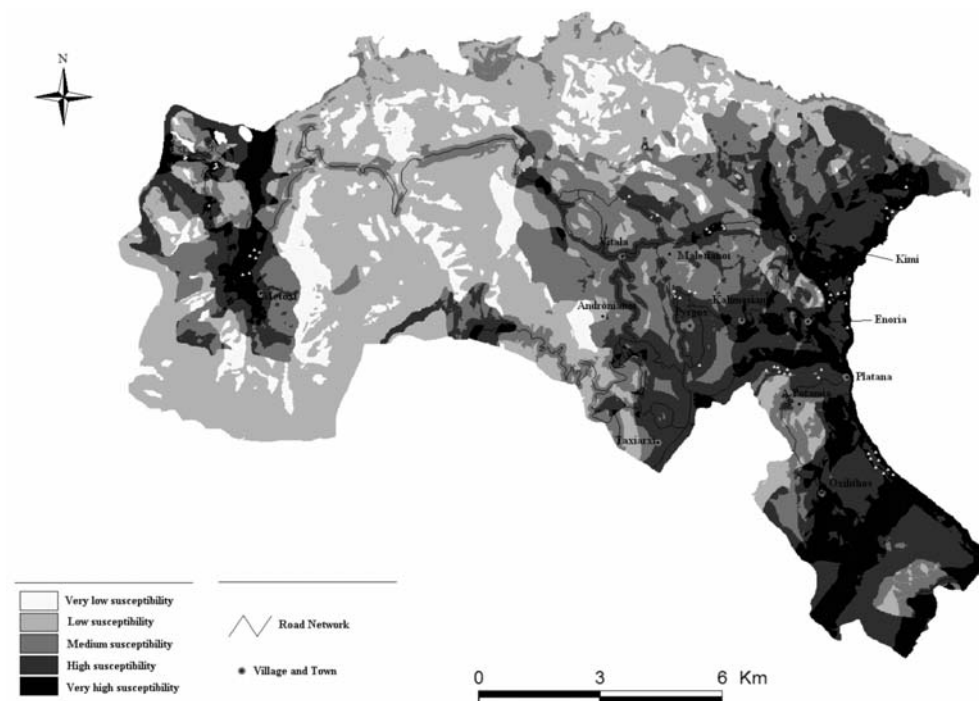


Fig. 2: Landslide Susceptibility map of Kimi municipality area

tionship and the contrast value between landslide-occurrence location and each of the variables were extracted. Table 2 shows in detail the landslide-influenced factors in which we could find the positively correlated with the landslide locations, and supposed to be significant causative factors that are likewise possible indicators for landslide manifestation.

$$Lsi = \sum_{i=1}^n C_i$$

The contrasts of each factor type were summed up to calculate the landslide susceptibility index (Lsi), as shown in the following equation, and by applying Spatial analysis techniques within GIS, a susceptibility landslide map is obtained (Figure 2).

Calculating the area, each class occupied by using only the Training set of data, the 8.45% of the studied area was classified as having very low susceptibility index, 36.48% was classified as having low susceptibility index, 21.76% was classified as having medium susceptibility index, 21.68% was classified as having high susceptibility index and 11.62% was classified as having very high susceptibility index. To validate the developed model, control points were used. Those control points are past landslide events that have not been included in the model, and are used as Test Data set. As already mentioned, about 15 % (10 landslide event, randomly distributed through the study area), where used to determine the Prediction rate. The three first classes, very low, low and medium susceptibility, include about 10% of the Test data set, while the 90% percent of the landslides where found in the areas of high and very high susceptibility index. The produced prediction rate (90%) was based on the random distributed control points and was accepted as satisfied.

6. Conclusion

In the presented study, the Weight of Evidence method was introduced in order to define the main factors contributing to the occurrence of landslides in Kimi, Euboea, Greece and to calculate the probability for future landslide manifestation. The results were used to produce a Landslide Susceptibility Map indicating areas of very low, low, medium, high, and very high susceptibility.

The analysis performed using the Weight of Evidence, proved that this method could be thought as an objective system that can discriminate the various parameters, in order to understand the importance of each one of them, in the development of landslide phenomena. It is also capable to calculate the weights, separately for each study area, allowing the selection of different weights, for the same parameters, when different settings exist. This process is an objective one and almost independent by the choices of the user.

The statistical method employed in this study determined several crucial factors for landslide susceptibility in the study area. Among them, slopes with angles from 0° to 17° facing NNW-NNE (315° - 45°) or (135° - 225°) SE-SW, consisting of Quaternary and Neogene sediments, located within a distance of 100m from the road network and with altitude value less than 220m were identified as indicators for high slope instability.

7. References

- Aleotti P, Chowdhury, R., 1999. Landslide hazard assessment: summary, review and new perspectives. *Bull Eng Geol Environ* 58:21-44.
- Ayalew, L. and Yamagishi, H., 2004. Slope movements in the Blue Nile basin, as seen from landscape evolution perspective, *Geomorphology* 57, pp. 95–116.
- Babu Sivakumar, G. L. and Mukesh M. D., 2002. Characterization of soil spatial variability and its influence on slope stability, *Indian Geotechnical Journal*, 32(2), 123-145.
- Bettian, N. and Birgit, T., 2007. Landslide susceptibility assessment using “weights-of-evidence” applied to a study area at the Jurassic escarpment (SW-Germany). *Geomorphology* 86, 12-24.
- Bonham-Carter, G.F., Agterberg, F.P., Wright, D.F., 1989. Weights of evidence modelling: A new approach to mapping mineral potential. *Statistical Applications in Earth Sciences* 89(9), 171-183.
- Bonham-Carter, G.F., 1994. *Geographic information systems for geoscientists: Modelling with GIS*. Pergamon Press, Canada, 398.
- Carrara, A., 1983. Multivariate models for landslide hazard evaluation: *Mathematical Geology*, v. 15, no. 3, p. 403-426.
- Carrara, A., 1984. Landslide hazard mapping: aims and methods, *Mouvements de Terrains*, Association Francaise Géographie Physique. Colloque de CAEN, pp. 141–151.
- Carrara, A., Cardinali, M., Detti, R., Guzzetti, F., Pasqui, V., Reichenbach, P., 1991. GIS techniques and statistical models in evaluating landslide hazard, *Earth Surface Processes & Landforms*, Volume 16, Issue 5, 427-445.
- Chung, C.F. and Fabbri, A.G., 2003. Validation of spatial prediction models for landslide hazard mapping. *Natural Hazards*, 30: 451-472.
- Dai, F.C. and Lee, C.F., 2002. Landslide characteristics and slope instability modeling using GIS, Lantau Island, Hong Kong, *Geomorphology*, Volume 42, Issue 3-4, 213-228.
- Dürr, S. T.-Altherr, R.-Keller, J. Okrusch, M. Seidel, E., 1978. The median Aegean crystalline belt: Stratigraphy, Structure, Metamorphism, Magmatism. In *Alps, Apennines, Hellenides*, 455-477.
- Guzzetti, F. Carrara, A., Cardinali, M., Reichenbach, P., 1999. Landslide hazard evaluation: a review of

- current techniques and their application in a multi-scale study, central Italy, *Geomorphology* 31, pp. 181–216.
- Huma, I., Radulescu, D., 1978. Automatic production of thematic maps of slope stability. *Bull IAEG* 11(17):95–99.
- Iliá, I., Koumantakis, I., Rozos, D., Markantonis, K., Tsagaratos, P., 2008. Landslide Phenomena in Kimi area, Evia Island, Central Greece. *Geophysical Research Abstracts*, Vol. 10, EGU2008-A-06831, 2008 SRef-ID: 1607-7962/gra/EGU2008-A-06831 EGU General Assembly 2008.
- Katsikatsos, G. 1976. La structure tectonique de Attique et de leile de Euboe. *Bull Soc Gool France* 19 : 211-228.
- Katsikatsos, G., De Bruijn, H., Van der Meulen, A. J., 1981. The Neogene of the island of Euboea (Evia): a review. *Geol Mijnb* 60 : 509-516.
- Katsikatsos, G., Migiros, G., Triantaphyllis, E. & Mettos, A., 1986. Geological structure of internal Hellenides (E. Thessaly SW Macedonia, Euboea Attica Northern Cyclades and Lesvos). *I.G.M.E., Geol. and Geoph. Res., Special issue*, 191-212.
- Kemp, L. D., Bonham-Carter, G. F., Raines, G. L., Looney, C.G., 1999. Arc-SDM: A review extension for Weight of Evidence Mapping, <http://gis.nrcan.gc>.
- Koukis, G. and Rozos, D. (1982). Geotechnical conditions and landslide movements in the Greek territory in relation to the geological structure and geotectonic evolution. *Mineral Wealth*, 16: 53-69.
- Koukis, G., 1988. Peloponnesus: History, Geology and Engineering Geology aspects. *Proceedings Int. Symposium on the Engineering Geology of Ancient Works, Monuments and Historical sites*, Marinós & Koukis (eds), Greece, 4, 2213 - 2234, Athens, Greece.
- Lee ,S., Choi, J., Min, K., 2002. Landslide susceptibility analysis and verification using the Bayesian probability model, *Environmental Geology*, Volume 43, 120-131.
- Lee ,S., Ryu, J-H., Won, J-S., Park, H-J., 2004. Determination and application of the weights for landslide susceptibility mapping: using an artificial neural network. *Engineering Geology*. v71. 289-302.
- Koumantakis, I., Rozos, D., Markantonis, K., Iliá, I., Tsagaratos, P., 2008. Landslide Phenomena of Kimi Municipality. Research Program founded by the Prefecture of Euboea Island.
- Mathew J., Jha V., Rawat G., 2007. Weights of evidence modelling for landslide hazard zonation mapping in part of Bhagirathi valley, Uttarakhand, *Current Science*, Vol. 92, no5, 628-638.
- Maharaja, R. 1993. Landslide processes and landslide susceptibility analysis from an upland watershed: a case study from St.Andrew, Jamaica, West Indies. *Engineering Geology*, Vol. 34, pp. 53-79.
- Pe-Piper, G. and Piper, D.J.W., 1994. Miocene magnesian andesites and dacites, Evia, Greece: adakites associated with subducting slab detachment and extension. *Lithos*, 31, 125-140.
- Raines, G. L., Bonham-Carter, G. F., Kemp, L., 2000. Predicting probabilistic modeling using Arcview GIS. *Arcuser*, April June 2000, p.45-48.
- Rozos D., Pygiotis, L., Skias, S., Tsagaratos, P., 2008. An implementation of rock engineering system for ranking the instability potential of natural slopes in Greek territory. An application in Karditsa County. *Landslides*, Vol. 5 no3, 261-270.
- Shaked Y., Avigad D. & Garfunkel Z. 2000. Alpine high-pressure metamorphism at the Almyropotamos window (southern Evia, Greece). *Geol. Mag.*, 137, 367-380.
- Soeters, R. and van Western, C.J., 1996. Slope instability recognition, analysis, and zonation. In: A.K. Turner and R.L. Schuster, Editors, *Landslides: Investigation and Mitigation*, Special Report vol.247, Transportation Research Board, National Academy Press, Washington, D.C. (1996).

THE USE OF THE GEOGRAPHICAL INFORMATION SYSTEMS (G.I.S) IN THE GEOLOGICAL – MINERALOGICAL MAPPING OF THE PARANESTI AREA

Karageorgiou M. M. D.¹, Karymbalis E.² and Karageorgiou D.E.³

¹ *Geographer, 62 Amisou str. 17123 N. Smyrni, Athens Greece, melaxroini_ka@yahoo.gr*

² *Harokopio University, Department of Geography, karymbalis@hua.gr*

³ *Department of Energy Solid Raw Materials, Institute of Geology and Mineral Exploration, Olympic Village, Entrance C 136 77 Acharnae Greece. dek@igme.gr*

Abstract

The aim of this study is to emphasize the role of the Geographical Information Systems (GIS) technology for the collection, organization, analysis, modeling and presentation of data required for the geological and ore-deposits mapping. As a case study area the region of Paranesti in Northern Greece was selected as it is of exceptional geological and uranium mining interest. For the geological and ore deposit mapping of the study area data derived from analogue maps at various scales (topographical and geological) along with detailed field geological observations and measurements were organized in a spatial database with a common geographical coordinate system utilizing GIS technology. This procedure revealed the relation between the geographical distribution of uranium deposits and the geological structure of the area as well as the effect of the active tectonics.

Key words: *(GIS) technology, uranium mining, mapping, Paranesti, Northern Greece.*

1. Introduction

The area of Paranesti is located in the northeastern part of the prefecture of Drama in Northern Greece. The natural relief of the broader area of Paranesti is characterized by intense mountainous morphology. The largest portion is covered by the west part of the Rhodopi mountain chain which is cut by the Nestos River valley and its tributaries.

The region of Paranesti was selected as a case study because it is of exceptional geological and uranium mining interest. For the geological and ore deposit mapping of the study area data derived from analogue maps at various scales (topographical and geological) along with detailed field geological observations and measurements were organized in a spatial database with a common geographical coordinate system. This applied methodology revealed the relation between the geographical distribution of uranium deposits and the geological structure of the area as well as the effect of the active tectonics.

GIS techniques have been used in similar studies such as the implementation of GIS in Santorini volcano for ground deformation analysis (Papageorgiou et al. 2010), the mineral potential map of the Singhbhum copper belt in Jharkhand by P. Sinha et al. (2002) and the creation of a geological database at the area of Kifisia in Athens by A. Zervakou (2004). It was concluded that the role of the Geographical Information Systems (GIS) technology for the collection, organization, analysis, modeling and presentation of data required for the geological and ore-deposits mapping is of great importance.

2. The case study area

The area of Paranesti, located at the northeastern part of the prefecture of Drama, is bordered to the north by Bulgaria, to the south by the prefecture of Kabala, to the west by the Community of Sidironero which belongs to the prefecture of Drama and to the east by the prefecture of Xanthi. It occupies an area of 788.394 acres, which corresponds to the 22,7% of the total area of the Drama prefecture. The municipality of Paranesti established with the unity of (P.D. 55/7-3-1994, OGI 39/21-33-1994) the Communities of Paranesti, Tholos and Sillis (Prasinada) and is one of the nine LGO (Local Government Organization) of the prefecture of Drama which belongs to the Constituency of the East Macedonia and Thrace. Paranesti's population is 1621 inhabitants, that mainly are refugees came to the area from the Pontos and the Mikra Asia (Asia Minor) since 1922. The capital of the municipality of Paranesti is 39 km far from the town of Drama and is consisted of 1439 inhabitants.

The area of Paranesti is characterized by intensely mountainous relief morphology. The largest portion is covered by the west part of the mountain chain of Rodopis and is crossed by Nestos River and its tributaries. It is impossible to give an accurate estimation or description of the climate conditions of the area because of the lack of meteorological station within the study area. A satisfactory idea about the climate of the area gives the temperature and rainfall data from the weather station at Sidironero. According to these data for the time period between 1977 and 1987, mean annual rainfall reaches 679 mm while mean annual temperature is 11,4° C. The minimum of the temperatures occur during the January and reaches up to -17° C and the maximum at July reaching 38,5° C. Generally, the climate in this area can be characterized as transitional between Mediterranean and European with the characteristics of the last one to be more intense. The largest part of the region is covered by forests since a small percentage was parceled out to agricultural cultivations, water surfaces, settlements and others land uses.

3. Methodology (GIS technology) - Results

Nowadays the main GIS software vendors have created integrated software packages to meet the need of a diverse user community (Longley, 2001). Specifically a GIS provides – among other capabilities - functions for terrain modelling and analysis (Digital Elevation Model creation from various sources, slope calculation, generation of topographic sections, etc.) as well as for geometric and spatial statistical calculations (Chalkias C., 2006).

The system created provides an advanced method to organize, analyze, compute and visualize spatial information and geologic and tectonic features for the geological and deposit mapping and analysis of the area of Paranesti. The core system consists of a commercial GIS software package (ArcGIS) supporting both vector and raster spatial data sets. This software is extended with special external functions (developed in a third generation programming language) implemented for the geological and the deposit analysis. The basic functions include the construction of geo-databases which provide the interaction of various data in a common coordinate system and a common scale. Additionally, functions and operations, among others uses, give the opportunity to create new thematic layers based on the correlation of attributes tables and creation of SQL questions while Spatial join operation is used to combine two or more dataset with respect to a spatial predicate. Finally, there are analysis procedures such as clip, union, intersect where data layers overlay producing new thematic layers.

As mentioned above the specific software that had been used is ArcGIS 9.0 and a prototype system has been developed as an outcome. The architecture of this prototype is illustrated in Fig. 1. The general concept is as follows. The core is a standard GIS. This system was enriched with functions developed especially for the geological and deposit analysis of the area of Paranesti. These functions are operating in relevant spatial datasets incorporated in the system and originated from analogue

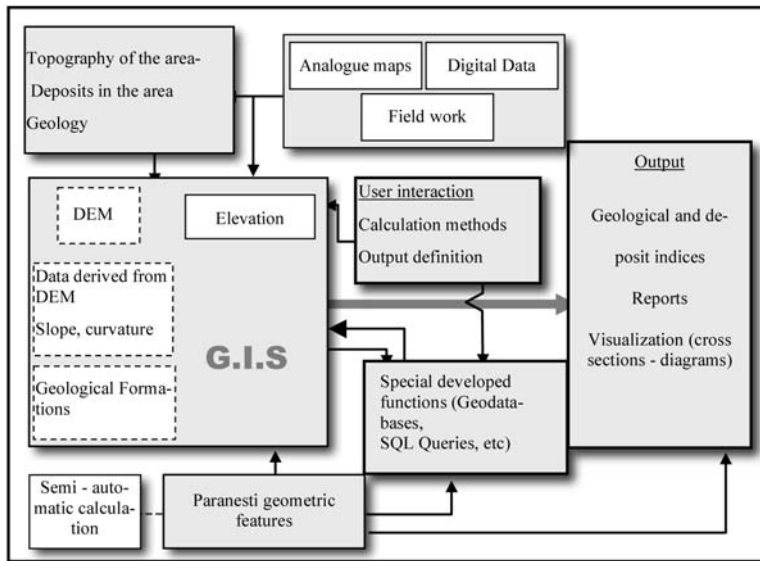


Fig. 1: Architecture of the prototype system.

maps, previous digital datasets and fieldwork. The geology as long as the deposits of the area is estimated through special computational procedures using mainly the DEM of the area geometry. The DEM - which is the main digital model used for the computations - is created by using the internal GIS functionality of the prototype. Features corresponding to Paranesti geometry cannot only manually be input but can also be calculated through semi-automated procedures of the system. The final outputs could be arithmetic features corresponding to specific geological and deposit indices - ratios, reports presenting morphology of the area, or advanced visualization.

In the present study for the detailed representation of the topography of the area of Paranesti two topographic maps of 1972 at a scale of 1:50000 obtained from the Greek Army Geographical Service (GAGS) of the area of Paranesti and Mesochori, were used. Additionally, geological maps of the area at the scale of 1:50000 by IGME were used in combination with detailed geological maps produced through extensive fieldwork.

All the analogue maps were scanned and transformed into .jpg files in order to demand less storage space. For the geo-reference of each one of the topographical and geological sheets four control points were choose and their co-ordinates were recorded. Before the geo-referencing the co-ordinates of the control points were transformed from Hatt to EGSA' 87. The aim of this action was to convert all data in the same projection system. The most often used projection system in Greece is the Greek Geodetic Projection System of 1987 (EGSA' 87). While the conversion of the co-ordinates materialized an error occurred in the region of ± 0.20 m. The software used for this conversion is the COORD_GR (Siggros, 2002). Generally, during the geo-reference of a map an error occurs due to the position of the cross on the right point of the map. In other words, it depends on whether the new point that has been created on the map has the same co-ordinates with the one on the real map or not. So it's obvious that the total RMS error differs from user to user. Also the mean value of the error has to correspond to the $\frac{1}{4}$ of the scale of the map (Chalkias, 2003). This means that for maps at a scale of 1:50000 the error should be less than 15 and for maps 1:5000 scaled should be less than 1.

Table 1. The thematic layers that had been created, its attributes and its source.

Thematic Layers	Form	Attributes	Data source
Contours	Line	Altitude	1:50000 GAGS
Geological Formations	Polygon	Geological Formations	1:5000 IGME
Geological Lines	Line	GEOLOGY_ID	1:5000 IGME
Drillings	Point	Drilling, EGSA87_X, EGSA87_Y	IGME

Afterwards, the geographical data of the area was organized into thematic layers in vector and raster form with which a geographical base was created. The attributes and the source of the data are represented in the following Table 1.

The procedure of digitizing was carried out with the head up digitizing method utilizing the respective functions and commands in order to reduce the errors. Then the values of each layer were imported in an attribute table. It was necessary to create the 3D Digital Elevation Model (DEM) in order to represent the general morphology and the curvature of the area. The DEM was created using appropriate vector data (contour lines) and specialized procedures (ANUDEM algorithm) in the framework of the used GIS. A number of secondary geographical variables, which are very significant in morphometric and geological analysis, were derived from the DEM. These variables are related to elevation measurements, slope, volumetric computations, geological formation outcrop and tectonic features such as faults.

A series of drillings were developed in the area of Paranesti by the Institute of Geology and Mineral Exploration (IGME) in order to study the geological and deposit characteristic of the area (Pergamalis et al., 1998). The process of creating the drillings began in December of 1978 and completed in December of 1996. The results were visualized in a map at a scale of 1:5000. The map was created between 1993 and 1996. It must be noted that the co-ordinates of the drillings were saved in a digital Excel file. This file was transformed in a data base (Access). Using the software ArcGIS 9.0 and the command Add xy data all the data and all the co-ordinates of the drillings are embodied in the program prepared to be computed.

According to the map the drillings were performed at the northwest and the southeast part of the area where the formations of “granite type Fteroto” and “granite type Dipotama” are developed. This happened because the aim of the exploration, part of which was the execution and the valuation of the drillings which was held by the Institute of Geology and Mineral Exploration (I.G.M.E.), was the discovery of uranium in this area. It was well-known, from previous explorations (regular and methodical stages), that uranium developed in these two geological formations and not in the “Middle type granite” (Pergamalis et al., 1998).

4. Geological Mapping

The methodology of combining all the data utilizing Geographical Information Systems lead to the construction of the following map (Fig. 2). This map depicts all the geological formations that seem to have the greatest mining interest in the area.

This map shows that in the area of Paranesti granite types are developed which can be grouped in three sub-categories: “granite type Fteroto”, “granite type Dipotama”, “granite Middle type”. Additionally, the area is composed of volcanic rocks, sedimentary-volcanic series, metamorphic rocks, limestone and limestone debris. The following table (Table 2) includes all the geological formations that the area consists of as well as the total area that each one of these formations occupies (in m²).

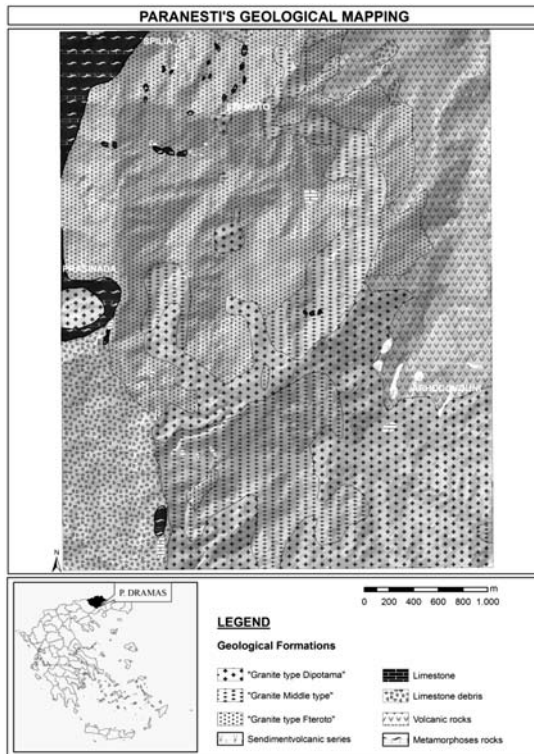


Fig. 2: The representation of all the geological formations which appear in the area of Paranesti.

Geological Formations	Area (m ²)
“Granite type Fteroto”	5.150.951,901
“Granite type Dipotama”	3.300.367,627
“Granite Middle type”	2.571.148,089
Volcanic rocks	2.387.990,000
Limestone debris	1.401.598,009
Metamorphoses rocks	492.907,886
Limestone	39.537,081

Table 2. The geological formations of the Paranesti region and the area occupied by each one of them.

The Comparative observation of Fig. 2 and Table 1 shows that the largest area of Paranesti, which is 5.150.951,901 m², is occupied by the formation called “granite type Fteroto” while the total area of “granite type Dipotama” and “granite Middle type” is 3.300.367,627 m² and 2.571.148,089 m² respectively. Additionally, 2,387.990,000 m² of the study area consists of volcanic rocks while the limestone debris and the metamorphoses rocks cover an area of 1.401.598,009 m², and 492.907,886 m² respectively. Finally a small part of the area of Paranesti is composed of limestone formations and the sedimentary-volcanic series with areas of 39.537,081 m² and 30.242,099 m² respectively. It has to be mentioned that this granite types rocks (the “granite type Fteroto”, the “granite type Dipotama” and the “Middle type”), which cover the wider area of Paranesti, are characterized as acid rocks. This is the main reason that leads the geologists to perform exploration activities for examining the opportunity of the existence of economical deposit of uranium.

5. Conclusions

The geology as long as the deposit of the area is estimated through special computational procedures using mainly the DEM of the area geometry. A series of drillings were developed in the area of Paranesti in order to study the geological and deposit characteristic of the area. A geological map of the study area was constructed through IGME geological previous maps and extensive detailed field-work mapping utilizing ArcGIS 9.0 software. The “granite type Fteroto” covers the largest part of the Paranesti area, then follow the “granite type Dipotama” and the “granite Middle type”. All these formations are of great economically importance for the deposit of uranium.

The methodology followed in this study is based on GIS technology. The use of GIS in all sectors of geo-sciences, gives solutions in problems that are related with the geological environment. Data procedure in the analytical context of GIS can produced useful variables and estimations. A fundamental element of a GIS is data integration which includes a common geographical reference system, common spatial and temporal coverage, and similar scale and quality of the data.

At the sector of digital cartography the interest focuses on the creation of a spatial database from where user can produce a geological map. Similarly at the sector of mineralogy the aim is to create a geodatabase where details for mineral outcrops can be stored. In this way, researches for mineral exploitations of oil and gas can be supported. Finally, at the sector of seismology GIS offer the possibility of, observing and earthquakes and researching the relation between earthquake events and fault zones. All these applications are owed in the particularities that GIS present. The most basic advantage of the GIS philosophy is the usefulness of the spatial data where the significance of spatial is incorporated with the attributes of data. Using spatial data is given the possibility for further analysis to qualitative data as long as quantitative.

GIS is not only a mean of producing maps but also a new completed technology essential for the analysis and the study of space and the decision-making concerning the terrain, the environment and the human.

6. References

- Chalkias C. 2003. *Geographical Information Systems II* (lecture notes), Harokopio University of Athens-Department of Geography.
- Chalkias C. 2006. *Terms and Meanings of Geographical Information*, Harokopio University of Athens-Department of Geography.
- Din A. 1993. *Interdisciplinary Research directions of GIS*, Mapping Awareness & GIS in Europe, vol 7, no 2, pp. 11-14.
- Haines Young, R. 1990. *GIS for Environmental Management*, Mapping Awareness, vol 4, no 9, pp 51-54.
- Longley 2001. *Geographic Information Systems and Science*, Wiley, England.
- Papageorgiou E., Vasilopoulou S., Lagios E., 2010. *Implementation of GIS in Santorini volcano for ground deformation analysis*. 8th Pan-hellenic Geographical Conference. Athens Greece, vol 1, pp 166-174.
- Pergamalis, Ph., Papachristopoulos, S., Karageorgiou, E., D. and Koukoulis, A., 1998. *Geological features of uranium and Rare Earths ores of Paranesti Drama areas*, Bulletin of Geological Society of Greece, vol. XXXII No3 pp.145-155.
- Siggros Y. 2002, *Transforming coordinates of the Greek spatial data*, Athens, Greece (http://users.auth.gr/kvek/coords_gr.zip).
- Sinha P., Nath M., De S., Misra R. 2002. *Mineral potential map by a knowledge driven GIS modelling: An example from Singhbhum copper belt, Jharkhand India* (<http://www.gisdevelopment.net/application/geology/mineral/geom0007.htm>).
- Zervakou A. 2004. *Educational material for applying GIS in geology. Theory and Practice. The case study of Kifissia*. NTUA, Greece.

MORPHOTECTONIC ANALYSIS OF THE NEOTECTONIC AND ACTIVE FAULTS OF BEOTIA (CENTRAL GREECE), USING G.I.S. TECHNIQUES

Sboras S.¹, Ganas A.², Pavlides S.¹

¹ Aristotle University of Thessaloniki, Department of Geology, 54124 Thessaloniki, Greece, pavlides@geo.auth.gr

² Institute of Geodynamics, National Observatory of Athens, aganas@gein.noa.gr

Abstract

We study the neotectonic regime and evolution of the central-eastern part of the Asopos River basin (Beotia, Central Greece) which is an area undergoing crustal extension. The main tools that were used in this research were a) field mapping of neotectonic and active normal faults and b) morphotectonic analysis of 59 catchments, which was carried out by GIS techniques. Our results include a) series of maps displaying the spatial variation of morphotectonic indices (sinuosity, asymmetry factor, valley-floor-to-height-ratio etc) and b) map of neotectonic fault segments with associated fault-slip data. The morphotectonic analysis indicates that if normal faults in this area are active, they are capable of generating earthquakes with $M > 6.0$.

Key words: *Morphotectonics, active faults, GIS, Asopos, Beotia, Greece.*

1. Geological setting

The study area lies between the Gulfs of Corinth and Evia, two major rift structures oriented WNW-ESE and NW-SE, respectively. The land between the two gulfs is an area of low strain where river Asopos flows along a longitudinal basin (striking E-W; Asopos basin) controlled by active faults. The southern margin of the basin forms the northern side of the Parnitha and Kitheronas mountains. The pre-rift rocks of the region belong to the Sub-Pelagonian zone of the Hellenides, the western slope of the Cimmerian microcontinent (Smith et al., 1979; Robertson et al., 1991). Geodetic, geological and seismological data suggest that the present tectonic regime of Central Greece is extensional in a N-S to NE-SW direction as a complex result related both to back-arc extension behind the Hellenic subduction zone and the transtensional tectonic regime that originates from the dextral strike-slip motion of the North Anatolian Fault and its extension to the North Aegean Trough (McKenzie, 1972; 1978; Le Pichon and Angelier, 1979; Jackson and McKenzie, 1988; Hatzfeld, 1993; Papazachos and Kiratzi, 1996; Kahle et al., 1998; Clarke et al., 1998; El-Fiky, 2000; Doutsos and Kokkalas, 2001; Jolivet, 2001; Papazachos 2002; Armijo et al., 2003; Hubert-Ferrari et al., 2003; Kreemer and Chamot-Rooke, 2004; Kreemer et al. 2004; Ganas et al., 2005; Kokkalas et al., 2006; Hollenstein et al., 2008; Jolivet and Brun, 2008).

The two prominent basins of the study area are the Thiva and Asopos basins. The first is restrained and partially drained by Yliki and Paralimni Lakes (Papanikolaou et al., 1988) and was not considered suitable for morphotectonic analysis. The Asopos basin, took its name from the homonymous

river, flows from the western part of Attiki Peninsula near Gulf of Corinth to the Gulf of Evia, running almost straight for a distance of about 50 km (Sboras et al., 2006). The basin started to form during Miocene according to Papanikolaou et al. (1988) and Mettos et al., (2000). Tectonic activity affects drainage patterns, causing several changes in the flow direction of Asopos River. According to a study of borehole data by Dounas et al. (1978), during Neogene times and near to the village Aghios Thomas the river was flowing 500-800 m southern from its present position. The evolution model of Asopos Basin, suggested by Papanikolaou et al. (1988), refers to a change in the tectonic regime during Quaternary causing uplift, erosion of the Miocene sediments and maintenance of terrestrial basin remnants. The topography of the northern side of Parnitha is characterized by high peaks with steep slopes, deep valleys and isolated highlands, while the low-lying sub-basin of Schimatari (mean elevation 100-200 m) is the main receiver of the eroded material from the surrounding mountains.

Two major lithological units occur in the study area. The first is pre-rift rocks comprising Mesozoic alpine carbonates (limestones and dolomites), and the second consists of post-alpine sedimentary formations divided into two sub-units: the Neogene sediments, that comprise from bottom to top lacustrine-lagoon formations and terrestrial-fluvial formations, respectively, and the Quaternary sediments consisting of alluvial, debris and colluvium (Dounas et al. 1978).

The first attempt for morphotectonic investigation was made by Papanikolaou et al. (1988). They analyzed the drainage network and the slope morphology of Asopos Basin concluding that the area is under active tectonic control with rotating blocks. Mariolakos et al. (1997; 2001) studied the neotectonic structures of Avlonas region and the broader Western Parnitha, suggesting a complex tectonic setting with a diverging tilting from the western and eastern part of Koukistras Stream. An active fault investigation was conducted by Goldsworthy et al. (2002) further more to the north, towards Thiva Basin. These authors describe a fault system in the local area of Kallithea village consisting of south dipping normal faults that bound the southern sides of low, parallel, limestone ridges. Exposed fault surfaces strike between N080°E and N115°E with striations indicating slip vector azimuths between 180–200°. Tsodoulos et al. (2008) performed a morphotectonic analysis in the Erythres-Dafni Fault zone which consists of two left-stepping overlapped segments. They used many geomorphic parameters which all conclude in fault's high activity. The region to the west of the Asopos basin was mapped by Ganas et al. (2007), who also report evidence of active faulting.

The broader region has suffered from several catastrophic earthquakes many of which are known from historical references. According to the earthquake catalogue of Papazachos and Papazachou (1997), the vicinity of Thiva was struck four times since 14th century: in 1321 ($M = 6.3$), in 1853 ($M = 6.8$), in 1893 ($M = 6.2$) and in 1914 ($M = 6.0$). Ambraseys and Jackson (1990) also give information about the 1893 and 1914 events. For the latter they suggest an E-W striking fault located between Kallithea and Asopia villages. For the broader area of Beotia - Attica, the known earthquakes are in 1938, Oropos ($M = 6.0$), in 1981, Alkyonides ($M = 6.7$) and in 1999, Athens ($M = 5.9$) (Ambraseys and Jackson, 1990; Ganas et al., 2004; Jackson et al., 1982; Papazachos and Papazachou, 1997). The first two events occurred inside the highly active grabens of Evia and Corinth Gulfs respectively, while the last one was an "unexpected" event occurred near the city's limits.

2. Methods

2.1 General

The neotectonic field mapping in the Tanagra-Avlona-Asopos region (scale 1:50000) indicates the existence of nine (9) major WNW-trending normal faults (Tanagra, Asopia-Asopos, Megalos Schi-

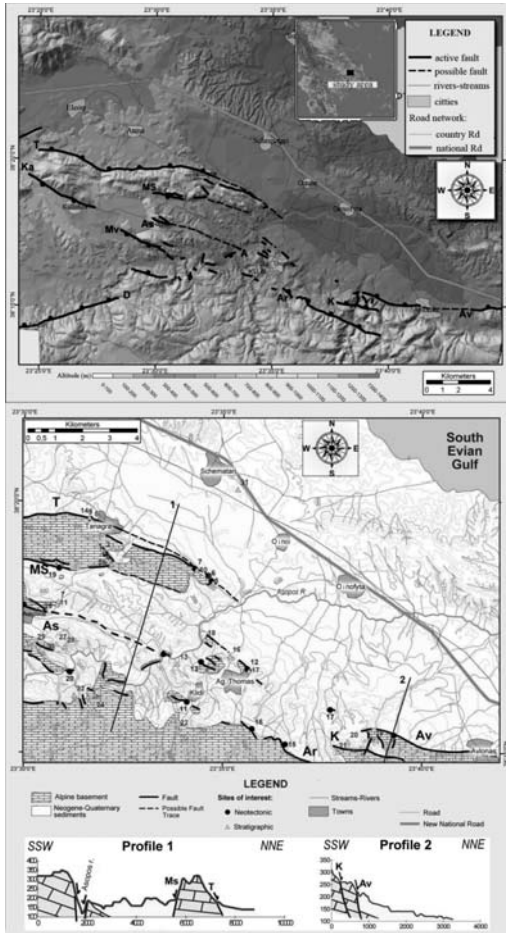


Fig. 1: Top: Neotectonic map of the study area, based on field mapping. T: Tanagra fault, Ka: Kallithea fault, Ar: Armakas fault, K: Koryfoula fault, Av: Avlonas fault, Mv: Mavrovouni fault, As and A: Asopia and Asopos fault, MS: Megalos Schinos fault and D: Dafne fault. Bottom: A more detailed geological map showing the investigated faults accompanied with two cross sections (numbered black lines). Lithological formations are simplified.

nos, Armakas, Koryfoula, Dafne, Avlona, Kallithea and Mavrovouni) with lengths more than 3 km. Many smaller fault segments are also present mainly striking WNW-ESE to NW-SE. The dominant dip direction is toward NNE. However, there are many antithetic faults that can also be observed, occupying the foothills of elongated limestone ridges. This pattern results in the formation of small parallel grabens and horsts. There are also a few conjugate normal faults striking (ENE-WSW) SW-NE, the largest of which is the Dafne fault (Figure 1).

Morphotectonic analysis is a powerful tool to help us detect and understand the processes that occur on the earth's surface. Tectonic movements and erosion leave their marks each in a different way and quantification of the morphological features is the key to associate the landscape with the neotectonic evolution of the region. Since morphotectonic analysis is a good indicator but not a stand-alone proof, it was performed after a morphotectonic-geological mapping. In order to achieve the most accurate results and their most distinctive presentation on different thematic maps, we used ArcGIS 8.1 software. The analysis was undertaken on a mosaic of four topographic maps in 1:50000 scale (HMGS). The maps were digitized, projected to the Greek National projection system (EGSA87) and a three-dimensional terrain model (DEM) was produced with a resolution of less than 20 m. We also used a SPOT 1 satellite image with 10-m resolution (Figure 3a) and 1:15000 scale aerial photo-

Table 1. Mathematical relationships for the morphotectonic indices that was applied in this paper (Keller and Pinter, 2002).

<i>Index</i>	<i>Relationship</i>
AF	$AF = (A_r / A_t) 100$
TTSF	$TTSF = D_a / D_d$
Hypsometric Integral (HI)	$HI = (H - H_{min}) / (H_{max} - H_{min})$
V_f	$V_f = 2 V_{fw} / (h_1 - h_3) + (h_2 - h_3)$
S_{mf}	$S_{mf} = L_{mf} / L_s$

Ar: area of the basin to the right of the trunk stream, At: total area of the drainage basin, Da: distance from mid-line of the drainage basin to the midline of the river, Dd: distance from the basin midline to the basin di-vide, H: mean elevation, H_{min} : minimum elevation, H_{max} : maximum elevation, V_{fw} : valley floor width, h_1, h_2 : elevations of left and right valley divides, h_3 : elevation of the valley floor, L_{mf} : length of the mountain front along the foot of the mountain, L_s : straight-line length of the mountain front.

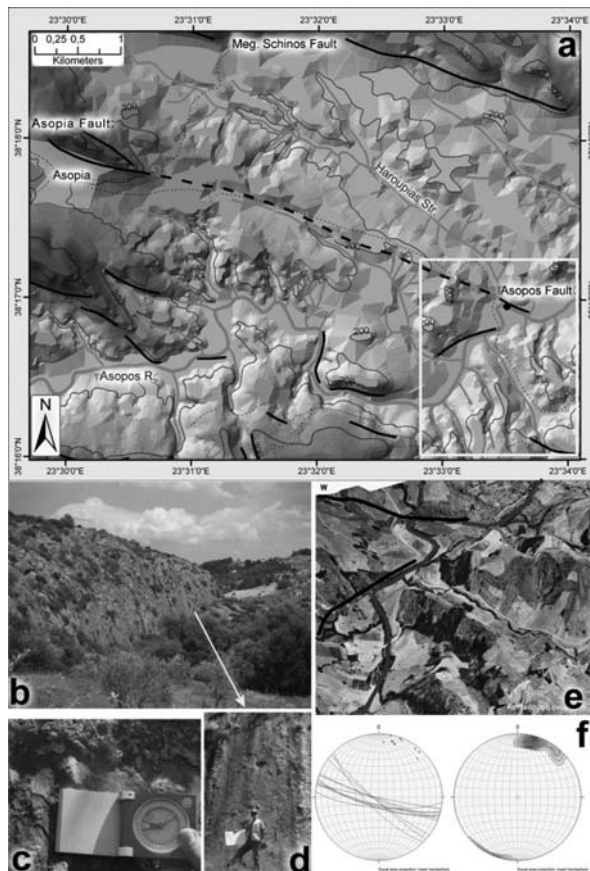


Fig. 2: a) DEM detail in the area of Asopia where the Asopia-Asopos Fault dominates. Contour lines every 100 m. Thin lines are the drainage and the thick line is Asopos River. Black lines are faults. The white outlined box refers to following images (b)-(f). b) The scarp of Asopos Fault lying on Mesozoic limestones. c) Evidences of slickensides indicating the normal character of the fault. d) Corrugations on the fault's free face. e) Detail of how Asopos Fault (A) affects the homonymous river with the use of DEM and aerial photograph (3x vertical exaggeration). The river, flowing northwards, is initially affected by a minor fault and then curves into an S shape in order to flow parallel to the scarp. At the end of the scarp, the river changes again its flow to its initial direction. f) Mesostructural analysis of the Asopos Fault portrayed on lower hemisphere equal-area projections. Left diagram shows plot of fault planes, right diagram shows contours of poles to fault planes. Data indicate a dominant SSW dip direction.

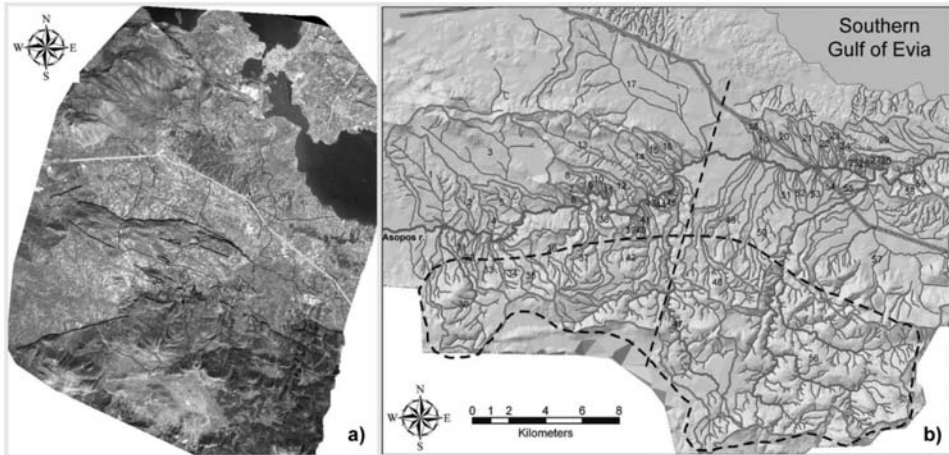


Fig. 3: a) DEM combined with a 10 m-resolution satellite image (SPOT 1). The major active tectonic structures are shown in black lines while the whitish line represents the National Road. b) DEM of the study area showing the drainage and the catchment deviation numbered. The National Road is also shown (thick grey line). The dashed outlined area and the dashed line are explained in the text.

graphs (HMGS) to locate precisely the fault segment boundaries (Figure 2e). The analysis comprised the calculation of morphotectonic indicators (asymmetry factor, transverse topographic symmetry, hypsometric curve, hypsometric integral, ratio of valley - floor width to valley height, mountain-front sinuosity – Table 1 shows the mathematical relationships) for 59 sub-basins in the central-eastern part of the Asopos basin, including also the cumulative one.

Some qualitative observations indicate a differentiation on the drainage network pattern and the shape and size of the catchments. The catchments south of Asopos River contain a denser, well-developed dendritic drainage network in contrast with the northern ones (curved dashed outlined area in Figure 3b) while their shape is larger and more complicated especially in the south-eastern part of the study area. In more detail, the main river seems to flow in the middle of the basin at the western part of the study area while it suddenly seems to flow nearer to the northern margin at the eastern part (left and right from the straight dashed line in Figure 3b, respectively). Some other local anomalies can be observed in the development pattern of some sub-basins, especially in the southern part of Asopos River. However, a more quantitative approach derives by calculating the following morphotectonic parameters.

2.2 Data analysis

The description of the analysed morphotectonic parameters and accompanied with short conclusions, follow below.

2.2.1 Slope and Mean Slope

An actual slope dipping distribution and a mean slope map of the sub-basins were produced in order to monitor abrupt morphological changes and to relatively compare each sub-basin. Results show that the catchments belonging to the southern part of Asopos Basin show greater values thus having a steeper relief. Here it should be noticed that high values in the actual or mean slope map are not seen

only in the areas where the erosion-resistant Mesozoic limestones appear (mostly in the southern part of the study area). Concerning the actual slope map, values higher than 9° and up to 15° can be observed in a large part of the region where mostly post-alpine sediments occur. As we move upwards the northern side of Parnitha Mountain a range between 15° to 30° is observed. Values higher than 30° appear only inside the narrow valleys and streams that lead to Asopos River, as well as in a part of the latter where Mavrovouni and Asopia-Asopos Faults control the local relief. The linear distribution of high values where active faults have been recognized and mapped can be also observed. The mean slope map shows that basins in the southern part of Asopos Basin have higher values suggesting a steeper morphology. Although high actual slope angles can be seen near mountains like Tefmissos and Kiryktion, the surrounding basins 3 and 13 show low mean slope angles. That can be interpreted as a subdued relief but with prominent scarps which in this case are the Kallithea and Megalos Schinos Faults.

2.2.2 Asymmetry Factor (AF)

This morphotectonic indicator, described by Keller and Pinter (2002), is helpful to understand if and how drainage has been developed under tectonic control in a quantitative manner. It is essential to insure that lithology (like dipping sedimentary formations) is taken out of the calculations in order to isolate only the tectonic effects. Since the study area is not very large, we consider a uniform microclimate. The value range corresponds from 0 to 100%. If the basin is not tilted then the AF is 50%. Values under and over 50% represent rightward and leftward tilting (according to the main river's flow), respectively. Sub-basin 3 shows high values of rightward tilting due to the existence of the NNE dipping Tanagra Fault north of the basin. The basin is situated on the footwall of the fault which causes a southern block rotation along a WNW-ESE trending axis. Sub-basin 14 shows an opposite rotation produced by the antithetic fault of the Tanagra Fault located at the southern foothills of Kiryquio Mt. Sub-basin 48 has a low AF (29.71%) due to the existence of Armakas Fault. The total basin of the study area has an AF of 65.1% which represents a northward rotation along an E-W trending axis, parallel to the Asopos River (Fig. 4). This means that the whole area is affected by the WNW-ESE striking faults.

2.2.3 Transverse Topographic Symmetry Factor (TTSF)

This is another quantitative index to evaluate basin asymmetry (Keller and Pinter, 2002; Figure 4). Absence of tectonics would cause the main river to flow evenly from both sides forming a perfectly symmetric basin with a TTSF value of 0. The TTSF value can be more than 0.0 and up to 1.0, depending on tectonic intensity, since lithological reasons are isolated. Values near to 1.0 indicate that the river flows closely to the margins of the basin, a result probably produced by intensive and recent tectonic activity. For the same reasons like in the Asymmetry Factor, sub-basin 3 has a high value of TTSF. High values in some of the basins from the southern side of Asopos River cannot be explained tectonically since the orientation of the local faults (Armakas, Koryfoula and Avlonas) is transverse to the longest axis of the sub-basins. On the other hand there is a lithological alteration in this area, having the water-resistant limestones in contrast with the post-alpine sediments probably affecting the drainage network. Concerning the broader Asopos basin, the TTSF could not be applied once since Asopos River flows in the middle of the basin during the first half distance of its flow, and near the northern margin during the second one. According to the division in the map of Figure 3 (dashed line), in the western part of the basin TTSF is approximately 0.1, while in the eastern part the value goes up to ca. 0.7. The distance between the two measurements are almost 10 km. This abrupt change can only be explained by tectonic activity.

2.2.4 Hypsometric Curve-Hypsometric Integral (HI)

Hypsometric Curve describes the distribution of elevations across an area of land and its Hypsometric Integral, which is defined as the area under the hypsometric curve, is the quantification of the curve's shape (Strahler, 1952; Pike and Wilson, 1971; Keller and Pinter, 2002). High values indicate a high topography relative to the mean, such as smooth upland surface cut by deeply incised streams, while low and intermediate values are associated with more evenly dissected drainage basins (Strahler, 1952; Keller and Pinter, 2002). A useful attribute of the latter is that it is independent of the basin size and relief. Sub-basins 1, 3, 17, 49, 50, 56 and 57 show low values of Hypsometric Integral indicating that these basins are in young stage (Figure 4). All these sub-basins are affected by many faults suggesting a possible uplift. The same happens to the Hypsometric Integral value of the broader basin ($H = 0.234$) suggesting a tectonic uplift of the whole study area.

2.2.5 Ratio of Valley – Floor Width to Valley Height (V_f)

This morphological indicator is useful to quantitatively differentiate the shape along a transverse section of a valley. High values of V_f indicate broad-floored U-shaped canyons, while low values indicate deep V-shaped valleys with streams that are actively incising (Keller and Pinter, 2002). The latter case can be related with uplifting. This parameter could not be applied in many sub-basins because the size was too small for the DEM's resolution. However, it is significant that almost all sub-basins located to the southern side of Asopos River have low ratio values (Figure 4). This can be interpreted as a tectonic uplift since these basins are situated on the footwall of the faults.

2.2.6 Mountain-front Sinuosity (S_{mf})

The Mountain-front Sinuosity index is a useful morphotectonic tool especially in our study area where mountains and hills mainly consist of limestones. It reflects the balance between erosional and tectonic forces (Keller and Pinter, 2002). According to Pavlides (2003), a range between 1.0 and 1.6 is considered to be a tectonically highly active mountain front, 1.6 up to 3.0 less active and 3.0 and above inactive. It is important to notice that the value is affected by the map scale. In the case of our mapped faults (Fig. 5), wherever it was possible for the method to be applied, the calculated values are less than 1.6. The lowest values in ascending order belong to Asopia, Mavrovouni, Megalos Schinos and Kallithea Faults, while the highest values belong to Tanagra and Avlonas Faults.

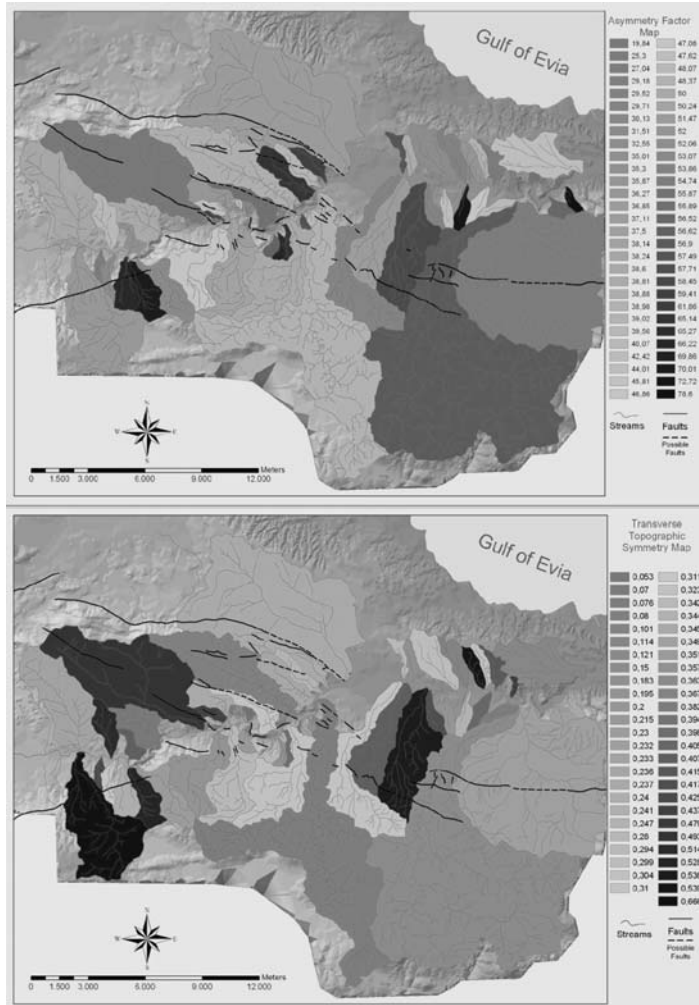
2.3 Evaluation of seismic potential

According to the length of the mapped faults, we used the empirical relationships of Wells and Coppersmith (1994), Ambraseys and Jackson (1998) and Pavlides and Caputo (2004) in order to estimate the seismic potential magnitude for each fault. At this stage we do not differentiate among the faults, i.e. active vs. inactive. It is clear that the Asopos Fault is active (Figure 2) because it controls drainage and shows linear, relatively uneroded scarps along its strike. However, other faults like the Tanagra fault seem less likely to be active because no such scarps were found during field work. No good quality seismological data (from local networks) exist, in order to show microseismic activity in south Beotia. Therefore, the estimates shown in Table 2 should be used with caution and with considerable uncertainty as more field work is necessary. In Table 2, the seismic potential magnitude is shown, according to the above mentioned empirical relationships (W & C, A & J, P & C respectively). Abbreviation of fault names like in Figure 1.

Table 2.

Fault	Length (km)	W & C	A & J	P & C
T	16.5	6.5 (± 0.6)	6.5	6.6 (± 0.5)
MS	6.5	5.9 (± 0.5)	6.1	6.2 (± 0.7)
As & A	5.0	5.8 (± 0.5)	5.9	6.1 (± 0.3)
Ar	7.0	6.0 (± 0.6)	6.1	6.2 (± 0.3)
Ka & Mv	10.8	6.2 (± 0.6)	6.3	6.4 (± 0.4)

The Asopia-Asopos Faults were considered segments of the same fault zone, thus we estimated the worst scenario for total activation. The same was considered for Kallithea-Mavrovouni Faults. Taking into account the results from Pavlides and Caputo (2004) relationship, each of the faults of table 2 is capable of earthquake magnitude > 6.0 . The Avlon fault (further East; Ganas et al., 2004) is not calculated since it was not studied in all of its length



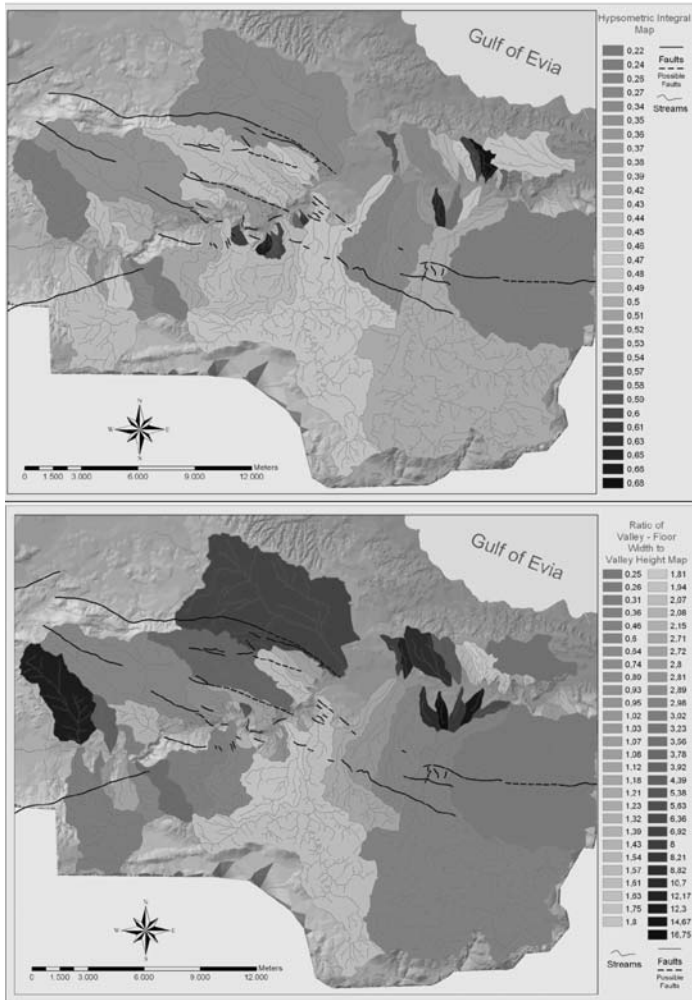


Fig. 4: Thematic maps produced after morphotectonic analyses in ARC GIS. The results of Asymmetry Factor, Transverse Topographic Symmetry Factor, Hypsometric Integral and Ratio of Valley-Floor Width to Valley Height are shown in order of appearance. Further explanation is found in the text.

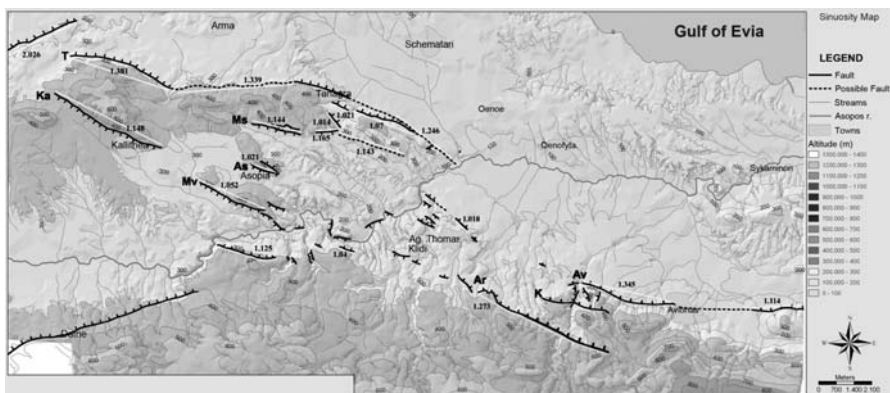


Fig. 5: Mountain Front Sinuosity map of the investigated area.

3. Conclusions

We applied detailed morphotectonic analysis in the region of the Asopos rift in central – south Beotia region, central Greece (Figures 3, 4 and 5). According to morphotectonic criteria, most mapped faults in the study area are considered as highly active, with the exception of Tanagra and Megalos Schinos faults (Figure 1), which display no clear geological and less geomorphological evidences of recent activity. Thus we characterized them as possible active in the sense that they can be triggered/activated as secondary structures. For the rest of the faults, on one hand our morphotectonic analysis and geological data suggest that they show evidence of recent and highly active tectonic movements, but on the other hand they have sparse seismic activity with long periods of quiescence as it derives from both historic and instrumental data. Evidence of high fault activity show the Avlona-Koryfoula-Armakas, Kallithea-Mavrovouni and Asopia-Asopos fault segments. Concerning the latter ones, Asopia fault segment although it seems morphologically less expressed than the Asopos Fault segment (southeastern extension; Figure 2) we suggest that they comprise two branches of the same fault.

4. References

- Ambraseys, N.N. and Jackson, J.A., 1990. Seismicity and associated strain of central Greece between 1890 and 1988. *Geoph. J. Int.*, 101, 663-708.
- Ambraseys, N. and Jackson, J., 1998. Faulting associated with historical and recent earthquakes in the Eastern Mediterranean region. *Geophys. J. Int.*, 133, 390-406
- Armijo, R., Flerit, F., King, G., and Meyer, B., 2003. Linear elastic fracture mechanics explains the past and present evolution of the Aegean. *Earth Plan. Sci. Lett.*, 217, 85-95
- Clarke, P.J., Davies, R.R., England, D.C., Parsons, B., Billiris, H., Paradissis, D., Veis, G., Cross, P.A., Denys, P.H., Ashkenazi, V., Bingley, R., Kahle, H.-G., Muller, M.V. and Briole, P., 1998. Crustal strain in central Greece from repeated G.P.S., measurements in the interval 1988–1997. *Geoph. J. Int.*, 135, 195-214
- Dounas, A., Kallergis, G., Morfis, A. and Pagounis, M., 1978. Hydrogeological investigation on the Asopos river valley. *IGME Publications*, 21, Athens
- Doutsos, T. and Kokkalas, S., 2001. Stress and deformation patterns in the Aegean region. *Journal of Structural Geology*, 23, 455-472
- El-Fiky, G.S., 2000. Crustal Strains in the Eastern Mediterranean and Middle East as Derived from GPS Observations. *Bull. Earthq. Res. Inst. Univ. Tokyo*, 75, 105-125
- Ganas, A., Pavlides, S.B., Sboras, S., Valkaniotis, S., Papaioannou, S., Alexandris, G.A., Plessa, A., and Papadopoulos, G. A., 2004. Active Fault Geometry and Kinematics in Parnitha Mountain, Attica, Greece. *J. Struct. Geol.*, 26, 2103-2118.
- Ganas, A., Drakatos, G., Pavlides, S.B., Stavrakakis, G.N, Ziazia, M., Sokos, E., and Karastathis, V.K., 2005: The 2001 Mw = 6.4 Skyros earthquake, conjugate strike-slip faulting and spatial variation in stress within the central Aegean Sea. *Journal of Geodynamics*, 39, 61–77.
- Ganas, A., Spina, V., Alexandropoulou, N., Oikonomou, A., and Drakatos, G., 2007. The Corini active fault in south-western Beotia region, central Greece: segmentation, stress analysis and extensional strain patterns. *Bull. Geol. Soc. Greece*, 40, 297-308.
- Goldsworthy, M., Jackson, J. and Haines J., 2002. The continuity of active fault systems in Greece. *Geophys. J. Int.*, 148, 596–618
- Hatzfeld, D., 1993. Geodynamics of the Aegean: A microseismotectonic approach. *Ann. Geofis.*, 36 (2), 215-228

- Hollenstein, C., Müller, M. D., Geiger, A. and Kahle H.-G., 2008: Crustal motion and deformation in Greece from a decade of GPS measurements, 1993–2003. *Tectonophysics*, 449, 17-40
- Hubert-Ferrari, A., King, G., Manighetti, I., Armijo, R., Meyer, B. and Tapponnier, P., 2003. Long-term elasticity in the continental lithosphere; modelling the Aden Ridge propagation and the Anatolian extrusion process. *Geophys. J. Int.*, 153, 111-132
- Jackson, J.A., Gagnepain, J., Houseman, G., King, G.C.P., Papadimitriou, P., Soufleris, C., Virieux, J., 1982. Seismicity, normal faulting, and the geomorphological development of the Gulf of Corinth (Greece): the Corinth earthquakes of February and March 1981. *Earth Plan. Sci. Lett.*, 57, 377-397
- Jackson, J. and McKenzie, D., 1988. Rates of active deformation in the Aegean Sea and surrounding regions. *Basin Research*, 1, 127-128
- Jolivet, L., 2001. A comparison of geodetic and finite strain pattern in the Aegean, geodynamic implications. *Earth Plan. Sci. Lett.*, 187, 95-104
- Jolivet, L. and Brun, J.-P., 2008. Cenozoic geodynamic evolution of the Aegean. *Int. J. Earth Sci.*, (Published online), doi: 10.1007/s00531-008-0366-4
- Kahle, H., Straub, C., Reilinger, R., McClusky, S., King, R., Hurst, K., Veis, G., Kastens, K. and Cross, P., 1998. The strain rate field in the eastern Mediterranean region, estimated by repeated GPS measurements. *Tectonophysics*, 294, 237–252
- Keller, A. and Pinter, N., 2002: Active Tectonics: Earthquakes, Uplift and Landscape. *Prentice Hall*, N. Jersey, Second Edition, pp 377
- Kokkalas, S., Xypolias, P., Koukouvelas, I., and Doutsos, T., 2006, Postcollisional contractional and extensional deformation in the Aegean region. In Dilek, Y., and Pavlides, S. (eds), Postcollisional tectonics and magmatism in the Mediterranean region and Asia: *Geol. Soc. Am. Special Paper*, 409, 97-123
- Kreemer, C. and Chamot-Rooke, N., 2004. Contemporary kinematics of the southern Aegean and the Mediterranean Ridge. *Geophys. J. Int.*, 157, 1377-1392
- Kreemer, C., Chamot-Rooke, N. and Le Pichon, X., 2004. Constraints on the evolution and vertical coherency of deformation in the Northern Aegean from a comparison of geodetic, geologic and seismologic data. *Earth Plan. Sci. Lett.*, 225, 329-346
- Le Pichon, X., and Angelier, J., 1979. The Hellenic Arc and trench system: a key to the neotectonic evolution of the Eastern Mediterranean area. *Tectonophysics*, 60, 1-42.
- McKenzie, D.P., 1972. Active tectonics of the Mediterranean region. *Geoph. J. R. Astr. Soc.*, 30, 2, 109-185
- McKenzie, D.P., 1978. Active tectonics of the Alpine–Himalayan belt: the Aegean Sea and surrounding regions. *Geoph. J. R. Astr. Soc.*, 55, 217–254.
- Mariolakos, I., Fountoulis, I. and Logos, E., 1997: The crucial role of the neotectonic deformation at the landfill site selection. The case study of Avlona (Attiki, Greece). *Proc. Int. I.A.E.G.*, 2, *Balkema, Rotterdam*, 2007-2010
- Mariolakos, I., Fountoulis, I., Sideris, C. and Hatoupis, T., 2001. The morphotectonic structure of Parnis Mt. (Attica, Greece). *Bull. Geol. Soc. Greece*, 34, 1, 183-190
- Mettos, A., Ioakim, C. and Rondoyanni, T., 2000: Palaeoclimatic and palaeogeographic evolution of Attica-Beotia (Central Greece). *Geol. Soc. Greece*, Special Publications, 9, 187-196.
- Papanikolaou, D.J., Mariolakos, I.D., Lekkas E.L. and Lozios, S.G., 1988. Morphotectonic observations on the Asopos Basin and the Coastal zone of Oropos. Contribution to the Neotektonics of Northern Attica. *Bull. Geol. Soc. Greece*, 20, 1, 251-267
- Papazachos, C.B., 2002. The active crustal deformation field of the Aegean area inferred from seismic-

ity and GPS data. *WEGENER 2002, Eleventh general Assembly of the Wegener Project, Athens, Greece, 12-14 June 2002*

- Papazachos, C.B. and Kiratzi, A.A., 1996. A detailed study of the active crustal deformation in the Aegean and surrounding area. *Tectonophysics*, 253, 129-153
- Papazachos, B. and Papazachou, C., 1997. The Earthquakes of Greece. Thessaloniki, *editions Ziti*, 304
- Pavlidis, S., 2003. The Geology of Earthquakes (in Greek). Thessaloniki, *University Studio Press*, 378
- Pavlidis, S and Caputo, R., 2004. Magnitude versus faults' surface parameters: quantitative relationships from the Aegean Region. *Tectonophysics*, 380, 159-188
- Pike, R.J. and Wilson, S.E., 1971. Elevation-relief ratio, hypsometric integral and geomorphic area-altitude analysis. *Bull. Geol. Soc. Am.*, 82, 1079-1083
- Robertson, A.H.F., Clift, P.D., Degnan, P., Jones, G., 1991. Palaeogeographic and palaeotectonic evolution of the Eastern Mediterranean Neotethys. *Palaeogeography, Palaeoclimatology, Palaeoecology*, 87, 289-344
- Sboras, S., Ganas, A., Pavlidis, S., 2006. Tectonic Geomorphology and active tectonics of the Asopos Rift valley, central Greece. 11th International Symposium on Natural and Human Induced Hazards & 2nd Workshop on Earthquake Prediction Abstract Volume, June 22-25, 2006, Patras, Greece, page 95.
- Smith, A.G., Woodcock, N.H., and Naylor, M.A., 1979. The structural evolution of a Mesozoic continental margin, Othris Mountain, Greece. *Jour. Geol. Soc. London*, 136, 589-603.
- Strahler, A.N., 1952: Hypsometric (area-altitude) analysis of erosional topography. *Bull. Geol. Soc. Am.*, 63, 1117-1142
- Tsodoulos, I.M., Koukouvelas, I.K. and Pavlidis, S., 2008. Tectonic geomorphology of the easternmost extension of the Gulf of Corinth (Beotia, Central Greece). *Tectonophysics*, 453, 211-232
- Wells, D.L. and Coppersmith, J.K., 1994. New empirical relationships among magnitude, rupture length, rupture width, rupture area, and surface displacement. *Bull. Seismol. Soc. Am.*, 84, 974-1002

DIGITAL ENGINEERING GEOLOGICAL MAP OF THE ATHENS PREFECTURE AREA AND RELATED DATABASE MANAGEMENT SYSTEM

**Kynigalaki M.¹, Nikolaou N.¹, Karfakis J.¹, Koutsouveli An.¹, Poyiadji El.¹,
Pyrgiotis L.¹, Konstantopoulou G.¹, Bellas M.¹, Apostolidis Em.¹, Loupasakis
K.¹, Spanou N.¹, Sabatakakis N.² and Koukis G.²**

¹ IGME / Engineering Geology Dpt., Entrance C, 1 Sp. Louis St, Olympic Village, 136 77 Acharnae, Athens, Greece nikolaou@igme.gr

² University of Patras, Department of Geology, Laboratory of Engineering Geology, 26500 Patras, Greece, g.koukis@upatras.gr

Abstract

A digital engineering-geological map of the Athens Prefecture area was compiled at an original scale of 1:10.000 by IGME in cooperation with Engineering Geology Laboratory of Patras University. The map is related to a database management system constructed according to the project's special needs, including geotechnical and geological data mainly obtained by boreholes and trial pits. The main map (11 sheets) is accompanied by three thematic maps at an original scale 1:50.000 (hydrogeological, tectonic) and 1:250.000 (seismic epicenters map). It constitute a basic tool for every activity of the Prefecture's services, in relation to urban development, civil and environmental protection policy, sustainable management of natural resources, continual data supply to citizens and to the technical world.

The main advantage of the digital map is the ability of constant updating of the related database, while this procedure should be established to serve social needs. As the mapping was based on a combination of conventional geological mapping techniques and the information from geotechnical database, it is considered to provide useful information for planners and decision makers at a preliminary planning level.

Key words: *engineering geological mapping, data base, urban development, Athens Prefecture.*

1. Introduction

The urban planning of the city of Athens was primarily based on economic and social determinants, without taking seriously into account the geological environment and the geodynamic factor. The problems that have been arisen due to this became more acute with the increase of the population and urban settlement expansion, the industrialization and the natural hazard impact (seismicity, floods) during the last decades. With the increasing demand for large engineering works construction (subways, freeways, metro, traffic links), the redevelopment of the broader area and the reconstruction of the inner city area, there was a need for up to date geological information and interpretation for planning purposes.

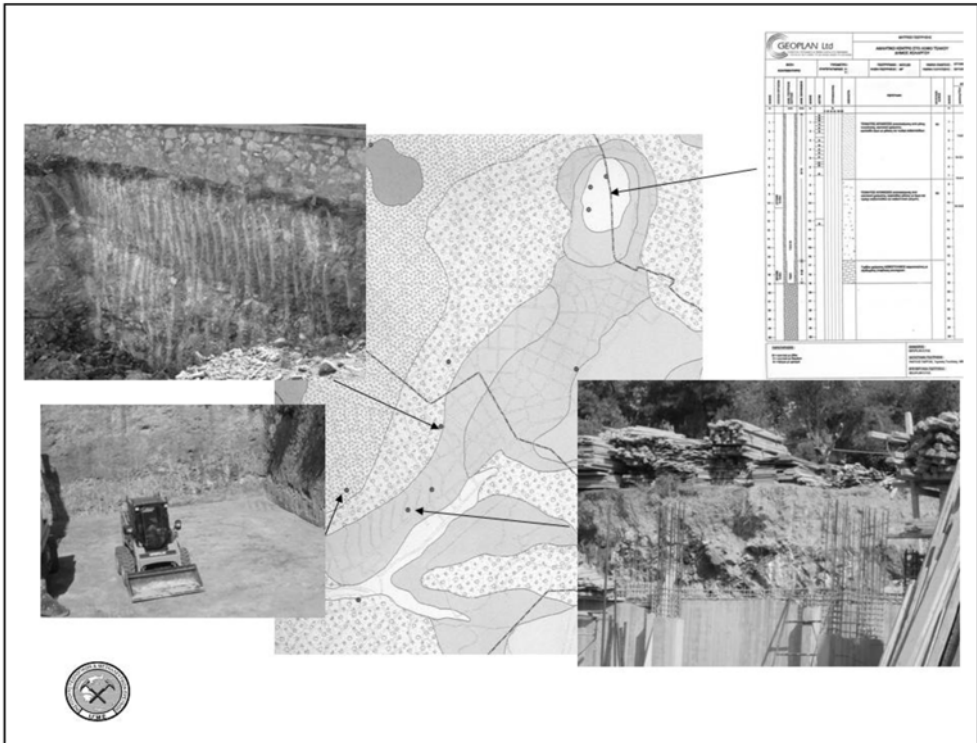


Fig.1: Part of a map sheet, accompanied by the relative information (excavation photos and borehole logs), introduced into the data base.

The geological, hydrogeological and geotechnical conditions prevailing the urban area must be generally well known for providing the necessary information to the local authorities, engineers and constructors, since they consist the framework for technical works planning. This information also constitutes the basic concept for the evaluation of the dynamic ground response in the case of seismic activity.

The IGME in cooperation with the University of Patras (Department of Geology - Laboratory of Engineering Geology), were commissioned to undertake the compilation of the digital engineering geological map of Athens Prefecture area at a scale of 1:10.000. The outcome (Fig. 1) was eleven (11) map sheets that cover the studied area (45 Municipalities and 3 Communities), accompanied by an extended legend and three (3) attached thematic digital maps, at various scales, as well as the relative data base. The work was coordinated by the Engineering Geology Department of IGME, while other Departments of IGME also collaborated for the creation of thematic maps, such as that of Geology and Geological Mapping Dept, as well as the Department of Hydrogeology.

2. Aims of the Project - The digital engineering geological map

In order to give a detailed description of engineering geological environment of the studied area, the working group placed the following objectives:

1. Digital management of the available geological and engineering geological information in the region of interest.

2. Relocation of the gathered information in a map of 1:10.000 scale with respect to the suitable accuracy.
3. Collection and handling of data, so that to obtain as possible homogeneity, density and reliability in geological – engineering geological information, all over the mapped area.
4. Reconsideration of configured information and update, according to the additional geological – engineering geological data obtained by the groups and companies involved in the area’s recent constructional activity.
5. Digital recording of a satisfactory number of borehole data in the created database obtained by public organizations and private consultants.

The engineering geological map compilation and the database creation, in combination with the attached set of thematic maps are considered to fulfil the engineering geological demands of Athens Prefecture responsibilities. More specifically it can constitute the basic tool for:

- Urban planning of infrastructure developmental works
- Mitigation of natural hazards and improvement of citizens’ safety
- Protection and upgrade of the environment
- Sustainable management of natural resources
- Citizens’ awareness
- Optimum exploitation of technical knowledge for advanced quality of life

It is pointed out that the information and data presented in an engineering geological map at 1:10.000 scale, does not substitute the site geotechnical investigation required for technical work constructions. Consequently, it does not withdraw the existing legal frame for public and private works, but offers guidance and technical support.

Moreover the advantage of digital maps is the continuous data updating which is strongly recommended to be established by the authorities in charge. Digital parameters also allow useful applications to be carried out, such as correlations, zonation, retrieval of selected data etc.

The topographic background of the engineering geological map at 1:10.000 scale was created from the digital background provided by the Prefecture of Athens, using Geographical Information Systems and more specifically ArcGIS 9.0. It has been produced with the accuracy of 1:5.000 scale map and it includes, apart from the road network, also the boundaries of 45 Municipalities and 3 Communities that belong to the Prefecture of Athens.

For the creation of digital data, the official Greek projection system (EGSA 87) has been used.

In order to obtain an accurate and up to date engineering geological map, the boundaries of the configured formations have been redrawn in the field. For this aim two main bibliographic sources have been implemented as guides, namely:

- a) the engineering geological maps at a scale of 1:25.000 of PhD thesis of N. Sabatakakis (1991), entitled “ Engineering geological research of Athens Basin” (University of Patras), as well as
- b) the Geological maps of the Institute of Geology and Mineral Exploration at 1:50.000 scale, sheets “ATHINAI - PIRAEUS”, “ATHINAI – ELEFSIS”, “ KIFISSIA” and “KOROPI - PLAKA”.

3. Legend of the engineering geological map

To describe in detail the engineering geological conditions of the urban area of the city the soil formations were grouped into twenty (20) individual geotechnical units, based on the evaluation of ex-

isting geotechnical database and the origin, relevant age, composition, physical state and engineering geological characteristics of the ground formations. In the full text description of each unit the particular characters of macroscopic observation are given, as well as qualitative and quantitative parameters from laboratory tests.

It is pointed out that the range of the given parameters has an indicative character and was determined by the bibliography of the wider area, as well as the selected studies of the Athens Prefecture area, that have been imported in the data base.

Finally, the classification of the engineering geological formations according to the Greek Seismic Regulation (E.A.K. – 2000) is also given in the legend.

A summarized description of soil units is given bellow:

1.	Man-made fill material.
2.	Recent materials of rivers, streams and coastal beds.
3.	Loose coastal deposits of grey sandy silts and soft clays.
4.	Loose deposits of mixed phases with predominance of fine materials
5.	Loose deposits of mixed phases with predominance of coarse materials.
6.	Scree materials moderately to well cemented.
7.	Moderately cemented breccia-conglomerates with brown-reddish cementing material.
8.	Semi-cohesive silts – clays of light brown colour
9.	Semi-cohesive to cohesive formations of thin layers of sandstones, micro-conglomerates, conglomerates and sands of marine facies, sub-white in colour.
10.	Cohesive red loams and moderately cemented conglomerates.
11.	Semi-cohesive to very cohesive formations of marls, sandstones, marly limestones, yellow-white in colour.
12.	Medium to thick bedded, intensely fissured, white-grey limestones of allochthonous series.
13.	Thin to medium bedded limestones, strongly tectonised, of yellow to white colour.
14.	Thick-bedded to massive, strongly tectonised and karstified limestones.
15.	Dolomites - dolomitic limestones.
16.	Schist-sandstone-marly series of the Athenian schists with limestone lenses.
17.	Athenian schists.
18.	Marbles with schist layers.
19.	Schists with marble layers.
20.	Semi-metamorphic to metamorphic undivided formations.

The physical and mechanical properties that are given in the full text legend of the engineering geological map are the following:

Soils: LL (%), IP (%), w (%), γ_b (t/m³), e, N_{SPT}, q_u (kPa), C_c, c_u (kPa), ϕ_u (°).

Rocks: ρ_d (kN/m³), σ_c (MPa), σ_t (MPa), I_{s(50)} (MPa), E_L (GPa), n (%), V_p (m/sec), I_{d2} (%), v, SHV

4. Atlas of thematic maps

A set of thematic maps was also compiled attached to the engineering geological map of 1:10.000 scale. Each map was drawn in particular individual scale according to the character of the special information shown. More specifically these maps are:

4.1 Hydrogeological map

Since the hydrogeological conditions constitute an important factor affecting the geotechnical behaviour of geological formations, it was considered necessary to compile a hydrogeological map at a scale of 1: 50.000. Indicative information with local character is given, while simple points of observation were also illustrated. Special effort was made in the recognition of places where high water level is expected affecting the foundation of common structures.

4.2 Tectonic map

A tectonic map of Athens Prefecture region was drawn at a scale of 1:50.000, in order to:

- a) Show the main tectonic lines and trends that characterize the structure of the studied region.
- b) Point out the areas where the geological formations are generally influenced by tectonics and probably appear differentiated geotechnical behaviour

It is noted that tectonic lines, drawn in the tectonic map, were indentified by at least two of the following ways:

- Field work
- Air photos interpretation
- Bibliographic reports and maps

4.3 Earthquake epicenters' map

A map of seismic epicenters was compiled at a scale of 1:250.000 in order to sketch out the seismic potential of the wider area around the study region. This map illustrates the distribution of shocks with magnitudes $\geq 4R$ which occurred in the area around the city.

5. Description of digital data

For the compilation of the engineering geological map of Athens Prefecture area at a scale of 1:10.000 including eleven (11) A0 size sheets, the following thematic levels were created for the relative sort of data:

- Sheets' connection diagram
- Boundaries of Athens Prefecture area
- Boundaries of Municipalities and Communities
- Greek territory boundaries
- City sector
- Road network
- Boundaries of engineering geological units
- Borehole's point
- Photo's point
- Underground water level

- Local underground water level
- Faults

The topographic contours (40 m interval) exported in raster format, originate from the vector digital data of the Hellenic Military Geographical Service. The thematic levels referring to the built environment (roads etc) were created from the digital data provided by the Prefecture of Athens, while further digital data used for the needs of the project originate from other sources such as the University of Patras and the Hellenic Mapping and Cadastral Organization.

The points illustrating either boreholes' or photos' sites are connected through hyperlink to relative picture files (Log records and Photos).

Two hundreds forty five (245) borehole points, were imported in the data base and marked on the map. They were selected after the evaluation of more than 2000 borehole records and considered to be most reliable and representative. They are well distributed over the map area and the different geological formations and originate from the Institute of Geology and Mineral Exploration, the Water Company of Athens, the Ministry of Environment and Public Works, the Prefecture of Athens, the University of Patras, as well as private companies.

Moreover five hundreds twelve (512) points, corresponding to photos taken during the recent field work, were marked on the map and imported in the data base.

In addition, for the compilation of the Earthquake epicenters' thematic map, digital data concerning earthquake epicenters of the wider region of Attiki were imported in the database. These data were obtained by Comninakis, P. - Papazachos, B. (1986) catalogue, up to 1949 and from the Geodynamic Institute of Athens Observatory records, for the time period 1950 – 2005.

6. Acknowledgments

The authors of the present article wish to thank Siemos N., Galanakis D. and Mourtas D. for the excellent cooperation.

7. References

- Andronopoulos, V., Koukis, G. 1976. Geological - Geotechnical study of Athens Acropolis region, Athens, Institute of Geology and Mineral Exploration, *Geotechnical Researches*, No 1.
- Anon., 1981. Rock and Soil description for Engineering Geological mapping, *Bulletin of I.A.E.G.*, 24, Report by the Commission of Engineering Geological Mapping.
- Comninakis, P.E., Papazachos, B.C., 1986. *A catalogue of earthquakes in Greece and surrounding area for the period 1901-1985*. Thessaloniki, University Publications 1, Geophysical Laboratory, 167pp.
- Dearman, W.R., Matula, M. 1976: Environmental aspects of Eng. Geological Mapping. *Bulletin of I.A.E.G.*, 14, 141-146.
- Dounas A., Kallergis G., Morfis A., 1976. Hydrogeological research for the Athens Metro study. Athens, Institute of Geology and Mineral Exploration.
- EPPO, 2000. *Greek Seismic Regulation* (and modifications)
- Gaitanakis, P. 1982. Geological map "Athinaï - Piraeus", scale 1:50.000, Athens, Institute of Geology and Mineral Exploration.
- Galanopoylos, A., 1989. The seismic danger in major and minor Attica region. Athens, *Proceedings of Athens Academy*, 63, 1st (1988).

- Kakkavas, N., Gioni-Staupoulou, G. 1978. Hydrogeological study of Peristeri Municipality, Attica. Problems of groundwater level uplift, Athens, Institute of Geology and Mineral Exploration, Researches No 23 ,18pp.
- Katsikatsos G., 2002. Geological map “Athinaí - Elefsis”, scale 1:50.000, Athens, Institute of Geology and Mineral Exploration.
- Katsikatsos, G., Mettos, A., Vidakis, M., Dounas, A. 1983. Geological map “Athinaí - Elefsis”, scale 1:50.000, Athens, Institute of Geology and Mineral Exploration.
- Katsikatsos, G., Migiros, G., Triantaphyllis M., Mettos A. 1986. Geological structure of internal Hellenides. Athens, Institute of Geology and Mineral Exploration, *Geol. and Geoph. Researches*, 191-212.
- Koukis, G., Sabatakakis, N. 2000. “Engineering geological environment of Athens, Greece”. Bulletin of Engineering Geology and the Environment, 59: 127 – 135
- Kounis G., 1980. Hydrogeological conditions of the region of Solar Village, No 3, (Lykovrysi), Athens, Institute of Geology and Mineral Exploration.
- Kounis G., 1981. Hydrogeological research for Athens Metro, Hydrogeological conditions Analysis II, Athens, Institute of Geology and Mineral Exploration.
- Kynigalaki, M., Nikolaou, N., Karfakis, J., Koutsouveli, An., Poyiadji, El., Pyrgiotis, L., Konstantopoulou, G., Apostolidis, Em., Bellas, M., Loupasakis, K., Spanou, N., Siemos, N., Galanakis, D. and Mourtas, D. 2006. Engineering geological map of Athens Prefecture region, at 1: 10.000 scale, with relative data base and Atlas of thematic maps, Athens, Institute of Geology and Mineral Exploration.
- Kynigalaki, M., Rozos, D., Vakondios, 2001. Seismic zonation study in the region of Anthoupolis, Peristeri Municipality. Athens, Institute of Geology and Mineral Exploration.
- Latsoudas, X. 2003. Geological map “Koropi - Plaka”, scale 1:50.000, Athens, Institute of Geology and Mineral Exploration.
- Marinos, P., Bouckovalas, G., Tsiambaos, G., Sabatakakis, N., Antoniou, A. (2001), “*Ground zoning against seismic hazard in Athens, Greece*”, Engineering Geology, 62: 343 – 356
- Mettos, A., 1992. *Geological and Paleogeographical study of terrestrial Neogene and Quaternary of formations of northeastern Attica and southeastern Viotia*. Athens, PhD Thesis, Athens University.
- Mouyiaris N., Andronopoylos V., et.al., 1989. Seismotectonic map of Greece, scale 1:500.000, Athens. Institute of Geology and Mineral Exploration.
- Mouyiaris N., 1994. *Seismic history of Aegea region (2400 B.C. - 1900 A.D.)*. Patras, PhD Thesis. Patras University.
- Papadeas, G. 2002. *Geological researches in Attica*, Athens, Athens University.
- Papanikolaou, D., 1986. *Geology of Greece*. Athens, Pentalofo Publications.
- Pian De, A. 1949. Aperche de la Mine de Peristeri, Athens, 12 pp.
- Report of the Commission of Engineering Geology Mapping, of the IAEG, 1979. Rock and Soil materials, Classification of rocks and soils for Engineering Geological Mapping. Part I: Rock and Soil Materials. *Bulletin of I.A.E.G.*, 19, Krefeld, 364-371.
- Rozos, D., Vakondios, I., Kynigalaki, M., Argyris, Ch., 1999. Geotechnical Study of subsidence phenomena in Anthoupoli, Peristeri Municipality, Athens, Institute of Geology and Mineral Exploration.
- Sabatakakis N., 1991. *Engineering geological research of Athens Basin*, PhD Thesis. Patras. Patras University.

- Siemos, N., Charmanidis, F., 2003. Hydrogeological - Drilling research of Olympic Works regions (Chaidari, Korydallos, Nikaia), Athens, Institute of Geology and Mineral Exploration.
- Siemos, N., Charmanidis, F., 2003. Hydrogeological - Drilling research of Olympic Works regions (Pedion Areos), Athens, Institute of Geology and Mineral Exploration.
- Siemos, N., Charmanidis, F., 2003. Hydrogeological - Drilling research of Olympic Works regions (OAKA, Markopoulo, Elliniko, Kallithea - Faliron), Athens, Institute of Geology and Mineral Exploration.
- Siemos, N., Charmanidis, F., 2003. Hydrogeological - Drilling research of Olympic Works regions (Ethnikos Kipos), Athens, Institute of Geology and Mineral Exploration.
- Trikalinos, I., Mousoulos, A. 1949. Coal mines of Peristeri, Athens, 34pp.
- UNESCO/IAEG 1976. *Engineering geological maps. A guide to their preparation*, Paris, UNESCO Press, 79 pp.
- Voreadis, G. 1940. *The lignite mines of Athens basin*, Athens.

AMELIORATING THE SPATIAL RESOLUTION OF HYPERION HYPERSPECTRAL DATA. THE CASE OF ANTIPAROS ISLAND

Nikolakopoulos K.¹, Gioti Ev.², Skianis G.³, and Vaiopoulos D.³

¹ *Institute of Geology and Mineral Exploration, Olympic Village Entrance C, 13677 Acharnae Athens, Greece knikolakopoulos@igme.gr,*

² *Department of Geography, Harokopio University of Athens 70, El. Venizelou Str, Athens 17671 Greece, gs20505@hua.gr*

³ *University of Athens, Department of Geology and Geoenvironment, 15784 Panepistimiopolis Zografou, Greece, skianis@geol.uoa.gr, vaiopoulos@geol.uoa.gr*

Abstract

In this study seven fusion techniques and more especially the Ehlers, Gram-Schmidt, High Pass Filter, Local Mean Matching (LMM), Local Mean and Variance Matching (LMVM), Pansharp and PCA, were used for the fusion of Hyperion hyperspectral data with ALI panchromatic data. The panchromatic data have a spatial resolution of 10m while the hyperspectral data have a spatial resolution of 30m. All the fusion techniques are designed for use with classical multispectral data. Thus, it is quite interesting to investigate the assessment of the common used fusion algorithms with the hyperspectral data. The study area is Antiparos Island in the Aegean Sea.

Key words: *Hyperion, Hyperspectral data, fusion, Antiparos Island.*

1. Introduction

The majority of the earth observing satellites such as SPOT, Landsat, Ikonos, Quickbird, EO-1 (ALI sensor) collect at the same time a panchromatic image with a higher spatial resolution and many multispectral bands with lower spatial resolution. This is due to technical reasons such as limited storage capacity, small data transfer rate and the limited energy autonomy of most of the satellites. These limitations affect more the hyperspectral sensors like Hyperion that collect more than 240 bands. Considering these limitations, it is clear that the most effective solution for providing high-spatial resolution hyperspectral remote sensing images is to develop effective image fusion techniques.

In this study seven fusion techniques and more especially the Ehlers, Gram-Schmidt, High Pass Filter, Local Mean Matching (LMM), Local Mean and Variance Matching (LMVM), Pansharp and PCA, were used for the fusion of Hyperion hyperspectral data with ALI panchromatic data. Both sensors are on onboard Earth Observing-1 satellite. Thus the data was collected simultaneously thus, there are no radiometric and atmospheric problems. The data was provided to IGME from USGS. The panchromatic data have a spatial resolution of 10m while the hyperspectral data have a spatial resolution of 30m. All the fusion techniques used in this study are designed for classical multispectral data and tested in previous studies (Chavez et al., 1991; Vaiopoulos et al., 2001; Nikolakopoulos, 2003; Aiazzi et al., 2002; Wang et al., 2005; Nikolakopoulos 2005; Laporterie-Dejean et al., 2005; Nikolakopoulos, 2008). Thus, it is quite interesting to investigate the assessment of the common used fusion algorithms with hyperspectral data.

2. Bands number reduction

The Hyperion data usually presents a low signal to noise ratio. Furthermore forty-six of the two hundred forty two Hyperion bands are uncalibrated so it is better not to be used. In order to reduce the total number of the bands a pre-selection based on optical and statistical criteria was done. Firstly, all the bands were examined visually. The optical control detected many bands dominated by noise and some other bands with no useful information (totally black or white images). Second, the histogram parameters of all the bands were examined. The statistical control of the minimum, maximum and the standard deviation values confirmed the existence of bands corrupted by noise. As a result only 155 bands (8-57, 78, 82-97, 99-119, 134-164, 182-184, 187-219) were used for the fusion processing. The spectral range of these bands is presented in Table 1.

3. Fusion techniques used in this study

The Ehlers algorithm (Ehlers, 2004; Ling et al., 2007; Ehlers et al., 2008) implemented in Erdas Imagine software is based on IHS transform and filtering in the Fourier Domain and should give the same quality results independently of the type of the images. The Gram Schmidt algorithm simulates a panchromatic band from the lower spatial resolution multispectral bands, performs a Gram-Schmidt transformation on the simulated panchromatic band and the multispectral bands, using the simulated panchromatic band as the first band, then swaps the high spatial resolution panchromatic band with the first Gram-Schmidt band and finally applies the inverse Gram-Schmidt transform to form the fused spectral bands. A limitation of the algorithm is that the low spatial resolution multispectral bands used to simulate the panchromatic band must fall in the range of the high spatial resolution panchromatic band or they will not be included in the resampling process (Laben and Brower, 2000; Envi, 2008).

The process of the High Pass Filter involves a convolution using a High Pass Filter (HPF) on the high resolution data, then combining this with the lower resolution multispectral data. More specially the algorithm read pixel sizes from image files and calculates the ratio of multispectral cell size to high-resolution cell size. Then it High-pass filter the high spatial resolution image, resample the multi-spectral image to the pixel size of the high-pass image and finally add the HPF image to each multi-spectral band. The HPF image is weighted relative to the global standard deviation of the multi-spectral band. The algorithm stretches the fused image to match the mean and standard deviation of the original multispectral image (ERDAS, 2008).

The LMM (Local Mean Matching) and the LMVM (Local Mean and Variance Matching), methods were specifically designed in order to minimize the difference between the fused image and the low-resolution MS channels (De Béthune et al., 1998), hence to preserve most of the original spectral information of the low-resolution channels. These filters apply normalization functions (Joly, 1986) at a local scale within the images in order to match the local mean and/or local mean and variance values of the PAN image with those of the original low-resolution spectral channel. The small residual differences remaining correspond to the high spatial information stemming from the high-resolution PAN image. This type of filtering drastically increases the correlation between the fused product and the low-resolution channel. By adjusting the filtering window sizes, the amount of spectral information preserved in the fused product can be controlled.

The Principal Component Analysis algorithm calculates principal components, remaps the high resolution image into the data range of PC-1 and substitutes it for PC-1, then applies an inverse principal components transformation. The Principal Component method is best used in applications that require the original scene radiometry (color balance) of the input multispectral image to be maintained as

Table 1.

Spectral bands no	Spectral Length (nm)	Full Width at Half the Maximum FWHM (nm)
8	426,82	11,38
57	925,41	11,27
78	922,54	11,04
82	962,91	11,04
97	1114,19	10,95
99	1134,38	10,92
119	1336,15	10,69
134	1487,53	11,04
164	1790,19	11,45
182	1971,76	10,93
184	1991,96	10,91
187	2022,25	10,90
219	2345,11	10,40

closely as possible in the output file. As this method scales the high resolution data set to the same data range as Principal Component 1, before the Inverse Principal Component calculation is applied, the band histograms of the output file closely resemble those of the input multispectral image.

The Pansharp fusion technique proposed by (Zhang, 1999) seems to have solved the two major problems in image fusion – colour distortion and operator dependency. A method based on least squares was employed for a best approximation of the grey value relationship between the original multispectral, panchromatic, and the fused image bands for a best colour representation. Statistical approaches were applied to the fusion for standardizing and automating the fusion process.

Some of the algorithms used in this study allow for various parameter settings. So many different tests were done. For every algorithm the best visual result was selected for the quality assessment. In all cases, the nearest neighborhood resampling method was applied.

For each fused image the following issues have been examined: a) the visual qualitative result, b) the statistical parameters of the histograms of the various frequency bands c) the correlation coefficient and d) the entropy of the original bands to the respective entropy of the fused bands was compared. Those criteria are in accordance with the general quality assessment criteria that were described in previous studies (Wald et al., 1997; Chavez et al., 1991).

4. Comparing the quality of seven fused images with the original Hyperion image

4.1. Visual Comparison

As already mentioned in this study, the quality of the fusion algorithms was evaluated both qualitatively and quantitatively. Visual comparison of all the possible band combinations of the fused images was used for the qualitative assessment, since it is the most simple but effective tool for showing the major advantages and disadvantages of a method.

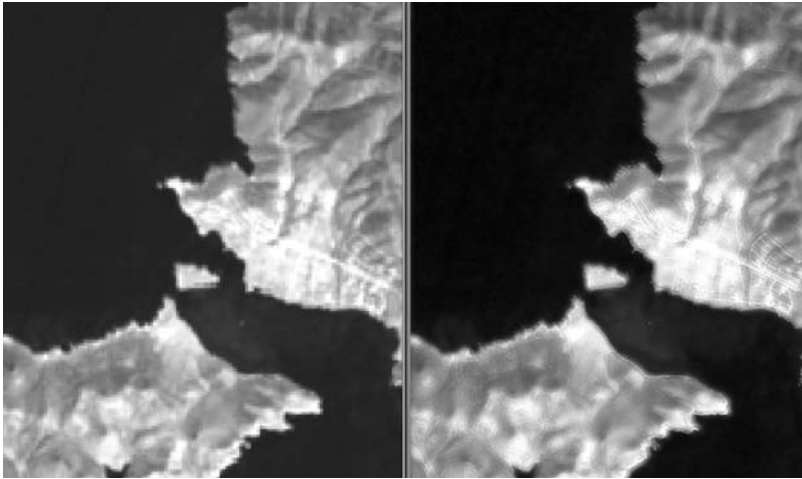


Fig. 1: (left): The original Hyperion image at 1/25.000 scale. A RGB combination of specific bands (2203, 844, 487 nm) is presented; (right): The same RGB combination of the Ehlers fused image.



Fig. 2: (left): The Gram-Schmidt fused image at 1/25.000 scale. A RGB combination of specific bands (2203, 844, 487 nm) is presented; (right): The same RGB combination of the HPF fused image.

A RGB combination of specific bands (2203, 844, 487 nm) of the original and the fused images are presented below (Figs 1-4). A first remark is that all the fusion algorithms ameliorate the spatial resolution of the original Hyperion data. The road network, the fields, the river network and the coastline can be more easily detected and mapped in the fused images. More particularly, the Ehlers fused image presents a much better spatial resolution, as some of the most important geomorphological characteristics can be easily discriminated. Moreover, it is obvious that the quality of the colours has been enhanced. Nevertheless, the contrast failed to give any better result. The Gram Schmidt fused image presents also a better spatial resolution. In that image, even the morphology of the sea bottom can be observed, which mean that bathymetrical information can be derived. Furthermore, there is a small amelioration in the contrast and a change in the quality of its colours as they became darker. Observing the HPF fused image, it can be easily seen that its spatial resolution is quite sat-



Fig. 3: (left): The LMM fused image at 1/25.000 scale. A RGB combination of specific bands (2203, 844, 487 nm) is presented; (right): The same RGB combination of the LMVM fused image.

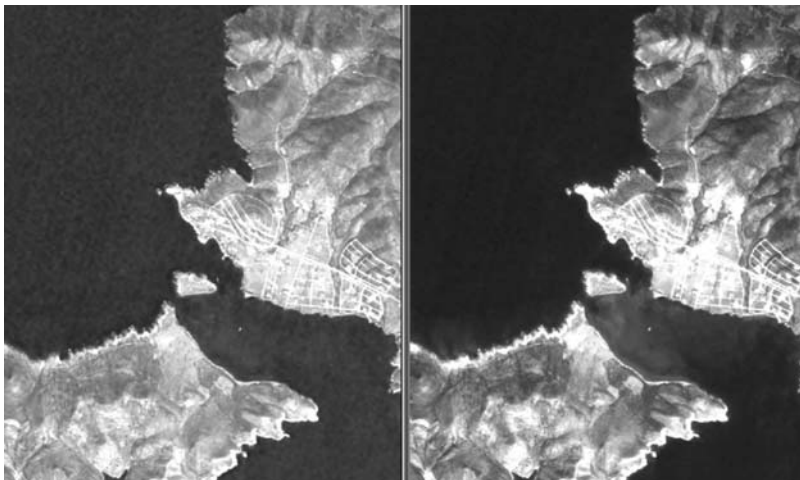


Fig. 4: (left): The Pansharp fused image at 1/25.000 scale. A RGB combination of specific bands (2203, 844, 487 nm) is presented; (right): The same RGB combination of the PCA fused image.

ified, comparing with Hyperion's. This image gives information about the road network, every field, the vegetation; even the coast line can be discriminated. The contrast of the image also presents a great enhancement but the quality of the colours isn't so representative. The LMM and the LMVM fused image also present better spatial resolution. They generally preserved the original colours and present a better contrast. The Pansharp fused image even if has also better spatial resolution than Hyperion's, doesn't give any further information about the morphology of the sea bottom. Moreover, the quality of the colour has changed and the contrast is presented with better results. The PCA fused image, has also a really satisfying spatial resolution as all the basic elements of the area, such as road network and vegetation are being illustrated. Bathymetrical information can also be retrieved. Meanwhile, the quality of the colour has been changed and now seems to be little darker and the contrast is at a better level.

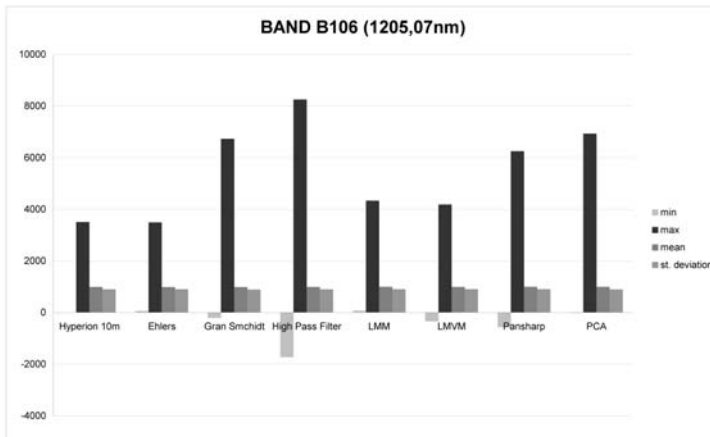


Fig. 5: The statistical parameters of the Hyperion band B106 and the respective fused bands.

4.2. Statistical Comparison

For all the images the statistical parameters of the histogram and especially the standard deviation of some specific bands were studied. The value of the standard deviation is vital in recognizing different unities. The higher the value of the standard deviation of a histogram is, the more different formations can be recognized. The statistical control is necessary in order to examine spectral information preservation. When the researcher wants to proceed to digital processing of the data (for example applying different ratios for mineral detection), an alteration to the original spectral characteristics wouldn't be appropriate, as it may influence the results.

As it can be observed all the fusion techniques didn't provoke significant changes to the standard deviation and the mean values (Fig. 5 and Fig. 6). There are only some changes at the value of minimum and maximum.

Particularly, it has to be pointed out that the Ehler's algorithm increases the minimum value of the bands 14, 21, 31, 41, 49, 55 and 87. The rate of the increase slows down for the bands 106, 116, 136 and 151 and finally there is no change for the minimum value of the bands 161, 195, 205, 218. At the maximum value of this algorithm it can't be distinguished any significant alteration.

The Gram Schmidt algorithm has also some variations at the minimum value, which are higher at bands 14, 21, 31. The maximum value differs from Hyperion's in all bands and there is a big difference at band 87. About the High Pass Filter fusion technique, the minimum value has changed in all cases and entails a negative number. The minimum value for the bands 49, 87, 106 has the greatest fluctuation from the others. The maximum value of this technique presents the same inclination with the one of Gram Schmidt where there were some remarkable changes in all bands and band 87 had the higher deviation. It is quite interesting to observe the LMM technique, which has the smallest changes in the minimum value comparing with the other algorithms. Only bands 14, 21, 31, 41, 49, 55, 87, 106, 116, 136, 151, present a negligible alteration and at the bands 161, 195, 205, 218 the value remains the same. The maximum value has also some negligible changes at lower bands and at higher bands there isn't any fluctuation at all. The LMVM algorithm has the same behaviour for the minimum values in all bands which mean that there is a small variation in all cases and all the values appears to have negative numbers. The maximum value only entails some small differences. The Pansharp technique presents a small deviation at the minimum value, which is almost at the same range. It is important to be marked that bands 14, 21, 31, 41 entail a positive number and the rest bands have a negative one. The maximum value presents some alteration in all bands. Band

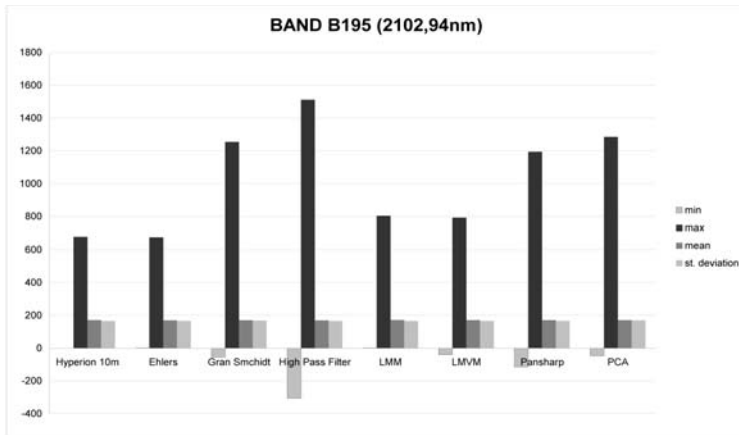


Fig. 6: The statistical parameters of the Hyperion band B195 and the respective fused bands.

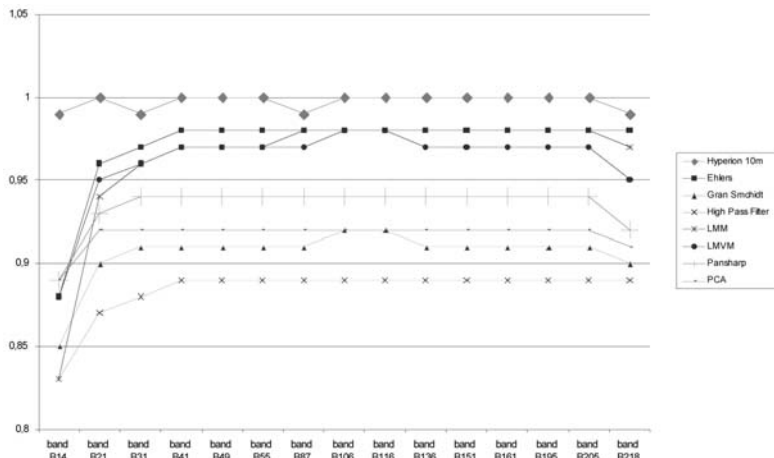


Fig. 7: The correlation value of specific fused bands and the respective original Hyperion bands.

14 has the smallest and band 87 has the biggest. Finally, PCA algorithm provokes some variations in the minimum value. Bands 106 to 218 present the smallest alteration. The maximum value also entails changes which are higher at band 87.

4.3. Correlation

The closeness between two images can be quantified in terms of the correlation function. The correlation coefficient ranges from -1 to 1. A correlation coefficient value of -1 indicates that the two images are highly correlated, i.e., very close to one another. A correlation coefficient of -1 indicates that the two images are exactly opposite to each other.

Each band of the original hyperspectral image has been correlated with the respective fused band. The correlation coefficients have been computed. The best spectral information is available in the hyperspectral image and hence the fused image bands should have a correlation closer to that of the hyperspectral image bands. The results are presented above (Fig. 7).

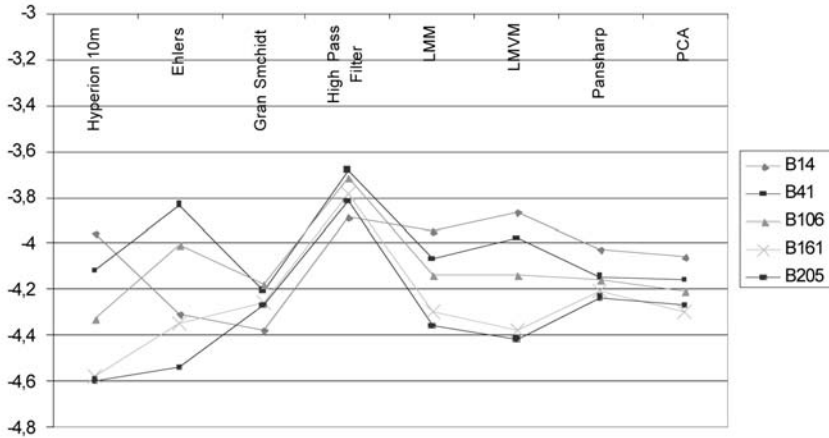


Fig. 8: The entropy of the Hyperion bands B14, B41, B106, B161, B205 and the respective fused bands.

The Ehlers fused image with a value close to 0,98 presents the highest correlation. The LMM and LMVM fused images have also a very satisfied correlation which it is close to 0,97. The High Pass Filter fused image presents the lower correlation to the original data. Its values are between 0,83 and 0,89. It is quite interesting to underline that all the fusion algorithms present the lower correlation values for the bands B14 and band B21. For the bands B31 to B205 the correlation is being increased. After the band 205 it can be observed that there is a decreasing tendency.

4.4 Entropy

The entropy H of an image may be defined:

$$H = \sum_{i=0}^L p_i \cdot \ln p_i$$

p_i is the percentage of the pixels of the image with digital number i . L is the quantization level (tonality range) of the image. For example if the digital number may take 28 different integer values from 0 to 255, L is equal to 255.

The entropy is generally considered to be a measure of the information content of the image. As long as the width of the image histogram increases, H also increases. Skewed image histograms have bigger entropy than symmetrical ones with the same standard deviation (Skianis & Nikolakopoulos 2008). Therefore the entropy value of a digital image contains information about the standard deviation and the shape of the histogram.

Observing band 14 (Fig. 8) it can be seen that High Pass Filter and LMVM fused images increase the entropy, LMM gives almost the same result with Hyperion's and all the other fusion techniques present a decrease in the entropy. The highest increase is presented in the high pass filter technique and the highest decrease in the Gram Schmidt. In Band 41 there are also some variations in the entropy as three of the fused images presents an increase (Ehler's, High Pass Filter and LMVM), three didn't give any fluctuation and two present a decrease from which Gram Schmidt's gives the greatest. About bands 106, 161 and 205 it can be observed that all the fused images present an increase in the entropy from which High Pass Filter has the highest and PCA the lowest. It would be inter-

esting to underline that High Pass Filter algorithm presents an important increase in all bands. Moreover, it can be observed that only bands 14 and 41 presented a decrease in certain fused images. All other bands give an increase in the entropy.

5. Conclusions

Seven fusion algorithms designed for multispectral data were tested on Hyperion hyperspectral data. The initial spatial resolution of Hyperion data (30m) has been ameliorated and the finally fused images have a spatial resolution of ten meters (10m). All the algorithms improve the target detectability of the Hyperspectral data. The road network, the fields and generally the formation boundaries can be more easily detected and mapped. All the algorithms keep almost invariable the mean and the standard deviation values of the original data. All the algorithms with the exception of the High Pass Filter provoke minor changes to the minimum value and a significant increase to the maximum value of the original data. All the fused images present a very high correlation to the original Hyperion bands. All the algorithms enhance the information contained in the original image as they increase the entropy value of most of the Hyperion bands.

The general conclusion is that the specific algorithms even if they were designed for use with classical multispectral data they can be used for the fusion of Hyperion Hyperspectral data.

6. References

- Aiazzi B., Alparone L., Baronti S. & Garzelli A., 2002. Context-Driven fusion of high spatial and spectral resolution images based on oversampled multiresolution analysis, *IEEE Transactions On Geoscience And Remote Sensing*, vol. 40, No. 10, October 2002, p. 2300-2312.
- Chavez, P.S. Jr., Sides, S.C., Anderson, J.A., 1991. Comparison of three different methods to merge multiresolution and multispectral data : Landsat TM and SPOT Panchromatic, *Photogrammetric Engineering and Remote Sensing*, Vol. 57, N° 3, pp. 295-303.
- De Bethune S., Muller F., Donnay J.P., 1998. Fusion Of Multispectral And Panchromatic Images By Local Mean And Variance Matching Filtering Techniques, *Fusion of Earth Data*, Sophia Antipolis, France, 28-30 January 1998.
- Ehlers M., 2004. Spectral characteristics preserving image fusion based on Fourier domain filtering, *Proc. of SPIE* Vol. 5574 p. 1-13.
- Ehlers M., Klonus S., Astrand P.J., 2008. Quality assessment for multi-sensor multi-date image fusion, *Proc. XXIIth Int. Congr. ISPRS*, Beijing, China p. 499-506.
- Envi, 2008. *Envi User's Guide Version 4.5* 2008, p 1152.
- Erdas, 2008. *Erdas Field Guide* p. 770.
- Joly, G., 1986. *Traitements des fichiers images*, Collection Télédétection satellitaire, No. 3, Paradigme, Caen, 137 p.
- Laporterie-Dejean F., De Boissezon H., Flouzat G., & Lefevre-Fonollosa M., 2005. Thematic and statistical evaluations of five panchromatic/multispectral fusion methods on simulated pleiades-hr images, *Information Fusion*, vol. 6, no. 3, pp. 193-212.
- Laben, C. A., Brower B. V., 2000. Process for Enhancing the Spatial Resolution of Multispectral Imagery Using Pan-Sharpener, US Patent 6,011,875.
- Ling Y., Ehlers M., Usery L., Madden M., 2007. FFT-enhanced IHS transform method for fusing high resolution satellite images, *ISPRS Journal of Photogrammetry & Remote Sensing* 61, 381-392.
- Nikolakopoulos K., 2003. Comparative study of fusing ETM data with five different techniques for the

- broader area of Pyrgos, Greece, *Proc of SPIE*, Vol. 5238, p. 84-95.
- Nikolakopoulos K., 2005. Comparison of six fusion techniques for SPOT5 data, *IEEE 2005 International Geoscience and Remote Sensing Symposium*, Seoul Korea 25-29 July 2005. Vol. 4, p. 2811- 2814.
- Nikolakopoulos K., 2008. Comparison of Nine Fusion Techniques for Very High Resolution Optical Data, *Photogrammetric Engineering & Remote Sensing*, Vol. 74 No 5, May 2008, pp.647-659.
- Skianis, G., Nikolakopoulos, K., 2009. The entropy as a measure of the performance of the NDVI vegetation index-a pilot study with an ALOS digital image. *Proc. of 'ALOS PI 2008 Symposium'*, Island of Rhodes, Greece 3-7 November 2008, ESA SP-664, January 2009. Unpaginated CDROM.
- Vaiopoulos D., Nikolakopoulos K., Skianis G., 2001. A comparative study of resolution merge techniques and their efficiency in processing images of urban areas. *IEEE/ISPRS Joint Workshop on Remote Sensing and Data Fusion over Urban Areas*, Rome, Italy, November 8-9th, 2001, p. 270-274.
- Wald, L., Ranchin, Th., Mangolini, M., 1997. Fusion of satellite images of different spatial resolutions: Assessing the quality of resulting images, *Photogrammetric Engineering and Remote Sensing*, Vol. 63, N° 6, pp. 691-699.
- Wang Z., Ziou D., Armenakis C., Li D., and Li Q., 2005. A comparative analysis of image fusion methods, *IEEE Transactions on Geoscience and Remote Sensing*, vol. 43, no. 6, pp. 1391-1402.
- Zhang, Y., 1999. A new merging method and its spectral and spatial effects, *International Journal of Remote Sensing*, vol. 20, pp. 2003-2014.

LANDSLIDE SUSCEPTIBILITY MAPPING OF THE NORTHEASTERN PART OF ACHAIA PREFECTURE USING ANALYTICAL HIERARCHICAL PROCESS AND GIS TECHNIQUES

Rozos D.¹, Bathrellos D. G.², Skilodimou D. H.²

¹Department of Geological Science, School of Mining and Metallurgical Engineering, NTUA, 9 Heroon Polytechniou str, 157 80 Zografou Athens, Greece, rozos@metal.ntua.gr

²Department of Geography & Climatology, Faculty of Geology & Geoenvironment, National & Kapodistrian University of Athens, University Campus, Zografou, 15784 Athens, Greece, gbathellos@geol.uoa.gr, hskilodimou@geol.uoa.gr.

Abstract

Landslides are one of the most frequent and disastrous natural hazards worldwide. Thus, the need of landslide susceptibility maps is of primary importance as they are both a useful tool for the land use planning and a necessary step for future development activities. This paper presents an integrated technique of analytical hierarchical process (AHP) and geographic information system (GIS) to create a landslide susceptibility map of the NE part of Achaia prefecture. The study area mainly consists of Neogene deposits and it is a part of the Corinthian graben, which characterized by intense neotectonic activity. Therefore, it is affected by many slope movements that usually cause serious damages in inhabitant areas and road networks. Based on field survey data analysis six parameters were chosen as major parameters that influence the stability of slopes to the direction of landslide manifestation. The AHP method identifies both the rate of the individual classes, and the weight of each factor. Spatial layers with their corresponding rates and weights were linearly combined to prepare the landslide susceptibility map, which includes four zones of slope movement's susceptibility, namely a low, a moderate a high and a very high zone. The evaluation and final confirmation of the map was based on a great number of recorded landslides in the area.

Key words: landslide susceptibility map, GIS, AHP method, Achaia prefecture, Peloponnesus.

1. Introduction

Landslides are among the most frequent and disastrous natural hazards worldwide, connected in many cases with huge economic and social welfare as well as with the loss of human lives. Therefore, as their manifestation has a great influence on population, constructions and environment, the evaluation of sliding risk is very important to their confrontation (Guzzetti et al., 1999). To this direction, landslide susceptibility maps, covering urban and rural areas and depicting sites with graduated risk levels, constitute a valuable tool for better understanding and confronting landslide's effects, but also for allocating areas prone to landslide manifestation (Castellanos et al., 2007). Moreover, they can be used in urban and rural planning and development (Bathrellos et al., 2009).

This study refers to the compilation of a landslide susceptibility map for the NE part of Achaia prefecture using GIS and the Analytical Hierarchy Process (AHP).

The AHP is multi-objective multi-criteria decision-making methodology (Saaty 1990; 2006) that has been used for compilation of sliding risk maps by many researchers (Ayalew et al., 2004; Komac 2006; Yoshimatsu and Abe 2006; Castellanos et al., 2007; Akgün et al., 2008). This process gives the ability of the correlation both the parameters that cause landslide manifestation and their classes, by using a table in which comparison of every two parameters and their classes is carried out.

Moreover, Geographic Information Systems (GIS) comprise a valuable tool for the compilation of landslide susceptibility maps (Saha et al., 2002; Lan et al., 2004). The use of GIS in such a case gives the advantage of a quick analysis, processing and correlation of a big volume of data.

As a great number of landslide phenomena is manifested in western Greece (Koukis and Rozos, 1982), the NE part of Achaia prefecture, was chosen for this study. This area mainly consists of Neogene deposits and it is a part of the Corinthian graben, which characterized by intensive neo-tectonic activity. So, it is affected by many slope movements that usually cause serious damages in inhabitant areas and road networks. For the above reasons, various studies have been done in the past regarding landslide examination in the Achaia prefecture (Koukis et al. 1997; Koukis et al. 2005; Sabatakakis et al., 2005; Rozos et al., 2006).

2. Geological setting

The North-eastern part of Achaia prefecture (study area), has an expanse of about 226km², while its altitude varies from 0 to 1760m. Formations from three geotectonic zones (Olonos - Pindos, Gavrovo - Tripolis and Ionian) participate in the geological structure of Achaia County. Also, the existence of Corinthian graben, with recent geodynamic evolution in its immediate vicinity, results in an increased seismic activity. Therefore, Achaia is characterized by a complicated geological structure with prevailing tectonic fracturing, as Pindos zone constitutes an extended overthrusting cup on Gavrovo zone formations (Rozos 1989).

The study area is constructed by (Rozos 1989; Koukis and Rozos 1982): (a) Fine-grained to coarse-grained loose Quaternary formations (clays, silts, siltstones and sands), as well as weathering products of older formations. Also, loose deposits of mixed phases, such as clayey silts, siltstones, and sands of various grain size distribution, and grits also present. (b) Coarse-grained loose Quaternary formations (pebbles and gravels of varying sizes with a minimum proportion of fine grained materials), screes and fans. (c) Coarse grained coherent Quaternary formations (polygenic conglomerates, usually of a poor gradation), and slope breccias, but also semi-cohesive conglomerates, sands with a low degree of diagenesis and rocky fragments, with red clay as a cementing material. All Quaternary deposits present a quick alteration of their phases, both vertically and horizontally.

(d) Fine – grained Plio-Pleistocene sediments with a variety of lithological horizons (clayey marls alternating with sands of a varying degree of diagenesis), and/or their mixed phases. (e) Coarse – grained Plio-Pleistocene sediments (conglomerates, usually strongly cemented, with pebbles of various and clayey - sandy cementing material). In general Plio-Pleistocene sediments can be subdivided into two main horizons. The lower one consisting of fine-grained facies (alternations of clayey marls, marls, silty sands and weak sandstones) prevails, with a progressive transition upwards to the coarser facies, finally giving coherent conglomerates of a great thickness.

(f) Flysch formations. Their main members are sandstones, siltstones and more rarely grit-conglomerates. They are cyclothematic and strongly folded sediments because of the tectonic action (nappes and upthrusts) and thus, they are in many places covered by weathering mantle of considerable thickness.

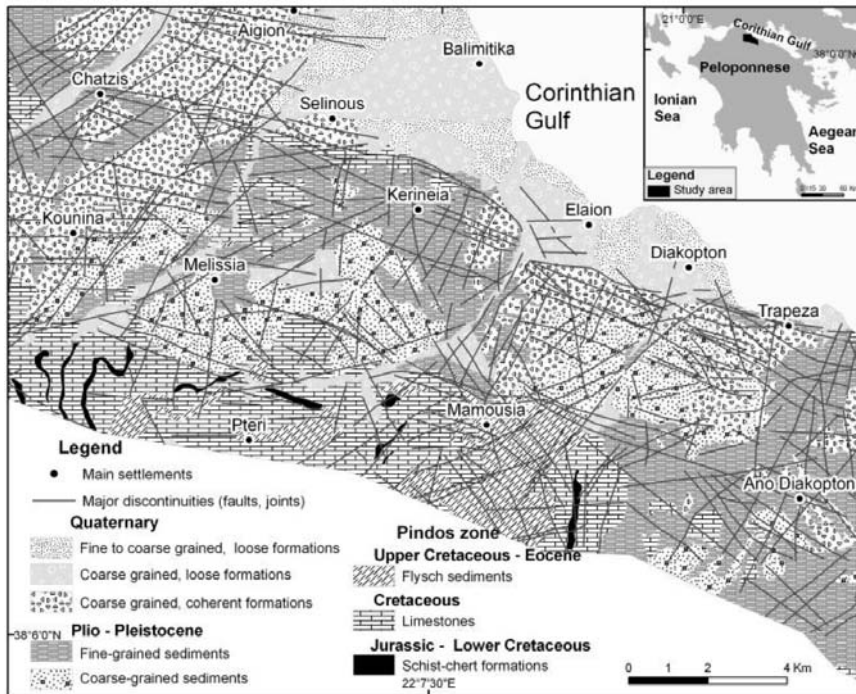


Fig. 1: The simplified geological map and the location map of the study area.

(g) Cretaceous limestones, which are usually moderate to thick-bedded, folded and karstified, with thin intercalations or nodules of silica lumps, but also with rare intercalations of claystones or siltstones.

(h) Schist - chert formations. They are alternations of cherts, siltstones, limestones and sandstones with rare occurrence of volcanic tuffs. Thus, thick weathering mantle is usually formatted, mainly in the cases of the surface occurrence of siltstones.

The surface distribution of the above engineering geological units is given in the map of Fig. 1.

Regarding the faults and major discontinuities encountered in the area, the examination of air photos and the field work revealed that their distribution and orientation show a rather dispersion, but with domination of these with $N70^{\circ}-90^{\circ}E$ and $N30^{\circ}-40^{\circ}W$ azimuths that are the oldest ones and resulted from the general uplifting of the area, as well as of these with $N40^{\circ}-50^{\circ}E$, $N70^{\circ}-80^{\circ}W$ and $N10^{\circ}-20^{\circ}E$ azimuths, which are connected with the migration of the Aegean arch (Doutsos et al., 1988).

3. Methods

3.1 Data analysis

For the application of the AHP method, a data base was firstly created using GIS software ArcGIS v.9.3. Then, all data used for the compilation of the sliding risk map were digitized and the various thematic layers were created. All the data layers were in vector format, transformed in grids with cell size 60×60 meters.

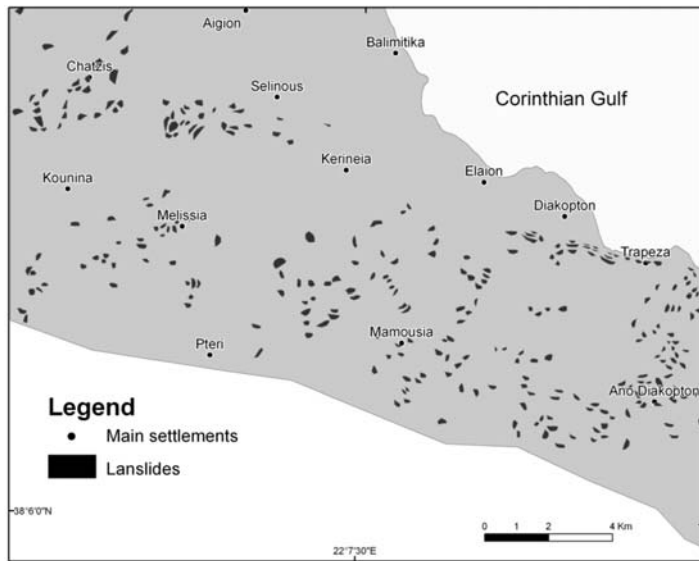


Fig. 2: Landslide events map in the study area.

Landslide inventory map

Landslide phenomena, for the necessities of the landslide inventory map compilation, were studied and recorded (Fig. 2), using previous works (Rozos 1989), but also field observations in the study area during 2008-2009. Finally, a number of 277 landslide events were recorded, with a varied size from 3.738m² to 83.356m². These events were engaged for the confirmation and evaluation of the landslide susceptibility map.

Based on the data analysis regarding the 277 landslide events in the area, lithology, distance from tectonic elements, slope's inclination, rainfall, land use, and geometry of main discontinuities, were chosen as major parameters that influence the stability of slopes to the direction of landslide manifestation.

Lithology

Lithology is one of the most determinative parameters regarding the landslide manifestation. For the study area the classes of lithology have arisen from its geological setting, based on literature (IGME 2005; Rozos 1989) and fieldwork. The distinctive geological formations were digitized and unified according to their engineering geological behaviour, in relation to landslide manifestation. Thus, lithology includes five classes as follows: (a) moderate to thick bedded limestones, (b) thin bedded schist chert formations, (c) Plio-Pleistocene coarse-grained sediments, (d) Cyclothemetic formations (Plio-Pleistocene fine-grained sediments and Flysch sediments), (e) Fine, fine-coarse to coarse and loose to semi-coherent Quaternary formations.

Distance from tectonic elements

The active tectonics in the study area plays an important role in the landslide manifestation. The various tectonic elements were also collected from the same sources as for lithology and fieldwork. All tectonic elements (faults, overthrusts and the rest lineaments) were digitized and buffer zones were formulated around them at distances of 50m, 100m, 150m and 200m. Thus, the classes of the buffer zones are five, namely: (i) the nearest (0-50m), (ii) the very near (51-100m), (iii) the near (101m-150m), (iv) the moderate distant (151m-200m) and (v) the distant (>200m).

Slopes' inclination

The inclination and the aspect of the slopes play a very important role in the manifestation of the landslides because they express the result of the combined influence of many agents (Rozos et al. 2008). The information on slope was obtained from topographical map (scale 1:50,000) developed by Hellenic Military Geographical Service. The grid map of the slopes' inclination was produced by means of the Digital Elevation Model. This map were classified into 5 classes, as follows: (i) 0°-5°, (ii) 6°-15°, (iii) 16°-30°, (iv) 31°-45°, and (v) > 45°.

Rainfall

As it is well known, precipitation is among the most usual triggering factors for landslide manifestation. Rainfall data were derived from four (4) meteorological stations, referred to mean annual precipitation for the period of 1975 – 2007. The mean annual precipitation of the area is between 665.98 to 870.93mm. For the necessities of this study, the precipitation map was produced, using the data of the meteorological stations in the area and applying the Inverse distance weighted (IDW) interpolation method. This map was separated into following classes: (i) <700mm, (ii) 701-750mm, (iii) 751-800mm, (iv) 801-850mm, and (v) >850mm.

Land use

The vegetation covering of the study area was taken from CORINE program (Bossard et al. 2000) and was saved as polygon layer. The variations of the vegetation in an area constitute an important parameter affecting the slope failures, as slope stability is very sensitive in changes on vegetation. For the necessities of this study, the land use, which reflects the vegetation covering, was classified into 5 categories as follows: (i) Barren areas, (ii) Urban areas, (iii) Forest areas, (iv) Shrubby areas – Natural grasslands, and (v) Cultivated areas.

Geometry of main discontinuities

The geometry of the main discontinuities in relation to slope geometry (aspect) is strongly related to the stability of hard soils, and soft rocks that dominate in the study area. Thus, the map of the main discontinuities was compiled using the relevant literature (Rozos 1989; IGME, 2005) and the observations during the fieldwork. The recorded dips and dip directions of the formations were digitized and saved as a map of GIS database. The formations without dip were characterized as “no data formations”. In a next step, the map was converted in raster format and combined to the aspect map for the correlation of the dip direction of strata with the slope aspect and classes like “drive against”, “drive sideways and vertical” “drive with” were formulated. Furthermore, the “drive with” class was combined with the angle of the slope and another three classes were created. Thus, the overall classes were as follows: (i) Drive against, (ii) Drive sideways and vertical, (iii) Drive with, having a dip of 1°-15°, (iv) Drive with, having a dip 16°-30°, (v) Drive with, having a dip of > 30°.

All the thematic layers of the instability parameters involved in this study are given in Fig. 3.

3. The Analytic Hierarchy Process (AHP) method

As a qualitative inhomogeneity is obvious in between the major parameters affecting slope stability, but also the influence of every one on landslide manifestation varies, the correlation and rating of these parameters and their classes were thought necessary.

This was done using Analytic Hierarchy Process (AHP) method, which includes a table with the numerical values of the binary comparison of the parameters. The binary comparison process is performed using a nine point scale, its numerical values of which with their corresponding level of im-

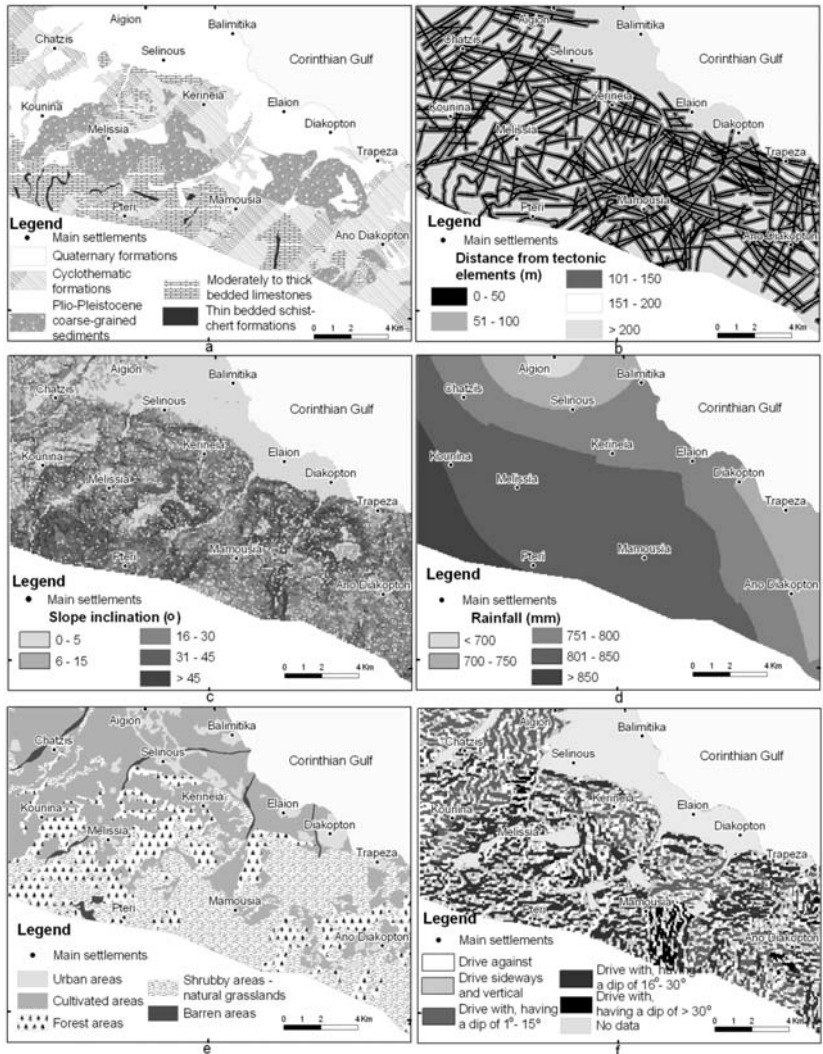


Fig. 3: Thematic maps of the instability parameters involved in this study and their classes. (a) lithology, (b) distance from tectonic elements, (c) slopes' inclination, (d) rainfall, (e) land use and (f) geometry of main discontinuities

portance are: 1 = equal, 3 = moderately, 5 = strongly, 7 = very strongly, 9 = extremely 2,4,6,8 = Intermediate values (Saaty, 1990). In the table used, every factor is weighted in relation to the others, and the derived numerical values, which range from 1/9 to 9, are placed in the correspondent cells. These values are subjective and represent the relative importance of one factor to the other regarding the adequacy for the seeking purpose. It is obvious that when the binary comparison is applied vice versa, the numerical value is the reciprocal of the initial. Then, the numerical values were normalized by diving each entry in a column by the sum of all the entries in that column, so that they sum up to 1. Following normalization, the values were averaged across the rows, in order to give the relative importance weight for each parameter.

The validity of AHP results is checked, by using consistency ratio (CR). This ratio is used in order to avoid the random choice in the AHP table. When CR is less than 0.1 the calculated weighting coefficients are acceptable. If the consistency ratio is higher than 0.1, a reassessment of judgements in the AHP table is demanded (Saaty, 1990). All the binary comparisons, the eigenvectors, the rates, the weights and the consistency ratio were calculated using the Expert Choice 11 software.

In this study, the instability parameters engaged and their classes were rated, engaging the experience and the field observations. The calculated ratings of the parameters and their various classes from the binary comparison and from CR of every matrix are shown in Table 1.

The aim of this analysis is every pixel of the thematic layers to gain a value, which represents the varied influence to landslide manifestation. For that reason the classes of every parameter were substituted by the numerical values derived from the rating. Next to that, the main parameters were interrelated with the same manner. Therefore, the weighting coefficients values were calculated. The results of the methods' application are shown in Table 2. As can be seen from this table, the parameter with the greater influence on landslide manifestation is slopes' inclination.

4. Results and discussion

Finally, and after the application of the AHP, a linear correlation was done between the weighting coefficients of the method and the raster layers of the principal parameters involved. The aim of this correlation was the total estimation of the ratings and thus, the compilation of the final landslide susceptibility map. This linear correlation is given by the formula:

$$O = \sum_{i=1}^n P_i W_i$$

Where, O = the overall score, n = the number of the parameters, Pi= the parameter i, and Wi = the weighting coefficient of the parameter i.

The produced landslide susceptibility map of the study area (Fig. 4) is territorially divided into four landslide susceptibility zones (low, medium, high, and very high), using the Quantile method, which was thought to be the proper one for the necessities of this study.

In this map the percentage extent of the susceptibility zones is 25.13% for the low zone, 25,22% for the moderate zone, 24,94% for the high zone, and 24,71% for the very high zone. The latter shows the higher territorial extent at the central and southwestern part of study area. The validity of the above map was checked by using the recorded landslides events in the area. For that purpose, the extent of landslides that laid on the distinguished landslide susceptibility zones, were counted using GIS capabilities. The derived percentages are: 9.33% for low zone, 29.19% for moderate zone, 28.83% for high zone, and 32.65% for very high one. These values, and especially for the last three zones, show a very good correspondence to those derived using AHP method, and thus revealing the validity of AHP application for compilation of landslide susceptibility maps.

5. Conclusions

From the above analysis and results, it is clear that a high percentage of the landslides in the study area belong to the zones of high to very high landslide susceptibility in the map, which was compiled, using AHP and GIS capabilities. The AHP is easy applicable, involves no complicated data, and its application is compatible with a GIS. Thus, the AHP and its methodology regarding the rat-

Table 1. The ratings of the classes of the major parameters used.

Parameters						Rating
Lithology	L1	L2	L3	L4	L5	
Moderately to thick bedded limestones(L1)	1	1/2	1/3	1/5	1/7	0,048
Thin bedded schist chert formations(L2)		1	1/2	1/4	1/6	0,073
Plio-Pleistocene coarse-grained sediments (L3)			1	1/3	1/5	0,115
Quaternary formations fine, fine –coarse to coarse, and loose to semi-coherent (L4)				1	1/3	0,253
Plio-Pleistocene fine-grained sediments and Flysch formations(L5)					1	0,510
<i>Consistency Ratio: 0,03</i>						
Distance from Tectonic elements	T1	T2	T3	T4	T5	
Nearest (0-50m)- (T1)	1	2	3	4	5	0,409
Very near (51-100m) - (T2)		1	2	3	4	0,256
Near (101-150m) - (T3)			1	3	4	0,183
Moderate distant (151-200m) - (T4)				1	3	0,097
Distant (>200m) - (T5)					1	0,053
<i>Consistency Ratio: 0,05</i>						
Slopes' inclination	S1	S2	S3	S4	S5	
0° – 5° (S1)	1	1/3	1/4	1/5	1/7	0,041
6° - 15° (S2)		1	1/4	1/6	1/8	0,060
16° - 30° (S3)			1	1/3	1/5	0,135
31° - 45° (S4)				1	1/3	0,259
> 45° (S5)					1	0,506
<i>Consistency Ratio: 0,08</i>						
Rainfall	R1	R2	R3	R4	R5	
< 700mm (R1)	1	1/2	1/3	1/4	1/5	0,062
700 - 750mm (R2)		1	1/2	1/3	1/4	0,097
751 - 800mm (R3)			1	1/2	1/3	0,160
801 - 850mm (R4)				1	1/2	0,263
>850mm (R5)					1	0,419
<i>Consistency Ratio: 0,06</i>						
Land use	LU1	LU2	LU3	LU4	LU5	
Barren areas (LU1)	1	1/2	1/2	1/4	1/6	0,063
Urban areas (LU2)		1	1/2	1/4	1/5	0,087
Forest areas (LU3)			1	1/2	1/3	0,143
Shrubby areas – Natural grasslands (LU4)				1	1/2	0,271
Cultivated areas (LU5)					1	0,437
<i>Consistency Ratio: 0,01</i>						
Geometry of main discontinuities	D1	D2	D3	D4	D5	
Drive against (D1)	1	1/2	1/4	1/5	1/3	0,057
Drive sideways and vertical (D2)		1	1/3	1/4	1/2	0,089
Drive with, having a dip of 1-15 (D3)			1	1/4	3	0,235
Drive with, having a dip 16-30°(D4)				1	4	0,490
Drive with, having a dip of > 30° (D5)					1	0,129
<i>Consistency Ratio: 0,06</i>						

Table 2. Weighting coefficients of every parameter involved.

	<i>P1</i>	<i>P2</i>	<i>P3</i>	<i>P4</i>	<i>P5</i>	<i>P6</i>	Weighting coefficient, W_i
P1	1	2	1/3	1/2	3	1	0,136
P2		1	1/3	1/2	2	1/2	0,090
P3			1	2	5	3	0,352
P4				1	4	2	0,218
P5					1	1/6	0,047
P6						1	0,158
Consistency Ratio: 0,03							
P1=Lithology, P2=Distance from Tectonic elements, P3= Slopes' inclination							
P4= Rainfall, P5= Land use, P6= Geometry of main discontinuities							

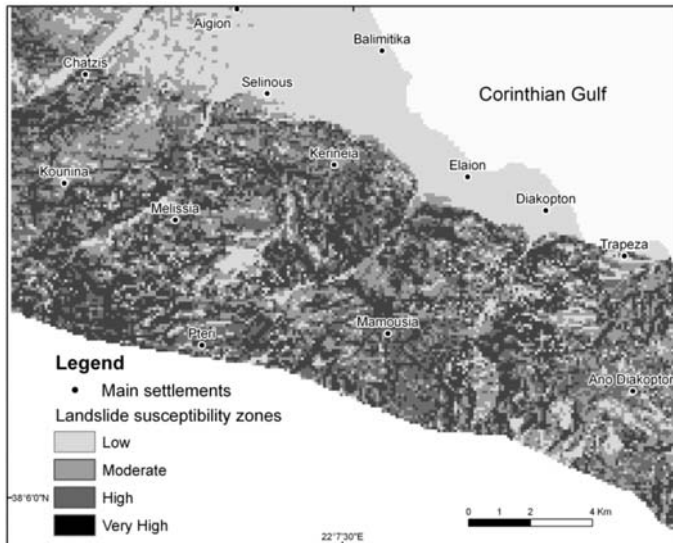


Fig. 4: Landslides susceptibility map

ing of the major parameters affecting landslides and their classes involved are valuable for compilation of a landslide susceptibility maps.

Therefore, AHP, supported by GIS capabilities, helps to the compilation of landslide susceptibility maps. This kind of maps can significantly helps in the urban planning and development of a site, a town or a county. To this direction, the landslide susceptibility map which was compiled during this study can be a useful guide for local Authorities, with regard to landslide confrontation and thus to the restriction of their damages in inhabited areas and technical works.

6. References

- Akgün, A., Dag, S., Bulut, F., 2008. Landslide susceptibility mapping for landslide-prone area (Findikli, NE Turkey) by likelihood-frequency ratio and weighted linear combination models. *Environmental Geology* 54, 1127-1143.
- Ayalew, L., Yamagishi, H. and Ugawa N., 2004. Landslide susceptibility mapping using GIS-based weigh-

- ted linear combination, the case in Tsugawa area of Agano River, Niigata Prefecture, Japan. *Landslides* 1, 73-81.
- Bathrellos, G.D., Kalivas, D.P., Skilodimou H.D., 2009. Landslide susceptibility mapping models, applied to natural and urban planning, using G.I.S. *Jou. Estudios Geológicos* 65(1), 49–65.
- Bossard, M., Feranec, J., Otahel, J., 2000. CORINE land cover technical guide – Addendum 2000. *European Environment Agency*, Copenhagen, p 104.
- Castellanos Abella, E.A. and Van Westen C.J., 2007. Generation of landslide risk index map for Cuba using spatial multi-criteria evaluation. *Landslides*, 4, 311–325.
- Doutsos, T., Kontopoulos, N., Poulimenos, E., 1988. The Corinth-Patras rift as the initial stage of continental fragmentation behind an active island arc (Greece). *Basin Research* p177-190.
- Guzzetti, F.; Carrara, A.; Cardinali, M. & Reichenbach, P., 1999. Landslide hazard evaluation: a review of current techniques and their application in a multi-scale study, Central Italy. *Geomorphology* 31, 181 – 216.
- IGME, 2005. Geological Map of Greece, at a scale of 1:50.000, Aigion sheet, Athens.
- Komac, M., 2006. A landslide susceptibility model using the Analytical Hierarchy Process method and multivariate statistics in perialpine Slovenia. *Geomorphology* 74, 17 – 28.
- Koukis, G. and Rozos, D., 1982. Geotechnical conditions and landslide movements in the Greek territory in relation to the geological structure and geotectonic evolution. *Mineral Wealth* 16, 53 – 69.
- Koukis, G., Rozos, D., Hatzinakos J., 1997. Relationship between rainfall and landslides in the formations of Achaia county, Greece. *Proc. of International Symposium of I.A.E.G. in Engineering Geology and the Environment, A.A. Balkema, Vol.1*, pp.793-798, Rotterdam.
- Koukis, G., Sabatakakis, N., Nikolaou, N., Loupasakis, C., 2005. Landslides hazard zonation in Greece. *Proc of open symp. on landslides risk analysis and sustainable disaster management by International Consortium on Landslides, Washington USA, Chapt 37* pp 291-296.
- Lan, HX., Zhou, CH., Wang, LJ., Zhang, HY., Li, RH., 2004. Landslide hazard spatial analysis and prediction using GIS in the Xiaojiang watershed, Yunnan, China. *Engineering Geology*, 76, 109 – 128.
- Rozos, D., 1989. Engineering-geological conditions in the Achaia County. Geomechanical characteristics of the Plio-pleistocene sediments. *Ph.D. Thesis, University of Patras*, 453p. Patras (in Greek, with extensive summary in English).
- Rozos, D., Pyrgiotis, L., Skias, S., Tsagaratos, P. 2008. An implementation of rock engineering system for ranking the instability potential of natural slopes in Grek territory. An application in Karditsa County. *Landslides* 5, 261–270.
- Rozos, D., Tsagaratos, P., Markantonis, K., Skias, S., 2006. An application of Rock Engineering System (RES) method for ranking the instability potential of natural slopes in Achaia County, Greece. *Proc. of XIth International Congress of the Society for Mathematical Geology*, S08-10, University of Liege Belgium.
- Saaty, TL., 1990. How to make a decision: The Analytic Hierarchy Process. *European of Operational Research* 48, 2–26.
- Saaty, TL., 2006. Rank from comparisons and from ratings in the analytic hierarchy/ network processes. *European of Operational Research* 168, 557–570.
- Sabatakakis, N., Koukis, G., Mourtas, D., 2005. Composite landslides induced by heavy rainfall in suburban areas. City of Patras and surrounding area, Western Greece. *Landslides, Springer Verlag* 2:202-211.
- Saha, AK, Gupta, RP., Arora, MK., 2002. GIS-based Landslide Hazard Zonation in the Bhagirathi (Ganga) Valley, Himalayas. *Int. J. Remote Sensing* 23(2), 357 – 369.
- Yoshimatsu, H. and Abe, S., 2006. A review of landslide hazards in Japan and assessment of their susceptibility using Analytical Hierarchy Process (AHP) method. *Landslides* 3, 149 -158.

A STUDY OF THE PERFORMANCE OF THE MODIFIED TRANSFORMED VEGETATION INDEX MTVI

Skianis G. Aim.¹, Gournelos Th.¹, Vaiopoulos D.¹, and Nikolakopoulos K.²

¹ University of Athens, Faculty of Geology and Geoenvironment, Department of Geography and Climatology, 157 84 Athens, Greece, skianis@geol.uoa.gr, gournelos@geol.uoa.gr, vaiopoulos@geol.uoa.gr

² Institute of Geological and Mineral Exploration (IGME), Olympic Village Entrance C, Aharnae 13 671, Greece, knikolakopoulos@igme.gr

Abstract

In the context of a recent research on the performance of vegetation indices we have shown, with the aid of probability theory, that the shape and width of the histogram of the Transformed Vegetation Index TVI is controlled by the ratio of the standard deviation of the Red band to that of the NIR band. Therefore a modification of the mathematical expression of the TVI vegetation index may produce images with a varying tonality contrast. In the present paper the modified transformed vegetation index MTVI is introduced, the value of which is controlled by a positive parameter c . A theoretical study of the effect of this parameter on the image histogram is first carried out and it is shown that changing c one can obtain MTVI images with different histograms and standard deviations. Experimentation with a satellite image over western Peloponnese verifies that the parameter c controls the shape of the MTVI histogram and, furthermore, the optical effect of the MTVI image as well as the spatial variation (semivariogram) of the pixel values. Therefore the proposed modified transformed vegetation index may help the potential user in broadening his/her choices to map the vegetation cover of the area under study.

Key words: vegetation index, TVI, MTVI, parameter c , standard deviation, semivariogram.

1. Introduction

The mapping of the land cover is essential for local and regional planning. Furthermore, studying the role of terrestrial vegetation is crucial in understanding how the earth functions as a system. A measure of the vegetation cover and green biomass may be obtained by calculating the vegetation index at each pixel of a multispectral image.

An abundance of vegetation indices have been proposed, in order to map vegetation cover. A comprehensive list of these indices is made by Jensen (2000). Most of the vegetation indices have been introduced and evaluated taking into account empirical criteria of response over land cover types of interest (Gitelson 2004, Malinis et al. 2004, Kale 2005, Silleos et al. 2006). Mathematical models which associate the vegetation cover with its reflectance at various spectral bands have also been developed (Goel 2008, Haboudaine et al. 2004). A probabilistic approach on the problem of the performance of a vegetation index has been proposed by Vaiopoulos et. al. 2004.

The transformed vegetation index TVI has been introduced by Deering et al. 1975. It has a particular interest, since it produces images with a strong tonality contrast, which may help in detecting burnt areas and soils with a poor vegetation (Skianis et al. 2007a, b).

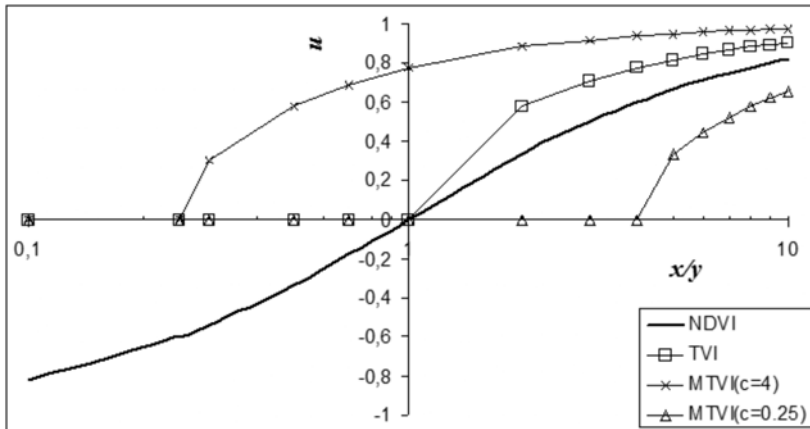


Fig. 1: NDVI, TVI and MTVI variation against x/y .

The TVI is defined by (Deering et al. 1975):

$$u = \begin{cases} \sqrt{\frac{x-y}{x+y}} & \text{for } x \geq y \\ 0 & \text{for } x < y \end{cases} \quad (1)$$

u is the value of the vegetation index x and y are the tonalities or reflectances of the Near Infrared and Red bands, respectively. This vegetation index may be alternatively expressed as $\sqrt{[(x-y)/(x+y) + 0.5]}$ in order to avoid negative values of the quantity under the square root, but in the present paper the definition of the TVI according to relation (1) is adopted.

Skianis et al. (2007b) have shown that modifying the expression for the TVI may produce images with a varying optical effect, which may be useful in recognizing targets of interest and mapping the land cover. The modified transformed vegetation index MTVI is defined by (Skianis et al. 2007b):

$$u = \sqrt{\frac{cx-y}{cx+y}} \text{ for } cx > y \quad (u = 0 \text{ if } cx \leq y) \quad (2)$$

c is a parameter which takes values between 0.1 and 10 and controls the tonality contrast of the image.

In Fig. 1 the variation of TVI and MTVI against x/y is presented, according to the relations (1) and (2). The behavior of the frequently used NDVI vegetation index, which has been introduced by Rouse et al. (1973) and is defined by $u = (x-y)/(x+y)$ is also presented. It can be observed that the MTVI takes higher values as long as c increases.

In this paper the statistical behaviour as well as the optical effect of the MTVI image is studied. First a mathematical expression for the MTVI histogram is derived, according to a probabilistic approach which has been developed by Vaiopoulos et al. (2004). The standard deviation is then calculated for various values of the c , in order to have a quantitative measure of the variation of the tonality contrast with this parameter. Then, the MTVI is applied on an ASTER image of the area of Olympia (western Peloponnese) in order to assess the optical effect and study the spatial variation of the produced MTVI images.

2. The MTVI histogram, according to the probabilistic approach

In order to study the statistical behaviour of the MTVI vegetation index, the histograms of the NIR and Red bands, x and y respectively, have to be simulated by a proper distribution. It is reasonable to assume that this distribution is zero for a null brightness value, presents a peak at a relatively low value of the tonality range and gets practically nullified at high brightness values. In practice, the histogram may be more complicated and present more than one peaks, but it is reasonable to be approximated by a simple distribution, which may help the mathematical analysis.

Vaiopoulos et al. 2004 have proposed distributions p of the form $p(x)$ (or $p(y)$) $\sim x \cdot \exp(-ax^2)$ (or $p(y) \sim y \cdot \exp(-ay^2)$), in order to describe the histograms of x and y bands. In the same paper, it has been derived the expression for the distribution $g(u')$ of the values u' of the MNDVI vegetation index, which is defined by (Vaiopoulos et al. 2004):

$$u' = \frac{cx - y}{cx + y} \quad (3)$$

c is the same parameter which appears in relation (2) for the MTVI vegetation index.

According to Vaiopoulos et al. 2004, $g(u')$ is given by:

$$g(u') = \frac{4\lambda c^2(1 - u'^2)}{[\lambda(1 + u')^2 + c^2(1 - u')^2]^2} \quad (4)$$

λ is given by (Skianis et al. 2007a):

$$\lambda = \left(\frac{\text{stdev}(y)}{\text{stdev}(x)} \right)^2 \quad (5)$$

The u values of the MTVI are related to the u' values of the MNDVI, by $u' = u^2$, for $u' \geq 0$ (or $cx \geq y$). According to Spiegel 1977, the distribution $g(u)$ of the MTVI values is related to $g(u')$ by:

$$g(u) = g[u'(u)] \cdot \left| \frac{du'}{du} \right| \quad (6)$$

Combining the relations (4) and (6) and taking into account that du'/du gives:

$$g(u) = \frac{8\lambda c^2(1 - u^2)u}{(1 + u^2)^3 \left[\lambda + c^2 \left(\frac{1 - u^2}{1 + u^2} \right)^2 \right]^2} \quad \text{for } u' \geq 0 \text{ (or } cx \geq y) \quad (7)$$

For $u' < 0$, or $cx < y$, u is equal to zero, according to relation (2). The percentage $g(0)$ of the null TVI values, is given by:

$$g(0) = \int_{-1}^0 g(u') du' \quad (8)$$

Combining relations (4) and (8) gives:

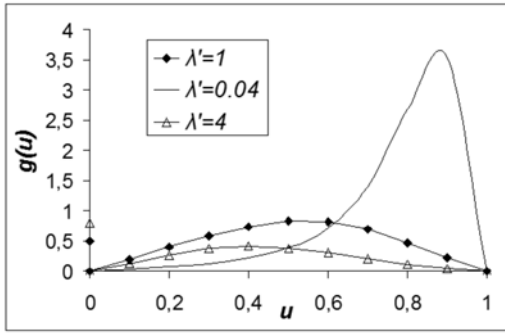


Fig. 2: The distribution $g(u)$ of the MTVI values, for various λ' values.

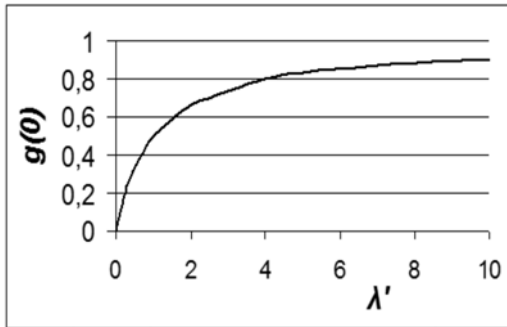


Fig. 3: The percentage $g(0)$ of the zero MTVI values against λ' .

$$g(0) = \frac{\lambda}{\lambda + c^2} \quad (9)$$

For convenience in the further statistical treatment, the quantity λ' is introduced, which is defined by:

$$\lambda' = \lambda c^2 \quad (10)$$

According to relations (7), (9) and (10), the expression for $g(u)$, which describes the histogram of the MTVI image, is:

$$g(u) = \begin{cases} g(0) = \frac{\lambda'}{\lambda'+1} & \text{for } cx < y \\ \frac{8\lambda'(1-u^2)u}{(1+u^2)^3 \left[\lambda' + \left(\frac{1-u^2}{1+u^2} \right)^2 \right]^2} & \text{for } cx \geq y \end{cases} \quad (11)$$

There is a remarkable similarity between the expression for the distribution $g(u)$ of the MTVI values (relation (11)) and that of the TVI values (Skianis et. al. 2007a). The only difference is that in the former the parameter λ' appears, while in the latter parameter λ appears instead.

In Fig. 2 the distribution $g(u)$ of the MTVI values for various λ' values is presented. As long as λ' decreases (which means that c increases) the peak of the distribution is shifted to the right. On the other hand, as it can be seen in Fig. 3, as long as c increases (λ' decreases), the percentage $g(0)$ of

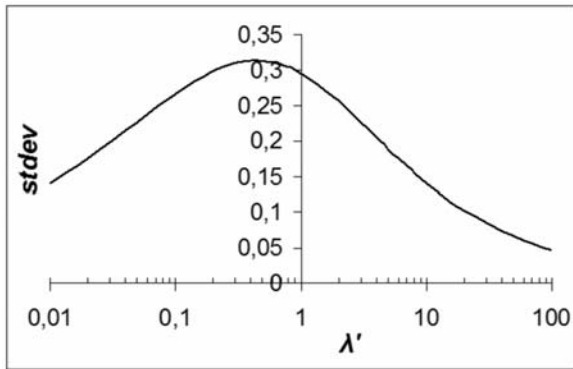


Fig. 4: The *stdev* variation of the MTVI values against λ' .

the null values -in other words the percentage of the image pixels with null tonality- decreases. Therefore for high c values the MTVI image is expected to be bright. Low c values are expected to produce dark images.

The standard deviation *stdev* of $g(u)$, which describes the MTVI image histogram, was numerically calculated for various λ' values. In Fig. 4, the *stdev* variation against λ' is presented. It can be observed that the *stdev* takes a maximum at $\lambda' \cong 0.5$, which, according to relation (10), gives $c \cong \sqrt{(2\lambda)}$. For this value of c the MTVI image is expected to have a maximum standard deviation, therefore the strongest tonality contrast.

The probabilistic approach gave a picture of how the parameter c influences the optical effect and statistical behavior of the MTVI image. Theoretical predictions have to be tested with real data, obtained by satellite images.

3. Experimentation with a satellite image



Fig. 5: A TVI ASTER image of a part of Western Peloponnese around Alfios river.

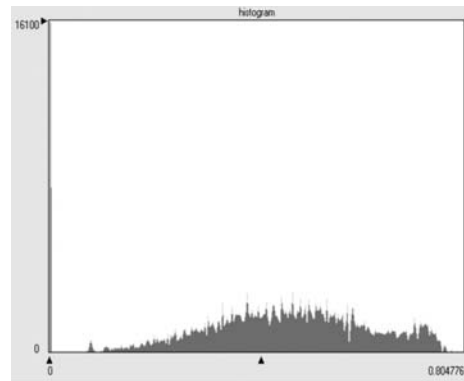


Fig. 6: The histogram of the TVI image.

The MTVI vegetation index, for various c values, was applied in a satellite ASTER image of July 2008, around the region of Olympia (western Peloponnese). The ratio λ of the satellite image was found to be equal to 1.006. The MTVI images were produced using ERDAS Imagine software. A special tool to calculate the MTVI values was developed, using the spatial modeller of this software. In Fig.5, the TVI image ($c = 1$) of the area is presented. Alfios river is expressed with a curved

line at the middle of the image, with direction East West. At the upper left and upper right part of the image the tonality is quite dark and expresses burnt areas (the fire took place one year before the acquisition of the image). Burnt areas with dark tonalities are also present at the middle of the image, below the river. Areas with dense vegetation and agricultural land are expressed with bright tones. In Fig. 6, the histogram of the image is presented. A great number of pixels have a null tonality and the others take values up to 0.885.

In Fig. 7 the MTVI image of the same area, for $c = 0.5$, is presented. It can be observed that the image has an overall dark tonality, which is also expressed in the image histogram of Fig. 8. The histogram is apparently blank because most pixels have null or very small tonalities. Therefore a small c value (less than unity) produces an MTVI image with dark tones and u values accumulated at zero point.

In Fig. 9 the MTVI image for a high c value equal to 4 is presented. The image is considerably brighter than those of Figs 5 and 7 and the MTVI histogram of Fig. 10 is shifted to the right.

The observation of the TVI and MTVI images shows that there is an accordance, in qualitative terms, between theoretical predictions and real data. Low c values produce dark images and histograms shifted to low u values, while high c values produce bright images with histograms shifted towards high u values.

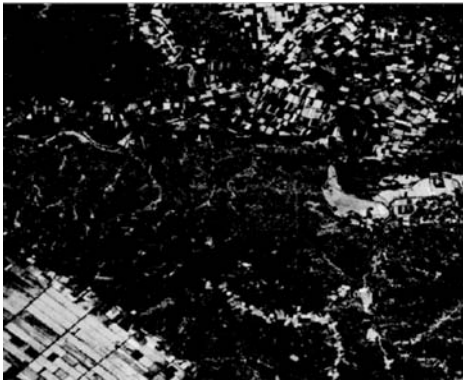


Fig. 7: The MTVI ASTER image for $c = 0.5$.

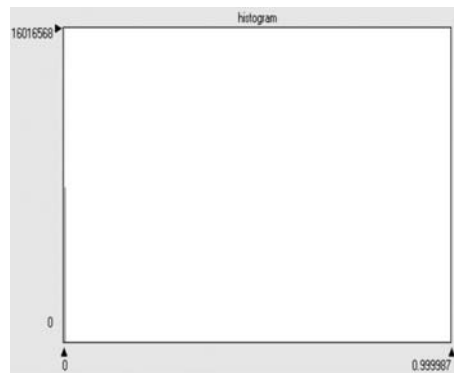


Fig. 8: The MTVI histogram for $c = 0.5$.



Fig. 9: The MTVI ASTER image for $c = 4$.

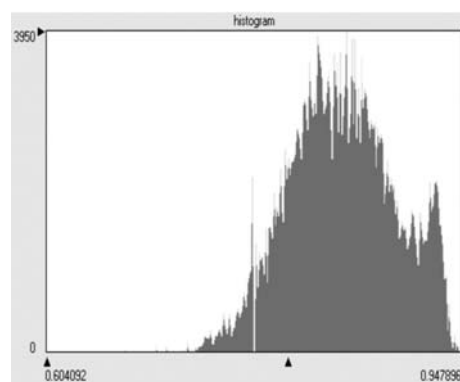


Fig. 10: The MTVI histogram for $c = 4$.

No histogram stretch was applied on the images of Figs 5, 7 and 9. The dark tonality of the MTVI image for $c = 0.5$ (Fig. 5) does not favour the different land cover types to be expressed clearly. If a

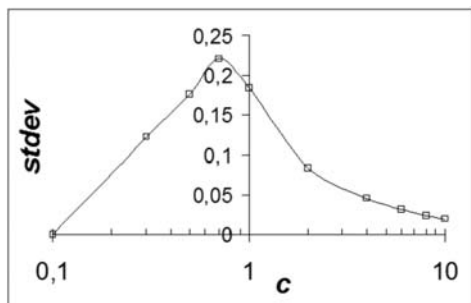


Fig. 11: The standard deviation of the MTVI ASTER images of part of western Peloponnese against c .

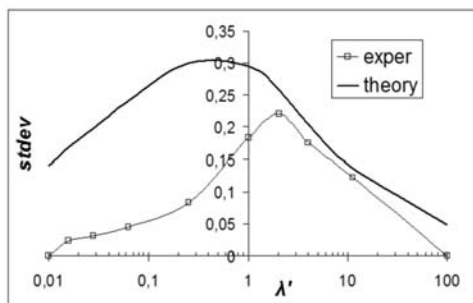


Fig. 12: Theoretically predicted and actual standard deviation values of the MTVI ASTER images against λ' .

linear histogram stretch is applied on this image, the vegetation cover, as well as the river zone, are expressed with very bright tonalities, in contrast to the dark tonality of the other formations.

In the MTVI image for $c = 4$ (Fig. 9) the eastern part of Alfios river is expressed with a dark tonality which is considerably lower than that of the other parts of the river. Particularly this tonality contrast is not so strong in the TVI image (Fig. 5). Actually a high c value (more than unity) produces images with a diversification in the tonalities of dark areas. Therefore the parameter c controls the contrast of the MTVI image, as well as the optical effect by which the various land cover types are expressed.

In order to study in quantitative terms the performance of the MTVI vegetation index on the ASTER image, the standard deviation (*stdev*) of the MTVI histogram for each c was calculated. In Fig. 11 the variation of the *stdev* of the produced MTVI images against c is presented. It can be observed that the *stdev* takes its maximum value for $c = 0.7$. According to the theoretical predictions, the peak should be at $c = \sqrt{2\lambda} = 1.4$ (since the λ value of the ASTER image is equal to unity). Actually, in quantitative terms, there are deviations between theoretically predicted and actual *stdev* values, as it can be seen in Fig. 12. The differences are smaller for high λ' ($=\lambda/c^2$) values and bigger for low λ' values.

The deviations between theory and actual data should be attributed to the assumptions upon which the probabilistic approach is based. The assumptions are: a) to describe the histograms of the NIR and Red bands can be described by simple distributions $p(x) \sim x \cdot \exp(-ax^2)$, b) the reflectances of the NIR and Red bands are independent each other (Vaiopoulos et al. 2004). Actual histograms are more complicated than the distribution p and a considerable correlation between NIR and Red values exists.

On the other hand there are similarities in the behaviour of the theoretical and actual *stdev* curves of Fig. 12. Both curves present a maximum around $\lambda' = 1$ and relatively high (low) actual *stdev* values correspond to high (low) theoretically predicted ones.

As a general comment, it can be stated that the probabilistic approach and the experimentation with the ASTER image showed that the parameter c in the expression for the MTVI tunes the optical effect and the standard deviation (in other words the tonality contrast) of the MTVI image.

Since the standard deviation is only a measure of the width of the contrast and does not provide any direct information about the spatial variation of the MTVI values, it is important to study this issue using a proper geostatistical function.

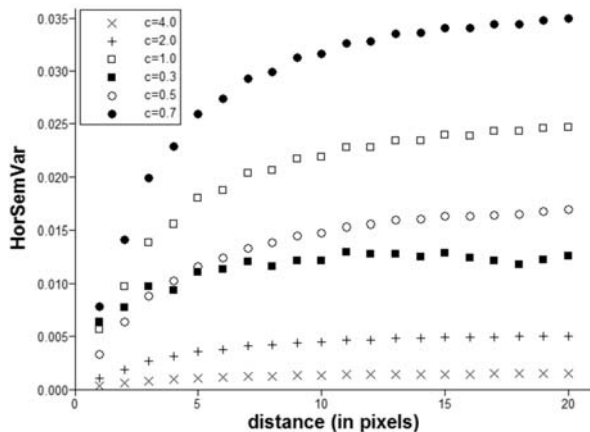


Fig. 13: The horizontal semivariograms of MTVI images for different c values.

4. The spatial variation of the MTVI images

The semivariogram of a digital image represents the variance of the tonality differences between pixels at various distances each other, therefore it provides information of the spatial variation of the tonality. The semivariograms of the MTVI images, for different c values were calculated, in order to see how the MTVI values vary in space. The ILWIS software was used for this purpose.

In Fig. 13 the horizontal semivariograms of MTVI images, for different values of c , are shown. The vertical semivariograms are not presented, since they have the same behaviour and small differences in the values of the semivariogram functions. It can be observed that the semivariogram of the MTVI image with $c = 0.7$ increases with distance more rapidly than all the others. Comparing Figs 11 and 13, one can see that the MTVI image of this c value has the biggest standard deviation. It can also be observed that as long as the standard deviation in Fig. 11 decreases, the values of the respecting semivariogram function also decrease. The same relation between standard deviation and spatial variation has also been observed in the case of an other vegetation index which was applied on a satellite image over a different area (Skianis et al. 2009). This remark indicates, without proving, that a high standard deviation of the image histogram corresponds to a strong spatial variation of the tonality of the image. If this is correct, then the probabilistic approach, although it is centered on the image histogram, may also provide information about the spatial variation of the image tonality. A further experimentation with satellite images of different areas, possibly combined with theoretical considerations, could be the subject of a future paper.

5. Conclusions

According to the mathematical analysis and the experimentation with the satellite image, two main conclusions can be drawn:

The standard deviation of the MTVI image depends on the ratio λ/c^2 . For a certain value of c , which does not differ much from λ , the standard deviation and spatial variation of the values of the MTVI image become maximum and the tonality contrast appears strong.

Changing c , MTVI images with different a different optical effect are produced. Targets that are not expressed clearly in an MTVI image with a certain c may appear with a more pronounced tonality contrast in an image of another c value.

The results and conclusions of this paper may help in the photointerpretation of the satellite image, in order to map burnt areas, different land covers and related morphological features. The MTVI may also serve as a tool to estimate important biophysical parameters such as leaf area index, percentage green cover and chlorophyll content, which control the behaviour and the evolution of an ecosystem, as well as the function of the system of the earth as a whole.

6. References

- D. Haboudane, J. R. Miller, E. Pattey, P. J. Zarco-Tejada, I. B. Strachan, 2004. Hyperspectral vegetation indices and novel algorithms for predicting green LAI of crop canopies: Modeling and validation in the context of precision agriculture. *Remote Sens. Environ.* 90, 337-352.
- Deering, D. W., Rouse, J. W., Haas, R. H., and Schell, J. A., (1975). Measuring Forage Production of Grazing Units from Landsat MSS Data. *10th International Symposium on Remote Sensing of Environment 2*, 1169-1178.
- Gitelson, A. A., 2004. Wide Dynamic Range Vegetation Index for Remote Quantification of Biophysical Characteristics of Vegetation. *Journal of Plant Physiology* 161, 165-173.
- Goel, N. S., 1988. Models of vegetation canopy reflectance and their use in estimation of biophysical parameters from reflectance data. *Remote Sens. Rev.* 4, 1-212.
- Jensen, J. R., 2000. *Remote Sensing of the Environment*. Prentice Hall. 544 pages.
- Kale, M., Singh, S. and Roy, P. S., 2005: Estimation of Leaf Area Index in dry deciduous forests from IRS-WiFS in Central India. *International Journal of Remote Sensing* 26(21), 4855-4867.
- Mallinis, G., Koutsias, N., Makras, A., Karteris, M., 2004. An assessment of the Information Content of Landsat -5 TM Bands for the estimation of forest stand parameters in Kassandra peninsula. *Proceedings of the 7th Panhellenic Geographical Congress*, Mytilini (Greece), October 14th-17th 2004, Vol. II, 415-422.
- Rouse, J. W., Haas, R. H., Schell, J. A., and Deering, D. W., 1973. Monitoring vegetation systems in the Great Plains with ERTS. *3rd ERTS Symposium*, Vol. 1, 48-62.
- Silleos, N. G., Alexandridis, T. K., Gitas, I. Z., and Perakis, K., 2006. Advances made in Biomasa Estimation and Vegetation Monitoring in the last 30 years. *Geocarto International* 21(4), 21-28.
- Skianis G. Aim., Vaiopoulos D., Nikolakopoulos K., 2009. Testing the performance of the MNDVI vegetation index. *SPIE Proceedings*, vol. 7472, *Remote Sensing of Agriculture, Ecosystems and Hydrology XI*, C. U. Neale, A. Maltese (Eds), 747204. DOI: 10.1117/12.830262.
- Skianis G., Vaiopoulos D., and Nikolakopoulos K., 2007a: A Comparative Study of the Performance of the NDVI, the TVI and the SAVI Vegetation Indices over burnt areas, using probability theory and spatial analysis techniques. *Proceedings of the 6th International Workshop of the EARSeL Special Interest Group on Forest Fires*, 27-29 September 2007, Thessaloniki-Greece, 142-145.
- Skianis, G. Aim., Vaiopoulos, D., Nikolakopoulos, K., 2007b. A Probabilistic Approach to the Problem of Assessing the Efficiency of the Transformed Vegetation Index. *Int. J. Sus. Dev. Plann.* 2(4), 461-480.
- Spiegel, M. R., 1977. *Probability and Statistics*. ESPI, Athens. 384 pages.
- Vaiopoulos, D. A., Skianis, G. A., Nikolakopoulos, K., 2004 . The contribution of probability theory in assessing the efficiency of two frequently used vegetation indices. *International Journal of Remote Sensing* 25(20), 4219-4236.

GIS- BASED APPLICATION FOR GEOTECHNICAL DATA MANAGING

Tsangaratos P.¹, Koumantakis I.², Rozos D.³

¹ National University of Athens, School of Mining and Metallurgical Engineering, Department of Geology, Laboratory of Engineering Geology and Hydrogeology, Iroon Polytechniou, 15780, Zografou, Greece, ptasag@metal.ntua.gr

² National University of Athens, School of Mining and Metallurgical Engineering, Department of Geology, Laboratory of Engineering Geology and Hydrogeology, Iroon Polytechniou, 15780, Zografou, Greece, mmgski@central.ntua.gr

³ National University of Athens, School of Mining and Metallurgical Engineering, Department of Geology, Laboratory of Engineering Geology and Hydrogeology, Iroon Polytechniou, 15780, Zografou, Greece, rozos@metal.ntua.gr

Abstract

The need to provide data management capabilities in geotechnical projects, makes data visualization in a more understanding way vital, while improvements in computer science, have created an opportunity to rethink the manner in which such data is archived and presented. Geographic Information Systems are considered nowadays as principal methods for analysis, utilizing their ability of manipulating, compiling and processing spatial data, such as geotechnical one.

In this paper, the development of Borehole Analysis System (BAS) a specific Graphical User Interface (GUI) application is proposed to access geotechnical data with the aim of a relational database and an open source GIS platform, embodied in the application. The BAS, is able to integrate multiple layers of gathered information and to derive additional knowledge by applying statistical and data mining algorithms with the use of spatial query tools. These can give reasonable conclusions and better representation in 2-D and 3-D environment.

The presented application is illustrated with an example from field practice, testifying its ability to be a useful tool for management and presentation of geological and geotechnical borehole data.

Key words: Geotechnical Data, Statistical Analysis, K-Means, GIS.

1. Introduction

The common practice was and in some extent still is, to report geotechnical data as borehole logs and laboratory spreadsheets as a supplement of geotechnical surveys that follows the planning, and designing of any civil engineering projects. 2-D graph or map is thought to be the basic tool of communication in geological science. However in the case of a borehole log, the most important document in a geological modelling, a 3-D environment is converted to a 2-D plane consequently with the loss of the third dimension, producing uncertain patterns of objects with similar properties. Geotechnical characterization of large civil engineering projects typically requires 3-D data such as stratification of soil types, elevation of water table, soil properties at various depths producing large

volumes of data that are difficult to manage and analyze (Adams, 1994). The applied procedure followed for manipulating multiple data from different locations involves, the opening of many different achieves, overlay series of papers, maps, photos, geotechnical surveys and spreadsheets, demanding a great amount of time and considerable effort. The common practice in order to be more productive implies averaging techniques with uncertain outcomes, which certainly influence the design and planning parameters of any project (Luna and Frost, 1998).

However, from that early practice, the introduction of Information Systems and Technology in geotechnical science had significantly changed the process of collecting, retrieving, analyzing and visualizing geotechnical data (Foster and Culshaw, 1990; Laxton and Becken, 1996; Bain and Giles, 1997; Pininska and Dziedzic, 2004; Denas et al, 2005; Lan and Martin, 2007). Moreover, Geographic Information System (GIS), has emerged to be a powerful computer-based technique that integrates spatial analysis, database management, and graphic visualization capabilities (MacCarthy and Graniero, 2006; Kaufmann and Martin, 2008). Many research tools and commercial software packages as those discussed by MacCarthy and Graniero (2006), have as main objective to discover similar patterns in spatially distributed geotechnical data. Those systems although they contain powerful features for statistical analysis, visualization and data exploration, in most cases they provide strict structural requirements for data input, limiting the user's freedom to structure his own data, while other software are developed on specific platforms or as an extension of commercial software narrowing its use and interoperation with other tools.

The Borehole Analysis System (BAS), a specific Graphical User Interface application, introduced in this paper, is presented as a tool to aid in the management, querying, data mining, and visualization of geotechnical data. It is capable to integrate multiple layers of gathered information, and to derive additional information visualizing them in a more easy-to-use way. This enables the production of maps with unlimited data, introduced in the form of attributes, layers and combinations of these. It fulfils the desire to visualize spatial patterns in data that may not be so obvious when presented in tabular format, establishing links with borehole and cross sections, processing spatially the data onto 2-D and 3-D environment. Finally data mining algorithms were applied, clustering data in such a manner that areas could be identified having certain characteristics or set of characteristics and seek knowledge from their locations and distribution.

2. Designing and compiling the application

The target was to develop an easy-to-use open source application, not to replace existing modelling techniques and known commercial software, but rather to serve as a geotechnical data manager assistant. In this way expert would be able to determine the geotechnical behaviour of the formations in a given research area, using interactive displays and visual correlation, but also saving time and working productive with considerable less effort.

The basic functions that it should supply the users, includes: a) a tool to import data in specific template or by structuring data manual according to users needs (Data Input Manager), b) a tool to apply simple data mining algorithms along with classical statistical analysis to identify similar physical or mechanical characteristics and draw correlations (Statistical / Data Mining Manager), c) a tool to indicate queries (Query Builder Manager) and finally d) a tool to visualize the outcomes in 2-D and 3-D environment (Visualization Manager).

The application has a graphical interface and has been developed with the use of Visual Basic 6.0 (VB6), a third – generation event driven programming language. The relational database, that is

constructed to contain geological, geotechnical and other related data, was embodied in the application by Structured Query Language (SQL) connection. It's implemented on the Microsoft Jet Engine, storing data in Microsoft Access Database, guarding an easy access, management and updating of data. Clustering algorithms (K-Means algorithm), written in VB6 code, were also embodied to source code in order to cluster data with similar characteristics providing an indication of the engineering behaviour. Finally the data were able to be manipulated and spatial analyzed by using the MapWindow GIS ActiveX Control. MapWindow project started in 1998 at Utah Water Research Lab at Utah State University as an alternative to using ESRI MapObjects LT 1.0 for custom applications. It is also defined as an open source GIS (mapping) code and set of programmable mapping components, capable for storing and spatial analysis, as well as properly modified and embodied in the applications source code (Dunsford and Ames, 2008).

3. Basic Functions and tools

Running BAS is practically a three step procedure. In the first step the user provides the application with all the available data, in the second step the application creates the needed files for analysis and in the final step the user is able to query, explore and analyse but also to visualize the data in 2-D or 3-D environment, through the appropriate functions and tools.

The obtained information is derived from existing borehole logs, field and laboratory test spreadsheets, geological, hydro-geological and geotechnical surveys, available topographic, hydrological, hydro-geological, and infrastructure information, aerial photos, boring photos, etc. The main objective during data pre-processing is to convert all the available data into digital format and import them to the system, such as maps, road infrastructure, topographic contours, and points of interest. Photos from boreholes are scanned and imported in the database. It is thought to be the most important phase as the quality and quantity of data determines the outcomes of the implementation of the system. The main functions and tools embodied in the BAS are described in more details in the following paragraphs.

3.1 Data Input Manager

The application provides a Data Input Manager which archives information concerning borehole identifiers and location data (x, y, z coordinates), such as columns containing sample depths, lithological and formation descriptions, columns with physical and mechanical properties, photos and scanned information maps. While using the Data Input Wizard the user has two options: to manually collect information by linking each data with the appropriate field names, or to import data using a specific template provided by the application. The database used, is built having five primary tables (project-info, borehole-info, physical-info, mechanical-info, description-info), which contained different types of information, categorical and numerical, but also spatial and non-spatial components. The key field to link each table was the Borehole Boring _ID (Tsagaratos, 2008). After the completion of the data input process the application creates the appropriate shapefile and adds it to the projects table as data point files. In addition, the user is able to create his own shapefiles by selecting the attributes of interest applying either Data mining Manager or Query Builder Manager.

3.2 Statistical and Data Mining Manager

By the utilization of statistical analysis the application could provide an indication of the range of variation and the distribution of geotechnical parameters in each lithostratigraphic unit, obtaining me-

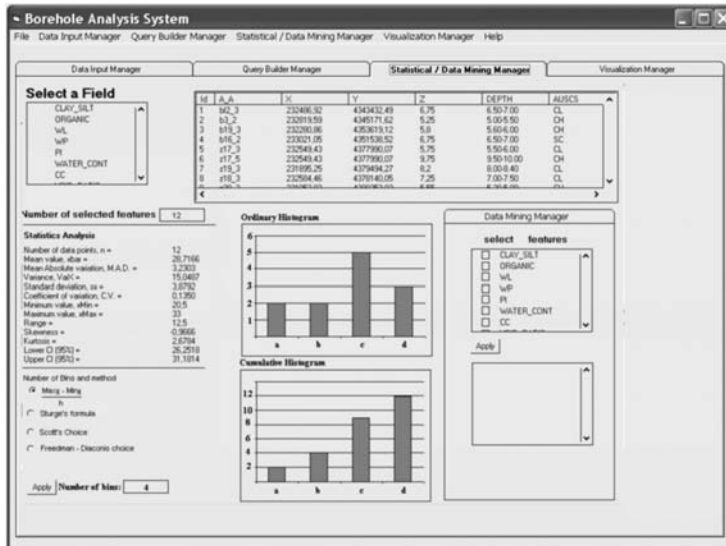


Fig. 1: Screenshot of Statistical / Data Mining Manager

dian, mode, mean, and standard deviation values. Moreover measuring asymmetry (skewness) and whether the data are peaked or flat relative to a normal distribution (kurtosis) is of valuable importance. High values of skewness and kurtosis indicate that data are not normally distributed, thus one could approximately expect that the variable in question tends not to cluster around the mean value. In addition more advanced statistical analysis could be initialized. Specifically by applying Pearson's test, the degree to which each one of the data parameters included in the database varies linearly with another could be calculated giving a more precisely knowledge of the geological environment. Moreover, Kendall's tau test (Daniel 1990), could be initialized when there is no linear relationship among the variables involved in the model. The Kendall' tau test measures the degree of concordance or discordance between two random variables, ranging also from -1 to +1, indicating respectively perfect, negative and positive correlation. The test can also be used to establish whether a random variable should be addressed as independent, if there is a significant spatial trend which would result in dependency (Jaska, 1995; Uzielli et al, 2004).

The statistical analysis and also graphical plots were used to prepare detailed reports and surveys describing the geotechnical properties of the materials, their engineering behaviour but also producing maps showing their distribution in the area of interest (Fig. 1).

The integration of data analysis and data mining techniques ultimately aims to the discovery of interesting, implicit and previously unknown knowledge hidden in the geotechnical database. The application provides an algorithm for clustering data. Clustering can be considered the most important unsupervised learning problem grouping sets of objects into clusters of similar objects. Applying these techniques on geotechnical data could be useful in identifying different lithology or formations with specific relative values and frequencies or distributions of certain attributes (Goktepe et al, 2005). In this application, K-Means algorithm (MacQueen, 1967) was utilized, which is considered as one of the simplest unsupervised learning algorithms that solve the well known clustering problem. The procedure follows a simple and easy way to classify a given data set (n observations) by implementing either the option that assumes a certain number of clusters (k clusters) fixed a priori,

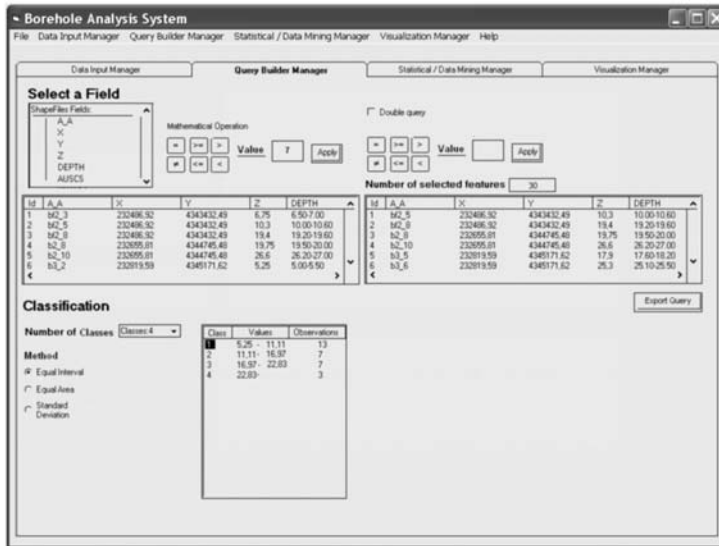


Fig. 2: Screenshot of Query Builder Manager

or the option of finding the optimum number through the data, in which each observation belongs to the cluster with the nearest mean.

3.3 Query Builder Manager

The Query Builder Manager along with the Statistical and Data Mining Manager are the most powerful tools in the developed application (Fig.2). The former can be helpful in identifying patterns of similar behaviour. It's used to combine categorical or numerical query terms into a single or complex query.

For example it could enable all boreholes that contain a particular formation or lie within a defined area, with relative information available at a point defined by grid coordinates, or within a defined lithostratigraphic unit. It could be also find a segment or lithostratigraphic unit with a particular set of physical or mechanical properties necessary to meet the design criteria for a specific engineering application. It's also the main tool to prepare the data for further analysis, as it builds the appropriate shapefiles.

3.4 Visualization Manager

The visualization tools were designed to visualize data, linking borehole photos, logs and cross-sections, physical and mechanical properties, based on a response to query parameters and data mining results or simply visualize the whole database (Fig. 3, 4). The application has also the ability of visualizing data in a 3D environment presenting the spatial distribution of the query or data mining results.

4. Applying the methodology and results

The database consisted of 39 boreholes data, derived from a civil engineering project located at the western part of Greece and involves the construction of the **Ionina Odos**, Ionian Highway. The total

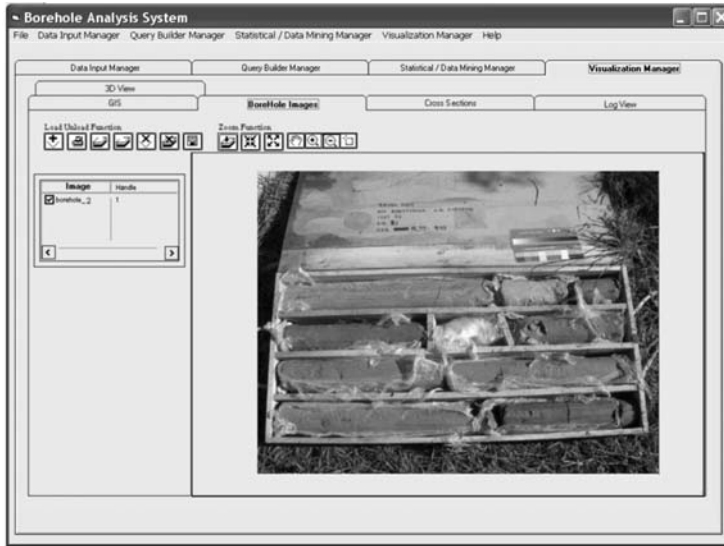


Fig. 3: Screenshot of Borehole Image / Visualization Manager

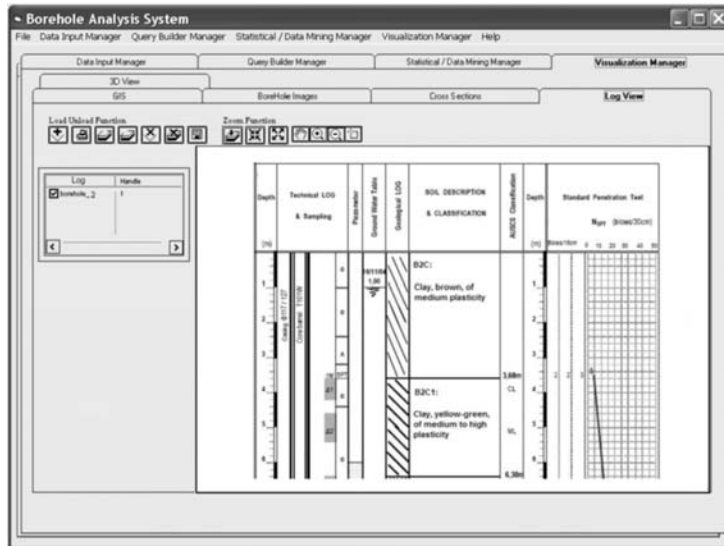


Fig. 4: Screenshot of Log View / Visualization Manager

length of the motorway will be 384 km, becoming part of the E55 highway in its full length. In the presented application we used data from the section that begins from Rio, Patras and ends at the town of Ioannina. It includes physical and mechanical properties obtained by engineering geological surveys, aerial photos, and log photos, collected and evaluated during the design phase of the project. After importing into the system the available data (1st phase), the aim was to quantify the degree of spatial variation of the physical and mechanical properties of the studied soils and thus obtain a more meaningful estimate at unsampled locations but also to provide input to reliability analyses. The main

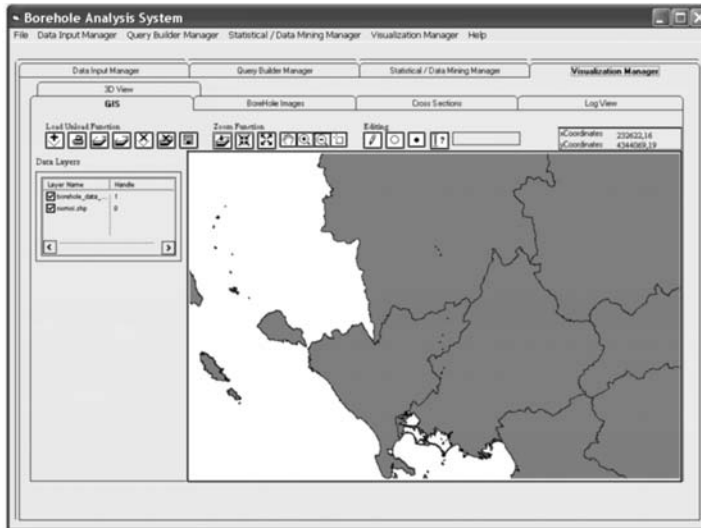


Fig. 5: Screenshot of GIS View / Visualization manager

steps were: a) perform statistical analysis for the entire database, describing the variation that the geotechnical parameters have and also using the Query Builder Manager to perform statistical analysis in specific areas, b) find the correlations between the variable used in the analysis, c) determine which variables would be included in the data mining process, and finally d) interpret the results in accordance with the available geotechnical surveys, evaluate and provide additional knowledge.

The mean value and the standard deviation, considered as the best estimate and the uncertainty of the best estimate respectively. In descriptive statistics the coefficient of variation, appears to be dimensionless. In most cases, it provides a more physically meaningful measure of dispersion relative to the mean value. When comparing between data sets with different units or widely different means, the coefficient of variation is better to be used instead of the standard deviation as can be illustrated below. Table 1 shows the results of the descriptive statistical analysis.

It seems that parameter of Plasticity Index PI, a parameter of great importance in geotechnical engineering, is the one with the higher value of coefficient of variation, while parameter Plastic Limit (W_p) the one with the lowest, having great spatial variation and varying behaviour response within the same area. The knowledge of variation for each parameter is more reliable when referred to each lithostratigraphic unit or within a specific segment of known depth. To focus our analysis in those areas the Query Builder Manager was used, following either the classification used in the log files, and applying the statistical analysis in the lithostratigraphic unit CH, or producing segments of certain depth, by applying simple methods of classification (equal intervals, equal area, and standard deviation). The lithostratigraphic unit CH refers to inorganic clay of high plasticity. It is used in the analysis as an example since it appears as the most dominate unit throughout the research area. During the first analysis, for the entire database, PI appeared with the highest value of coefficient of variation. However, it does not appear as such, within the CH lithostratigraphic unit, but also within the 10m depth segment that was produced by the Query Builder. From the above analysis it is obvious that each parameter varies differently in respect to different lithostratigraphic units, or within different segments of certain depth.

Table 1.

Statistical Analysis applied to the entire database						
Parameters	W_L	W_p	P_I	W_c	C_c	V_r
Mean Value	45,38	23,40	21,98	26,536	0,153	0,723
Variance	168,24	14,394	115,719	47,588	3,3711E-02	3,2724E-02
Standard Deviation	12,97	3,794	10,757	6,898	5,8061E-02	0,1808
Coefficient of variance	0,285	0,1620	0,4894	0,2599	0,3774	0,2501
Minimum	20,2	14,1	1,3	8,3	0,051	0,238
Maximum	66,2	32,3	36,2	42,6	0,279	1,15
Range	46	18,2	34,9,6	34,3	0,228	0,911
Skewness	-0,3429	0,1628	-0,4215	-0,4418	0,2281	-0,3349
Kurtosis	2,1118	3,1251	1,8546	3,5297	2,2985	3,5596
Statistical Analysis applied to the CH lithostratigraphic unit						
Parameters	W_L	W_p	P_I	W_c	C_c	V_r
Mean Value	57,207	25,615	31,593	29,115	0,174	0,785
Variance	25,672	7,963	12,184	3,265	3,4673E-03	1,3711E-02
Standard Deviation	5,0667	2,8218	3,4905	4,2537	5,9048E-02	0,117
Coefficient of variance	8,8568E-02	0,1101	0,1104	0,1461	0,338	0,149
Minimum	50,4	22,2	24,6	18,5	0,057	0,51
Maximum	66,2	32,3	36,2	34,9	0,279	0,955
Range	15,8	10,1	11,6	16,4	0,222	0,455
Skewness	0,23	0,796	-0,3298	-1,0269	8,047E-03	-0,7931
Kurtosis	1,7177	3,2236	0,1614	3,7637	2,5736	3,2263
Statistical Analysis applied to the 10m depth segment						
Mean Value	50,583	24,458	26,125	28,716	0,152	0,776
Variance	62,765	13,22447	37,53296	15,04879	3,0666E-02	1,1636E-02
Standard Deviation	7,922	3,636	6,126	3,879	5,5377E-02	0,107
Coefficient of variance	0,1566	0,1486	0,2345	0,135	0,3631	0,1389
Minimum	38,1	20,8	15,1	20,5	0,057	0,54
Maximum	66,2	32,3	35,4	33,0	0,235	0,908
Range	28,1	11,5	20,3	12,5	0,178	0,368
Skewness	0,3554	0,8821	-0,2967	-0,9666	0,1006	-0,8570
Kurtosis	2,4855	2,4761	2,0671	2,6784	2,0558	2,6982

W_L: Liquid Limit, W_p: Plasticity Limit, P_I: Plasticity Index, W_c: Water Content, C_c: Compression Index, V_r: Void ratio

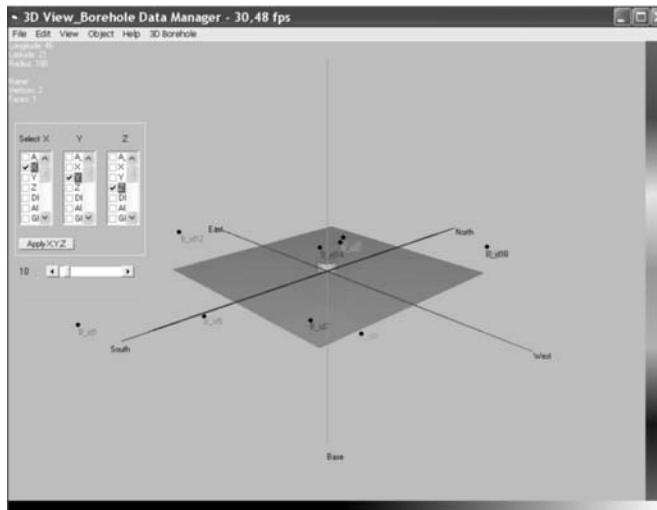


Fig. 6: Screenshot of 3D View / Visualization manager

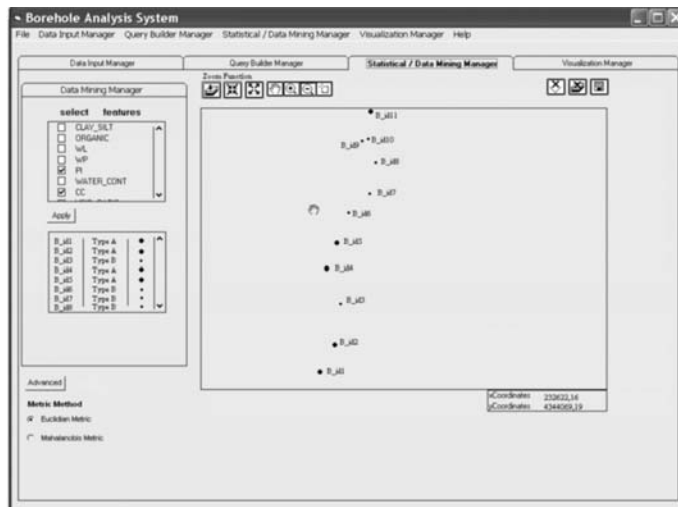


Fig. 7: Visualizing the Data Mining Manager results

By the end of each performed analysis the BAS provides the user within a second the statistical reports and exports data into word or excel format. Moreover the results were encoded as shapefiles and introduced in the Visualization Manager. There the user could produce 2D views of the spatial distribution of the borehole database, showing the values of each parameter in a formulated list-view object (Fig. 5). When ever the user needs to visualize the log photos or the log profile, he could do so just by clicking in the appropriate tab, which illustrates the image data.

The application can commute the features into 3D shapefiles, where x, y, z values are imported by the user, while the application converts those values in such a manner that the new values of x,y,z are within a space of [-1, 1]. This conversion provides a better visualization perspective of the boreholes location and the spatial variances of the geotechnical parameters (Fig.6).

The problem of classifying formations according to certain variables becomes more complicated in areas where few experimental data exist. However data mining algorithms could server as an appropriate tool, in order to perform clustering and classification (Chen et al, 1996; Kanungo et al, 2002). In our case the existing data could be used to identify areas with similar characteristics by clustering them into classes that appear minimum coefficient of variance within each class and maximum coefficient of variance among classes. The outcomes of the initialization of data mining algorithms, were in accordance with those described by the geotechnical surveys and indicate that certain areas could be identify having similar geotechnical profile, according to their Euclidean distance (Fig.7).

5. Conclusions

The developed application is based on structuring and storing in digital formats the various geotechnical data of different types (borehole logs, cross-section, geological maps, and in-situ and laboratory test parameters). It can also be used to answer specific enquiries concerning the variables that characterized the material in question, to aid to the production of engineering geological maps, geotechnical summaries, and assessments of engineering behaviour for the soils and rocks of an area.

It could be used as a simple querying tool to answer simple questions about geological and geotechnical characteristics in a spatial context or as an advanced investigation tool, identifying spatial patterns in their data based on any attribute through querying, data mining and visual explore them in 2-D and 3-D environment.

The application of data mining algorithms in the available geotechnical database proved to be a very powerful technique, identifying spatial patterns of similar geotechnical parameters that were much more difficult to identify following the classical procedure applied in geotechnical investigation.

The final product is for use both to engineers and geologists, providing a better understanding of engineering geological conditions, but also to planners identifying areas that may geologically constrain development.

6. References

- Adams M., Bosscher J., 1994. Integration of GIS and knowledge-based systems for subsurface characterization. *In ASCE Monograph on Integration of Expert Systems*, eds. M.L. Maher and I.Tommelein, ASCE.
- Ames, D.P., C. Michaelis, A. Anselmo, L. Chen, and H. Dunsford, 2008. *MapWindow GIS. Encyclopedia of GIS*. New York, Sashi Shekhar and Hui Xiong (eds). Springer, 633-634.
- Bain A., Giles A., 1997. A standard model for storage of geological map data. *Computers & Geosciences* Vol.23, No 6, 613-620.
- Chen M.-S., Han, J., Yu, P.S., 1996. Data mining: An overview from a database perspective. *IEEE Transactions on Knowledge and Data Engineering*, Vol.8, Issue 6, 866-883.
- Daniel, W. W., 1990. *Applied non parametric statistics*. Boston, 2nd edition: PWS-Kent, 635pp.
- Denas Z., Belickas J., Sliupa S., 2005. Intergrated approach and application of GIS for management of geological data. *The Current Role of Geological Mapping in Geosciences*, S. Ostaficzuk (eds), 135–150.
- Foster A., Culshaw G., 1990. The Use of Site Investigation Data for Preparation of Engineering Geological Maps and Reports for Use by Planner and Civil Engineer. *Engineering Geology*, Vol.29, 347-354.
- Goktepe B., Altun S., Sezer A., 2005. Soil clustering by fuzzy c-means algorithm, *Advances in Engi-*

- neering Software*, Vol.36, Issue 10, 691-698.
- Jaksa, M.B., 1995. The Influence of Spatial Variability on the Geotechnical Design Properties of a Stiff, Overconsolidated Clay. Ph.D. Thesis, University of Adelaide.
- Kanungo, T., Mount, D.M., Netanyahu, N.S., Piatko, C.D. Silverman, R., Wu, A.Y., 2002. An efficient k-means clustering algorithms: Analysis and implementation. *IEEE Transactions on Pattern Analysis and Machine Intelligence*, Vol.24, Issue 7, 881-892.
- Kaufmann O., Martin T., 2008. 3D geological modelling from boreholes, cross section and geological maps, application over former natural gas storages in coal mines. *Computers & Geosciences*, Vol. 34, 278-290.
- Lan H., Martin D., 2007. A digital approach for integrating geotechnical data and stability analyses. *Rock Mechanics: Meeting Society's Challenges and Demands*, E.Eberhardt, D. Stead & Morrison, T. (eds), London, Taylor and Francis Group.
- Laxton L., Becken K., 1996. The Design and implementation of a spatial database for the production of geological maps. *Computers & Geoscience*, Vol. 22, 123-733.
- Luna R., Frost D., 1998. Spatial Liquefaction Analysis System. *Journal of Computing in Civil Engineering*, ASCE, Vol. 12, No. 1, 48-56.
- McCarthy D., Graniero A., 2005. A GIS-based borehole data management and 3D visualization system. *Proceedings of the 2005 Annual Conference of the International Association for Mathematical Geology, Toronto*, 267-272.
- MacQueen B., 1967. Some Methods for classification and Analysis of Multivariate Observations. *Proceedings of 5-th Berkeley Symposium on Mathematical Statistics and Probability*, Berkeley, University of California Press, 1:281-297.
- Pininska J., Dziedzic A., 2004. GIS application for geomechanics—a Polish example, *Bulletin of Engineering Geology and the Environment*, Vol.63, No 1, 83-87.
- Tsagaratos P., 2008. Development of a graphical user interface (GUI) application for the management of borehole data, *Geophysical Research Abstracts*, Vol. 10, EGU2008-A-06732.
- Uzielli M., Vannucchi G., Phoon K., 2004. Assessment of weak stationarity using normalized cone tip resistance. *Proceedings of the 9th ASCE Specialty Conference on Probabilistic Mechanics and Structural Reliability, Albuquerque, New Mexico, July 26–28*.

ΕΥΡΕΤΗΡΙΟ ΣΥΓΓΡΑΦΕΩΝ AUTHOR INDEX



- Adamaki A.K.: 1984
Agalos A.: 2005
Aidona E.: 1888
Albanakis K.: 2383
Alexandratos V.G.: 2310
Alexandri M.: 1056
Alexandropoulou S.: 989
Alexandrou M.: 1888
Alexopoulos A.: 1792
Alexopoulos J.D.: 1898
Alexouli-Livaditi A.: 737
Alkalais E.: 1286
Amerikanos P.: 1149
Anagnostou Ch.: 2426
Anagnostoudi Th.: 548
Angelopoulos A.: 1094
Antonakos A.: 1821
Antonarakou A.: 568, 613, 620, 763
Antonelou A.: 876
Antoniou A.A.: 1104
Antoniou Var.: 320
Antoniou Vas.: 320
Apostolaki Ch.: 2570
Apostolidis Em.: 1418, 1619, 1850
Apostolidis N.: 2532
Apostolidis N.: 2597
Arapogiannis E.: 2229
Argyraki A.: 1737, 2319, 2510
Argyriadis I.: 264
Arvanitidis N.D.: 2437
Arvanitis A.A.: 1907, 2246
Astiopoulos A.C.: 1994
Athanassouli E.: 939
Avgerinas A.: 276
Avramidis P.: 558, 654
Ballas D.: 1056, 1737
Baltzois V.: 1149
Bantekas I.: 829
Barbera G.: 663
Barbu O.: 594
Baskoutas I.: 2125
Bathrellos D.G.: 1637
Bathrellos G.D.: 1572
Batsalas A.: 697
Baziotis I.: 2485, 2522, 2667
Behrends T.: 2310
Bel-lan A.B.: 2338
Bellas M.: 1619
Bellas S.: 579
Beshku H.: 1777
Birke M.: 2338, 2350
Bizoura A.: 1314
Bloukas S.: 1149
Bonsall T.A.: 2406
Bourliva A.: 2532
Bourouni P.: 2540
Brachou C.: 907
Brauer R.: 1267
Brusca L.: 2327
Burgess W.: 1716
Caputo R.: 400, 486
Carey S.: 1056
Catalano S.: 400
Chailas S.: 1919
Chalkias D.: 1335
Charalambopoulos S.: 1878
Chatzaras V.: 387
Chatziangelou M.: 1112
Chatzipanagis I.: 2702
Chatzipetros Al.: 486, 1131, 1383
Chiotis E.: 1539, 1549
Chousianitis K.G.: 1572, 2005
Christanis K.: 224, 2218
Christaras B.: 1112, 1122, 1131, 1267, 1672
Christidis G.E.: 2553, 2562, 2570
Christofides G.: 2680
Christoforidou P.: 1678
Çina A.: 2577
Codrea V.: 594
D' Alessandro W.: 2327
Daftsis E.: 1737
Dasaklis S.: 737
De Vos W.: 2350
Delagrammatikas G.: 2485
Delimani P.: 1074
Demetriades A.: 2338, 2350
Depountis N.: 1138, 1210
Dermitzakis M.D.: 86, 978
Diakakis M.: 1323
Diamantis I.: 1697
Diasakos N.: 1149
Dilalos S.: 1898
Dimitrakopoulos D.: 1688
Dimitriou D.: 2229
Dimiza M.D.: 602, 763
Dominic Fortes A.: 2726
Dotsika E.: 886, 958, 1840, 2265, 2383
Doutsou I.: 1350
Doveri M.: 1840
Drakatos G.: 1994
Drinia H.: 613, 620, 763
Dunkl I.: 276
Duris M.: 2338
Economou G.: 804, 2485
Economou N.: 1802
Eikamp H.: 918
Epitropou N.: 939
EuroGeoSurveys Geochemistry Expert Group: 2338, 2350
Exioglou D.: 1230
Fadda S.: 2446, 2588
Fakiris E.: 1064
Falalakis G.: 276
Fassoulas C.: 746
Fassoulas C.: 781, 896, 918
Ferentinos G.: 176, 1018, 1064
Fermeli G.: 978, 989
Fernandez-Turiel J.L.: 2373
Fikos I.: 1953
Filippidis A.: 2373, 2532, 2597, 2762
Filippidis S.: 2597
Fiori M.: 2446, 2588
Foscolos A.E.: 8, 2294
Fotopoulou M.: 2218
Foumelis M.: 1301
Foundas P.: 989
Fountoulis I.: 1046
Frisch W.: 276
Gaki-Papanastassiou K.: 409, 418, 506
Galanakis D.: 1428, 1465
Galbenis C.T.: 2485
Ganas A.: 1607
Garver J.J.: 309
Gawlick H-J.: 276
Georgakopoulos A.N.: 1230, 2236, 2274
Georgiadis I.K.: 2606
Georgiadis P.: 1406
Georgiou A.: 2492
Georgiou Ch.: 1428

Georgiou P.: 1056
 Georgoulas A.: 1074
 Geraga M.: 1018, 1064
 Germenis N.: 989
 Gerogianni N.: 2786
 Gerolymatou E.: 1438
 Gialamas J.: 1777
 Giannakopoulos A.: 958
 Giannouloupoulos P.: 1438, 1447
 Gimeno D.: 2373
 Gioti Ev.: 1627
 Gkadi E.: 548
 Gkiolas A.: 1272
 Gkiougkis I.: 1697
 Golubović Deligani M.: 1582
 Gospodinov D.: 1994
 Gournelos Th.: 1335, 1647
 Hademenos V.: 1539
 Hagiou E.: 1157
 Haidarlis M.: 907
 Hamdan H.: 1802
 Handler R.: 299
 Hatzipanagiotou K.: 876, 2501,
 2540, 2617, 2712
 Helly B.: 845
 Iatrou M.: 1018
 Iliá I.: 1590, 1688
 Iliopoulos G.: 746, 781, 918
 Īnaner H.: 2218
 Ioakim Chr.: 1035
 Ioannidis N.: 1888
 Janikian Z.: 939
 Jenkyns H.C.: 627
 Jipa-Murzea C.: 594
 Kacandes G.: 2562
 Kadetova A.V.: 1341
 Kafkala I.G.: 2390
 Kafousia N.: 627
 Kalantzi F.: 1350
 Kalisperi D.: 654
 Kallergis G.: 1821
 Kallioras A.: 69, 1697
 Kalogerogiannis G.: 1149
 Kamberis E.: 289, 715
 Kanaris D.: 1202, 1230
 Kantiranis N.: 2762
 Kapetanidis V.: 2015
 Karageorgiou D.E.: 1457, 1601,
 2229, 2236, 2274, 2692
 Karageorgiou M.M.D.: 1601, 2236,
 2274
 Karagianni A.: 1165
 Karagianni E.: 495
 Karakaisis G.F.: 46, 2026
 Karakitsios V.: 627, 634, 663
 Karakonstantis A.: 2043
 Karakostas V.G.: 1984, 1994, 2053,
 2064, 2075, 2093, 2114
 Karalemas N.: 1707
 Karamanos Ch.K.: 2053, 2075
 Karapanos E.: 1716
 Karastathis V.K.: 1438
 Karfakis J.: 1619
 Kargiotis E.: 2257
 Karipi S.: 2617, 2712
 Karmis P.D.: 1393, 1438, 1447,
 1919
 Karoutzos G.: 1165
 Karydakís Gr.: 2246, 2265
 Karymbalis E.: 409, 418, 1601
 Kastanioti G.: 2786
 Kastanis N.: 169
 Katagas Ch.: 247
 Kati M.: 2786
 Katrivanos D.E.: 999
 Katsanou K.: 1726, 1878, 2218
 Katsiki P.: 2562
 Katsikis J.: 2692
 Katsonopoulou D.: 812
 Kaviris G.: 2084
 Kelepertsis A.: 1858
 Kelepertzis E.: 1737
 Kementzetzidou D. A.: 2053
 Keupp H.: 579
 Khak V.A.: 1192
 Kidd W.S.F.: 309
 Kiliás A.: 276, 2075, 2114
 Kiliás S.P.: 2646
 Kiratzi A.: 2135, 2144
 Kitsopoulos K.: 2455, 2625
 Kokinou E.: 289
 Kokkalas S.: 368, 428
 Kokkidis N.: 548
 Kolaiti E.: 1286
 Kolios N.: 2246
 Kondopoulou D.: 1888, 1972
 Konstantinidi-Syvridi E.: 804
 Konstantopoulou G.: 1157, 1619
 Kontakiotis G.: 763
 Kontogianni V.: 886, 1202
 Kontopoulos N.: 558, 643, 654
 Koravos G.Ch.: 2193
 Koroneos A.: 2606, 2680, 2752
 Koskeridou E.: 613
 Kosmidis E.: 1812
 Kossiaris G.: 939
 Kostopoulou V.: 726
 Kotsovinos N.: 1074
 Kougemitrou I.: 804
 Kouki A.: 1169, 1177, 1184
 Koukidou I.: 1747
 Koukis G.: 1138, 1165, 1210, 1508,
 1619
 Koukoulis A.: 1457
 Koukouvelas I.: 368, 1350
 Koulouris S.: 1210
 Koumantakis I.: 1590, 1656
 Kounis G.D.: 1758, 1767, 1821
 Kounis K.G.: 1758, 1767
 Kourkouli P.: 1301
 Kourkounis S.: 643
 Koutsinos S.: 2246
 Koutsios A.: 654
 Koutsopoulou E.: 2635
 Koutsouveli An.: 1418, 1619
 Kozireva E.A.: 1341
 Kozyreva E.A.: 1192
 Kranis H.: 1919
 Kritikou S.: 1007
 Ktena S.: 1165
 Ktenas D.: 548
 Kurz W.: 299
 Kynigalaki M.: 1202, 1619
 Kyriakopoulos K.G.: 309, 663,
 2327, 2361, 2726
 Kyrousis I.: 1406
 Lagios E.: 344, 2005
 Lainas S.: 1138, 1210
 Lalechos N.S.: 442
 Lalechos S.N.: 442
 Lambrakis N.: 1716, 1726, 1878,
 2218
 Lampropoulou P.: 2465
 Laskaridis K.: 2475
 Lasocki S.: 2114
 Lazaridis A.: 1840, 2383
 Lazaris S.: 2390
 Lehmann P.: 1831
 Leivaditi A.: 1406
 Lekkas E.: 1361
 Lekkas S.: 1707
 Lelli M.: 1840
 Lemesios I.: 1878
 Leone G.: 886
 Leontakianakos G.: 2485
 Leptokaropoulos K.M.: 2093
 Liakopoulos S.: 1438
 Limnios N.: 2200
 Locutura J.: 2338
 Lois A.: 2183
 Loukaidi V.: 737
 Loupasakis C.: 1219, 1230, 1465,
 1619, 1850
 Lycourghiotis S.: 1029
 Lykakis N.: 2646
 Lykoudi E.: 1314, 1406
 Lykousis V.: 1046
 Magganas A.: 2786

Makri K.: 169, 999
 Makris J.: 32, 357
 Makrodimitras G.: 675
 Makropoulos K.C.: 216, 2005, 2015, 2084, 2104, 2163
 Malandraki V.: 1094
 Malandrakis E.: 1149
 Malegiannaki I.: 1007
 Maneta V.: 685
 Manoutsoglou E.: 697, 1314, 2492
 Maramathas A.: 1777
 Marinos P.V.: 1238, 1248, 1259
 Marinov S.P.: 2398
 Mariolakos I.D.: 92, 821, 829, 1785
 Markantonis K.: 1406
 Maroukian H.: 409, 418, 506
 Marsellos A.E.: 309
 Martelli M.: 2327
 Matiatos I.: 1792
 Mavromatis T.: 1131
 Mazzoleni P.: 663
 Melfos V.: 845, 948
 Mertzaniides Y.: 1802, 1812, 1962, 2257
 Metaxas A.: 2229, 2236, 2265, 2274
 Metaxas Ch.P.: 442
 Michail K.: 939
 Michailidis K.: 2532, 2657
 Midoun M.: 264
 Migiros G.: 320
 Mirek J.: 2114
 Mitropoulos A.: 2257
 Mitropoulos D.: 1474
 Monaco C.: 400
 Moraiti E.: 1267
 Moshou A.: 2104
 Moumou Ch.: 706
 Mountrakis D.M.: 276, 495
 Mourtzas N.D.: 453, 1272, 1286
 Mpalsats I.: 2501
 Mposkos E.: 2522, 2667
 Mwila G.: 1697
 Nastos P.T.: 1335
 Neuweiler I.: 1831
 Nicolaou E.: 939
 Nikas K.: 1821
 Nikolaidis A.: 989
 Nikolakopoulos K.: 1486, 1627, 1647
 Nikolaou N.: 1202, 1393, 1619
 Nikolaou P.: 706
 Nikolopoulos V.: 829
 Nomikou P.: 464, 1056
 Novikova T.: 1438
 Ntontos P.: 264
 Oikonomopoulos I.: 2284
 Or D.: 1831
 Orlecka-Sikora B.: 2093
 Palyvos N.: 829
 Pambuku A.: 1777
 Panagiotakopoulou O.: 643
 Panagiotaras D.: 558
 Panagiotopoulos V.: 548
 Panagopoulos A.: 1678, 1747
 Panagopoulos G.: 2492
 Panoussi P.: 634
 Pantelaki O.: 697
 Papadimitriou E.: 1994, 2200
 Papadimitriou E. E.: 1984, 2053, 2064, 2075, 2093, 2114
 Papadimitriou P.: 2005, 2015, 2043, 2084, 2104
 Papadopoulos A.: 2680
 Papadopoulos G.A.: 1438
 Papadopoulou L.: 845
 Papadopoulou S.: 548
 Papaefthymiou S.: 2465
 Papafotiou A.: 1831
 Papageorgiou E.: 331, 344
 Papakonstantinou K.: 1840
 Papamantellos D.: 2465
 Papamarinopoulos S.P.: 105
 Papanastassiou D.: 1438
 Papanicolaou C.: 2294
 Papanikolaou D.: 72, 464, 475
 Papanikolaou G.: 2236, 2265, 2274
 Papanikolaou I.: 320
 Papanikolaou M.: 475
 Papanikos D.: 939
 Papastamatiou D.: 2510
 Papastefanou C.: 2680
 Papastergios G.: 2373, 2597, 2762
 Papathanassiou G.: 486, 1122, 1131, 1373, 1383
 Papatheodoropoulos P.: 989
 Papatheodorou G.: 1018, 1064
 Papazachos B.C.: 46
 Papazachos C.B.: 46, 495, 1930, 2026, 2064
 Papoulia J.: 357
 Papoulis D.: 558, 876, 2635
 Paradisopoulou P.M.: 2114
 Paragios I.: 2597
 Paraskevopoulos K.M.: 2752
 Parcharidis I.: 1301, 1582
 Parpodis K.: 2390
 Pasadakis N.: 2294
 Pashos P.: 939
 Passas N.: 1286
 Patronis M.: 2475
 Pavlides S.: 169, 486, 1122, 1373, 1383, 1607
 Pavlides Sp.: 1131
 Pavlidou S.: 939
 Pavlopoulos A.: 715
 Pavlopoulos K.: 1582
 Pechlivanidou S.: 706
 Perdikatsis V.: 2570
 Perissoratis C.: 1035
 Perraki M.: 804
 Perraki Th.: 2284
 Persianis D.: 2692
 Petrakaki N.: 2319
 Photiades A.: 726, 1495
 Pikoulis V.E.: 2183
 Pitsonis I.S.: 2193
 Plessa A.: 2193
 Pliakas F.: 1697
 Ploumis P.: 2702
 Pomoni-Papaioannou F.: 620, 726, 793
 Pomonis P.: 2617, 2712
 Pontikes Y.: 856
 Popandopoulos G.: 2125
 Poulakis N.: 1149
 Poulos S.E.: 506
 Poutoukis D.: 886, 2383
 Poyiadji El.: 1393, 1619
 Pratikakis A.: 2562
 Pretti S.: 2446, 2588
 Psarakis E.Z.: 2183
 Psomiadis D.: 886, 958, 1840, 2383
 Puglisi D.: 663
 Pyliotis I.: 548
 Pyrgakis D.: 1138
 Pyrgiotis L.: 1619
 Raco B.: 1840
 Rathossi C.: 856
 Rausch R.: 69
 Reimann C.: 2350
 Rigopoulos I.: 2501, 2617, 2712
 Rizzo A.: 2327
 Romagnoli G.: 400
 Rondoyanni Th.: 379, 1406
 Roumelioti Z.: 1438, 2135, 2144
 Rousakis G.: 1056
 Rozos D.: 1177, 1184, 1219, 1406, 1465, 1590, 1637, 1656, 1850
 Sabatakakis N.: 1138, 1165, 1210, 1619
 Sabatakakis P.: 1508
 Sakelaris G.: 2786
 Sakellariou D.: 1046, 1056
 Salminen R.: 2350
 Sarris A.: 289
 Sboras S.: 486, 1607
 Schüth C.: 69

- Schütz C.: 1831
 Scordilis E.M.: 46, 2026, 2154
 Sdrolia S.: 845
 Seeber L.: 2075
 Segou M.: 2163
 Serelis K.G.: 2390
 Serpetsidaki A.: 2174
 Siavalas G.: 2218
 Sideri D.: 1850
 Sifakis A.: 907
 Sigalos G.: 737
 Sigurdsson H.: 1056
 Sikalidis C.: 2373, 2532, 2597, 2762
 Skarlatoudis A.A.: 1930
 Skarpelis N.: 2417, 2510, 2553
 Skianis G.Aim.: 1627, 1647
 Skilodimou H.D.: 1572, 1637
 Skordas K.: 1858
 Smith D.C.: 804
 Sofianska E.: 2657
 Sokos E.: 989, 2174, 2183
 Soldatos T.: 2752
 Solomonidou A.: 2726
 Sotiropoulos P.: 344
 Sotiropoulos S.: 715
 Soulios G.: 196
 Soulis V.J.: 1094
 Soupios P.: 654
 Spanos D.: 368
 Spanou N.: 1230, 1619
 Spassov S.: 1972
 Spry P.G.: 2406
 Spyridonos E.: 1314, 1785, 2492
 Spyropoulos N.: 886
 St. Seymour K.: 2406
 Stamatakis G.: 2739
 Stamatakis M.: 2606, 2739, 2773
 Stamatis G.: 1868, 1878
 Stamboliadis E.: 697
 Stampolidis A.D.: 1907
 Stefanova M.: 2398
 Stiros S.: 886, 1029
 Stivanakis V.: 2465
 Stoulos S.: 2680
 Stoykova K.: 675
 Stratikopoulos K.: 1726
 Svana K.: 746
 Symeonidis K.: 1286
 Syrides G.: 1131
 Tagkas Th.: 1149
 Tarvainen T.: 2350
 Tassiou S.: 1520
 Theocharis D.: 821
 Theodorou D.: 1335
 Theodorou G.: 763
 Theodosiou Ir.: 926, 939
 Theodosoglou E.: 2752
 Thomopoulos Ach.: 1112
 Thomopoulos K.: 1064
 Tombros S.F.: 2406
 Tortorici G.: 400
 Tortorici L.: 400
 Tougiannidis N.: 2284
 Tranos M.D.: 495, 2064
 Triantafyllidis S.: 2417
 Triantafyllou G.: 2294
 Triantaphyllou M.: 475, 602, 634, 715, 754, 763,
 Trontzios G.: 2657
 Tryfonas G.: 1149
 Tsagas D.: 1335
 Tsaklidis G.M.: 1984, 2200
 Tsanakas K.: 418, 506
 Tsangaratos P.: 1406, 1590, 1656, 1688
 Tsapanos T.M.: 2193
 Tsaparas N.: 620
 Tselentis G–A.: 2174
 Tselepidis V.: 379
 Tsiambaos G.: 183, 1104, 1259
 Tsikouras B.: 876, 2501, 2540, 2617, 2712
 Tsimas S.: 2485
 Tspoura–Vlachou M.: 663
 Tsirambides A.: 2606, 2762
 Tsirigotis N.: 1149
 Tsobanoglou C.: 1812
 Tsokas G.N.: 1907
 Tsolakis E.: 763
 Tsolis–Katagas P.: 856, 2635
 Tsombos P.: 1438, 1447, 1486, 1528, 1539, 1547, 1539, 1548, 1559
 Tsoukala E.: 958
 Tsourlos P.: 1962
 Tzamos E.: 2762
 Tzanaki I.: 289
 Tzani A.: 344, 1919, 1941
 Tzavidopoulos I.: 886
 Tzevelekou Th.: 2465
 Tziritis E.: 1858
 Tzortzaki E.: 613
 Vafidis A.: 1802
 Vagenas N.: 1165
 Vagenas S.: 1210
 Vagioteu E.: 1149
 Vaiopoulos D.: 1627, 1647
 Vakalas I.: 675, 697
 Vako E.: 1777
 Valera P.: 2446, 2558
 Valiakos I.: 965
 Valkaniotis S.: 486, 1383
 Vamvakaris D.: 495
 Van Cappellen P.: 2310
 Varaggouli E.: 1074
 Vargemezis G.: 1953, 1962
 Varnavas S.: 234
 Varvarousis G.: 2229, 2265
 Vasilatos Ch.: 2773
 Vassiliades E.: 1520
 Vassiliou E.: 1688
 Vassilopoulou S.: 516
 Vaxevanopoulos M.: 948
 Vitsas T.: 989
 Vlachopoulos I.: 1165
 Vlachou–Tspoura M.: 2773
 Vogiatzis D.: 2762
 Vontobel P.: 1831
 Votsi I.: 2200
 Voudouris K.: 1678
 Voudouris P.: 685, 845, 2786
 Vougioukalakis G.: 939
 Voulgaris N.: 2163
 Vouvalidis K.: 706, 1122
 Vrettos K.: 2236
 Vythoulkas N.K.: 2193
 Wölfler A.: 299
 Xeidakis G.: 1074
 Xypolias P.: 368, 387
 Zagana E.: 1726, 1878
 Zambetakis–Lekkas A.: 773
 Zananiri I.: 1474, 1539, 1549, 1972
 Zanchetta G.: 886
 Zeligidis A.: 643, 675, 697, 793
 Zerefos C.S.: 2
 Zervakou A.D.: 1528, 1539, 1549, 1559
 Zevgitis T.: 989
 Ziannos V.: 1812
 Zidianakis G.: 781
 Zisi N.: 958, 1840, 2383
 Zorba T.: 2752
 Zoumpoulis E.: 793
 Zouridakis N.: 1792
 Zouros N.: 159, 896, 965
 Zygouri V.: 527